PROCEEDINGS OF
09th INTERNATIONAL CONFERENCE ON
Smart Manufacturing and Environmental Engineering
Bhubaneswar, India

Organized by:

DEPARTMENT OF MECHANICAL ENGINEERING
&
DEPARTMENT OF CIVIL INGINEERING

Date of Event:

18th - 19th December, 2017

VENUE:

NM INSTITUTE OF ENGINEERING & TECHNOLOGY,
BHUBANESWAR, ODISHA, INDIA.

Published by : International journal of engineering sciences paradigms & researches, ISBN 2319-6564

CORE MEMBERS

ADVISORY COMMITTEE

1. Dr. Mihir Mohanty, Asso. Prof., SOA University
2. Dr. Rajat Giri, Asso. Prof., IIT BBSR
3. Dr. Anup Panda, Prof., NIT Rourkela
4. AMIYA RATH, BPUT
5. Dr. Alok Jagdev, KIIT university

ORGANIZING COMMITTEE

1. Dr. R C Parida, Chairmam, NM Group of Institutes.
2. Dr. Niranjan Mishra, Principal, NMIET
3. Prajnadipta Sahoo, Head of the Department, Electrical Engineering
4. Rashmi Ranjan Rath, Asso. Prof., Dept of Electronics and Communication Engineering
5. Chinmaya Ranjan Pradhan, Asso. Prof., Dept. of electrical engineering
6. Santosh kumar Sharma, Asso. Prof., Dept. of Computer Science

EDITORIAL COMMITTEE

1. Sukanya Nayak, Asst Prof , Dept of ECE
2. Subhendu Sahoo, Asso. Prof. , Dept Of EE
3. Dr. Khirod Kumar Rout, Professor, Dept of EEE

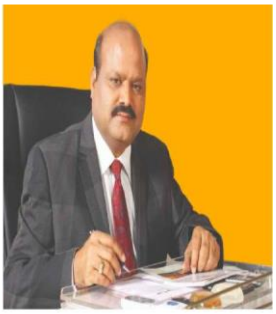

I am happy to know that the 9th International conference on **Smart Manufacturing and Environmental Engineering** is organized by the Department of CIVIL and Mechanical Engineering of NMIET Bhubaneswar from 18th and 19th December 2017 at NMIET Campus Bhubaneswar.

Green tech or green technology is an umbrella term that describes the use of technology and science to create products that are more environmentally friendly. The goal of green tech is to protect the environment and in some cases, to even repair past damage done to the environment.

I convey my very best wishes to both the organizers and the participants, and hope that this sharing of ideas will lead to better world.

(Dr. Ramesh Chandra Parida)
Patron and Chairman,
NM Group of Institutions

It is a great pleasure and honor to know that **NM Institution of Engineering and Technology is organizing the international Conference on "Green Technology and Material Research" during** 18th and 19th December 2017, at Bhubaneswar.

Welcome to the **9th International Conference on Smart Manufacturing and Environmental Engineering** being held in NMIET, Bhubaneswar, India from 18th Sept. till 19th December 2017. The International Conference on Smart Manufacturing and Environmental Engineering is held annually. The Organizing and Program Committees have worked hard to produce a first class technical conference and a pleasing and enjoyable social event. On behalf of the Organizing and Program Committees I welcome you all to Odisha and hope that you enjoy the scenery of Bhubaneswar and are rewarded by the technical challenges of the Sixth International Conference on Information Fusion.

(Principal)
NMIET BHUBANESWAR

I am happy to know that the 9th International conference on **Smart Manufacturing and Environmental Engineering** is organized by the Department of CIVIL and Mechanical Engineering of NMIET Bhubaneswar from 18th and 19th December 2017 at NMIET Campus Bhubaneswar.

Green tech or green technology is an umbrella term that describes the use of technology and science to create products that are more environmentally friendly. he goal of green tech is to protect the environment and in some cases, to even repair past damage done to the environment.

I convey my very best wishes to both the organize and the participants, and hope that this sharing of ideas will lead to better world.

Chairman
Organizing Committee

The **9TH International conference on Smart Manufacturing and Environmental Engineering** will be held on 18th and 19th December 2017 at NMIET BBSR. The organizing committee has done an excellent job and this conference promises to be another great success. I extend a personal invitation for you to participate and I look forward to seeing many of you in Bhubaneswar.

(Chief Guest)

On behalf of the organizing committee, I welcome all of you to the **09th International Conference on Smart Manufacturing and Environmental Engineering** at NMIET Bhubaneswar. The Organizing and Program Committees have worked hard to produce a first class technical conference and a pleasing and enjoyable social event. On behalf of the Organizing and Program Committees I welcome you all to Australia and hope that you enjoy the scenery of Cairns and are rewarded by the technical challenges of the Seventh International Conference.

Convener

TABLE OF CONTENTS

★★★

ARRANGEMENT OF SOFT CLAYEY SOILS AND THEIR STRESS ANALYSIS UNDER DIFFERENT CONDITIONS

[1]CHANNABASAVARAJ WOLLUR, [2]RAGHUPATRUNI BHIMA RAO, [3]BIPESH MOHANTY

[1]Professor, Department of Civil Engineering, NMIET, BBSR, India
[2]Department of Civil Engineering, AIET, Bhubaneswar, India
[3]Department of Civil Engineering, CEC, Bhubaneswar, India
E-mail: [1]mishra.s.c@nmiet.ac.in

Abstract - Development of structural designing constructions on delicate clayey grounds expects architects to consider the combination conduct of these stores. On account of the regular thickness of clayey soils, their combination is significantly affected by vertical pressure and furthermore because of natural substance. Because of an ever increasing number of developments being focused on in profoundly populated metropolitan territories, there is a developing requirement for development of structures and geotechnical structures on delicate clayey surfaces, that normally produce unmistakable drag misshaping. Notwithstanding an immense exploration work being done related to the optional combination conduct of a characteristic dirt materials, there are as yet numerous inquiries regarding this marvel.

Keywords - Delicate Earth, Solidification, Creep, Thickness.

I. INTRODUCTION

Increasing population and dire shortage of land area has caused its reclamation in many of the developed countries. For the ease of sea transport, many big cities worldwide are located on clayey deposits around coastal areas, hence large number of structures are constructed on soft soils. For all the civil engineering projects related to soft clayey deposits, engineers of necessity have to contemplate the consolidation behaviors of a deposit. Consolidation generally is a phenomenon by which a soil mass decreases in volume by squeezing out pore water by means of slow dissipation of the excess hydrostatic pressure due to an imposed total stress. As per Karl Terzaghi's theory, "consolidation is a process which is characterized by reduction in water content of the saturated soils without the replacement of water by air." Terzaghi shown the consolidation process in a clay soil subjected to loading is analogous to the behavior of the spring – piston model. Springs represent soil skeleton. Spring surrounded by water represents saturated soil. Perforations in a piston are analogous to the voids which provide permeability to soil. As the stress is withdrawn from the consolidated soil, it rebounds, restoring some of its volume it had lost in the consolidation process. On stress being applied again, the soil will consolidate again but now along the recompression curve, represented by the recompression index. The soil with its load removed is referred as over-consolidated, while highest stress to have acted upon it is referred to as the pre-consolidation stress.

1.2 Need and Scope:

The importance of secondary consolidation is predominant for highly plastic soils. Fundamental understanding of the compressibility of soil with a wide range of plasticity index is essential for developing theories of consolidation data for any foundation project. An assessment of the behavior of secondary compression index Cawith time is urgently wanted. Determination of the primary compression index (Cc) and secondary compression index (Ca) of soils with wide margin of plasticity indices (Ip) may help in this regard.

1.3 Literature Review:

Hanna (1950) carried out research at Fouad I University, Cairo. The calculated and the theoretical settlements, according to the results from consolidation tests were relatively very close; but numerically, theoretical settlements in many buildings were 3–4 times the observed values. Mesri (1973) investigated considerable importance of secondary or delayed compression and noted that coefficient of secondary compression is the powerful tool to explain the secondary compression. Mineral composition and physicochemical environment have significant influences on the co-efficient of secondary compression. Sridharan and Jayadeva(1982) explained that the compressibility of the pure clay soils under external loading not only relies on the negative charges and the crystallite structures of clayey minerals but it also relies on the ion concentrations, temperature , dielectric constants and cationvalency of the pore fluid. Barbour and Fredlund (1989) stressed on smectite behavior of clay, which is significantly controlled by pore liquid composition. The interactions of clay soil with pore fluid cause changes in volume and shear strength by ion diffusion under constant external stresses. Sridharan and Prakash (1998) proposed estimation of secondary settlement based on secondary compression factor ($m = \Delta \log e / \Delta \log t$) is more realistic for soil which exhibit non-linear secondary compression behavior. Muntohar (2003) carried out laboratory one- dimensional consolidation tests and stressed on the swelling and compressibility characteristics of soil–bentonite mixtures. The swelling and compressibility characteristics generally increase with increase in bentonite percentage in bentonite, kaolinite and sand mixtures. Bhattacharya and Basack (2011) suggested Installation of prefabricated vertical drains, followed by preloading that accelerates the consolidation of soft soil having low hydraulic conductivity and low shear strength thereby reducing the timeperiod.

1.4 Experimental Investigation:

Material used in this study are Na bentonite and Cabentonite that are commercially available in market, along with silt.

1.5 MaterialCharacterization:

1.5.1 Atterberg limits:

Atterberg limits were determined as per IS: 2720-Part 5 (1985) and the results are tabulated below.

Soil	Liquid limit (*wl* %)	Plastic limit (*wp*%)	Plasticity Index (*Ip* %)
Na-Bentonite	407	42	365
Ca- Bentonite	140	61	79
Silt	27	22	5

1.5.2 Special gravity: The specific gravity of Na-bentonite and Ca-bentonite, silt were determined as per IS: 2720-Part 3 (1980) and their values were found to be 2.7, 2.67 and 2.6 respectively.

1.6 Apparatus Used:

The mineral composition of bentonite is obtained by using X- ray diffraction method. According to Bragg's law, the XRD identifies the minerals based on the relationship between the angle of incidence of X-rays (θ) to the c-axis spacing (d). A Philips automated powder diffractometer was used for XRD analysis in this study. Consolidation test under varied load and plasticity indices is done by using a one-dimensional consolidometeroroedometer.

1.6.1 X-ray diffraction method(EDX):

Fine grained bentonite power and silt of 1.5 g was kept in oven drying for 2 hours and allowed to cool in room temperature. Then, sample is filled in the sample holder of diffractometer and the XRD pattern is obtained by scanning over angles between 5° to 90°, 2θ at 5°/min. In the step mode, a 0.05° - 2θ step for 2 s was given. Results are analyzed using X-pert High Score software. From the results of XRD analysis mineral composition such as Illite, Kaolinite, Montmorillonite, Muscovite are found in Na bentonite sample. Similarly, the analyses were carried out for Cabentonite and silty soil and the mineral composition were determined.

1.6.2 One-dimensional consolidometer Test:

One-dimensional consolidation testing method was first given by Terzaghi in 1925. The test is carried out using a consolidometeror (oedometer). Figure 3.14 represents a one dimensional consolidometeror oedometer. The soil specimen is kept in a metal ring having two porous stones, one is at top of the said specimen and another one at the bottom of it. The load is imposed by a lever arm, and compression is read through the dial gauge. The specimen remains under water during the coarse of test. Every load increment is normally kept for at least 24 hours. Following that the load is doubled and the compression measurement is done and continued.

1.6.2.1 Test Procedure:

One-Dimensional consolidation test was done in in conformity with ASTM D2435/ (ASTM, 1999). Standard fixed ring type consolidometer was used with ring diameter 75mm and 25mm height to perform the experiment. The soil specimen was kept inside the metal ring having a porous stone at the top and bottom. All specimens were tested at moisture content of extracted soil sample. Utmost care was taken to prevent air entrapment in soil specimens remolded in the rings. The specimen was kept under water throughout the test. The load to the specimen was exerted through a leverarm, and the compression of the specimen was measured by a dial gauge. The deformation of the soil sample was noted from the dial gauge starting from 0 s, 30 s, 1min, 1.5min, 2min, 4min, 6min, 8min, 10min, 15min, 30 min, 60 min, 90 min, 120 min, 150 min, and 1440 min. The load was usually doubled every 24 h (i.e. incremental loading of 60, 120, 240, 480, 960, 1920 kPa were applied).

1.7 Result:

Various tests were carried out on ten different type of clays based on their plasticity, prepared by having different proportions of silt mixed in commercially obtainable sodium and calcium bentonite to aquire representative samples of various plasticity indices. As one dimensional consolidation tests were done for each of these soil samples at different vertical effective stresses. Dial gauge readings corresponding to each incremental loading were noted down. The primary compression index (C_c) was calculated from the slope of e versus log σ' curve and the secondary compression index(C_a) was obtained from the slope of settlement versus time plot (δ-logt).

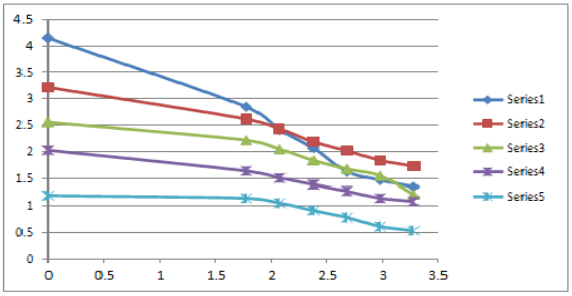

Series: 1-IP=98 2-IP=75 3-IP=42 4-IP=20 5-IP=14.

Figure 4.1 e - $log\ \sigma'$ curves for the consolidation test conducted for soil with Na bentonite mixed with silt.

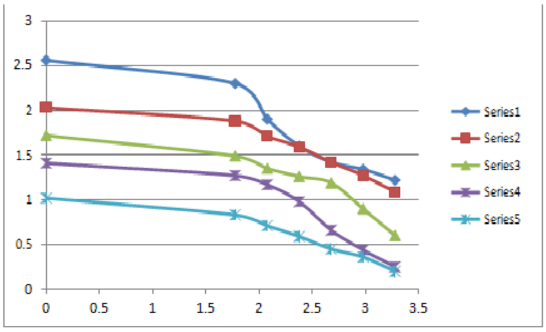

Series : 1-IP=51 2-IP=40 3-IP=29 4-IP=18 5-IP=10.
Figure 4.2 e - $log\ \sigma'$ curves for the consolidation test conducted for soil with Ca bentonite mixed with silt

II. CONCLUSION AND FUTURESCOPE

Tests reported in this thesis suggest primary compression index (Cc) increase with increase in the plasticity of the soil. Also a correlation was made between primary compression index (Ca) and plasticity index (Ip). The equation so developed can be considered to be reasonably accurate for consolidation problem. Secondary compression index (Ca) decreases with rise in stress range but the case is opposite with increase in plasticity index. Based on the outcome of this investigation following future works may be suggested:

- More investigation is required to establish correlation between primary compression index (Cc) and secondary compression index (*C*a) with permeability (*k*), coefficient of consolidation (*Cv*), coefficient of volume compressibility(*mv*).
- Tests may be conducted to study different minerals, pore fluid present in soft soil and their effect on primary and secondary consolidation.
- Tests may be conducted at low and elevated temperature.

REFERENCES

[1] Hanna, W. S. (1950). “Settlement studies in Egypt.” Geotechnique; 2(1),33-45.
[2] Mesri, G. (1973). “Coefficient of Secondary Compression,” J. of the soil mech. and found. Div; 99(1), pp. 124-128.
[3] Jain, S.K; and Nanda, A. (2010). “Nature of the Secondary Compression inSoil.”
[4] Ind. Geotech. Conf; IGS Mumbai Chapter & IIT Bombay,1121-1124.
[5] Lambe, T. W., and R. V. Whitman. (1969). "Soil Mechanics.” New York:Wiley.
[6] Indian Standard. IS: 2720 (Part 5) –1985 –Method of test for soils (Part 5 - Determination of liquid and plasticlimit).
[7] Indian Standard. IS: 2720 (Part 5) –1985 –Method of test for soils (Part 5 - Determination of liquid and plasticlimit).
[8] Sheeran, D. E., and Krizek, R.J. (1971). “Preparation of homogeneous soil samples by slurry consolidation.” J. Materials; 6(2), 356.

★★★

CHANGE OF MECHANICAL BEHAVIOR OF A COMPACTED WELL-GRADED GRANULAR MATERIAL WITH AND WITHOUT CEMENT

[1]DEVI PRASAD SINGH, [2]SWARUP RANJAN SAHOO, [3]JYOTIRMAYEE PANDA

[1]Professor, Department of Civil Engineering, NMIET, BBSR, India
[2]Department of Civil Engineering CEC, Bhubaneswar, India
[3]Department of Civil Engineering, AIET, Bhubaneswar, India
E-mail: [1]acharya.jyotikusum@nmiet.ac.in

Abstract - Concrete increases improve the presentation of granular soils. Be that as it may, most writing instances of concrete augmentations are in inadequately evaluated sands, either to imitate the conduct of sandstones or to complement the mechanical differences among established and uncemented soils. In this article, the conduct of an all around evaluated granular soil, utilized for base and sub-base of streets, was concentrated by doing triaxial tests on solidified and uncemented tests. Tests were compacted to accomplish a thick texture and tried at stresses ordinarily utilized in prac-tice. Sieving was utilized to comprehend if breakage is significant and to decide the grain size disseminations of the examples after compaction and shearing. The outcomes show that the expansion of little rates of concrete extraordinarily increment stiffness and widening. Along these lines, creating bigger qualities; this is especially significant at low confining stresses in streets and stopping regions, where this material is usually utilized. Everywhere strains, the outcomes show that different Critical State Lines exist for both the uncemented and solidified soils. Each line has a different slant, which is accepted to be the aftereffect of the development of the grain size appropriation of the established soil. The standardized information demonstrate that an extraordinary state limit surface can be resolved for every one of the three tried soils.

Keywords - Cemented soil; Compacted soil; Triaxial test; Critical state; Base and sub base; Granular soil

I. INTRODUCTION

Research in uncemented granular material has highlighted the importance of breakage, where the onset of breakage in the NCL is a function of the mineralogy of the grains [12]. Breakage is important as it also marks the location of the CSL, and many researchers have shown that by changing the grain size distribution, the CSL will also change (Thevanayagam et al., 2002, Carrera et al., 2011; Xiaoet al., 2016). In structured sands, only a few researchers considered the changes in particle size distribution (PSD) and its effect on altering the location of the CSLs and NCLs, when compared to the uncemented samples (Cuccovillo and Coop, 1997a; Marri et al., 2012). Certain results have shown that due to cementation, the resultant CSL would have a reduced gradient (Cuccovillo andCoop, 1997a), whilst others have shown that the cementation increases the gradient of CSL (Schnaid et al., 2001). In the aforementioned research, it is not clear if the alterations of the CSL gradient are due to particle breakage, bond degradation or a combination of both. Different critical state lines for the same samples with different cement con- tents are also reported by Cruz et al. (2011). The DEM results have shown that alterations in the CSL are due to the breakage of the bonds and the generation of a different grain size distribution, as some of the particles are still cemented together (Yu et al., 2014; Yu et al., 2015). The alteration of the CSL due to breakage was also investigated by Ghafghazi et al. (2014), where they claimed that break- age causes a downward parallel shift in the CSL, and according to Bandini and Coop (2011), large amounts of breakageareneededforsignificantchangestooccur.

In the majority of the research encountered so far, the samples were prepared using poorly graded granular mate- rials (sands of aeolian origin) or with lower densities; this was done in order to accentuate the breakage or the improvement caused by the binding agent added. In a cou- ple of articles (Rios et al., 2014; Consoli et al., 2014) well graded residual soils are reinforced with cement, however some of them have fines and there is no attempt to measure or determine the breakage.

When well graded soils are used the research tends to concentrate on the mechanical properties of the material at small strains i.e. stiffness and strength up to peak, using multiple-step loading triaxial tests (Kongsukprasert and Tatsuoka, 2007and Taheri et al., 2012). These tests have the advantage of allowing the use of a single sample to cover a large range of stresses, however it is unclear what the effect of damage to the cement bonds and particle breakage is from the previous loading steps. Hence, the effect of the addition of cement on manmade materials used forengineeringpurposesisnotverywellunderstood. The purpose of this paper is then to study the effect of small levels of cementation on a very dense fabric, created by compaction of a well graded granular material, under monotonic loading, on commonly used soils. The improve- ment of the mechanical properties and examines the effects of cementation within the Critical State framework is also explored.

II. MATERIAL TESTED

The soil used in this research was a crushed limestone with 88% CaCo3, collected from a depot in South London and is currently used commercially for the bases of roads in Southern England. The soil was wet sieved and each parti- cle size range was stored in separate bags. The main prop- erties of this material are summarised in Table 1, with the particle size distribution (PSD) shown in Fig. 1, together with the range defined by the UK Highways Agency (2016)forabaseandsub-basetype.

The idealised grading curve proposed by Fuller andThompson (1907) is based on the idea that when larger par- ticles are in contact with each other, larger voids are gener- ated and occupied by intermediate particles; this procedure is then followed to the smallest size available. Theidealised curve generates dense fabrics and was then used to correct the initial grading curve of the soil, given that the particles are not spherical, it is argued that it then does not generate the densest possible fabric. Given the sizes of the particles available, the PSD named ‘‘Adjusted grading” (Fig. 1) was used for all the tests. This curve follows the Fuller curvefor the largest sizes, and below the size 3.35 mm it was trans- lated downwards as not enough material was available. For the same reason, sizes below 0.425 were chosen to make sure that all samples would have the same grain size distribution and the grading within the Type 1, as defined by the UK Highway Agency (2016)for a base and sub- base. As the triaxial equipment used is capable to test sam- ples up to 100 mm diameter and 200 mm high, the grain size distribution was truncated at 20mm.

Cemented samples were created by adding Portland cement classified as CEM1, in accordance to the British Standards (BSEN 1197-1:2011). Given the high strength of the compacted samples, only small percentages of cement (1 and 2%) were used to generate modest changes instrengththatcouldbetestedinatriaxialequipment.

III. APPARATUS AND SAMPLE PREPARATION

A computer-controlled triaxial apparatus, with a local strain measurement system capable of measuring 10-6 strain, similar to Cuccovillo and Coop (1997b), was used for the conventional triaxial tests (Fig. 2). The system uses RDP electronics LVDTs (model D6/05000) attached to a modulator/demodulator (model S7DC) that allow the full configuration of the output electric signal. At the beginning of the shearing, the local instruments are reset to zero to take advantage of the 16-bit auto scale of the data logger. The volumetric strain was measured using the volume gauge and the localinstrumentation.

The desired amount of each fraction of soil was thor- oughly mixed in a tray, with different moisture contents, before being compacted in 5 layers, using 27 blows of a 5 kg hammer falling from a height of 450 mm (BS1377-4, 1990). A compaction curve for the uncemented soil was determined inorderto definethe optimum moisture content. Given that the cemented and uncemented sampleswere tested, a decision was made to compact all sampleswith a moisture content of around 10%, providing enoughwater for cement hydration at the cost of a lower dry den- sity. Table 2 contains the properties of every sample tested.After compaction, the uncemented samples were trans-ported to the pedestal of the triaxial equipment for testing. Suction maintained that the sample was intact before theconfining pressure was applied and the percolation proce- dure started. The cemented samples were prepared with two different percentages of cement (45 g for 1% and 90 g for 2% cement); where an equivalent mass was removed from the smallest grading of the samples’ PSD. The sample prepara- tion followed a similar procedure to the one described above, except that the cement and dry soil were thoroughly

Table 1
The index properties of research material from dry sieving.

Description	Crushedlimestone
Max density-vibratinghammer(g/cm^3)	2.24
Maxvoidratio	0.83
Mindensity(g/cm^3)	1.51
Minvoidratio	0.23
Particledensity(gr/cm^3)	2.76
Max dry density-automatic heavy compaction (g/cm^3)	2.24
Optimum water content (modifiedproctor)	6%
Typeofsoil	GW
D_{10}(mm)	0.2
D_{30}(mm)	1.5
D_{50}(mm)	3
D_{60}(mm)	4
Uniformity coefficient C_u¼$\frac{D_{60}}{D_{10}}$	20
Curvature coefficient- C_c¼ $D^{30}\frac{D^2}{10 \times D_{60}}$	2.8

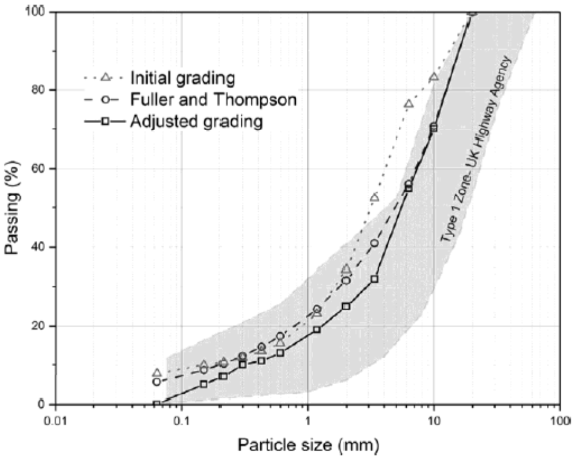

Fig. 1. Particle size distributions: Initial grading; Fuller and Thompson(1907) and the Adjusted grading. The grey band defines the range of type1 (UK Highway Agency,2016).

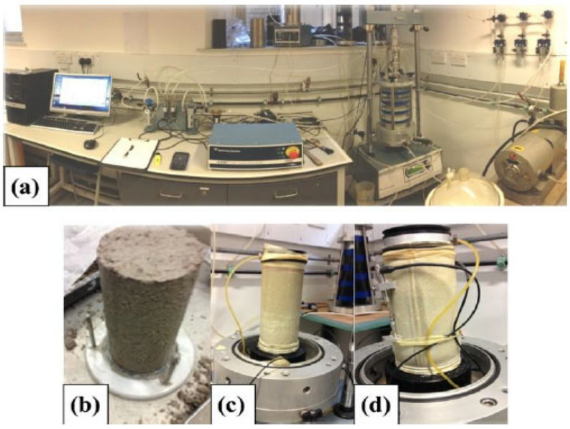

Fig. 2. Picture of the equipment and samples: (a) triaxial equipment in the lab; (b) compacted sample in the pedestal and sample with local instrumentation before closing the triaxial chamber.

mixed together before adding the same wateramount, mix-ing was then continued until homogeneity was achieved. After compaction the sample and mould were put inside of a plastic bag and allowed to cure for24 h. The sample was then placed inside of a tank withwaterat22◦Candallowedtocure,submerged,foranother4days.Atday5the sample was removed from the tank, mounted onthetri-axial pedestal and prepared for testing. This procedure was followed to guarantee that the cement couldhydratefully. Avolumeinexcessof2000ccofwaterwaspercolatedthroughthesampletoremoveairbubbles.Thepressureapplied was around 18 kPa, caused by thedifferencein height between a water containerlocatedapproximately2 m above the sample and the outlet from thepedestal.Thewatercomingfromthesamplewasclearandtheauthors believe that no cement particleswereremovedfromthesampleduringpercolation.Thesamplewasthensaturated, maintaining an effective stress of 15 kPa.AB-parametertestwasperformedatdifferentbackpressures,from 100 to 350 kPa on the first sample. Whilstitincreasedslightlyupto250kPa,theincreasesat300and350kPawhere negligible (values measured were of the orderof 0.86to0.92). Itisimportanttomentionthatthevolume gauge only changed slightly during the increase in pres- sures, being fairly constant once the required pressures were maintained. This indicated that the sample was satu- rated and the B-parameters would not reach the required value. Therefore, a minimum back pressure of 250 kPa was used in all drained tests and monitored by another transduceratthetopofthesample.

In the consolidation stage the effective stress was raised to the value used in the test. This procedure would take around 2 to 3 days before shearing; however, the cemented samples were all sheared in a drained way at the end of day 7.

Table 2 Properties of the samples tested: the name indicates the cement percentage and the confining stress used during shearing.

Properties of the samples tested: the name indicates the cement percentage and the confining stress used during shearing.

Test Name	W_0 (%)	e_0 *	e_{con} **	c_{Dry} (g/cm^3)	q_{max}(kPa)
M-0%-020	9.61	0.379	0.378	1.952	301
M-0%-050	8.63	0.376	0.370	1.961	482
M-0%-100	9.66	0.417	0.405	1.938	804
M-0%-200	10.03	0.404	0.388	1.978	1177
M-0%-400	9.71	0.400	0.374	1.973	2067
M-1%-050	9.59	0.397	0.392	1.958	941
M-1%-100	8.44	0.367	0.357	1.974	1219
M-1%-200	8.72	0.392	0.364	1.968	1910
M-1%-300	9.83	0.410	0.381	1.943	2247
M-1%-400	9.03	0.393	0.350	1.965	2755
M-2%-020	9.21	0.380	0.380	1.961	809
M-2%-050	8.74	0.388	0.383	1.960	1359
M-2%-100	8.61	0.371	0.361	1.972	1656
M-2%-200	9.04	0.396	0.380	1.951	2157
M-2%-300	8.67	0.388	0.360	1.973	2718

* e_0 – initial void ratio.

** e_{con} is the void ratio after consolidation, before shearing.

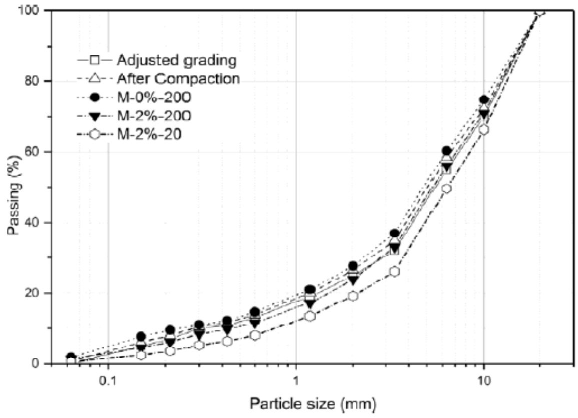

Fig. 3. Particle size distributions of the samples: original and after the compaction and monotonic shearing.

Therefore, the consolidation stage was extended even if the volume change wasnegligible. During drained shearing a constant confining pressure was maintained throughout the test. The sample was sheared at a constant rate of strain of 0.016 mm/min, this was determined based on the capacity of the data acquisi- tion system to interpret strains of 10-6. Well after peak strength, the speed was doubled until the test was termi- nated. Tests were terminated either by achieving a constant strength and a constant volume, or by reaching an axial strain of30%. The moisture content was determined by using left over soil from the tray, and the initial void ratio of each sample was calculated in five different ways: an average of the ini- tial dimensions, the volume of voids and solids, the dry unit weight and the final water content. Outliers were removed and an average of the values deemed acceptable was used. Although the samples were carefully prepared, a variation in the initial void ratio was unavoidable (Table 2).

IV. BREAKAGE

The idea of having a balance between particle breakage and particle rearrangement at critical state has been reported by many authors [(Chandler 1985, Daouadjiet al. 2001, Coop et al. 2004, Salim and Indraratna 2004,Muir Wood and Maeda 2008; Rubin and Einav 2011). The literature review has also shown that the level of breakage in dense granular materials, at lower pressures, is rarely investigated. It is often disregarded and assumed not to affect critical state, particularly when a large number of contacts is expected. Therefore, samples were sieved to evaluate breakage after shearing, whilst extra samples were prepared to determine if compaction caused particle breakage (Fig.3). The results showed that after compaction small amounts of breakage can be seen in all sizes. Breakage was alsoseen after shearing, where the largest changes in PSD were seen in sizes ranging from 1 to 7 mm, where the increase inpassing percentage is in the order of 8%. The smaller sizes have also increased, perhaps indicating the shearing of the asperitiesatthesmallconfiningstressesused.

An attempt to determine the PSD for the cemented samples was carried out by breaking the cement bonds before sieving, samples were put on individual sealed bags andthe bonding destroyed by hand. Larger pieces that were kept intact were removed by hand, and only the soil that seemed not to have bonds was used. The results showed that the PSD curve of sample M 2%-200 is slightly above the original curve for sizes above 3 mm and below the original curve for sizes below 3 mm; whilst the M 2%-20 is below the original size tested (Fig. 3). Thisdemonstrates

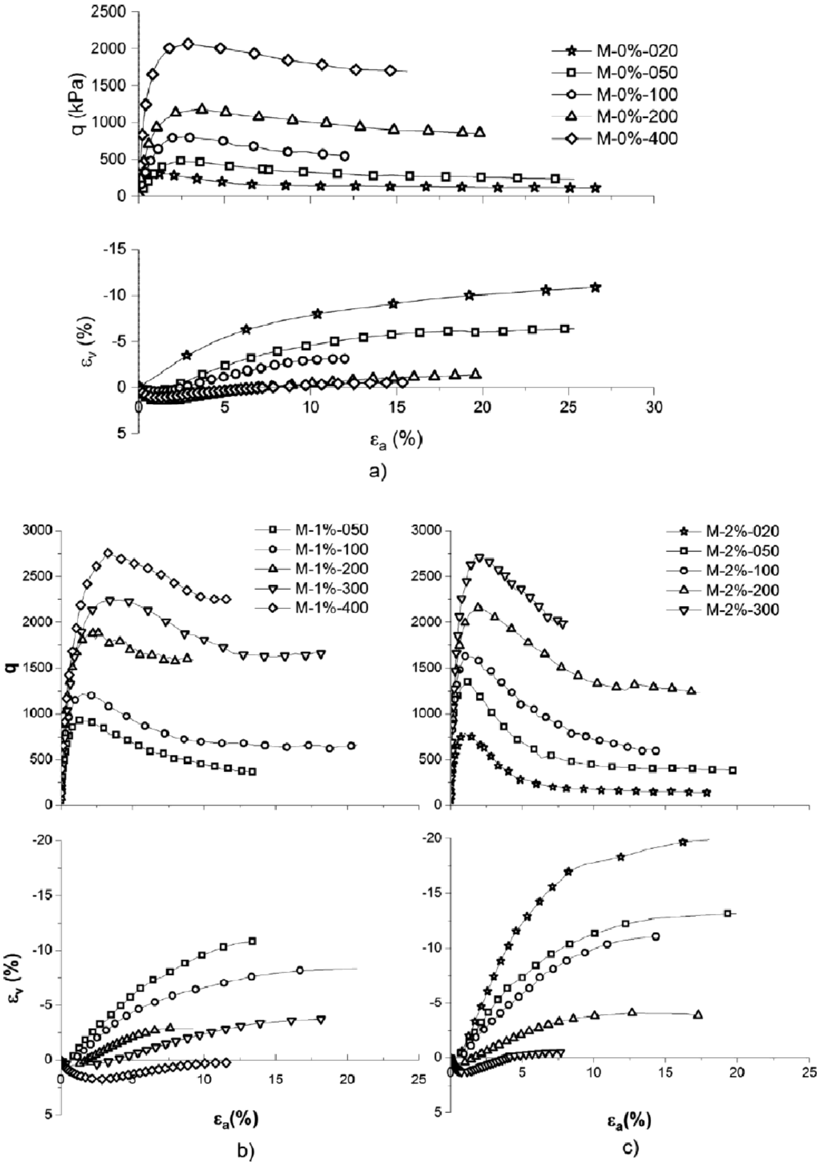

Fig. 4. Stress-strain and volumetric response of the soils tested with: a) 0%, b) 1% and c) 2% cement content.

the effect of the confining stress on the destruction of the bonds and the difficulty to destroy by hand, the bonds on the smallest sizes, even after a monotonic shearing has taken place.

V. TRIAXIAL TESTS (STRESS-STRAINBEHAVIOUR)

The triaxial test results are shown on Fig. 4, where the stress-strain and the volumetric curves of 15 tests are plot- ted. As expected, all samples showed a strain-softening behaviour towards a constant strength after peak stress. The volumetric behaviour is similar; after a large dilation that reduces with the confining stress, it is possible to visu- alise a steady state, where no change in volume and strength is seen with the increase in shear strain. Large vol- umetric strains are also seen particularly at low stresses, where there are sharp changes in the volumetric behaviour, possibly indicating the occurrence of localisation. How- ever, all samples have failed in barrelling and only in a few samples signs of localisation were noticed. A couple of tests were terminated earlier, due to small punctures on the membrane given the large strains. The axial strain, ea, was measured by two local displacement transducers up to a certain point (usually peak stress) switching to the external transducerafterwards.

The effect of the addition of cement in the strength is clear, as the peak values increase with the addition of cement for all confining stresses tested. Simultaneously, there is also an increase in the brittleness index (the ratio between the peak shear strength and the shear strength at large strains) of the samples. Fig. 5shows the brittleness index calculated for all of the samples. The samples with 2% cement have a much larger brittleness index when com- pared to the other samples. It is also clear that the values of brittlenessindexcalculatedforthe1%cementsampleshave little deviation from the 0% samples; i.e., the addition of 1%cementcausessmallchangestothisparameter.

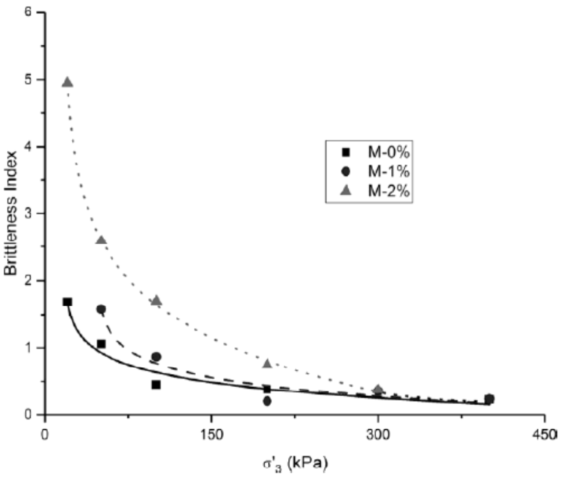

Fig. 5. The relationship between brittleness index and confining pressure.

The results also show that increasing thecementcontentreduces the level of strain required to reach thepeakstress.Thisistrueforeveryconfiningstresstested, confirmingthatthereisanincreaseinstiffnesswiththeadditionof cement. Fig. 6shows a direct comparisonbetweenthecemented and uncemented samples forcertainconfiningstresses, to better show the effect of cementation inthepeakshearstrengthandthevolumetricbehaviour,wherehigher cement content generates larger dilativevolumetricstrains.For the uncemented soil, the area correspondenttothemaximum rate of dilation directlycorresponds to thepeakstrength,whilstthecementedsamplesexperience peakslightly before the maximum rate of dilation.Thechangeseen is not large, but enough to demonstratethatsmalladditions of cement can generate a structure that affectthestrengthofevenverydensefabrics,asshowninFig.7.Fig.8showsthetangentstiffnesscurves(slopeofthestress-strain curves) with arrows indicating thepointswereachangeinshearingratewasperformedtoacceleratethetests. The gross yield points, regarded as the onsetofbond-ing degradation and the locus wheresignificantplasticdeformations start to occur, are also indicated inthecurveswith the use of a black square. Theseweredeterminedusing the method proposed by Malandraki and Toll(1996) and Alvarado et al. (2012b)and are marked bythe start of the change in direction of the stiffnesscurve.Itisclearthattheadditionofcementincreasesthetangentstiffness;thetangentstiffnessoftheuncementedsamplesstartatvalueslowerthan1GPa,whilstthesampleswith1%cementstartatvalueslowerthan2to3GPa,andthesampleswith2%showvalueslowerthan7or8GPa.Itcanalsobeseenthatincreasingthestrainreducesthetangent stiffness and that the rate of reductionin stiffnessisrelatedtothepercentageofcement(i.e.lowercementper- centages lower reductions and highercementpercentageshigher reductions). Comparing tests in each group, itis also seenthatincreasingtheconfiningpressurealsoresultsin higherstiffnesses,despitethefactthatincertainsamplesthisisnotveryclearanditislikelytobetheeffectofthe scales used in the graph.

5.1. Stress-Dilatancy

A stress-dilatancy analysis was performed and Fig. 9contains the plots of all 15 uncemented and cemented sam- ples, shown with the respective cement percentage. Oneach graph, the peak strength, the gross yield and last test point are represented by different symbols. The uncemented samplesshowanincreaseintheratioq/p0withdilation,uptoapeak, reached at the same time as the highest dilation rate. From that point onwards, dilation rate reduces together with the q/p0ratio. Asthevolumestopschanging,auniquevalue of M =

1.76 can be determined, corresponding to a friction angle at critical state u´cs =43◦. Theeffectofthecementpercentagecanbeseenbythe initial change in the shape of the curve. At the start of shearing,asdilationdevelops,thesamplesquicklyreach higherratiosofq/p0,indicatingthatthecementationisnow active and allowing a stiffer response from the sample. This difference is proportional to the cement percentage; i.e., the highercementpercentage,thehighertheratioq/p0.Theeffects of cementation are also visible in the location of the peak stress, as it occurs before the maximum rate of dilation; this is similar to what was observed previously in Fig. 7and described by Leroueil and Vaughan (1990). However,thedifferencebetweentheratioq/p0,measured at the peak stress and at the maximum rate of dilation is verysmall,indicatingthatthepeakislargelygovernedby dilation rather than by cement content. The samples with 1% cement do not show this as clearly as the samples with 2% cement. Another expected behaviour is the reduction in dilation rate with the confining stress, seen in all cement and uncemented samples, similar to the behaviour of cemented sands, demonstrated by Coop and Willson(2003),Consolietal.(2012)andAlvaradoetal.(2012b).

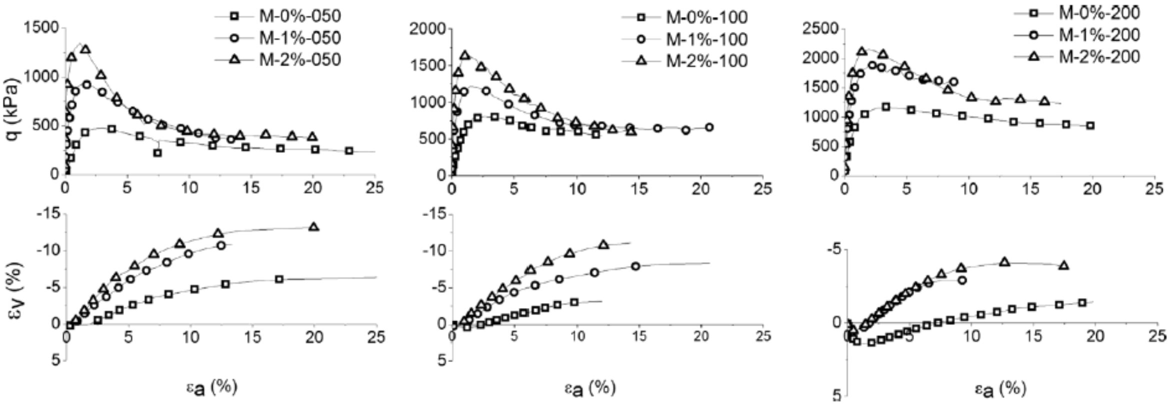

Fig. 6. Comparison of the stress-strain and volumetric responses of the samples with 0%, 1% and 2% cement, under different confining pressures.

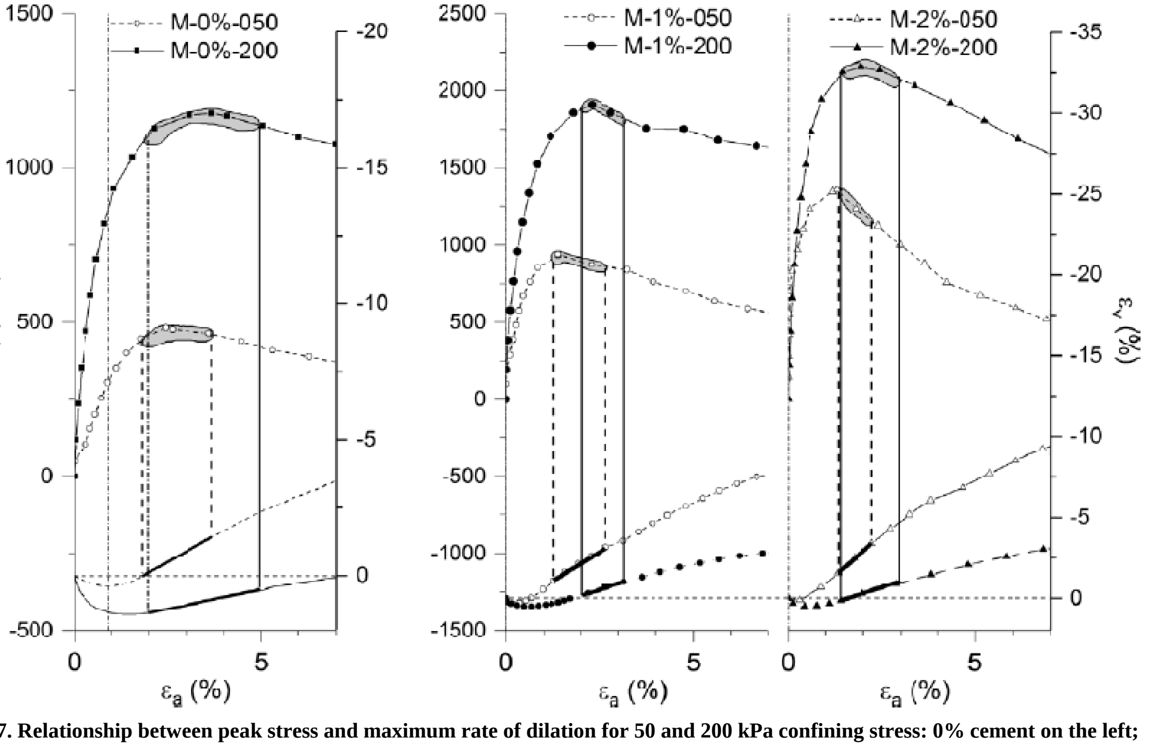

Fig. 7. Relationship between peak stress and maximum rate of dilation for 50 and 200 kPa confining stress: 0% cement on the left; 1% in the middle and 2% on the right.

The same authors have pointed out that after the max- imum dilation rate the samples seem to follow a linear fric- tional trend, however, as the stress ratio reduces, the dilationrateseemstoreducemuchquicker,i.e.volumetric

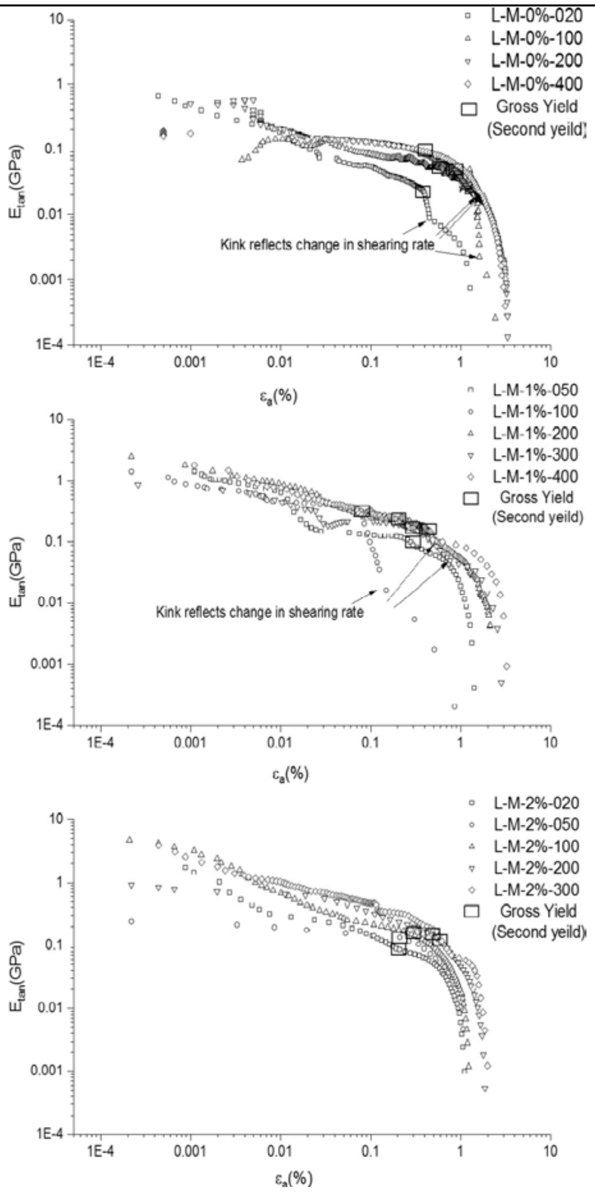

Fig. 8. Tangent stiffness against axial strain in log scale, together with the gross yield points for: (a) 0%, (b) 1% and (c) 2% cement.

strainschangeatalargerrate,andthepathmovesinwardsand away from the frictional trend. Theauthorsattributethisbehaviourtotheoccurrenceoflocalisationandtherapidreductionofvolumetricstrains.Inthecaseofthesamplestestedhere,asimilarbehaviourwasobservedafterpeak, however, as the shearing continues thistrendisreversedandthesamplesseemtoconvergetoauniquevalueofM:M=2.00for1%cementandM=2.05for2%cement.AscanbeseeninFig.9band9c,ifthelineartrend line is followed, a higher value of Misdeterminedfor the same percentages of cement, whilst in thecaseofCoopandWillson(2003),alowervaluewouldbedefined.TheworkdonebyMu¨hlhausandVardoulakis(1987)andFinnoetal(1997),showthatthethicknessoftheshearband is proportional to the particle sizedistribution. Authors mention values of 16 and 10 to 25 times d50 respectively. Given that the triaxial sample has a finite vol- ume this implies that the volumetric strains measured in a triaxial sample are a function of the grain size distribution. Therefore, variations in the grain size distribution during shear, will cause large changes in the dilation ratio. The samples tested are lightly cemented and the grain size dis- tribution curve obtained after shearing, shows that the final grading has larger intermediate particles than the original grading. This indicates that there is an evolution of the par- ticle size distribution during the shearing process. The DEM work done by Wang and Leung (2008a, 2008b), clearly shows that despite the shearing, there are still clus- ters of particles that remain intact within the sample. The authors, therefore, believe that as bonds degrade due to shearing there is a constant change in the particle size dis- tribution. The consequence are seen as different volumetric strain rates that bring the dilation path inwards. As shear- ing continues, a more stable grading is achieved and a dif- ferentvalueofMisreachedatcriticalstate.

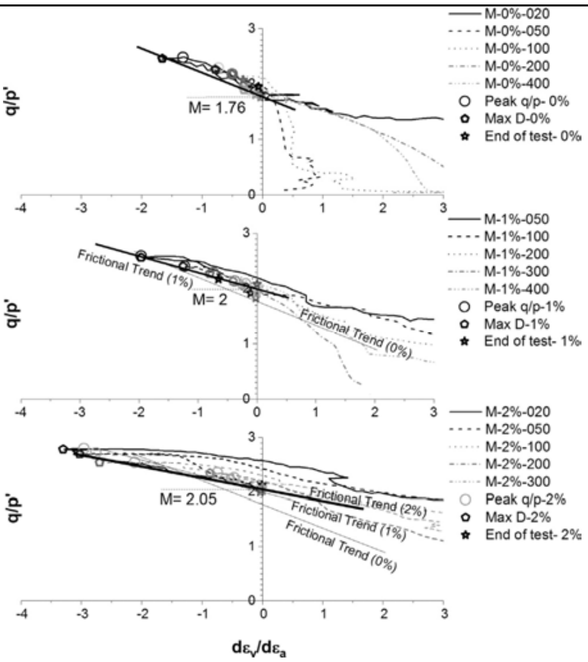

Fig. 9. Stress-dilatancy analysis: (a) 0%, (b) 1% and (c) and 2% cement content.

VI. CRITICAL STATE

The points correspondent to the peak strength and the end of tests were plotted in Fig. 10, together with the results obtained from the Indirect Tensile tests (ITS) (BSEN13286-42:2003), as well as Unconfined Compressive tests (UCS) (BSEN 13286-41:2003), on samples of the same size, prepared using the same methodology. These samples are not shown on Table 2 but fall within the same

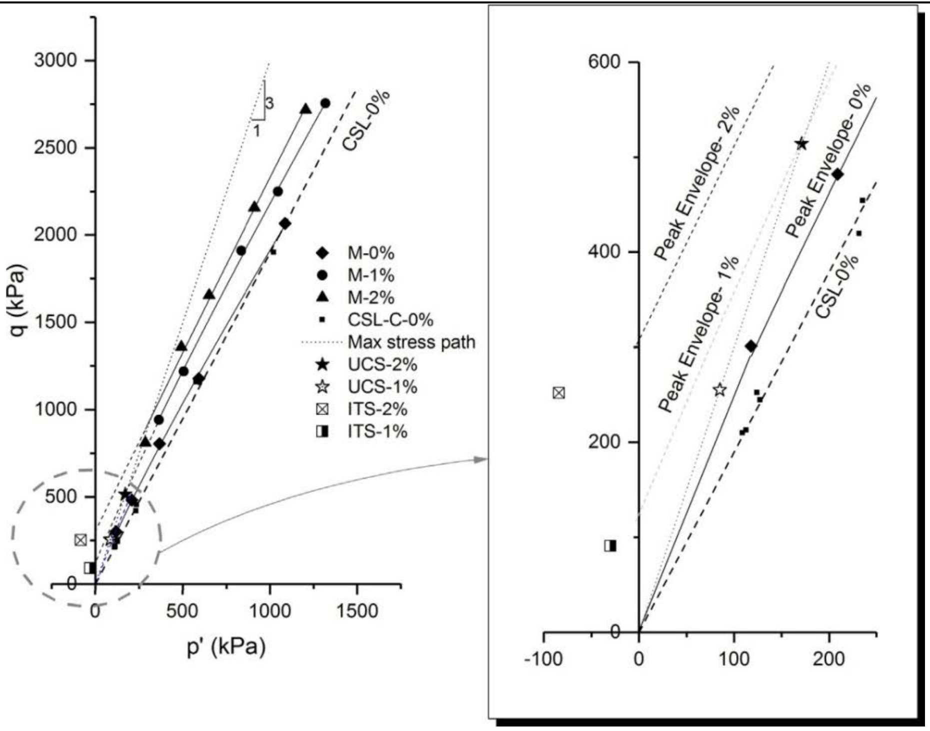

Fig. 10. Peak envelop on q versus p´ diagram; the inset shows the small stresses region.

	Critical state				Peak		
Type of crushed limestone	k	C	M	$/'_{cs}$(°)	q/p'	q Intercept	$/'_{p}$(°)
Uncemented	0.053	1.747	1.77	43.1	1.81	0	46.6°
1% cement	0.101	2.054	2.00	48.6	1.90	265	45.9°
2% cement	0.122	2.218	2.05	49.8	2.03	299	46.7°

Table 3 Specification of peak and critical state line.

average values. These results served to plot the peak envel- opes, as the cemented samples have a small tensile strength anditmustbeconsideredwhendefiningthepeakenvelopes of the cemented soils. The failure envelopes plottedsuggest values of M that are very similar to the values determined in the dilation plots above. Fig. 10b shows the small stress area with more detail. It is also important to point out that the peak envelope for the uncemented soil is curved and seemstojointheCSLatp0ofaround1100kPa.Theprop- erties of the strength envelopes are shown on Table 3, where the peak friction angle for the uncemented soil was calculated assuming nocohesion.

Been et al. (1991)have shown that within the normal range of engineering stresses, sands show a steady stateline at small stresses that is much shallower than at high stres- ses. Therefore, the paths followed by the tested samples whereplottedonthespecific volume,lnp0spaceonFig. 11, with the final point of each test indicated by a sym- bol. Although the arrows indicate the direction the tests were following when they were terminated, Fig. 4shows that the magnitude of this movement was very small for most of the tests. The results show that there is no unique CSL for the cemented and uncemented soils. Instead, the results point clearly to the location of three distinct CSLs, one for each type of soil tested. The results also show that the addition of cement increases the slope of the CSL when compared to the uncemented soil. The larger dilative beha- viour seen in the cemented samples is responsible for the steeper curve gradient shown by the cemented samples. A summary of the parameters obtained for the steady state lines in Fig. 11 is shown in Table 3.

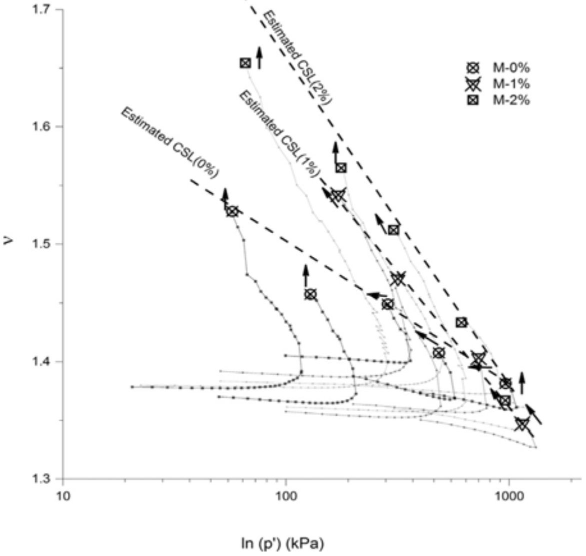

Fig. 11. Location of critical state lines for samples with 0%, 1% and 2% cement content on the specific volume ,m, versusthelogarithmofthemean effectivestress,ln(p0).

Thesteadystatelinesdeterminedforthecementedsoils seem to reach a common point at stresses of around p0=1000kPa.Thisiscompatiblewiththeresultsshown by the grain size distribution curves, where the PSD of cementedsamplesshearedatlargestressesisverysimilar tothePSDoftheuncementedorоriginalgrainsizedistribution. As the percentages of cement content used inthis research were very small, the effect on the strength of the samples is likely to be felt only at small stresses. At larger confining stresses, the resultant frictional strength mobi- lised is much larger than the contribution of the cement. At that point the changes in the critical state lines caused by the cementation are verysmall.

6.1. Normalisedbehaviour

Given that the stresses used to consolidate the samples were very low and it was not possible to determine a Nor- mal Compression Line (NCL), each set of tests was nor- malised with respect to M and the equivalent pressure on the CSL, by using Eq. (1) (k is the slope of the CSL, C is thespecificvolumeatp0=1kPaandmisthespecificvolume, on the CSL and p´cs is the mean effective stress on theCSL):

$$p^{0}_{cs}\ ¼\exp\ \frac{^{-}\ C—m\ ^{\Sigma}}{k} \qquad (1)$$

The normalised stress paths show that it is possible to determine a state boundary surface for the peak states for each set of test up to the critical state line (broken line on Fig. 12). The normalised gross yield points determined from the stiffness curves for each set of tests was also plot- ted in Fig. 11. The gross yield envelopes are fully enclosed within the respective SBSs indicating that the cement per- centages generated a very weak bonding. At low stresses, the yield surface seems to coincide with the SBS, however, as the stresses increase the yield surface moves inside and awayfromtheSBS.Theeffectofthecementpercentage

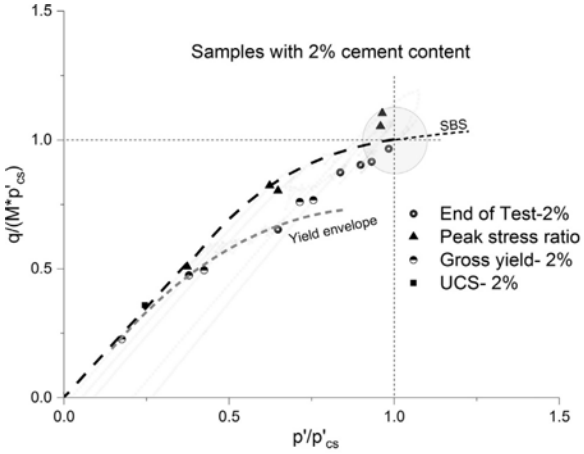

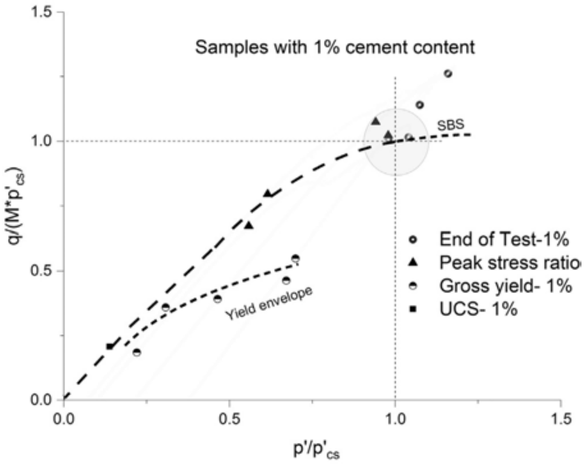

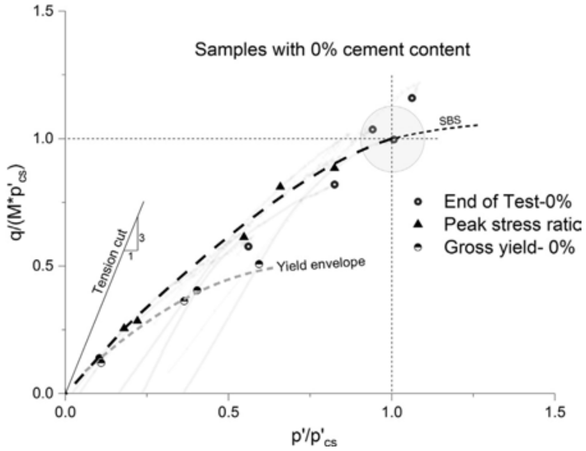

Fig. 12. Normalised yield and strength envelopes: (a) 0%, (b) 1% and (c) 2% cement. is seen in the proximity between the gross yielding surface and the SBS, as the larger cement content keeps the yield surface closer to the SBS.

In Fig. 13 all the state boundaries and yield surfaces wereplottedtogether.Theresultsshowthatthesearevery

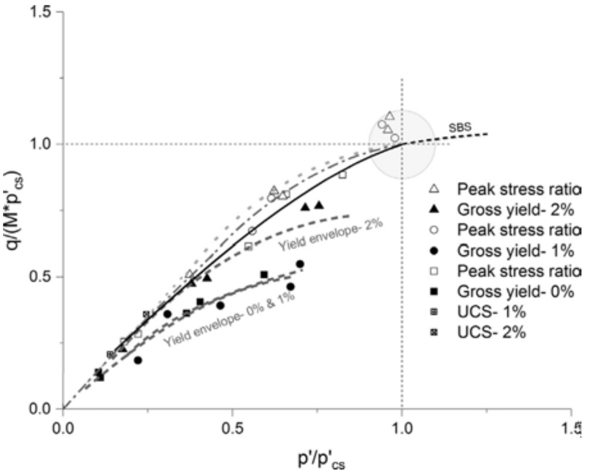

Fig. 13. Comparison of the normalized data for the uncemented and cemented soils.

similar, and a unique SBS could be used to represent the effect of the cemented and uncemented tests, when nor- malised by the CSL and the value of M. The gross yield surface of the uncemented and the

1% cement are coinci- dent, however, a unique surface cannot be assumed as the 2% cement results have shown a significantly higher gross yieldsurface.

VII. CONCLUSIONS

This work presents the findings of a study conducted in cemented and uncemented samples of a well graded com- pacted granular material, used for base and sub-base con- struction in the UK. The following conclusions can be drawn from thiswork:

The mechanical properties of a well graded compacted granular material traditionally used in construction, can be further improved with the addition of small per- centages ofcement.

The addition of cement also increases the dilative ten- dency of these soils, providing better results particularly when small confining stresses are used as is the case of base and sub-base for road construction.

The results show that it is possible to determine a unique Critical state line for the uncemented material and that the addition of cement will increase the slope of this line within the range of stresses commonly observed in engineering practice.

When the data is normalised by the equivalent pressure on the CSL and the value of M, it is possible to deter- mine a unique state boundary surface for the cemented and uncemented soils used in this research. The gross yield surface, however, is not unique and will depend on the cementpercentage.

REFERENCES

[1] Alvarado, G., Coop, M.R., Willson, S., 2012a. On the role of bondbreakage due to unloading in the behaviour of weak sandstones.Ge´otechnique62(4),303–316.

[2] Alvarado,G.,Lui,N.,Coop,M.R.,2012b.Effectoffabriconthebehaviour of reservoir sandstones. Can. Geotech. J. 49(9),1036–1051.Bandini,V.,Coop,M.R.,2011.Theinfluenceofparticlebreakageonthelocationofthecriticalstatelineofsands.SoilsFound.51 (4),591–600.

[3] Been, K., Jefferies, M.G., Hachey, J., 1991. The critical state of sands.

[4] Ge´otechnique41(3),365–381. BS 1377-4: 1990. Soils for civil engineering purposes — Part 4: Compaction-related tests, London: British Standard Institute. BS EN 13286-41: 2003. Unbound and hydraulically bound mixtures. Test method for determination of the compressive strength of hydraulically bound mixtures. London: British Standard Institute. BS EN 13286-42: 2003. Unbound and hydraulically bound mixtures. Test method for the determination of the indirect tensile strength of hydraulically bound mixtures. London: British StandardInstitute. BSEN1197–1:2011.Cement.Composition,specificationsandconformity criterua for common cements. London: British StandardInstitute.

[5] Carrera, A., Coop, M.r., Lancellotta, R., 2011. Influence of grading on themechanical behaviour of Stava tailings. Geotechnique 61 (11), 935–

[6] 946.

[7] Chandler, H.W., 1985. A plasticity theory without drucker's postulate,suitable for granular materials. J. Mech. Phys. Solids 33 (3), 215–226.

[8] Coop, M.R., Atkinson, J.H., 1993. The mechanics of cemented carbonatesands. Geotechnique 43 (1), 53–67.

[9] Coop, M.R., Willson, S.M., 2003. Behavior of Hydrocarbon ReservoirSands and Sandstones. J. Geotech. Geoenviron. Eng. 129 (11), 1010–1019.

[10] Coop, M.R., Sorensen, K.K., Freitas, T.B., Georgoutsos, G., 2004.Particlebreakageduringshearingofacarbonatesand.Ge´otechnique54 (3),157–163.

[11] Cuccovillo, T., Coop, M.R., 1997a. Yielding and pre-failure deformationofstructuredsands.Ge´otechnique47(3),491–508.

[12] Cuccovillo, T., Coop, M.R., 1997b. The measurement of local axialstrainsintriaxialtestsusingLVDTs.Ge´otechnique47(1).

[13] Consoli, N.C., Dalla Rosa Johann, A., dos Santos, V.R., Corte, M.B.,Moretto, R.L., Gauer, E.A., 2012. Key parameters for tensile andcompressivestrengthofsilt–limemixtures.Ge´otechniqueLett.2(May),81–85.

[14] Consoli, N.C., Silva Lopes, L., Consoli, B.S., Festugato, L., 2014. MohrCoulomb failure envelopes of lime-treated soils. Geotechnique 64 (2),165–170. Cruz, N., Rodrigues, C., Viana da Fonseca, A., 2011. The influence of cementation in the critical state behaviour of artificial bonded soils. In: International Symposium on Deformation Characteristics of Geoma- terials. pp. 730–737.

[15] Daouadji, A., Hicher, P.-Y., Rahma, A., 2001. An elastoplastic model forgranular materials taking into account grain breakage. Eur. J. Mech.A. Solids 20 (1),113–137.

[16] Delfosse-Ribay, E., Djeran-Maigre, I., Cabrillac, R., Gouvenot, D., 2004.Shear modulus and damping ratio of grouted sand. Soil Dynam.Earthq. Eng. 24 (6),461–471.

[17] Finno, R.J., Harris, W.W., Mooney, M.A., Viggiani, G., 1997. Shearbandsinplanestraincompressionofloosesand.Ge´otechnique47(1),149–165.

[18] Fuller, W.B., Thompson, S.E., 1907. The laws of proportioning concrete.

[19] Trans. Am. Soc. Civil Eng., 59

[20] Ghafghazi, M., Shuttle, D.A., DeJong, J.T., 2014. Particle breakage andthecriticalstateofsand.SoilsFound.54(3),451–461.

[21] Haeri, S.M., Hamidi, A., Hosseini, S.M., Asghari, E., Toll, D.G., 2006.Effect of cement type on the mechanical behavior of a gravely sand.Geotech. Geol. Eng. 24 (2), 335–360.

[22] Huang, J.T., Airey, D.W., 1993. Effects of cement and density on anartificially cemented sand. Geotechnical Engineering of Hard Soils-Soft Rocks. Balkema, Rotterdam, Athens, pp. 553–560.

[23] Kongsukprasert, L., Tatsuoka, F., 2007. Small strain stiffness and non-linear stress-strain behaviour of cemented-mixed gravelly soil, SoilsFound. 47 (2), 375–394.

[24] Leroueil, S., Vaughan, P.R., 1990. The general and congruent effects ofstructureinnaturalsoilsandweakrocks.Ge´otechnique40(3),467–488.

[25] Lohani, T.N., Kongsukprasert, K., Watanabe, K., Tatsuoka, F., 2004.Strength and deformation properties of compacted cement-mixedgravelevaluatedbytriaxialcompressiontest.SoilsFound.44(5),95–108.

[26] Marri, A., Wanatowski, D., Yu, H.S., 2012. Drained behaviour ofcemented sand in high pressure triaxial compression tests. Geomech.Geoeng. 7 (3), 159–174.

[27] Malandraki, V., Toll, D.G., 1996. The definition of yield for bondedmaterials. Geotech. Geol. Eng. 14 (1), 67–82.

[28] Mu¨hlhaus,H.B.,Vardoulakis, I.,1987. Thethicknessofshearbandsingranularmaterials.Ge´otechnique 37(3),271–283.

[29] Muir Wood, D., Maeda, K., 2008. Changing grading of soil: effect oncritical states. Acta Geotech. 3 (1), 3–14.

[30] Rios, S., Viana da Fonseca, A., Baudet, B., 2014. On the shearing behaviour of an artificially cemented soil. Acta Geotech. 9 (2), 215– 226. https://doi.org/10.1007/s11440-013-0242-7.

[31] Rubin, M.B., Einav, I., 2011. A large deformation breakage model ofgranular materials including porosity and inelastic distortional defor-mation rate. Int. J. Eng. Sci. 49 (10), 1151–1169.

[32] Salim, W., Indraratna, B., 2004. A new elastoplastic constitutive modelforcoarse granular aggregates incorporating particle breakage. Can.Geotech. J. 41 (4),657–671.

[33] Schnaid, F., Prietto, P.D.M., Consoli, N.C., 2001. Characterization ofcemented sand in triaxial compression. J. Geotech. Geoenviron. Eng.127 (10), 857–868.

[34] Shafabakhsh, G., Rezaeian, M., 2010. Analysis of the effects of applyingdifferent quantities and types of additives on strength parameters ofcold in-situ recycled mixtures made of bitumen foam. J. Transport.Res. 7 (122),53–66.

[35] Taheri, A.Y., Sasaki, Y., Tatsuoka, F., Watanabe, K., 2012. Strength anddeformation characteristics of cemented-mixed gravelly soil in multi-ple-step triaxial compression. Soils Found. 52 (1), 126–145.

[36] Tang, C., Shi, B., Gao, W., Chen, F., Cai, Y., 2007. Strength andmechanical behavior of short polypropylene fiber reinforced andcement stabilized clayey soil. Geotext. Geomembr. 25 (3), 194–202.

[37] Thevanayagam, S., Shenthan, T., Mohan, S., Liang, J., 2002. Undrainedfragility of clean sands, silty sands, and sandy silts. J. Geotech.Geoenviron. Eng. 128 (10), 849–859.

[38] UK Highway Agency, 2016. Manual of contract documents for highway works volume 1 specification for highway works- road pavements — unbound, cement and other hydraulically bound mixtures (series0800). Highway Agency. Available at: http://www.standardsforhigh-ways.co.uk/mchw/vol1/ (Accessed July 18,2016).

[39] Wang, Y.-H., Leung, S.-C., 2008a. A particulate-scale investigation ofcemented sand behavior. Can. Geotech. J. 45 (1), 29–44.

[40] Wang, Y.H., Leung, S.C., 2008b. Characterization of cemented sand byexperimental and numerical investigations. J. Geotech. Geoenviron.Eng. 134 (7), 992–1004.

[41] Xiao, Y., Liu, H., Ding, X., Chen, Y., Jiang, J., Zhang, W., 2016.Influence of particle breakage on critical state line of rockfill material.Int. J. Geomech. 16 (1),04015031. Yu, Y., Cheng, Y.P., Xu, X., Soga, K., 2014. DEM Study on the Mechanical Behaviours of Methane Hydrate Sediments: Hydrate Growth Patterns and Hydrate Bonding Strength. In: Proceedings of the 8th International Conference on Gas Hydrates (ICGH8-2014). Beijing,China.

[42] Yu,Y.,Cheng,Y.P.,Xu,X.,Soga,K.,2015.Shapeeffectofelongat edsoilparticles on Discrete Element Modelling of methane hydrate soilsediments. Geomech. Micro to Macro,207–212.

★★★

CORROSIVE INITIATED MUDS: MATERIALS IN CEASELESS INTEREST

[1]JASWANTH GANGOLU, [2]OSIN SANGHAMITRA PATEL, [3]JAGRUTI JAGATANANDINI SWAIN

[1]Assistant Professor, Department of civil Engineering, NMIET, BBSR
[2]Department of Civil Engineering AIET Bhubaneswar
[3]Department of Civil Engineering CEC BBSR
E-mail: [1]Rout.suryaleen@nmiet.ac.in,

Abstract -
Corrosive initiation is a synthetic treatment generally utilized on dirts, normally bentonites in hydrochloric or sulphuric corrosive, to get mostly broken down materials with upgraded surface properties appropriate for new applications or showing intriguing new conduct. This paper depends generally on the aftereffects of long-running experiments in our research centers, enhanced by distributed information from somewhere else. An audit of ongoing writing shows that interest in these materials stays far reaching, with a few new improvements of ecological importance and in the region of mud polymer nanocomposites. Corrosive treatment of vermiculites and of non-growing mud materials is likewise included.

I. INTRODUCTION

One application of calcium bentonite with a significant market is the decolourization of vegetable, animal and mineral oils. Most of the calcium bentonite used for filtering and decolourizing oils is acid activated (Odom, 1984). Acid treatment with sulphuric or hydrochloric acid removes the calcium cations from the surfaces and edges of the layers, which increases the overall negative charge. In industry, sulphuric acid is preferred to hydrochloric because it is less expensive and is not as harsh as HCl (Murray, 2007). This makes the acid-activated clays more effective at removing coloured anions from theoil.

The term ‘acid-activated clays’ has generally been reserved in the industrial literature for partly dissolved bentonites. Bentonite has always had a multitude of markets, and acid-activated bentonite has been a standard product for many decades. Usually a Ca^{2+}-bentonite is treated with inorganic acids to replace divalent calcium cations with monovalenthydrogenionsandtoleachoutferric,ferrous,aluminium,and magnesium cations, thus altering the smectite layers and increasing the specific surface area (SSA) and porosity. The overview of the abbreviations used in this contribution is in Table 1. This results in the production of bleaching earths, that is, clays suitable for a range of bleaching or decolourizing applications, in which they compete against naturally-occurring bleaching earths (Siddiqui, 1968; Kendall, 1996;Christidisetal.,1997;Falarasetal.,1999;Hussinetal.,2011).Themechanism of decolourization of crude maize and sunflower oils has been studied by means of adsorption of β-carotene by a low-grade bentonite, containing 50–60% mixed-layered illite (I)-smectite with80–85% expandable layers. The decolourization depended on temperature, being a two-step process (Christidis and Kosiari, 2003).

Salemetal.(2015a,b)investigatedindetailthetreatments ofused oils.Intheregenerationofwastelubricantoil(Salemetal., 2015a)the nano-porousadsorbentswereinitiallyproducedbyacidtreatmentof naturalclay.Theeffectsofseveralfactors,suchasacidtype,concentrationandresidencetime,ontheporousstructureoftheadsorbentwere evaluated.Areductionofabout0.27nmwasobservedinthedistance betweenmontmorillonitelayersinthepresenceofsulfuric acid,due toprotonationofthelayers.Promisingresultsconcerningreductionof adsorbentcontentintheregenerationofwastelubricantoil wereobtained.FortheregenerationofwasteengineoilbyactiveCa-bentonite powder,theporousadsorbentswerepreparedbyacidificationusingnitricandsulfuricacidsolutions.Theoptimumpropertiesformethylene blueadsorptionbyclaysactivatedinthepresenceofnitricandsulfuric acids were specific surface areas (SSA) of 109 and 89 m2 g−1, respectively.ThechangeinSSAvalues(obtainedfromtheN2adsorptionisotherms) on treatment with acid was due to the formation of new nano-pores of size 10–12 nm (Salem et al.,2015b).

Taxiarchou and Douni (2014)activated a bentonite from Milos, Greece,withoxalicacidandinvestigatedtheeffectofacid activation conditionsonthebleachingofsunfloweroil.Theactivated materials hadexcellentbleachingpropertiesandweresuitableforindustrialuse as bleaching earths. Optimum bleaching properties were achieved using a variety of combinations of reaction parameters, sometimes with bleaching ability equivalent to that of the known commercial bleaching earth Tonsil Optimum 210FF.

HarveyandMurray(1997)declaredintheiroverviewofthehistory anddevelopmentofindustrialclaysthatacidactivationisaveryuseful procedureforobtainingsophisticatedclaymaterials,eveninthe21st centuryinthedevelopingcountries.Murrayreassertedandsupported thisconclusionseveraltimesinhispapersandbooks(Murray,1999,2000, 2007; Harvey and Lagaly, 2013). This treatment is one of the mostcommonchemicalmodificationsofclayminerals,usedforbothindustrialandscientificpurposes(KomadelandMadejová, 2013–areferencewhichformsthebasisofthecurrentcontribution,supplemented by inclusion of several manuscripts published in2013–2015).

Table 1
The abbreviations used.

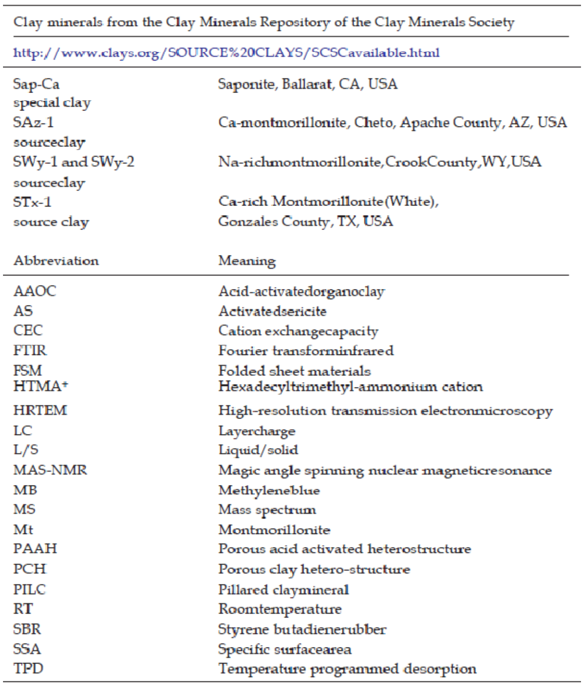

Clay minerals from the Clay Minerals Repository of the Clay Minerals Society	
http://www.clays.org/SOURCE%20CLAYS/SCSCavailable.html	
Sap-Ca special clay	Saponite, Ballarat, CA, USA
SAz-1 sourceclay	Ca-montmorillonite, Cheto, Apache County, AZ, USA
SWy-1 and SWy-2 sourceclay	Na-richmontmorillonite,CrookCounty,WY,USA
STx-1 source clay	Ca-rich Montmorillonite(White), Gonzales County, TX, USA
Abbreviation	Meaning
AAOC	Acid-activatedorganoclay
AS	Activatedsericite
CEC	Cation exchangecapacity
FTIR	Fourier transforminfrared
FSM	Folded sheet materials
HTMA$^+$	Hexadecyltrimethyl-ammonium cation
HRTEM	High-resolution transmission electronmicroscopy
LC	Layercharge
L/S	Liquid/solid
MAS-NMR	Magic angle spinning nuclear magneticresonance
MB	Methyleneblue
MS	Mass spectrum
Mt	Montmorillonite
PAAH	Porous acid activated heterostructure
PCH	Porous clay hetero-structure
PILC	Pillared claymineral
RT	Roomtemperature
SBR	Styrene butadienerubber
SSA	Specific surfacearea
TPD	Temperature programmed desorption

Acid activation consists of the reaction of clay minerals with a min- eral acid solution, usually HCl or H_2SO_4. The goal of this is to obtain a partlydissolvedmaterialwithincreasedSSA, porosity andsurfaceacid- ity (Komadel, 2003; Carrado and Komadel, 2009). The materials thus manufactured are widely available, relatively inexpensive solid sources ofprotons,andeffectiveinanumberof industriallysignificantreactions and processes. Clay minerals are affordable adsorbents for the removal of industrial contaminants (Zhao et al., 2015b). The authors used HCl as an acid modifier to activate Akadama clay, and adsorption experi- ments were conducted to evaluate the Cr(VI) adsorption. The optimum application pH was broadened from 2 to3–9.

Acidattackonclaymineralsalsooccursnaturally,forexampleinthe interactionofacidminedrainagewithclayminerals(Galánetal.,1999;Dubíkováetal.,2002).Miningwastecontainingsulphidesisthemost commonandmostsignificantanthropogenicsourceofacidity.Progres- sive oxidation leads to the production of protons and sulphates in leachingwaters,whichgenerallyalsomobilizelargeamountsofmetal cationsbydissolutionofminerals.Thesewatersinfluence thecompositionofsurfacewatersbutalsohaveanimpactonthesurroundingsoils and terrestrial ecosystems (Komadel and Madejová,2013).

Very early acid-dissolution studies based on solution analysis of dioctahedralsmectitesinHClbyOsthaus(1954,1956)indicatedfaster dissolution of octahedral than tetrahedral sheets. However, in the 1990s,assaysofsolidreactionproductsemployingadvancedspectroscopictechniquesprovidedclearexperimentalevidencethatacidtreat- ments dissolved central atoms from the tetrahedral and octahedral sheetsatsimilarrates.LucaandMacLachlan(1992)studiedthedissolutionoftwonontronitesin10%HClbyMössbauerspectroscopy,fitting thespectraeitherwithtwooctahedralFe^{3+}doubletsonly,orwithan additionaltetrahedralFe^{3+}doublet.Acidtreatmentremovedoctahe- dral and tetrahedral Fe^{3+}from the structure at about the same rate. MössbauerandIRspectroscopiesandXRDindicatedthattheremaining undissolvedparthadthestructureoftheuntreatednontronite.A^{27}Al and^{29}SiMAS-NMRstudy(Tkáčetal.,1994)onremovaloftetrahedral and octahedral Al^{3+} from Mt by 6 M HCl led to very similar conclusions. The rates of dissolution of tetrahedral and octahedral Al^{3+} were also comparable. Three different types of structural units were identified in acid-treated samples, including $(SiO)_3SiOH$ units which, as a result of poor ordering of the framework, have no possibility of cross-linking.

Upon acid treatment, protons penetrate into the mineral layers and attack the structural OH groups. The resulting dehydroxylation is con- nected with the successive release of the central atoms from the octahe- dra as well as with the removal of Al from the tetrahedral sheets. Simultaneously, a gradual transformation of the tetrahedral sheets intoathree-dimensionalframeworkproceeds.Dependingontheextent of acid activation, the resulting solid product contains unaltered layers andamorphoussilica,whiletheambientacidsolutioncontainscations accordingtothechemicalcompositionoftheclaymineral andtheacid used.Thereareseveralclaymineralsincludingtrioctahedralsmectites (Vicente et al., 1995a; Komadel et al., 1996b), dioctahedral smectites (Komadeletal.,1990;Tkáčetal.,1994;Heetal.,2002),illite-smectite (Pentráketal.,2010),sepiolite(Vicenteetal.,1995b)andpalygorskite (Suárez Barrios et al., 1995), and the final product consists of amor- phous, porous, protonated and hydrated silica with a three- dimensional cross-linked structure (Komadel,1999).

A complex approach to investigation of acid activation of clays is seen in the papers of Kooli and co-authors. Kooli and Jones (1997)acid-activated a natural saponite at room temperature (RT) or 90 °C with different acid/clay ratios and characterized the products by XRD, IRspectroscopyandthermogravimetry.Theleachingof Mgfromtheoc- tahedral sheets was enhanced by increasing the acid/clay ratio and by raising the temperature at which the process was carried out. Textural properties were strongly correlated to the presence of a noncrystalline silica phase formed during the acid activation process. Kooli and Jones(1998) used acid-treated saponite for the preparation of Al- and Zr- pillared acid-activated clays, which incorporated less Al and Zr than the parent saponite, in consequence of the reduced cation exchange ca- pacity (CEC) of the matrix followingacid-activation.

Koolietal.(2005)reportedontheintercalationproperties ofacid-activatedmontmorillonitestreatedatdifferentacid/clayratioswith thecationicsurfactantcetyltrimethylammonium(C16TMA)hydroxide. Theacidactivationcausedareductioninthenumberofcationexchange sites and improved the exfoliation of the silicate sheets at higherpH values.Thebasalspacingincreasedfrom1.54to3.80nm,depending ontheextentofacidactivation.The^{13}CCP/MAS-NMRspectraindicated thattheintercalatedsurfactantsexhibitedasignificantdegreeofgauche conformation in the acid-activatedclays.

FurtherstudyoftheintercalationofC16TMAintotheinterlayersofa synthetic layered silicate, Na-magadiite, was made by Kooli et al.(2006a)inthepresenceofdifferentanions,resultinginevidencethat theamountofintercalatedhexadecyltrimethylammonium(C16TMA) cation depends on the anion type, the maximum content achieved being1.16mmol/g.TherawNa-magadiiteexhibitedabasalspacingof 1.54 nm, increasing to 3.12 nm on intercalation of C16TMA cations.

Koolietal.(2006b)discussedporousclayheterostructures(PCH)as anewclassofsolidacidsexhibitingporesizesintherarely-observed supermicroporetosmallmesoporeregion,formedbythesurfactant- directed assembly of mesostructured silica within the two-dimensionalgalleriesofsmectites.Acidactivationwaseffectiveinimprovingtheacidityandthemesoporosityoftherawclaymineral.The effect of the clay mineral type on the properties of porous acid-activatedclayheterostructures(PACHs)wasanalysed.In mostcases, softextractionofthesurfactantsviachemicalmethodsdid notimprove thestabilityandthepropertiesofPCHandPACHmaterials.

Kooli et al. (2009) analysed the acid-activated montmorillonites pre- pared from the Ca^{2+}-montmorillonite STx-1 and H_2SO_4 at different acid/montmorillonite ratios. On reaction with C16TMA bromide solu- tion, the acid-treated Mt incorporated smaller amounts of the surfac- tants than the parent Mt, due to the lower CEC after acid treatment. The powder XRD patterns exhibited a similar basal spacing of 3.80 nm but with a less ordered structure at higher acid\montmorillonite ratios. Some conformational heterogeneity was observed by ^{13}C CP NMR spectroscopyduetodifferentlocalenvironmentsoftheC16TMA^{+}cationsin the interlayer space. The stability of the surfactant decreased when in- tercalated into the montmorillonites, compared to that of pure C16TMABr. This indicates that the interlayer space influenced the de- composition steps.

KooliandYan(2013)consideredthechangesthatacidactivationef- fectsonthephysico-chemicalpropertiesoftherawclayminerals.The extentofthesemodificationsdependedonthetypeandoriginofthe claymineralsandtheconditionsoftheacidactivation.Intheirstudy, abentoniteexhibitedstrongstabilitytowardsacidtreatmentat90°C andathigheracid/claymineralratios,withslightdepletion ofMg^{2+}, Fe^{3+}andAl^{3+}cations(about5%).Theresultingorgano-acidactivated clays, prepared after reaction with C16TMA hydroxide solution, containedbetween0.80and0.70mmol/gofsurfactantand exhibited interlayerspacingof2.20nmand1.80nm,independentoftheinitial concentrationsoftheorganicmolecules.Theseorganoclayswerestable inacidicandbasicsolutions.However,onheatingto200°C,theinterlayerspacingshrank,withthermogravimetricanalysisin dicatingthis tobeduetothedegradationoftheorganicsurfactants.Therehydration ofthecalcinedorganoclaysattemperaturesbelow200°Cdidnotleadto anincreaseofthebasalspacing,duetochangesintheconfigurationof theC16TMA$^+$cations.

Kooli (2015) explored the thermal stabilities of polyvinylpyrroli- done (PVP)-organoclays and organo-acid-activated clay composites preparedbychemicalexchangereactions.Therawclaymineralwas acid-activatedpriortoexpansionbycetyltrimethylammonium surfactants.Theacidactivationprocessaffectedtheintercalated amountof C16TMA$^+$cationsintheresultingorganoclays,andthus,theamount ofPVPinthecomposite.Thecationcontentdecreasedwithextent of acidactivation.Theorganophilicmodificationoftheclay mineralwas an important step in the intercalation of the PVP molecules and, hence,intheexpansionofthesilicatesheetsfrom3.80nmto4.20nm. Thecompositesexhibitedbettercrystallineorderthanthestartingmaterial,withintensereflectionsatlowerangles.Thethermal stabilityof organoclays,acid-activatedclays,andcompositeswasstudiedusing thermogravimetricanalysisandinsituX-raydiffraction.Thedecompositionofintercalatedsurfactantsoccurredatlowertemperaturesthan thatoftheneatsurfactantsalt,andthebasalspacingoftheorganoclays (oracid-activatedclays)shrunkto2.0nmat215°C.However,thebasal spacingofcompositesexhibitedgreaterstabilityandcollapsedto 2.0nmonlyat300°C.Thistypeofmaterialcouldofferanalternative stable product for engineering purposes in the design of new composites.

Koolietal.(2015a,b)investigatedremovalofthedyebasicblue41 usingmodifiedclaymaterials.Modificationofbrickwastebyacidor basesolutionswascarriedouttoenhanceitsphysicochemicalproperties.Treatingbrickwastewithaciddidnotimproveitscapacityforre- moval of basic blue 41. However, treatment with base increased the removal capacity twofold. The adsorption capacity decreased from 100%to10%whentheinitialconcentrationsofbasicblueanddoseof thebrickwasteincreasedfrom25to900mg/L.Theparticle sizeofthe untreated brick waste also affected the removal capacity – for the sameinitialdyeconcentrations,moredyewasremovedwithasmaller particle diameter. The resulting experimental equilibrium data were well-representedbytheLangmuirisotherm,andthekineticdatafita pseudo-secondordermodelwell.Themaximumremovalofbasicblue 41dyewas60–70mg/g(Koolietal.,2015a).Koolietal.(2015b)alsoactivatedaclayfromtheKhulaisareaofSaudiArabiaat90°C atdifferent acid to clay mineral ratios. The clay contained mostly smectite, with ka- olinite and quartz admixtures. Upon acid activation, structural changes occurred for the smectite only; the other phases were not affected, as indicatedbypowderXRDandFTIR.AdecreaseintheAl_2O_3, MgO,Fe_2O_3, and Na_2O contents accompanied a relative increase in SiO_2. The acid- activated clays exhibited a lower CEC and higher SSA. These changes in chemical composition and other properties were related to the extent of the acid activation process. The acidity was enhanced up to a certain level of activation, and then it decreased gradually. The increase in sur- face area was not the main factor in the removal capacity of the acid ac- tivated clays for basic blue-41 dye. Up to a certain point, acid activation improved the removal capacity of the raw clay, from 50 mg/g to a maximumof73mg/g.Higheracid/clayratiosdecreasedthiscapacity,dueto the destruction of the removal sites during the acid activation. The recycling of spent acid activated clay was achieved by sulphate radical oxidation, and about 85% of dye removal could still be retained after six recycle runs (Kooli et al.,2015b).

Theextentofthedissolutionreactiondependedonboththeclay mineraltypeandthereactionconditions,suchastheacid/claymineral ratio, acid concentration, time and temperature of the reaction (Komadel,2003;Sakizcietal.,2011).Thecompositionoftheclayminerallayerssubstantiallyaffectedtheirstabilityagainstacidattack; trioctahedrallayersdissolvedmuchfasterthantheirdioctahedralcounterparts.Theresultsofseveralstudiesapplyingcomplexsetsoftech- niques showed that higher substitutions of $Mg^{2+}$and/or $Fe^{3+}$for Al^{3+}indioctahedralsmectitesincreasedtheirdissolutionrateinacids (Vicenteetal.,1994,1995a,1995b;Komadeletal.,1996b; Madejováetal.,1998,2009b;Steudeletal.,2009a),supportingthefindingsof Novák and Číčel, (1978), who found a good correlation ofthe $Mg^{2+}$and Fe^{3+} contents in dioctahedral smectites with the half-time of dissolution in HCl. Similar half-times (or dissolution rates) were ob- tained for reactions in 6 M acid for a Mg-rich Mt at 95 °C and an Fe- beidellite at 60 °C. More details are given in the original paper and in Table 10.1.1 of Komadel and Madejová (2013).

Thispaperwillmainlyreviewtheacidtreatmentofsmectit es,the dominantmineralsinbentonites.Butwewillalsoconsider othermineralswhosetreatmentwithacidyieldsenvironmentally-benigncatalystsortheirsupports,andwhichhavebeenusedinvarious chemical reactions such as Friedel–Crafts alkylation and acylation, dimerization and polymerization of unsaturated hydrocarbons (Adams, 1987;Brown,1994),andascolourdevelopersincarbonlesscopyingpapers (FahnandFenderl,1983).Morerecenttrendsincatalysisalsoinclude green catalysts in which the properties of certain chemicals are enhanced.Modificationoftheclaystructurebyacidactivationandim- pregnation of transition metals, such as chromium and vanadium, enhancedtheredoxpropertiesandincreasedtheLewisand Bronsted acidities. Various samples of vanadia supported on chromium- containingacid-activatedbentonitewerepreparedandcharacterized bydiffuse-reflectanceUV–visspectroscopy,surfaceacidity(determined byFT-IR),XRD,N_2adsorption-desorptionisotherms,andSEMcoupled withEDX.Thebehaviourofthesecatalystswasstudiedinthecyclohex- eneepoxidationreactionusingtert-butylhydroperoxideastheoxidant (Belaidi et al.,2015). Zaghouane-Boudiaf et al. (2014) spectrophotometrically investigat- ed the adsorption of 2,4,5 trichlorophenol (TCP) from aqueous solution onto the surface of organo-bentonites. Natural bentonite was activated with H_2SO_4 at 90 °C and exchanged with a series of four alkyltrimethylammonium bromides (alkyl = C12, C14, C16 and C18) to evaluate the effect of carbon chain length on the TCP adsorption. XRD was used to study the change in the structural properties of the samples. The basal spacing of the activated bentonite (AB) was in- creased from 1.34 to 2.15 nm by intercalation of the cationic surfactants into the interlayer space. The intercalated cationic surfactants were characterized by FTIR. The surface areas of the organo-bentonites were much lower than that of AB. The adsorption of TCP onto organo- bentonites followed pseudo-second-order kinetics, and theadsorption isothermsfitwellwiththeLangmuirmodel.Theadsorptioncapacityof organo-bentonite increased with increasing alkyl chain length. TCP strongly interacted with AB exchanged with octadecyltrimethylammonium$^+$(C18)cations.

The hydrolysis of hemicellulosic oligosaccharides (OS) was investi- gated using acid-activated clays as catalysts by Vilcocq et al. (2015). Acid activation was performed in HCl solution or with aluminium exchange. The clay catalysts were characterized by XRD, N_2 adsorption isotherms, CEC, FTIR, titration of acid sites in water, and adsorption of sugars and disaccharides. The HCl-activated clays were the most effi- cient catalysts for maltose hydrolysis. Hydrolysis of OS into monomer sugars over a clay catalyst proved technically feasible, yielding simpler xylo-oligosaccharide chains.

Acid-treated clay minerals pillared with (hydr)oxy aluminium specieshavealsobeenusedtoprepareclaymineral-modifiedelectrodes (Falarasetal.,2000a),asadsorbentsforoilclarification(Mokayaetal.,1993; Falaras et al., 2000b; Pagano et al., 2001), and as catalysts (Mokaya and Jones, 1994; Bovey and Jones, 1995; Bovey et al., 1996;Zhao, et al.,2015a).

II. METHODS OF INVESTIGATION

Themethodsemployedtocharacterizetheacid-activatedsilicates includechemicalanalysis;X-raydiffraction(XRD);Fouriertransform infrared (FTIR), magic angle spinning nuclear magnetic resonance (MAS-NMR), and Mössbauer spectroscopies; scanning (SEM), transmission(TEM),andhigh-resolutiontransmissionelectron(HRTEM)microscopies; and acidity, surface area, and pore-size measurements.

Usually,acombinationofseveralmethodsisneededforsufficientchar- acterization of the materials obtained (Číčel and Komadel, 1994;Vicenteetal.,1994,Vicenteetal.,1996b;Breenetal.,1995b;Komadelet al., 1996b; Gates et al., 2002; Klika et al., 2011; Scarletti et al.,2011; Ramesh et al., 2012, Khalili et al., 2015).

Chemicalanalysesofsolidand/orliquidreactionproducts andMAS-NMRandIRspectroscopiesareverysensitivetothenature andcontent oftheoctahedralsitesandthusalsotothechangesthatoccur indifferentstagesofacidattack(Breenetal.,1995a,b).Theextentofthedisso- lution of different chemical components of the sample can be determinedbychemicalanalysisofthestartingmaterialandbyanalysis oftheacidsolutionsreactedforspecifictimes.Thefiltrateandwashing solutions are combined and usually analysed by atomic absorption spectroscopy (Pentrák et al.,2010).

Spectroscopyinthemid-IR(MIR)regionisaroutinecharacteriza- tion technique for acid-treated clay minerals. As protons penetrate intotheclaymineralayersandattacktheOHgroups,theresultingdehydroxylationconnectedwiththesuccessivereleaseoftheoctahedral atomscanbereadilyfollowedbychangesinthecharacteristicabsorptionbandsattributedtovibrationsofOHgroupsand/oroct ahedralcations.ComparativeIRstudiesofacidtreatedsmectites(Madejováetal.,1998) as well as saponites, sepiolite and palygorskite (Vicente et al.,1996a) have been published.

InadditiontothespectraobtainedintheMIRregion,thespectra measuredinthenear-infrared(NIR)regioncanprovideusefulinformationaboutthedecompositionofclaymineralsininorganic acidssince theobservedbandscorrespondingtothevibrationsofOHgroupsare sensitivetovariationsinthemineralstructure.However,despitethe non-destructive character of NIR spectroscopy and the simplicityof sample preparation, its application to acid-treated clay minerals re- mains rather rare (Madejová et al., 2007, 2009a; Pentrák et al., 2009,2010; Tomić et al.,2012).

III. H^+-EXCHANGED CLAY THINERALS

The acidity of non-acid-treated smectites has two sources: (i) the compensatingcations,whichmayhaveastrongpolarizingeffectonco-ordinatingwatermolecules,mostofwhichareintheinterlayerspaces and may not be easily accessible and (ii) specific sites at the layer edges,whichmaybecompensatedbyOHgroupformation,leadingto Brønsted acid sites such as Si–OH. Also, coordinativelyunsaturated $Al^{3+}$and $Mg^{2+}$are easily formed at the edges and act as Lewis acid sites (Lambert and Poncelet,1997).

Duringacidtreatment,theprotonsfirstreplacetheexchangeable cations; after that they attack the layers (Číčel and Komadel, 1994). Theexchangereactionwasfastifthesmectitehadalargesurfacearea for the acid to interact with, and if the quantity of available protons wassufficient.Thesubstitutionratewasindependentofthesmectite iftheclaymineralcontainedonlyswellinglayers.Incontrasttosmectitessaturatedwithmetalcations,proton-saturatedsmectiteswereunstable. The layers were attacked by surface and interlayer hydrated protons,evenafterdryingtheseparatedactivatedmineral, similarlyto whatoccurredinsolution.Thisprocess,knownas‘auto-transformation’, spontaneouslychangedH^+-smectitestotheirAl^{3+},Fe^{3+},orMg^{2+}formsonageing(BarshadandFoscolos,1970).Inaqueousdispersion at 90 °C, the process was completed within 4 days (Janek andKomadel,1999).

TostudythepropertiesofH^+-claymineral,maximalsaturation by protons and maximum stability of the product were required. Various preparation methods were tested. The best results were obtainedbypassingtheclaydispersionthroughasuccession ofH^+, OH^-,andH^+ion-exchangeresins.H^+-formsofb2mmfractionsof bentonites with various Fe^{3+}contents were thus prepared. Potenti- ometric titrations of proton-saturated fine fractions of bentonites were used to characterize the acid sites at the smectite–water inter- face in dispersions. The titration curves revealed that the number of strongacidsitesvaried,andaccountedfor60–95%ofthetotalacidity inthefreshlypreparedH^+-forms(Janeketal.,1997).Thelayer-charge (LC) distributions of all samples were inhomogeneous. This distribution changed after oxalate pre-treatment of the samples, duetotheremovalofreadilysolublephasesthatmighthaveblocked exchange sites. After auto-transformation, the alkylammonium exchangemethod(Lagaly,1994)revealedinhomogeneous chargeden- sity distributions; the fraction of layers of the highest charge decreased. Comparison of the CEC obtained frompotentiometric curvesandtheCECcalculatedfromthemeanLCconfirmedthatthe protonattackoccurredattheparticleedges.However,forseveral samples, the structural attack may also occur from within the inter- layerspace.Auto-transformationoftheH^+-smectitesalsodecreased themeanLC.ProtonspreferentiallyattackedtheoctahedralMg^{2+}during the auto-transformation. The number of strong acid sites de- creased and the number of weak acid sites increased onageing.

The titration data obtained were used in a thermodynamic calcula- tion of proton affinity distribution. Numerical solution of an integral adsorption equation indicated a continuous distribution of proton interaction sites. The proton affinity distributions clearly showed up to five different proton interaction sites in the smectite–water systems, within the accessible experimental range of pH between 2 and 12. The strongest acid “sites” were those of the free protons present in the dis- persion, while the weaker acid sites were the released structural Al^{3+}, Fe^{3+}, or Mg^{2+} cations and/or their hydrolyzed species and deproton- ation of SiOH groups. These results indicated the sources of acidity in acid-activated bentonites (Janek and Komadel, 1993). Hydrated alumin- ium cations in fresh proton-saturated dispersions contributed to a group of weak acid sites, which also included oligomeric hydroxoaluminum cations. The number of these sites increased during auto- transformation. Freshly prepared proton-saturated dispersions showed low pH values and the particles interacted by edge-to-face contacts. This increased the viscosity in comparison with the sodium forms which had pH close to 7 (Janek and Lagaly, 2001). A kinetic study of proton-promoteddissolutionofK^+-MtinsolutionswithconstantKCl concentrations, using both titration and batch equilibration experiments, showed that adsorption of protons and dissolution of Al^{3+}occurred (Zysset and Schindler,1996).

IV. ACID DISSOLUTION OF STHECTITES

Acidtreatmentofclaymineralswithstronginorganicacidsresulted in solid products containing unaltered layers and amorphousthree- dimensionalcross-linkedsilica,dependingontheextentofacidactivation.TheIRspectraoftheSWy-1(smectiteWyoming,fromtheClay Minerals Repository of the Clay Minerals Society) Mt after reaction with6MHCl(KomadelandMadejová,2013)indicatedchangesofthe chemicalbondsintheMtstructure.Thegradualdecreaseintheintensi- tiesoftheOHbending(930–800cm^{-1})andAl–O–Si(524cm^{-1})bands indicateddecompositionoftheoctahedralsheets.Changesinthetetra- hedral sheets were reflected in the position and shape of the Si–O stretching band. In addition to the tetrahedral Si–O band near 1048cm^{-1},theMIRspectraoftheacid-treatedsamplesshowedapro- nounced absorption near 1100 cm^{-1}, assigned to Si–O vibrations of amorphoussilicawithathree-dimensionalframeworkformedduring acid treatment. The position of the Si–O band at 1103 cm^{-1}together with the weak inflection near 524 cm^{-1} observed for the sample dissolvedfor30hreflectedsignificantyetincompletedissolutionofMt in6MHCl(Madejováetal.,1998).TheNIRspectrumofSWy-1Mtpresentedabroad,complexbandat7083cm^{-1}correspondingtothefirst overtones($2\nu_{OH}$)ofthestructuralOHgroupsandH_2Omolecules.The intense band near 5251 cm^{-1}was attributed to the combination mode $(\nu + \delta)_{H2O}$ of the water molecules and the band at 4533 cm^{-1} to combination modes $(\nu + \delta)_{OH}$ of the structural OH groups (KomadelandMadejová,2013).Uponacidtreatment,the intensities ofthesebandsgraduallydecreasedasaresultofthedecompositionof theMtlayers.Anewbandat7311cm^{-1}assignedto$2\nu_{SiOH}$confirmed the presence of SiOH groups (Pálková et al.,2003).

Li$^+$dissolvedslightlyfasterthanMg^{2+}fromhectoritelayersatlow acidconcentrations(Komadeletal.,1996b).Thus,protonswerepreferentiallyattractedbythemorenegativesitesclosetoLi$^+$(intheoctahe- dral sheet) rather than by the sites adjacent to Mg^{2+}. This difference disappearedathighacidconcentrationswherethereactionrateswere high.Similarly,octahedrally-coordinatedMg^{2+}cationswerepreferen- tially released by HCl in comparison with Fe^{3+}and Al^{3+}(Christidisetal.,1997;Gatesetal.,2002).Theeffectoftheacidanionondissolutionof hectorite is complex and uncertain (Komadel et al., 1996b; VanRompaeyetal.,2002).Theeffectsofsmectitetype,acidconcentration, andtemperatureonthehalf-timeofdissolutionin0.2LHCl/gsmectite acid/claymineralratioinclosedsystems(nosubstancesbeingaddedor removed)appearintheoriginalpaperandtheyarealsosummarizedby KomadelandMadejová(2013).Therateofdissolutionofvariousatoms obtainedfromchemicalanalysisoftheliquidreactionproductsprovidedinformationondifferentphasesoratomtypesinthestructure,byindicatingtherelativeamountsofoctahedralandtetrahedralsubstituents which were readily soluble even without acid, soluble on treatment withacid,andinsoluble(ČíčelandKomadel,1994).Thereadilysoluble portionsincludedexchangeablecationsandeasilysoluble admixtures such as goethite (Komadel et al., 1993) and calcite (Komadel et al.,1996b).Themostcommon‘insoluble’phasesfoundin thefinefractions of bentonites were kaolinite, quartz, anatase and volcanic glass. Halloysitewasthemostdecomposedmineralafterreactioninsulphuric acid of different concentrations, followed by montmorillonite,pyrophylliteandkaolinite(Katoetal.,1966).Theobservedlow dissolution rateofpyrophyllitecomparedwithMtwasduetolowoctahedralsubstitutionandthepresenceofcollapsednon-swellinginterlayerspaces in pyrophyllite.

Pentrák et al. (2010) investigated the influence of chemical compositionandswellingabilityofthreedioctahedralclaymineralsfromthe Mt-Iseriesontheirdissolutionin6MHCl.Mtwascompletelydissolved within 18 h, while after 36 h the residues of non-decomposed illite couldbedistinguishedinbothsampleswithprevailingnon-swellinginterlayerspaces.Thechemicalcompositionofdioctahedralclayminerals hadagreatereffectonthedissolutionratethanswellability.Thepureil- lite, with a higher degree of substitution of Mg^{2+} and Fe^{3+} for Al^{3+}in the octahedral sheets and of Al^{3+}for Si^{4+}in the tetrahedral, was moreeasilysolubleinHClthantheillite-smectitewith30%swellinginterlayerspaces.Aseriesofreduced-chargeMtwaspreparedviaLi$^+$fix- ation at elevated temperatures (the Hofmann–Klemen effect) to explorehowtheexpandabilityoftheinterlayerspacesinfluencedthe extentofdissolution.AsthenegativeLCdecreased,thenon-swellinginterlayerspacecontentincreased(Komadeletal.,1996a).Thedissolu- tion of reduced-charge Mt in HCl indicated that pyrophyllite-like layerssurroundedbynon-swellinginterlayerspacesdissolvedmore slowlythanMtlayersofsimilarchemicalcompositionlocatedbetween swellinginterlayerspaces(KomadelandMadejová,2013).Thisclearly showed that protons attacked the layers from the swolleninterlayer spacesalso.Non-swellingilliteandkaolinitewerealsomoreresistant toHClattackthanMtorvermiculite(JozefaciukandBowanko,2002).

Bentonites are widely available and abundant natural materials, serving as low cost adsorbents for water and wastewater treatment (Tooretal.,2015).Onestudywasdirectedtowardsidentifyingacost-effectiveactivationprotocolforenhancingtheadsorption capacityof AustralianbentoniteforremovalofCongoredfromwastewater.Combinedacidandthermalactivationprovidedverypromisingresultsfor this purpose. Bhattacharyya et al.(2014)and Bhattacharyya et al.(2015) activated kaolinite and montmorillonite with 0.25 and 0.50M H_2SO_4toremoveRhodamineBandCongoredfromwater. Theyfound thatthedyemoleculeswereheldtotheclaymineralsurface byweak bondsandtheacid-treatedclaymineralsshowedbetteradsorptionca- pacity for the dyes than did the parent clays. Cottet et al.(2014) pre- pared a montmorillonite modified with iron oxide for use as an adsorbentofmethylenebluedye.TheymodifiedthepHofthesolution fortheadsorptionexperimentsandusedasetoftechniques toobtain also the activationparameters.

An in situ observation by AFM showed that the dissolution of hectorite and nontronite in acid solutions occurred inward from the edges;thebasalsurfaceswereunreactive.Thehectorite(010)facesdissolvedmoreslowlythanthelathends.Theedgesdissolved onallsides androughened.Therate-limitingstepofthedissolutionprocesswasthe breaking of the bonds of connecting oxygen atoms (Bickmore et al.,2001).

V. ACID DISSOLUTION OF ORGANO-STHECTITES

Thehydrophilicsurfaceofswellingclaymineralshasbeen rendered hydrophobicbyexchangingthenaturallyoccurringinorganiccations with organic (mostly alkylammonium) cations. The size and the amountoftheorganiccationssignificantlyaffectthedissolutionrate of smectites in acids (Breen et al., 1997a). Both the MIR spectra and thecarboncontentrevealedthatonlyasmallproportionof dodecyl- or octadecyl trimethylammonium was displaced during HCl treatment of organo-smectites, and the remaining alkylammonium cations protected the smectite from acid attack. The long-chain alkylammoniumcationsrestrictedtheaccessofprotonsto thelayers, and the extent of acid attack wasreduced.

Dissolutionoforgano-smectitesinHClcouldalsobeeffectively followedbyNIRspectroscopy(Madejováetal.,2009b;Tomićetal.,2012).ThespectraofSAz-1(smectiteArizona,fromtheClayMinerals Repository of the Clay Minerals Society) Mt saturated with tetramethylammonium(TMA^+)andhexadecyltrimethyl ammonium ($HDTMA^+$)cationsshowedthe$2\nu_{OH}$and$2\nu_{H2O}$bands(7060cm^{-1}), $(\nu + \delta)_{H2O}$ (5246 cm^{-1}), and $(\nu + \delta)_{OH}$ (4515 cm^{-1}), as well as the first overtones (6100–5500 cm^{-1}) and combination modes (4500–4000 cm^{-1}) of the CH_3 and CH_2 groups (Madejová et al.,2009b,KomadelandMadejová,2013).ThespectrumofTMA$^+$-SAz-1Mtdissolvedfor2hin6MHClat80°Cshowedthedisappearanceof all bands in the $2\nu_{CH3}$ region, but the shoulders near 4445 and 4321cm^{-1}indicatedthatnotallTMA$^+$cationswereexchangedbyprotons.Theappearanceofaweak$2\nu_{SiOH}$bandat7316cm^{-1}confirmed theacidificationoftheTMA$^+$-SAz-1Mtsurface.After6hofdissolution, theabsenceofCH_3bands,theincreasedintensityofthe$2\nu_{SiOH}$band,the reducedintensityofthestructuralOHovertoneband,andtheappearanceofthe$(\nu+\delta)_{SiOH}$bandat4551cm^{-1},confirmedthatTMA$^+$-SAz-1Mthadbeenconvertedtoprotonatedamorphoussilica.

VI. ACID ACTIVATION OF VERTHICULITES

Likesmectites,vermiculitesareexpandableminerals.Theexpansion ofvermiculitesismorerestrictedbecausetheirlayerchargeishigher andthischargeislargelylocatedinthetetrahedralsheet.Thedistinctionofvermiculitefromsmectiteisarbitrary,basedonalayercharge of0.6eq/$O_{10}(OH)_2$.Thesetwogroupsofswellingminerals canbetreatedasacontinuum,foralthoughMtisadioctahedralmineralwhilemost vermiculites are trioctahedral (de la Calle and Suquet, 1988), dioctahedralvermiculitesareknown(MallaandDouglas, 1987).How- ever, there is enough to be said about vermiculites for them tomerit their ownsection.

Themostwidelyacceptedoperationaldefinitionofavermiculiteis that of the ca. 1.45 nm basal spacing for the Mg^{2+}-exchanged form aftertreatmentwithglycerol,togetherwiththecollapseoftheK$^+$-formto1.0nmonheatingat300°Cfor1h.Purevermiculite shoulddisplayarationalseriesofverynarrowreflections,butsuchmineralsare very rare. The glycerol test distinguishes vermiculite from smectite, and the heating test distinguishes vermiculite from chlorite (the 1.4-nmbasalspacingofchloriteisnotaffectedbyheatinginsuchconditions).Theheatingtestcanbeusedtodetectvermiculiteinthepresence ofchlorite.Theapplicationofdifferentteststosoilvermiculiteshasbeen described in detail by Malla and Douglas(1987).

TwosamplesofpristinevermiculiteswerereactedwithHNO_3under controlled conditions. Structural and textural studies were performed using chemical composition analysis, XRD, ^{29}Si and ^{27}Al NMR, adsorp- tion/desorption nitrogen measurements, SEM and TEM. Acid activation increasedthespecificsurfaceareaandporosityofthesamplesandledto partial leaching of Fe, Al and Mg from the octahedral sheets. Acid leaching of the two vermiculite samples with 3 and 4 M HNO_3 at 80 °C for 4 h removed nearly all the MgO, Al_2O_3 and Fe_2O_3, and left behind a SiO_2-containing residue, as could be expected. Low-crystallinity prod- ucts were obtained for both vermiculites when treated with high acid concentrations (Santos et al.,2015). Grindingofclaysmodifiestheirsurfacesandcansignificantlyaffect theirleachingbehaviour.Thereactionofvermiculitefrom SantaOlalla (Huelva, Spain) with HCl at various concentrations was affected by grindingandacidconcentration.Theacidleachingofgroundvermiculite for3minwith1MHClsolutionat80°Cfor24hremovedMgOandAl_2O_3almostcompletely,leavingaresiduecontainingSiO_2andFe_2O_3.XRD analysisshowedthepresenceofakaganeite(β-FeOOH)andanamorphoussilicaphase.Porositystudiesshowedaveryhighspecificsurface areaforgroundsamplescomparedwithungroundvermiculite,attributedtothepresenceofstructuralironintheresidue.Highresolutiontransmissionelectronmicroscopy(HRTEM)confirmedthepresenceofiron oxyhydroxidesembeddedinthesilicamaterial.Theparticlemorphology oftheironoxidescorrespondedwelltothatofakaganeitemicrocrystals precipitated from solution. The leached vermiculite residue also contained $Cl^-$and a small amount of Ti^{4+}, which were incorporated into the akaganeite microcrystals (Maqueda et al.,2009). Afterannealing,thematerialobtainedafteracidtreatmentofground vermiculiteconsistedamorphoussilicaandakaganeite.TheXRDpat- terns of the starting sample, measured at temperatures from 30 to 1200 °C, showed that the crystalline phase was present until about 300 °C, whereas between 300 and 800 °C the sample was practically amorphous. This is in agreement with previous observations thatβ-FeOOHdecomposestoanamorphousorpoorlycrystallinephase,β-Fe_2O_3,andtransformsonlyslowlytocrystallineα-Fe_2O_3.At850°Cthe firstsignsofacrystallinephasewererecognized,whichwasfullydevelopedby1050°C,consistingofquartz,cristobalite,α-Fe_2O_3andε-Fe_2O_3. Thiseffectshowedthatwell-crystallizedironoxidenanoparticles embeddedinthesilicamatrixareusuallyformedat~1000°C.Element mappingofaparticleofthecompositeobtainedbyannealingthesam- pleatthehighesttemperatureshowedwell-separatedFe_2O_3andSiO_2particlesinacompositematerial.AlandMgimpuritiesfromtheoriginal vermiculiteaccompaniedthesilicacomponents,andthepresenceof TiO_2 associated with Fe_2O_3 grains (Perez-Rodriguez et al., 2011). Perez-Maquedaetal.(2012)provedthatacidleachingofvermiculite isaprocedurewhichleadstothepreparationofporoussilicawitha highsurfacearea.Thethermalbehaviourofgroundandungroundvermiculitesaftertheacidtreatmentwasanalysed.Fortheacid-treatedungroundvermiculite,dehydratedvermiculite,enstatiteand cristobalite were formed during the heating, while for the ground mineral the only phases observed wereof iron oxides and cristobalite. Chmielarzetal.(2012)reactedvermiculitewith0.8Msolutionsof HCl and H_2SO_4 for up to 24 h, characterized the obtained materials witharangeofmethods,andconfirmedpartialleachingof Fe^{3+},$Al^{3+}$and Mg^{2+} cations from the octahedral sheets. The efficiency of the leachingprocessdependedonitsdurationandtheacidused.Thetreatmentstronglymodifiedthevermiculitestructure,leadingtoadistinctin- crease of its catalytic activity in the selective catalytic reduction of nitric oxide.Thebestcatalyticperformancewasfoundforvermiculitereacted withsulphuricacidfor8h.Temuujinetal.(2003)obtained highsurface areasilicabyselectivelyleachingvermiculite.Leaching with2MHClat 80 °C for 2 h produced a maximum value of surface area (672 m^2/g) withtotalporevolumeof0.44ml/g.The^{29}SiMASNMRspectraofthe leachedproductsindicatemainlyQ^3andQ^4structuralunits,assigned aslayerandframeworkstructures,respectively.Thelayer structureisresponsibleforformingmicroporesandtheframeworkstructureforms mesopores.Thenumberofmicroporesdecreasedwithlon gerleaching time,themicroporescondensingtoincreasetheframeworkstructure.

Thecharacteristicsoftheporoussilicaobtainedfromvermiculiteare compared with those from other clayminerals.

Kupkováetal.(2015)treatedtwovermiculiteswithsimilarchemicalcompositionsandslightlydifferentlayerchargeswith differentconcentrationsofHClsolutionstoanalysethechangesintheir structural and chemical properties. Both (untreated) samples represented a mixed-layerstructureafterincompletetransformationofbiotitetovermiculite.Theacidificationwasmoreeffectiveatleaching Mg^{2+}cations fromthelessvermiculatedsample,andatleaching$Fe^{2+}$and $Fe^{3+}$from the octahedra and Al^{3+} from the tetrahedra of the othervermiculite.

Hashemetal.(2015)chemicallyactivatedvermiculitefromEgyptby leaching with 0.5 M HCl or with 30% H_2O_2 solutions. SEM andXRD showedthatleachingwithHClresultedinpartialtransformationofits orderedlayersintoadelaminatedstructure,whilereaction withH_2O_2 ledtoseparationandfragmentationofthelayersbutwithoutstructural change.ThechemicallyactivatedvermiculitetreatedwithCd^{2+}orPb^{2+}cationsshowedhigherthermalstabilitythantherawvermiculite.The removalefficiencyofperoxide-activatedvermiculitewashigherthan that of the acid-activated vermiculite for bothcations.

Jin and Dai (2012) treated vermiculite with H_2SO_4 and HNO_3 aque- ous solutions of different concentrations. The modified materials were used as supports to immobilize TiO_2. The TiO_2/vermiculite composites were characterized by X-ray diffraction, scanning electron microscopy, and nitrogen absorption. Their photocatalytic activity was evaluated by removal of MB. The anatase-type crystalline phase was well deposit- ed on the supports. The concentrations of acid for treatment had a sig- nificant influence on the pore sizes and surface area of vermiculite. The treatment process changed the microstructure of vermiculite, mod- ified its characteristics, and improved the catalytic activity and absorp- tion capacity of the composites. The effect of treatment with nitric acid was superior to that of sulfuricacid.

VII. PROPERTIES OF ACID-ACTIVATED STHECTITES

Mudrinicetal.(2015)examinedhowadditionofNiaffects theelec-trochemicalactivityofFeinHCl-treatedMacjiDobentonite(Serbia). Incorporation of nickel into acid-treated bentonite at 70 °C for 30 min was achieved. A wealth of information on the system was obtained via application of a set of analytical methods. The electrocatalytic test showed that the current response of the Fe^{2+}/Fe^{3+}oxidation/reduction process increased on GC electrodes separately modified with each of the acid treated samples, in comparison with the current obtained on the GCelectrodemodifiedwithanuntreatedsample.Theappliedacidtreat- ment probably increased the accessibility of the electroactive iron with- in smectite. Further modification of the selected acid-treated sample with nickel species resulted in a decreased current response of the Fe^{2+}/Fe^{3+}oxidation/reductionprocessandimprovedthereversibility of thisprocess.

7.1 Layer charge(LC)

The structural modification of smectites upon acid treatmenthas beenfoundtobecloselyconnectedwiththeLCalteration. LCinacid- treated samples was compensated mostly by the protons that had substitutedtheexchangeablecations.UV–visspectroscopyofthesmectitedispersionswithmethylenebluewasusedforexaminingthemodificationofLC(Madejováetal.,2007;Pentráketal.,2012). Differentdye species – monomers, dimers, H-aggregates and J-aggregates – were adsorbedonthesamplesasaresultofthevariationsinLC.Asaconse- quence of the acid treatment, the amount and/or size of the H-aggregatesofMBdecreased,whilethecontentofthemonomericform oftheadsorbeddyecationincreased.ThechangesinLCobservedin thesmectitespectrashowedthattherateofdissolutioninHClvaried withthetypeofcentralatoms.TheMBspectraofSWy-2Mtrevealed apronouncedheterogeneityoftheLCdistributioninthislow-charge Mt. Thechargeoftheclaymineralstructure,alreadyhighlyvariable,was furthermodifiedbydecompositionofthestructureuponacidoralkalinetreatment(Jozefaciuk,2002).Differentclaymineralswerereacted withHClorNaOHatroomtemperature(RT)for2weeks.Boththreat- ments increased the surface charge, but the overall chargeincreased or decreased depending on the mineral and the reaction conditions. Charge-generatingsurfacegroupswereheterogeneous.Duringacid treatment, the number of weakly acidic surface groups increased, whilethenumberofgroupsofstrongeracidiccharacterdecreased.

7.2 Specific surface area

Themostimportantphysicalchangesinacid-activatedsmectitesincludeincreaseoftheSSAandaverageporevolume.Theextentofthese changeshasbeenfoundtodependontheacidstrength,lengthofthe treatmentandontheheatingmethod.Microwaveirradiation-assisted acidactivationofsmectiteswasfasterthanconventionalheating.The SSAandporosityofthesampleswassimilarforcomparablydissolved materials (Korichi et al., 2012). A mathematical modelincorporating therelationshipsbetweentime,acidconcentration,microwaveheating powerandthestructuralandtexturalpropertiesofacidactivatedbentoniteshowedthatthedurationofmicrowaveirradiationwaslesssig- nificantthantheothertwofactors (Petrovićetal.,2012).

Acid activation of bentonites caused a splitting of the particles along with an increase of the SSA and decrease of CEC of the bentonites (Tomić et al., 2011). The SSA of acid activated samples was several times larger than for untreated materials. Christidis et al. (1997) report- ed a 4- to 5-fold increase of the SSA of two HCl-activated bentonites. As in some cases mentioned above, treatment increased the SSA only up to a point (typically under intermediate activation conditions), then de- creased with further treatment.

Twosaponitesandaferroussaponite(griffithite)werereactedwith b2.5% HCl at 25 °C for periods of up to 48 h. Most of the octahedral sheetsofthemineralsweredissolved,aswasindicatedbythehighextentofremovalofMg^{2+},thechangesintheIRspectra,andtheTGA-DTA curvesoftheactivatedsaponites.Destructionofthesaponitestructure yielded free silica, and the SSA of the saponites doubled even after mild acid activation (Vicente et al., 1996b; Suárez Barrios et al., 2001). The SSA of griffithite samples increased massively after activation, with values of up to ten times higher than the SSA of the untreated sam- ple. The creation of microporosity had a substantial influence on the SSA. Free silica had a very important contribution to the SSA of leached samples (Vicente et al., 1995b). The high SSA of 197 m^2/g of a natural saponite was related to the very small particle size because of its sedi- mentary origin. Reaction of sedimentary saponites at RT with 0.62% HClforupto48horwith1.25%HClforupto6hproducedpartialdis- solutionoftheclaymineral. Amixture ofunalteredsaponiteandfreesil- ica was obtained. The solid products consisted mainly of delaminated layers, free silica, and insoluble impurities. The SSA was 462 m^2/g and thenumberofacidcentreswas0.98mmolH$^+$/g(Prietoetal.,1999).

7.3 Porous structure

Texturalcharacteristicssuchasporevolumeorporesizedistribution have played a significant role in the applications of clay minerals. JovanovićandJanaćković(1991)foundthattheporestructureandad- sorption properties of an HCl-activated Serbian bentonite at 75 °C dependedontheconcentrationoftheacidused.Theratioofthemass ofclaytothevolumeofacidsolutionwas1:10g/cm^{3}andthe adsorbent withoptimalporosityandadsorptionpropertieswasobtainedfrom treatmentwith2Macid.Babakietal.(2008)reportedthatthephysical andchemicalpropertiesofbentonites,suchasadsorptionandcatalytic activity,dependedextensivelyonthemicro- andmesopores.Though themacroporeswereaccessiblefromthesurfaceoftheparticles,their effectontheadsorptivepropertiesofasolidwasminorcompared to thatofthemicroporesandmesoporeslocatedwithintheparticles.Varioustechniquessuchasacidtreatmentorpillaringhavebeenusedto improve smectitemesoporosity.

Short-timesynthesisroutesforpreparationofmesoporousorFolded SheetMaterials(FSM)havebeendevelopedfromHCl-leachedsaponite samples.Theacidtreatmentwasperformedunderstirring for24hat25 and100°Cin6–10and3–7MHClsolutions.Theleachedsilicatepowderswerewashed,dispersedinhexadecyltrimethylammoniumbro- mide solution as a structure-directing agent, stirred at pH =12.3 for 3 h at 70 °C and afterwards at pH = 8.5 for an additional 3 h at RT, andfinallycalcinedat550°Ctoobtainthemesoporousmaterials.AgeneralimprovementofthemesoporousFSMstructurewasobtainedwhen afiltrationstepwasaddedtothesynthesisrouteafterthedissolutionat pH=12.3,byremovingalldissolvedsilicatesandthuspreventingthe formation of amorphous silica. The material synthesised after acid leachingby8MHClatRThadthemostcondensedstructure,thehighest unitcelldimensions,SSAandporevolume,andthenarrowestpore-size distribution(Linssenetal.,2002).ThepropertiesoftheFSMprepared from saponite samples by different HCl treatments are reported in Table10.1.2ofKomadelandMadejová(2013).Formostpreparations obtainedat25°C,theBETSSAweremuchhigherandmore sensitive to the acid concentrations than for the materials prepared at 100 °C. Thematerialobtainedafterleachingwith5MHClat100°C hadthe highest porevolume.

AcidactivationofaCa^{2+}-Mtbyreactionwithsulphuric-acidsolutionsandsubsequentpillaring(intercalationofoligomericAl(hydr)ox- ides – 'Keggin ions' – and calcination at temperatures up to 500 °C) producednewmaterialsforbleachingcottonseedoil,with bleaching propertiesdependentontheextentofactivationpriortopillaring.The pillaredacid-activatedMtpossessedahigherbleachingefficiencythan the pillared non-activated clay minerals. Mild activation of the Mt followedbypillaringproducedmaterialswiththebestfractionaldegree of bleaching (Falaras et al.,2000b).

FaghihianandMohammadi(2014)preparedpillaredcatalystsby pillaringofMtandcharacterizedthembyXRD,FTIR,N$_2$adsorptioniso- therms, NH$_3$temperature programmed desorption, SEM, and elemental andthermalanalysistechniques.Theacid-treatedsamplehadalower Al content and its total pore volume and SSA were higher. The acid- activated pillared catalyst, due to its higher surface acidity, showed en- hanced catalytic activity for the alkylation of benzene with linear olefins compared to the untreated sample.

DetailedstudyofpreparationandcharacterizationofanAl PILCde- rived from an acid-treated Mt showed that careful selection of the levelofacidtreatmentwasnecessarytooptimisetheSSA, porevolume, surfaceacidityandthermalstabilityofthefinalPILC.Theoptimumlevel ofacidtreatmentcorrespondedtotheremovalofbetween19and35% oftheoctahedralcations.However,thesevaluesdepended ontheclay mineral.ThePILCmadefromacid-activatedmaterialshadsignificantly higherporevolumeandaciditythanconventionalPILC,butsimilar basalspacings,SSAandthermalstability.Thehigheraciditywasmainly duetoanincreaseofBrønstedacidsitesarisingfromthetreatmentbeforethepillaringprocedure.Thehigheracidityofthepreviouslyacid- activated PILC was reflected in better catalytic activity for acid-catalysedreactionsthandisplayedbyotherPILC(MokayaandJones,1995). Porous clay heterostructures (PCH) with enhanced acidity couldalsobepreparedfromsuitablyacid-activatedMt.TheirhighacidityarosefromBrønstedacidsites(PichowiczandMokaya, 2001).

PCHexhibitedporesizesintherarely-observedsupermicroporeto smallmesoporeregion,formedbythesurfactant-directedassemblyof mesostructuredsilicawithinthetwo-dimensionalgalleriesofsmectites (Koolietal.,2006a,b).Acidactivationofthesmectiteisaneffectiveway toimprovetheacidityandthemesoporosityoftherawclay mineral.

Thetypeoftheoriginalclaymineralaffectedtheproperties ofporous acid activated heterostructures (PAAH). Synthesis of PACH was achieved and the samples were characterized by powder XRD, N$_2$ adsorption-desorptionandacidityusingcyclohexylamineasaprobe molecule.Ashort-rangeorderinthestructurewasrevealedbyXRDof PACHmaterials.Theoriginortypeofclaymineralaffectedthefinal properties of the derivedmaterials.

7.4 Catalytic properties

Acid-activated clay minerals are well established as both solid acid catalysts and catalyst supports. The nature of the exchangeable cations substantially affects the acidity of clay mineral catalysts. The high cata- lytic activity of A1^{3+}-exchanged Mt has been attributed to the en- hanced polarization of water molecules in the primary coordination sphere around the Al^{3+} cations, giving rise to strong Brønsted acidity (Varma, 2002; Jankovič and Komadel, 2003b).

H$^+$-saturatedMtofconsiderablecatalyticactivitycouldbeprepared by thermal decomposition of ammonium-exchanged clay minerals (JankovičandKomadel,2000,2003a).However,amoretypicalmethod wasacidactivationofclaymineralswithamineralacid.Acid-activated claymineralsareofinterestashighsurfaceareasupportsforenvironmentallybenigncatalysts.Commercialproductsarenormallyreacted withafixedamountofacid,sufficienttoremovetherequirednumber ofoctahedralcationstooptimisetheSSAandBrønstedacidityforaparticularapplication.However,onlyafewsystematicstudieshavebeen reportedonhowtheextentofacidactivationoftheparentmineralcon- tributes to the catalyticactivity.

Several studies have illustrated the application of commercial acid- activated Mt (K-10) catalysts. Flessner et al. (2001) investigated the sur- face acidity of a series of K-catalysts (commercial Süd Chemie acid- treated montmorillonite clays) using a wide range of complementary experimental techniques. The different methods applied allowed a com- prehensive characterization of the surface acidity. The strength and density of Brønsted acid sites were correlated with trends in isobutene conversion. Further activation of the K-10 Mt commonly used as a heterogeneous acid catalyst (Wallis et al., 2007) with HCl of varying concentrations increased its catalytic activity in three test reactions: tetrahydropyranylation of ethanol, diacetylation of benzaldehyde, and esterification of succinic anhydride.

The catalytic activity of acid-activated Mt for Brønsted acid-catalysed reactions was highly dependent on the extent of acid treatment. Two contrasting model reactions were used. The first, involving highly polar reactants, was the acid-catalysed addition of 3.4-dihydropyran to methanol. The dihydropyran molecule was protonated to give a stabilized carbocation that reacted with methanol to form tetrahydropyranyl ether as the only product. The second reaction, involving a non-polar, hydrophobic reactant was the acid-catalysed rearrangement of α-pinene to camphene. The optimum activation conditions depended on the type of reaction being catalysed (Rhodes and Brown, 1994). AcidactivationofCa^{2+}-Mtsignificantlyincreaseditseffectivenessas asupportfor$ZnCl_2$Friedel-Craftsalkylationcatalysts.Optimumtreatmentconditionswereestablishedandtherewasevidenceforasynergistic interaction between the adsorbed salt and the acid-activated claymineral(Rhodesetal.,1991).Thehighestactivitywas associated with long acid treatment times. Structural characterization by XRD, 29SiMAS-NMRspectroscopy,andelementalanalysissuggestedthat the amount of residual clay mineral in the most active supportswas small (Rhodes and Brown,1992). Aseriesofacid-activatedmontmorilloniteswerepreparedandevaluatedasactivecatalystsforthecrackingofrosinbyTonget al.(2014). AllthesampleswerecharacterizedbyXRD,FTIR,nitrogenadsorption- desorption, temperature-programmed desorption of NH_3, SEM and thermalanalysis.Theacidtreatmentofmontmorilloniteimprovedthe specificsurfaceareaandtheamountofsurfaceSi^+groups. ThemoderateBrønstedacidityontheacid-activatedmontmorillonitemightbe responsible for the cracking ofrosin. Differentclayminerals,suchasmagnesium-oraluminium-richMt,a ferruginous smectite, an iron-rich beidellite, and a hectorite, were leached with H_2SO_4 or HCl. The extent of activation was controlled by the acid concentration and temperature. The elemental composition of the starting materials did not significantly influence the catalytic reaction of 2.3-dihydropyran and methanol to tetrahydropyranyl ether. The Brønsted acidity and catalytic activity of the activated clay minerals were highest for the samples prepared with the mild acid treatments but decreased with increased leaching of octahedral cations. The acid sites of acid-activated Mt were strong enough to produce tetrahydropyranyl ether in 80% yield. However, the acid-activated hectorite showed no catalytic activity. The octahedral depletion correlated well with the acidity (determined from thermal desorption of cyclohexylamine) and the catalytic activity for the chosen test reaction (Breenetal.,1995a,1995b,1997b;Komadeletal.,1997). Thecatalyticactivityforthedimerizationofoleicacidincreasedafter mildactivationofMtinHCl.However,theactivityoftheactivatedMt withabout50%ofoctahedralAl^{3+}removedwascomparabletothatof theuntreatedmineral(Číčeletal.,1992).Acidactivatedsmectitescan convertalkenesformedbythermaldecompositionofhigh-densitypolyethylene into light gases and aromatic species. Total conversion increased with both the extent of acid treatment and the temperature. Theproportionofaromaticproductswaslargestforcatalystsprepared using short activation (Breen et al., 2000). Acid-activated bentonite (andkaolin)coulddebutylate2-tert-butylphenolandshoweddifferent debutylationvsisomerizationselectivitydependingonthepreparation conditions.Theresultingcatalyticactivityofthesesampleswasdependentonthetypeofacidused.Samplesactivatedwithaceticacidshowed relativelylowconversion,whereasthosetreatedwithhydrochloricor phosphoric acids were very active catalysts (Mahmoud and Saleh,1999). doNascimentoetal.(2015)consideredacidtreatmentofclaymineralsoneofthemosteffectivemethodsforproducingactivematerials. Theydiscussedtheroleofactivatedclaysintheproductionofbiodiesel, OH_2 arenewable,biodegradableandenvironmentallyfriendlyfuel,which canbeobtainedfromesterificationreactions,transesterification,and pyrolysis. A Brazilian montmorillonite was treated with 0.2–0.8 M H_2SO_4,characterizedbyXRDandFTIR,andappliedinthe catalyticesterification of oleic acid. The results revealed that the clay treatedwith 0.8MH_2SO_4hadpromisingcatalyticactivityinthestudied reaction, withamaximumconversionofoleicacidof65%at30°C. Two Terra Rossa soils collected in the Mediterranean region of CroatiaandTurkeywerecomprehensivelytestedbyStipicevicetal.(2014)intheirnatural,acid-activated,andsurfactant-modifiedforms as sorbents for hydrophobic triazine groundwater pollutants with a viewtopotentialapplicationinthemultiminerallandfillbarriers.The soilswerepredominantlycomposedofkaolinite,followedbyquartz, calcite,iron-bearingoxides/oxyhydroxides,andotherclayminerals. Thenaturalsoilswerepoorinorganiccarbon,similarinchemicalcomposition,anddifferentinCEC.Sorptionexperimentswere conducted with hydrophobic, weakly basic and ionisable triazine herbicides (atratone,ametryn,andatrazine)andthreedealkylatededegradation products of atrazine. The enrichment of natural soils with hexadecyltrimethylammonium (HDTMA) bromide was more efficient in soil with higher CEC. The sorption capacities of the HDTMA-modifiedsoilsweregreaterformostcompoundsthanthecapacitiesof the acid-activated soils. The acid-activated or surfactant-modified forms of Terra Rossa soils could be applicable as components of an organophiliclayerinmulti-mineralbarriersforretentionoftriazines and similar chemicals (Stipicevic et al.,2014).

Acidactivationoftetralkylammonium(TMA$^+$)-smectitesproduced hybridcatalystsfortheisomerisationofα-pinenetocamphene.This catalyticactivitywasattributedtotheenhancedhydrophobicityofthe organo-smectites.Acid-activatedTMA$^+$-smectiteswerethemostactive catalystsandyielded60–90%conversionofα-pinene.Theyieldswere comparablewiththoseobtainedwithothersolidcatalystssuchaszeolitesandPILCs.Theiron-substitutedsmectitesweremoreactivethan the aluminium counterparts. The dodecyl trimethylammonium and octadecyl trimethylammonium smectites were generally less active (Breen et al., 1997a). SWy-2 Mt and SAz-1 Mt loaded with various amounts of the polycation magnafloc were reacted with 6 M HCl at 95°C.Thesesmectiteswereactivecatalystsfortheisomerisationofα-pinenetocampheneandlimonene.Theconversionbythepolycation-exchangedSAz-1Mtwaslargerthanbytheunloadedactivatedcounterpartbecausetheformermaterialwasmorehydrophobic.ForSWy-2Mt theyieldsintheabsenceandpresenceofpolycationsweresimilar,suggestinggooddispersionofbothsamplesintheunpolarα-pinene.The yields,basedontheinitialamountofα-pinene,forthemostactivecatalystswerebetween80and90%.Theseyieldsweredirectlycomparable with those obtained by using zeolites and PILC, although the acid- activatedpolycation-treatedclaymineralsweremarginallylessselective towards camphene (Breen and Watson, 1998). Catrinescu et al.(2013, 2015) reported in detail on the selective synthesis of α-terpinyl methyletherfromlimoneneandα-pinene.Acidsitesandtheirstrength playacrucialroleinthesecatalysts.Mildacidactivationwith1MHCl for 30 min and with reflux of the raw SAz-1 clay leads to a material withagoodcatalyticbehaviour,whileanyincreaseintheseverityof theacid-treatmentcausedamarkeddecreaseincatalyticactivity.The catalyst based on the high layer-charge SAz-1 montmorillonite was themostactive.Ion-exchangewithAl^{3+},followedbythermalactivation at150°C,affordedthehighestnumberofBrønstedacidsites-asignificantproportionofwhichwerelocatedintheclaygallery-andthiscoincidedwiththemaximumcatalyticactivity,whileanyincreaseinthe severity of the acid-treatment caused a marked decrease in catalytic properties.

TheSTx-1andSWy-2Mtwereactivatedwithdifferentamountsof 12MHClandthenexchangedwithafixedamountof1MTMA$^+$chloridesolutionatRT,givingrisetoH$^+$/TMA$^+$montmorillonites.Inaddition,TMA$^+$/H$^+$sampleswereobtainedbyacidactivationofTMA$^+$-exchangedMt.Theaciditywasdeterminedbyadsorption ofcyclohexyl- amine and the catalytic activity by the isomerization of 1-butene at 300 °C to yield cis- and trans-2-butene. The total conversion for the isomerizationof1-butenewas higherfortheTMA$^+$/H$^+$-samplesthan fortheH$^+$/TMA$^+$-catalysts.TMA$^+$cationsadsorbedontheclaymineralswereextremelyresistanttoexchangebyprotons,but protons wereeasilydisplacedbyTMA$^+$cations(Morontaetal.,2002).BreenandMoronta(1999)investigatedtheeffectoflayerchargeofmontmo- rillonitesSWy-2,STx-1,SAz-1andsaponiteSap-Catreatedwithdiffer- ent amounts of 12 M HCl and 1 M tetramethylammonium chloride solution at room temperature. The catalytic activity of these hybrid acid-activatedorganoclays(AAOC)wasmeasuredusingtheisomeriza- tion of α-pinene at 120 °C for 1 h to yield camphene, limonene, and otherminorproductsandcomparedtoacid-treatedclaysintheabsence ofTMA$^+$cations.Thetotalconversionfortheisomerizationofα-pinene wasexcellentforAAOCformedfromSWy-2(88%)andSTx-1(73%), moderateforSap-Ca(50%),andlowforSAz-1(20%).Samplestreated withTMA$^+$alonehadnomarkedcatalyticactivity.Acid-treatedSap-CaandSTx-1,whichcontainednoTMA$^+$cations,werealsoeffectivecatalysts.TMA$^+$cationswereunexpectedlyresistanttoexchangebypro- tons. Breen and Moronta (2000)used the same three montmorillonitesandasaponiteastheydidintheirpaperBreenandMoronta (1999). Here they were activated with different amounts of Al^{3+}andtetramethylammoniumTMA$^+$cationstoobtain materials withacombinedAl^{3+}andTMA^{+}contentequaltotheirCECs.Thecata- lytic activity was evaluated by reacting α-pinene at 120 °C for 1 h to yieldcamphene,limonene,andotherminorproductsandcompared toclayspreparedwithoutTMA^{+}.ThetotalconversionoverSap-Ca, STx-1,SWy-2,andSAz-1was90%,80%,65%,and25%,respectively,in samples treated with Al^{3+}alone. Similar yields were obtained over theAl^{3+}/TMA^{+}-exchangedformswhentheTMA^{+}contentwasb20% CEC,butthepresenceofTMA^{+}significantlyreducedthetotalconver- sion.TheactivityoftheAl^{3+}-exchangedclaysforthetestreactionwas attributed to their ability to remain expanded at the temperature of theactivationprocess,thuspermittingeasyaccessofthereagent.SAz-1montmorilloniteshowedthelowestcatalyticactivity,forwhichtwo differentreasonscouldbegiven.Firstly,thehighMgcontentintheminerallayersgaveitthelowestlayerstabilityduringactivationbyHCl.Sec- ondly, its high layer charge of SAz-1 caused cations to attach to the layers,restrictingaccessofthereagentstotheactivecentresinthein- terlayer galleries.

The effect of short alkyl chain cations on the modification of the structural, surface and textural properties of organo-montmorillonites uponacidtreatmentwasinvestigatedbyPálkováetal.(2011).Samples preparedfromCa-SAzmontmorilloniteandtetramethylammonium (Me_4N^+-),tetraethylammonium(Et_4N^+-).tetrapropylammonium (Pr_4N^+-)andtetrabutylammonium(Bu_4N^+-)saltsweretreatedin 6MHClat80°Cfor2–8handanalyzedbydifferentmethods.Acidtreat-mentoforgano-montmorillonitescausedgradualreleaseofAlandMg fromtheoctahedralsheetsanddestructionoftheirlayeredstructure. The extent of the changes depended significantly on the size of the organocation.Whilethelargeplate-likeparticlesofCa-SAzandMe_4N- SAz were disintegrated during acid treatment, creating smaller fine grains,themorphologyofBu_4N-SAzwasmodifiedonlyslightly.Pore size analysis showed generation of a pore network upon organo-montmorillonitedissolution.Withlongeracidattack,porevolumein- creased and the pore size distribution curves were shifted, showing poreswithdiameterN2.5nm.Thesurfaceareaofacid-treatedsamples increasedduetodestructionofthemontmorillonitelayers andforma- tion of the SiO_2-rich reaction product. A maximum value 475 m^2/g wasobservedforMe_4N-SAzafter4hoftreatment.Thesurfaceareas ofEt_4N-SAz,Pr_4-SAzandBu_4N-SAzwere441,419and293m^2/g,respec-tively,after8htreatments.Asimilardecompositionlevel wasobserved forCa-SAzandMe_4N-SAz,withlesslayerdestructionfoundforEt_4N- SAz,Pr_4-SAzandverylittleforBu_4N-SAz.ThoughBu_4N^+isashort-chainalkylcation,itssizeislargeenoughtocovertheinner andouter surfaces of montmorillonite and thus to protect the clay layers from acidattack.

Madejováetal.(2012)investigatedtheeffectofsurfactant sizeon the extent of montmorillonite decomposition in HCl. Na-SAz montmo- rillonite and tetraalkylammonium salts of varying alkyl chain(from methyl,Me_4N,topenthyl,Pe_4N)wereusedforpreparation oforgano-montmorillonites.Decreasingintensityofthed$_{001}$diffractionindicated thedestructionofmontmorillonitestructureduetogradualsurfactant release.AshiftoftheSiOstretchingbandto1097cm^{-1}confirmedthe formationofanamorphoussilicaphase.Anewbandnear7315cm^{-1}correspondingtotheSiOHovertoneindicatedthepresenceofprotonat-edsilica.Thisbandwasobservedinthespectraofallacid-treatedsam-ples,includinginthosewithminordecompositionofthelayers.Thesize ofthecationssignificantlyaffectedthedecompositionof montmorillon- itesintheacid.TheleaststablewereNa-SAzandMe_4N-SAz,inwhich the octahedral atom content dropped to around 5% of their original values upon 8 h treatments. Et_4N-SAz and Pr_4N-SAz were slightly more resistant at short treatment times. Bu_4N-SAz and Pe_4N-SAz showedtheleaststructuralmodifications,asonly50%and 35%ofocta-hedralatoms,respectively,werereleasedintosolutionover8hoftreat-ment.Thisobservationprovedthatthebulkyalkylammoniumcations obstructingtheinnerandoutersurfacesofmontmorilloniteareeffec-tiveatpreventingprotonaccesstothelayers,protectingthe mineral from degradation by theacid.

Pálkováetal.(2013)examinedtheeffectoftetrabutylammonium (Bu_4N^+)andtetrapenthylammonium(Pe_4N^+)cationsonthemodifica- tion of the organo-montmorillonite structure upon acid treatment. SampleswerereactedwithHClfor2–12h.Theprincipaltoolforfollow-ingstructuralchangeswasMAS-NMRspectroscopy.The^{29}SiMAS-NMR spectraoftheinitialNa-saturatedform(Na-SAz)showedagradualde-creaseoftheintensityoftheresonanceassignedtoSiO_4cross-linkedin thetetrahedralsheetsQ^3(0Al),whilesignalsarisingfromthereaction products Q^{3}1OH and Q^4(0Al) became more pronounced upon acid treatment.TheQ^3(0Al)signalalmostcompletelydisappe aredforNa- SAztreatedfor8h,unlikeBu$_4$N-SAzandPe$_4$N-SAz,whichdisplayeda signalofrelativelyhighintensityevenafter12hofreaction .The^{27}Al MAS-NMR measurement showed that more than one half of the Al remainedinthereactionproductofBu$_4$N-SAzandPe$_4$N-SAzafter8h treatments,whileAlcontentdroppedbelow5%forNa-SAz.Theformationofacidsiteswasinvestigatedviapyridineadsorption. Onlyphysically adsorbed and H-bonded pyridine was detected for acid-untreatedsamples.Incontrast,theIRspectraofthesamplespartially decomposedinHClrevealedbandsofpyridineadsorbedonBrønsted acid sites. The pyridine was strongly bonded and did not desorb even on heating to 230 °C.

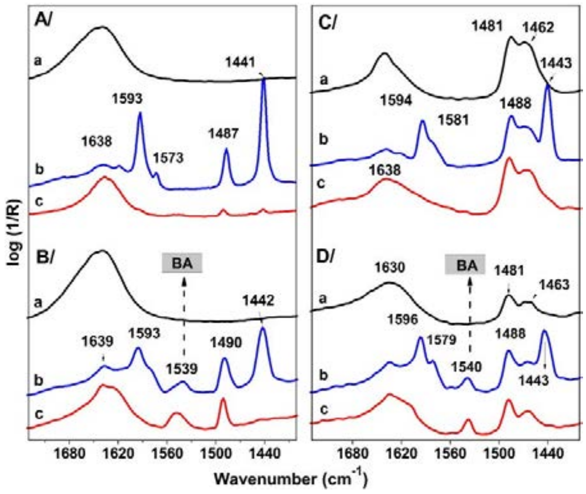

Fig.1.ThisfigureisbasedonthedataprovidedbyPálkováetal.(2013) andMadejováetal.(2015). MIR DRIFT spectra of acid treated and not acid treated Na–SAz and Bu$_4$N–SAz beforeandafterpyridineadsorption;moredetailsareinthefigure.A/Na-SAznotacid treated, B/ Na-SAz-2h, acid treated for two hours, C/ Bu$_4$N-SAz not acid treated, D/ Bu$_4$N-SAz-12h acid treated for 12 h, a - prior to pyridine adsorption, b - after pyridine adsorption,c-afterpyridineadsorptionandsubsequentheatingat230°C.

TheeffectofHCltreatmentincreationofacidsitesinMtwasinvestigated by NIR spectroscopy using pyridine as a probe molecule (Madejová et al., 2015). The Na-form of SAz-1 Mt was treated in 6M HCl for 2–8 h at 80 °C. A gradual decrease of the intensities of the bandsrelatedtostructuralOHgroupsinboththeMIRandNIRspectra reflectedthereleaseoftheoctahedralatomsfromNa-SAzuponproton attack. A new band near 7315 cm^{-1}due to the SiOH overtone confirmed the formation of protonated silica. After exposure of the Na-SAz to pyridine vapours the intensity of the $(\nu + \delta)_{H_2O}$combination banddiminished,indicatingthepartialreplacementofwatermolecules by pyridine. More details appear in (Madejová et al.,2015).

Fig. 1 is based on the data provided by Pálková et al. (2013) and Madejová et al. (2015) from their investigation of the spectra in the 1700–1400 cm^{-1}region after pyridine adsorption. The acid sites in untreated and acid-treated Na-SAz and Bu$_4$N-SAz were analyzed. The spectrum of Na-SAz-py contained well-resolved bands at 1593, 1573, 1487 and 1441 cm^{-1} (Fig. 1A, spectrum b). The most intense bands at 1441 and 1593 cm^{-1} corresponded to the hydrogen-bonded pyridine, and the band near 1487 cm^{-1}indicated the presence of weak BA sites. The vibration at 1573 cm^{-1} has been attributed to the physisorbed pyridine(Yariv,2002).TheIRspectrumofSAz-2h-py(Fig.1B,spectrum b)showedadecreaseoftheintensitiesofthebandsrelatedtoH-bondedandphysisorbedpyridinecomparedtoNa-SAz-py.Inaddition,thewell-resolvedbandat1539cm^{-1}wasassignedtotheN$^+$–Hdeformationvibrationofthepyridiniumcation(Yariv,2002).ThepyridinemoleculesacceptedprotonsfromH$_3$O$^+$,presentinthesampleafterHCltreatment, thusconfirmingtheexistenceofstrongBAsitesontheSAz-2hsurface.Though the reaction product contained also silanolgroupstheiraciditywasnotstrongenoughtoprotonatepyridine.Instead,itisbelievedthatthesilanolOHgroupsweremerelyH-bondedtopyridine.Afterheatingthesampleat230°C(Fig. 1)noabsorptionbandsofpyridinecouldbeobservedinthespectrum.TheexchangeofNa$^+$withBu$_4$N$^+$cationsmodifiedtheshapeoftheIRspectrumintheregion wheretheringvibrationsofpyridineoccurred(Pálkováetal.,2013).Inadditiontothebroadwaterbandnear1630cm^{-1},bandsrelatedtodeformation (δ) vibrations of CH$_3$ (1481 cm^{-1}) and CH$_2$(1462cm^{-1})groupswerealsoobservedforBu$_4$N–SAz(Madejováetal.,2012).Afterpyridineadsorption,bandsrelatedtotheringvibrationsofpyridineappearedinthespectrum.Thebandsat1594and1443cm^{-1}wereduetoH-bonded pyridine. A broad shoulder in the 1580–1570cm^{-1}regionarosefromphysisorptionofpyridineontoseveraldifferentactivesitesonBu$_4$N–SAz,thesamplewiththemorehydrophobicsurfacecomparedtoNa–SAz.Theidentificationofthebandnear1487cm^{-1}asrelatedtoweakBAsiteswasdifficulttomakeduetothestrongδ_{CH_3}band.Theforces holding the pyridine on the surface of Bu$_4$N–SAz wererather weak, as shown by the spectra after thermal treatment.

Acid treatment changes the IR pattern in the 1650–1400 cm^{-1} region(Fig.1).TheIRspectraofBu$_4$N–SAz–12hafterpyridineadsorption showedthebandspreviouslyassignedtoskeletalvibrationsofpyridine partiallyoverlappingthebandscorrespondingtodeformationCH$_3$and CH$_2$ vibrations. The well-developed band at 1581 cm^{-1}belongs to physisorbed pyridine, while the bands at 1594 and 1443 cm^{-1}are due to pyridine hydrogen-bonded to the residual water molecules and/or to the SiOH groups of the reaction product. The band at 1539cm^{-1}unambiguouslyconfirmstheformationofthepyridinium cation.StrongBAsitesariseathydratedH^{+}-donorsitesonthemineral surface, as well as from metal cations released from the octahedral sheetsofmontmorilloniteuponacidtreatmentandentrappedonthe surfaceoftheparticlesofthepartlydecomposedsample.Thechanges tothepyridinebandsuponheatingBu$_4$N–SAzfor8hweresimilarto thosefoundfor2hheatingofNa–SAz,with^{29}SiMASNMRshowing thesameextentofdecompositioninbothcases(~55%).TheIRspectrumofBu$_4$N–SAz–8hheatedto110°Cshoweddisappearanceofthe 1581cm^{-1}bandduetodesorptionofphysisorbedpyridine anda decrease of the intensities of the 1594 and 1443 cm^{-1}bands resultingfromaslightdecreaseintheamountofH-bondedpyridine. In addition, a new shoulder can be seen near 1610 cm^{-1}due to the shrinking of the 1596 cm^{-1}band. This band is even better resolved after the release of H-bonded pyridine upon heating to 170 °C. Be- cause the 1610 cm^{-1}band remains in the spectrum even after heating to 230 C, and because of the diagnostic band of strong BA sites at 1539 cm^{-1}, the absorption at 1610 cm^{-1}can be attributed to the ring vibration of pyridiniumcation.

Although upon 12 h acid treatment of Bu$_4$N–SAz the amount of decomposedmontmorillonitelayersincreased(Fig.1B),thechanges observed in the spectra of pyridine-treated samples were almostthe sameasfoundforBu$_4$N–SAz–8h.ItfollowsthattheBrønstedacidity ofthesamplewithb40%ofmontmorilloniteishighenoughtoproton- ate pyridine, which is strongly physisorbed onto the sample evenat 230°C.

Zimowskaetal.(2013)discussedthepreparationandpropertiesof Al-containing porous clay heterostructures (PCH). These were synthe- sised from laponite by post-synthesis alumination usingaluminium isopropoxideandaluminiumnitrateasAlsources(Si/Al= 30and10). Thesolidswerecharacterizedby^{27}Aland^{29}SiMAS-NMR,FTIR,nitrogen adsorption/desorption at −196 °C, NH$_3$-TPD-MS, pyridine adsorption monitoredbyFTIR,andcatalyticdecompositionofethanol.

Alumination resulted in substitution of Al for Si in the mesoporous silica component of PCH and in formation of extra-lattice Al species. A more uniform distribution of Al sites was obtained with the use of alu- minium nitrate. Alumination caused a decrease in the textural parame- ters, which was more pronounced upon impregnation with Al-isopropoxide. The parent PCH-L possessed little capacity for sorption of basic molecules. Alumination enhanced the sample acidity. Pyridine adsorption showed that the acidity, especially at elevated temperatures, was primarily determined by the presence of Lewis acid sites. Brønsted acid centres were less abundant and rather weak.

Clay–polymer nanocomposites are heterogeneous materials in whichatleastoneofthecomponentdomains,thereinforcingphase, hasadimensionontheorderofnanometres.Thesematerialsareattractivebecausetheirpropertiescanbesignificantlydifferentfromthoseof theindividualcomponents,withtheresultantcomposites sometimes displayingsynergisticproperties,e.g.CarradoandBergaya(2007)and Carrado and Komadel(2009).

Zha et al. (2014) showed that strong interfacial interaction and nanodispersion were necessary for polymer nanocomposites to have good mechanical performance. Mt was first structurally modi- fied by acid treatment to produce more silanol groups on the layer surface.Thiswasfollowedbychemicalmodificationbycovalently grafting the gamma-methacryloxy propyl trimethoxysilanemole- cule on the silanol groups. ^{29}Si and ^{27}Al MAS-NMR resultsrevealed microstructural changes in Mt after acid treatment andconfirmed the proliferation of silanol groups on acid-treated Mt surfaces. Thermogravimetric analysis indicated an increase in the grafted amount of organosilane on the Mt surface. XRD showed that the functionalization process changed the highly-ordered stacking structureoftheMtintoahighlydisorderedstructure,indicatingsuc- cessful grafting of organosilane to the interlayer surface of the sheets.Styrenebutadienerubber(SBR)/Mtnanocompositeswere further prepared by co-coagulating SBR latex and grafted-Mt aque- ous suspension. During vulcanization, a covalent interface between modified Mt and rubber was established through peroxide radical-initiatedreactions,andlayeraggregationwaspreventedeffectively. TheSBR/MtnanocompositeshadhighlyanduniformlydispersedMt layers, and covalent interfacial interaction wasachieved.

D'Amico et al. (2014) analysed different strategies for modification ofanArgentinianbentoniteofCEC=0.939meq/g,combiningthereac- tions of cationic exchange, silylation, and acid activation with H$_2$SO$_4$. XRD, TG, FTIR and water absorption tests were used to characterize the samples prepared. A combination of all three –acid-activation, silylationandcationicexchange–providedthebiggestbasalspacing, aswellaslowequilibriumwateruptake,makingtheresultingbentonite a promising material for clay-polymernanocomposites.

Lin et al. (2014)prepared bentonite-supported nanoscale zero-valentironforthepurposeofremovingacidvioletredBfromaqueous solution.Bentonitedecreasedtheaggregationoftheironnanoparticles andincreasedtheirreactivity,leadingtotheremovalofN95%ofacidvioletredBcomparedtoN75%removedbythenanoscalezero-valentiron in the absence ofsmectite.

Borah et al. (2014)described in situ generation of Cu^0- nanoparticles into the nanopores of modified montmorillonite and theircatalyticperformanceinthethree-componentcouplingreactions of aldehyde, amine and alkyne to synthesize propargylamines. The modificationofmontmorillonitewascarriedoutwithHCl undercontrolledconditionsinordertogeneratenanoporesintothematrix,and these pores acted as a “host” for the in situ generation of Cu^0- nanoparticles.

Rasouli et al. (2014)activated commercial K10 Mt with H_2SO_4, followed by modification with cetyltrimethylammonium bromide (CTAB).Theconditionsoftheactivationprocesswereoptimizedfor decolourizationefficiency,withthemostfavourableactivationparametersforMtfoundtobeacontacttimeof2.2hwith3.6MH_2SO_4at50°C. TheMt-K10thusobtainedwascharacterizedbyFTIR,XRD,SEM and TEM. FTIR analysis confirmed that acid activation andmodification causedtheintercalationofCTA$^+$cationsintotheMt-K10interlayers and an increase inSSA.

JeenpadiphatandTungasmita(2014)evaluatedtheperformanceof variousacid-activatedbentonitesascatalystsintheesterificationreactions of oleic acid with methanol and of a high acid content palm or *Jatropha* oil with methanol or ethanol. Na-bentonite was acid-activatedbyeitherH_2SO_4atvaryingconcentrationsfrom0.25to2.0M orby0.5MHNO_3.Thecharacterizationoftherawandacid-activated bentonites was then conducted by nitrogen adsorption, XRD, XRF, SEMandacid-basetitrationanalysis.The0.5MH_2SO_4acid-activated bentoniteexhibitedthebestcatalyticactivitywith100%methyloleate yield and 99% free fatty acid conversion in the esterification of pure oleicacidandoleicacidinpalmoilwithmethanol.Bothconversions were higher than that obtained by esterification via the commercial Amberlyst-15catalyst.

Various2:1typeclaymineralswereactivatedbyH_2SO_4treatment andtheirsolidaciditieswereevaluatedbyNH_3-TPD.Clayminerals withvariousdegreesofAlsubstitutioninthetetrahedralsheetswere usedasthestartingmaterials.Theseincludedmontmorillonite(ideally notetrahedralAl),saponite(lowtetrahedralAlcontent),vermiculite (intermediatetetrahedralAlcontent)andphlogopite(hightetrahedral Alcontent).Allofthesesamplesshowedincreasedsolidacidityafter selective leaching, the solid acidities varying in the order phlogopitebmontmorillonitebvermiculitebsaponite.TheNH_3-TPD spectra were deconvoluted into two peaks; the L-peak at b 200 °C corresponded to a weak acid site and the H-peak at N 250 °C correspondedtoastrongacidsite.ThetemperatureoftheH-peakwas lowestinphlogopite(252°C)andhighestinsaponite(305°C).Thegenerationofsolidacidityinthesesampleswasfoundtoberelatedtothe evolutionofnewtetrahedralAlsitesshowingaslightlydifferent^{27}Al MAS NMR chemical shift from the original tetrahedral Al NMR resonance.

VIII. ACID DISSOLUTION OF NON-SWELLING CLAY THINERALS

8.1 Aciddissolutionofnon-swellingclaymineralssuchasillites,ka- olinites or fibrous clay minerals (sepiolite and palygorskite) has been a widely studied method for improving their surface and cata- lytic properties (Cai et al., 2007; Lenarda et al., 2007; Steudel et al.,2009b; Bibi et al., 2011; Valášková et al., 2011; Worasith et al.,2011; Yanik et al.,2012). *Kaolinite group minerals*

The dissolution rates of natural kaolinites of different origins, of halloysite,andofilliticclaysinH_2SO_4andHClweredeterminedbymea- suring the release rate of aluminium. The dissolution rate of kaolinitein 0.5MH_2SO_4at25°Cwasapproximatelythreetimeshigher thaninHCl ofequivalentprotonconcentration.Thedissolutionin5M $H_2SO_4$was eight times faster when the solid phase was periodically separated fromtheacidsolution,washedbydistilledwateranddried. Thealuminiumreleaseratedecreasedastheamountofclay-sizemicasinkaolinitic claysincreased.Theratewasalsoaffectedbythecrystallinityoftheclay mineral(Hradiletal.,2002).Forlessorderedkaolinite,the dissolution processwasfaster,notonlyinHClbutalsoinKOHsolution (Pentrák et al.,2009).

Thesolubilityofkaoliniteinacidsvariedwiththenatureandcon- centrationoftheacid,theacid-to-kaoliniteratio,thetemperature,and thedurationoftreatment.Thereactionofnaturalkaolinrefluxedwith 1 M–10 M H_2SO_4 at 110 °C for 4 h followed by calcination at 500 °C for2hyieldedamorphoussilica.TheleachingofAl^{3+}cationsincreased withacidconcentration.Treatmentwith10MacidincreasedtheSi/Al ratiofrom0.65to8.09,theSSAfrom23to143m^2/g,andtheporevolumefrom0.36to1.18cm^3/g.Thesolidphasesthusobtainedshowed promise as adsorbents and catalyst supports (Panda et al.,2010).

Proton adsorption and desorption could be computed from potenti- ometric titration data over the range of pH 2–12 using surface complex- ation models. The pH for zero proton charge was close to 5.5. The positive charge that developed below pH 5.5 was due to proton adsorp- tion on aluminium sites of the octahedral sheet. The external hydroxyl groups of the octahedral sheet were the first to be protonated, while secondary protonation took place on either the inner hydroxyl groups or the edge aluminol groups. Above pH 5.5 the kaolinite surface underwent two successive deprotonations, the first at about pH 5.5 and the second at around pH 9 (Huertas et al., 1998). The dissolution mechanism of kaolinite was mainly determined by the aluminol surface sites (external and internal structural hydroxyl groups and aluminol groups at the particle edges) under both acidic and alkaline conditions (Huertas et al.,1999).

KaolinitedissolutionratesatpH2to4andtemperaturesof25,50 and70°Cwereobtainedusingstirredandnon-stirredflow-throughreactors.Theratesincreasedwithincreasingstirringspeedandthestirringeffectwasreversible.Theeffectofstirringspeedonthekaolinite dissolutionratewashigherat25°Cthanat50and70°CandatpH4 than at pH 2 and 3. Stirring induced the formation of fine particles. TheratioofreactivesurfaceareatoSSAincreased,andthedissolution rateofkaolinitewasenhanced.Anequilibriumbetweentheproduction anddissolutionofthefineparticlescouldexplainthereversibilityas wellasthetemperatureandthepHdependenceofthestirringeffect (Metz and Ganor,2001).

PyridineandNH$_3$adsorptionindicatedthatthestrongacidsiteson activated kaolinite were of the Lewis type (Tabak and Afsin, 2001). Acidactivationincreasedtheamountofprotonatedspeciesonakaolin- itesurfaceattheexpenseofcoordinatively-boundNH$_3$.Thepresenceof NH$^+$cationsonanactivatedsampledidnotprovethepresenceofprotonicacidsitesonitsown,sincetheaddedprotoncouldhavecomefrom theresidualwaterintheinterlayerspace.Progressivedehydrationof thesurfaceresultedinastrongincreaseinchemisorbedNH$_3$.

Solidacid-activatedmetakaoliniteshaveshownpromiseasadsorbentsandcatalystsupports.Metakaoliniteswerepreparedbycalcina- tion of kaolinites at 600–900 °C and were more reactive than the parentkaoliniteafteracidactivationwith6MHClat90°C. 6hofreactionwithacidremovedmostoftheoctahedralAl^{3+}cationsandyielded anamorphoussilicaphasewithhighSSA.Acidtreatmentfor24halso removedtheoctahedralcations,butledtotheformationofamorphous silicawithamuchlowerSSA.Metakaolinitepreparedbycalcinationat 900°Chadalowerreactivitythanthematerialsobtainedatlowertem- peratures (Belver et al.,2002).

Theactivatedmetakaoliniteswereactivecatalystsforthealkylation of benzene with benzyl chloride, giving N 75% conversion of the alkylatingagent.Metakaoliniteactivatedwith4MHNO$_3$ achieved87% conversionofbenzylchloridetodiphenylmethanewith100%selectivity within30minofreactiontime.Thismightbetheresultofthegreater surfaceacidityofthissample.Extremelyefficientsolidcatalystswithre- markable acidic properties could be produced by the activation of metakaolinitewithH$_2$SO$_4$,HNO$_3$andHClO$_4$(Sabuetal.,1999).

Aungetal.(2015)investigatedtheeffectofacidactivationofkaolin intermsofaluminalosses,surfaceareachanges,andoilbleachingperformance.Groundkaolinwastreatedwithhydrochloricorcitricacid andbleachingtestswereperformedonricebranoil.Adsorptionstudies showedthattheoptimalbleachingachievablewas~83and~81%foractivationwith0.5Mhydrochloricorcitricacid,respectively,whereas bleaching with a commercial clay was ~ 82%. The highest bleaching valuewasnotassociatedwiththemaximumclaysurfaceareaorporos- ity–theformationofhighlyamorphoussilicawasactuallyfavourable fortheadsorptionofanionicpigments,suchaschlorophyll-*a*.

Aung et al. (2014) focused on the effects of thermal treatment be- tween 80 and 700 °C of kaolins from Thailand and chemical activation with 0.3–2 M H$_2$SO$_4$, regarding the ability to remove the undesirable colour of rice bran oil. The mineralogical, physical and physicochemical properties of the initial and activated kaolins were discussed in relation to the bleaching effectiveness of the activated sample. Generally, the greater the temperature used before the activation step and the greater theconcentrationofsulfuricacidusedduringactivation,thegreaterwas the structural degradation of the kaolinite. Al was removed from the oc- tahedral sheets of kaolinite and amorphous SiO_2dominated in the sam- ples. The measured maximum bleaching capacity was not necessarily obtained when using the activated kaolin of the highest specific surface area and pore volume; rather, the bleaching capacity was dependent on boththealuminacontentandtheproportion ofkaoliniteinthesamples. Partial preservation of the kaolinite structure was crucial for obtaining good bleaching capacity, as this meant the preservation of the aluminol sites likely to be involved in the adsorption of unsaturated molecules present in the rice bran oil. Partial leaching of Al from the octahedral sheets of kaolinite was also an important factor in obtaining good bleaching capacities.

Several physico-chemical methods, including XRD, ATR FTIR spectroscopy,andwavelengthdispersiveX-rayfluorescence,wereusedin thecomplexstudyofSzczepaniketal.(2015)tocharacterizetheprocessofchemicalmodificationofhalloysitefromthePolish stripmine Dunino.Halloysite,kaolinite,hematite,andcalcitewereidentifiedin therawsample.Bleachingthehalloysiteremovedorsignificantlyreducedthecontentofothermineralspresentintherawhalloysite.Mod- ification with 4-chloro-aniline caused progressive incorporation of amine into thesample.

Wang et al. (2014) systematically investigated the effects of acid- and heat-treatments on the physicochemical properties, structure and morphologyofhalloysiteusingXRD,FTIR,SEMandTEM.HCltreatment had no influence on the tubular mineral structure, but it became amor- phous after calcination at N500 °C. Ofloxacin (OFL) was adsorbed onto halloysite via electrostatic interaction between the protonated OFL and the negative halloysite surface. Acid-activation proved an effective way to improve mineral's rate of adsorption and release of cationic drug molecules.

Al Bakain et al. (2014) activated kaolin with 1.0 MH_2SO_4 at mini- mumliquid-to-solidratiousingmicrowaveheating.Theoptimumconditionsforactivationwereanl/Sratioof3.0mL1MH_2SO_4 pergram kaolin, microwave input power 500–600 W and heating time of 5–10min.ActivationatlowerL/Swasinefficient,indicatingthatthesol- vent played a role by absorbing microwaves more intensively and thus improving activation. Microwave-heated kaolin had better adsorptionoftartrazinedyeduetoimprovementsinthetexturalandchemical propertiesofthekaolinite.Fillingtheporesofkaolinbyacidsolutionin- creasedthemicrowaveabsorptionanddealuminationofkaolinite.

8.2 Sepiolite and palygorskite

Thefibrousclaymineralssepioliteandpalygorskitehavehadwide-rangingindustrialandmedicalapplications,particularlyasadsorbents, catalystsandcatalystsupports,becauseoftheirstructuralcharacteris- tics and physico-chemical properties. Heating and acid activation have often been used to enhance their properties (Valentín et al., 2007). Donmezetal.(2015)foundthattheadsorptivepropertiesofnaturalsepioliteintheremovalofCu^{2+}ionfromaqueoussolutionincreasedwith theinitialcopperconcentration,contacttime,andsolution pH.Adsorptionatdifferentoperatingconditionsfollowedapseudo-secondorder model. The equilibrium adsorption results were fitted better with a Langmuirisothermthanbyothermodels;theLangmuirmonolayeradsorptioncapacityofsepiolitewas9.64mg/gatpH6.0and20°C.Increasingthetemperatureassistedthesorptionprocess.Acidactivationof palygorskitefollowedbyinsituhydrothermaltreatmentwassuccess- fully utilized in zeolite A synthesis (Jianget al., 2012).

When sepiolite and palygorskite were activated by HCl, the octahe- dral sheets progressively dissolved. The content of silica increased, and that of octahedral cations decreased, with the acid strength. In both cases, fibrous free silica was obtained. Sepiolite decomposed more rap- idly than palygorskite because its octahedral sheets contained more $Mg^{2+}$and the structural microchannels were larger. The removal of the cations and disaggregation of the particles, as well as the increase in the micropore volume, caused enlargement of the SSA (Myriamet al., 1998). A substantial increase in the SSA was observed for HCl- treated palygorskite. The obtained free silica had the fibrous morpholo- gy of natural palygorskite but no microporosity was detected (SuárezBarrios et al.,1995).

LalhmunsiamaandLee(2015)reportedonacidactivationofsericite,amica-basednaturalclay.Itwasannealedat800°Cfor4hfollowedbyacidactivationwith3.0MHClat100°Ctoobtainactivatedsericite(AS).Theactivationofsericitecausedasignificantincreaseinthespecificsurfacearea.Further,SEMimagesoftheASshowedadisorderedandheterogeneoussurfacestructurewithmesoporesonitssurface,whereasthepristinesericitepossessedacompactlayeredstructure.ThematerialswerefurtheremployedintheremovalofSr(II)fromaqueoussolutionsinabatchreactorsystem.RemovalofSr(II)wasstudiedasafunctionofpH,concentrationofadsorbate,contacttime,backgroundelectrolyteconcentrationanddoseofads orbentusingpristinesericiteandAS.TheremovalofSr(II) wasenhancedbyincreasingthepHofthesolutionandtheextentofSr(II)removalwasincreasedbyincreasingthesorbateconcentration.ThisstudysuggestedthatAScanbeproductivelyappliedtotheremovalofSr(II)fromtheaquaticenvironment.OndissolutionofsepiolitesamplesinHCl,theproductsoftreatmentwithmildacidwerenotinfluenced muchbythepresenceoffreesilica.However,theinfluence ofsilicabecameimportantwhensamplesweresubjectedtomoreintenseacidtreatment(Vicenteetal.,1995b).Astheamountofironandaluminiumextractedfromsepioliteincreased,theSSAofthemineralgrewfrom195to306m^2/gandtheoriginalmicroporous structure became mesoporous. TheCECofsepiolitewaseliminatedbyacidtreatment,whichhad theeffectofprogressivelytransformingthemineralstructureintoan amorphoussilica-alumina(Dékanyetal.,1999).TheSSAoftheoriginal sepioliteincreasedfrom148to263m^2/ganddecreasedafterwards.Approximately16%ofthetotalvolumewastakenupbymicropores.Acid activation restricted particle deformation during thermal treatment. Themicroporevolumeincreasedby20%andtheSSAreachedvalues N500 m^2/g for the acid-treated samples (Balci, 1999).

Naturalandacid-activatedsepiolitesandpalygorskiteshaveoften beenusedasadsorbentsfortheremovalofheavymetalsfromaqueous solutions(Chenetal.,2007,Wangetal.,2007).Frini-SrasraandSrasra(2008)studied the surface acidity of raw and acid-activated palygorskite using acid-base potentiometric titrations. The average numberofprotonsreactedpersurfacesitewerecalculated, showing thatthetreatmentincreasedtheclayacidityandmodifiedthesurface charge.Frini-SrasraandSrasra(2010)reportedapronouncedincreaseoftheSSAofHCl-treatedTunisianpalygorskiteduetodissolutionofoctahedralsheetsandthecreationofmesoporosity.Theacid-activated samplesshowedahigheradsorptioncapacityofCd^{2+}thanthenatural palygorskite.

IX. CONCLUSIONS

Acidactivationofclaysandclaymineralsremainsanattractivemod- ification for research and applications. These include the traditional bleaching and decolourization of vegetable and other oils by materials based on bentonites, but numerous other clays can be profitably modi- fied in this way, such as swelling vermiculites and various non-swelling minerals. The final reaction products contain amorphous, porous, pro- tonated and hydrated silica with a three-dimensional cross-linked structure.

ACKNOWLEDGEMENTS

ThefinancialsupportoftheSlovakGrantAgencyforScienceVEGA (grant no. 2/0132/13) and of the Slovak Research andDevelopment Agency(grantAPVV-0362-10)isgreatlyappreciated.Thispublication istheresultoftheprojectimplementation“Centreformaterials,layers, and systems for applications and chemical processes under extreme conditions–StageII,”supportedbytheResearchandDevelopmentOp-erationalProgrammefundedbytheERDF.L.Petraisacknowledgedfor preparationoftheGraphicalabstractandH.PálkováforprovidingFig.1, and J. Asher forproofreading.

REFERENCES

[1] Adams,J.M.,1987.Syntheticorganicchemistryusingpillared, cation-exchangedandacid-treated montmorillonite catalysts — a review. Appl. Clay Sci. 2,309–342.

[2] AlBakain,R.Z.,Al-Degs,Y.S.,Issa,A.A.,Jawad,S.A.,AbuSafieh,K.A.,2014.Activationofka-olin with minimum solvent consumption by microwave heating. Clay Miner. 49,667–681.

[3] Aung,L.L.,Tertre,E.,Worasith,N.,Suksabye,P.,Thiravetyan, P.,2014.Thecapacityofac-tivatedkaolinstoremovecolourpigmentsfromricebranoil:theeffectsofacidcon-centration and pre-heating prior to activation. Clay Miner. 49,513–526.

[4] Aung,L.L.,Tertre,E.,Suksabye,P.,Worasith,N.,Thiravetyan, P.,2015.Effectofaluminacontentandsurfaceareaofacid-activatedkaolinonbleachingofricebranoil.

[5] J. Am. Oil Chem. Soc. 92, 295–304.

[6] Babaki,H.,Salem,A.,Jafarizad,A.,2008.Kineticmodelfortheisothermalactivationofbentonite by sulfuric acid. Mater. Chem. Phys. 108,263–268.

[7] Balci,S.,1999.Effectofheatingandacidpre-treatmentonporesizedistributionofsepi-olite. Clay Miner. 34,647–655.

[8] Barshad, I., Foscolos, A.E., 1970. Factors affecting the rate of interchange reaction ofadsorbed H$^+$on the 2:1 clay minerals. Soil Sci. 110, 52–60.

[9] Belaidi, N., Bedrane, S., Choukchou-Braham, A., Bachir, B., 2015. Novel vanadium-chromium-bentonite green catalysts for cyclohexene epoxidation. Appl. Clay Sci.107,14–20.

[10] Belver,C.,BañaresMuñoz,M.A.,Vicente,M.A.,2002.Chemicalactivationofakaoliniteunder acid and alkaline conditions. Chem. Mater. 14,501–506.

[11] Bhattacharyya,K.G.,Sen,G.S.,Sarma,G.K.,2014.Interactionsofthedye,rhodamineBwithkaolinite and montmorillonite in water. Appl. Clay Sci. 99,7–17.

[12] Bhattacharyya,K.G.,Sen,G.S.,Sarma,G.K.,2015.Kinetics,equilibriumisothermsandther-modynamicsofadsorptionofCongoredontonaturalandacid-treatedkaoliniteandmontmorillonite. Desalin. Water Treat. 53,530–542.

[13] Bibi,I.,Singh,B.,Silvester,E.,2011.Dissolutionofilliteinsaline-acidicsolutionsat25°C.Geochim. Cosmochim. Acta 75,3237–3249.

[14] Bickmore,B.R.,Bosbach,D.,Hochella,M.F.,Charlet,L.,Rufe,E.,2001.Insituatomicforcemicroscopy study of hectorite and nontronite dissolution: implications forphyllosilicateedgesurfacestructuresanddissolutionmechanisms.Am.Mineral.86,411–423.

[15] Borah,B.J.,Borah,S.J.,Saikia,L.,Dutta,D.K.,2014.Efficientt

hree-componentcouplingre-actions catalyzed by Cu^0-nanoparticles stabilized on modified montmorillonite. Catal.Sci. Technol. 4,1047–1054.

[16] Bovey, J., Jones, W., 1995. Characterization of Al-pillared acid-activated clay catalysts.

[17] J. Mater. Chem. 5, 2027–2035.

[18] Bovey,J.,Kooli,F.,Jones,W.,1996.PreparationandcharacterizationofTi-pillaredacid-activated clay catalysts. Clay Miner. 31,501–506.

[19] Breen,C.,Moronta,A.,1999.Influenceoflayerchargeonthecatalyticactivityofmildlyacid-activatedtetramethylammonium-exchangedbentonites.J.Phys.Chem.B103,5675–5680.

[20] Breen, C., Moronta, A., 2000. Characterization and catalytic activity of aluminum-andaluminum/tetramethylammonium-exchangedbentonites.J.Phys.Chem.B104,2702–2708.

[21] Breen,C.,Watson,R.,1998.Acid-activatedorganoclays:preparation,characterisationandcatalyticactivityofpolycation-treatedbentonites.Appl.ClaySci.12,479–494.

[22] Breen,C.,Madejová,J.,Komadel,P.,1995a.Correlationofcatalyticactivitywithinfrared,Si-29MASNMRandaciditydataforHCl-treatedfinefractionsofmontmorillonites.Appl. Clay Sci. 10,219–230.

[23] Breen, C., Madejová, J., Komadel, P., 1995b. Characterization of moderately acid-treated,size-fractionated montmorillonites using IR and MAS NMR-spectroscopy andthermal-analysis. J. Mater. Chem. 5, 469–474.

[24] Breen,C.,Zahoor,F.D.,Madejová,J.,Komadel,P.,1997a.Characterizationandcatalyticac-tivityofacid-treated,size-fractionatedsmectites.J.Phys.Chem.B101,5324–5331.

[25] Breen, C., Watson, R., Madejová, J., Komadel, P., Klapyta, Z., 1997b. Acid-activatedorganoclays: preparation, characterization and catalytic activity of acid-treatedtetraalkylammonium-exchanged smectites. Langmuir 13, 6473–6479.

[26] Breen,C.,Last,P.M.,Taylor,S.,Komadel,P.,2000.Synergicchemicalanalysis-thecouplingofTGwithFTIR,MSandGC–MS2.CatalytictransformationofthegasesevolvedduringthethermaldecompositionofHDPEusingacid-activatedclays.Thermochim.Acta363,93–104.

[27] Brown,D.R.,1994.Review:claysascatalystandreagentsupports.Geol.Carpath.Ser.Clay45,45–56.

[28] Cai, Y.F., Xue, J.Y., Polya, D.A., 2007. A Fourier transform infrared spectroscopicstudyofMg-rich, Mg-poor and acid leached palygorskites. Spectrochim. Acta A66,282–288.Carrado,K.,Bergaya,F.,2007.Clay-basedpolymernanocomposites(CPN).CMSWorkshop

[29] Lectures 15. The Clay Minerals Society, Chantilly, VA, USA (278 pp.).

[30] Carrado,K.A.,Komadel,P.,2009.Acidactivationofbentonitesandpolymer-claynano-composites. Elem. 5,111–116.

[31] Catrinescu,C.,Fernandes,C.,Castilho,P.,Breen,C.,Carrott,M.M.L.R.,Cansado,I.P.P.,2013. Selective methoxylation of limonene over ion-exchanged and acid-activated clays.Appl. Catal. A Gen. 467,38–46.

[32] Catrinescu,C.,Fernandes,C.,Castilho,P.,Breen,C.,2015.Selectivemethoxylationofα-pinene to α-terpinyl methyl ether over Al^{3+}ion-exchanged clays. Appl. Catal. AGen. 489,171–179.

[33] Chen,H.,Zhao,Y.,Wang,A.,2007.RemovalofCu(II)fromaqueoussolutionbyadsorptiononto acid-activated palygorskite. J. Hazard. Mater. 149, 346–354.

[34] Chmielarz,L.,Wojciechowska,M.,Rutkowska,M.,Adamski, A.,Wegrzyn,A.,Kowalczyk, A., Dudek, B., Boron, P., Michalik, M., Matusiewicz, A., 2012. Acid-activated vermiculitesascatalystsoftheDeNO(x)process.Catal.Today191,25–31.

[35] Christidis,G.E.,Kosiari,S.,2003.Decolorizationofvegetableoils:astudyofthemecha-nismofadsorptionofβ-carotenebyanacid-activatedbentonitefromCyprus.ClayClay Miner. 51,327–333.

[36] Christidis,G.E.,Scott,P.W.,Dunham,A.C.,1997.Acidactivationandbleachingcapacityofbentonites from the islands of Milos and Chios, Aegean, Greece. Appl. Clay Sci. 12,329–347.

[37] Číčel, B., Komadel, P., 1994. Structural formulas of layer silicates. In: Amonette, J.E.,

[38] Zelazny,L.W.(Eds.),QuantitativeMethodsinSoilMineralogy.SoilScienceSocietyofAmericaMiscellaneousPublication, Madison,WI,pp.114–136(SoilScienceSocietyofAmerica).

[39] Číčel,B.,Komadel,P.,Nigrin,M.,1992.Catalyticactivityofsmectitesondimerizationof

[40] oleic-acid. Collect. Czechoslov. Chem. Commun. 57, 1666–1671.

[41] Cottet,L.,Almeida,C.A.P.,Naidek,N.,Viante,M.F.,Lopes,M.C.,Debacher,N.A.,2014.Ad-sorption characteristics of montmorillonite clay modified with iron oxide with respecttomethyleneblueinaqueousmedia.Appl.ClaySci.95,25–31.

[42] D'Amico,D.A.,Ollier,R.P.,Alvarez,V.A.,Schroeder,W.F.,Cyras,V.P.,2014.Modificationofbentonite by combination of reactions of acid-activation, silylation and ionic ex-change. Appl. Clay Sci. 99,254–260.

[43] delaCalle,C.,Suquet,H.,1988.Vermiculite.In:Bailey,S.W.(Ed.),HydrousPhyllosilicates(Exclusive of Micas)Reviews in Mineralogy 19. Mineralogical Society of America,Washington, DC, pp.455–496.

[44] Dékany, I., Turi, L., Fonseca, A., Nagy, J.B., 1999. The structure of acid treated sepiolites:small-angle X-ray scattering and multi MAS-NMR investigations. Appl. Clay Sci. 14,141–160.

[45] doNascimento,A.R.,Alves,J.A.B.L.,Melo,M.A.D.,Melo,D.M.D.,deSouza,M.J.D.,Pedrosa, A.M.G., 2015. Modification of bentonite by combination of reactions of acid-activation,silylationandionicexchange.Am.J.Mater.18,283–287.

[46] Donmez,M.,Camci,S.,Akbal,F.,Yagan,M.,2015.Adsorptionofcopperfromaqueoussolutionontonaturalsepiolite:equilibrium,kinetics,thermodynamics,andregenera-tion studies. Desalin. Water Treat. 54,2868–2882.

[47] Dubíková, M., Cambier, P., Šucha, V., Čaplovičová, M., 2002. Experimental soil acidifica-

[48] tion. Appl. Geochem. 17, 245–257.

[49] Faghihian, H., Mohammadi, M.H., 2014. Acid activation effect on the catalytic perfor-mance of Al-pillared bentonite in alkylation of benzene with olefins. Appl. Clay Sci.93-94, 1–7.

[50] Fahn,R.,Fenderl,K.,1983.Reactionproductsoforganicdyemoleculeswithacid-treatedmontmorillonite. Clay Miner. 18,447–458.

[51] Falaras, P., Kovanis, I., Lezou, F., Seiragakis, G., 1999. Clay Miner. 34, 221–232.Falaras,P.,Lezou,F.,Pomonis,P.,Ladavos,A.,2000a.Al-pillaredacid-activatedmontmoril-

[52] lonite modified electrodes. J. Electroanal. Chem. 486, 156–165.

[53] Falaras,P.,Lezou,F.,Seiragakis,G.,Petrakis,D.,2000b.Bleachingpropertiesofalumina-pillared acid-activated montmorillonite. Clay Clay Miner. 48,549–556.

[54] Flessner, U., Jones, D.J., Roziere, J., Zajac, J., Storaro, L., Lenarda, M., Pavan, M., Jimenez-Lopez,A., Rodriguez-Castellon, E., Trombetta, M., Busca, G., 2001. A study of the surface acidityofacid-treatedmontmorilloniteclaycatalysts.J.Mol.Catal.AChem.168,247–256.

[55] Frini-Srasra,N.,Srasra,E.,2008.Determinationofacid-basepropertiesofHClacidactivat-ed palygorskite by potentiometric titration. Surf. Eng. Appl. Electrochem. 44,401–409.

[56] Frini-Srasra,N.,Srasra,E.,2010.AcidtreatmentofsouthTunisianpalygorskite:removalofCd(II) from aqueous and phosphoric acid solutions. Desalination 250,26–34.

[57] Galán, E., Carretero, M.I., Fernandez-Caliani, J.C., 1999. Effects of acid mine drainage onclay minerals suspended in the Tinto River (Rio Tinto, Spain). An experimental approach. Clay Miner. 34, 99–108.

[58] Gates,W.P.,Anderson,J.S.,Raven,M.D.,Churchman,G.J.,2002.MineralogyofabentonitefromMiles,Queensland,Australiaandcharacterisationofitsacidactivationproducts.Appl. Clay Sci. 20,189–197.

[59] Harvey,C.C.,Lagaly,G.,2013.Industrialapplications.In:Bergaya,F.,Lagaly,G.(Eds.),De-velopments in Clay ScienceTechniques and Applications 5B. Handbook of Clay Sci-ence. Elsevier, Amsterdam, pp.453–490.

[60] Harvey,C.C.,Murray,H.H.,1997.Industrialclaysinthe21stcentury:aperspectiveofex-ploration, technology and utilization. Appl. Clay Sci. 11,285–310.

[61] Hashem,F.S.,Amin,M.S.,El-Gamal,S.M.A.,2015.Chemicalactivationofvermiculitetoproduce highly efficient material for $Pb^{2+}$and Cd^{2+}removal. Appl. Clay Sci. 115,189–200.

[62] He, H.P., Guo, J.G., Xie, X.D., Lin, H.F., Li, L.Y., 2002. A microstructural study of acid-activated montmorillonite from Choushan, China. Clay Miner. 37, 337–344.

[63] Hradil,D.,Hostomský,J.,Soukupová,J.,2002.Aluminiumreleaseratesfromacidifiedclaystructures: comparative kinetic study. Geol. Carpath. 53,117–121.

[64] Huertas,F.J.,Chou,L.,Wollast,R.,1998.Mechanismofkaolinitedissolutionatroomtemperatureandpressure:part1.Surfacespeciation.Geochim.Cosmochim.Acta62,417–431.Huertas,F.J.,Chou,L.,Wollast,R.,1999.Mechanismofkaolinitedissolutionatroomtem-perature and pressure part II: kinetic study. Geochim. Cosmochim. Acta63, 3261–3275.

[65] Hussin, F., Aroua, M.K., Daud, W.M.A.W., 2011. Textural characteristics, surface chemistryand activation of bleaching earth: a review. Chem. Eng. J. 170, 90–106.

[66] Janek,M.,Komadel,P.,1993.AutotransformationofH-smectitesinaqueoussolution.Ef-fect of octahedral iron content. Geol. Carpath. Ser. Clay 44,59–64.

[67] Janek,M.,Komadel,P.,1999.Acidityofprotonsaturatedandautotransformedsmectitescharacterized with proton affinity distribution. Geol. Carpath. 50,373–378.

[68] Janek,M.,Lagaly,G.,2001.Protonsaturationandrheologicalpropertiesofsmectitedis-persions. Appl. Clay Sci. 19,121–130.

[69] Janek,M.,Komadel,P.,Lagaly,G.,1997.Effectofautotransformationonthelayerchargeofsmectites determined by the alkylammonium method. Clay Miner. 32,623–632.

[70] Jankovič, Ľ., Komadel, P., 2000. Catalytic properties of a heated ammonium-saturated dioctahedral smectite. Collect. Czechoslov. Chem. Commun. 65, 1527–1536.

[71] Jankovič, Ľ., Komadel, P., 2003a. Metal cation-exchanged montmorillonite catalyzed pro-tection of aromatic aldehydes with Ac2O. J. Catal. 218, 227–233.

[72] Jankovič,Ľ.,Komadel,P.,2003b.Microwaveassistedsynthesisofsubstitutedindolesusing montmorillonite as catalyst. Solid State Phenom. 90–91, 481–486.

[73] Jeenpadiphat,S.,Tungasmita,D.N.,2014.Esterificationofoleicacidandhighacidcontentpalmoiloveranacid-activatedbentonitecatalyst.Appl.ClaySci.87,272–277.

[74] Jiang,J.L.,Feng,L.D.,Gu,X.,Qian,Y.H.,Gu,Y.X.,Duanmu,C.S.,2012.SynthesisofzeoliteAfrompalygorskiteviaacidactivation.Appl.ClaySci.55,108–113.

[75] Jin,L.,Dai,B.,2012.TiO_2activationusingacid-treatedvermiculiteasasupport:character-istics and photoreactivity. Appl. Surf. Sci. 258,3386–3392.

[76] Jovanović, N., Janaćković, J., 1991. Pore structure and adsorption properties of an acid-activated bentonite. Appl. Clay Sci. 6, 59–68.

[77] Jozefaciuk,G.,2002.Effectofacidandalkalitreatmentsonsurface-chargepropertiesofselected minerals. Clay Clay Miner. 50,647–656.

[78] Jozefaciuk,G.,Bowanko,G.,2002.Effectofacidandalkalitreatmentsonsurfaceareasandadsorption energies of selected minerals. Clay Clay Miner. 50,771–783.

[79] Kato,C.,Suzuki,T.,Fujiwaraa,T.,1966.Decompositionandstructuralchangeofclaymineralsbyacid.MemoriesoftheSchoolofScienceandEngineering,WasedaUniversity,pp.13–24.

[80] Kendall, T., 1996. Smectite clays. In: Kendall, T. (Ed.), Industrial Clays. Industrial MineralsInformation Ltd., London, pp. 1–12.

[81] Khalili,F.I.,Sultan,M.,Robl,C., Al-Ghouti,M.A.,2015.Insightsinto theremediationcharacterization of modified bentonite in minimizing organosulphur compounds fromdiesel fuel. J. Ind. Eng. Chem. 28,282–293.

[82] Klika, Z., Pustkoví, P., Dudova, M., Čapková, P., Kliková, C., Grygar, T.M., 2011. The adsorp-tion of methylene blue on montmorillonite from acid solutions. Clay Miner. 46,461–471.

[83] Komadel, P., 1999. Structure and chemical characteristics of modified clays. In: Misealides,P.,Macášek,F.,Pinnavaia,T.J.,Colella,C.(Eds.), NaturalMicroporousMaterialsinEn-vironmental Technology. Kluwer, The Netherlands, pp.3–18.

[84] Komadel, P., 2003. Chemically modified smectites. Clay Miner. 38, 127–138.

[85] Komadel,P.,Madejová,J.,2013.Acidactivationofclayminerals.In:Bergaya,F.,Lagaly,G.(Eds.), Handbook of Clay Science. Elsevier, Amsterdam, pp.385–409.

[86] Komadel, P., Schmidt, D., Madejová, J., Číčel, B., 1990. Alteration of smectites by treatments with hydrochloric acid and sodium carbonate solutions. Appl. Clay Sci. 5, 113–122.

[87] Komadel,P.,Stucki,J.W.,Číčel,B.,1993.ReadilyHCl-solubleironinthefinefractionsofsome Czech bentonites. Geol. Carpath. Ser. Clay 44,11–16.

[88] Komadel, P., Bujdák, J., Madejová, J., Šucha, V., Elsass, F., 1996a. Effect of non-swelling layers on the dissolution of reduced-charge montmorillonite in hydrochloric acid.Clay Miner. 31, 333–345.

[89] Komadel,P.,Madejová,J.,Janek,M.,Gates,W.P.,Kirkpatrick,R.J.,Stucki,J.W.,1996b.Dissolutionofhectoriteininorganicacids.ClayClayMiner.44,228–236.

[90] Komadel, P., Janek, M., Madejová, J., Weekes, A., Breen, C., 1997. Acidity and catalytic ac-tivity of mildly acid-treated Mg-rich montmorillonite and hectorite. J. Chem. Soc. Far-aday Trans. 93, 4207–4210.

[91] Kooli,F.,2015.Theeffectsofacidactivationonthethermalpropertiesofpolyvinylpyrrol- idone and organoclay composites. J. Chem. Art.#919636.

[92] Kooli,F.,Jones,W.,1997.Characterizationandcatalyticpropertiesofasaponiteclaymod-ified by acid activation. Clay Miner. 32,633–643.

[93] Kooli,F.,Jones,W.,1998.AlandZrpillaredacid-activatedsaponiteclays:characterizationand properties. J. Mater. Chem. 8,2119–2124.

[94] Kooli,F.,Yan,L.,2013.Chemicalandthermalpropertiesoforganoclaysderivedfromhigh-ly stable bentonite in sulfuric acid. Appl. Clay Sci. 83−84,349–356.

[95] Kooli,F.,Khimyak,Y.Z.,Alshahateet,S.F.,Chen,F.,2005.Effectoftheacidactivationlevelsofmontmorilloniteclayonthecetyltrimethylammoniumcationsadsorption.Lang-muir 21,8717–8723.

[96] Kooli,F.,Mianhui,L.,Alshahateet,S.F.,Chen,F.,Yinghuai,Z.,2006a.Characterizationandthermal stability properties of intercalated Na-magadiite withcetyltrimethylammonium(C16TMA)surfactants.J.Phys.Chem.Solids67,926–931.Kooli, F., Hian, P.C., Weirong, Q., Alshahateet, S.F., Chen, F., 2006b. Effect oftheacid-activated clays on the properties of porous clay heterostructures. J. Porous.Mater. 13, 319–324.

[97] Kooli,F.,Liu,Y.,Alshahateet,S.F.,Messali,M.,Bergaya,F.,2009.Reactionofacidactivatedmontmorillonites with hexadecyltrimethylammonium bromide solution. Appl. ClaySci. 43,357–363.

[98] Kooli,F.,Yan,L.,Al-Faze,R.,AlSuhaimi,A.,2015a.Removalenhancementofbasicblue41bybrickwastefromanaqueoussolution.Arab.J.Chem.

8,333–342.
[99] Kooli, F., Liu, Y., Al-Faze, R., Al Suhaimi, A., 2015b. Effect of acid activation of Saudi localclay mineral on removal properties of basic blue 41 from an aqueous solution.Appl. Clay Sci. 116,23–30.
[100] Korichi,S.,Elias,A.,Mefti,A.,Bensmaili,A.,2012.Theeffectofmicrowaveirradiationandconventional acid activation on the textural properties of smectite: comparativestudy. Appl. Clay Sci. 59–60,76–83.
[101] Kupková,J.,Honek,D.,Vallová,S.,Valášková,M.,2015.Characterizationoftwolowcharge vermilulites after hygrochloric acid treatment. Geodyn. Geomater. 12, 299–306.
[102] Lagaly, G., 1994. Layer charge determination by alkylammonium ions. In: Mermut, A.R.(Ed.),LayerChargeCharacteristicsof2:1SilicateClayMinerals.ClayMineralsSocietyWorkshop Lectures 6, Boulder, CO, USA, pp.1–46.
[103] Lalhmunsiama, T.D., Lee, S.M., 2015. Physico-chemical studies in the removal of Sr(II)from aqueous solutions using activated sericite. J. Environ. Radioact. 147, 78–84.
[104] Lambert,J.F.,Poncelet,G.,1997.Acidityinpillaredclays:originandcatalyticmanifesta-tions. Top. Catal. 4,43–56.
[105] Lenarda,M.,Storaro,L.,Talona,A.,Moretti,E.,Riello,P.,2007.Solidacidcatalystsfromclays: preparation of mesoporous catalysts by chemical activation of metakaolinunder acid conditions. J. Colloid Interface Sci. 311,537–543.
[106] Lin,Y.M.,Chen,Z.X.,Chen,Z.L.,Megharaj,M.,Naidu,R.,2014.Decolorationofacidvioletred B by bentonite-supported nanoscale zero-valent iron: reactivity, characterization,kinetics and reaction pathway. Appl. Clay Sci. 93-94,56–61.
[107] Linssen,T.,Cool,P.,Baroudi,M.,Cassiers,K.,Vansant,E.F.,Lebedev,O.,VanLanduyt,J., 2002.Leachednaturalsaponiteasthesilicatesourceinthesynthesisofaluminosili-cate hexagonal mesoporous materials. J. Phys. Chem. B 106,4470–4476.
[108] Luca,V.,MacLachlan,D.J.,1992.Siteoccupancyinnontronitestudiedbyaciddissolutionand Mossbauer-spectroscopy. Clay Clay Miner. 40,1–7.
[109] Madejová,J.,Bujdák,J.,Janek,M.,Komadel,P.,1998.ComparativeFT-IRstudyofstructuralmodifications during acid treatment of dioctahedral smectites and hectorite.Spectrochim. Acta A 54,1397–1406.
[110] Madejová, J., Andrejkovičová, S., Bujdák, J., Čeklovský, A., Hrachová, J., Valúchová, J.,
[111] Komadel, P., 2007. Characterization of products obtained by acid leaching of Fe-bentonite. Clay Miner. 42, 527–540.
[112] Madejová, J., Pentrák, M., Pálková, H., Komadel, P., 2009a. Near-infrared spectrosco-py: a powerful tool in studies of acid-treated clay minerals. Vib. Spectrosc. 49,211–218.
[113] Madejová,J.,Pálková,H.,Pentrák,M.,Komadel,P.,2009b.Near-infraredspectroscopicanalysis of acid-treated organo-clays. Clay Clay Miner. 57,392–403.
[114] Madejová, J., Pálková, H., Jankovič, Ľ., 2012. Degradation of surfactant-modified montmo- rillonites in HCl. Mater. Chem. Phys. 134, 768–776.
[115] Madejová,J.,Pálková,H.,Jankovič,Ľ.,2015.Near-infraredstudyoftheinteractionofpyr-idine with acid-treated montmorillonite. Vib. Spectrosc. 76, 22–30.
[116] Mahmoud,S.,Saleh,S.,1999.Effectofacidactivationonthede-tert-butylationactivityofsome Jordanian clays. Clay Clay Miner. 47,481–486.
[117] Malla,P.B.,Douglas,L.A.,1987.Identificationofexpandinglayersilicates:layerchargevs.expansionproperties.In:Schultze, L.G.,vanOlphen,H.,Mumpton,F.A.(Eds.),Pro-ceedingsoftheInternationalClayConference,Denver,1985.TheClayMineralsSoci-ety, Bloomington, IN, pp.277–283.
[118] Maqueda, C., Perez-Rodriguez, J.L., Šubrt, J., Murafa, N., 2009. Study of ground and un-ground leached vermiculite. Appl. Clay Sci. 44, 178–184.
[119] Metz, V., Ganor, J., 2001. Stirring effect on kaolinite dissolution rate. Geochim.Cosmochim. Acta 65, 3475–3490.
[120] Mokaya, R., Jones, W., 1994. Pillared acid-activated clay catalysts. J. Chem. Soc. Chem.Commun. 1994, 929–930.
[121] Mokaya,R.,Jones,W.,1995.Pillaredclaysandpillaredacid-activatedclay:acomparativestudy of physical, acidic and catalytic properties. J. Catal. 153,76–85.
[122] Mokaya,R.,Jones,W.,Davies,W.,Whittle,M.E.,1993.Preparationofalumina-pillaredacid-activated clays and their use as chlorophyll adsorbents. J. Mater. Chem. 3,381–387.
[123] Moronta, A., Ferrer, V., Quero, J., Arteaga, G., Choren, E., 2002. Influence of preparationmethod on the catalytic properties of acid-activated tetramethylammonium-exchanged clays. Appl. Catal. A Gen. 230, 127–135.
[124] Mudrinic, T., Mojovic, Z., Milutinovic-Nikolic, A., Mojovic, M., Zunic, M., Vukelic, N., Jovanovic, D., 2015. Electrochemical activity of iron in acid treated bentonite and in-fluence of added nickel. Appl. Surf. Sci. 353, 1037–1045.
[125] Murray,H.H.,1999.Appliedclaymineralogytodayandtomorrow.ClayMiner.34,39–49.
[126] Murray, H.H., 2000. Traditional and new applications for kaolin, smectite, andpalygorskite: a general overview. Appl. Clay Sci. 17, 207–221.
[127] Murray,H.H.,2007.Appliedclaymineralogy.Occurrences,processingandapplicationofkaolins, bentonites, palygorskite-sepiolite, and common clays. Developments inClay Science 2. Elsevier, B. V. (180pp.).
[128] Myriam,M.,Suarez,M.,Martin-Pozas,J.M.,1998.Structuralandtexturalmodificationsofpalygorskiteandsepioliteunderacidtreatment.ClayClayMiner.46,225–231.
[129] Novák, I., Čičel, B., 1978. Dissolution of smectites in hydrochloric acid: II. Dissolution rateas a function of crystallochemical composition. Clay Clay Miner. 26, 341–344.
[130] Odom,I.E.,1984.Smectiteclayminerals:propertiesanduses.Philos.Trans.R.Soc.Lond.A311,391–409.
[131] Osthaus, B.B., 1954. Chemical determination of tetrahedral ions in nontronite and mont-morillonite. Clay Clay Miner. 2, 404–417.
[132] Osthaus,B.B.,1956.Kineticstudiesonmontmorilloniteandnontronitebytheaciddisso-lution technique. Clay Clay Miner. 4,301–321.
[133] Pagano, T., Sergio, M., Glisenti, L., Diano, W., Grompone, M.A., 2001. Use of pillared mont-morillonites to eliminate chlorophyll from rice bran oil. Ing. Quím. 11–19.
[134] Pálková,H.,Madejová,J.,Righi,D.,2003.Aciddissolutionofreduced-chargeLi-andNi-montmorillonites. Clay Clay Miner. 51,133–142.
[135] Pálková, H., Jankovič, Ľ., Zimowska, M., Madejová, J., 2011. Alterations of the surface and morphology of tetraalkyl-ammonium modified montmorillonites upon acid treat-ment. J. Colloid Interface Sci. 363, 213–222.
[136] Pálková, H., Hronský, V., Jankovič, Ľ., Madejová, J., 2013. The effect of acid treatment on the structure and surface acidity oftetraalkylammonium-montmorillonites.
[137] J. Colloid Interface Sci. 395,166–175.
[138] Panda,A.K.,Mishraa,B.G.,Mishrac,D.K.,Singha,R.K.,2010. Effectofsulphuricacidtreat-ment on the physico-chemical characteristics of kaolin clay. Colloids Surf. APhysicochem. Eng. Asp. 363,98–104.
[139] Pentrák,M.,Madejová,J.,Komadel,P.,2009.Acidandalkalitreatmentofkaolins.ClayMiner. 44,507–519.
[140] Pentrák,M.,Madejová,J.,Komadel,P.,2010.Effectofchemicalcompositionandswellingon acid dissolution of 2:1 clay minerals. Philos. Mag. 90,2387–2397.
[141] Pentrák,M.,Czímerová,A.,Madejová,J.,Komadel,P.,2012.Changesinlayerchargeofclayminerals upon acid treatment as obtained from their interactions with methyleneblue. Appl. Clay Sci. 55,100–107.
[142] Perez-Maqueda, L.A., Maqueda, C., Perez-Rodriguez, J.L., Šubrt, J., Černý, Z., Balek, V., 2012.
[143] Thermalbehaviourofgroundandungroundacidleachedvermiculite.J.Therm.Anal.Calorim. 107,431–438.

[144] Perez-Rodriguez, J.L., Maqueda, C., Murafa, N., Šubrt, J., Balek, V., Pulišová, P., Lančok, A.,

[145] 2011. Study of ground and unground leached vermiculite II. Thermal behaviour ofground acid-treated vermiculite. Appl. Clay Sci. 51, 274–282.

[146] Petrović, S., Rožić, L., Vuković, Z., Novaković, T., Stanisavljev, D., 2012. Response surface optimization for activation of bentonite using microwave irradiation. Clay ClayMiner. 60, 32–39.

[147] Pichowicz, M., Mokaya, R., 2001. Porous clay heterostructures with enhanced acidityobtained from acid-activated clays. Chem. Commun. 2001, 2100–2101.

[148] Prieto, O., Vicente, M.A., Bañares Muñoz, M.A., 1999. Study of the porous solidsobtained by acid treatment of a high surface area saponite. J. Porous. Mater. 6,335–344.

[149] Ramesh,S.,Bhati,Y.S.,JaiPrakash,B.S.,2012.Microwave-activatedp-TSAdealuminatedmontmorillonite—a new material with improved catalytic activity. Clay Miner.47,231–242.

[150] Rasouli,F.,Aber,S.,Salari,D.,Khataee,A.R.,2014.Optimized removalofreactivenavyblueSP-BRbyorgano-montmorillonitebasedadsorbentsthroughcentralcompositede-sign. Appl. Clay Sci. 87,228–234.

[151] Rhodes, C.N., Brown, D.R., 1992. Structural characterization and optimization of acid-treatedmontmorilloniteandhigh-porositysilicasupportsfor$ZnCl_2$alkylationcata-lysts. J. Chem. Soc. Faraday Trans. 88,2269–2274.

[152] Rhodes,C.N.,Brown,D.R.,1994.Catalyticactivityofacid-treatedmontmorilloniteinpolarand nonpolar reaction media. Catal. Lett. 24,285–291.

[153] Rhodes,C.N.,Franks,M.,Parkes,G.M.B.,Brown,D.R.,1991. Theeffectofacidtreatmentonthe activity of clay supports for $ZnCl_2$alkylation catalysts. J. Chem. Soc. Chem.Commun. 12,804–807.

[154] Sabu, K.R., Sukumar, R., Rekha, R., Lalithambika, M., 1999. A comparative study on H_2SO_4,$HNO_3$and $HClO_4$treated metakaolinite of a natural kaolinite as Friedel-Crafts alkyl-ation catalyst. Catal. Today 49, 321–326.

[155] Sakizci, M., Erdoğan Alver, B., Yörükoğulları, E., 2011. SO_2adsorption on acid-treated ben-

[156] tonites from Turkey. Clay Miner. 46, 73–83.

[157] Salem, S., Salem, A., Babaei, A.A., 2015a. Application of Iranian nano-porous Ca-bentonitefor recovery of waste lubricant oil by distillation and adsorption techniques. J. Ind.Eng. Chem. 23, 154–162.

[158] Salem,S.,Salem,A.,Babaei,A.A.,2015b.Preparationandcharacterizationofnanoporousbentoniteforregenerationofsemi-treatedwasteengineoil:appliedaspectsforen-hanced recovery. Chem. Eng. J. 260,368–376.

[159] Santos,S.S.G.,Silva,H.R.M.,deSouza,A.G.,Alves,A.P.M.,daSilvaFilho,E.C.,Fonseca,M.G., 2015. Acid-leached mixed vermiculites obtained by treatment with nitric acid. Appl.Clay Sci. 104,286–294.

[160] Scarletti,N.V.Y.,Raven,M.,Madsen,I.,2011.PowderX-raydiffractionstudyofthehydra-tion and leaching behavior of nontronite. Clay Clay Miner. 59,560–567.

[161] Siddiqui, M.H.K., 1968. Bleaching Earths. Pergamon Press, London (86 pp.).

[162] Steudel,A.,Batenburg,L.H.,Fischer,H.R.,Weidler,P.G.,Emmerich,K.,2009a.Alterationofnon-swelling clay minerals and magadiite by acid activation. Appl. Clay Sci. 44,105–115.

[163] Steudel,A.,Batenburg,L.H.,Fischer,H.R.,Weidler,P.G.,Emmerich,K.,2009b.Alterationofswelling clay minerals by acid activation. Appl. Clay Sci. 44,95–104.

[164] Stipicevic, S., Sekovanic, L., Drevenkar, V., 2014. Ability of natural, acid-activated,andsurfactant-modifiedTerraRossasoilstosorbtriazineherbicidesandtheirdegrada-tion products. Appl. Clay Sci. 88-89,56–62.

[165] SuárezBarrios,M.,FloresGonzález,L.V.,Vicente,M.A.,MartínPozas,J.M.,1995.Acidacti-vation of a palygorskite with HCl: development of physico-chemical, textural andsurface properties. Appl. Clay Sci. 10,247–258.

[166] SuárezBarrios,M.,Buey,C.S.,GarciaRomero,E.,MartínPozas,J.M.,2001.Texturalandstructural modifications of saponite from Cerro del Aguila by acid treatment.ClayMiner. 36,483–488.

[167] Szczepanik,B.,Slomkiewicz,P.,Gamuszek,M.,Czech,K.,Banas,D.,Kubala-Kukus,A., Stabrawa,I.,2015.Theeffectofchemicalmodificationonthephysico-chemicalcharacteristicsofhalloysite:FTIR,XRF,andXRDstudies.J.Mol.Struct.1084,16–22.

[168] Tabak,A.,Afsin,B.,2001.Firmlyadsorbedammoniaandpyridinespeciesatactivatedka-olinite surfaces. Adsorpt. Sci. Technol. 19,673–679.

[169] Taxiarchou, M., Douni, I., 2014. The effect of oxalic acid activation on the bleaching prop-erties of a bentonite from Milos Island, Greece. Clay Miner. 49, 541–549.

[170] Temuujin,J.,Okada,K.,MacKenzie,K.J.D.,2003.Preparation ofporoussilicafromvermic-ulite by selective leaching. Appl. Clay Sci. 22,187–195.

[171] Tkáč,I.,Komadel,P.,Müller,D.,1994.Acid-treatedmontmorillonites-astudyby^{29}Siand27Al MAS NMR. Clay Miner. 29,11–19.

[172] Tomić,Z.,Logar,V.P.,Babic,B.M.,Rogan,J.R.,Makreski,P., 2011.Comparisonofstructural,textural and thermal characteristics of pure and acid treated bentonites fromAleksinac and Petrovac (Serbia). Spectrochim. Acta A 82,389–395.

[173] Tomić, Z., Ašanin, D., Antić-Mladenović, S., Poharc-Logar, V., Makreski, P., 2012. NIR and

[174] MIRspectroscopiccharacteristicsofhydrophilicandhydrophobicbentonitetreatedwith sulphuric acid. Vib. Spectrosc. 58,95–103.

[175] Tong,D.S.,Zheng,Y.M.,Yu,W.H.,Lin,M.W.,Chun,H.Z.,2014.Catalyticcrackingofrosinover acid-activated montmorillonite catalysts. Appl. Clay Sci. 100,123–128.

[176] Toor,M.,Jin,B.,Dai,S.,Vimonses,V.,2015.Activatingnatural bentoniteasacost-effectiveadsorbentforremovalofCongo-redinwastewater.J.Ind.Eng.Chem.21,653–661.

[177] Valášková,M.,Barabaszová,K.,Hundaková,M.,Ritz,M.,Plevová,E.,2011.Effectsofbrief

[178] millingandacidtreatmentontwoorderedanddisorderedkaolinitestructures.Appl.Clay Sci. 54,70–76.

[179] Valentín,J.L.,Lopéz-Manchado,M.A.,Rodríguez,A.,Posadas,P.,Ibarra,L.,2007. Novelan-hydrousunfoldedstructurebyheatingofacidpre-treatedsepiolite.Appl.ClaySci.36,245–255.

[180] VanRompaey,K.,VanRanst,E.,DeConinck,F.,Vindevogel, N.,2002.Dissolutioncharacteristicsofhectoriteininorganicacids.Appl.ClaySci.21,241–256.

[181] Varma,R.S.,2002.Clayandclay-supportedreagentsinorganicsynthesis.Tetrahedron58,1235–1255.

[182] Vicente,M.A.,SuárezBarrios,M.,López-González,J.D.,Bañares-Muňoz,M.A.,1994.Acid activation of a ferrous saponite (griffithite): physicochemical characterization andsurface area of the products obtained. Clay Clay Miner. 42, 724–730.

[183] Vicente, M.A., López González, J.D., Baňares Muňoz, M.A., 1995a. Preparation of micropo-rous solids by acid treatment of a saponite. Microporous Mater. 4, 251–264.

[184] Vicente, M.A., López González, J.D., Baňares-Muňoz, M.A., 1995b. Influence of the free sil-ica generated during acid activation of a sepiolite on adsorbent and textural proper-ties of the resulting solids. J. Mater. Chem. 5, 127–132.

[185] Vicente,M.A.,Suárez,M.,Baňares-Muňoz,M.A.,LópezGonzález,J.D.,1996a.ComparativeFTIR study of the removal of octahedral cations and structural modifications duringacidtreatmentofseveralsilicates.Spectrochim.ActaA52,1685–1694.

[186] Vicente, M.A., Suárez Barrios, M., López González, J.D., Baňares-Muňoz, M.A., 1996b. Char-acterization, surface area, and porosity analyses of the solids obtained by

acidleaching of a saponite. Langmuir 12, 566–572.
[187] Vilcocq,L.,Spinola,V.,Moniz,P.,Duarte,L.C.,Carvalheiro,F.,Fernandes,C.,Castilho,P., 2015.Acid-modifiedclaysasgreencatalystsforthehydrolysisofhemicellulosicoli-gosaccharides. Catal. Sci. Technol. 5, 4072–4080.
[188] Wallis,P.J.,Gates,W.P.,Patti,A.F.,Scott,J.L.,Teoh,R.,2007. Assessingandimprovingthecatalytic activity of K-10 montmorillonite. Green Chem. 9,980–986.
[189] Wang,W.,Chen,H.,Wang,A.,2007.Adsorptioncharacteristicsof Cd(II)fromaqueousso-lution onto activated palygorskite. Sep. Purif. Technol. 55,157–164.
[190] Wang,Q.,Zhang,J.P.,Zheng,Y.,Wang,A.Q.,2014.Adsorptionandreleaseofofloxacinfromacid-andheat-treatedhalloysite.ColloidsSurf.B:Biointerfaces113,51–58.
[191] Worasith,N.,Goodman,B.A.,Neampan,J.,Jeyachoke,N.,Thiravetyani,P.,2011.Character-izationofmodifiedkaolinfromtheRanongdepositThailandby XRD,XRF,SEM,FTIRand EPR techniques. Clay Miner. 46,539–559.
[192] Yanik, G., Cleylantekin, R., Tasci, E., Ozcay, U., 2012. The Sahin village (Kutahya, Turkey)clay deposit and its possible utilization. Clay Miner. 47, 1–10.
[193] Yariv, S., 2002. In: Yariv, S., Cross, H. (Eds.), Organo-Clay Complexes and Interactions.
[194] Marcel Dekker, Inc., New York, pp. 345–462.
[195] Zaghouane-Boudiaf,H.,Boutahala,M.,Sahnoun,S.,Tiat,C.,Gomri,F.,2014.Adsorptioncharacteristics,isotherm,kinetics,anddiffusion ofmodifiednaturalbentoniteforre-moving the 2,4,5-trichlorophenol. Appl. Clay Sci. 90,81–87.
[196] Zha,C.,Wang,W.C.,Lu,Y.L.,Zhang,L.Q.,2014.Constructingcovalentinterfaceinrubber/clay nanocomposite by combining structural modification and inter lamellarsilylationofmontmorillonite.ACSAppl.Mater.Interfaces6,18769–18779.
[197] Zhao,Y.H.,Wang,Y.J.,Hao,Q.Q.,Liu,Z.T.,Liu,Z.W.,2015a. Effectiveactivationofmontmo-rilloniteanditsapplicationforFischer-Tropschsynthesisoverrutheniumpromoted cobalt. Fuel Process. Technol. 136,87–95.
[198] Zhao,Y.X.,Qi,W.F.,Chen,G.Y.,Ji,M.,Zhang,Z.Y.,2015b.BehaviorofCr(VI)removalfromwastewater by adsorption onto HCl activated Akadama clay. J. Taiwan Inst. Chem.Eng. 50,190–197.
[199] Zimowska,M.,Pálková,H.,Madejová,J.,Dula,R.,Pamin,K., Olejniczak,Z.,Gil,B.,Serwicka, E.M., 2013. Laponite-derived porous clay heterostructures: III. The effect ofalumination. Microporous Mesoporous Mater. 175,67–75.
[200] Zysset, M., Schindler, W., 1996. The proton promoted dissolution kinetics of K-montmorillonite. Geochim. Cosmochim. Acta 60,921–931.

★★★

EXAMINATION OF SQUARE ESTABLISHMENTS LAYING ON SOIL ROCK AND ROCKEROCK MEDIA UNDER COUPLED VIBRATIONS

MANGALASHRITA PARIDA

Asst Prof., Department of Civil Engineering NMIET BBSR

Abstract -
In the current examination, the powerful reaction of square establishments of various comparable range to mass (Ro/m) proportions under coupled vibrations is researched for different homogeneous and layered frameworks. The recurrence subordinate solidness and damping of establishment laying on homogeneous soils and shakes are resolved utilizing the half-space hypothesis. The unique reaction attributes of establishment laying on the layered framework considering rockerock mix are assessed utilizing finite component program with sending limits. Frequencies versus adequacy reactions of square establishment are acquired for both translational and rotational movement. Another approach is proposed for assurance of dynamic reaction of square establishments laying on soil rock and endured rockerock framework as conditions and diagrams. The varieties of dimensionless characteristic recurrence and dimensionless full sufficiency with shear wave speed proportion are examined for various thicknesses of top soil/endured rock layer. The powerful practices of square establishments are likewise examined for various rockerock frameworks by thinking about sandstone, shale and limestone underlain by basalt. The varieties of firmness, damping and amplitudes of square establishments with recurrence are appeared in this investigation for different rockerock mixes. In the examination, two thunderous pinnacles are seen at two distinct frequencies for both translational and rotational movement. It is seen that the dimensionless thunderous amplitudes abatement and characteristic frequencies increment with increment in shear wave speed proportion. At long last, the parametric examination is performed for block establishments with measurements of 4 m × 3 m × 2 m and 8 m × 5 m × 2 m by utilizing summed up charts. The varieties of regular recurrence and pinnacle relocation adequacy are likewise read for various top layer thicknesses and unpredictable minutes.

I. INTRODUCTION

The geology of the Earth consists of all types of soils, rocks and minerals belonging to different geological periods. Due to its diversity in nature, geotechnical engineers and geologists are exposed to completely new set of problems. They encounter the problem related to nonhomogeneity because of the presence of discontinuities such as bedding planes of varying strength, fissures, joints and faults. Due to the presence of such geological structures, the studies related to the foundations constructed on such surfaces become most important. Normally, block foundations are required tosupportmachines,machinetoolsandheavyequipment onsuch nonhomogeneous surfaces. These types of machinefoundationsareprovided in heavy industries like nuclear powerplant,hydropowerplant,andpetrochemicalindustrytoensurethesatisfactoryoper-ationofthemachines,whichhaveawiderangeofoperating speeds, dynamic loads and operating conditions. Todesignthemachinefoundationsuccessfully,itiscrucialtocarryoutcareful engineering analysis to understand the responseof blockfounda-tiontothedynamicloads.Theblockfoundationsaresubjectedtoeitherstaticload,orcombinationofstaticanddynamicloadrepetitivelyoveralongperiodoftime.Thisloadleadstothegen-erationofdynamicforcessuchasbalancedandunbalancedforcesdue to the operation of rotating type or reciprocatingtypema-chinery.Inthecaseofthecoupledvibrations,horizontalandrocking motions are generated simultaneously under theactionofunbalanced horizontal dynamic forces of rotating typeofmachines.In the Indian scenario, most of the heavy constructionisinprogress on the Deccan trap rocks. These rocksaremostlycomposed of weathered basalt underlain by fresh basalt.Apart from this, the rocks which are slightly weathered at present may become weaker in future due to the environmental action. Many researchers (Xiao et al., 2014a, b, 2015; 2016; Xiao and Desai,2016) investigated the characteristics of the weathered rocks and granular soils related to their dilatancy, particle breakage and transitional behaviors. It is found that the density and pressure have great influences on the strength and stressestrain behaviorsofweatheredrocksandgranularsoils.Thesematerials exhibit strain hardening, postpeak strain softening, volumetric contraction, and expansion with a range of densities and pres- sures. Hence, the shear wave velocity, stiffness and damping values are significantly influenced by the state of the material, which varies from hard rocks to highly weathered rocks or granular soils. Therefore, the foundations for heavy machinery and structures on such type of ground conditions must be studiedthoroughlyforthefuturesafety.Ingeneral,theselayered combinations can be classified as (i) soilerock/weathered rockerock system and (ii) rockerock system. The dynamic analysis of block foundations resting on these layered systems is very complex.Fewstudiesareavailableintheliteratureregardingthe methodology of determination of the natural frequencies and resonant amplitudes of block foundation under coupled horizontal and rockingvibration.

Hence,inthepresentstudy,anattemptismadetoanalyzethe effect of various soilerock and rockerock foundation systems on dynamic response of block foundations of different mass and equivalent radii under coupled mode of vibrations. Thedynamic response characteristics of foundations are studied by using the theoriesproposedbyVeletsosandWei(1971)andKausel(1974)for homogenous and layered system, respectively. The variations of naturalfrequencyandresonantamplitudewithshearwave velocity are investigated for different top layer thicknesses. The dynamic behaviorsofblockfoundationsareanalyzedfordifferentrockerock systemsbyconsideringsandstone,shaleandlimestoneunderlain by basalt. The variations of stiffness, damping and amplitudesof foundation with frequency are shown in this study for various rockerock combinations. The variations of natural frequencyand peak displacement amplitude are also studied for different top layer thicknesses and eccentric moments. Finally, the parametric study is carried out to determine the natural frequency and resonant amplitude for block foundations with dimensionsof 4 m 3 m 2 m and 8 m 5 m 2 m using generalized relations proposed in thestudy.

II. THEORETICAL INVESTIGATION

The classical work on vibratory response of foundations was carried out by Lamb (1904). Subsequently, Reissner (1936) developed an analytical solution to periodic vertical displacement at the centerofthecircularloadedareawithelastichalf-spacemathematicalmodel.Arnoldetal.(1955)extendedtheelastichalf-space theorytoincludeothermodesofvibrationsusingrigidbase type contact stress distribution and weighted average displacement condition. Hsieh (1962) obtained the expressions for the frequency- dependent stiffness and geometrical damping in terms of displacement functions. Lysmer (1965)and Lysmer and Richart(1966)showed that vertical vibration of a rigid circular footing can be represented by a simplified analog consisting of a simple damped oscillator with physical parameter that gives good agreement with the response curve obtained from the elastic half-space theory. It is well established now that the dynamic response of foundations depends on several factors, i.e. size and shape of the foundation, depth of embedment, soil profile, soil properties, fre-quency of loading, and mode of vibration (Richart et al., 1970;Gazetas and Stokoe, 1991). The finite element approach has been usedtocalculatethestiffnessanddampingofembeddedfoundationsbyanumberofinvestigators(UrlichandKuhlemeyer,1973;Kausel and Ushijima, 1979). Beredugo and Novak (1972)and Novak and Sachs (1973)presented the stiffness and damping for thecoupledandtorsionalmodeofvibrationofembeddedfootings, and it was found that both the stiffness and damping values increaseduetotheembedmentoffooting.VeletsosandVerbiˇc(1973)andVeletsosandNair(1974)proposedstiffness anddampingparameters of embedded footing for different modes of vibrations. Furthermore, Warburton (1957), Hadjian and Luco(1977)and Kagawa and Kraft (1981)studied the dynamic response of foundations considering the heterogeneities of thesoil.

The dynamic impedance of block foundation resting on homogenousdepositconsideredashalf-spaceisevaluatedusingthe theory proposed by Veletsos and Wei (1971). Furthermore, the theory proposed by Kausel(1974)is used for the layered system analysisinwhichtoplayeristreatedasstratumandbottomlayeris consideredashalf-space.Dynamicresponsesofblockfoundationin soilerock and rockerock system under vertical vibrations were studied by Kumar et al. (2013)and the natural frequency and amplitudewerecorrelatedwithshearwavevelocityratio. Dimensionlessgraphsandvariousequationswereproposedtodetermine the stiffness and damping of block foundation under vertical vibrations in soilerock/rockerock system. However, there are no similarstudiesmadetoinvestigatethedynamicresponseofblock foundation in soilerock and rockerock system under coupled vibrations (horizontal and rockingmotion).

2.1 Homogenous medium

In the present study, an approximate solution proposed by Veletsos and Wei (1971) is used to study the steady-state response of rigid circular disk of infinitesimal thickness supported at the surface of a non-dissipative, homogeneous, linear elastic half-space. The weight of the disk is assumed to be negligible. The exciting forces considered include a harmonically varying lateral force directed along the *x*-axis, and harmonically varying moment acting about the*y*-axis. The following assumptions are proposed:

(i) the normal component of the contact pressure is assumed to be zero due to horizontal force, and (ii) the horizontal or shearing components of the interface pressure are assumed to be zero due to overturning moment. Thus, it permits the horizontal translational motion of the disk to be evaluated independently. The surrounding region of disk is assumed to be stress free.

In order to compute the coupled displacements, the amplitudes of the steady-state horizontal displacement and rotation of the disk,*u*andf,stateas

$$\begin{Bmatrix} u \\ \phi r_o \end{Bmatrix} = \begin{bmatrix} f_{11} + ig_{11} & f_{12} + ig_{12} \\ f_{21} + ig_{21} & f_{22} + ig_{22} \end{bmatrix} \begin{Bmatrix} u_{st} \\ \phi_{st} r_o \end{Bmatrix} \tag{1}$$

$$u_{st} = \frac{2 - \nu}{8Gr_o} P \tag{2}$$

$$\phi_{st} = \frac{3(1 - \nu)}{8Gr_o^3} M \tag{3}$$

where*f*and*g* arethedimensionlessflexibilitycoefficients;iisthe imaginary unit, satisfying i^{2}¼ —1; u_{st} is the horizontal displacementbystatichorizontalforce,*P*;f_{st}istherotationofdiskdueto staticmoment,*M*;nisthePoisson’sratioformaterialofhalf-space; r_o is the equivalent radius; and *G* is the shear modulus. The flexibilitycoefficients*f*and*g*arethefunctionsofnanddimensionless frequencyparameter(a_o),anda_o¼ur_o/V_s,whereuisthecircular frequency of the excitation, and V_s is the shear wave velocity in the half-space.

The force amplitudes, *P* and *M*, corresponding to the displace- mentamplitudes,*u*andf,canbeexpressedas

$$\begin{Bmatrix} P \\ \dfrac{M}{r_o} \end{Bmatrix} = K_x \begin{bmatrix} k_{11} + ia_o c_{11} & k_{21} + ia_o c_{21} \\ k_{21} + ia_o c_{o21} & \dfrac{2 - \nu}{3(1 - \nu)} (k_{22} + ia_o c_{o22}) \end{bmatrix} \begin{Bmatrix} u \\ \phi r_o \end{Bmatrix} \tag{4}$$

where*k* and *c* are the dimensionless stiffness coefficient and damping coefficient, respectively, depending on a_o and r_o; $K_x$rep- resents the horizontal static force necessary to produce¼ a unit horizontal displacement of the disk, and K_x *P*/u_{st}.

If the off-diagonal terms of the flexibility matrix areneglected, f_{12}, f_{21}, g_{12}, and $g_{21}$are assumed to be zero, the forceedisplacement relationship for the disk can be obtained from thefollowing equations:

$$\begin{Bmatrix} P \\ M \end{Bmatrix} = \begin{bmatrix} (k_1 + ia_o c_1)K_x & 0 \\ 0 & (k_2 + ia_o c_2)K_\phi \end{bmatrix} \begin{Bmatrix} u \\ \phi \end{Bmatrix} \tag{5}$$

where*K*frepresentsthestaticmomentnecessarytorotatethedisk byaunitamount¼withnorestrictiononthevalueofthehorizontal displacement,and*K*f*M*/f_{st}.

The stiffness function for horizontal and rocking motion are calculated from Eq. (5). The above methodology is used to inves- tigate the dynamic response of block foundation resting on homogeneous medium by using the computer program DYNA 5 (Novak et al., 1999).

2.2 Layered medium

The analysis is carried out using finite element method based formulation and computer program developed by KauselandUshijima (1979). A three-dimensional (3D) axisymmetric finite element model with transmitting boundaries is used to model a rigidcircularfoundationrestingonahomogeneousrockstratumof finite depth lying on a much stiffer rock-like material. The trans-mittingboundariesusedweredevelopedbyKausel(1974) tothe3D case with axisymmetricgeometry.

Kausel and Ushijima (1979) presented a numerical method for the dynamic analysis of axisymmetric foundation resting on viscoelastic soil layers over rock of infinite horizontal extent. The solution technique developed by Lysmer and Waas (1972)was extended for the analysis of axisymmetric systems subjected to arbitrary non-axisymmetric loading using Fourier expansion method.

For the plane symmetric displacement modes, the forced hori- zontal displacement is referred to as swaying and the forced rota- tion about horizontal axis is referred to as rocking. The stiffness functions can be given as

$$K_s = K_{so}(k_1 + ia_o c_1)(1 + 2i\beta_{h1}) \tag{6}$$

$$K_\psi = K_{\psi o}(k_2 + ia_o c_2)(1 + 2i\beta_{h2}) \tag{7}$$

whereKsisthehorizontalstiffnessfunction,Kjistherocking stiffnessfunction,KsoandKjoaretherealpartsofthestiffness functions in the static case, and bis the internal damping coefficient.

Using the methodology proposed by different researchers, the analyses are carried out to determine the dynamic response of block foundation in soilerock system, weathered rockerocksystem and rockerock system. The methodology involved in this study is incorporatedinthecomputerprogramDYNA5(Novaket al.,1999). This program is used to present the dynamic behavior of block foundation in terms of frequency response curves fordisplacement, stiffness, and damping constants for layered system.

III. RESULTS AND DISCUSSIONS

Theanalysesarecarriedoutforthreeeccentricmoments,i.e. 0.45 N m, 0.366 N m, 0.278 N m for both homogeneous and layered media. The results of translational amplitude, rotational amplitude and frequency are then respectively plotted in dimensionless form using the following equations:

$$A_x = \frac{xm}{m_e e} \tag{8}$$

$$A_\psi = \frac{I_\psi}{m_e e Z_e} \tag{9}$$

$$a_o = \frac{\omega r_o}{V_s} \tag{10}$$

where*x* is the amplitude of system, *m* is the total mass of the footingandmachine,*I*jisthemomentofinertia,$m_e$isthemassof eccentricrotatingpartofoscillator,*e*istheeccentricityofrotating partofoscillator,j$_o$istherotationalmoment,anduistheang ular operatingfrequency.

Two different ratios of equivalent radius to mass of block foundation, i.e. $(R_o/m)_1$ 2.85 $10^{-5}$and $(R_o/m)_2$1.74 10^{-5}, are considered to study the effect of mass and size of foundation on the dynamic response of block foundation, where R_o is the equivalent radius of footing in meter. The properties of soil and rocks consideredfortheanalysisareshowninTable1(Zhao,2010).

3.1 Homogeneous medium

In the case of homogenous medium, the theory proposed by Veletsos and Wei (1971)has been used for the analysis of block foundation resting on homogeneous soil and four types of homo- geneous rocks, i.e. sandstone, shale, limestone and basalt. The stiffness and damping constant are normalized as

$$k_h;\ k_r ¼\ k_o ¼\ \frac{k}{k_{soil}\ ða_o¼ 0Þ} \quad (11)$$

$$c_h;\ c_r¼\ c_o¼\ \frac{c}{k_{soil}ða_o\ ¼0Þ} \quad (12)$$

where$k_o$isthenormalizedstiffnessconstant,whichistermedask_h and$k_r$forhorizontalstiffnessandrockingstiffness,respectively;c_o is the normalized damping constant, which is c_h and c_r for hori- zontaldampingandrockingdamping,respectively;andk_{soil}(a_o¼0) is the stiffness of soil at a_o¼0.

Table 1
Properties of soil and rocks (Zhao, 2010).

Medium	Shear wavevelocity(m/s)	Unit weight (kN/m³)
Soil	185	16
Weatheredrock	1680	20.81
Sandstone	1110	22
Shale	2220	23
Limestone	2960	25
Basalt	3700	26

The variations of normalized horizontal stiffness (k_h) with dimensionless frequency (a_o) for all types of homogeneous soil and rocks are shown in Fig. 1a and b for $(R_o/m)_1$ and ¼$(R_o/m)_2$, respec- tively.¼ The variation of normalized rocking stiffness (k_r) with dimensionless natural frequency (a_o) are shown in Fig. 2a and b for $(R_o/m)_1$ and $(R_o/m)_2$, respectively. It has been observed that both horizontal and rocking normalized stiffness values are maximum for the basalt among all materials considered here. Hence, the foundation resting on basalt has higher resistance for both hori- zontal and rocking displacements as compared to other rocks and soil.

The variations of normalized horizontal damping (c_h) with dimensionless frequency (a_o) are shown in Fig. 3a and b for $(R_o/m)_1$ and $(R_o/m)_2$, respectively. The variations of normalized rocking damping (c_r) with dimensionless frequency (a_o) are also shown inFig. 4a and b for $(R_o/m)_1$ and $(R_o/m)_2$, respectively. It is noted that

the normalized damping increases significantly as dimensionless frequency decreases at low frequency condition for both horizontal and rocking motion because of the conversion of frequency- independent material damping (b) to the equivalent viscous damping coefficient (c) as c 2b/u. It is also observed that the normalized horizontal and rocking damping values for soil are much lower than those of the homogeneous rocks.

The variations of dimensionless translational amplitude (A_x) and dimensionlessrotationalamplitude(Aj)withdimensionlessfre- quency(a_o) are shown in Fig. 5a and b for both $(R_o/m)_1$and $(R_o/m)_2$, respectively. It is observed from these figures that there are two dimensionless amplitude peaks at two different dimensionless fre- quencies. For $(R_o/m)_1$, the maximumvalue of dimensionless frequency is lower and the maximum dimensionless amplitude is higher than the $(R_o/m)_2$for both horizontal and rocking motion. The maximum value of dimensionless amplitude is higher for soil as compared to

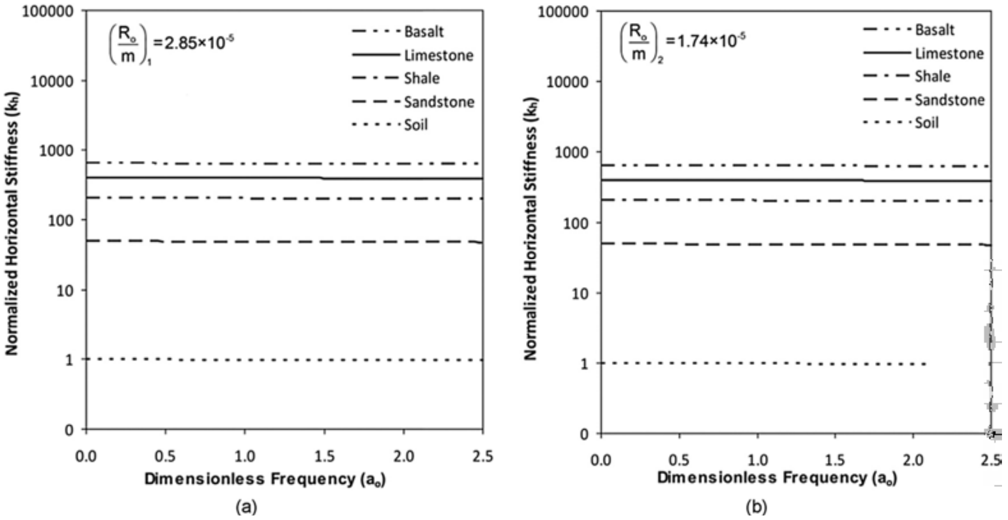

Fig. 1. Variations of normalized horizontal stiffness (k_h) with dimensionless frequency (a_o) for (a) $(R_o/m)_1$ and (b) $(R_o/m)_2$ ratios.

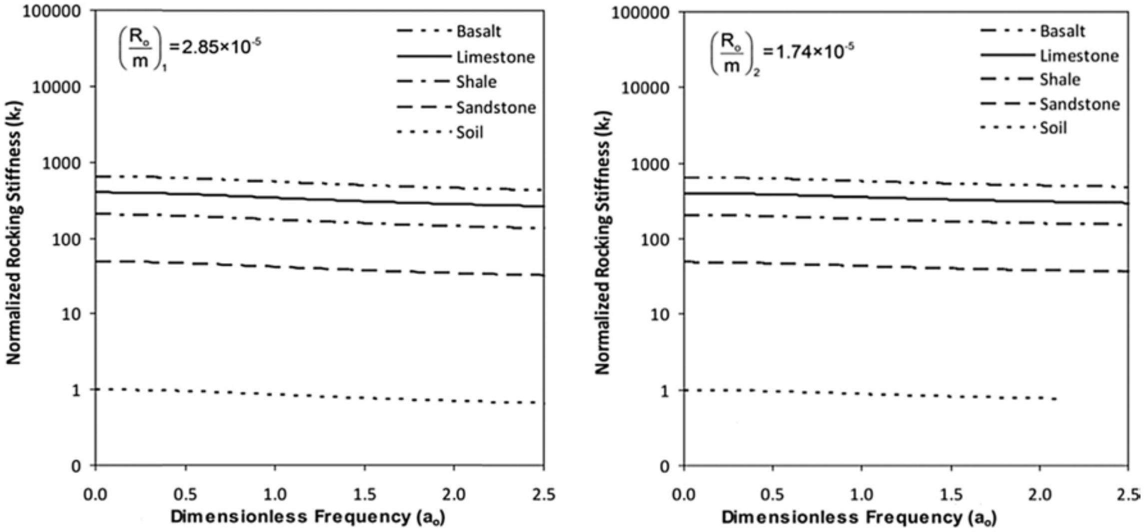

(a) (b)

Fig. 2. Variations of normalized rocking stiffness (k_r) with dimensionless frequency (a_o) for (a) $(R_o/m)_1$ and (b) $(R_o/m)_2$ ratios.

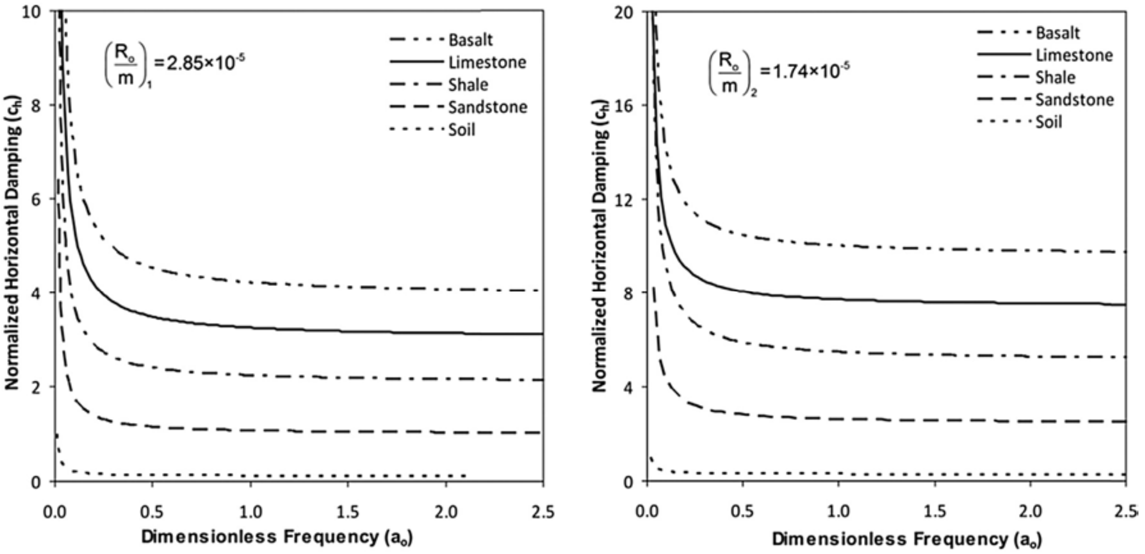

(a) (b)

Fig. 3. Variations of normalized horizontal damping (c_h) with dimensionless frequency (a_o) for (a) $(R_o/m)_1$ and (b) $(R_o/m)_2$ ratios.

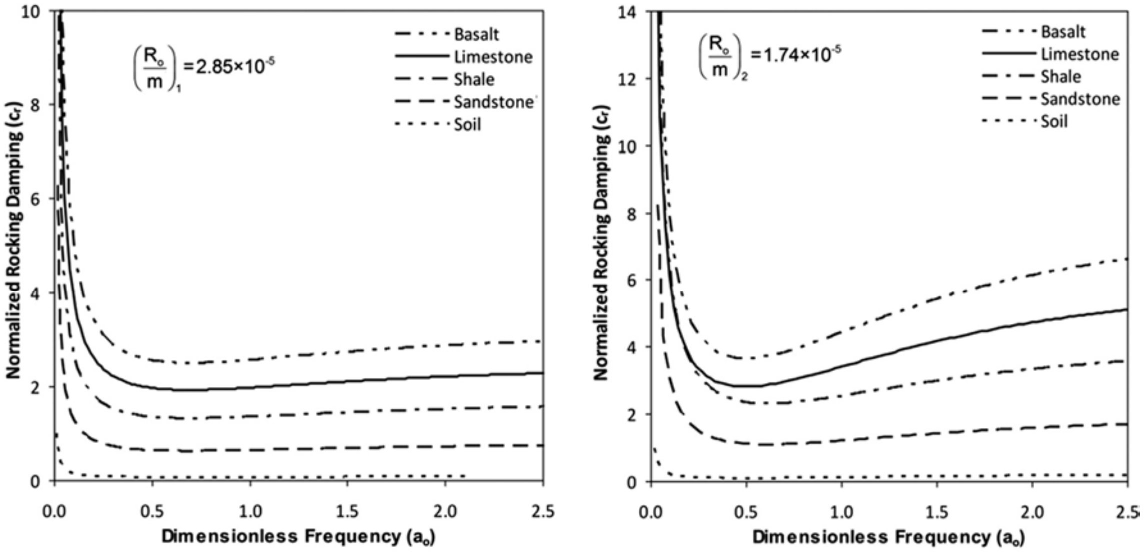

(a) (b)

Fig. 4. Variations of normalized rocking damping (c_r) with dimensionless frequency (a_o) for (a) $(R_o/m)_1$ and (b) $(R_o/m)_2$ ratios.

those of the rocks for both translational and rotational cases. It can also be seen that the dimensionless frequency (a_o) corresponding to themaximumvalueofdimensionlessamplitudeforsoilislowerthan those of the rocks for both translational and rotationalmotion.

3.2 Layered medium

By using the theory proposed by Kausel (1974), the analyses are carried out to study the dynamic response of block foundations resting on layered soilerock and rockerock systems. In the case of layered medium, the dimensionless parameter which appreciably influences the dynamic response of block foundation is the H/B ratio, where H is the depth of top layer and B is the width of foundation. In the present study, three different H/B ratios, i.e. 0.5, 1 and 1.5, are considered. The results of dynamic impedance of foundations, pertaining to all possible translational and rotational modes of vibration, are plotted in the form of dimensionless parametersofstiffness,dampingandamplitude.Theratiosof stiffness and damping of the layered system to the stiffness of homogeneous igneous rock are taken to obtain the normalized stiffness and damping of layeredsystem:

kk ¼ k ¼ k / k_{basalt}ða_o¼0Þ (13)

c / c;c¼c¼ hr o k_{basalt}ða_o¼ 0Þ (14)

wherek_{basalt}(a_o ¼ 0) is the stiffness of basalt at the zero dimensionlessfrequency.

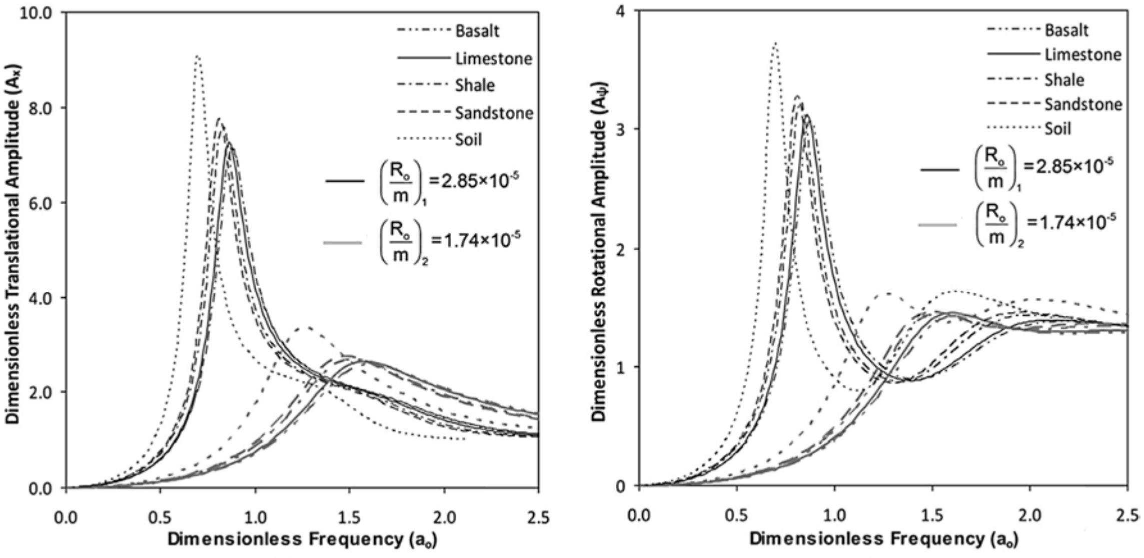

(a) (b)

Fig.5.Variationsof(a)dimensionlesstranslationalamplitude(A_x)and(b)dimensionlessrotationalamplitude(Aj)withdimensionlessfrequency(a_o)for(R_o/m)$_1$and(R_o/m)$_2$ratios.

3.2.1 Soilerock and weathered rockerock systems

It is well established that the shear wave velocity is greatly influenced by the state of the material, which varies from hard rock to highly weathered rock or granular soils. Therefore, in the case of soilerock and weathered rockerock systems, the analyses are carried out by considering shear wave velocity as an important parameter. In the layered system, the soil or weathered rock layeris normally underlain by hard rock and hence the layered medium can be defined by two shear wave velocities, i.e. V_{s1} and V_{s2} (where V_{s1} is the shear wave velocity of top layer, and V_{s2} is the shear wave velocity of bottom half-space). Therefore, in the present study, the dynamic behavior of block foundation on layered medium is investigatedintheformofshearwavevelocityratio(V_{s1}/V_{s2}).

Three different shear wave velocity ratios, i.e. 0.8, 0.6 and 0.3, are considered in the analyses to represent limestoneebasalt, shaleebasaltandsandstoneebasaltsystems,respectively. Thenthevariations of natural frequency and resonant amplitudeof translational and rotational modes of vibration are obtained for H/B 0.5, 1 and 1.5. The maximum dimensionless amplitude with its subsequent ¼dimensionless natural frequency is obtained for all shear wave velocity ratios. The trend lines are plotted for twocases:

(i) natural frequency and shear wave velocity, and (ii) resonant amplitude and shear wave velocity ratios. The shear ⩽wave velocity ratio (V_{s1}/V_{s2}) 0.5 is normally considered to represent the soilerock and weathered rockerock systems (Gupta and Rao, 1998). Therefore, the extrapolation is done for shear wave velocity ratio (V_{s1}/V_{s2})upto0.5byusingtheequationoftrendline.

The variation of dimensionless natural frequency for the first peak with shear wave velocity ratio is shown in Fig. 6a for both (R_o/ m)$_1$ and (R_o/m)$_2$. Similarly, the variation of dimensionless natural frequency for the second peak with shear wave velocity ratio is shown in Fig. 6b for both $(R_o/m)_1$ and $(R_o/m)_2$. The trend lines shown in the graph are the variations of the first and second natural frequencieswithshearwavevelocityratiosforthecoupledvibration.It is observed from the figures that the trend lines show decrement with the decrease in shear wave velocity ratio. The variations of dimensionlesstranslationalamplitude(A_x)withshearwave velocity ratio is shown in Fig. 7a and b for $(R_o/m)_1$ and $(R_o/m)_2$, respectively. Similarly,thevariationsofdimensionlessrotationalamplitude(Aj) with shear wave velocity ratio is shown in Fig. 8a and b for $(R_o/m)_1$ and $(R_o/m)_2$, respectively. It can be seen from these figures that the values of dimensionless natural frequency are higher and dimensionless translational and rotational amplitudes are lower for $(R_o/ m)_2$ as compared to $(R_o/m)_1$. It can be seen from Figs. 7 and 8 that as H/B ratios increase, the dimensionless rotational and translational amplitudesdecrease.Aconvergingtrendisfoundforthetrendlines representing resonance frequency and amplitudes for various H/B ratios as the values of V_{s1}/V_{s2} increase. Therefore, the effect of H/B ratio reduces as the shear wavevelocity ratio increases.

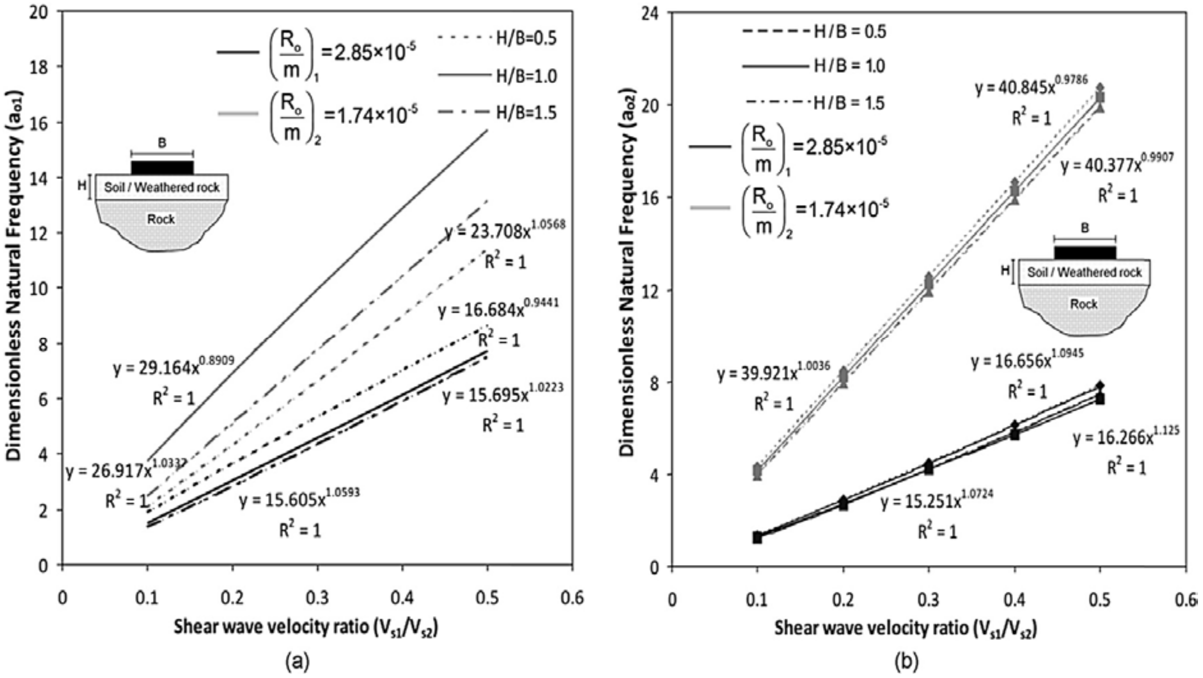

Fig. 6. Variations of dimensionless natural frequency with shear wave velocity ratio (V_{s1}/V_{s2}) for $(R_o/m)_1$ and $(R_o/m)_2$: (a) First peak, a_{o1}, and (b) Second peak, a_{o2}.

It is observed that with the increase in shear wave velocity ratio, the dimensional natural frequencies increase and the dimensionless resonant amplitudes decrease. Therefore, the dimensionless natural frequencies are found lower and the dimensionless resonant amplitudes are found higher in the case of soilerock system than those in weathered rockerock system.

3.2.2 Rockerock system

In the present study, the rockerock combinations considered are limestoneebasalt, shaleebasalt and sandstoneebasalt with shear wave velocity ratio of 0.8, 0.6 and 0.3. The variations of dimensionless frequency, dimensionless translational and rotationalamplitudesarestudiedforvariousH/Bratiosandshearwave velocityratios.

The variations of normalized horizontal stiffness (k_h) with dimensionlessfrequency(a_o)areshowninFig.9aandbfor $(R_o/m)_1$ and $(R_o/m)_2$, respectively, for sandstoneebasalt, shaleebasalt and limestoneebasaltsystems.Similarly,thevariationsofnormalized rockingstiffness(k_r)withdimensionlessfrequency(a_o)areshown

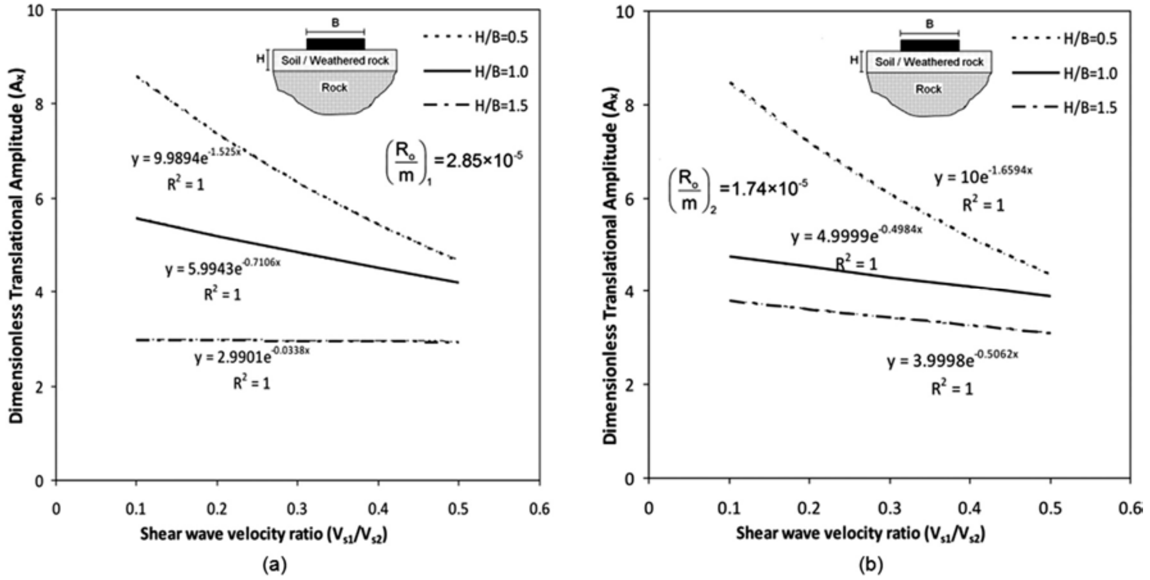

Fig. 7. Variations of dimensionless translational amplitude (A_x) with shear wave velocity ratio (V_{s1}/V_{s2}) for (a) $(R_o/m)_1$ and (b) $(R_o/m)_2$ ratios.

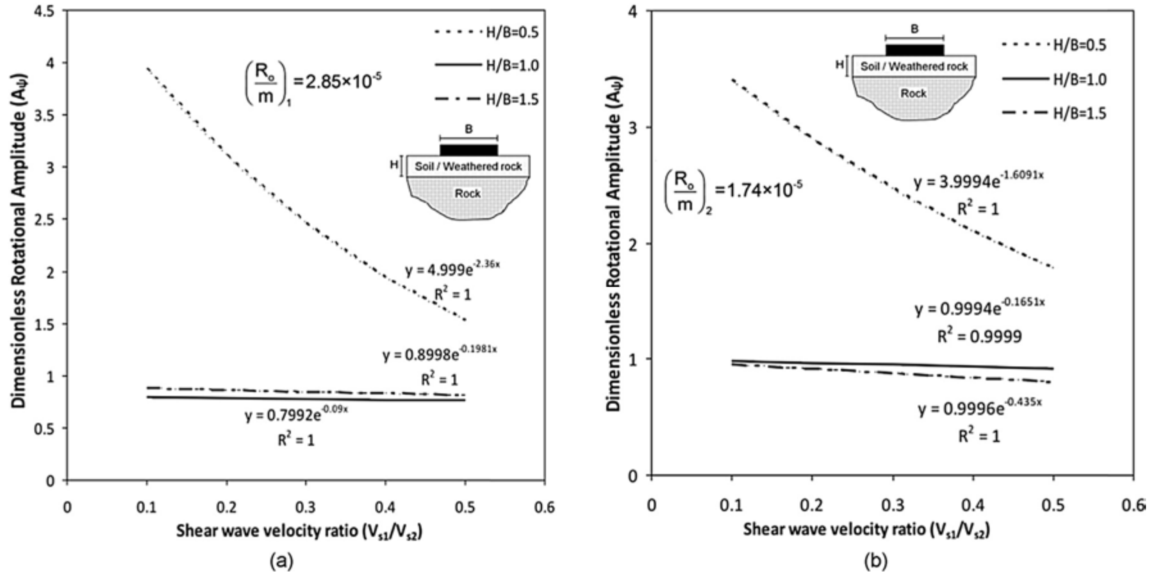

Fig.8.Variationsofdimensionlessrotationalamplitude(Aj)withshearwavevelocityratio(V_{s1}/V_{s2})for(a)$(R_o/m)_1$and(b)$(R_o/m)_2$ratios.

inFig.10aandbfor$(R_o/m)_1$and$(R_o/m)_2$,respectively.Itcan beseen that the normalized horizontal and rocking stiffness values are higherforlimestoneebasaltsystemthanthoseforothertworockerocksystems,becauseofhighershearwavevelocityratiooflime-stoneebasaltsystem.Also,thenormalizedhorizontalandrocking stiffnessvaluesofshaleebasaltsystemarelargerthanthoseofthe sandstoneebasalt system. It is also observed that the normalized stiffness values decrease with the increase in H/B ratios approxi-matelyuptodimensionlessfrequency(a_o)of1.5forbothhorizontal and rockingmotion.

The variations of normalized horizontal damping (c_h) with dimensionless frequency (a_o) are shown in Fig. 11a and b for $(R_o/m)_1$ and $(R_o/m)_2$ respectively for all rockerock systems. Similarly, the variations of normalized rocking damping (c_r) with dimensionless natural frequency (a_o) are shown in Fig. 12a and b for $(R_o/m)_1$ and $(R_o/m)_2$, respectively. It is found that both normalized horizontal and rocking damping (c_h and c_r) values increase as shear wave velocity ratio increases. It is also noted that the normalized dampingisverylowforsandstoneebasaltsystemascomparedto those for other rockerock systems. It can also be seen that the variationsofnormalizeddamping($c_h$andc_r)valueswithH/Bratio are very less for lower dimensionless frequency, a_o<0.2. The normalizeddampingincreaseswiththeincreaseinthicknessoftop layer approximately up to dimensionless frequency (a_o) of1.5 for both horizontal and rockingmotion.

Thevariationsofdimensionlesstranslationalamplitude(A_x)and rotationalamplitude(Aj)withdimensionlessfrequency(a_o)for sandstoneebasaltsystemareshowninFig.13aandbforboth(R_o/ m)$_1$ and (R_o/m)$_2$, respectively. Similarly, the variations of dimensionless translational and rotational amplitudes withdimensionlessfrequencyareshowninFig.14a andbrespectivelyforshaleebasaltsystem.Further,thevariationsofdimensionlesstranslational androtationalamplitudeswithdimensionlessfrequencyareshown inFig.15aandbrespectivelyforlimestoneebasaltsystem. Itis

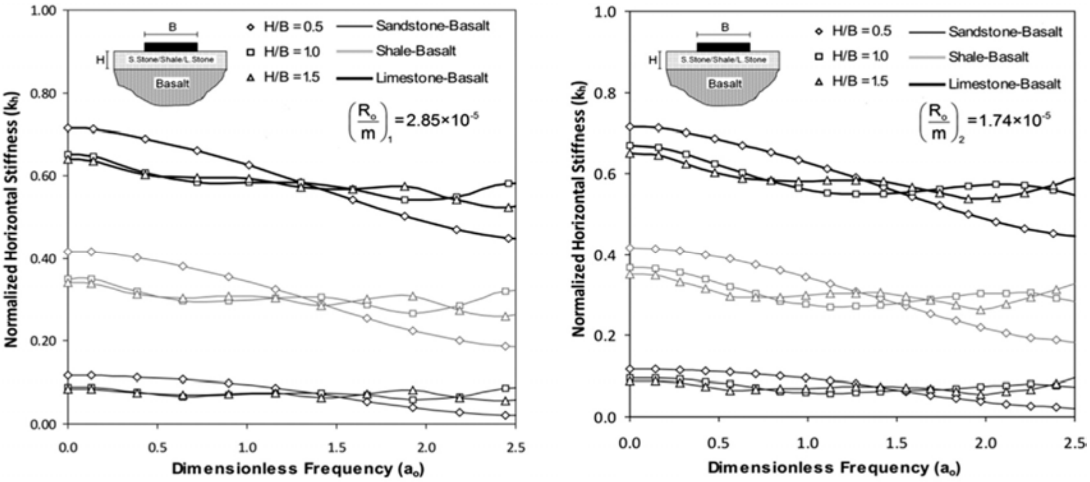

(a) (b)

Fig. 9. Variations of normalized horizontal stiffness (k_h) with dimensionless frequency (a_o) for (a) (R_o/m)$_1$ and (b) (R_o/m)$_2$ ratios.

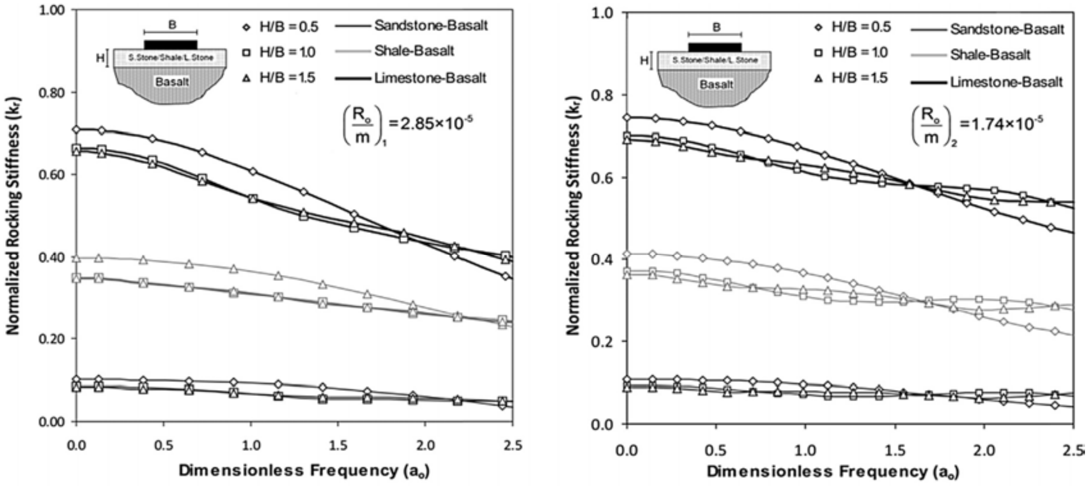

(a) (b)

Fig. 10. Variations of normalized rocking stiffness (k_r) with dimensionless frequency (a_o) for (a) (R_o/m)$_1$ and (b) (R_o/m)$_2$ ratios.

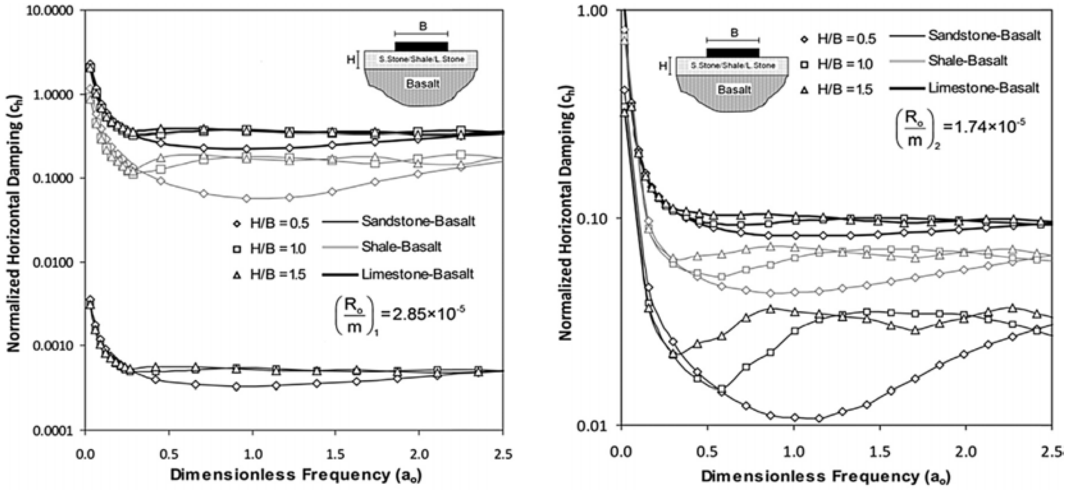

(a) (b)

Fig. 11. Variations of normalized horizontal damping (c_h) with dimensionless frequency (a_o) for (a) (R_o/m)$_1$ and (b) (R_o/m)$_2$ ratios.

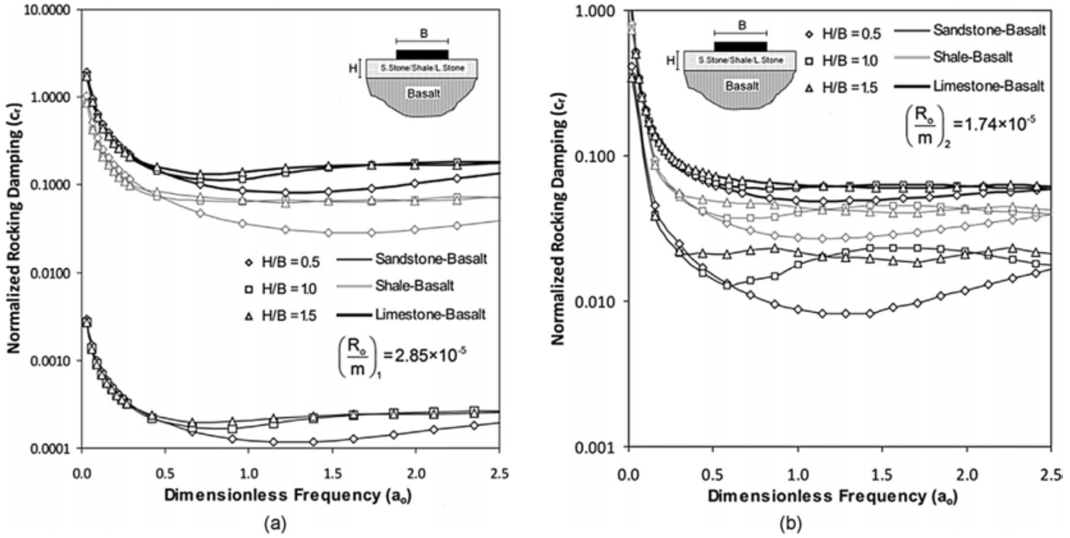

Fig. 12. Variations of normalized rocking damping (c_r) with dimensionless frequency (a_o) for (a) $(R_o/m)_1$ and (b) $(R_o/m)_2$ ratios.

found that in most of the cases, the response is dominated by the first resonant peak and the second resonant peak is entirely sup- pressed for both translational and rotational motion. It is alsofound that the dimensionless natural frequencies increase and the dimensionless resonant amplitudes decrease with the increase in shear wave velocity ratio. It is observed that the maximum value of dimensionless frequency is lower and the maximum dimensionless amplitude is higher for $(R_o/m)_1$ than that for $(R_o/m)_2$ for all rockerock systems in the case of both horizontal and rocking motion.

IV. PARAMETRIC STUDIES

The parametric study is carried out for two block foundations with dimensions of 4 m × 3 m × 2 m and 8 m 5 m 2 m, sub- jected to coupled horizontal and rocking vibrations. The values of horizontal and rotational amplitudes corresponding to their natural frequencies are shown in Tables 2 and 3 for block foundationswith dimensions of 4 m 3 m 2 m and 8 m 5 m 2 m, respectively.

Thefrequencyandamplitudevaluesarepresentedfortwo different eccentric moments ($m_e e$0.028 N m and 0.045 N m). The values ¼ listed in Tables 2 and 3 are obtained with the help of generalized graphs proposed in the presentstudy.

The natural frequencies for soilerock and weathered rockerock systems are found by using Fig. 6a and b. Similarly, Fig. 7a and b are used for determining the values of translational am- plitudes and Fig. 8a and b are used for rotational amplitudes for soilerock and weathered rockerock systems. It is observed from Tables 2 and 3that the values of both natural frequency and maximum amplitude vary with mass and size of block founda- tions. For soilerock system, the resonant amplitudes are found higher and the natural frequencies are found lower as compared to those for other rockerock systems. It is also observed that the values of natural frequencies are higher and theresonantamplitudesarelowerforlimestoneebasaltsystem

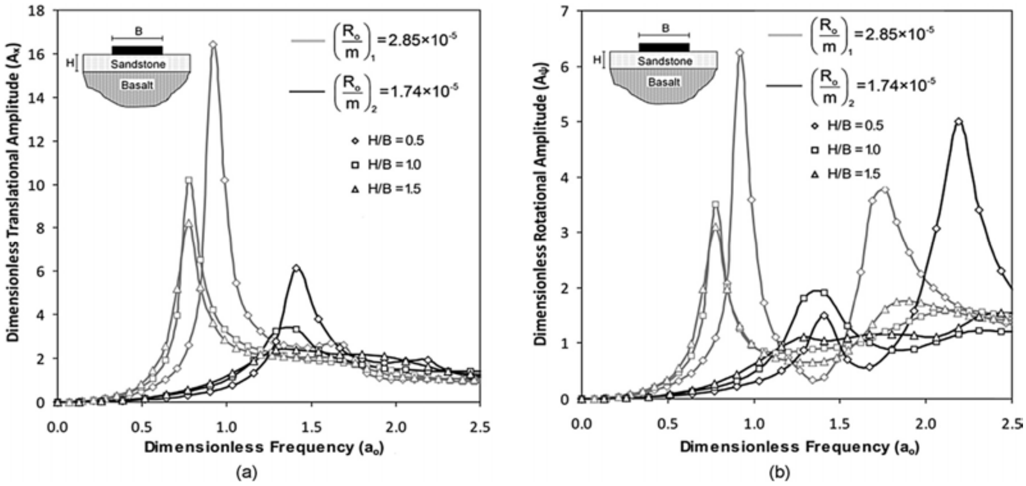

Fig.13.Variationsof(a)dimensionlesstranslationalamplitude(A_x)and(b)dimensionlessrotationalamplitude(Aj)withdimensionlessfrequency(a_o)forsandstoneebasaltsystem for $(R_o/m)_1$ and $(R_o/m)_2$ ratios.

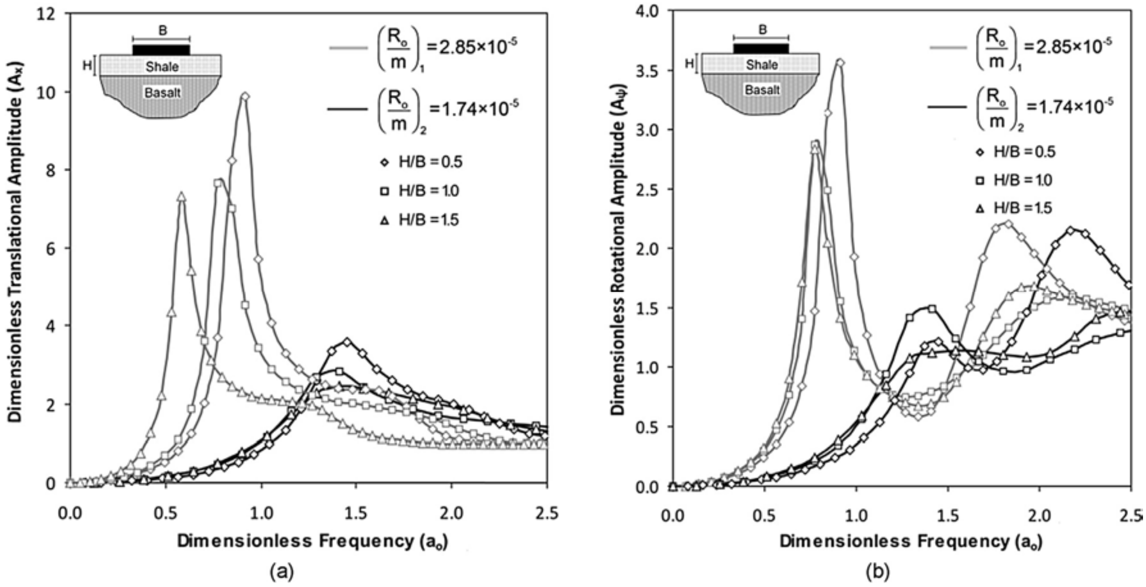

Fig.14.Variationsof(a)dimensionlesstranslationalamplitude(A_x)and(b)dimensionlessrotationalamplitude(Aj)withdimensionlessfrequency(a_o)forshaleebasaltsystemfor (R_o/m)$_1$ and (R_o/m)$_2$ ratios.

as compared to those for all other systems. Therefore, the lime- stoneebasalt system can be considered as the best foundation medium for block foundation among all other systems consid- ered in this study, because the limestoneebasalt system is suit- able for machines with high operating frequencies and low amplitude of vibration.

V. CONCLUSIONS

In the present study, an effort is made to study the dynamic response of block foundations resting on homogeneous andlayered media under coupled horizontal and rocking vibrations. Two different R_0/m ratios are considered to investigate the effect of size and mass of block foundation. Analyses are carried out to studythe variations of stiffness, damping and amplitude with frequency of block foundation for three different media: (i) homogeneous soil and rocks, (ii) soil/weathered rockerock system, and (iii) rockerock system. For all the cases, the response is dominated by the first resonant peak and the second peak is entirely suppressed in the case of translational motion. However, the reverse trends are found in the case of rotational motion.

In the case of homogeneous medium, it is found that the normalized horizontal and rocking stiffness values for block foun- dations on soil are lower than those for the block foundations on rocks.Itisalsoobservedthatthenormalizedhorizontaland rocking damping values for soil is much lower than those for the homo- geneous rocks. Therefore, the dimensionless translational and rotational amplitudes for soil are found higher than those forrocks

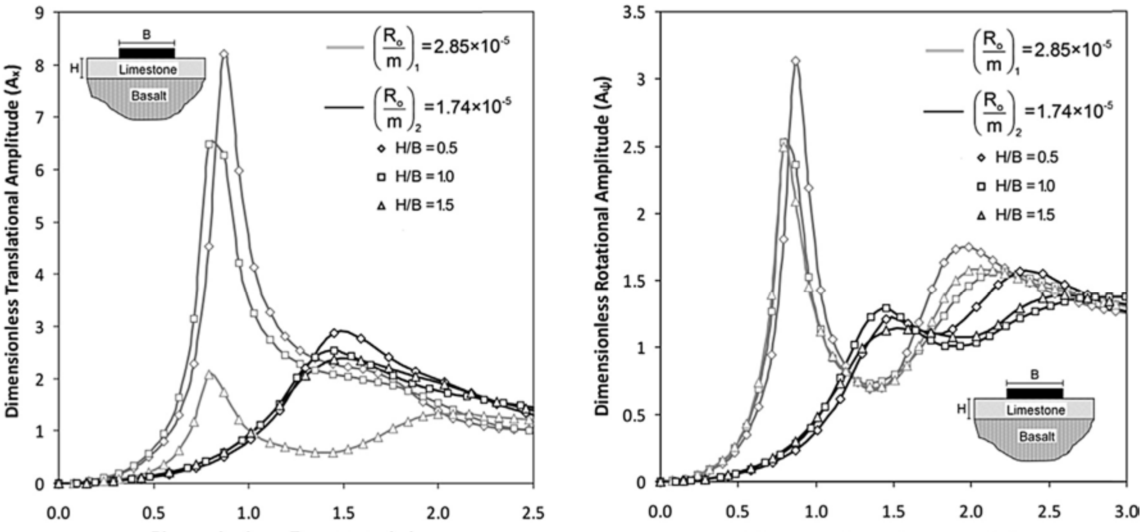

Fig.15.Variationsof(a)dimensionlesstranslationalamplitude(A_x)and(b)dimensionlessrotationalamplitude(Aj)withdimensionlessfrequency(a_o)forlimestoneebasaltsystem for (R_o/m)$_1$ and (R_o/m)$_2$ ratios.

Table 2
Observed natural frequency and resonant amplitude for different eccentric moments for foundation with dimensions of 4 m × 3 m × 2 m.

System	Type of rockand soil	H/B	$m_e e$¼ 0.028Nm						$m_e e$¼ 0.045 Nm					
			f_{n1} (Hz)	$A_{H1\text{-res}}$ (mm)	$\mathbf{j}_{r1\text{-res}}$ (rad)	f_{n2} (Hz)	$A_{H2\text{-res}}$ (mm)	$\mathbf{j}_{r2\text{-res}}$ (mm)	f_{n1} (Hz)	$A_{H1\text{-res}}$ (mm)	$\mathbf{j}_{r1\text{-res}}$ (rad)	f_{n2} (Hz)	$A_{H2\text{-res}}$ (mm)	$\mathbf{j}_{r2\text{-res}}$ (mm)
Soilerock/ weathered rockerock	Soilebasalt (V_{s1}/V_{s2}¼0.05)	0.5	15.7	0.0092	0.0369	34.6	0.0288	0.00184	15.7	0.0147	0.0593	34.6	0.0462	0.00295
		1	32.1	0.00487	0.00099	33	0.000598	0.000692	32.1	0.00782	0.00144	33	0.000961	0.00111
		1.5	19.3	0.00389	0.00097	31.4	0.000598	0.000598	19.3	0.00625	0.00155	31.4	0.000961	0.00111
	Weathered rockebasalt(V_{s1}/V_{s2}¼0.45)	0.5	163	0.0047	0.0192	300	0.00212	0.000969	163	0.00755	0.0308	300	0.034	0.00155
		1	229	0.00398	0.00092	293	0.000587	0.000634	229	0.00639	0.00147	293	0.000943	0.00101
		1.5	189	0.00317	0.00082	287	0.000587	0.00059	189	0.00509	0.00131	287	0.000943	0.00948
Rockerock	Sandstoneebasalt (V_{s1}/V_{s2}¼0.3)	0.5	85.9	0.00719	0.0022	155	0.00966	0.00134	85.9	0.77652	0.28421	155	1.0432	0.17311
		1	71.6	0.004449	0.001246	195	0.000489	0.000555	71.6	0.48049	0.16096	195	0.05281	0.07169
		1.5	70	0.00343	0.001084	170	0.000582	0.000617	70	0.37044	0.14003	170	0.06285	0.0797
	Shaleebasalt (V_{s1}/V_{s2}¼0.6)	0.5	159	0.004653	0.001445	324	0.000734	0.000769	159	0.46887	0.18667	324	0.07396	0.09934
		1	146	0.003575	0.001099	388	0.000498	0.000554	146	0.36024	0.14197	388	0.05018	0.07156
		1.5	140	0.00305	0.0009889	356	0.00056	0.000584	140	0.30734	0.12775	356	0.05643	0.07544
	Limestoneebasalt (V_{s1}/V_{s2}¼0.8)	0.5	210	0.003415	0.001093	472	0.00061	0.00061	210	0.36882	0.01412	472	0.06588	0.0788
		1	200	0.003048	0.0009763	534	0.0005	0.000545	200	0.32918	0.12612	534	0.054	0.0704
		1.5	195	0.00272	0.000895	496	0.000571	0.000553	195	0.29376	0.11562	496	0.06166	0.07144

Note: f_{n1} and f_{n2} are the first and second resonant frequencies, respectively; $A_{H1\text{-res}}$ and $A_{H2\text{-res}}$ are the first and second resonant amplitudes for horizontal motion, respectively; $\mathbf{j}_{r1\text{-res}}and\mathbf{j}_{r2\text{-res}}$arethefirstandsecondresonantamplitudesforrockingmotion,respectively.

Table 3
Natural frequency and resonant amplitude for different eccentric moments for foundation with dimensions of 8 m × 5 m × 2 m.

System	Type ofrock andsoil	H/B	$m_e e$¼0.028Nm						$m_e e$¼ 0.045 Nm					
			f_{n1} (Hz)	$A_{H1\text{-res}}$ (mm)	$\mathbf{j}_{r1\text{-res}}$ (rad)	f_{n2} (Hz)	$A_{H2\text{-res}}$ (mm)	$\mathbf{j}_{r2\text{-res}}$ (mm)	f_{n1} (Hz)	$A_{H1\text{-res}}$ (mm)	$\mathbf{j}_{r1\text{-res}}$ (rad)	f_{n2} (Hz)	$A_{H2\text{-res}}$ (mm)	$\mathbf{j}_{r2\text{-res}}$ (mm)
Soilerock/ weathered rockerock	Soilebasalt (V_{s1}/V_{s2}¼0.05)	0.5	15.6	0.000925	0.0000781	9.97	0.000291	0.000444	15.6	0.00148	0.000125	9.97	0.000467	0.000712
		1	11.6	0.0000578	0.0000953	8.89	0.000101	0.000089	11.6	0.0000927	0.000152	8.89	0.000161	0.000142
		1.5	10.4	0.0000298	0.0000603	9.75	0.000201	0.000079	10.4	0.0000477	0.0000733	9.75	0.000322	0.000126
	Weathered rockebasalt (V_{s1}/V_{s2}¼0.45)	0.5	126	0.000499	0.0000648	111	0.000231	0.000171	126	0.000801	0.000104	111	0.00037	0.000273
		1	111	0.0000434	0.0000647	106	0.000112	0.000082	111	0.0000696	0.000103	106	0.00018	0.000131
		1.5	107	0.000294	0.0000628	104	0.000211	0.000076	107	0.0000471	0.0001	104	0.000338	0.000121
Rockerock system	Sandstoneebasalt (V_{s1}/V_{s2}¼0.3)	0.5	70	0.000852	0.0000788	108	0.000269	0.000265	70	0.27604	0.06697	108	0.087150.22522	
		1	66.8	0.000502	0.00011	152	0.00015	0.0000778	66.8	0.16264	0.09349	152	0.0486	0.06612
		1.5	66.8	0.000339	0.0000577	122	0.000176	0.0000815	66.8	0.10983	0.04903	122	0.05702	0.06926
	Shaleebasalt (V_{s1}/V_{s2}¼0.6)	0.5	152	0.000263	0.0000534	203	0.000217	0.0000857	152	0.08521	0.04538	203	0.0703	0.07283
		1	133	0.000399	0.0000802	292	0.000161	0.0000759	133	0.12927	0.06816	292	0.05216	0.0645
		1.5	152	0.000332	0.0000603	248	0.000182	0.0000776	152	0.10756	0.05124	248	0.05896	0.06595
	Limestoneebasalt (V_{s1}/V_{s2}¼0.8)	0.5	195	0.000404	0.0000649	310	0.000203	0.0000831	195	0.13089	0.055159	310	0.06577	0.07062
		1	190	0.000353	0.0000684	381	0.00017	0.0000732	190	0.11437	0.058133	381	0.05508	0.06223
		1.5	195	0.000332	0.0000605	339	0.000187	0.0000738	195	0.10756	0.051419	339	0.06058	0.06272

and the dimensionless natural frequencies for soil are found lower than those for rocks.

In the case of layered medium, i.e. soilerock and weathered rockerock systems, different equations are proposed to calculate the dimensionless natural frequency and resonant amplitudes for both translational and rotational motion in terms of *H*/*B* ratios and shear wave velocity ratio. It is observed that the dimensional natural frequencies increase and the dimensionless resonant amplitudes decrease with the increase in shear wave velocity ratio. Therefore, the dimensionless natural frequencies are found higher in the case of weathered rockerock system than those for soilerock system and the dimensionless resonant amplitudes are foundhigher in the case of soilerock system than those for the weathered rockerock system. These parameters are presented in the form of shear wave velocity, as the testing for strength parameters of these weathered rocks is very difficult in laboratory. The graphs presented can directly be used by the practicing engineers for estimation of natural frequency and resonant amplitude of block type machine foundations resting on different layered combinations like soilerock and weathered rockerocksystems.

For rockerock systems, it is observed that the normalized stiffness decreases and the damping increases with increase in thickness of top layer approximately up to dimensionless frequency of 1.5 for both horizontal and rocking motion. It is found that both normalized stiffness and damping increase with increase in shear wave velocity ratio. Therefore, the dimensionless resonant amplitudes decrease and the natural frequencies increase with increasein shear wave velocity ratio for both translational and rotational motion. It is also found that both the dimensionless resonant amplitudes and natural frequencies decrease with increase in *H*/*B* ratio.

The effect of R_o/m ratio on the frequency-amplituderesponseis alsoinvestigatedforhomogeneousandlayeredsystems.It is observed that the maximum value of dimensionlessfrequencyis lower and the maximum dimensionless amplitude is higherfor$(R_o/m)_1$thanthosefor$(R_o/m)_2$forbothhorizontal androckingmotion.Theparametricstudyisalsocarriedoutforthecaseofblock foundation with dimensions of4 m 3m 2 m and8m 5m 2 m, using normalized graphs proposed in the presentwork.Thevaluesoftranslationalandrotationalamplitudescorrespondingtotheir natural frequencies are presented. It is observed fromTables2and3thatthenaturalfrequenciesareloweran dtheresonantamplitudesarehigherforsoilebasaltsystem ascomparedtothosefor all other rockebasalt systems, because of the lowshearwavevelocityratioofsoilebasaltsystem.Thebestpossibleoptiontobeconsideredasfoundationmediumforblockfoundationistheonehaving high natural frequency and low resonantamplitude.

Therefore,thelimestoneebasaltsystemcanbeconsidered asgood foundation medium for the blockfoundation.

REFERENCES

[1] Arnold RN, Bycroft GN, Warburton GB. Forced vibrations of a body on an infiniteelastic solids. Journal of Applied Mechanics 1955;77:391e401.

[2] Beredugo YO, Novak M. Coupled horizontal and rocking vibration of embeddedfootings. Canadian Geotechnical Journal 1972;9(4):477e97.

[3] Gazetas G, Stokoe KH. Free vibration of embedded foundations: theory versusexperiment. Journal of Geotechnical Engineering 1991;119(9):1382e401.

[4] Gupta AS, Rao KS. Index properties of weathered rocks: inter-relationships andapplicability. Bulletin of Engineering Geology and the Environment 1998;57(2):161e72.

[5] Hadjian AH, Luco JE. On the importance of layering on impedance functions. In:Proceedings of the 6th WCEE, New Delhi; 1977.

[6] Hsieh TK. Foundation vibrations. Proceedings of the Institution of Civil Engineers e

[7] Civil Engineering 1962;22:211e26.

[8] Kausel E. Forced vibrations of circular foundations on layered media. PhD Thesis.

[9] Cambridge,MA,USA:MassachusettsInstituteofTechnology(MIT); 1974.

[10] Kausel E, Ushijima R. Vertical and torsional stiffness of cylindrical footing. CivilEngineeringDepartmentReportR79e6.Cambridge,MA,USA:MIT;1979.

[11] KagawaT,KraftLM.Machinefoundationsonlayeredsoildeposits.In:Proceedingsof the 10th international conference on soil mechanics and foundation engi-neering; 1981. p.249e52.

[12] KumarA,MannaB,RaoKS.Dynamicresponseofblockfoundationsrestingonsoilerock and rockerock system under vertical excitation. Indian GeotechnicalJournal2013;43(1):83e95.

[13] Lamb H. On the propagation of tremors over the surface of an elastic solid. Philo-sophical Transactions of the Royal Society A 1904;203:1e42.

[14] Lysmer J. Vertical motion of rigid footings. Report No. 3. Vicksburg, MS, USA: U.S.Army Engineer Waterways Experiment Station; 1965.

[15] Lysmer J, RichartJr FE. Dynamic response of footings to vertical loading. Journal ofSoil Mechanics and Foundation Engineering Division 1966;92(1):65e91.

[16] Lysmer T, Waas G. Shear waves in plane infinite structure. Journal of EngineeringMechanics 1972;98(1):85e105.

[17] Novak M, Sachs K. Torsional and coupled vibrations of embedded footings. Inter-national Journal of Earthquake Engineering and Structural Dynamics 1973;2(1):11e33.

[18] Novak M, El-Naggar MH, Sheta M, El-Hifnawy L, El-Marsafawi H, Ramadan O.DYNA5da computer program for calculation of foundation response to dy-namic loads. London, UK: Geotechnical Research Centre, University of WesternOntario;1999.

[19] Richart FE, Hall JR, Woods RD. Vibrations of soils and foundations. Englewood Cliffs,NJ, USA: Prentice-Hall, Inc.; 1970.

[20] Reissner E. Stationare, axialsymmetrischedurcheineschuttelnde masse erregtoschwingungeneineshomogenenelastischenhalbraumes. Ingenieur 1936;7(6):381e96 [in German].

[21] Urlich CM, Kuhlemeyer RL. Coupled rocking and lateral vibrations of embeddedfootings. Canadian Geotechnical Journal 1973;10(2):145e60.

[22] Veletsos AS, Wei YT. Lateral and rocking vibration of footings. Journal of Soil Me-chanics and Foundation Division 1971;97(9):1227e48.

[23] VeletsosAS,Verbiˇc B.Vibrationofviscoelasticfoundations.EarthquakeEngineeringand Structural Dynamics1973;2(1):87e102.

[24] Veletsos AS, Nair VVD. Torsional vibration of viscoelastic foundation. Journal ofGeotechnical Division1974;100(3):225e46.

[25] Warburton GB. Forced vibration of a body upon an elastic stratum. Journal ofApplied Mechanics1957;24(1):55e8.

[26] Xiao Y, Liu H, Chen Y, Jiang J. Bounding surface model for rockfill materialsdependent on density and pressure under triaxial stress conditions. Journal ofEngineering Mechanics 2014a;140(4):04014002.

[27] Xiao Y, Liu H, Chen Y, Jiang J. Bounding surface plasticity model incorporating thestate pressure index for rockfill materials. Journal of Engineering Mechanics2014b;140(11):04014087.

[28] Xiao Y, Liu H, Sun Y, Liu H, Chen Y. Stress-dilatancy behaviors of coarse granularsoils in three-dimensional stress space. Engineering Geology 2015;195:104e10.Xiao Y, Desai CS. General stress-dilatancy relation for granular soils. Journal of

[29] Geotechnical and Geoenvironmental Engineering 2016;142(4):02816001.

[30] Xiao Y, Liu H, Ding X, Chen Y, Jiang J, Zhang W. Influence of particle breakage oncritical state line of rockfill material. International Journal of Geomechanics2016;16(1):04015031.

[31] Zhao J. Handbook on rock mechanics for civil engineers. Lausanne, Switzerland:DepartmentofCivilandEnvironmentalEngineering,SwissFederalInstituteofTechnology;2010.

★★★

EXECUTION EXAMINATION OF PIEZO-CLAY COMPONENTS I SOIL: A REVIEW

[1]MINAKSHEE MAHANANDA, [2]NAYAN KISHOR GIRI, [3]NILANCHALA SWAIN

[1]Assistant Professor, Department of Civil Engineering, NMIET, BBSR
[2]Asst Professor, Department of Civil Engineering CEC Bhubaneswar
[3]Asst Professor, Department of Civil Engineering AIET Bhubaneswar

Abstract -
Piezoceramic components are the electro-mechanical transducers which produce shear and pressure waves. Utilization of these piezoceramic drinking spree/extender components is an arising pattern in geotechnical designing for deciding different soil properties. Nonetheless, wave speeds utilizing piezoceramic elements are influenced by different factors, for example, the drinking spree soil communication, sorts of info waves, molecule size and shape, measurement of soil example, contact conduct, reflection and refraction wonders and different hardware boundaries, for example, recurrence, plentifulness, electro-mechanical properties and math of drinking spree/extender components. Keeping this in view, a point by point audit and examination of the outcomes from drinking spree/extender component testing as accessible in writing was done and is introduced in this paper. Butt-centric ysis of the test outcomes accessible in writing has been finished regarding different components influencing wave speed and the strategy for translation. Result from the current work should be helpful for determination of different estimating boundaries during drinking spree/extender tests in soils.

I. INTRODUCTION

The concept of piezo-electricity was first discovered by Jacques and Pierre Curie in 1880 [1]. Based on this concept later on, var- ious Piezoceramic actuators and sensors were developed which havewideapplicationsinvariousfieldsofengineering,medicaland interdisciplinary research for non-destructive testing of different materials [2]. Bender/extender elements are one of these electro- mechanical transducers which work on piezo-electric effect [3,4].These are small sized cantilever beams made up of pure semicon- ductors such as quarts (natural) or Lead zirconate-titanate/Barium titanate (man-made) to generate shear and compression waves in the laboratory [5,6]. The material experiences a change inits physical dimensions in the form of bending or extending with the application of electric potential across it and vice-versa [4,7–9].Behaviour of the element, thus acting as a bender or extender (and hence generating shear and compression waves, respectively) depends upon the direction of polarization (same/opposite) and the types of connection (series/parallel) of two individual piezo-ceramic plates sandwiched to a central electrode. During theinitial stages of research, one set of piezoceramic elements (trans-mitter and receiver) was used to act either as a bender or an extender. Later on, some of the researchers developed novel ben-der/extender element that allows a single set of transducers to function both as bender and extender with the help of a master control box[10]. Since last few decades, use of these piezoce- ramic bender elements is becoming more and more popular in advanced geotechnical investigations because of its simplicity and non-destructive nature [11–14]. Researchers have incorporated the bender elements in various laboratory testing equipments like tri- axial cell, oedometer, resonant column apparatus and torsional shear testing devices [14–20]. Shear wave velocity thus obtained, hasbeencorrelatedwithvariousengineeringpropertiesof soilsviz., unconfined compressive strength, undrained shear strength, pois- son's ratio, shear modulus, SPT (Standard Penetration Test) valueetc [16,21–23]. Moreover, researchers have developed empirical relationships between the shear wave velocity and various index properties of soil viz, void ratio, compression index, liquid limit etc. [24].

However, applicability of bender/extender elements for in-situ testing is still questioned by many of the researchers due to itsfunc-tioninthesmallstrainrangeandthepresenceofhighnoiselevelsin the signals caused by surrounding effects. Nonetheless, some of the researchers [25]. have proposed the use of portable bender element device as a non-destructive technique in the field for sample quality assessment of soft clayey soils. On the other hand, bender element tests have been performed by some of the researchers on different soil specimens with various confining stresses to simulate the real field conditions in the laboratory [21,26–29]. However, interpreta- tion of waves obtained from the bender/extender elements in these soils has been a challenging task always because, there are many factors which largely affect signal interpretation viz., soil proper- ties and its geometry, material properties of bender element and its dimensions, reflection/refraction of waves from boundary wall of soil sample and various electro-mechanical parameters like fre- quency, amplitude etc. [14,16,17,21,30]. Influence of these factors causes various types of complications in the waveforms like sig-nal noise, wave attenuation, electro-magnetic coupling, near field effect etc., which in turn make it difficult to interpret the signals in a proper manner.

As such, no guidelines, standards or any methodology exists as on date to overcome these limitations. Therefore, it is highly recommended to study the parameters affecting wave velocities and get the solutions related to problems in wave inter-pretations in different types of soil and under different laboratory conditions. This will help to come up with some outputs that canbeacceptableuniversally.Forthispurpose,itisveryessentialto assemble,compileandanalysetheavailabledatafromliteraturein a precisemanner. Keeping this in view, an extensive review of literature related to bender/extender testing and signal interpretation in different types of soils was carried out and data collection was done for further analysis. The properties of soil samples and its geometry,soilfabricanisotropy,geometryofbender/extenderelement, frequency of excitation and its amplitude, types of input waves, soil-elementinteraction,wavereflectionandrefractionhavebeen studiedinrelationtodifferentwavevelocitymeasuringtechniques such as time domain, frequency domain and cross-correlation. Problems associated with travel time measurement such as wave attenuation,electro-magneticcoupling,nearfieldeffectshavebeen discussed briefly and efforts have been made to minimize these problems from literature survey. The outcome from the present workissupposedtobeveryusefulinselectingdifferentmeasuring parameters during bender/extender tests insoils.

II. WORKING PRINCIPLE OF PIEZOCERAMIC BENDER/EXTENDER ELEMENTS

Forthefirsttime,piezo-electricmaterialwasusedbyShirleyand Hampton in 1978 [5,31–33] as bender/extender elements in exper-imental soil mechanics. As mentioned earlier, bender/extender elements are the transducers used to transmit and receive shear (S-) and compression (P-) waves through soil sample [10,32]. It com- prise of two strips/plates of ceramic material bonded together by a conductive central metal shim and two conductive outer electrodes as shown in Fig. 1(a). Depending upon the elemental polarization and wiring configuration, the transducers can act as a transmitter (actuator) or receiver (sensor)[34].

When, an instantaneous and strong electric field is applied to the ceramic plates, it get polarized [13,33]. Direction of this polar- ization (same or opposite) in two plates of the bender/extender and its wiring configuration (series or parallel) has been investigated by many of the researchers [34,35] for optimization of results in differ- ent soils under different laboratory testing conditions. It has been foundthat,wiringconfigurationinparallelandpolarizationinsame direction makes the piezoceramic elements to behave as bender and it can be used as a transmitter (actuator) for S- waves as shown inFig.1(b).Similarly,wiringconfigurationinseriesandpolarization in opposite direction also makes the elements to behave as bender but that can be used as a receiver (sensor) for S- waves as shown in Fig. 1(c). On the other hand, elements with wiring configuration in parallel and polarization in opposite direction act as P- wave trans- mitter (extender) as shown in Fig. 1(d) whereas; elements with wiring configuration in series and polarization in same direction acts as P- waves receiver (extender) as shown in Fig. 1(e). Stud- ies reveals that the elements with parallel type connection exhibit twice the displacement as that of series type connection and hence the parallel type connection is best suited to act as a transmitters and series type as receiver [35]. Fig. 1 shows bender/extenders and its motions upon triggering the transmitter for S- and P- waves. However,itcanbementionedherethatthestrainlevelcausedin thesoilsamplesduetopropagationofwavesfrombender/extender is very less and is in the range of 10−4 which does not induce any deformation in the soil specimen.

III. MEASUREMENTOFWAVEVELOCITYUSINGBENDER/EXTENDER ELEMENT

Bender/extender elements are generally incorporated in con- ventional apparatus in order to measure the P- or/and S- wave velocity [5,36,37]. The transmitter and receiver elements are insertedatthetwooppositeendsofsoilspecimensandthetime lag (*t*), between the input and output wave signals are measured by triggering and propagating a wave impulse through the soil spec- imen at certain frequency and voltage [11]. Wave velocity is then computed using Eq. (1) as follows:

$$V = L_{tt}/t \qquad (1)$$

Where, *V* denotes wave velocity ($V_s$for shear wave and $V_p$for compressionwave)andL_{tt}isthetip-to-tipdistancebetweentrans-mitter and receiver as shown in Fig. 2[29,31,38].

Consideringsoilasanelastic,isotropic,infiniteandhomogenous continuum,researchers[39,40]haveproposedEq.(2)forcompres-sion waves asfollows:

$$\frac{\iota^2 u_x}{\iota t^2} = \frac{M}{p} \cdot \frac{\iota^2 u_x}{\iota x^2} (\text{P} - \text{waveequation}) \qquad (2)$$

Where, $u_x$is the particle motion in x- direction and *M* is the con-strainedmodulus.Similarly,Eq.(3)isproposedforshearwavesas follows:

$$\frac{\iota^2 u_y}{\iota t^2} = \frac{G}{p} \cdot \frac{\iota^2 u_y}{\iota x^2} (\text{S} - \text{waveequation}) \qquad (3)$$

Where,$u_y$istheparticlemotioniny−directionand*G*istheshear modulus.Bysubstituting,u_x=$Ae^{j(mt-kx)}$andu_y=$Ae^{j(mt-kx)}$inEqs.(2)

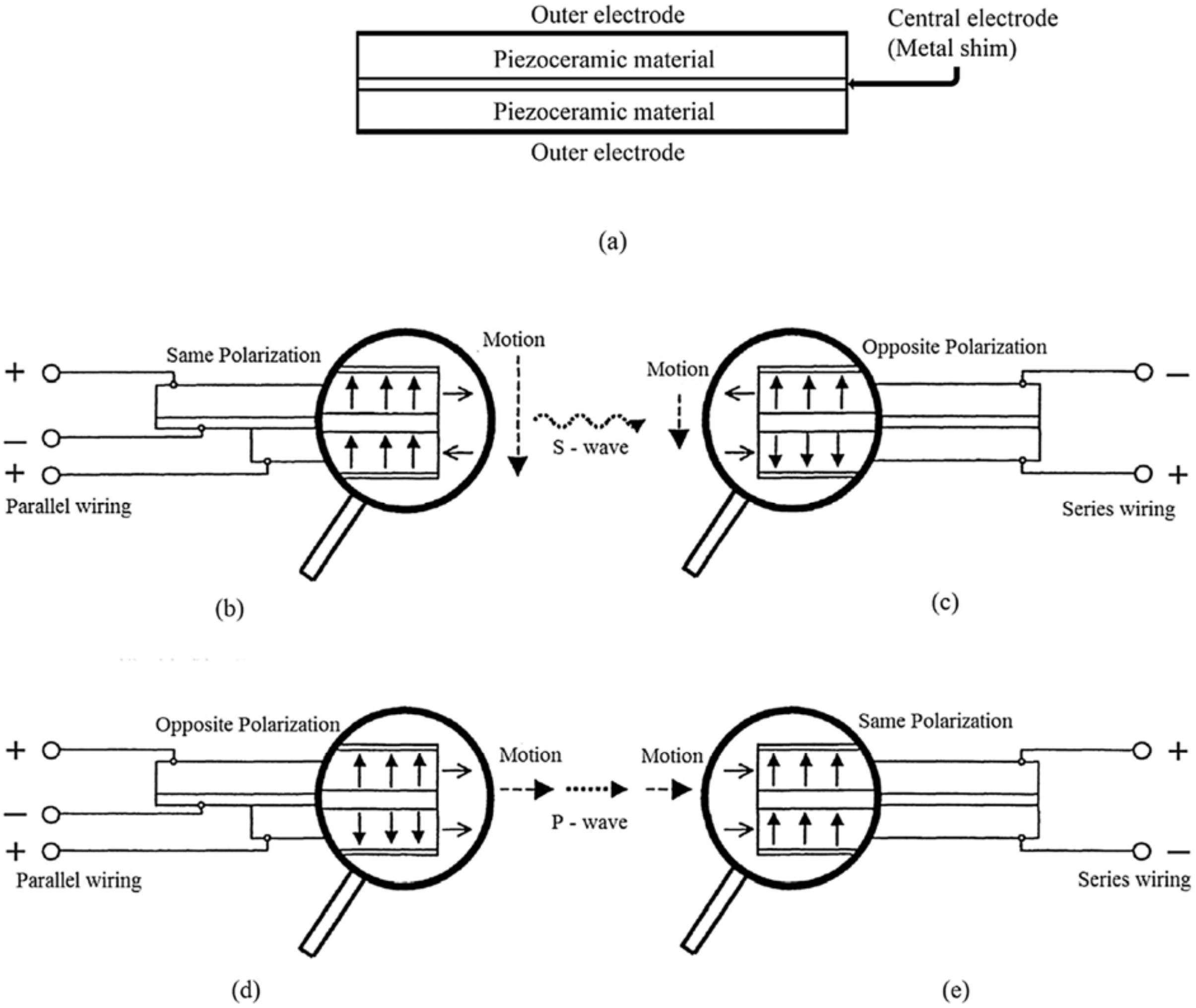

Fig. 1. Piezoceramic Elements [10]: a>) General Schematic representation, (b) Bender transmitter (c) Bender receiver (d) Extender transmitter (e) Extender receiver.

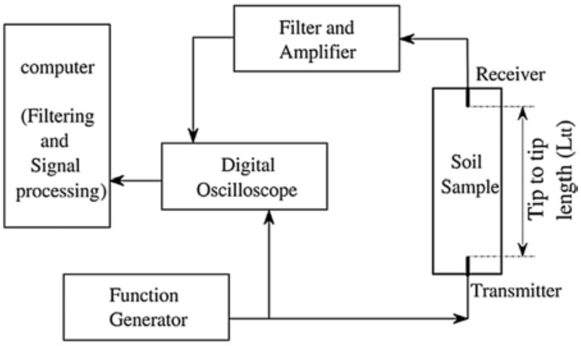

Fig. 2. Schematic representation of bender element test setup.

and(3),itisfoundthatm/k= $\sqrt{M/p}$ andm/k= $\sqrt{G/p}$ forP- and S- waves, respectively.

where, t is the time, p is the density of material, A is the maximum amplitude of motion, $>m = 2w/T$ is the temporal angular frequency, $k = 2w/h$ is the spatial frequency or wave number, T is the time period and h is the wavelength. However, $>\omega/k = T$ which represents the wave velocity. Hence,

$$V_P = \sqrt{M/p} \tag{4}$$

$$V_s = \sqrt{G/p} \tag{5}$$

Some researchers have considered end-to-end length of thesoil specimen for calculating the wave velocity, while a few of them have adopted the tip-to-tip distance [34,35,41]. As the bender/extenderelementprotrudesintosoilspecimenfromsurfaceof theendcap,itisdifficulttodecidewhetherthetravellengthisconsideredasfullspecimenlengthortiptotipdistanceorsome other intermediateeffectivedistance.Inthisregard,Dyvicand Madshus in 1985[42]through their studies concluded that, tip-to-tip distance measurement technique gives best agreement as compared to other techniques. This is due to the reason that waves first get transferred from the tip of transmitter element to the soil specimenandisfirstreceivedbystrikingtothetipofreceiverelement. ViggianiandAtkinson[4]havealsoperformedtestsbyvaryingthe lengthofsoilspecimensandreachedthesameconclusion. Thetestsetupsformeasuringwavevelocities($V_p$andV_s)comprise ofafunctiongeneratortosupplyandcontroltheinput voltage and excitation frequency to the transmitting element. To pro- cess the output signal from the receiver, a filter-amplifier unit is required so as to get a clear waveform which is free from noise anddistortion.Interpretationoftheseinput(I/P)andoutput(O/P) signals from the transmitter and receiver can be done by simple eyeobservationsusinganoscilloscope.Further,analysisofwaveformusingdigitalfilterprogramsthroughnumericalanalysiscan beperformedbyusingFastFourierTransformation(FFT) andCross Correlation(CC)techniquesasexplainedinthefollowing sections [34,43]. Moreover, the circuitry system can be modified so as to measure the wave velocities in two different directions, simultaneously.SuchatestsetupisillustratedinFig.3[44]thatconsistsof two sets of transmitters and receivers, inserted both laterally and vertically.Ontheotherhand,someoftheresearchershave adopted disctypepiezoceramicelements,wherethediscsaremade ofLead Zirconate-Titanate(PZT)material(20mmdiaand2mmthick).A typical test setup using disc type piezoceramic element is illus- trated in Fig. 4(a) [28]. Bending discs are generally modelled to transmitandreceivecompressionwavesbutitisworthmentioning that the mounting technique for bending discs is totallydifferent from bender/extender strip element. Bender element ismounted asafixedcantileverbeamwhereasbendingdiscisrestrainedlike hingealongthecircumferenceasshowninFig.4(b).When bending discisexcited,centreofthediscmovesbackandforthsoastoapply impactonthematerialgeneratingcompression(P-)waves[45].In future, bending discs can be proved to be useful for testing rock specimensifpropercouplingbetweenthediscandrockspecimen is achieved. This is because of making groove in rock specimens for bender element insertion is difficult and hence there aremore chances of getting unrealisticwaveforms.

IV. STRAIN LEVEL IN BENDER/EXTENDERTESTING

The shear (S-) and compression (P-) wave velocities depend mainly on soil stiffness and hence are related to the shear modulus(*G*)andconstrainedmodulus(*M*),respectively[46–48].Onthe otherhand,theelasto-plasticbehaviourofsoilincludingtheshear andconstrainedmoduluslargelydependsuponappliedstrainlevel [49].Since,thereisavariationintheappliedstrainlevelexhibited bydifferenttechniques;theresultobtainedfromdifferent methods alsovariesfromeachother.Variousfieldtestssuchasthedownhole seismic tests, cross hole test, seismic reflection and refractiontest andthespectralanalysisofsurfacewaves(SASW)generatesdata athigherstrainlevels[49–51].Resonantcolumntestandthecyclic triaxialtestsuptosomeextent,measuresoilpropertiesatsmallto mediumstrainslevel.Ontheotherhand,bender/extenderelement test is non-destructive in nature which measure soil properties at verysmallstrainlevel.Therangeofstrainlevelduringthe measurementofsoilpropertiesinvariousfieldandlabtestsisdepictedin Fig.5.Itistomentionherethatmaterialbehavesalmostaslinearly elastic within very small strain range and it behavesnon-linearly withfurtherincreaseinshearstrain.Finally,thematerialtendsto fail at larger strain at which the deformation is non-recoverable [52,53]. Hence, shear modulus that is related to the shear wave velocity, $V_s$in bender element tests is comparatively higher than the shear modulus obtained from other methods[11,27,37,54,55].

V. GEOMETRY OF BENDER/EXTENDER ELEMENTS USED BY PREVIOUS RESEARCHERS

Depending upon the physical and electrical properties of piezoceramic materials, different dimensions and shape of bender/extenderelementshavebeenadoptedorfabricatedby different researchers for their experimental studies. It is found that, for a given configuration of bender/extender element, tip deflection and hence the output signal strength depends upon the protrusion length as well as the width (*w*) of bender/extender elements [21].As such, length of the bender/extender elements adopted by the previous researchers varies from 7 to 31.8 mm and the width from2 to 17 mm. The dimensions of a list of bender elements used by previous researchers during the last three to four decades are pre- sented in Table. 1. Moreover, a graphical representation of aspect ratio corresponding to the numbers of articles available in litera- ture is presented in Fig. 6. The larger the width of bender/extender, higher will be the transmitting force but lower the output voltage at receiver. On the other hand, narrow width of receiver element causes higher output voltage for the given input force [21]. Similarly, larger the thickness of bender/extender element, lower willbe the deflection of tip element and hence the output voltage at receiver. As such, the thickness of bender/extender elements adopted by the previous researchers ranges from 0.38 to 6.1 mm, although, most of them have adopted a thickness of 0.5–0.7 mm. Moreover, it is reported that the bender elements with higher aspect ratio yield low resonance frequency [33]. Nonetheless, some researchers have suggested to use bender element with higher aspect ratio enabling it to exhibit different resonant frequency in different soils and thus enhancing its energy transmission ability [3]. Measurement of wave velocity in soil samples with higher length requires high power waves to reach the receiver. In such cases, higher aspect ratio of the piezoceramic elements is required to generate high input power and excitation frequency to achieve large deflections [45]. In addition, the length to thickness ratio of the bender element governs its stiffness and behaviour as transmitter, whereas, the length to width ratio governs the output voltage at receiver element, which ultimately affects its performance during the experiments. However, it is also to be noted that the performance of bender element depends mainly on the types of piezoceramic material, its microstructure and porosity [56,57].Also, resonant frequency of bender/extender element affects the size of near field in travel time determination and hence is an important design parameter for bender/extender installations [48].Likewise, resonant frequency (f_r), length of bender/extender element (L_b), moment of inertia (I) and elastic modulus (E_b) are largely dependent on physical and mechanical properties of bender/extenderelements.Whenbenderelementdeflectsinair(ref

Table 1
Soil and bender/extender element properties and wave parameters adopted by various researchers

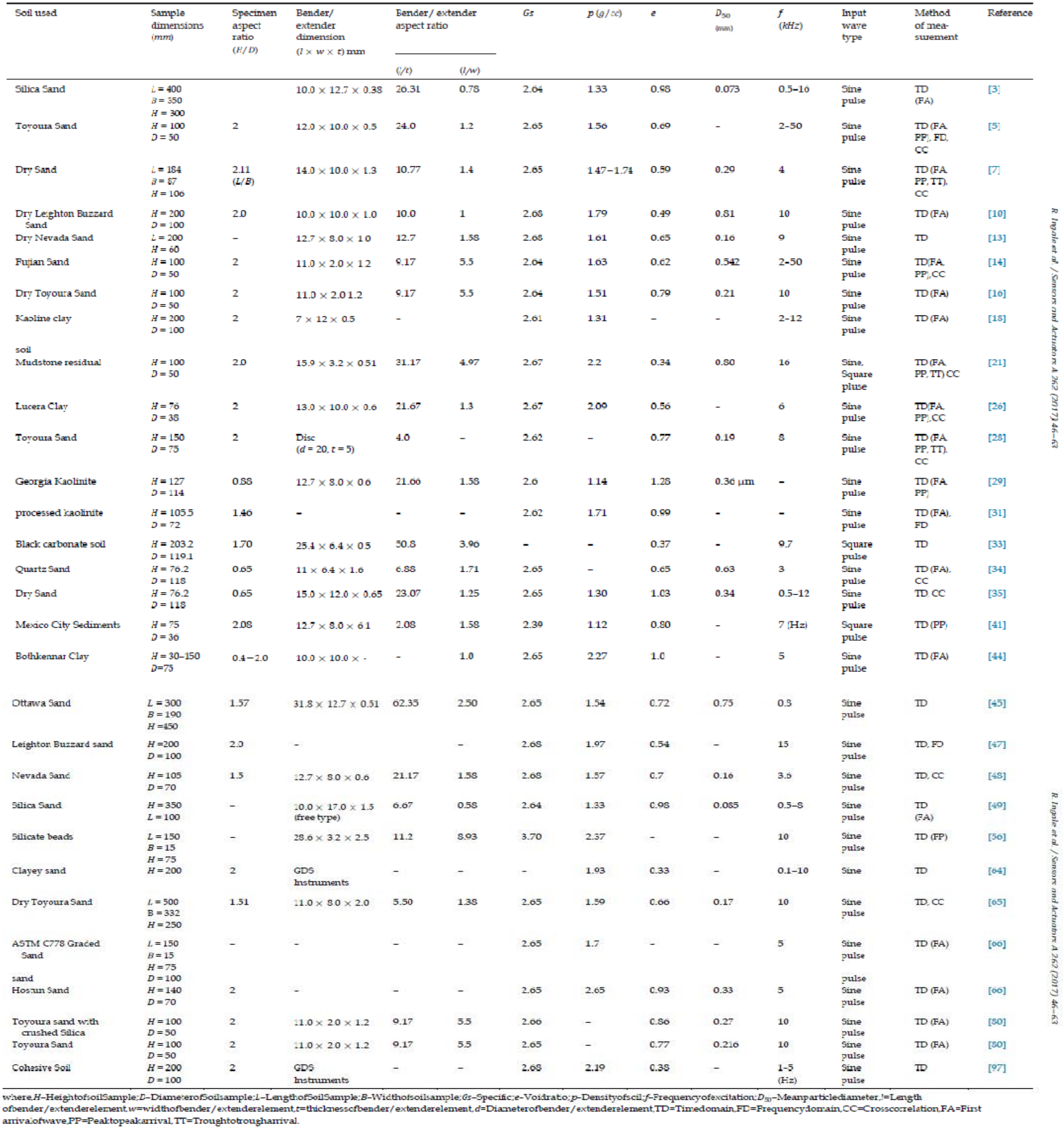

Soil used	Sample dimensions (mm)	Specimen aspect ratio (H/D)	Bender/ extender dimension (l × w × t) mm	Bender/ extender aspect ratio		Gs	ρ (g/cc)	e	D_{50} (mm)	f (kHz)	Input wave type	Method of mea- surement	Reference
				(l/t)	(l/w)								
Silica Sand	L = 400 B = 350 H = 300		10.0 × 12.7 × 0.38	26.31	0.78	2.64	1.33	0.98	0.073	0.5–16	Sine pulse	TD (FA)	[3]
Toyoura Sand	H = 100 D = 50	2	12.0 × 10.0 × 0.5	24.0	1.2	2.65	1.56	0.69	–	2–50	Sine pulse	TD (FA PP), FD, CC	[5]
Dry Sand	L = 184 B = 87 H = 106	2.11 (L/B)	14.0 × 10.0 × 1.3	10.77	1.4	2.65	1.47–1.74	0.59	0.29	4	Sine pulse	TD (FA PP, TT), CC	[7]
Dry Leighton Buzzard Sand	H = 200 D = 100	2.0	10.0 × 10.0 × 1.0	10.0	1	2.68	1.79	0.49	0.81	10	Sine pulse	TD (FA)	[10]
Dry Nevada Sand	L = 200 H = 60	–	12.7 × 8.0 × 1.0	12.7	1.58	2.68	1.61	0.65	0.16	9	Sine pulse	TD	[13]
Fujian Sand	H = 100 D = 50	2	11.0 × 2.0 × 1.2	9.17	5.5	2.64	1.63	0.62	0.542	2–50	Sine pulse	TD(FA PP),CC	[14]
Dry Toyoura Sand	H = 100 D = 50	2	11.0 × 2.0 1.2	9.17	5.5	2.64	1.51	0.79	0.21	10	Sine pulse	TD (FA)	[16]
Kaoline clay	H = 200 D = 100	2	7 × 12 × 0.5	-		2.61	1.31	–	-	2–12	Sine pulse	TD (FA)	[18]
soil Mudstone residual	H = 100 D = 50	2.0	15.9 × 3.2 × 0.51	31.17	4.97	2.67	2.2	0.34	0.80	16	Sine, Square pluse	TD (FA PP, TT) CC	[21]
Lucera Clay	H = 76 D = 38	2	13.0 × 10.0 × 0.6	21.67	1.3	2.67	2.09	0.56	-	6	Sine pulse	TD(FA PP),CC	[26]
Toyoura Sand	H = 150 D = 75	2	Disc (d = 20, t = 5)	4.0	–	2.62	–	0.77	0.19	8	Sine pulse	TD (FA PP, TT), CC	[28]
Georgia Kaolinite	H = 127 D = 114	0.88	12.7 × 8.0 × 0.6	21.66	1.58	2.6	1.14	1.28	0.36 μm	-	Sine pulse	TD (FA PP)	[29]
processed kaolinite	H = 105.5 D = 72	1.46	-	-	-	2.62	1.71	0.99	-	-	Sine pulse	TD (FA), FD	[31]
Black carbonate soil	H = 203.2 D = 119.1	1.70	25.4 × 6.4 × 0.5	50.8	3.96	-	-	0.37	-	9.7	Square pulse	TD	[33]
Quartz Sand	H = 76.2 D = 118	0.65	11 × 6.4 × 1.6	6.88	1.71	2.65	–	0.65	0.63	3	Sine pulse	TD (FA), CC	[34]
Dry Sand	H = 76.2 D = 118	0.65	15.0 × 12.0 × 0.65	23.07	1.25	2.65	1.30	1.03	0.34	0.5–12	Sine pulse	TD CC	[35]
Mexico City Sediments	H = 75 D = 36	2.08	12.7 × 8.0 × 6.1	2.08	1.58	2.39	1.12	0.80	–	7 (Hz)	Square pulse	TD (PP)	[41]
Bothkennar Clay	H = 30–150 D=75	0.4–2.0	10.0 × 10.0 × -	–	1.0	2.65	2.27	1.0	–	5	Sine pulse	TD (FA)	[44]
Ottawa Sand	L = 300 B = 190 H =450	1.57	31.8 × 12.7 × 0.51	62.35	2.50	2.65	1.54	0.72	0.75	0.3	Sine pulse	TD	[45]
Leighton Buzzard sand	H =200 D = 100	2.0	–		–	2.68	1.97	0.54	–	15	Sine pulse	TD, FD	[47]
Nevada Sand	H = 105 D = 70	1.5	12.7 × 8.0 × 0.6	21.17	1.58	2.68	1.57	0.7	0.16	3.5	Sine pulse	TD, CC	[48]
Silica Sand	H = 350 L = 100	–	10.0 × 17.0 × 1.5 (free type)	6.67	0.58	2.64	1.33	0.98	0.085	0.5–8	Sine pulse	TD (FA)	[49]
Silicate beads	L = 150 B = 15 H = 75	–	28.6 × 3.2 × 2.5	11.2	8.93	3.70	2.37	–	–	10	Sine pulse	TD (FP)	[56]
Clayey sand	H = 200	2	GDS Instruments	–	–	–	1.93	0.33	–	0.1–10	Sine	TD	[64]
Dry Toyoura Sand	L = 500 B = 332 H = 250	1.51	11.0 × 8.0 × 2.0	5.50	1.38	2.65	1.59	0.66	0.17	10	Sine pulse	TD, CC	[65]
ASTM C778 Graded Sand	L = 150 B = 15 H = 75	–	–	–	–	2.65	1.7	–	–	5	Sine pulse	TD (FA)	[66]
sand	D = 100										pulse		
Hostun Sand	H = 140 D = 70	2	–	–	–	2.65	2.65	0.93	0.33	5	Sine pulse	TD (FA)	[66]
Toyoura sand with crushed Silica	H = 100 D = 50	2	11.0 × 2.0 × 1.2	9.17	5.5	2.66	–	0.86	0.27	10	Sine pulse	TD (FA)	[80]
Toyoura Sand	H = 100 D = 50	2	11.0 × 2.0 × 1.2	9.17	5.5	2.65	–	0.77	0.216	10	Sine pulse	TD (FA)	[80]
Cohesive Soil	H = 200 D = 100	2	GDS Instruments	–	–	2.68	2.19	0.38	–	1-5 (Hz)	Sine pulse	TD	[97]

where,H–HeightofsoilSample;D–DiameterofSoilsample;L–LengthofSoilSample;B–Widthofsoilsample;Gs–Specific;e-Voidratio;p–Densityofsoil;f–Frequencyofexcitation;D_{50}–Meanparticlediameter,l=Length ofbender/extenderelement,w=widthofbender/extenderelement,t=thicknessofbender/extenderelement,d=Diameterofbender/extenderelement,TD=Timedomain,FD=Frequencydomain,CC=Crosscorrelation,FA=First arrivalofwave,PP=Peaktopeakarrival,TT=Troughtotrougharrival.

R. Ingale et al. / Sensors and Actuators A 262 (2017) 46–63

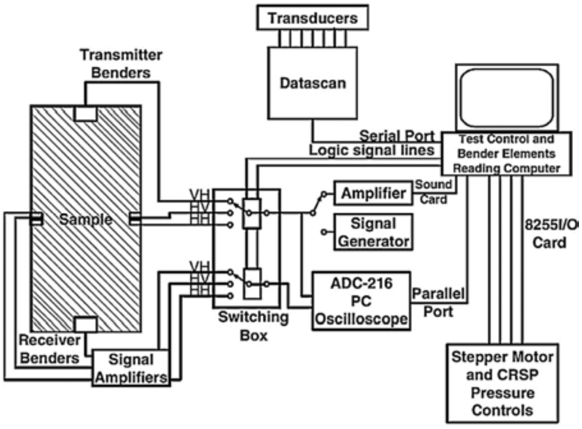

Fig. 3. Schematic representation of modified bender element test setup [44].

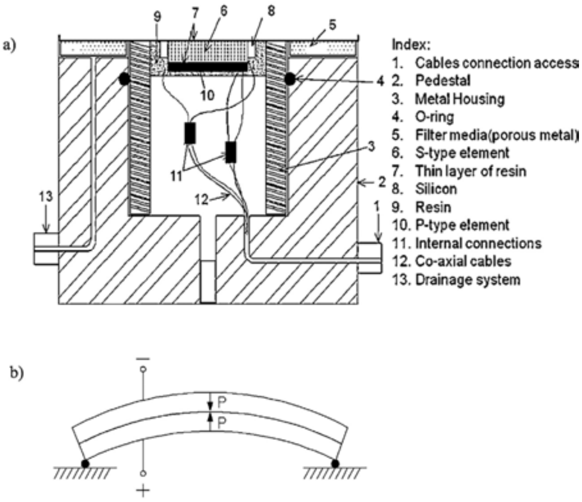

Fig. 4. (a) Disc type piezoceramic element housed in pedestal (b) working mechanism of disc element [28].

Fig. 7), its resonant frequency can be described with fixed-free boundary conditions for first mode [48] as follows:

$$f_r = \frac{\omega}{2w} = \frac{1}{2w}\frac{k_b}{m_b} = \frac{1}{2w}\frac{1.875\ E_b I}{m(\,L_b)^4}\ 4 \tag{6}$$

Where, $k_b$is the equivalent spring constant, $m_b$is the cantilever mass of piezoceramic element ($m_b= mL_b$), $L_b$is the cantilever length,*m*ismassperunitlengthandaistheeffectivelengthfactor affected by the anchor efficiency (a = 1 for perfectly rigid anchor andgreaterthan1forsoftanchor)and$k_b=1.8754E_bI/(\,L_b)$ 3.Themassofbenderelementis$m_b=pbbt$.where,(aL_b)where,*b*and*t*are width and thickness of benderelement.

The behaviour of the bender element when buried in soil sample gets affected by several soil parameters such as density, stiffness, modulus of elasticity etc. The soil stiffness $k_s$can be obtained by using Mindlins solution for point load integrated to rectangular geometry [58] as follows:

$$k_s = yE_sL_b \tag{7}$$

Where,µ=2andisthemeandisplacementinfluencefactor atthe soil–elementinterface.$E_s$istheelasticmodulusofsoilwhichcanbe

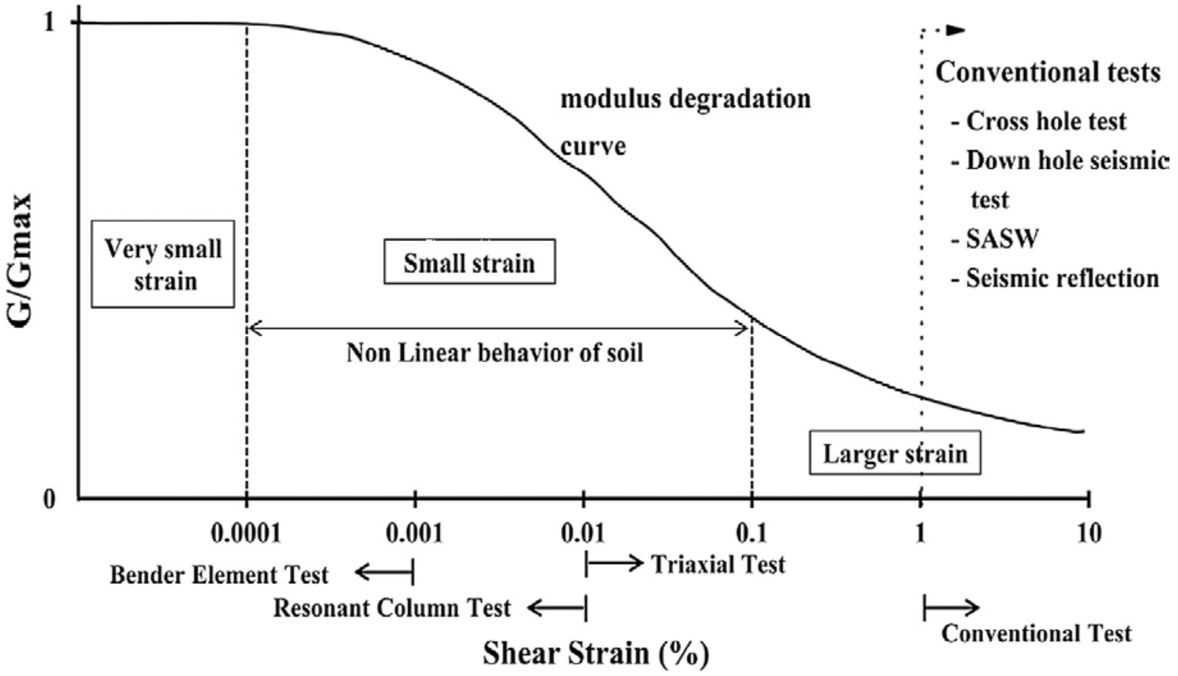

Fig. 5. Normalized stiffness degradation curve with increasing shear strain.

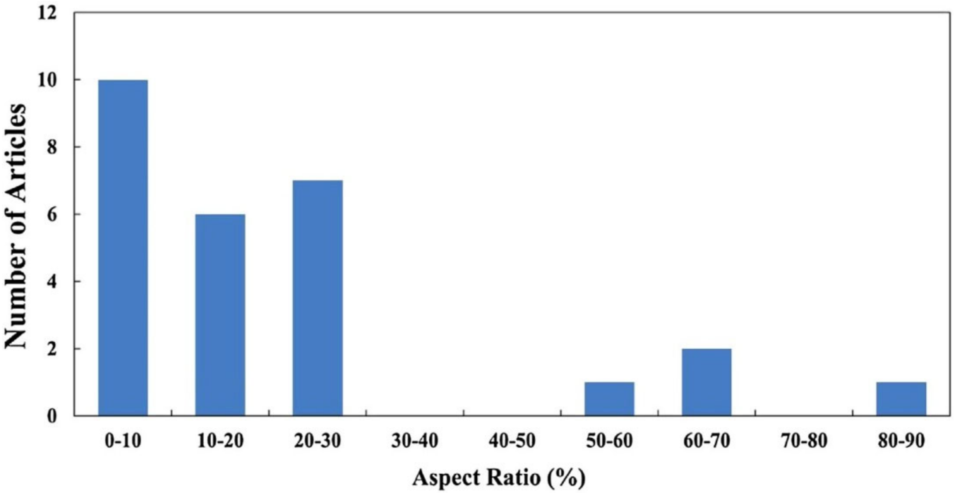

Fig. 6. Graphical representation of aspect ratio as used by previous researchers.

calculatedfrompoisonsratio(τ)anddensity(p)ofthesoil. Then,theequivalentspringconstant$K_s$willbecome

$$K_s=2yV^2p_s(1+T)L_b \tag{8}$$

Theeffectivesoilmass,$m_s$isrelatedtothevolumeb^2L_basfollows:

$$m_s= p_sb^2L_b \sum \tag{9}$$

Finally,thefirstorderresonantfrequencyofbenderelement in soil is herein obtained by combining the mass and stiffness ofthe benderelementandaffectedsoil,resultinginanequivalentspring constant$k_{eq}=k_b+k_s$andequivalentmass$m_{eq}=m_b+m_s$.

$$f_r= \frac{1}{2w}\left[\frac{\frac{1.875^{4Eb^I}}{(L_b)}+2yV^2p(1+T)L_s}{p_b bt(L_b)+p_s b^2L_b}\right]^{\sum} \tag{10}$$

However, performance of the bender/extender element is largely affected by the material properties, insertion technique in soil, shielding and grounding processes and obviously the anisotropic nature of the soilsamples.

VI. BENDER/EXTENDER AND SOIL INTERACTION

The bender/extender element configuration in experimental test setup creates various uncertainties due to mechanical and electrical defects [59]. The measurement of wave travel time is therefore largely affected by the electro-mechanical behaviour of soil-elementssystem.Although,theelectricaleffectscanbeassessed by placing the bender/extender elements in direct contact with eachother(tip-to-tip)andgettingtheresponseoftraveltime[15], mechanicalpropertiesaredifficulttoassessduetoenergyabsorbingcapacityofsoilandthesoilanisotropy.Assuch,theresponse of bender element as transmitter is controlled by the properties of piezoceramic material, unsupported length of the elementand its fixity to soil, properties of surrounding soil and the coupling between bender element and soil [48]. The response of receiver element,ontheotherhand,isnotonlyaffectedbystiffness, energy absorption characteristics and dispersive nature of soil but also by the attenuation phenomena, distance between transmitter and receiver element, boundary wall reflection, refraction and wavelength of the signals [60,61]. Moreover, impedance mismatch is a common problem associated with bender element testing in stiff soil [62]. Hence, researchers have investigated the effects of bender element installation in clay soil specimen and observed that thebenderelementcausessomelocaldisturbanceswhenit bends andthusaffectingthesurroundingsoil.Asaresult,thebenderelement also generates a P-wave component at sides of sample that disturbs the original S-wave. Hence, sometimes it is suggestedto addsomesaltsurroundingthebenderelementthatcanstrengthen thesoil.Moreover,benderelementstudiesonfullandhalf-length samples have been performed by some of the

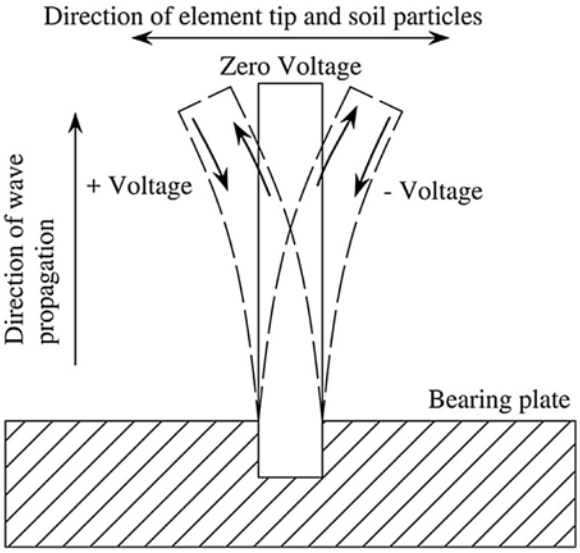

Fig. 7. Piezoceramic bender element and its movement w.r.t. applied voltage.

researchers and existence of some local effects (called near field effect) close to bender elements has been found resulting in lower velocities of about20%inhalf-lengthsamples[63].Incaseofsurfacemounted bender elements with side to side measurement of wave velocity,benderelementlengthisfoundtoinfluencethewavevelocity when centre-to-centre distance between transmitter and receiver wereadopted.Insuchcases,howeveracombinedbenderelement andaccelerometerisfoundtominimizetheimpedancemismatch between transducer and tested materials. However, in all these cases,waveattenuationisgenerallyfoundtoincreasewith increase in soil stiffness[64].

VII. METHODS FOR DETERMINATION OF WAVE TRAVEL TIME

Wave velocity can be determined by knowing the tip-to-tip distance between transducer and receiver and time required to travelthisdistance.Dependinguponthelevelofcomplexitiessuch as crosstalk effect or electro-magnetic coupling [35], near field effect [48,65] and wave attenuation [61] observed in different soil specimens,severalwavemeasuringapproacheshavebeendeveloped.Basedonthemodeofoperation,thesemethodsareclassified as time domain analysis, frequency domain analysis and cross-correlation[11,36,49,66,67].Assuch,nostandardmethodhasbeen developedtilldatefortestingandinterpretationofthetestresults. Hence,theresultsobtainedfrombender/extendertestsare highly subjectiveinnatureandinvolveshighdegreeofuncertainty.

7.1 Time domain analysis

Time domain (TD) analysis is the most commonly and widely accepted method for determination of the travel time in bender/extendertests[49,65,66].Inthismethod,thefirststart-to-start, firstpeak-to-peak,firsttrough-to-troughorzerocrossingofinput-outputwavesareusedtodeterminethetraveltimeofwaves as showninFig.8.Thismethodprovidesreasonableresultsfortravel timebutislargelyaffectedbythenearfieldeffectinlowinputfrequencyrange[61,68].However,ithasalsobeenfoundthat, when frequencyoftheinputsignalapproachestheresonantfrequencyof bender-soilsystem,thefirstarrivalmethodisnotmuchinfluenced by the input frequency and yields quite good results [49].

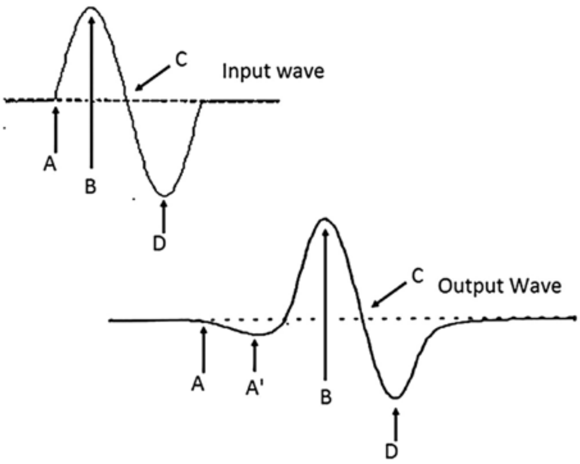

Fig. 8. Typical input and output wave: (A, A) first start-to-start; (B, B) first charac- teristic peak; (C, C) zero crossing; (D, D) first characteristic deflection.

More- over, traveltimeobtainedfromthe firstarrivalmethodisfoundto be in good agreement with the cross-correlation method in sand samplesforboththesurfacemountedandtip-to-tiparrangement of bender elements [3]. The first arrival method is still debatable due to the existence of near field effect which creates barrier in obtaining clearer waveform [5]. In addition, the S- wave velocity measurementusingfirstarrivalmethodisquietcumbersomedue to downward movement of output wave indicating the presence nearfieldcomponent[16].Inthisregard,however,somecontradictorystatementsarepresentedinliterature.ViggianiandAtkinson [4]haveconsideredthefirstarrivalofshearwaveasthepointoffirst deflection,whereas,Sanchez-salinero[61]concludedthispointof first detection as the arrival of near field components. Further, it issuggestedtoconsiderasuitableL_{tt}/hratiotominimizethe near field effect [69]. However, in the absence of any particular crite- ria for wave identification, time domain analysis is not suitable in stiff geo-materials as reported in literature [37,44,50]. Further, if the output wave signal is distorted with noise, the first arrival method is found to be unsuitable for determination of the travel time. Some of the researchers [17,54] have adopted the peak-to-peakmethodorevenconsideredthesecondarrivalofoutputwave for the determination of traveltime.

7.2 Frequency domain analysis:

The time domain method is not an effective technique to describe the dispersive nature of waves which is more or less frequency dependent [70]. On the other hand, frequency domain analysis(FD)recognisesthefrequencycontentofthetransmitted and received signals as cross-spectrum using Fourier transfor- mation [8]. This method generally assumes identical frequencies of input and output waves and compares the phase difference between corresponding Fourier components of the signals from transmitterandreceiverelements[50,54].Thetraveltime(t_t)can be computed by considering the best fitted slope of frequency (*f*) and unwrapped phase (∗) of transfer function [54] as follows:

$$t_{t} = \frac{1}{\frac{d\$2w}{df}} \tag{11}$$

Although, the frequency domain method is found to yield lower velocities as compared to the time domain method [5,50,54,71], it provides an improved understanding of the behaviour of bender-soil interaction [4]. A term named as coherence function (μ2) is normally used to describe linearity and dependencies between transmitted x(t) and received y(t) signals [72].The value of coher- ence function varies from 0 to 1, whereas, the ideal constant for linear system of single input x(t) and single output y(t), it is restricted to 1. Maximum value of coherence does not ensure the unwrapped phase function with constant slope [50]. Wave veloc- ity is decoded directly from the relative phase of transmitted and received waves signal as illustrated in Fig. 9(a) and (b) [54,72]. In case of frequency domain analysis, higher frequencies are more ideal as it mainly focuses on spectral frequency breakdown and the phase shifts[18].

7.3. Cross-Correlation

Similarity between the input and output signals as a function of the lag of one signal relative to the other can be determined usingcross-correlation.Thecross-correlationbetweentwosignals is given by Eq. (12) as follows:

$$CCxy(\imath) = \lim_{T\to\infty} \frac{1}{T} \int_{0}^{T} x(t)\,y(t+\imath)\,dt \tag{12}$$

Where, x(*t*) and y(*t*) are the transmitted and received signals, *T*is the total travel time and *ı* is the time shift between two signals. Alternatively, the cross-spectrum of input-output signals can be expressed by Eq. (13) as follows:

$$CC_{xy}(f) = X(f)\,Y(f)^{*} \tag{13}$$

Where,$CC_{xy}(f)$,$X(f)$and$Y(f)$aretheFouriertransformsof CC_{xy}(v), x(t) and y(t) respectively and the asterisk denotes complex con- jugate [3,44,50].The inverse Fourier transform of Eq. (13)yields cross-correlation between the two signals. However, this method isconsideredasatimedomaininterpretationtechnique,although, calculations need to be executed in frequency domain [37].The measurement assumes the presence of plane wave fronts and therefore the absence of reflected and refracted waveforms [17].Insoftsoils,wheresignalinterpretationisverydifficult,thecross-correlationmethodcanyieldreasonableresultsforthetraveltime bymaximumpeakpoints,iftheinputfrequencyandcharacteristics pointscorrespondingtothewavesarrivalischosencorrectly.Some researchers have validated the applicability of cross-correlation techniquewithtimedomaintechniquebyexaminingthesimilarity between the transmitted and received waveforms [21,73].How- ever, the first peak point method in cross-correlation technique doesnotprovidereasonableresultsinsandysoilsandinsuchcases the first peak method is considered to be more effective [5,37,71].Also, it is observed that the cross-correlation technique does not workasanalternativetotimedomaintechniqueincaseofsandand artificially treated soil due to discontinuities in waveformsignals duringexperimentalinvestigations[5].Itisnoteworthyto mention that, velocity obtained from cross-correlation technique is gener- ally lower than that obtained from the peak to peak method at higher excitationfrequencies[5].

VIII. FACTORS AFFECTING WAVE INTERPRETATION AND REMEDIAL MEASURES

8.1 *Wave attenuation*

Spreading of wave energy generally called as radial damping andtheenergydissipationresultingfromfrictionallossesinmate- rial causes amplitude reduction, known as wave attenuation or damping[61].Likewise,amplitudeofthearrivalsignaldecaysas the distance between source (transmitter) and target (receiver) increases.Characteristicsofmaterialandthetypesofwavelargely affecttheattenuationphenomena.Thedampingcharacteristics of different materials depends upon the capacity of the material to storeelasticstrainenergy[61].Becauseofthedampingcharacter- istics of soils, it makes the high energy transmitted waves to low energyoutputwavesignalscausingreductioninwaveamplitude [74]. Damping in soils generally increases with increase its mois- turecontent[75].Moreover,theP-waveattenuationislargerthan S-waveattenuationasobservedbyresearchersinKaolinand mudstonesoilspecimenatdifferentconfiningpressure.However,shear wave shows multiple wave attenuation characteristics than the compressionwaves.Further,theattenuationisfasterathig herexci-tation frequencies and thus creating problems to measure travel timeinsoilslikesediment,wherehigherfrequencyisrequired[51].SimilarobservationhasalsobeenmadebyChanin2012[76].Itis reportedinliteraturethat,inputwaveswithhigherexcitationfrequency(>29kHz)leadstotheovershootingofwaveswhichresults inimproperfunctioningoftheelements[30,35].Ontheotherhand, instiffandcompactedsoil,thewaveattenuationisfoundto bemore because of the greater stiffness impedance between transducers andtestedmaterials.Thisphenomenaisillustratedin Fig.10(a) [68]and Fig. 10(b) [27,35]. The attenuation generally decreases with increase in confining pressure [51]. In order to minimize wave attenuation, some of the researchers have suggestedadoptinghigherlengthtothicknessratiotohavelowresonantfrequency [33].

8.2 Electro-magnetic coupling

As already mentioned, in bender/extender elements (either transmitterorareceiver)theoutersurfaceofthetwopiezoceramic plates are provided with conductive electrodes which converts electrical energy into mechanical energy and vice-versa, causing elements to bend or extend. Electro-magnetic coupling generally takes place due to the capacitive, inductive or conductive cou- pling from one element to another [77]. It is also called as the crosstalk phenomena because of the undesirable effect of trans- mitted waves. The cross talk is nothing but the leakage between transmittedandreceivedchannelwhichcontaminatesthe received signalwithsomecontentsofthetransmittedone[78].Thecrosstalk effect is more prominent in wet soil which are highly conductive [35,48,79]. In such cases, the transmitted signal is electricallyconductedthroughwaterpresentinsoil,andthusreachingthereceiver element almost instantaneously [78].Fig. 11(a) shows a typical crosstalkeffectobservedincaseofdrysand[35].Fig.11(b) showsa similar effect when both the transmitter and receiver are inseries connections[48].

In order to minimize the electro-magnetic coupling, various researchershaveappliedshieldingandgroundingtothepiezoceramictransducerswithpolyurethanecoatinganditisprovedtobe very useful [48,77,80]. In some cases, researchers have suggested to adopt a frequency in the range of 2–5 kHz and the L_{tt}/h ratio (whereL_{tt}isthetiptotipdistancebetweentransmitterandreceiver and$h$isthewavelength)aslessthan1inordertogetclearsignals [35,48].Inaddition,paralleltypeofconnectionhelpstoreducethe effectofelectro-magneticcoupling.Thewavelengthratiosadopted

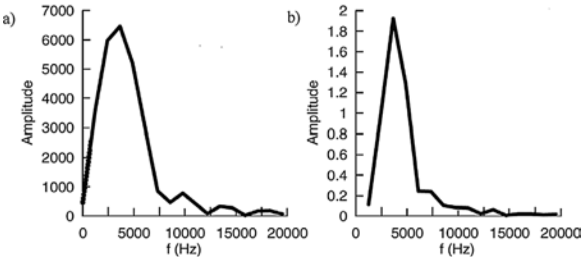

Fig. 9. Wave signals from (a) Transmitter and (b) Receiver in frequency domain[26].

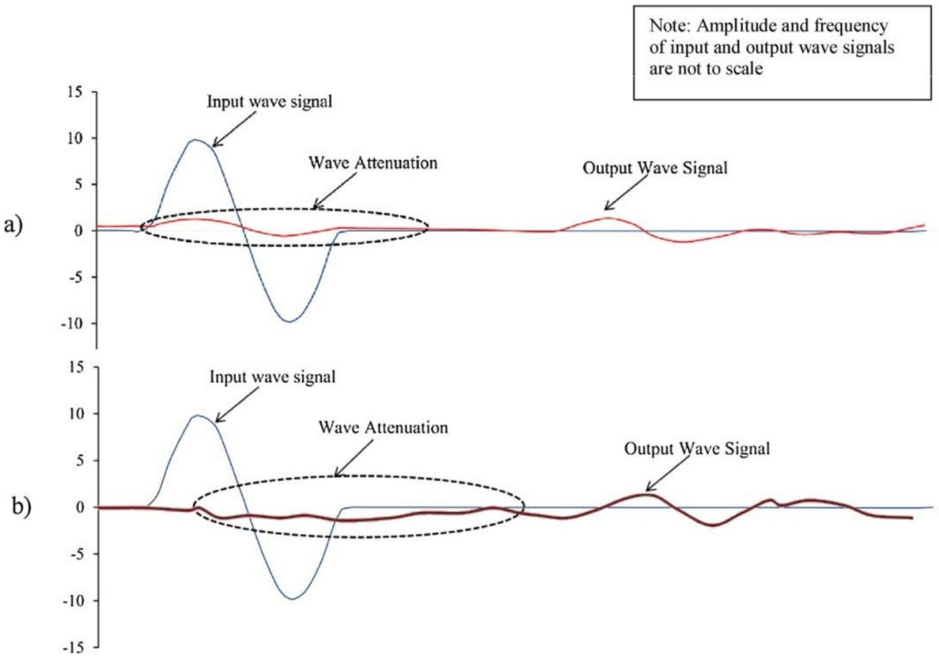

Fig. 10. Typical S-wave attenuation phenomena in (a) stiff clay [68] (b) soft clay[35].

bypreviousresearcherstominimizetheeffectofelectro-magnetic coupling are summarized in Table2.

8.3 Near field effect

Problem occurs in shear (S-) wave travel time determination, whenanunknowncomponentofwavetravellingwiththespeedof compression (P-) wave encounters the transmitting wave [14,65].Thisphenomenonisknownasnearfieldeffect.Thenearfieldcomponentofwavecausestransmittedwavetobedistortedatitsorigin point and wave starts with downward or upward deflection as observed in Fig. 11[35,48,54,65]. Whentheshearwavetravels,twodifferentwavesignalsappear, one component of this signal wave travels in longitudinal directionandtheothertravelsasshearwave,makingitdifficultto distinguishtheS-wavetraveltimeduetoearlyarrivalofP-wave component [48,61].This effect is more prominent when transmitterandreceivercomescloser.Wang[65]hassuggestedaspacing equalto2$h$betweenthetransmitterandreceiverinordertoavoid thenearfieldeffect.Ontheotherhand,Sanchez-Salinero[61]has developed a closed form solution for transverse and longitudinal movingwavesignalsinlinearelasticandhomogenousmedia.Some have suggested to adopt cross-correlation technique tointerprets thesignalandtominimizethedispersivecomponentstoobtained clearer waveforms [61,69]. The near field effect obtained bysome researcherindrysandsample,whenmeasuringtheS-wavevelocity is presented in Fig. 12(a) [16]. Similarly, a typical waveform havingnearfieldcomponent,whenmeasuringP-wavevelocityis presentedinFig.12(b)[35].Nearfieldeffectcanalsobeobserved inreceivedwaveasshowninFig.12(c),whenusingmultireceiver transducers during the bender element tests[65]. Someauthors[15,61,74,81]havesuggestedtousehigherinput frequency and wavelength ratio to minimize the near field effect [65].Clearwaveformsareobtainedinsilicasandspecimenwhen thetriggeringfrequencyiskepthigherthan2kHz[3].Apartfrom this,theL_{tt}/hratiomustbegreaterthan4tocompletelyseparate theP-andS-wavesignals[61].ItisduetothefactthatgreaterL_{tt}/h ratioincreasesthedifferencebetweenP-andS-wavearrivaltime and thus helps to get clear S- wave at

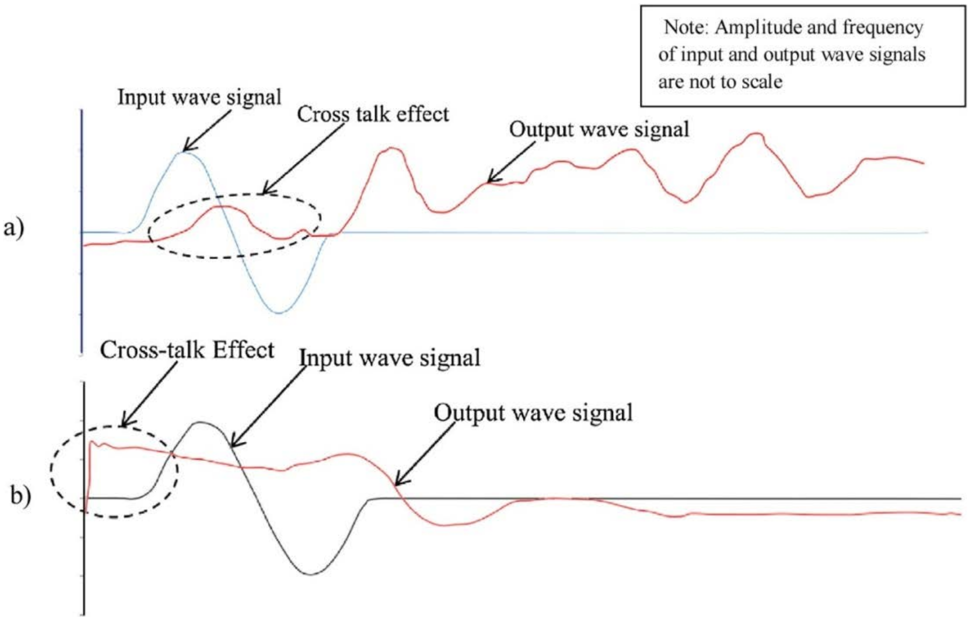

Fig. 11. Typical crosstalk (Electro-magnetic coupling) phenomena in S-wave for (a) Wet sand [35] (b) Dry Sand [48].

Table 2
Wavelength ratio for different types of soils as suggested by previous researchers

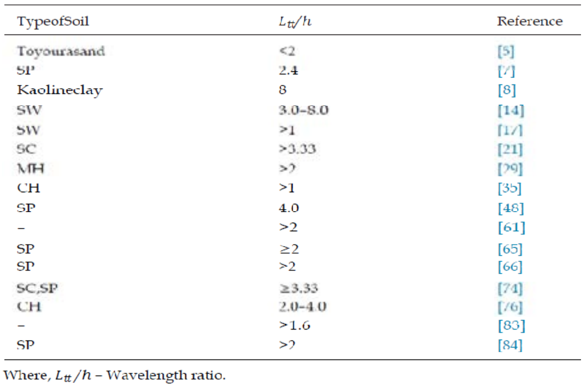

TypeofSoil	L_{tt}/h	Reference
Toyourasand	<2	[5]
SP	2.4	[7]
Kaolineclay	8	[8]
SW	3.0–8.0	[14]
SW	>1	[17]
SC	>3.33	[21]
MH	>2	[29]
CH	>1	[35]
SP	4.0	[48]
–	>2	[61]
SP	≥2	[65]
SP	>2	[66]
SC,SP	≥3.33	[74]
CH	2.0–4.0	[76]
–	>1.6	[83]
SP	>2	[84]

Where, L_{tt}/h – Wavelength ratio.

the receiver [5,15,30,61,82].The values of wavelength ratio (L_{tt}/h) in different types of soils usedbypreviousresearchersaresummarizedinTable2.It canbe observed that, most of the researchers have adopted wavelength ratio value between 1 and 4 [17,21,35,48,61,66,74,76,83,84]. Some of the researchers have suggested to keep the wavelength ratio greater than 1.6 to minimize near field effect[83], whereas, some otherhavesuggestedittokeepmorethan2[65,74].Assuch ,studies have been done to know the combined effects of frequency andamplitudeonwaveattenuation,electro-magneticcouplingand nearfieldeffectduringthemeasurementofS-wavevelocityindifferenttypesofsoils.Thesuggestedcombinationofthesefrequency andamplitudeforbetterresultshasbeensummarizedinTable3. It is to mention here that, different materials exhibit dissimilar arrangement of particles and fabric anisotropy and hence shows different responses to the transmission of waves [85]. From the graphical representation of the data in Fig. 13, it is observed that near field effect can be minimized by adopting frequencies rangingfrom5–6kHzandamplitude15–20V(peaktopeak)inCHsoils [8,18,35,44]. In case of SP type soils, the range of frequency and amplitudeare3–8kHzand4–20V,respectively.Veryfewexperimentshavebeenperformedincaseof CL,SMandSCtypes ofsoil andhenceitrequiresfurtherinvestigationinthisdirection.

IX. EFFECT OF THE TYPES OF WAVEFORM ON WAVEVELOCITY

Severalmethodologiesviz.,timedomain,frequencydomainand cross-correlationhavebeendevelopedbyresearchersfortheinterpretationofwavevelocities.However,someoftheresearchersare in favour of using different waveforms to ascertain clear output waves. Different waveforms as adopted by previous researchers are summarized in Table 4. Although, the square wave in bender/extender test is adopted by some researchers [19,41,42], it is least favourable. This is because, the square wave contains spectrum of different frequencies and hence the received signalsdoes not resembles the output signal of similar nature. Moreover, the received square wave signal seems to be more distorted at the beginningandthusmakingthesignalinterpretationmoredifficult. Contrarytothis,someresearchers[21]haveobtainedclear signals in kaolin clay using square waves. On the other hand, sine wave has been more popular due to reliable results, in spite of the fact thatitcausesgreaterambiguityinthetraveltimedeterminationas compared to square waves[4,21,30,86,87].

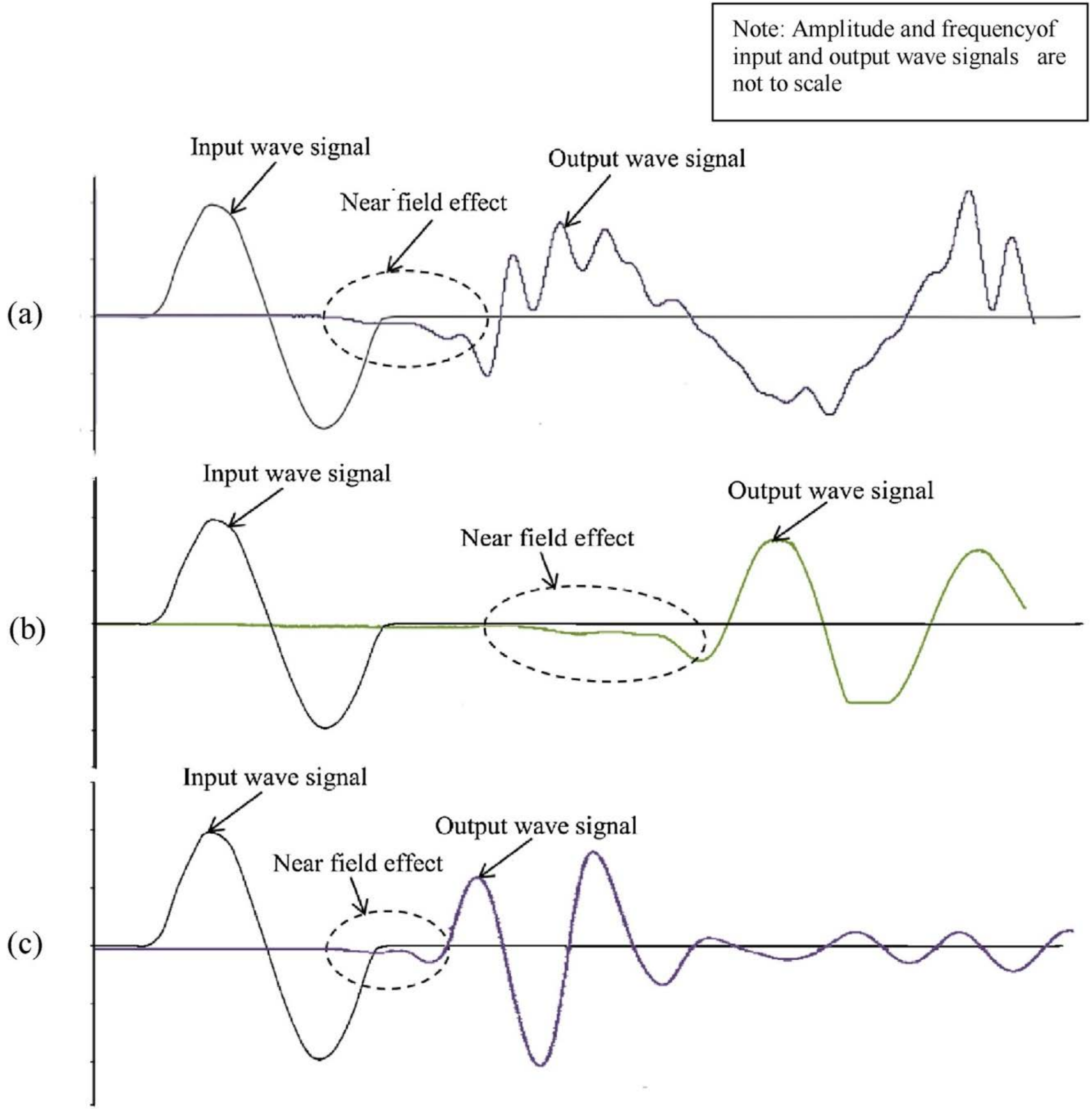

Fig. 12. Typical near field effect in sands as observed by different researchers [16,35,65].

Table 3
Frequency and amplitude for different types of soils as suggested by previous researchers

Soil Type (USCS)	Soil Sample aspect ratio	Bender/extender Size *(l × w × t) (mm)*	Suggested Frequency *(kHz)*	Amplitude *(V)*	Reference
SP	2.28	14.0×10.0×1.3	4.0	20	[7]
CH	–	–	5.0	20	[8]
SM	2	10.0×10.0×1.0	10.0	20	[11]
SW		12.7×8.0×1.0	9.0	9	[13]
CH	2	7.0×12.0×0.5	6.0	16	[18]
SW	0.65	11 × 6.4 × 1.6	3.0	12	[34]
CL	1.7	25.4 × 6.4 × 0.5	10.0	20	[35]
CH	0.65	15.0×12.0×0.65	5.0	20	[36]
SP	0.65	15.0×12.0×0.65	3.0	20	[36]
SC	–	–	4.0	10	[46]
CH	0.4−2.0	10.0 × 10.0 × -	5.0	20	[47]
SP	–	10.0×17.0×1.5	4.0	10	[49]
SP	2	–	7.0	12	[50]
SP	1.5	12.7×8.0×0.6	3.6	4	[51]
SP	2	–	5.0	20	[61]
SW	2	–	10.0	20	[77]

(Where, CL- Low Plasticity Clay; SM –Silty Sand; SP: Poorly graded Sand; CH- High Plasticity Clay; SC- Clayey Sand; SW: Well Graded Sand).

Table 4
Types of input waveform adopted by previous researchers.

Input waveform		Reference
	Sine wave (single pulse)	[4,15]
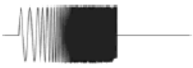	Continuous sine sweep of frequencies	[5,43,54]
	Square or step signal	[19,42]
	Impulse signal wave	[48]
	Continuous sine wave (constant frequency)	[54]
	Distorted sine wave pulse	[98]
	Forced oscillation	[98]
	Sine pulse (90>° Phase shift)	[99]
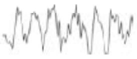	Random wave signal	[100,101]

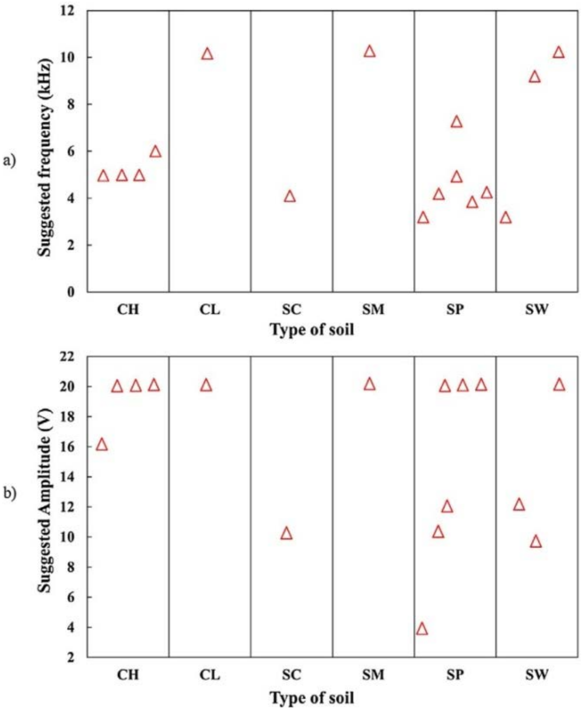

Fig.13.Rangeof(a)frequencyand(b)amplitudeasreportedbyvariousresearchers for different types ofsoils.

X. EFFECT OF REFLECTION AND REFRACTION OF WAVES

Inbenderelementtest,reflectionandrefractionfromthespec- imen boundaries may produce some waves other than thedirect S wave. Identification of these multiple reflected and refracted waves becomes most difficult due to the near field effect, wave attenuation and dispersion of waves [61,88]. S- wave generates in the direction of bender element plane and P- wave in the direc- tion perpendicular to the bender element plane upon deflection of the piezoceramic element (refer Fig. 14). The reflected P- wavestravel faster than the S- waves due to lateral boundaries which in turn causes disturbance in S- wave measurements [6]. This effect of boundary reflection/refraction depends upon the poisson's ratio of soil [48]. In case of highly confined or stiff geo-materials, refracted waves with higher velocities that travel along the rigid boundary wall mask the S- wave arrival when the distance between trans- mitter and receiver increases. The refraction phenomenon of waves through soil specimen is illustrated in Fig. 14. Since, the measure- ment of S- wave velocity assumes a straight travel length between transmitter and receiver, there may be a wrong interpretation in the arrival of direct S-wave due to boundary wall refractions. Hence, it is suggested to place the bender elements at a minimum distance of 0.4 times the length of the soil specimen to avoid the effects of refracted waves [89]. Moreover, some of the researchers have usedthermocolaroundtheboundarywallsofsampletoavoidwave reflections [7]. Researchers have found the effect of wave reflection higher in sandy soils than in soft soils because of long replications and lower damping[5].

XI. EFFECT OF PARTICLE SIZE, SHAPE AND CONTACT BEHAVIOUR ON WAVEVELOCITY

Rearrangementofparticlesandthefabricstructuretakesplace with application of loading in medium to large strain levels. This rearrangement of particles and fabric structure depends on sur- face roughness, particle size distribution, inter-particle contact and the material properties [41,90,91]. In this regard, some of the researchers have studied the effect of wave velocity at low strain levelfordeterminingthestiffnessandenergydissipationusingparticlecontactbehaviourbyassumingelastic,visco-plasticandbrittle

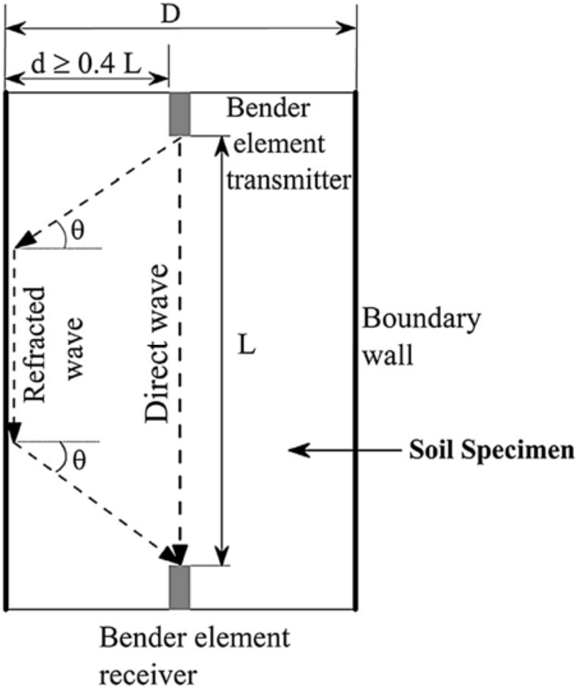

Fig. 14. Schematic illustration of wave refraction from boundary wall of soil speci- men.

contacts behaviour [90]. The soil fabric structure appears to have verylowimpactonshearwavevelocityofsoftkaolinitesediments with water content in the range of 0.6 to 6 times its liquid limit [19,92]. A study on the effect of particle surface roughness shows that,increaseinsurfaceroughnesscausesdecreaseinshear wavevelocity[93].Also,asperastudyinfineglassbeads, mediumcoarse glass beads and coarse glass beads [16,80] the characteristic signaloutputandhencewavevelocityisfoundtobeaffectedbythe frequency of input signals, mean particle size of the material and confining stress level. Moreover, the small strain shear modulus (G_0)isfoundtodecreasewithincreaseincoefficientofuniformity (C_u=D_{60}/D_{10}), where, D_{60} and D_{10} denotes the mean diameter of soilparticlesforwhich60and10percentoftheparticlesare finer than D_{60} and D_{10},respectively[94,95].

XII. EFFECT OF SAMPLE GEOMETRY AND BOUNDARY CONDITIONS

Shear waves are generally affected by the boundary wall reflec- tions which results in signal distortion [83]. Moreover, it has also been observed that when waves interact with boundary walls of the specimens, it results in conversion of shear wave to compression wave and vice-versa [21]. Distortion due to this signal reflection mainlydependsupontheaspectratioandhencethediameterofsoil specimen. Zhou et al. [3] have concluded that a change in different travel distances does not cause any change in shear wave velocity but it is the distance between the bender/extender element and lateral boundaries which creates signal distortions and makes it difficult for interpretation of test results. Table 1 shows the geome- tries of different soil samples considered by previous researchers. It can be noted that the aspect ratio of soil specimen as used by the researchers generally varies from 0.4 to 2.28 in different types of soil. However, most of the researchers (about 70%) have adopted the aspect ratio as 2 that can be also observed in Fig. 15. Studies reveal that the boundary wall effects can be minimized by inser- tion of bender element at the centre of soil specimen duringtesting [65]. Assuming the specimens as an infinite medium, ASTM D 2845 [96] suggests the specimen diameter as 5 times the wavelength of transmitted waves.

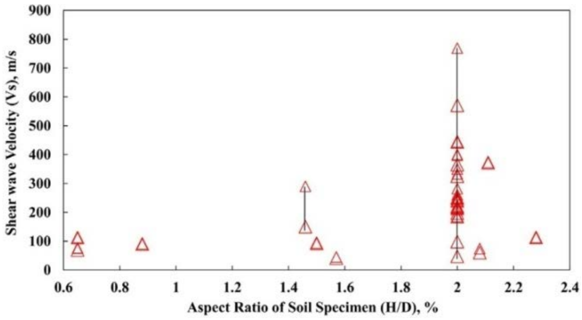

Fig. 15. Sample aspect ratio in soils with different shear wave velocity.

XIII. EFFECT OF SOME SOIL PARAMETERS ON WAVE VELOCITY

Wave velocity depends on various soil parameters viz., con- fining stress, void ratio, moisture content etc. Confining stress represents the real time field conditions which create an impact on the strength of signal waveforms. Although, shear wave veloc- ity generally increases with increase in confining stress, quality ofwaveforms progressively get degraded. Some of the researchers have found the shear wave velocity to decrease with increase in confiningstressinsoilwithfinecontent(<0.075mm)lessthan20% [14]. However, this effect has not been observed in case of compres- sion waves[10,28]. Moreover, higher confining stress yields higher shear modulus in soil specimens and results in decreased Poisson’s ratio [16,81]. As per a research on saturated Fujian sand, a compo- nent of compression wave is always found to travel through the soil samples that reach the receiver element before the arrival of shear wave [14]. Hence, in saturated sands, sometimes it becomes morecomplicated to interpret the shear wave velocity from bender elementtests.Studieshavealsorevealedthattheeffectofvoid ratio (e)onshearmodulus(G_0)ismoreprofoundthanconstrainedmod- ulus (M_0) in sands[16], where, G_0 and M_0 can be calculated from shearwaveandcompressionwavevelocities,respectively.

XIV. CONCLUSION

Some of the major findings from the present review are as follows:

1. Discshapedpiezoceramicelementscanbeusefulformeasuring wavevelocitiesinstiffsoilsandrockspecimensif modifications aredonetoachieveadequatecouplingbetweensoil/rockspeci- mens and theelements.
2. Function of bender/extender element largely depends upon its geometry and material types. Length and thickness are the governing factors when the element vibrates in air. But,after insertion in soil specimen, width of the element governs the transmitting capacity of the element and the output signal strength. The effective length, width and thickness of piezoce- ramic elements are limited to 9.0–13.0 mm (length), 6.0–8.0 mm (width) and 0.5–0.7 mm (thickness). Depending upon the length ofsoilspecimenandhencethewavetravellingdistance,elements can be manufactured with higher aspect ratio for high power input waves and thus giving larger deflections. Eq. (6) and (10) canbeusefultodetermineresonantfrequencyandinturnthegeometry of bender/extender element, when the element is in air and when embedded in a soil specimen, respectively.
3. Timedomainanalysisusingfirstarrivaltechniqueissuitablefor measuring travel time of P- waves but not for S- waves due to presence of near fieldcomponent.
4. Nearfieldeffectandtheeffectofelectro-magneticcouplingcan becontrolledbyadoptingasuitablewavelengthratio.
5. Wave attenuation, electro-magnetic coupling and near field effect can be minimized by adopting a suitable combination of frequencyandamplitudebasedupontheypesof soil.
6. An aspect ratio of 2 for soil specimen is found to be ideal in minimizing the effect of boundary wallreflections.

Itisbelievedthattheoutcomeoftheanalysisfrompresentwork will help the upcoming researchers to develop properguidelines andsuitablemethodologyforbenderelementtestinginsoils.

FUNDING

The work is supported by the research project funded by SERB, Department of Science and Technology, New Delhi (Project ID: SB/FTP/ETA-0371/2012).

REFERENCES

[1] J.Curie,P.Curie,Developmentviacompression,ofelectricpolarizationin hemihedral crystals with inclined faces, Bull. La Soc. Minerol. Fr. 91 (1880)90–93.

[2] R. Brosse, A. HosseiniKamal, R. Jardine, Measuring the static and dynamic small strain stiffness of UK mudrocks, in: Proc. 15 th ECSMGE, Athens, 2011,pp. 137–142.

[3] Y. Zhou, Y. Chen, Y. Asaka, T. Abe, Surface-mounted bender elements for measuring horizontal shear wave velocity of soils, J. Zhejiang Univ Sci. A 9(2008) 1490–1496,http://dx.doi.org/10.1631/jzus.A0820323.

[4] G.Viggiani,J.Atkinson,TechnicalNoteInterpretationofbenderelement tests, Geotechnique 45 (1995) 149–154, http://dx.doi.org/10.1680/geot. 1995.45.1.149.

[5] T.Ogino,T.Kawaguchi,S.Yamashita,S.Kawajiri,Measurementdeviations for shear wave velocity of bender element test using timedomain, cross-correlation, and frequency domain approaches, Soils Found. 55 (2015) 329–342, http://dx.doi.org/10.1016/j.sandf.2015.02.009.

[6] J.C. Santamarina, A. Klein, M.A. Fam, Soils and waves:Particulate materials behavior, characterization and process monitoring, J. Soils Sedim. 1 (2) (2001), http://dx.doi.org/10.1007/BF02987719,130–130.

[7] A.Juneja,M.Endait,Advancesinsmallstrainmeasurementusingbender, Proc. Indian Geotech. Conf. (2013)1–8.

[8] D.Nash,J.Sukolrat,P.Greening,N.Benahmed,Comparisonofshearwavevelocity measurements in a soft clay specimen using time and frequency domain techniques, Riv. Ital. Di Geotec. 5 (2007)56–68.

[9] K.Uchino,IntroductiontoPiezoelectricActuatorsandTransducersKenjiUchino, International Center for Actuators and Transducers, Penn State University,2003.

[10] M.L. Lings, P.D. Greening, A novel bender/extender element for soil testing, Géotechnique 51 (2001) 713–717, http://dx.doi.org/10.1680/geot.2001.51.8. 713.

[11] J.O.Donovan,G.Marketos,C.O.Sullivan,NovelMethodsofBenderElementTest Analysis, 2015, pp.311–316.

[12] D.C. Presti, M. Jamiolkowski, R. Lancelotta, L. Vercelli, Maximum shear modulus measurement using bender elements in oedometer tests, Riv. Ital.Di Geotec. (1993)1–9.

[13] J.C.Santamarina,S.J.Brandenberg,S.Choi,B.L.Kutter,D. W.Wilson,Benderelement system for measuring shear wave velocities in centrifuge models, Phys. Model. Geotech. (2006) 165 (ICPMG-Ng, ZhangWang).

[14] Y. Cai, Q. Dong, J. Wang, C. Gu, C. Xu, Measurement of small strain shear modulus of clean and natural sands in saturated condition using bender element test, Soil Dyn. Earthq. Eng. 76 (2015) 100–110, http://dx.doi.org/10. 1016/j.soildyn.2014.12.013.

[15] E. Brignoli, M. Gotii, K. Stokoe, Measurement of shear waves in laboratory specimens by means of piezoelectric transducers, Geotech. Test. J. 19 (1996)384–397(1996).

[16] X. Gu, J. Yang, M. Huang, Laboratory measurements of small strain properties of dry sands by bender element, Soils Found. 53 (2013) 735–745,http://dx.doi.org/10.1016/j.sandf.2013.08.011.

[17] R.Arulnathan,R.W.Boulanger,M.F.Riemer,Analysisofbenderelement tests, Geotech. Test. J. 21 (1998) 120–131, http://dx.doi.org/10.1520/ GTJ10750J.

[18] Black, S. Stanier, S. Clarke, Shear wave velocity measurement of kaolin duringundrainedunconsolidatedtriaxialcompression,Geo Halifax2009,Proc. 62 nd Can. Geotech. Conf. (2009)1–8.

[19] M. Fam, C. Santamarina, Study of geoprocesses with complementary mechanical and electromagnetic wave measurements in an oedometer, Geotech.Test.J.18(1995)307–

314,http://dx.doi.org/10.1520/GTJ10999J.

[20] C.Valle-Molina,K.H.Stokoe,Seismicmeasurementsinsandspecimenswith varyingdegreesofsaturationusingpiezoelectrictransducers,Can.Geotech. J. 49 (2012) 671–685,http://dx.doi.org/10.1139/t2012-033.

[21] E.C.Leong,S.Yeo,H.Rahardjo,Measuringshearwavevelocityusingbender element, Geotech. Test. J. 28 (2005) 488–498, http://dx.doi.org/10.1520/ GTJ12196.

[22] N.Yesiller,J.L.Hanson,M.Usmen,Ultrasonicassessmentofstabilizedsoils,Proc. ASCE Geo-Institute Soft Gr. Technol. Conf. (2001)170–181.

[23] S.Oh,D.Park,B.Kim,Y.Mok,Laboratorymeasurementsofstiffnessofsoftclay using bender elements, 14th World Conf Earthq. Eng. (2008) 1–8.

[24] M.P.Kulkarni,A.Patel,D.N.Singh,Applicationofshearwavevelocityfor characterizing clays from coastal regions, KSCE J. Civ Eng. 14 (2010) 307–321, http://dx.doi.org/10.1007/s12205-010-0307-1.

[25] M.M.Landon,D.J.Degroot,T.C.Sheahan,NondestructiveSampleQuality Assessment of a Soft Clay Using Shear Wave Velocity, 133, 2007, pp. 424–432.

[26] G.Mitaritonna,A.Amorosi,F.Cotecchia,Multidirectionalbenderelementmeasurements in the triaxial cell: equipment set-up and signal interpretation, Rev. Ital. Di Geotec. (2010)21.

[27] C. Ferreira, J.P. Martins, A.G. Correir, Determination of the small-strain stiffness of hard soils by means of bender elements and accelerometers, Proc.15thEur.Conf.SoilMech.Geotech.Eng(2011)179–183,http://dx.doi. org/10.1017/CBO9781107415324.004.

[28] L.P.Suwal,R.Kuwano,Diskshapedpiezo-ceramictransducerforPandS wave measurement in a laboratory soil specimen, Soils Found. 53 (2013) 510–524,http://dx.doi.org/10.1016/j.sandf.2013.06.004.

[29] X. Kang, G.C. Kang, B. Bate, Measurement of stiffness anisotropy in kaolinite using bender element tests in a floating wall consolidometer, Geotech. Test. J. 37 (2014),http://dx.doi.org/10.1520/GTJ20120205.

[30] M.R.Coop,V.Jovicic,M.Simic,ObjectivecriteriafordeterminingGmaxfrom bender element tests, Géotechnique 46 (1996) 357–362, http://dx.doi.org/ 10.1680/geot.1996.46.2.357.

[31] J.F. Camacho-tauta, J. David, J. Alvarez, Comparisonbetween resonant-column and bender element tests on three types of soils, Dyna 80 (182) (2013) 163–172 http://www.scielo.org.co/pdf/dyna/v80n182/v80n182a20.pdf.

[32] J.Carvalho,M.Arroyo,G.Cascante,M.F.Amaral,A.V.Fonseca,Compression and shear wave propagation in cemented-sand specimens, Géotech. Lett. 1 (2011) 79–84,http://dx.doi.org/10.1680/geolett.11.00032.

[33] D.J. Shirley, L.D. Hampton, Shear-wave measurements in laboratory sediments,J.Acoust.Soc.Am.63(1978)607,http://dx.doi.org/10.1121/1. 381760.

[34] P.P.Bartake,A.Patel,D.N.Singh,Instrumentationforbenderelementtesting of soils, Int. J. Geotech. Eng. 2 (2008) 395–405, http://dx.doi.org/10.3328/ IJGE.2008.02.04(395–405).

[35] Patel, D.N. Singh, K.K. Singh, Performance analysis of piezo-ceramic elementsinsoils,Geotech.Geol.Eng.28(2010)681–694,http://dx.doi.org/ 10.1007/s10706-010-9328-2.

[36] J.Rio,P.Greening,L.Medina,Influenceofsamplegeometryonshearwave propagation using bender elements, Deform. Charact. Geomater. (2003) 963–967,http://dx.doi.org/10.1201/NOE9058096043.ch121.

[37] D. Airey, A.K.M. Mohsin, Evaluation of shear wave velocity from bender elements using cross-correlation, Geotech. Test. J. 36 (2013) 1–9, http://dx.doi.org/10.1520/GTJ20120125.

[38] L.R. Hoyos, E.A. Suescun-Florez, A.J. Puppala, Stiffness of intermediate unsaturated soil from simultaneous suction-controlled resonant column andbenderelementtesting,Eng.Geol.188(2015)10–28,http://dx.doi.org/10.1016/j.enggeo.2015.01.014.

[39] J.C. Santamarina, A. Klein, M.A. Fam, Soils and waves. Particulate materials behavior, characterization and process monitoring, J. Soils Sedim. 1 (2001) 130,http://dx.doi.org/10.1007/BF02987719.

[40] A.Patel,K.K.Singh,D.N.Singh,Applicationofpiezoceramicelementsfor determining elastic properties of soils, Geotech. Geol. Eng. 30 (2012) 407–417, http://dx.doi.org/10.1007/s10706-011-9476-z.

[41] J.A. Diaz-rodriguez, P. Moreno-carrizales, L. Lpez-flores, A study of soil microstructureusingBenderelementtests,FourthInt.Conf. RecentAdv.Geotech. Earthq. Eng. Soil Dyn. (2001)2–6.

[42] C. Dyvik, R. Madshus, Lab measurements of Gmax using bender element, in:Adv. Art Test. Soils under Cycl. Cond. ASCE, New York, 1985, pp.186–196.

[43] C.Ferreira,A.Fonseca,J.A.Santos,Comparisonofsimultaneousbenderelements and resonant column tests on porto residual soil, Soil Stress. Behav. Meas. Model. Anal. 146 (2007)523–535.

[44] J. Sukolrat, D. Nash, M. Lings, The assessment of destructuration of BothkennarclayusingbenderelementsSoftSoilEngTaylor Fr.Gr.7(2007) 471–480,http://dx.doi.org/10.1017/CBO9781107415324.004.

[45] E.Eseller-Bayat,S.Gokyer,M.K.Yegian,R.O.Deniz,A.Alshawabkeh,Bender elements and bending disks for measurement of shear and compression wave velocities in large fully and partially saturated sand specimens, Geotech. Test. J. 36 (2013),http://dx.doi.org/10.1520/gtj20120024.

[46] J.O.Donovan,C.O.Sullivan,G.Marketos,Two-dimensionaldiscreteelement modellingofbenderelementtestsonanidealisedgranularmaterial,Granul. Matter 14 (2012) 733–747,http://dx.doi.org/10.1007/s10035-012-0373-9.

[47] M.Theron,C.R.I.Clayton,A.Best,Interpretationofside-mountedbenderelement results using phase shift and group velocity, Deform. Charact. Geomaterials.3rdInt.Symp.Pre-FailureDeform.Charact.Geomaterials (2003)127–132.

[48] J.S. Lee, J.C. Santamarina, Bender elements: performance and signal interpretation, J. Geotech. Geoenviron. Eng. 131 (2005) 1063–1070, http:// dx.doi.org/10.1061/(ASCE)1090-0241(2005)131:9(1063).

[49] Y.Zhou,Y.Chen,Y.Shamoto,Freetypebenderelementsfor characterising soilincentrifugemodeltests,Phys.Model.Geotech.Springman,TaylorFr. (2010) 417,http://dx.doi.org/10.1017/CBO9781107415324.004.

[50] A.V. Fonseca, C. Ferreira, M. Fahey, A framework interpreting bender element tests, combining time-domain and frequency-domain methods, Geotech.Test.J.32(2009)91–107,http://dx.doi.org/10.1520/GTJ100974.

[51] E.C. Leong, S.H. Yeo, H. Rahardjo, Measurement of wave velocities and attenuation using an ultrasonic test system, Can. Geotech. J. 41 (2004) 844–860,http://dx.doi.org/10.1139/t04-041.

[52] S. Likitlersuang, S. Teachavorasinskun, C. Surarak, E. Oh, A. Balasubramaniam, Small strain stiffness and stiffness degradation curve of Bangkok Clays, Soils Found. 53 (2013) 498–509, http://dx.doi.org/10.1016/j. sandf.2013.06.003.

[53] J. Martins, A. Gomes Correia, Comparison between laboratory and field stiffnessbywavemeasurements,J.Test.Eval.43(2015)1–13,http://dx.doi. org/10.1520/JTE20140087.

[54] P.Greening,D.Nash,Frequencydomaindeterminantionof Gousingbender elements, Geotech. Test. J. 27 (2003) 1–

7, http://dx.doi.org/10.1520/ GTJ11192.

[55] M.Aris,N.Benahmed,Effectofdifferentsamplepreparation methodsonthe behavior of granular materials using bender elements, Springer Ser. Geomech. Geoengin. 53 (2011) 339–344, http://dx.doi.org/10.1017/CBO9781107415324.004.

[56] X. Yu, A. Pradhan, Bender Element Testing and Discrete Element Modeling ofShear Wave in Granular Media, IFCEE, 2015, pp.1993–2002.

[57] E.V. Barabanova, O.V. Malyshkina, A.I. Ivanova, E.M. Posadova, K.M. Zaborovskiy,A.V.Daineko,Effectofporosityontheelectricalpropertiesof PZTceramics,IOPConf,Ser.Mater.Sci.Eng.49(2013)12026,http://dx.doi. org/10.1088/1757-899X/49/1/012026.

[58] E.H.Poulos,H.G.Davis,ElasticSolutionsforSoilandRock Mechanics,Wiley,New York,1974.

[59] J.R. Phillips, Piezoelectric Technology Primer, CTS Wireless, Albuquerque,NM, 2000.

[60] P.D.Greening,L.Medina,J.Rio,M.Arroyo,D.M.Wood,Effectsofsamplesizeon bender-based axial G0 measurements, Geotechnique 56 (2006) 39–52,http://dx.doi.org/10.1680/geot.2006.56.1.39.

[61] I.Sanchez-Salinero,J.M.Roesset,K.H.Stokoe,H.Kenneth,Analytical Studiesof Body Wave Propagation and Attenuation, 1986, pp.272.

[62] K.H.Chan,T.Boonyatee,T.Mitachi,Effectofbenderelementinstallationinclaysamples,Géotechnique60(2010)287–291,http://dx.doi.org/10.1680/ geot.7.00135.

[63] M.Knutsen,OnDeterminationofGMaxbyBenderElementandCross-Hole Testing,NorwegianUniversityofScienceandTechnology, 2014http://hdl. handle.net/11250/233301.

[64] C. Ferreira, A.V. Fonseca, D.F.T. Nash, Shear wave velocities for sample quality assessment on a residual soil, Soils Found. 51 (2011) 683–692,http://dx.doi.org/10.3208/sandf.51.683.

[65] Y.H.Wang,K.F.Lo,W.M.Yan,X.B.Dong,Measurementbiasesinthe Bender element test, J. Geotech. Geoenvironmental Eng. 133 (2007) 564–574, http://dx.doi.org/10.1061/(ASCE)1090-0241(2007)133:5(564).

[66] M.Aris,N.Benahmed,S.Bonelli,Experimentalgeomechanics:alaboratory studyonthebehaviourofgranularmaterialusingbenderelements,Eur.J. Environ. Civ. Eng. 16 (2012) 97–110, http://dx.doi.org/10.1080/19648189. 2012.668031.

[67] M. Arroyo, Pulse Tests in Soil Samples, 2001, http://dx.doi.org/10.13140/2.1. 3249.9848.

[68] J.S. Lee, A.L. Fernandez, J.C. Santamarina, S-wave velocity tomography: small-scale laboratory application, Geotech. Test. J. 28 (2005) 336–344,http://dx.doi.org/10.1520/GTJ12638.

[69] F. Mancuso, C. Simonelli, A. Vinale, Numerical analysis of in-situ S wave measurements,in:proceedings,in:TwelfthInt.Conf.SoilMech.Found.Eng.,Rio de Janeiro, 1989, pp.277–280.

[70] G. Alvarado, M.R. Coop, On the performance of bender elements in triaxial tests, Géotechnique 62 (2012) 1–17,http://dx.doi.org/10.1680/geot.7.00086.

[71] S. Yamashita, T. Kawaguchi, Y. Nakata, T. Mikami, T. Fujiwara, S. Shibuya, Interpretation of international parallel test on the measurement of G_{max} using Bender elements, Soils Found. 49 (2009) 631–650, http://dx.doi.org/ 10.3208/sandf.49.631.

[72] J.F. Camacho-Tauta, G. Cascante, A. Viana, D. Fonseca, J.A. Santos, Time and frequency domain evaluation of bender element systems, Geotechnique 65 (2015) 548–562, http://dx.doi.org/10.1680/geot.13.P.206.

[73] J.C.Fam,M.Santamarina,Astudyofconsolidationusingmechanicalandelectromagnetic waves, Geotechnique 47 (1997)203–219.

[74] E.C. Leong, J. Cahyadi, H. Rahardjo, Measuring shear and compression wave velocities of soil using bender-extender elements, Can. Geotech. J. 46 (2009) 792–812,http://dx.doi.org/10.1139/T09-026.

[75] B.Madhusudhan,J.Kumar,Dampingofsandsforvaryingsaturation,J. Geotech.Geoenviron.Eng.139(2013)1625–1630,http://dx.doi.org/10. 1061/(ASCE)GT.1943-5606.0000895.

[76] C.Chan,Ontheintepretationofshearwavevelocityfrombenderelementtests, Acta Tech. Corviniensis Bull. Eng. 5 (2012)29.

[77] A.Palczynska,A.Wymyslowski,T.Bieniek,G.Janczyk,D. Pasquet,T.Dinh, Crosstalkphenomenaanalysisusingelectromagneticwavepropagationby experimental an numerical simulation methods, 15th Int. Conf. Therm. Mech. Multi-Physics Simul. Exp. Microelectron. Microsystems (2014)1–10.

[78] J. Rio, Advances in Laboratory Geophysics Using Bender Elements, 2006http://discovery.ucl.ac.uk/1348997/.

[79] K. Senetakis, B.N. Madhusudhan, A. Anastasiadis, Wave propagation attenuation and threshold strains of fully saturated soils with intraparticle voids, J. Mater. Civ. Eng. ASCE (2015) 1–11, http://dx.doi.org/10.1061/(ASCE)MT.1943-5533.0001367.

[80] X.Liu,J.Yang,Effectoffinescontentonthesmallstrainstiffnessofsand,Adv. Civil Environ. Mater. Res. (2012) 1951–1961 (ACEM'12).

[81] X. Gu, J. Yang, Laboratory measurement of shear stiffness of decomposed granite,15thEur.Conf.SoilMech.Geotech.Eng.(2011)191–196,http://dx. doi.org/10.1017/CBO9781107415324.004.

[82] G.Vilhar,V.Jovicic,Measurementandinterpretationofthesmallstrainstiffness of boston silty sand, Acta Geotech. Slov. 6 (2009)57–75.

[83] M.Arroyo,M.Wood,P.D.Greening,Sourcenearfieldeffects andpulsetests in soil samples, Géotechnique 53 (2003) 337–345, http://dx.doi.org/10. 1680/geot.2003.53.3.337.

[84] J. Marjanovic, J.T. Germaine, Experimental study investigating the effects of setup conditions on bender element velocity results, Geotech. Test. J. 36 (2013) 1–11,http://dx.doi.org/10.1520/GTJ20120131.

[85] S.D.Gumaste,K.R.Iyer,S.Sharma,D.N.Singh,Determinationofthefabricalteration of marine clays, Acta Geotech. Slov. 11 (2014)21–31.

[86] Z. Cheng, E.C. Leong, A hybrid bender element-ultrasonic system for measurementofwavevelocityinsoils,Geotech.Test.J.37(2014),http://dx. doi.org/10.1520/GTJ20120158.

[87] J. Blewett, I.J. Blewett, P.K. Woodward, Phase and amplitude responses associated with the measurement of shear-wave velocity in sand by bender elements, Can. Geotech. J. 37 (2000) 1348–1357, http://dx.doi.org/10.1139/ t00-047.

[88] D. Fratta, J.C. Santamarina, Wave propagation in soils: multi-mode, wide-band testing in a waveguide device, Geotech. Test. J. 19 (1996) 130–140,http://dx.doi.org/10.1520/GTJ10336J.

[89] Sawangsuriya, M. Fall, D. Fratta, Wave-based techniques for evaluating elastic modulus and poisson's ratio of laboratory compacted lateritic soils, Geotech. Geol. Eng. 26 (2008) 567–578, http://dx.doi.org/10.1007/s10706- 008-9190-7.

[90] G. Cascante, C. Santamarina, N. Yassir, Flexural excitation in a standard torsional-resonant column device, Can. Geotech. J. 53 (1998) 478–490,http://dx.doi.org/10.1139/t98-012.

[91] J.C.Santamarina,D.Fratta,Shearwavepropagationinjointedrock:stateof stress, Géotechnique 52 (2002) 495–505, http://dx.doi.org/10.1680/geot. 2002.52.7.495.

[92] K.Klein,J.C.Santamarina,Softsediments:wave-basedcharacterization,Int. J. Geomech. 5 (2005) 147–157, http://dx.doi.org/10.1061/(ASCE)1532-3641(2005)5:2(147).

[93] C. Santamarina, G. Cascante, Effect of surface roughness on wave propagation parameters,

Geotechnique 48 (1998) 129–136, http://dx.doi.org/10.1680/geot.1998.48.1.129.

[94] T. Wichtmann, T. Triantafyllidis, Influence of the grain-size distribution curveofquartzsandonthesmallstrainshearmodulusGmax,J.Geotech. Geoenviron. Eng. 135 (2009) 1404–1418, http://dx.doi.org/10.1061/ (ASCE)GT.1943–5606.0000096.

[95] T.Iwasaki,F.Tatsuoka,Effectsofgrainsizeandgradingondynamicshear moduliofsands,SoilsFound.17(1977)19–35,http://dx.doi.org/10.2355/ isijinternational.38.559.

[96] ASTM D-2845-05, Standard Test Method for Laboratory Determination of Pulse Velocities and Ultrasonic Elastic Constants of Rock, ASTM, 2005, pp. 5–11,http://dx.doi.org/10.1520/D2845-08.2.

[97] W. Sas, K. Gabrys, A. Szymanski, Comparison of resonant column and Bender elements tests on selected cohesive soil from warsaw, Electron. J. Polish Agric. Univ. 17 (2014)1–12.

[98] V.Jovicic,M.R.Coop,M.Simic,Objectivecriteriafordetermining Gmaxfrom bender element tests, Geotechnique 46 (1996) 357–362, http://dx.doi.org/10.1680/geot.1996.46.2.357.

[99] D.S. Pennington, D.F.T. Nash, M.L. Lings, Horizontally mounted Bender elements for measuring anisotropic shear moduli in triaxial clay specimens, Geotech.Test.J.24(2001)133–144,http://dx.doi.org/10.1520/GTJ11333J.

[100] S.K.Roesler,Anisotropicshearmodulusduetostressanisotropy,ASCEJ.Geotech. Engng Div. 105 (1979)871–880.

[101] J.A.Santos,J.Camacho-Tauta,M.Parodi,A.V.Fonseca,C.Ferreira,Useofrandomvibrationstomeasurestiffnessofsoils,Exp.Vib.Anal.Civ.Eng. Struct. 1978 (2007) 1169–1178.

★★★

EXPULSION OF ARSENIC FROM CONTAMINATED WATER: REVIEW

[1]SAMAPTIKA MOHANTY, [2]AKASHPRAVA PANDA, [3]SATYA PRAKASH MISHRA

[1]Assistant Professor, Department of Civil Engg. NMIET, BBSR
[2]Asst Professor, Department of Civil Engineering AIET Bhubaneswar
[2]Asst Prof, Department of Civil Engineering CEC Bhubaneswar
E-mail: [1]Mahananda.minakshee@nmiet.ac.in

Abstract - Arsenic tainting in water, particularly groundwater, has been perceived as a significant issue of cataclysmic extents. As the total populace builds, quite possibly the most key assets for human endurance, clean water, is diminishing. The rising requests for water frequently can't be met by surface water supplies. This has prompted expanded reliance on ground-water assets in numerous pieces of the world. Arsenic is available in the world's outside, the outcomes of ground-water improvement frequently incorporate over drafting, land subsidence. Arsenic can be effectively solubilized in ground waters depending onpH, redox conditions, temperature, and solutioncomposition and henceforth it is available in ground water in some arsenic affected areas.Arsenic in drinking water past breaking point can do mischief to human wellbeing and the utilization of ground water ill suited for human utilization in those territories. Anthropogenic wellsprings of arsenic incorporate modern cycles (specifically, mining and purifying), debris deposits from power plants, pesticide and compost applications, wood additives, inorganic arsenical pesticides and herbicides mechanical and city waste, and sewage sludge.In this paper, a wide outline of the accessible innovations for arsenic expulsion has been introduced based on writing study. The principle treatment strategies included coagulation-sedimentation, adsorption division, particle trade, film strategy, which have the two points of interest and weaknesses. It reasoned that the determination of treatment cycle ought to be site explicit and winning conditions and no interaction can fill the need under different conditions as every innovation has its own restrictions.

I. INTRODUCTION

Arsenic (atomic number 33, atomic weight 74.9; specific gravity 5.73, melting point 817oC (at 28 atm), boiling point 613oC and vapor pressure 1mm Hg at 372◦C.) is a silver- grey brittle crystalline solid. Arsenic exists in the −3, 0, +3 and +5 oxidation states [6,8]. Two forms are common in natural waters: arsenite (AsO3 3−) and arsenate (AsO4 3−), referred to as arsenic (III) and arsenic(V)[3,5,8]. Arsenic contaminants present in our drinking water supply may be from natural (geogenic) and/or anthropogenic sources. Naturally arsenic is present in the earth‘s crust as the 20th most abundant element, it is typically associated with igneous and sedimentary rocks in an inorganic form, such as arsenopyrite and Anthropogenic sources of arsenic include industrial processes (in particular, mining and smelting), ash residues from power plants, pesticide and fertilizer applications, wood preservatives, inorganicarsenical pesticides and herbicides industrial and municipal waste, and sewage sludge[6]. However, the main cause of groundwater contamination is geogenic.The World Health Organization (WHO) had recommended a maximum contaminant level (MCL) of arsenic in drinking water of 10 ppb [3, 11,12]. The acute toxicity of arsenic at high concentrations has been known about for centuries. It was only relatively recently that a strong adverse effect on health was discovered to be associated with long-term exposure to even very low arsenic concentrations. Drinking water is now recognized as the major source of human intake of arsenic in its most toxic (inorganic) forms. The presence of arsenic, even at high concentrations, is not accompanied by any change in taste, odor or visible appearance of water. The presence of arsenic in drinking water is therefore difficult to detect without complex analytical techniques. The effects of arsenic are serious and ultimately life-threatening. Arsenic in drinking water is a global problem affecting countries on all five continents. The most serious damage to health has taken place in Bangladesh and West Bengal, India[12].Several treatment technologies have been adopted to remove arsenic from drinking water under both laboratory and field conditions. Technologyshouldprovidecommunities with asustainable,continuous, affordable, safewater supply in all cases and also technologies should not have anundueadverse effect on the environment. Technologies meeting these technical criteria canbeevaluated underseveralsocioeconomiccriteria. First,thesystemsmust be economically feasible.

II. METHODS FOR ARSENIC REMOVAL

Most of arsenic present in the nature water is in inorganic forms. The most common valence states of arsenic, As(V) or arsenate is more prevalent in aerobic surface waters and As(III) or arsenite is more likely to occur in anaerobic ground waters. As(V) includes H_3AsO_4, $H_2AsO_4^-$, $HAsO_4^{2-}$, AsO_4^{3-} in which the negatively charged arsenate accounts for more and As(III) includes H_3AsO_3, $H_2AsO_3^-$, in which the uncharged H_3AsO_3accounts for more [2].Knowledge of the speciation of arsenic i.e. the repartition of the different species as a function of pH, is fundamental to understand the removal process. In the typical pH range of natural waters, arsenate ions are present as $H_2AsO_4^-$,$HAsO_4^{2-}$ and $AsO_4^{3-}$and arsenite is found mostly as the uncharged species H_3AsO_3, which is shown in the following figures.

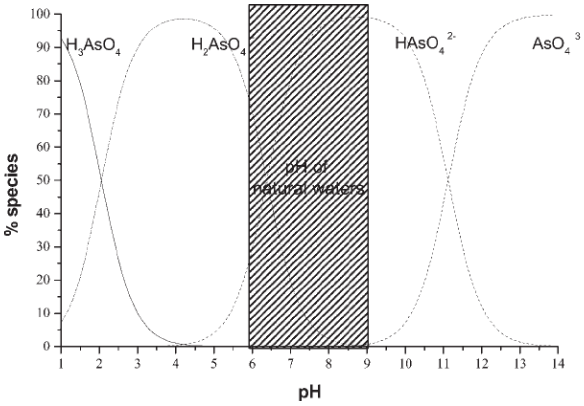

Figure 1: As(V) species repartition as function of pH [4].

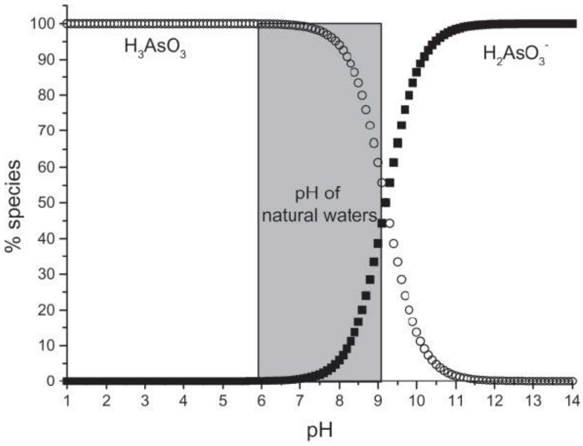

Figure 2: As(III) species repartition as function of pH [4].

Removal efficiencies for As(III) are poor compared to removal As(V) by any of the technologies evaluated due to the negative charge on As(V) and hence the technologies under review perform most effectively when treating arsenic in the form of As(V). If not so then As (III) may be converted through pre-oxidation to As(V). Data on oxidants indicate that chlorine, ferric chloride, potassium permanganate, ozone and hydrogen peroxide are effective in oxidizing As(III) to As(V). Pre-oxidation with chlorine may create undesirable concentrations of disinfection byproducts. Ozone and hydrogen peroxide should oxidize As(III) to As(V), but no data are available on performance[5].

Table 1: Showing performance and limitations of arsenic oxidants[13].

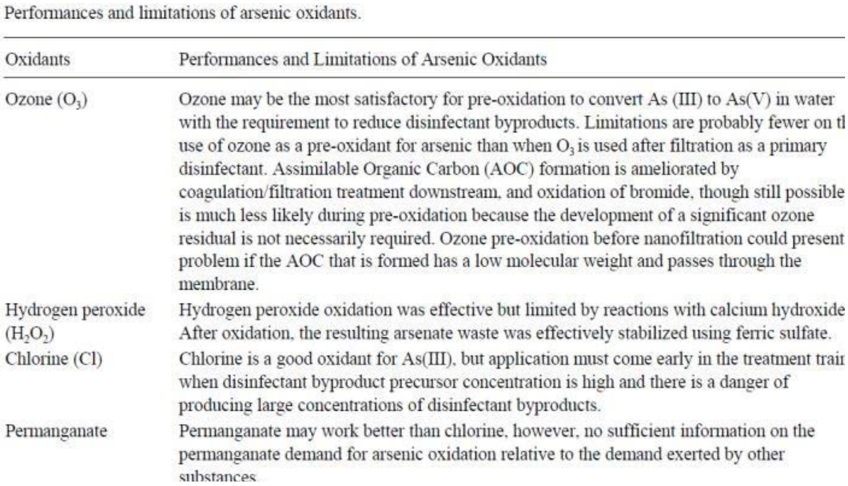

Performances and limitations of arsenic oxidants.

Oxidants	Performances and Limitations of Arsenic Oxidants
Ozone (O_3)	Ozone may be the most satisfactory for pre-oxidation to convert As (III) to As(V) in water with the requirement to reduce disinfectant byproducts. Limitations are probably fewer on t use of ozone as a pre-oxidant for arsenic than when O_3 is used after filtration as a primary disinfectant. Assimilable Organic Carbon (AOC) formation is ameliorated by coagulation/filtration treatment downstream, and oxidation of bromide, though still possible is much less likely during pre-oxidation because the development of a significant ozone residual is not necessarily required. Ozone pre-oxidation before nanofiltration could present problem if the AOC that is formed has a low molecular weight and passes through the membrane.
Hydrogen peroxide (H_2O_2)	Hydrogen peroxide oxidation was effective but limited by reactions with calcium hydroxide After oxidation, the resulting arsenate waste was effectively stabilized using ferric sulfate.
Chlorine (Cl)	Chlorine is a good oxidant for As(III), but application must come early in the treatment trai when disinfectant byproduct precursor concentration is high and there is a danger of producing large concentrations of disinfectant byproducts.
Permanganate	Permanganate may work better than chlorine, however, no sufficient information on the permanganate demand for arsenic oxidation relative to the demand exerted by other substances

All of the technologies for arsenic removal rely on a few basicchemicalprocesses, most common methods used for arsenic removal are elaborated here:

Precipitation processes: Precipitation processes involving coagulation/ filtration have been studied extensively for the removal of arsenic from water. Adsorption co-precipitation with hydrolyzing metals such as Al^{3+} and Fe^{3+} is the most commonly used treatment technique for removing arsenic from water. The precipitate formed after coagulation or in situ oxidation of iron and manganese present in water could be removed by sedimentation followed by rapid sand filtration or direct filtration or microfiltration.Coagulation with iron and aluminum salts and lime softening has been considered the most effective treatment process for removing arsenic from water to meet the interim primary drinking water regulations standard. Oxidation of As(III) to As(V) and removal using one of the processes described above has been recommended (USEPA 2000a & b). Atmospheric oxygen, hypochlorite and permanganate are commonly used for oxidation of As(III) to As(V). However, oxidation with air (atmospheric oxygen) is very slow. The effectiveness of this technology is less likely than other treatments to be reduced by characteristics and contaminants other than arsenic. It is also capable of treating water characteristics or contaminants other than arsenic, such as hardness or heavy metals. Systems using this technology generally require skilled operators, for this reason, precipitation/co- precipitation is more cost-effective at large scale where labour costs are spread over a larger quantity of treated water. The As is removed in the formation of the insoluble compounds $Al(AsO_4)$ or$Fe(AsO_4)$[12].

Sorption Technology:Sorption is a common word use for both adsorption and absorption. Some materials with big specific surface area and high surface energy which have strong adsorption ability can separate and remove the contaminant to purify water in the process of adsorption. This adsorption action may be chemistry effect such as surface chemistry coordination or complex or physical effect such as static-electric attraction. Adsorption is one of the most effective methods to remove the arsenic in the water; the common adsorbents included activated alumina, activated carbon, function resinand metal oxide, etc.[2].Adsorption involves the use of granular adsorptive media for the selective removal of arsenic from water with or without pH adjustment and with or without spent media regeneration. Several granular adsorptive filter media have shown high effectiveness in arsenic removal from water. These include activated alumina, activated carbon, iron oxide coated or based filter media including some commercial media like Aqua-Bind MP, ArsenX,Bayoxide E33 ferric oxide, Granular Ferrichydroxide (GFH), MEDIA G2, manganese greensand etc. These technologies are consistently capable of removing arsenic to below the required standard level (USEPA 2002).The effectiveness of adsorption for arsenic treatment is more likely than precipitation processes to be affected by characteristics and contaminants other than arsenic. Small capacity systems usingthesetechnologiestendtohaveloweroperatingand maintenance costs and require less operator expertise. Adsorption and ion exchange therefore tend to be used more often when arsenic is the only contaminant to be treated, for relatively smaller systems, and as an auxiliary process for treating effluent from larger systems[12]. Several adsorptive media like activated alumina, activated carbon, iron and manganese coated sand, kaolinite clay, hydrated ferric oxide, activated bauxite, titanium oxide, silicium oxide and many natural and synthetic media have been reported to remove arsenic from water. The efficiency of adsorptive media depends on the use of oxidizing agents as aids to provoke the adsorptive of arsenic on the media[10].

Activated Alumina:

Activated alumina (Al_2O_3) has a good adsorptive surface, in the range of 200-300 m^2/g. The large surface area gives the material a very large area for adsorption of arsenic. When water passes through a packed column of activated alumina, the impurities including arsenic present in water are adsorbed on the surfaces of activated alumina grains. Eventually, the columnbecomes saturated, first at its upper zone and later downstream towards the bottom end, and finally the column gets totally saturated. Regeneration of saturated alumina is carried out by exposing the medium to 4% caustic soda (NaOH) either in batch or by flow through the column resulting in highlyarsenic contaminated caustic wastewater. Arsenic removal by activatedalumina is controlled by pH and the arsenic content of water. The efficiency drops as the point of zero charge is approached and at pH 8.2 where the surface is negatively charged, the removal capacities are only 2-5% ofthe capacity at optimal pH.Some examples of activated alumina basedadsorptive media are: the –BUET Activated Alumina‖,the–AlcanEnhancedActivatedAlumina‖andthe –ApyronArsenicTreatmentUnit‖[10].

Metal (hydrogen) oxide:

Iron oxide with high surface energy and surface area hasstrong adsorption capability with respect to many inorganicions and organic matters. Lots of literatures have reportedthat heavy metal ions and organic contaminate can beremovedby iron (hydrogen) oxide. Several iron oxides removedarsenic effectively such as amorphous hydrous ferricoxide, crystalline hydrous ferric oxide (ferrihydrite), hematite, magnetite and goethite. The iron hydroxide and its polymer with high adsorption and fast kinetic whichhave the biggest capability of adsorption were the mosteffective. However, some shortcomings with iron hydroxidestillexists,for example, some anions have an adverseinfluence on the arsenic removal such as SO42-, Cl-, F-,PO4- and SiO3-. The latter two have relatively strongerimpact than the former three. In addition, the arsenic removalwas influenced by pH markedly. The removal efficiencydecreased quickly as pH is over 8.5. Arsenateremoval is much better than arsenite by iron hydroxide. Also iron hydroxide had poor adsorption to arsenite. Lakshmipathiraj et al (2006) combined the advantages of Mn and Fe, synthesize a suitable adsorbent, Mn-substituted iron oxyhydroxide (MIOH), which could remove both arsenite and arsenate from aqueous solutions with considerable efficiency[8].

Activated Carbon:

Activated carbon (AC) has been extensively used for the removal of organic contaminants in water. Results regarding arsenic removal are quite controversial but most of them show that activated carbon can remove As(V) but not As(III). However, As(V) uptake capacities were low, reaching 20 mg/g on granular activated carbon. The performance of Activated carbon depends on its chemical composition. It has been demonstrated that a fly ash content of activated carbon was a critical parameter in arsenate removal. In another study, As(V) sorption was correlated to Activated Carbon zeta potential values but fly ash content was not consistent with As(V) removal. As(III) was removed significantly only at high initial concentration (.700 mg/L), which was explained by an oxidation from As(III) to As(V) by the oxygenated functional groups present at the surface of the sorbent. Furthermore, Jubinka and Rajakovic demonstrated that activated carbon did not remove As (III) in the pH range of2–10[4]. Chemically treated activated carbon exhibits high adsorption capacity for arsenic. The factors (such as solution pH, carbon type and carbon pretreatment and elution of the arsenic from loaded carbon) that affect the mechanism of the adsorption of arsenic species on activated carbons. It is found that As(V) is more effectively removed from solution by using activated carbon with high ash content and pre-treatment of the carbon with Cu(II) solutions improves its arsenic removal capacity. In these studies, commercially available activated carbons were used. The use of commercial activated carbon is not suitable for developing countries because of its high cost[13].

Strong Base Anion (SBA) Exchange Resin:

Strong base anion (SBA) exchange resins have quaternary ammonium groups connected to the polymer matrix and differ by the nature of the group attached to the nitrogen. They can be classified in two classes: type I resins with three methyl groups connected to the nitrogen and type II with two methyl and one ethanolamine group. Anion exchange resins have more affinity for divalent anions than monovalent anions, therefore, HAsO42-will be preferentially adsorbed over H2AsO4-. Thus, according to the speciation diagram reported in Fig.1, arsenate removal is expected to increase between pH 6 and 9. On the other hand, due to its weak dissociation constant, As(III) cannot be removed. A pre- oxidation step is necessary to treat an arsenite solution with ion exchange technology[4].

Metal-Loaded Polymers:

Metal-loaded polymers were described four decades ago by Helfferich to separate ligands of different coordination. These materials have been used only recently for the treatment of water contaminated with toxic anions like arsenic, selenite, or fluoride. Another domain of application is analytical chemistry, where these sorbents are used to pre-concentrate very dilute solutions of arsenic before analysis. One attractive feature of these polymers is that most of the time, they overcome interferences with chloride and sulfate ions generally observed with strong anion exchange resins. Due to the strong interaction between the metal bound onto the polymer and arsenic, uptake capacities can alsobe increased. The most interesting property may be the possibility to remove both As(III) and As(V). Operating pH conditions can also be less restricted than with SBA because arsenic species do not have to be negatively charged to be removed. However, sorbent has to be carefully designed to avoid any release of the metal in solution and adversely affect the quality of water. Metal-loaded polymers are usually prepared by passing a metal ion solution at a given concentration and pH through a packed column of resins in a down flow or up flow mode. With this method, the operator has control ofthe pH and concentration of the feed solution. pH is one of the most important parameter to study because it affects both the nature of arsenic species in solution and the surface of the adsorbent. Whenever possible, buffers should be avoided as they can interfere with Sorption Technologies for Removal of Arsenic in Water. Some of metal loaded polymers are: Fe(III)-Resins, Cu(II)-Resins, Zr(IV)-Resins, La(III)-Resins, Ce(IV)-Resins etc. [4]. Most of the work on metal-loaded polymers has been done with Fe(III) but these sorbents have limitations for drinking water treatment due to their low operating pH for As(V) removal and a low affinity for As(III). Zr(IV)-loaded chelating resins are promising because they are selective and have an high affinity for arsenite ions at neutral pH[4].

Granular Ferric Hydroxide:

Granular ferric hydroxide is also used for the adsorptive removal of arsenate, arseniteandphosphate from water. Granular ferric hydroxide reactors are fixed bed absorbers operate like a conventional filter with a downward flow of water. The water containing high dissolved iron and suspended matters should be aerated and filtered through a gravel/sand bed as a pretreatmentto avoid clogging of the adsorption bed[10].

Hydrous Cerium Oxide:

Hydrous cerium oxide is also a good adsorbent. Laboratory test and field testing of the materials at several sites showed that the absorbent is highly efficient in removing arsenic fromgroundwater[10].

Iron Coated Sand and Brick Chips:

Iron coated sand and iron coated brick chips are effective in removing bothAs(III) and As(V).The ‗Shaplaarsenicfilter (Shapla arsenic filter has been developed and tested widely use in Bangladesh. This is flow through system in which arsenic contaminated water flows through a bucket containing active arsenic removal material prepared by a specialized chemical treatment of ordinary brick particles to incorporate activated iron oxide in the brick particles)‖ and ‗SurokkaArsenic Filter(TheSurokkafilter is a house hold arsenic filter made out of local components and materials. The filter operates on the properties of locally available iron containing yellow sands to absorb arsenic from ground water. The water flows through the filter at a predetermined rate so that almost 100% removal of As(III) and As (IV) is obtained. The operation of the filter is very simple, just pouring water to the container containing 20 kg active material and collecting water in a receiver)‖ are example of a household arsenic removal filter based on iron coated brick chips developed and promoted by the International Development Enterprises (IDE). Thebrick chips are treated with ferrous sulphate solution for iron coating. The water collected from contaminated tube wells passes through the filter media placed in earthen container having a drainage system underneath. The Na2CO3-rich water may be used for leaching of arsenic from As loaded brick chips/sands.

Membrane filtration: Membrane processes can remove arsenic through filtration, electric repulsion, and adsorption of arsenic-bearing compounds. The effectiveness of microfiltration and ultrafiltration as a technique for arsenic removal is highly dependent on the size distribution of arsenic bearing particles in the source water. Nano-filtration membranes are capable of removing significant portions of the dissolved arsenic compounds in natural waters. Reverse Osmosis (RO) is a technology proven through several bench- and pilot-scale studies, and is very effective in removing dissolved constituents. Since arsenic in groundwater is typically 80- 90% dissolved, RO is a suitable technology for arsenic removal in groundwater. Membrane filtration is effective in removing both As(III) and As(V) species. However, efficiency in removing As(V) is higher than for As(III).The effectiveness of membrane filtration for arsenic removal is sensitive to a variety ofuntreated water contaminants and characteristics. It also produces a larger volume of residuals and tends to be more expensive than other arsenic treatment technologies. It is therefore used less frequently than precipitation/ co-precipitation, adsorption, and ion exchange (USEPA2002).

Biological removal processes:In the present study, an alternative technology for the removal of both trivalent and pentavalent arsenic species was examined based on the established biological iron oxidation from groundwater.Iron oxidation can be catalyzed by several microorganisms, which are indigenous in most groundwater, such asGallionellaferruginea and Leptothrixochracea. Arsenic can be removed by direct adsorption or co-precipitation on the preformed biogenic iron oxides, whereas there was anindicationof As(III) oxidation by iron oxidizing bacteria, leading to improved overall removal efficiency. The objective of the present research was to study the mechanism of As(III) removal during biological iron oxidation, as well as to establish the optimum conditions for efficient arsenic (IIIand
V) removal, in order to meet the new standard of 10 mg/L. Furthermore, investigations using living, dead or resting cells have been performed, in order to obtain additional information regarding the role of bacteria and the mechanism of trivalent arsenic removal. In addition, the removal of pentavalent arsenic has been examined, in order to obtain an integrated view on the applicability of this technology in groundwater treatment, when both inorganic forms of arsenic are present. It is considered as an innovative treatment approach, which can be summarized under the term
‗‗biological adsorptive filtration‘‘.The removal of arsenic was examined simultaneously to biological iron oxidation. The treatment process was based on a fixed-bed up flow filtration unit. A schematicdiagramof experimental set-up is shown in Fig. 3. The apparatus consisted of a(Plexiglas) column, which was filled with appropriate filtration media (polystyrene beads). The indigenous microorganisms after 3 months of operation have been deposited and accumulated in the filtration column. The oxidation of iron resulted in the formation of a biofilm. In particular, Gallionellaferruginea forms stalks andLeptothrixochracea sheaths, when present in an oxidizing environment rich in ferrous iron. It is proposed that the formation of stalks and sheaths may serve as a protective mechanism against the increasing reducing capacity of ferrous iron as it becomes unstable in an environment that becomes oxidized. By this way these bacteria accumulate in the filtration media and grow by obtaining their energyeither by the oxidation of ferrous iron (Gallionella) or by consumption of organic matter (Leptothrix)[7].

Figure 3: Schematic representation of biological oxidation and filtration unit [7].

(1) Continuous flow of contaminated groundwater, (2) arsenic stock solution, (3) peristaltic (feeding) pump, (4) influent sampling vessel, (5) air injection, (6) aeration column, (7) filtration column and (8)effluent.

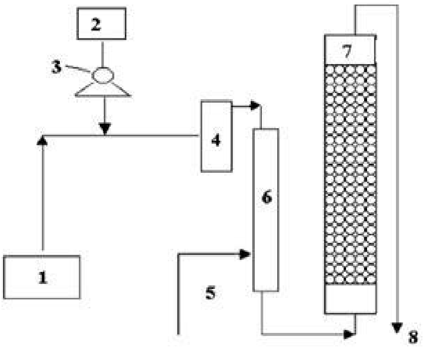

Fig. 1. Schematic representation of biological oxidation and filtration unit. (1) Continuous flow of contaminated groundwater, (2) arsenic stock solution, (3) peristaltic (feeding) pump, (4) influent sampling vessel, (5) air injection, (6) aeration column, (7) filtration column and (8) effluent. *Column characteristics*: active height: 1 m, inner diameter: 68 mm, surface area: 0.0036 m^2, bed volume: 3.6 L, total bed porosity: 0.37, bead diameter 3–4 mm.

Column characteristics: active height: 1m, inner diameter: 68 mm, surface area: 0.0036m2, bed volume: 3.6 L, total bed porosity: 0.37, bead diameter 3–4mm.

Table 2: Efficiency of conventional arsenic removal techniques[11].

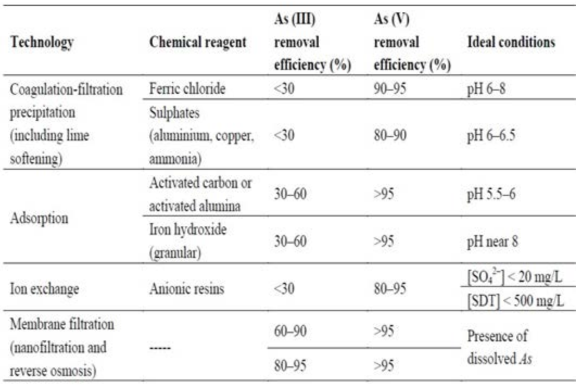

Technology	Chemical reagent	As (III) removal efficiency (%)	As (V) removal efficiency (%)	Ideal conditions
Coagulation-filtration precipitation (including lime softening)	Ferric chloride	<30	90–95	pH 6–8
	Sulphates (aluminium, copper, ammonia)	<30	80–90	pH 6–6.5
Adsorption	Activated carbon or activated alumina	30–60	>95	pH 5.5–6
	Iron hydroxide (granular)	30–60	>95	pH near 8
Ion exchange	Anionic resins	<30	80–95	[SO_4^{2-}] < 20 mg/L [SDT] < 500 mg/L
Membrane filtration (nanofiltration and reverse osmosis)	-----	60–90	>95	Presence of dissolved *As*
		80–95	>95	

Emerging Physico-Chemical Technologies:
The conventional technologies for arsenic removal referred above are fairly well documented, although some of the systems have only come into prominence in recent decades. Nowadays, extensive research has been conducted towards identifying new technologies for arsenic removal. These focus particularly on low-cost systems that can be applied to smallwater supply systems, in order to increase efficiency and improve the cost-benefit balance of arsenic removal. Technology research has also focused on the improvement of existing conventional technologies such as adsorption, by modifying or using novel adsorbent materials, or by introducing new chemical oxidation processes. Most of these technologies rely on the oxidation of arsenite followed by filtration through a porous material, where arsenic is removed through adsorptionand co-precipitation. TiO2 immobilization, on a PET (poly ethylene terephthalate) surface, combined with co-precipitation of arsenic on iron (III) hydroxides (oxides), could be an efficient way for total inorganic arsenic removal from waters. Because of their very strong affinity for arsenic, iron compounds are used by many removal systems. This is also the case for the application implemented and described in the case study presented below. Recent research work was developed to find a suitable iron (II) to arsenic ratio in water to reduce arsenic to 5 ppb (or lower) through slow sand filtration. It was found that a ratio of 40:1 was necessary to ensure the desired arsenic concentration in the treated effluent[11].

Alternative Technologies: Some alternative safe water options applied in West Bengal and Bangladesh include clay filters, deep tube wells, dug wells, surface and rainwater harvesting and solar distillation. Solar distillation techniques use the sun's energy to evaporate water, which is then re-condensed. This process of evaporation and re-condensation separates all chemicals, including arsenic, from the water. The SORAS (Solar Oxidation and Removal of Arsenic) process has been used in the rural Andes regions in Latin America. It is based on the adsorption of As(V) onto iron oxides and hydroxides using UV radiation and the addition of citrate as a catalyst for the formation of oxidizing radicals that allow the conversion of arsenite to arsenate. In this context, the combination of solar oxidation with one of the conventional adsorption processes might be a pertinent development towards yet another promissory alternative to arsenic removal. The goal would be to optimize the SORAS process by incorporating complementary conventional techniques, thereby increasing its reliability. To that effect, it was proposed that a UV radiation measurement cell be programmed so that the water to treat is automatically re- routed to a chemical oxidation process, whenever the available UV radiation is less than that required for arsenite oxidation. This alternative technology appears as particularly suitable for small and medium-size water supply systems. By integrating a solar radiation (renewable energy source) oxidation technology with conventional reactive filtration or adsorption processes, it is also aiming for the reduction of arsenic removalcosts[11].

II. SLUDGE DISPOSAL

All the arsenic treatment technologies ultimately concentrate arsenic in sorption media, sludge or liquid media and indiscriminate disposal of these mayleadto environmental pollution.Hence, environmentally safe disposal of sludge, saturated media and liquid wastes rich inarsenic is of high concern. Experiments were conducted to assess transformation of arsenicfrom aqueous solutions in the presence of cow dung. Some studies suggested that bio-chemical(e.g., bio-methylation) process in the presence of fresh cow-dung may led to significant reduction of arsenic from arsenic rich treatment wastes. Another optionwould be to blend the arsenic contaminated material into stable waste or engineeringmaterials such as glass, bricks, concrete or cement blocks. However, there is also possibility of air pollution or water pollution downstream of kilns burning bricks containing arseniccontaminatedsludgedue to volatilization of arsenic during burning at high temperature [10].

III. CONCLUSION

To remove arsenic from wastewaters, the most commonly used technologies are adsorption onto activated alumina, and precipitation or adsorption by metals oxides, predominantly Fe(III) and membranes. These technologies for removal of arsenic from wastewaters are most suited to dealing with relatively low concentrations of arsenic, i.e. the low µg/l level. However, the technique of precipitation, generally using Fe (III) or lime softening is suited to higher concentrations, normally at the low mg/l levels. Adsorption is a method that has been an important method used in arsenic removal. Most studies are focused on the type of adsorbent mediums and the economics of their regeneration. Membrane technology, especially Nano filtration, becomes a promising method in arsenic removal and is also widely considered as the methods that can be used to meet regulations for lowered arsenic concentrations in drinking water. Also the biotic oxidation of iron by the microorganisms is found to be a promising technology for effective removal of arsenic from groundwater. During this process, iron oxides were deposited in the filter medium, along with the microorganisms, which offer a favorable environment for arsenic to be adsorbed and removed from the aqueous streams. This technology offers several advantages towards the Conventional physicochemical treatment processes, applied in the removal of arsenic. It avoids the use of chemical reagents for the oxidation of trivalent arsenic; therefore, it is more economical and environment friendly. Other alternative methods also studied for their feasibility in replacing the current available methods. Future needs on arsenic removal technology should take into considerations of reducing the treatment cost, simplifying the operational complexity of the technology and disposal of arsenic bearing treatment residual.

REFERENCES

[1] Birgit Daus, Rainer Wennrich, Holger Weiss, 2004, Sorption materials for arsenic removal from water:a comparative study. Water Research38,2948–2954.

[2] Darrell Kirk Nordstrom,2002,Worldwide Occurrences of Arsenic in Ground Water, SCIENCE VOL 296,2143-2145.

[3] D. Mohan, C.U. Pittman Jr., 2007, Arsenic removal from water/wastewater usingadsorbents—A critical reviewJournalof Hazardous Materials 142,1–53.

[4] Dr. Laurent Dambies, 2005, Existing and Prospective Sorption Technologiesfor the Removal of Arsenic in Water, Separation Science and Technology-Vol. 39, No. 3, pp.603–627.

[5] EPA,2001,–ArsenicinDrinkingWater-Treatment Technologies‖: Removal,1-5.

[6] Erin Valentine, Michael George, and Lisa McIntosh, 2003,–Arsenicindrinkingwater‖.

[7] Ioannis A Katsoyiannis, AnastasiosZouboulis, 2004,Applicationof Biological Processes for the Removal ofArsenicfrom Groundwater–ARTICLE in Water Research 38,17–26.

[8] Liu Zhenzhong, Deng Huiping& Zhan Jian, 2007, Arsenic in Drinking Water and Its Removal, Chinese Journal of Population Resources and Environment-5,23-28.

[9] R. Nickson , C. Sengupta , P. Mitra , S. N. Dave, K. Banerjee , A.Bhattacharya , S. Basu , N. Kakoti,N.S.Moorthy,M.Wasuja,M.Kumar,

[10] D.S. Mishra , A. Ghosh , D. P. Vaish, A. K. Srivastava , R. M. Tripathi , S. N. Singh ,R. Prasad ,

[11] S. Bhattacharya & P. Deverill, 2007, Journal of Environmental Science and Health Part A 42, 1707– 1718.

[12] SSWM, 2004, Arsenic Removal Technologies, compiled by:Household sand filter operated by a family in the red river delta.Source: LUZI etal.

[13] Sustainability, 2009, Emerging and Innovative Techniques for Arsenic Removal Applied to a SmallWater Supply System,1288-1304.

[14] Thematic Overview Paper 17 by BranislavPetrusevski, Saroj Sharma, Jan C. Schippers (UNESCO-IHE), and Kathleen Shordt (IRC), Reviewed by: Christine van Wijk(IRC). –Arsenic in drinking water‖. IRC International Water and Sanitation Centre, March2007.

[15] Thomas S.Y. Choonga, T.G. Chuaha, Y.Robiaha,

[16] F.L. Gregory Koaya, I. Aznib, 2007, Arsenic toxicity, health hazards and removal techniques from water: an overview,139–166.

★★★

EXTENSION AND STRENGTH PROPERTIES OF CEMENT CONTAINING REUSED SOLID TOTAL

[1]SUBHALIPSA PRADHAN, [2]ALIVASAKHI MISHRA, [3]NILGRIB MOHANTY

[1]Assistant Professor, Department of Civil Engg., NMIET, BBSR
[2]Asst Prof, Department of Civil Engineering CEC BBSR
[3]Asst Prof, [3]Department of Civil Engineering AIET BBSR
E-mail: [1]Bagchi.suchampa@nmiet.ac.in

Abstract - In the Middle East locale, inside dividers of structures are generally put with gypsum. Hence, the destruction squanders are presumably gypsum sullied, which may prompt inward sulfate assault in new cements containing reused concrete. This examination gives the findings of a test examination on cement made with reused solid totals defiled with development gypsum (unhydrous calcium sulfate). For this, four gatherings of blends were readied. In the first gathering, the characteristic sand was part of the way and completely supplanted by tainted fine reused solid total. In the subsequent gathering, the regular rock was incompletely and completely subbed by debased coarse reused solid total. In the third gathering, both sand and rock were subbed by polluted reused solid total, while the fourth gathering was coordinated to examine the impact of silica rage on cement made with reused solid total. The deliberate properties were development, compressive strength, parting rigidity and modulus of burst. The outcomes demonstrated that the higher the rate level of tainted reused totals the lower the strength and the higher the extension. The best outcomes were recorded for the second gathering of blends. In all cases, the development didn't surpass the restriction of 0.05%.

Keywords - Contaminated; Aggregate; Recycled Aggregate; EXPANSION; Strength; Gypsum; Silica Fume

I. INTRODUCTION

Theoutputofhugeamountsofsolidwastesisoneofthemostunfavorableconsequencesoftheglobalpopulationand economygrowth.ConstructionandDemolitionWastes(CDW)areoneofthemostcommonandlargestmunicipalwastes thatimposeenormouscostsoflandfillmanagementandtransportationbesidestheirnegativeimpactontheenvironment.In Europe for example, 34% of more than 2500 million tons of annual solid wastes is CDW [1]. On the other hand, the huge constructionworksleadtoconsumehugequantitiesofnaturalfineandcoarseaggregates.Thedemandofnaturalaggregate for construction industry has been doubled during the last 10 years reaching an annual of 40 billion tons [2]. A remedy solution to these problems is the recovery and the recycling of old concretes to produce concrete aggregates. The annual global CDW output exceeds 2000 million tons with an average recovery percentage of more than 50% [2]. The recovery percentage ranges from less than 10% in some developing countries to more than 90% in countries like Taiwan, Japan, Denmark and Netherlands[2,3].

ThepropertiesofnewconcretemadewithRecycledConcreteAggregate(RCA)mayvarydependingon(1)thestrengthof oldconcretefromwhichtheRCAisderived,(2)theprocedureofproducingRCA,and(3)themoistureconditionofthe RCA. Accordingly, there is a contradiction between the authors regarding some properties of concrete produced withRCA. Thevastoftheliteraturereviewshowedthatusing50%RCAormorewouldadverselyaffectthemechanicalpropertiesof concrete.However,somestudiesshowedthattheuseofRCAinconcreteisnotalwaysunfavorableandgoodpropertiesmay be achieved when the mix proportions are selected carefully [4–8]. Indeed, the material characteristics like strength, modulusofelasticity,dryingshrinkage,waterabsorption, totalporevolumeandcarbonationarenotsignificantlyaltered whenabout20%ofvirginaggregateisreplacedbyRCA[9–15].Otherpreviousresearchersshowedthatcompressive strength may be comparable or slightly greater when recycled aggregate from better quality concrete sources is used [16–20]. However,theuseoffineRCAmayincreasethetimedependentstrainsincludingcreepanddryingshrinkagebecausethis typeofrecycledaggregatecontainsoldmortarsandcementpastes[10]. SomereinforcedconcretememberssuchaswallsandslabsarefinishedwithconstructiongypsumandplasterofParis. Therefore,thedemolitionwastesderivedfromthesemembersarecontaminatedwithgypsum.Thepresenceofgypsummayleadtocompositioninducedinternalsulfateattack.Thistypeofattackisgeneratedatnormaltemperaturesduetotworeactions.ThefirstreactiontakesplaceandoccursbetweengypsumandC_3Awiththepresenceofwaterproducingettringite,whilethesecondhappensbetweencalciumsulfatefromgypsumandthemonosulfatephasethatpresentinthehydratedcementpasteproducingexpansiveettringite.Theformerreactioninitiatesdirectlyaftermixinganditisnecessarytocontrolsetting, it becomes unfavorable when it generates beyond setting stages because of the formation ofexpansiveettringite.Some previous researches were found in the literature about the effect of internal attack of sulfate onthemechanicalpropertiesanddurabilityofconcretesandmortars[9,21–23].Astudycarriedoutontheexpansionofmortarsincorporatedwithfine RCAshowedthattheexpansionofmortarsdidnotexceedtheexpansionlimitof0.1%availableintheliteraturethoughtheSO$_3$contentinthesandwas2.9%[9].Thisencouragingfindingwasvalidirrespectiveofthetypeofcementused.Otherstudies[22,23]usedfineaggregatewithdifferentgypsumcontaminationcontentsasareplacementofsilicasandinultra-highperformanceconcrete.Theyshowedthatlowgypsumcontentscouldslightlyincreasethecompressiveandsplittingstrengthsofconcretesamples,whilesuchresultswasnotobservedforordinarymortars.Theyalsoshowedthatthe expansion of contaminated mortars was noticeably higher as the gypsum content increased.

II. RESEARCH SIGNIFICANCE

Asintroduced,manystudieswerecarriedoutoneitherRCAorgypsum-contaminatedaggregate.However,verylimited informationisavailableregardingthebehaviorofconcretewhenRCAiscontaminatedwithgypsum.Theselimitedstudies were focused on mortars rather than concretes. Besides, the effects of RCA contaminated with gypsum on the strength properties were not previously studied. Therefore, further information is still required dealing with the strength and durabilityofthistypeofconcrete.Thepresentstudyhasinvestigatedthestrengthanddurabilitycharacteristicsofconcrete made with gypsum contaminated fine and coarse RCA with different replacement dosages ranging from 0 to 100%. The sourceofthecontaminatedrecycledaggregatewascrushedgypsum-plasteredconcretecubes.Theinvestigatedproperties wereexpansion,compressivestrength,splittingtensilestrength,andmodulusofrupture.

III. EXPERIMENTAL WORK

3.1 Materials

TheordinaryPortlandcement(ASTMtypeI)havingafinenessof312m^2/kgandspecificgravityof3.15g/cm^{3}wasusedin thisstudy,whilesilicafumewithafinenessof21,100m^2/kgandspecificgravityof2.2g/cm^{3}wasalsoutilizedinsomemixes. LocalgradednaturalfineandcoarseaggregatesfromWasitprovince/Iraqwereadoptedintheexperimentalwork.Gypsum-contaminatedRCAswerealsousedasfineandcoarseaggregates.Inordertosatisfytherequiredworkability,highrange water reducer admixture was added to somemixes.


(a) plastering molds (b) preparing cubes for plastering

Fig. 1. Gypsum-plastering of cubes made as source contaminated recycled concrete.

3.2 Preparing gypsum contaminated RCA

Theproducingmethodofgypsum-contaminatedRCAwasasfollows:(1)asufficientnumber ofconcretecubeswerecast fromnaturalaggregatetoproduceaconcretewithacubecompressivestrengthof25MPa.(2)Thecubeswerecuredupto28 days,thentheywereplasteredwithgypsum(unhydrouscalciumsulfate)fromaonesidewithathicknessof12mm.Fig.1showstheprocessofpreparationandplasteringofthesourceconcretecubes.(3)Afterthat,thecubeswerecrushedtoobtain thegypsum-contaminatedRCA.Toassurethatalltheplasteringgypsumisincludedintherecycledaggregate,thecubes werefirstkeptinplasticbagsandcrushedinacompression machinebeforecrushingtofinerparticles.Fig.2showsapatchof sourcegypsum-plasteredcubes,whileFig.3showstheinitialcrushingprocessofthesecubes.ThegradationofRCAswas adjusted manually so that it became similar tothat of natural aggregates. The sieve analysis of the recycled aggregates is presentedinFig.4.Thecontentofacidsolublesulfates,SO$_3$inthegypsumcontaminatedRCAwas1.5%byweight.In orderto compensateforthehighwaterabsorptionofRCAs,theywerepre-soakedinwaterfor24hpriortocasting.

3.3 *Preparing, mixing and testing*

Thereferencemixhasbeendesignedwithatargetcompressivestrengthof25MPa.Theconcretemixesareclassifiedinto fourgroups.AsshowninTable1,threetypesofaggregatereplacementmethodswereadopted,namelysandreplacement, gravelreplacementaswellasbothsandandgravelreplacement.Thereplacementlevelswere20,40,60,80,and100%.In otherwords,thenaturalsandwaspartiallyandfullyreplacedbyfineRCAinaGroupAmixes.InGroupBmixes,thegravel wassubstitutedbycoarseRCAatvariouslevels.InGroup C,bothsandandgravelwerereplacedwithfineandcoarse RCAs.In thefourthgroup(GroupD)andtomonitortheinfluenceofsilicafume,itwasincorporatedinthemixeswiththehighest replacementlevel.

The concretes were mixed in a drum type mixer of 0.1 m^3 capacity. Initially, aggregates with a small quantity of water were mixed. Thereafter, the cement and silica fume with the rest of water were added and mixing was resumed until a homogenous mixture wasachieved.

The testing methods of hardened concretes involved expansion, compressive strength, splitting tensile strength, and modulus of rupture for third point bending samples. The specimens used were 100 mm cubes for compressive strength,

150 300 mm cylinders for splitting tensile strength and 100 100 400 mm for both expansion and modulus ofrupture. The strength properties were measured after 7, 28, and 90 days of curing in water, while the expansion was measured at specified ages up to 6 months of curing in water. Immediately after demolding, two demec points were glued on each expansionsampletomeasurethelengthchangeviaextensometeratthespecifiedages.

IV. RESULTS AND DISCUSSION

4.1 Compressive strength

Figs.5–7toshowtheeffectofreplacementlevelofsand,gravelandbothofthembyRCAonthecompressivestrengthofconcrete.Itcanbeseenthat,thecompressivestrengthdecreasedwithincreasingtheRCAreplacementlevelirrespectiveof thereplacementtype.However,thehighestdecrease,whichvariedfrom6to38%,wasrecordedformixesofGroupC in whichboththesandandgravelwerereplacedbyrecycledaggregates.ThespecimensofgroupA,inwhichsandwasreplaced byfineRCA,showedthesecondhighestdecreaseincompressivestrengthof7to31%.Ontheotherhand,thecompressive strengthoftheGroupBmixeswaslessaffectedbythesubstitutionofcoarseaggregatebycoarseRCAsuchthatthehighest recorded percentage decrease was27%.

Fig. 2. A batch of source gypsum-plastered cubes.

Fig. 3. Initial crushing of source cubes.

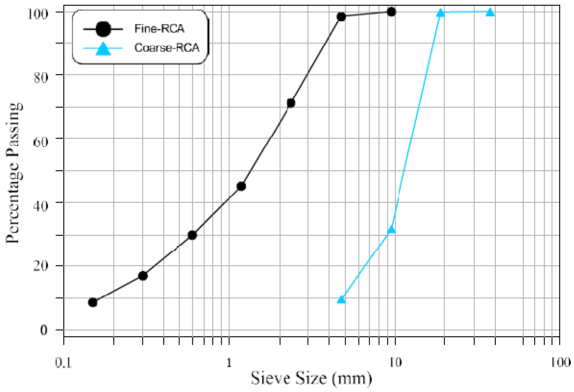

Fig. 4. Sieve analysis of fine and coarse RCA.

ThecompressivestrengthbehaviorofthenewconcretederivedfromRCAcouldberelatedtothelowqualityofsourceconcreteaswellastheporousinterfacialtransitionzonebetweenaggregateandcementpaste.Manypreviousstudiesalso provedtheadversenessofthestrengthofconcretemadefromrecycledconcreteaggregate[11,12,14,24–26]. Inthepresent studythecombinationeffectofgypsumandrecycledconcreteaggregatealsoledtodecreasethecompressivestrengthofthe new concrete. Furthermore, the decrease in compressive strength was higher in sand replacement as comparedto gravel replacement. Gesoglu et al. [23] reported a continuous decrease with the increase of gypsum content in the compressive strengthofcementmortarsmadeofcontaminatedfineaggregates.Theyshowedthatthestrengthdecreasereachedupto approximately40%foragypsumcontentof11.5%.Thehigherspecificsurfaceareaofgypsumparticlesthatwerepresentin fine recycled aggregate compared to those present in coarse aggregate accelerates the interaction between fine gypsum particlesandC_3Aandleadstoproducemoreettringite.Furtherstrengthdeteriorationoccurredwhenbothsandandgravel were substituted by contaminated RCA because of the accumulated higher gypsum content in theseaggregates.

When the strength development of the mixes was considered, it can be seen that all the mixes even those with high gypsum content developed strength with age as shown in Figs. 5–7. The growth in strength could be related to the continuousinteractionofcementandcuring water.Moreover,someporeswereeventuallyfilledwithettringite.Ouyang et al. [27] found that the compressive strength increases with age initially and then dropped depending on the C_3A and cement content in the mix. The apparent contradiction between both studies could be related to the much higher SO_3 contentusedinthepreviousone(7%)ascomparedtothecurrentone(2%).

Table 1
Mix proportion of concrete (kg/m^3).

Specimen'sGroup	CodeNumber	Cement	Silicafume	Water	SP	Coarseaggregate		Fineaggregate		w/b	Slump(mm)
						NCA	RCA	NFA	RFA		
Reference	CM	380	0	210	0	980	0	790	0	0.55	95
A	MRC20	380	0	210	0	784	196	790	0	0.55	90
	MRC40	380	0	210	1.9	588	392	790	0	0.55	95
	MRC60	380	0	210	1.9	392	588	790	0	0.55	90
	MRC80	380	0	210	2.28	196	784	790	0	0.55	85
	MRC100	380	0	210	2.28	0	980	790	0	0.55	85
B	MRF20	380	0	210	0	980	0	632	158	0.55	90
	MRF40	380	0	210	0	980	0	474	316	0.55	85
	MRF60	380	0	210	2.28	980	0	316	474	0.55	80
	MRF80	380	0	210	2.66	980	0	158	632	0.55	85
	MRF100	380	0	210	3.42	980	0	0	790	0.55	85
C	MRCF20	380	0	210	1.9	882	98	711	79	0.55	85
	MRCF40	380	0	210	2.28	784	196	632	158	0.55	80
	MRCF60	380	0	210	3.04	686	294	553	237	0.55	80
	MRCF80	380	0	210	3.42	588	392	474	316	0.55	75
	MRCF100	380	0	210	2.8	490	490	395	395	0.55	70
D	MRC100S	342	38	210	1	0	980	790	0	0.55	80
	MRF100S	342	38	210	1	980	0	0	790	0.55	80
	MRCF100S	342	38	210	1.1	490	490	395	395	0.55	75

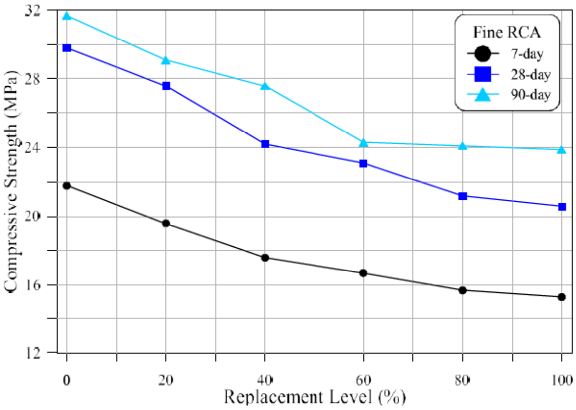

Fig. 5. Variation of compressive strength with contaminated fine RCA.

4.2 Splitting tensile strength and flexural strength

Concrete is known for its weakness in tension. One of the tests used to evaluate the tensile strength of concrete is the splittingtest.Thesplittingtensilestrengthofconcreteissensitivetotheaggregatetypeandisrelatedtothecompressive strength. On the other hand, the flexural beam test (modulus of rupture) can be used as an indicator for reductionsinsplittingtensilestrengthwereapproximatelyintherangesof8–17%,16–21%,20–31%and22–33%,respectively, while strength gain was recorded for some samples at a replacement level of 20%. The better results of the specimens in

both theflexural strengthandindirectlythetensilestrength.Therefore,boththesplittingtensileandtheflexuraltestswereconductedinthis researchtoevaluatetheeffectoftheincorporationofsulfate-contaminatedRCA. Thetestresultsofthesplittingtensilestrengthfortheconcretemadewithcontaminated RCAarepresentedinFigs.8–10. Aswiththecompressivestrength,thesplittingtensilewasadverselyaffectedbytheinclusionofRCAandthehigherthe substitution level the lower the retained strength. In all cases, the reduction in strength was increased as thesubstitution level increased. Fig. 8 shows that for fine RCA replacement and for the three ages of concrete, the reductions in splitting tensilestrengthwereintherangesofapproximately9–13%,17–20%,21–28%,28–35%and31–35%forreplacementlevelsof 20,40,60,80and100%,respectively.Ontheotherhand,lowerreductionlevelswererecordedforcoarseRCAreplacementsas showninFig.9.ForcoarseRCAreplacementlevelsof40,60,80and100%andforthethreetestages,thepercentage

whichthegravelwaspartiallyandtotallyreplacedbycontaminatedcoarseRCAareattributedtotheslowdissolutionof coarsegypsumparticlesinwater,whichisnotenoughtopromoteettringiteformation.

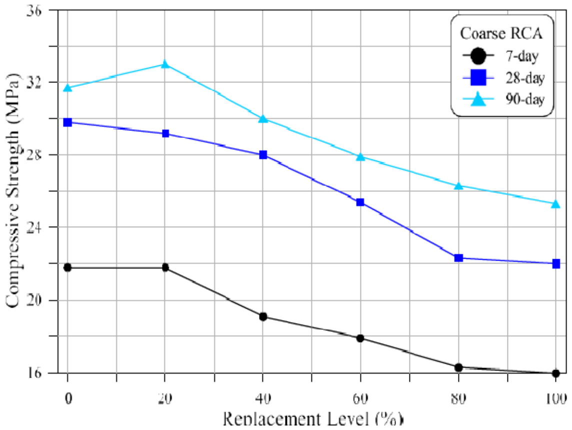

Fig. 6. Variation of compressive strength with contaminated coarse RCA.

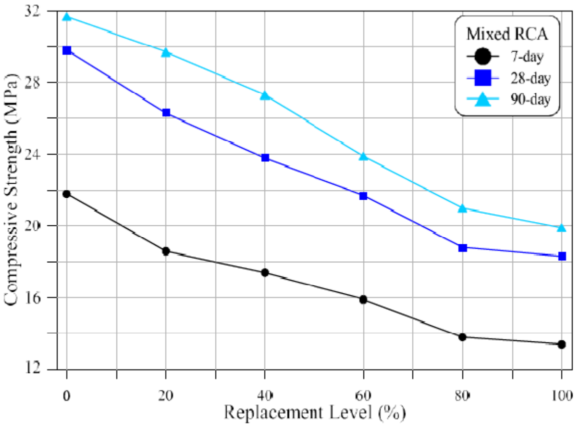

Fig. 7. Variation of compressive strength with contaminated mixed RCA.

Fig.10showsthedeclinedsplittingstrengthofspecimens withmixedsubstitutionoffineandcoarseRCA(GroupC). This caseofreplacementledtothehighestlevelsofstrengthreductionamongthethreegroupsofspecimens.Forthethreetest ages, the strength reduction values were 7–39% when both natural aggregates were replaced by fine and coarse RCA comparedto9–35%foronlyfineRCAreplacementand6–33%forcoarseRCAreplacement.

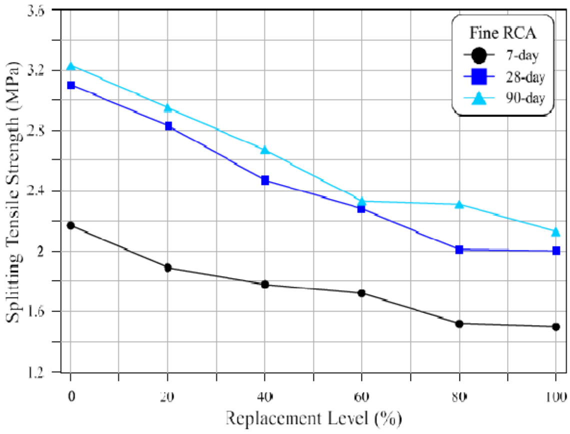

Fig. 8. Variation of splitting tensile strength with contaminated fine RCA.

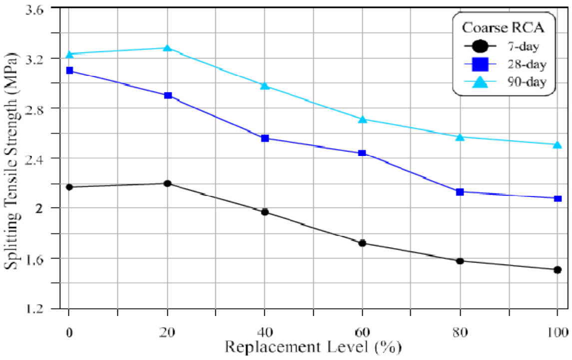

Fig. 9. Variation of splitting tensile strength with contaminated coarse RCA.

Figs.11–13 showthattheflexuralstrength(modulusofrupture)showedsimilartrendofdeclinewiththeincreaseofRCA replacement level. Similar to the splitting tensile strength, the fine RCA replacement was found of larger impact on the flexuralstrengththanofcoarseRCAreplacement,whilethelargestreductionlevelsinflexuralstrengthwererecordedforthe caseofmixedRCAreplacement.Forthethreecuringages, therangesofpercentagereductionintheflexuralstrength were6–33%,0–28%and6–41%forfine,coarseandmixedRCAreplacements,respectively.Thisagaincanbeattributedtothefaster dissolution of the fine gypsum particles, which maximizes their negative impact by the formation of the undesirable ettringiteformation.

It is worth noting that the RCA which is resulting from old concrete contains both original particles as well as mortar adheredonthem.ThenewmortarincorporatedwithRCA, therefore,consistsoftwointerfacialtransitionzones;one ofthem ispositionedbetweentheoriginalparticlesandtheadheredmortarwhiletheotheroneislocatedbetweenthenewmortar andRCA.Thisgeneratestheweaknessregionsinthemicrostructureofthenewconcretesparticularlyunderthebending loads, and thus reducing the flexural strength and fracture energy of concrete. Some recent researches have investigated theseinterfacialtransitionzonesusingadvancedtechniques[28–31].

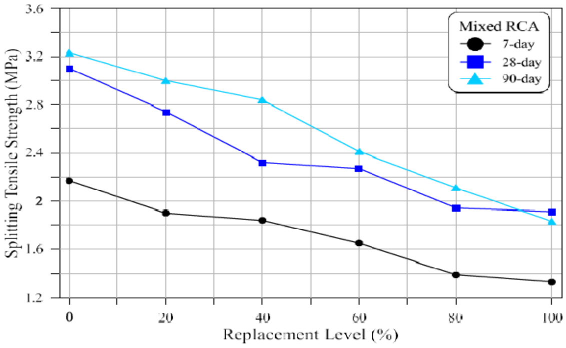

Fig. 10. Variation of splitting tensile strength with contaminated mixed RCA.

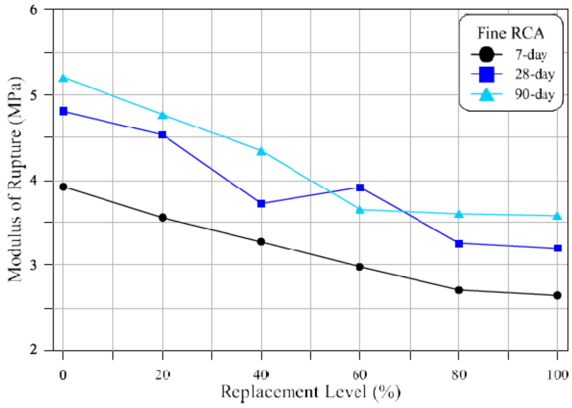

Fig. 11. Variation of modulus of rupture with contaminated fine RCA.

4.3 Expansion

Figs.14–16showthevariationofexpansionofconcretemadewithRCAwithage.Obviously,theexpansionofconcrete increasedwithtime.Thisisbecausewhilemaintainingthe concretesamplesinwater,theCSHgelabsorbswaterandthe moleculesofwatercausetheparticlesofgeltofurtherapart.Withcuringtime,furthersmallswellingoccursasaresult of decliningthesurfacetensionoftheCSHgel[32].Ineachgroupofmixes,theexpansionstrainwashigherwithincreasing thereplacementlevelofvirginaggregatebycontaminated RCA.However,thehigheststrainswereobservedforGroupC mixes,wheremixedRCAwasused,becauseoftheirhighestSO$_3$contentinaggregatefollowedbythegroupoffineRCA (Group A), while the specimens of the Group B where coarse RCA was used showed the lowest strains. The maximum recordedexpansionsforthethreegroupswithreplacementsoffineRCA,coarseRCAandmixedRCAwere0.046,0.026,and 0.048%, respectively. Thus, the results of expansion test fully support the results trend of the compressive and tensile strengths discussed earlier. Indeed, increasing gypsum content in the mix leads to form further ettringite. The ettringite generated at early ages (beforesetting)isnotharmfulandevennecessarytocontrolsetting.However,itbecomesadversenesswhenitdevelopslater (athardenedstage)becauseexpansionofhardenedmatrix developscracksandhenceweakensthesystem[32].Asreported by [33], the use of recycled concrete aggregates instead of natural aggregate increases the expansion of concrete, so the relativelyhigherexpansivestrainsofmixeswithcontaminatedaggregatesascomparedtocontrolmixeswerenotonlydue to the existence of excessive sulfates in aggregate but also due to recycled concrete aggregates. However, it is difficult to distinguishtheeffectoftheadheredmortarontherecycled aggregateparticlesfromtheeffectofthegypsumbecauseeach oneofthemmayincreasetheexpansionstrain.

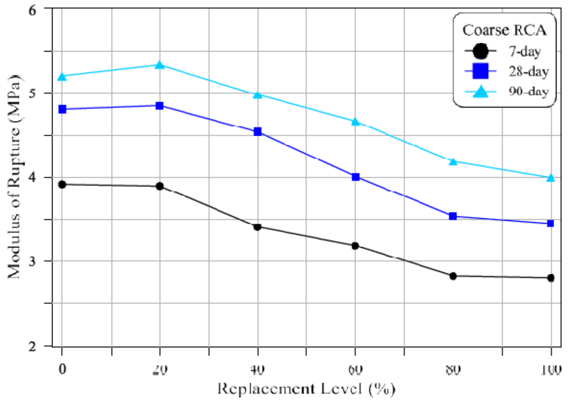

Fig.12.VariationofmodulusofrupturewithcontaminatedcoarseRCA.

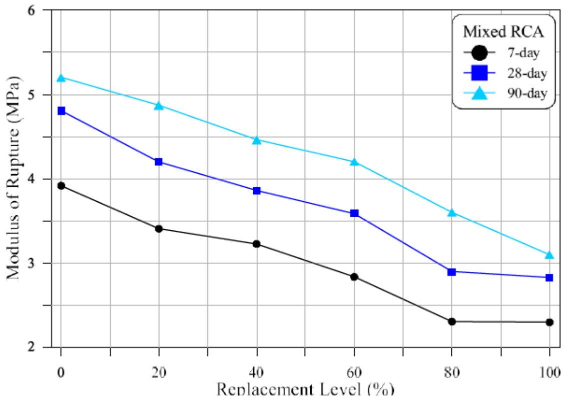

Fig. 13. Variation ofmodulus of rupture with contaminated mixed RCA.

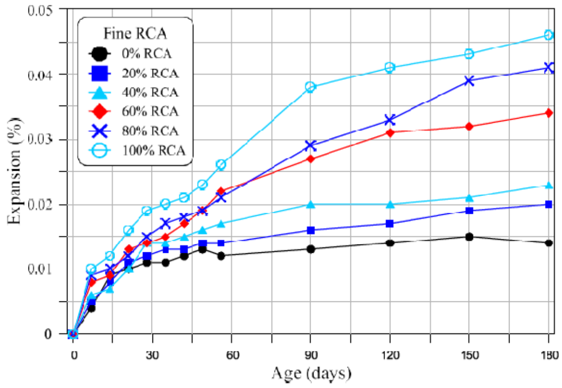

Fig. 14. Expansion with time for concrete with different contaminated fine RCA contents.

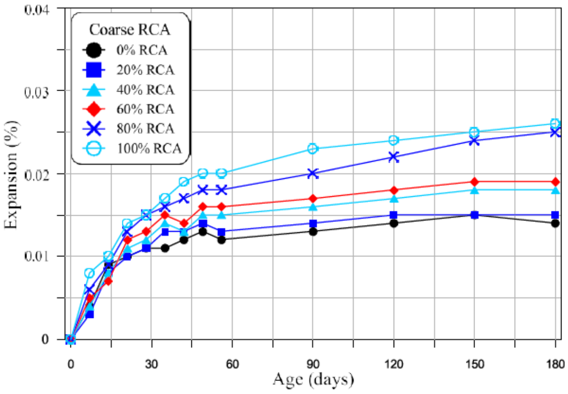

Fig. 15. Expansion with time for concrete with different contaminated coarse RCA contents.

SomestandardsprovidelimitsforsulfatecontentinaggregateexpressedasSO_3.Regardingnaturalaggregate,thislimit is 0.5%forfineaggregateand0.1%forcoarseaggregateintheIraqistandards[34],whileASTMandENstandardsdonotprovide any limitations. The reason may be due to the absence of appreciable sulfates in the natural aggregate of their regions. However, the EN standard requires that the SO_3 content in recycled aggregate must not exceed 1%. On the other hand, researchers [9,35,36] have adopted the expansion strain to determine the quality of concrete made with gypsum contaminated aggregate even in all cases the SO_3 level in aggregate exceeds the standard limits. They reported that the concrete or mortar is acceptable whenever the expansion is not higher than 0.1% after one year of immersing in water or 0.05% after 6 months of immersing in water. In the present study, the expansion did not exceed 0.048% in all cases, morepromisingresultswereachievedingroupsAandBwhereeithersandorgravelwerepartiallyorfullyreplacedbyRCA.Otherstudyalsosuggestedagreatpotentialforuseofcontaminatedrecycledaggregateinconstructionindustrythoughthatstudywasfocusedonexpansionofmortarsonly[9].

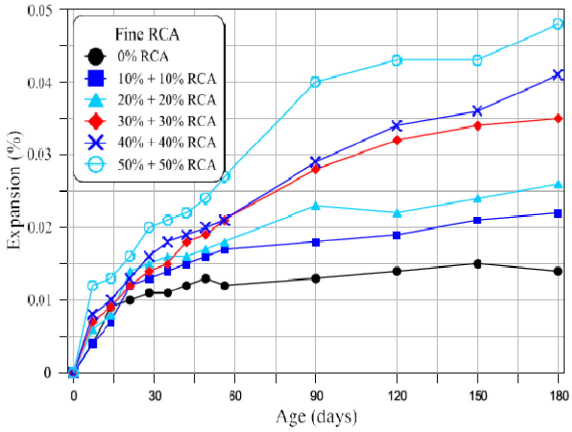

Fig. 16. Expansion with time for concrete with different contaminated mixed RCA contents.

4.4 Effect of silicafume

Silica fume is a very reactive pozzolanic material because of its physical and chemical features. When using this by- product material in concrete, a significant development in compressive and tensile strengths is expected. Figs. 17–19illustrate the influence of silica fume on the compressive strength, splitting tensile strength and modulus of rupture of concrete when sand, gravel and both of them were fully replaced by recycled fine (F), coarse (C) and mixed (M) RCA aggregates.Thefiguresshowcomparisonsbetweenthestrengthofconcretewith100%contaminatedRCAwithand without the10%cementsubstitutionbysilicafume.ThelittersSFinFigs.17–19refertothepresenceofsilicafume.

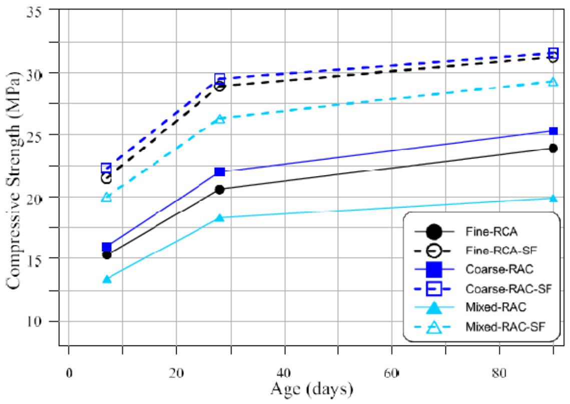

Fig. 17. Effect of silica fume on compressive strength of specimens with 100% RCA.

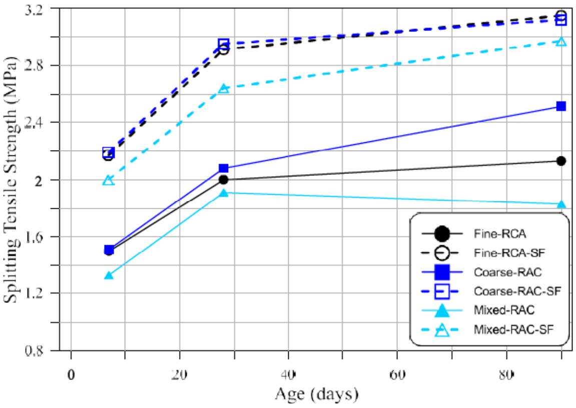

Fig. 18. Effect of silica fume on splitting tensile strength of specimens with 100% RCA.

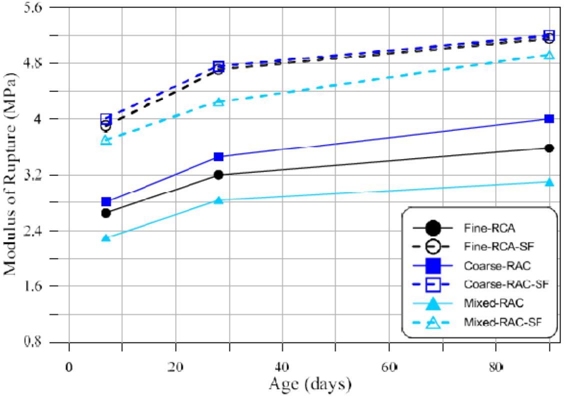

Fig. 19. Effect of silica fume on modulus of rupture of specimens with 100% RCA.

Figs. 17–19 show that the retained compressive strength, splitting strength and modulus of rupture were significantly improvedbytheadditionofsilicafume.Obviously,thesilicafumecompensatedforthestrengthreductioncausedbythe present of waste concrete aggregate such that both traditional concrete and that made with RCA showed almost similar strengths. The enhanced aggregate-matrix interfacial transition zone could be the reason behind such behavior because silicafumemakesthiszonedenserandstructurallystronger.Thepercentagedevelopmentincompressivestrengthdueto silicafumeadditionforthethreegroupswithfine,coarseandmixedcontaminatedRCAandforthethreeagesrangesfr om approximately25to50%.Similarly,thedevelopmentsinsplittingtensilestrengthandmodulusofrupturerangefrom 24to 62%and30to61%,respectively.Theresultsofthecurrentresearchareinconsistentwithpreviousresearches[37,38]that showedbetterstrengthanddurabilityperformanceofRCAspecimensincorporatedsilicafumecomparedtothosewithout silicafume.

V. CONCLUSIONS

1. Fromtheresultsoftheexperimentalworkconductedinthisstudy,thefollowingsconclusionscanbedrawn,
2. The compressive strength was lower with increasing the replacement level of virgin aggregate by contaminated RCA. However, the lowest strengths were recorded for Group C mixes in which the sand and gravel were replaced by contaminatedRCA,followedbyGroupAinwhichsandwasreplacedbycontaminatedRCA.Ontheotherhand,GroupB showedthebestresultsamongthethreegroupsofmixes.
3. The splitting tensile strength and flexural strength generally exhibited trend similar to compressive strength. The maximum reductions in splitting tensile strength due to the use of fine, coarse and mixed RCA were 35%, 33% and 39%, respectively,whiletheywere33%,28%and41%for flexuralstrength,respectively.
4. IncreasingthereplacementlevelofcontaminatedRCAledtoincreasetheexpansionstrainofconcreteofthe threegroups ofmixtures.However,thelargeststrainsweregenerallyobservedforGroupCmixesbecauseoftheirhighestSO_3content in aggregate, followed by group A and Group B. In all cases, the maximum recorded expansion was0.048%.
5. The use of silica fume counterbalanced the strength reduction and strain increment due to the replacement of natural aggregatebycontaminatedRCA.Thepercentagedevelopmentincompressive,tensileandflexuralstrengthsduetosilica fume inclusion ranged from 24 to62%.

REFERENCES

[1] R.V.Silva,J.Brito,R.K.Dhir,Establishingarelationshipbetweenmodulusofelasticityandcompressivestrengthofrecycledaggregateconcrete,J.Clean. Prod. 112 (2016)2171–2186.

[2] V.W.Tam,M.Soomro,A.C.Evangelista,Areviewofrecycledaggregateinconcreteapplications(2000-2017),Constr.Build.Mater.172(2018)272–292.

[3] J.Barritt,Anoverviewonrecyclingandwasteinconstruction,ICE Proc,Constr.Mater.169(2015)1–5.

[4] J.M.Khatib,Propertiesofconcreteincorporatingfinerecycledaggregate,Cem.Concr.Res.35(2005)763–769.

[5] L.Evangelista,J.deBrito,Mechanicalbehaviorofconcretemadewithfinerecycledconcreteaggregates,Cem.Concr.Comp.29(2007)397–401.

[6] V.Corinaldesi,G.Moriconi,Behaviorofcementitiousmortarscontainingdifferentkindsofrecycledaggregate,Constr.Build.Mater.23(2009)289–294.

[7] L.F.R.Miranda,S.M.S.Selmo,CDWrecycledaggregaterenderings,PartII–Analysisoftheeffectofmaterialsfinerthan75lmunderaccelerated aging performance,Constr.Build.Mater.20(2006)625–633.

[8] C.Shi,Y.Li,J.Zhang,W.Li,L.Chong,Z.Xie,Performanceenhancementofrecycledconcreteaggregate-Areview,J.Clean.Prod.112(2016)466–472.

[9] G.T.Rodríguez,M.Barra,S.Pialarissi,D.Aponte,E.Vázquez,Expansionofmortarswithgypsumcontaminatedfinerecycledaggregates,Constr.Build. Mater. 38 (2013)1211–1220.

[10] M.Alexander,S.Mindess,Aggregatesinconcrete,ModernConcreteTechnologySeries(2010)435.

[11] B.H.Hamad,A.H.Dawi,Sustainablenormalandhighstrengthrecycledaggregateconcretesusingcrushedtestedcylindersascoarse aggregates,Case Stud, Constr. Mater. 7 (2017)228–239.

[12] D.Carro-Lopez,B.Gonzalez-Fonteboa,J.Brito,F.Martinez-Abella,I.Gonzalez-Taboada,P.Silva,Studyoftherheologyofself-compactingconcretewith

[13] fine recycled concrete aggregates, Constr. Build. Mater. 96 (2015) 491–501.

[14] C. Alexandridou, G.N. Angelopoulos, F.A. Coutelieris, Mechanical and durability performance of concrete produced with recycled aggregates from Greek construction and demolition waste plants, J. Clean.Prod. 176 (2018) 745–757.

[15] C.Medina,W.Zhu,T.Howind,M.I.Rojas,M.Frias,Influenceofmixedrecycledaggregateonthephysical-mechanicalpropertiesofrecycledconcrete,J. Clean. Prod. 68 (2014)216–225.

[16] F.Liu,W.Feng,Z.Xiong,G.Tu,L.Li,Staticandimpactbehaviourofrecycledaggregateconcreteunderdailytemperaturevariations,J.Clean.Prod.191(2018)283–296.

[17] C.S.Poon,Z.H.Shui,L.Lam,EffectofmicrostructureofITZoncompressivestrengthofconcretepreparedwithrecycledaggregates, Constr.Build.Mater.18 (6) (2004)461–468.

[18] Z. Wang, L. Wang, Z. Cui, M. Zhou, Effect of recycled coarse aggregate on concrete compressive strength, Trans. Tianjin Univ. 17 (3) (2011)229–234.

[19] K.Yang,H.Chung,A.Ashour,Influenceoftypeandreplacementlevelofrecycledaggregatesonconcreteproperties,ACIMater.J.105(3)(2008)289–296.

[20] R.V. Silva, J. Brito, R.K. Dhir, Performance of cemenetitious renderings of masonry mortars containing recycled aggregates from construction and demolition wastes, Constr. Build. Mater. 105 (2016)2171–2186.

[21] C.Thomas,J.Setien,J.A.Polanco,Structuralrecycledconcreteaggregatemadewithprecastwastes,Constr.Build.Mater.114(2016) 536–546.

[22] F.Debieb,L.Courard,S.Kenai,R.Degeimbre,Mechanicalanddurabilitypropertiesofconcreteusingcontaminatedrecycledagregates,Cem.Concr. Comp 32 (2010)421–426.

[23] M. Gesoglu, E. Guneyisi, A. Nahhab, H. Yazici, Properties of ultra-high performance fiber reinforced cementitious composites made with gypsum-contaminatedaggregatesandcuredatnormalandelevatedtemperatures,Constr.Build.Mater.93(2015)427–438.

[24] M.Gesoglu,E.Guneyisi,A.Nahhab,H.Yazici,Theeffectofaggregateswithhighgypsumcontentontheperformanceofultra-highstrengthconcretes and portland cement mortars, Constr. Build. Mater.110 (2016) 346–354.

[25] T.Ozturan,C.Cecen,Effectofcoarseaggregatetypeonmechanicalpropertiesofconcreteswithdifferentstrengths,Cem.Concr.Res. 27(2)(1997)165–170.

[26] M.Tokyay,Effectofaggregatetypeonmechanicalpropertiesofhighstrengthconcrete,Tek.Dergi9(2)(1998)1627–1638.

[27] N.Bui,T.Satomi,H.Takahashi,Improvementofmechanicalpropertiesofrecycledaggregateconcretebasingonanewcombination methodbetween recycled aggregate and natural aggregate, Constr. Build. Mater.148 (2017) 376–385.

[28] C.Ouyang,A.Naani,W.F.Chang,Internalandexternalsourcesofsulfateionsin Portlandcementmortar:twotypesofchemicalattack, Cem.Concr.Res.18 (5) (1988)699–709.

[29] W.G.Li,Z.Y.Luo,C.Long,C.Q.Wu,W.H.Duan,S.P.Shah,Effectsofnanoparticleonthedynamicbehaviorsofrecycledaggregateconcreteunderimpact loading, Mater. Des. 112 (2016)58–66.

[30] W.G. Li, Z.Y. Luo, Z.H. Sun, Y. Hu, W.H. Duan, Numerical modelling of plastic-damage response and crack propagation in RAC under uniaxial loading, Mag. Concr. Res. 70 (2017)459–472.

[31] W.G. Li, Long Chu, V. Tam, C.S. Poon, W.H. Duan, Effects of nanoparticles on failure process and microstructural properties of recycled aggregate concrete, Constr. Build. Mater. 142 (2017)42–50.

[32] B. Lie, W.G. Li, Z. Tang, V. Tam, Z. Sun, Durability of recycled aggregate concrete under coupling mechanical loading and freeze-thaw cycle in salt- solution, Constr. Build. Mater. 163 (2018)840–849.

[33] A.M. Neville, Properties of Concrete, Longman, New York,1995.

[34] J.M.Khatib,Propertiesofconcreteincorporatingfinerecycledaggregate,Cem.Concr.Res.35(2005)763–769.

[35] IraqiOrganizationofStandards,IOS45:1984,forAggregate.

[36] N.J.Crammond,Examinationofmortarbarscontainingvaryingpercentagesofcoarselycrystalinegypsumasaggregate,Cem.Concr.Res.14(2)(1984) 225–230.

[37] H.N.Atahan,D.Dikme,Useofmineraladmixturesforenhancedresistanceagainstsulfateattack,Constr.Build.Mater.25(2011)3450–3457.

[38] R.V.Silva,J.Brito,R.Neves,R.Dhir,Predictionofchlorideionpenetrationofrecycledaggregateconcrete,Mater.Res. 18(2)(2015)427–440.

[39] D. Pedro, J. Brito, L. Evangelista, Mechanical characterization of high performance concrete prepared with recycled aggregates and silica fume from precast industry, J. Clean. Prod. 164 (2017) 939–949.

* * *

FLY ASH IN CONCRETE TO IMPROVE CONCRETE FUNCTIONING

AHMAD OMAR

Asst Prof, Department of Mechanical Engineering NMIET

Abstract - Endless supply of power through warm course including combination of pounded coal, simultaneous age of fly debris in enormous amounts involves genuine concern not just on account of issues related with its removal and usage yet additionally in view of its danger to public security and nature. As of now, enormous amount of fly debris is being unloaded in slurry structure in huge territories close to the force plants without being put to profitable use in India. Just an extremely low rate (<49) of fly debris produced in India is being utilized for profitable applications though the relating figures of different nations may fluctuate from 45% to 67%.

Albeit fly debris offers ecological points of interest, it additionally improves the exhibition and nature of cement. Fly debris influences the plastic properties of cement by improving usefulness, decreasing water interest, lessening isolation and dying, and bringing down warmth of hydration. Fly debris expands strength, decreases penetrability, lessens erosion of fortifying steel, builds sulfate opposition, and diminishes soluble base total response. Fly debris acquire its greatest strength more lower than concrete made with just portland concrete. The technique for working with this sort of cement are standard for the plant and won't influence the spending plan of working . As a Civil Engineer we attempt to utilize fly debris in development, as it assists protection climate with decreased its unfriendly effect with numerous different favorable circumstances, however now question ascends how much or rate fly debris could be utilized in cement for development works, and to answer this current investigation have been made.

I. INTRODUCTION

Concrete, typically composed of gravel, sand, water, and Portland cement, is an extremely versatile building material that is used extensively worldwide. Reinforced concrete is very strong and can be cast in nearly any desired shape. Unfortunately, significant environmental problems result from the manufacture of Portland cement. Worldwide, the manufacture of Portland cement accounts for 7-9% of the total carbon dioxide (CO2) produced by humans, adding the greenhouse gas equivalent of 330 million cars driving 19,900 miles peryear.

A waste part Fly Ash could be for large portions of Portland cement, significantly rising concrete’s environmental characteristics. Fly Ash, carrying mostly of silica, alumina forms a compound similar to Portland cement when mixed with lime and water. Fly ash is a non- combusted by-product of coal-fired power plants and generally ends up in a landfill. However, when high volumes are used in concrete (displacing more than 35% of the cement), it creates a stronger, more durable product and reduces concrete’s environmental impact considerably. Due to its strength and lower water content, cracking is reduced.

In the HVFAC mechanism, physical and chemical factors combine at all ages to densify and bind the paste. In the early age of concrete, the important factors of strength developmentare

(i) Physical effect - fine particles of fly ash act as micro aggregates and densify themass

(ii) Chemical contribution of the formation of ettringiteor related sulpho-aluminate production.

25% (weight of cement) would be considered high volume fly ash concrete. With high volume fly ash concrete, you will see less early age strength, but the long-term strength is about the same as with normal concrete. investigated the influence of activated fly ash on the compressive strength of concrete. Various activation techniques, such as physical, thermal and chemical were adopted. Concrete specimens were prepared with 13, 19, 28 and 47% of activated fly ash replacement levels with cement. Compressive strength was determined at 7, 14, 21,28 and 90days.

1) Activation of fly ash improved the strength of concrete. However, the compressive strength of fly ash concrete was less than that of ordinary portland cement even after 87 days ofcuring.

2) Among the activation systems, chemically activated coal fly ash (CFA) improved the compressive strength to a certain extent, only with 10 and 20% replacements. Since the CFA surface layer is etched by a strong alkali to facilitate more cement particles to join together and also the addition of CaO which is further promoting the growth of CSH gel and Ca(OH)2 which is more advantageous to enhance have a 28- day cube compressive strength of 26.4 MPa. Based on the results, it was concluded that:

1) Compressive strength of fine aggregate (sand) replaced fly ash concrete specimens was higher than the plain concrete (control mix) specimens at all the ages. The strength differential between the fly ash concrete specimens and plain concrete specimens became more distinct after 28-days.

2) Compressive strength continued to increase with age for all fly ash replacementlevels.

3) The maximum compressive strength occurs with 50% fly ash content at all ages. It was 40.0 MPa at 28-day, 51.4 MPaat 91-day, and 54.8 MPa at365-day.

4) Splitting tensile strength, and flexural strength of fine aggregate (sand) replaced fly ash concrete

specimens was higher than the plain concrete (control mix) specimens at all the ages. The strength differential between the fly ash concrete specimens and plain concrete specimens became more distinct after28-days.
5) Both splitting and flexural strengths continued to increase with age for all fly ashpercentages.
6) At all the ages, the maximum splitting tensile strength was observed with 50% fly ash content. It was 3.5 MPa at28-day, 4.3 MPa at 91-day, and 4.4 MPa at 365-days.
7) Maximum flexural strength was found to occur with 50% fly ash content at all ages. It was 4.3 MPa at 28-day, 5.2 MPa at 91-day, and 5.4 MPa at365-days.
8) Modulus of elasticity of fine aggregate (sand) replaced fly ash concrete specimens was higher than the plain concrete (control mix) specimens at all the ages. The differential between the fly ash concrete specimens and plain concrete specimens became more distinct after28-days.
9) Modulus of elasticity of fine aggregate (sand) replaced fly ash concrete continued to increase with age for all fly ash percentages.
10) At all ages, the maximum value of modulus of elasticity occurs with 50% fly ash content. It is 24.5 GPa at28-day, 28.0 GPa at 91-day, and 29.0 GPa at 365-day.

Atis et al. (2004) in their paper " Strength and shrinkage properties of mortar containing a nonstandard high-calcium fly ash" assessed the drying shrinkage of mortar mixtures containing high calcium nonstandard fly ash up to the age of 5 months. Five mortar mixtures including control Portland cement and fly ash mortar mixtures were prepared. Fly ash replaced cement on mass basis at the replacement ratios of 10, 20, 30 and 40%. Water–cementitious materials ratiowas 0.4. Mixtures were cured at 65% relative humidity and 20 ± 2O C. They reported that shrinkage of Portland cement mortar at 5 months was 0.1228%. Shrinkage of fly ash mortar decreased with the increase in fly ash content. Shrinkages of mortar containing 10, 20 and 30% fly ash were 25, 37 and 43%, lower than the shrinkage of Portland cement mortar at the end of 5 months. The reduction in shrinkage with the use of fly ash in mortar could be explained by the dilution effect of fly ash. The expansive property of fly ash most probably contributed to the reduction in dryingshrinkage.
investigated the Thermal Conductivity (TC) of HVFA concrete at the age of 28 days. Cement was replaced with 0, 50, 60, and 70% of Class C fly ash. They concluded that TC of concrete decreased to 32, 33, and 39% for 50, 60 and 70% fly ash replacement, respectively.Siddique, R. (2003) in his paper " Effect of fine aggregate replacement with class F fly ash on the abrasion resistance of concrete " studied the abrasion resistance of concrete proportioned to have four levels of fine aggregate replacement (10, 20, 30 and 40%) with Class F fly ash. A Control mixture with ordinary Portland cement was designed to have 28 days compressive strength of 26 MPa. Concrete specimens were made for the purpose. The abrasion resistance of concrete mixtures was determined at the ages of 28, 91, and 365 days in accordance with Indian Standard Specifications. It was measured in term of depth of wear. The variation of depth of wear versus percentage of fine aggregate replacement with Class F fly ash, at 60 min of abrasion time concluded that with the increase in fly ash content, depth of wear decreased, which indicated that the abrasion resistance of concrete increased with the increase in fly ash content. Thisshowed that for a particular percentage of fine aggregate replacement with fly ash, depth of wear decreased with increase in age, which means that abrasion resistance increased with age. This could be primarily attributed to the increase in compressive strength resulting from increased maturity of concrete with age.

Chalee et al. (2007) in their paper " Effect of W/C ratio on covering depth of fly ash concrete in marine environment" studied the effect of W/C ratio on covering depth required against the corrosion of embedded steel of fly ash concrete in marine environment up to 4-year exposure. Fly ash was used to partially replace Portland cement type I at 0, 15, 25, 35, and 50% by weight of cementitious material. Water-to- cementitious material ratios (w/c) of fly ash concretes were varied at 0.45, 0.55, and 0.65. Tests were conducted for corrosion of embedded steel bar after being exposed to tidal zone for 2, 3, and 4 years.

Based on the tests, they concluded that:

1) Covering depth required for the initial corrosion of embedded steel bar in concrete could be reduced with fly ash.
2) Decrease in W/C ratio resulted in reducing the covering depth required for initial corrosion, and generally affected the cement concrete rather than the fly ashconcrete.
3) Fly ash concretes with 35 and 50% replacements and W/C ratio of 0.65, provided the result of corrosion resistance at 4- year exposure as good as cement concrete with W/C ratio of 0.45.
4) Concrete with compressive strength of 30 MPa could reduce the covering depth from 50 to 30 mm by using fly ash to replace Portland cement of 50%.
From the above observations, it can be seen that there is an immense need to carry out systematic and comprehensive research on the utilization of fly ash and other industrial wastes, like gypsum, to develop a binder of sufficient strength by exploiting their inherent pozzolanic /cementing characteristics at normal temperature and evaluate the strength and durability characteristics of concrete, based on such a binder, to determine the potential use, in Civil Engineering constructions.

II. IMPORTANCE OF TODAY STUDY

The scope of present study aims at providing the M40 concrete with that optimum quantity of fly ash content which could be used in structure or road construction with acceptable strength values so, that the cost of construction can be reduced to a great extent and also by achieving this the harmful impact of fly ash on environment could be reduced.

III. REQUIREMENT

Consequent upon increased generation of electricity through thermal route involving combustion of pulverized coal/ignite, concurrent generation of fly ash in bulk quantities is a matter of serious concern not only because of issues associated with its disposal and utilization but also because of its threat to public health and ecology. At present, large quantity of fly ash is being dumped in slurry form in largeareasclosetothepowerplantswithoutbeingputto gainful use in India. Only a very small percentage (<35%) of fly ash generated in India is being used for gainful applications whereas the corresponding figures of other countries may vary from 60 to 100% Although fly ash offers environmental advantages, it also improves the performance and quality of concrete. Fly ash affects the plastic properties of concrete by improving workability, reducing water demand, reducing segregation and bleeding, and lowering heat of hydration. Fly ash increases strength, reduces permeability, reduces corrosion of reinforcing steel, increases sulphate resistance, and reduces alkali-aggregate reaction. Fly ash reaches its maximum strength more slowly than concrete made with only portland cement. The techniques for working with this type of concrete are standard for the industry and will not impact the budget of a job. So as a Civil Engineer we should effectively try to use fly ash in construction, as it helps in saving environment with reduced construction cost along with many other advantages, but now question rises to what extent or percentage fly ash could be used in concrete for construction works, and to answer this present study have beenmade.

3.1 BENEFITES OF FLY ASH INCONCRETE

The advantages of the fly ah in concrete are listed below:

1) Fly Ash is a pozzolana: A pozzolana is a siliceous or luminosities product that, in finely divided form and in the presence of moisture, chemically reacts with the calcium hydroxide released by the hydration of Portland Cement to form additional calcium silicate hydrate and other cementitious compounds. The hydration reactions are similar to the reactions occurring during the hydration of Portland Cement. Thus, concrete containing Fly Ash pozzolana becomes denser, stronger and generally more durable long term as compared to straight Portland Cement concrete mixtures.

2) Fly Ash improves concrete workability and lowers water demand: Fly Ash particles are mostly spherical tiny glass beads. Ground materials such as Portland Cement are solid angular particles. Fly Ash particles provide a greater workability of the powder portion of the concrete mixture which results in greater workability of the concrete and a lowering of water requirement for the same concrete consistency. Pump ability is greatlyenhanced.

3) Fly Ash generally exhibit less bleeding and segregation: than plain concretes. This makes the use of Fly Ash particularity valuable in concrete mixtures made with aggregates deficient infines.

4) Sulfate and Alkali Aggregate Resistance: Class F and a few Class C Fly Ashes impart significant sulfate resistance and alkali aggregate reaction resistance to the concrete mixture.

5) Fly Ash has a lower heat of hydration: Portland Cement produces considerable heat upon hydration. In mass concrete placements the excess internal heat may contribute to cracking. The use of Fly Ash may greatly reduce this heat build up and reduce externalcracking.

6) Fly Ash generally reduces the permeability and adsorption of concrete: By reducing the permeability of chloride ion egress, corrosion of embedded steel is greatlydecreased. Also, chemical resistance is improved by the reduction of permeability and adsorption.

7) Fly Ash is economical: The cost of Fly Ash is generally less than Portland Cement depending on transportation. Significant quantities may be substituted for Portland Cement in concrete mixtures and yet increase the long-term strength and durability. Thus, the use of Fly Ash may impart considerable benefits to the concrete mixture over a plain concrete for lesscost.

IV. ACCUSATIVE OFSTUDY

The main objective of the present study is to compare the strength characteristics of M40 concrete by using sample of different percentages of fly ash by mass of cementitious material, and also comparison is made between there cost. To achieve this objective following step are to befollowed:

1) Design of M30 concrete mix to gain the ratio of different components ofconcrete.

2) By using the above calculated ratio samples for compressive and flexural strength test for 27%, 47%, 75% replacement of cement by fly ash is to bemade.

3) Compressive strength of 3,7 and 21 days is to be calculated by casting cubes for M30 mix at 28%, 50% and 70% fly ash replacement bycement.

4) Flexural strength of 28 and 56 days is to be calculated by casting beam shaped samples of M30 mix at 26%, 54% and 68% fly ash replacement bycement.

5) Comparison of the compressive and the flexural

strength obtained at different percentages of fly ash is to bemade.

6) Cost comparison of 26%, 40% and 75% fly ash concrete is to bemade.

V. EXPERIMENTAL PROGRAMME

The following test programme was planned to investigate the results:

1. To obtain the physical properties of the concrete constituents i.e. Pozzolanic Portland cement ,fine aggregates, coarse aggregate and flyash.
2. Development of various mix combinations forconcrete.
3. Casting andcuring.

5.1 SUBSTANTIAL.

The properties of product used in concrete are determined in laboratory as per relevant code of practice. Different materials used in the present study were cement, coarse aggregates, fine aggregates, fly ash, water and admixture. Result of the test conducted to determine physical properties of materials are reported and discussed in the section. The materials used were having the following characteristics:

5.1.1 Cement

Cement is a fine, grey powder. It is mixed with water and materials such as sand, gravels and crushed stone to make concrete. The cement and water forms a paste that binds the other materials together as the concrete hardens. The ordinary cement contains the two basic ingredients namely argillaceous and calcareous. In argillaceous materials clay predominates and in calcareous materials calcium carbonate predominates. The basic composition is provided in table 1.1.

In the present work Ambuja PPC was used for casting cubes and beam samples for all concrete mixes. The cement was of uniform colouri.e grey with a ligh greenish shade and was free from any hard lumps. All tests on cement were conducted, as per procedure laid down in code IS: 1489 (Part-I): 1991[36]. Summary of the results of various tests conducted on cement is provided in table1.2

Table 1.1 Composition Limits of Portaland Cement Ingradient

Ingradients	Percent of Ingradientst
Lime	61-65
Silica	18-26
Alumina	2-9
Iron Oxide	0.8-8
Magnesia	0.2-5
Alkalies	0.5-1.5
Sulphur	1-2

REFERENCES

[1] Rubenstein, M (2013): “Emission From The Cement Industry”, State of The Planet Blogs From The Earth Institute, Columbia University, pp.1-2.

[2] Alam, J, Akhtar, M.N (2011): “Fly Ash Utilization in Different Sectors in Indian Scenario”, International Journal of Emerging Trends in Engineering and Development, Issue 1, Vol. (1), pp. 2-3.

[3] NTPC Ltd. (2007): “Fly Ash for Cement”, Ash Utilization Department, pp.32.

[4] Brown, J.H. (1982): "The strength and workability of concrete with PFA substitution", In: Proceedings International Symposium on the Use of PFA in Concrete, pp.151–161.

[5] Gebler, S. H., Klieger, P. (1983): "Effect of fly ash on the air-void stability of concrete (No. RD085. 01T)", Portland CementAssociation.

[6] Owens, P. L. (1979): “Fly ash and its usage in concrete”, Concrete International, 13(7), pp45-50.

[7] Sivasundaram, V., Carette, G. G. & Malhotra, V. M. (1990): "Selected properties of high volume fly ash concretes", Concrete International, 12(10), pp. 47- 50.

[8] Carette, G. G., Malhotra, V. M. (1984): "Characterization of Canadian fly ashes and their performance in concrete", Division Report, MRP/MSL, pp.84-137.

[9] Joshi, R. C., Lohtia, R. P. (1993): "Effects of premature freezing temperatures on compressive strength, elasticity and microstructure of high volume fly ash concrete", Third Canadian Symposium on Cement and Concrete, Ottawa, Canada.

[10] Lohtia, R. P., Nautiyal, B. D. & Jain, O. P. (1976): "Creep af Fly Ash Concrete" In ACI Journal Proceedings (Vol. 73, No. 8).ACI.

[11] Haque, M.N., Langan, B.W. & Ward, M.A. (1998): "High fly ash concretes”, ACI Material.8(1), pp. 54–60

[12] Saraswathy, V., Muralidharan, S., Thangavel, K. & Srinivasan, S. (2003): "Influence of activated fly ash on corrosion-resistance and strength of concrete", Cement and Concrete Composites, 25(7), pp. 673-680.

[13] Siddique, R. (2003): "Effect of fine aggregate replacement with Class F fly ash on the mechanical properties of concrete", Cement and Concrete Research, 33(4), pp.539-547.

[14] Atiş, C. D., Kilic, A. &Sevim, U. K. (2004): "Strength and shrinkage properties of mortar containing a nonstandard high-calcium fly ash". Cement and Concrete Research, 34(1), pp.99-102.

[15] Demirboğa, R., Türkmen, İ. &BurhanKarakoç, M. (2007): "Thermo-mechanical properties of concrete containing high-volume mineral admixtures", Building and Environment, 42(1), pp.49-354.

[16] Ho, D. W. S., Lewis, R. K. (1983): “Carbonation of concrete incorporating fly ash or a chemical admixture”, ACI Special Publication, pp.79.

[17] Virtanen, J. (1983): “Freeze-thaw resistance of concrete containing blast-furnace slag, fly ash or condensed silica fume”, ACI Special Publication, pp. 79.

[18] Mehta, P. K. (2000): "Sulfate attack on concrete: separating myths from reality", Concrete International 22(8): pp.57-61.

[19] Naik, T. R., Singh, S. S. & Hossain, M. M. (1994): "Permeability of concrete containing large amounts of fly ash", Cement and Concrete Research, 24(5), pp. 913-922.

[20] Siddique, R. (2003): "Effect of fine aggregate replacement with Class F fly ash on the abrasion resistance of concrete", Cement and concrete research, 33(11), pp.1877-1881.

[21] Chalee, W., Teekavanit, M., Kiattikomol, K., Siripanichgorn, A., &Jaturapitakkul, C. (2007): "Effect of W/C ratio on covering depth of fly ash concrete in marine environment", Construction and Building Materials, 21(5), pp.965-971.

[22] Managing Coal Combustion Residues in Mines, Committee on Mine Placement of Coal Combustion Wastes, National Research Council of the National Academies,2006.

[23] ASTM C 618: “Standard Specification for Coal Fly Ash and Raw Pozzolanafor Use in Concrete”, American Society for

Testing andMaterials.

[24] ASTM C216: “Specifications for Facing Brick.” American Society for Testing andMaterials.

[25] ASTM C 55: “Specificaionsfor Concrete.” American Society for Testing andMaterials,

[26] IS: 3812 (Part-I) 2003: “Pulverized Fuel Ash- Specification (For Use as PozzolanaInCement, Cement Mortar and Concrete).” Bureau of Indian Standards, New Delhi. 2003.

[27] NTPC Ltd. (2007): “Fly Ash for Cement”, Ash Utilization Department, pp.6-10.

[28] Dunn, S.: “Decarbonizing the Energy Economy”, State of the World 2001: A World Watch Institute Report on Progress Toward a SustainableSociety.

[29] W.W. Norton and Company, 2001, pp. 83-102.

[30] Mehta, P.K.: “Concrete Technology for Sustainable Development”, Concrete International 21(11), 1999, pp. 47-52.

[31] Mehta, P.K.: “Durability: Critical Issues for the Future”, Concrete International 19(7), 1997, pp. 69- 76.

[32] IS: 1489 (Part-I)-1991: “Portland-Pozolana Cement-Specifications (Fly Ash Based)”, Bureau of Indian Standards, New Delhi.1991.

[33] "Construction Materials”, teaching.ust.hk/~civl111/CHAPTER3.pdf, pp. 1-8.

[34] IS: 2386 (Part-I)-1963: “Methods of Test of Aggregates for Concrete (Particle Size and Shape).” Bureau of Indian Standards, New Delhi.1963.

[35] IS: 2386 (Part-IV)-1963: “Methods of Test of Aggregates for Concrete (Mechanical Properties).” Bureau of Indian Standards, New Delhi.1963.

★★★

FROM PROJECTING TO 3D PRINTING GEOPOLYMERS: A PROOF OF IDEA

[1]AJAYA KUMAR BEURA, [2]SHRADHANANDA GHADEI, [3]BIJAYALAXMI BEHERA,
[4]SIKENDER SHARMA

[1]Assistant Professor, Department of Mechanical Engineering
[2]Asst Prof, Department of Civil Engineering AIET BBSR
[3]Asst Prof, Department of Civil Engineering CEC BBSR
[4]Prof, Department of Civil Engineering REC BBSR
E-mail: [1]kumar.anjan@nmiet.ac.in

Abstract - The target of this paper is to characterize a blend plan methodology permitting the execution of geopolymer in powder bed 3D printing. In a particular cover approach, an aluminosilicate powder bed is enacted through the store of a basic silicate arrangement. We first show that, in contrast with projecting, this innovation requires dominating the spreading of the fluid into the powder bed to guarantee that the response happens where it is required. A progression of examinations at the drop level, emulating the 3D printing measure, were performed to decide the printing arrangement piece for a given powder bed pressing. We at that point feature the connection between the compressive strength of the printed geopolymer and the powder bed immersion, constrained by the printing boundaries. At last, SEM/EDX examination affirm the development of geopolymer with wanted Si/Al and Na/Al proportions in the subsequent literature.

Keywords - Powder bed 3D printing Geopolymers, Mix design Sustainability

I. INTRODUCTION

Construction industry is a large consumer of resources. More than 40%ofresourcesconsumedworldwideareusedforconstruction[1]and good quality resources such as gravel or sand are becoming scarce in someplaces[2,3].Areductionofresourceconsumptionhasthereforetobecombinedwithareductionofgreenhousegasemissions.Overthelast decades, efforts have been made to build more energy efficient build- ings, which has reduced the energy needed for operating the buildings. However, the embodied energy associated with the production of building materials was not thoroughly considered [4–6], and its reduction is becoming the new challenge in sustainable construction [7,8]. To reduce the greenhouse gas emissions, we can use lessmaterial by better designing the structure [9–11], extend the service life of the existing structure to avoid the use of new materials (work on durability ofbuildings[12–15])orusematerialswithlowercarbonintensity,such as earth, bamboo or straw[16–20].

3D printing represents a promising technique to meet thesere- quirements [10]. Parts can be built locally and material is efficiently applied where it is needed, which allows to use less of it by optimizing the design. 3D printing is an additive technique, not subtractive; therefore, less waste is produced during the production. Small complex partscanbeprintedallowingfortargetedreplacementwhichcanextend theservicelifeofstructures[21].Furthermore,itopensalargevarietyof potential materials to be used. Because the technology allows theirusein a controlled environment, materials or processes that would be too complexortoodangeroustouseonsitecanbeprefabricated.Thesystem is very flexible (sake binder and plaster based powder [22] as well as many types of waste such as plastic, construction waste or paper pulp [23–25]):itshouldthusbepossibletoprintmaterialswithlower carbon intensity.

In construction, a lot of research is done on extrusion based 3D printing [26–28], where a material paste is extruded through a nozzle and deposited layer by layer to build up the object. This is the most spread 3D printing technique because it is cheap and prototypes or replacement parts can easily be printed. The drawbacks of this method are that overhangs can only be printed with the help of support struc- tures and the accuracy is low due to the layered structure.

These printing limitations are not problematic with binder jet 3D printing, where a powder bed is glued layer by layer at given positions. Actually, the underlying powder serves as a support structure for over- hangs and may be reused if it has not been printed. In construction, researchisdoneonpowderbed3Dprintingwithcement[29,30]aswell as on sand with phenolic binders. The latter one is used to print structurallyoptimizedelementsthatareassembledtoafloorsystem[9]ortoprintlostformworksforcomplexelementsfilledwithhighperformance concrete[10].

Commerciallyavailablebindersforbinderjettingaremostlyorganic[31].Theepoxybasedresinsarehardandsetfast.However,theyarenotfireresistantandtheyreleasevolatileorganiccarbon(VOC)duringtheiruse [32–34], which makes them quite difficult to apply in construction. Alternatively, sodium silicate is used as an inorganic binder [31] for sandpowderbeds,butitneedsheattosetanditiswater-soluble.Forthe current application in metal moulding, this is perfectly fine (the mould canbedissolvedandthesandreused),butnotforconstructi onpurposes. To combine lower CO_2 emissions with a reduction of material con- sumption, the raw materials currently used in 3D printing need to be replaced by materials with a lower carbon footprint: recycled or waste materials as a powder bed and an inorganic binder, which does not require energy for setting. A good candidate that fulfills the criteria in termsofperformanceandembodiedenergyisgeopolymer binder,since itcanbebuiltfromwastematerialssuchasslag,flyashorglasswasteas aluminosilicatesource.Thegeopolymerreactionisdescribedasfollows: analuminosilicateisactivatedwithanalkalinesolution,whichallowsto dissolve and rearrange the aluminates and silicates [35]. Geopolymers have indeed many advantages for powder bed 3D printing. They havea low embodied carbon intensity [36], they are water and fire resistant [37],strongerthantheorganicbinder,theycausenoVOCemissions,no heat is needed for curing and they can be synthesized from waste ma- terials [38,39]. For instance, waste materials like blast furnace slag [40,41], fly ash [42], glass waste [43], brick powder [44,45] and many more are regularly used as aluminosilicates in geopolymer concrete applications.Thefinalpropertiesofgeopolymerslikestrengthorsetting time strongly depend on the silica, alumina, sodium and water ratios, whichhavetobetakenintoaccountinthemixdesign[46,47].

Previous work has been done in using geopolymers for powder bed 3D printing applications [48–50]. D-Shape [50] developed a printer to prints building parts by distributing a geopolymer slurry on a powder bed. Xia et al. [48] showed that it is possible to reach a strength of 0.9 MPaafterprintingand16.5MPaafterapost-processingwithanhydrous sodium metasilicate at elevated temperatures. In these applications, the authorsmixthealuminosilicateaswellasthealkalineactivatorwiththe aggregates in the powder bed and print by adding water only. Thereare some limitations in this method as it means that the powder canalready react when exposed to air humidity and makes it difficult to reuse the non-printedpowder.

Other possibilities of mixing or separating aggregates, aluminosilicatebinderandactivatorscanbetested:theactivatorcanbe inthesolid phase or in the liquid phase [30]. As the activator is often theexpensive part of the mix (from an economic and environmental perspective), it seemsinterestingtohaveitintheliquidpartratherthandispersedinthe sandbed.Furthermore,inordertoavoidtheproblemofthesettingtime limitation when activator and binder are mixed together, it might be bettertoseparatethebinderandtheactivator,followingabinderjetting approach [30]. Therefore, in this work, the aluminosilicate binder is mixed in the powder bed and the activator, in liquid form, is deposited onit.AccordingtotheRILEMMAPP[51],thismethodcan beclassified asparticle-bedbinding,whichisanadditiveshapingprocesstoproduce freeform parts out of geopolymer offsite.

Powder bed 3D printing allows to produce complex formwork and therefore to save structural material. Its use with alkali activation of wastematerialcanfurtherreducethecarbonintensityofthestructureas well as its virgin materialconsumption.

The objective of this research is thus to define a mix designstrategy toallowtheimplementationofgeopolymersinpowderbed3Dprinting. In the mix design of geopolymers, the silica, aluminum, sodium and water ratios are important for the workability of the paste as well as the final properties of the geopolymer [46,47]. Contrary to a casting pro- cess, in 3D printing, these ratios depend on the penetration behavior of theprintingsolutionintothepowderbed[52,53].Tomodel theprinting process,experimentswithsingledropsonpowderbedswereperformed andtheliquidtosolidratioinasingledropwasdetermined. Fromthis

II. MATERIALS

2.1 Mineral powder

Alltheexperimentswereconductedonmineralpowdermixesoffine quartz sand (FS003 from Strobel Quartz Sand GmbH) and metakaolin sourced from Imerys (referred to here as MK) mixed at varying mass ratios. Their respective mean grain size (d_{50}) analyzed with a laser particle-sizeanalyzer(ParticaLA-950,Horiba,Germany),specificden- sity (SG) determined by helium pycnometry (AccuPyc II 1340 Micromeritics)specificsurfacearea(SSA_{BET})measuredbynitrogenadsorption (Micromeritics Tristar II 3020) and SiO_2 and Al_2O_3 contents obtained through X-ray fluorescence spectrometry (XRF), are given in Table1.

2.2 Activating solution

An alkaline solution (sodium silicate solution, referred to here as NaSil)wasusedastheactivatingsolutionforthemetakaolin.TheNaSil solution was prepared by mixing deionized water at 20 ◦C to sodium hydroxide (NaOH) in pellet form and to silica gel, both sourced from Sigma Aldrich (Switzerland), in a closed plastic bottle to prevent evap- oration and cooled for 24 h. The solution was prepared with a SiO_2/Na_2Omolarratioof1.69,optimalmolarratioforafastinitialstrengthof thegeopolymer[47],requiredfortheprintingofthenextla yerinthe3D printingprocess.However,toensureconnectionbetween consecutive layers,anintermediatefinalsettingtimeisneeded:aH$_2$O/Na$_2$Oratioof 12.93waschosen[47].Thespecificdensityofthesolution(1.46g/cm3) was measured with a Densito 30 PX from Mettler Toledo andits apparent viscosity (0.06 Pa.s at 20 ◦C) was measured using a Malvern Kinexus Lab stress-controlled rheometer equipped with parallelplates (Malvern Instruments,Switzerland).

III. EXPERIMENTAL PROCEDURES

Experiments on two scales were performed in this work. In order to get an insight of the local liquid to solid ratio in powder bed 3D printed parts, single droplets of printing solution were dropped on powderbeds withvaryingcomposition.Thefindingsofthisdropexperimentshelped to set up the printing parameters at bigger scale. With the help of SEM/ EDX analysis of single drops, 3D prints and casted geopolymer, the validity of the use of single drops as a model for prints will betested.

3.1 Powder bedpacking

To determine the optimal powder bed composition in 3D printing, the random loose and dense packing of powder mixes containing different proportions of sand and MK were measured according to Sedranetal.andL´ed´eeetal.[54,55].Tomeasuretheloose packing fraction, the powder mix was filled in a metallic cylinder of a given volume and the weight wasrecorded. ForpowdermixeswithalowMKcontent(below20wt%),thedense packing fraction was obtained following the protocol of [55]. The cylinderwasfilledinthreetimes:aftereverytime,thecylinder wasplaced on a shocking table and twenty shocks were applied. After the last filling,aweightof5kgwasplacedonthepowdersurfaceandadditional fortyshockswereapplied.Attheendoftheprocedure,the massandthe finalvolumeofthepowder$V_t$weredetermined,andthepackingfraction (ϕ) wascalculated.

Table 1
Specification of the mineral powders used in this study.

	d_{50} [µm]	SSA [m^2/g]	SG [g/cm^3]	SiO$_2$ [wt %]	Al$_2$O$_3$ [wt %]
Sand	240	0.09	2.6	>99.1	<0.2
Metakaolin	4	13.17	2.58	51.63	44.37

Since MK is a very fine powder, the measurement of the dense packing according to Sedran et al. [54] is more appropriate for mixes with a high MK content. An increasing amount of water was added to 250gofpowderandmixedwithafourbladedmixingtoolconnectedto a mechanical stirrer (Heidolf, Switzerland) during 2 min at 350 rpm. Aftermixing,theVicattruncatedcone(Vicatronic,Matest,Switzerland) wasfilledwiththematerialandplacedundertheconsistencyneedle(10 mm diameter). The penetration depth of the needle in free fall was measured.Accordingtotheprotocolfrom[54],amixwith apenetration depth of 6 mm is at the maximum packing. The amount of added water for a 6 mm penetration is extrapolated and the maximum packing fraction of the mix can be calculated. The dense and random loose packingofthedifferentpowdermixesareplottedinFig.1asafunction of the MKcontent.

3.2. Sample Preparation

3.2.1. Drop Experiment

Togetaninsightofthespreadingoftheliquidintodifferent powder bed compositions [53,56,57], first experiments consisted in simulating the 3D printing process by dropping NaSil solution on different non-compacted quartz sand/MK mixes (Fig. 2). The volume of the NaSil solutionwascontrolledto5,10and20µlwithanaccuracypipettefrom EppendorfResearchPlus(Switzerland),displayingasystematicerrorof 0.12 µl. Accordingly, dried geopolymer drops were produced and characterized. Through the analysis of the dried drop weight after removal and knowing the powder bed composition, the liquid to solid ratio as well as the theoretical Si/Al and Na/Al molar ratios in the dried geopolymer drop were calculated. The height and the diameter of the final drops were determined with image analysis (Matlab, ImageJ) on picturestakenwithaDSLRcamera(CanonEOS500D)fromthesideand amicroscope(LeicaS9i,LeicaMicrosystemsAG,Switzerland)fromthe top. The images were transferred into binary images before analysis. In thesideview,theheightofeachdropwasdeterminedbyevaluatingthe maximumdistancebetweenthelowestandthehighestpixelofthedrop. In the top view, the surface of the drop area was determined and the corresponding diameter assuming a circle was calculated. The measurements were repeated on three samples of each mix (Fig.3).

With an envelope density analyzer (Geopyc 1360, Micrometrics, Germany), the average volume of the dried drops (Vdd) was measured and with the dry drop weight (mdd), the packing state of the powder in the drop Cdwas calculated as following:

$$C_d = \frac{m_{pd}/\rho_p}{V_{dd}} - \frac{m_{dd} - m_{wd} + m_{H2O}}{V_{dd}\cdot\rho_p} \tag{1}$$

Wherem_{pd}isthemassofthepowderincorporatedinthedrydrop,ρ_p thespecificdensityofthepowder,m_{dd}themassofthedrydrop,$m_{wd}$the

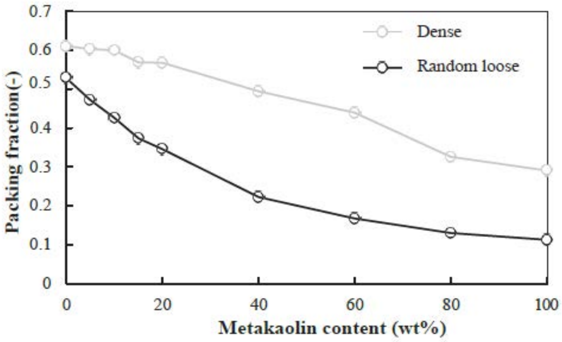

Fig. 1. Random loose and dense packing fraction of the different powder bed compositions.

massofthewetdrop,andmH2Othemassoftheevaporated waterduring the dryingprocess.

The microstructure was qualitatively studied in X-Ray micro tomography(RXSolutions,France),usingavoxelsizeof25 µmanda160 kV X-ray source applying 70 kV and 70µA.

3.2.2.

Samples were printed with a custom-built binder jet 3D printer [58,59] (Fig. 4) with a selective binder activation approach [30]: a liquid binding agent (alkaline solution) is deposited on a powder bed (mixofMKandsilicasand)previouslydistributedonaplatform(Fig.4). Where the alkaline solution gets in contact with MK, a geopolymer is built. Overtime, layers of powder are bonded with the geopolymer to form anobject.

The custom-built printer allows the control of different parameters (Fig. 4):

- NozzlediameterDn(mm):anynozzlecanbemountedontheprinter.
- Moving speed V (m/min): the current setup can be safely operatedatlinear speeds up to 20 m/min along X and Y axes. The Z axis is notparticularly relevant as it is actuated only once per layer and forrelatively short travel distances (layer height h): to avoid misalig- ments of the printing frame it was operated at2 m/min.
- Injectionvolumeperdistancel(µl/mm):theflowratecanbeadjusted
- between <0.005 ml/min and >40 ml/min by controlling therotating speed (100 rpm) and the tubing diameter
- Layer height h (mm): no specific limitations are derived from thesetup itself, rather the process requires a layer thickness that isminimum 2–3 times the average diameter of the inertgrains.
- -Spacing s (mm) between the printed lines: it controls the overallsaturation of the print bed and is usually indicated as a multiple ofthe nozzle diameter. The resulting saturation is function of themovingspeedV,theinjectionvolumeperdistancel,andthespacing s.

In this study, most of the parameters were kept constant and two werevaried.TheoptimalnozzlediameterDnisaffectedby theviscosity and by the surface tension of the injected solution: a valid compromise between achievable resolution and practical machine operation was foundin0.25mm.Theprintedlayerheighthdependsonthe penetration depth of the liquid in the powder bed, which in turn depends on the powder bed composition. As seen in the drop experiment, with increasing metakaolin content,thepenetrationdepthincreasesupto 3.4 mm until 20 wt% MK and decreases afterwards. To ensure the interconnection between two layers, a layer height of 3 mm waschosen forthepowdermixcontaining20wt%MK.ThemovingspeedVofthe printheadwassetto30m.min—1.Eitherthevolumeperdistancelorthe line spacing *s* (*s*=D_n. *a*, with *a* being a multiplier factor) were varied from one sample to another: these variations are discussed in the relevant sections of this manuscript. By varying these two parameters, the volumeofliquidprinted(V_l)onacertainvolumeofpowder(V_t)mixcan becontrolled:

$$\frac{V_l}{V_t}=\frac{l}{(D_n.a.h)} \qquad (2)$$

Bars of dimension 4 4 16 cm3 were printed (Fig. 5) and demoulded from the powder bed after 24 h. The bars were stored at ambient room temperature and humidity, and were subjected to mechanicaltestssevendaysafterprintingwithoutanypostprocessing.The compressive strength was measured with a mechanical press equipped with a 50 KN cell, applying 0.1 KN/mm perpendicular to the printing planes,inz-direction(Matest,Switzerland),accordingtoASTMC349.

3D printed samples

3.3. Phaseidentification

Static Nuclear Magnetic Resonance (NMR) 27Al measurements

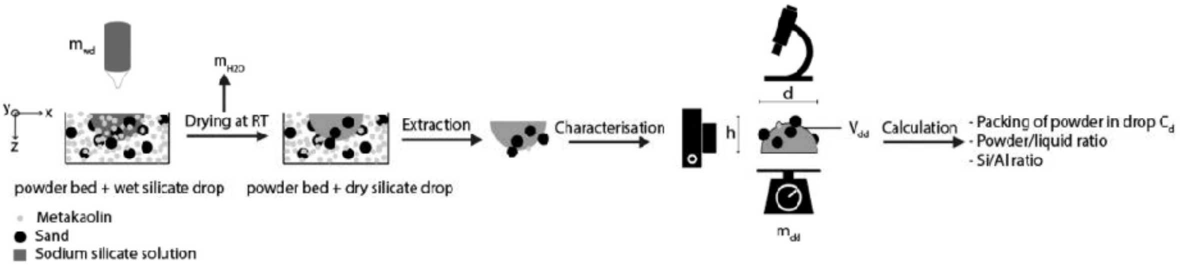

Fig. 2. Production of geopolymer drops.

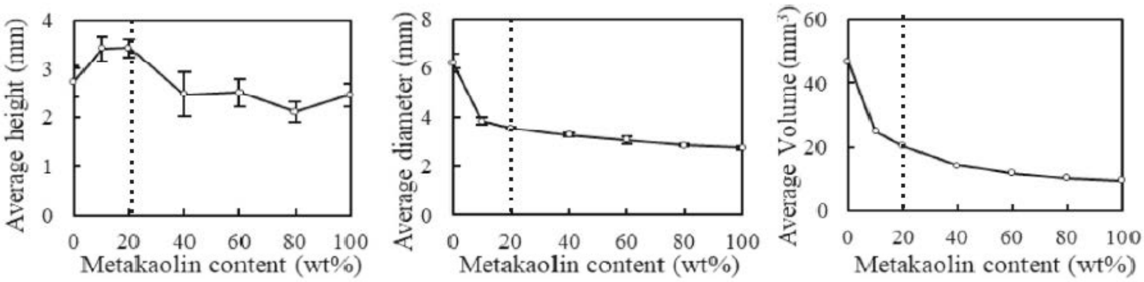

Fig. 3. Height, diameter and volume of dried drops produced on powder beds with varying compositions. The dashed line represents the transition to water proofdrops.

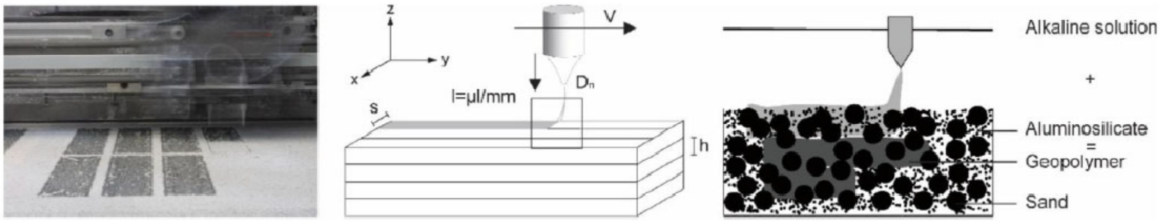

Fig. 4. Deposition of alkaline solution on powder bed with the custom-built 3D printer and the variable parameters.

Fig. 5. 3D printed geopolymer bar with 0.2 µl/mm3.

(Bruker Avance500 spectrometer at 11.74 T) were performed on raw and produced materials to prove that a geopolymer is built in each considered process. With a scattering electron microscope (Quanta 200 3DSEM-FIB)includinganEDAXSystemthelocalelementcomposition ofthedrops,piecesof3Dprintedandcastsampleswasdetermined.The sampleswerecut,embeddedinepoxy(EPO-TEK®301)andpolishedto 1 µm. For ideal conductivity, a carbon coating was applied. An EDX point analysis with an accelerating voltage of 15 kV was performed on up to 10 points on the geopolymer matrix of each sample to determine the Si, Al and Na atomic percentages. From these values, the Si/Al and Na/Al ratios on the corresponding points werecalculated.

IV. RESULTS AND DISCUSSION

4.1. Porosity and liquid penetration

In Fig. 6.a, the dried drops produced with 10 µl NaSil solution deposited on loosely packed powder beds containing an increasing MK amount are presented, as well as the corresponding images obtained by X-Raymicrotomography(Fig.6.b).Itcanbenotedthat,when noMKis introducedinthemix,theresultingdropisnotspherical(diskofaround 3mmthickness)whereasintroducing10wt%and20wt%ofMKinthe mix results in the formation of more spherical drops. Above 20 wt% of MK in the mix, the volume of the resulting drops decreases with an increasing MK content. The decreasing volume with increasing MK content is in line with the compacity measurement of the powder bed, which shows lower packing for higher amounts of MK. The lower packingresultsinmorevoids,thereforethesameamountofliquidfinds

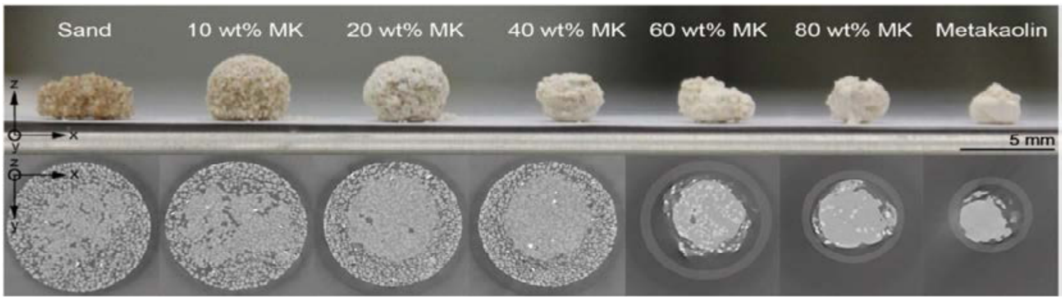

Fig. 6. a) Dried drops produced with 10 µl NaSil solution deposited on powder beds containing an increasing MK amount. b) X-Ray Microtomography images of the dried drops in the x y plane indicated in a).

place in a smaller powder volume. From an ecological and economical point of view the metakaolin content should be minimized [36,60,61]. To evaluate the minimum amount of metakaolin required to build a geopolymer, an easy qualitative test was conducted: the drops were immersed in water. Since geopolymer is supposed to be waterproof, dropsthatsustaintheimmersioninwatercanbeconsidered tocontaina geopolymerbinder.Dropsproducedfrommixescontaining10wt%MK and less totally dissolve when immersed in water. The lack of water resistance shows that 10 wt% of MK is not enough to properly build a geopolymer. This observation suggests that 20 wt% of MK is the optimumMKcontentforthecurrentapplication,sincetheuseofMKshould be reduced to a minimum. Additionally, the sample with 20 wt% MK results in the largest volume of the final drop, which helps to increase the printingspeed.

This decision is also supported by the trend of the Si/Al ratio with varying MK content. The Si/Al ratio obtained in produced drops canbe calculated from the mass of the introduced solution and from the final mass of the dried geopolymer drop (Fig. 7). On powder bed mixeswith MK contents higher than 20 wt%, the Si/Al ratio in the resulting geopolymerdropremainsconstantaround2.Therefore,itcan besuggested that20wt%MKistheminimumamountleadingtoastrong geopolymer. However,thesystemgivesusthefreedomtoincreasetheMKcontentin ordertoadaptthedropsizewhilekeepingtheSi/Alratioconstant.

Considering the X-Ray microtomography images (Fig. 6.b), it is possibletoconfirmthattheincreasingcontentofMKinthe mixleadsto adensificationofthedropinternalstructure.Novoidsarenoticedinthe center of the drops: locally, at small scale, the material is in a dense compactstate.Below20wt%MK,theinternalstructureis notfully compact, voids are observed. As the penetration of a single drop into a porous substrate depends on the structure of the substrate (the porosity, the size of the pores, the orientation of the pores, and the surface chemistry [53,56,57]), the observed behavior can be explained by the shape of the particles. The MK particles have a platelet shape [62] and, consequently, bond across large flat surfaces. The binder has to wet a bigger surface compared to spherical particles, where the binder onlystaysattheneckbetweentwograins[56].Inordertoreducetheamount of MK to a minimum but still build a strong geopolymer and a dense packedpowderbedformaximumstrength,aMKcontentof20wt%was chosen for the following printingexperiments.

By comparing the dense packing fraction of the different powder mixes with the calculated packing fraction of the powder mix in the drops(Fig.8.Comparisonbetweenthedensepackingfractionmeasured for the powder bed and the calculated packing fraction in the drops.), a correlation can be found. It can be seen that the calculated packing fraction in the drops corresponds to the dense packing of the corre- sponding powder mix. Since the powder bed is in a random loose packing state when the drop is placed, the conclusion can be drawnthat theliquidpenetrationintothepowderbedleadstoadensificationofthe material. This densification can be explained by the presence of the platelet like shape of the metakaolin powder. As stated by Sachs et al. [56], the platelets will be bond across the flat surfaces, allowing for a denser packing. The internal structure of the mixes prepared with more than 20 wt% MK is full of matter and no voids are noticed (cf. Fig. 6). This dense state is thus taken into consideration for the following

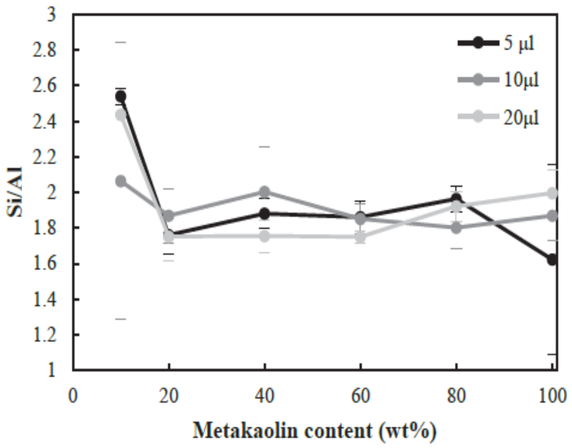

Fig. 7. Si/Al ratio ingeopolymer drops with varying MK content in pow- derbeds.

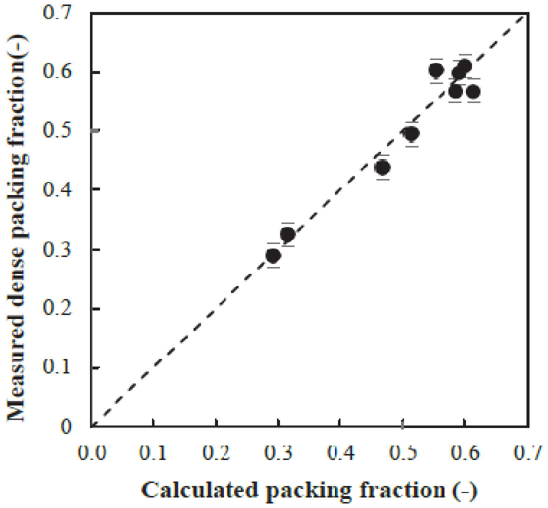

Fig. 8. Comparison between the dense packing fraction measured for the powder bed and the calculated packing fraction in the drops.

experiments even if, initially, the powder bed is loosely placed in the printer. The packing of the powder bed seems then to control the final internal structure of the material, as the porous network influences the ability of the liquid to penetrate.

Thankstotheseresults,itispossibletoassumethat,forthis mixand during the printing process, the liquid deposited at the surface of the powder bed penetrates and fills all the voids existing between the par- ticles. The porosity ε is the ratio of the volume of voids Vvbetween particlestothetotalvolumeofthepackingVtandtheyarelinkedbythe following relationship:

$$\varepsilon = \frac{V}{V_t} = 1-\phi \tag{3}$$

And

$$V_s = V_t{}^*\phi = V_t{}^*(1-\varepsilon) \tag{4}$$

Where $V_s$is the specific volume of the powder. Therefore, based on the assumption that the liquid fills the existing voids and with Eqs. (3)and (4), the volume of the liquid, at the drop scale, can be defined as follow:

$$V_l = V_v = V_t{}^*\varepsilon \tag{5}$$

Thetotalporosityεofthepowderbediscalculatedfromthepacking fraction by considering a dense packing of the powder bed With the total volume $V_t = V_s + V_l$, it is then possible to calculate the liquid to solid ratio in the drop fully geopolymerized (Fig. 9), depending on the porosity (ε) of the powderbed:

$$\frac{V_l}{V_s} = \frac{\varepsilon}{1-\varepsilon} \tag{6}$$

Knowing the specific densities of the liquid and the powder ($\rho_l$and ρ_p), the liquid to solid ratio can be determined as follow:

$$\frac{m_l}{m_p} = \frac{\varepsilon^*\rho_l}{\rho_p(1\quad\varepsilon)} \tag{7}$$

4.2. Optimal mix design composition

Thankstothepreviousexperimentsandassumingthatlocally,atthedropscale,theliquidpenetratesandfillsallthevoidsinthepowderbed,theamountofliquidtosolidcontentforagivenpowderbedcomposition is determined to be equal to0.4.

Thisratiowasusedtocastandprintcomparablesamples.In casting, all the components are combined: the NaSil solution was added to the powder mix (20 wt% MK 80 wt% sand) and mechanically mixed with a stirrer during 3 min. The obtained geopolymer paste was cast in three moulds of dimension 4 4 16 cm3 and demolded after 2 days. To reachtheliquidtosolidratioequalto0.4intheprintedsample,the printing parameters were adapted to reach the right amount of printed liquidpervolumeofpowder.Withthespecificdensityoftheliquidand the density of the dense packing of the powder bed (ρm), Eq. (2) canbe expressed in terms of mass:

$$\frac{m_l}{m_p} = \frac{\rho_l}{\rho_m(D_n.a.h)}\frac{l}{} \tag{8}$$

The maximum liquid per distance l is limited by the capacity of the pump, whereas the lower limit is given by the maximum moving speed oftheaxis.Asapreliminarytest,anlof0.6µl/mmandalinespacingsof 0.5 mm (a 2) was chosen.

InFig.10,thecompressivestrengthoftheprintedandcastedsamples are compared to geopolymer printed in selective binder activation [48] and organic binder printed in a commercial powder bed printer [9].The casted samples exhibit the highest strength (35 MPa) whereas 3Dprin-ted bars reach 5.3 MPa with a standard deviation of 0.7 MPa. The densitiesintheprintedandthecastedpartsaresimilar,1.6g/cm3and1.8 g/cm3, respectively. Therefore, the difference in strength cannot be explained only with the density. It can be suggested that the heteroge- neities or defects created during the printing process predominantly influence the strength. Further experiments have to be performed to improve the bonding between lines and layers.

Withapost-processingstep, Xiaetal.[48]showedthatitispossible toincreasesignificantlythestrengthoftheprintssfrom0.9 to16.5MPa. In the present work, the environmental impact of the print is kept to a minimum,thereforenopost-processingwasapplied.Incomparison,the resulting parts are five times stronger than parts printed with selective binderactivationwithoutpost-processing[48].Sincetheorganicbinder exhibits a compression strength of only 5 MPa [9], the presentedbinder jetting technique with geopolymers is suitable to print building parts loadedonlyoncompression,eventhoughthe3Dprintedsamplesare less strong than the casted geopolymer.

However, even if the printed sample reaches the required compres- sivestrength,thecriteriaintermsofdimensionandshapeofthesample isnotfulfilled(Fig.11).Comparedtoa4 4cm2square,thecrossSectionoftheprintedbarshowsinaccuraciesespeciallyinthebottomof the sample. Indeed, at sample scale, it seems that the amount of liquid deposited, calculated from the local material at the drop scale, is in excess and cannot penetrate all the available porosity.

Therefore, only the locally printed material can be considered to have a similar composition as the casted material. For printing, the overall liquid to solid ratio is thus not the only parameter to take into account,likeincasting.Incasting,thelocalgeopolymercompositionis the same as the overall mix, whereas in 3D printing, the overall composition differs from the local geopolymer composition due to the inclusion of voids with unprinted powder (Fig.12).

In comparison with the casting process of geopolymer, where the local liquid to solid ratio depends on what is initially introduced in the mix, the overall liquid to solid ratio in 3D printing depends on the penetration behavior and distribution of the liquid through the powder bed.

The penetration of the liquid in the powder bed then results in a certain saturation (S) of the powder bed, which can be defined as the fraction of the pore volume (V_v) that is filled with liquid (V_l) [63]:

$$S = \frac{V_l}{V_v} \tag{9}$$

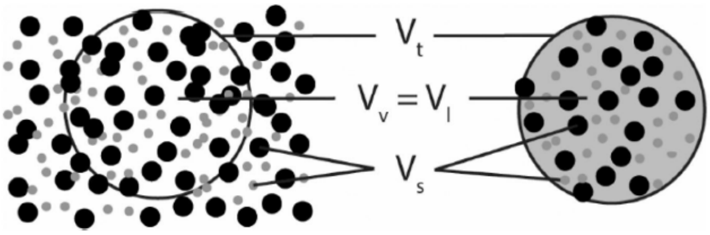

Fig. 9. Liquid penetration in powder bed filling all accessible voids.

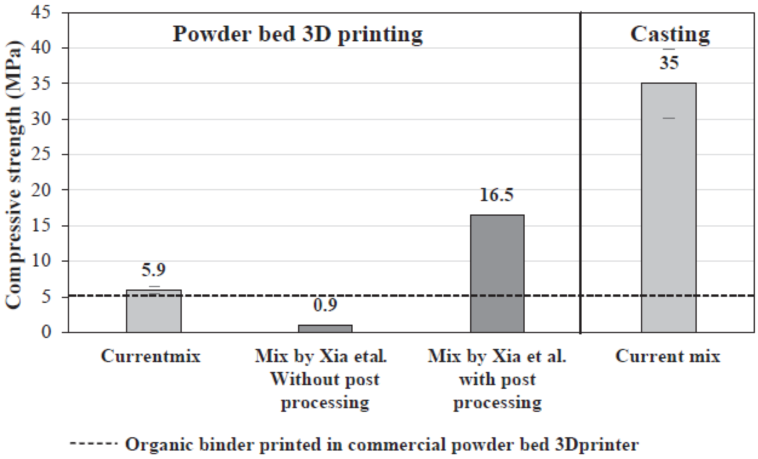

Fig. 10. Compressive strength of printed and casted samples compared to geopolymer printed with selective binder activation and organic binder printed with commercial binder jetting (dotted line) [9,48].

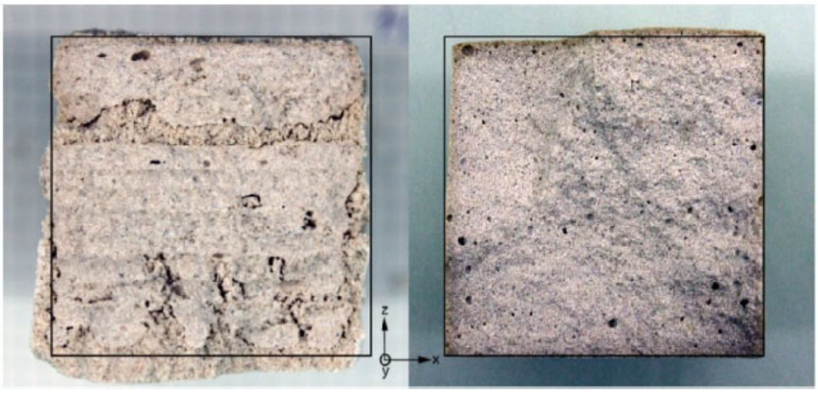

Fig.11.Printedsample(left)andcastedsample(right).Shapeanddimension-flooding. Theblacksquarerepresentsthetargeteddimensionandshape(section4 4cm2).

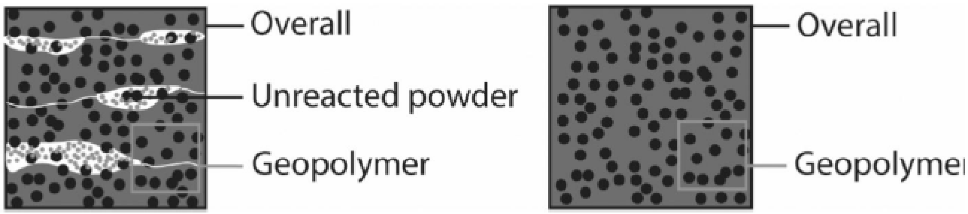

Fig. 12. Close up sketch of a 3D printed sample (left) compared to a cast of the same material (right).

Below saturations of 100%, the powder bed behaves like a porous solid, partially filled with liquid. Getting closer to, or even exceeding, 100%, the liquid starts to be the dominating medium and the slurry can flow. In 3D printing, this flow leads to excessive dimensional inaccuracies.

Consequently, by varying the amount of liquid deposited per dis- tance l and the spacing s between the printed lines, samples with decreased powder bed saturations were printed. The different printing parameters allowing these variations are gathered in Table 2. Asshown inFig.13,thecompressivestrengthincreaseswithincreasingsaturation of the powder bed with liquid. The higher saturation of the pores in the powderbedwithprintingsolutionleadstoaprintelementwithahigher density, therefore a higher compression strength. However, with satu- rations exceeding 70% the liquid starts to dominate the system and the dimensional accuracy drops. As the 3D printed parts in Table 2 show, saturations below 70% lead to more accurate prints.

Whereasinthecastedsampleweconsiderthatafullsaturationofthe porosity in the powder is reached, in the overall volume of the printed sample the unreacted powder between layers and the remaining porosityhastobetakenintoaccount,leadingtoaporousfinalpart.

Table 2
Printingliquidperpowdervolume(inbrackets:powderbedsaturationin%)forvaryingprintingparametersandthe sectionofthecorrespondingprintedsamples.Theblacksquarerepresentsthetargeteddimensionandshape(section4 × 4 cm2).

		s = D_n.a (mm)		
		0.5	0.75	1
l (µl/mm)	0.6	 0.40 µl/mm³ (92%)	 0.27 µl/mm³ (62%)	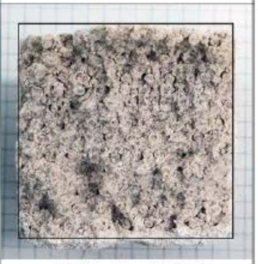 0.20 µl/mm³ (46%)
	0.7	 0.47 µl/mm³ (108%)	 0.31 µl/mm³ (72%)	 0.23 µl/mm³ (54%)

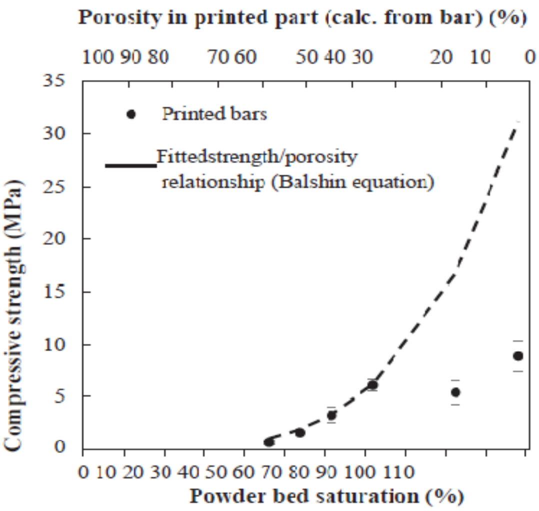

Fig. 13. Compression strength of printed bars with varying saturation.

It is well known that an increasing porosity leads to a decreasing compression strength. For engineering materials, several models were developed in order to relate the porosity of a part with its strength [64,65], such as Ryshkewitch [66] or Balshin [67]. Therefore, considering the unreacted powder in the printed part as pores, the macroporosity *M* of the printed part can be expressed as the ratio of the volume of the unreacted powder (V_{up}) and the total print volume:

$$= M \quad \frac{V_u}{{}_pV_t} \tag{10}$$

Assumingthatthelocallyprintedmaterialisthesamegeopolymerasthecastedmaterial,itwasfoundthatthestrengthoftheprintedpartsuntil 70% powder bed saturation can be modelled with the Balshin equation [67]:

$$\sigma = \sigma_0(1—\varepsilon)^b \tag{11}$$

where σ is the compression strength of the print, σ0 the compression strengthofthesamematerialbutcasted,ϵthemacroporosityoftheprint and b a constant (here b4).

Above 70% powder bed saturation, the compression strengths are lowerthanexpectedfromtheBalshinmodel(Fig.13).This fallstogether with the transition to the liquid dominated state of the powder bed, where it starts to flow out. The behavior of the printed sample is thus controlled by the amount of liquid per volume, which is related to the printer parameters, and not only to the initial liquid to solid ratio as for casting.

The line spacing s and distributed liquid per distance l parameters were combined in one parameter, the liquid per volume, assuming that different parameter combinations will lead to the same saturation level. The fact that the strength of a print with 92% saturation is lower than optimized printing parameters, a trade-off between strength of the part with72%saturation,showsthatthisassumptionmightnot holdtruefor saturations higher than 70%. Extensive work on the influence of the single parameters line spacing s and liquid per distance l should be performed.

4.3. Proof of concept

As shown in Section 4.2, the compressive strength of a 3D printed geopolymer strongly depends on the printing parameters, and with optimized printing parameters, a trade-off between strength of the part and dimensional accuracy can be found. In general, the strength of a geopolymer depends on the Si/Al and Na/Al ratios [46]. Therefore, it is expected that with the optimization not only of the printing parameters but also of the geopolymer composition, the strength of a 3D printed geopolymer should further increase. From the mass calculation, determined with the drop experiment, it was shown that the Si/Al ratio is independentfromthepowderbedcompositionwithMKcontentshigher than20wt%.Thus,theprintingsolutionneedstobeadaptedinorderto obtain stronger geopolymer. Assuming that the composition of the locallyprintedgeopolymercorrespondstothecompositionofthesingle drop,fromEq.(7)thelocalliquidtosolidratioisknown.Withthisdata and a fixed aluminosilicate content (here MK) in the powder bed, the composition of the printing liquid can be adapted to obtain Si/Al and Na/Al ratios that should lead to highly resistant geopolymer. The Si/Al and Na/Al ratios can be expressed asfollow:

$$\frac{Si}{Al}=\frac{n(SiO_2)_l+n(SiO_2)_{MK}}{2n(Al_2O_3)_{MK}} \tag{12}$$

$$\frac{Na}{Al}=\frac{n(NaOH)_l}{2n(Al_2O_3)_{MK}} \tag{13}$$

From these equations, the required SiO_2/Na_2O ratio can be obtained:

$$\frac{SiO_2}{Na_2O}=\frac{n(SiO_2)_l}{n(Na_2O)_l}=\frac{\frac{Si}{Al}*2n(Al_2O_3)_{MK}-n(SiO_2)_{MK}}{2*\frac{Na}{Al}*2n(Al_2O_3)_{MK}} \tag{14}$$

With the molar masses and Eq. (7), the moles are converted into masses,thereforethemasspercentageofNaOHandSiO_2inthesolution can be calculated. The mass of water in the printing solution and the H_2O/Na_2O ratio can bedetermined:

$$m(H_2O)_l= m_l-m(NaOH)_l-m(SiO_2)_l \tag{15}$$

$$\frac{H_2O}{Na_2O}=\frac{n(H_2O)_l+n(H_2O)_{NaOH}}{n(Na_2O)_l} \tag{16}$$

TheexpectedSi/AlandNa/Alratiosintheprintedpartfrom agiven printingsolutioncanthenbecalculated,aswellastherequiredsolution compositionfordesiredSi/AlandNa/Alratios.TheexpectedSi/Al,and Na/Alinthegeopolymerfortheprintingsolutionusedinthisworkwere calculated to be 2, and 1.2, respectively. These values are close to the optimum ratios providing the highest geopolymer strength according to [46]. To test whether the calculated values meet the compositions in singledrops,printsandcasts,SEMimagesweretakenofcrosssectionsof thecorrespondingsamples(Fig.14).WithEDXtheelementcomposition in several points was measured. In Fig. 15, the average of themeasured Si/Al and Na/Al ratios for the singledrop (2.20.3;0.7 0.4), the 3D printedbar(2.1 0.1;0.6 0.1), and the castedbar(2.2 0.2; 0.8 0.2)areplotted.TheyshowaclosefittothecalculatedSi/Al valueof2, whereasthemeasuredNa/Alratioislowerthanexpected(0.7insteadof 1.2). TheSi/AlandNa/AlratiosmeasuredwithEDXaresimilar inallthe threesamples,theylayineachother’sstandarddeviation. Thereforethe same composition is present, no matter whether only a single drop or a fullpartisprinted,andthesingledropcanbeusedasanexampleforfast testing of solutions. The fact that the 3D printed andthe casted sample

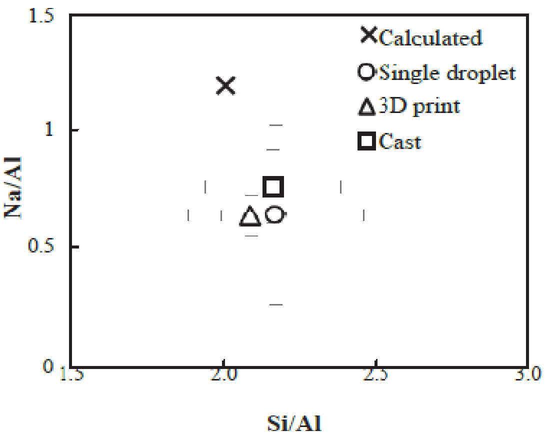

Fig. 15. Si/Al and Na/Al ratios of single drops, printed and casted samples, measured by EDX.

have the same composition confirms the theoretical assumption for the liquid to solid ratio in the 3D print. However, it is important to note that this only applies to a local level of the print (cf. Fig. 12). Overall, the print is more porous than the casted material, due to the unreacted powderpresentinthesample.Nevertheless,theresultsshowthatwhere the binder is printed, the composition can be modelled by the behavior of a singledrop.

The calculated values for Si/Al and Na/Al ratios correspond to the initialmixcompositionofthecastedsamples.Thediscrepancybetween this value and the values measured with EDX is similar as found by Rowles et al. [46]: the Si/Al ratios are higher, and the Na/Al ratios lower as expected form the initial composition of the mix. The slight shift towardshigherSi/Alratioscouldbeexplainedbythepresenceofnotfully reacted MK. The measured Na/Al ratios are lower than the calculated value.Duetotheevaporationoflightweightatomsunderelectronbeam impact, the Na content might be underestimated, resulting in a measured Na/Al ratio lower thanexpected.

With EDX the elemental composition of the samples could be determined, but not the conformation of the elements. To prove thatthe present elements build the structure of a geopolymer, an Al-NMRanal- ysis of unprinted powder mix, a printed and a casted bar wasconducted (Fig. 16). In the geopolymer reaction, aluminum (V) is rearranged into aluminum(IV)conformation,whichischaracteristicforthegeopolymer structure. Indeed, this shift is present for the casted and for the printed bars: a geopolymer is properly built even in the printedsample.

Thanks to these results, we could successfully proof the concept of powder bed 3D printing geopolymers in an approach where the binder and the activator are separated. The new mix design strategy, wherethe composition of the printed binder is calculated depending on the com- pacity of the powder bed and the desired composition in the printed geopolymer,helpstooptimizethepropertiesonthematerial level.On the larger scale, the hardware of the printer needs to be upgraded in order to ensure more homogeneous printing. The printing parameters need to be refined in order to improve the binding between lines and layers and therefore decrease the porosity and improve the strength of the printed parts. More experiments with varying printing parameters, such as nozzle diameter or layer height, will be conducted.

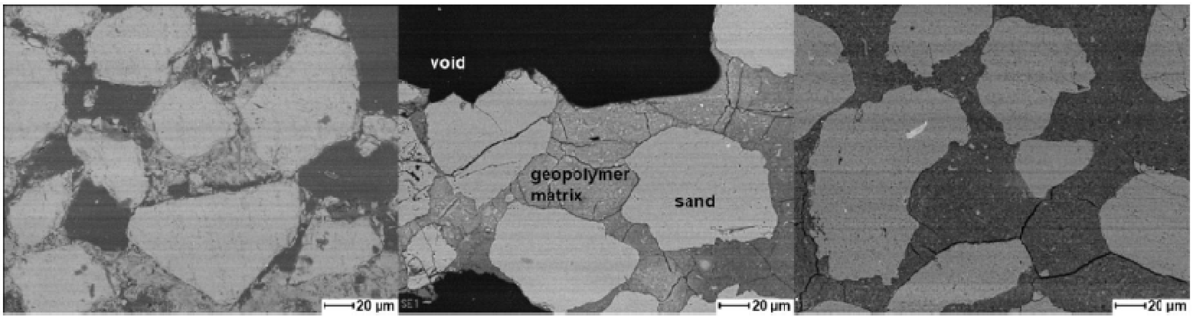

Fig. 14. SEM images of single drop (a), 3D printed bar (b), and a casted bar (c).

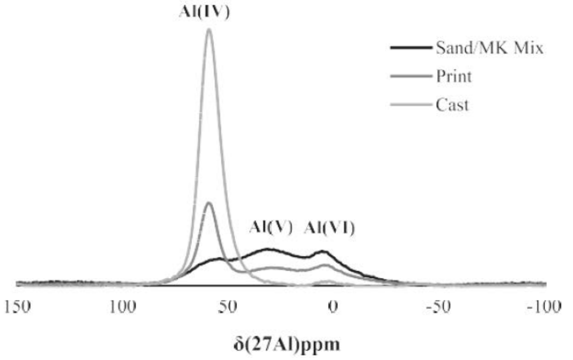

Fig.16.^{27}AlNMR spectrum of the 3D printed sample and of the casted sample.

V. CONCLUSION

The mix design in 3D printing differs from usual mix design in casting. In casting, the desired ingredients are mixed to the right pro- portions and the final cast has the same composition. In powder bed3D printing the mix design of the material is more complicated, since the ratio between the liquid part and the solid part depends on the pene- tration behavior. To get an insight on the penetration behavior, the printingprocesswasmimickedbysingledropsofliquidon powderbeds.

Theresultsoftheseexperimentsperformedatthedropscaleshowedthat the addition of liquid to the powder bed with 20 wt% MK compactsthe powder to a dense packing. From micro tomography images of the drops,itcanbeassumedthattheliquidoccupiesallvoidspresentinthis dense packing, allowing the determination of the local liquid to solid ratiobythepackingdensityofthepowderbed.Knowingthelocalliquid tosolidratioaswellasthepowderbedcompositionandtheformulation oftheliquid,theSi/AlandNa/Alratiosintheresultinggeopolymercan bedetermined.Thenewproposedmixdesignstrategyuses thistheother way round: knowing the composition and the packing of the powder bed,thecompositionoftheliquidcanbeadaptedtoobtaindesiredSi/Al and Na/Al ratios in the resultinggeopolymer.

Nevertheless, the printed material is characterized by a poorer mechanical response than the corresponding casted material, due to the high porosity. The macro porosity in the printed part can be controlled by the printing parameters. The strength of parts increases with increasing powder bed saturation but, once reached the critical value, the precision decreases. Until this point, the strength can be modelled with a Balshin equation taking into account the casted strength and the macro porosity of the printed material. Further research should be performed to analyse the void distribution and its influence on the mechanicalperformanceof3Dprintedgeopolymer.This newmixdesign strategy allows us to potentially replace the metakaolin and the sand easilybymoreenvironmentallyfriendlyalternative,possiblyrecycledor waste materials such as slag, fly ash, or brick waste for the aluminosilicate and gneiss quarry or concrete waste for the solid particles. As a result, it is possible to combine a material efficient manufacturing process with a low carbon footprintmaterial.

CREDIT AUTHORSHIP CONTRIBUTION STATEMENT

VeraVoney:Conceptualization,Methodology,Investigation,original draft preparation, Writing and-Reviewing,
Pietro Odaglia: Conceptualization, Methodology, Resources,

INVESTIGATION

Coralie Brumaud: Conceptualization, Methodology, supervision, original draft preparation, Writing-Reviewing and Editing
Benjamin Dillenburger: Conceptualization, Methodology, supervision,
Guillaume Habert: Conceptualization, Methodology, Supervision, Reviewing

DECLARATION OF COMPETING INTEREST

The authors declare that they have no known competing financial interests or personal relationships that could have appeared toinfluence the work reported in thispaper.

ACKNOWLEDGEMENTS

TheauthorswouldliketothanktheClaylabgroup(IGT,ETHZurich) for the technical support for Accupyc, Geopyc and BETmeasurements. WarmthanksalsogotoEmmanuelKeita(IFSTTAR,Paris),AselMaria AguilarSanchez(IfB,ETHZurich)andRen´eVerel(LAC,ETHZurich)for the help to conduct, respectively, microtomography, SEM/EDX, and NMR measurements. The Swiss National Fund (SNF, project N◦200020_169359) and the NCCR in digital fabrication are gratefully acknowledged for their financialsupport.

REFERENCES

[1] A. Horvath, Construction materials and the environment, Annu. Rev. Environ. Resour. 29 (2004)181–204.
[2] D. Ioannidou, G. Meylan, G. Sonnemann, G. Habert, Is gravel becoming scarce? Evaluating the local criticality of construction aggregates, Resources, Conservation and Recycling 126 (2017)25–33.
[3] P.Peduzzi,Sand,rarerthanonethinks,EnvironmentalDevelopment11(2014) 208–218.
[4] M. Hegger, J. Hartwig, M. Keller, L. Elschen, P. Pick, EcoEasy - Abschlussbericht, 2012.
[5] I. Sartori, A.G. Hestnes, Energy use in the life cycle of conventional andlow-energy buildings:areviewarticle,Energyandbuildings39(3)(2007)249–257.
[6] A. Passer, C. Ouellet-Plamondon, P. Kenneally, V. John, G. Habert, The impact of future scenarios on building refurbishment strategies towards plus energy buildings, Energy and Buildings 124 (2016)153–163.
[7] IEA,"Materialefficiencyincleanenergytransitions,"March2019 2017.
[8] M.Ro¨ck,etal.,EmbodiedGHGemissionsofbuildings– thehiddenchallengeforeffective climate change mitigation, Appl. Energy 258 (2020)114107.
[9] M. Rippmann, A. Liew, T. Van Mele, P. Block, Design, fabrication and testing of discrete 3D sand-printed floor prototypes, Materials Today Communications 15 (2018)254–259.
[10] A. Jipa, M. Bernhard, B. Dillenburger, and M. Meibodi, "3D-Printed Stay-in-Place Formwork for Topologically Optimized Concrete Slabs," in *2016 TxA Emerging Design Technology conference*, 2016: Texas Society ofArchitects.
[11] G.Habert,D.Arribe,T.Dehove,L.Espinasse,R.LeRoy,Reducing environmental impactbyincreasingthestrengthofconcrete:quantificationoftheimprovementto concrete bridges, J. Clean. Prod. 35 (2012)250–262.
[12] U.M.Angst,"Challengesandopportunitiesincorrosionofsteelinconcrete,"
[13] *Materials and Structures*, vol. 51, no. 1, p. 4, 2018.
[14] R. Klis, E.N. Chatzi, Data recovery via hybrid sensor networks for vibration monitoring of civil structures, International Journal of Sustainable Materials andStructural Systems 2 (1–2) (2015)161–184.
[15] E. Brühwiler, "UHPFRC Technology to enhance the performance of existing concrete bridges," in *Proceedings of the Ninth International Conference on Bridge Maintenance, Safety and Management (IABMAS 2018): Maintenance, Safety, Risk, Management and Life-Cycle Performance of Bridges*, 2018, no. CONF, pp. 318–324: Taylor & FrancisGroup.
[16] A.Hajiesmaeili,F.Pittau,E.Denari´e,andG.Habert,"LifeCycleAnalysisof Strengthening Existing RC Structures with R-PE-UHPFRC," *Sustainability*, vol. 11, no. 24, p. 6923, 2017.

[17] C. Ouellet-Plamondon, G. Landrou, M. Palacios, Earth Concrete as a Promising Building Material,2015.

[18] G. Landrou, C. Brumaud, G. Habert, Influence of magnesium on deflocculated kaolinite suspension: mechanism and kinetic control, Colloids Surf. A Physicochem. Eng. Asp. 544 (2018)196–204.

[19] E.Z. Escamilla, G. Habert, Environmental impacts of bamboo-based construction materials representing global production diversity, J. Clean. Prod. 69 (2014) 117–127.

[20] F. Pittau, F. Krause, G. Lumia, G. Habert, Fast-growing bio-based materials as an opportunity for storing carbon in exterior walls, Build. Environ. 129 (2018) 117–129.

[21] Landrou, C. Brumaud, F. Winnefeld, R. J. Flatt, and G. Habert, "Lime as an anti- plasticizer for self-compacting clay concrete," *Materials*, vol. 9, no. 5, p. 330,2016.

[22] M. Despeisse, et al., Unlocking value for a circular economy through 3D printing: a researchagenda,Technol.Forecast.Soc.Chang.115(2017)75–84.

[23] RepRap. *Powder Printer Recipes*. Available:https://reprap.org/wiki/Powder_Printer

[24] _Recipes.

[25] PreciousPlastic.*Startcollaborating,boostplasticrecycling*.Available:https://p reciousplastic.com/.

[26] Winsun.*Chinesecompany3Dprints10buildingsinadayusingconstructionwaste*. Available: https://www.dezeen.com/2014/04/24/chinese-company-3d-prints-bui ldings-construction-waste/.

[27] B. Holthuis. *Paper Pulp Printer*. Available:http://www.beerholthuis.com/.

[28] N. Roussel, Rheological requirements for printable concretes, Cem. Concr. Res.112 (2018)76–85.

[29] L.Reiter,T.Wangler,N.Roussel,R.J.Flatt,Theroleofearlyagestructuralbuild- up in digital fabrication with concrete, Cem. Concr. Res. 112 (2018)86–95.

[30] R.A. Buswell, W.L. de Silva, S. Jones, J. Dirrenberger, 3D printing using concrete extrusion:aroadmapforresearch,Cem.Concr.Res.112(2018)37–49.

[31] V. Colla and E. Dini, "Large scale 3D printing: From deep sea to the moon," *Low-Cost 3D Printing, for Science, Education & Sustainable Development; Canessa, E., Fonda,C.,Zennaro,M.,Eds*,pp.127–132,2013.

[32] D.Lowke,E.Dini,A.Perrot,D.Weger,C.Gehlen,B.Dillenburger, Particle-bed3D printing in concrete construction–possibilities and challenges, Cem. Concr. Res. 112 (2018)50–65.

[33] Exone. *3D Printing Binders*. Available:https://www.exone.com/Resources/Binders.

[34] M. Upadhyay, T. Sivarupan, M. El Mansori, 3D printing for rapid sand casting—a review, J. Manuf. Process. 29 (2017)211–220.

[35] N. Bakhiya, K.E. Appel, Toxicity and carcinogenicity of furan in human diet, Arch. Toxicol. 84 (7) (2010)563–578.

[36] I. Agustí-Juan, A. Jipa, G. Habert, Environmental assessment of multi-functional building elements constructed with digital fabrication techniques, Int. J. Life Cycle Assess. (2018)1–13.

[37] C.Sotelo-Pin˜a,E.N.Aguilera-Gonza´lez,andA.Martínez-Lu´evanos,"Geopolymers: Past, Present, and Future of Low Carbon Footprint Eco-Materials," in *Handbook of Ecomaterials*: Springer, 2018, pp.1–21.

[38] G. Habert, C. Ouellet-Plamondon, Recent update on the environmental impact of geopolymers, RILEM technical Letters 1 (2016)17–23.

[39] R.E. Lyon, P. Balaguru, A. Foden, U. Sorathia, J. Davidovits, M. Davidovics, Fire-resistantaluminosilicatecomposites,Fireandmaterials21(2)(1997)67–73.

[40] P.Duxson,A.Ferna´ndez-Jim´enez,J.L.Provis,G.C.Lukey,A.Palomo,J.S.vanDeventer, Geopolymer technology: the current state of the art, J. Mater. Sci. 42 (9) (2007)2917–2933.

[41] J.L. Provis, J.S.J. Van Deventer, Geopolymers: Structures, Processing, Properties and Industrial Applications, Elsevier,2009.

[42] T. Cheng, J. Chiu, Fire-resistant geopolymer produced by granulated blast furnace slag, Miner. Eng. 16 (3) (2003)205–210.

[43] M.Palacios,F.Puertas,Effectofcarbonationonalkali-activatedslagpaste,J.Am. Ceram. Soc. 89 (10) (2006)3211–3221.

[44] A.Fern´andez-Jim´enez,A.Palomo,M.Criado,Microstructuredevelopmentof

[45] alkali-activated fly ash cement: a descriptive model, Cem. Concr. Res. 35 (6)(2005) 1204–1209.

[46] N.Paszek,M.Go´rski,MechanicalParametersofMetakaolin-BasedGeopolymerwith CRT Glass Waste Fine Aggregate, Proceedings of the InternationalConference onSustainableMaterials,SystemsandStructures(SMSS,2017,p. 2017.

[47] M.Tuyan,O¨.Andiç-Çakir,K.Ramyar,Effectofalkaliactivatorconcentrationand

[48] curingconditiononstrengthandmicrostructureofwasteclaybrick powder-basedgeopolymer, Compos. Part B 135 (2018)242–252.

[49] P.Rovnaník,B.Rˇezník,P.Rovnaníkov´a,Blendedalkali-activatedflyash/brickpowder materials, Procedia Engineering 151(2016) 108–113.

[50] M.Rowles,B.O'connor,Chemicaloptimisationofthecompressivestrengthof aluminosilicate geopolymers synthesised by sodium silicate activation of metakaolinite, J. Mater. Chem. 13 (5) (2003)1161–1165.

[51] A.Favier,M´ecanismedepriseetrh´eologiedeliantsg´eopolym`eresmod`eles,Universit´eParis-Est,2013.

[52] M. Xia, J. Sanjayan, Method of formulating geopolymer for 3D printing for constructionapplications,Mater.Des.110(2016)382–390.

[53] R. Ramakrishnan, B. Griebel, W. Volk, D. Günther, and J. Günther, "3D printing of inorganic sand moulds for casting applications," in *Advanced Materials Research*, 2014,vol.1018,pp.441–449:TransTechPubl.

[54] D-Shape. Available:https://d-shape.com/.

[55] R.A. Buswell, et al., A process classification framework for defining and describing digital fabrication with concrete, Cem. Concr. Res. 134 (2020)106068.

[56] E.W.Washburn,"Thedynamicsofcapillaryflow,"*Physicalreview*,vol.17,no.3,p. 273,1921.

[57] K.P.Hapgood,J.D.Litster,S.R.Biggs,T.Howes,Droppenetrationintoporous powder beds, J. Colloid Interface Sci. 253 (2) (2002)353–366.

[58] T.Sedran,F.DeLarrard,L.LeGuen,D´eterminationdelacompaci t´edescimentset

[59] additionsmin´eralesa`lasondedeVicat,2007.

[60] V.L´ed´ee,F.DeLarrard,T.Sedran,andF.Brochu,"Essaidecomp acit´edesfractions granulairesa`latable`asecousses,"*LaboratoireCentraldesPonts etChauss´ee–IST Diffusiondes´editions,Juillet2004*,Paris,2004.

[61] E. Sachs, et al., Three-dimensional printing: the physics and implications of additive manufacturing, CIRP Annals-Manufacturing Technology 42 (1) (1993) 257–260.

[62] T.Nguyen,W.Shen,K.Hapgood,Droppenetrationtimeinheterogeneouspowder beds, Chem. Eng. Sci. 64 (24) (2009)5210–5221.

[63] P. Odaglia, V. Voney, D. Benjamin, G. Habert, "Open Hardware Additive ManufacturinginBinderJet3DPrinting,"*Proceedingsofthe1stInternational Conference on 3D Construction Printing*,2018.

[64] V. Voney, P. Odaglia, C. Brumaud, B. Dillenburger, G. Habert, "Geopolymer Formulation for Binder Jet 3D Printing," *Proceedings of the 2nd International Conference on Digital Concrete*, 2020.

[65] B.K. Diffo, A. Elimbi, M. Cyr, J.D. Manga, H.T. Kouamo, Effect of the rate of calcination of kaolin on the properties of metakaolin-based geopolymers, Journal ofAsianCeramicSocieties3(1)(2015)130–138.

[66] A. Heath, K. Paine, M. McManus, Minimising the global warming potential of clay basedgeopolymers,J.Clean.Prod.78(2014)75–83.

[67] P.Duxson,J.L.Provis,G.C.Lukey,S.W.Mallicoat,W.M.Kriven, J.S.VanDeventer, Understanding the relationship between

geopolymer composition, microstructure and mechanical properties, Colloids Surf. A Physicochem. Eng. Asp. 269 (1–3) (2005)47–58.

[68] J. Frederic, Bredt, *Binder stability and powder/binder interaction in three dimensional printing*,1995.

[69] X. Chen, S. Wu, J. Zhou, Influence of porosity on compressive and tensile strength ofcementmortar,Constr.Build.Mater.40(2013)869–874.

[70] L. Li, M. Aubertin, A general relationship between porosity and uniaxial strength of engineeringmaterials,Can.J.Civ.Eng.30(4)(2003)644–658.

[71] E. Ryshkewitch, Compression strength of porous sintered alumina and zirconia: 9th communicationtoceramography,J.Am.Ceram.Soc.36(2)(1953)65–68.

[72] M. Y. Balshin, "Relation of mechanical properties of powder metals and their porosity and the ultimate properties of porous metal-ceramic materials," in *Dokl AkadNaukSSSR*,1949,vol.67,no.5,pp.831–834.

★★★

IMPACT OF PLASTIC WASTE ON STRENGTH OF CLAYEY SOIL MIXED WITH FLY ASH

[1]ANWAY MAITI, [2]SARUK MALLICK, [3]SUBHARANSHU KUMAR MUDULI

[2]Assistant Professor, Department of Mechanical Engineering, NMIET, BBSR
[2]Asst Prof, Department of Civil Engineering REC Bhubaneswar
[3]Asst Prof, Department of Civil Engineering AIET Bhubaneswar
E-mail: [1]Singh.deviprasad@nmiet.ac.in

Abstract - This paper present the impact of plastic waste as a strips on the strength of clayey soil and dirt fly debris blend and the outcomes are introduced in term of compressive strength, shear strength, california bearing proportion CBR) attributes. The distinctive level of plastic waste 0.5%, 1.0%, 1.5% and 2.0% by dry load of 10mm length also, 5 mm width) and 5%, 10%, 15% and 20% fly debris by weight were blended into the clayey soil. With increment in level of waste plastic there is expanding pattern in MDD upto the 1.5% of waste plastic after that diminishing pattern in MDD is noticed. However, an expansion in OMC has been seen with increment in level of waste plastic. The expansion in fly debris rate the MDD having expanding pattern up to 10% and assist expansion of fly debris the MDD shows diminishing pattern. However, an expansion in OMC has been seen with increment in level of fly debris. With increment in level of waste plastic there is expanding pattern in UCS upto the 1.5% of waste plastic after that diminishing pattern in UCS is noticed. The increment in fly debris rate the UCS having expanding pattern up to 10% and assist expansion of fly debris the UCS shows diminishing pattern. With increment in level of waste plastic there is expanding pattern in CBR upto the 0.5% of waste plastic after that diminishing pattern in CBR is noticed. The increment in fly debris rate the CBR having expanding pattern up to 10% and advance expansion of fly debris the CBR shows diminishing pattern .The current examination will help in burning-through the significant amount of waste plastic in this manner decreasing the natural danger.

I. INTRODUCTION

Soil Stabilization is the process of blending and mixing materials with a soil to improve certain properties of the soil. The process may include the blending of soils to achieve a desired gradation or the mixing of commercially available additives that may alter the gradation, texture or plasticity, or act as a binder for cementation of the soil. The long term performance of any construction project depends on the soundness of the under laying soils. Unstable soil scan create significant problems for pavements. Lack of adequate road network to cater to the increased demand and increase distress in road leading to frequent maintenance have always been big problem in our country. Evolving new construction materials to suit various traffic and site conditions for economic and safe design is a challenging task in road construction. Effective utilization of local weak soils by imparting additional strength using stabilization materials enable reduction in construction cost and improved performance for roads. Fly ash is the residue produced from the thermal power plants. Its composition basically depends on the type of coal which is fused during combustion in the power plant. It is a pozzolanic material. Nowadays fly ash has found its application in many areas like manufacturing of cement and bricks, landfiiling, construction of roads and embankments etc. and is thus moved from the category of ―hazardous waste‖to ―useful waste material‖in the year 2009 by the government of India. Similarly a large percentage of tile waste is produced in the country arising the need of its proper disposal. Stabilization of poor soil is a rapidly emerging area which can be used for proper utilization of wastematerial.

The Properties of a soil are very uncertain when it is subjected to variable moisture. It shows huge volumetric change when exposed to dry and wet conditions. This is due to presence of active clay mineral. When water occupies large space in the voids of soil the strength of soil changes. These changes create challenges for civil engineers doing work on site specially while constructing foundations. Though black cotton soil is unfit for infrastructural development, they are useful to protect environment and waste disposal. For the construction of any kind of structure resting on weak soil, various available methods are used to improve the bearing capacity and reduce the settlement of soils. One of the methods is using reinforcement. The concept reinforcement of soil by using fibres was developed in the 19th century. The main objective of reinforcing the soil was to upgrade its properties. The reinforcing material introduced in the soils alters the strength and deformation characteristics of the soil. Plastic is considered as one of the best invention in many aspects of life. The amount of plastic waste is increasing year by year. Due to this the need of plastic waste management has increased so that it can be used as soil stabilizer and in other ground improvement techniques as it behaves like reinforcing material. Hence to make the development path sustainable the use of plastic waste in geotechnical engineering needs to be encouraged. By doing so, Properties of soil will be improved and reuse of plastic can also be madeefficiently.

Plastics waste is of two types:

- Pre-use plastic (productionscrap)
- Post-use plastic Pre-useplastic

That plastic which does not fulfil the desired requirement during casting and assembly i.e. material that has the mismatching colour, undesirable hardness, or wrong processing characteristics are called Pre-use plastic waste. This material is easy to use for other applications and has the property to get recycled. Pre-use plastic waste is the ultimate source of plastics which are suitable for reprocessing from manufacturers of plastic products. Processing of Pre-used plastic is less as compared to post-use hence Pre-use is more valuable then Post-use plastic.

II. OBJECTIVE OF THESTUDY

To check and improving the CBR and shear strength value by adding plastic waste and fly ash. Moreover pavement on clayey soil requires a greater thickness of base and sub-base course which results increases the expenditure of project. To set right this problem it becomes mandatory to increase the strength of the soil which in-turn will help in lessening the thickness of the pavement layers and thus project cost.The common additives which are widely used in stabilizing the soil are cement and lime. Lime is preferred over cement stabilization because lime is cheaper than cement and Carbon-Di-Oxide (C02), which causing detrimental to the environment, is emitted during the production of cement. Lime stabilization is requires adequate clay content and a relatively high curing temperature and hence it is more suitable for tropical and sub-tropical countries like India. Cement is generally used where clay content in soil is comparatively less and the temperature is relatively less. Researchers are going on for alternative by-products to cement ,fly ash and lime which not only satisfy the engineering requirements and cause no pollution but also be cost effective. Present thesis makes the use of plastic waste and fly ash with the soil and finds the changes in the soil properties.

III. LITERATUREREVIEW

PalakChopra , G.S Bath , Amanpreet Singh Virk [1] In this study, Fly ash, by-product of thermal power plant, is used for stabilization of expansive soils. The disposal of Fly Ash is a big problem for environment, so it should be used for good cause. In this research paper, fly ash is added in the clayey soil in the proportion of 5%, 10%, 15%, 20% and 25% by weight of soil and the properties are compared with parent soil. The properties studied are liquid limit, plastic limit, plasticity index, california bearing ratio (CBR) and unconfined compressive strength. With the increase in Fly ash OMC is decreased from 20.75% 17.18% , whereas MDD of the soil has shown an increasing path from 1.614 gm/cc to 1.693gm/cc

Saket Dixit [2]. In this study different types of waste plastic were randomly mixed with the soil, then a series of California Bearing Ratio (CBR) tests were conducted to evaluate the strength of subgrade soil. High density polyethylene (HDPE), Low density polyethylene (LDPE) and Polypropylene (PP) at various percentages were used for improving soil strength. Results from the CBR tests established that addition of these materials in subgrade soil gives efficient strength to subgrade soil. It was observed that the CBR value increases with increase in fiber content up to a certain percentage but decreases with further addition of waste plastic content. The pavement sections has been designed with the modified subgrade using HDPE, LDPE & PP and the critical strain values at the top of the subgrade and at the bottom of the bituminous layer has been analysedand

compared with the allowable values as per IRC: 37-2012 for the traffic loading of 150 msafor the four lane divided state highway project. The reduction in the crust thickness and saving in the project cost has been compared for the different subgrade with different waste plastics and by varying plastic contents.

Vijay Kumar Patidar, Dr. SuneetKaur [3]. Soil stabilization alters the physical properties of soil in order to improve its strength, durability, or other qualities to meet the engineering requirements. It can be achieved by adding suitable admixtures like cement, lime and waste material like fly ash, gypsum etcor by other suitable stabilization method. the cost of adding these additives has tremendously increased in past few years; there for there is need for the development of other kinds of soil additive such as plastic, bamboo etc and these new techniques of soil stabilization using plastic waste which can be effectively used to solve the challenges of society, thereby reducing the amount of waste plastic material.

Wajid Ali Butt, Karan Gupta and J.N.Jha [4]. This experimental studyhas revealed that the addition of SDA results a significant increase in CBR and unconfined compressive strength. Furthermore the values of CBR obtained are within the limits recommended by the Asphalt Institute for Highway sub-base andsub-grade. Thus from the present study it is concluded that SDA, an industrial waste, is a cheap satisfactory stabilizing agent for sub-baseandbase course in clayey fills; although its performance can be improved by combining it with other bonding materialssuch as lime, and becomes an alternatives use of industrial waste to reduce the construction cost of road particularly in the rural areas of the country

Dr. A.I. Dhatrak [5] after reviewing performance of plastic waste mixed soil as a geotechnical material, it was observed that for construction of flexible pavement to improve the sub grade soil of pavement using waste plastic bottles chips is an alternative method. In his paper a series of experiments are done on soil mixed with different percentage of plastic (0.5%, 1%, 1.5%, 2 % & 2.5%) to calculate CBR. on the basis of experiments that he concluded using plastic waste strips will improve the soil strength and can be used as sub grade . It is economical and eco-friendly method to dispose waste plastic because there is scarcity of good quality soil for embankments andfills.

Akshat Malhotra and HadiGhasemain [6] studied the effect of HDPE plastic waste on the UCS of soil. In a proportion of 1.5%, 3%, 4.5% and 6% of the weight of dry soil, HDPE plastic (40 micron) waste was added. They concluded that the UCS of black cotton soil increased on addition of plastic waste. When 4.5 % plastic waste mixed with soil strength obtained was optimum mixes. These optimum mixes obtained through the experimental investigation carried were further checked for strength characteristics through California bearing ratio test. A considerable improvement in the CBR value was obtained for these optimum mixes in comparison to that of pure clay. The results of experimental investigation reveals that soil:sand::70:30,soil:sand:flyash::63:27:10 and soil:sand:flyash:tile waste::63:27:10:9 are the best optimum mixes on the basis of compaction characteristics and for every optimum mix CBR value shows an increasing trend. Basic purpose of this study is to use the waste materials (river sand, fly ash and tile waste) as additives so as to solve the problem of disposing them and producing a cheaper construction material. Also, the gainful effects of these waste materials when used in a composite form on the geotechnical properties of locally available clayey soil can be visualized from thisstudy.

Murat Olgun[8] Anexperimental investigation was conducted to evaluate the effects of polypropylene fiber inclusions on the geotechnical characteristics of a clayey soil that was chemically stabilized with 287.32KN/m2 which is maximum because for natural soil it was71.35KN/m2.

Babita Singh , Amrendra Kumar and Ravi Kumar Sharma[7] In this paper an attempt has been made in the direction of improving the lacking geotechnical properties of locally available clayey soil by adding admixtures i.e. sand, fly ash and tile waste in suitable proportion. The suitable proportion in which the admixtures are to be added in the clay is decided with the help of proctor compaction test to obtainthe cement and fly ash. For all stabilized soils, cement and fly ash were added at 8% and 30%, respectively. Reinforced stabilized soil specimens were prepared at four different percentages of fiber content (0.25%, 0.50%, 0.75%, 1.0%) and three differentfiber lengths (6 mm, 12 mm, 20 mm). Unconfined compressive and split tensile strength tests were carried out after 7- and 28-day curing periods. The volume change characteristics of the reinforced stabilized soil were determined using shrinkage limit and crack reduction values. The interactions between the fiber surface and the stabilized soil were analyzed by means of scanning electronmicroscopy.

IV. MATERIAL USED

SOIL :- Nearly 100 Kg of locally available clayey soil was collected from Mathana. Then the soil was sieved through 4.75mm sieve to remove the gravel fraction. The soil is classified as Intermediate compressible clay, CI, as per IS: 1498 (1970). The physical properties of soil are reported in Table 1.

Table 1 physical properties

S. No.	Parameters	Result
1.	Modified Compaction Test MDD (gm/cc) OMC (%)	1.73 17.69
2.	Liquid Limit (%)	48.38
3.	Plastic Limit (%)	23.59
4.	Plasticity Index (%)	24.79
5.	Specific Gravity	2.74
6.	Indian Soil Classification	CI

WASTE PLASTIC

Waste Plastic have been purchased from the market of Ambala. The Plastic are cut into pieces of approximately 10mm lengths & 5mm width and are mixed in percentage of 0.5 %, 1.0%, 1.50% and 2.0% by dry weight ofsoil.

FLY ASH

The fly ash was collected from the Thermal Power Plant, Panipat. The fly ash was oven dried and was passed through 300 micron sieve. The fly ash was mixed with parent soil in percentage of 5%, 10%,15% and 20%. The chemical properties of Fly ash is given in Table 2.

Table 2 chemical properties

Sr. No.	Parameter	%age
1	SiO_2	56.33
2	Al_2O_3	23.45
3	Fe_2O_3	5.19
4	TiO_2	0.94
5	CaO	3.47
6	MgO	0.63
7	SO_3	0.44
8	K_2O	1.30

EXPERIMENTAL PROCEDURE

Following are the tests which have been carried out in laboratory: -

CHARACTERISTICS TESTS

- Moisture ContentDetermination.
- Atterberg LimitsDetermination.
- Specific Gravity Test byPycnometer.

STRENGTH TESTS

- Heavy Compaction Test - IS : 2720 (Part 8) - 1983
- Unconfined Compression Test - IS : 2720 (Part10) – 1991

Test & Unconfined Compressive Strength Test. This test confirms to IS: 2720 (Part 8) 1983.

SAMPLE PREPARATION

For parent soil 5 kg of oven dried soil sample is taken on tray and thoroughly mixed with water. For the blended mixtures the quantity of soil depends upon the ratio at which it is desired to be mixed with other additives. The amount of water mixed at first trial may vary according to the soil samplecomposition.

PROCEDURE

The mixed sample is placed in previously weighted ($m_l$gm) mouldof capacity 2250 cc. in five layers. Each layer is given 25 blows with a 4.9 kg rammer with free fall height of 450 mm. After five successive layers collar is removed and excess soil is trimmed off. The weight of mould with soil is taken ($m_2$gm). This process is repeated for other water content also until there is a decrease in $m_2$value. For each trial a portion of soil is taken for moisture content determination.

CALCULATION

Bulk density of soil, $\gamma = (m_2 - m_l)/2250$ Dry density of soil, $\underline{\ }\gamma_a$
$= \gamma / (1+w)$
Where w = moisture content present in soil.

UNCONFINED COMPRESSIVE STRENGTH TEST

This test confirms to IS 2720 (Part 10): 1991

SAMPLE PREPARATION

Cylindrical specimen is compacted by static compaction in 3.8 cm diameter and 7.6 cm high mould. The inner surface of the mould is lubricated with mobile oil so as to extrude the sample from mouldwith minimum disturbance. The sample is placed inside the specimen mould in seven layers using spoon, leveled and gently compacted. Pressure pad will be inserted into the mould and the whole assembly will be statically compacted in loading frame to the desired density. The sample is to be kept under static load for not less than 10 minutes in order

- California bearing ratio (CBR) test - IS : 2720 (Part 16) – 1987

V. METHODOLOGY

Compaction Test

This Phase of Study involved a detailed investigation of the compaction characteristics of the parent soil and blended sample containing different percentage of waste plastic and fly ash contents, in order to obtain the optimum moisture contents and maximum dry densities. The optimum moisture contents thus obtained is used in preparing samples for CBR

to account for any subsequent increase in height of sample due to swelling. The sample will then be removed from the mouldwith the help of sample extruder. Initial dimensions aremeasured.

PROCEDURE

The sample is placed on the pedestal of the Strain controlled tri-axial cell with non- pervious discs at the top and bottom. A loading platen will be placed at the top which is connected through loading piston to the proving ring. The sample arrangements are brought in the contact of deformation dial gauge. The axial strain rate is chosen as 1.0 mm/minute by appropriate setting of turret lever and strain setting lever. The compressive stress taken by the sample will be recorded at various strain levels until the sample fails. The dimensions are noteddown.
For measurement of compressive stress taken by the sample, 50kg capacity provingringwithprovingringconstantof 0.25 kg/division. Proving ring and deformation dial gauge installed in the testing programme is having least count of 0.002 mm and 0.01 mm respectively.

CALCULATION

Axial strain, $e = (\Delta L / Lo)$
Where, ΔL = change in length after failure L = initial length of the specimen
Average cross-sectional area afterfailure,
Where, A_o = Initial Average cross-sectional area of Specimen. Compressive Stress, $\sigma_o = (P/A)$

CALIFORNIA BEARING RATIO (CBR) TEST

The CBR is a measure of resistance of a material to penetration of standard plunger under controlled density and moisture conditions. The CBR test may be conducted in re- mouldedor undisturbed specimen in the laboratory. The test is simple and has been extensively investigated for field correlations of flexible pavement thickness requirement. The test is conducted by causing a cylindrical plunger of some diameter to penetrate a pavement component material at 1.25mm/minute. The loads, for 2.5mm and 5mm are recorded. This load is expressed as a percentage of standard load value at a respective deformation level to obtain C.B.R. value. The values are given in the table

Table 3 Standard Load Value at a Respective Deformation to obtain C.B.R. Value

Penetration, mm	Standard Load, kg	Unit Standard Load, Kg/Cm^2
2.5	1370	70
5.0	2055	105
7.5	2630	134
10.0	3180	162
12.5	3600	183

PROCEDURE

Place the mould assembly with the surcharge weights on the penetration test machine. Seat the penetration piston at the center of the specimen with the smallest possible load, but in no case in excess of 4 kg so that full contact of the piston on the sample is established. Set the stress and strain dial gauge to read zero. Apply the load on the piston so that the penetration rate is about 1.25 mm/min.

Record the load readings at penetrations of 0.5, 1.0, 1.5, 2.0, 2.5, 3.0, 4.0, 5.0, 7.5, 10 and 12.5 mm. Note the maximum load and corresponding penetration if it occurs for a penetration less than 12.5 mm. Detach the mould from the loading equipment. Take about 20 to 50 g of soil from the top 3 cm layer and determine the moisturecontent.

The C.B.R. values are usually calculated for penetration of 2.5 mm and 5 mm. Generally the C.B.R. value at 2.5 mm will be greater that at 5 mm and in such a case/the former shall be taken as C.B.R. for design purpose. If C.B.R. for 5 mm exceeds that for 2.5 mm, the test should be repeated. If identical results follow, the C.B.R. corresponding to 5 mm penetration should be taken fordesign.

VI. RESULTS AND DISCUSSIONS

Moisture-density relationship

Modified Proctor tests have been conducted to determine optimum moisture content (OMC) and maximum dry density (MDD) of soil stabilized with various percentages of waste plastic and fly ash as reported in Table A.1. Fig B.1 to B.4 shows comparison of OMC and MDD respectively for parent soil stabilized with different percentages of waste plastic and fly ash.

For parent clay OMC and MDD have been observed as 17.69% and 1.73 g/cc respectively.

For soil stabilized with waste plastic and 5% fly ash, OMC varies from 15.28 to 18.05% and MDD varies from 1.77 to 1.70 g/cc , with increase in percentage of waste plastic from 0.5% to 2.0%.

For soil stabilized with waste plasric and 10% fly ash, OMC varies from 15.76 to 18.39% and MDD varies from 1.78 to 1.75 g/cc , with increase in percentage of waste plastic from 0.5% to 2.0%.

For soil stabilized with waste plastic and 15% fly ash, OMC varies from 16.58 to 18.32% and MDD varies from 1.74 to 1.69 g/cc , with increase in percentage of waste plastic from 0.5 % to 2.0%.

For soil stabilized with waste plastic and 20% fly ash, OMC varies from 17.05 to 18.65% and MDD varies from 1.72 to 1.68 g/cc , with increase in percentage of waste plastic from 0.5 % to 2.0%.

With increase in percentage of waste plastic there is increasing trend in MDD upto the 1.5% of waste plastic after that decreasing trend in MDD is observed. Though, a increase in OMC has been observed with increase in percentage of wasteplastic.

The increase in fly ash percentage the MDD having increasing trend up to 10% and further addition of fly ash the MDD shows decreasing trend . Though, a increase in OMC has been observed with increase in percentage of fly ash.

Stress- Strain Relationship

Unconfined Compressive Strength tests have been conducted to determine UCS of soil stabilized with various percentages of waste plastic and fly ash as reported in Table A.2 to A.18 and B.9 to B.31 show comparison of stress and strain respectively. For parent clay UCS have been observed as 1.06 kg/cm^2 .

For Soil stabilized with waste plastic and 5% fly ash, the UCS value has been increasing trend upto 1.5% waste plastic and after that the UCS value start to decreasing with respect to parentsoil.

For Soil stabilized with waste plastic and 10% fly ash, the UCS value has been observed increasing trend up to 1.5% waste plastic and after that the UCS value start to decreasing with respect to parentsoil.

For Soil stabilized with waste plastic and 15% fly ash, the UCS value has been observed increasing trend up to 1.5% waste plastic and after that the UCS value start to decreasing with respect to parentsoil.

For Soil stabilized with waste plastic and 20% fly ash, the UCS value has been observed increasing trend up to 1.0% waste plastic and after that the UCS value start to decreasing with respect to parentsoil.

With increase in percentage of waste plastic there is increasing trend in UCS upto the 1.5% of waste plastic after that decreasing trend in UCS is observed.

The increase in fly ash percentage the UCS having increasing trend up to 10% and further addition of fly ash the UCS shows decreasing trend.

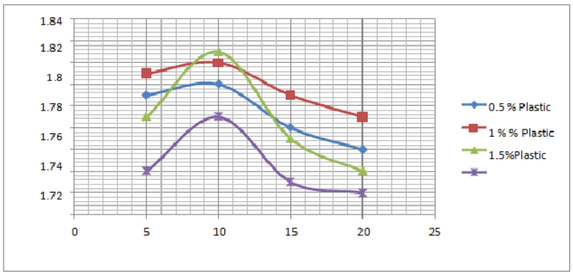

Graph 1 Showing Maximum Dry Density Relationship with Different Percentage of Waste plastic and Fly ash with Parent Soil

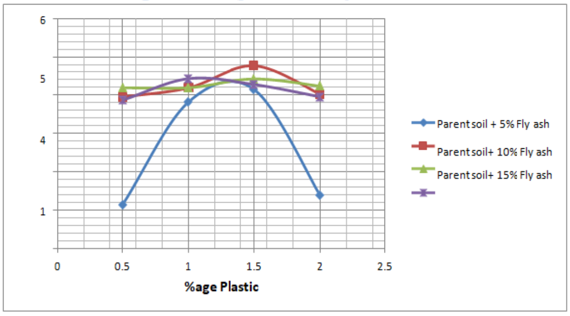

Graph 2 Showing Unconfined Compressive Strength Relationship with Different Percentage of Waste Plastic

CBR Result

The CBR tests were conducted as per IS 2720(Part 16) - 1987. CBR is the prime factor which determines the thickness of each pavement layer in the designof pavement

.It is the ratio expressed in percentage of force per unit area required to penetrate a soil mass. The load values to cause 2.5mm and 5mm penetration are noted. These loads are expressed as standard load values. The standard load values are 1370kg and 2055 kg at 2.5mm and 5.00mm respectively. Generally, the CBR value at2.5mm penetration will be greater than that at 5mm penetration. The soaked CBR value is determined by subjecting the specimen in the mould for four day soaking. California Bearing Ratio test was performed on the soil sample mixed with varying amount of waste plastic and fly ash at MDD and OMC determined from compaction test. From this test the strength characteristics of the soil samples are studied by determining California Bearing Ratio value. The CBR result of various samples mixed with different percentage of waste plastic with fly ash are noted.

For parent clay CBR have been observed as 0.89 % .

For Soil stabilized with waste plastic and 5% fly ash, the CBR value has been increasing trend upto 1.5% waste plastic and after that the CBR value start to decreasing with respect to parent soil.

For Soil stabilized with waste plastic and 10% fly ash, the CBR value has been observed decreasing trend for waste plastic with respect to parent soil.

For Soil stabilized with waste plastic and 15% fly ash, fly ash, the CBR value has been observed decreasing trend for waste plastic with respect to parentsoil.

For Soil stabilized with waste plastic and 20% fly ash, the CBR value has been observed increasing trend up to 1.0% waste plastic and after that the CBR value start to decreasing with respect to parent soil.

With increase in percentage of waste plastic there is increasing trend in CBR upto the 0.5% of waste plastic after that decreasing trend in CBR is observed.

The increase in fly ash percentage the CBR having increasing trend up to 10% and further addition of fly ash the CBR shows decreasing trend .

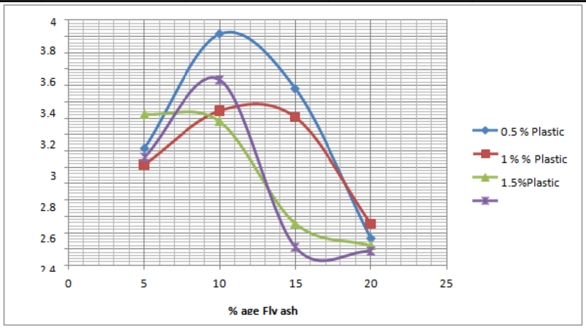

Graph 3 Showing CBR with Different Percentage of Fly Ash

VII. CONCLUSION

The study demonstrates the influence of waste plastic on the CBR and stress strain characteristics of compressible locally available clay. The following conclusions have been drawn based on the laboratory investigations carried out in this study:

- With increase in percentage of waste plastic there is increasing trend in MDD upto the 1.5% of waste plastic after that decreasing trend in MDD is observed. Though, a increase in OMC has been observed with increase in percentage of waste plastic.
- The increase in fly ash percentage the MDD having increasing trend up to 10% and further addition of fly ash the MDD shows decreasing trend . Though, a increase in OMC has been observed with increase in percentage of flyash.
- It has been observed that there is increasing trend up to 1.50 % waste plastic after that having decreasing trend in the UCS value with the addition of waste plastic and Fly ash to the parentsoil.
- The increase in fly ash percentage the UCS having increasing trend up to 10% and further addition of fly ash the UCS shows decreasing trend.
- It has been observed that there is increasing trend up to 0.50 % waste plastic after that having decreasing trend in the CBR value with the addition of waste plastic and Fly ash to the parent soil. These values of CBR for soil treated with various percentages of waste plastic and fly ash will help in proper designing of the Pavement on the basis of strength criteria.
- It has been observed that there is increasing trend up to 10 % Fly ash after that having decreasing trend in the CBR value with the addition of Fly ash and Plastic to the parent soil. These values of CBR for soil treated with various percentages of waste plastic and fly ash will help in proper designing of the Pavement on the basis of strength criteria.

SCOPE OF FURTHER RESEARCH

A number general research suggestions are listed herein that should increase this knowledge and enable the waste plastic and fly ash to become more useful engineering materials.

- For advance research, it is recommended that the effect of combining the waste plastic with additives such as lime or cement can be investigated that can further improve the properties of stabilizedsoil.
- Comparative study on soil treated with waste plastic and man-made fibres may bedone.
- Further research may be done in this direction to know the exact cause and remedial measures against the failure of structures resting on expansivesoils.
- Experimental studies can be done on soil stabilized waste plastic to determine other properties such as strength, permeability etc.

REFERENCES

[1] IS:1498(1970),–IndianStandardMethodsofTest for Soils: Classification and Identification of Soil for General Engineering Purposes‖, Bureau of IndianStandards.

[2] IS:2720(Part8)-1983–IndianStandardMethods of Test for Soils: Determination of Moisture Content-Dry Density Relation using Heavy Compaction‖, Bureau of IndianStandards.

[3] Singh, Alam and Chowdhary, G.R. (1994), –Soil Engineering in Theory and Practice‖, Geotechnical Testing and Instrumentation, Vol. 2, CBS Publishers and Distributors,Delhi.

[4] Ranjan,GopalandRao,A.S.R.(2000),–Basicand Applied Soil Mechanics‖, New AgeInternational (P) Ltd., New Delhi.

[5] Ru,ZhangJiandXing,Cao,(2002),–Stabilization of Expansive soil by Lime and Flyash‖, Journal of Wuhan University of Technology, Vol.17,No.4.

[6] Cai, Yi,Shi, Bin, Ng, Charles W.W., Tang, Chao- sheng (2006), –Effect of polypropylene fibreand lime admixture on engineering properties of clayey soil‖, Engineering Geology, 87, pp230–240.

[7] Tang, Chaosheng, Shi, Bin, Gao, Wei, Chen, Fengjun,Cai,Yi(2007),–Strengthandmechanical behavior of short polypropylene fiber reinforced and cement stabilized clayey soil‖, Geotextiles and Geomembranes, 25, pp194–202.

[8] Naeini, S.A. and Sadjadi, S. M. (2009), ― Effect of waste polymer materials on shear strength of unsaturated clays‖, 2ndInternational Conference on New Developments in Soil Mechanics and Geotechnical Engineering, Near East University, Nicosia, North Cyprus, pp.350-358.

[9] Maheshwari, KalpanaVinesh, Desai, Atul K. and Solanki, ChandreshH. (2011), –Performance of Fiber Reinforced Clayey Soil‖, EJGE, Vol. 16, pp.1067-1082.

[10] Estabragh, A. R.,Bordbar, A. T. andJavadi, A. A. (2011) –Mechanical Behavior of a Clay Soil Reinforced with Nylon Fibers‖, GeotechGeolEng, 29, pp. 899–908.

[11] Pradhan, Pradip Kumar, Kar, Rabindra Kumar and Naik, Ashutosh (2012), –Effect of Random Inclusion of Polypropylene Fibers on Strength Characteristics of Cohesive Soil‖, GeotechGeolEng, 30, pp.15–25.

[12] Sharma,R.K.(2012),–SubgradeCharacteristicsof Locally Available Soil Mixed With Fly Ash and Randomly Distributed Fibers‖, International Conference on Chemical, Ecology and Environmental Sciences (ICEES'2012), Bangkok, pp. 177-181.

[13] Sayyed Mahdi Hejazi, Mohammad Sheikhzadeh, SayyedMahdi Abtahi, Ali Zadhoush(2012), –A simple review of soil reinforcement by using natural and synthetic fibers‖, Construction and Building Materials, 30, pp.100-116.

[14] AkshatMehrotra, HadiGhasemian, D.R. Kulkarni, and N.R. Patil(2014):"effect of HDPE plastic on the unconfined compressive strength of black cotton soil" IJIRSET January 2014/vol. 3/issue1

[15] Babita Singh, Amrendra Kumar, Ravi Kumar Sharma (2014):"effect of waste materials on strength characteristics of local clay " International Journal of Civil Engineering Research 2014 vol.5.

[16] Dr. A.I. Dhatrak, S.D. Konmare (2015): "performance of randomly oriented plastic waste in flexible pavement" IJPRET march 2015/vol. 3/no. 9/193-202.

[17] Vijay KumarPatidar, Dr. SuneetKaur (2016) –A Review Literature on the Use of Waste Plastic to Improve Geotechnical Properties of Soil‖, International Research Journal of Engineering and Technology (IRJET), Volume: 03 Issue:06.

[18] PalakChopra , G.S Bath , Amanpreet Singh Virk (2017),–Influence of Waste Fly Ash on Characteristics of Clayey Soil‖, International Journal of Engineering Science andComputing.

[19] SharanVeer Singh, MahabirDixit (2017),– Influence Stabilization of Soil by Using Waste Plastic Material‖, International Journal of Innovative Research in Science, Engineering and Technology, Vol. 6, Issue 2, February2017.

[20] SaketDixit(2017),–EffectofWastePlasticon the Strength Characteristics of the Subgrade for the Flexible Pavement‖, Global Research and Development Journal for Engineering, Vol. 2, Issue 11, October2017.

[21] TinkuKalita,AnitaSaikia,BhaskarjyotiDas (2017),– Effect of Fly ash on the Strength Behaviourof the Clayey Soil‖, International Research Journal of Engineering and Technology (IRJET), Volume:04 Issue: 07. July 2017

[22] R.R Pandya, A.J Shah (2017),–Effect Alkali activated Fly ash on the Strength of Clayey Soil‖, Indian Geotechnical Conference , December2017

★★★

IMPACT OF WASTE MARBLE POWDER TO IMPROVE ENGINEERING CHARACTERISTICS OF EXPENSIVE SOIL

ASHES DAS

Asst Prof, Department of Mechanical Engineering NMIET BBSR

Abstract - Expansive soils happening in bone-dry and semi-dry environment locales of the world reason major issues on structural designing constructions. Such soils swell when given an admittance to water and therapist when they dry out. A few endeavors are being made to control the swell-recoil conduct of these dirts. Soil adjustment utilizing synthetic admixtures is the most seasoned and most far and wide strategy for ground improvement. In this investigation, squander limestone residue and waste dolomitic marble dust, results of marble industry, were utilized for adjustment of extensive soils. The sweeping soil is set up in research facility as a combination of kaolinite and bentonite. Squander limestone residue and waste dolomitic marble dust were added to the sweeping soil with foreordained level of stabilizer shifting from 0 to 30 percent. Grain size dissemination, consistency cutoff points, synthetic and mineralogical organization, expanding rate, and pace of swell were resolved for the examples. Growing rate diminished and pace of swell expanded with expanding stabilizer rate. Likewise, tests were restored for 7 days and 28 days prior to applying swell tests. Relieving of tests influences swell rates and pace of swell in certain manner.

Keywords - Expansive Soil, Soil Stabilization, Swelling Potential, Waste Limestone Dust, Waste Dolomitic Marble Dust

I. INTRODUCTION

Expansive soil deposits occur in the arid and semi arid regions of the world and are problematic to engineering structures because of their tendency to heave during wet season and shrink during dry season (Mishra et al.2008).

Expansive soils are a worldwide problem that poses several challenges for civil engineers. They are considered a potential natural hazard, which can cause extensive damage to structures if not adequately treated (Al-Rawas, 2002). Expansive soils cause more damage to structures, particularly light buildings and pavements, than any other natural hazard, including earthquakes and floods (Jones and Holtz,1973).

During the last few decades damage due to swelling action has been observed clearly in the semi arid regions in the form of cracking and breakup of pavements, roadways, building foundations, slab-on-grade members, and channel and reservoir linings, irrigation systems, water lines, and sewer lines (Çokça, 2001).

Clay Mineralogy

The term clay can refer both to a size and to a class of minerals. As a size term, it refers to all constituents of a soil smaller than a particular size, usually 0.002 mm in engineering classifications. As a mineral term, it refers to specific clay minerals that are distinguished by (1) small particle size, (2) a net electrical charge, (3) plasticity when mixed with water and (4) high weathering resistance (Mitchell and Soga,2005).

The basic idealized crystalline structural unit of a clay mineral is composed of a silica tetrahedron block and an aluminum octahedron block. Aluminum octahedron block may have Aluminum (Al3+) or magnesium (Mg2+). If only aluminum is present, it is called gibbsite [Al2(OH)6]; if only magnesium is present, it is called brucite [Mg3(OH)6]. Various clay minerals are formed as these sheets stack on top of each other with different ions bonding them together (Oweis and Khera, 1998). A silica tetrahedron and a silica sheet, also an octahedron and an octahedron sheet are presented in Figure 1.1. Also, these figures consist of schematic representations of silica and octahedronsheets.

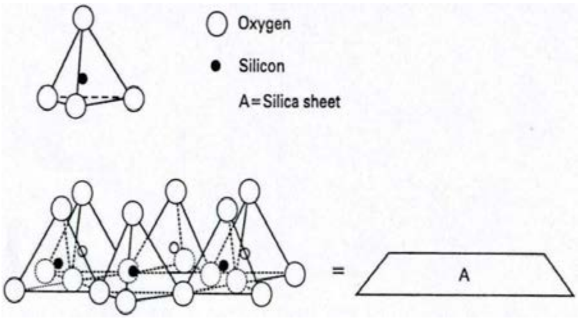

Figure 1.1 A Silica Tetrahedron and a Silica Sheet Kaolinite group

Kaolinite crystals consist of tetrahedron and octahedron sheets. The bonding between successive layers is by van der Waals forces and hydrogen bonds. The bonding is sufficiently strong that there is no interlayer swelling in the presence of water (Mitchell and Soga,2005).

Mica-like group

Illite has a basic structure consisting of a sheet of alumina octahedrons between and combined with two sheets of silica tetrahedrons. In the octahedral sheet there is partial substitution of aluminum by magnesium and iron, and in the tetrahedral sheet there is partial substitution of silicon by aluminum. The combined sheets are linked together by fairly weak bonding due to (non - exchangeable) potassium ions held between them (Craig, 1997).

Smectite group

Montmorillonite is formed from weathering of volcanic ash under poor drainage conditions or in marine waters. The basicbuildingsheetsforsmectitearethesameasforillite except there is no potassium ion present. The space between the combined sheets is occupied by water molecules and exchangeable cations. There is a very weak bond between the combined sheets due to these ions. Considerable swelling of montmorillonite can occur due to additional water being absorbed between the combined sheets (Craig, 1997; Oweis and Khera, 1998).

Mechanism of Swelling

Swelling of clay minerals is directly related with diffused double layer and cation exchange capacity of them.

Double Layer of Clay Minerals

The negatively charged clay particle surface and the concentration of positive ions in solution adjacent to the particle form what is referred to as a diffuse double layer or DDL (Bohn et al. 1985). Overlapping DDLs between clay particles generate interparticle repulsive forces or microscale “swelling pressures”. Interaction of the DDL and, hence, swelling potential, increases as the thickness of the DDL increases (Mitchell, 1976). The thickness of DDL is associated with valence of cations, concentration of cations, temperature and pH.

II. LITERATURE REVIEW

Al-Rawas, A.A., Taha et al, “A Comparative Evaluation of Various Additives Used in the Stabilization of Expansive Soils”. Geotechnical Testing Journal, Vol. 25,2002 :- This paper investigates the effectiveness of using cement by-pass dust, copper slag, granulated blast furnace slag, and slag- cement in reducing the swelling potential and plasticity of expansive soils. The soil used in this study was brought from Al-Khod (a town located in Northern Oman) where structural damage was observed. The first stage of the experimental program dealt with the determination of the chemical, mineralogical, and geotechnical characteristics of the untreated soil. The soil was then mixed with the stabilizers at 3, 6, and 9% of the dry weight of the soil. The treated samples were subjected to liquid limit, plastic limit, swell percent, and swell pressure tests. Furthermore, the cation exchange capacity, exchangeable cations (Na+, Ca++, Mg++, and K+), and pH of the treated samples were also measured.

Almeida N. et al.“Recyclingof Stone Slurry in Industrial Activities: Application to Concrete Mixtures, Building and Environment”, Vol. 42, 2007:- In recent years, large amounts of stone waste have been generated in natural and artificial stone industry with significant environmental impacts. To solve the problems, stone waste in different forms could be used in different industrial activities in particular construction industry and other activities such as paper, ceramics industry (faience), paints, plastics and polymers, glass. Rubber, siderurgy, sugar, pharmaceutics, textiles or in articles such as soaps or candles. Further it could be applied as agriculture soil corrective, acid water treatment and dumpsites sealing . This paper reveals an overview of current solutions of reducing environmental and economical disadvantages of this kind ofby-product.

Çelik, M.Y. at all “Marble Deposits and the Impact of Marble Waste on Environmental Pollution”, Journal of Environmental Management, Vol. 87, 2008:- The Portland cement manufacturing process is a major contributorto greenhouse gas emissions and depletion of natural resources. Waste Marble Dust (WMD) on the other hand is cheap and environmental demeaning form of marble processing units, which if used in civil works will create Sustainable Structures (SS) and will save our environment from degradation with positive impact on our country’s Gross Domestic Product(GDP).

Çetiner, S. et al. Stabilization of Expansive Soils byÇayırhan Fly Ash and Desulphogypsum, M.S. Thesis, METU, Turkey, 2004 :- Expansive soils are one of the most serious problems which the foundation engineer faces. Several attempts are being made to control the swell-shrink behavior of these soils. One of the most effective and economical methods is to use chemical additives. Fly ash and desulphogypsum, both of which are by-products of coal burning thermal power plants, are accumulating in large quantities all over the world and pose serious environmental problems

Çokça, E. et al. “Use of Class C Fly Ashes for the Stabilization of an Expansive Soil”, Journal of Geotechnical and Geoenvironmental Engineering, Vol. 127, 2001 :- Excessive heave associated with swelling of expansive soils can cause considerable distress to lightweight civil and highway engineering structures. Several methods have been suggested to control this problem.

III. METHODOLOGY

Chemical Stabilization

Soil stabilization using chemical admixtures is the oldest and most widespread method of ground improvement. Chemical stabilization is mixing of soil with one of or a combination of admixtures of powder, slurry, or liquid for the general objectives of improving or controlling its volume stability, strength and stress-strain behavior, permeability, and durability (Winterkorn and Pamukçu, 1990).

Pozzolanic Reactions

Time depending pozzolanic reactions play a major role in the stabilization of the soil, since they are responsible for the improvement in the various soil properties (Show et al., 2003). Pozzolanic constituents produces calcium silicate hydrate (CSH) and calcium aluminate hydrate (CAH).

Ca^{2+} + $2(OH)^{-}$ + SiO_2 (Clay Silica) @ CSH Ca^{2+} + $2(OH)^{-}$ + Al_2O_3 (Clay Alumina) @CAH

The calcium silicate gel formed initially coats and binds lumps of clay together. The gel then crystallizes to form an interlocking structure thus, strength of the soils increases (Hadi et al, 2006; Sivapullaiah, 2006).

Marble and Production of Waste Marble Dust

Stone-masons often apply the term marble to any rock predominantly of calcite and/or dolomite (cited in Dietrich and Skinner, 1979). Marble may be considered as metamorphosed limestone (i.e. limestone which has been fully re-crystallized and hardened under hydrothermal conditions) (Oates, 1998). In this study waste dolomitic marble dust wasused.

Production of Waste Marble Dust

The production of fine particles (<2 mm) while cutting marble is one of the major problems for the marble industry. When 1 m³ marble block is cut into 2 cm thick slabs, the proportion of fine particle production is approximately 25 % (Kun, 2000).

While cutting of marble blocks water is used as cooler. But, the fine particles can be easily dispersed after losing humidity, under atmospheric conditions, such as wind and rain. Thus, fine particles can cause more pollution than other forms of marble waste (cited in Çelik and Sabah,2007).

Figure - Views from waste marble dust disposed sites

Soil Stabilization Using Waste Marble Dust

Extensive literature is available on soil improvement by the application of additives, notably cement and lime. Lately, many researchers have reported on additives that could substitute lime as a soil modifier. Such materials include fly ash (Çokça, 1999; Indraratna et al. 1991, 1995), rice husk (Muntohar, 1999); (Muntohar and Hantoro 2000), marble dust (Okagbue and Onyeobi, 1999), and limestone ash (Okagbue and Yakubu, 2000) (Cited in Okagbue,2007).

Oedometer Methods to Determine Swell Properties

The most satisfactory and convenient method of determining the swelling properties of an expansive clay is by direct measurement. Direct measurement of expansive soils can be achieved by the use of the conventional one-dimensional consolidometer (Chen, which can be easily polished (Oates, 1998). Limestones, schistes, travertinesor even granites can be considered as marble in the business world (Onargan et al., 2005). Waste marble dust produced from marble plants can be either of these natural stones' dust. Thus, in order to distinguish the stabilizers used, stabilizers were named as waste limestone dust and waste dolomitic marble dust in thisstudy.

Marble (Real Marble)

Marble or real marble is a metamorphic rock that consists
1975).

According to ASTM D4546 - 03 (Standard Test Methods for One- Dimensional Swell or Settlement Potential of Cohesive Soils), test methods for swell properties can be grouped into three; Method A, Method B and Method D. Initially, the terminology of experiments is presented.

Swell, L = Increase in elevation or dilation of soil column following absorption of water

Free swell, % = Percent heave, h hx/100 water at the seating pressure.

Primary swell, L = An arbitrary short-term swell usually characterized as being completed at the intersection of the tangent of reverse curvature to the curve of a dimensional change-logarithm of time plot with the tangent to the straight line portion representing long-term or secondary swell (Fig. 3.2).

Secondary swell, L = An arbitrary long-term swell usually characterized as the linear portion of a one dimensional change-logarithm of time plot following completion of short-term or primary swell (Fig. 3.2).

Swell Pressure, kPa: A pressure preventing the specimen from swelling.

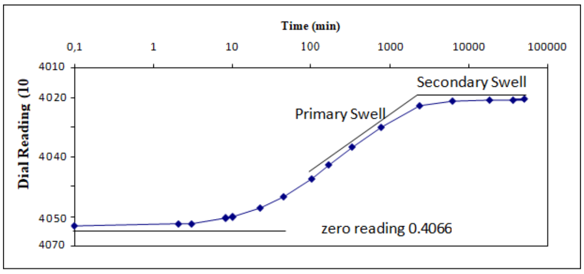

Figure - Time - Swell Curve

IV. EXPERIMENTAL INVESTIGATIONS

Purpose

The purpose of this experimental study is to investigate the effects of the addition of waste limestone dust and waste dolomitic marble dust on Atterberg limits, grain size distribution, swell percentage, and rate of swell of an expansive soil sample; and also, to investigate the effect of curing on swell percentage and rate of swell of an expansive soil stabilizated with waste limestone dust and waste dolomitic marble dust.

Preparation of the Test Samples

In nature, expansive soils are widely present. However, possible non- homogeneity or disturbance of these soils may prevent to show actual effects of the stabilizers. Thus, an artificially expansive soil sample (Sample A) was prepared using kaolinite and bentonite in laboratory.

By dry mass, Sample A was composed of 85% kaolinite and 15% bentonite. In the beginning of the preliminary studies, waste limestone dust and waste dolomitic marble dust as stabilizer, were pre-tested and the results showed that these materials could be considered as stabilizing agents for SampleA.

Each sample was prepared by addition of waste limestone dust or waste dolomitic marble dust to Sample A with different percentages to obtain a sample with predetermined percentage of stabilizer varying from 0 to 30 percent (by dry weight of the sample).

Free Lime Content Test on Stabilizers

Pozzolanic activity is the one of the main factors using of waste limestone dust and waste dolomitic marble dust. Lime content of these stabilizers plays major role for pozzolanic activity. ASTM C 25 (Standard Test Methods for Chemical Analysis of Limestone, Quicklime and Hydrated Lime) was used as a reference to determine the hydrated lime content of test samples.

To determine hydrated lime in stabilizers, the following steps can be summarized;

Neutralized sugar solution is prepared. (40 g sugar is dissolved in 100 ml CO2-free water, several drops of 4% phenolphthalein indicator and 0.1 N NaOH is added to sugar solution).

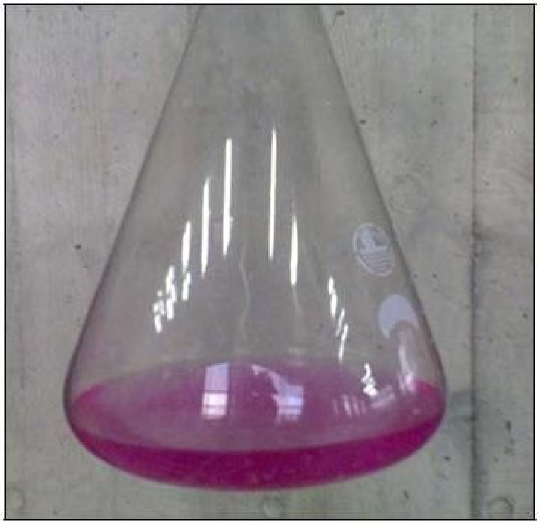

Figure - A view of neutralized sugar solution

2.804 g of sample is brushed in 40 ml of CO_2-free water and 100 ml of neutralized sugar solution is added to this mixture. The mixture is left for reactions for 15 min. and in 5 min. intervals it is swirled.

After 15 min. the mixture is titrated with HCl, until the first disappearance of the pink color, which persists for 3 s.

Available lime [$Ca(OH)_2$], % = $\underline{NxVx3.704}W$

Where; N: normality of acid solution (= 1 in this study) V: standard HCl (1.0 N), ml

W: weight of sample, g (= 2.804 g in this study)

Experimental Program

Experimental study was conducted in seven phases:

- Free lime content test was performed onstabilizers
- Analyses for stabilizers were performed by METU Central Laboratory and General Directorate of Mineral Research and Exploration(MTA).
- Hydrometer tests, Atterberg limit tests, and specific gravity tests were applied to thesamples.
- Free Swell Ratio Test was applied to thesamples.
- Free swell tests were applied to the samples without cure.
- Free swell tests were applied to the 7 days cured samples.
- Free swell tests were applied to the 28 days cured samples

V. RESULT & DISCUSSIONS

Test Results

Results of available lime test are presented in Figure .free swell ratio test results are presented. Effect of addition of waste limestone dust and waste dolomitic marble dust on liquid limit (LL), plastic limit (PL), plasticity index (PI = LL- PL), shrinkage limit (SL) and shrinkage index (SI = LL - SL) are presented in Fig.5.3, 5.4, 5.5, 5.6 and 5.7, respectively.

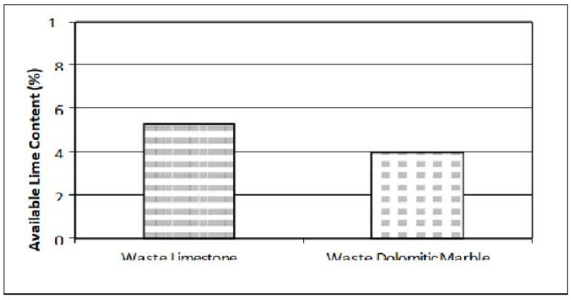

Figure - Results of Available Lime Test

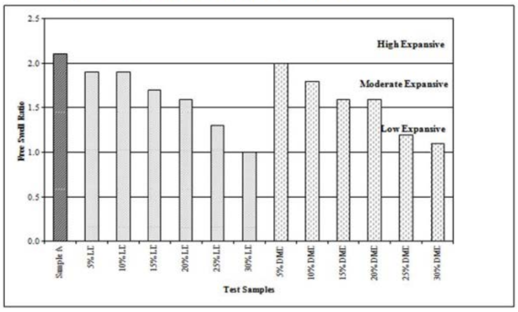

Figure - Effect of Addition of Waste Limestone Dust and Waste Dolomitic Marble Dust on Free Swell Ratio of the Samples

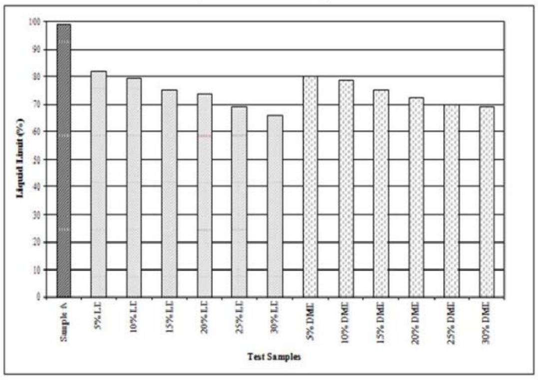

Figure - Effect of Addition of Waste Limestone Dust and Waste Dolomitic Marble Dust on the Liquid Limit (LL) of the Samples

Swell percentage vs. time relationship for Sample A, a typical swell percentage vs. time graph, is presented in Figure. For swell percentage calculations dial readings recorded in free swell test were subtracted by initial readings and ΔH/H vs. time graph was plotted. Swelling percentage vs. time relationships of the waste limestone dust and waste dolomitic marble dust added samples are presented in AppendixB.

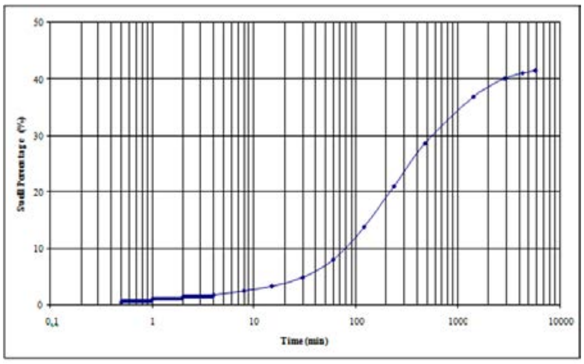

Figure - Swelling Percentage versus Time Relationship for Sample A

Calculations for Prediction of Swell Percentage

A typical log time vs. percent swell relationship generally follows a standard “S” shape. This “S” shape curve can be divided into 3 phases; Initial, primary and secondary swelling. Initial swelling is generally less than 10% of total swelling. This is essentially due to swelling of the bentonite clay particles within the voids of the coarser non-swelling fractions. This swelling of particles does not cause an increase in the volume of the sample. Primary swelling develops when the voids can no longer accommodate further clay particle swelling. After the primary swelling complete slow continued swelling, secondary swelling occurs. In time/free swell vs. time graphs after some time elapsed, a straight-line relationship is apparent (Sivapullaiah, et.al, 1996). The slope of straight-line part of time/free swell vs. time graphs can be used to predict maximum swell. Swelling percentage vs. time graph and time/free swell vs. time graph for 7 days cured 25% LD sample as examples are presented in Fig. , respectively. Predicted and measured free swell percentages and difference between them are presented in Table and those graphs are presented in Figure.

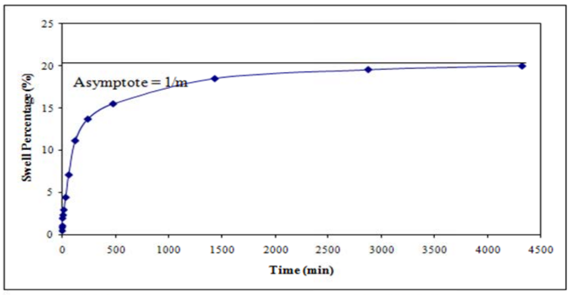

Figure - Swell Percentage vs. Time Graph of 7 days Cured 25 % LD Sample

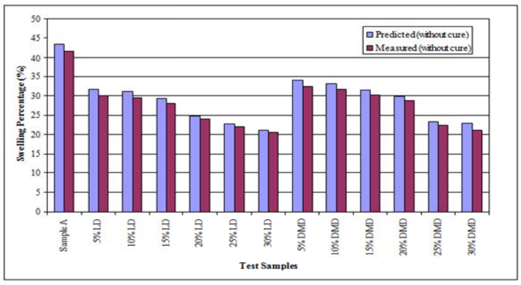

Figure - Measured and Predicted Swelling Percentage Graph for Test Samples

Table 5.1 Predicted and Measured Swell Values for the Test Samples

Sample	Samples without Cure			7 Days Cured Samples			28 Days Cured Samples		
	Measured Swell (%)	Predicted Swell (%)	fference (%)	Measured Swell (%)	Predicted Swell (%)	ifference (%)	Measured Swell (%)	Predicted Swell (%)	Difference (%)
Sample A	41.5	43.5	2.0	38.4	40.2	1.8	37.3	38.9	1.6
5% LD	30.0	31.6	1.6	26.1	27.6	1.5	23.5	24.2	0.7
10% LD	29.6	31.2	1.6	24.8	26	1.2	21.6	21.9	0.3
15% LD	28.1	29.3	1.2	22.8	23.5	0.7	19.1	19.6	0.5
20% LD	23.9	24.9	1.0	20.9	21.3	0.4	17.5	17.8	0.3
25% LD	22.1	22.8	0.7	20.0	20.6	0.6	16.5	16.8	0.3
30% LD	20.6	21.1	0.5	19.0	19.5	0.5	15.7	16.1	0.4
5% DMD	32.4	34.0	1.6	27.1	28.6	1.5	26.9	27.8	0.9
10% DMD	31.6	33.1	1.5	26.1	27.1	1.0	25.8	26.8	1.0
15% DMD	30.2	31.5	1.3	24.9	25.7	0.8	24.5	25.1	0.6
20% DMD	28.7	29.9	1.2	23.3	24.0	0.7	22.2	22.7	0.5
25% DMD	22.4	23.3	0.9	20.2	20.9	0.7	19.6	20.0	0.4
30% DMD	21.1	22.9	1.8	19.5	19.9	0.4	18.1	18.2	0.1
(%) Mean of Differences	**1.3**			**0.9**			**0.6**		
(%) Standard Deviation of Differences	**0.440**			**0.457**			**0.396**		

VI. CONCLUSIONS

In this study, the suitability of waste limestone dust and waste dolomitic marble dust as stabilizers for swelling potential of an expansive soil was studied. Waste limestone dust and waste dolomitic marble dust added to Sample A. According to test results, the following outcomes can be summarized:

- Addition of waste limestone dust and waste dolomitic marble dust decreased liquid limit, plasticity index and shrinkage index, increased plastic limit and shrinkage limit of

SampleA.

- Activity of samples decreased by addition of stabilizers. Activity of Sample A decreased more as waste limestone dust percentage increased. However, there is no consistent relationship between activity and the percentage of waste dolomitic marbledust.
- Free swell ratio of Sample A decreased with addition of stabilizers. As the percentage of stabilizer increased, free swell ratiodecreased.
- By addition of stabilizers, the swelling percentage decreased considerably. The reduction was higher for waste limestone added samples having more limecontent.
- By addition of stabilizers, the t_{50} values were decreased. In other words, samples having more stabilizers reached the 50 % of total swellquicker.
- Swelling percentage and rate of swell of samples decreased by curing. Curing was more effective for waste limestone dust added samples. Also, curing was more effective for rate of swell of samples than swelling percentage.

REFERENCES

[1] Al-Rawas, A.A., TahaR., Nelson, J.D.,Al-Shab,

[2] T.B. and Al-Siyabi, H., A Comparative Evaluation of Various Additives Used in the Stabilization of Expansive Soils, Geotechnical Testing Journal, Vol. 25, No. 2, pp. 199-209,2002.

[3] Almeida N., Branco, F., Santos, J.R., Recycling of Stone Slurry in Industrial Activities: Application to Concrete Mixtures, Building and Environment, Vol. 42, pp. 810–819,2007.

[4] ASTM, Standard Test Method for One-Dimensional Consolidation Properties of Soils, Annual Book of ASTM Standards, D 2435-90, Vol. 04 - 08, pp. 313- 323, 1993.

[5] ASTM, Standard Test Methods for One- Dimensional Swell or Settlement Potential of Cohesive Soils, Annual Book of ASTMStandards, D4546 - 03, Vol. 04 -08, pp. 1-7,1999

[6] ASTM, Standard Test Methods for Chemical Analysis of Limestone, Quicklime and Hydrated Lime, Annual Book of ASTM Standards, C 25-93a, Vol.04.01, pp. 9-36, 1993

[7] Bohn, H. L., McNeal, B.L. and O'Conner, G. A., Soil Chemistry, 2nd Edition, John Wiley Inc., New York, 1985.

[8] Craig, R.F., Soil Mechanics, 6th Edition, Spon Press, London,1997.

[9] Chen, F. H., Foundations on ExpansiveSoils, Elsevier Scientific Pub. Co., Amsterdam, 1975

[10] Çelik, M.Y., MermerAtıklarının (Parça-Tozların) Değerlendirilmesi, M. S. Thesis, AfyonKocatepe University, Natural and Applied Sciences, 119 pages,1996.

[11] Çelik, M.Y., Sabah, E., Geological and Technical Characterization of İscehisar (Afyon-Turkey) Marble Deposits and the Impact of Marble Waste on Environmental Pollution, Journal of Environmental Management, Vol. 87, No.1, pp. 106-116,2008.

[12] Çetiner, S., I., Stabilization of Expansive Soils by Çayırhan Fly Ash and Desulphogypsum, M.S. Thesis, METU, Turkey, 107 pages,2004.

★★★

NUCLEAR MAGNETIC RESONANCE SPECTROSCOPY OF CEMENT IN SOLID STATE

[1]BHAGWAT T. DHEKWAR, [2]AMLAN PATTNAYAK, [3]SMITA SUBHADARSHINI

[1]Asst Prof, Department of Mechanical Engineering NMIET BBSR
[2]Assistant Professor, Department of Civil Engineering AIET Bhubaneswar
[3]Asst Prof, Department of Civil Engineering REC Bhubaneswar

Abstract -
Concrete is the universal material whereupon present day civilisation is assembled, giving long haul strength, impermeability and sturdiness for lodging and foundation. The central compound connections which control the design and execution of concretes have been the subject of extreme exploration for quite a long time, yet the complex, crystallographically scattered nature of the key stages which structure in solidified concretes has brought difficulty up in getting nitty gritty data about nearby construction, response instruments and energy. Strong state atomic attractive reverberation (SS NMR) spectroscopy can resolve key nuclear underlying subtleties inside these materials and has arisen as a critical instrument in portraying concrete construction and properties. This audit gives an exhaustive outline of the utilization of multinuclear SS NMR spectroscopy to comprehend compositionestructureeproperty connections in concretes. This remembers anhydrous and hydrated stages for Portland concrete, calcium aluminate concretes, calcium sulfoaluminate concretes, magnesia-based concretes, antacid actuated and geopolymer concretes and manufactured model frameworks. Progressed and multidimensional tests test 1H, 13C, 17O, 19F, 23Na, 25Mg, 27Al, 29Si, 31P, 33S, 35Cl, 39K and 43Ca cores, to contemplate nuclear construction, stage advancement, nanostructural improvement, response systems and energy. Accordingly, the components controlling the actual properties of concretes would now be able to be settled and perceived at an uncommon and fundamental degree of detail.

Keywords - Solid-State NMR; Spectroscopy; Portland Cement; Calcium Aluminate Cements; Calcium Sulfoaluminate Cements; Magnesia-Based cements; Alkali-Activated Cements

I. INTRODUCTION

Modern society is heavily reliant on cementitious materials in constructing our built environment. Second only to water interms ofcommodityuse[1,2],theworldwideproductionofconcreteex- ceeds10billiontonnesperannum. Themostcommoncementused toproduceconcreteisPortlandcement(PC)[3],acomplex material made up of multiple calcium-rich mineral phases that react with water and harden to provide strength, impermeability and resis- tance to thermal, mechanical and chemical stresses over long timescales[4].TheexcellentphysicalpropertiesofPChaveresulted in its incorporation into virtually all of the modern built environment.

However, PC production results in large associated CO2 emissions,approximately0.73e0.99tCO2/tPC,whichis~8% ofcurrent globalanthropologicalCO2emissionswhenconsidering aPCpro- ductionvolumearound4Gtperannum[5,6]. Consequently, low- moments(i.e.non-zerospin) andappliedmagneticfieldsanden- ables determination of the local chemical environments of NMR- active nuclei, regardless of the level of crystallographic order or disorder, and this is essential in its application to the study of ce- ments. In cements, nuclei of interest include ^{1}H, ^{13}C, ^{17}O, ^{19}F, ^{23}Na, ^{25}Mg, ^{27}Al, ^{29}Si, ^{31}P, ^{33}S, ^{35}Cl, ^{39}K and ^{43}Ca (Table 1). Solid-state (SS) NMR is ideally suited to study both anhydrous and hydrated solid phasesincementitiousmaterials.Itsapplicationtocement samples ofdifferentagesisinvaluableinresolvingthereactionmechanisms, kinetics and structural evolution that dictate the properties and performanceofcements(andthusalsoconcretesmadeusingthese cements).NMRcanalsobeappliedasapowerfultoolprobingthe dynamics of mobile ions and water within cementitious materials, in particular through the use of ^{1}H NMR relaxometry which pro- vides information about water mobility and pore size distribution [8,9]. These various applications and nuclei will be discussed in detail in the sections which follow

CO2cementitiousmaterialshaveemergedasattractive,moresus- tainablealternativestoPC[4].Supplementarycementitiousmate- rials (SCMs) such as coal fly ash (FA), blast furnace slag,calcined clays, finely ground limestone and silica fume are widely used in concrete.ByblendingPCwithSCMs,itispossibletoenhanceand control physical properties, e.g. strength, durability, phaseforma- tion and reaction kinetics, and also to improve sustainability by reducingassociatedCO2emissionsandvalorisingindustrialwastes [7].PC-freebinderssuchascalciumaluminatecements(CACs)and calcium sulfoaluminate (CSA) cements, magnesia-based cements, alkali-activatedmaterials(AAMs)andgeopolymers,amongoth ers, have also received significant attention from academia and in- dustry due to the enhanced technical properties and/or sustain- ability that they can provide, when compared with PC[4].

Thecomplexchemicalnatureofcementsystems,whichoften involvecrystallographicallydisorderedphasesandwhichcontinue to evolve as a function of time for many years after initial mixing.

II. SOLID-STATE NMR SPECTROSCOPY

An NMR experiment involves holding a sample in a magnetic field(denotedB0)andapplyingpulsesofradiofrequencyradiation to induce precession of the nuclear spin and measuring theelec- tromagnetic response produced as the nuclei relax back to their equilibriumstates.Theelectromagneticsignalismeasuredasafree inductiondecay,whichisthenconvertedtoanNMRspectrumby applying a Fourier transform. The NMR spectrum contains reso- nances characteristic of near-neighbour atomic environments [10,11]. Terms representing the magnetic dipolar interaction, chemicalshieldingandquadrupolarinteractionsbetween thenu- cleus and its environment are of particular interest in the study of cements.

NMR spectra of solids are broadened (compared to those of liquids) due to dipolar interactions, anisotropy of the chemical shielding and quadrupolar interactions between the intrinsic nu- clear electric quadrupolar moment and the surrounding electric field gradient [10]. This necessitates the application of sample spinning methods to reduce broadening.

Magic angle spinning (MAS) requires spinning a sample at an angleofcos2(qMAS)¼1/3(qMASz54.74○) withrespecttothestatic magneticfield(B0) sothat dipolar interactionsaresuppressed,and both chemical shielding anisotropy and first-order quadrupolar interactions are removed [10,11], narrowing spectral lineshapes. This means that the local chemical environments of spin S ½ nuclei (which do not experience second-order quadrupolar in- teractions) can be represented in terms of the isotropicchemical shift (diso) in MAS NMR spectra. Quadrupolar nuclei (S > ½) expe- rience additional second-order quadrupolar interactions, so the quadrupolarinteractiontermoftheHamiltonianisnon-zerounder MAS conditions. This limits spectral resolution due to anisotropic broadening of the signals. However, these second-order quad-rupolarinteractionsareinverselyproportionaltothestrengthofB0 andcanthusbereduced throughtheuseofhighmagneticfields [10,11]. Owing to the disordered structure of many cementitious phases,significantlinebroadeningoccursatallpractically achiev- able MAS rates, and so the spectra for relevant nuclei are often poorlyresolved

The presence of paramagnetic species within cementitious materials can limit the applicability of SS NMR for their charac-terisation;thesespeciesinfluencetherelaxationandchemicalshift ofnearbynuclearspins,whichcanseverelydampenandshiftthe NMR signal of these nuclei [10]. This is particularly problematic in standard ‘grey’ PC and in ferrite-containingsulfoaluminate cements, which each contain tetracalcium aluminoferrite (4CaOAl2O3Fe2O3,C4AF),aswellasinbinderscontainingcoalFA (containing Fe2O3) [13]. The use of Fe2O3-free cement systems for spectroscopicanalysis[14e16]can,therefore,beadvantageous.

Recent advances in this understanding of the chemistry and materials science of cements, in which the application of SSNMR hasplayedapivotalrole,arediscussedinthefollowingsection.

III. TERMINOLOGY USED IN DEFINING THE LOCAL STRUCTURE OF SILICATES AND ALUMINATES

Si sites are generally identified using notation of the type Qn(mAl) (represented by Q) is bonded to n other tetrahedral atoms (m of which are Al) via oxygen bridges. Qn(mAl) Si sites within cemen- titious materials typically resonate in the region from 60 ppm to120 ppm relative to tetramethyl silane, with significant overlap between the broad resonances observable in disordered solid phases, but a more negative chemical shift induced by a higher connectivity (i.e. higher n) (Fig. 1) [11,16e18].Each additional tetrahedral Al atom which replaces an Si neighbouring aQn(mAl) silicon site also increases the chemical shift by approximately 5 ppm [11], and this provides an important point ofdifferentiation betweenQn(mAl)sitesasafunctionofnandm,althoughtheeffects of the two parameters cannot always straightforwardly be discriminated without application of multinuclear NMR techniques.

Bridges betweentwotetrahedral Alsitesaredisfavoured (acrystallographic and thermodynamic observation known as ‘Loewenstein's princi- ple’ [19]). Tetrahedral and octahedral Al sites typically resonate within the regions 80e50 ppm and 20 - 0 ppm, respectively, rela- tive to Al(H2O)3þ(aq), while resonances assigned to five- coordinated Al and highly distorted tetrahedral Al environments have been observed in the region 50e20 ppm, Fig. 2[11,17,20e22].

IV. CHARACTERISATION OF CEMENTITIOUS MATERIALS

4.1. MAS NMR of anhydrous cementitiousmaterials

4.1.1. Portlandcement

PC primarily comprises the ‘clinker’ phases tricalcium silicate (3CaOSiO2, C3S, in numerous polymorphs), dicalcium silicate (2CaOSiO2, C2S; the a and b polymorphs of this composition are preferredincementsduetotheirhydraulicnature,whereas g-C2S isunreactive),tricalciumaluminate(3CaO$Al2O3,C3A)andtetra- calcium aluminoferrite. This assemblage of clinker minerals is producedfromlimestoneandsilicatemineralsinarotarykiln,then rapidly cooled and interground with calcium sulphate to formPC [23]. Among these clinker minerals, tricalcium silicate (or a slightly impure form of this phase, containing Al and/or Mg among other substituents,whichiscommonlydescribedas‘alite’inthe cements literature [24]) is the predominant constituent of modern PC, definingitshydraulicnatureandhighearlystrengthdevelopment uponcementhydration.Theexpectedvaluesofdobs,diso andCQfor different nuclei in various phases in PC are shown in Table 2 and discussed in the followingtext.

4.1.1.1. Tricalcium silicate (alite, hartrurite). C3S is known to exist in seven polymorphs: three triclinic, three monoclinic and one trigonal. The alite present in PC crystallises from the melt in a trigonal form and upon rapid cooling, transforms into metastable

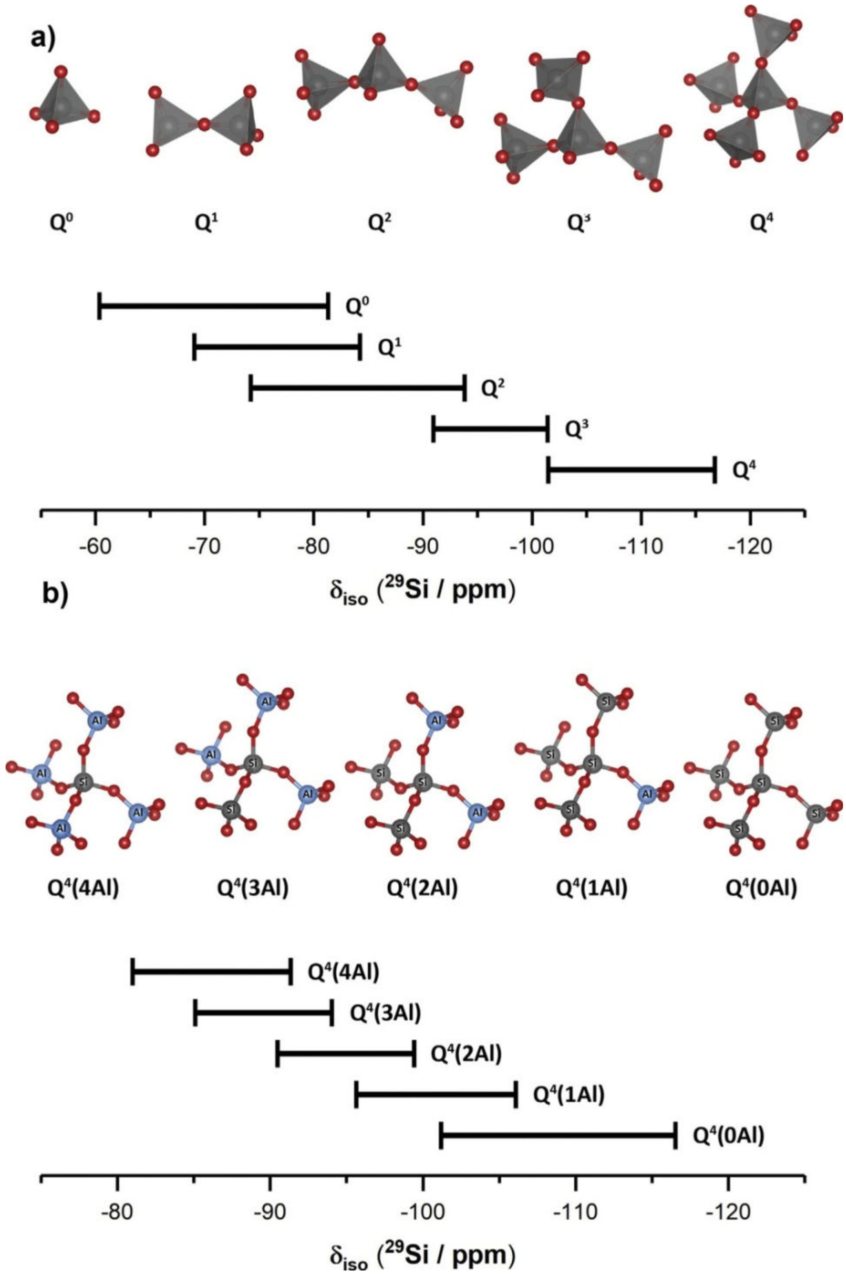

Fig. 1. Typical ranges of 29Si chemical shifts for (a) Qn and (b) Q4(mAl) sites in solid silicates [11]. Si, Al and O atoms are represented by grey, blue and red spheres, respectively.

polymorphs, predominantly, the two monoclinic polymorphs MI and MIII[25]. 29Si MAS NMR analysis of the MI polymorph of alite has shown that Si exists within nine crystallographically distinct sites, approximately within the range from 69 to 75 ppm [26,27], while 29Si MAS NMR spectra of the MIII polymorph exhibit overlappingresonancesbetween—66and—78ppmcorresponding to eighteen distinct SiO4 tetrahedra (Fig. 3)[27,28].

The calcium silicate chainsinalite can accommodate a number of guest ions which substitute for silicon (e.g. AlO5—or PO3—for SiO4—[30e32]) or oxygen (e.g F—for O2—[31]). Substitution of AlO5—for SiO4—in C S chains has been identified crystallographically since the 1950s [24,33]and was first subjected to NMR analysis in 1994 by Skibsted et al. [34] using 27Al MAS NMR [30], then later confirmed unambiguously using 27Al multiple quantum (MQ)MAS NMR.

Reduction of the temperature at which alite forms, whichis desirableforbotheconomicandenvironmentalreasonsin cement production, is often achieved by adding ‘mineralising’ additives such as fluoride and phosphate, which substitute into the alite structure.Tranetal.[31]used29Siand27AlMAS,19F-29Sicrosspolarisation (CP) MAS and 19F-29Si CP rotational-echo double-resonance (REDOR) MAS NMR techniques to show that F—sub-stitutesforO2—ionsinthealitephasealone,accordingtoacoupled substitutionmechanismSiO4—þO2—/AlO5—þF—[35], with a strong preference for F—substitution into interstitial oxygen sites notinvolvedincovalentSi-Obonds.Poulsenetal.[32]showedvia 31P and inversion recovery 31P MAS NMR that PO3—ions substitute for SiO4—tetrahedra in alite; a substitution level of 1.3 mol. % was identified in the sample studied. MASNMRspectroscopytoaseriesofCaF2-modifiedPCscontaining between 0.23 and 0.77wt% fluorine, demonstrating that increased fluorine content drives increased fluorine substitution into alitevia

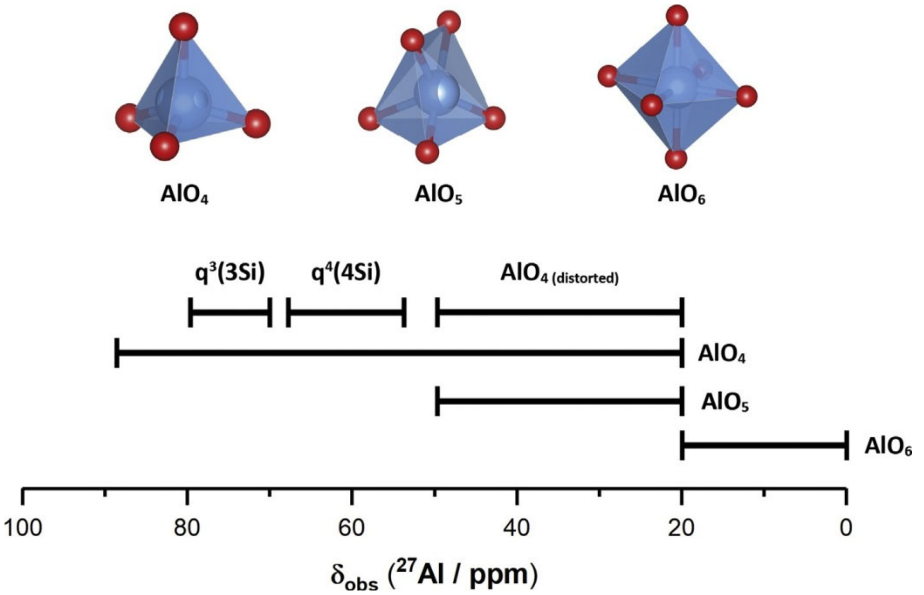

Fig. 2. Typical ranges of 27Al chemical shifts for different aluminium sites in aluminates and aluminosilicates [11]. Al and O atoms are represented by blue and red spheres, respectively.

Table 2
Coordination states, dobs, disoand CQ for different nuclei in the major constituents of Portland cement.

Phase	Nucleus	Site	Coordination	d_{obs}(ppm)	d_{iso}(ppm)	C_Q(MHz)	Magneticfield(T)	Reference
Tricalciumsilicate(C_3S)[a]	29Si	Q^0 (Si^{IV}_{1-9})inM_I	4	—69to—75	—69to—75	e	4.70, 7.5and8.45	[26,27]
		Q^0(Si^{IV}_{1-18}) in M_{III}	4	—66to—78	—66to—78	e	7.5	[27]
		43Ca		CainM_I	e	60e110	e	e
			21.1	[38]CainM_{III}	e	60e110	e	e
							21.1	[38]
Dicalciumsilicate(**b**-C_2S)	17O	Si-<u>O</u>-Ca(NBO)	2	116.2	116.2	e	11.7	[43]
	29Si	Si-$(OCa)_4$	4	—71.3	—71.3	e	7.5,11.7	[27,42e44]
	43Ca	Ca_1	e	e	33.7	2.41	21.1	[38]
		Ca_2	e	e	53.8	2.98	21.1	[38]
Tricalciumaluminate (C_3A)	27Al	Al^{IV}_1	4	e	79.5	8.69	7.1,9.4and11.7	[52]
	43Ca	Ca	4	e	78.3	9.3	7.1, 9.4and11.7	[52]
Tetracalciumaluminoferrite(C_4AF)	27Al	Al^{IV}_1	4	61e71	e	e	9.4	[55]
		Al^{VI}_1	6	0e20	e	e	9.4	[55]
Gypsum(C<u>$</u>$H_2$)	33S	S	e	328	e	e	19.6	[59]
	43Ca	Ca	e	—28	e	e	8.6	[40]

[a] M_I and M_{III} are the monoclinic polymorphs of alite comprising nine and eighteen crystallographically distinct Si sites, respectively.

adoublesubstitutionmechanismandthatF— andAl3þionsinalite are likely to be clusteredtogether. Recently, 17Oe29Si CP heteronuclear correlation (CP-HETCOR)

MAS NMR was used to resolve oxide ion sites bonded to one Si4þfrom those bonded to Ca2þin synthetic tricalcium silicate for the first time [37]. Oxide ion sites bonded to Ca2þplay an important roleinthestructureandreactivityofC3Sbuthaveprovendifficult to resolve. 43Ca MAS NMR analysis of alite was first reported by Moudrakovskietal.[38],withthehigh-field(21.14T)natural abundance 43CaMASNMR spectrumofthemonoclinicpolymorph showing a broad, asymmetric resonance consistent with overlapping43Caresonancesfromthe36non-equivalentsitesforCain this phase and deviations from a perfect lattice (Fig. 4) [28]. This contrasts with the 43Ca MAS NMR spectrum of the triclinic polymorph, which exhibited well-separated 43Ca resonances despite the29non-equivalentsitesforCainthisphase[39],suggestingthat some of these non-equivalent sites are quite similar. This work demonstrates the power of SS 43Ca MAS NMR to resolve polymorphism,whichisvaluableinidentification,characterisationand quantification of metastable polymorphs within cement systems, although the time and instrumentation required to collect high-resolution43Caspectramayprovetobealimitationinapractical sense. Differences in 43Ca MAS NMR spectra have also been exploited for spectroscopic analysis of the CaCO3 polymorphs calcite, aragonite and vaterite [40,41], which are also present in many cementsystems.

4.1.1.2. Dicalcium silicate (belite, larnite). The 29Si and 17O MAS NMR analysis of b-C2S (also known as belite and the dominant polymorph of dicalcium silicate found in PCs) has shown that Si

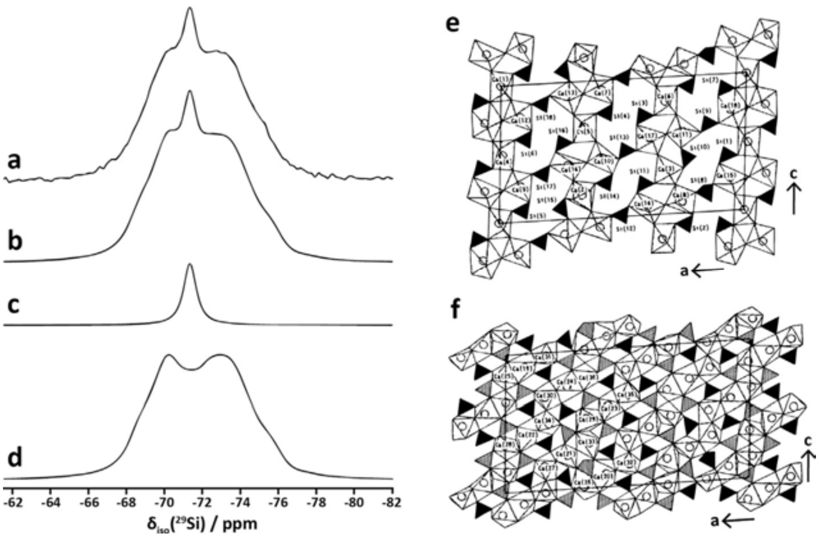

Fig. 3. 29Si MAS NMR spectrum (9.4 T, spinning speed nR¼ 13.0 kHz) of (a) grey PC and (b) its deconvolution, which is composed of the subspectra for belite and alite shown in (c) and(d).AdaptedfromPoulsen etal.[29].Parts(e)and(f)showtwodifferentsections takenthroughthemonoclinicsuperstructureof theMIIIpolymorphofalite,vieweddowntheb axis,showingpolyhedralocatedin(e)andabove(f)thea,0,cplane.AdaptedfromNishietal.[28].

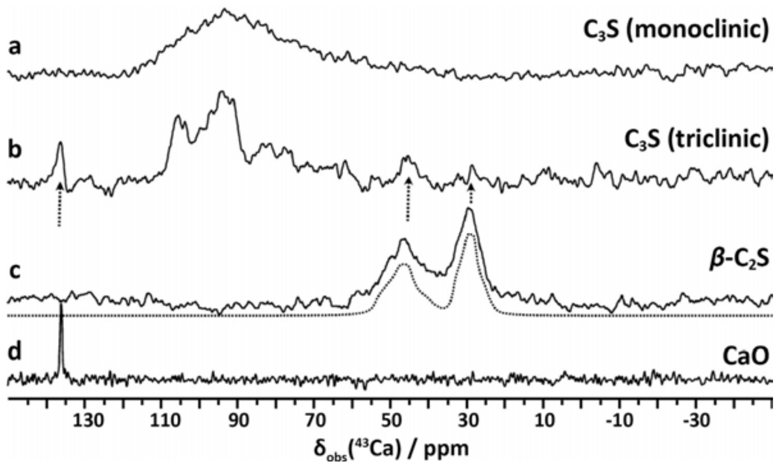

Fig. 4. Natural abundance 43Ca MAS NMR spectra (21.4 T) of (a) monoclinic C3S, (b) triclinic C3S, (c) b-C2S and (d) CaO. The dotted line below spectrum (c), for b-C2S, shows the spectralsimulationforthesecond-orderquadrupolarinteractions.Theverticalarrowsbelowspectrum(b),fortriclinicC3S,indicatethepositionsofthesignalsduetoCaOandb-C2S impurities.AdaptedfromMoudrakovskietal.[38].

exists within a single Q0 (isolated SiO4 tetrahedron) environment which exhibits a single 29Si resonance at 71.3 ppm [27,42e44], coordinatedtocalciumviafourSi-O-Calinkages[43].SomePCsalso containtheapolymorphsofC2S,butthesedonotappearto have been analysed specifically by high-resolution SS NMR in theavail- able body of literature, so the focus here will be on the bform.

Despitethefactthattherearefourcrystallographicallydistinct oxygensiteswithinb-C2S[42],asinglebroadresonanceisobserved in the 17O MAS NMR spectrum [43], suggesting that there is some degreeofdisorderinthisphase.Asforthecaseofalite,substitution of Al3þfor Si4þin C2S has been identified crystallographically since the 1950s [45,46]. In 1994, 27Al MAS NMR was used to providethe in C2S in PC [30], which has significant consequences for the dissolution and hydration reactions of this phase, given the ther- modynamic preference for dissolution of Al from calcium alumi- nosilicates [47]. Skibsted et al. [30]determined quadrupole coupling parameters and the isotropic chemical shift for this unique Al3þguest ion in belite, which exhibited the most deshiel- ded chemical shift (diso96.1 ppm) yet reported for a tetra- coordinatedAl environmentbondedtofouroxygenatoms,further SiO_4^{4-} tetrahedra for the sample studied) in PCs containing between 0.08and0.45wt%P_2O_5,withasimilarcoupledsubstitutioncharge balancing mechanism proposed as described previously foralite, whereCa^{2þ}ispartiallyreplacedbyFe^{3þ}viaSiO^{4-}þ2Ca$_4^{2þ}$/ PO$_4^{3-}$þFe^{3þ}þ . Ca·

The 43Ca MAS NMR spectrum of belite was first reported by Moudrakovski et al. [38], Fig. 4. The high-field (21.14 T) natural abundance43CaMASspectrumexhibitedtwodistinctresonances consistentwiththecrystalstructureofthisphaseandcalculations from density functional theory (DFT) (Table 2). Both sites exhibited extensive asymmetry in Ca-O bondlengths.

4.1.1.3. Tricalcium aluminate. The investigation of C3A by 27Al MAS andMQMASNMRatmultiplefieldshasshownthatitcontainstwo inequivalent Al tetrahedral sites, which resonate at diso79.5 ppm and 78.25 ppm, respectively, arranged in six-membered rings of AlO4 tetrahedra in the cubic (pure) polymorph of C3A (Fig. 5) [34,49]. disovalueswithin±6ppmofthosedeterminedbySkibsted etal.[49]havealsobeenreportedfortheseAlIVsiteswithinC3Aby other workers, although with some variability in reported reso- nance positions [50e52]. Four of the six crystallographically non- equivalent calcium sites in C3A were resolved using high-field (21.1 T) single-pulse 1D43Ca MAS NMR by Moudrakovski et al.[38].

4.1.1.4. Tetracalcium aluminoferrite (brownmillerite). The analysis of C4AFbyNMR,andparticularlyby27AlMASNMR,isconstrained by the nuclear-unpaired electron dipolar couplings betweenthe 27Al nucleus and paramagnetic Fe3þions [53e55], which severely broadenthe27AlMASNMRspectraanddampenthesignal[52,55], examining Ca2AlxFe2-xO5 with x 0.93, 1 and 1.33 (Fig. 6). Increasing Fe content dramatically dampenedand broadenedtheobserved resonances,butdespitethesedifficulties, it was possible to observe that the central transitions showed a dominant resonance for AlIV species at 61 ≤ dobs≤ 71 ppm, with increased shielding at higher Fe content, and AlVI species at 0 ≤ dobs≤ 20ppm.

Asmentionedinsection2,thepresenceofC4AFinPCalso has significant implications for acquisition of 29Si MAS NMR data for C3S and C2S phases. A dramatic decrease in the longitudinal relaxation time, T1, in grey PC has been attributed to the close proximity of these diamagnetic phases to paramagnetic C4AF [56,57]. However, Poulsen et al. [29] attributed this effectprimarily toFe3þionsincorporatedasguestionswithinCSandCSphases, rather than intermixing with ferrite phases. These effects need to beconsideredcarefullywhenattemptingtoquantifyC3SandC2S phases in PC via deconvolution of 29Si MAS NMR spectra as pref- erential incorporation of Fe3þions within either of the silicate phases will result in a dampening of the 29Si MAS NMR signal for thatphaseandconsequentlyleadtoincorrectquantification[57]. Further discussion of methods to mitigate this issue is provided insection4.3 dehydrated forms, is interground with PC clinker in small quanti- tiestocontrolthesettingrateofthehydratingcement.DuringPC hydration,C3Areactswithgypsumtoformettringite(AFt)whichis subsequently converted (in part or in full) to monosulfoaluminate (AFm), starting a few hours after initial hydration [23]. In the absenceofgypsum,C3Awouldhydraterapidlyandsettingcould occur within minutes (i.e. ‘flashsetting’).

The first application of NMR to any of the cement phases dis-cussedinthisarticlewasundertakenbyPake,whoin1948applied 1H NMR to single crystals and powdered hydrates of gypsum, demonstrating that the splitting observed in the spectrum (the Pake doublet) reflects the dipolar coupling of two 1H nuclei and therefore the internuclear distance between H atoms within the watermoleculesofgypsum[58].Naturalabundance43CaMASNMR (8.6T,nR¼2kHz)hasrevealedasingleCasiteingypsumre of gypsum (both natural abundance and enriched with 33S) revealed a single S site in gypsum resonating at diso328 ppm (Fig. 7) [59]. However, it was noted that acquisition of natural abundance33SMASNMRspectraforPCsamplesisnotpracticaldue to extremely long acquisition times, and consequently, this tech- nique does not appear useful for field samples or those without isotopicenrichment.

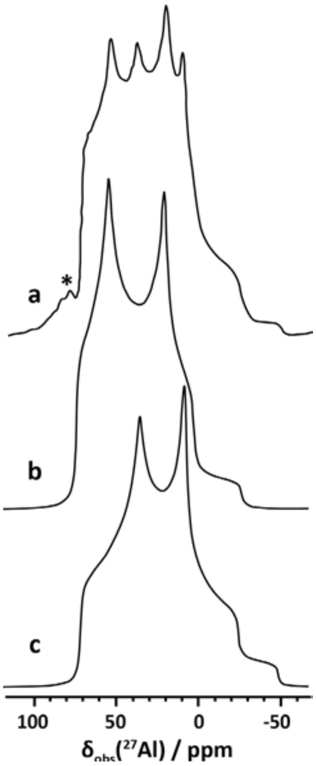

Fig. 5. ^{27}Al MAS NMR spectra (9.4 T, nR¼ 18.0 kHz) of cubic C3A (3CaO$Al2O3): (a) showing the resonance from the central transition. Simulations for each of thetwo AIO4 sites are shown in (b) and (c). *Resonances from satellite transitions. Adapted from Skibsted et al., 1991[49]

4.1.2. Innovation in cements to reduce CO2emissions

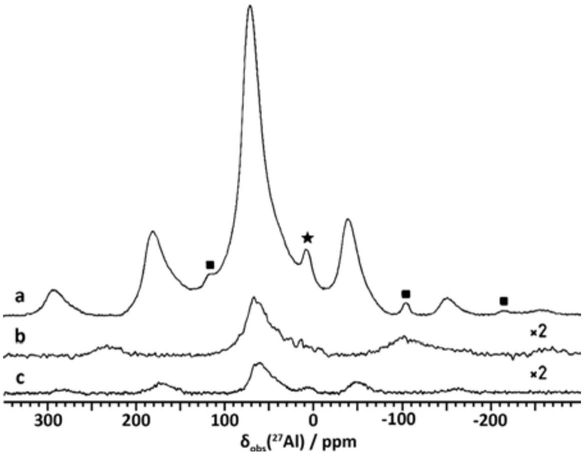

Fig.6. ^{27}AlMASNMRspectra(9.4T) forthesyntheticferrites (a)Ca2Al1$33Fe0$67O5, (b)Ca2AlFeO5and (c)Ca2Al0$93Fe1$07O5,acquiredusingbetween18,000and76,000 scansand spinningspeeds of11.6,17.5and11.5kHz,respectively.The spectrain(b) and(c)areshownonidenticalintensityscales, whichcorrespondtoaverticalexpansion byafactoroftwo relativetothespectrumin(a).Theasteriskandsquaresin(a)indicate theresonancefromthecentraltransitionandspinningsidebandsfor theAlVIsite.AdaptedfromSkibstedetal. [55].

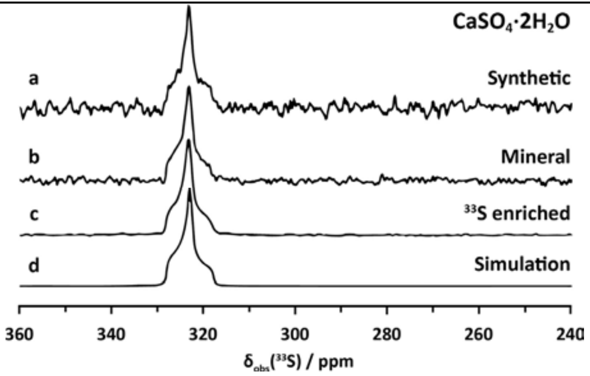

Fig. 7. 33S MAS NMR spectra (19.6 T, nR¼ 6e8 kHz) of (a) synthetic, (b) mineral and (c) 33S-enriched gypsum (CaSO4$2H2O) and (d) a second-order quadrupolar model of the central transition adjusted to the experimental data using DMFIT [60] and the NMR parameters reported in Ref. [59]. Adapted from d'Espinose de Lacaillerie et al. [59].

Commercially produced cements contain a worldwide average of~20%, butupto95% insomecases, replacementofPCclinker by SCMs, while maintaining similar performance to existing cements [61]. The SCMs used are primarily fine limestone, ground granulated blast-furnace slags (GGBFSs), coal FAs and silica fume, with recent developments also focussing on ternary blends, e.g.those containingbothcalcinedclaysandgroundlimestone[61]. Theuse of non-PC hydraulic clinkers such as CACs, CSA cements, belite- ye'elimite-ferriteclinkersandmagnesia-basedcements,aswellas non-clinkerebased cements such as AAMs, can also offer significant reductions in CO2 emissions.

The materials used as SCMs are often crystallographically disordered, compositionally variable and multiphase in nature.SS NMR has consequently been instrumental in characterising the local structure of these materials, which are used both as SCMsin blendswithPCandalsoasprecursorsforalternativecements. The expected dobs, disoand CQ for different nuclei in the main phases foundincommonSCMsareshowninTable3anddiscussedinthe followingtext.

4.1.2.1. Supplementary cementitious materials

4.1.2.1.1. Limestone. Limestone used as an SCM comprises primarilytheCaCO3polymorphscalciteandaragonite,aswellassome dolomite (CaMg(CO3)2). Calcite and aragonite, as well as the additional CaCO3 polymorph vaterite, are also generated within cementsinserviceasthecalcium-richcement hydratephasesreact withatmospheric CO2inaprocess knownascarbonation[62].43Ca MAS NMR analysis of calcite, aragonite and vaterite [40,41]has revealed substantially different chemical shifts and quadrupolar coupling constants for each polymorph, diso¼ 21.6, 12.6 and 26 ppm and CQ1.39, 3.7 and 0.68 MHz for calcite, vaterite and aragonite, respectively. 13C MAS NMR spectra of crystallographically pure calcite and aragonite show single resonancesin each phase at approximately diso168 ppm and 170 ppm, respectively [63,64], while crystallographically pure vaterite exhibitstwo13CMASNMRresonancesatdiso170ppmand 169ppm [65].

4.1.2.1.2. Blast furnace slag. GBFS GGBFS is generated as a secondaryproductofpigironproductioninablastfurnace;the liquid silicate slag is tapped from the furnace, rapidly cooled by granulationandthengroundtoaparticlesizesimilartothat ofPC. It can be blended with PC at replacement ratios as high as 95% under current European standards (EN 197-1) [66]and is also aprimary precursor for low-CO2 cements[4].

GGBFS consists primarily of depolymerised calcium silicate glasses, as well as small amounts of low-crystallinity phases within the melilite group [18,67e70]. The composition of GGBFS is dependentonthecharacteristicsoftheironproducedandoreused, aswellastheoperationaldetailsoftheblastfurnace[69],withCaO, Al2O3, SiO2 and MgO contents typically varying between 35e42 wt %, 7e13 wt %, 34e36 wt % and 6e15 wt % respectively [67e69,71e73]. The Al in the depolymerised silicate glass ischarge balanced mainly by Ca2þcations, with excess calcium cations contributing to the depolymerisation of the aluminosilicate framework [67e69]. As in most glasses, the reactivity of GGBFS is dependentonthelevelofdepolymerisationofthealuminosilicate framework [67,68]. 29Si and 27Al MAS NMR studies of GGBFS were interpretedasindicatingthatsiliconispresentmainlyasadimeric tetrahedral species, and Al is present in tetrahedral coordination [74]. Shimoda et al. [75e78]examined local structures in an amorphous synthetic slag using isotopic enrichment and multi-nuclear MAS and MQMAS NMR, probing 27Al, 29Si, 25Mg, 17O and 43Ca nuclei (Fig. 8), and showed that the amorphous slag frame- work structure can be generally described as a depolymerised chain-like network of SiO4 tetrahedra branched with AlO4 tetrahedra,withoxygenatomsoccupyingstructurallyinequivalentsites (dependentontheirbondingnature),andmultisiteoccupancyof Mg and Ca ions. These observations are supported by molecular dynamics simulations [79]. The structure and chemicalcharacteristicsofGGBFSareanalogoustothoseofnumerousothercalcium aluminosilicateglasseswhichhavebeenexaminedindetailusing MAS NMR[80e86].

4.1.2.1.3. Coal FA. Coal FA, a by-product of thermoelectriccoal combustion, comprises primarily Al2O3 and SiO2 within an assemblageofaluminosilicateglassyphases,withsomeadditional minor crystalline constituents, which can include quartz, mullite, ferrite spinels, calcium aluminates and others [87e89]. The characteristicsofcoalFAs(composition,extentofheterogeneityinthe glass and the local structure of each phase within the ash) vary widelybetweensourcesandasafunctionoftimeandaredependentonthetypeofcoalusedandthecombustionprocessthrough which it passes [90e92]. Mineral constituents in coal (mostly sili- cates and aluminosilicates) are melted as the coal is burned, become entrained in the flue gas as small droplets and are then cooledandcollectedasafinepowder,byelectrostaticprecipitators inthechimneystacksofthepowerstation.FAisblendedwithPCat replacementfractionsupto~50%inmanypartsoftheworldasits reactivesilicatefractioncanreactwithcalciumhydroxide through

Table 3

Coordination type and expected dobs, disoand CQ ranges for different nuclei in various supplementary cementitious materials

Phase	Nucleus	Site	Coordination	d_{obs}(ppm)	d_{iso}(ppm)	C_Q (MHz)	Magneticfield(T)	Reference
Limestone	^{13}C	CaCO$_3$(calcite)	4	168	168	e	8.45,9.4	[63,64]
		CaCO$_3$(aragonite)	4	170	170	e	8.45,9.4	[63,64]
		CaCO$_3$ (vaterite) site1	4	169	169	e	8.45,9.4	[65]
		CaCO$_3$ (vaterite) site2	4	170	170	e	8.45,9.4	[65]
	^{43}Ca	CaCO$_3$(calcite)	6	e	21.6	1.39	8.45,11.75,21.1	[40,41]
		CaCO$_3$(aragonite)	9	e	12.6	3.7	8.45,14.1,18.8	[40,41]
		CaCO$_3$(vaterite)	e	e	—26	0.68	8.45,11.75,21.1	[40,41]
Blast furnaceslag	^{17}O	Mg-NBO	2	e	55	2.2	16.4	[75]
		(Mg,Ca)-NBO	2	e	66	2.4	16.4	[75]
		Si-<u>O</u>-Al	2	e	68	3.3	16.4	[75]
		(Ca,Mg) NBO	2	e	81	2.8	16.4	[75]
		(Ca,Mg)-NBO	2	e	92	2.7	16.4	[75]
		Ca-NBO	2	e	120	2.9	16.4	[75]
	^{25}Mg	(MgO$_6$)$_1$	6	e	17	2.7	16.4	[75]
		(MgO$_6$)$_2$	6	e	10	4.6	16.4	[75]
	^{27}Al^a	Al^{IV}	6	55e68	76	4.3	9.4,14.1, 16.4	[18,20,73,75,199,438]
	^{29}Si^a	Q^1	1	—73e—91	—73e—91	e	7.05, 9.4, 14.1, 16.4	[18,20,71e73,75,199,206,438]
	^{43}Ca	Ca	e	25	e	e	16.4	[75]
Coalflyash	^{27}Al	Al^{IV}	4	40e60	e	e	14.1	[20,88,103e105]
		Al^{VI}	6	10to10	e	e	14.1	[20,88,103e105]
	^{29}Si	Q^4(mAl), m¼ 0-4	4	— 90 to—120	e	e	14.1	[20,88,103e105]
Metakaolin	^{27}Al	Al^{IV}	4	56e60	e	e	7.05,11.7	[107,110e113]
		Al^{V}	5	30e40	e	e	7.05,11.7	[107,110e113]
		Al^{VI}	6	0e10	e	e	7.05,11.7	[107,110e113]
	^{29}Si	Q^4(1Al)	4	—103	—103	e	11.7	[110]
Silicafume	^{29}Si	Q^4	4	—110	—110	e	7.1,9.4	[8,119,120]

[a] Thedistributionof^{27}Aland^{29}SiMASNMRresonancesforslagtypicallyspansbetween60and80ppm:forclarity,onlytheresonanceinthisdistributionexhibitingthe maximum intensity isprovided.

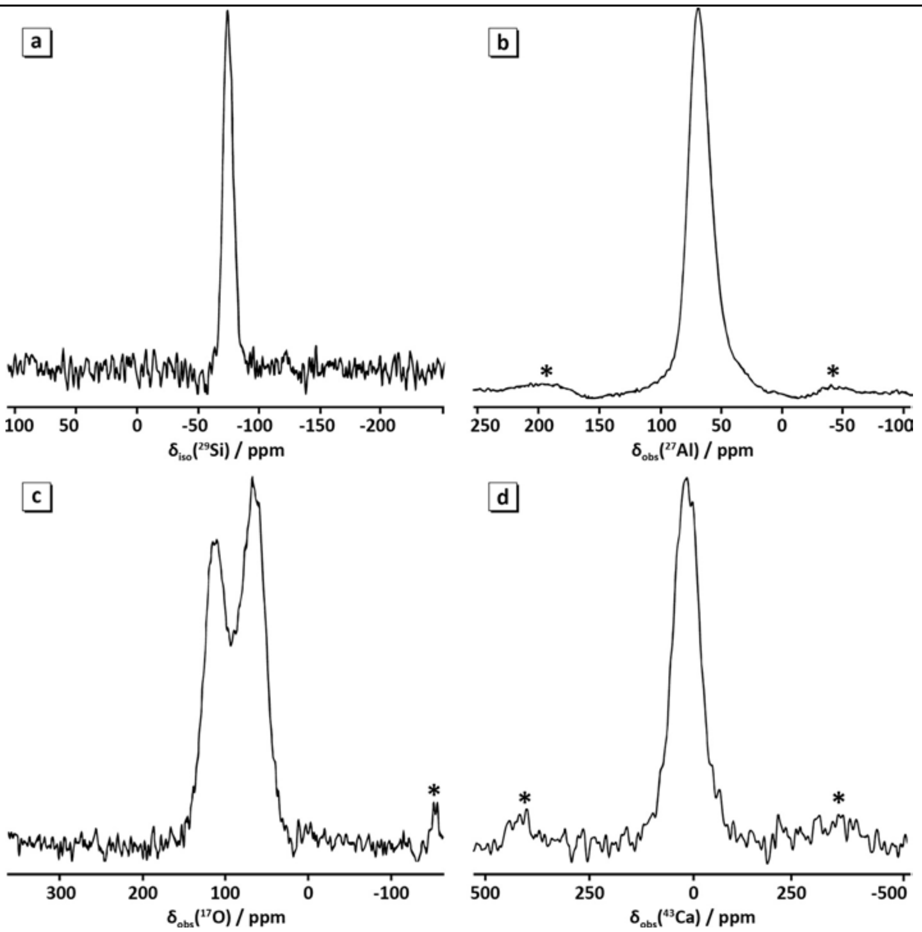

Fig. 8. (a) 29Si, (b) 27Al, (c) 17O and (d) 43Ca MAS NMR spectra (16.4 T, nR¼ 18 kHz) of synthetic slag enriched in 17O and 43Ca. Adapted from Shimoda et al., 2008 [75]. *Spinning sidebands.

the ‘pozzolanic’ reaction (Ca(OH)2 reactive silicates /calcium silicate hydrate) to produce desirable binding phases, while reducingtheoverallenvironmentalimpactofthecementandalso valorising this ash which would otherwise be a problematic high- volume waste requiringlandfilling.

Phasesegregationuponcoolingoccursoverthemajorityofthe relevantcompositional rangeforalumino silicateglasses, andsoas the molten aluminosilicate materials are quenched rapidly asthe flue gas cools, the various phases formed are finely interspersed within the FA particles. The result is a highly heterogeneous ma- terial,asdifferent FAparticlescoolatdifferentratesandarederived from different mineral matter entrained in the coal [93], resulting in both inter- and intra-particle variation in local phase composi- tion [94]. As a result, FA reactivity when used as an SCM (i.e. blended with PC) or as a precursor for AAM varies significantly between ashes, and between phases within each particular ash [95e102].

The crystalline phases presentin FAoccurinsmall amounts;in thelow-calciumasheswhichareconsidered mostdesirablefor blendingwithPC, thesephases (predominantlyquartz,mulliteand ferritespinels) arerelativelyunreactivewhencomparedtothe aluminosilicate glassy phase. Consequently, knowledge ofthe compositionoftheglassyphaseisimportantforcorrectformula- tion when designing cements containing FA, and SS MAS NMR (usedinconjunction withelectronmicroscopy) isakeytechnique thatcanprovidethisinformation,aslongastheashisnottoo rich iniron.

29Si and 27Al MAS NMR studies of FA have shown that the vit- reous aluminosilicate phase contains a distribution of Q4(mAl) Si species, with aluminium mainly present in poorly ordered tetra- hedral coordination, and also revealed the presence of a small amount of Al in octahedral coordination in mullite-like crystallites and glasses (Fig. 9) [20,88,103e105]. The quantity of each Q4(mAl) Si species, as well as the distribution of AlIV and AlVI sites, is dependentonthelocal phasechemicalcomposition.17OMASNMR studies have shown that alkali and alkali earth metals (mainly Na and K in FA) can act as network modifiers and form non-bridging oxygen sites if present in high enough concentrations in alumino-silicateglasses[106]whichareanalogoustotheglassyphaseinFA.

4.1.2.1.4. Metakaolin. Metakaolin is a layered aluminosilicate material which is used in cements as a pozzolanic additive andis producedby dehydroxylationofkaoliniteclayat temperaturesof

500ee800 ○C [107,108]. It is frequently used as an SCM in blends withPC[61,109].29Siand27AlMASNMRstudiesofmetakaolinhave shownthatitconsistsofalternatingbuckledsilicateandaluminate layers [68], with silicon in tetrahedral coordination (Fig. 10a) [110]and aluminium in a distribution of tetrahedral, pentahedral and octahedral coordination (Fig. 10b and c) [107,110e113], with each siteexhibitingasignificantdegreeofasymmetryinthelocalelec- tric field gradient [113]. It has been suggested that metakaolin containsapproximatelyequalamountsoftetrahedral(AlIV),octahedral(AlVI)andpentahedralAl(AlV)[111,114,115];howeverothers havefoundthroughcrystallographicanalysisthatsomeof theAlis tricoordinated[116].

Fig. 9. (a) 29Si and (b) 27Al MAS NMR spectra (14.1 T, nR¼ 10 kHz) of fly ash. Adapted from Bernal et al. [20]. Note that the spectra are significantly broadened by the presence of iron (5.2 wt% represented as Fe2O3 by X-ray fluorescence analysis) in the ash.

4.1.2.1.5. Silica fume. Silica fume is an amorphous form of SiO2 with extremely small (tens of nm) particle size, produced as a byproductofsemiconductorSimanufacture[118].Itiscommonly blendedwithPCatrelativelylowlevels(upto10wt%)topromote strength development and durability. Published work examining silicafumeviaNMRisfocussedon29SiMASNMRofPC-silicafume blends, which has shown that silica fume comprises a distribution of Si atoms in tetrahedral coordination (Q4 units), connected by oxygen bridges [8,119,120]. Because silica fume is a pure silica source with a 29Si resonance that is clearly distinct from that of eitherPCoranyofitshydrationproducts,itispossibletoaccurately determine the extent of reaction of silica fume within a blended cement through 29Si MAS NMR; this is much more accurate for silica fume than for any other siliceous SCMs, as the other SCMs haveresonanceswhichatleastpartiallyoverlapthesignal dueto the PC or its reaction products[121].

4.1.2.2. Non-PC hydraulicclinkers

4.1.2.2.1. Calcium aluminate cement. CACs consist primarily of monocalciumaluminate(CaAl2O4,CA),whichtypicallyaccountsfor40e60%wt.%ofcommercialCACs,along withsmallerquantitiesof C12A7 and CA2[23,122]. While considerably more expensive than PC,thesecementsareintendedforuseinapplicationswhererapid hardening is useful and/or when resistance to thermal stresses, chemical(particularlyacid)attackandimpactorabrasionisdesired [122],e.g.refractoryconcretes,cementsandconcretesfor effluent treatment infrastructure, blended cements for marine applications and other demanding service environments. CACs are now restricted from bulk use in structural concrete due to a series of material failures in past decades [123], but this does not limit theiruseinspecialistapplications.Theexpecteddobs,diso andCQfor different nuclei in CAC are shown in Table 4 and discussed in the followingtext.

4.1.2.2.1.1. Monocalcium aluminate, CaAl2O4

Monocalciumaluminate, CA ,is the principalreactivephase whichcontrolstheperformanceofCAC. ThecrystalstructureofCA consists of AlO4 tetrahedra forming six-membered rings in a tridymite-like structure [124]. 27Al MAS NMR isotropic chemical shiftsandquadrupolarcouplingparametersforeachofthe sixnon-equivalentAlO4tetrahedrainCAhavebeendeterminedby27Al MASNMRatmultiplefields (7.1,9.4 and 11.7TinRefs.[50,52] and 18.8 T in Ref. [84]), giving 81.9 ppm ≤ diso≤ 83.8 ppm and

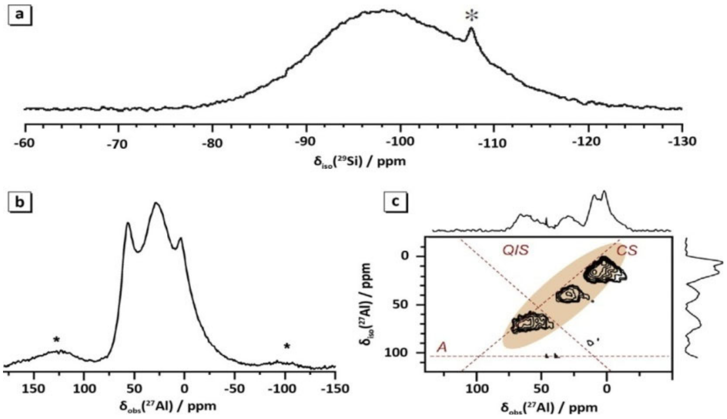

Fig. 10. (a) 29Si MAS NMR (9.4 T, nR6 kHz, adapted from Dai et al. [117]), where *indicates a resonance from a quartz impurity), (b) 27Al MAS NMR (11.7 T, nR15 kHz, adapted fromDuxsonetal.[111])and(c)27Altriplequantum(3Q)MASNMR(11.7T,adaptedfromKoberaetal.[113])spectraofmetakaolin.

Table 4
Coordination, expected dobs, disoand CQ for different nuclei in calcium aluminate cements.

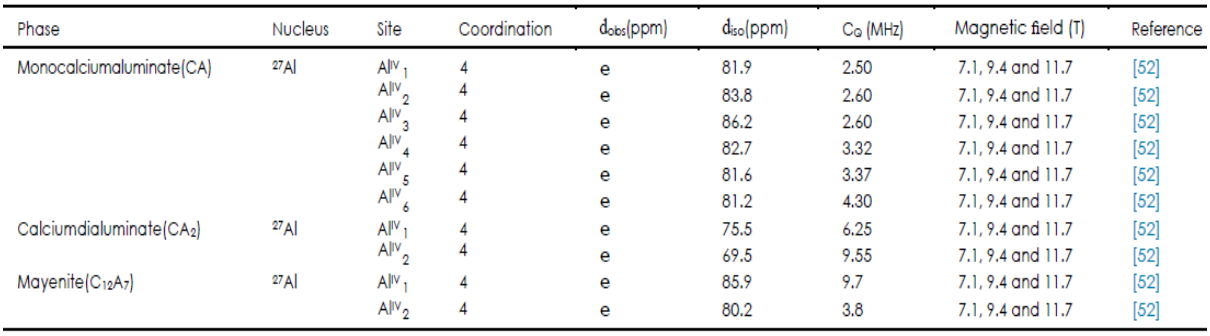

Phase	Nucleus	Site	Coordination	d_{obs}(ppm)	d_{iso}(ppm)	C_Q (MHz)	Magnetic field (T)	Reference
Monocalciumaluminate(CA)	^{27}Al	$Al^{IV}{}_1$	4	e	81.9	2.50	7.1, 9.4 and 11.7	[52]
		$Al^{IV}{}_2$	4	e	83.8	2.60	7.1, 9.4 and 11.7	[52]
		$Al^{IV}{}_3$	4	e	86.2	2.60	7.1, 9.4 and 11.7	[52]
		$Al^{IV}{}_4$	4	e	82.7	3.32	7.1, 9.4 and 11.7	[52]
		$Al^{IV}{}_5$	4	e	81.6	3.37	7.1, 9.4 and 11.7	[52]
		$Al^{IV}{}_6$	4	e	81.2	4.30	7.1, 9.4 and 11.7	[52]
Calciumdialuminate(CA_2)	^{27}Al	$Al^{IV}{}_1$	4	e	75.5	6.25	7.1, 9.4 and 11.7	[52]
		$Al^{IV}{}_2$	4	e	69.5	9.55	7.1, 9.4 and 11.7	[52]
Mayenite($C_{12}A_7$)	^{27}Al	$Al^{IV}{}_1$	4	e	85.9	9.7	7.1, 9.4 and 11.7	[52]
		$Al^{IV}{}_2$	4	e	80.2	3.8	7.1, 9.4 and 11.7	[52]

2.5 MHz CQ 4.3 MHz by deconvolution of both the resonance from the central transition and the spinning sidebands. Variations inthegeometryoftheAlO4tetrahedra(primarilydifferencesinAl- O bond lengths [124]) are primarily reflected in the 27Al MAS NMR quadrupolar parameters rather than in chemical shifts. This work contrasted earlier assertions that the resonance from the central transition could be simulated with a single set of quadrupolarpa- rameters and two isotropic chemical shifts[51].

High-field (18.8 T) 17O MAS NMR of CA has resolved eight resonancesduetoOatomsinAlIV-O-AlIVlinkages[84]withchemical shiftsbetween50and90ppmandCQvalueslessthan2MHz,with the tricluster oxygen site exhibiting the largest CQ (Fig. 11). This work demonstrated the benefits of utilising high fields which can narrow resonances sufficiently to resolve additional sites; eight of thetwelvecrystallographicallydistinct17OsitesinCAwereabletoberesolvedat18.8T[84],whileonlyfiveofthese17Ositescouldbe resolved at 14.1 T[125].

4.1.2.2.1.2. Calcium dialuminate,CaAl4O9

Calcium dialuminate (CA2) is found in relatively alumina-rich CAC clinkers that are used as refractory cements and is a slowly reacting cement constituent. Its structure comprises two tetrahe- drally coordinated Al atoms; one AlO4 tetrahedron contains two tricoordinated oxygen atoms and the other contains a single tricoordinatedoxygenatom,withtheremainingoxygenseachcon- nected to two Al atoms (Fig. 12) [126,127]. 27Al MAS NMR data collected at multiple fields (7.1 T, nR¼ 18.0 kHz; 9.4 T, nR¼ 18.0 kHz and 11.7 T, nR¼ 15.2 kHz) resolved single resonances for each tetrahedrally coordinated Al atom, with diso¼ 75.5 ppm and 69.5 ppm [52], and significant CQ values (6.25 MHz and 9.55 MHz, respectively)duetoelectricfieldgradient(EFG)asymmetrycaused bythenearbytricoordinatedoxygens.EarlierworkbyMülleretal. [51]determinedsimilardisoandCQvaluesforthesiteneighbouring twotricoordinatedoxygenscomparedtothoseobtainedbySkibstedetal.[52],butthosefortheAlO4tetrahedracontaininga single tricoordinated oxygen atom exhibited larger discrepancies,likely becauseoftheinsufficientresolutionandnotabledistortionofthe centraltransitioncausedbythemuchlowerspinningspeed utilised in those earlyexperiments.

17O MAS NMR (18.8 T) resolved four distinct oxygen sites in CA, resonating between 40 and 72 ppm [84], including a tricluster oxygen atom with three AlIV neighbours (i.e. an O(AlIV) site) resonating at approximately 40.6 ppm and with quadrupolar pa- rameters CQ¼ 2.5 and h ¼0.4.

4.1.2.2.1.3. Dodecacalcium hepta-aluminate (mayenite), C12A7

Mayenite, (Ca12Al14O33, C12A7), is generally present as a minor phaseinmorecalcium-richCACclinkers.Ithasalsobeendiscussed in the past as a potential constituent of PC clinkers but is now considered unlikely to form under realistic commercial PC pro- duction conditions [23]. 27Al MAS NMR at high spinning speed (17.8 kHz) resolved two distinct AlIV sites within C12A7, with diso85.9 and 80.2 ppm, respectively, in close agreement with the known crystal structure [129]and other 27Al MAS NMR in- vestigationsofthisphase[50,51].Differencesbetweenthedisoand quadrupolar parameters (3.8 MHz and 9.7 MHz) of these two AlIV sites arise due to distortions in one of the tetrahedra [50], which result in oxygen mobility [130]. Consequently (althoughmaybe

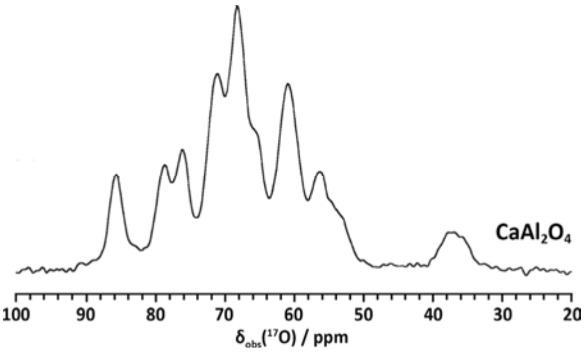

Fig. 11. 17O MAS spectrum of CaAl2O4 at 18.8 T. Adapted from Stebbins et al. [84].

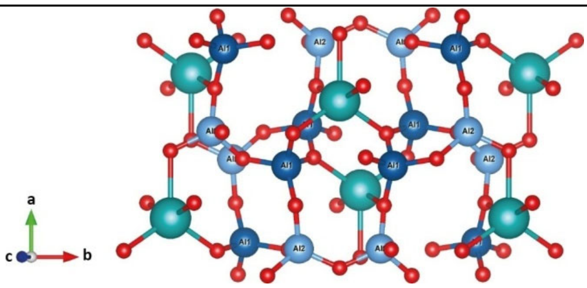

Fig. 12. Illustration of the local environments in the crystal structure of CA2, based on information obtained from single-crystal diffraction data [127]. The two AlO4 tetrahedra are denotedbyAl1(containingtwotricoordinatedoxygenatoms)and Al2(containingasingletricoordinatedoxygenatoms).Caatomsare representedbycyanspheres,Alatomsarerepresentedbydarkandlightbluespheres(denotingAl1andAl2,respectively)andOatomsare representedbyredspheres.PreparedusingtheVESTAsoftwarepackage[128].

incidentallyinthecontextofcementchemistry),mayenite hasalso received significant attention as a high-performance oxygen ion conductor[131].

4.1.2.2.2. CSA cements. CSA cements comprise calcium sulfoaluminate(ye'elimite,Ca4(AlO2)6SO4,C4A3$)andotherclinkerpha- ses such as belite, C4AF, ternesite (C5S2$) and/or calcium aluminates and are typically blended with calcium sulphate to regulate the rate of their setting [61,132]. 27Al MAS NMR investigations of commercially produced CSA and synthetic ye'eli- mite showed nearly identical spectra, consisting of a single peak (with maximum intensity at approximately 68 ppm) with two high-field shoulders at approximately 60 and 52 ppm[34,133e135]. Evidence enabling discrimination of two of the eight non-equivalentAlsitespresentinthecrystalstructureofye'elimite (which is an aluminate analogue of the sodalite framework)[136]was identified in this broad peak [133]. Recent work by Skibsted etal.[137]reportedthatthe27AlMASNMRspectralregionforAlIV in ye'elimite (~80 50 ppm) is dominated by overlapping reso- nances from the eight different Al sites. Isotropic projections from27AlMQMASNMRspectraobtainedbythesameauthorsrevealed four distinct resonances with very similar isotropic chemical shifts and quadrupole coupling parameters[34,138].

Ternesite, sometimes also called sulfospurrite, is a common minor constituent in modern CSA cements that is now being un- derstood to have some hydraulic activity but also forms withinPC kilns as an undesirable deposit on the refractory that reduces kiln performance. Ternesite exhibits a single, well-defined 29Si MAS NMR resonance at 73.0 ppm [139], consistent with its crystal structure [140] in which double layers of silicate tetrahedra alter- nate with single layers of sulphate tetrahedra, with calcium 7-coordinated to oxygenatoms.

The application of NMR spectroscopy to the belite and tetra- calcium aluminate phases present in CSA cements has been dis- cussed in detail in sections 4.1.1.2 and 4.1.1.4, respectively.

4.1.2.2.3. Magnesia-based cements. Magnesium silicate hydrate (M-S-H) cementsaretypicallyformedfromasourceofmagnesium andasourceofhighlyreactivesilica,suchassilicafume[141].The magnesiumsourceistypicallylight-burnedMgO,andMg(OH)2can also be used [142]. Although M-S-H was initially identified as a degradationproductinPCexposedtochemicallyaggressivecon- ditions [141,143], subsequent work has shown that M-S-H gels can also form a cementitious mass to generate high compressive strength [144e148]. These gels will be discussed in detail in section 4.2.6.

The25MgMASNMRspectrumofpolycrystallineMgOexhibitsa single sharp resonance at diso26 ppm [149,150], while the 17O MASNMRspectrumofthiscompoundenrichedwith17O containsa single sharp resonance at 47 ppm [150,151], consistent with octa-hedralMgO6sitesinthecubiccrystalstructureofthisphase,andin good agreement with first-principles calculations using DFT [152]. The 25Mg MAS NMR spectrum of Mg(OH)2 (brucite) exhibits a typical quadrupolar resonance with diso¼ 14.1 ppm and CQ3.15 MHz [153]. Application of NMR spectroscopy to silica fume has been discussed in detail in section 4.1.2.1.5. Many other magnesia-based cements also exist, including those based onmagnesium carbonates, phosphates and oxysalts (both chloride and sulphate) [141]; MgO is the primary Mg source used in the production of most of thesecements.

4.2. MASNMRofkeycementitiousbindingphases

ThevastmajorityofSSMASNMRinvestigationsofcementitious binding phases, which are often complex, disordered silicates [17,18,20,21,104,154,155], have probed 29Si and 27Al nuclei, yielding information about the coordination states of Al and the connec-tivityofSi(viaoxygenbridgestoSiorAlortonon-bridgingoxygen sites).Thelownaturalabundanceof29Si(4.7%)resultstheneedfor long data acquisition times for non-enriched samples, but the wealth of information obtainable from this technique has meant that it is nonetheless widely used[22].

4.2.1. Calcium silicate hydrategels

Calcium silicate hydrate (C-S-H) is the main product of PC hy- dration. It displays low crystallinity and variable composition and comprises(ingeneralterms)Q2Sichainsofvaryinglengthswith Q1 Si sites at chain termination points, as shown by 29Si MAS NMR [17,54,156,157]. These silicate chains are flanked by an interlayer containingconfinedH2Omolecules,aqueouscationicspecies(Ca2þand Hþin pure C-S-H, but with scope for substitution, particularly by alkali metals) and a calcium oxide sheet (Fig.13) [158,159]. The silicatechainsarearrangedina‘dreierketten’structure,basedona repeatingchainunitofthreetetrahedralsites,two‘pairing’ andone ‘bridging’,wherevacanciesinthebridgingsitesleadtocharacter- istic chain lengths of (3n 1) for integer values of n [160]. The two pairing SiIV units (Q2(p)) are linked with the calcium oxide sheet [159]. The expected dobs, disoand CQ for different nuclei in C-S-H, aluminium-substituted C-S-H (C-(A)-S-H) and alkali-and aluminium-substitutedC-S-H(C-(N,K)-A-S-H)areshowninTable5and discussed in the followingtext.

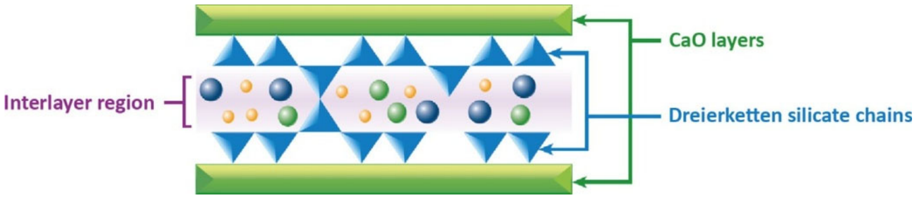

Fig.13. Schematicrepresentationofthestructuralfeaturesofcalcium-silicatehydrate(C-S-H)gels,adaptedfromProvisandBernal[4].TetrahedralSisitesandCaOlayersare shownbybluetrianglesandgreenrectangles,respectively.Circlesdenotevariousinterlayerspecies(waterorcations).

Numerous structural models for C-S-H have been proposed, including those based on jennite [161,162]and tobermorite [159,163], with recent SS NMR work probing both 29Si [164e167]and 17O [168] nuclei indicating strong structural similarity of C-S- H with a distorted tobermorite-like structure. 29Si MAS NMR spectroscopyincombinationwithothertechniqueshasshownthat C-S-H forms a structural series which shows both continuity and diversity, with phase-pure C-S-H exhibiting Ca/Si ratios at least between 0.55 and 2.0 [167,169,170]. Recent work combining dy- namic nuclear polarisationeenhanced (29Si)29Si double quantum coherence(theIncredibleNaturalAbundanceDoubleQuantum Transfer Experiment, INADEQUATE) and (1H)29Si HETCOR MAS NMRanalysisapproaches,withatomisticmodelling,determineda series of atomic level structures for C-S-H based on defective tobermorite with Ca/Si ratios of 1.25e2.0 [170]. These models include a structurally important interlayer calcium site which bridgesQ1silicatespeciesandisassociatedwithstronghydrogen bonding that stabilises the C-S-H, allowing high Ca/Si ratios to be reached in a phase-pureC-S-H. Despiteexperimentalandanalyticaldifficultiesarisingfromthe lownaturalabundanceandlargequadrupolemomentof17O,MAS NMR spectroscopy probing this nucleus has revealed valuableinformationregardingtheroleofoxygenspeciesinC-S-Hgels.Cong et al. [43,168] used 17O MAS NMR to study C-S-H in both synthetic gelsandhydratedb-C2S,identifyingtwonon-bridgingoxygensites (linking a Si atom with two or three Ca2þions, Si-O-Ca2þ), a single bridging oxygen site (linking two Si atoms, Si-O-Si), oxygen atoms within surface hydroxyl groups linked with either Ca2þ(Ca-OH) or framework Si atoms (Si-OH) and a single site corresponding to oxygenwithininterlayerH2Omolecules.Theobservationsofthese 17O MAS NMR resonances (and their relative intensities) support theRichardsonandGroves[159]defect-tobermoritemodelforC-S-H. Both non-bridging and bridging oxygen sites were observed to become less shielded with increasing Ca/Si ratio and decreasing polymerisation,indicatingadecreaseintheaverageSi-O-Sibond angles,consistentwithpreviousobservationsofadecreaseintheb axis of the pseudo-unit cell of C-S-H [167] at a higher Ca/Siratio.

As mentioned previously, natural abundance 43CaMASNMRexperiments face inherent difficulties due to thelownaturalabundance(0.145%),highquadrupolemomentandsmallmagnetogyricratioofthisnucleus,Table1.Consequently,veryfewstudiesprobing 43Ca in C-S-H via MAS NMR have beenperformed.Moudrakovskietal.[38]used43CaMASNMRtostudyaseries ofC-S-HgelsofdifferingCa/Siratios,aswellasC-S-Hproducedbyhydratingtriclinic C3S, crystalline 11 Å tobermorite and portlandite(Fig.14).ThecoordinationstateofCa2þinC-S-Hiscomplexandnotyetfullyresolved, but the work of Richardson [171] indicatestheexpectationthatthemostprobablecoordinationnumbersinplausibleC-S-Hstructuresare6or7dependingonthesitetypeandoccupancy.PairedSiO4chainsites(Q2(p))andbridgingSiO4chainsites(Q2(b)) in C-S-H in hydrated PC exhibit overlapping 29SiMASNMRresonances[16,172]andthereforecannotberesolvedindividually

Table 5
Coordination states and expected dobs, disoand CQ values for different nuclei in C-S-H, C-(A)-S-H and C-(N,K)-(A)-S-H.

Nucleus	Site	Coordination	d_{obs}(ppm)	d_{iso}(ppm)	C_Q (MHz)	Magnetic field (T)	Reference
^{1}H	Ca-OH	1	1.0	e	e	7.04, 9.4, 11.7	[164,180e182,310]
	Si-OH	1	4.5	e	e	7.04, 9.4, 11.7	[164,180e182,310]
	H_2O	1	5.2			7.04, 9.4, 11.7	[164,180e182,310]
^{17}O	Si-$\underline{O}$-Ca	2	e	104e112	2.4	11.74	[43,168]
	Si-$\underline{O}$-Si	2	e	60e82	4.5	11.74	[43,168,366]
	Si-$\underline{O}$-Al	2		45.5	0.5	14.1	[366]
	Ca-OH	2	e	70	6.5e7.2	11.74	[43,168]
	Si-OH	2	e	4e10	4.4e5.6	11.74	[168]
	Interlayer H_2O	2	e	0	0	11.74	[43,168]
^{23}Na	InterlayerNa^{þ}	e	—3	—3.7	1.0	14.10	[14,366]
^{27}Al	q^{2} charge balanced by interlayer Ca^{2þ}, Na^{þ}or H^{þ}cations	4	66	e	e	9.4, 17.5	[190,193]
	q^{2} charge balanced by interlayer or surface Al^{V} or Al^{VI} cations	4	e	74.6	4.5	17.5	[193]
	q^{3}	4	65	60	4.1	9.4, 11.7, 14.1	[14,20,188,201,366]
	Interlayer Al^{IV}	5	e	39.9	9.1	7.1, 9.39 and 17.5	[192e194]
^{29}Si	Q^{1}	4	—80 ±4	—80 ±4	e	7.1,9.4	[17,157]
	Q^{2a}	4	—85 ±4	—85 ±4	e	7.1,9.4	[16,17,172]
	Q^{2}(1Al)^{a}	4	—80 ± 4	—80 ± 4	e	9.4, 14.1	[20,21,199]
	Q^{2}(b)	4	—83.4	—83.4	e	9.4, 11.7, 17.5	[15,172,188,190,193]
	Q^{2}(p)	4	—85.3	—85.3	e	9.4	[15,172,188,190,193]
	Q^{2}(p)(1Al)		—80.5e—82.0	—80.5e—82.0	e	9.4	[15,172,188,190,193]
	Q^{3}	4	—95 ± 4	—95 ± 4	e	7.1, 9.4, 14.1	[20,188,199]
	Q^{3}(1Al)	4	—90 ± 4	—90 ± 4	e	9.4, 14.1	[20,21,199]
^{43}Ca	Ca-Osheet	6	10e45	e	e	21.14	[38]
	Interlayer Ca^{2þ}	~7	35e85	e	e	21.14	[38]

[a] Q^{2} resonances in these studies are not specified as bridging or pairing tetrahedra.

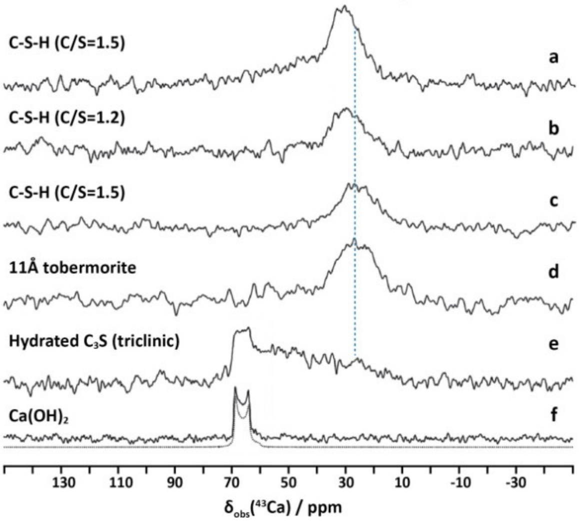

Fig. 14. Natural abundance 43Ca MAS NMR spectra of (a) C-S-H (Ca/Si ¼ 1.5), (b) C-S-H (Ca/Si ¼ 1.2), (c) C-S-H (Ca/Si ¼ 1.2), (d) 11 Å tobermorite, (e) hydrated triclinic C3S and (f) portlandite (Ca(OH)2). The dotted line below the spectrum of Ca(OH)2 is the simulation for the second-order quadrupolar interactions, and the blue vertical line indicates the centreband position of 11 Å tobermorite. Adapted from Moudrakovski et al. [38].

usingthistechnique;however,thesesitescanoftenberesolvedby their differing 29Si MAS NMR chemical shifts in synthetic C-S-H gels (Fig. 15)[173e177]. 43CaMASNMRspectraofthesyntheticC-S-Hgelsshowbroad resonances at approximately 27e31 ppm, very similar to the spectrumof11Åtobermorite[178].AnincreasedCa/Siratioleads todecreasedshieldingof43Caions(i.e.resonancesmovetohigher chemicalshift),consistentwithadecreaseinthemeanchainlength (MCL) of the silicate, and also in good agreement with 29Si MAS NMR data[167]. The43CaMASNMRspectrumofhydratedtriclinicC3Scontainsa broadresonanceacrossachemicalshiftrangethatincludes thatof the main resonances from C-S-H gels with 0.8 Ca/Si 1.5, indicatingthatC-S-Hinhydratedcementsystemsmaycontainvarious locallydifferentchemicalcompositions[38].Combining theseobservationswithanalysisof43CaMASNMRsignalintensityvs.delay time,Moudrakovskietal.[38]proposedthatCaintheCa-Osheets resonatesat10ppm≤dobs≤45ppmandinterlayerCa2þions resonate at35ppm dobs 85 ppm at a field B0of 21.14T. BowersandKirkpatrick[179]usednaturalabundance43 CaMAS

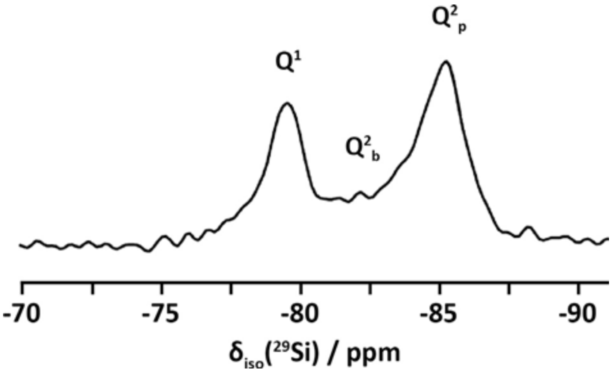

Fig. 15. 29Si MAS NMR spectra of synthetic C-S-H (Ca/Si 1) showing resonances from pairing(Q2(p)) andbridging(Q2(b))silicontetrahedra.AdaptedfromLothenbach etal., 2015[177].

NMRtodemonstratethatdespitebroadspectra,six-coordinateCa(aspresentinjennite)andseven-coordinateCa(aspresentin11Å tobermorite) may be resolved by differences in chemical shift resonate at35ppm dobs 85 ppm at a field B0of 21.14T. BowersandKirkpatrick[179]usednaturalabundance43 CaMAS (dobs ¼24ppmvs.—9ppm,at21.1T). By using this approach, itmay be possible to resolve the various locally different chemical com- positions (i.e. those with differing Ca/Si ratios) within C-S-H gels.

Despiteseverelinebroadeningin1HMASNMRspectrawhich resultsfrom1H-1Hdipolarcouplings,thehighsensitivityof1H,and thedevelopmentofmultipulsedecouplingsequenceswhichreduce linebroadening,haveledtotheapplicationofthistechniqueto studyprotonenvironmentsinC-S-H[157].However,theinforma-tionobtainablefrom1HMASNMRspectraofC-S-Hisgenerally limited,duetothedistributionofprotonsacrossmanychemical sitesandthesmallchemicalshiftrange(approximately20 ppm) over which 1H in solid phases can resonate [157]. 1H MAS and combined rotation and multiple pulse sequence (CRAMPS) NMR techniqueshavebeenusedtomonitorhydrationofsyntheticC3S duringtheearlystagesofhydrationandatlongerintervalsupto28 daysofcuring[180e182].Itwasdemonstratedthatitispossibleto resolvearesonancefromprotonsinCa-OHatdobs5.2fromthe overlapping broad resonances of protons in Si-OH andmobile water molecules at dobs0.5e1 ppm (B07.04 and 9.44 T). Recently,quantitative29SiMASand1H-29SiCPMASNMRexperi- ments have been used to monitor hydration of 29Si-enriched triclinicC3Sin-situoverthefirst24hofreaction[183].Theseresults were correlated with isothermal calorimetry measurements to identify the previously unobserved phenomenon of partial passivationofthesurfaceofC3Swhichdrivesdecelerationofthe reaction.

4.2.1.1. C-(A)-S-H gels. 29Si MAS NMR has revealed important in- formation regarding incorporation of Al in CeSeH (i.e. forming C- (A)-S-H) in hydrated PC [16,57,167,172,184e186], PCeSCM blends[117,187,188]and2000-yearoldRomanseawaterharbourconcrete [189]. Application of 29Si MAS NMR has allowed observation of resonancesfromQ1,Q2andQ2(1Al)siteswhichmakeupthesilicate chainsintheC-(A)-S-Hgel[16,167,172].TheMCLcanbecalculated fromtheintensitiesofQn(mAl)resonancesobtainedfrom29SiMAS NMRspectraldeconvolutionsbyusingequation(1),whilethede- greeofAl-Sisubstitutioninthetetrahedralchainscanbeobtained fromtheintensitiesoftheQ1,Q2andQ2(1Al)resonances(equation (2)),asdemonstratedbyRichardsonetal.[184,185]andAndersen et al.[186].

$$MCL_{aluminosilicate}\ ¼\ \frac{\Sigma\quad 1\quad 2\quad \frac{3}{2}2}{\frac{1}{2}Q^{1}\qquad \Sigma\ 2} \qquad (1)$$

$$\frac{Al^{IV}}{Si}¼\ \frac{\Sigma\quad \frac{1}{2}Q^{2}ð1Alþ}{Q^{1}þ\ Q^{2}þ\ Q^{2}ð1Alþ\ \Sigma} \qquad (2)$$

Using29SiMASNMR,Andersenetal.[186]showedthattheAlIV/ Si ratio in C-(A)-S-H in hydrated white PC is dependent on the availabilityofdissolvedAl3þions,butindependentofhydration time.Richardsonetal.[190]used29SiMASNMRtodeterminethat AlpreferentiallysubstitutesintoQ2(b)sitesandthattheMCLof aluminosilicate chains in C-(A)-S-H is dependent on both the availabilityofAl3þionsinsolutionandhydrationtime,findingsthat weresubsequentlyconfirmedbyAndersenetal.[184,186].Ithas alsobeensuggestedthatAlmaysubstituteforSiinsmallamounts in pairing sites [188,191,192], although this isthermodynamically disfavouredcomparedtothebridgingsites[191].
Al readily substitutes for Si in the bridging position in alumi- nosilicate chains in C-(A)-S-H up to a ratio of Al/Si 0.1, while at higherAl/Siratios,katoiteand/orstr€atlingitearealsoformed[15]. Analysis by 29Si and 27Al MAS NMR has shown that the AlIV/Si ratio in C-(A)-S-H in hydrated PC can be increased significantly bythe presence of alkali cations (Naþor Kþ) [16]via a mechanism in which the charge deficit introduced by Al-Si substitution is balancedbyadsorptionorbondingofalkalicationsintheinterlayer region. The role of alkalis in these structures will be discussed further in section 4.2.1.2.
^{27}Al MAS NMR experiments, particularly at high field (B014.1 T), have proven particularly useful in gaining detailed structuralinformationregardingtheroleofAlinC-(A)-S-H,inboth synthetic gels and hydrated PC. 27Al MAS NMR experiments at multiplefields(e.g.Fig.16)haveshowninsyntheticgelsandhy- drated PC that the AlIV bridging sites in C-(A)-S-H are charge balanced by interlayer Ca2þ, Naþor Hþions (dobs¼ 66 ppm, B0¼17.5T)[190,193]orbyinterlayerorsurfaceAlVorAlVIions (diso¼ 74.6 ppm, CQ¼ 4.5 MHz) [193]. AlV sites in theC-(A)-S-H interlayer can potentially substitute for Ca2þions (diso¼ 39.9 ppm, CQ5.1 MHz) [192e194]. From these studies, and others, it was concludedthatAldoesnotentertheCa-Osheet,northepairing tetrahedral sites in the silicate chains of C-(A)-S-H [22,172,184,190,193,194].

4.2.1.2. C-(N,K)-A-S-H gels. Synthesis of C-(A)-S-H gels in an environmentcontaininghighalkalimetalconcentrations,suchasinthe productionofAAMsfromGGBFS[154,160],yieldsaC-(N,K)-A-S- H gel. This is structurally similar to C-S-H, but with Alsubstitution inbridgingtetrahedralsitesandintheinterlayerasdiscussedinthe precedingsection,andwithchargebalancingbyalkalications(Naþand Kþ) in the gel interlayer, with additional alkalis able to sorb to the gel surfaces [74,154,185,195e197]. The structural characteristics ofthiscomplexgelhavebeenelucidatedlargelybytheapplication of SS NMR; representative spectra of alkali-activated GGBFS are showninFig.17,whileaschematicrepresentationoftheC-(N,K)-A-S-Hgelexhibitsadisorderedstructuresimilartothatofcrosslinked and/or non-crosslinked, structurally imperfect tobermorite [17,74,195]. As noted previously, there is a strong thermodynamic preference for Al substitution into bridging tetrahedra in the C- (N,K)-A-S-H gel [198].

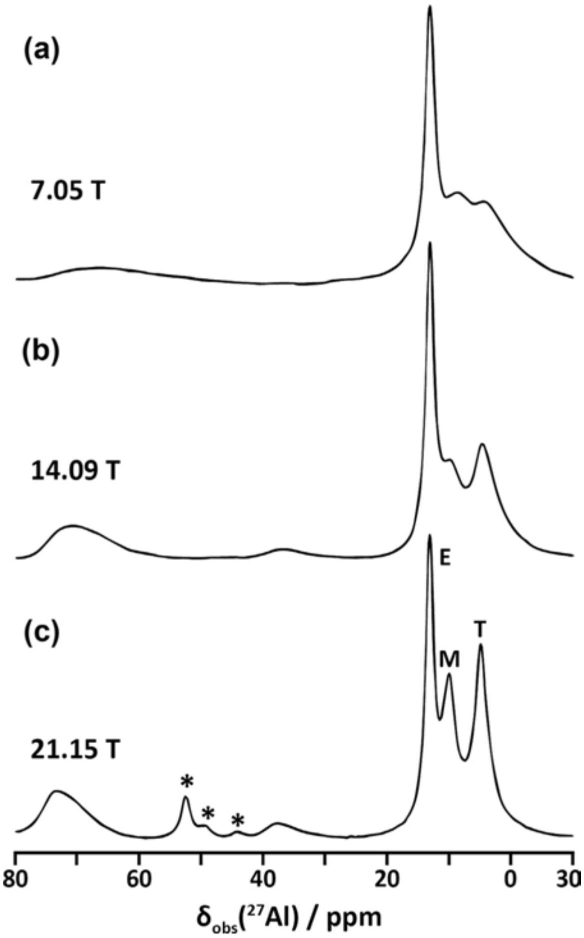

Fig. 16. 27Al MAS NMR spectra of the central transition for white PC hydrated for 12 weeksrecordedat(a)7.05T(nR¼13.0kHz),(b)14.09T(nR¼13.0kHz)and(c)21.15T (nR¼ 9.5 kHz), using 1H decoupling. Spinning sidebands are indicated by *. The resonancesfromthecentraltransitionofettringite,monosulphateandthethirdaluminate hydrate phase (described in section 4.2.8) are indicated by E, M and T, respectively. Adapted from Andersen et al. [172].

29Si MAS NMR has provided extensive evidence of thepres- ence of cross-linked (Q3 and/or Q3(1Al)) sites within2000-year-oldRomanseawaterharbourconcrete[189],alkali-activatedslag cements [20,188,199]and synthetic analogues[14,15,200e203]. The structure of these C-(N,K)-A-S-H gels was described by Myers et al. [195]as a mixture of cross-linked and non-cross-elinked silicate chains within a defect-tobermorite structure, with crosslinking occurring through partially Al-substituted bridging sites [21,188,193,196]. Using this model and 29Si MAS NMRspectraldeconvolutions,itispossibletocalculatetheMCL and AlIV/Si ratio of the cross-linked C-(N)-A-S-H gel structures usingthefollowingequations(3)and(4)[195].

$$\mathrm{MCL}_{\mathrm{crosslinked}}\ ¼\ \frac{4\sum Q^1 þ Q^2 þ Q^2 ð1AlÞ þ Q^3 þ 2Q^3 ð1AlÞ \sum}{Q^1} \qquad (3)$$

$$\frac{\mathrm{Al}^{IV}}{Si}\ ¼\ \frac{Q^3 ð1AlÞ}{\sum Q^1 þ Q^2 þ Q^2 ð1AlÞ þ Q^3 þ 2Q^3 ð1AlÞ} \qquad (4)$$

Crosslinking occurs predominantly in low-Ca C-(N,K)-A-S-H gels,and29Siand27AlMASNMRresultsindicatethatthe extentof crosslinking is promoted by increased overall Al content up to a ratioofapproximately1Alper6chainsites[21,204].However,the extentofcrosslinkinghasbeenobservedtodecreaseovertimeas thereactionproceeds,attributedtothelowerAl-bindingcapacity ofcrosslinkedgelcomponents[21].Studyoflaboratorysynthesised gels has shown that the amount of Al which is able to substitute into the C-(N,K)-A-S-H gel appears to be limited toapproximately Al/Si 0.2, with C-(N,K)-A-S-H gel compositions typically within the range 0.5 <Ca/(Al Si) 1 and 0 <Al/Si 0.2 [15,192,193,205]. The MCL of the aluminosilicate chains is often 7e10 tetrahedra for C-(N,K)-A-S-H gels produced by sodium silicate or potassium silicateactivationofslag[18,206];however,thisdependsontheCa/ (Al Si)ratio. Thereareconflictingreportsregardingthemechanismofalkali uptake and relationship with Al content of the C-(N,K)-A-S-H gel. 23Na MAS NMR analysis has indicated that alkali cations exist in two distinct environments within C-(N,K)-A-S-H gels [164,207,208]; the spectra show a sharp resonance at dobs¼ —7.6 ppm (7.05 T, nR¼ 10 kHz) [164] attributed to either a

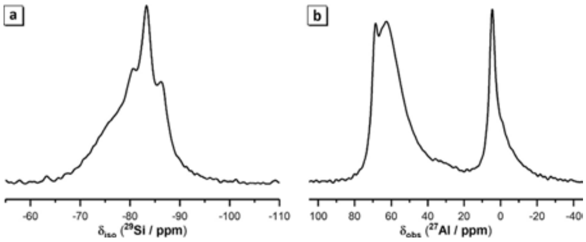

Fig. 17. (a) 29Si MAS NMR spectra (14.1 T, nR¼ 10 kHz) and (b) 27Al MAS NMR spectra (14.1 T, nR¼ 10 kHz) of an alkali-activated slag cured for 7 days. Adapted from Bernal et al., 2013[20].

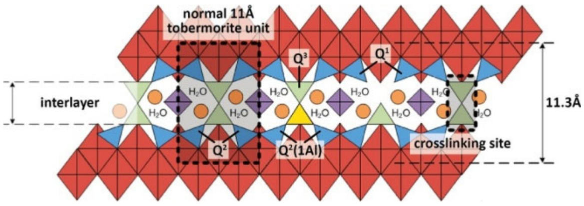

Fig.18.SchematicrepresentationofthestructuralfeaturesofC-(N)-A-S-Hgels,adaptedfromMyersetal.[195].PairedandbridgingSitetrahedraarerepresentedbyblueandgreen triangles,respectively,andintralayercalcium,charge-balancingalkalicationsandinterlayerprotonsand/orcalciumcationsbythereddiamonds,orangecirclesandpurplesquares, respectively.TheyellowtriangleindicatesAlsubstitutingforSiinabridgingtetrahedralsite.

highly symmetric bound alkali site or mobile alkali ions. An additional broad resonance at approximately dobs¼ —3 ppm (14.1 T, nR10 kHz) [14] to dobs10 ppm (7.05 T, nR10 kHz) [164]attributed to low-mobility Na within a disordered phase, possibly sorbed to the surface of the nanostructuredgel.

Some observations suggest a direct correlation between Al content and alkali uptake [16,209], supported by an intuitive rationaleofincreasedAlcontentdrivinganincreaseinalkaliuptake tochargebalancetheAlO—4tetrahedra.However,otherobservations suggest an inverse proportionality between Al content and alkali uptake[210]orthatAlcontentdoesnotaffectalkaliuptakeinthe C-(N,K)-A-S-H gel [204,211,212]. Alkali uptake in C-A-S-H gels has been observed to be promoted by lower Ca/Si ratios and higher alkali concentration [213], presumably because lower levels of charge balancing Ca2þincrease the requirement for charge balancing by alkali cations. It has been suggested that charge balancing alkali cations in the C-(N,K)-A-S-H gel interlayerinduce additional structural disorder by reducing the periodicity of the interlayerandreducingtheregularityofthestackingofthelayers due to differences in ionic size, indicating that incorporation of alkalis into C-(N,K)-A-S-H has a significant effect on gel nanostructure [13,214]. However, when 29Si MAS NMR was used to investigate compositionesolubilityestructure relationships in syntheticC-(N,K)-A-S-Hgels[204],itappearedthattheC-(N,K)-A- S-H gel structure was actually becoming more (rather than less) crystalline in the presence of alkalis, with both Na and K incorporated into its interlayer space [213]. The additional structural disorder was observed in C-(N,K)-A-S-H gel systems with lower pH (~13 [214]) than those in which greater ordering was observed (pH >13.5 [204,213]); it is, therefore, likely to be the higher pH of the more alkali-rich systems which drives rearrangement to more crystalline structures, rather than the alkali cations themselves. Elevated temperature also drives increased polymerisation, ordering and phase purity of synthetic C-(A)-S-H gel structures [215].

4.2.1.3. Other guest ions in C-S-H gels (C-S-(X)-H). In addition to Al3þandNaþ,otherionicspeciesmaybeincorporatedinto theC-S- H gel structure. Owing to the 100% natural abundance and high magnetogyric ratio of 19F and 31P, SS NMR experiments probing thesenucleihavebeenveryusefulinelucidatingthestructuralsites in which these atoms can exist within the C-S-H gel. 19F MAS NMR has shown that interlayer hydroxyl species may be substituted by F—[36,216]. Further analysis of F—speciation in C-S-Hby
19F-29Si-
19Fforthandback(FB)CPMASNMR(amodifieddouble CP
MAS NMR experiment which transfers polarisation forth and back between high- and low-g spin nuclei [217]) confirmed the aforementionedobservationofF—forOH—substitutionintheinterlayer, aswellasrevealingasecondFsiteattributedtoF—ionsassociated with CaO6 layers of a jennite-like part of the C-S-H gel[216,217].

PO3—ions can also be incorporated in the interlayer of C-S-H gels.31PMASNMRanalysisofinterlayerPO3—ionsexhibitsabroad resonance which has the same chemical shift as the PO3—ions in alite,somustbeselectivelydetectedusing1H-31PCPMASNMRto enable it to be distinguished from the signal of remnant clinker in an incompletely hydrated paste[32,34].

4.2.1.4. C-S-H e X interactions. SS NMR has also found applications investigating sorption of ions onto cement binding gels[173,218,219]. Static 35Cl NMR experiments and measurement of35Cl spinelattice relaxation time constants (T1) and spinespin relaxationtimeconstants(T2)wereusedtostudychloridesorption
onto jennite (used as a model C-S-H phase) suspended in lime- saturated NaCl solution [218]. This was intended to simulate hydratedPCinserviceinmarineenvironmentsandshowedthat
chlorideundergoesrapidexchangebetweensurfaceandbulkso- lution sites and exists predominantly in a hydrated, solution-like chemicalenvironment.

High-resolution 29Si, 23Na and 133Cs MAS NMR was used to study the interaction of sodium and caesium chloride salts with synthetic C-S-H [173]; this work is of particular relevance to the nuclear industry as some caesium isotopes are important fission product radionuclides. This work showed that both Naþand Csþcluster in hydrated C-S-H, while in dry C-S-H Naþ, formed outer- sphere complexes (adsorbed with their hydration sphere) and Csþformedinnerspherecomplexes(bounddirectlytothesurface with no intervening watermolecules).

1H,13C,27Aland29SiMASNMRhasbeenusedtoinvestigatethe structureoftheCaCO3polymorphscalcite,aragoniteand vaterite [65,220],aswellasK2CO3[220],andtheirformationinhydratedPC (i.e.throughcarbonation)andinteractionwithPChydrate phases [221].ThisworkshowedthatcarbonationofhydratedPCoccursin twostages:gradualdecalcificationofC-S-Hbyremovalofcalcium from the interlayer and defect sites until Ca/Si 0.67 is reached (corresponding to infinite silicate chains in a tobermorite-like structure), followed by further decalcification by removal of calcium from the gel layers and formation of a layered or three- dimensional silicate gel. The amount of carbonates formed is directlyproportionaltotheCa/Siratioofthegel.Theapplicationof 13CMASand1H-13CPMASNMRalsoenabledcarbonateanionsin hydrous and anhydrous phases to be distinguished[65,220].

SS MAS NMR has been used to examine the interaction between a variety of organic additives and PC during hydration. Natural abundance 43Ca and 13C MAS NMR was used to examine the interaction between a poly(ethylene-vinyl acetate) (PEVAc) admixture,addedtocementmortarstoimprovefracturetoughness andimpermeability,andhydratedwhitePCoverthefirst3 months ofhydration.PEVAchydrolysisoccursimmediatelyasPChydration commences,andinducesminorstructuralchangestothehydrated PC, primarily formation of a small amount of amorphous, low- coordinated calcium sites [222]. This demonstrates that PEVAc admixtures do not induce significant structural changes to hydratedwhitePCandarethereforeunlikelytobedetrimentaltothe performance of these cements. Conversely, 1H-13C CP MAS NMR showed that when mixed with 15 wt % poly (vinyl alcohol) and 10 wt % mineral antiblocking agents, PEVAc does not hydrolysein the alkaline solution of hydrating PC and was adsorbed to the surface of the cement binder [223,224]. This is particularly impor- tant in the context of both chemical and physical durability as PEVAc and other similar latex dispersions are commonly used as waterproofing agents and sealants incements.

4.2.2. Alkali aluminosilicate ((N,K)-A-S-H)gels

SS MAS NMR studies of hydrous alkali aluminosilicate in the contextofcementsarerelativelyrecentcomparedtothose exam- ining C-S-H and related phases in hydrated PC, with the first application probing 29Si speciation in alkali hydroxide/silicate activated metakaolin cements in 1988 [115,225,226]. Since these first experiments, SS MAS NMR analysis probing 29Si and 27Al has playedapivotalroleindeterminingthestructureofalkali-activated aluminosilicatecements,includingthoseknownas‘geopolymers’ [68,227]. The main reaction product of alkali activation of aluminosilicateprecursorshasbeenrevealedtobeathree-dimensional hydrous alkali aluminosilicate gel, consisting of highly crosslinked (predominantlyq4/Q4)AlO— 4andSiO4tetrahedralinkedviabridging oxygen atoms, with a small number of terminal hydroxyl groups forming Q3 sites. This structure is consistent across alkali alumi- nosilicate gels produced from reagent chemicals [228e231], calcined clays such as metakaolin [104,232e235], and aluminosilicate-rich waste materials such as coalFA [104,105,236e238]. This three-dimensional alkali aluminosilicate gelframeworkisoftendescribedasahighlycrosslinked,disordered pseudo-zeolitic structure [13,239e243], and nanocrystallinezeolite phaseshavebeenobservedaslocalisedregionsofordering

Table 6
Coordination, expected d_{obs}, d_{iso} and CQ for different nuclei in (N,K)-A-S-H.

Nucleus	Site	Coordination	d_{obs}(ppm)	d_{iso}(ppm)	C_Q (MHz)	Magnetic field (T)	Reference
^{17}O	Si-O-Si	2	e	39.0	1.26	14.10	[252,255,371]
	Si O Al	2	c	33.0	1.00	14.10	[252,255,371]
	H_2O	2	e	—9.8	0.55	14.10	[252,255,371]
^{23}Na	ChargebalancingNa[b]	6	—3to—5	—1.26 to—2.60	0.70e1.41	11.7,14.10	[112,255]
^{27}Al	q^4	4	58e60	61.0e66.3	1.4e1.9	14.10	[112,255,256]
^{29}Si	Q^4	4	—110 ±6ppm	—110 ±6ppm	e	7.5,9.4, 14.1	[112,236,237,250,251]
	Q^4(1Al)	4	—102 +5ppm	—102± 5ppm	e	7.5, 9.4, 14.1	[112,236,237,250,251]
	Q^4(2Al)	4	—95 ±4ppm	—95± 4ppm	e	7.5, 9.4, 14.1	[112,236,237,250,251]
	Q^4(3Al)	4	—90 ±4ppm	—90± 4ppm	c	7.5, 9.4, 14.1	[112,236,237,250,251]
	Q^4(4Al)	4	—86 ±4ppm	—86± 4ppm	e	7.5, 9.4, 14.1	[112,236,237,250,251]

within the broadly less-ordered gel framework [239]. The short-range ordering has been observed by 29Si and 27Al MAS NMR spectros- copy [20,112,244,245]together with X-ray and neutron pair dis- tribution function analysis [246e249] to extend to approximately 2e3 nearest neighbour shells. The expected dobs, disoand CQ for different nuclei in (N,K)-A-S-H gels are shown in Table 6 and dis- cussed in the followingtext.

27Aland29SiMASNMRhaveshownthatAlandSiarepresentin tetrahedral coordination, with Si existing in Q4(mAl) environments wheremisbetween1and4dependingontheAl/Siratioofthegel, andAlpredominantlyinq4(4Si)environmentsduetotheenergetic penalty associated with Al-O-Al bonding (Fig. 19) [236,237,250,251]. Reports of the observation of AlIV-O-AlIV bonds withinalkali-activatedmetakaolinhavealsobeenmadeformate- rials with Si/Al close to 1.0 using 17O triple quantum (3Q) MAS NMR [252], despite these bonds being significantly less thermodynami- cally favourable than AlIV-O-SiIV bonds, as entropic effects cause some violation of strict Si-Al ordering [250]. The negative charge associatedwithAlsubstitutionforSiisbalancedbyhydratedalkali cations(Fig.20)andisthoughttobedelocalisedacrossalloxygen atoms,withtheoxygenatomclosesttothechargebalancingalkali cation carrying the majority of this delocalised negative charge [114,252]. The (N,K)-A-S-H gel nanostructure is significantly influ-encedbykineticlimitationsonsilicaandaluminareleasefromsolid precursors if these are used [253,254]and consequently evolves overtimeasthereactionprocessproceeds[237].Schematicrep- resentations of the disordered N-A-S-H gel based on recent struc- tural descriptions are shown in Fig.20.

23Na MAS NMR analysis of metakaolin-derived (N,K)-A-S-H gels (Fig. 21a) [111,257] identified a single disordered Na environment withinthegelattributedtoNaþinacharge-balancingrole,whose chemicalshift(dobs¼—3.5to—6ppm,B0¼11.7T)wasindependent oftheSi/Alratio.AqueousNaþ(dobs¼0ppm,B0¼11.7T) wasalso observedwithintheporesolution,charge-balancingAl(OH)—4(aq)species, in samples with Si/Al ≤ 1.40. Charge balancing Naþsites resonating at a similar frequency (dobs4 ppm, B014.1 T) have alsobeenobservedinalkalialuminosilicategelsproducedfrom synthetic precursors [228]. These sites resonate at similar fre- quencies to those of hydrated Naþions in hydrothermally altered glass [258], providing opportunities to draw structural parallels to betterunderstandthenatureofthecementitiousgels.Kþionsin alkalialuminosilicategelsbalancethechargedeficitfrom Al3þ⇔

Si4þsubstitutionwithinthealuminosilicateframeworkandbehave

similarlytocharge-balancingNaþions[259,260](Fig.21b),andthe incorporation of Kþions into the (N,K)-A-S-H gel is preferential compared to Naþions when both arepresent.

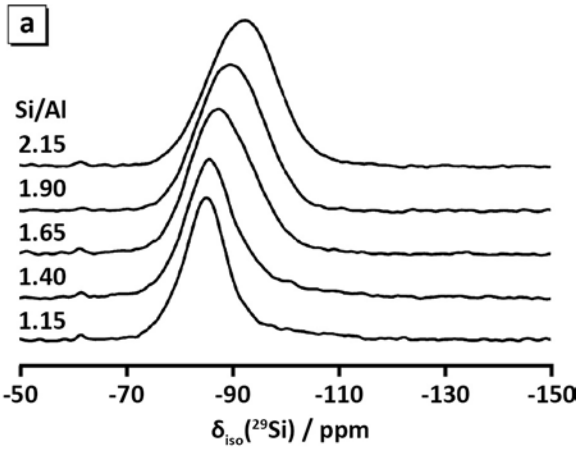

Fig. 19. (a) 29Si MAS NMR spectra (7.05 T, nR¼ 5 kHz) and (b) 27Al MAS NMR spectra (11.7 T, nR¼ 15 kHz) of N-A-S-H gels produced by reacting metakaolin with a sodium silicate solution (with Si/Al ratios as marked) and curing for 14 days. Adapted from Duxson et al.[111,112].

Related to this selectivity for larger alkali cations, SS NMR has also been applied to study the interaction of caesium with alkali aluminosilicate gels, to investigate their applicability in nuclear waste immobilisation applications. 133Cs MAS NMR spectra of Cs- doped alkali aluminosilicate gels produced from metakaolin and sodiumsilicateexhibitasinglebroadasymmetricresonanceat approximately d¼ 0 ppm (B ¼ 9.4 T) [261] consistent with that of Cs bound tightly to an aluminosilicate surface (such as that in kaolinite and illite [208,262]), strengthening the appeal of alkali aluminosilicate gels in nuclear waste immobilisation applications.

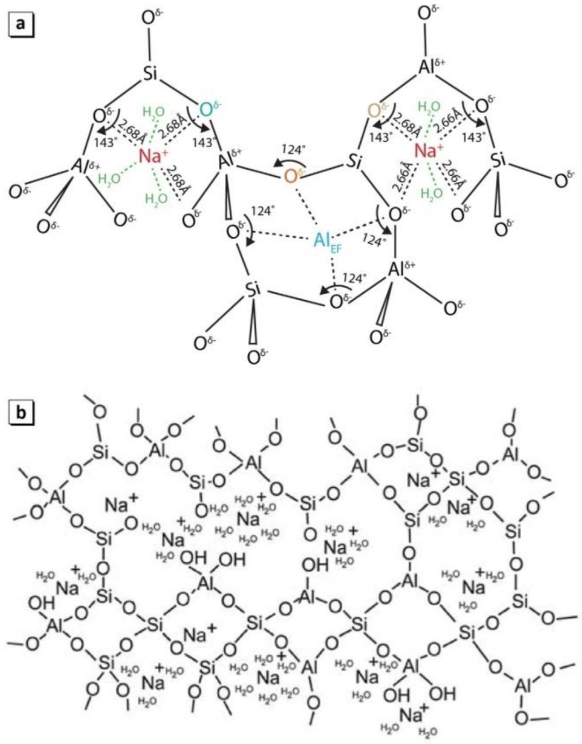

Fig. 20. (a) Schematic representation of a section of N-A-S-H gel adapted from Walkley et al. [255] showing charge-balancing sodium, charge-balancing extra-framework Al (AlEF), bridgingoxygenchargebalancedbyNaþandassociatedwiththreeH2Omolecules,bridgingoxygenchargebalancedbyAlEFandbridgingoxygenchargebalancedbyNaþand associatedwithtwoH2Omoleculesand(b)schematicrepresentationofasectionofN-A-S-HgeladaptedfromRowlesetal.[256].

4.2.3. Multiphase C-(N,K)-A-S-H/(N,K)-A-S-Hgels

Coexistence of C-(N,K)-A-S-H and (N,K)-A-S-H gel frameworks occursinmanycementsystems,includingAAMsbasedonblendsof high-calcium and low-calcium reactive precursors [20,263e265](Fig. 22), and the gels appear to be stable in coexistence [14,20,231,266e268], as long as there is sufficient alkali content [117,266,269e271]. SS NMR has proven particularly useful in determiningthestructureand compositionofthesecoexistinggel frameworks which are otherwise very difficult to discriminate. Owing to the structural similarity between these two gels, many resonancesintheirSSNMRspectraoverlap;however,thesecanbe distinguished and attributed appropriately with sound chemical reasoningandspectral deconvolution (discussedinsection4.3).

Using 27Al and 29Si MAS NMR, the growth of an N-A-S-H gel within alkali silicate-PC-dehydroxylated halloysite blends was shown to preferentially consume available Si within the system through rapid reactions involving the initially dissolved silica[270]. ^{27}Al and ^{29}Si MAS NMR of AAMs based on GGBFS-metakaolin blends [266], combined with high-resolution X-ray diffractometry [272,273], has also shown significant phase coexistence in these binders, although the dissolution of Ca2þfrom the GGBFS, and subsequentreactionmechanisms, dependson bothalkalinity and precursorchemistry.

Structural analysis via 29Si, 1H-29Si CP MAS, 27Al, 23Na and 1H MAS NMR of multiphase C-(N)-A-S-H and N-A-S-H gel frameworks within synthetic AAMs has also revealed strong dependence of reaction kinetics, gel composition and structure on precursor composition [14]. This work demonstrated that increased Cacon- tent of the solid precursor (or blend of precursors) promotes the formationoflow-Al,high-CaC-(N)-A-S-HwithlowerMCL,whereas increased Al content promotes Al inclusion and reduced cross-linking within C-(N)-A-S-H, formation of an additional N-A-S-H gel and increased presence of secondary alumina-rich hydrate phases.

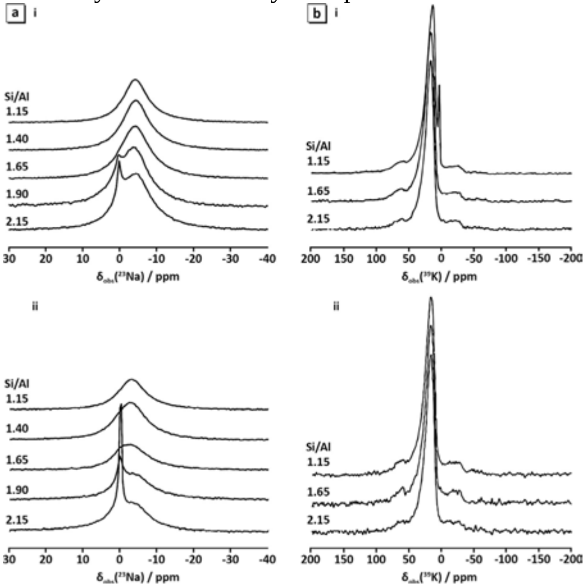

Fig.21.(a)23NaMASNMRspectraof(i)N-A-S-Hand(ii)N-K-A-S-HgelswithSi/Alratiosasmarkedand(b)39KMASNMRspectraof(i)K-A-S-Hand(ii)N-K-A-S-HgelswithSi/Al ratiosasmarked.Allmixed-alkaligelshaveNa:K¼1:1onamolarbasis,andallgelswereproducedbyalkaliactivationofmetakaolin.AdaptedfromDuxsonetal.[111] andDuxson et al.[259].

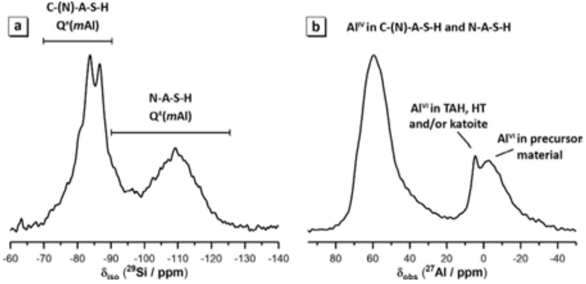

Fig.22.(a)29SiMASNMRspectra(14.1T,nR¼10kHz)and(b)27Al MASNMRspectra(14.1T,nR¼10kHz)ofanalkali-activated50%wt.slag/50%wt.flyashblendcuredfor14days, withcoexistenceofC-(N)-A-S-Hand(N,K)-A-S-Hgels.The29SiMASNMRspectrumshownin(a)exhibitsresonancesduetoQn(mAl)(1≤n≤3andm ≤n)speciesinC-(N)-A-S-H andQ4(mAl)(m≤n)inN-A-S-H,whilethe27AlMASNMRspectrumshownin(b)exhibitsresonancesduetoAlIVspeciesinbothC-(N)-A-S-HandN-A-S-H,aswellasAlVIspeciesin unreactedprecursormaterialandtheadditionalreactionproducts hydrotalcite(HT),thethirdaluminatehydrate(TAH)andkatoite.AdaptedfromBernaletal.[20].

4.2.4. HydratedCACs

CACs comprising primarily CA (with smaller quantities of CA2 and/or C12A7) hydrate to form mixtures of the microcrystalline metastablephasesCAH10andC2AH8,followedbyconversiontothe stablephasesC3AH6andamorphousAH3[122,274].The expected d_{obs}, d_{iso} and CQfor27AlinhydratedCACsareshowninTable7and discussed in the following text; information for other nuclei within these phases is not available in the openliterature.

Table 7
Coordination, expected d_{obs}, d_{iso} and CQ for different nuclei in hydrated calcium aluminate cements.

Nucleus	Site	Coordination	d_{iso}(ppm)	C_Q (MHz)	Magnetic field (T)	Reference
^{27}Al	Al inCAH_{10}	6	10.2	2.4	7.1, 9.4 and 11.7	[52]
	Al in C_2AH_8	6	10.3	1.2	7.1, 9.4 and 11.7	[50,276]
	Al in C_3AH_6	6	12.36	0.71	7.1, 9.4 and 11.7	[52]
	Al^{IV}_{1} in AH_3	6	10.4	1.97	7.1, 9.4 and 11.7	[52]
	Al^{IV}_{2} in AH_3	6	11.5	4.45	7.1, 9.4 and 11.7	[52]

Skibsted et al. [52] used 27Al MAS NMR to identify overlapping resonancesattributedtooctahedralAlenvironmentsinthe stable C3AH6 (diso¼ 12.3 ppm, CQ¼ 0.705 MHz) and amorphous AH3 (dobs¼8ppmatB0¼9.4T)phasesinCAChydratedfor28 days;the isotropicchemicalshiftforC3AH6wasdeterminedviasimulationof the spinning sidebands associated with this phase. Analysis of synthetic CAH10 at multiple fields exhibited a broad resonance in the octahedral Al region of the 27Al MAS NMR spectrum and allowed determination of diso¼ 10.2 ppm and 1.9 MHz CQ 2.6 MHz for this site. These results are consistent withpreviousdataacquiredatlowerfield[275]. Subsequentwork examinedCAChydratephasesusing27AlMAS[50,276] andMQMAS [276]NMR, enabling determination of diso¼ 10.3 ppm and CQ¼ 1.2 MHz for the octahedral Al site in the metastable C2AH8 phase and diso11.9 ppm and CQ 4.3 MHz for the amorphous AH3 phase.

Becauseofthecleardistinctionbetweenalenvironmentsin hydrated(AlVI)andanhydrous(AlVI)CAC,thedegreeof hydrationof this cement may be readily determined from 27Al MAS NMR (Fig. 23) [44,50,51]. This, however, relies on the assumption thatall Alresonanceswithinthe27AlMASNMRspectraareobservableand quantifiedcorrectly;thisisnotalwaysthecaseduetothepresence of ‘NMR invisible’ Al species (see section4.3).

27Al, 31P and 1H-31P CP MAS NMR has also been used to show thatmodificationofCACbyadditionofphosphatepreventstheloss of material performance which is caused by the conversion from themetastablecalciumaluminatehydratestostableC3AH6inhy- drated CAC. Instead, phosphate modification yields an apparently stableamorphouscalciumaluminophosphategelcomprisingboth AlIVandAlVIsites[277].Inthesematerials,phosphorusispresentin hydrous environments with varying, but mostly low, degrees of crosslinking.

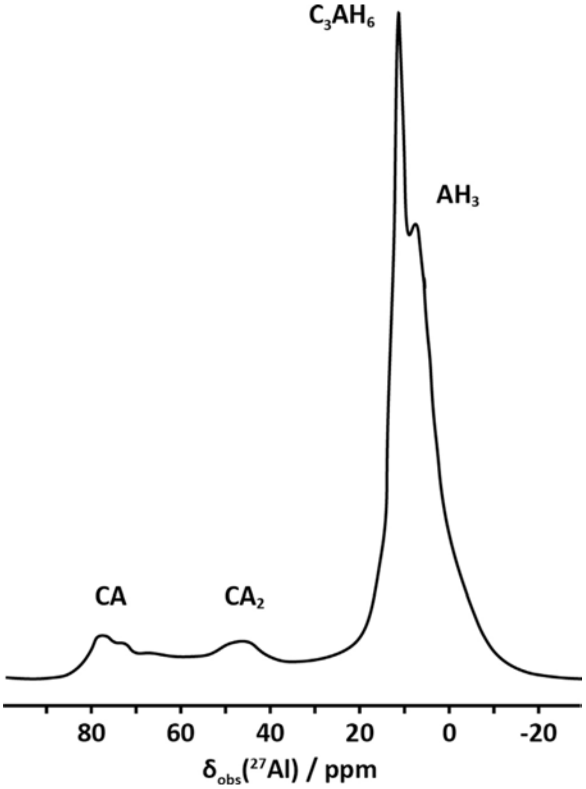

Fig. 23. 27Al MAS NMR spectrum (9.4 T, n ¼ 13.1 kHz) of a calcium aluminate cement hydratedfor28days.Thedegreeofhydration,estimatedbyintegrationoftheAlIV AlVI spectral regions, is 86 ± 1%. Adapted from Skibsted et al.[52].

4.2.5. Hydrated CSAcements

Ye'elimite (C A $) hydrates in the presence of calcium sulphate (C$, added as gypsum or in dehydrated forms) to form ettringite (‘AFt’, Ca Al (SO) (OH) $26H O, see section 4.2.8.2), calcium monosulfoaluminate hydrate (‘monosulphate AFm’, 3CaO$(Al,Fe)2O3$CaSO4$nH2O, see section 4.2.8.3) and microcrystallinealuminiumhydroxide(Al(OH)3),withtheproportionofeach phasedependentontheC4A3$/C$ratio[278].Thepresenceofbelite along with these phases in a CSA cement, which is common because of the prohibitive cost of Si-free Al sources for cement manufacture,resultsintheformation ofstra€tlingite(2CaO$SiO2$Al2O3$8H2O;asilica-substitutedAFmphase,seesec- tion 4.2.8.3) and/or C-S-H as additional reaction products. As mentionedinsection4.1.2.2.2,CSAclinkerscanalsocontainC5S2$ (ternesite), which hydrates along with alumina-bearing clinker constituentstoformstr€atlingite[279,280].MostcommercialCSAcements also contain C4AF (section 4.1.1.4) as the economically viablealuminasourcesusedincementmanufacturealsocontain significant quantities of Fe; this will typically hydrate (in both CSA and PC cements) more slowly than the hydraulic aluminate phases and yields Fe-substituted forms of many of the same AFm and AFt hydrate phases[281e283].

SSNMRstudiesofhydratedCSA(syntheticandcommercial)and CSA/PCblendshaveshownnarrow27AlMASNMRresonancesfor octahedral Al in ettringite and monosulphate at approximately dobs¼13ppmand10.2ppm(B0¼14.1T),respectively,aswellasa broad low-intensity resonance at dobs¼ 9 ppm at the same field which is attributed to Al(OH)3[133e135,284,285], consistent with the resonances of pure phases in synthetic samples, section 4.2.4[52,286,287]. AswithCAC, thecleardistinctionbetweenAlenvironments in hydrated (AlVI) and anhydrous (AlVI) CSA allows the degreeofhydrationofaluminium-containingphases tobereadily determined from 27Al MAS NMR. This has shown that aluminium- containing phases generally react to form hydrates within 24 h [133e135,284]. Monitoring the degree of hydration in CSA/PC blendsissignificantlymore difficultduetothe presenceofAlIVsites inC3AandC-(A)-S-Hphases[133],aswellasthepresenceofFe which can severely dampen and shift the NMR signal of these nuclei[10];however,itismadepossiblebyspectraldeconvolution using appropriate models and constraints (see section4.3).

4.2.6. Magnesium silicate hydrate (M-S-H)gels

Magnesium silicate hydrate (M-S-H) cements are commonly producedfromMgOandsilicafumeviahydrothermalorambient- temperature processes [288e292], and generally comprise atalc- like or serpentine-like phase [141,293], although there remains somedebatearoundthemostappropriatestructuralmodel forM- S-H. 29Si MAS NMR spectra of M-S-H cements exhibit as many as five distinct 29Si MAS NMR resonances, attributed to Q1, Q2, two Q3 and Q4 sites [142,146,292,294e298]. The major component of the 29Si MAS NMR spectra is a Q3 resonance at approximately diso93 ppm and the Q1 and Q2 resonances are typically broad [142,292], indicating the disordered nature of the gel. These envi- ronmentshavebeenattributedto Sisiteswithinadisordered phase structurally similar to talc (Mg3Si4O10(OH)2) [296]and/or serpentine-group minerals (polymorphs of Mg3(Si2O5)(OH)4, such as chrysotile, lizardite and antigorite) [142], with Mg/Si ratios ranging from 0.57 to 1.3[291,293,298].

Alkaline earth aluminosilicate hydrate gel (magnesium alumi- nosilicate hydrate, M-A-S-H) has also been reported [299]. MAS NMR of these materials synthesised from sepiolite (Mg4Si6O15(OH)2$6H2O) and chrysotile (Mg3(Si2O5)(OH)4) resolved similar Q329Si MAS NMR resonances at 90 ppm, and tetrahedral Mg sites from 25Mg MAS NMR.

4.2.7. Magnesium potassium phosphate cements(MKPC)

Magnesium potassium phosphate cement (MKPC) is aclinker- free acidebase cement which reacts to form struvite-K (MgKPO4$6H2O) as a crystalline main strength-giving phase; this phase is structurally analogous to the natural mineral struvite, NH4MgPO4$6H2O, but without requiring the presence of ammo- nium cations for its synthesis [141,300e302]. Application of SS NMR to investigate structural and phase evolution in MKPC is relatively recent, with the most extensive analysis probing 25Mg, 27Al, 29Si, 31P and 39K nuclei in MKPC blended with FA and with GGBFS [303]. Struvite-K exhibits a31P resonance at dobs6.2 ppm [303], which correlates well with the chemical shift of struvite, dobs6.1 ppm [304]. A shoulder on this resonance at dobs4 ppm was observed in MKPC/FA blends (but not MKPC/GGBFS blends)andwassuggestedtoresultfromthepresenceofadisor- dered and/or partially substituted struvite-K phase. The predomi- nant crystalline struvite-K phase exhibits 25Mg and 39K resonances at diso¼ —1.0 ppm (CQ¼ 3.8 MHz) and diso¼ —73.1 ppm (CQ 2.2 MHz), consistent with previous observations for synthetic versions of this phase [305,306]. An amorphous orthophosphate environmentwasalsoidentified,whichhasnointimateinteraction with hydrogen and no measurable Al interactions[303].

4.2.8. Additional reactionproducts

Manyadditionalreactionproductsarealsoformedalongwith the main silicate gels during hydration of the cements discussed previously and will be discussed in turn in this section. These additional reaction products are often intimately mixed with the dominant silicate gel frameworks [7,231] and can significantly in- fluence the phase evolution and nanostructural development of thesehydratephases.Theexpecteddobs,disoandCQfordifferent nucleiintheadditionalreactionproductsobservedinhydratedPC, CAC,CSAandmagnesia-basedcements,aswellascementsbased onalkalimetaloralkaliearthaluminosilicatechemistry,areshown in Table8.

4.2.8.1. Portlandite. Portlandite (CaOH2), also called slaked lime, is acommonreaction productinhydratedPCandisalsopresentasa reaction productorremnantprecursorinpozzolanicorslag-based bindersactivatedwithlime.Ingeneral,portlanditeforms whenthe Ca/Siratioissignificantly higherthancanbe accommodatedbyC-S-H or related phases [307]. It consists of layers of octahedrally coordinated Ca bound to oxygen atoms in tetrahedralcoordination [23] with hydrogen occupying a single crystallographic site. It isa keyparticipantinlongertermphaseevolutionofC-(A)-S-Hgelsin blended PC cements via the pozzolanic reaction [308]. High-field natural abundance 43Ca MAS NMR of portlandite [179]and 43Ca MAS NMR of isotopically enriched portlandite at multiplefields [309]have shown a single quadrupolar resonance centred at approximately dobs50e60 ppm (7.04, 11.7 and 21.1 T) corre-spondingtoasingleCaenvironmentwhereCaisoctahedrallyco- ordinated by six hydroxyl groups. Correspondingly, 1H MAS NMR spectra of portlandite exhibit a single resonance at diso0.7 ppm from the single Ca-O-H site [180,182,310]. Chloride sorption onto portlanditeinportlandite suspensionshasbeenstudiedusingstatic 35Cl NMR experiments and measurement of 35Cl spinelattice relaxation time constants (T1) and spinespin relaxation time con- stants (T2) [218]. Chloride on portlandite exists predominantly in a hydrated, solution-like chemical environment and is rapidly exchanged between the surface and bulk solution. Portlandite quantification in hydrated cements by NMR is not usually attempted,asneither43Canor17Onucleiareparticularlystraight- forward to use in such studies, and other techniques such asther- mogravimetry and X-ray diffraction (XRD) can give reliable quantitativeresultsforthisphasemuchfasterandlessexpensively.

4.2.8.2. ‘Aluminate ferrite trisulphate’etype phases. Ettringite is the archetypal ‘aluminate ferrite trisulphate’ (AFt) phase, with a columnarhydrousCSAstructureandaveryhighwatercontent(up to 32 water molecules per formula unit) [311]. Ettringite forms rapidlyintheearlieststagesofhydrationofPC,asC3Areactswith gypsum, or equivalently through hydration of ye'elimite with excess gypsum in CSA cements. Early 27Al MAS NMR experiments (9.4 T) examining ettringite displayed a resonance at diso13 ppm thatappearedcharacteristicofasingleoctahedrallycoordinated AlO6 site [52], which contrasted with the then-proposed crystal structureofettringitewhichcontainedtwodistinctoctahedralAlO6 sites [312]. Recent work using ultraehigh-field (22.3 T) 27Al MAS and MQMAS NMR (Fig. 24) has in fact been able to resolve two distinct octahedrally coordinated AlO6 sites in syntheticettringite

Table 8

Coordination, expected dobs, disoand CQ values for different nuclei in various additional reaction products in hydrated PC, CAC, CSA and magnesia-based cements, as well as cements based on alkali metal or alkali earth aluminosilicate chemistry.

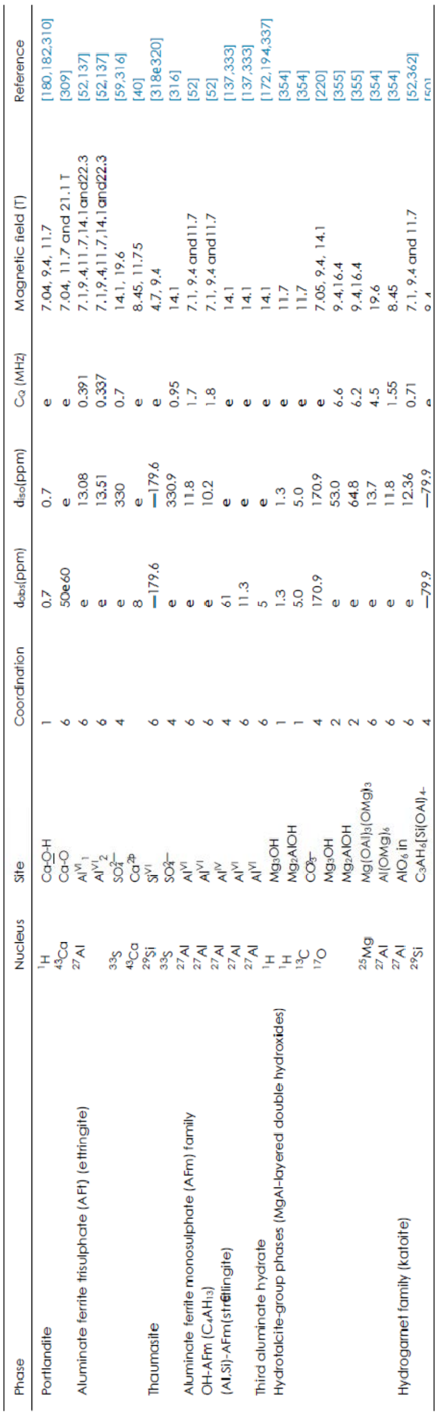

Phase	Nucleus	Site	Coordination	d_{obs}(ppm)	d_{iso}(ppm)	C_Q (MHz)	Magnetic field (T)	Reference
Portlandite	^{1}H	Ca-O-H	1	0.7	0.7	e	7.04, 9.4, 11.7	[180,182,310]
	^{43}Ca	Ca-O	6	50e60	e	e	7.04, 11.7 and 21.1 T	[309]
Aluminate ferrite trisulphate (AFt) (ettringite)	^{27}Al	Al^{VI}_{1}	6	e	13.08	0.391	7.1,9.4,11.7,14.1and22.3	[52,137]
		Al^{VI}_{2}	6	e	13.51	0.337	7.1,9.4,11.7,14.1and22.3	[52,137]
	^{33}S	SO_4^{2-}	4	e	330	0.7	14.1, 19.6	[59,316]
	^{43}Ca	Ca^{2+}		8	e	e	8.45, 11.75	[40]
Thaumasite	^{29}Si	Si^{VI}	6	−179.6	−179.6	e	4.7, 9.4	[318e320]
	^{33}S	SO_4^{2-}	4	e	330.9	0.95	14.1	[316]
Aluminate ferrite monosulphate (AFm) family	^{27}Al	Al^{VI}	6	e	11.8	1.7	7.1, 9.4 and11.7	[52]
OH-AFm (C_4AH_{13})	^{27}Al	Al^{VI}	6	e	10.2	1.8	7.1, 9.4 and11.7	[52]
(Al,Si)-AFm(strätlingite)	^{27}Al	Al^{IV}	4	61	e	e	14.1	[137,333]
	^{27}Al	Al^{VI}	6	11.3	e	e	14.1	[137,333]
Third aluminate hydrate	^{27}Al	Al^{VI}	6	5	e	e	14.1	[172,194,337]
Hydrotalcite-group phases (MgAl-layered double hydroxides)	^{1}H	Mg_3OH	1	1.3	1.3	e	11.7	[354]
	^{1}H	Mg_2AlOH	1	5.0	5.0	e	11.7	[354]
	^{13}C	CO_3^{2-}	4	170.9	170.9	e	7.05, 9.4, 14.1	[220]
	^{17}O	Mg_3OH	2	e	53.0	6.6	9.4,16.4	[355]
		Mg_2AlOH	2	e	64.8	6.2	9.4,16.4	[355]
	^{25}Mg	$Mg(OAl)_3(OMg)_3$	6	e	13.7	4.5	19.6	[354]
	^{27}Al	$Al(OMg)_6$	6	e	11.8	1.55	8.45	[354]
Hydrogarnet family (katoite)	^{27}Al	AlO_6 in	6	e	12.36	0.71	7.1, 9.4 and 11.7	[52,362]
	^{29}Si	$C_3AH_6[Si(OAl)_{4-}$	4	−79.9	−79.9	e	9.4	[50]

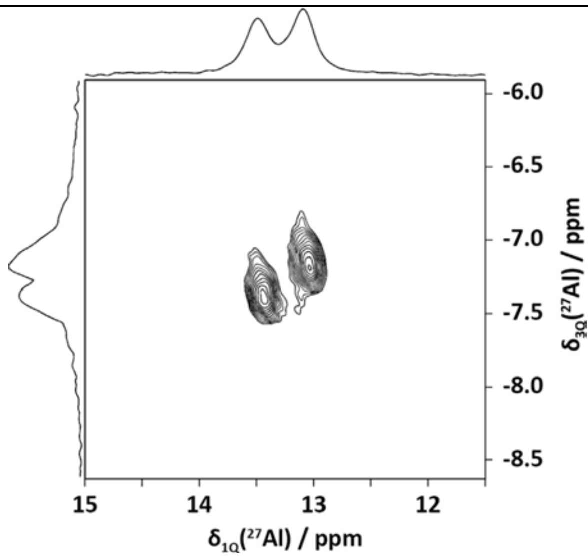

Fig. 24. 27Al MQMAS NMR spectrum (23.3 T, nR15 kHz, 5 ○C sample temperature) of ettringite showing two distinct AlIV sites. Adapted from Skibsted et al.[137].

[137], consistent with the now well-accepted crystal structure solved by Moore and Taylor [312]. The two AlO6 sites resonate at diso¼ 13.08 and 13.51 ppm and are highly symmetric, displaying verysmallquadrupolarcouplingparametersofCQ0.391 MHzand 0.337 MHz, respectively. The high symmetry and very similar isotropicchemicalshiftsoftheseresonancesareduetoverysmall variations in Al-O bond lengths between sites, consistent with high-resolution powder XRD [313], single-crystal XRD and DFT calculations [311]. As a consequence of the small distinction in isotropic chemical shift values, these resonances remained unre- solved for more than two decades in 27Al MAS NMR spectra ac- quired at lower fields [22,52,57,117,135,186,187,314,315]. This demonstrates the importance of acquiring high-field spectra for quadrupolar nuclei in complex phases, even where crystallinity is high (as in the case of ettringite) and for relatively ‘accessible’ nuclei such as27Al.

Natural abundance 43Ca MAS NMR analysis of ettringite also resolved only a single 43Ca resonance (dobs8 ppm) [40] despite the existence of two Ca sites in the crystal structure; this can be attributed to the structural similarity between the two Ca sites in ettringite and the poor signal-to-noise ratio of the spectrum resultinginpoorlydefinedoverlappingquadrupolarlineshapesfor each site. High-field natural abundance 33S MAS NMR [59]and single-enhanced wideband uniform rate smooth truncation (WURST) and hyperbolic secant (HS) MAS NMR spectroscopy probing 33S [316]identified a single narrow resonance (diso330 ppm, CQ 0.7 MHz) attributed to the single sulphur site in ettringite, which has a high degree of symmetry as it is within a discrete sulphateanion.

Thaumasite (Ca3Si(OH)6(CO3)(SO4)$12H2O) is a silicate- and carbonate-substituted AFt phase which can form by reaction of sulphate and carbonate ions with cement minerals (i.e. during sulphate attack of PC systems) [317]. This similarity has caused difficulty distinguishing thaumasite from ettringite using XRD, infraredspectroscopyorthermogravimetrictechniques. However, thaumasite exhibits a 29Si MAS NMR resonance at diso179.6 ppm [318e320], corresponding to Si in a veryunusual sixfold coordination, meaning that it is readily identifiable by this technique. 1H-29Si CP MAS NMR has been used to identify and quantify thaumasite in PC systems containing carbonate andsul- phate additives and revealed that significant quantities of thau- masite can form in cements with negligible Al content [320]. WURST and HS MAS NMR spectroscopy probing 33S [316] in thau- masite identified a single narrow resonance (diso¼ 330.9 ppm, CQ 0.95 MHz), consistent with its crystal structure in which sulphur exists in a single SO2—crystallographic site [321], asin ettringite.

4.2.8.3. ‘Aluminate-ferrite-monosulphate’etypephases.Calcium monosulfoaluminateandsimilarhydrocalumite-likeAFmphasesare observedinmanytypesofcements,includingPC[117,322,323],CSA cements[133e135,284,285] andmanyalkali-activatedslagcements [154,324e326].AFmphasesarelayereddoublehydroxide(LDH)e type structures, with positively charged portlandite-like layers con- tainingone-thirdofAl3þorFe3þcationsassubstituentsforCa2þ, balancedbyanionicspecies(commonlySO2—,CO2—andOH—),and with significant interlayer H2O [327e330](Fig. 25). They can be represented by the general formula [Ca2(Al,Fe)(OH)6]XxH2O, where X represents an exchangeable singly charged (e.g. OH—) anionorhalfofadoublychargedanion(e.g.SO2—,CO2—)[322].With theexceptionofOH—/SO2—substitution(upto50mol%)[322],these phasesgenerallydonotformextensivesolidsolutionsbutrathercan coexistasseparatephaseswithcloselyrelatedstructuresbut differing interlayer anions. Consequently, many hydrated cement systemscontainmixturesofdistinctAFmphases.AFmphasesin hydratedPCtypicallycontaintheanionsSO2—(termedmono-sulphate), CO2—(monocarbonate) and/or OH—(hydrocalumite, C4AH13) in the interlayer [52,117,322,323,331], while those in alkali-activatedslagsandmetakaolin-richPCblendscommonlycontain interlayerdivalentaluminosilicateanions,[AlSi(OH)]2—,formingan AFmstructure,whichisalsogiventhemineralnamestra€tlingite [154,324]. Substitution by multiple anions in ordered positions is also possible, for example, 1:1 hydroxide and carbonate to form hemicarbonateor1:1sulphateandchloridetoformKuzel'ssalt [322]. Friedel's salt (3CaO$Al2O3$CaCl2$10H2O) is also observed in hydratedPC,whichhasbeenexposedtoasourceofchloride,e.g. whenservinginmarineenvironmentsorcoldclimateswithroad salting.

Thesephaseseachexhibitasingle

27AlMASNMRresonanceat approximately dobs10e12 ppm, depending on field strength [52,117,133], in accordance with their crystal structures containing AlVI[327,332]. Owing to similarities in structure, each of these AFm phasesexhibitsverysimilar27AlMASNMRresonancesatstandard fieldstrengths,andsotheyaremoreoftendistinguishedfromeach other via complementary techniques, e.g. XRD, where their differentbasalspacingscanbeobserved.Themonosulphateand monocarbonate 27Al MAS NMR resonances are severely over- lapping (dobs12 ppm), but evidence for more than one peak in this region has been observed by ultraehigh-field 27Al MAS NMR (23.3 T) [137], suggesting that it may be possible to resolve these resonances,andthoseofC4AH13,atultrahighfield.Thesorptionof chlorideontothemonocarbonateAFmphaseC4ACH11 wasinves- tigated by static 35Cl NMR experiments and measurement of 35Cl spinelattice relaxation time constants (T1) and spinespin relaxa- tion time constants (T2) [218], showing that chloride is in rapid exchangebetweenadsorbedsurfacesitesandbulksolutionsitesin each phase and exists predominantly in a hydrated, solution-like chemical environment on the monocarbonate surface. This behaviour is similar to chloride sorption onto portlandite andonto jennite, as discussedpreviously.

Stra€tlingite(Ca4Al2(OH)12[AlSi(OH)8]2$2H2O)isanAFmphase which forms as a hydration product of aluminium-rich cements including PC-metakaolin blends and some non-Portland binders. 27AlMASNMRanalysisofhydratedwhitePC-metakaolinblends [117]andhydratedCSA[137],aswellassyntheticstra€tlingite[333], revealedtworesonancesatdobs61ppmand11.3ppm(14.1T) attributedtoAlIVandAlVIsites,respectively.Theseresonancesare characteristic ofthecrystalstructureofstr€atlingite[334],which containsAlIVinadouble-tetrahedralenvironmentaspartofthe

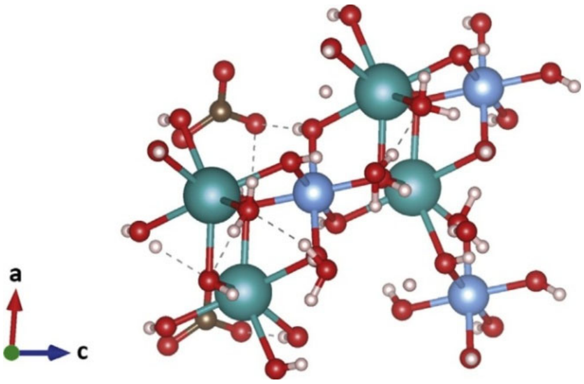

Fig. 25. Illustration of the local environments in the crystal structure of the mono-carbonateAFmphase[Ca4Al2(OH)12]CO3$5H2Oobtainedfrom single-crystaldiffraction data[329].Caatomsarerepresentedbycyanspheres,Alatomsarerepresentedbyblue spheres,OatomsarerepresentedbyredspheresandHatomsarerepresentedbylight pinkspheres.PreparedusingtheVESTAsoftwarepackage[128].

aluminosilicateinterlayeranion([(T,,)(OH,O)$0.25HO]—,T¼Si orAl,, vacancy),aswellastheAlVIinthebrucite-typelayer ([Ca2Al(OH)6$2H2O]þ)thatdefinestheAFmstructure. TheAlVIsiteinstr€atlingiteresonatesatasimilarfrequencytoAlVIsitesin monosulphate,andconsequentlystr€atlingiteismoreconclusively identifiedfromitsAlIVresonance,unlessworkingatextremelyhigh fields. The 27Al MAS NMR spectrum of hydrated CSAcollectedatB022.3 T appears to contain contributions from severalindividualoverlappingAlVIresonances[137],suggestingthatmonosulphate,monocarbonateandstra€tlingitemaybeabletoberesolvedin27Al MASorMQMASNMRspectraacquiredatultra-highmagneticfield.The29SiMASNMRspectrumofsyntheticstr€atlingiteexhibitsa broad resonance atapproximatelydobs 86.5 ppm,containing contributions from resonances resulting from Q3(3Al), Q2(2Al), Q2(1Al) and Q2 sites [333,335], consistent with the crystal structure [334]ofstra€tlingite which containsdoubletetrahedralsilicatering structures. The presence of these resonances is often used to monitor hydration in PC-CSA blends [133].

Asmentionedpreviously,Friedel'ssaltisanAFmphasewithCl—as its interlayer ion. Variable temperature static 35Cl NMR has shownthatinterlayerCl—inFriedel'ssaltexhibitsaresonanceat diso¼ 30 ppm with a quadrupolar coupling constant CQ 2.22e2.87 MHz, indicating uniaxial symmetry above 0 ○C resulting from dynamically averaged interlayer species [336]. Below0○C,theCl—inthissiteexhibitsreduced(triaxial)symmetry resultingfromarigidcrystalstructure,asindicatedbyaresonance at diso¼ 26 ppm with a quadrupolar coupling constant CQ¼ 3.0MHz.

4.2.8.4. Third aluminate hydrate. The ‘third aluminate hydrate’ (TAH)phaseisanamorphousnanoscalealuminatehydratephase which precipitates at the surface of the C-S-Hetype gels formed duringPChydration[172,194,337]andwhichhasalsobeennotedin sodium silicateeactivated GGBFS [18,20,155,324]. TAH is to date onlyidentifiablebyNMR,andconsequently,thetechniqueiskeyto thediscoveryofitsexistence.TAHisdescribedasapoorly ordered $Al(OH)_3$ phase [194,337]which is intimately mixed with other hydrate phases. Stoichiometric arguments and thermodynamic modellingsuggestthatthepresenceofTAHislikelytobelinkedto high concentrations of available Ca and Al [154,338,339], as the opposingchargesonCeSeHandAFmphasesmayproduce strong mutual attractions and physically destroy the AFm crystals [22,340], which would then result in low-crystallinity aluminate (AFm-like) layers being dispersed throughout the CeSeH gel while being undetectable by XRD [22]. This hypothesis is supported by transmission electron microscopy observations [337]. TAH phases exhibit a ^{27}Al MAS NMR resonance at dobs5 ppm (14.1 T) in the spectra of C-S-Hetype gels [172,194,337]and of sodium silicate-eactivatedGGBFS[18,20,155,324].Broadeningofthe^{29}SiMASNMR resonanceattributedtoQ^1Sispeciesinsodiumsilicateeactivated slags [155] is attributed to the presence of Al^{VI}-O-Si linkages be- tween TAH andC-S-H.

4.2.8.5. Hydrotalcite-groupphases.Hydrotalcite($Mg_6Al_2CO_3(OH)_{16}[CO_3]\$4H_2O$),Fig.26)isanMg-AlLDHmineralwithaprimarylayerof positivelychargedbrucite-likesheets(seesection4.1.2.2.3), comprisingoctahedrallycoordinatedMgboundtooxygenatomsin tetrahedral coordination, with partial replacement of Mg2þby trivalentoctahedrallycoordinatedcations,whichareAlin thecaseof truehydrotalcite[341].TheAlatomsarerandomlydistributedwithin these layers at low concentrations [342] but take on a significantly moreorderedconfigurationatthehigherconcentrationswhichare morecharacteristicofhydrotalcite-groupphasesobservedincements[23].AsecondarylayercontainsH_2Omoleculesandanions, mostcommonlycarbonate,CO_2—,andhydroxyl,OH—,whichare intercalatedandchargebalancethenetpositivechargesinducedin the sheets by incorporation of trivalent cations to replace Mg2þ[341,343]. More than 40 identified mineral species conform to this generaldescription(butwithdifferentcationandanionsubstituents anddegreesofsubstitution)andarecollectivelydenoted hydrotalcite-supergroupphases.

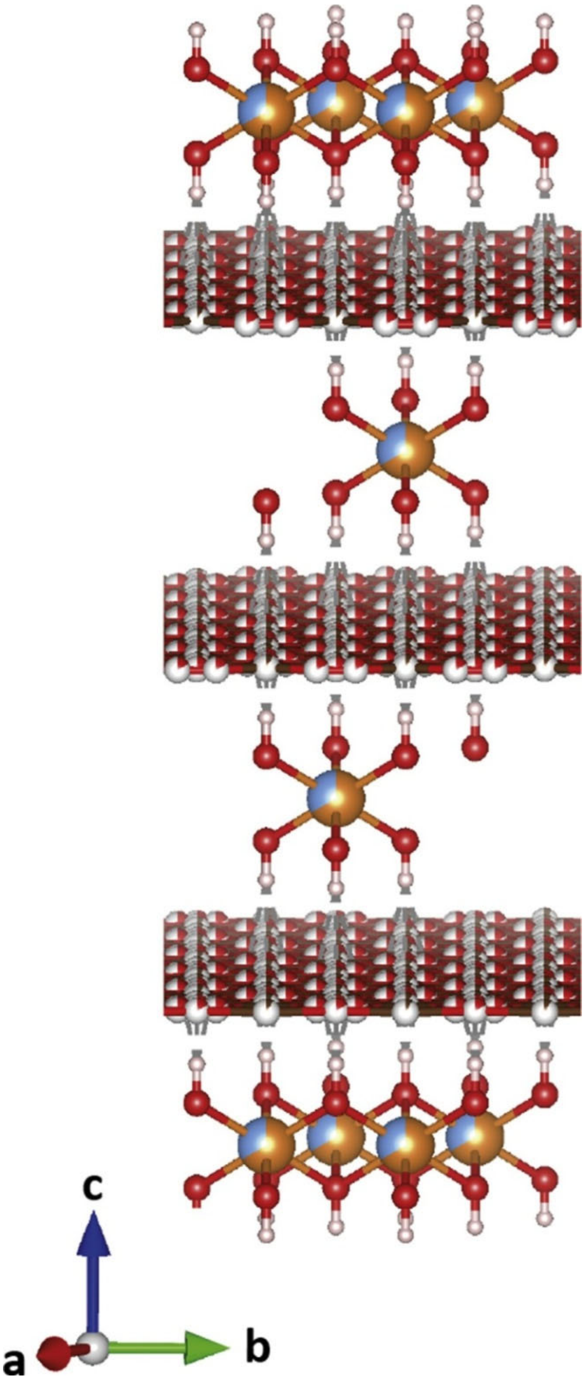

Fig. 26. Illustration of the local environments in the crystal structure of hydrotalcite ($Mg_6Al_2CO_3(OH)_{16}[CO_3]\$4H_2O$) obtained from single-crystal diffraction data [352]. Mg, Al, C, O and H atoms are represented by orange, blue, red and light pink spheres, respectively. Partial colouring of spheres indicates the average proportion of each respectiveatomoccupyingaspecificsiteinthehydrotalcitecrystalstructure.Prepared using the VESTA software package[128].

Quintinite-groupphases, whichareasubsetofthe hydrotalcite- supergroup with Mg/Al 2, have been observed on a sub- micrometrescaleinhydratedPC-GGBFSblends[99,220,344]andin cementsproduced frommetallurgicalslagsactivatedwithsodium silicate or sodium hydroxide [71,72,154,190,324,325,345e348], typically occurring when slags with Mg content 5% are used, consistent with predictions from thermodynamic modelling [349]. ThesephasesgenerallycontainhigherAlcontent(Mg/Al ¼2)than true hydrotalcite (Mg/Al ¼ 3) [341]. Previous work identified a phasethatwasdenoted‘M4AH13’andproposedthatitmaybean analogue of the AFm-structured C4AH13, however, this phase has since been shown to be OH-quintinite (Mg4Al2(OH)13$4H2O)) [350,351].

27AlMASNMRspectraofsodiumsilicateeactivatedslag cements exhibit a resonance at dobs9 ppm (9.4 T) attributed to a hydrotalcite-like phase containing AlVI sites [325,353], consistent with 27Al MAS NMR analysis of synthetic hydrotalcites [342,353]. Simulation of 27Al MAS NMR spectra of synthetic hydrotalcite- group phases has determined the isotropic chemical shift of this site to be diso11.8 ppm, attributed to a single Al environment surrounded by Mg atoms in octahedral coordination [354], with broadening of this resonance indicating increased disorder as Al content is decreased. A broad shoulder on this resonance at dobs3 ppm (8.45 T) is observed when the intercalated anion is CO2— [354]. High-field (19.6 T) 25Mg MQMAS NMR of these hydrotalcite-group phases resolved a single 25Mg resonance at diso13.7 ppm assigned to Mg symmetrically surrounded by 3 Mg and 3 Al ions, Mg(OAl)3(OMg)3[354]. 1H MAS NMR data acquired with high spinning speeds have also been used to resolve two distinct hydroxyl resonances in these phases at diso¼1.3 and 5.0ppm,respectively,attributedtoMg3OHandMg2AlOHwhichare observedatMg/Al4and3,respectively[354].Recently,17OMAS and MQMAS NMR resonances attributed to oxygen sites in these two hydroxyl groups were also observed in isotopically enriched synthetic hydrotalcite-group phases [355]. 1H-13C CP MAS NMR of synthetic hydrotalcite revealed a single 13C resonance at diso170.9 ppm attributed to a single CO3 site [220]. This work also utilised 13C MAS and 1H-13C CP MAS NMR to resolve carbonate anionsinanhydrous(e.gCaCO3)andhydrousorhydroxylated(e.g. hydrotalciteormonocarbonate)phasesinhydratedPCelimestone blends. The observation of a 1H-13C CP MAS NMR resonance in a hydrated PCelimestone blend exhibiting a chemical shift consis- tent with that of pure hydrotalcite (diso170.9 ppm) measured on thesameinstrumentshowedexplicitlythathydrotalciteformedin this hydrated cement contained carbonate anions[220].

4.2.8.6. Hydrogarnets. The hydrogarnet series (Ca3(AlxFe(1- x))2(SiO4)y(OH)4(3-y); 0 x 1 and 0 y 3) describes a group of garnet minerals where the (SiO4)4—tetrahedra are partially or completelyreplacedbyhydroxylions.InPChydratedatambient temperatures, the formation of siliceous hydrogarnet is minimal[331,356];however,formationofthesephaseshasbeenobserved in PC hydrated at higher temperatures [357e360] or in the pres- enceofexcessFespecies[357,361],andwater-richmembersofthe grossular - katoite hydrogrossular series (Ca3Al2(SiO4)y(OH)4(3-y); 0 ≤ y ≤ 3) are major hydration products in CACs[52].

Katoite (Ca3Al2(SiO4)y(OH)4(3-y); 0 y 1.5, often denoted C3AH6) exhibits a 27Al MAS NMR resonance with an isotropic chemical shift of diso¼ 12.4 ppm and a quadrupolar coupling constantCQ0.6MHz[52,362]duetooctahedralAlsurroundedby six hydroxyl groups in the hydrogarnet structure [51]. Increased substitution of silica into this structure results in a 27Al MAS NMR resonance at approximately diso¼ 4e6 ppm, with thisresonance shifting towards lower frequencies and exhibiting increased quadrupolar broadening with increasing silica content[50,362].

27AlMASNMRresonancesattributedtokatoitehavebeenobserved in CACs [50,52]and alkali-activated slags [20,155,197]. 29Si MAS NMR analysis of hydrated CAC attributed a broad resonance at approximately diso79.9 ppm to Si sites in [Si(OAlVI)4-x] (OCa)x species(classifiedasQ0inthenomenclatureofFig.1asthereareno bondstotetrahedralspecies;alloftheAlsubstituentsareoctahedral) andusedspectraldeconvolutiontoquantifythisphaseinthe hydrated CAC[50].

4.3. Spectraldeconvolution

4.3.1.Deconvolutionstrategiesandpitfallsrelatedtospectraof cementitiousmaterials

MathematicaldeconvolutionofMASNMRspectraallowsresolution of individual resonances which contributeto theoverallspectraandcanenablequantificationoftheresonatingspecies[60].Thesimplestcaseinwhichdeconvolutioncanbeperformedisfornon-quadrupolar(spins ½)nuclei,thespectraofwhichcanbedeconvolutedusingaseriesofGaussian,Lorentzianormixed(Voigtor pseudo-Voigt) peaks to simulate individual resonancesusingaleastsquaresfittingmethod[363].Thisisperformedroutinelyinthestudyofanhydrousandhydratedcementsandrelatedphases.The most appropriate lineshape to simulate theindividualres-onances forspinS ½ nuclei depends on the orderinganddy- namics of the material under investigation [364,365];fororderedandrigidSSsystems,aGaussian(statistical)distributionbestrep-resents the resonance lineshape as interatomicdistancesaregenerallyconstant.Forhighlydynamicsystems(e.g.solutionsorgases),aLorentziandistr ibution(basedoncollisiontheory)bestrepresents the resonance lineshapeas mobility is high[365].Consequently, resonance lineshapes forspinS ½ nucleiindynamicSSsystemsmaybebestrepresentedbyVoigtorpseudo-Voigt distributions weighted heavily towards aGaussianprofile.Inreality,dynamicsofsolidsincementitioussystemsareextremelyslow relative to those in solution, and a Gaussian distribution provides a suitable approximation for the resonance lineshapes.

Deconvolutionofthespectraofquadrupolarnuclei(S>½) isalsopossible;however,quadrupolarinteractionsmustbetaken into account when simulating the spectra (Fig. 27). Quadrupolar parameterscanbeestimated[21]; however,owingtothelarge variationinNMR parametersacrosssamplesandinstruments,this approach is prone to error must be appropriately justified. It is oftenmoreappropriate todeterminethequadrupolarparameters directly.

Quadrupolarinteractionscanbedeterminedbyacquiring single-pulseMASNMR spectraatmultiplefieldsandsimulatingthe NMR resonancesobservedforthecentraltransitionateachfield withaconsistentsetofNMRparameters(diso,CQandtheasymmetryparameterh)[30,172]; thisisoftenthemostreadilyimplementableapproachifinstrumentsatmultiplefieldsareavailableas itdoesnotrequirecomplex experimentsorfittingapproaches. Quadrupolar parameters canalsobe determined(alongwithdisoand h) at a single field by simulation of manifolds of spinning sidebandsobservedforsatellitetransitionsinMASNMRspectra [367e369],typicallyacrossspectralwidthsontheorderof 2MHz.

Thismethodcanbecomputationallyexpensiverelativeto simula- tion of single-pulse MAS NMRspectra.

Two-dimensional experiments such as MQMAS NMR techniques[242,255,370]arealsousedtodeterminediso,CQandh,and thus aid in deconvolution of NMR spectra for quadrupolar nuclei. MQMAS achieves high resolution by conversion of symmetricMQ coherence (pQ) to the single quantum (1Q) detectable central transition and plotting pQ and 1Q correlations in two dimensions [371].Consequently,chemicalshiftanisotropyisremovedfromthe MQ dimension, and disocan readily be determined from the two dimensionalMQMASspectrum.CQandhcanthenbedetermined by simulating the two-dimensional MQMAS spectrum or the pQdimension of this spectrum using readily available software (e.g. DMFit[60]orQuadfit[372]),informationwhichcaninturnbeused to simulate the single-pulse MAS NMR spectrum. A suitablemodel which incorporates these interactions should be used, e.g. the Czjzek model[373].

When performing any spectral deconvolution, the minimum possiblenumberofconstituentsubpeaksshouldbeusedto enable an accurate and meaningful interpretation of the spectra [363]. Subpeakwidthsshouldbesetinarationalmanner,consideringthe expecteddisorderwithineachsitetype,andtheirpositions mustbe consistentwithliteraturedataforspecificsitetypesinpure

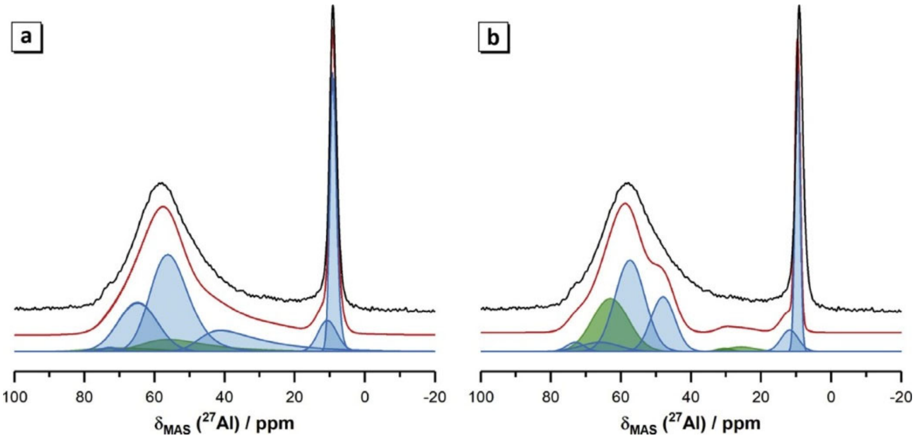

Fig. 27. 27Al (S 5/2) MAS NMR data of a synthetic (calcium, alkali) aluminosilicate gel deconvoluted using (a) the Czjzek isotropic model with quadrupolar parameters determined from 27Al MQMAS NMR data [366]and (b) Gaussian distributions. Deconvoluted resonances (bottom curves) attributed to sites within the precursor are shaded in green, deconvoluted resonances attributed to newly formed sites in the reaction product are marked in blue, the simulated spectrum is marked in red (middle curve) and the 27Al MAS NMR spectrum is marked in black (top curve). The distributions of chemical shifts (as defined by disoand FWHM) are the same in the deconvolutions in both (a) and (b); however, the simulated spectrum in (a) correctly accounts for quadrupolar broadening by using the Czjzek isotropic model, while the simulated spectrum in (b) is deconvoluted incorrectly usingGaussian distributionsanddoes notaccount forquadrupolar broadening.Asaresult,theintensitiesoftheresonancesattributedtoeach newlyformedsitediffer between(a)and(b),andadditionalresonancesmustbeaddedtothedeconvolutionin(b)toprovideasatisfactoryfit.Consequently,anyquantificationobtainedfrom(b)isincorrect.Adapted from Walkley et al.,[366].

materials.Therelativedeconvolutedsubpeakintensitiesshouldbe consistent with a mass balance for all elements, the structural constraintsdictatedbydatafromadditionalanalyticaltechniques (e.g.quantitativeXRD)andthosedescribedbyrelevantstructural models,e.g.the‘substitutedgeneralmodel’forC-S-Hgels[159],the ‘crosslinked substituted tobermorite model’ for C-(N)-A-S-Hgels [195]andthethermodynamicsofastatisticaldistributionofSiand Al sites within a Q4 aluminosilicate network for N-A-S-H products [250].

To provide an accurate representation of binder chemistry, andconsideringthattheconversionofsolidcementitious phasestohydrateproductsisalmostneverfullycompleteina practical cementing binder (even after decades or more), the contributionoftheremnantunreactedprecursortothespectra must be taken into account [13]. This can be achieved either through selective isotopic labelling of the binder [371], by subtraction of a scaled component spectrum for the remnant unreactedprecursorduringdeconvolutionifcongruentdisso- lution is assumed [18,20,345](Fig. 28) or by using the spec- trum of a leached residue (obtained via selective dissolution) to represent a residual precursor component if congruency is uncertain [315,345]. For quantitative analysis, the congruency and kinetics of dissolution and reaction processes involving cementitious precursor materials must be carefully considered and modelled appropriately [14,20]as the underlying assumptionscandramaticallyaffectthefinaldeconvolution.This canbeachievedbyavarietyofmethods,includingthoseused to measure the degree of reaction of SCMs in PCeSCM blends [374].Methodsincludeselectivedissolution[375],scanning electron microscopy [323,376], thermogravimetry [374]and XRD with iterative Rietveld refinement (e.g. the ‘partial or no knowncrystalstructure’,PONKCS,method[377])approaches.

Inapracticalsense,GGBFSisahighlydepolymerisedglassthat is likely to dissolve close to congruently [325], whereas FA is a much more complex mineral assemblage that dissolves incongruently[101,102].

Quantificationofindividualresonancescanoftenbecomplex, even with seemingly simple spectra of non-quadrupolar nuclei suchas29Si(seethefollowingsection).Quantificationof 27Al resonancescanbeparticularlydifficultduetothepresence ofAl specieswhichexhibitresonancessobroadthattheyareoften undetectable.‘NMRinvisible’Alspecieshavebeendescribed, largely in older literature, in zeolites, minerals and gels; up to 30% of all Al species in some zeolites could not be observed at 9.4 T [378].However,theseresonancesweredetectableathigh field (18.8T)[378],highlightingtheimportanceofacquiringSSNMR spectraatthehighestfieldpossibleifquantificationisdesired.

4.3.2. Complexities in quantification of tricalcium and dicalcium silicate inPC

The29Sispinelatticerelaxationtimeconstants(T01)for beliteareapproximately30timesthoseofaliteatthesame magneticfield[29],andconsequently,itiscrucialtoensure thatsufficientrecycledelaysareusedduringNMRdata acquisitiontoallowforcompleterelaxationofbothaliteand belite.Thiscanbeachievedviainversion-recovery29Si spinelatticerelaxationMASNMR[27,29](e.g.Fig.29)or T01-relaxation-time-filtered29SiMASNMR[57].Deconvolutionof suchdataallowsindependentquantification,andhencevalidation,oftherelativeproportionsofaliteandbelitewithin PC [27,29]. This work has shown that the determination of alite andbelitecontentinPCusingtraditionalBoguecalculations [379]strongly overestimates the belite content at the expense ofalite,consistentwith resultsfromXRDandothertech- niques; the modified Taylor-Bogue calculation [380]provides a much better match to the alite/belite ratio determined by 29Si MAS NMR spectral deconvolution [27].

4.4. DFT computation of NMR spectra andparameters

Isotropicchemicalshifts,couplingconstantsandelectric fieldgradientsofmoleculescanalsobepredictedabinitio from calculations using DFT [381,382]and used to simulate NMR spectra. Computation of NMR parameters from DFT is widelyusedtodeterminethecrystalstructure andorderingin ceramics, zeolites and other crystalline materials; however, therehasbeenlittleapplicationofthisapproachtothephases in cementitious materials. Rejmak et al. [165,166]performed simulations of various C-S-H gel structures based on 14 Å tobermoriteandjennitemodelsandcalculatedtheresultant isotropic29Sichemicalshifts.Calculatedchemicalshifts forQ2siteswerefoundtobelargelyindependentofthestructural modelused,andQ1andQ2siteseachshowedalargedisper- sion of calculated chemical shifts. The calculated 29Si MAS NMRchemicalshiftswerefoundtobeingoodagreement with those of 14 Å tobermorite. This work also showed that terminalsilicatesites(Q1),andpairedsilicatetetrahedrawith an AlO4 unit within the first coordination sphere (Q2(1Al)), which exhibitsimilarisotropicchemicalshifts,maybedistinguished easily by large differences between their chemical shift an- isotropies[166].

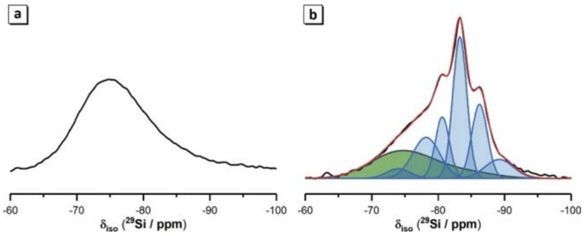

Fig. 28. 29Si MAS NMR spectra (14.1 T, nR¼ 10 kHz) of (a) an anhydrous slag and (b) a sodium silicateeactivated slag cement (shown in black) with associated deconvolutions (individualresonancesareshowninblueandthesimulatedspectrumisshowninred).Theshadedgreenresonanceisarepresentationoftheunreactedanhydrousslagcomponent andisbased onthe29Si MASNMRspectrumofthe anhydrousslag,withtheintensityof thisresonancerescaledbyasinglefactorontheassumptionofcongruentdissolution ofslag. Adapted from Bernal et al.[20].

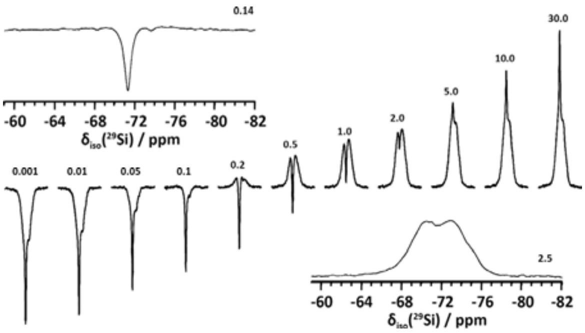

Fig. 29. Inversion-recovery 29Si MAS NMR spectra (9.4 T, nR12.0 kHz) of white PC, illustrating the differences in spinelattice relaxation for alite and belite. The left and right expansionsshowsubspectraofbeliteandaliteobtainedatthezero-crossingsfor29Siinaliteandbelite,respectively.Therecoverytimes insecondsareindicatedfortheindividual spectra. Adapted from Poulsen et al.[29].

Ab initio prediction of NMR parameters from calculations using DFT is yet to be applied extensively to cementitious materialsand represents an important opportunity for further advancement. In particular, combining DFT predictions with experimental dataac- quired at high field of synthetic model systems will reveal impor- tant new structural insights which may then be used to untangle many remaining questions in more complex, heterogeneous systems.

4.5. Application of advanced NMR experiments to cementitious materials

4.5.1. Spin-echo MASNMR

MASNMRspectracontainingbroadresonances,suchasthoseofdisorderedcementitioussystems,canexperienceartefactsanddistortionintroducedinthefirstfewmicrosecondsofinstrumentaldeadtimeatthebeginningofthefreeinductiondecay[10].Spin-echopulsesequences[383]canbeusedtoovercomethisby refocussingthespinsystem.Thespinsystemisgivenaninitialnon-selective(90○)pulse,afterwhichthespinsareallowedtoprecess anddephase(duetothevaryingprecessionratesofindividualnuclearmomentswithinthesystem).Applyinga180○ pulseaftera timeTflipsthespinsystemandrestoresphasecoherencetotheprecessionatatime2Tafterthefirst90○pulse,refocussingthespin system[10,383].Asmallnumberofauthorshaveusedspin-echo pulsesequencesanalysing cementitiousmaterialstoaccuratelyquantifythesitespresentinthesesystems[8,260,299,384].

4.5.2. Cross polarisation MASNMR

CPMASNMRinvolvestransferofmagnetisationfromanucleus with more abundant spins to a nucleus with less abundant spins, allowing acquisition of the NMR spectrum of the less abundant nucleus with a much higher signal-to-noise ratio than would be obtained by MAS NMR [10]. This is achieved by irradiation of the two nuclei at their correct Larmor frequencies in fulfilment of the HartmanneHahn condition [385]. The signal from the less abundantnucleusinclosestproximitytothemoreabundantnucleusis preferentially enhanced, and so additional structural information canbegainedbycomparisonofCPMASandMASspectra ofthe samesample.1Histhemostcommonhigh-abundancenucleusin cementitious materials, and consequently, this technique canbe particularly advantageous for probing local environments in cementitious materials where the structural role of water is of interest.

4.5.2.1. 1H-X CP MAS. 1H-29Si CP MAS was used to examine hy- dration of b-C2S and show that the initial hydration products contain monomeric silicate hydrates, the amount of which de- termines the initial hydration rate [386], while 31P MAS and 31P-1H CP MAS NMR were used to demonstrate that the very small quantity of PO3—ions involved in the hydration of white PC are accommodated within the interlayer of C-S-H [32,34]. Interlayer PO3—ions exhibit a broad 31P resonance with the same chemical shift as that of PO3—guest ions in alite, so must be selectively detected using 31P-1H CP MAS techniques. 1H-29Si CP MAS NMR (Fig.30)hasalsobeenusedtoidentifySispeciescloselyassociated withwater(i.e.Si-OHlinkages) thatarelikely toexistaspart ofthe C-S-H gel [43,167,185,386e392], C-(N)-A-S-H gel or AFm phases in alkali-activated slag [154,196], metakaolin [242] and synthetic C-(N)-A-S-H gels [14], while 1H-27Al CP MAS NMR has also been used to identify Al-OH linkages in synthetic analogues of PC hydration products[393].

13CMASand1H-13CCPMASNMR havealsobeencombinedto studycarbonation ofsyntheticC-S-HandC-A-S-Hgels[221]andto determinetheNMRparameters ofinorganiccarbonates relevantto cement chemistry [220]. During early studies of TAH, 1H-27Al CP MAS NMR revealed Al(OH)3—units closely associated with C-S-H, leadingtotheidentificationoftheTAHasanamorphousaluminate hydroxide or calcium aluminate hydrate produced either as a separatephaseorananostructuredprecipitateonthesurfaceofthe C-S-H gel [194]. 1H-29Si and 1H-27Al CP MAS NMR experiments are also particularly useful for constraining 29Si and 27Al MAS NMR spectral deconvolutions of the C-S-H model system tobermorite and C-A-S-H gels[14,393].

4.5.2.2. X-Y CP MAS. Studies using X-Y CP MAS NMR experiments (thatis,thoseCPexperiments whichdonotprobeprotons) tostudy cementitious materialsarefewer; however,theyhavestillrevealed new insight into the interactions in these materials. 17O-27Al CP MAS NMR has been used to support a claim that Al atoms within GGBFSareconnectedonlytobridgingoxygenatomsand notnon- bridgingoxygenatoms [75].19F-29SiCPMASand19F-29SiCPREDOR MASNMRtechniqueshavebeenusedtoshowthatF— substitutes for O2—ions in only the alite phase in white PC, as discussed pre- viously in section 4.1.1.1, aligning with the proposed Si4þO2—/ Al3þF— coupled substitution mechanism [35], with 19F-29Si CP REDORMASNMR indicatingastrongpreference forF—substitution into interstitial oxygen sites not involved in covalent Si-Obonds.

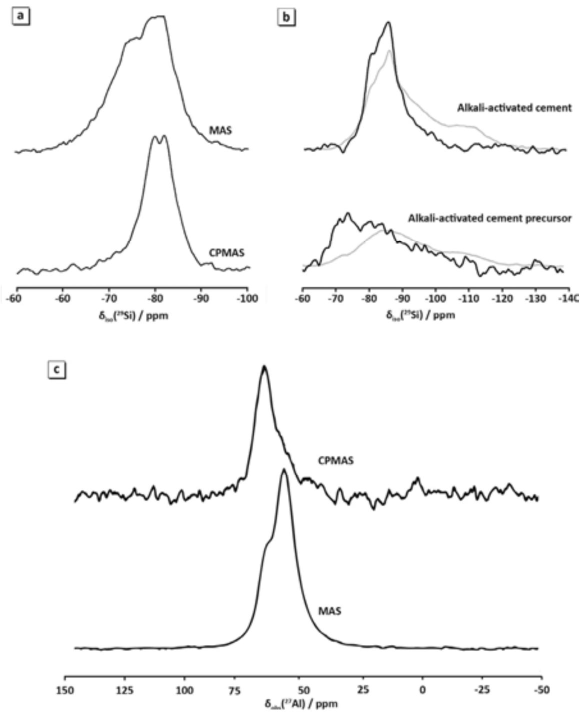

Fig.30.(a)1H-29SiCPMASandMASNMRspectraofblastfurnaceslagactivated with 4MNaOHandcuredfor1day.AdaptedfromWangetal.[154].(b)Single-pulse29Si(grey)and 1H-29SiCP(black)MASNMRspectraofasyntheticcalciumaluminosilicateprecursorandofasyntheticalkali-activatedcementproducedfromit(containingC-(N)-A-S-H),curedfor 3days.Allspectraarenormalisedtoconstanttotalintensity.AdaptedfromWalkleyetal.[14].(c)1H-27AlCP-MASNMRoftobermorite.AdaptedfromHoustonetal.[393].

4.5.3. Multiple quantum MASNMR

Recently,MQMASspectroscopy[394,395],probinghalfinteger quadrupolarnucleiincluding17O,23Na,and27Al,hasbeenusedto obtain high-resolution NMR spectra of synthetic C-S-H [188], CAC [276], AAM [113,242,252,256,276,370,371,396], related reaction products [137,276,354,355,397]and precursors [34,36,75,138]. MQMAS achieves high resolution by conversion of symmetricMQ coherence (pQ) to the single quantum (1Q) detectable central transition, and plotting pQ and 1Q correlations in two dimensions [371]. Consequently, chemical species with similar localstructures andcoordinationenvironments,whichwouldotherwiseresultin overlapping resonances in one-dimensional MAS NMR spectra, may be resolved.

27Al 3Q MAS NMR has been used to examine symmetry of Al siteswithinsyntheticcalciumaluminatehydratesandtoobtainthe isotropic chemical shift, quadrupolar coupling constant and asymmetry parameter of these sites [276]. 27Al 3QMAS NMR spectraofthesematerialsresolvedadditionalAlsitestothosethat could not be obtained by 27Al MAS NMR alone, including two Al sites within C4AH13[276]. 27Al 3Q MAS NMR has also been used to probe Al substitution in C-S-H gels [276,393], identifying two distinct tetrahedral Al sites that were attributed to Al substitution forSiintobothbridgingandnon-bridgingpositions[276],although other studies (as discussed in section 4.2.1.1) have shown that bridging positions are a strongly preferred environment. 27Al 3QMASNMRhasprovidedadditionalinsightintocoordinationand symmetry of Al environments within N-A-S-Hetype gels (Fig. 31a and b), including determination of the isotropic chemical shift (diso), quadrupolar coupling constant (CQ) and asymmetry (h) parameter of the electric field gradient tensor

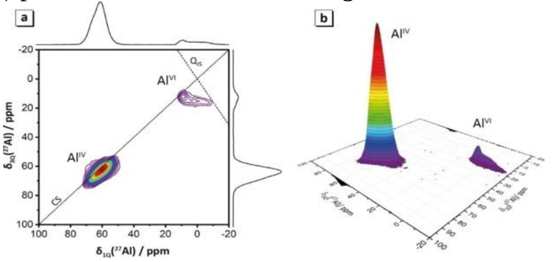

Fig. 31. (a) 27Al MQMAS NMR spectrum (14.1 T, nR¼ 20 kHz, room temperature) of a synthetic alkali-activated cement containing a N-A-S-H gel (adapted from Walkley et al. [255]) and (b) a three-dimensional representation of the spectrum shown in (a).

[113,242,255,256,370,371,396] and also Al environments in C-A-S- H/N-A-S-H gel blends [396]. Both 27Al 3QMAS NMR [276] and 25Mg 3QMASNMR[354]havealsobeenusedtoresolveindividualAland Mg sites within Mg-containing LDHs, while recent work used 27Al MQMAS NMR to resolve for the first time 8 distinct Al sites in ye'elimite [34,138] and high-field 27Al MQMAS NMR to resolve for the first time two distinct octahedrally coordinated AlO6 sites in synthetic ettringite [137](see section 4.2.8.2‘Aluminate ferrite trisulphate’etype phases). MQMAS NMR, therefore, appears to offersignificantscopeforfutureadvancesintheunderstandingthe atomic structure ofcements.

Processing of MQMAS spectra using standard single-axial isotropic shearing (iso-shearing) in the indirect dimension removes the second-order quadrupolar term and leaves the projectionofthespectraontotheindirectdimensionaxisasapure function of isotropic variables such as the isotropic chemicalshift (diso)andthequadrupolar-inducedshift(dQIS), allowingchemically distinct sites to be resolved in the indirect (pQ) dimension [242,371,398,399].Themorerecentlyintroducedmethodofbiaxial Q-shearing [371] in both the indirect and direct dimensions allows orthogonalseparationofdisofromthequadrupolarparametersdQISand the quadrupolar coupling constant (CQ) and is particularly useful for disordered materials which typically give MQMAS spectradisplayingadistributionofchemicalshiftandquadrupolar parameters, that can be difficult to interpret for identification of chemically distinct sites[113,371].

4.5.4. Multiple resonance experiments

4.5.4.1. REDOR, TEDOR, TRAPDOR and REAPDOR. REDOR [400e402]and transferred-echo double-resonance (TEDOR) [403e405] are multiple resonance MAS NMR experiments whichexploitheteronucleardipolarcouplinginspin-½nuclei and provide both qualitative and quantitative information about the proximity of the two spins. Transfer of population in double-resonance (TRAPDOR) [406,407] and rotational-echo adiabatic passage double-resonance (REAPDOR) [400,408]experiments extend the principlesofREDORandTEDORtoquadrupolarnuclei.Itshouldbe noted that the X{1H} REDOR and 1H-X CP MAS NMR techniques (where X 27Al or 29Si) provide complementary data; X{1H} REDOR MAS NMR experiments selectively suppress resonances of protonatedspecies,while1H-XCPMASNMRexperimentsenhance thesignalsofspeciesexperiencingdipolarcouplingwithrigid

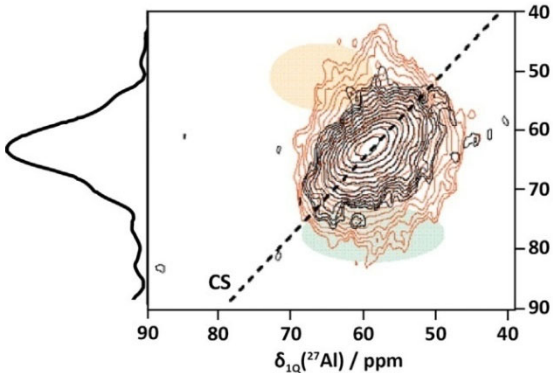

Fig.32.Isosheared ^{27}Al{1H}REDOR3Q/MASNMRspectrum(blackcontours)overlaid onanisosheared ^{27}AlMQMASNMRspectrum(redcontours)ofasodiumsilicate-reactivated metakaolin cement. Adapted from Brus et al. [242]. The main resonance resultspredominantlyfromAlO—4tetrahedrachargebalancedbyNaþions,andthe shadedorangeandgreenareasindicateregionswhereAlO—4tetrahedraconnectedto SiO4tetrahedraviabridginghydroxylgroups(AlIVeOHþeSiIV)andAlO—4tetrahedra chargebalancedbyextra-frameworkAlspeciesareexpectedtoresonate,respectively.

proton species (i.e. terminal hydroxyl groups, strongly bound H2O etc.) [242].

Brus et al. [242] applied 27Al{1H} REDOR 3Q MAS NMR (Fig. 32) to identify bridging hydroxyl groups connecting AlIV and SiIV tetrahedrainaseriesofalkali-activatedmetakaolincements,supporting the identification (see section 4.2.2) of charge balancing extra-framework Al species in these systems. 29Si{1H} REDOR 3Q MAS NMR has also been applied to a series of aluminosilicate geopolymers[370]toshowthatthesematerialscontainaheterogeneousdistributionofcharge-balancingNaionsandassociated water molecules, with the Na ions and water molecules preferentially clustered around fully polymerised Q4(4Al) Sispecies.

Recently, Greiser et al. [409] used 29Si{27Al} TRAPDOR NMR, 27Al {29Si} and 27Al{1H} REDOR NMR experiments to reveal new information regarding the phase assemblage and nanostructure of cementitious sodium aluminosilicate gels produced via the one-part alkali-activation route using variety of silica sources. This workshowedtheextentofformationofanamorphoussodium aluminosilicate gel, coprecipitation of an amorphous hydrous aluminagel(Al(OH)3)andformationofzeoliticphasesaredependent on the silica source, despite very similar Si/Al of the starting reactionmixtures.TheidentificationofamorphousAl(OH)3hasnot beenpreviouslyreportedanddemonstratestheimportanceofusing double-resonance NMR techniques to resolve multiple overlapping 27Al resonances that are often present in single-pulse 27Al MAS NMR spectra (Fig.33).

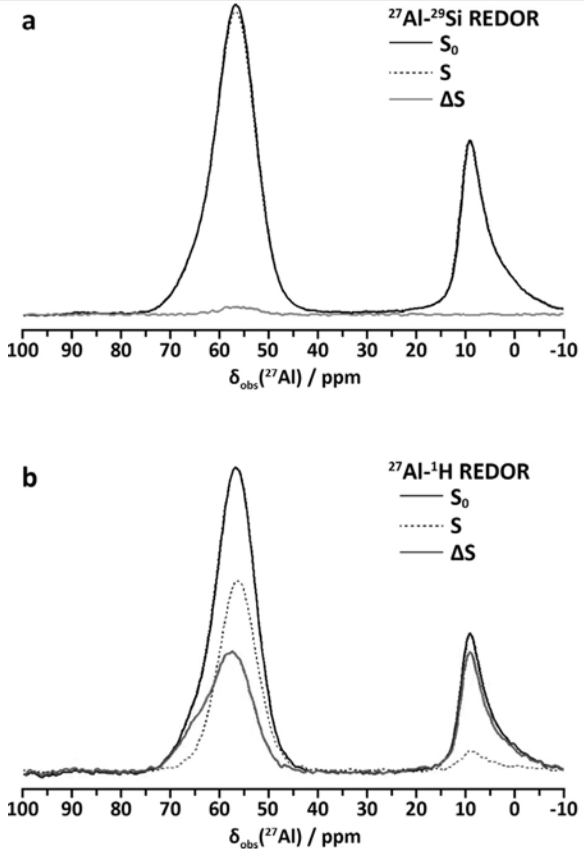

Fig. 33. (a) 27Al{29Si} and (b) 27Al{1H} REDOR NMR spectra (S, dashed line) overlaid with 27Al MAS NMR spectra (S0, black line) and difference spectra (DS ¼ S0e S, grey or blue lines) of a cementitious sodium aluminosilicate gel produced via one-part alkali- activation of rice husk ash. Adapted from Greiser et al. [409]. The AlO6 resonance (dobs¼ 8 ppm) does not show a discernible 27Al—(29Si) REDOR NMR effect and shows a strong 27Al—(1H) REDOR interaction, demonstrating that this resonance is due toAlO6 within a hydrous alumina gel (Al(OH)3) with little or no Si in proximity.

Tran et al. [396] used a 29Si{27Al} REAPDOR NMR technique to distinguish between Si-O-Al connectivity environments in alkali- activated metakaolin and to identify the number of Al atoms substituted in the second coordination sphere of each probed Si site. The same authors also used 29Si and 27Al MAS, 19F-29Si CP MAS and 29Si{19F} CP REDOR MAS NMR techniques to show that F—substitutesforO2—ionsinonlythealitephaseinwhitePC,with29Si {19F} CP REDOR MAS NMR indicating a strong preference for F—substitution into interstitial oxygen sites not involved in covalent Si-Obonds,demonstratingalimitationontheachievabledegreeof fluoridesubstitutionintoalite.31P-27AlREAPDORNMRhasalsobeenusedtodemonstratetheexistenceofaluminiumephosphorus interactions within phosphate-modified CACs [277], where no other analytical technique was able to provide direct evidence about the existence (or otherwise) of these bonds within the disorderedgelsystemsofinterest.TheuniversalREAPDORcurve [410]which is commonly used to fit REAPDOR NMR data and determineinternucleardistancesis,however,specifically designed foranisolatedspinpair(i.e.monodentatestructures)whichlimits itsapplicability(inaquantitativesense)tothepolydentate struc- tures which comprise mostcements.

4.5.4.2. 2D homonuclear correlation MAS NMR spectroscopy. 2D homonuclear correlation MAS NMR spectroscopy (COSY) is a multiple resonance MAS NMR experiment involving transfer of magnetisationbetweentwonucleiofthesameisotopeandisuseful for determining connectivity between different sites when many resonances are present. Double quantum 29Si-29Si COSY experi- ments on synthetic C-S-H isotopically enriched with 29Si has resolvedbothdimeric(Q1-Q1)andchainendgroup(Q1-Q2)Sisites as well as (Q3-Q3) and (Q3-Q2) bridging linkages [176], confirming the presence of these sites in C-S-H as discussed in section4.2.1.

4.5.4.3. 2D heteronuclear correlation MAS NMR. 2D HETCOR MAS NMRisamultipleresonanceMASNMRexperimentwhichinvolves transfer of magnetisation between two heteronuclei and isuseful fordeterminingconnectivitybetweendifferentnucleiwhenmany resonances are present. This experiment is similar to the X-Y CP MAS NMR experiment; however, in the X-Y 2D HETCOR experi- ment, the magnetisation of nucleus Y is allowed to evolve for a (variable) time t1 prior to being transferred to nucleus X, whose response is measured directly during the detection period t2[10]. Significantsensitivityenhancementcanbegainedbycombining MQMAS with the HETCOR experiment (HMQC) [411]. Rawal etal.

[57] used 1H-29Si and 1H-27Al HETCOR MAS NMR with different 1H spin-diffusion times to probe correlations between different mo- lecular moieties in hydrated white PC: both short (10 ms, probing strongly coupled species with internuclear distance <1 nm) and long (30 ms for 29Si and 20 ms for 27Al, probing more weakly coupled species over several nm), Fig. 33. 1H-29Si HETCOR MAS NMR experiments were able to resolve chemically bonded -OH groups,adsorbedwaterandstrongly hydrogenbonded-OHgroups associatedwith Q1,Q2andQ2(1Al) Sisites,withchemicallybonded -OHgroupsandadsorbed waterprimarilyassociated withQ1and Q2(1Al)sites,aswellaswaterstronglyadsorbedtosix-coordinateSi siteswithinathaumasite-likephasethatwasclaimedtobepresent inthehydratedPC[57],althoughtheidentificationofthis mineral incementsthathavenotbeensubjectedtochemicaldamag

eis extremelyuncommon.
ResonancesfromprotonsinH2O,Ca-OHandSi-OHgroupshave also been identified by 1H-29Si HETCOR MAS NMR analysis of synthetic C-S-H [176], with both types of hydroxyl sites correlating with all Si sites in C-S-H and water molecules correlating with Q1 and both bridging and pairing Q2 sites. 1H-27Al HETCOR MAS NMR experiments resolved hydroxyl groups chemically bound to AlVI sites within ettringite and TAH and an absence of correlation be- tween 1H species and four-coordinate 27AlIV moieties. Enhanced resolution provided by the 1H-29Si and 1H-27Al HETCOR MAS NMR experiments allowed resolution of 29Si-OH and 27Al-OH bonds which were not resolved in single-pulse MASNMR experiments.

4.5.4.4. Satellite transition spectroscopy. Accurate determinationof diso, CQ and h is crucial for an accurate and unambiguous interpretation of SS MAS NMR spectra. Determination of these parameters from single-pulse MAS NMR spectroscopy observing the central transition (mS± ½) between nuclear spin states, however, is hindered due to the second-order quadrupolar shift. Satellite transition spectroscopy involves observing the satellite transitions in MAS NMR spectra of quadrupolar nuclei, where residualsecond-orderquadrupolareffectsunderMAS(quadrupolar broadeningandthesecond-orderquadrupolarshift)arereduced relative to the central transition [367]. The dependence of the second-order quadrupolar shift for a particular spin S on the nu- clear spin state transition (m) results in a different net isotropic chemicalshiftforeachm;consequently,bysimulatingall observed transitions, it is possible to determine the isotropic chemical shift from a single spectrum [367e369]. Jakobsen et al. [412]and Skibsted et al. [368] demonstrated simulation of all transitions in MAS NMR spectra of crystalline powders toaccurately determine CQ and h for 17O, 23Na and 27Al in systems with large CQ values (CQ>2 MHz), as well as applying this method to accurately determinethe27AlCQvalueof1.9MHzforAlVIinhydratedwhitePC [44]. Skibsted et al. [52]also applied this method to a series of calciumaluminatephasesinCACandinPC(Fig.34),determining 27Aldiso,CQandhvaluesanddistributions.Thesewerethenusedto describelinearrelationshipsbetweenCQandthemeandeviationof bondanglefromidealtetrahedralsymmetry,aswellasbetweenCQandacalculatedestimateofthegeometricaldependencyoftheEFG tensor. This method has also been used to identify the two crys- tallographically distinct octahedrally coordinated Al sites in kaolinite [413], as specified by its crystal structure[414].

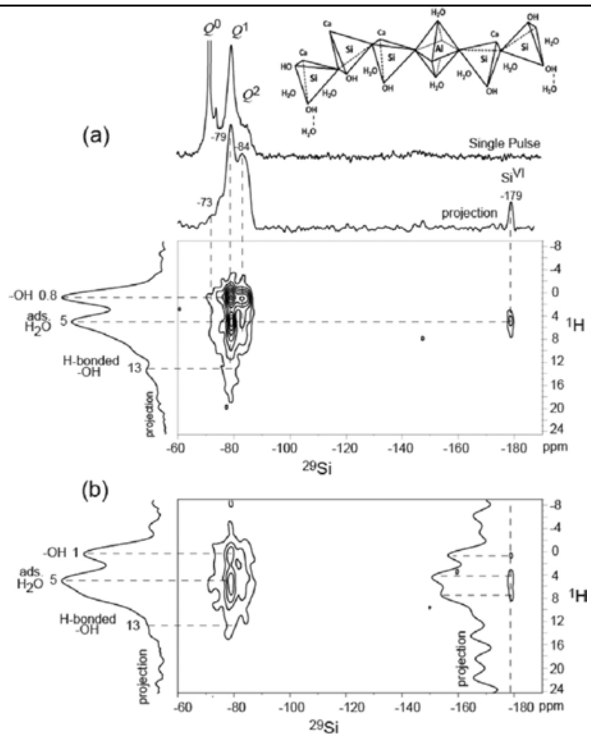

Fig. 34. 1H-29Si HETCOR MAS NMR (11.7 T, nR¼ 6.5 kHz) of white PC with 1H spin- diffusion times of (a) 10 ms and (b) 30 ms. Adapted from Rawal et al. [57].

4.5.5. 1H relaxationNMR
1Histhemostsensitivenucleusincementitiousmaterials which maybeprobedusingNMR;however,1H-1Hdipolarcouplingscause severe line broadening which limits the resolution of 1H MAS NMR spectra, which is further compounded by the small chemicalshift range(approximately20ppm)overwhich1Hnucleiinsolidphases resonate. These limitations have impeded the widespread appli- cation of single-pulse MAS NMR experiments probing 1H in cementitiousmaterials.However,1Hrelaxationrates(spinelattice, 1/T1, and spinespin, 1/T2) are sensitive to proton mobility in hy- dration products and water in the vicinity of solideliquid interfaces and can therefore provide extensive information regarding porosity, pore size distributions and tortuosity in these cementitiousmaterials.
EarlyworkusedprotonNMRrelaxometrytomonitorhydration of C3S and PC by measurement of T1 and T2 relaxation times [415e421],identifyinganinductionperiod(~3h)[417]aswellas waterinvarioushydratephases[416],mobilewaterinmicropores and water with restricted mobility in a solid gel component [420,421].
Spinespinrelaxationratesaremodulatedbythemotionofthe speciesonwhichthespinsresideandvarybyseveralorders of magnitudeforprotonsinrigid(e.g.solidhydrates)ormobile(e.g. molecular water) species. Rapid measurements

of spinespin relaxationratesare,therefore,particularlyattractivetomonitor reactionin-situ[22].Thisapproachhasbeenusedtomonitorhydrationofwhite PC,andsyntheticC3SandC3A[422e424],andled toidentificationoffivecomponentswithdistinctT2values corre- spondingtocapillaryporewater,solid-likecrystallinewaterand OH—groups(i.e.inportlandite,gypsum,andettringite),mobile water molecules incorporated in CeSeH, water moleculeswith restrictedmobilityintheCeSeHinterlayerandsecondary hydrationwaterreleasedbythedecompositionofettringite(Fig. 35).

Spinespin relaxation times have also been used to observethe retardationofPChydrationinthepresenceofvariousorganicad- ditives [425]. 1H relaxation rates can also be exploited to link the structureandkineticsattheatomiclevelofcementitiousmaterials to microscale and macroscale engineering properties such as porosity, pore size distributions and tortuosity in hydrated cement pastes, mortars and concretes. Measurement of spinelattice relaxationrateshasbeenusedtodeveloprelaxationmodelsforthe dependencyofT1ontheporesurfacetothevolumeratioandthe presence of nearby paramagnetic ions [426e429], while T1-T2[427,428] and T2-T2[430,431] correlation NMR experiments have been used to identify discrete pores (e.g. large capillary pores or smallergelpores,Fig.36)inhydratedwhitePCandsyntheticC-S- H and measure exchange of water between these locations, by exploitationofthefactthatincreasedporesizeresultsinincreased relaxation times. Variable temperature proton NMR relaxometry experiments have also been used to monitor freezeethaw phe- nomena in hydrated PC and C-S-H[432,433].

More recently, 1H NMR relaxometry has been used toquantify all the water present, as well as the size and volume of discrete population of pores containing this water, in hydrated white PC both with [8]and without [434,435]silica fume additions. This work showed that addition of silica fume alters the chemical composition of the C-S-H formed, but does not alter the density, and identified four discrete populations of liquid water: water in the C-S-H interlayer in pores approximately 1 nm in diameter, waterintheC-S-Hgelinporesapproximately3nmindiameterand waterinsmall(~10nmindiameter)andlarge([10nmin diameter)capillarypores.Correlationof1HNMRrelaxometrywith results from mercury intrusion porosimetry (MIP) has shown that MIPcanaccuratelydeterminetheporosityofcementpastes[436].

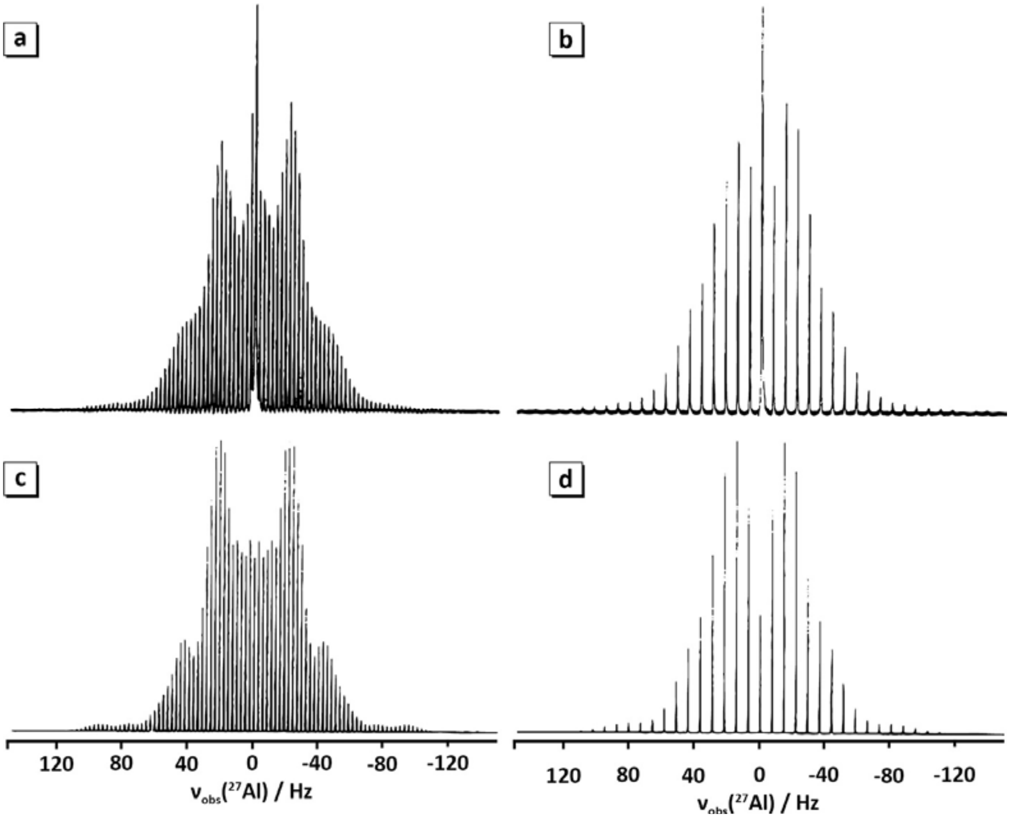

Fig. 35. 27Al MAS NMR spectra of ettringite (C6A$3H32) recorded at (a) 9.4 T, nR¼ 6.5 kHz, and (b) 9.4 T, nR7.5 kHz. Simulations of the satellite transitions in parts (a) and (b) are shownin(c)and(d).AdaptedfromSkibstedetal.[52].

V. CONCLUSIONS AND PERSPECTIVES

SS NMR spectroscopy has played a pivotal role understanding the complex compositionestructureeproperty relationships in cementsandrelatedmaterials.Inparticular,SSNMRspectroscopy hasaffordedalevelofinsightintotheiratomicstructure,reaction mechanisms, kinetics of formation and structural evolution which hasbeenpreviouslyunattainableandhasprovidedthebasisforthe currentstateoftheartinunderstanding,modellingandpredicting compositionestructureeproperty relationships, reaction mechanism and kinetics in PC, CAC, CSA, magnesia-based, AAM and geopolymer-basedcements. ApplicationofadvancedMASNMRexperimentsprobing1H,13C, 17O,19F,23Na,25Mg,27Al,29Si,31P,33S,35Cl,39Kand43Canucleihave beenusedtostudytheatomicstructure,phaseevolution,nano-structuraldevelopment,reactionmechanismsandkineticsoccurring in these cementitious systems, including multidimensional, multiresonance and in-situ experiments. Single-pulse MASNMR experiments probing 27Al and 29Si nuclei are by far the most routinelyappliedNMRexperimentsusedtostudycementsand have been instrumental in building our current understanding. However,owingtotheextensivestructuralinformationtheseexperimentshaveprovidedtodate,theirroleincontinuedadvancement of the understanding of compositionestructureeproperty relationships in cementitious materials islimited.

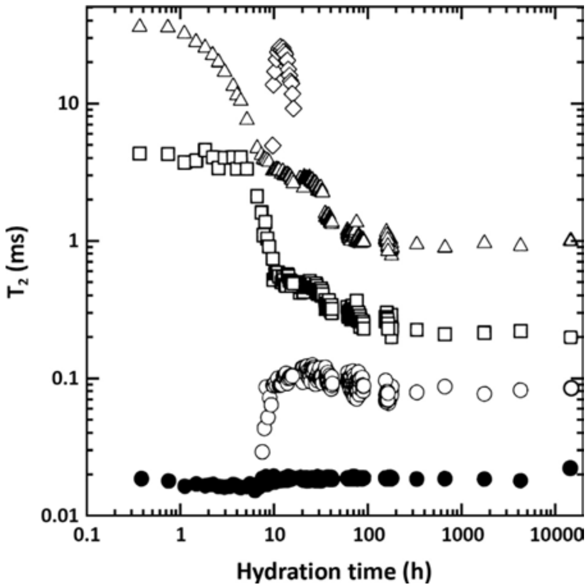

Fig. 36. Proton spinespin relaxation times (T2) vs. hydration time of white PC hydrated at 20 ○C. Proton signals come from water molecules in the pore solution (triangles), crystalline water and OH—groups (filled circles) in C-S-H and portlandite, more mobile water molecules in the interlayer of C-S-H (squares) and secondary hydration water released by the decomposition of ettringite (diamonds). Adapted from Holly et al. [422].

Performing NMR experiments at high field (B020.0 T), probing less commonly investigated nuclei such as 17O and 43Ca in isotopically enriched samples and application of less commonly used techniquesincludingCPMAS,MQMASandmultiresonanceexperiments (e.g. SEDOR, REDOR, TEDOR, REAPDOR and TRAPDOR) presents the best opportunity for elucidation of information regardingthemechanismswhichcontrolthestructureand physical properties of cementitious materials, that has been previously unattainable. The difficulty in conducting these experimentsandinterpretationofthespectraobtained,however, islikely tobethelargestobstacletotheirroutineapplication.Thispresents a key challenge which must be overcome and will require a concerted,collaborativeeffortfrombooththeSSNMRspectroscopy and cement materials chemistrycommunities.

CONFLICT OF INTEREST

The authors declare no conflict of interest.

ACKNOWLEDGEMENTS

The authors thank and acknowledge Dr John Hanna, Dr Greg Rees,DrFre´de´ricBlanc,DrMarc-AntoineSani,DrPeterDuxson,Dr JohnGehman,DrSusanBernalandDrRupertMyersforveryhelpful and insightful discussions over many years regarding theapplication of SS NMR to cementitious materials. The research leading to these results has received funding from the Engineering and Physical Sciences Research Council (EP/P013171/1) and from the European Research Council under the European Union's Seventh FrameworkProgramme(FP/2007-2013)/ERCGrantAgreementStG 335928(GeopolyConc).

APPENDIX A. SUPPLEMENTARY DATA

Supplementary data to this article can be found online at https://doi.org/10.1016/j.mtadv.2019.100007.

REFERENCES

[1] P.-C. Aïtcin, Cements of yesterday and today: concrete of tomorrow, Cement Concr. Res. 30 (2000)1349e1359.

[2] World Business Council for Sustainable Development, Cement Industry En-ergy and CO2Performance: ‘Getting the Numbers Right’,2009.

[3] P. Hewlett, Lea's Chemistry of Cement and Concrete, Elsevier Science,1998.

[4] J.L. Provis, S.A. Bernal, Geopolymers and related alkali-

activated materials, Annu.Rev.Mater.Res.44(2014)299e327.

[5] L. Bernstein, J. Roy, K.C. Delhotal, J. Harnisch, R. Matsuhashi, L. Price, et al., Industry, in: B. Metz, O.R. Davidson, P.R. Bosch, R. Dave, L.A. Meyer (Eds.), Climate Change 2007: Mitigation. Contribution of Working Group III to theFourth Assessment Report of the Intergovernmental Panel on ClimateChange, Cambridge University Press, Cambridge, United Kingdom,2007.

[6] J.G.J. Olivier, G. Janssens-Maenhout, J.A.H.W. Peters, Trends in Global CO2 Emissions; 2012 Report, PBL Netherlands Environmental AssessmentAgency, The Hague, Netherlands,2012.

[7] B. Lothenbach, K. Scrivener, R.D. Hooton, Supplementary cementitious materials,CementConcr.Res.41(2011)1244e1256.

[8] A.C.A. Muller, K.L. Scrivener, J. Skibsted, A.M. Gajewicz, P.J. McDonald, In-fluence of silica fume on the microstructure of cement pastes: new insights from1HNMRrelaxometry,CementConcr.Res.74(2015)116e125.

[9] A.M. Gajewicz, E. Gartner, K. Kang, P.J. McDonald, V. Yermakou, A 1H NMR relaxometry investigation of gel-pore drying shrinkage in cement pastes, Cement Concr. Res. 86 (2016)12e19.

[10] K.J.D. Mackenzie, M.E. Smith, Multinuclear Solid-State Nuclear Magnetic Resonance of Inorganic Materials, Pergamon, Elsevier, Oxford,2002.

[11] G. Engelhardt, D. Michel, High-resolution Solid State NMR of Silicates andZeolites, Wiley, Chichester,1987.

[12] S.E. Ashbrook, Recent advances in solid-state NMR spectroscopy of quadrupolarnuclei,Phys.Chem.Chem.Phys.11(2009)6892e6905.

[13] J.L. Provis, A. Palomo, C.J. Shi, Advances in understanding alkali-activated materials,CementConcr.Res.78(2015)110e125.

[14] B.Walkley,R.SanNicolas,M.-A.Sani,G.J.Rees,J.V.Hanna,J.S.J.vanDeventer, et al., Phase evolution of C-(N)-A-S-H/N-A-S-H gel blends investigated viaalkali-activation of synthetic calcium aluminosilicate precursors, CementConcr. Res. 89 (2016)120e135.

[15] E´.M.L'Ho^pital,B.Lothenbach,G.LeSaoût,D.Kulik,K.Scrivener,Incorpora-

[16] tionofaluminiumincalcium-silicate-hydrates,CementConcr.Res.75(2015)91e103.

[17] J. Skibsted, M.D. Andersen, H. Jennings, The effect of alkali ions on the incorporation of aluminum in the calcium silicate hydrate (C-S-H) phaseresulting from portland cement hydration studied by 29Si MAS NMR, J. Am. Ceram. Soc. 96 (2013)651e656.

[18] I.G. Richardson, The calcium silicate hydrates, Cement Concr. Res. 38 (2008)137e158.

[19] G. Le Saoût, M. Ben Haha, F. Winnefeld, B. Lothenbach, C. Jantzen, Hydration degree of alkali-activated slags: a 29Si NMR study, J. Am. Ceram. Soc. 94 (2011)4541e4547.

[20] W.Loewenstein,Thedistributionofaluminuminthetetrahedraofsilicates and aluminates, Am. Mineral. 39 (1954)92e96.

[21] S.A. Bernal, J.L. Provis, B. Walkley, R. San Nicolas, J.D. Gehman, D.G. Brice, et al., Gel nanostructure in alkali-activated binders based on slag and fly ash,and effects of accelerated carbonation, Cement Concr. Res. 53 (2013) 127e144.

[22] R.J.Myers,S.A.Bernal,J.D.Gehman,J.S.J.vanDeventer,J.L. Provis,TheroleofAl in cross-linking of alkali-activated slag cements, J. Am. Ceram. Soc. 98(2015)996e1004.

[23] J. Skibsted, C. Hall, Characterization of cement minerals, cements and their reaction products at the atomic and nano scale, Cement Concr. Res. 38 (2008) 205e225.

[24] H.F.W.Taylor,CementChemistry,ThomasTelford,London, 1997.

[25] J.W. Jeffery, The tricalcium silicate phase, in: Proceedings of the Third In-ternational Symposium on the Chemistry of Cement, Cement and Concrete Association, London,1952.

[26] T.Staneˇk,P.Sulovský,Theinfluenceof thealitepolymorphismonthestrengthofthePortlandcement,CementConcr.Res.32(2002)1169e1175.

[27] M. Magi, E. Lippmaa, A. Samoson, G. Engelhardt, A.R. Grimmer, Solid-state high-resolution silicon-29 chemical shifts in silicates, J. Phys. Chem. 88(1984)1518e1522.

[28] J.Skibsted,H.J.Jakobsen,C.Hall,Quantificationofcalciumsilicatephasesin Portland cements by 29Si MAS NMR spectroscopy, J. Chem. Soc. Faraday Trans. 91 (1995)4423e4430.

[29] F.Nishi,Y.Take´uchi,I.Maki,TricalciumsilicateCa3O[SiO4]:themonoclinicsuperstructure,Z.fürKristallogr.Cryst.Mater.172(1985)297e314.

[30] S.L.Poulsen,V.Kocaba,G.LeSaoût,H.J.Jakobsen,K.L.Scrivener,J.Skibsted, ImprovedquantificationofaliteandbeliteinanhydrousPortlandcementsby29Si MAS NMR: effects of paramagnetic ions, Solid State Nucl. Magn. Reson. 36 (2009)32e44.

[31] J. Skibsted, H.J. Jakobsen, C. Hall, Direct observation of aluminium guestionsinthesilicatephasesofcementmineralsby27AlMAS NMRspectroscopy,

[32] J. Chem. Soc. Faraday Trans. 90 (1994) 2095e2098.

[33] T.T. Tran, D. Herfort, H.J. Jakobsen, J. Skibsted, Site preferences of fluoride guest ions in the calcium silicate phases of Portland cement from 29Si{19F}CP-REDORNMRspectroscopy,J.Am.Chem.Soc.131(2009)14170e14171.

[34] S.L.Poulsen,H.J.Jakobsen,J.Skibsted,Incorporationofphosphorusguestionsin the calcium silicate phases of Portland cement from 31P MAS NMR spec- troscopy, Inorg. Chem. 49 (2010)5522e5529.

[35] J.Jeffery,Thecrystalstructureoftricalciumsilicate,ActaCrystallogr.5(1952) 26e35.

[36] J. Skibsted, T.F. Sevelsted, S.L. Poulsen, T.T. Tran, Studies on guest-ion incorporation in Portland cement - part 2, ZKG Int. (2013)46e52.

[37] G.K. Moir, H.F.W. Taylor, F. Massazza, J.E. Bailey, S. Chanda, P. Pichat, et al., Improvements in the early strength properties of Portland cement [anddiscussion], Philos. Trans. Roy. Soc. Lond. A Math. Phys. Sci. 310 (1983) 127e138.

[38] J. Skibsted, T.F. Sevelsted, S.L. Poulsen, T.T. Tran, Studies on guest-ion incorporationinPortlandcementdPart1,ZKGInt.(2013)66e72.

[39] Hung, Z. Gan, P.L. Gor'kov, D.C. Kaseman, S. Sen, M. LaComb, et al.,Detection of “free” oxide ions in low-silica Ca/Mg silicate glasses: resultsfrom17O/29SiHETCORNMR,J.NonCryst.Solids445e446(2016)1e6.

[40] I.L. Moudrakovski, R. Alizadeh, J.J. Beaudoin, Natural abundance highfield43Ca solid state NMR in cement science, Phys. Chem. Chem. Phys. 12 (2010) 6961e6969.

[41] N.I.Golovastikov,R.G.Matveeva,N.V.Belov,Crystalstructureoftricalcium silicate, Kristallografiya 20 (1975)721e729.

[42] R. Dupree, A.P. Howes, S.C. Kohn, Natural abundance solid state 43Ca NMR, Chem. Phys. Lett. 276 (1997)399e404.

[43] D.L.Bryce,Calciumbindingenvironmentsprobedby43CaNMRspectroscopy, Dalton Trans. 39 (2010)8593e8602.

[44] K.H.Jost,B.Ziemer,R.Seydel,Redeterminationofthestructureofb-dical-

[45] cium silicate, Acta Crystallogr. B 33 (1977) 1696e1700.

[46] X. Cong, R.J. Kirkpatrick, 17O and 29Si MAS NMR study of beC2S hydrationandthestructureofcalcium-silicatehydrates,CementConcr.Res.23(1993) 1065e1077.

[47] J. Hjorth, J. Skibsted, H.J. Jakobsen, 29Si MAS NMR studies of Portland cement components and effects of microsilica on the hydration reaction, CementConcr. Res. 18 (1988)789e798.

[48] K.T. Greene, Dicalcium silicate solid solutions, J. Res. Natl. Bur. Stand. 32(1944)1e10.

[49] R.W. Nurse, The dicalcium silicate phase, in: Proceedings

of the Third In-ternational Symposium on the Chemistry of Cement, Cement and Concrete Association, London,1952.

[50] E.H. Oelkers, S.R. Gislason, The mechanism, rates and consequences ofbasaltic glass dissolution: I. An experimental study of the dissolution rates ofbasalticglassasafunctionofaqueousAl,Siandoxalicacidconcentrationat25○C and pH3 and 11, Geochem. Cosmochim. Acta 65 (2001)3671e3681.

[51] R.J. Mccarty, J.F. Stebbins, Constraints on aluminum and scandium substi-tution mechanisms in forsterite, periclase, and larnite: high-resolution NMR,Am. Mineral. 102 (2017)1244e1253.

[52] J. Skibsted, H. Bildsøe, H.J. Jakobsen, High-speed spinning versus highmagnetic field in MAS NMR of quadrupolar nuclei. 27Al MAS NMR of 3CaO$Al2O3, J. Magn. Reson. 92 (1991)669e676.

[53] P. Pena, J.M. Rivas Mercury, A.H. de Aza, X. Turrillas, I. Sobrados, J. Sanz,Solid-state27Aland29SiNMRcharacterizationofhydratesformedin calcium aluminateesilica fume mixtures, J. Solid State Chem. 181 (2008)1744e1752.

[54] D. Müller, W. Gessner, A. Samoson, E. Lippmaa, G. Scheler, Solid-state 27Al NMR studies on polycrystalline aluminates of the system CaO-Al2O3, Poly- hedron 5 (1986)779e785.

[55] J. Skibsted, E. Henderson, H.J. Jakobsen, Characterization of calcium alumi-nate phases in cements by 27Al MAS NMR spectroscopy, Inorg. Chem. 32 (1993)1013e1027.

[56] S.Geller,P.M.Raccah,Phasetransitionsinperovskitelikecompoundsoftherare earths, Phys. Rev. B 2 (1970)1167e1172.

[57] P. Colombet, H. Zanni, A.-R. Grimmer, P. Sozzani, Nuclear Magnetic Reso-nanceSpectroscopyofCement-BasedMaterials,Springer,Berlin,Heidelberg, 1998.

[58] J. Skibsted, H.J. Jakobsen, C. Hall, Quantitative aspects of 27Al MAS NMR of calcium aluminoferrites, Adv. Cem. Based Mater. 7 (1998)57e59.

[59] C.L. Edwards, L.B. Alemany, A.R. Barron, Solid-state 29Si NMR analysis of cements: comparing different methods of relaxation analysis for deter-mining spinlattice relaxation times to enable determination of the C3S/C2S ratio,Ind.Eng.Chem.Res.46(2007)5122e5130.

[60] Rawal, B.J. Smith, G.L. Athens, C.L. Edwards, L. Roberts, V. Gupta, et al., Molecular silicate and aluminate species in anhydrous and hydrated ce-ments,J.Am.Chem.Soc.132(2010)7321e7337.

[61] G.E. Pake, Nuclear resonance absorption in hydrated crystals: fine structure oftheprotonline,J.Chem.Phys.16(1948)327e336.

[62] J.-B.d'EspinosedeLacaillerie,F.Barberon,B.Bresson,P.Fonollosa,H.Zanni,

[63] V.E.Fedorov,etal.,Applicabilityofnaturalabundance33Ssolid-stateNMRto cementchemistry,CementConcr.Res.36(2006)1781e1783.

[64] D.Massiot,F.Fayon,M.Capron,I.King,S.LeCalve´,B.Alonso,etal.,Modellingone- and two-dimensional solid-state NMR spectra, Magn. Reson. Chem. 40(2002)70e76.

[65] K.L. Scrivener, V.M. John, E.M. Gartner, Eco-efficient Cements: Potential, Economically Viable Solutions for a low-CO2, Cement-Based Materials In-dustry,UnitedNationsEnvironmentProgramme,Paris,2016.

[66] D.W.S. Ho, R.K. Lewis, Carbonation of concrete and its prediction, Cement Concr. Res. 17 (1987)489e504.

[67] J.Feng,Y.J.Lee,R.J.Reeder,B.L.Phillips,Observationofbicarbonateincalcite byNMRspectroscopy,Am.Mineral.91(2006)957e960.

[68] H.W. Papenguth, R.J. Kirkpatrick, B. Montez, P.A. Sandberg, 13C MAS NMRspectroscopy of inorganic and biogenic carbonates, Am. Mineral. 74 (1989)1152e1158.

[69] H. Nebel, M. Neumann, C. Mayer, M. Epple, On the structure of amorphous calciumcarbonateeadetailedstudybysolid-stateNMRspectroscopy,Inorg. Chem. 47 (2008)7874e7879.

[70] European Committee for Standardization, EN 197-1:2011, Cement. Compo-sition,SpecificationsandConformityCriteriaforCommonCements,2011.

[71] P. Duxson, J.L. Provis, Designing precursors for geopolymer cements, J. Am.Ceram. Soc. 91 (2008)3864e3869.

[72] J.L. Provis, J.S.J. van Deventer, Geopolymerse Structure, Processing, Prop-ertiesandIndustrialApplications,WoodheadPublishing,Abingdon,2009.

[73] C.J. Shi, P.V. Krivenko, D.M. Roy, Alkali Activated Cements and Concretes, Taylor and Francis, New York,2006.

[74] Y. Li, X. Liu, H. Sun, D. Cang, Mechanism of phase separation in BFS (blastfurnace slag) glass phase, Sci. China Technol. Sci. 54 (2011)105e109.

[75] M. Ben Haha, B. Lothenbach, G. Le Saoût, F. Winnefeld, Influence of slag chemistry on the hydration of alkali-activated blast-furnace slagd part I:effectofMgO,CementConcr.Res.41(2011)955e963.

[76] S.A. Bernal,R.San Nicolas,R.J.Myers,R.MejíadeGutie´rrez,F.Puertas,

[77] J.S.J.vanDeventer,etal.,MgOcontentofslagcontrolsphaseevolutionandstructural changes induced by accelerated carbonation in alkali-activated binders,CementConcr.Res.57(2014)33e43.

[78] M. Ben Haha, B. Lothenbach, G. Le Saoût, F. Winnefeld, Influence of slag chemistry on the hydration of alkali-activated blast-furnace slag d part II:effectofAl2O3,CementConcr.Res.42(2012)74e83.

[79] P.J. Schilling, L.G. Butler, A. Roy, H.C. Eaton, 29Si and 27AI MAS-NMR of NaOH- activatedblast-furnaceslag,J.Am.Ceram.Soc.77(1994)2363e2368.

[80] K. Shimoda, Y. Tobu, K. Kanehashi, T. Nemoto, K. Saito, Total understanding of the local structures of an amorphous slag: perspective from multi-nuclear (29Si, 27Al, 17O, 25Mg, and 43Ca) solid-state NMR, J. Non Cryst. Solids 354 (2008)1036e1043.

[81] K.Shimoda,K.Kanehashi,M.Hatakeyama,Y.Tobu,T.Shimizu,K.Saito,Ul- tra-highmagneticfield(21.8T)solid-statenuclearmagneticresonanceforinorganic materials, Chem. Lett. 36 (2007)834e835.

[82] K.Shimoda,Y.Tobu,K.Kanehashi,T.Nemoto,K.Saito,Local environmentsofslags: the first application of 43Ca 3QMAS NMR technique, Chem. Lett. 34(2005)1588e1589.

[83] K. Shimoda, Y. Tobu, K. Kanehashi, T. Nemoto, K. Saito, First evidence of multiple Ca sites in amorphous slag structure: multiple-quantum MAS NMRspectroscopy on calcium-43 at high magnetic field, Solid State Nucl. Magn.Reson. 30 (2006)198e202.

[84] K. Shimoda, K. Saito, Detailed structure elucidation of the blast furnace slag bymoleculardynamicssimulation,ISIJInt.47(2007)1275e1279.

[85] S.K. Lee, J.F. Stebbins, Disorder and the extent of polymerization in calcium silicate and aluminosilicate glasses: O-17 NMR results and quantum chem-ical molecular orbital calculations, Geochem. Cosmochim. Acta 70 (2006)4275e4286.

[86] S.K. Lee, J.F. Stebbins, C.A. Weiss, R.J. Kirkpatrick, 17O and 27Al MAS and 3QMAS NMR study of synthetic and natural layer silicates, Chem. Mater. 15(2003)2605e2613.

[87] J.R. Allwardt, S.K. Lee, J.F. Stebbins, Bonding preferences of non-bridging O atoms:evidencefrom17OMASand3QMASNMRoncalcium aluminateand low-silicaCa-aluminosilicateglasses,Am.Mineral.88(2003)949e954.

[88] S.K. Lee, J.F. Stebbins, Extent of intermixing among framework units in sili-cate glasses and melts, Geochem. Cosmochim. Acta 66 (2002)303e309.

[89] J.F.Stebbins,J.V.Oglesby,S.Kroeker,Oxygentriclustersincrystalline CaAl4O7 (grossite) and in calcium aluminosilicate glasses: 17O NMR, Am. Mineral. 86 (2001)1307e1311.

[90] S.K. Lee, J.F. Stebbins, The structure of aluminosilicate glasses: high-resolution 17O and 27Al MAS and 3QMAS NMR study, J. Phys. Chem. B 104 (2000)4091e4100.

[91] S.K. Lee, J.F. Stebbins, AleOeAl and SieOeSi sites in framework alumino- silicate glasses with Si/Al1: quantification of framework disorder, J. NonCryst. Solids 270 (2000)260e264.

[92] W. Bumrongjaroen, I. Muller, R.A. Livingston, J. Davis, A performance-basedfly ash classification system using glassy particle chemical composition data,WorldofCoalAshConference,Denver,Colorado,USA,2011.

[93] S. Gomes, M. François, Characterization of mullite in silicoaluminous fly ashbyXRD,TEM,and29SiMASNMR,CementConcr.Res.30 (2000)175e181.

[94] S. Gomes, M. François, M. Abdelmoula, P. Refait, C. Pellissier, O. Evrard, Characterization of magnetite in silico-aluminous fly ash by SEM, TEM, XRD,magneticsusceptibility,andMo€ssbauerspectroscopy, CementConcr.Res.29(1999)1705e1711.

[95] N.Koukouzas,J.H€am€ala€inen,D.Papanikolaou, A.Tourunen,T.J€antti,Mineralogicalandelementalcompositionofflyashfrompilotscalefluidised bed combustion of lignite, bituminous coal, wood chips and their blends,Fuel 86 (2007)2186e2193.

[96] K.Erdogˇdu,P.Türker,Effectsofflyashparticlesizeonstrength ofPortlandcementflyashmortars,CementConcr.Res.28(1998)1217e1222.

[97] S.V. Vassilev, R. Menendez, D. Alvarez, M. Diaz-Somoano, M.R. Martinez- Tarazona, Phase-mineral and chemical composition of coalfly ashes as abasis for their multicomponent utilization. 1. Characterization of feed coalsand fly ashes, Fuel 82 (2003)1793e1811.

[98] R.T. Hemmings, E.E. Berry, On the glass in coal fly ashes: recent advances,in: GJ McCarthy, FP Glasser, DM Roy, RT Hemmings (Eds.), Materials researchsociety symposia proceedings, vol 113, Cambridge University Press, NewYork, USA, 1987, pp.3e38.

[99] S.Diamond,Particlemorphologiesinflyash,CementConcr.Res.16(1986) 569e579.

[100] Diaz-Loya, M. Juenger, S. Seraj, R. Minkara, Extending supplementary cementitious material resources: reclaimed and remediatedfly ash andnaturalpozzolans,CementConcr.Compos.101(2017)44e51.

[101] E.I. Diaz, E.N. Allouche, S. Eklund, Factors affecting the suitability of fly ash assourcematerialforgeopolymers,Fuel89(2010)992e996.

[102] K.L.Aughenbaugh,R.T.Chancey,P.Stutzman,M.C.Juenger, D.W.Fowler, Anexamination of the reactivity of fly ash in cementitious pore solutions, Mater.Struct. 46 (2013)869e880.

[103] K.L.Aughenbaugh,P.Stutzman,M.C.Juenger,Assessmentof theglassyphasereactivity infly ashes used for geopolymer cements, in: L. Struble, J. Hicks (Eds.), Geopolymer Binder Systems, ASTM STP 1566, ASTM International, West Conshohocken, PA, 2013, pp.11e20.

[104] P.T.Durdzin´ski,M.BenHaha,M.Zajac,K.L.Scrivener,Phase assemblageofcompositecements,CementConcr.Res.99(2017)172e182.

[105] P.T.Durdzin´ski,C.F.Dunant,M.BanHaha,K.L.Scrivener,A newquantifica-tionmethodbasedonSEM-EDStoassessflyashcompositionandstudythereactionofitsindividualcomponentsinhydratingcementpaste,Cement Concr. Res. 73 (2015)111e122.

[106] P.T.Durdzin´ski,R.Snellings,C.F.Dunant,M.B.Haha,K.L.Scrivener,Flyashasanassemblageofmodel CaeMgeNa-aluminosilicateglasses,CementConcr.Res. 78 (2015)263e272.

[107] R.T. Chancey, P. Stutzman, M.C.G. Juenger, D.W. Fowler, Comprehensivephase characterization of crystalline and amorphous phases of a Class F fly ash,CementConcr.Res.40(2010)146e156.

[108] A.Fern´andez-Jime´nez,A.Palomo, Characterisationof flyashes. Potentialreactivity as alkaline cements, Fuel 82 (2003)2259e2265.

[109] C.Ruiz-Santaquiteria,J.Skibsted,A.Ferna´ndez-Jime´nez,A.Palomo,Alkalinesolution/binder ratio as a determining factor in the alkaline activation ofaluminosilicates,CementConcr.Res.42(2012)1242e1251.

[110] A.Palomo, S.Alonso,A.Fern´andez-Jime´nez,I.Sobrados, J.Sanz,Alkalineactivation offly ashes: NMR study of the reaction products, J. Am. Ceram.Soc. 87 (2004)1141e1145.

[111] J.F. Stebbins, Z. Xu, NMR evidence for excess non-bridging oxygen in analuminosilicate glass, Nature 390 (1997)60e62.

[112] K.J.D. MacKenzie, I.W.M. Brown, R.H. Meinhold, M.E. Bowden, Outstanding problems in the kaolinite-mullite reaction sequence investigated by 29Si and 27Al solid-state nuclear magnetic resonance: I, Metakaolinite, J. Am. Ceram. Soc. 68 (1985)293e297.

[113] C.E. White, J.L. Provis, T. Proffen, D.P. Riley, van Deventer JSJ, Density func-tional modeling of the local structure of kaolinite subjected to thermal dehydroxylation,J.Phys.Chem.A114(2010)4988e4996.

[114] F. Wang, K. Kovler, J.L. Provis, A. Buchwald, M. Cyr, C. Patapy, et al., Meta-kaolin,in:N.DeBelie,M.Soutsos,E.Gruyaert(Eds.),PropertiesofFreshand

[115] Hardened Concrete Containing Supplementary Cementitious Materials:State-of-the-Art Report of the RILEM Technical Committee 238-SCM,WorkingGroup4,SpringerInternational,Cham,2018,pp.153e179.

[116] D.Kolouˇsek,J.Brus,M.Urbanova,J.Andertova,V.Hulinsky, J.Vorel,Prepa-ration, structure and hydrothermal stability of alternative (sodium silicate-free)geopolymers,J.Mater.Sci.42(2007)9267e9275.

[117] P.Duxson,G.C.Lukey,F.Separovic,J.S.J.vanDeventer,Effectofalkalications on aluminum incorporation in geopolymeric gels, Ind. Eng. Chem. Res. 44(2005)832e839.

[118] P. Duxson, J.L. Provis, G.C. Lukey, F. Separovic, J.S.J. van Deventer, 29Si NMR study of structural ordering in aluminosilicate geopolymer gels, Langmuir 21(2005)3028e3036.

[119] L.Kobera,J.Brus,P.Klein,J.Dedecek,M.Urbanova,BiaxialQ-shearingof27Al 3QMAS NMR spectra: insight into the structural disorder of framework aluminosilicates,SolidStateNucl.Magn.Reson.57e58(2014)29e38.

[120] P.Duxson,A.Ferna´ndez-Jime´nez,J.L.Provis,G.C.Lukey,A.Palomo,J.S.J.vanDeventer, Geopolymer technology: the current state of the art, J. Mater. Sci.42 (2007)2917e2933.

[121] J.Davidovits,Geopolymerseinorganicpolymericnewmaterials,J.Therm.Anal. 37 (1991)1633e1656.

[122] C.E. White, J.L. Provis, T. Proffen, D.P. Riley, J.S.J. van Deventer, Combining density functional theory (DFT) and pair distribution function (PDF) analysis to solve the structure of metastable materials: the case of metakaolin, Phys.Chem. Chem. Phys. 12 (2010)3239e3245.

[123] Z. Dai, T.T. Tran, J. Skibsted, Aluminum incorporation in the CeSeH phase ofwhite Portland cementemetakaolin blends studied by 27Al and 29Si MAS NMRspectroscopy,J.Am.Ceram.Soc.97(2014)2662e2671.

[124] R.C. Lewis, Silica fume, in: N. De Belie, M. Soutsos, E. Gruyaert (Eds.), Properties of Fresh and Hardened Concrete Containing SupplementaryCementitious Materials: State-of-the-Art Report of the RILEM Technical Committee 238-SCM, Working Group 4, Springer International, Cham,2018, pp.99e121.

[125] H.Hilbig,F.H.Ko€hler,P.Schie0l,Quantitative29SiMASNMRspectroscopyofcementandsilicafumecontainingparamagneticimpurities,CementConcr.Res. 36 (2006)326e329.

[126] X.J.Wang,X.Y.Wang,H.F.Zhu,C.Qian,29SiNMRcharacterizationofsilica tetrahedron in the silica fume simulate hydration, Key Eng. Mater. 539(2013)1e4.

[127] K.L.Scrivener,B.Lothenbach,N.DeBelie,E.Gruyaert,J.Skibsted,R.Snellings, et al., TC 238-SCM: hydration and microstructure of concrete with SCMs,Mater. Struct. 48 (2015)835e862.

[128] K. Scrivener, Calcium aluminate cements, in: B.S. Choo (Ed.), Advanced ConcreteTechnology,Butterworth-Heinemann,Oxford,2003,pp.1e31.

[129] A.Neville,Historyofhigh-aluminacement.Part1:problemsandthestonereport,Proc.Instit.CivilEng.Eng.Hist.Herit.162(2009)81e91.

[130] W.Ho€rkner,H.Müller-Buschbaum,ZurkristallstrukturvonCaAl2O4,J.Inorg.Nucl. Chem. 38 (1976)983e984.

[131] J.F. Stebbins, S.K. Lee, J.V. Oglesby, Al-O-Al oxygen sites in crystalline alu-minates and aluminosilicate glasses: high-resolution oxygen-17 NMR re-sults, Am. Mineral. 84 (1999)983.

[132] V.I.Ponomarev,D.M.Kheiker,N.V.Belov,Crystalstructureofcalciumdia-luminate, Kristallografija 15 (1970)1140.

[133] D.W. Goodwin, A.J. Lindop, The crystal structure of CaO$2Al2O3, Acta Crys- tallogr. B 26 (1970)1230e1235.

[134] K. Momma, F. Izumi, VESTA 3 for three-dimensional visualization of crystal, volumetric and morphology data, J. Appl. Crystallogr. 44 (2011)1272e1276.

[135] H.Bartl,T.Scheller,Zurstrukturdes12CaO$7Al2O3,NeuesJahrbuchMineral. Monatsh. (1970)547e552.

[136] M.Teusner,R.A.DeSouza,H.Krause,S.G.Ebbinghaus,B.Belghoul,M.Martin, Oxygendiffusioninmayenite,J.Phys.Chem.C119(2015)9721e9727.

[137] M.Lacerda,J.T.S.Irvine,F.P.Glasser,A.R.West,HighoxideionconductivityinCa12Al14O33, Nature 332 (1988)525.

[138] F.Winnefeld,B.Lothenbach,Hydrationofcalciumsulfoaluminatecementsdexperimentalfindingsandthermodynamicmodelling,CementConcr.Res.40 (2010)1239e1247.

[139] G. Le Saoût, B. Lothenbach, A. Hori, T. Higuchi, F. Winnefeld, Hydration ofPortland cement with additions of calcium sulfoaluminates, Cement Concr.Res. 43 (2013)81e94.

[140] J.T. Song, J.F. Young, Direct synthesis and hydration of calcium aluminosulfate(Ca4Al6O16S),J.Am.Ceram.Soc.85(2002)535e539.

[141] S. Allevi, M. Marchi, F. Scotti, S. Bertini, C. Cosentino, Hydration of calciumsulphoaluminate clinker with additions of different calcium sulphate sour-ces, Mater. Struct. 49 (2016)453e466.

[142] N.J. Calos, C.H.L. Kennard, A.K. Whittaker, R.L. Davis, Structure of calcium aluminatesulfateCa4Al6O16S,J.SolidStateChem.119(1995)1e7.

[143] J. Skibsted, M.T. Pedersen, J. Holzinger, Resolution of the two aluminum sitesin ettringite by 27Al MAS and MQMAS NMR at very high magnetic field (22.3 T),J.Phys.Chem.C121(2017)4011e4017.

[144] M.T. Pedersen, J. Skibsted, 27Al MAS and MQMAS NMR study of ye'elimite at different magneticfields, in: Proceedings of EUROMAR. Aarhus, Denmark,2016.

[145] L.Bonafous,C.Bessada,D.Massiot,J.-P.Coutures,B.L.Holland,P.Colombet, 29Si MAS NMR study of dicalcium silicate: the structural influence of sulfate andaluminastabilizers,J.Am.Ceram.Soc.78(1995)2603e2608.

[146] P. Brotherton, J. Epstein, M. Pryce, A. White, Crystal structure of ‘calcium sulphosilicate’,Ca5(SiO4)2SO4,Aust.J.Chem.27(1974)657e660.

[147] S.A.Walling,J.L.Provis,Magnesia-basedcements:ajourneyof150years,and cementsforthefuture?Chem.Rev.116(2016)4170e4204.

[148] S.A. Walling, H. Kinoshita, S.A. Bernal, N.C. Collier, J.L. Provis, Structure and properties of binder gels formed in the system Mg(OH)2eSiO2eH2O for immobilisation of Magnox sludge, Dalton Trans.44 (2015) 8126e8137.

[149] D.C.Menashi,B.Arnon,DurabilityofPortlandcement-silicafumepastesin magnesium and sodium sulfate solutions, ACI Mater. J. 85 (1988) 148e157.

[150] J.Szczerba,R.Prorok,E.S´niez_ek,D.Madej,K.Ma´slona,Influenceoftimeand

[151] temperature on ageing and phases synthesis in the MgOeSiO2eH2O system,Thermochim. Acta 567 (2013) 57e64.

[152] J. Wei, Y. Chen, Y. Li, The reaction mechanism between MgO and microsilica at room temperature, J. Wuhan Univ. Technol. Mater. Sci. Ed. 21 (2006)88e91.

[153] J.Wei,Q.Yu,W.Zhang,H.Zhang,ReactionproductsofMgOandmicrosilica cementitious materials at different temperatures, J. Wuhan Univ. Technol. Mater. Sci. Ed. 26 (2011)745e748.

[154] C. Ødegård, Z. Chen, B. Myhre, MgOeSiO2eH2O bonded MgO castables, in: Unified International Technical Conference on Refractories (UNITECR'01), American Ceramic Society, 2001, pp.4e7.

[155] B. Myhre, C. Ødegård, H. Feldborg, Periclase castables based on the bondMgOeSiO2eH2O: properties and current status, in: INREFCON (5th India InternationalRefractoriesCongress)inBhubaneswar,India,2002.

[156] R. Dupree, M. Smith, Solid-state magnesium-25 NMR spectroscopy, J. Chem.Soc. Chem. Commun. (1988)1483e1485.

[157] P.S. Fiske, J.F. Stebbins, I. Farnan, Bonding and dynamical phenomena inMgO: a high temperature 17O and 25Mg NMR study, Phys. Chem. Miner. 20 (1994)587e593.

[158] A.V.Chadwick,I.J.F.Poplett,D.T.S.Maitland,M.E.Smith,OxygenspeciationinnanophaseMgO from solid-state 17O NMR, Chem. Mater. 10 (1998)864e870.

[159] S. Rossano, F. Mauri, C.J. Pickard, I. Farnan, First-principles calculation of 17O and 25Mg NMR shieldings in MgO at finite temperature: rovibrational effect insolids,J.Phys.Chem.B109(2005)7245e7250.

[160] K.J.D. MacKenzie, R.H. Meinhold, Thermal decomposition of brucite, Mg(OH)2:a25MgMASNMRstudy,Thermochim.Acta230(1993)339e343.

[161] S.-D. Wang, K.L. Scrivener, 29Si and 27Al NMR study of alkali-activated slag, Cement Concr. Res. 33 (2003)769e774.

[162] F. Bonk, J. Schneider, M.A. Cincotto, H. Panepucci, Characterization bymultinuclear high-resolution NMR of hydration products in activated blast-furnaceslagpastes,J.Am.Ceram.Soc.86(2003)1712e1719.

[163] P. Colombet, A.R. Grimmer, Applications of NMR Spectroscopy to Cement Science, Taylor &Francis,1995.

[164] J. Skibsted, C. Hall, H.J. Jakobsen, Nuclear magnetic resonance spectroscopy and magnetic resonance imaging of cements and cement-based materials, in: J. Bensted, P. Barnes (Eds.), Structure and Performance of Cements, seconded.,SponPress,London&NewYork,2002,pp.457e476.

[165] C.Labbez,I.Pochard,B.Jo€nsson,A.Nonat,C-S-H/solutioninterface:experimentalandMonteCarlostudies,CementConcr.Res.41(2011) 161e168.

[166] I.G.Richardson,G.W.Groves,Theincorporationofminorandtraceelements into calcium silicate hydrates (C-S-H) gel in hardened cement pastes, Cement Concr. Res. 23 (1993)131e138.

[167] I.G. Richardson, Tobermorite/jennite- and tobermorite/calcium hydroxide- based models for the structure of C-S-H: applicability to hardened pastes of tricalcium silicate, b-dicalcium silicate, Portland cement, and blends ofPortlandcementwithblast-furnaceslag,metakaolin,orsilicafume,Cement Concr. Res. 34 (2004)1733e1777.

[168] D.A. Kulik, Improving the structural consistency of C-S-H solid solution thermodynamic models, Cement Concr. Res. 41 (2011)477e495.

[169] H.F.W. Taylor, Proposed structure for calcium silicate hydrate gel, J. Am.Ceram. Soc. 69 (1986)464e467.

A. Nonat, The structure and stoichiometry of C-S-H, Cement Concr. Res. 34 (2004)1521e1528.

[170] G. Renaudin, J. Russias, F. Leroux, C. Cau-dit-Coumes, F. Frizon, Structural characterization of CeSeH and CeAeSeH samplesdpart II: local environmentinvestigatedbyspectroscopicanalyses,J.SolidStateChem.182(2009) 3320e3329.

[171] P. Rejmak, J.S. Dolado, M.J. Stott, A. Ayuela, 29Si NMR in cement: a theoreticalstudyoncalciumsilicatehydrates,J.Phys.Chem.C116(2012)9755e9761.

[172] P.Rejmak,J.S.Dolado,M.J.Stott,A.Ayuela,29Sichemicalshiftanisotropiesin hydrated calcium silicates: a computational study, J. Phys. Chem. C 117(2013)8374e8380.

[173] X. Cong, R.J. Kirkpatrick, 29Si MAS NMR study of the structure of C-S-H, Adv. Cem. Based Mater. 3 (1996)114e156.

[174] X. Cong, R.J. Kirkpatrick, 17O MAS NMR investigation of the structure of calciumsilicatehydrategel,J.Am.Ceram.Soc.79(1996)1585e1592.

[175] C.S. Walker, S. Sutou, C. Oda, M. Mihara, A. Honda, Calcium silicate hy- drate (C-S-H) gel solubility data and a discrete solid phase model at 25○Cbased on two binary non-ideal solid solutions, Cement Concr. Res. 79 (2016)1e30.

[176] A.Kumar,B.J.Walder,A.KunhiMohamed,A.Hofstetter,B.Srinivasan,

[177] A.J. Rossini, et al., The atomic-level structure of cementitious calcium silicate hydrate, J. Phys. Chem. C 121 (2017) 17188e17196.

[178] I.G. Richardson, Model structures for C-(A)-S-H(I), Acta Crystallogr. B 70(2014)903e923.

[179] M.D. Andersen, H.J. Jakobsen, J. Skibsted, Incorporation of aluminum in the calcium silicate hydrate (CSH) of hydrated Portland cements:A high-field 27Al and 29Si MAS NMR investigation, Inorg. Chem. 42 (2003) 2280e2287.

[180] H.Viallis,P.Faucon,J.C.Petit,A.Nonat,Interactionbetweensalts(NaCl,CsCl)and calcium silicate hydrates (CSH), J. Phys. Chem. B 103 (1999) 5212e5219.

[181] J.J.Chen,J.J.Thomas,H.F.W.Taylor,H.M.Jennings,Solubilityandstructureof calciumsilicatehydrate,CementConcr.Res.34(2004)1499e1519.

[182] I.G. Richardson, J. Skibsted, L. Black, R.J. Kirkpatrick, Characterisation ofcement hydrate phases by TEM, NMR and Raman spectroscopy, Adv. Cem.Res. 22 (2010)233e248.

[183] F. Brunet, P. Bertani, T. Charpentier, A. Nonat, J. Virlet, Application of 29Si homonuclear and 1H29Si heteronuclear NMR correlation to structural studies of calcium silicate hydrates, J. Phys. Chem. B 108 (2004) 15494e15502.

[184] B. Lothenbach, A. Nonat, Calcium silicate hydrates: solid and liquid phasecomposition,CementConcr.Res.78(2015)57e70.

[185] K.J.D. MacKenzie, M.E. Smith, A. Wong, A multinuclear MAS NMR study of calcium-containing aluminosilicate inorganic polymers, J. Mater. Chem. 17(2007)5090e5096.

[186] G.M. Bowers, R.J. Kirkpatrick, Natural abundance 43Ca NMR spectroscopy of tobermorite and jennite: model compounds for CeSeH, J. Am. Ceram. Soc. 92(2009)545e548.

[187] B. Bresson, S. Masse, H. Zanni, C. Noik, Tricalcium silicate hydration at high temperature. A 29Si and 1H NMR Investigation, in: P. Colombet, H. Zanni, A.-

[188] R. Grimmer, P. Sozzani (Eds.), Nuclear Magnetic Resonance SpectroscopyofCement-BasedMaterials,SpringerBerlinHeidelberg,1998,pp.209e215.

[189] D. Heidemann, W. Wieker, Characterization of protons in C-S-H phases bymeansofhigh-speed1HMASNMRinvestigations,in:P.Colombet,A.-

[190] R. Grimmer, H. Zanni, P. Sozzani (Eds.), Nuclear Magnetic Resonance Spec-troscopy of Cement-Based Materials, Springer-Verlag, Berlin, 1998,pp.169e180.

[191] D. Heidemann, Proton high-resolution solid-state NMR spectroscopy usingCRAMPS techniques for studies in silicate and cement science,in:

[192] P. Colombet, A.R. Grimmer (Eds.), Applications of NMR Spectroscopy to Cement Science, Gordon and Breach, Amsterdam, 1994, pp. 77e102.

[193] E.Pustovgar,R.P.Sangodkar,A.S.Andreev,M.Palacios,B.F. Chmelka,

[194] R.J. Flatt, et al., Understanding silicate hydration from quantitative analyses of hydrating tricalcium silicates, Nat. Commun. 7 (2016) 10952.

[195] I.G. Richardson, G.W. Groves, The structure of the calcium silicate hydrate phases present in hardened pastes of white Portland cement/blast-furnace slagblends,J.Mater.Sci.32(1997)4793e4802.

[196] I.G. Richardson, A.R. Brough, G.W. Groves, C.M. Dobson, The characterization of hardened alkali-activated blast-furnace slag pastes and the nature of thecalcium silicate hydrate (CeSeH) paste, Cement Concr. Res. 24 (1994) 813e829.

[197] M.D.Andersen,H.J.Jakobsen,J.Skibsted,Characterizationof whitePortland cement hydration and the C-S-H structure in the presence of sodium aluminate by 27Al and 29Si MAS NMR spectroscopy, Cement Concr. Res. 34 (2004)857e868.

[198] C.A. Love, I.G. Richardson, A.R. Brough, Composition and structure ofCeSeH inwhitePortlandcemente20%metakaolinpasteshydratedat25○C,Cement Concr. Res. 37 (2007)109e117.

[199] X.Pardal,F.Brunet,T.Charpentier,I.Pochard,A.Nonat,27Aland29Sisolid-stateNMRcharacterizationofcalcium-aluminosilicate-hydrate,Inorg.Chem.51 (2012)1827e1836.

[200] M.D. Jackson, J. Moon, E. Gotti, R. Taylor, S.R. Chae, M. Kunz, et al., Material and elastic properties of Al-tobermorite in ancient roman seawater concrete, J.Am.Ceram.Soc.96(2013)2598e2606.

[201] I.G.Richardson,A.R.Brough,R.Brydson,G.W.Groves,C.M. Dobson,Location of aluminum in substituted calcium silicate hydrate (C-S-H) gels as deter-mined by 29Si and 27Al NMR and EELS, J. Am. Ceram. Soc. 76 (1993) 2285e2288.

[202] L.Pegado,C.Labbez,S.V.Churakov,Mechanismofaluminiumincorporation intoCeSeHfromabinitiocalculations,J.Mater.Chem.A2(2014)3477.

[203] P. Faucon, A. Delagrave, C. Richet, J.M. Marchand, H. Zanni, Aluminum incorporation in calcium silicate hydrates (CSH) depending on their Ca/Siratio,J.Phys.Chem.B103(1999)7796e7802.

[204] G.K. Sun, J.F. Young, R.J. Kirkpatrick, The role of Al in CeSeH: NMR, XRD, and compositionalresultsforprecipitatedsamples,CementConcr. Res.36(2006) 18e29.

[205] M.D. Andersen, H.J. Jakobsen, J. Skibsted, A new aluminium-hydratespecies in hydrated Portland cements characterized by 27Al and 29Si MAS NMR spectroscopy, Cement Concr. Res. 36 (2006)3e17.

[206] R.J.Myers,S.A.Bernal,R.SanNicolas,J.L.Provis,Generalizedstructuraldescriptionofcalcium-sodiumaluminosilicatehydrategels:thecross-linked substituted tobermorite model, Langmuir 29 (2013)5294e5306.

[207] A.Ferna´ndez-Jime´nez,F.Puertas,Structureof calciumsilicatehydratesformedinalkaline-activatedslag:influenceofthetypeofalkalineactivator, J.Am.Ceram.Soc.86(2003)1389e1394.

[208] J. Schneider, M.A. Cincotto, H. Panepucci, 29Si and 27Al high-resolution NMR characterizationofcalciumsilicatehydratephasesinactivated blast-furnace slagpastes,CementConcr.Res.31(2001)993.

[209] H. Manzano, J.S. Dolado, A. Ayuela, Aluminum incorporation to dreierketten silicate chains, J. Phys. Chem. B 113(2009) 2832e2839.

[210] F. Puertas, M. Palacios, H. Manzano, J.S. Dolado, A. Rico, J. Rodriguez, A modelfor the C-A-S-H gel formed in alkali-activated slag cements, J. Eur. Ceram. Soc. 31 (2011)2043e2056.

[211] S. Grangeon, F. Claret, C. Roosz, T. Sato, S. Gaboreau, Y. Linard, Structureof nanocrystallinecalciumsilicatehydrates:insightsfromX-raydiffraction,synchrotronX-rayabsorptionandnuclearmagneticreso-nance, J. Appl. Crystallogr. 49 (2016)771e783.

[212] E.M.L'Ho^pital,B.Lothenbach,D.A.Kulik,K.Scrivener,Influenceofcalciumtosilica ratio on aluminium uptake in calcium silicate hydrate, Cement Concr. Res. 85 (2016)111e121.

[213] E´.M.L'Ho^pital,AluminiumandAlkaliUptakeinCalciumSilicateHydrates(C-

[214] S-H),Ph.D.thesis,E´colePolytechniqueFe´de´raledeLausanne, Lausanne,Switzerland, 2014.

[215] B. Walkley, J.L. Provis, R. San Nicolas, M.A. Sani, J.S.J. van Deventer, Stoi- chiometrically controlled Ce(A)eSeH/NeAeSeH gel blends via alkali-activationofsyntheticprecursors,Adv.Appl.Ceram.114(2015)372e377.

[216] R.J.Myers,E´.M.L'Ho^pital,J.L.Provis,B.Lothenbach,Composition-solubility-

[217] structurerelationshipsincalcium(alkali)aluminosilicatehydrate(C-(N,K-)A-S-H), Dalton Trans. 44 (2015)13530e13544.

[218] X. Pardal, I. Pochard, A. Nonat, Experimental study of SieAl substitution in calcium-silicate-hydrate (C-S-H) prepared under equilibrium conditions, Cement Concr. Res. 39 (2009)637e643.

[219] I.G. Richardson, S. Li, Composition and structure of an 18-year-old 5 M KOH- activated ground granulated blast-furnace slag paste, Constr. Build. Mater.168 (2018)404e411.

[220] H. Viallis-Terrisse, A. Nonat, J.-C. Petit, Zeta-potential study of calcium silicatehydratesinteractingwithalkalinecations,J.ColloidInterfaceSci.244(2001)58e65.

[221] Y. Kim, R. James Kirkpatrick, 23Na and 133Cs NMR study of cation adsorption on mineral surfaces: local environments, dynamics, and effects of mixedcations, Geochem. Cosmochim. Acta 61 (1997)5199e5208.

[222] S.-Y. Hong, F.P. Glasser, Alkali sorption by C-S-H and C-A-S-H gels: Part II. Role of alumina, Cement Concr. Res. 32 (2002)1101e1111.

[223] H. Stade, On the reaction of C-S-H(di, poly) with alkali hydroxides, Cement Concr. Res. 19 (1989)802e810.

[224] T.T.H.Bach,E.Chabas,I.Pochard,C.CauDitCoumes,J.Haas, F.Frizon,etal.,Retention of alkali ions by hydrated low-pH cements: mechanism and Naþ/ Kþselectivity,CementConcr.Res.51(2013)14e21.

[225] T.Chappex,K.Scrivener,AlkalifixationofCeSeHinblendedcementpastes and its relation to alkali silica reaction, Cement Concr. Res. 42 (2012)1049e1054.

[226] E´.M.L'Ho^pital,B.Lothenbach,K.Scrivener,D.A.Kulik,Alkaliuptakeincal-

[227] cium alumina silicate hydrate (C-A-S-H), Cement Concr. Res. 85 (2016)122e136.

[228] C.E. White, L.L. Daemen, M. Hartl, K. Page, Intrinsic differences in atomic ordering of calcium (alumino)silicate hydrates in conventional and alkali- activated cements, Cement Concr. Res. 67 (2015)66e73.

[229] R.J.Myers,E´.M.L'Ho^pital,J.L.Provis,B.Lothenbach,Effectoftemperatureand

[230] aluminium on calcium (alumino)silicate hydrate chemistry under equilib-rium conditions, Cement Concr. Res. 68 (2015) 83e93.

[231] K. Enemark-Rasmussen, T.T. Tran, J. Skibsted, Fluoride ions as structural probe-ions in 19F MAS NMR studies of cement materials and thermally activatedSCMs,Adv.Cem.Res.26(2014)233e246.

[232] T.T. Tran, H. Bildsøe, H.J. Jakobsen, J. Skibsted, Double cross-polarization MASNMR in the assignment of abundant-spin resonances: 19Fe{29Si}e19F FBCP/ MAS NMR of fluoride ions incorporated in calcium silicate hydrate (CeSeH)phases,J.Magn.Reson.221(2012)19e23.

[233] P. Yu, R.J. Kirkpatrick, 35Cl NMR relaxation study of cement hydrate sus-pensions,CementConcr.Res.31(2001)1479e1485.

[234] J.V.Hanna,L.P.Aldridge,E.R.Vance,Csspeciationincements,MRSProc.663 (2011)89e96.

[235] T.F. Sevelsted, D. Herfort, J. Skibsted, 13C chemical shift anisotropies for carbonate ions in cement minerals and the use of 13C, 27Al and 29Si MAS NMR in studies of Portland cement including limestone additions, Cement Concr. Res. 52 (2013)100e111.

[236] T.F. Sevelsted, J. Skibsted, Carbonation of CeSeH and CeAeSeH samples studied by 13C, 27Al and 29Si MAS NMR spectroscopy, Cement Concr. Res. 71 (2015)56e65.

[237] J.L. MacDonald, U. Werner-Zwanziger, B. Chen, J.W. Zwanziger, D. Forgeron, A 43Ca and 13C NMR study of the chemical interaction between poly(-ethyleneevinylacetate)andwhitecementduringhydration,SolidStateNucl.Magn. Reson. 40 (2011)78e83.

[238] J. Rottstegge, M. Wilhelm, H.W. Spiess, Solid state NMR investigations on the roleoforganicadmixturesonthehydrationofcementpastes,CementConcr.Compos. 28 (2006)417e426.

[239] J. Rottstegge, M. Arnold, L. Herschke, G. Glasser, M. Wilhelm, H.W. Spiess, etal., Solid state NMR and LVSEM studies on the hardening of latex modified tilemortarsystems,CementConcr.Res.35(2005)2233e2243.

[240] Z.Gabelica,J.Davidovits,H.J.Jakobsen,Geopolymerisationofpolysialates,in:

[241] J. Davidovits, J. Orlinski (Eds.), Geopolymer'88: First European Conference onSoftMineralurgy.Compie`gne,TheGeopolymer Institute;TheUniversityofTechnologyofCompie`gne,France,1988.

[242] J. Davidovits, Structural characterization of geopolymeric materials with X-ray diffractometry and MAS-NMR spectroscopy, in: J. Davidovits, J. Orlinski (Eds.), Geopolymer'88: First European Conference on Soft Mineralurgy.Compie`gne,TheGeopolymer Institute;TheUniversityof TechnologyofCompie`gne,France,1988.

[243] C.A.Rees,J.L.Provis,G.C.Lukey,J.S.J.vanDeventer,Attenuatedtotalreflec- tance Fourier transform infrared analysis of fly ash geopolymer gel aging, Langmuir 23 (2007)8170e8179.

[244] B. Walkley, R. San Nicolas, M.A. Sani, J.D. Gehman, J.S. vanDeventer,

[245] J.L. Provis, Phase evolution of Na2O-Al2O3-SiO2-H2O gels in synthetic aluminosilicate binders, Dalton Trans. 45 (2016) 5521e5535.

[246] X-m Cui, L-p Liu, G-j Zheng, R-p Wang, J-p Lu, Characterization of chemo-syntheticAl2O3e2SiO2geopolymers,J.NonCryst.Solids356 (2010)72e76.

[247] G.Zheng,X.Cui,W.Zhang,Z.Tong,Preparationofgeopolymerprecursorsbysolegel method and their characterization, J. Mater. Sci. 44 (2009)3991e3996.

[248] I.García-Lodeiro,A.Palomo,A.Fern´andez-Jime´nez,D.E.Macphee,Compat-ibility studies between N-A-S-H and C-A-S-H gels. Study in the ternary di- agram Na2OeCaOeAl2O3eSiO2eH2O, Cement Concr. Res. 41 (2011) 923e931.

[249] J. Davidovits, Properties of geopolymer cements, in: First International ConferenceonAlkalineCementsandConcretes,ScientificResearchInstitute onBindersandMaterials,Kiev,Ukraine,1994,pp.131e149.

[250] P. Duxson, S.W. Mallicoat, G.C. Lukey, W.M. Kriven, J.S.J. van Deventer, The

effectofalkaliandSi/Alratioonthedevelopmentofmechanical properties of metakaolin-based geopolymers, Colloid. Surf. A Physicochem. Eng. Asp.292 (2007)8e20.

[251] C. Li, H. Sun, L. Li, A review: the comparison between alkali-activated slag(SiCa) and metakaolin (SiAl) cements, Cement Concr. Res. 40 (2010)1341e1349.

[252] J. Melar, G. Renaudin, F. Leroux, A. Hardy-Dessources, J.M. Nedelec, C. Taviot- Gueho, et al., The porous network and its interface inside geopolymers as afunction of alkali cation and aging, J. Phys. Chem. C 119 (2015) 17619e17632.

[253] M.Criado,A.Ferna´ndez-Jime´nez,A.Palomo,I.Sobrados,J.Sanz,Effectofthe SiO2/Na2O ratio on the alkali activation of fly ash. Part II: 29Si MAS-NMRsurvey,MicroporousMesoporousMater.109(2008)525e534.

[254] A.Ferna´ndez-Jime´nez,A.Palomo,I.Sobrados,J.Sanz,Theroleplayedbythe reactive alumina content in the alkaline activation of fly ashes, Microporous Mesoporous Mater. 91 (2006)111e119.

[255] K.Ikeda,Preparationofflyashmonolithsconsolidatedwithasodiumsilicate binderatambienttemperature,CementConcr.Res.27(1997)657e663.

[256] J.L. Provis, G.C. Lukey, J.S.J. van Deventer, Do geopolymers actuallycontain nanocrystalline zeolites? A reexamination of existing results, Chem. Mater.17 (2005)3075e3085.

[257] F.Sˇkva´ra, T.Jílek,L.Kopecký, Geopolymer materialsbasedonflyash, Ce-

[258] ramics-Silikaty 49 (2005) 195e204.

[259] A.Fern´andez-Jime´nez,M.Monzo´,M.Vicent,A.Barba,A.Palomo, Alkalineactivation of metakaolinefly ash mixtures: obtain of zeoceramics andzeocements,MicroporousMesoporousMater.108(2008) 41e49.

[260] J.Brus,L.Kobera,M.Urbanov´a,D.Kolouˇsek,J.Kotek,Insightsintothestructural transformations of aluminosilicate inorganic polymers: acomprehensive solid-state NMR study, J. Phys. Chem. C 116 (2012) 14627e14637.

[261] J.E. Oh, Y. Jun, Y. Jeong, Characterization of geopolymers from compositionallyandphysicallydifferentClassFflyashes,CementConcr.Compos.50(2014)16e26.

[262] I.García-Lodeiro,A.Ferna´ndez-Jimenez,A.Palomo,D.E.Macphee,Effectonfresh C-S-H gels of the simultaneous addition of alkali and aluminium, Cement Concr. Res. 40 (2010)27e32.

[263] I.García-Lodeiro, A.Ferna´ndez-Jime´nez,A.Palomo, D.E.Macphee,Effect ofcalcium additions on NeAeSeH cementitious gels, J. Am. Ceram. Soc. 93 (2010)1934e1940.

[264] J.L. Provis, J.S.J. van Deventer, Direct measurement of the kinetics of geo- polymerisation by in-situ energy dispersive X-ray diffractometry, J. Mater.Sci. 42 (2007)2974e2981.

[265] C.E. White, J.L. Provis, A. Llobet, T. Proffen, J.S.J. van Deventer, Evolution of local structure in geopolymer gels: an in situ neutron pair distribution functionanalysis,J.Am.Ceram.Soc.94(2011)3532e3539.

[266] C.E. White, J.L. Provis, T. Proffen, J.S.J. Van Deventer, The effects of temper- ature on the local structure of metakaolin-based geopolymer binder: aneutron pair distribution function investigation, J. Am. Ceram. Soc. 93 (2010) 3486e3492.

[267] C.E. White, B. Bloomer, J.L. Provis, N.J. Henson, K. Page, The synergy be-tween total scattering and advanced simulation techniques in understandinggeopolymergelevolution:quantifyingextentofreactionusingin situ X-ray pair distribution function analysis, in: NICOM4: 4th InternationalSymposium on Nanotechnology in Construction. Agios Nikolaos,Greece,2012.

[268] J.L.Provis,P.Duxson,G.C.Lukey,vanDeventerJSJ,Statisticalthermodynamic model for Si/Al ordering in amorphous aluminosilicates, Chem. Mater. 17(2005)2976e2986.

[269] I.Lecomte,C.Henrist,M.Lie´geois,F.Maseri,A.Rulmont,R. Cloots,(Micro)-structural comparison between geopolymers, alkali-activated slag cementandPortlandcement,J.Eur.Ceram.Soc.26(2006)3789e3797.

[270] P.Duxson,TheStructureandThermalEvolutionofMetakaolin Geopolymers, PhD thesis, The University of Melbourne, Melbourne, Australia,2006.

[271] Hajimohammadi, J.L. Provis, J.S.J. van Deventer, Effect of aluminarelease rateonthemechanismofgeopolymergelformation,Chem.Mater.22(2010) 5199e5208.

[272] Hajimohammadi, J.L. Provis, J.S.J. van Deventer, The effect of silica avail- ability on the mechanism of geopolymerisation, Cement Concr. Res. 41(2011)210e216.

[273] Walkley, G.J. Rees, R. San Nicolas, J.S.J. van Deventer, J.V. Hanna, J.L. Provis, New structural model of hydrous sodium aluminosilicate gels and the role ofcharge-balancing extra-framework Al, J. Phys. Chem. C 122 (2018)5673e5685.

[274] M.R.Rowles,J.V.Hanna,K.J.Pike,M.E.Smith,B.H.O'Connor,29Si,27Al,1Hand 23Na MAS NMR study of the bonding character in aluminosilicate inorganic polymers,Appl.Magn.Reson.32(2007)663e689.

[275] V.F.F. Barbosa, K.J.D. MacKenzie, C. Thaumaturgo, Synthesis andcharacteri- sation of materials based on inorganic polymers of alumina and silica: sodiumpolysialatepolymers,Int.J.Inorg.Mater.2(2000)309e317.

[276] A.Y. Wang-hong, R. James Kirkpatrick, Hydrothermal reaction of albite and asodium aluminosilicate glass: a solid-state NMR study, Geochem. Cosmo-chim. Acta 53 (1989)805e819.

[277] P. Duxson, J.L. Provis, G.C. Lukey, J.S.J. van Deventer, 39K NMR of free potassiumingeopolymers,Ind.Eng.Chem.Res.45(2006)9208e9210.

[278] V.F.F. Barbosa, K.J.D. MacKenzie, Synthesis and thermal behaviour of potassiumsialategeopolymers,Mater.Lett.57(2003)1477e1482.

[279] M.G. Blackford, J.V. Hanna, K.J. Pike, E.R. Vance, D.S. Perera, Transmission electron microscopy and nuclear magnetic resonance studies of geopolymers for radioactive waste immobilization, J. Am. Ceram. Soc. 90 (2007)1193e1199.

[280] Y. Kim, R.J. Kirkpatrick, R.T. Cygan, 133Cs NMR study of cesium on the sur- faces of kaolinite and illite, Geochem. Cosmochim. Acta 60 (1996) 4059e4074.

[281] S.A. Bernal, E.D. Rodriguez, R. Mejia de Gutierrez, M. Gordillo, J.L. Provis, Mechanicalandthermalcharacterisationofgeopolymersbasedonsilicate-activatedmetakaolin/slagblends,J.Mater.Sci.46(2011)5477e5486.

[282] I.Ismail,S.A.Bernal,J.L.Provis,R.SanNicolas,S.Hamdan,J.S.J.vanDeventer, Modification of phase evolution in alkali-activated blast furnace slag by theincorporationofflyash,CementConcr.Compos.45(2014)125e135.

[283] C.K. Yip, G.C. Lukey, J.S.J. van Deventer, The coexistence of geopolymeric geland calcium silicate hydrate at the early stage of alkaline activation, Cement Concr. Res. 35 (2005)1688e1697.

[284] Buchwald, H. Hilbig, C. Kaps, Alkali-activated metakaolin-slag blendsdperformance and structure in dependence of their composition,J. Mater. Sci. 42 (2007)3024e3032.

[285] F. Puertas, S. Martinez-Ramirez, S. Alonso, T. Vazquez, Alkali-activatedfly ash/slag cemente strength behaviour and hydration products, Cement Concr. Res. 30 (2000)1625e1632.

[286] F.Puertas,A.Fern´andez-Jime´nez,Mineralogicalandmicrostructuralchar-acterisationofalkali-activatedflyash/slagpastes,CementConcr.Compos.25(2003) 287e292.

[287] A.V.Gir~ao,I.G.Richardson,R.Taylor,R.M.D.Brydson,Composition,morphology and nanostructure of CeSeH in 70% white Portland cemente30%flyashblendshydratedat55○C,CementConcr.Res.40(2010) 1350e1359.

[288] J. Tailby, K.J.D. MacKenzie, Structure and mechanical properties of alumi-nosilicate geopolymer composites with Portland cement and its constituent minerals,CementConcr.Res.40(2010)787e794.

[289] K. Dombrowski, A. Buchwald, M. Weil, The influence of calcium content on the structure and thermal performance offly ash based geopolymers, J. Mater. Sci. 42 (2007)3033e3043.

[290] S.A. Bernal, J.L. Provis, V. Rose, R. Mejia de Gutierrez, Evolution of binder structureinsodiumsilicate-activatedslag-metakaolinblends,CementConcr.Compos. 33 (2011)46e54.

[291] S.A. Bernal, R. Mejia de Gutierrez, J.L. Provis, V. Rose, Effect of silicate modulus and metakaolin incorporation on the carbonation of alkali silicate-activatedslags,CementConcr.Res.40(2010)898e907.

[292] L. Black, P. Purnell, J. Hill, Current themes in cement research, Adv. Appl.Ceram. 109 (2010)253e259.

[293] W. Gessner, D. Müller, H.J. Behrens, G. Scheler, Zur Koordination des Alu- miniums in den Calciumaluminathydraten 2CaO$Al2O3$8H2O und CaO$Al2O3$10H2O,Z.Anorg.Allg.Chem.486(1982)193e199.

[294] P. Faucon, T. Charpentier, D. Bertrandie, A. Nonat, J. Virlet, J.C. Petit, Char-acterization of calcium aluminate hydrates and related hydrates of cement pastesby27AlMQ-MASNMR,Inorg.Chem.37(1998)3726e3733.

[295] M.A.Chavda,S.A.Bernal,D.C.Apperley,H.Kinoshita,J.L.Provis,Identification ofthehydrategelphasespresentinphosphate-modifiedcalciumaluminate binders,CementConcr.Res.70(2015)21e28.

[296] F. Winnefeld, B. Lothenbach, Phase equilibria in the system Ca4Al6O12- SO4eCa2SiO4eCaSO4eH2O referring to the hydration of calcium sulfoalu- minate cements, RILEM Tech. Lett. 1 (2016)10e16.

[297] F. Bullerjahn, M. Zajac, M. Ben Haha, CSA raw mix design: effect on clinker formationandreactivity,Mater.Struct.48(2015)3895e3911.

[298] T. Hanein, I. Galan, F.P. Glasser, S. Skalamprinos, A. Elhoweris, M.S. Imbabi, etal., Stability of ternesite and the production at scale of ternesite-based clinkers,CementConcr.Res.98(2017)91e100.

[299] B.Z.Dilnesa,B.Lothenbach,G.LeSaout,G.Renaudin,A.Mesbah,Y.Filinchuk, etal.,IronincarbonatecontainingAFmphases,CementConcr. Res.41(2011) 311e323.

[300] B.Z. Dilnesa, B. Lothenbach, G. Renaudin, A. Wichser, E. Wieland, Stability ofmonosulfate in the presence of iron, J. Am. Ceram. Soc. 95 (2012) 3305e3316.

[301] B.Z.Dilnesa,E.Wieland,B.Lothenbach,R.D€ahn,K.L.Scrivener,Fe-containingphasesinhydratedcements,CementConcr.Res.58(2014)45e55.

[302] Cuesta, A.G. De la Torre, I. Santacruz, P. Trtik, J.C. da Silva, A. Diaz, et al., Chemistry and mass density of aluminum hydroxide gel in eco-cements byptychographic X-ray computed tomography, J. Phys. Chem. C 121 (2017)3044e3054.

[303] G.Paul,E.Boccaleri,L.Buzzi,F.Canonico,D.Gastaldi,Friedel'ssaltformation in sulfoaluminate cements: a combined XRD and 27Al MAS NMR study, Cement Concr. Res. 67 (2015)93e102.

[304] T. Isobe, T. Watanabe, J.-B. d'Espinose de la Caillerie, A. Legrand, D.Massiot, Solid-state1Hand27AlNMRstudiesofamorphousaluminumhydroxides,

[305] J. Colloid Interface Sci. 261 (2003) 320e324.

[306] Vyalikh, K. Zesewitz, U. Scheler, Hydrogen bonds and local symmetry inthecrystalstructureofgibbsite,Magn.Reson.Chem.48(2010)877e881.

[307] T.Zhang,L.J.Vandeperre,C.R.Cheeseman,Formationofmagnesiumsilicate hydrate (M-S-H) cement pastes using sodium hexametaphosphate, CementConcr. Res. 65 (2014)8e14.

[308] T.Zhang,L.J.Vandeperre,C.R.Cheeseman,Magnesium-silicate-hydratece-mentsforencapsulatingproblematicaluminiumcontainingwastes,

[309] J. Sustain. Cem. Based Mater. 1 (2012) 34e45.

[310] T.Zhang,C.R.Cheeseman,L.J.Vandeperre,DevelopmentoflowpHcement systems forming magnesium silicate hydrate (M-S-H), Cement Concr. Res. 41(2011)439e442.

[311] Roosz, S. Grangeon, P. Blanc, V. Montouillout, B. Lothenbach, P. Henocq, et al., Crystal structure of magnesium silicate hydrates (M-S-H): therelation with 2:1 MgeSi phyllosilicates, Cement Concr. Res. 73 (2015) 228e237.

[312] D.R.M. Brew, F.P. Glasser, Synthesis and characterisation of magnesium sil-icatehydrategels,CementConcr.Res.35(2005)85e98.

[313] E.Bernard,B.Lothenbach,D.Rentsch,I.Pochard,A.Dauze`res,Formationofmagnesium silicate hydrates (M-S-H), Phys. Chem. Earth Parts A/B/C 99(2017)142e157.

[314] J. Temuujin, K. Okada, K.J. MacKenzie, Formation of layered magnesium sil-icate during the aging of magnesium hydroxideesilica mixtures, J. Am.Ceram. Soc. 81 (1998)754e756.

[315] J.-B.d'EspinosedelaCaillerie,M.Kermarec,O.Clause,29SiNMRobservation of an amorphous magnesium silicate formed during impregnation of silicawithMg(II)inaqueoussolution,J.Phys.Chem.99(1995) 17273e17281.

[316] M. Tonelli, F. Martini, L. Calucci, E. Fratini, M. Geppi, F. Ridi, et al., Structural characterization of magnesium silicate hydrate: towards the design of eco-sustainablecements,DaltonTrans.45(2016)3294e3304.

[317] Pedone, F. Palazzetti, V. Barone, Models of aged magne-siumesilicateehydrate cements based on the lizardite and talc crystals: aperiodicDFT-GIPAWinvestigation,J.Phys.Chem.C121(2017)7319e7330.

[318] B.Lothenbach,D.Nied,E.L'Ho^pital,G.Achiedo,A.Dauze`res,Magnesiumandcalciumsilicatehydrates,CementConcr.Res.77(2015)60e68.

[319] K.J.D.MacKenzie,S.Bradley,J.V.Hanna,M.E.Smith,Magnesiumanaloguesofaluminosilicate inorganic polymers (geopolymers) from magnesium min-erals,J.Mater.Sci.48(2013)1787e1793.

[320] A.D. Wilson, J.W. Nicholson, Acid-Base Cements: Their Biomedical andIn-dustrial Applications, Cambridge University Press,2005.

[321] M. Mathew, L.W. Schroeder, Crystal structure of a struvite analogue, MgKPO4$6H2O,ActaCrystallogr.B35(1979)11e13.

[322] S.Graeser,W.Postl,H.-P.Bojar,P.Berlepsch,T.Armbruster,T.Raber,etal., Struvite-(K), KMgPO4$6H2O, the potassium equivalent of struvitee a new mineral, Eur. J. Mineral. 20 (2008)629e633.

[323] L.J. Gardner, S.A. Bernal, S.A. Walling, C.L. Corkhill, J.L. Provis, N.C. Hyatt, Characterisationofmagnesiumpotassiumphosphatecements blendedwithfly ash and ground granulated blast furnace slag, Cement Concr. Res. 74(2015)78e87.

[324] S.N. Scrimgeour, J.A. Chudek, G.A. Cowper, C.H. Lloyd, 31P solid-state MAS-NMRspectroscopyofthecompoundsthatforminphosphate-bondeddentalcasting investment materials during setting,

Dent. Mater. 23 (2007)934e943.

[325] D.Laurencin,C.Gervais,H.Stork,S.Kra€mer,D.Massiot,F.Fayon,25Mgsolid-state NMR of magnesium phosphates: high magnetic field experimentsand density functional theory calculations, J. Phys. Chem. C 116 (2012)19984e19995.

[326] L.J. Gardner, S.A. Walling, S.A. Bernal, C.L. Corkhill, D. Iuga, J.L. Provis, et al.,Characterisation of struvite-K, MgKPO4$6H2O, an analogue of struvite (manuscript in preparation),2017.

[327] B. Lothenbach, F. Winnefeld, Thermodynamic modelling of the hydration ofPortlandcement,CementConcr.Res.36(2006)209e226.

[328] S.-Y. Hong, F.P. Glasser, Alkali binding in cement pastes: part I. The C-S-H phase, Cement Concr. Res. 29 (1999)1893e1903.

[329] H. Zanni, R. Rassem-Bertolo, S. Masse, L. Fernandez, P. Nieto, B. Bresson, AspectroscopicNMRinvestigationofthecalciumsilicatehydratespresentincementandconcrete,Magn.Reson.Imag.14(1996)827e831.

[330] F.Me´ducin,B.Bresson,N.Lequeux,M.-N.deNoirfontaine,H.Zanni,Calciumsilicate hydrates investigated by solid-state high resolution 1H and 29Si nuclear magnetic resonance, Cement Concr. Res. 37 (2007)631e638.

[331] E.Scholtzov´a,L.Kuckova´,J.Ko˘zí˜sek,D.Tunega,Structuralandspectroscopiccharacterization of ettringite mineral-combined and DFT experimentalstudy,J.Mol.Struct.1100(2015)215e224.

[332] Moore, H. Taylor, Crystal structure of ettringite, Acta Crystallogr. B 26(1970)386e393.

[333] F. Goetz-Neunhoeffer, J. Neubauer, Refined ettringite (Ca6Al2(- SO4)3(OH)12·26H2O) structure for quantitative X-ray diffraction analysis, Powder Diffr. 21 (2006)4e11.

[334] Katz, A. Brough, R. Kirkpatrick, L. Struble, G. Sun, J. Young, Cement so- lidification of simulated off-gas condensates from vitrification of low-levelnuclearwastesolutions,WasteManag.21(2001)543e553.

[335] G.LeSaout,E.Le´colier,A.Rivereau,H.Zanni,Chemicalstructureofcementaged at normal and elevated temperatures and pressures: part II: lowpermeabilityclassGoilwellcement,CementConcr.Res.36(2006)71e78.

[336] M.R. Hansen, M. Brorson, H. Bildsøe, J. Skibsted, H.J. Jakobsen, Sensitivity enhancement in natural-abundance solid-state 33S MAS NMR spectroscopy employing adiabatic inversion pulses to the satellite transitions, J. Magn.Reson. 190 (2008)316e326.

[337] W.Lukas,SubstitutionofSiinthelatticeofettringite,CementConcr.Res.6(1976)225e233.

[338] A.-R. Grimmer, W. Wieker, F.V. Lampe, E. Fechner, R. Peter, G. Molgedey,Hochauflo€sende29Si-NMRanfestenSilicaten:anisotropiederchemischenVerschiebungimThaumasit,Z.Chem.20(1980)453.

[339] Lippmaa, M. Maegi, A. Samoson, G. Engelhardt, A.R. Grimmer, Structural studies of silicates by solid-state high-resolution silicon-29 NMR, J. Am.Chem. Soc. 102 (1980)4889e4893.

[340] J. Skibsted, L. Hjorth, H.J. Jakobsen, Quantification of thaumasite in cemen- titious materials by 29Si{1H} cross-polarization magic-angle spinning NMR spectroscopy, Adv. Cem. Res. 7 (1995)69e83.

[341] R.A. Edge, H.F.W. Taylor, Crystal structure of thaumasite, [Ca3Si(OH)6$12H2O](SO4)(CO3), Acta Crystallogr. B 27 (1971)594e601.

[342] T. Matschei, B. Lothenbach, F.P. Glasser, The AFm phase in Portlandcement, Cement Concr. Res. 37 (2007)118e130.

[343] C.Famy,A.Brough,H.Taylor,TheCSHgelofPortlandcementmortars:PartI. The interpretation of energy-dispersive X-ray microanalyses from scanning electron microscopy, with some observations on CSH, AFm and AFt phasecompositions,CementConcr.Res.33(2003)1389e1398.

S.D. Wang, K.L. Scrivener, Hydration products of alkali-activated slag cement, CementConcr.Res.25(1995)561e571.

[344] X. Ke, S.A. Bernal, J.L. Provis, Controlling the reaction kinetics of sodiumcarbonate-activated slag cements using calcined layered double hydroxides,Cement Concr. Res. 81 (2016)24e37.

[345] S.A. Bernal, J.L. Provis, R.J. Myers, R. San Nicolas, J.S.J. van Deventer, Role of carbonates in the chemical evolution of sodium carbonate-activated slagbinders, Mater. Struct. 48 (2015)517e529.

[346] R. Allmann, Refinement of the hybrid layer structure [Ca2Al(OH)6]þ$[1/2SO4$3H2O]—, Neues Jahrb. Mineral. Monatsh. 1977 (1977) 136e143.

[347] G. Renaudin, M. Francois, O. Evrard, Order and disorder in the lamellar hy-drated tetracalcium monocarboaluminate compound, Cement Concr. Res. 29(1999)63e69.

[348] M. François, G. Renaudin, O. Evrard, A cementitious compound withcomposition 3CaO$Al2O3$CaCO3$11H2O, Acta Crystallogr. Sect. C Cryst. Struct. Commun. 54 (1998)1214e1217.

[349] Buttler, L. Dent Glasser, H. Taylor, Studies on 4CaO$Al2O3$13H2O and the related natural mineral hydrocalumite, J. Am. Ceram. Soc. 42 (1959) 121e126.

[350] B.Lothenbach,G.LeSaoût,E.Gallucci,K.Scrivener,Influenceoflimestoneon thehydrationofPortlandcements,CementConcr.Res.38(2008)848e860.

[351] S. Ahmed, H. Taylor, Crystal structures of the lamellar calcium aluminate hydrates, Nature 215 (1967)622e623.

[352] S.Kwan,J.LaRosa,M.W.Grutzeck,29Siand27AlMASNMR stra€tlingite,J.Am.Ceram. Soc. 78 (1995)1921e1926.

[353] R.Rinaldi,M.Sacerdoti,E.Passaglia, Str€atlingite:crystalstructure,chemistry,and a reexamination of its polytype vertumnite, Eur. J. Mineral. (1990) 841e850.

[354] W.Geßner,D.Müller,Festko€rper-NMR-untersuchungenamgehlenithydrat2CaO$Al2O3$SiO2$8H2O, Z. Chem. 29 (1989)344e345.

[355] R.J. Kirkpatrick, P. Yu, X. Hou, Y. Kim, Interlayer structure, anion dy- namics, and phase transitions in mixed-metal layered hydroxides; var-iabletemperature35ClNMRspectroscopyofhydrotalciteand Ca-aluminatehydrate(hydrocalumite),Am.Mineral.84(1999)1186e1190.

[356] R. Taylor, I.G. Richardson, R.M.D. Brydson, Composition and microstructure of 20-year-old ordinary Portland cementeground granulated blast-furnaceslag blends containing 0 to 100% slag, Cement Concr. Res. 40 (2010) 971e983.

[357] B. Lothenbach, A. Gruskovnjak, Hydration of alkali-activated slag: ther-modynamic modelling, Adv. Cem. Res. 19 (2007)81e92.

[358] J.L. Provis, J.S.J. van Deventer, Alkali Activated Materials. State-of-the-Art Report,RILEMTC224-AAM,Springer,Dordrecht,2014.

[359] H.F.W.Taylor,Sulfatereactionsinconcreteemicrostructuralandchemical aspects, Ceram. Trans. 40 (1994)61e78.

[360] S.Mills,A.Christy,J.-M.Ge´nin,T.Kameda,F.Colombo,Nomenclatureofthehydrotalcitesupergroup:naturallayereddoublehydroxides,Mineral.Mag.76 (2012)1289e1336.

[361] K.J.D. MacKenzie, R.H. Meinhold, B.L. Sherriff, Z. Xu, 27Al and 25Mg solid-state magic-anglespinningnuclearmagneticresonancestudyofhydrotalciteanditsthermaldecompositionsequence,J.Mater.Chem.3(1993)1263.

[362] R.K.Allada,J.D.Pless,T.M.Nenoff,A.Navrotsky,Thermochemistryof

[363] hydrotalcite-likephasesintercalatedwithCO2-,NO-,Cl-,I-,andReO-,Chem.

[364] A.Samoson,Satellitetransitionhigh-resolutionNMRofquadrupolarnuclei in powders, Chem. Phys. Lett. 119 (1985)29e32.

[365] J. Skibsted, N.C. Nielsen, H. Bildsøe, H.J. Jakobsen, Satellite transitions in MAS NMRspectraofquadrupolarnuclei,J.Magn.Reson.95(1991)88e117.

[366] C.J€ager,Satellitetransitionspectroscopy of quadrupolarnuclei,in:

[367] B. Blumich, R. Kosfeld (Eds.), NMR Basic Principles and Progress: Solid-State NMR II, Springer-Verlag, Berlin, 1994, p. 135.

[368] J.Brus,S.Abbrent,L.Kobera,M.Urbanova´,P. Cuba,Advancesin27AlMASNMRstudiesofgeopolymers,Annu.Rep.NMRSpectrosc.88(2016)79e147.

[369] J.D. Gehman, J.L. Provis, Generalized biaxial shearing of MQMAS NMRspectra, J. Magn. Reson. 200 (2009)167e172.

[370] T.F.Kemp,M.E.Smith,QuadFitdanewcross-platformcomputerprogramfor simulation of NMR line shapes from solids with distributions ofinteractionparameters,SolidStateNucl.Magn.Reson.35(2009)243e252.

[371] J.-B. d'Espinose de Lacaillerie, C. Fretigny, D. Massiot, MAS NMR spectra ofquadrupolar nuclei in disordered solids: the Czjzek model, J. Magn. Reson. 192 (2008)244e251.

[372] P.T.Durdzin´ski,M.BenHaha,S.A. Bernal,N.DeBelie,E.Gruyaert,

[373] B.Lothenbach,etal.,OutcomesoftheRILEMroundrobinondegreeof

[374] reaction of slag and fly ash in blended cements, Mater. Struct. 50 (2017)135.

[375] Mater. 17 (2005) 2455e2459.

[376] J. Lumley, R. Gollop, G. Moir, H. Taylor, Degrees of reaction of the slagin

[377] R. Snellings, T. Paulhiac, K. Scrivener, The effect of Mg on slag reactivity inblendedcements,WasteBiomassValoriz.5(2014)369e383.

[378] H.M. Dyson, I.G. Richardson, A.R. Brough, A combined 29Si MAS NMR and selective dissolution technique for the quantitative evaluation of hydrated blast furnace slag cement blends, J. Am. Ceram. Soc. 90 (2007)598e602.

[379] R.Brydson,I.G.Richardson,G.W.Groves,Determiningthelocal coordinationof aluminium in cement using electron energy loss near-edge structure, Microchim. Acta 114 (1994)221e229.

[380] I.G. Richardson, Clarification of possible ordered distributions of trivalent cationsinlayereddoublehydroxidesandanexplanationfortheobserved variation in the lower solid-solution limit, Acta Crystallogr. B 69 (2013) 629e633.

[381] X.Ke,S.A.Bernal,J.L.Provis,UptakeofchlorideandcarbonatebyMg-AlandCa-Al layered double hydroxides in simulated pore solutions of alkali-activatedslagcement,CementConcr.Res.100(2017)1e13.

[382] R.J. Myers, B. Lothenbach, S.A. Bernal, J.L. Provis, Thermodynamic modelling ofalkali-activatedslagcements,Appl.Geochem.61(2015)233e247.

[383] D.M.Roy,E.Sonnenthal,R.Prave,Hydrotalciteobservedinmortarsexposed to sulfate solutions, Cement Concr. Res. 15 (1985)914e916.

[384] Mascolo, Hydration products of synthetic glasses similar to blast-furnace slags,CementConcr.Res.3(1973)207e213.

[385] R. Allmann, H. Jepsen, Die struktur des hydrotalkits, Neues Jahrb. Mineral. Monatsh. 1969 (1969)544e551.

[386] J.Rocha,M.delArco,V.Rives,M.A.Ulibarri,Reconstructionoflayereddoublehydroxides from calcined precursors: a powder XRD and 27Al MAS NMR study,J.Mater.Chem.9(1999)2499e2503.

[387] P.J. Sideris, F. Blanc, Z. Gan, C.P. Grey, Identification of cation clustering inMgeAl layered double hydroxides using multinuclear solid state nuclear magnetic resonance spectroscopy, Chem. Mater. 24 (2012)2449e2461.

[388] L. Zhao, Z. Qi, F. Blanc, G. Yu, M. Wang, N. Xue, et al., Investigating localstructure in layered double hydroxides with 17O NMR spectroscopy, Adv. Funct. Mater. 24 (2014)1696e1702.

[389] B. Lothenbach, E. Wieland, A thermodynamic approach to the hydration ofsulphate-resistingPortlandcement,WasteManag.26(2006)706e719.

[390] N.C. Collier, N.B. Milestone, J. Hill, I.H. Godfrey, Immobilisation of Fe floc: part2, encapsulation offloc in composite cement, J. Nucl. Mater. 393 (2009)92e101.

[391] G.LeSaout,E.Le´colier,A.Rivereau,H.Zanni,Chemicalstructureofcementaged at normal and elevated temperatures and pressures: part I. Class Goilwellcement,CementConcr.Res.36(2006)71e78.

[392] B.Lothenbach,T.Matschei,G.Mo€schner,F.P.Glasser,Thermodynamicmodelling of the effect of temperature on the hydration and porosity ofPortlandcement,CementConcr.Res.38(2008)1e18.

[393] N.Neuville,E.Le´colier,G.Aouad,A.Rivereau,D.Damidot,Effect of curingconditionsonoilwellcementpastebehaviourduringleaching:experimentalandmodellingapproaches,Compt.Rendus Chim.12(2009)511e520.

[394] N.C.Collier,N.B.Milestone,J.Hill,I.H.Godfrey,Thedisposal ofradioactive ferric floc, Waste Manag. 26 (2006)769e775.

[395] J.M. Rivas Mercury, P. Pena, A.H. De Aza, X. Turrillas, I. Sobrados, J. Sanz, Solid-state 27Al and 29Si NMR investigations on Si-substituted hydrogarnets, Acta Mater. 55 (2007)1183e1191.

[396] J. Mahler, A. Sebald, Deconvolution of 29Si magic-angle spinning nuclear magnetic resonance spectra of silicate glasses revisitede some critical comments,SolidStateNucl.Magn.Reson.5(1995)63e78.

[397] L. Petrakis, Spectral line shapes: Gaussian and Lorentzian functions inmagnetic resonance, J. Chem. Educ. 44 (1967)432.

[398] J.H.VanVleck,Line-breadthsandthetheoryofmagnetism,IlNuovoCimento6 (1957)993e1014.

[399] B. Walkley, S.J. Page, G.J. Rees, J.L. Provis, J.V. Hanna, Nanostructural devel-opment of synthetic CaO-(Na2O)-Al2O3-SiO2-H2O gels revealed by multinu-clearMQMASNMR(manuscriptinpreparation),2017.

[400] Some blends with Portland cements, Cement Concr. Res. 26 (1996) 139e151.

[401] J. Rossen, K. Scrivener, Optimization of SEM-EDS to determine the CeAeSeH composition in matured cement paste samples, Mater. Char. 123 (2017) 294e306.

[402] N.V. Scarlett, I.C. Madsen, Quantification of phases with partial or no knowncrystalstructures,PowderDiffr.21(2006)278e284.

[403] C.A.Fyfe,J.L.Bretherton,L.Y.Lam,Detectionofthe‘invisible aluminium’andcharacterisation of the multiple aluminium environments in zeolite USY byhigh-fieldsolid-stateNMR,Chem.Commun.(2000)1575e1576.

[404] R.H.Bogue,TheChemistryofPortlandCement,Reinhold,1955.

[405] H.F. Taylor, Modification of the Bogue calculation, Adv. Cem. Res. 2 (1989) 73e77.

[406] M. Kaupp, B. Michael, V.G. Malkin, Calculation of NMR and EPRParameters: TheoryandApplications,JohnWiley&Sons,2006.

[407] L.B. Casabianca, A.C. de Dios, Ab initio calculations of NMR chemical shifts, J. Chem. Phys. 128 (2008)052201.

[408] E.L. Hahn, Spin echoes, Phys. Rev. 80 (1950)580e594.

[409] D. Nied, K. Enemark-Rasmussen, E. L'Hopital, J. Skibsted, B. Lothenbach, Properties of magnesium silicate hydrates (M-S-H), Cement Concr. Res. 79(2016)323e332.

[410] S.R. Hartmann, E.L. Hahn, Nuclear double resonance in the rotating frame, Phys. Rev. 128 (1962)2042e2053.

[411] Y. Tong, H. Du, L. Fei, CP/MAS NMR studies of the initial hydration processes of activated and ordinary beta-dicalcium silicates, Cement Concr. Res. 20(1990)986e991.

[412] X. Cong, R.J. Kirkpatrick, 1Hd 29Si CPMAS NMR study of the structure of calcium silicate hydrate, Adv. Cem. Res. 7 (1995)103e111.

[413] S.A. Rodger, G.W. Groves, N.J. Clayden, C.M. Dobson, Hydration of tricalcium silicate followed by 29Si NMR with cross-polarization, J. Am. Ceram. Soc. 71 (1988)91e96.

[414] R. Rassem, H. Zanni-Theveneau, I. Schneid, M. Regourd, 29Si high-resolution NMR study of tricalcium silicate hydration, J. Chim. Phys. 86 (1989)1253e1264.

[415] J.F. Young, Investigations of calcium silicate hydrate structure using silicon- 29 nuclear magnetic resonance spectroscopy, J. Am. Ceram. Soc. 71 (1988) C118eC120.

[416] Y. Okada, H. Ishida, T. Mitsuda, 29Si NMR spectroscopy of silicate anions inhydrothermallyformedC-S-H,J.Am.Ceram.Soc.77(1994)765e768.

[417] I.G.Richardson,ThenatureofC-S-Hinhardenedcements,CementConcr. Res. 29 (1999)1131e1147.

[418] J.R. Houston, R.S. Maxwell, S.A. Carroll, Transformation of meta-stable cal-cium silicate hydrates to tobermorite: reaction kinetics and molecular structure from XRD and NMR spectroscopy, Geochem. Trans. 10 (2009) 1e14.

[419] L. Frydman, J.S. Harwood, Isotropic spectra of half-integer quadrupolar spinsfrom bidimensional magic-angle-spinning NMR, J. Am. Chem. Soc. 117(1995)5367e5368.

[420] Medek, J.S. Harwood, L. Frydman, Multiple-quantum magic-angle spinningNMR:anewmethodforthestudyofquadrupolarnucleiinsolids,J.Am.Chem. Soc. 117 (1995)12779e12787.

[421] T.T. Tran, S.A. Bernal, D. Herfort, J. Skibsted, Characterization of the network structure of alkali-activated aluminosilicate binders by single- and double-resonance 29Si {27Al} MAS NMR experiments, in: M.A.T.M. Broekmans (Ed.),Proceedingsofthe10thInternationalCongressforAppliedMineralogy. Trondheim, 2011, pp.707e715.

[422] T.-J. Park, S.-S. Choi, Y. Kim, 27Al solid-state NMR structural studies ofhydrotalcite compounds calcined at different temperatures, Bull. KoreanChem. Soc. 30(2009).

[423] D. Massiot, B. Touzo, D. Trumeau, J.P. Coutures, J. Virlet, P. Florian, et al.,Two- dimensional magic-angle spinning isotropic reconstruction sequences forquadrupolarnuclei,SolidStateNucl.Magn.Reson.6(1996) 73e83.

[424] I.Hung,J.Tre´bosc,G.L.Hoatson,R.L.Vold,J.-P.Amoureux,Z.Gan,Q-sheartransformation for MQMAS and STMAS NMR spectra, J. Magn. Reson. 201(2009)81e86.

[425] T. Gullion, Measurement of dipolar interactions between spin-12 andquadrupolar nuclei by rotational-echo, adiabatic-passage, double-resonanceNMR,Chem.Phys.Lett.246(1995)325e330.

[426] T. Gullion, J. Schaefer, Rotational-echo double-resonance NMR, J. Magn.Reson. (1969) 81 (1989)196e200.

[427] E.R.H. van Eck, W.S. Veeman, Spin density description of rotational-echo double-resonance,transferred-echo double-resonance and two-dimensional transferred-echo double-resonance solid state nuclear magneticresonance,SolidStateNucl.Magn.Reson.2(1993)307e315.

[428] E.R.H. van Eck, W.S. Veeman, The determination of the average 27Al-31P distance in aluminophosphate molecular sieves with SEDOR NMR, SolidStateNucl.Magn.Reson.1(1992)1e4.

[429] A.W. Hing, S. Vega, J. Schaefer, Transferred-echo double-resonance NMR,J.Magn.Reson.96(1992)205e209.

[430] A.W. Hing, S. Vega, J. Schaefer, Measurement of heteronuclear dipolar coupling by transferred-echo double-resonance NMR, J. Magn. Reson. A 103(1993)151e162.

[431] C.P. Grey, W.S. Veeman, The detection of weak heteronuclear couplingbe- tween spin 1 and spin 1/2 nuclei in MAS NMR; 14N/13C/1H triple resonance experiments,Chem.Phys.Lett.192(1992)379e385.

[432] C.P. Grey, W.S. Veeman, A.J. Vega, Rotational echo 14N/13C/1H triple reso- nance solid-state nuclear magnetic resonance: a probe of 13Ce14N internucleardistances,J.Chem.Phys.98(1993)7711e7724.

[433] T. Gullion, Detecting 13Ce17O dipolar interactions by rotational-echo, adia- batic-passage, double-resonance NMR, J. Magn. Reson. A 117 (1995)326e329.

[434] S.Greiser,G.J.G.Gluth,P.Sturm,C.Ja€ger,29Si{27Al},27Al{29Si}and27Al{1H}double-resonance NMR spectroscopy study of cementitious sodium alumi-nosilicate gels (geopolymers) and gelezeolite composites, RSC Adv. 8(2018) 40164e40171.

[435] Goldbourt, S. Vega, T. Gullion, A.J. Vega, Interatomic distance measure- ment in solid-state NMR between a spin-1/2 and a spin-5/2 using a universal REAPDORcurve,J.Am.Chem.Soc.125(2003)11194e11195.

[436] Bax, S. Subramanian, Sensitivity-enhanced two-dimensional hetero- nuclear shift correlation NMR spectroscopy, J. Magn. Reson. 67 (1986)565e569.

[437] H.J.Jakobsen,J.Skibsted,H.Bildsøe,N.C.Nielsen,Magic-anglespinningNMRspectra of satellite transitions for quadrupolar nuclei in solids, J. Magn.Reson. 85 (1989)173e180.

[438] J. Rocha, J.D. Pedrosa, D.E. Jesus, 27Al satellite transition MAS-NMR spectroscopyofkaolinite,ClayMiner.29(1994)287e291.

[439] D.Bish,R.VonDreele,Rietveldrefinementofnon-hydrogenatomicpositions in kaolinite, Clays Clay Miner. 37 (1989)289e296.

[440] R. Blaine, Proton magnetic resonance (NMR) in hydrated Portland cements, Natl.Bur.Stand.Monogr.43(1960)501e511.

[441] D. Lasic, J. Corbett, J. Jian, J. MacTavish, M. Pintar, R. Blinc, et al., NMR spin grouping in hydrating cement at 200 MHz, Cement Concr. Res. 18 (1988)649e653.

[442] R.Blinc,M.Burgar,G.Lahajnar,M.Roˇzmarin,V.Rutar,I.Kocuvan,etal.,NMRrelaxationstudyofadsorbedwaterincementandC3Spastes,J.Am.Ceram. Soc. 61 (1978)35e37.

[443] K. Kawachi, M. Murakami, E. Hirahara, The hydration and hardening ofcement. The nuclear magnetic resonance absorption of water molecules incement,Bull.Fac.Eng.HiroshimaUniv.4(1955)95e100.

[444] P.Seligmann,Nuclearmagneticresonancestudiesofthewaterinhardened cementpaste,PortlandCem.Assoc.Lab.Bull.222(1968).

[445] L. Miljkovic, D. Lasic, J. MacTavish, M. Pintar, R. Blinc, G. Lahajnar, NMR studies of hydrating cement: a spin-spin relaxation study of the early hydrationstage,CementConcr.Res.18(1988)951e956.

[446] L.Schreiner,J.Mactavish,L.Miljkovi´c,M.Pintar,R.Blinc,G. Lahajnar,etal.,NMR line shape-spin-lattice relaxation correlation study of Portland cement hydration,J.Am.Ceram.Soc.68(1985)10e16.

[447] R. Holly, E. Reardon, C. Hansson, H. Peemoeller, Proton spinespin relaxation studyoftheeffectoftemperatureonwhitecementhydration,J.Am.Ceram. Soc. 90 (2007)570e577.

[448] J. Greener, H. Peemoeller, C. Choi, R. Holly, E.J. Reardon, C.M. Hansson, et al.,Monitoring of hydration of white cement paste with proton NMR spinespinrelaxation, J. Am. Ceram. Soc. 83 (2000)623e627.

[449] R. Holly, H. Peemoeller, M. Zhang, E. Reardon, C. Hansson, Magnetic reso-nance in situ study of tricalcium aluminate hydration in the presence ofgypsum,J.Am.Ceram.Soc.89(2006)1022e1027.

[450] M. Gussoni, F. Greco, F. Bonazzi, A. Vezzoli, D. Botta, G. Dotelli, et al., 1H NMR spin-spin relaxation and imaging in porous systems: an application to themorphological study of white Portland cement during hydration in thepresenceoforganics,Magn.Reson.Imag.22(2004)877e889.

[451] A.Plassais,M.-P.Pomie`s,N.Lequeux,J.-P.Korb,D.Petit,F.Barberon,etal.,Microstructure evolution of hydrated cement pastes, Phys. Rev. 72 (2005) 041401.

[452] P. McDonald, J.-P. Korb, J. Mitchell, L. Monteilhet, Surface relaxation andchemical exchange in hydrating cement pastes: a two-dimensional NMRrelaxationstudy,Phys.Rev.72(2005)011409.

[453] P.J.McDonald,J.Mitchell,M.Mulheron,P.S.Aptaker,J.-P.Korb,L.Monteilhet, Two-dimensional correlation relaxometry studies of cement pastes per-formed using a new one-sided NMR magnet, Cement Concr. Res. 37 (2007) 303e309.

[454] P.S. Wang, M. Ferguson, G. Eng, D. Bentz, C. Ferraris, J. Clifton, 1H nuclear magnetic resonance characterization of Portland cement: molecular diffu-sion of water studied by spin relaxation and relaxation time-weighted im-aging, J. Mater. Sci. 33 (1998)3065e3071.

[455] L.Monteilhet,J.-P.Korb,J.Mitchell,P.McDonald,Observationofexchangeof micropore water in cement pastes by two-dimensional T2T2nuclear magneticresonancerelaxometry,Phys.Rev.E74(2006)061404.

[456] Valori, V. Rodin, P. McDonald, On the interpretation of 1H 2-dimensional NMR relaxation exchange spectra in cements: is there exchange between pores with two characteristic sizes or Fe3þconcentrations? Cement Concr. Res. 40 (2010)1375e1377.

[457] J.-Y.Jehng,D.Sprague,W.Halperin,Porestructureofhydratingcementpaste bymagneticresonancerelaxationanalysisandfreezing,Magn. Reson.Imag.14 (1996)785e791.

[458] R. Valckenborg, L. Pel, K. Kopinga, Combined NMR cryoporometry andrelaxometry,J.Phys.DAppl.Phys.35(2002)249.

[459] A.C.A. Muller, K.L. Scrivener, A.M. Gajewicz, P.J. McDonald, Densification of CeSeH measured by 1H NMR relaxometry, J. Phys. Chem. C 117 (2013) 403e412.

[460] A.C.A.Muller,K.L.Scrivener,A.M.Gajewicz,P.J.McDonald ,Useofbench-topNMR to measure the density, composition and desorption isotherm ofCeSeHincementpaste,MicroporousMesoporousMater.178(2013)99e103.

[461] A.C.A. Muller, K.L. Scrivener, A reassessment of mercury intrusion porosim-etry by comparison with 1H NMR relaxometry, Cement Concr. Res. 100 (2017)350e360.

[462] G.H. Fuller, Nuclear spins and moments, J. Phys. Chem. Ref. Data 5 (1976)835e1092.

[463] Walkley, A. Kashani, M.A. Sani, T.D. Ngo, P. Mendis, Examination of alkali- activated material nanostructure during thermal treatment, J. Mater. Sci. 53(2018)9486e9503.

★★★

OPENINGS AND FUTURE HEADINGS FOR VISUAL SOIL ASSESSMENT TECHNIQUES IN SOIL STRUCTURE RESEARCH

[1]BHARAT CHEDE, [2]JHARANA PRADHAN, [3]SMITA SAHOO

[1]Assistant Professor, Department of Mechanical Engineering, NMIET, BBSR
[2]Asst Prof, Department of Civil Engineering REC BBSR
[3]Asst Prof, Department of Civil Engineering AIET BBSR
E-mail: [1]palai.priyadarshini@gmail.com

Abstract -
As the utilization of visual soil assessment (VSE) strategies has spread universally, they have been presented to various climatic and pedological situations, bringing about the need to explain restrictions, empower refinements and open up new roads of examination. The primary target of this paper is to layout the capability of VSE techniques to create novel soil structure examination and how this potential could be created and incorporated inside existing exploration. We give a concise outline of VSE techniques to sum up the dirt data that is acquired by VSE. More definite VSE techniques could be created to give spatial data to soil measure models, for example compaction models. VSE could be joined with detecting procedures at the field or scene scale for better administration of fields with regards to accuracy cultivating. Further work ought to be never really plant life, roots and soil fauna into VSE strategies to give general pointers of soil quality and for assessment of ecological danger factors identified with soil C stockpiling, GHG outflows and supplement filtering, with specific reference to fleeting changes. There is an incredible potential in consolidating (instead of contrasting) VSE with estimations of soil structure, for example incorporating VSE in soil design and compaction research, as these techniques give spatial data that is difficult to acquire with different strategies.

I. INTRODUCTION

Soil structure comprises the physical habitat of soil living organisms, and controls many important physical, chemical and biological soil functions and associated ecosystem services. Soil structure is typically defined as the spatial arrangement of soil constituents and voids (i.e. soil pores), which may also be defined as the spatial distribution of soil properties (Dexter, 1988). However, soil structure is more than just the physical arrangement of particles and pores (that was referred to as “structural form” by Kay and Angers (2001)), and includes structural stability (i.e. the ability to resist external stresses) and structural resilience (i.e. the ability to recover upon stress removal) (Kay and Angers, 2001).

Different methods can be used to evaluate the different aspects of soil structure. For example, computed tomography (CT) imaging is excellent at visualizing and quantifying the form of soil structure (foranoverview,seeTainaetal.,2008;Peth, 2011; WildenshildandSheppard, 2013) and can be used to study the dynamics of soil structural pore spaces (i.e. the dynamics of the form of soil structure) by multiple scanning as demonstrated by Peth et al.(2013), but cannot directly assess soil structure stability or resilience. Visual soil evaluation (VSE) cannot reveal as much information on the geometrical arrangement of pores and constituents as CT imaging does, but assesses both the structural form and the structural stability (e.g. DVWK, 1995a, 1997; ATV-DVWK, 2001; Boizard et al., 2007; Guimarães et al., 2011), and may reveal information on the resilience through biological indicators (e.g. Boizard et al., 2017). Unlike the texture of a soil that can be considered a static property, the soil structure is a dynamic trait. Soil structure is influenced by bothnatural and anthropogenic processes. The natural processes include abiotic processesinduced by drying-wetting and freeze-thaw phenomena, as well as biotic processes leading to the creation of new pore spaces by the penetration of plant roots and burrowing fauna, soil aggregate stabilization by plant roots, fungi, and soil fauna (enmeshing, excretions), and soil shrinkage due to plant water uptake (Kay,1990; Dexter, 1991; Horn et al., 1994; Horn, 2003; Hallett et al.,2013). Anthropogenic influences on soil structure are primarily related to soil management including soil tillage, soil compaction due to vehicle traffic, incorporation of organic fertilizers and amendments, as well as crop selection and fertilization (for an overview, see Kay, 1990; Bronick and Lal, 2005; Kay andMunkholm, 2011). Such aspects have significant influence on structural stability and resilience as well as structural form, all of which influencesoil function (Horn,1990; Hornetal.,1994).

Despite the recognized importance of soil structure for soil functioning, its characterization and quantification of the complex interactions (as stated above) that drive soil structure formation remain a challenge (e.g. Hallett et al., 2013; Peth et al., 2013). Visual soil evaluation (VSE) methods have been developed to assess the structural state of soil (for a review see Boizard et al., 2007). Most VSE methods were developed as a practical diagnostic tool in agricultural extension service. Various visual methods to assess soil structure and soil quality have been developed and used for many years in different parts of the world, and these have mainly been published in reports, booklets and notes (e.g. Görbing, 1947;Peerlkamp, 1959; Preuschen, 1983; Gautronneau and Manichon,1987; DVWK, 1995a; Shepherd, 2000; Munkholm, 2000; McKen-zie, 2001; Nievergelt et al., 2002). More recently, methods have been refined, combined, and published in scientific journals (for an overview see e.g. Ball et al., 2015). In the remainder of this paper, we use 'visual soil evaluation (VSE) methods' as a general term for all methods, whereas specific methods (e.g. 'Profil Cultural'; Gautronneau and Manichon, 1987) will be referred to by their specific name. Furthermore, there has been a growing interest to (re-)use VSE methods in research, that primarily have been used to characterize the impact of soil management on soil structure and to help identify the type and location of measurements for further characterization of soil physical properties (Ball et al., 2015; this special issue).

Only a few studies have used VSE methods with regards to soil structure dynamics. Roger-Estrade et al. (2000)used the 'Profil Cultural' method (Gautronneau and Manichon, 1987) to quantify the temporal evolution of soil structure under contrasting tillage systems, and Boizard et al. (2013) used the same method to study recovery after compaction in a reduced tillage experiment. Ball andMunkholm (2015)showed that the 'Visual Evaluation of Soil Structure' (VESS) method (Guimarães et al., 2011) was able to reveal variations in soil quality and recovery, over a four-year period of evaluation, when assessing compaction by tractor and animal trampling. These authors also highlighted that repeating VSE measurements over time enables the monitoring of soil quality evolution.

All VSE methods are mainly used within an agronomic context, with the purpose of assessing soil management effects and providing soil management recommendations. Thus, it is impor- tant that VSE scores have veracity and are nearly reproducible. Therefore, soil structure is systematically evaluated according to manuals and instruction videos to reduce operator dependence for most VSE methods. In general, different operators typically find very similar scores (e.g. Ball et al., 2007; Guimarães et al.,2011). Subjectivity is, however, still considered a modest limitation to VSE methods, e.g. in relation to the isolation of structural units and the assessment of their properties and efforts to further reduce this limitation continue. Other limitations include possibly confusing soil moisture effects on soilstrength with those of compaction and difficulty in use in soils of extreme textures and insufficient emphasis on porosity, particularly with spade methods (Ball and Munkholm, 2015; Munkholm andHolden, 2015). Scale is also an important aspect to take account for any soil structure description method. Babel et al. (1995)proposed an initial description of soil structure (shape and surface of the structural units, geometrical arrangement, aggre- gate strength, bioturbation, etc.) at a given scale, and then to reproduce observations at various scales applicable across land uses and across scientific disciplines.

VSE methods yield information on the vertical thickness and depth of natural and anthropogenic soil layers, and on the spatial arrangement of structural features (profile methods) or the size distribution of soil fragments (spade methods). Such information is not available, for example, from sampling at discrete (pre-defined) depths with small volumes (e.g. undisturbed cylindrical soil cores that may have a typical volume of 100 cm3), which are typically used in soil structure research. Several studies have demonstrated significant correlations between the various structural features (as e.g. obtained by VSE methods) and a range of soil properties (mainly soil physical properties such as, bulk density, penetration resistance, saturated hydraulic conductivity, among others; see e.g.Horn, 1990; Shepherd, 2003; Dörner and Horn, 2009; Guimarães et al., 2013; Moncada et al., 2014; Ball et al., 2017). Moreover, the shape of the fragments and an estimate of the tensile strength of thefragmentsisobtainablefrom VSEmethods. The'ProfilCultural' reports detailed information regarding the spatial arrangement and distribution of soil properties (e.g. aggregates, pores, roots, organic residues), whereas other methods such as VESS (Guimar- ães et al., 2011), the Visual Soil Assessment (VSA) method (Shepherd, 2009) and SOILpak (McKenzie, 1998), for example, combine this information into a score or soil quality index, either for each layer or for a whole soil profile. The reason for combining this information into a single index is that such an index will be useful for assessing the overall physical quality of a soil, for comparing soil quality across soils, and for providing soil management recommendations. However, valuable information on soil structure can be lost through the combination process. We will argue in this paper that this information could be useful in research aiming at better understanding the impact of soil structure on soil functioning (including plant growth) and better understanding of soil structure dynamics.

A joint workshop of the ISTRO working groups on Visual Soil Examination and Evaluation (VSEE) and Subsoil Compaction held in May 2014 brought together scientists dealing with characteri- zation of soil structure and its dynamics with a focus on soil management impacts (soil tillage, soil degradation by compac- tion). A main aim of the workshop was to jointly discuss and possibly outline (i) research needs of visual soil evaluation methods, new approaches (ii) to combine VSE methods with "traditional" soil physical methods and analysis as well as with remote and proximal sensing techniques, and (iii) to integrate VSE in soil structure research for better quantification of soil structure and better understanding of soil structure dynamics caused by soil management. This article summarizes and synthesizes the discussions from the workshop. Although the workshop had an emphasis on tropical conditions, most of the discussions were relevant to all soils.

The main objectives of this paper are to outline (i) research needs for improvement of VSE methods, and (ii) the opportunities of VSE methods in soil structure research. We will provide a brief overview of VSE methods, in order to summarize the soil information that is obtained by VSE. We will describe research needs for further development of VSE methods and their better integration in soil structure research. Finally, we propose ways of using and integrating the spatial information obtained by VSE in research on soil structure dynamics and soil compaction.

II. BRIEF OVERVIEW OF VISUAL SOIL ASSESSMENTMETHODS

2.1. General approach of visual soil evaluation methods

Many visual soil evaluation (VSE) methods have been developed worldwide to evaluate the soil structural quality of topsoils and whole soil profiles. As mentioned above, many different methods have been developed and used in various parts of the world, but description of many methods may not be readily available for the international scientific community because they are often published in institutional reports, notes or as booklets. However, most methods share similar soil quality assessment criteria related to visible soil porosity as well as the size, shape and strength of aggregates. Please consult Boizard et al. (2007) for an overview of 10 different methods presented at the ISTRO 2005 workshop at Péronne, France. The methods generally divide into topsoil-focused spade methods and topsoil and subsoil focused profile methods. The most commonly used spade methods in research are the VSA method (Shepherd, 2009) and the VESS method developed from the Peerlkamp method (Ball et al., 2007;Guimarães et al., 2011) (Munkholm and Holden, 2015). Among the soil profile methods, ‘Profil Cultural’ (Gautronneau and Manichon,1987; Peigné et al., 2013), SOILpak (McKenzie, 1998) and, most recently, the numeric visual evaluation of subsoil structure methods (SubVESS) (Ball et al., 2015) are used in research (Munkholm and Holden, 2015). These five spade and profile methods are described in detail by Batey et al. (2015). It is also important to mention methods that integrate information from different methods into an overall soil quality rating such as the MuenchebergSoilQualityRatingsystem(Muelleretal.,2013).

The five different VSE methods mentioned above all include assessment of size, shape and strength of soil aggregates and of visible porosity (Batey et al., 2015). These features yield information on the quality of soil as plant growth medium, habitat for soil biology and on conditions for nutrient cycling, and water and gas storage and transport. Other commonly evaluated features are soil colour (e.g. VESS, SubVESS and VSA), earthworms in terms of numbers, sizes, species and burrows (e.g. VSA and Munkholm spade method (Munkholm, 2000)), rooting in terms of proliferation and architecture, depth, and distortion (e.g. VESS, VSA, SOILpak and SubVESS), porosity (all methods) and water stable aggregates (SOILpak). Most methods include an evaluation of distinct soil layers or zones but often evaluation scores are assessed across different layers. The importance of specific evaluation of limiting layers such as hardpans is highlighted in the profile methods (SOILpak, SubVESS and ‘Profil Cultural’) and in some spade methods (VESS, Guimarães et al., 2011). The VSE methods differ markedly in terms of the level of details regarding the evaluation. The more detailed the analysis (as for ‘Profil Cultural’) the longer it takes to complete an evaluation. In general the simple spade methods such as VESS are fastest (5–15 min per sample) and the detailed profile methods take the longest time (1–3 h) (Boizard et al., 2007; Batey et al., 2015). The fast and easy to use spade methods make it possible to make many replicates in the same time as it takes to do one detailed profile evaluation. Thereby, a larger area and more treatments can be covered within the same time interval. On the other hand this may be at the expense of more detailed understanding of specific land use or management effects on soil structure. In many cases a combina- tion of fast and simple methods with a few more detailed evaluations may be beneficial in order to obtain both general knowledge on spatial differences and in depth knowledge of the impact of specific land use or soil management. Pleaseconsult Batey et al. (2015) for more details on similarities and differences between the commonly used methods.

2.2. Application of visual methods inpractice

VSE methods are used in many countries by agricultural advisors, teachers, and farmers, even though detailed knowledgeof the use of the VSE methods in practice is often lacking. More detailed VSE methods will require specialized soil knowledge for successful application, while simple spade methods only requiresome methodological training for successful application by students or farmers, for example. Weexpect that the methods are most widely used in Western Europe, Australia, New Zealand and Brazil, where most of today's known methods have been developed. To illustrate the interest in VSE methods in practice, the VESS manual has been translated into a number of languages, including Spanish, French, Portuguese, Norwegian and Danish, primarily byadvisors.

2.3. Application of visual methods in soil research

The VSE methods are increasingly being used in soil research to evaluate effects of land use and soil management, primarily. Munkholm and Holden (2015)listed 29 VSE papers on arable soil and 10VSEpapersongrasslandsoilsinarecentreviewandmos tof them had been published since 2010. In general, VSE methods have been useful to detect effects of land use and management on soil structure. Most VSE papers also include comparative quantitative soil structure data e.g. soil pore characteristics, bulk density, soil strength, soil structural stability and hydraulic conductivity. Strong correlations have been found in many cases as outlined by e.g. Batey et al. (2015). Significant correlations with crop yield have also been shown in some studies (Mueller et al., 2009; Munkholmet al.,2013).

The VSE methods have primarily been used for comparative studies where effects of land use and management has been investigated at a specific time. In a few cases the VSE methods have been applied to study soil structure dynamics, i.e. spatio-temporal changes in soil structure after e.g. animal or field traffic induced soil compaction (Ball and Munkholm, 2015; Boizard et al., 2013).Boizard et al. (2013) showed that the “Profil Cultural” was a useful tool to assess soil recovery after heavy compaction. They detected thedevelopmentofaplaty structurelayerinthe yearsafteraheavy compaction treatment. The above mentioned studies suggest that there is a great potential for more widespread application of VSE methods in studies of soil structure dynamics. However, VSE methods are destructive by nature and this has to be taken into account when choosing VSE as a tool to study temporal evolution of soil structure, especially within fieldexperiments.

3. Research needs for further development of visual soil assessment methods

3.1. Improving the quality of scoring by including the impact ofsoil moisture content atsampling

Soil aggregate fragmentation is an integral component of many visual evaluation methods (see previous section). However, fragmentation is strongly affected by the soil moisture (for an overview, see e.g. Dexter and Bird, 2001; Munkholm, 2011), and hence the soil moisture, measured in terms of water content or in terms of matric potential, at the time of assessment can influence the result of the test (Fig. 1). Water strongly affects the consistency and the strength of soil (e.g. Atterberg, 1911; Horn, 2003), consequently, a drier soil is generally harder and more difficult tobreakup, and therefore, extra pressure is required to fragment dry aggregates. Especially, it is important that the soil is not dried to conditions drier than it has ever experienced before, as this is associated with irreversible soil structural changes, when smaller aggregatesmaybreakupduetoporeweakening(Hornetal. ,2014). This may not be a problem under many conditions, but could be crucial when evaluating subsoils in temperate climates. A wet soil is weak, and beyond a certain moisture content soils no longer break-up, instead the aggregates plastically deform when a pressure is applied. Both, a too dry and a too wet soil may result in a false interpretation of its structure. Soil friability describes the tendency of a soil to break down into fragments of desired sizes upon application of a stress (Utomo and Dexter, 1981). A range of water contents can be defined within which soil friability is satisfactory (see Munkholm, 2011). The upper (i.e. wet) limit of this range is typically defined from soil consistency and often assumed at w=PL(lowerplasticlimit). AshortcomingofusingPLasalimitis that it is determined on remoulded soils, and natural soil may behave differently. The lower (i.e. dry) limit is less well defined but related to energy requirement for fragmentation. Soil friability is maximum at intermediate soil water contents, with the maximum friability at a water content, w, at around 0.9 PL, see Munkholm(2011). Similarly, we can define a range of suitable water contents for visual soil evaluation (Fig. 1). It may be assumed that the range of water contents for satisfactory friability and satisfactory visual soil evaluation coincide. For this reason, it is generally recom- mended that visual tests are conducted while the soil is within the friable range (Ball et al., 2017), to avoid misinterpretation of the sample. The ease of fragmenting an aggregate is one of the key factors evaluated by VESS. We suggest that the optimum range of water contents for visual soil evaluation could be investigated in future research. The range of suitable water contents may be affected by climatic conditions (e.g. rainfall patterns) and soil type

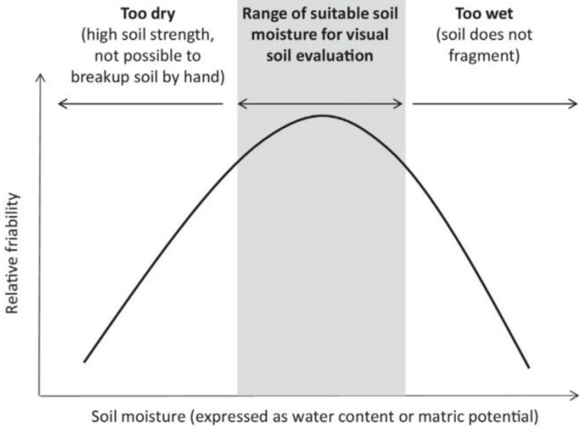

Fig. 1. Schematic illustration of the suitable range of soil moisture (expressed as water content or matric potential) for visual soil evaluation, in analogy to the relationship between soil friability and soil water content. Adapted from Munkholm(2011).

(e.g.differentforsandsoilsvsclaysoils).Thelatterproblemmaybe overcome by specifying a range in matric potentials rather than in water content. Another strategy could be to develop methods to normalize VSE results to a standardized water content (e.g. by using w/PL) or matric potential. This would require that the water content and/or matric potential at the time of VSE is measured, as suggested by Babel et al. (1995). Furthermore, it could be interesting to perform VSE at various water contents/potentials. We hypothesize that the change in soil quality (e.g.score) as assessed by VSE as a function of soil water status may carry some information on the resilience of a certain soil (structure).

3.2. Extending the scope of VSE by integrating biological indicators

Macrofauna and root activity, which are also assessed in VSE methods, play a major role in soil structural quality, mainly by improving macroporosity, by promoting aggregation, and by stabilizing structures (e.g. Lynch, 1984; Kay, 1990; Dexter, 1991;Uteau et al., 2013; Han et al., 2015; Pagenkemper et al., 2015). Some methods, such as the VSA, include the number of earthworms as an indicator of soil quality (Shepherd, 2009), while Munkholm (2000)uses the number of earthworm holes as another quality aspect to be evaluated. Munkholm (2000)highlights the difficulty of evaluating soil macrofauna as it can be difficult to observe the fauna before they escape the soil block extracted for evaluation. VESS does not currently include faunal presence as part of its evaluation, however, the presence of distinct biopores (resulting from earthworm and root activity) is a criterion for attributing a score and counting of earthworms within the block is proposed as an extension of the method. Franco et al. (2017)showed positive correlations between VESS and reduction in Isoptera and Coleoptera abundance, while earthworm activity has been shown to have an important impact on soil structural quality (Piron et al., 2012). Therefore, the improvement and incorporation of faunal assess- ments in visual methods and the evidence of their action in soil structure dynamics should be a future research goal, as also highlighted by Boizard et al. (2007)and Munkholm and Holden(2015).

3.3. Combining visual soil assessment methods with remote and proximal sensing and interactive tools for mobile devices

Remote sensing techniques can be used to show diagnostic indicators of soil properties, such as soil texture (Peng et al., 2014), organic matter content (Viscarra Rossel and Hicks, 2015; Aldana-Jague et al., 2016), organic matter quality (Ben-Dor et al., 1997), iron content, soil texture or particle size distribution, clay mineralogy, water content, soil contamination (Peng et al.,2016), cation exchange capacity and calcium carbonate content through imaging spectroscopy (Ben-Dor et al., 2009; Stenberget al., 2010; Soriano-Disla et al., 2014) and soil moisture through RADAR sensing (Zribi et al., 2011). Estimates of these properties by means of remote sensing typically rely on relationshipsestablished from standard measurements on pre-treated and remoulded soil samples in the laboratory. However, actual in situ properties of structured soils may differ from apparent properties measured on homogenized samples. Therefore, there is a risk of misinterpretationofdata.Forexample,Hartmannetal.(1998)showedthatthere is a difference in the observed cation exchange when comparing homogenized samples with in situ structured soil. Multispectral sensing can be used to estimate land cover and use, vegetation indices and degradation (Dewitte et al., 2012; Mulder et al., 2011). Here we differentiate remote sensing that is airborne or satellite basedatthelargescale fromproximalsensingthatisground-based for finer scales (Wulf et al.,2015).

Proximal sensors utilize a variety of electromagnetic radiations to infer information on salinity, organic composition, mineralogy, moisture content, topsoil thickness and clay content (Samouelianet al., 2005; Viscarra Rossel et al., 2006). These and other sensing techniques can be used to differentiate the landscape or plot intoscaled units of sensory output that can be related to site properties through field sampling (Paradelo et al., 2016). Good correlations have been observed between the results of remote or proximal sensing and soil variables such as bulk density, penetration resistance, soilorganiccarbonand soilmoisture and, forVIS-NIR sensing of soil quality, has been related to visual quality scores for VESS (Askari et al., 2015).

A promising area of future study is the correlation of electromagnetic spectrum sensing results with visual evaluation scores as it would allow the interpolation of a limited number ofSq scores (from VESS) over the sensed areas, reducing the burden of sampling. This would be of particular relevance in precision farming where inputs are related to soil variables. Aerial photography, now available at low cost using Unmanned Aerial Vehicle (UAV/drone) technology, could be used to identify areas of compacted or degraded soil for further investigation via VSE. Combining techniques of remote and ground-based sensing and yield mapping could be used to delineate areas with similar soil properties and/or adverse yield productivity (Fig. 2), and thereby assist in selecting locations for more detailed investigation using VSE. In addition, use of handheld devices with various sensors (e.g. NIR to detect moisture content) could complement VSE and make soil quality scoring more robust (cf. Section3.1).

Another promising area of developing technology is the use of interactive tools for mobile devices, such as smart phones and tablets, that include instructional help videos, methodologies and scoringapplications,whichallowfieldobservationstoberelatedto reference photographic guides, to make soil quality scoring more relevant or for easy transmission to experts available online. This would allow more information to be available than from a chart or fieldguide,reducingerrorsandtheinfluenceoftheoperator.

3.4. Integrating VSE with other properties to provide more holistic estimation of soilquality

The measurement of soil hydraulic properties is a useful indicator of a drainage or aeration limitation of the cropping potential, however, inferring these properties via visual methods canbedifficult.Manysoilfeaturescloselyrelatedtosoilhydraulics, such as surface crusting, large cloddy structure, soil colour, surface deformation, surface ponding, soil erosion and surface microrelief can be scored visually using ad hoc keys (Murphy et al., 2013;Guimarães et al., 2015; Shepherd, 2009). Including surface features in visual methods could be of particular value by enabling improved inferences regarding hydraulic properties. For example, recordingthepresenceofsealingorsurfacecrustingorplatylayers could imply restricted infiltration or water drainage. The development of visual assessments such as the erosion toolkits that relate soil texture and slope to soil structure and thereby to risk of erosion (Regan, 2012; Guimarães et al., 2015) could enable more objectivity when linking surface features with soil structural quality.

Profile methods, such as SubVESS, "Profil Cultural" andSOILpak (topsoil and subsoil) give an overall status of soil structure to a greater soil depth than the spade methods. A vertical continuous pore network is important for soil functions, such as drainage and aeration and as a conduit for root growth, all of which are key factors for crop productivity and profile methods are suitable when tracking macropore continuity (Munkholm and Holden, 2015). Identifying and distinguishing man-made from naturally com- pacted layers will enable profile methods to be more useful for identifying subsoil layers that require loosening. Munkholm andHolden (2015) reported that identifying the layer that limits plant growth is crucial for subsoils, therefore, reporting evaluations for individual layers is recommended by Ball et al. (2015)and McKenzie (1998).

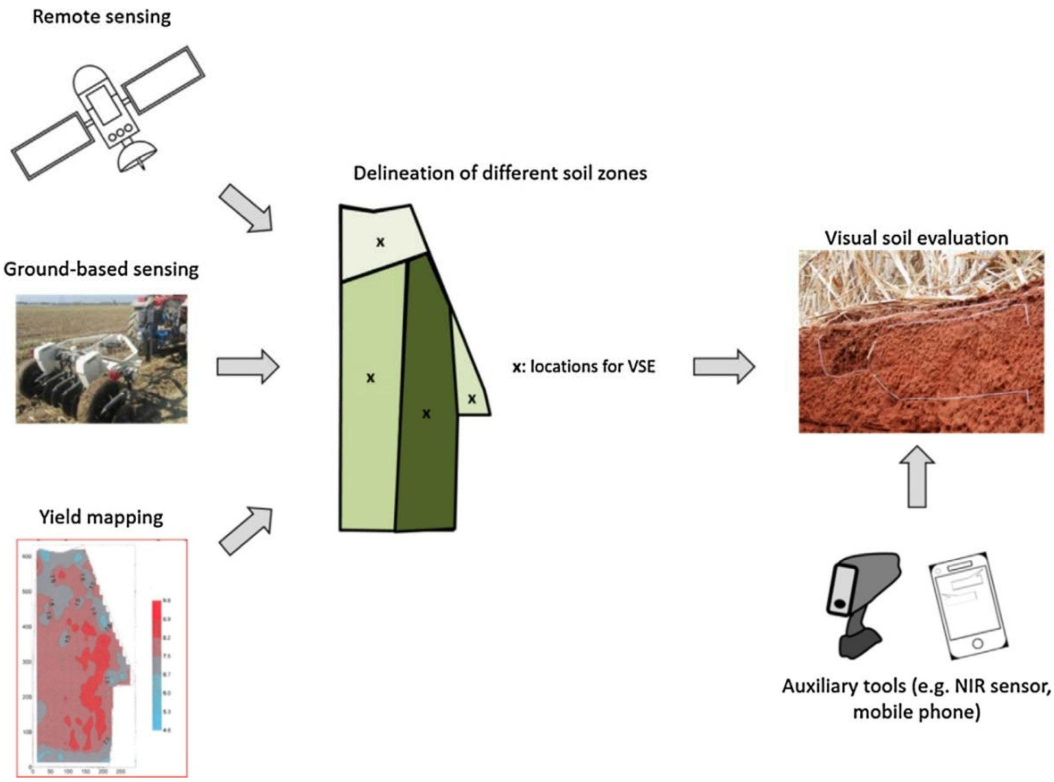

Fig.2.Conceptualfigureshowingtheuseofremoteandproximalsensingandinteractivetoolsformobiledevicestogetherwithvisualsoilevaluation.Remotesensingand ground-basedsensingcanidentify variationsinsoilpropertiesandyield-limitingfactors(e.g.soiltexture,nitrogenavailability,soilmoisture,soilcompaction), whileyield mapping reflects the spatial variability of productivity. For example, combining areas of poor soil conditions and restricted productivity reveals zones that require further evaluation by VSE in order to deduce specified soil management recommendations for soil improvement. Ground-based sensing photo from Naderi-Boldaji et al. (2014).VisualsoilevaluationphotofromDr.CraigD.Rogers.

Assessment of agricultural land in terms of soil quality and soil structure using quick VSA and VESS techniques has been shown to provide an indication of the potential for soils to store C, release GHGs and lose nutrients, and are therefore important for identifying problems as well as to combat environmental change (Cloyetal.,2015).VSAandVESSwerealsousedtoestimatetherisk of soil emissions of nitrous oxide from pastures where compaction damage was present and rates of mineral N fertilizer were high. Visual assessments also have the potential to assess the risk of surface water runoff and nutrient loss. Such assessments which combine detailed soil and crop visual evaluations with fertilizer management history are areas for potential development. The potential role of soil colour was shown for the further extension of visual evaluation techniques to a soil carbon storage index. These methods show clear potential for further development and research to provide validation of scored soil and crop qualities with measured properties of soil C storage, GHG emissions and nutrientleaching (Cloyetal.,2015; Balletal.,2017).

Extending and combining visual methods with other simple quantitative or qualitative field methods will give a more general soilqualityindicator, suchasin VSA and SOILpak(Muelleretal., 2014; Munkholm and Holden, 2015). Govaerts et al. (2006)proposed a minimum data set to assess soil quality that should take into account soil and climatic conditions for the specific agro- ecological zone and their interaction with land use. Mueller et al.(2014)also proposed the combination of quantitative and qualitative field based methods with visual evaluation of soil methods. Combination of VSE methods with visual crop evaluation may also extend the agronomic relevance of VSE for identifying limiting soilconditions.

IV. POTENTIAL OF VISUAL SOIL EVALUATION METHODS TO ADVANCE SOIL STRUCTURE RESEARCH

4.1. Accounting for spatial variability in soil modelling

Quantification of the form of soil structure can be achieved through imaging (e.g. Peth et al., 2013) or indirect measurements (i.e. water and gas transport, aggregate size distribution, etc.; e.g. Ball et al., 1988). All imaging techniques and physical measure- ments are limited to a given size of observation, which makes our understanding of soil structure discontinuous and incomplete. Thus, extrapolation from measurements on soil samples to soil profile or to field is uncertain (e.g. Etana et al., 2013). Usually, averaged measurements on randomly sampled soil cores (10—2m) are used to explain soil functioning at the profile (100 m) or field scale (102 m), or to parameterize models. The issue of upscaling observations at core or smaller scale to field, landscape and global scale was highlighted as one of the essential challenges for soil modelling in a recent extensive review (Vereecken et al., 2016).

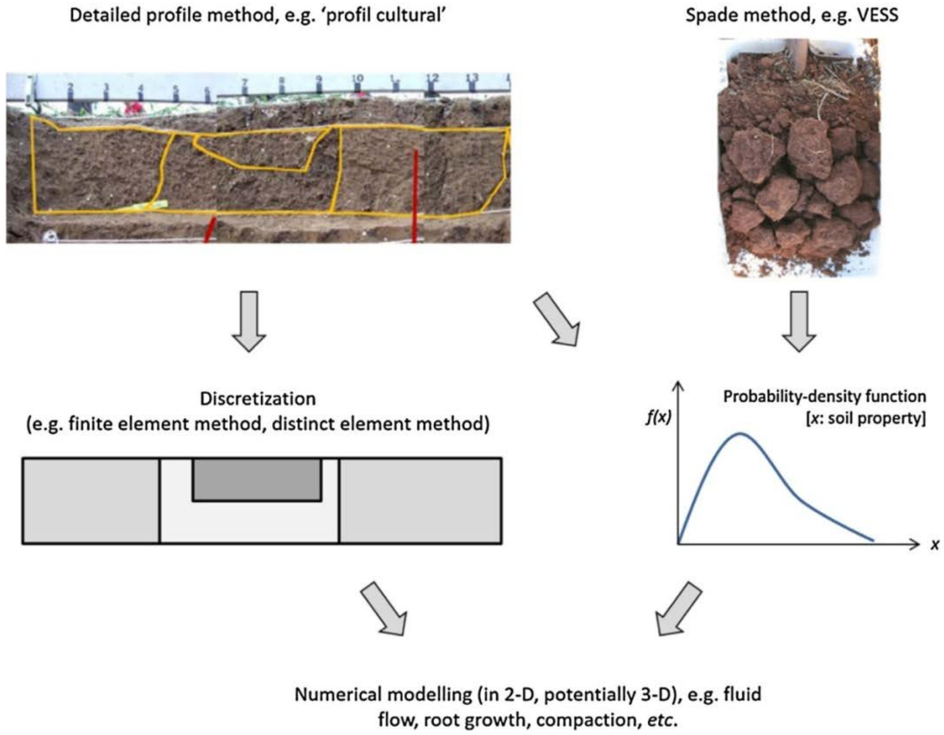

Fig. 3. Conceptual figure illustrating how the spatial information obtained from visual soil evaluation could be used in soil process modelling. We outline two ways of incorporating structural information in models, either via localization of areas of different soil properties (left) or via a statistical approach (right). Detailed profile methodscan be used for either method, while spade methods are limited to incorporation of spatial information via statistical means. Different levels of grey in the lower left picture representdifferentsoilqualityscoresordifferentvaluesofagivensoilproperty.ProfilCulturalphotofromBoizardetal.(2017).VESSphotofromRachelM.L.Guimarães.

The variability of a soil property can be described using probabilistic models (Perfect and Kay, 1994; Chun et al., 2008). However, simulation and evaluation of the effect of agricultural practices on soil functions often need maps of the spatial organization of the different structural features. Geophysical methods including electrical resistivity tomography, ground penetrating radar and seismic methods can be used to obtain two- or three-dimensional maps of soil physical properties thatcan be related to parameters relevant for soil models (Besson etal.,2004; Petersen et al., 2005). Further information on spatial variation of soil structural features can be readily assessed in situ by visual soil evaluation methods. VESS has been used to determine the minimum sampling density of VESS and of other assessmentsof soilqualitytocapturethe spatialvariationinafield. This involved sampling at up to 16 points per ha and mapping the data sets by kriging at decreasing sampling density to determine the optimum sampling density. This was 0.9–1 per ha for the two agricultural fields assessed (Laura Thomas and Bryan Griffiths, SRUC Edinburgh, personal communication). This corroborates similarresultsfoundbyRachelM.L.Guimarães(unpublisheddata), who evaluated 36 blocks per ha and concluded that one VESS evaluation per ha was the minimum sample density required to accurately represent a field's soil quality via VESS, however, it is suggested that three replicates should be taken per ha for statisticalpurposes.

Few studies have attempted to integrate soil structure spatial variability at the profile scale as described by visual soil evaluation methods into models, but some exceptions are the studies by Benjamin et al. (1990), Coutadeur et al. (2002)and Ndiaye et al.(2007). The methodology was the same for all these studies: physical measurements were performed in the laboratory or in the field for the different structural zones as identified on the soil profile by VSE, and measured soil parameters were used to model heat or water transport in two dimensions. However, none ofthese works took into account the temporal variation in soil structure, which would need also a model of structure dynamics, e.g. ‘Sisol’ developed by Roger-Estrade et al. (2009). For the studies mentioned above, VSE methods were used to give information on the spatial distribution of different zones, but soil properties needed to model the process in question (e.g. water transport) were obtained by measurements. VSE methods were used to choose the position of the sampling, which might lead to an overestimationofthedifferencesbetween,forexample, loose and compacted zones, as transitions between these zones might be difficult to sample.

The DVWK bulletins 234 and 235 (DVWK, 1995b,1997) showed that prediction of soil functions (e.g. soil strength) requires knowledge of in situ soil structural features related to aggregation, in addition to intrinsic soil properties (e.g. texture). Similarly, in a recent study, Moncada et al. (2014)showed that pedotransfer functions could benefit from integrating a VSE score. All these results might be due to the more holistic approach of VSE methods as compared with specific physical measurements. It is well known that soil structure changes over time due to natural and antrophogenic factors. Despite this, dynamic changes in soil structureareignoredinmost soilmodels(Vereeckenetal.,2016)— most likely due to lack of empirical data. VSE methods aresensitive to temporal changes (Boizard et al., 2013; Ball and Munkholm,2015)andmaybeusedastooltoassessinsituchangesataggregate to pedon scale and at different depths. Qualitative information from a VSE method at different times before and after tillage could be successfully used to model soil structural dynamics as affected by tillage (Roger-Estrade et al., 2000). Fig. 3illustrates how the spatial information obtained from visual soil evaluation could be used in soil process modelling. The qualitative information from VSE may be supplemented with quantitative data at selected times and depths, which may be used in more mechanistic soil modelling.

4.2. Improving the description of compaction propagation by including spatial description of soil structure within the soil profile

Compaction is a major soil threat due to ongoing intensification of agricultural practices: farmers and contractors choose large machinery to increase efficiency of field operations, and industry designs machinery that can perform on weak soils to increase flexibility of field operations planning (Schjønning et al., 2015). Description of the stress-strain processes during compaction of agricultural soils is typically based on geotechnical frameworks using continuum mechanics (Nawaz et al., 2013). However, agricultural soils present a three-dimensional organization of various components (mineral and organic particles, plant residues, stones) (e.g. Horn, 1990). Although approaches from continuum mechanics have been shown to produce fairly good estimations of stress transmission in arable soils (Keller et al., 2014), especially tilled topsoils, these may rather resemble a granular material

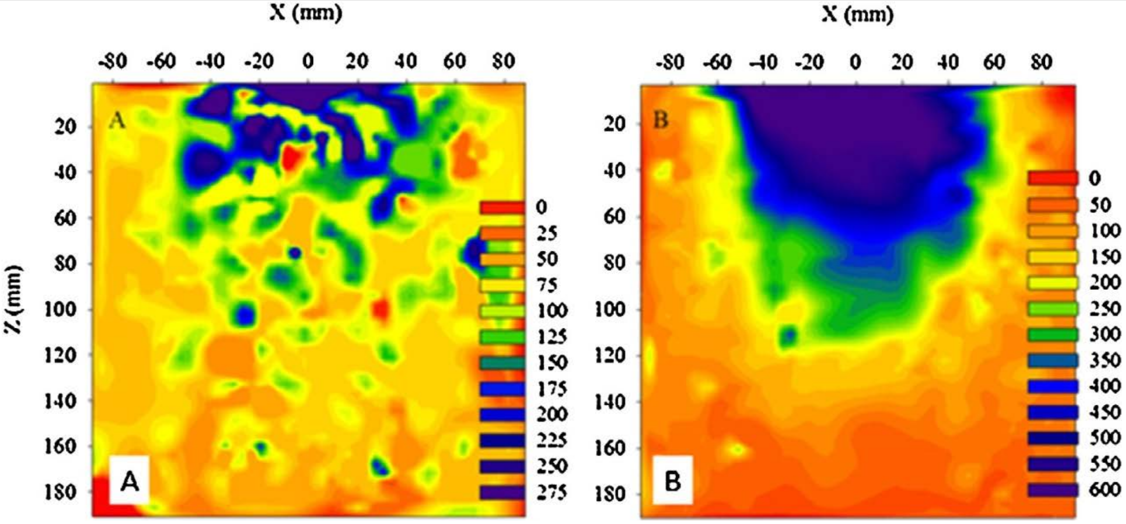

Fig. 4. The importance of including structure information for predicting stress propagation. Stress transmission in an undisturbed soil column (0.2 m high and 0.2 m in diameter) derived from X-ray computed tomography at applied stresses of 275 kPa (A) and 620 kPa (B). Source: Adapted from Naveed et al. (2016).

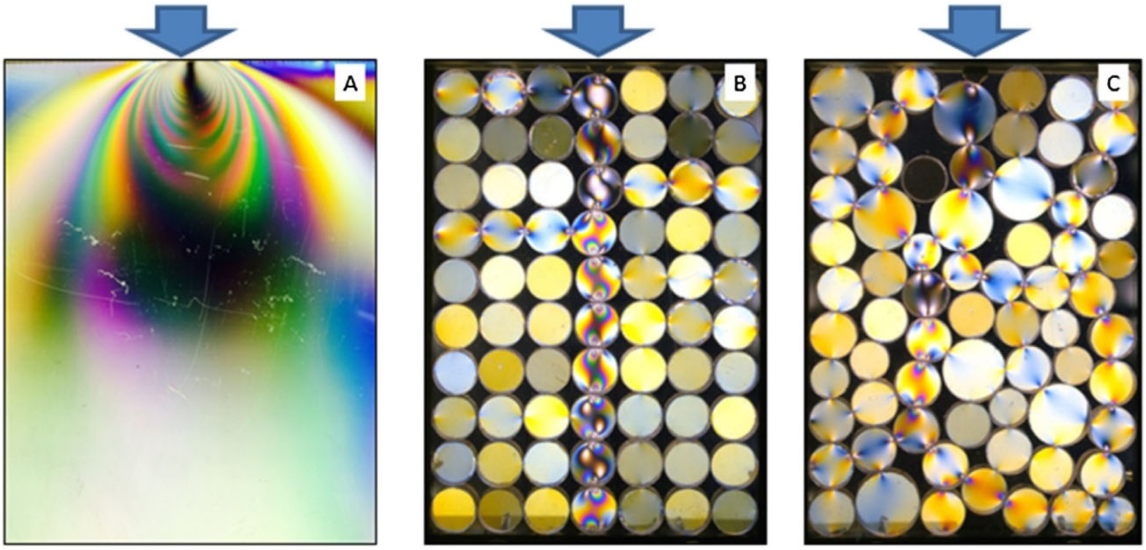

Fig.5.SpatialinformationonsoilstructureprovidedbyVSEcouldpotentiallyleadtoabetterrepresentationofstresspropagation.(A)Aphotoelasticviewofaplate,(B)a regularpackingofmono-sizeddiscsand(C)arandompackingofdiscswiththreedifferentsizes.Allaresubjectedtoapointloadof600N.Theplateandthediscsweremade of polycarbonate,whichhasaYoung'smodulusof2.0GPaandaPoisson'sratioof0.37.

(assembly of aggregates) than a continuum. Horn (1990)showed that stress transmission is affected by soil aggregation, readily assessed in some VSE techniques. The model described andapplied by Richards et al. (1997)and Richards and Peth (2009)could accommodate heterogeneity of soil properties and accounts for their evolution due to mechanical and hydraulic stresses. Naveedet al. (2016) recently observed that, in topsoils, stress propagation was heterogeneous and occurred through specific paths as long as the macro-structures were not deformed (Fig. 4). Thus, mechanics of tilled soil layers may be better described by granular matter physics than continuum physics. The mechanical behaviour of granular materials largely depends on grain size distribution (Voivret et al., 2007) and grain shapes (Azéma et al., 2009). By analogy, soil aggregate size distribution and aggregate shapes are expected to influence soil mechanical behaviour. Fig. 5A illustrates the elastic mode of stress propagation under a point load in an isotropic and continuous matter as described by Boussinesq(1885), which might be enough to describe stress propagation under certain soil conditions. Bulk measurements of soil physical parameters (such as measurements on soil cores) average soil properties for the volume of the sample, and measurements on replicated soil samples are typically averaged to represent properties at the pedon scale. Using average soil properties for a collection of aggregates may lead to an oversimplified description ofsoilpropertieswithina profilethatwould result in an unrealistic stress propagation (Fig. 5B). Introducing some information about the aggregate properties (size distribution) and how the collection of aggregates is spatially organized would improve description of stress propagation and therefore help better understanding of the mechanical behaviour of structured soil (Fig. 5C). Therefore, information from VSE methods associated with granular physics would help to better understand stress-strain relationships of aggregated soillayers.

V. CONCLUSIONS

Since their inception VSE methods have grown to become important tools in research. However, VSE methods still need better harmonization and reduction in subjectivity in aggregate exposure and the influence of soil moisture content at sampling for more accurate scoring. Handheld sensors and ICT devices may also help in this area. The spatial distribution of structural features recorded by VSE methods is often integrated into a score or soil quality index. We argue that VSE provides important information regarding spatial distribution of soil structure, particularly aggregation and macro-porosity, which could be disaggregated andusedtobetterunderstandvarioussoilprocesses,especiallythe process of soil compaction. More detailed VSE methods, such as ‘Profil Cultural’, could be developed (simplified, disaggregated and made more accessible) so that the spatial information is more easily provided. VSE could be combined with sensing techniques at field or landscape scale for better management of fields in the context of precision farming. Combining VSE methods with visual crop evaluation may extend the agronomic relevance of VSE for identifying limiting soil conditions. Further work should be done to integrate plant vigour, roots and soil fauna into VSE methods to provide general indicators of soil quality and environmental indicatorsofgreenhousegasemission,carbonstorageand nutrient transport. Forthispurposemorecomparisons betweenscoringand field/laboratory measurements are needed. However, we see a great potential in combining (rather than comparing) VSE with measurementsofsoilstructure,i.e.integratingVSEinsoil structure research, as these methods provide repeatable spatial information on large-scale aspects of soil structure that are difficult to obtain with othermethods.

ACKNOWLEDGEMENTS

This paper is an output from the workshop on Soil structural quality of tropical soils: Visual evaluation methods and soil compaction prevention strategies that was held 26–30 May 2014 inMaringá,Paraná,Brazil.Theworkshopwasfinancially supported by the International Soil Tillage Research Organization (ISTRO), which is gratefully acknowledged. The workshop was organized as a joint meeting of the ISTRO working groups on Visual Soil Examination and Evaluation (VSEE) and on Subsoil Compaction. LJM would like to acknowledge support from the Danish Ministry of Environment andFoodthroughtheOptiPlantproject. BCB would like to acknowledge financial Support from the Rural & Environ- ment Science & Analytical Services Division of the Scottish Government (R033003). ML and TK gratefully acknowledge financial support from the Danish Research Council for Technology and Production Sciences (Project No. 11-106471 “StressSoil”). RMLG would like to acknowledge Dr. Craig D. Rogers for providing photographs for Fig. 2.

REFERENCES

[1] Aldana-Jague, E., Heckrath, G., Macdonald, A., van Wesemael, B., Van Oost, K., 2016.UAS-based soil carbon mapping using VIS-NIR (480–100 nm) multi-spectralimaging: potential and limitations. Geoderma 275, 55–66.

[2] Askari, M.S., Cui, J., O’Rourke, S.M., Holden, N.M., 2015. Evaluation of soil structuralquality using VIS-NIR spectra. Soil Till. Res. 134, 1–10.

[3] Atterberg, A., 1911. Über die physikalische Bodenuntersuchung und über diePlastizität der Tone. Int. Mitt. Bodenkd. 1, 10–43.

[4] ATV-DVWK, 2001. Gefügestabilität ackerbaulich genutzter Mineralböden Teil III:Methoden für eine nachhaltige Bodenbewirtschaftung. ATV-DVWK-M 901.3935669704 27 pp..

[5] Azéma,E.,Radjai,F.,Saussine,G.,2009.Quasistaticrheology, forcetransmissionandfabricpropertiesofapackingofirregular polyhedralparticles.Mech.Mater.41,729–741.

[6] Babel,U.,Benecke,P.,Hartge,K.H.,Horn,R.,Wiechmann,H., 1995.Determinationofsoil structure at various scales. In: Hartge, K.H., Stewart, B.A. (Eds.), SoilStructure–ItsDevelopmentandFunction,AdvancesinSoilScience.CRC Press1-56670-173-2, pp.1–10.

[7] Ball,B.C.,Batey,T.,Munkholm,L.J.,2007.Fieldassessmentofsoilstructuralquality–adevelopmentofthePeerlkamptest.SoilUseManag.23,329–337.

[8] Ball, B.C., Batey, T., Munkholm, L.J., Guimarães, R.M.L., Boizard, H., McKenzie, D.C.,Peigné, J., Tormena, C.A., Hargreaves, P., 2015. The numeric visual evaluation ofsubsoil structure (SubVESS) under agricultural production. Soil Till. Res. 148,85–96.

[9] Ball, B.C., Guimarães, R.M.L., Cloy, J.M., Hargreaves, P., Shepherd, T.G., McKenzie, B. M., 2017. Visual soil evaluation: a summary of some applications and potential developments for agriculture. Soil Till. Res. 173, 114–124 (http://dx.doi.org/10.1016/j.still.2016.07.006).

[10] Ball, B.C., Munkholm, L.J., 2015. The expanding discipline and role of visual soilevaluation. In: Ball, B.C., Munkholm, L.J. (Eds.), Visual Soil Evaluation: RealizingPotential Crop Production with Minimum Environmental Impact. CABInternational, Wallingford, pp. 142–154.

[11] Ball,B.C.,O'Sullivan,M.F.,Hunter,R.,1988.Gasdiffusion,fluidflowandderivedporecontinuityindicesinrelationtovehicletrafficandtillage.J.SoilSci.39,327–339.

[12] Batey, T., Guimarães, R.M., Peigné, J., Boizard, H., 2015. Assessing structural qualityfor crop performance and for agronomy (VESS, VSA, SOILpak, Profil Cultural,SubVESS). In: Ball, B.C., Munkholm, L.J. (Eds.), Visual Soil Evaluation: RealizingPotential Crop Production with Minimum Environmental Impact. CABInternational, Wallingford, pp. 15–30.

[13] Ben-Dor, E., Chabrillat, S., Demattê, J.A.M., Taylor, G.R., Hill, J., Whiting, M.L.,Sommer,S.,2009.Usingimagingspectroscopytostudysoilproperties.RemoteSens. Environ. 113,S38–S55.

[14] Ben-Dor,E.,Inbar,Y.,Chen,Y.,1997.Thereflectancespectraoforga

nicmatterinthevisible near-infrared and short wave infrared region (400–2500 nm) during acontrolleddecompositionprocess.RemoteSens.Environ.61, 1–15.

[15] Benjamin, J.G., Blaylock, A.D., Brown, H.J., Cruse, R.M., 1990. Ridge tillage effectsonsimulatedwaterandheattransport.SoilTill.Res.18,167–180.

[16] Besson, A., Cousin, I., Samouëlian, A., Boizard, H., Richard, G., 2004. Structuralheterogeneityofthesoiltilledlayerascharacterizedby2Delectricalresistivitysurveying.SoilTill.Res.79,239–249.

[17] Boizard,H.,Batey,T.,McKenzie,D.C.,Richard,G.,Roger-Estrade,J.,Ball,B.C.,Bradley,I., Cattle, S., Hasinger, G., Munkholm, L.J., Niewergelt, J., Peigné, J., Shepherd, G.,2007. Field meeting “Visual Soil Structure Assessment” held at the INRAResearch Station, Estrées-Mons, France, April 25–May 2, 2005 34 pp..

[18] Boizard, H., Peigné, J., Sasal, M.C., Guimarães, M.F., Piron, D., Tomis, V., Vian, J.F., Cadoux, S., Ralisch, R., Tavares Filho, J., Heddadj, D., Battista, J., Duparque, A., Franchini, J.C., Roger-Estrade, J., 2017. Developments in the “profil cultural” method for an improved assessment of soil structure under no-till. Soil Till. Res. 173, 92–103 (http://dx.doi.org/10.1016/j.still.2016.07.007).

[19] Boizard,H.,Yoon,S.W.,Leonard,J.,Lheureux,S.,Cousin,I.,Roger-Estrade,J.,Richard,G., 2013. Using a morphological approach to evaluate the effect of traffic andweather conditions on the structure of a loamy soil in reduced tillage. Soil Till.Res. 127,26–33.

[20] Boussinesq, J., 1885. Application des Potentiels à l’étude de l’équilibre et duMouvement des Solides Élastiques. Gauthier-Villars, Paris, pp. 30.

[21] Bronick,C.J.,Lal,R.,2005.Soilstructureandmanagement:areview.Geoderma124,3–22.

[22] Chun, H.C., Gimenez, D., Yoon, S.W., 2008. Morphology, lacunarity and entropy ofintra-aggregate pores: aggregate size and soil management effects. Geoderma146, 83–93.

[23] Cloy,J.M.,Ball,B.C.,Shepherd,T.G.,2015.Evaluatinglandqualityforcarbonstorage,greenhouse gas emissions and nutrient leaching. In: Ball, B.C., Munkholm, L.R.(Eds.), Visual Soil Evaluation: Realising Potential Crop Production withMinimum Environmental Impact. CABI, Wallingford, UK, pp.103–121.

[24] Coutadeur,C.,Coquet,Y.,Roger-Estrade,J.,2002.Variationofhydraulicconductivityinatilledsoil.Eur.J.SoilSci.53,1–10.

[25] Dewitte, O., Jones, A., Elbelrhiti, H., Horion, S., Montanarella, L., 2012. Satelliteremote sensing for soil mapping in Africa: an overview. Prog. Phys. Geogr. 36,514–538.

[26] Dexter, A.R., 1988. Advances in characterization of soil structure. Soil Till. Res. 11,199–238.

[27] Dexter,A.R.,1991.Ameliorationofsoilbynaturalprocesses.SoilTill.Res.20,87–100.Dexter,A.R.,Bird,N.R.A.,2001.Methodsforpredictingtheoptimumandtherangeofsoilwatercontentsfortillagebasedonthewaterretentioncurve.SoilTill.Res.

[28] 57, 203–212.

[29] Dörner, J., Horn, R., 2009. Direction-dependent behaviour of hydraulic andmechanical properties in structured soils under conventional and conservationtillage. Soil Till. Res. 102, 225–232.

[30] DVWK, 1995a. Bodenkundliche Untersuchungen im Felde zur Ermittlung vonKennwerten zur Standortcharakterisierung. Teil I: Ansprache der Böden.DVWK-Regel 129/1995. 3-89554-024-2.

[31] DVWK, 1995b. Gefügestabilität ackerbaulich genutzter Mineralböden. Teil 1:Mechanische Belastbarkeit. DVWK Merkblatt 234, ATV-DVWK, Hennef..

[32] DVWK, 1997. Gefügestabilität ackerbaulich genutzter Mineralböden. Teil 2:Auflastabhängige Veränderung von bodenphysikalischen Kennwerten. DVWKMerkblatt 235, ATV-DVWK, Hennef..

[33] Etana, A., Larsbo, M., Keller, T., Arvidsson, J., Schjønning, P., Forkman, J., Jarvis, N.,2013.Persistentsubsoilcompactionanditseffectsonpreferentialflowpatternsinaloamytillsoil.Geoderma192,430–436.

[34] Franco, A.L.C., Cherubin, M.R., Cerri, C.E.P., Guimarães, R.M.L., Cerri, C.C., 2017.

[35] Relating the visual soil structure status and the abundance of soil engineeringinvertebratesacrosslandusechange.SoilTill.Res. 173,49–52.doi:http://dx.doi.org/10.1016/j.still.2016.08.016.

[36] Gautronneau,Y.,Manichon,H.,1987.Guideméthodiquedupr ofilcultural.GEARAetCEREF, 1987. Mimeografado..

[37] Görbing, J., 1947. Die Grundlagen der Gare im praktischen Ackerbau (Band I und II).

[38] Landbuch Verlag GMBH, Hannover.

[39] Govaerts, B., Sayre, K., Deckers, J., 2006. A minimum data set for soil qualityassessment of wheat and maize cropping in the highlands of Mexico. Soil Till.Res. 87, 163–174.

[40] Guimarães, R.M.L., Ball, B.C., Tormena, C.A., 2011. Improvements in the visualevaluation of soil structure. Soil Use Manag. 27, 395–403.

[41] Guimarães, R.M.L., Ball, B.C., Tormena, C.A., Giarola, N.F.B., da Silva, A.P., 2013.

[42] Relatingvisualevaluationofsoilstructuretootherphysicalpropertiesinsoilsofcontrasting texture and management. Soil Till.Res. 127, 92–99.

[43] Guimarães, R.M.L., Fenton, O., Murphy, B., Tormena, C.A., 2015. Soil structure underadverse weather/climate conditions. In: Ball, B.C., Munkholm, L.J. (Eds.), VisualSoil Evaluation: Realizing Potential Crop Production with MinimumEnvironmental Impact. CAB International, Wallingford, pp. 15–30.

[44] Hallett, P.D., Karim, K.H., Bengough, A.G., Otten, W., 2013. Biophysics of the vadosezone: from reality to model systems and back again. Vadose Zone J. 12 doi:http://dx.doi.org/10.2136/vzj2013.05.0090.

[45] Han,E.,Kautz,T.,Perkons,U.,Uteau,D.,Peth,S.,Huang,N.,Horn,R.,Köpke,U.,2015.Root growth dynamics inside and outside of soil biopores as affected by cropsequence determined with the profile wall method. Biol. Fertil. Soils 51, 847–856.

[46] Hartmann, A., Gräsle, W., Horn, R., 1998. Cation exchange processes in structuredsoilsatvarioushydraulicproperties.SoilTill.Res.47,67–72.

[47] Horn, R., Taubner, H., Wuttke, M., Baumgartl, T., 1994. Soil physical properties andprocessesrelatedtosoilstructure.SoilTill.Res.30,187–216.

[48] Horn, R., 2003. Stress–strain effects in structured unsaturated soils on coupledmechanical and hydraulic processes. Geoderma 116, 77–88.

[49] Horn, R., 1990. Aggregate characterization as compared to soil bulk properties. SoilTill. Res. 17, 265–289.

[50] Horn,R.,Peng,X.,Fleige,H.,Dörner,J.,2014.Porerigidityinstructuredsoils—onlyatheoreticalboundaryconditionforhydraulicproperties? SoilSci.PlantNutr.60,3–14.

[51] Kay,B.D.,Angers,D.A.,2001.Soilstructure.In:Sumner,M.E.(Ed.),HandbookofSoilScience. CRC Press, Boca Raton, pp.229–276.

[52] Kay, B.V., 1990. Rates of change of soil structure under different cropping systems.

[53] Adv. Soil Sci. 12, 1–52.

[54] Kay, B.V., Munkholm, L.J., 2011. Managing the interactions between soil biota andtheir physical habitat in agroecosystems. In: Ritz, K., Young, I. (Eds.), TheArchitectureandBiologyofSoils:LifeinInnerSpace.CAB International,pp.170–195.

[55] Keller,T.,Lamandé,M.,Arvidsson,J.,Berli,M.,Ruiz,S.,Schjønning,P.,Selvadurai,A.P.S.,2014.Transmissionofverticalsoilstressunderagriculturaltyres:comparingmeasurementswithsimulations.SoilTill.Res.140,106–117.

[56] Lynch, J.M., 1984. Interactions between biological processes, cultivation and soilstructure. Plant Soil 76, 307–318.

[57] McKenzie, D., 1998. SOILpak for Cotton Growers, 3rd edition Orange, New SouthWales, Australia.

[58] McKenzie, D.C., 2001. Rapid assessment of soil compaction damage.I. The SOILpakscore, a semi-quantitative measure of soil structural form. Aust. J. Soil Res. 39,117–125.

[59] Moncada, M.P., Penning, L.H., Timm, L.C., Gabriels, D., Cornelis, W.M., 2014. Visualexaminations and soil physical and hydraulic properties for assessing soilstructural quality of soils with contrasting textures and land uses. Soil Till. Res.140, 20–28.

[60] Mueller,L.,Kay,B.D.,Hu,C.,Li,Y.,Schindler,U.,Behrendt,A.,Shepherd,T.G.,Ball,B.C.,2009.Visualassessmentofsoilstructure:evaluationofmethodologieson sitesin Canada, China and Germany. Part I: comparing visual methods and linkingthem with soil physical data and grain yield of cereals. Soil Till. Res. 103, 178–187.

[61] Mueller,L.,Saparov,A.,Lischeid,G.,2014.NovelManagementandAssessmentToolsfor Monitoring and Management of Land and Water Resources in AgriculturalLandscapes of Central Asia. Springer International, Switzerland, pp.115–142.

[62] Mueller, L., Shepherd, G., Schindler, U., Ball, B.C., Munkholm, L.J., Hennings, V.,Smolentseva,E.,Rukhovic,O.,Lukin,S.,Hu,C.,2013.Evaluationofsoilstructureintheframeworkofanoverallsoilquality rating.SoilTill.Res.127,74–84.

[63] Mulder, V.L., deBruin, S., Schaepman, M.E., Mayr, T.R., 2011. The use of remotesensing in soil and terrain mapping—a review. Geoderma 162, 1–19.

[64] Munkholm,L.J.,2000.TheSpadeAnalysis—AModificationoftheQualitativeSpadeDiagnosisforScientificUse.Tjele,Denmark,pp.1–40.

[65] Munkholm,L.J.,2011.Soilfriability:areviewoftheconcept,assessmentandeffectsof soil properties and management. Geoderma167–168, 236–246.

[66] Munkholm, L.J., Heck, R.J., Deen, B., 2013. Long-term rotation and tillage effects onsoil structure and crop yield. Soil Till. Res. 127, 85–91.

[67] Munkholm, L.J., Holden, N.M., 2015. Visual evaluation of grassland and arablemanagement impacts on soil quality. In: Ball, B.C., Munkholm, L.J. (Eds.),VisualSoil Evaluation: Realizing Potential Crop Production with MinimumEnvironmentalImpact.CABInternational,Wallingford,pp.49–65.

[68] Murphy, B.W., Crawford, M.H., Duncan, D.A., McKenzie, D.C., Koen, T.B., 2013. Theuse of visual soil assessment schemes to evaluate surface structure in a soilmonitoring program. Soil Till. Res. 127, 3–12.

[69] Naderi-Boldaji,M.,Sharifi,A.,Hemmat,A.,Alimardani,R.,Keller,T., 2014.Feasibilitystudy on the potential of electrical conductivity sensor Veris13100 for fieldmapping of topsoil strength. Biosyst. Eng. 126,1–11.

[70] Naveed, M., Schjønning, P., Keller, T., de Jonge, L.W., Moldrup, P., Lamandé, M., 2016.Quantifying vertical stress transmission and compaction-induced soil structureusing sensor mat and X-ray computed tomography. Soil Till. Res. 158, 110–122.

[71] Nawaz,M.F.,Bourrié,G.,Trolard, F.,2013. Soilcompactionimpactandmodelling.Areview. Agron. Sust. Dev. 33,291–309.

[72] Ndiaye, B., Molénat, J., Hallaire, V., Gascuel, C., Hamon, Y., 2007. Effects ofagricultural practices on hydraulic properties and water movement in soils inBrittany (France). Soil Till. Res. 93, 251–263.

[73] Nievergelt, J., Petrasek, M., Weisskopf, P., 2002. Bodengefüge: Ansprechen undBeurteilenmitvisuallenMitteln.SchriftenreihederFAL,vol.41.3-905608-62-694pp.

[74] Pagenkemper, S.K., Athmann, M., Uteau, D., Kautz, T., Peth, S., Horn, R., 2015. Theeffect of earthworm activity on soil bioporosity—investigated with X-raycomputed tomography and endoscopy. Soil Till. Res. 146A, 79–88.

[75] Paradelo, M., Hermansen, C., Knadel, M., Moldrup, P., Greve, M.H., de Jonge, L.W.,2016. Field-scale predictions of soil contaminant sorption using visible-nearinfrared spectroscopy. J. Near Infrared Spectrosc. 24, 281–291.

[76] Peerlkamp, P.K., 1959. A visual method of soil structure evaluation. Meded. v.d.

[77] LandbouwhogeschoolenOpzoekingsstationsvandeStaatteGent.XXIVNo.24.,pp.216–221.

[78] Peigné, J., Vian, J.F., Cannavacciuolo, M., Lefevre, V., Gautronneau, Y., Boizard, H.,2013. Assessment of soil structure in the transition layer between topsoil andsubsoil using the profil cultural method. Soil Till. Res. 127, 13–25.

[79] Peng,Y.,BouKheir,R.,Adhikari,K.,Malinowski,R.,Greve,M.B.,Knadel,M.,Greve,M.H., 2016. Digital mapping of toxic metals in Qatari soils using remote sensingandancillarydata.RemoteSens.8,1003.

[80] Peng, Y., Knadel, M., Gislum, R., Schelde, K., Thomsen, A., Greve, M.H., 2014.

[81] Quantification of SOC and clay content using visible near-infrared reflectance-mid-infrared reflectance spectroscopy with Jack–Knifing partial squaresregression. Soil Sci. 179, 325–332.

[82] Perfect, E., Kay, B.D., 1994. Statistical characterization of dry aggregate strengthusing rupture energy. Soil Sci. Soc. Am. J. 58, 1804–1809.

[83] Petersen, H., Rabbel, W., Horn, R., Fleige, H., 2005. Applicability of geophysicalprospecting methods for mapping of soil compaction and variability of soiltexture on farm land. J. Plant Nutr. Soil Sci. 168, 1–12.

[84] Peth, S., 2011. Noninvasive quantification of 3D pore space structures in soils. In:Glinski, J., Horabik, J., Lipiec, J. (Eds.), Encyclopedia of Agrophysics. Springer,Berlin, pp. 516–519.

[85] Peth, S., Nellesen, J., Fischer, G., Tillmann, W., Horn, R., 2013. Dynamics of soilmacropore networks in response to hydraulic and mechanical stressesinvestigatedbyX-raymicrotomography.In:Logsdon,S.,Horn,R.,Berli,M.(Eds.),Advances in Agricultural Systems Modeling, Quantifying and Modeling SoilStructure Dynamics, vol. 3. , pp.121–153.

[86] Piron, D., Pérès, G., Hallaire, V., Cluzeau, D., 2012. Morphological description of soilstructurepatternsproducedbyearthwormbioturbationattheprofilescale.Eur.

[87] J. Soil Biol. 50, 83–90.

[88] Preuschen, G., 1983. Die Spatendiagnose und ihre Auswertung. In: Böhm, W.,Kutschera,L.,Lichtenegger,E.(Eds.),RootEcologyandIts PraciticalApplication.

[89] International Symposium Gumpenstein, 1982, Bundesanstalt Gumpenstein, A-8952 Irdning, , pp. 355–368.

[90] Regan, J.T., 2012. The erodibility and surface runoff potential of a selection of Irishtillage soils. (PhD thesis). National University of Ireland, Galway, Ireland.

[91] Richards, B.G., Baumgartl, T., Horn, R., Gräsle, W., 1997. Modelling the effects ofrepeated wheel loads on soil profiles. Int. Agrophys. 11, 177–187.

[92] Richards, B.G., Peth, S., 2009. Modelling soil physical behaviour with particularreference to soil science. Soil Till. Res. 102, 216–224.

[93] Roger-Estrade, J., Richard, G., Boizard, H., Boiffin, J., Caneill, J., Manichon, H., 2000.

[94] Modelling changes in the tilled layer structure over time as a function ofcropping systems. Eur. J. Soil Sci. 51, 455–474.

[95] Roger-Estrade,J.,Richard,G.,Dexter,A.R.,Boizard,H.,DeTourdonnet,S.,Bertrand,M., Caneill, J., 2009. Integration of soil structure variation with time and spaceinto models for crop management. A review. Agron. Sustain. Dev. 29,135–142.

[96] Samouelian, A., Cousin, I., Tabbagh, A., Bruand, A., Richard, G., 2005. Electricalresistivity survey in soil science: a review. Soil Till. Res. 83, 173–193.

[97] Schjønning,P.,vandenAkker,J.J.H.,Keller,T.,Greve,M.H.,Lamandé,M.,Simojoki,A.,Stettler, M., Arvidsson, J., Breuning-Madsen, H., 2015. Driver-Pressure-State-Impact-Response(DPSIR)analysisandriskassessmentforsoilcompaction—aEuropean perspective. Adv. Agron. 133,183–237.

[98] Shepherd, T.G., 2000. Visual soil assessment, Field Guide for Cropping and PastoralGrazing on Flat to Rolling Country. 1st edition 1. horizons.mw & LandcareResearch, Palmerston North, New Zealand.

[99] Shepherd, T.G., 2003. Assessing soil quality using visual soil assessment. In: Currie,L.D., Hanly, J.A. (Eds.), Tools for Nutrients and Pollutant Management:Applications to Agriculture and Environmental Quality. Occasional Report No.

[100] 17. Fertilizer and Lime Research Centre, Massey University, Palmerston North, pp. 153–166.

[101] Shepherd, T.G., 2009. Visual Soil Assessment, 2nd edition Field Guide for PastoralGrazing and Cropping on Flat to Rolling Country, vol. 1. Horizons ResearchCouncil, Palmerston North, New Zealand, pp. 120.

[102] Soriano-Disla, J.M., Janik, L.J., Viscarra Rossel, R.A., Macdonald, L.M., McLaughlin, M.J., 2014. The performance of visible, near-, and mid-infrared reflectancespectroscopy for prediction of soil physical, chemical, and biological properties.Appl. Spectrosc. Rev. 49, 139–186.

[103] Stenberg, B., Viscarra Rossel, R.A., Mouazen, A.M., Wetterlind, J., 2010. Visible andnear infrared spectroscopy in soil science. Adv. Agron. 107, 163–215.

[104] Taina,I.A.,Heck,R.J.,Elliot,T.R.,2008.ApplicationofX-raycomputedtomographytosoilscience:aliteraturereview.Can.J.SoilSci.88, 1–20.

[105] Uteau, D., Pagenkemper, S.K., Peth, S., Horn, R., 2013. Root and time dependent soilstructure formation and its influence on gas transport in the subsoil. Soil Till.Res. 132, 69–76.

[106] Utomo, W.H., Dexter, A.R., 1981. Soil friability. J. Soil Sci. 32, 203–213. Vereecken,H.,Schnepf,A.,Hopmans,J.W.,Javaux,M.,Or,D.,Roose,T.,Vanderborght,

[107] J., Young, M.H., Amelung, W., Aitkenhead, M., Allison, S.D., Assouline, S.,Baveye,

[108] P., Berli, M., Brüggemann, N., Finke, P., Flury, M., Gaiser, T., Govers, G., Ghezzehei,T., Hallett, P., Hendricks Franssen, H.J., Heppell, J., Horn, R., Huisman, J.A., Jacques, D., Jonard, F., Kollet, S., Lafolie, F., Lamorski, K., Leitner, D., McBratney, A., Minasny, B., Montzka, C., Nowak, W., Pachepsky, Y., Padarian, J., Romano, N.,Roth,K.,Rothfuss,Y.,Rowe,E.C.,Schwen,A.,Šimu○nek, J.,Tiktak,A.,VanDam,J.,van der Zee, S.E.A.T.M., Vogel, H.J., Vrugt, J.A., Wöhling, T., Young, I.M., 2016.Modeling soil processes: review, key challenges, and new perspectives. Vadose Zone J. 15 doi:http://dx.doi.org/10.2136/vzj2015.09.0131.

[109] Viscarra Rossel, R.A., Hicks, W.S., 2015. Soil organic carbon and its fractionsestimated by visible?near infrared transfer functions. Eur. J. Soil Sci. 66, 438–450.

[110] Viscarra Rossel, R.A., Walvoort, D.J.J., McBratney, A.B., Janik, L.J., Skjemstad, J.O.,2006. Visible, near infrared, mid infrared or combined diffuse reflectancespectroscopyforsimultaneousassessmentofvariussoilproperties.Geoderma131,59–75.

[111] Voivret, C., Radjai, F., Delenne, J.-Y., El Youssoufi, M.S., 2007. Space-filling propertiesof polydisperse granular media. Phys. Rev. E 76, 021301.

[112] Wildenshild, D., Sheppard, A.P., 2013. X-ray imaging and analysis techniques forquantifying pore-scale structure and processes in subsurface porous mediumsystems. Adv. Water Resour. 51, 217–246.

[113] Wulf, H., Mulder, T., Schaepman, M.E., Keller, A., Jörg, P., 2015. Remote Sensing of Soil: Project Report from the Federal Office of the Environment (FOEN/BAFU). University of Zurich Avaiable at: http://www.geo.uzh.ch/fileadmin/files/content/abteilungen/rsl1/Remote_sensing_of_soils_BAFU_report_dpi300_v.pdf(assessed 28.04.16).

[114] Zribi, M., Baghdadi, N., Nolin, M., 2011. Remote sensing of soil. Appl. Environ. Soil Sci. 2 pp..

★★★

STANDARDS AND UTILIZATIONS OF DIRECT CONTACT LAYER REFINING (DCMD): A FAR REACHING SURVEY

[1]BIKASH NAIK, [2]ABHIPSA MOHANTY, [3]ATUL KUMAR MALLIK

[1]Assistant Professor, Department of Mechanical Engineering, NMIET, BBSR
[2]Asst Prof, Department of Civil Engineering REC BBSR
[3]Asst Prof, Department of Civil Engineering AIET BBSR
E-mail: [1]mohanty.samaptika@nmiet.ac.in,

Highlights -
DCMD innovation has acquired a gigantic measure of interest throughout the long term. Momentum examination and late uses of DCMD are audited in this dad per. Recent concerns, for example, layer fouling and working conditions are talked about. Combination of DCMD with environmentally friendly power, for example, sunlight based energy is additionally introduced.

Graphical Abstract -

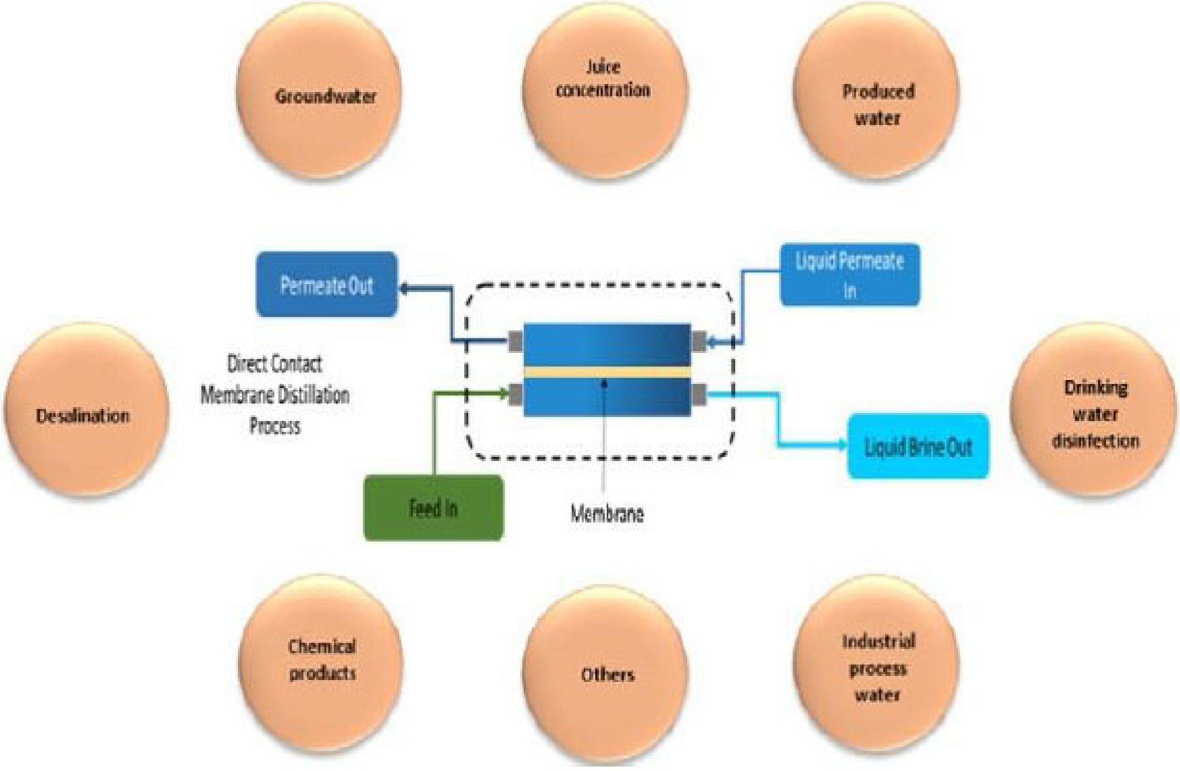

Abstract -
In this paper, the current and latest utilizations of direct contact layer refining (DCMD) are examined. Aside from its quickly expanding use for the desalination of profoundly saline feed water, the DCMD is gradually turning into a favored innovation for delivered water treatment, purification of groundwater, recovery of modern interaction water, expulsion of micro-pollutants from drinking water, juice fixation, and creation of synthetic items. The essentials of the DCMD and administering conditions (from warmth and mass exchange rules) that portray execution boundaries are first clarified. Recent concerns in the DCMD tasks, for example, the influence of layer type, film fouling, and working conditions on the DCMD execution or profitability are likewise examined in this paper. Crossover frameworks and environmentally friendly power incorporation with DCMD frameworks have been introduced as feasible arrangements that would improve the maintainability of the DCMD activities.

I. INTRODUCTION

Membrane technology is gradually becoming the first-line choice for manyphysicalandchemical processesintheindustries [1,2].Membrane processes are currently of prime importance in the water treatment sector oftheeconomiesof manynations becauseofthe numerous benefits of membrane separation over thermal technologies[3–5]. Some of these benefitsincludethe avoidanceofcostlyandinefficientthermalenergy [3,6], reduction of environmental impacts associated with fuel combus- tion for thermal energy production, lower pumping and capital require- ments, and huge ecological footprints required in many thermal distillation plants [7]. However, established membrane separation pro- cessesincluding reverseosmosis(RO) havealsobeen showntobesusceptibletochallengessuchasanearinverserelationshipbetween membrane selectivity and permeability [2,5,8,9], higher levels of energy requirement and membrane fouling when membrane technology is usedforcertainapplicationssuchasdesalinationofhighly salinefeed [10], highlevelsoffeed pretreatmentrequirements[11,12],andinability ofmany membrane storemovemicropollutants andcontaminantsof emerging concern from feed water because membranes only concentrate thesepollutants(butdonotdestroythem)[13,14].Therefore,attempts havebeenmadetointegrate membraneseparationwiththermaldistilla- tioninorder tocombinethe comparativeadvantages ofbothapproaches inwhatisknownasmembrane distillation(MD)[15–19]. MDisather- mallydriven separation processin whichahydrophobicmicroporous membraneseparatesafeedstreamandareceivingphasehavinga lowertemperature[16]. Thedrivingforceofheattransportisthe temperature gradient acrossthemembrane whichresultsinawatervaporpres- sure differential that causes transport of water vapor through the membranepores[20].Themaincompetitiveadvantageof MDisthatdis- tillationoccursbelow thenormalboiling pointofthefeedsolution[21].

Thisseparationmethodisbased onequilibriumbetween the vaporand liquid molecules of the liquid mixture[19].

Therefore,in MD, separationoccursasaresult ofphasechangearising fromthepartialvaporpressure differencebetweenthefeedandreceiving phase[22]. Thebarrierimposed by themembranetotheliquid(feed) phaseallowsonlythevaporphasetopassthroughthemembranepores.

Asaresult,volatilemoleculeswillevaporateatthehotliquid/vaporinter- face,thevaporswillcrossthe membrane pores and condenseonthecold liquid/vaporinterface insidethemembranemodule[23–25]. Forfeeds containingvolatilesolutes,thesesoluteswillpassthrough themembrane whentheirboilingpointsare lessthanthatofwater[19].Because MDisa nonisothermal processinwhichthehydrophobic membraneisnotwetted bywater,itislesspronetomembrane fouling, itexhibitshigherrejection of soluteswhencomparedwithconventionalmembranetechnologies suchasRO,anditisunaffectedby highosmoticpressureofhighlysaline feed[16]. Inaddition,whenMDiscompared withfull-scalethermaldistil- lationapproaches, MDcanbecarried outatloweroperatingtemperatures and pressures becauseitrequireslowervaporspace(duetomembrane barrier),ithasgoodcompatibilitywithwasteheatsources orrenewable energy,anditcanbeusedfordecentralizedapplicationsbecauseofits lesscomplexconfigurations[20,26].Therehasbeenasurge inMDresearch inthelastdecade. Fig.1showsasignificantincreaseinthenumberof GooglesearchresultsforMDsincethebeginningofthe21stcentury.Despitethe increasing researchefforts, MDisnotappliedonanindustrial scaleyet. Themainreasonsarethelackofcommerciallyavailablemem- branes and energy cost[18].

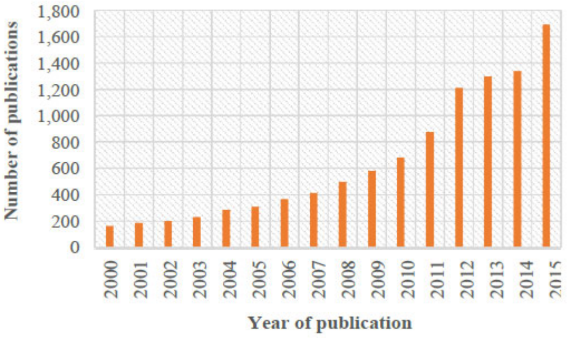

Fig. 1. Number of Google search results since 2000.

MD membranes are attractive becausetheyallow retentionofliquid waterandpassageofwatervapor. Theliquidwaterdoesnotenterthe non-polarmembrane poreseventhoughtheaverageporesizeofmicro-porousmembranesissignificantlyhigherthanthediameterofaliquid watermoleculebecauseof high surface tension of water[27]. Aconvex meniscusisformed inthe membrane poreasaresultofthehighwater surfacetension–knownascapillaryaction–which restricts themem- brane from porewetting.

Porewettingoccurswhenthepressureoftheliquidfeedisableto propeltheliquidthroughthemembranepores[28,29].Thispressure isknownasLiquidEntryPressure(LEP).LEPismeasured bythecontact angleandusedtodescribethehydrophobicityofthemembrane.Sometimes,itisthemembranesupport,ratherthantheactivelayer,thatis wetted[28].Thewatercontactangleofhydrophobicmembranetends tobeabove90upto150°(ormoreforsuperhydrophobicmembranes) toensurethatwaterdropletslieonthemembranesurfacewithoutwettingit[30].HighLEPisfavoredbymembranepropertiesincludingsmall poresize,lowsurfaceenergy,highsurfaceroughnessandhighsurface tension [31,32]. Operating temperature and feed composition might alsoinfluencetheLEPindirectlybyalteringtheliquidcontactangle andsurfacetension[33].Liquidfeedcontainingorganic,i norganicand amphiphiliccomponentscanacceleratemembranewetting[29]and microstructureevolutionathightemperaturecanenhancethepropensityofmembranewetting[34].Therefore,theproductivityandselectivityofMDmembranesarelimitedbythewettingpressure. Meanwhile, thedepositionofnanoparticlesonmembranesurfaceshas been showntoimprovethesuperhydrophobicityorporewettingresistance ofmembranes[32,35,36].SiO_2nanoparticlesgraftedonthesurfaceof commercialpolypropylene(PP)MDmembranehavebeenshowntoincreasethesurfaceroughnessandhydrophobicityofthemembrane[32]. When compared with the virgin membrane, the nano-coatedmembraneexhibitedhighersurfaceroughnesswhichpreventedporewetting,asinspiredby lotusleafeffect[32].Thelotusleafisasocial symbolofpurityinBuddhistculturebecauseitresistsdirtandmud. Therefore,theimpartationofwater-repellingpropertiestoamembrane throughthemodificationofitssurfaceroughnessinawaysimilartothe pronouncedroughnessofalotusleafisknownas—lotuseffect‖bio-inspiration[37].Polyvinylidenefluoride(PVDF)nanofibermembranes thatweremodifiedwithsilvernanoparticleordopaminehavealso shown anti-wetting property when compared with un-altered membranes[35].Usinga3.5wt%NaClasthefeedsolution,anintegrally-modifiedPVDFnanofibermembranewasabletoachieveastableflux of31.6L/m^2hbecauseofthemodificationsofitsmorphologyandtopologycausedbythehierarchicalnanostructures[35].Thecoatingofnano- TiO_2onPVDFmembranesthroughalow-temperaturehydrothermal processandsubsequentfluorosilanizationofthemembraneshasalso beenshowntoimpartanti-wettingpropertyonthemembranesbyincreasingthewatercontactanglefrom125to166°[36]. CurrentissuesintheuseofMDforseparationprocessesrevolve aroundthelowproductivityofMDmembranesasaresultoflimitations thatmustbeimposedontheexternalpressureloadonthefeedtoavoid pore wetting [22]. To avoid pore wetting, the transmembranehydrostaticpressureshouldnotbegreaterthantheliquidentrypressure–thelowestpressureneededtowetthehydrophobicmembrane.Anattempttoincreasetheexternalpressurebeyondtheacceptablelimit wouldcausesevereporewetting,membranefouling,andlowsolutere- jection[23,25].Lackofcustom-mademembranesspecificallyfabricated forcommercialMDapplicationsispartlyresponsibleforcurrentissues affecting MD membrane performance, as membranes designed for conventionalmembranetechnologies(suchasmicrofiltrationorMFandultrafiltrationorUF)arecurrentlybeingusedformostMDinvestigations. Inaddition,energyinefficiencyisasourceofconcerninmanyMD applicationscurrentlybecauseenergyislostduetotemperaturepolarizationatthemembraneandheatofcondensationatthecold(perme- ate) side. Although the partial vapor pressure of the feed can be improvedbyusingrenewableenergy,especiallysolarthermalenergy, thethermalenergycontentofthepermeateisnotreusedforincreased productwaterrecoveryinmanyapplications[19,28]. MDtechnologiesincludedirectcontactmembranedistillation(DCMD) whereacoldliquidisindirectcontactwiththemembraneatthepermeate side,airgapmembranedistillation(AGMD)whereanairgapactsasthe condensingsurfaceatthepermeateside,sweepgasmembranedistillation (SGMD)whereagasisforcedthroughthegapatthepermeatesidetoaid theevaporationoflessvolatilesubstancesofinterest,andvacuummem- brane distillation (VMD) where gap channel configuration issubjected to vacuum[16,23].DCMDhasreceivedgreaterattentionbecauseitdoes notrequireanexternalcondenseranditismoresuitableforwater-basedapplications[28].DCMDhasthesimplestMDconfiguration.TheoperationofDCMDisrelativelyeasyandhighfluxcanbeobtainedatthe rightoperatingconditions[38].However,DCMDischaracterizedbylow thermal energy efficiency because the evaporator and condenser surfaces arecloseleadingtoloweffectivedrivingforce(ascomparedtothemuch higherbulktemperaturedifferenceacrossthemembrane)[39].AGMDexhibitshighefficiencyofthermalenergyutilizationbutlowflux.SGMDalso showshighthermalefficiencybutrequirelargeflowsofsweepinggasto producehighpermeaterecovery.VMDcanbeusedtoobtainbothconsiderablethermalefficiencyandpermeateflux[40].LikeDCMD,theproductivityofVMDcanalsobeimprovedbyincreasingthefeedt emperatureand flowrate[16].ThecascadingofVMDmembraneswiththe aimofreducing feedpressureinamultistagestepwiseconfigurationandrecoveringenergyforfeedpreheatinghasalsobeencarriedoutinordertoshowtheeconomicviabilityofVMD[41].However,itisinterestingtonoteherethatthe set-upprocedureforVMDisquitecomplicated,mainlybecauseofthevacuumandexternalcondensers[38].ThisisaseriousdrawbackforVMD. VMDremainsoneoftheleastinvestigatedMDconfigurationsfordesalinationbecauseofthisdrawback[38].Also,thecomplexityofVMDconfiguration,ascomparedtoDCMD,doesnotguaranteehigherproductivityat lowertemperatures.DCMDperformsbetterthanVMDin termsofpermeateproductionrateatlowtemperaturesinspiteofitssimple configuration [40].TheeffectofvacuuminVMDonlybecomesnoticeableathighertemperaturesorhighflowrateconditions.Attheselevels,theresistanceto masstransfercausedbymolecule-moleculecollisionisremoved[42].In addition,unlikeinDCMD,thedirectcontrolofpermeatetemperatureis notpossibleinVMDbecausethevacuumpressurecanonlybeachieved throughavacuumpump[3].Asignificantlyhighpressure variation mightalsobenoticedonthemembranesurfaceinVMDbecauseoftheapplicationofvacuum,whichmighteventuallyresultinwettingorreduction inhydrophobicityofthemembrane[39].Therefore,mostresearchon VMDhasfocusedmainlyontheremovalofvolatileorganiccompounds suchasethanol,withonlyminimalstudiesondesalination [39].

Therefore,inthispaper,thecurrentandrecentlydevisedapplicationsofDCMDhavebeendiscussed.TheaforementionedissuesassociatedwithMDhavealsobeenpresented(inthecontextofmainly DCMD). Viable solutions in terms of hybridization of DCMD with existingtechnologiesandincorporationofrenewableenergywith DCMDinasustainablemannerhavealsobeenproposed.

Wangand Chung[18],Alkhudhirietal.[16],Driolietal.[15]andZhangetal.[43]recently reviewed the main principles, possible configurations, opportunitiesandchallengesofmembranedistillation.However,noneof thesereviewsdiscussedtheapplicationsofDCMDandcurrentissuesassociatedwithDCMDindetail.Eachofthesereviewsdiscussedspecific issuesaffectingMDingeneralwithoutanexpositiononthe currentissues,applications,challenges,andviableopportunitiesavailableto DCMDinparticular.ThisreviewprovidesmoredetailsintotheapplicationsofDCMDandsummarizestherecentadvancementsofdifferent aspectsofDCMDsuchasmembranematerials,operating conditions, andenergyrequirements.Challengesandopportunitiesavailablefor improvementofDCMDarealsodiscussedinthisreview. Asthisreview willelaborateontheemergingtrendsinthedevelopmentof DCMDin termsofexperimentalworkandmodeling;thesustainabilitysectionattemptstoclarifythestrengthsandweaknessesofthetechnologyasit triestogainafootholdagainstmorecommondesalination options.

II. FUNDAMENTALS OF DCMD

MD was first introduced in the 1960s. It was first patented by Bodel in1963[22,28]. Itwasnotdevelopedformanyyears(Fig.1)duetounfavorableeconomicpurposesandanestimatedlowtemperaturepolarizationcoefficient. Thiscoefficientiscalculatedusing Eq.(1).

$$\tau\ ¼\ \frac{Tfm-Tpm}{Tfb-Tpb} \qquad (1)$$

where,Tfmisthetemperatureofthefeedonthemembraneside, Tpm isthetemperature ofthe permeateonthe membraneside, Tfb isthe temperatureofthebulkfeed and Tpbisthetemperatureofthebulkpermeate. This coefficientrepresentsthelossofthethermaldrivingforce duetothethermalboundarylayerresistances.Anestimationofthe temperature polarization effect allows a better understanding ofthe heatandmass transferresistances. Forexample,inamodeldeveloped byJensenetal.[44]aimedatestimatingthetransmembranewater fluxduringtheconcentration ofblack currantjuice, polarizationeffects wereshowntohave decreased the waterflux significantly.

Later in the 1980s, newmembrane developmentallowedforabetter understanding oftheheat and mass transfer principles through research.

Thispermittednewapplicationssuchaswastewaterincluding producedwatertreatment[45]. Therearefour different types of MD thatdifferintwoways:1-thewayinwhichthevaporpressuregradient ismaintainedand2-thecondensationmethodofthe permeatevapor. ThesefourmethodsareDCMD, AGMD,SGMD,andVMD. InDCMD, boththefeedsolution and an aqueous solutions thatiscolderthan thefeedsolution willbeindirectcontactwiththemembrane; the former at the feed sideandthelatteratthepermeatesideofthe membrane.DCMDmethodisthemostwidelyusedinresearchdue toitssimplicityandeaseofapplication. TheAGMDcontainsastagnantairgapbetweenthemembraneandacondensationsurface wheretheevaporated volatilemoleculescross boththemembrane poresandtheairgap tocondenseover acoldsurface inthe membranemodule. AsfortheSGMD, aflowingstreamofgassweepsthe membraneatthepermeatesidewhichisfollowedbythecondensation of thevapormolecules outside the membranemodule. Inthe VMD, usingavacuumpump, vacuumisappliedtothepermeate sidewheretheapplied pressureislessthanthevolatilemolecules saturation pressure. TheairgapinAGMD,thesweepgasSGMDand thevacuumin VMDwereaddedinorderto reducetheheat loss dueto conduction and themass transferresistance[19]. Configurations of these distillation methods are shown in Fig. 2.

In DCMD, sensibleheatlossresults inadifferenceinthe bulk and membrane interface temperatures. Fig. 3 shows the temperatures of thedifferentpartsofatypical DCMD configuration. Duetothe lowering of temperature asthefeed movesfromthefeedchannel throughthe membranetothepermeatechannel asaresultoftemperaturepolarization, thedriving forceof heattransferbecomesnegativelyaffected. In DCMD, thereissimultaneoustransfer of bothheatandmass determined bytheheatfluxandtransfer coefficientsinboth feed and permeate sides[47].

2.1. Heat and mass transfer equations

There are three regions within a typical DCMD process where heat is transferred (Fig.3).

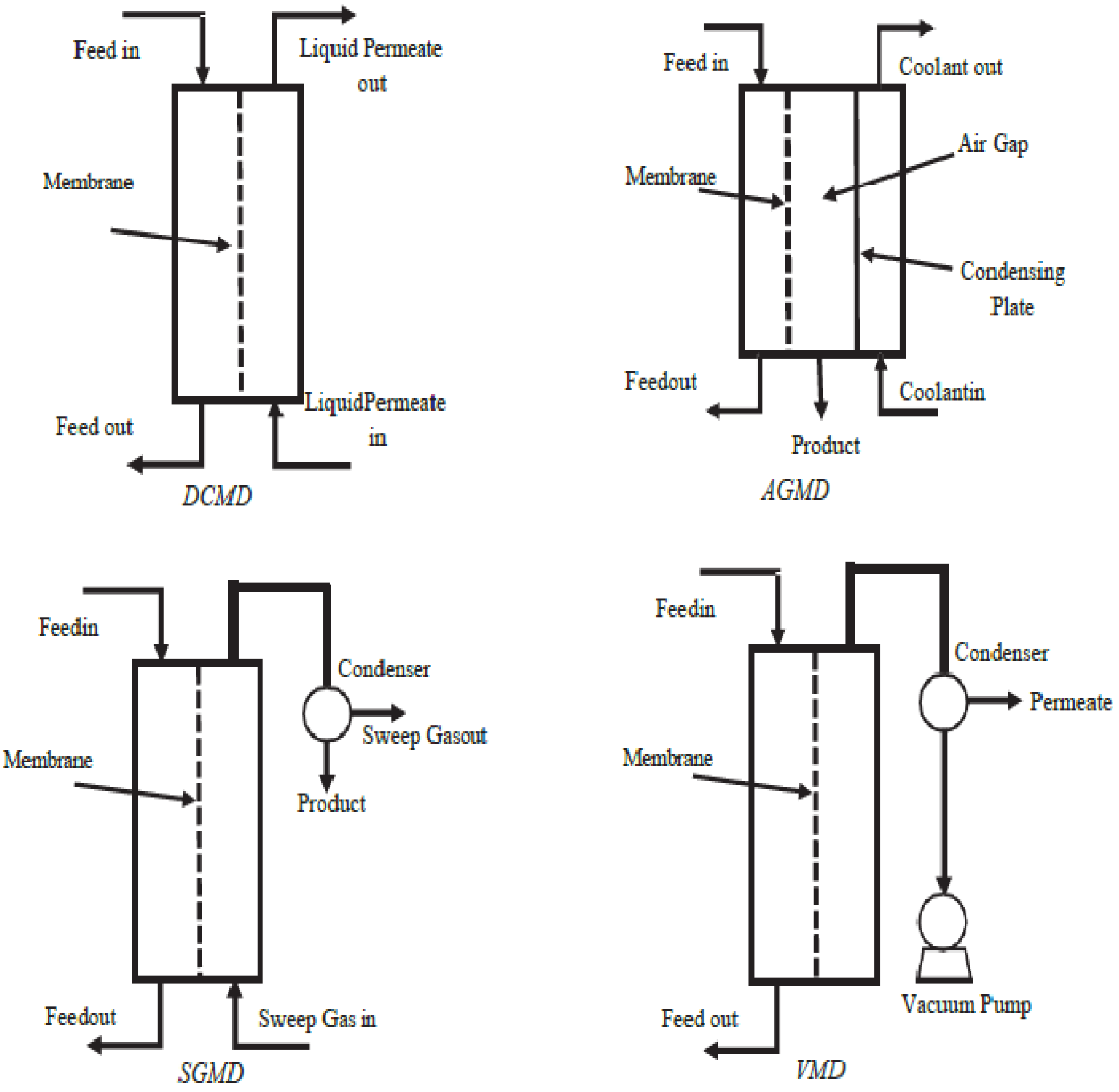

Fig.2.ThefourMDconfigurations[46].

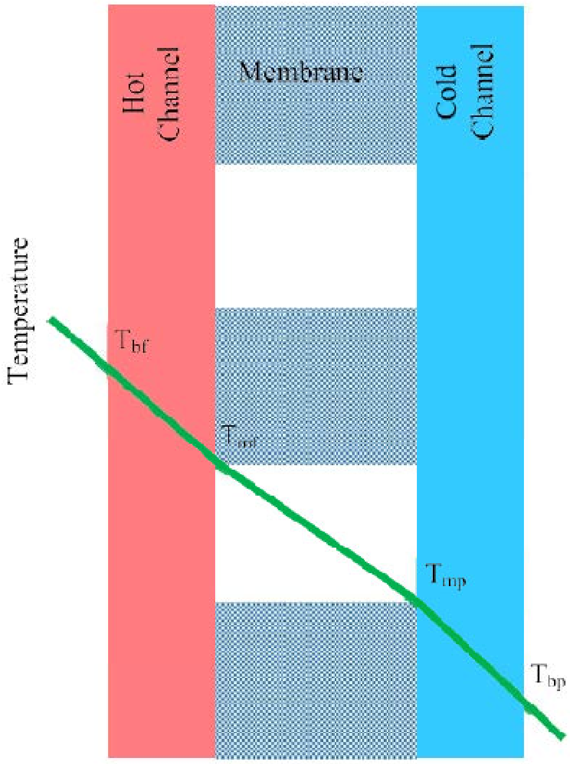

Fig. 3. The bulk and membrane interface temperatures where *Tbf*is the bulk feed temperature, *Tmf*isthemembraneinterfacetemperatureatthefeedside, *Tmp*isthe membraneinterface temperatureatthepermeateside, and *Tbp*isthebulkpermeate temperature[48].

1. Throughthefeedsolutionthermalboundarylayerwherethereis convection-heattransferinthefeedboundarylayer($Q_{f,conv.}$)and heattransferduetomasstransferacrossthefeedthermalboundary layer ($Q_{f,M.T.}$),i.e.

$$Q_f = Q_{f,conv.} + Q_{f,M.T.} = h_f\left(T_{bf} - T_{mf}\right) + J_w\left\{H_{L,f}\left(\frac{T_{bf}+T_{mf}}{2}\right)\right\} \tag{2}$$

2. Throughthemembranewhereacombinationofconductiveheat transfer($Q_{m,cond.}$)andheattransferduetowatervapormigration throughthemembranepores($Q_{m,M.T.}$) exist,i.e.

$$Q_m = Q_{m,cond.} + Q_{m,M.T.} = h_m\left(T_{mf} - T_{mp}\right) + J_w H_v \tag{3}$$

3. Throughthepermeatesolutionthermalboundarylayerwherethere isconvectionheattransferinthethermalpermeateboundarylayer ($Q_{p,conv.}$),andheattransferduetomasstransferacrossthepermeate thermal boundary layer($Q_{p,M.T.}$)

$$Q_p = Q_{p,conv.} + Q_{p,M.T.} = h_p\left(T_{mp} - T_{bp}\right) + J_w H_{L,p}\left(\frac{T_{mp}+T_{bp}}{2}\right) \tag{4}$$

In Eqs.(2)–(4), h_f is the heat transfer coefficient of feed boundary layer, $H_{L,f}$ is the enthalpy of the feedsolution which is evaluated at the average temperature of feed and membrane/feed interface(T_{bf}+T_{mf})/2, h_m is the heat transfer coefficient of the hydrophobicmembrane, h_p. is the heat transfer coefficient of permeate boundary layer, J_w is the permeate flux, H_v is the enthalpy of the vapor and $H_{L,p}$ is the enthalpy of the permeate solution which is evaluated at the average temperature of permeate and membrane/permeate interface(T_{bp}+T_{mp})/2..

Asformasstransfer,thereisalinearrelationshipbetweenthemass flux(J_w) and watervapor pressure difference. This relationship is shown in Eq.(5).

$$J_w = B_m\left(P_{mf} - P_{mp}\right) \tag{5}$$

where, P_{mf} and P_{mp} are the partial pressures of water at the feed and permeate sides which can be calculated from Antoine equation shown in Eq.(6).

$$P_v = \exp\left(23.328 - \left(\frac{3841}{T-45}\right)\right) \tag{6}$$

where,$P_v$isthewatervaporpressurein Pa and T is theequivalent temperatureinK[47]. Anincreasein feedtemperatureresultsina significant increaseinthe massflux. The use of higher operating temperatures ispreferableforanenhancementintheheatandmasstransferof the DCMD[49]. However, thereisalwaysathreshold for feed temperature becauseofthe liquidentry pressure (or wetting pressure).

2.2. Recent DCMD models

Somemodelshavebeendevelopedrecentlybyresearchersin ordertoimprovetheunderstanding of the fundamentalsof DCMD andestimatesome processparameters. Forexample,duetothecompressiblestructure, changingtheporosity, thicknessand poresize of themembraneofacommonly used membrane in DCMD (i.e. polytetrafluoroethyleneor PTFEmembrane), amodelwaspresented byZhangetal.[50] forfluxand evaporation ratiopredictions. Assumingthattortuosity remains constantduringmembranecompression, the DCMD model for flux prediction with changing pressureswasadvancedthroughmassandheattransferbalances. This model is applicable at high temperatures where there is a greatvariationinmembrane compression.Itwassuggestedthat thepressuredropalongtheDCMDmodulecouldbereducedbyreducingthemembrane lengthandusing compressible membranes. Inastudycarried outbyMartinezetal.[51],itwasobservedthat thenarrow poresize distributionsincommercialmembranesmake

Themolecularand Knudsen resistances tobesignificantin the presence ofstagnantair, whereasintheabsenceofstagnantair, viscous and Knudsen contributions are important. Still, for membranes with smaller pores at low temperatures, low vapor pressures, the viscous contribution is minimal. Some of the recently developed models can becategorized into: blackbox, grey box,and two dimensional models.

2.2.1. Black box models

Raoetal.[52]usedasimplifiedfluxpredictionforDCMD modeling usingamembrane structuralparameter. Theyclaimthatmanyofthe complex models for DCMD are based on unreliable mass transferas- sumptions. Correlation between 18 structural membraneparameters and permeate flux were proposed. Four parameters (ε(porosity)/ δ(thickness),$\varepsilon/\tau\delta$,$1/\tau\delta$,andanewparameterintroducedby them i.e. coupled membrane structural property or Cm) were observed tohavethemostsignificant influenceonpermeateflux. Cm was developed inamannerthatitissimpleandnotcostlyto measure. Predictions that weremore accurate thanthe dusty gas model(DGM) were obtained.

Knudsen and Browniandiffusioncoefficients havebeencombined withBosanquet'sassumptioninarecentstudytoinvestigatethefunda- mentalaspectsofheat and masstransferin DCMD[53].Asagainstmany theoreticalstudieswhichhaveemployedtheuseofsoftwareorcompu- tationalapplication, thesolutionof Fick'slawwascarriedoutinitsoriginaldifferential form inthisstudysoastoobtainthemolarfluxof water vapor throughaDCMDmembranepore.An effective diffusion Coefficientwasobtainedfromthecombination of Knudsen and Brownian diffusion coefficients. Theresultsobtainedshowedthattherequired heatfluxmonotonouslyincreasedwiththevaporfluxthroughmem- braneporesandthetheoretical predictionof permeate fluxagrees withexperimentalobservations reportedintheliterature.

2.2.2. Grey-boxmodels

Amodelingtechniquethathasbeenusedinsomerecentstudiesfor the evaluation of DCMD performance based on some operating parametersisDGM.ThreedifferentformsofDGMhavebeencreatedrecently toinvestigatetheDCMDmasstransportacrossGEAspireQL833membrane[54].TheresultsobtainedfromthisstudyshowedthatKnudsen-moleculardiffusiontransitionmodelyieldedthebestprediction.This studyalsorecommendedthatheattransfercorrelationsandKnudsen-molecularmasstransportequationcanbeusedinthepredictionof heatandmasstransferforflatsheetDCMDexperiments.To obtain some parameters, DCMD experiments were performed using deionizedwaterandaqueoussaltsolutionsofNaClwithconcentration levelsupto15pptasfeed.Jensenetal.[44]modeledaDCMDvariant forblackcurrantjuice.Mostofthephysicalparameterswerebasedon literatureorcorrelations.Whenliteraturedatawasnotavailable,they fittedtheirparameterstotheexperimentaldata.Theirmodelincluded aDGMandachievedapredictionoftemperatureandflowinexperimentaldatawithaverageerrorssmallerthan10%.Andrjesdóttiretal. [54]optimized a DCMD model with experimental data. Up to 15,000ppmNaClconcentrationindistilledwaterwasusedasfeed. TheyevaluatedthreedifferentformsofDGMandconcludedthatthe Knudsen-moleculardiffusiontransitionmodelachievesthebestresults. Inaddition,themostaccurateheattransfercorrelationswerefoundto betheLévêqueequationandtheDittus–Boelterequationforlaminarflow and turbulent flow,respectively. Responsesurfacemethodology(RSM)hasalsobeenused recently forthemodelingandoptimizationoftheDCMDprocess.Boubakri etal.[55]developedamodelfortheoptimizationofoperatingparametersaffectingwaterdesalinationinDCMDusingRSM.PPmembrane withlowporesizewasused.Thedevelopedmodelforpermeateflux responsewasstatistically validatedby theanalysisofvariance (ANOVA)whichshowedahighvalueofcoefficientofdetermination (R2= 0.989). The obtained optimum operating parameters were foundtobevaporpressuredifferenceof0.355×105Pa,feedflow rateof73.6L/h, permeateflowrateof17.1L/h, andfeedionicstrength of309mM. Undertheseoptimumconditions,thepermeatefluxwas 4.191 L/m2 h.

Manawietal.[56]studiedtheeffectofoperationalparametersondistillatefluxinDCMD.Theirmodelwasbasedondividingthemembraneareainto10elements,whichweremodeledashotand coldcontrolvolumesconnectedbysimultaneousmassandheattransferusinga flatsheetsystem.Theirmodelwasuniqueinpredictingtemperature andfluxprofilesthatarenotmeasurablealongthemembrane.Their modelpredictedtemperaturepolarizationthatcanbereducedbyhigh flowsorbytheuseofspacers.Themodelpredictedthatfluxcanbeincreasedbyusingcountercurrentflowandspacers.Manawietal.also studied the temperature polarization effect in DCMD desalination of highsalinityfeed[57].Thetemperaturepolarizationeffectisareduction influxduetobuildingupofsoluteonthemembranecausing atemper- ature difference between the liquid and membrane. This model was basedontheirpreviousmodel[56].Thebesttemperaturepolarization coefficient(TPC)valueof0.82wasachievedforaflowrate of3L/min andafeed–permeatetemperaturesystemof 60–20°C. Ramezanianpour andSivakumar[58]havealsoworkedonafluxdeclinemodelforfouling predictionsinDCMD.Theyintroducedasystemdependentconstantas anempiricalfunctionoftemperatureandpressure.Theyvalidatedtheir modelwiththreesetsofexperiments,andverifieditwithtwosetsof experimentsand4setsofliteraturedata.Theyconcludedfromtheir modelthatrapidfluxdeclinehighlydependsonparticlesizeanddensity,aswellastheflowrate.

2.2.3. Two-dimensional dynamic model

Most DCMD processes have been modeled as steady-state one-dimensionalsystemsusingempiricalheatandmasstransferequations. Stationarytwo-dimensionalDCMDmodelshavebeenconsideredonly inveryfewstudies.BinAshooretal.[59]havedevelopeda dynamic modelofadirectcontactmembranedistillation(DCMD)processin plate-and-frameconfiguration. Thismodelaimsatgiving insight into theunderlyingcoupledphysicochemicalphenomena.ThemodelisimplementedinthemodelingpackagegPROMS.InDCMD, bothmassand heattransferoccursimultaneouslyandbothtemperatureandconcentrationpolarizationeffectsshouldbetakenintoconsideration.Most modelingworksinliteratureonDCMDprocessesusuallyfocusonthe masstransferresistanceofvaporacrossamembraneattributedtothe membrane characteristics (i.e. pore size, porosity and tortuosity)and heattransferresistancestoobtainthemeantemperatureon themembranesurface.Theconcentrationpolarizationphenomenaareusually ignored to simplify the calculation procedure. Only few publications usestationaryoneortwo-dimensionalheat-transferequationtosimulateaparticularapplicationmoreaccurately.Althoughmanysemi- empiricalmodelshavebeendeveloped, adetailedmodelfor temperature polarizationon flat-plate DCMD processesisstilllacking.Intheir study,BinAshooretal.[59]developedadynamictwo-dimensional flat-platemathematicalmodelforDCMDprocessesinordertoobtain thetemperatureandconcentrationdistributionsinthehotandcold channelsandthelocalmassfluxatthemembranesurfaces. Theavailabilityofsuchamodelforsimultaneousenergyandmassbalances willbeanimportantbasisfortheanalysis,designandoptimizationof DCMDprocessesforsalinewaterdesalination.Table1summarizes these models and their benefits. A 2-D dynamic model from advection-diffusionequationhasalsobeenanalyzedanddiscretized viaanunconditionallystablealgorithmandusedforthepredictionof temperatureprofileinDCMD[60].Temperaturedistributionsalong themembraneandfluxvariationswerepredicted.Inaddition,temporal variationsoftemperatureinthefeedandpermeatecontainerswereobtained.TheAlternatingDirectionImplicitmethod(ADI) wasemployed andtheerrorbetweenthemodelresultsandexperimentaldatawas b5%[60].Inarelatedpaper,Eleiwietal.[61]alsoemployedthe2D Advection–DiffusionEquationtostudythetemporalbehaviorof DCMDprocess,especiallywhenitisdrivenbysolarenergy.Feed,permeateandmembranecharacteristicsweremodeled.The modelwasexperimentallyvalidatedinthesteadystatephase.Themodelresultswere experimentallyvalidated.Whenthefeedinlettemperatureswerevariedbetween30°and75°withastepincrementof0.1°every 2min, therelativeerrorwaslessthan±5%[61].

III. CURRENT APPLICATIONS OF DCMD

DCMDhasbeenusedformanypurposesotherthanthedesalination ofsalinewaterinordertoproduceproductwaterofhighquality.Some oftheseapplicationsarewastewatertreatment,groundwaterand drinkingwaterpurification,productionofchemicals,crystallizationof salts,concentrationoffruitjuices,removalofwaterfrombloodandproteinsolutionsinbiomedicalindustries,removalofdyesintextileindustries,andremovalofboronandarsenicfromaqueoussolutions.For wastewatertreatment,DCMDhasbeenappliedforthetreatmentof producedwater,pharmaceuticalwastewater,andradioactivewastewater[18].Theuseoftreatedwastewaterisbecomingveryimportantfor thesustainabilityofwaterresourcesandmanyadvancedwastewater treatmenttechnologieshavebeendevelopedrecently[62

–67].TheapplicationofDCMDforwastewaterinvolvesreductionand removalof suspendedsolids,biodegradableorganics,andpathogenicbacteria. ThemodelingofwastewatertreatmentusingtheDCMDprocesshas alsoshownsomeimpressiveresults.Thecalculationofmasstransfer mechanismsandpermeatefluxinthetheoreticalanalysisofradioactive wastewatertreatmentusingtheDCMDhasbeencarriedout[68]where DGMwasusedtoobtainthemodelingresults.Itwasdiscoveredthatthe DCMDprocesscanseparatealmostallCs+,Sr2+andCo2+fromradioactivewastewater.ItwasconcludedthattheDCMDisapromisingseparationprocessforlow-levelradioactivewastewatertreatment. DCMDhas alsobeensuccessfully appliedtotreatcoolingtowerblowdownwater (CTBD). Yuetal.[69]examinedtheperformanceofDCMDfordesalinating simulatedCTBD. Bothsilica-freeandsilica-containingsimulated waterweretested. Apermeatefluxofabout30L/m2handsaltrejection ofN99.95%wereachievedunderafeedsidetemperatureofabout60°C. Membranescaling wasstudiedanditwas foundthatinsolublecalcium carbonatescaleswereformed onthemembraneata concentrationfactorof about 3.7–4.0 for silica-free simulated CTBD water(Fig.4). However, forsilica-containingsimulated CTBDwater,scalesfrom silica, calciumcarbonateand sulfatewere precipitated togetherunderaconcentrationfactorof about 3.2–5.0. Meanwhile, anantiscalantwas addedresulting intheenhancementofwaterrecoverytoabout87%. TheapplicationofDCMDforproducedwatertreatmentandchemical processesareexemplified inthefollowing sections.

Table 1
DCMD models for performance prediction

Model	Parameters	Prediction	Reference
Blackbox	ε(porosity)/δ(thickness), $\varepsilon/\tau\delta$,$1/\tau\delta$, Cm (coupled membrane structural property)	Permeateflux	
	[52]Blackbox	Knudsen and Browniandiffusioncoefficients	
	Molar flux of water vapor through a DCMD membrane pore [53]		
Greybox	Knudsen-molecularmasstransport	Heat and mass transfer for flatsheetDCMD	
	[54]Grey box (RSM) Vapor pressure difference, feed flow rate,	permeate flow rate, feed ionic strength Permeateflux	
	[55]Greybox	Flow andspacerproperties	
	Permeate flux andtemperaturepolarization	[56]	
Greybox	Particle sizeanddensity	Flux decline duetofouling	
	[58]2Ddynamic		
	Poresize,porosity,tortuosity,heattransferresistances,concentrationpolarization	Massflux,temperatureandconcentrationdistribution	[59]

3.1. Produced water treatment

Asignificantamountofoilywastewaterisstillbeingproducedfrom oilexploitation andprocessing[70]. Pollutionresultingfromtherelease ofuntreatedoilywastewatertotheenvironmentisstillaconcern. However, DCMDprocesshasrecently beenappliedforoilywastewatertreatmentsothatthe deleterious components inthewastewatercanbe removedbeforethedischargeofthefinaleffluentintotheenvironment. Producedwater isthenamegiventotheby product produced along with thegasand oilfrompetroleumcompanies. Thiswatercontainsdissolvedorganiccompounds, heavymetals, and radioactive components. Produced waterhasthreemain sources: 1-Water injected intothereservoirtoenhanceoil recovery,2-Flowback waterfromhydraulicfracturingactivities,and3-Amixtureofboth.Thiswaterisofmainconcern duetothe problems associatedwithitsproduction suchassurface and groundwater pollution resulting from its constituents.

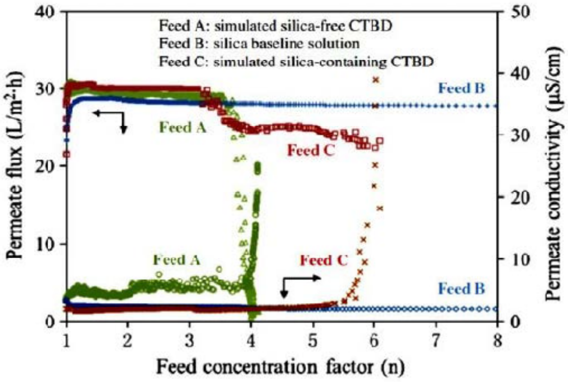

Fig.4.DCMDfluxandpermeateconductivityfordifferenttypesofsimulatedCTBDfeedas afunctionoffeed concentrationfactor. FeedA:simulatedsilica-freeCTBD;feedB: simulatedsilica watersolutionasbaselineandfeedC:simulatedsilica-containingCTBD [69].

Inaddition, industriesproduceitinlarge quantitieswhere there isan estimated dailyglobalproduction of250millionbarrels.Thisnumberisestimated tobearoundthreetimesthatofproducedoil.Largevolumesofproducedwaterareassociatedwithwater-stressed countries[71]. Produced water resulting from oil companies is composed ofaromaticcompounds, cationsandanions,heavymetals,solidsanddissolvedgases. Thearomaticcompounds presentinproduced waterare ethylbenzene, xylenes,naphthalene,phenantherene,polyaromatichydrocarbons,andphenols.Asforthecationsandanions,Na+,K+,Ca2+,Mg2+,Ba2+,Sr2+,Fe2+,Cl−,SO2−,CO2−, HCO– Are the ions present inproduced water. HeavymetalssuchasCd,Cr,Cu,Pb,Hg,Ni,Agand Zncanbefound.Solidssuchasbacteria,waxesandasphaltenesanddissolvedgasessuchasCO2,O2andH2Scanalsobefoundinproduced water[72].Producedwaterresultingfromgascompanies differsfrom thatobtainedfromoilcompaniesbasedonitsacidity,volumeofproduction,treatmentchemicalsandconcentrationofvolatilecomponents. Producedwaterfromgascompaniesaremoreacidicandcontainsa higherconcentrationofvolatilecomponents.Inaddition, one-thirdof thechemicalsusedingastreatmentsuchasmethanolandethyleneglycolarepresentinthewater.Furthermore,thevolumeofproduced waterfromgascompaniesislessthanthatproducedfromoilcompanies [72].

Inthepast,physical,chemicalandbiologicalmethodswereusedto treatproducedwater.Thephysicalmethodinvolvedtheuseofdifferent chemicalssuchasactivatedcarbon,copolymersandzeolitetoadsorb carbonandtheuseofsandfilterstoremovemetals.Thechemicalmethodwasusedtoremovesuspendedandcolloidalparticlesthrough chemicalprecipitation,photocatalytictreatmentandtreatmentwith ozone.Asforthebiologicalmethod,differentaerobicandanaerobicmicroorganism treatment techniques were employed. However, these methodssufferfromdisadvantagessuchashighcost,useofhazardous chemicals and their large environmental footprint. These drawbacks leadtotheproposalofmembrane-basedmethodstotreatproduced waterinthe21stcentury.ExamplesofthesemethodsareMF,UFand RO.Nonetheless,downsidesofthesemethodsareexistent.MFrequires highenergyanditisnotveryefficientfordivalentsalts,monovalent saltsandviruses.UFundergoesmembranefoulingandislimitedto feed containing low molecular weight organics and salts, inaddition toitshighenergyconsumption.AsforRO,ithasahighpressurerequirementandeventraceamountsofoilandgreasecancausemembrane fouling[2].Hence,analternativemethodwassuggestedforproduced water treatment that is more feasible for this type of application, whichisDCMD[72].DCMDisapromisingtechnologybecauseitoffers ahighsoluterejection(N99%)and70%producedwaterrecovery.Therefore,thismethodisveryattractiveforproducedwatertreatment.Inaddition,duetoitslargemembranepores,itsufferslessfromfouling.

DCMDcanalsobecombinedwithotherseparationprocessessuchas UFandROtherebycreatinganintegratedseparationsystemanditis capableofusingalternativesourcesofenergysuchassolarenergy.It effectivelyremovesorganics,heavymetalsandradioactivesubstances fromaqueoussolutions,makingitasuitablemethodforthistypeof treatment[72].

ThecapabilityofDCMDtowithstandhighfeedsalinitywithoutasignificantdecreaseinwaterfluxacrossthemembranemakes itwellsuitedtotreatproducedwater.AnaddedadvantagetotheDCMDmethod forproducedwatertreatmentisthatitdoesnotrequireadditionalenergyforcoolingthefeed[73].Furthermore,DCMDmethodisattractivefor thetreatmentofproducedwaterbecauseofitsrelativelysmallenvironmentalfootprint[74].However,therearesomedrawbacks associated withtheapplicationofDCMDforproducedwatertreatment.Insome cases,producedwateriscomposedofsmallorganiccompoundsand dissolvedgasesexertingpartialvaporpressuresthatmight exceed thatofwaterhence,allowingthemtobetransportedwiththewater vaporfluxacrossthemembrane.Thismightresultinthecontamination ofthepermeate;makingtheuseofDCMDtotreatproducedwatera challenge.Anotherchallengetothisapplicationisthewettingcaused bythefeedcomponentssuchasalcoholsandsurfactants,therebylowering thefeedliquidsurfacetension.Thisallowsthefeedsolutionto crossthemembranetothepermeateside,affectingthequalityofthe permeate.EventhoughmembranefoulingislowerinDCMD,highlyvolatilecomponentsinproducedwatermightleadtothewettingofmembranepores,reducesofwaterflux,andinterferencewiththemassand heattransfer.Fouling,whetherorganicorbiofouling,wouldreduce theproductivityofDCMDmethod.Henceforthesecases,apretreatmentstepwouldbeneeded.Thispretreatmentstepwouldnotonly maintaintheproductivityofthemethodbutalsoremovecomponents thatpromotemembranewettingfromtheproducedwater. Inaddition, certainproductwaterstandardsneedtobemet,sotheuseof post-treatmenttoremovevolatilecompoundsfromthefeedsolutionmight also be a necessary step. As a result of the pretreatment, post-treatmentandmembranecleaningsteps,thechemicaland energy costsoftheprocesswillbeelevated.Anaddeddisadvantageisthevariability in the produced water composition so the pre- and post-treatmentstepsaswellascleaningandthemembranedesignwill havetobechosenaccordinglybasedonthequalityoftheproduced water[74].

PolymericmembranessuchasPVDFhavedisplayedstableandreliableresultsforproducedwatertreatmentinastudycarried outby Macedonioetal.[71].TheresultsobtainedindicatedthatDCMDisa suitable method for this kind of treatment. However, these results wereobtainedonlyfromalaboratoryscalesetupwithatestingperiod that was roughly about 200 min. The long-term viability of this approachinapilotordemonstration-scalestudywasnotcarriedoutand cannotbeverified.TheoverallsaltrejectionwasfoundtobeN99% withatotalcarbonrejectionN90%.Witha70%recovery, watercosts of0.72USD/m3and1.28USD/m3,respectivelywereobtainedfromthe economicevaluationoftheprocesswhentheproducedwatertemperaturewas50°Cand20°C,respectively.However,real-lifedatafromthe testedunitwasnotusedfortheeconomicestimationbecausethetested unitwasnotevaluatedforlonghoursandexperimentswere carriedout foronlyabout200min.Theeconomicdatausedwereassumedfrom previousstudiesandadaptedfora100m3/hDCMDplant.Inaresearch articlebySinghetal.[75],DCMDwasusedtotreatdifferenttypesof deoiledproducedwaterobtainedfromChevronCorporation.Thedistilledwaterobtainedfromthoseproducedwatersamplescontained verylowTDSvaluesandwaterrecoverywasaround80%. TheseTDS valueswererepresentedintheformofconductivityatdifferenttemperaturesandareshowninFig.5.Withanincreasedfeedflowrateat80°C, thewatervaporfluxwas15kg/m2h,increasingto20kg/m2hwhere novelcoatedmembranesandahollowfibercross-flowmoduledesign wereused.

DCMDhasalsobeensuggestedforthetreatmentofproducedwater comingfromSteamAssistedGravityDrainage(SAGD). Singhetal.[75]designedasteamassistedgravitydrainage (SAGD)processwithatemperaturerangeof80–130°Cforimproveddesalinationofasalinefeed with10,000ppmTDS.AporousflatsheetPTFEDCMDmembranewas testedusingapressurerangeof2–3atm.Thefeedsolutioncontained 3000ppmNaCl,45ppmphenol,45ppmcresoland10ppm naphthenic acid.Thecompositionofthewaterproducedwasobtained throughthe SAGDprocess.Thewatervaporfluxachievedwas195kg/m2hwhich wasafewtimeslargerthanthatobtainedfromtheseawater ROprocess.

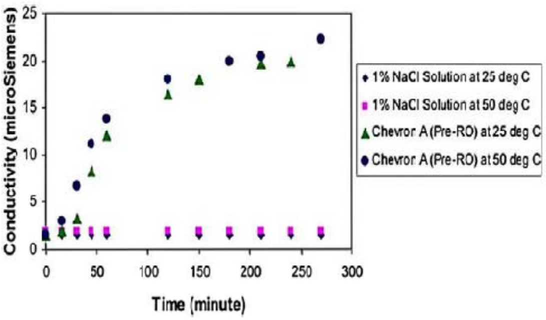

Fig.5.Temporalchangesindistillateconductivityfora1%NaClsolutionandChevronA (pre-RO) water at 25 and 50 °C[75].

Shafferetal.hasshownthatMDiswellsuitedforthedesalinationof high-salinityshalegasproducedwater[74]-thereasonbeingthatan increase in the TDS concentration of the feed from 35,000 to 75,000 mg/L reduces the permeate flux by only 5%. The ability of DCMDtoutilizelow-gradeheatofthefeedstreamtoproduceacceptablewaterfluxesmakesthislow-energytechnologyanattractiveone forthiskindoftreatmentshowingfuturepromiseintermsofthisproduced water treatmentapplication.

Recently,DCMDhasbeenattractiveforthetreatmentofRObrine fromcoalseamgas(CSG).ThecontrolofscalingduringtheDCMDtreatmentofCSGRObinehasbeenstudiedbyDuongetal.[76]. Theeffectof scalecleaningchemicalsonwaterfluxwasinvestigated,wherebythe cleaningpotentialofachemicalagentknownas MC3wastested.Scale removalisessentialfortherestorationofmembranesurfacehydrophobicity.Thisagentwas,however,foundtolacktheabilityof chemicaldepositremoval.ThiswasduetothecomplexityoftheCSGRObrine scalants.Therewasanobservedreductionintheperformanceofthe membraneintermsofthewaterfluxandsaltrejectionasaresultof theremainingscalants.Hence,chemicalscalingshouldbeprevented throughpretreatment,ratherthancuredinordertoavoidtheneedfor chemicalcleaningduringthecourseofsuchatreatment.Temperature wasalsofoundtoinfluencescaling,i.e.areducedfeedtemperaturereducesmembranescaling.ThroughthetreatmentofCSGRObrine usingtheDCMD,80%waterwasrecoveredintheabsenceofanyobservedmembranescalingatafeedtemperatureof35°Cwithawater flux of 10 L/m2 h[76]. Theuseofanother MDtechnology(AGMD)forCSGRObrinetreatmenthasalsoevolvedlatelyanditwouldbeappropriatetodiscuss the results obtained by researchers in this field in the context of accessingitsviability.InacombinedUF/ROandspiral-woundAGMD pilotscalestudyperformedbyDuongetal.[77],RObrinereleased fromCSGwastreated.Usingamembraneareaof7.2m2,amodule heightof0.5mandmodulediameterof0.4m,anoverallsystemrecoveryof95%wasobtained.75%ofthefeedCSGwaterwasrecoveredby UF/ROwhile80%wasrecoveredbyAGMD.Distillateflowrateof10L/hwithaGORof2.5wereobtained.Thermalandelectricenergyconsumedwere250kWh/m3and1.1kWh/m3,respectively.Inastudyperformedonthissystem inNewSouthWales(Australia),1haofflat-plate solarthermalcollectorarrayswasusedtoachievewaterproductionof 472m3/dfromCSGproducedwater[77].ThetreatmentofRObrineproducedfromcoalseamgas(CSG)usingAGMDresultsinthevolumereductionofthebrine[78,79].Thefabricationofgraphene/PVDF membranesusingthephaseinversiontechniquehasbeencarriedout forthetreatmentofRObrinefromCSGproducedwaterbyAGMD.The performanceofthismembranewasfoundtobebetterthanthatofthe commercialPVDFmembraneintermsoffluxandsaltrejection[78]. For a feed temperature of 60.0 °C and permeate temperatureof 20.0°C,afluxof20.5L/m2handsaltrejectionof99.99%wereobtained fora24hoperation.Furthermore,itwasobservedthatthewetting resistanceaswellasstrengthofthemembranewereincreasedbyincorporating graphene in PVDF[78].

3.2. Concentration of juice and food wasteeffluent

Apartfromtheproductionofpurewaterfromsalinewaterortreated waterfromproducedwater,DCMDhasbeensuccessfullyusedforother applicationsovertheyears.Jensenetal.hastheoreticallyusedDCMDto concentrateblackcurrantjuice[44]whereadustygasmodel(DGM) wasdeveloped.Theconcentrationpolarizationatthemembranesurfacewasestimatedbyempiricalcorrelationsformassandheattransfer coefficients.Thismodelwascapable ofpredictingfluxesin DCMDon blackcurrantjuicebasedon concentrationpolarizationatthemembranesurface withan averagepercentageerrorbelow10%.Theconcentrationofwasteeffluentshasalsobeencarriedoutusing DCMD.Kezia etal.hasusedflatsheet PTFEmembranesof nominalporesizes 0.05mm,0.22mm, and 0.45mminDCMD to concentratethewasteeffluent from salty wheyby-productfromthecheesemakingindustry[80].Afinaltotal solidsconcentrationof±30%w/wandwaterrecovery of37–83%wasreported.Thepressure-dropacrossthechannellength was alsopredicted, accountingforthefeedspacer.Foranincreaseof 1minthechannellength,theuseofthesmallestmembrane poresize of0.05μmwouldberequired fortheDCMDoperation,unlessvery lowcross-flowvelocitiesareused. Itwasalsodemonstratedthatthe foulingofthemembraneswasprimarilygovernedbyprecipitationof calciumphosphatesalt. Afurtherobservationwasthattheoperation atalow pHdoesnotsignificantly improvethefluxorthefinalsalt concentration.

DCMDhasbeenused forapplejuiceconcentration[19]. 50%ofthe juicewas concentratedand apermeatefluxof9kg/m2hwasachieved. PTFEmembraneswereusedforthisDCMDtreatmentand alcohol-watersolutionswereused fortheorangejuiceconcentration.Theeffectsoffactors suchfeedflowrate,temperaturedifference,andfeed concentrationonthetransmembranefluxwerestudied.Throughthe increaseinflowrate, thefluxcanbeimprovedwhilereducingtheimpactofconcentrationpolarization. Throughalcoholic treatment, hydrophilicmembranescanbe madeintohydrophobiconeshence, enhancingthemembranesurfaceforsuchanapplication[19]. DCMD hasalsobeenused fortheconcentrationof wholemilk,skimmilk, wheyandpurelactosesolution[81]. Flatsheet PTFE membraneswere testedforthisapplication.

ThisstudywasperformedinAustraliaand conducted fortheevaluationofsustainabilityaspectofdairymilkprocessing.Afluxof10kg/m2hwasobtainedfortheconcentrationof wheysolution. Thisvaluewas foundtobetwiceasgreatas that of the treated skim milk (5 kg/m2 h)[81].

3.3. Chemical production and removal

DCMDhasbeencoupledwithachemicalreactorinorderto convert KClinto$KHSO_4$[82]. Thefeedtemperatureattheinletofthemembrane module mounted to333Kor343Kandthe permeatetemperaturewas 293K.PureHClacidreaching aconcentrationof43g/dm3wasalsoobtained. Theresultsobtainedshowedthattheconversionat343Kwith the reaction mixture containing KCl and H_2SO_4 in the molar ratio of 1:2 yielded a high efficiency of $KHSO_4$ production. Also,DCMD hasbeenappliedforheavymetalremovalusinghybridPTFEmem- brane. Bhattacharya et al. [83] investigated different membranes to removetoxicchromium(VI)fromsimulatedwater.Theresults showedthatthehydrophobicPTFEmembraneincorporatedwith polyethyleneterephthalate (PET) exhibited improved performance in terms of normalized flux. A two-dimension mathematical model was developed using a modified coupled Knudsenand Poiseuille flow models. The modeling results obtained were veri- fied with experimental results. The PTFE/PET membrane was also compared with PTFE/PP membrane and it was shown thatPTFE/PP membrane showed better performance in terms of normalized flux (Fig. 6).

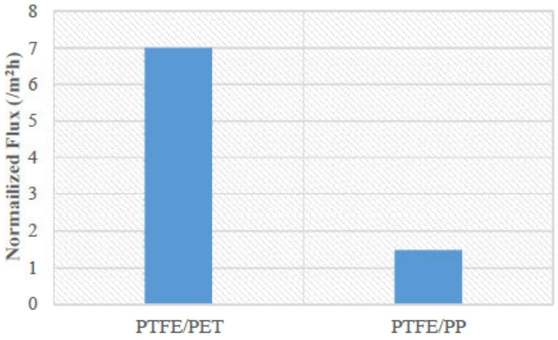

Fig.6.ComparisonofnormalizedfluxofPTFE/PETandPTFE/PP membranesfortoxic chromium (VI) from simulated water[83].

DCMDhasalsobeenappliedforammoniaremoval.Quetal.[84]car- riedoutacomparativeinvestigation foracceleratingammoniaremoval from aqueoussolution. Theprocessesusedinthisstudyinclude a modifiedDCMD (MDCMD) withreceiving solutioninthepermeateside, and a hollow fiber membrane contactor (HFMC). Experimental results showedthattheammoniaremovalefficiencyofDCMD,HFMCand MDCMD were 52, 88, and 99.5% within 105 min, respectively. In MDCMD,feedpHvaluewasprovedtobethemostdominantoperating factorandtheoptimalfeedpHwas12.20.Itwasalsodemonstratedthat increaseinfeedtemperatureand flowrateledtohigherammoniamass transfercoefficient, ammoniaremovalefficiency,andpermeateflux. DCMDhasalsobeenusedtoremovearsenic,atoxicsubstance,from contaminated groundwater[85].Solar-drivenDCMD(SDMD) wasap- pliedandthree differenttypes ofhydrophobicflatsheetmembranes madeofPTFEandPPwithsurfaceareaof120×10−4m2weretested. Thestudyshowed thatfeedanddistillate temperatureconstitutesignif- icanteffectonthefluxand almost 100%arsenic separationwasachieved without wetting the membrane pores, evenafter120hof operation. The PTFE membrane with a fluxof49.80kg/m2hwasfoundtobethe best out of differenttestedmembranes.Thestudyshowedalsothat theSDMDcaneffectivelyseparatearsenicfromgroundwater.Arsenic removalfrom contaminatedground waterhasalsobeeninvestigated byYarlagaddaetal.[86]. Inthisstudy,thecapabilityoftheDCMDprocesstoremovearsenic, uraniumandfluoridefrom contaminatedsaline groundwaterwasexamined usingtwotypesofmembranes,PPand PTFE, underdifferent operating conditionsand membranecharacteris- tics.Theremovalofsalts, arsenic,fluoride, and uranium fromsynthetic brackishwatercontaining1000–10,000ppmsalts,10–400ppbarsenic anduranium,and1–30ppmfluoridewas demonstrated. Itwasfound thatDCMD isabletoachieveover99%rejectionofthesalts,arsenic, fluorideanduraniumcontaminantswhileproducingahighqualityper- meate.Theauthorsalsoobserved that the abilityto utilizelowgrade heatsourcesmakesthe DCMDprocessaviableoptiontorecoverpotable water fromavariety ofimpairedgroundwaterfeeds. DCMDhasbeenusedfortheremovaloffluoridefrombrackish groundwater using a self-prepared PVDF membrane [87]. Fluoride, if consumedabovetheacceptablelimit,canresultincripplingbonedis- easesanddamagetosensitivebody organs suchasheart, kidney,and liver.Inthisstudy, amaximumpermeatefluxof35.6kg/m2hwasobtainedwiththefeedsolutionat80°Candthecolddistillate waterat 20°C. Usingacidifiedgroundwaterasfeed,theexperimentalresultsob- tainedshowed thatthepermeateflux anddistillatequalitywerekept stablebeforethe concentration factorreached5.0.Whena300-hcontinuousfluorideremovalexperimentoftheacidifiedgroundwaterwas carriedoutwiththe concentrationfactor of4.0,thepermeateflux remainedstableand nofluoridewasdetectedintheproducedperme- ate. Permeateflux,productwaterquality,andthermalefficiencywere alsoinvestigatedtheoretically to demonstrate the performance of PVDFDCMDmembraneforfluorideremovalatafeedtemperatureof 71°C.TheexperimentaldatawasobtainedusingthetheoreticalKnudsenmoleculardiffusionmodelwherethepermeatefluxan dthermalefficiencywereobtainedas 22.38kg/m2hand69.19%respectively. A fluoride removal of N98.6% was achieved makingthePVDFDCMD membranesapplicable fortheproductionoffluoride-freewaterforpotable andindustrialprocessapplications.

3.4. Resource recovery

DCMDhasbeenappliedforphosphorusextractionfromwastewater. A hybrid FO-DCMD system was able to extract phosphorus from digestedsludge[88]. Inthecourseofthisprocess,FOwasabletoconcentrateorthophosphateandammoniumthroughtherecoveryofphosphorusasstruvite(MgNH4PO4·6H2O). FOwasusedasthepretreatment stepwhileDCMD wasusedfortherecoveryofthedrawsolutionaswell ascleanwaterextractionfromthesludge.MgCl2wasused asanFO drawsolution. Theobtainedstruvitecrystalprecipitatewasinvestigated foritscrystalmorphology,elementalcomposition,andcrystalstructure. ItwasconcludedthatFO-DCMDsystem isa suitable approachforphosphorus extraction from wastewater[88].
DCMDhasalso been investigated foritspotency infreshwaterrecoveryfromwastewater. DCMDhasbeenusedforthetreatmentofenvironmentally hazardousolivemillwastewater(OMW)[89].Duringthe courseofthistreatment,threecommercialPTFEmembranesofpore sizes0.2μm,0.45μm,and1.0μm werestudiedusingdifferentoperatingtemperatures.This studyaimedattheproductionofpurewateraswell astheconcentrationofnaturalpolyphenolspresentinOMW.Theeffect ofmembraneporesizeontheseparationcoefficientofpolyphenols wasfoundtobeinsignificant.DCMDhasalsobeenusedfortheeffectivetreatmentofcoolingwaterblowdowncontainingsilicaand hardness [69]. In this work [69], distillate flux of 30 L/m2 h and salt rejection of 99.95% were achieved where the feed temperaturewas around 60°C.
Ammoniareleasedasapollutantintowaterbodiesfrommunicipal andindustrialwastewaterscauseseutrophicationandoxygendepletion.DCMDhasbeeneffectivefortheremovalofammoniafromwater [46,84,90].Forexample,theuseofcapillaryPVDFmembranewith80% porosity,averageporesizeof0.22μm,andLEPof250kPaforammonia removalfromwastewaterhasbeeninvestigated[84].Ammoniaremovalefficiencieswerecomparedusingthreeapproaches- conventional DCMD, hollow fiber membrane contactor, and a modified DCMD apparatus–andtheresultsobtainedwere52%,88%and99.5%respectively.
ThemodifiedDCMDshowedthehighestammoniaremovalefficiency becauseithadareceivingsolutioncontaining0.01mol/Lsulfuricacid inthepermeateside.TheeffectsoffeedpH,temperature,flowrate, andammoniaconcentrationonthesystemperformancewerealsostudied.IncreaseinpHallowedimprovementsinremovalefficiencyanddistillateflux.Furthermore,ariseinthefeedtemperatureandflowrate resultedinenhancedremovalefficiencyofammonia,ammoniamass transferrateanddistillateflux[84].Table2summarizesall thedifferent applicationsofDCMDinthissection.

Table 2
Recent applications of DCMD.

Reference	Application	Polymer	Operating conditions	Results
[71]	Oilfield produced water treatment	PVDF	Feedtemperatureof50°C	Overall salt rejection N 99%; Total carbon rejection N 90%; 70% recovery; Water cost of 0.72 USD/m^3
[71]	Oilfield produced water treatment	PVDF	Feedtemperatureof20°C	Water cost of 1.28 USD/m^3
[75]	Chevron Corporation produced water treatment	/	1%NaClsolutionandChevronA(pre-RO)waterat25°Cand50°C	Distillate of very low TDS; 80% recovery; Flux was 15 to 20 kg/m^2 h
[74]	SAGD produced water treatment	PTFE	Temperaturerangeof80-130°Ctreatingfeedof10,000ppmTDS containing 3000 ppm NaCl, 45 ppm phenol, 45 ppm cresol and 10 ppm naphthenic acid	Flux of 195 kg/m^2 h (greater than that obtained from RO)
[74,91]	High-salinity shale gas produced water treatment	/	Feed temperature of 55 °C; permeate temperature of 25 °C; Feed and permeate flow velocities set to 0.39 m/s and 0.28 m/s, respectively	Increase in the TDS concentration of the feed from 35,000 ppm to 75,000 ppm
[80]	Saline dairy waste concentration	PTFE	Use of Flat Sheet PTFE membranes of minimal pore sizes 0.05 mm, 0.22 mm and 0.45 mm	Final total solids concentration of ±30% w/w and water recoveryof37–83%;Foulinggovernedby precipitation of calcium phosphate salt
[19,92]	Apple juice concentration	PTFE	Feed temperatures 50 °C, 60 °C and 70 °C and permeate temperatures of 10 °C, 20 °C and 30 °C	Permeate flux of 9 kg/m^2 h for 50% juice concentration; Permeate flux of 3.0-3.8 kg/m^2 h for 60%–65%juice concentration
[19,81]	Whole milk, skim milk, whey and a pure lactose solution concentration	PTFE	Feed and permeate temperatures of 54 °C and 5 °C, respectively	Whey solution concentration produced a flux of 10 kg/m^2 h while treated skim milk produced 5 kg/m^2 h
[82]	Chemical production	PP	Feed temperature of 333 K or 343 K and a permeate temperature of 293 K	Conversion at 343 K with the reaction mixture containing KCl and H2SO4 in the molar ratio of 1:2 yielded a high efficiency of $KHSO_4$ production
[83]	Chromium (VI) removal from simulated water	PTFE/PET	Feed temperature varying from 40 °C to 70 °C; Permeate temperature ranging from 18 °C to 25 °C; Feed flow rate ranging from 50 L/h to 125 L/h; Feed concentration increasing from 200 ppb to 2000 ppb	2-D model developed for experimental verification

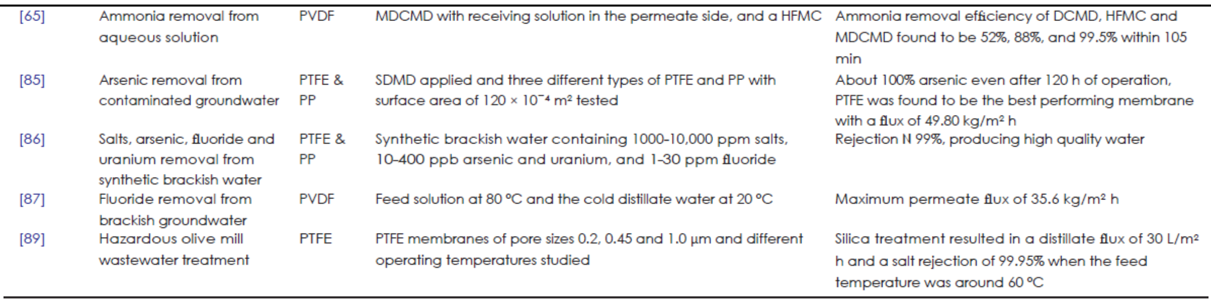

[65]	Ammonia removal from aqueous solution	PVDF	MDCMD with receiving solution in the permeate side, and a HFMC	Ammonia removal efficiency of DCMD, HFMC and MDCMD found to be 52%, 88%, and 99.5% within 105 min
[85]	Arsenic removal from contaminated groundwater	PTFE & PP	SDMD applied and three different types of PTFE and PP with surface area of 120 × 10^{-4} m^2 tested	About 100% arsenic even after 120 h of operation, PTFE was found to be the best performing membrane with a flux of 49.80 kg/m^2 h
[86]	Salts, arsenic, fluoride and uranium removal from synthetic brackish water	PTFE & PP	Synthetic brackish water containing 1000-10,000 ppm salts, 10-400 ppb arsenic and uranium, and 1-30 ppm fluoride	Rejection N 99%, producing high quality water
[87]	Fluoride removal from brackish groundwater	PVDF	Feed solution at 80 °C and the cold distillate water at 20 °C	Maximum permeate flux of 35.6 kg/m^2 h
[89]	Hazardous olive mill wastewater treatment	PTFE	PTFE membranes of pore sizes 0.2, 0.45 and 1.0 μm and different operating temperatures studied	Silica treatment resulted in a distillate flux of 30 L/m^2 h and a salt rejection of 99.95% when the feed temperature was around 60 °C

IV. RECENT ADVANCES AND CURRENT ISSUES WITH DCMD

4.1. Membrane development, design and fabrication

Thechoiceofmembranematerialusedisaverysignificant deter- miningfactoroftheefficiency ofDCMD[18]. Duetothewiderange of DCMD applicationssuchas ground water, seawater,wastewater,producedwater,radioactivewater,coolingwater,boilerblow down,and industrialprocesswatertreatment, membraneshavebecomeincreasinglycrucial fortheoverallsuccessofDCMDoperations.Hence,dependingonthetargetcontaminantspresentinspecificapplications, hydrophobicmembranesare tobechosen accordingly.Severalmembraneshaverecently beendesigned, fabricated, andtestedforprocess performanceusingpolymerssuchasPP,PVDF,polysulfone(PSf),and PTFE.PVDFmembraneshave moderatethermalstability,goodchemical resistance with asurfaceenergyof30.3×10^{-3}N/m.AsforPPmembranes,theyhavealowermembraneperformanceduetotheirmoderatethermalstabilityatelevated temperaturesandtheirsurfaceenergy is30.0×10^{-3}N/m. PTFEmembranesareoneofthemost commonly used membranesinMD.Theyresultinhighwatervaporpermeability and highwettingresistancedue totheirhighporosity,ofabout90%, and high hydrophobicity. Theirsurfaceenergyisthelowestwitha value of 9.0×10^{-3}N/m to 20.0×10^{-3}N/m [50]. Membranes with lowsurfaceenergy, highporosity(withlowmeanporesizeandnarrow poresizedistribution),andlowthermalconductivityaremostpreferredfor MD applications. Low thermal conductivity of MDmembrane isdesiredtoavoid lossofheatacrossthemembrane. The characteristics ofpolymericmaterialsthathavebeentestedforDCMDapplicationsin termsofsurfaceenergy,thermalconductivity,thermalandchemical stability are summarized in Table3.

4.1.1. PVDFmembranes

PVDFmembranesexhibitrelativelyhighsurfaceenergy. However, PVDFmembranesshow highcontactanglewhichisanecessarycondi- tionto preventmembraneporewettingandhighselectivitybuthigh contactanglehasnodirect roleintheimprovement ofthepermeability ofthemembrane[93]. Theuseofnanomaterialssuchasnanofiber membranes asmembranepolymermaterialsisofgrowinginterest duetotheirpropertiesthatmakethemtobesuitableforDCMDapplica- tion.Thesemembranesarecharacterized bytheirhighporosity,low tortuosity,largesurface poresize, andhighsurfacehydrophobicity [94]. Therefore,somerecenteffortshavebeengearedtowardsthe functionalizationofthesurfacesof PVDFmembranesbyintegrating PVDFwithother functional groupsandnanomaterialsinordertoim- prove thermal diffusivity through the membranes and optimize membranepermeability. MembranessuchascompositePVDF-surface modifyingmacromolecules(PVDF-SMM)nano-fibermembraneshave beenfabricatedandtestedfor DCMDprocessforthe treatment ofsaline feed containing 3.5wt%NaCl[95]. Resultsobtained showed that the hydrophobicSMM-modified PVDFelectrospun nano-fiber membranes are verypromisinginDCMD forseawaterdesalination afterrunningfora 48 h operational timeframe. Electrospun nanofiber membranes consistingofPVDF blendedwithclaynanocompositeshavealso been prepared andtestedfor DCMDoperation[96]. Theresultsobtained showedthat theincorporation ofclaynanocompositesincreases the hydrophobicity ofthemembranesas doestheincrease in the concentrationofclaynanocomposite.Theconclusionofthestudywas thatthePVDF–claynanocomposite nanofibermembranesshowedim- proved performance in DCMD applicationsinadditiontothefactthatit restrictsporewettingintheDCMDprocess.Recently,the blendingof multi-walledCNTs(MWCNTs) withPVDFinflatsheetmembranesby phaseinversionmethodhasbeenusedtoproduceDCMD membranes forthedesalinationofsalty watercontaining 35g/LNaCl[97]. Ahigher permeate flux of 9.5×10^{-3}kg/m2 s was achieved while using the blended membrane, as compared with a commercial PVDF membrane thatgaveapermeatefluxofonly 7.8×10^{-3}kg/m2s. PVDFhollow fiberDCMD membraneshavealsobeendevelopedbySongetal.[98]usingnon-solventinducedphase

Table 3
Summaryofmembranepolymercharacteristics[18].

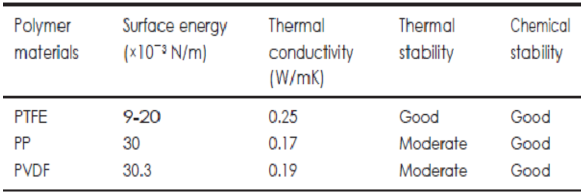

Polymer materials	Surface energy ($\times10^{-3}$ N/m)	Thermal conductivity (W/mK)	Thermal stability	Chemical stability
PTFE	9-20	0.25	Good	Good
PP	30	0.17	Moderate	Good
PVDF	30.3	0.19	Moderate	Good

inversiontechnology.Taguchiexperi- mentaldesign witha threelevelL9orthogonalarray(OA)andstatistical analyseswereemployedtoidentifytherelationshipbetweenthecondi- tionsselectedforthehollow fiber membranesformationandthemembrane performance. Theresultsshowedthatthehighestwaterflux achievedindesalinating3wt%NaClaqueoussolutionwas higherthan 20kg/m^2 hatanaveragefeedtemperatureof 64.5°Cwith99.9%salt rejection.

Non-solventinducedphaseinversion throughhydrophobiccalcium carbonatenanoparticles dispersioninthePVDFcastingsolutionhasalso beenemployedforthefabricationofPVDFDCMDmembrane[99].This hydrophobicnanoparticle additionimproved themembraneporosity, increased themembranesurfaceroughnessandcontactangleandled tothefurtherenhancementofthecrystallinitydegreeandthermalsta- bilityofthehollowfiber. Furthermore, thecompositemembranes displayedagreatermechanical strengthcompared tothefiberswithout thenanoparticles. Usingthefabricatedmembranesindesalinatinga 3.5wt%sodiumchloridesolution,themaximumtransmembranepermeatefluxwas foundtobe46.3kg/m2h withalowerthermalloss whenthehotfeedinlet temperatureand colddistillateinlettempera- turewere kept at 80.5°Cand20.0°C, respectively. Throughrunning 30dayscontinuous desalinationexperiments,thecompositemembraneexhibitedsatisfyingperformancestabilitycomparedwiththe purePVDFmembraneindicatingitsgreatpotentialusefor desalination using the DCMD[99].

Duetotheunsatisfactoryperformanceofthenanofibermembranes intheMDprocess,intermsofstability,Liaoetal.[94]developedcompositenanofibermembraneswithrobustsuperhydrophobicityand highporositythatissuitableforMDapplication.Usingthesemembranes,theDCMDtestsdeterminedastablehighperformanceovera periodof50h[94].Inanotherstudy,electrospunsuperhydrophobicorganicandinorganiccompositenanofibrousmembraneswerefabricated usingsilicananoparticles(SiO2NPs)andhydrophobicsilica/PVDF. ThesemembranesdisplayedexcellentDCMDperformance.Themem- branes were characterized by high porosity, an extremely highliquid entrypressureofwater(LEPw,2.40±0.10bar),robustnanofibermorphologyofPVDFimmobilizedSiO2NPs,remarkablemechanicalproperties,thermalstability,andcorrosionresistance.Thesefeaturesresulted inthelong-termstabilityanddesalinationcapacityofthemembranes. TheobtainedresultswerefoundtobebetterthanthoseusingPVDF and PVDF ENMs where the permeate vapor flux was found tobe 41.1kg/m2hwithastablelowpermeateconductivityofaround 2.45µS/cmusing3.5wt%NaClsaltfeedwithΔT=40°CoveraDCMD testperiodof24h.Furthermore,membraneporeswetting wasnotde- tected[100].

Inanotherrecentinvestigationaimedatexaminingtheperformance ofhybridPVDFmembranesforDCMDoperation,adual-layeredstruc- tureofpolyvinylidenefluoride-co-hexafluoropropylene(PVDF-HFP) nanofibersandpolyacrylonitrile(PAN)microfiberswere fabricatedby electrospinning[101]. Morphologicalcharacterizationofthefabricated membraneshowedslightlybeadedcylindricalPVDF-HFPnanofibers withporosityofabout90%.ThecontactanglesofPVDF-HFPandPANfiberswere150°and100°,respectively.Waterfluxesof45and30L/m2h wereobtainedusingDL2membrane(i.e.25/75PH/PANthicknessratio) whendistilledwaterand35gNaClsolutionswereusedasfeed, respectively.Inasimilarstudy,flatsheetPVDF-HFPmembraneshave beenpreparedandinvestigatedforDCMDperformanceusingastatisticalapproach[102].Factoriallinearmodelsweredevelopedtodescribe themaineffectsoffactorssuchaspurewaterpermeationfluxandsalt rejectioncoefficientofthepreparedmembranesontheDCMDresponses.Analysisofvarianceshowedthatallfactorshavesignificanteffectsontheresponses.Resultsobtainedshowedthattheintegrationof thepolymericmembranematerialshasthegreatesteffects onbothpermeatefluxandsaltrejectioncoefficient.Optimizationof membrane preparationconditionswascarriedoutusingaminimumnumberofexperimentsandbyapplyingLagrangemultipliersoptimizationmethod. Theobtainedoptimumconditionswere:19.1wt%PVDF-HFPconcentration,4.99wt%polyethyleneglycol(PEG)concentration, and35°Ccoag- ulation bath temperature. Under these conditions, the prepared membraneexhibitedthehighestsaltrejectioncoefficient of99.95% andapermeatefluxof4.41L/m2h.PVDFelectrospunnanofibrous membranes(ENMs)withdifferentthicknesseshavealsobeenfabricatedandexaminedforDCMDperformance[103].Itwasdiscoveredthat membranesasthinas27µmgaveatransmembranefluxashighas 60L/m2h.Amodelwasalsodevelopedfortheestimationoftheoptimal membranethicknessoftheseENMsforDCMDoperations.Theresults showedthatthevalueofoptimalthicknessincreasedwithreduced heat transfer coefficients, decreased feed inlet temperature, increased membranepermeability,andincreasedsalinity.Thepredictedoptimum thicknesswasestimatedtobe13µm.Laliaetal.[104]preparedPVDF-HFPmembranesthroughelectrospinningusingthreesets ofmats, with different fiber diameters and physical properties. Thesemats wereobtainedbyvaryingpolymerconcentrationfrom10to15wt%. Themembraneswereformedviahotpressingthepreparedmatsin ordertofusefibers.Theeffectofthisontheporesizedistribution,porosity,contactangleandLEPwasstudied.Themeanporesize wasfoundto be0.26µmwithaporosityof58±5%,acontactangleof125°±2.41 andLEPof19.1psi.WhentestedontheDCMDfordesalinationpurposes,thewaterfluxwasfoundtobe20–22L/m2handthesaltrejection ratio was98%. Interconnectedsponge-likestructuresoffabricatedhollow-fiber PVDFmembraneshavealsoshownhighpermeabilitiesduringDCMD operation[105].Theporesizeandporosityofthesefabricatedmembraneswereintherangeof0.20–0.40µmand61.07–79.36%,respectivelyandthemaximumworkablestrengthobtainedwas6.941MPa.The fluxreached77.6kg/m2husingtheDCMDprocess.Thestudyconcluded thatthemembranespreparedfromthismethodaresuitable forDCMD. HollowfiberandnanofibrousPVDFmembranesfabricatedviadry-jet wet spinning and electrospinning techniques by Ghaffour et al.[106]forDCMDapplicationhavealsoshownwaterfluxashighas31.6L/m2hand36L/m2hforthehollowfibersandelectrospunnanofibrous membranes,respectively.Afeedinlettemperatureof80°Candpermeatetemperatureof20°Cweremaintained. ItispertinenttonoteherethatthecommercialviabilityofPVDF membranesforlarge-scaleindustrialDCMDoperations(foranoperationalperiodofupto1000hormore)isstillquestionable.ManystudiesthathaveemployedPVDFmembranesforDCMDapplicationsdidnot providedetailedresultsintermsofoperationalperiodandmembrane life.ThestabilityofPVDFmembranesforlongperiodsof DCMDoperations,rangingfromseveralweekstomonths,canstillnotbeascertained fromDCMDstudies.AlthoughsomecommerciallyavailablePVDFmembraneshavebeentestedforDCMDapplications[107–113],thestability ofthesemembranesforcommercialproductioninreal-lifeplantoperationswasnotascertained.AlthoughKhayetetal.[110]reportedstable fluxeswhileusingaPVDFmembraneforthetreatmentof30mg/LsolutionofhumicacidunderpHofabout7,experimentaldatawereobtainedforaperiodb2000min.Liaoetal.[94]alsoreportedastabilityperiod ofonlyover50hwhentheirsuperhydrophobicsilica-PVDFnanocompositemembranewasscouredwithsalinewater.AndalthoughGryta andBarancewicz[114]triedtousecompositecapillaryPVDFmembraneswithanadmixtureofPTFEparticlesforlong-termdesalination of1000ppmofsalinefeed(i.e.foraperiodof1000h),thepermeate fluxdecreasedbyhalfandthediameterandwallthicknessofthemembraneschangedby10–20%duringtheprocess.Therefore,thereisneed formoreresearchactivitiesinthisareasothattheeconomic lifeofPVDF membranes for large-scale DCMD operations can be ascertained. Some commercialPVDFmembraneswhichhavebeenusedfor DCMDapplications are shown in Table4.

4.1.2. PTFEmembranes

OutofallmembranematerialsthathavebeentestedforDCMDapplications,PTFEshowsexcellenthydrophobicityinadditiontoitsgood thermalstabilityandresistancetochemicalattack.However,amajor drawbackassociatedwiththeuseofPTFEmembranesforDCMDisthe degreeofcomplexityinvolvedinitsfabrication.PTFEmembranesare mostlypreparedbydifficultextrusion,sinteringorstretching[20,28]. ArecentattempthasbeenmadetoimprovethefluxacrossPTFE DCMDmembranesthroughmembranesurfacemodificationbyplasma treatment[117].CompositePTFEDCMDmembranesdesignedfordesalinationandconsistingofporouswovensupportandadensePTFElayer havebeenmodifiedusingplasmatreatment[117].Theresultsobtained indicatedthattheplasmatreatmentstronglyaffectedthesu rfacehydrophilicityofthemembranesenhancingtheirdesalinationperformance. Moreover, extending the plasma treatment time and increasing the plasma power significantly decreased the water contact angle and significantlychangedthesurfacemorphologyofthemodifiedmembranes. A further discovery was that this plasma treatment only slightly changedtheroughnessandsurfaceporosityofthemembrane.Such changesinthesurface morphologyand polarityenhancedthehydrophilicityofthemodified membranes significantly improvingthepermeationfluxwhilereducingthesaltrejection.

PTFEpolymerhasalsobeen employed for high-temperature DCMD operation using hollow fibers membranes[118].Theresultsobtainedfromthisstudyshowedthat therewasnoleakageofsaltfromtheprocessunderanycondition.Inaddition,thehighestwatervaporfluxachievedwas115kg/m2hat118°C, whichwasclosetothat achieved forseawater RO processes.

Table 4
TestedcommerciallyavailablePVDFmembranes

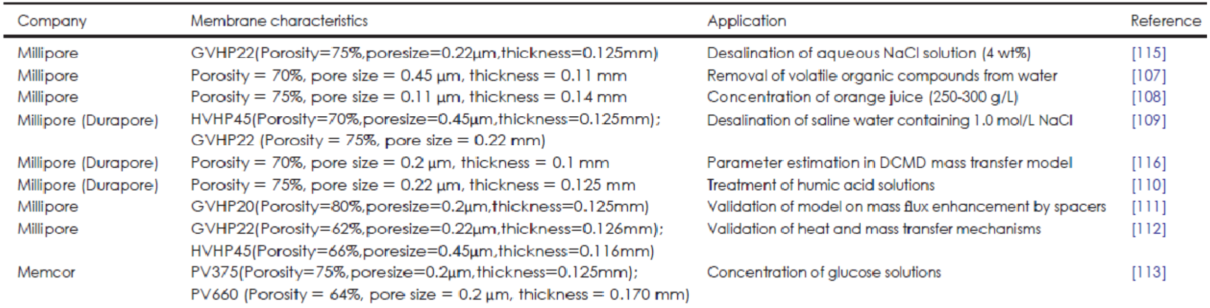

Company	Membrane characteristics	Application	Reference
Millipore	GVHP22(Porosity=75%,poresize=0.22µm,thickness=0.125mm)	Desalination of aqueous NaCl solution (4 wt%)	[115]
Millipore	Porosity = 70%, pore size = 0.45 µm, thickness = 0.11 mm	Removal of volatile organic compounds from water	[107]
Millipore	Porosity = 75%, pore size = 0.11 µm, thickness = 0.14 mm	Concentration of orange juice (250-300 g/L)	[108]
Millipore (Durapore)	HVHP45(Porosity=70%,poresize=0.45µm,thickness=0.125mm); GVHP22 (Porosity = 75%, pore size = 0.22 mm)	Desalination of saline water containing 1.0 mol/L NaCl	[109]
Millipore (Durapore)	Porosity = 70%, pore size = 0.2 µm, thickness = 0.1 mm	Parameter estimation in DCMD mass transfer model	[116]
Millipore (Durapore)	Porosity = 75%, pore size = 0.22 µm, thickness = 0.125 mm	Treatment of humic acid solutions	[110]
Millipore	GVHP20(Porosity=80%,poresize=0.2µm,thickness=0.125mm)	Validation of model on mass flux enhancement by spacers	[111]
Millipore	GVHP22(Porosity=62%,poresize=0.22µm,thickness=0.126mm); HVHP45(Porosity=66%,poresize=0.45µm,thickness=0.116mm)	Validation of heat and mass transfer mechanisms	[112]
Memcor	PV375(Porosity=75%,poresize=0.2µm,thickness=0.125mm); PV660 (Porosity = 64%, pore size = 0.2 µm, thickness = 0.170 mm)	Concentration of glucose solutions	[113]

PTFEhasbeenshowntoproducehigherfluxthanPVDFas aDCMD membranematerial[119].Zhangetal.[119]studieddifferentmembranesincludingPVDFMFmembranewithanon-wovensupport layer,PTFEMFmembranewithanon-wovensupportlayer,andthree MDmembranesmadefromPTFEallwithastructuredscrimsupport layerbutwithdifferentporesizes[119]. Theresultsobtainedshowed thatPTFEmembranesproducedmuchhigherfluxthanPVDFMFmembraneatthesameoperatingconditions. Itwasdiscoveredthatthesupportlayeraffectednotonlytheflux,butalsotheenergyefficiency (0.51–0.24). Theresultsalsoshowedthatincreasingthefeedvelocity andinlettemperaturefurtherincreasedtheflux,buttherate offluximprovementwasreducedatveryhighvelocities. Duringthecourseofthis study,therewasan improvementin the mass transfercoefficientfor thinnersupportandactivelayermembranes,leadingtofluxesashigh as46L/m2hat80°C. Furthermore,theheattransfercharacteristics werefoundtobesuperiorfortheopenscrimbackedmembranescomparedtothenon-wovensupportmembranes, resultinginasignificantly greaterthermalefficiency forthescrimbackedmembranes.

Meanwhile,thecombinationofhydrophobicPVDFwith PTFEparticleshasbeenstudiedto determine the influence of PTFEonPVDFmembrane [114]. Hydrophobic PVDF capillary membranes with an admixtureofPTFEparticlesweredesignedandtestedfor DCMD[114]. Long-term DCMDinvestigations werecarriedoutanditwas demonstrated that the amountof wettedpores wasgraduallyincreasedduring theprocess.Asaresult,theprocessefficiencydecreasedsignificantly. AfterrunningtheDCMD processforover 1000h, thepermeatefluxdecreasedbymorethanhalf forthemajorityofinvestigatedmembranes. Inspiteofthis,thesaltrejectiondidnotdeteriorate,whichindicated thattheporeslocatedmainlyonthe membranesurfacewerewetted. Aslowerrate of wettability was observedforthemembraneswith sponge-likestructures. TheincorporationofPTFEparticlesintothe polymer matrix, however, enhanced the hydrophobicity of thePVDF membrane (watercontactangleincreased from88to103°). Moreover, itwasfoundthatthediameter and wallthicknesso fthe investigated capillary membranes changed by10–20% duringthe DCMDprocess.

4.1.3. Other DCMD membrane materials

OtherDCMDmembranematerialsincludePP,PSf,and Polyetherimide(PEI).Manyofthesematerialshavealsobeenfunctionalizedwithnanomaterials andspecificfunctionalgroupsinrecentstudiesinorderto improve membrane fluxorsoluterejection.Royetal. [120]hasfabricatedandtestedaPP-basedDCMD membrane integrated withfunctionalized carbonnanotube(CNT)forwatervaporfluxenhancement.TheeffectofspecificinteractionsofCNTfunctionalgroups with water moisture on the enhancement of water vapor flux in DCMD (viathealterationofthepolar–nonpolarnatureofthemembranesurface)washighlightedanddiscussed.Thewatervaporfluxobtainedwas36.8kg/m2hat70°CforCNT–COOH–PPhybrid,whichwas 51.5% higher thanthe value obtainedfromanunmodifiedPPmembrane atfeedsaltconcentrationof10,000ppm.Saltrejectionwas foundtobe N99.9%.ThefabricatedCNT–COOH–PPmembranealsoyieldedanin- creaseofabout1.5-timesinthemasstransfercoefficient.Theeffective- ness of CNTs for improved DCMD operation has also been shown throughtheuseself-supportingCNTBuckyPapers.Duméeetal.[121]studied membranesmadefromself-supportingCNTBucky-Papersina DCMD processanddiscovered thatthesemembraneswerehighlyhydrophobic(contactangleof113°C),highlyporous(90%), andexhibited thermalconductivityof2.7kW/m2h.Self-supportingCNTBucky-Paper membranesdemonstratedeffectivenessofuseforDCMD with99%salt rejectionandfluxrateof~12kg/m2hatawatervaporpartialpressure differenceof22.7kPa.However,theperformanceofthese membranes wasfoundtobelimitingduetotheageingofthemembranes bydelam- ination. It was recommended that membrane ageing may be addressed through the fabrication of composite membrane materialstructures. CNT Bucky-Paper membranes have also characterized for their suitable separationpropertiessuchastheirnaturalhydrophobicity,highporosityandveryhighspecificsurfacearea[122].Ina studycarried outbyDuméeetal.[122],thesenanotubesweremodifiedthrough (1)UV/ozonetreatmentcreatinghydroxylgroupsand(2)reacting withthosegroupsthroughthesubstitutionwithalkoxysilanebased groups.Thisstudyconcludedthatlargercontactanglewouldresult from Bucky Papers(140°).

TheenhancementofPSfforDCMDapplicationhasbeencarriedout bypreparingaCF4-plasmaporousflatsheetPSfmembranemodified atacontactangleof144°[123].Asaresultoftheplasmamodification, anenhancedfluxof53.33kg/m2hwasobtainedacrossthe prepared membraneatafeedtemperatureof70.3°C.Thisfluxwas80%higher thanthatobtainedfromacommercialPVDFmembranewithcomparable performancestability.Heatandmasssimulationmodelingwascarriedoutinthesamestudyanditwasshownthattortuosityofthe PSf membraneswascloseto1incontrastto2.5forthecommercialPVDF membranes.Pengetal.hasalsofabricatedPSfflat-sheetmembranes usingavapor-inducedphaseseparation(VIPS)[124].ThebestPSf membranehasthefollowingcharacteristics:meanporeradiusof 0.32μm,watercontactangleof106.4°,liquidentrypressureofwater of300kPaandtotalporosityof82.1%. Theuseofthismembranematerial inDCMDresultedinafluxof30.0kg/m2hwithafeedsalinityof 35g/LNaCl.Inaddition,distillatewateroflow-conductivitywaspro- ducedwithhot-feedandcold-distillatesidetemperaturesof 73°Cand 25 °C, respectively.

AnothermaterialthathasshowntobeeffectiveforpolymericDCMD membranefabricationisPEI.Afluorinatedsurfacemodifyingmacro-molecule(SMM)hasbeensynthesizedandblendedintothecastingso- lution of PEI used as the host polymer in order to membrane hydrophobicityandwatervaporflux[125].Thefabricated composite poroushydrophobic/hydrophilicmembranewaspreparedby the phaseinversiontechniqueinasinglecastingstep.During membrane formation,theSMMmigratedtothetopmembranesurface,therebyincreasingitshydrophobicityanddecreasingitsporesize,nodulesizeand roughnessparameters.Thethicknessoftheporoushydrophobiclayer wasfoundtobearound4mm.Performanceexperimentswerecarried out using different aqueous NaCl solutions and operatingconditions. ThewaterproductionratewasfoundtobehighforDCMDdesalination becauseofthelowresistancetomasstransportachievedbythediminutionofthewatervaportransportpathlengththroughthehydrophobic thin top-layer of themembrane.

ThecharacteristicsandperformanceofsomerecentlydevelopedmembranesforDCMDdesalinationintermsoffluxandsaltrejection are summarized in Table5.

Thefabricationofpolymericmembranesthathavebeenconventionallyusedin MDhasbeenperformedusingtechniquessuchasnon-solventinducedphaseseparation(NIPS),thermallyinducedphaseseparation(TIPS),meltextrusionstretching,sinteringandelectro-spinning [18].Lately,inorganicmembranessuchasthoseinvolvingtheuseofceramics,carbonnanotubes(CNTs)andmetalshavebeenstudiedforMD applications[121,128–130].Ceramicmembranessuchaszirconia,alu-minaandtitaniumhavebeenmodifiedaccordinglyforenhancedhydrophobicityandimprovedMDapplication[131,132].Theuseofself-supportingCNTmembranesinDCMDapplicationhasresultedina fluxof12L/m2hwith99%saltrejection,whenthewatervaporpartial pressuredifferencewas22.7kPa[121].Theincreaseinporehydrophobicityasaresultof CNTmodificationhasallowed anenhancementof the performance ofthe DCMD, asevidentinflux improvement by 1.85 times the original flux. Due to the observed ageing of the self-supporting membrane, surfacegraftingandcoatingcan be implemented for improved membrane durability.

Table 5
PerformanceofrecentlydevelopedDCMDmembranes

Reference	Polymer	Membrane characteristics	Feed	T_{feed} (°C)	$T_{permeate}$ (°C)	Stable operation (h)	Flux (kg/m²h)	Salt rejection
[94]	Electrospun silica-PVDF composite	Contact angle 156.3°; bulk porosity 82%; 0.69 μm mean pore size	3.5 wt% NaCl	60	20	50	18.1	Permeate water b5.0 μS/cm
[94]	Electrospun PVDF with superhydrophobic skin	0.32 μm mean pore size; contact angle 154°	3.5 wt% NaCl	60	20	40	24.6	N 99.99%
[100]	PVDF-based membranes	0.26-0.64 μm mean pore size; contact angle 128-154°	1-3.5 wt% NaCl	50–80	17-24	8–40	4 28	98–99.99%
[126]	PVDF-HFP with different solvents and solvent mixtures	Mean pore size: 0.064-0.071 μm	3 wt% NaCl	50–80	25	/	2.88-6.84	N 99.3%
[127]	TiO_2 and fluoro-silanecompound coating on PTFE membraneswith PET support	Mean pore size: 0.25 μm	Up to 10 wt% NaCl	60	25	130 for coated capillary membrane	4–6	/
[101]	Nano fibrous PVDF-HFP-PAN	Porosity: 90%; contact angle of PVDF-HFP:150°; contact angle of PAN:100°	35 g NaCl solution	/	/	/	PH: 45 PAN:30	/
[102]	PVDF-HFP	/	/	/	/	/	4.41	99.95

Other surface modified membranes includehydrophilicpolyethersufone(PES)ultrafiltration(UF) hollowfibermembranesthat canbetransformedintohydrophobic MDmembranes throughCF4 plasmamodification[133].Themodified membranesgaveastablewaterfluxof66.7L/m2hwithsalt rejection of99.97%at73.81°Cfora DCMDoperationof54h. Thesurfacetreatmentof polyethersulfone(PES) canbeperformed throughthe addition ofgraftingagentssuchastetraethylorthosilicate(TEOS)and trimethylchlorosilane(TMSCl).Theidentificationandcharacterization of these modified membranes was performed in a study by Rastegarpanahetal.[134]usingmultipletechniques.Theseincludedattenuatedtotalreflectioninfraredspectroscopy(ATR\\IR),scanning electron microscopy (SEM) coupled with energy-dispersive X-ray spectrometer(EDX),atomicforcemicroscopy(AFM),andopticalcontact angle measurement (OCA). These membranes, having contact angle of 150°,wereusedinDCMDoperationfordesalinationpurposes. Aseparationfactorof99.7%aswellaspermeatefluxesclosetothoseobtained fromacommercialmembranewereobtained[134]. MembranemodificationhasalsobeenperformedviaTiO2nanoparticlesincorporation[36].Thecontactangleofthismembranewasfound toincreasefrom125°to166°andwastestedonseawaterandhumic acidsolutions.TiO2-modifiedmembraneshavealsobeeninvestigated fortheDCMD treatment of phenolicsolution[135]. Studiesonthesepārationefficiency andfoulingtendency of these membranes were carried outinthe presenceandabsenceofsilane. TheadditionoftheTiO2 to PVDFcastingsolutionwas performed through the method of phase inversion.Thepremodifiedmembranehadacontactangle of151° whereas the post-modified membrane had a contact angle of 140°. Overaperiodof8h,thesemembranesachieved99%rejectionwith membranefluxreductionof17%forthepre-modifiedmembranesand 12%forthepost-modifiedones.Thepost-treatedmembranesgavea higherpermeatefluxbecausetheyexhibitedhigherporosity.The inner pores within the unmodified PVDF/TiO2 membrane can be blockedasaresultofmembranewetting[135]. Dependingonthetypeofmembrane,thefluxandconductivityof permeatedifferforaDCMDoperation.Testedmembranescanbecharacterizedintermsof LEP,CA,andgaspermeability.Themoduleswould alsodifferinaccordancewiththetestedoperatingparameterssuchas flowmode,flowrate,temperature,andconcentration.For example, whiletestingninetypesofcommerciallyavailablemembranesfor drinkingwaterproductionfromsalinewater,Heetal.[136]observed thatpermeateconductivitywasbelow8mS/cmforallthestudiedconditions. However, the individual performance of the membranes dependedonthetypeofsalinewater,hotandcoldsidetemperature, andpropertiesofmembranes. Fluxvalueof23.76L/m2hwasobtained from seawater treatment whileusingfeed temperatureof60°C, permeatetemperatureof20°C, andflowratesof0.6L/min for PTFE membranes withporesizeof0.22mm. Afteraonemonthperiod,thisvalue dropped to 14.36 L/m2h. Roughpolystyrene(PS)micro/nano-fibrousmembranes prepared throughthemethod ofelectrospinning haveshownsuperhydrophobicity andhighporosity which makethemwellsuitedfor DCMDdesalination [137]. Different concentrations of the polymer ranging from 15 to 30wt%werestudied. TwoPSnanofibrousmembranesofdifferentthicknesses(60μmand120μm)weretestedforDCMDdesalinationapplication (Fig.7).

For thethinner membrane withathicknessof 60μm,20g/LNaClsalt feedwastreatedresulting inaflux of 104.8±4.9kg/m2h. Asforthe thicker membrane with a thickness of 120 μm, a feed solution of 35g/LNaClwastreatedresultinginafluxof51±4.5kg/m2 h.Temperaturedifferencebetween thehotand coldstreams wassetat50°Cfor bothmembranes over a10hperiodintheabsence ofsignificantwetting. Recently developedmembranesprepared fromsurfacemodificationof polymersand nanomaterials havebeensummarizedinTable6.

4.1.4. Measurement and control of membranefouling

OneofthemainchallengesassociatedwithDCMDisitsfoulingeffect [139].Thisoccurswhensubstancessuchas$CaSO_4$and$CaCO_3$knownas scalantsdepositonthesurfaceof themembraneorinitsporesreducing thepermeatefluxwithtime[140].Otherkindsoffoulantsincludeparticulates,organicmatter, andbiofilmwhichcanalsocausefluxdecline. Anotherrnegative impactofthesefoulantsin DCMD operationsis their tendency to adversely modify membrane surface properties and reduce thequalityofthepermeate[139].Onetypeoffoulingofseriousconcern to DCMD is organicfouling. Ononeinstance,Naiduetal.[141]observed a40–50%fluxdeclinewhenasyntheticsolutionofhumicacid(HA),alginateacid(AA) and bovineserumalbumin(BSA) wasfedtoaDCMD system.OrganicfoulingdevelopmentindicatedthatBSA andHAshow dominantfoulingtendencies. TheHAfeedsolutionshowedthermaldisaggregationtolowmolecularweight-HA(LMW-HA) organicswithin-creased feed temperature(50to70°C). Inaddition,theBSAfeed solution showed more significant deposits on the membranesurface (35.2%highercarbonmasscompared toHAfoulant)withlesssignificant pore penetration. However, minimal fouling was observed with AAduetoitshydrophilicnature.Thisstudyhighlightsthefactthat DCMDoperationsarestill verymuchinfluencedbyorganicfouling agentswhichresultinsignificantadverseeffectsonmembranelife andoperatingcost. Theextentof foulinghasalsoshowntobeinfluencedbyDCMD operating conditionssuchasfeedandpermeatevelocities.DifferentfeedandpermeateflowvelocitieshavebeentestedinaDCMDsysteminordertostudy thesystemperformanceandscaling pattern[142]. Ithasbeen concludedthatacombinationsettingi.e. feed and permeatevelocities of0.8m/sand1.1m/s,respectivelyresultedina30% higher recoveryratioand60%lowerpumpingenergy,as comparedwith when bothvelocities weremaintainedat1.1m/s.Membraneanalysis demonstratedbulkcrystallizationtendencyathighflow velocityranges(1.1–2.2m/s) whilemembranesurfacecrystallization

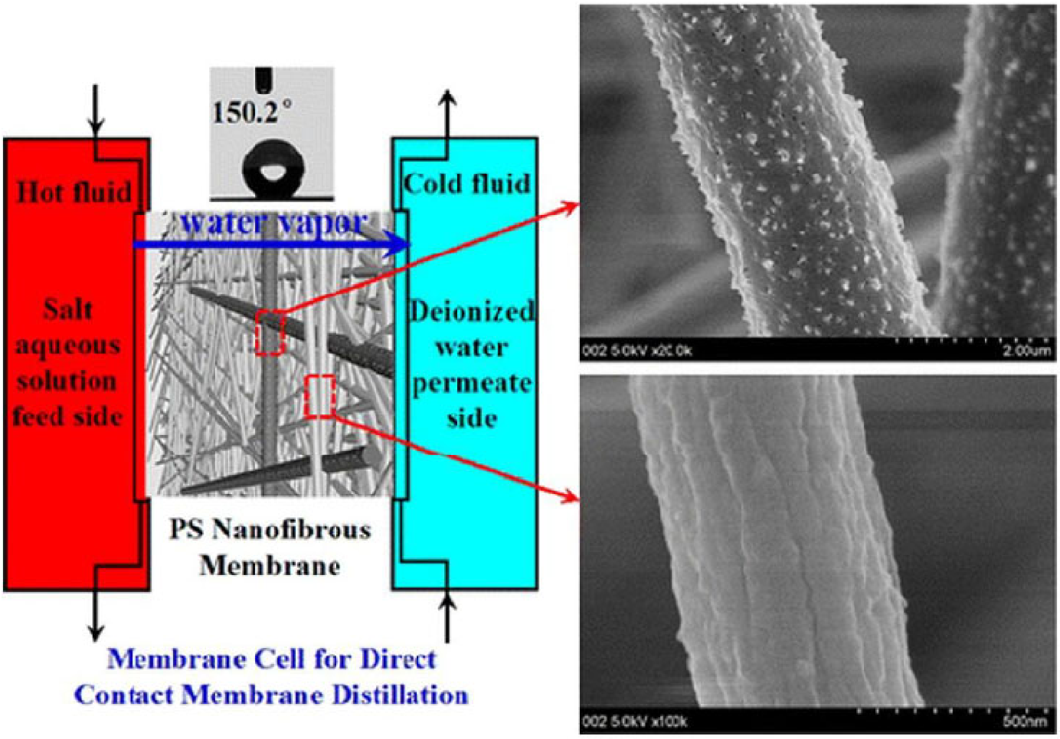

Fig. 7. PS for DCMD treatment of saline feed [137].

wasdominantatlowerflowvelocities(0.5–0.8m/s). Moreover,the combination setting showed beneficial outcome of reduced tendency ofmembranesurfacecrystallization.

Otherthanorganicfouling,amajorproblemforDCMDmembranes isscaling,especiallyscalingcausedbycalciumprecipitantsathightemperatures.Nghiemetal.[143]investigatedmembranescalinginDCMD andrevealedthatmembranescalingcausedbyCaSO4was moresevere thanthatcausedbyCaCO3orsilicateatfeedtemperatureof 40°Cand distillatetemperatureof20°C[143].Atasaturationindexofupto1.5, CaSO4scalingoccurredonlyafterasufficientlylonginductiontimeof upto25h.Theresultsshowedadecreaseintheinductionperiodand anincreaseinthesizeoftheCaSO4crystalsasthefeedtemperatureincreasedwithregularmembraneflushing/cleaninguntilit was completelyfreeofanylargecrystalstoresettheinductionperiod.The studyconcludedthatthereisinterplaybetweeninductiontimeand thesaturationindex.AnotherfactoraffectingthescalingofaDCMD membraneisthebubblesizearoundthemembranewherethemixing andmembranesurfaceshearratewouldbeenhancedbysmallmean bubblesizeandnarrowdistribution[144].Anoptimalgasflowrateof 0.2L/min,upto2.30and2.13-foldenhancementcanbereachedfor heattransferandtemperaturepolarizationcoefficients(TPC),respectivelywhereatahighgasflowrate,negativeeffectcanbeobserved.

Shearstressandhydrodynamicsinducedbygasbubblesimproves localscalingresistanceasdeterminedbyChenetal.[144].Thestudy observedthatmeanbubblesizeandnarrowersizedistributionarethe preferreddryingconditions.Asaresultofbrineconcentrationprocess, 131%oftotalwaterremovalwasimproved.

Themodelingoffoulingmechanismsandresistancetotransportin thefoulinglayerhasalsobeenstudiedinarecentinvestigation[145]. Dingetal.[145]studiedthetransportresistanceoffoulinglayerformed whileconcentratingtheextractoftraditionalChinesemedicine(TCM) byDCMD.Anempiricalmodelwasdevelopedtodescribe theconcentrating process. The result showed that membrane fouling in this studywasmainlycausedbythedepositionofsuspendedsolidparticles inTCMextract.Thefluxdeclinesfasterwithincreasingfeedtemperatureandfeedflowvelocityresultinginafasterincreaseoffoulant concentrationinthefeed.However,thecomparisonoftherelationships betweenfoulingresistance and concentration ratio obtainedunderdifferentconditionsrevealedthatthegrowthoffoulinglayercanbeeffectivelylimitedbyoptimizingeitherthefeedtemperatureorfeedflow velocity.

Table 6
Surface-modified and new DCMD membranes from nanomaterials

Membranematerial	Fabricationmethod	Performance	Reference
PESUF	CF_4 plasmasurfacemodification	Fluxof66.7L/m^2hwithasaltrejectionof99.97%at73.81°Cforanoperational period of 54 h	[133]
PVDF/TiO_2	Phaseinversion	99%rejection,loweringofmembranefluxreductionfrom17to12%over8h	[135]
PS superhydrophobic micro/nano-fibrous	Electrospinning	For membrane thickness of 60 μm: 20 g/L NaCl salt feed was treated resulting in a flux of 104.8 ± 4.9 kg/m^2 h; For 120 μm, a feed solution of 35 g/L NaCl was treated resulting in a flux of 51 ± 4.5 kg/m^2 h at ΔT = 50 °C for 10h	[137]
Graphene/PVDF	Phaseinversion	G/PVDF-0.5membranedisplayedthehighestfluxwithacontactanglegreaterthan that of G/PVDF-0.1 and G/PVDF-0.3	[78]
PVDF/TiO_2	Lowtemperaturehydrothermalprocess	Contactangleincreasefrom125°to166°	[36]
Cellulosenitrate	Octafluorocyclobutane plasmasurface modification	Good performance with PTFE, PP andPVDFpolymers	[138]
PES	Phase inversion and grafting agents addition (TEOS andTMSCl)	Contactangleof150°;Separationfactorof99.7%	[134]
CNT	Chemicalvapordeposition	Fluxof12L/m^2hwith99%saltrejectionandwatervaporpartialpressure difference of 22.7 kPa	[121]

InastudycarriedoutbyNguyenetal.[139],theeffectsofoperating parameterssuchasthefeedtemperatureandhydrodynamicconditions ontheformationofmembranefoulinglayerwerestudied. Thecompositionandmorphologyoffoulantswerestudiedusingmultipleanalyticaltechniques. Theseincludescanningelectronmicroscopycoupled withenergydispersive X-ray(SEM-EDS),X-ray diffraction(XRD), Fouriertransforminfrared spectrometry(FTIR),AFMandcontactangle.The results showedtheoccurrenceofmoreseveremembranefoulingand wettingathigherfeedtemperatures. Foulingresulting fromtheseawaterRObrinefeeddisplayed alargeamountofbothinorganicfoulants suchas $CaCO_3$ and$CaSO_4$ andorganicfoulantssuchaspolysaccharides andproteins.Furthermore,testsdisplayedareductioninthefouling andwettingeffectupon theadditionof NaOCltothefeed asapretreat- mentstep. Coupling thistreatmentwiththerinsingofthemembrane witha3%HClsolutionsshowedarestorationoffluxaswell asagood-qualitypermeateproduction[139]. Inanotherstudy, areducedfeed temperatureand enhanced feedflowratewerefoundtoreducethe fouling effect[146].

Across-flowbenchscaleDCMD unithasalsobeentested toinvesti- gatetheeffectoffoulingonpermeateflux, intermsofchoosingthemost suitablemembranefortheunitoperation[31].ThroughSEMimagery andcontactanglemeasurements, themembranecharacteristicsand morphologywereobservedinordertostudythesuitability ofthemem- branesforDCMDoperation. PTFE membrane was foundtohaveacon- tact angle of 127° with highly porous surface supported with less porousandbiggerpore-sizePPmembrane. Furthermore,theresults fromthisstudyindicatedthat,inthepresenceofantiscalants,themembraneswereoperationalforoveraperiodof17hwithoutseverefouling [31].

4.2. Operating conditions and their effects on DCMD productivity

MajordeterminantsoftheperformanceoftheDCMDareitsdesign, configuration,andoperating conditions. DCMD systemperformancein termsofproductivity andcapacityarelargelyaffectedbyflowpathof thefeedandpermeate(countercurrentorconcurrent),materialofsys- temconstruction, meansofheatexchange, mechanicalandthermal properties offeedandpermeate, andsystemconfiguration.Theselected operating conditionsaffecttheoverallefficiencyoftheDCMDprocess [56].InmanyDCMDstudies, temperaturegradienthasbeenidentified asan importantoperatingcondition.However,valuesoftemperature forthehotandcoldsidesare veryimportantfactorsashigheroperating temperature forthehotsidemightresultintomorefluxes,providedthatliquidentrypressureisnotreached.However,thesefluxes would alsoultimatelydepend onthesourceoffeedwater, typeofmembrane, and feed flow rate or velocity[74,75,87]. Fig.8(a)and(b)showthevariation of fluxwithtemperature,asobtainedfromdifferentstudieswith different temperaturerange.

Fig.8(a)and(b)showthatalthoughhighfeedsidetemperatureis desired for higher flux, feed flow properties such as the flow rate woulddeterminethefluxataparticularoperatingtemperature.Theinfluenceofoperating conditions suchasfeedtemperature,feedflowrate, coldstream flowrate, andfeedconcentrationontheperformanceof ninecommerciallyavailablehydrophobicflatsheetPTFE DCMD membranes hasbeenstudiedby Mahdietal.[147]. Theresultsobtained from this experimental study revealed that increasing the feed temperature,feedflowrate,andmoduledepthonthecoldsideresultedinan increaseinpermeateflux.Bahmanyaretal.[148]simulatedandstudied theeffectofoperatingconditionssuchasfeedtemperature,feedcirculationrate,andfeedinletconcentrationonpermeatefluxinaDCMD process. Mass and energy models were developed andsolved numericallyusingMATLAB.Heattransferduetomassflux,heatlost byconduction,aswellastheircontributions totheoverallheatflux throughthemembranewere shown tobesignificantoperatingfactors. Thisstudyconsidered thevariationofphysicalandflowpropertieswith temperatureandconsequentlyheattransfercoefficients.

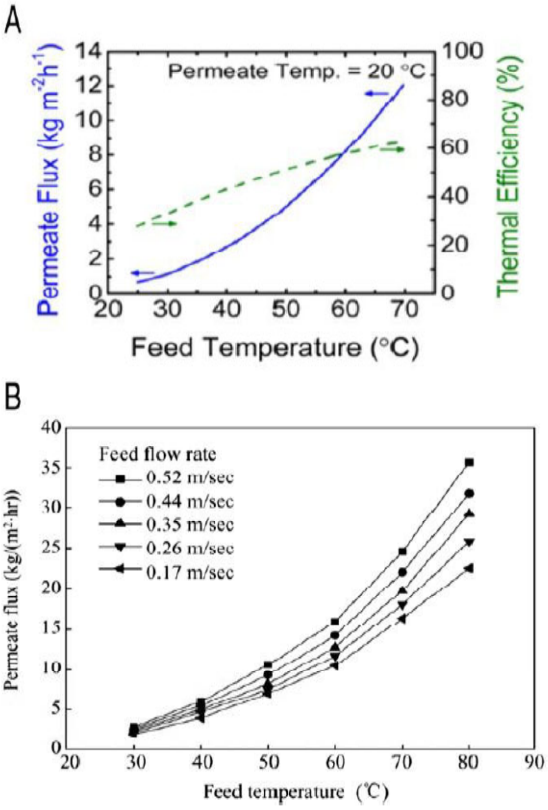

Fig.8.(a)Variationofpermeatefluxandthermalefficiencywithfeed temperature fora typicalcommercialPPmembrane (atfeedtemperatureuptoapproximately70°C, permeate temperature of 20 °C) [74]. (b). Variation of permeate flux with feed temperature and flow velocity[87].

AspenPlus softwarehasalsobeenusedrecently to theoretically investigatethe criticalmembraneareaasa crucial operatingconditionfortheDCMD process[149]. Energyefficiencyandeconomicanalyseswerecarried usingtheAspenPlusapplication.Theresultsshowedthata critical membrane area existed, below which, significant increases ofwater productionand gainoutputratio(GOR)wereobserved.Operating belowthecriticalmembraneareawouldalsoleadtosignificantdrop in waterproductioncost(WPC). Whenthetemperaturedifferencein theheatexchanger wasincreasedto6°C,WPCwasconsiderablyreduced because the heat exchanger cost was cut down. However,optimumfluidvelocities beyondwhichthere wassignificantpenaltyof more electrical energy consumption resulting from pumpingwere observed.

4.2.1. Effect oftemperature

Manawietal.[57]hasalsodemonstratedthattemperatureisavery important operating factor which needs serious considerationduring thedesignofDCMDoperationsinordertoavoidtemperaturepolarization.ADCMDmodelwasdevelopedtoestimatethetemperaturepolarizationcoefficientacrossaDCMDmembrane[57].Thelocalfluxand localtemperaturepolarizationcoefficientsatdifferentoperatingconditionswereobtained.Itwasdiscoveredthatthehighesttemperaturepolarizationcoefficientof0.82wasachievedataflowrateof3L/minand feedandpermeatetemperatureof60°Cand20°C,respectively.Itwas alsoobservedthatthecoefficientincreasedfrom0.66fora spacer-filledchannelto0.47foraspacer-freeoperationat1.5L/minflowcondition,whenthetemperatureofthefeedandpermeatewas 70°Cand 30°C,respectively.TemperaturepolarizationcoefficientinDCMDhas alsobeenshowntodependlargelyontheintrinsicmasstransfercoefficientofthemembraneused(Cvalue).Yuetal.[49]hasinvestigatedthe effect of membrane Cvalue on the performance enhancement of both non-baffledandbaffledmodulesusingCFD.Theresultsobtained showedthattemperaturepolarizationcoefficientdecreasedsignificantlywithincreasingCvalueregardlessoftheexistenceofbaffles.However, itwasconcludedthattheintroductionofbafflesintoDCMDmembrane modulecangreatlyenhancethemassfluxandtemperaturepolarization coefficientforamembranewithahighCvaluewherethemainheat transferresistanceisdeterminedbythefluidsideboundarylayers. Thetemperaturepolarizationcoefficientwasalsoobservedtodecrease generallywithincreasingoperatingtemperaturesandthemassfluxincreasedsignificantlywhentheoperatingtemperaturewasincreased. Therefore,higheroperatingtemperaturesweresuggestedtobepreferableforasubstantialimprovementintheheat/masstransferandthermalefficiency inDCMDoperations,evenwitharelativelysmall transmembranetemperaturedifference.SinghandSirkar [73]alsoobservedthatthethermalconductivityofmembranematerialisastrong determiningfactorofDCMDperformance.Meanwhile,inordertoinvestigatetheeffectofthermalconductivityofhydrophobic/hydrophilic hollowfibermembranesonvaporflux,anexperimentalandmathematicalmodelingstudyhasbeencarriedoutbySuetal.[150].A significant increaseinvaporfluxfrom31.4to78.5kg/m2hunderfeedanddistillate temperaturesof80°Cand20°C,respectively,whenthethermalconductivityoftheinnerhydrophiliclayerwasvariedfrom0.2to1.4W/mKwaspredicted.MWCNTswithgraphiteparticleswereembedded intothehollowfiberhydrophiliclayertoimproveitsthermalconductivity. By incorporating both graphite and MWCNTs, the thermalconductivity wasincreasedfrom0.59to1.30W/mK.Thethermal conductivityobtainedwasstillrelativelylowanditwasfoundthat thisincreaseinthermalconductivity,actualizedthroughtheaddition ofnanomaterials,ledtoasignificantincreaseinvaporfluxfrom41.2 to66.9kg/m2hwhentheinletfeedanddistillatetemperatureswere maintainedat80.4°Cand15.3°C,respectively.

4.2.2. Effect of flowdeflector

Thedirectionofinletvelocityalsoinfluencestheperformanceof DCMD.Wangetal.[151]investigatedtheinfluenceofaflowdeflector onDCMDefficiency.Atotalofsevenmodules,including asmoothmembranemoduleandsixflowdeflectormoduleswerefabricatedandtested.Thesmoothmodulerevealedacomparativelyabruptchangeofwaterfluxwhentheinletvelocitywasaround0.25m/s.Usingthe samepumpingpower,thetestresultsshowedthatthewaterfluxforsmoothmoduleweresmallerthanthatobtainedfor allmodulescontainingaflowdeflectoratalltemperatures.Itwasalsodiscoveredthat moduleswithmoredeflectorsbecamemorecompetitiveatahigher feedtemperaturebutwerelesseffectivewhenthevelocity washigh.

OperatingaDCMDprocessbyusingroughened-surfaceflowchannel in a countercurrent configuration has been shown to enhance heat transferandsystemperformance[152].Hoetal.[152]enhancedheat transferinsalinewaterdesalinationviaDCMDbyusingroughened-surfaceflowchannelonacountercurrentparallel-plateDCMDmodule. Anincreaseinthepurewaterproductivitywasachievedwhencomparedwithconcurrent-flowoperationwithoutroughened-surfaceeffects.Roughened-surfaceeffectshavedemonstratedthetechnical feasibilityofperformanceimprovementsandupto42.11 %ofperformanceenhancementwasachievedforthiscountercurrent-flowDCMD system.Inasimilarstudy,Hoetal.[153]alsotheoretically proposed roughened-surfaceflowchannelforenhancementofpurewaterproductivityinsalinewaterDCMDprocess.Aheattransfercoefficientcorrectionfactorwasobtainedfromheatandmasstransfermechanisms andthisfactorwasincorporatedwiththeexperimentaldataobtained. Thecorrectionfactorwasexpressedasrelativeroughness andcanbe usedforpredictingtheheattransfercoefficientforroughened-surface channels.

4.2.3. Effect of membraneproperties

Certainly,differentoperatingfactorshavedifferenteffectsonthe performanceoftheDCMDprocess. Therefore, effortshave alsobeen directedtowardsthe investigationofthesensitivityofDCMDperformancetodifferentfactors.ThesensitivityofDCMDtovariousoperating conditionshasalsobeentheoreticallystudiedbyHayeretal.[154]using theCFDmethodinordertodeterminethemostcrucialconditions.The globalsensitivityanalysistechniquewasusedtomeasuretheeffectsof differentparametersonthetransmembranefluxandtemperaturepolarizationcoefficient.Theresultsobtainedindicatedthatthemostsignificantdesignparametersin DCMDaremembranethicknessandfeed temperature.Raoetal.[155]hascarriedoutamechanisticinvestigation ofthefactorscontributingtohigherwaterfluxusingDCMD,vacuum- enhanced direct-contact MD (VEDCMD), and pressure-enhanced DCMD(PEDCMD) configurations.Theonedominantfactorcontributing toimprovedwaterfluxwasreducedmembranecompaction.Theother dominantfactorwasthereducedairpressureinsidethemembrane pores.Thepressuredifference,inbothPEDCMDandVEDCMD,was foundtohaveaminimaleffectonwaterflux.Asimplified modelthat canbeusedtopredicttherelativemagnitudesofwaterfluxeswas alsodeveloped[52]. Thefourparametersε/δ,ε/τδ,1/τδ,[relationships betweenδ(thickness),ε(porosity)andτ(tortuosity)]andCmwere foundtobehighlycorrelatedwithwaterflux. Thisstudyprovidedadetailedcollectionof MDmembranepropertiesandtheirwaterfluxvalues thatwillassistothersinmembraneselection,developmen, and application. Meanwhile, forgeneralDCMD applications, the dominantfactor depends onthescaleofoperation,configurationofDCMD,andthe nature of feed to be purified [24]. For DCMD integrated with salt-gradientsolarpond(SGSP), forexample,thesurfaceareaofthesolar pondwasfound tostrongly influencetheproductivityofthesystem [156]. AtheoreticalinvestigationbySuarezetal.[156]fortheproduction ofsustainablefreshwater fromatterminallakes usinga SGSP-DCMDprocessrevealed thatfreshwaterflowswereofthesameorder ofmagnitudeasevaporation,andtheintegratedsystemwouldonlybe successfuliftheSGSP isconstructed insidetheterminallakesothat thereislittleornonet increaseinthesurfacearea. Forthestudied site,waterproductionoftheorderof2.7×10−3m3/m2dwasachieved. Thestudyconcludedthatthemajoradvantagesofthissystemwerethe use of renewable thermal energy, requirement of little electrical energy, requirementoflow maintenance, and provisionofsalts bytheterminal lakessothatstratification canbe createdinthe SGSP.

4.3. Sustainability of DCMD

4.3.1. Economics and cost of waterproduction

Througheconomicevaluation,themaincontributingfactorstothe waterproductioncostcanbebetterunderstood.Therelationshipsbetweenthewaterflux/production, GORand thewater productioncost (WPC)inrelevancetothe DMCDsystemdesignandoperatingparametershave been investigatedby Zouetal.[149].Itwasshownthatthere existsacritical membrane areabelow whichthereisanobservedincreaseofwaterproductionandGOR,whichresultedinasignificant dropintheWPC. Afurtherobservation wasthepositiveeffectofincreasingthefeedtemperature onthewaterfluxandtheGOR.Inaddition,thewaterflux, waterproductionandtheGORhavebeenshown toincreasewithanincreaseinthefeedandpermeatevelocities.This studyconcludedthatthroughreducingthe costofheatexchange,the WPCcanbesignificantly reduced.Inanotherstudy,theeconomicperformanceofDCMDwasanalyzedfortheestimationofthe massflux andtheheatefficiencythrough the consideration of parameterssuch asmembranestructural properties. Itwasfoundthattrans membrane fluxand thermalefficiencycanbeenhancedthroughanincreasein thetemperaturegradient. TheestimatedwatercostoftheDCMDwith heat recovery was1.17USD/m3.

Thisvaluewasrelativelyclosetothat ofwaterproduced byconventionalthermalprocesses,forexample costofwaterproducedfromMEDwasaround1.00USD/ m3andcost ofwaterproducedfrom MSFwasaround 1.40USD/m3.However,the water production cost of this low-grade thermal energy methodcan besignificantlyreduced approachingthecostof RO produced water, about0.50USD/m3, henceleadingtomajorsavings[91].

An economic study aimed at comparingthesolarpowered-MDsys- temshasalsobeen carriedoutby Saffarinietal.[157].Threesystems-DCMD,AGMD,andVMD-weremodeledand economically analyzed. Theresultsshowed a significantincreaseinwater productionandre- ductionin thecostthrough anincreaseinthefeedinlettemperature. Furthermore, itwasobservedthatthewatercostcanbe reduced throughamoreeffectivemembranelengthand feedchanneldepth. Therefore, theselectedoperatingconditionsinDCMDhaveaconsiderableimpactonthefinal costofwaterproduction. However,anincrease infeedinlettemperaturewithouta corresponding increaseinthermal energyutilizationefficiencywouldresultinhighercostsof waterpro- duction,asshowninFig.9.

ForthereductionofwaterproductioncostsinDCMDoperations,energyconsumptionneedstobereduced.Thismakesenergyconsumption asignificantfactorthatneedstobeconsideredwhenapplyingDCMDfor freshwaterproduction[158].AcomputationalframeworkhasbeenformulatedbyNguyenetal.[159]forthesimulationandoptimizationof DCMDinordertominimizetheenergyconsumedduringthisprocess. Thestudyalsousedalab-scaleDCMDsystemtoconcentratea1.5kg glucosesolutionfrom30to60%w/w.DynamicoptimizationwasperformedtominimizetheenergyexpensesofthisDCMDprocess.Theenergyconsumedaccountedfortheheatexchangebetweenthefeedand permeate streams, within the membrane module, and the pumping powerforpumpingofstreams,whilemaintainingaminimummass flux of 0.5 kg/m2 h. The optimal operating conditions found in this study wereobservedtoreducethetotalenergy consumptionby 26.3%.TheresultsobtainedshowedthatthehighestachievableenergyefficiencyofDCMDwithinthetestedrangewasabout49.9%.EnergyefficiencyinDCMDoperationhasalsobeeninvestigatedthroughtheuse ofalow-gradeheatsource.Linetal.[160]usedlow-gradeheatcoupled withaheatexchanger(HX)toevaluatethemassrecoveryrate(fraction offeedwaterrecovered)andspecificheatduty(energyinputperunit massofproductwater)ofDCMDdesalinationthroughthethermodynamic analysis.Fromthisanalysis,acriticalrelativeflowratethat limitsDCMD operationbetweenpermeatelimitingregimeandfeedlimitingregime wasrevealedwhenthemasstransferkineticsarenotlimiting.Theresultsobtainedshowedthatthehighestmassrecoveryrateandlowest specificheatdutyachievableweredeterminedbythethermodynamic propertiesofthesystemandoccurredatthecriticalrelative flowrate. Thethermodynamiclimitsformassrecoveryrateandspecificheat dutywere6.4%and27.6kJ/kg,respectivelyforseawaterdesalination bysingle-passDCMDat60°C.Thestudyconcludedthatheattransfer acrossathermally-conductiveDCMDmembranereducestherecovery rateandenergyefficiencyoftheprocessandthishasimplicationsfor theoptimizationoftheDCMDprocess.Theuseofmembraneshaving highheat-transferresistancewouldhelptoimprovetheGORupto 32%[161]exceptpolymermembraneshavinghighthermalcanbe incorporated with nanomaterials to improve their surface characteris- tics [150].

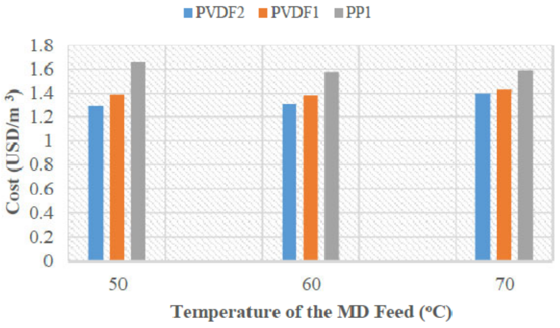

Fig.9.Watercostatvariousfeedinlettemperaturesfordifferentmembranes(membrane life-time=5years, recoveryrate=70%,permeatetemperature=25°C)[71].

4.3.2. Integration of DCMD with renewableenergy

4.3.2.1. Solarenergycoupling. Lately,attemptshave been madetoincor- porateDCMD withrenewable energy inordertorestricttheuseofcon- ventionalfossil-fuelenergyforthegenerationofthermalenergyin DCMD,hencereducingitsenvironmentalfootprint.Solar energyisone ofthemajorrenewableenergy sourcesthathavebeenappliedforther- mal energy generation in DCMD. Solar-driven membrane distillation (SDMD)and DCMDcoupledwithSGSParetwoftherecentstudies thatwerefocusedonsustainableDCMD through theexploitation of environmentally-friendly solarenergy[85,156,162]. Threemembranes (C02,C07 andC12; basedontheporesizesof0.2,0.7,and1.2μm,respectively)havealsobeenexperimentallytestedfordesalinationvia the solar-assisted DCMD process [163]. Desalination of real seawater withouttemperaturecontrolwascarriedoutunderthefollowingconditions:feedinlettemperatureof65.0°C, permeateinlettemperatureof 25.0 °C and flow rate of 2.5 L/min. Long-term experimental runs (150days)usingbothsolarand electricpowershowedthatpermeate fluxwasonlyreducedfrom28.48to26.50L/m2hwhensolarpower wascombinedwithconventionalelectricpower toruntheprocess [163]. Shim et al. [164]has developed a 2-dimensional model for solar-assistedDCMDsystemforseawaterdesalination.Themodelwas verifiedwithexperimentalresults.Thesolar-DCMDsystemrancontinuouslyforN150daysforseawaterdesalinationinKorea.Duringday time,N77.3%oftheheatingenergywassuppliedbysolarenergy.Inparticular,inthemonthofSeptember,95.3%oftheheatingenergywassuppliedbysolarenergy.Inanotherstudy,theperformanceof asolar drivenDCMDplantwasinvestigatedbyBouguechaetal.[165]using twoarrangements,onewithheatrecovery device(HRD)andthe other without. For the arrangement without HRD, the distillate per modulewasfoundtobe3.31L/handforthatwithHRDwasfoundto be 4.59L/h.

Theremovalofarsenicfromacontaminatedgroundwaterresource hasbeenstudiedusingPVDFmembranesinasolardriven DMCDconfig- uration. Thisresultedinapproximately 100%arsenic-freewaterwith highfluxesandreduced temperaturepolarization.Duetohighfluxes of 74kg/m2hata feed water temperatureof40°C and95kg/m2hat afeedwatertemperatureof60°C, Mannaetal.[85]concludedthat thisdesigncouldbeused effectivelyinthevastarsenic-affectedrural areas of South-East Asian countries with abundant availability ofsun- lightenergy.Furthermore, Chenetal.[166]hasdesignedacombined solar absorberasan energysourceforwaterdesalinationby DCMDpro- cess.Experimentaltestswerecarried outatatemperaturerangeof about35–50°C. Thesolarabsorber wasinsertedbetweenaglasscover and the DCMDmembrane toheattheflowingfluidwhichwas passed underneath the absorber plate. A two-dimensional mathematical energymodelandageneralnumericalmethodwerealsousedto obtainthe waterproductivity, absorberplateand flowconduittemperaturedistri- butions. The results obtained showed that the theoretical predictions agreedfairlywellwiththeexperimentalresultsusingacombination ofKnudsendiffusion andviscousflow models formembranecoefficient estimation. The maximumtransmembrane flux incrementinthis study wasobtainedas16.56%andthedistillationabilitypotentiallwas4.1kg/ m2h. Renewableenergy(mainlysolar) hasproven tobeeffectivefor thermalenergysupplyto DCMDsystems.However,thecostsofsolar collectors and otherthermalenergycollectingdevicesstillremainahugechallenge[17]andfurtherresearchdevelopmentsinthisarea areneeded.

ADCMD system coupled withasolarphotovoltaic(PV) cellhasbeen usedinthetreatmentoftapwaterinorder toreducethesalinityofthe wateranddecreasethehealthrisksassociatingwithconsumingthe water[167]. DCMDwasreportedtobe themostsuitablefortheproductionofsmallquantityof cleandrinkingwaterforhouseholdapplicationsbecauseit consumeslessenergythanRO.PeopleinIndiarelyontap waterfordrinkingpurposeswherethesewaterstendtobehighlycontaminatedwithfluorideandarsenicresultinginassociated healthrisks [167]. Throughaperformedchemicalanalysisofthewaterproduced fromDCMD, thecleanwaterproduced wasfoundtobeofgreatquality.

Comparingthethermalefficiency ofthePV-DCMDwithPV-RO, the solarPV-drivenDCMDwas foundtoproducemoredrinkingwater [167].Afewsolarenergy-drivenplants havealsobeen developed. The development of a solar thermally-driven standalone MD plant witha capacityof200–20,000L/dhasbeencarriedoutbyFraunhoferInstitute forSolarEnergySystemsISE,Germany[168].Theheatsourceforthis plantcanbeathermal collectorthatis corrosionfree, orastandard flatplate, orvacuumtube collector integratedwithaheatexchanger. Several experimental and simulationstudieswerecarried outtoinves- tigatetheapplicabilityofthis systemfor potential installation locations. Itwasobservedthat thissystemcanbeusedtoprovidepotablewaterto rural areasorremotelocations.Forexample,accordingtosimulationre- sults,acollectorwithanareab6m2 withoutheatstoragecanprovide 120to160L/dofwaterin thesummerperiod[168].Apilot-scalesolar DCMDunit (Fig.10)hasalsobeendevelopedbyFathetal.[169].The unitwaslocatedattheMechanicalEngineeringDepartmentsite,Alex- andriaUniversity,Alexandria,Egypt. Onasunnyday(7.25kWh/d), theunitcanproduceabout 11.2L/d for everym2ofcollectorarea.A PVpanelwas used torunthe feedpumpwhilesolarcollectorswere usedtosupplythermalenergytothefeedwater.Condensationenergy wasrecoveredinthe condenserchanneloftthe membraneinorderto preheatthefeedwater. Thesolarcollectorefficiencywasabout50% whilethe processefficiencywasabout90%.Itwasconcludedthatthe systemwasverysuitableforuseinaridareas such as Arab and North Africanregions. DCMDhasbeen integrated withsolarpondsbyUniversityofTexas atElPasoinaprojectsponsoredbytheUSBureauofReclamationincol- laborationwiththe Swedishfirm SCARAB[170].Thesystemhadbeen previouslytestedat SandiaNationalLaboratory.Heatwassuppliedby hotbrinethatwaspumpedfromthebottomofthesolarpond and passedthroughaheatexchanger. Ontheotherhand, coldwaterwas suppliedfromthesurfaceof thesolarpondand passedthroughaheat exchangertoprovide cooling. Processdatawere registered byusing DaqView®software. Thefluxobtainedrangedfrom0to6L/m2h.The fluxwasmeasureddowntohotsidetemperaturesaslowas 13°C, whichmeansthatthesystem canworkeffectively withalowgrade heat source[170].

Fig.10.ApictureofAlexandria'scompactMDsystem[169].

Solarthermalcollectorshavebeenintegratedwithpilotplants inSpainandMexicobythe MEDESOL[171]. AmultistagesolarMDsys- temwasexperimentally accessed. Thisprojectwasaimedatproducing 500–50,000L/dofwaterbyminimizingenergyconsumptionin amulti- stageMDsystem. Anadvancedcompound parabolicsolarconcentrator wasdevisedasthe heatsourceand thepreventionofscalingthrough theuseofanti-foulingcoatingsonmembrane surfaceswasconsidered [171]. In a 4-month trial of the MEDESOL project, fluxes ofup to 6.5kg/m2handthermalconsumptionof810kWh/m3wereported [19].

AquastillNetherlandhasalsodevelopedseveralkindsof mem- branemoduleswhichcanbeusedinpilot-scaleDCMDsystems depending onthefeed watercompositionanddesiredqualityoftheeffluent[172]. Changingthenumberofchannelsinthemoduleprovidesa range of capacities, with membrane surface area that can extendfrom 1m2to120m2permodule. Flexibilityintermsofmembranelength andcross-flowvelocityprovidesasystemthatcanbeadaptedtoobtain to obtaintheoptimum performance intermsof fluxandthermalefficiency. Astate-of-the-artMDsystem has been builtby Aquastillinthe beginningof 2016withacapacityofproducing100m2/d[172].

4.3.2.2. Membrane distillation-crystallization. Membrane distillation-crystallization(MDC)methodhasbeenusedtorecoverwaterthrough theprecipitationof crystalsaltsenabled bytheconditionsofsupersatu- rationinacrystallizer. Theeffectsofoperatingfactorsontheperformanceofthe MDCsuchastemperatureandsaturationlevelhave beenstudiedand foundtobethe criticalparameters[173]. Fortwo saltsolutions-sodiumsulfate(Na2SO4) andsodiumchloride(NaCl), theimpactoffeedtemperatureonthefluxwasinvestigated.Athigh saltconcentrationsandfeed temperaturesof 50and60°C, fluxvalues ashighas20L/m2h wereobtained. Whenthecriticaldegreeofsaturationofthecrystalswasexceeded,scaleswereformedonthe membrane andthefluxwasrapidlyreducedasaresult ofreducedmembraneper- meability.Thismethodwas usedfortheproductionofanhydroussodiumsulfatecrystals[173].BrinethatisdischargedasabyproductofRO desalinationplantscanbeused asthefeedforMDC.Thisapproachhas beentested onsyntheticRObrineonabenchscaleMDplant[174]. Themanufacturingof21kg/m3ofNaClcrystalswasachievedthrough thismethodandtherecoveryof waterfactorwasincreaseduptoto90%. Fornatural RObrines,therewasanobservedreductionof20%inthe saltcrystalformationandatransmembranefluxdeclineof 8%dueto theexistenceofdissolvedorganicmatter. Therateofgrowthoftheso- diumchloridecrystalswas foundtobereducedby15–23%fornatural brines.TheMDCoperationswasalsofoundtobestableovera100hpe- rioddueto thecontrolofsupersaturation, polarization,nucleation course and hydrodynamics[174].

The use of a recently developed simultaneous membrane distillation–crystallization(SMDC) technologyfortheproductionof purewaterandsalt crystal hasalsobeenstudiedfor NaClcrystallization [175].Whileincreasingthefeedtemperaturefrom40to70 °C,anin- creaseinfluxwasobserved butthisincrease wassignificantlydimin- ishedattemperaturevaluesof 60°Cand70°C.Thiswasaresultof membranescalingand wettingthatresultedfromtheoversaturation ofsaltattheboundarylayer. Thismembranescalingchallengecan, however, bepreventedthroughcriticalfluxcalculationsusingReynolds numbers and crystallizer temperatures. The membrane performance can bestabilizedfora continuous operationof5000minbymaintaining operation belowthecriticalflux. Overa2000minoperation,anincrease in the feedtemperaturefrom40°Cand70°Callowedforanincreasein NaClcrystalproductionfrom 7.5kg/m3 solutionto34kg/m3.Thistem- peratureincrease inturnincreased thenucleationratereducingthe crystalsizesfrom87.40μmto48.82μm[175].

4.3.2.3. Waste heat coupling. Thefuturepotentialofcouplingwasteheat withDCMD hasbeenstudiedthroughpilotandbenchscaletests[38,11

9,170].Wasteheatfromnuclearreactorscanalsobeused[176].In pilotandbenchscaletestscarried outby Jansenetal., distillateof excellentqualitywasproduced therebyreducingtheneedforpretreatmentand primaryenergyforthermalenergyproduction[177].Athermalenergynecessityofabout520MJ/m3 wasrequired fromwasteheat forpollutedbrackishwaterdesalination. Asaresultofthelowenergy requirementofthis technology, cheapwasteheatcanbeusedforthe treatmentof saline streams resulting intheproductionofhighquality distillate. Withlargescalesystemsforseawaterorbrackishwaterdesalination,theuseofwasteheat canensureenergy consumptionofonly 300–400MJ/m3(similartothat obtainedinlargescaleMSFandMED processes)andestimatedproductioncostsof0.3–0.5USD/m3[177].

4.3.2.4. Geothermal energy coupling.

Bundschuhetal.[178]observed that geothermalcouplingwithDCMDwasabetteroptionthan solarcoupling.Thereasonbeingthatlow-costgeothermalheatprovidesastable heatsourcethatisreadilyaccessible,ascomparedtosolarenergy.The possibilityofup-scalingduetothesteadyheatsourceforgeothermal makesitabetteralternativetosolar.Solar-geothermalhybridarrangementshave,however,beensuggestedasanappropriateoptionwhereverthesetwosourcesarereadilyobtainabletocushiontheproblemsof intermittencyassociatedwithsolarenergy.Theuseofgeothermal waterorheatinthetreatmentofwaterusingtheDCMDis,therefore, a feasiblemethod. AnexperimentalstudyperformedbyAmalietal.[179]compared thecouplingofgeothermalenergywithDCMDandAGMD.Thiswas donethroughtheanalysisofoperatingparameterssuchasfeedconcentration,feedflow,feedtemperatureandtheairgapwidth.Duetothe lowerenergyrequirementsintheAGMD,itwasdeemedas themore suitable method for seawater desalination through geothermalenergy coupling[179].Resultsobtainedfromseveralworksrelatedtothecoupling ofrenewableenergywith DCMDare summarizedinTable7.

4.3.3. Hybrid DCMDsystems

Duetotheworldwidegrowingissueofwaterscarcityandfluctuatingfossiloilprice, researchinterestsfocusingon hybrid DCMDsystems drivenby renewable/wasteenergy andcombining DCMDwithother technologiesforenergy efficiencyandcostreductionarenecessary [180,181]. Onestudyfocusingonafreezedesalinationmembranedistillation,FD–MD,hybridsystemattempted tousethewastecoldenergy releasedfromtheprocessofre-gasifyingliquefiednaturalgas(LNG). Thiswasdoneusingindirectcontactfreezedesalination(ICFD)and DCMDconfigurations. Throughthe optimizationoftheICFDoperation parameterssuchas operationdurationandfeedconcentration,there wasproductionofhighqualitydrinkablewaterwithalowsalinity around0.144g/L.Simultaneously,theDCMDwasusedto obtainultra-purewaterthroughtheoptimizationofthehollowfibermodulelength andpackingdensity.Ahightotalwaterrecoveryof71.5% wasachieved wherethequalityofthewaterobtainedwaswithinthedrinkingwater standards. Furthermore, this hybrid system has been proven, through specificenergycalculations,tobeanenergysavingprocessthrough theutilizationofcoldenergyhence,reducingtheamountofconsumed energy[182].Ahybridphotocatalysis–DCMDsystemwasstudiedfor theremoval ofibuprofensodiumsalt(IBU) fromtapwater. Overa long term process, theeffectofthecomposition offeedonthepermeate fluxandmembranescaling wasstudied.Aftera54hoperationofthe photocatalyticmembranereactor,PMR,thefluxdecline wasfoundto be7%comparedtopurewaterflux.However,aftera188hoperation, thefluxwasreducedby86%.Calciteandaragonitecrystalsdeposited onthemembranesurface'sthinporousTiO2layerwherethe CaCO3scaledepositwascleanedwithHClandthefluxrecovered.Therewas noobservednegativeinfluenceoftheoperationmodeontheproduct (distillate)qualityandthisoperationalmethodwasrecommendedfor full scale applications[183]. HybridsystemofUFandMDwasalsoinvestigatedbyGrytaetal. [184]forthetreatmentofoilywastewater.Watercollected fromaharborwastreatedwithoutpretreatmentusingPVDFmembranesintheUF moduleandPPmembranesintheMDmodule.TheuseofaUF/MDhybridsystemtotreatoilwastewaterresultsinthecompleteremovalof oil,averyhighreductioninthetotalorganiccarbonof99.5%andin thetotaldissolvedsolids,99.9%.Inthisprocess,thepermeatereleased fromtheUFisheatedinaheatexchangerbeforeitissenttotheMD module.ThefinalproductsofthishybridsystemaretheMDdistillate andtheUFretentate.Aforwardosmosis–membranedistillation(FO–MD)hybridsystemusedforthefirsttimetoconcentrateproteinsolutions,specificallyabovineserumalbumin(BSA)solution,hasbeen demonstratedbyWangetal.[185].UsingafabricatedPVDF-PTFEmembrane,aconcentratedNaClsolutionwasusedasadrawsolutetodehydrateproteinsinFO,whileinMD,thedistillatewaterisaby-product duringthere-concentrationofdilutedNaCldrawsolution.Appropriate operatingconditionsweredeterminedforthissystemusingdifferent NaClconcentrationsasdrawsolutesinFOanddifferentfeedtemperaturesinMD.Theresultsshowedsystemstabilitywhenthe dehydration rateacrosstheFOmembraneisthesameasthewatervaporrateacross theMDmembrane.Throughtheestablishmentofsimple mathematical modelsshowingconsistencywiththeexperimentalresults,itwasconcludedthatthenewlydevelopedFO–MDhybridsystemdisplaysfuture promisefortheconcentrationofpharmaceuticals/protein solutions.The resultsofthehybridMDsystemsarepresentedinTable8below.

Table 7
DCMD coupling with renewable energy

Renewable energy source	Application	Findings	Reference
Solar	Seawaterdesalination	Flux up to 28.48L/m^2 h	[163]
Solar	Seawaterdesalination	77.3%oftheheatingenergywassuppliedbysolarenergy;solar-DCMDsystemwasruncontinuallyfor N 150 days; 40.9 L/hm^2 fresh water flux at 60 °C feed temperature and 20 °C permeate temperature	[164]
Solar	Seawaterdesalination	Distillate per module for system with HRD was4.59L/h	[165]
Solar	Arsenic removal from contaminatedgroundwater	Nearly 100% arsenic-free water with a flux of 95 kg/m^2 h at a feed water temperature of60 °C	[85]
Solar	Seawaterdesalination	Maximumtransmembranefluxincrementof16.56%withadistillationpotentialof4.1kg/m^2h	
	[166]Solar	Tapwater treatment	
	Excellent quality water production,	More water productionthanRO	[167]
Wasteheat	Desalination of differentlevels of saline water	Energyrequirementsof300-400MJ/m^3andestimatedcostsof0.3-0.5USD/m^3	[177]
Geothermal	Viability of geothermalenergy for DCMD and AGMD.	AGMD was more suitable due to the lowerenergyrequirements	[179]

Table 8 Applications of hybrid DCMD systems.

Type	Application	Operating parameters	Findings	Reference
FD-MD	Use of waste cold energy released from the process of re-gasifying LNG	Operation duration and feed concentration	High quality drinkable water of low salinity (0.144 g/L); Water recovery of 71.5%	[182]
Photocatalysis–MD	Removal of ibuprofen sodium salt (IBU) from tap water	Feed composition	Flux reduction by 86% after 188 h operation; Calcite and aragonite crystals deposition on the membrane surface's thin porous TiO_2 layer	[183]
UF-MD	Oily wastewater treatment	TOC of the feed	Total organic carbon reduction of 99.5%; 99.9% TDS removal	[184]
FO-MD	Protein solutions concentration (BSA)	NaClconcentrationindraw solute; Feed temperature	System was stable when dehydration rate across FO membrane is the same as the water vapor rate across the MD membrane	[185]

V. CONCLUSIONS AND FUTURE DIRECTION

MDtechnologyhasgainedatremendousamountofinterestoverthe yearsintermsofitsdesign, testingparameters, modelingandapplications. Thesimple DCMD configuration plays abigroleinthisimproved interestwhereitisexpectedtogainfurtherattentionduetoitsabilityto beusedasasolutionto currentwaterscarcity issues. Thismeansthat, notonlyisthistechnology deemedsuitablefortheremovalofcontaminantssuchas salts, heavymetals, organics,radioactivesubstances, it can also be used to treat wastewater and concentrate substances. Wastewate rproduced from bothoilandgasindustriesposerealenvironmental threats but DCMD displays a strong potential intheir treatment.Producedwaterresultingfromoilindustriesdifferfromthat producedfromgasindustriesin termsoftheir composition. Thetreatmentofproducedwaterfrom gasindustriesusingDCMDisapotential applicationwith futurepromisethathasnotyetbeenimplementedby oilandgascorporations.Thispresentsagreatpotentialfor massive freshwaterrecoveryfromproduced water. Thetreatmentofthistoxic rawwaterallowsforthereuseof waterfordifferentpurposessuchas drinkingwaterwhich isacrucial needofwaterstressedcountries.Duringthe course ofthisreview,thetreatmentofthis wastewateras well as brinewasbrieflydiscussed butthereisneed formore futureworkfor the pilot and commercial evaluations of the applications. This article hasalsoexaminedthedifferentmembranepolymersandnanomaterials usedin DCMDaswellasthevarious recentapplicationsofDCMD.However,future developments onthefabricationofmembranes throughthe useofnovelmaterials thatwillbe applied specifically forthe DCMDprocessarerequiredsoasto improvethe processperformanceandensure widespread commercialandindustrialimplementation ofDCMD.In termsofimproving thepermeatefluxaswellastheoverallperformance oftheDCMD, futureresearchthrough theuseofhighly permeable membranesandsuitable moduleswith improved hydrodynamics needtobeused. Furthermore, focusshould bedirectedtowardsthereductionofDCMDmembranewettingbyimprovingmembranehydrophobicity and poregeometry. Inregardstotemperaturepolarization,moreresearchneedstobe carriedoutinordertoimprove theenergy efficiencyof DCMDoperations.Alargenumberof experimentalparametersarealsorequiredtodeterminem embraneselectivityandfluxeswithhighaccuracy.Inaddition, robust mathematical models are essential for describing the DCMD processandfordevelopinga bettertechnicalunderstandingofDCMD. Optimization studies of DCMDshouldbecarriedoutwithrobustdetailedmodelsfordesignandscaleup.Thecapabilityofthe DCMDtobeintegratedwithwasteheatandrenewableenergyfortheminimum useofthermalenergy and reductioninelectricalenergyrequirementhasallowedDCMDtogainalotofinterestinthisageofsustainability. Althoughtheestimatedcostofwaterproducedfrom DCMDintegrated withwasteheatenergy orrenewableenergy islessthancostofwater producedfromRO or conventionalthermalprocesses, futuredevelopmentsshouldbefocusedonsolvingthelowfluxandwettingwhich havebeenassociated with DCMD process integrated withwasteheat.

ACKNOWLEDGMENTS

The authors would like to acknowledge the support, guidance, and assistance provided by the Masdar Instituteof Science and Technology, AbuDhabi, UnitedArabEmirates, in compiling the review paper.

REFERENCES

[1] S.A. Deowan, S.I. Bouhadjar, J. Hoinkis, Advances in Membrane TechnologiesforWater Treatment, Elsevier, 2015, http://dx.doi.org/10.1016/B978-1-78242-121-4.00005-8.

[2] A.Giwa,N.Akther,V.Dufour,S.W.Hasan,Acriticalreviewon recentpolymericand nano-enhancedmembranesforreverseosmosis,RSCAdv.6(2016)8134–8163, http://dx.doi.org/10.1039/C5RA17221G.

[3] K.Jevons,M.Awe,Economicbenefitsofmembranetechnologyvs.evaporator,Desalination250(2010)961–963,http://dx.doi.org/10.1016/j.desal.2009.09.081.

[4] K.P.Lee,T.C.Arnot,D.Mattia,Areviewofreverseosmosismembranematerialsfor desalination-developmenttodateandfuturepotential,J.Memb.Sci.370(2011) 1–22,http://dx.doi.org/10.1016/j.memsci.2010.12.036.

[5] S.Daer,J.Kharraz,A.Giwa,S.W.Hasan,Recentapplicationsof nanomaterialsin waterdesalination:acriticalreviewandfutureopportunities,Desalination367 (2015)37–48,http://dx.doi.org/10.1016/j.desal.2015.03.030.

[6] N.Misdan,W.J.Lau,A.F.Ismail,SeawaterReverseOsmosis(SWRO)desalinationby thin-filmcompositemembrane—currentdevelopment,challengesandfuture prospects, Desalination 287 (2012) 228–237, http://dx.doi.org/10.1016/j.desal. 2011.11.001.

[7] T.Mezher,H.Fath,Z.Abbas,A.Khaled,Techno-economicassessmentandenvironmentalimpactsofdesalinationtechnologies,Desalination266(2011)263–273,http://dx.doi.org/10.1016/j.desal.2010.08.035.

[8] G.M.Geise,H.B.Park,A.C.Sagle,B.D.Freeman,J.E.McGrath,Waterpermeability andwater/saltselectivitytradeoffinpolymersfordesalination, J.Memb.Sci.369 (2011)130–138,http://dx.doi.org/10.1016/j.memsci.2010.11.054.

[9] N.Akther,A.Sodiq,A.Giwa,S.Daer,H.A.Arafat,S.W.Hasan, Recentadvancements inforwardosmosisdesalination:areview,Chem.Eng.J.281(2015)502–522, http://dx.doi.org/10.1016/j.cej.2015.05.080.

[10] M.Elimelech,W.a.Phillip,Thefutureofseawaterdesalination: energy,technology, andtheenvironment,Science333(2011)712–717,http://dx.doi.org/10.1126/science.1200488.

[11] S.Jamaly,N.N.Darwish,I.Ahmed,S.W.Hasan,Ashortreview onreverseosmosis pretreatmenttechnologies,Desalination354(2014)30–38,http://dx.doi.org/10.1016/j.desal.2014.09.017.

[12] I.Sutzkover-Gutman,D.Hasson,Feedwaterpretreatmentfordesalinationplants, Desalination264(2010)289–296,http://dx.doi.org/10.1016/j.desal.2010.07.014.

[13] A.R.D.Verliefde,RejectionofOrganicMicropollutantsbyHighPressureMembranes(NF/RO),TUDelft,DelftUniversityofTechnology,2008.

[14] M. Petrovic, Analysis and removal of emerging contaminants in wastewaterand drinking water, TrAC Trends Anal. Chem. 22 (2003) 685–696,http://dx.doi.org/10.1016/S0165-9936(03)01105-1.

[15] E.Drioli,A.Ali,F.Macedonio,Membranedistillation:recentdevelopmentsand perspectives,Desalination356(2015)56–84,http://dx.doi.org/10.1016/j.desal. 2014.10.028.

[1] Alkhudhiri, N. Darwish, N. Hilal, Membrane distillation: a comprehensivereview,Desalination287(2012)2–18,http://dx.doi.org/10.1016/j.desal.2011.08.027.

[16] M.R.Qtaishat,F.Banat,Desalinationbysolarpoweredmembranedistillationsystems, Desalination 308 (2013) 186–197, http://dx.doi.org/10.1016/j.desal.2012.01.021.

[17] P.Wang,T.-S.Chung,Recentadvancesinmembranedistillationprocesses: membranedevelopment,configurationdesignandapplicationexploring,J.Memb.Sci. 474(2015)39–56,http://dx.doi.org/10.1016/j.memsci.2014.09.016.

[18] L.M.Camacho,L.Dumée,J.Zhang,J.DeLi,M.Duke,J.Gomez,etal.,Advancesin membranedistillationforwaterdesalinationandpurificationapplications,Water (Switzerland)5(2013)94–196,http://dx.doi.org/10.3390/w5010094.

[19] P.Onsekizoglu,Membranedistillation:principle,advances,limitationsandfutureprospectsinfoodindustry,Adv.fromModel.toAppl.(2012)233–266.

[20] F.A.Banat,M.Al-Shannag,Recoveryofdiluteacetone-butanol-ethanol(ABE)solventsfromaqueoussolutionsviamembranedistillation,BioprocessEng.23 (2000)643–649,http://dx.doi.org/10.1007/s004490000214.

[21] H. Susanto, Towards practical implementations of membrane distillation, Chem. Eng.Process.ProcessIntensif.50(2011)139–150,http://dx.doi.org/10.1016/j.cep.2010.12.008.

[22] L.D.Tijing,Y.C.Woo,J.-S.Choi,S.Lee,S.-H.Kim,H.K.Shon,Foulinganditscontrolin membranedistillation\\areview,J.Memb.Sci.475(2014)215–244,http://dx.doi.org/10.1016/j.memsci.2014.09.042.

[23] I.Hitsov,T.Maere,K.DeSitter,C.Dotremont,I.Nopens,Modellingapproachesin membrane distillation: a critical review, Sep. Purif. Technol. 142 (2015) 48–64,http://dx.doi.org/10.1016/j.seppur.2014.12.026.

[24] D.M. Warsinger, J. Swaminathan, E. Guillen-Burrieza, H.A. Arafat, J.H. Lienhard V, Scaling and fouling in membrane distillation for desalination applications: a review, Desalination 356 (2014) 294–313, http://dx.doi.org/10.1016/j.desal.2014. 06.031.

[25] B.L.Pangarkar,M.G.Sane,M.Guddad,Reverseosmosisandmembranedistillation fordesalinationofgroundwater:areview,ISRNMater.Sci.2011(2011)1–9, http://dx.doi.org/10.5402/2011/523124.

[26] K.Y.Y.Wang,T.S.Chung,M.Gryta,HydrophobicPVDFhollowfibermembranes withnarrowporesizedistributionandultra-thinskinforthefreshwaterproductionthroughmembranedistillation,Chem.Eng.Sci.63(2008)2587–2594,http:// dx.doi.org/10.1016/j.ces.2008.02.020.

[27] M. Khayet, Membranes and theoretical modeling of membrane distillation: areview, Adv. Colloid Interf. Sci.

164 (2011) 56–88, http://dx.doi.org/10.1016/j.cis.2010.09.005.

[28] S.Goh,J.Zhang,Y.Liu,A.G.Fane,Foulingandwettinginmembranedistillation (MD)andMD-bioreactor(MDBR)forwastewaterreclamation,Desalination 323 (2013)39–47,http://dx.doi.org/10.1016/j.desal.2012.12.001.

[29] Y.Yuan,T.R.Lee,ContactAngleandWettingProperties,Surf. Sci.Tech,Springer,BerlinHeidelberg2013,pp.3–34.

[30] A.K. Fard, Y. Manawi, Seawater desalination for production of highly pure waterusingahydrophobicptfemembraneanddirectcontactmembranedistillation(DCMD),Int.J.Environ.Chem.Ecol.Geol. Geophys.Eng.8(2014)398–406.

[31] M.Rezaei,W.Samhaber,Wettingbehaviourofsuperhydrophobicmembranescoatedwithnanoparticlesinmembranedistillation,Chem.Eng.Trans.47(2016).

[32] K.W. Lawson, D.R. Lloyd, Membrane distillation, J. Memb. Sci. 124 (1997)1–25,http://dx.doi.org/10.1016/S0376-7388(96)00236-0.

[33] R.B.Saffarini,B.Mansoor,R.Thomas,H.A.Arafat,Effectoftemperature-dependent microstructureevolutiononporewettinginPTFEmembranesundermembrane distillationconditions,J.Memb.Sci.429(2013)282–294,http://dx.doi.org/10.1016/j.memsci.2012.11.049.

[34] Y.Liao,R.Wang,A.G.Fane,Engineeringsuperhydrophobicsurfaceon poly(vinylidenefluoride)nanofibermembranesfordirectcontactmembranedis- tillation,J.Memb.Sci.440(2013)77–87,http://dx.doi.org/10.1016/j.memsci.2013.04.006.

[35] A.Razmjou,E.Arifin,G.Dong,J.Mansouri,V.Chen,Superhydrophobicmodification of TiO2 nanocomposite PVDF membranes for applications in membrane distillation,J.Memb.Sci.415-416(2012)850–863,http://dx.doi.org/10.1016/j.memsci.2012.06.004.

[36] C.Dorrer,J.Rühe,Somethoughtsonsuperhydrophobicwetting,SoftMatter5 (2009) 51, http://dx.doi.org/10.1039/b811945g.

[37] M.S.El-Bourawi,Z.Ding,R.Ma,M.Khayet,Aframeworkforbetterunderstanding membranedistillationseparationprocess,J.Memb.Sci.285(2006)4–29,http:// dx.doi.org/10.1016/j.memsci.2006.08.002.

[38] A.Basile,HandbookofMembraneReactors:ReactorTypesandIndustrialApplica-tions, vol. 2 o,2013.

[39] J.Koo,J.Han,J.Sohn,S.Lee,T.M.Hwang,Experimentalcomparisonofdirectcontactmembranedistillation(DCMD)withvacuummembranedistillation(VMD), Desalin.WaterTreat.51(2013)6299–6309,http://dx.doi.org/10.1080/19443994.2013.780817.

[40] E.Summers,CyclePerformanceofMulti-StageVacuumMembraneDistillation (MS-VMD)Systems,Proc.2013IDAWorldCongr.Desalin.WaterReuse,Tianjin, China,2013.

[41] Z.Lei,B.Chen,Z.Ding,SpecialDistillationProcesses(2005),http://dx.doi.org/10.1016/B978-044451648-0/50004-5.

[42] Y.Zhang,Y.Peng,S.Ji,Z.Li,P.Chen,Reviewofthermalefficiencyandheatrecycling inmembranedistillationprocesses,Desalination367(2015)223–239,http://dx.doi.org/10.1016/j.desal.2015.04.013.

[43] M.B.Jensen,K.V.Christensen,R.Andrésen,L.F.Søtoft,B.Norddahl,Amodelofdirectcontactmembranedistillationforblackcurrantjuice,J.FoodEng.107 (2011)405–414,http://dx.doi.org/10.1016/j.jfoodeng.2011.06.014.

[44] A.Giwa,S.Daer,I.Ahmed,P.R.Marpu,S.W.Hasan,Experimentalinvestigationand artificialneuralnetworksANNsmodelingofelectrically-enhancedmembranebioreactorforwastewatertreatment,J.WaterProcessEng.11(2016)88–97,http:// dx.doi.org/10.1016/j.jwpe.2016.03.011.

[45] M. Khayet, T. Matsuura, Introduction to Membrane Distillation, Membr. Distill.Princ.Appl.,Oxford,UK2011,pp.1–13.

[46] M.Qtaishat,T.Matsuura,B.Kruczek,A.Khayet,Heatandmass transferanalysisin directcontactmembranedistillation,Desalination219(2008)272–292,http://dx.doi.org/10.1016/j.desal.2007.05.019.

[47] D.U.Lawal,A.E.Khalifa,Fluxpredictionindirectcontactmembranedistillation,Int. J.Mater.Mech.Manuf.2(2014)302–308,http://dx.doi.org/10.7763/IJMMM.2014.V2.147.

[48] H.Yu,X.Yang,R.Wang,A.G.Fane,AnalysisofheatandmasstransferbyCFDfor performanceenhancementindirectcontactmembranedistillation,J.Memb.Sci.405-406(2012)38–47,http://dx.doi.org/10.1016/j.memsci.2012.02.035.

[49] J.Zhang,S.Gray,J.Li,ModellingheatandmasstransfersinDCMDusingcompress-iblemembranes,J.Memb.Sci.387-388(2012)7–16,http://dx.doi.org/10.1016/j.memsci.2011.08.034.

[50] L.Martínez,Characterisationofthreehydrophobicporousmembranesusedinmembranedistillationmodellingandevaluationoftheirwatervapourpermeabilities,J.Memb.Sci.203(2002)15–27,http://dx.doi.org/10.1016/S0376-7388(01)00719-0.

[51] G.Rao,S.R.Hiibel,A.E.Childress,Simplifiedfluxpredictionindirect-contactmembranedistillationusingamembranestructuralparameter,Desalination351(2014)151–162,http://dx.doi.org/10.1016/j.desal.2014.07.006.

[52] A.S. Kim, A two-interface transport model with pore-size distribution forpredictingtheperformanceofdirectcontactmembranedistillation(DCMD), J. Memb. Sci. 428 (2013) 410–424, http://dx.doi.org/10.1016/j.memsci.2012.10.054.

[53] Ó.Andrjesdóttir,C.L.Ong,M.Nabavi,S.Paredes,A.S.G.Khalil,B.Michel,etal.,An experimentallyoptimizedmodelforheatandmasstransferindirectcontactmembranedistillation,Int.J.HeatMassTransf.66(2013)855–867,http://dx.doi.org/10.1016/j.ijheatmasstransfer.2013.07.051.

[1] Boubakri, A. Hafiane, S.A.T. Bouguecha, Application of response surface methodologyformodelingandoptimizationofmembranedistillationdesalinationpro- cess,J.Ind.Eng.Chem.20(2014)3163–3169,http://dx.doi.org/10.1016/j.jiec.2013.11.060.

[54] Y.M.Manawi,M.Khraisheh,A.K.Fard,F.Benyahia,S.Adham,Effectofoperationalparametersondistillatefluxindirectcontactmembranedistillation (DCMD):comparisonbetweenexperimentalandmodelpredictedperfor- mance,Desalination336(2014)110–120,http://dx.doi.org/10.1016/j.desal.2014.01.003.

[55] Y.M.Manawi,M.A.M.M.Khraisheh,A.K.Fard,F.Benyahia, S.Adham,Apredictive modelfortheassessmentofthetemperaturepolarizationeffectindirectcontact membranedistillationdesalinationofhighsalinityfeed,Desalination341(2014) 38–49,http://dx.doi.org/10.1016/j.desal.2014.02.028.

[56] M.Ramezanianpour,M.Sivakumar,Ananalyticalfluxdecline modelformembrane distillation, Desalination 345 (2014) 1–12, http://dx.doi.org/10.1016/j.desal.2014.04.006.

[57] B.BinAshoor,H.Fath,W.Marquardt,A.Mhamdi,DynamicModelingofDirectCon- tact Membrane Distillation Processes, Comput. Aided Chem. Eng 2012, pp.170–174,http://dx.doi.org/10.1016/B978-0-444-59507-2.50026-3.

[58] F.Eleiwi,T.M.Laleg-Kirati,DynamicModelingandOptimizationinMembraneDistillationSystem,19thIFACWorldCongr.,theInternationalFederationofAutomaticControl, Cape Town, South Africa 2014, pp.3327–3332.

[59] F.Eleiwi,N.Ghaffour,A.S.Alsaadi,L.Francis,T.M.Laleg-Kirati,Dynamicmodel- ing and experimental validation for

direct contact membrane distillation (DCMD) process, Desalination 384 (2016) 1–11, http://dx.doi.org/10.1016/j.desal.2016.01.004.

[60] A.Giwa,S.W.Hasan,Theoreticalinvestigationoftheinfluence ofoperatingconditionsonthetreatmentperformanceofanelectrically-inducedmembranebioreactor,J.WaterProcessEng.6(2015)72–82,http://dx.doi.org/10.1016/j.jwpe.2015.03.004.

[61] A.Giwa,I.Ahmed,S.W.Hasan,Enhancedsludgepropertiesanddistributionstudy ofsludgecomponentsinelectrically-enhancedmembranebioreactor,J.Environ. Manag.159(2015)78–85,http://dx.doi.org/10.1016/j.jenvman.2015.05.035.

[62] A.Giwa,S.W.Hasan,Numericalmodelingofanelectricallyenhancedmembrane bioreactor (MBER) treating medium-strength wastewater, J. Environ. Manag. 159 (2015)78–85,http://dx.doi.org/10.1016/j.jenvman.2015.08.031.

[63] S.W.Hasan,M.Elektorowicz,J.A.Oleszkiewicz,Correlations betweentrans- membrane pressure (TMP) and sludge properties in submerged membrane electro-bioreactor (SMEBR) and conventional membrane bioreactor (MBR), Bioresour.Technol.120(2012)199–205,http://dx.doi.org/10.1016/j.biortech.2012.06.043.

[64] S.W.Hasan,M.Elektorowicz,J.A.Oleszkiewicz,Start-upperiodinvestigation of pilot-scalesubmergedmembraneelectro-bioreactor(SMEBR)treatingrawmunicipalwastewater,Chemosphere97(2014)71–77,http://dx.doi.org/10.1016/j.chemosphere.2013.11.009.

[65] A.Giwa,S.M.Jung,W.Fang,J.Kong,S.W.Hasan,Bio-electrochemicalprocesscoupled with novel Mno2nanowires for wastewater treatment, Intl. J. Environ.Ecol.Eng.3(2016)520–523.

[66] M.Khayet,Treatmentofradioactivewastewatersolutionsbydirectcontactmembranedistillationusingsurfacemodifiedmembranes,Desalination321(2013) 60–66,http://dx.doi.org/10.1016/j.desal.2013.02.023.

[67] X.Yu,H.Yang,H.Lei,A.Shapiro,Experimentalevaluationon concentratingcooling towerblowdownwaterbydirectcontactmembranedistillation, Desalination323 (2013)134–141,http://dx.doi.org/10.1016/j.desal.2013.01.029.

[68] S.Jamaly,A.Giwa,S.W.Hasan,Recentimprovementsinoilywastewatertreatment:progress,challenges,andfutureopportunities,J.Environ.Sci.37(2015) 1–16,http://dx.doi.org/10.1016/j.jes.2015.04.011.

[69] F.Macedonio,A.Ali,T.Poerio,E.El-Sayed,E.Drioli,M.Abdel-Jawad,Directcontact membranedistillationfortreatmentofoilfieldproducedwater, Sep.Purif.Technol. 126(2014)69–81,http://dx.doi.org/10.1016/j.seppur.2014.02.004.

[70] A.Fakhru'l-Razi,A.Pendashteh,L.C.Abdullah,D.R.A.Biak,S.S.Madaeni,Z.Z.Abidin, Reviewoftechnologiesforoilandgasproducedwatertreatment,J.Hazard.Mater. 170(2009)530–551,http://dx.doi.org/10.1016/j.jhazmat.2009.05.044.

[71] D.Singh,K.K.Sirkar,Desalinationofbrineandproducedwater bydirectcontact membrane distillation at high temperatures and pressures, J. Memb. Sci. 389 (2012)380–388,http://dx.doi.org/10.1016/j.memsci.2011.11.003.

[72] D.L.Shaffer,L.H.AriasChavez,M.Ben-Sasson,S.Romero-VargasCastrillón,N.Y.Yip,

[73] M.Elimelech,Desalinationandreuseofhigh-salinityshalegasproducedwater: drivers,technologies,andfuturedirections,Environ.Sci.Technol.47(2013) 9569–9583,http://dx.doi.org/10.1021/es401966e.

[74] D.Singh,P.Prakash,K.K.Sirkar,Deoiledproducedwatertreatmentusingdirect-contactmembranedistillation,Ind.Eng.Chem.Res.52(2013)13439–13448, http://dx.doi.org/10.1021/ie4015809.

[75] H.C.Duong,S.Gray,M.Duke,T.Y.Cath,L.D.Nghiem,Scalingcontrolduringmembranedistillationofcoalseamgasreverseosmosisbrine,J.Memb.Sci.493(2015) 673–682,http://dx.doi.org/10.1016/j.memsci.2015.07.038.

[76] H.C.Duong,A.R.Chivas,B.Nelemans,M.Duke,S.Gray,T.Y.Cath,etal.,Treatmentof RO brine from CSG produced water by spiral-wound air gap membrane distilla- tion—apilotstudy,Desalination366(2015)121–129,http://dx.doi.org/10.1016/j.desal.2014.10.026.

[77] Y.C. Woo, Y. Kim, W.-G. Shim, L.D. Tijing, M. Yao, L.D. Nghiem, et al., Graphene/ PVDFflat-sheetmembraneforthetreatmentofRObrinefromcoalseamgas pro- duced water by air gap membrane distillation, J. Memb. Sci. 513 (2016) 74–84,http://dx.doi.org/10.1016/j.memsci.2016.04.014.

[78] H.Geng,J.Wang,C.Zhang,P.Li,H.Chang,HighwaterrecoveryofRObrineusing multi-stageairgapmembranedistillation,Desalination355(2015)178–185, http://dx.doi.org/10.1016/j.desal.2014.10.038.

[79] K.Kezia,J.Lee,M.Weeks,S.Kentish,Directcontactmembranedistillationforthe concentrationofsalinedairyeffluent,WaterRes.81(2015)167–177,http://dx.doi.org/10.1016/j.watres.2015.05.042.

[80] A.Hausmann,P.Sanciolo,T.Vasiljevic,E.Ponnampalam,N. Quispe-Chavez,M. Weeks,etal.,Directcontactmembranedistillationofdairyprocessstreams,Mem- branes(Basel)1(2011)48–58,http://dx.doi.org/10.3390/membranes1010048.

[81] M.Tomaszewska,A.Łapin,Theinfluenceoffeedtemperatureandcompositionon theconversionofKClintoKHSO4inamembranereactorcombinedwithdirect contactmembranedistillation,Sep.Purif.Technol.100(2012) 59–65,http://dx.doi.org/10.1016/j.seppur.2012.08.022.

[82] M.Bhattacharya,S.K.Dutta,J.Sikder,M.K.Mandal,Computationalandexperimentalstudyofchromium(VI)removalindirectcontactmembrane distillation,J. Memb.Sci.450(2014)447–456,http://dx.doi.org/10.1016/j.memsci.2013.09.037.

[83] D.Qu,D.Sun,H.Wang,Y.Yun,Experimentalstudyofammoniaremovalfrom waterbymodifieddirectcontactmembranedistillation,Desalination326(2013) 135–140,http://dx.doi.org/10.1016/j.desal.2013.07.021.

[84] P.Pal,A.K.Manna,Removalofarsenicfromcontaminatedgroundwaterbysolar-drivenmembranedistillationusingthreedifferentcommercial membranes, WaterRes.44(2010)5750–5760,http://dx.doi.org/10.1016/j.watres.2010.05.031.

[85] S.Yarlagadda,V.G.Gude,L.M.Camacho,S.Pinappu,S.Deng, PotablewaterrecoveryfromAs,U,andFcontaminatedgroundwatersbydirectcontactmembrane distillationprocess,J.Hazard.Mater.192(2011)1388–1394,http://dx.doi.org/10.1016/j.jhazmat.2011.06.056.

[86] D.Y.Hou,J.Wang,B.Q.Wang,Z.K.Luan,X.C.Sun,X.J.Ren,Fluorideremovalfrom brackishgroundwaterbydirectcontactmembranedistillation, WaterSci.Technol. 61(2010)3178–3187,http://dx.doi.org/10.2166/wst.2010.878.

[87] M.Xie,L.D.Nghiem,W.E.Price,M.Elimelech,Towardresourcerecoveryfrom wastewater:extractionofphosphorusfromdigestedsludgeusingahybridfor- wardosmosis–membranedistillationprocess,Environ.Sci.Technol.Lett.1 (2014)191–195,http://dx.doi.org/10.1021/ez400189z.

[88] M.M.a.Shirazi,A.Kargari,Areviewonapplicationofmembranedistillation(MD)processforwastewatertreatment,98(2015)101–112.

[89] R.Sarbatly,C.-K.Chiam,AmmoniaRemovalfromSalineWaterbyDirectContact Membrane Distillation, Sustain. Membr. Technol. Energy, Water, Environ, John

Wiley&Sons,Inc,Hoboken,NJ,USA2012,pp.309–317,http://dx.doi.org/10.1002/9781118190180.ch27.

[90] S.Alobaidani,E.Curcio,F.Macedonio,G.Diprofio,H.Alhinai,E.Drioli,Potentialof membrane distillation in seawater desalination: thermal efficiency,sensitivity studyandcostestimation,J.Memb.Sci.323(2008)85–98,http://dx.doi.org/10.1016/j.memsci.2008.06.006.

[91] S.Gunko,S.Verbych,M.Bryk,N.Hilal,Concentrationofapple juiceusingdirect contactmembranedistillation,Desalination190(2006)117–124,http://dx.doi.org/10.1016/j.desal.2005.09.001.

[92] L.F.Dumée,S.Gray,M.Duke,K.Sears,J.Schütz,N.Finn,Theroleofmembranesurfaceenergyondirectcontactmembranedistillationperformance,Desalination323(2013)22–30,http://dx.doi.org/10.1016/j.desal.2012.07.012.

[93] Y.Liao,R.Wang,A.G.Fane,Fabricationofbioinspiredcompositenanofiber membraneswithrobustsuperhydrophobicityfordirectcontact membrane distillation,Environ.Sci.Technol.48(2014)6335–6341,http://dx.doi.org/10.1021/es405795s.

[94] J.A.Prince,D.Rana,G.Singh,T.Matsuura,T.JunKai,T.S.Shanmugasundaram,Effect ofhydrophobicsurfacemodifyingmacromoleculesondifferentlyproducedPVDFmembranesfordirectcontactmembranedistillation,Chem.Eng.J.242(2014)387–396,http://dx.doi.org/10.1016/j.cej.2013.11.039.

[95] J.A.Prince,G.Singh,D.Rana,T.Matsuura,V.Anbharasi,T.S.Shanmugasundaram, Preparationandcharacterizationofhighlyhydrophobicpoly(vinylidenefluoride)claynanocompositenanofibermembranes(PVDF–clayNNMs)fordesalination usingdirectcontactmembranedistillation,J.Memb.Sci.397-398(2012)80–86,http://dx.doi.org/10.1016/j.memsci.2012.01.012.

[96] T.L.S. Silva, S. Morales-Torres, J.L. Figueiredo, A.M.T. Silva, Multi-walled carbonnanotube/PVDFblendedmembraneswithsponge-andfinger-likeporesfordirect contactmembranedistillation,Desalination357(2015)233–245,http://dx.doi.org/10.1016/j.desal.2014.11.025.

[97] Z.W.Song,L.Y.Jiang,OptimizationofmorphologyandperformanceofPVDFhollowfiberfordirectcontactmembranedistillationusingexperimentaldesign, Chem.Eng.Sci.101(2013)130–143,http://dx.doi.org/10.1016/j.ces.2013.06.006.

[98] D.Hou,J.Wang,X.Sun,Z.Ji,Z.Luan,PreparationandpropertiesofPVDFcomposite hollowfibermembranesfordesalinationthroughdirectcontact membranedistil-lation,J.Memb.Sci.405-406(2012)185–200,http://dx.doi.org/10.1016/j.memsci.2012.03.008.

[99] X.Li,X.Yu,C.Cheng,L.Deng,M.Wang,X.Wang,Electrospunsuperhydrophobic organic/inorganiccompositenanofibrousmembranesformembranedistillation,ACSAppl.Mater.Interfaces7(2015)21919–21930,http://dx.doi.org/10.1021/acsami.5b06509.

[100] L.D.Tijing,Y.C.Woo,M.A.H.Johir,J.-S.Choi,H.K.Shon,Anoveldual-layerbicomponentelectrospunnanofibrousmembranefordesalinationbydirectcontactmembranedistillation,Chem.Eng.J.256(2014)155–159,http://dx.doi.org/10.1016/j.cej.2014.06.076.

[101] M.Khayet,C.Cojocaru,M.C.García-Payo,Experimentaldesignandoptimizationof asymmetricflat-sheetmembranespreparedfordirectcontactmembranedistillation,J.Memb.Sci.351(2010)234–245,http://dx.doi.org/10.1016/j.memsci.2010.01.057.

[102] P.Wang,T.-S.Chung,Designandfabricationoflotus-root-likemulti-borehollow fibermembranefordirectcontactmembranedistillation,J.Memb.Sci.421-422(2012)361–374,http://dx.doi.org/10.1016/j.memsci.2012.08.003.

[103] B.S. Lalia, E. Guillen-Burrieza, H.A. Arafat, R. Hashaikeh, Fabrication andcharacterizationofpolyvinylidenefluoride-co-hexafluoropropylene(PVDF-HFP)electrospun membranesfordirectcontactmembranedistillation,J.Memb.Sci.428(2013) 104–115,http://dx.doi.org/10.1016/j.memsci.2012.10.061.

[104] Z.Wang,L.Sun,Q.Wang,B.Li,S.Wang,Anovelapproachtofabricateinterconnectedsponge-likeandhighlypermeablepolyvinylidenefluoridehollowfiber membranesfordirectcontactmembranedistillation,Eur.Polym.J.60(2014) 262–272,http://dx.doi.org/10.1016/j.eurpolymj.2014.09.015.

[105] L.Francis,N.Ghaffour,A.S.Alsaadi,S.P.Nunes,G.L.Amy,PVDFhollowfiberand nanofibermembranesforfreshwaterreclamationusingmembranedistillation,J. Mater.Sci.49(2014)2045–2053,http://dx.doi.org/10.1007/s10853-013-7894-4.

[106] F.A.Banat,MembraneDistillationforDesalinationandRemovalofVolatileOrganicCompounds from Water, McGill University,1994.

[107] V.Calabro,B.L.Jiao,E.Drioli,Theoreticalandexperimentalstudyonmembranedistillationintheconcentrationoforangejuice,Ind.Eng.Chem.Res.33(1994) 1803–1808,http://dx.doi.org/10.1021/ie00031a020.

[108] L.Martínez,F.J.Florido-Díaz,Theoreticalandexperimentalstudiesondesalination usingmembranedistillation,Desalination139(2001)373–379,http://dx.doi.org/10.1016/S0011-9164(01)00335-6.

[109] M.Khayet,A.Velázquez,J.I.Mengual,Directcontactmembranedistillationof humicacidsolutions,J.Memb.Sci.240(2004)123–128,http://dx.doi.org/10.1016/j.memsci.2004.04.018.

[110] J.Phattaranawik,R.Jiraratananon,A.G.Fane,C.Halim,Massfluxenhancement usingspacerfilledchannelsindirectcontactmembranedistillation,J.Memb.Sci. 187(2001)193–201,http://dx.doi.org/10.1016/S0376-7388(01)00344-1.

[111] J.Phattaranawik,R.Jiraratananon,A.G.Fane,Heattransportandmembranedistillationcoefficientsindirectcontactmembranedistillation,J.Memb.Sci.212(2003) 177–193,http://dx.doi.org/10.1016/S0376-7388(02)00498-2.

[112] V.A.Bui,M.H.Nguyen,J.Muller,Alaboratorystudyonglucoseconcentrationbyosmoticdistillationinhollowfibremodule,J.FoodEng.63(2004) 237–245,http:// dx.doi.org/10.1016/j.jfoodeng.2003.07.005.

[113] M.Gryta,M.Barancewicz,InfluenceofmorphologyofPVDFcapillarymembranes ontheperformanceofdirectcontactmembranedistillation,J.Memb.Sci.358 (2010)158–167,http://dx.doi.org/10.1016/j.memsci.2010.04.044.

[114] C. Yang, X.-M. Li, J. Gilron, D. Kong, Y. Yin, Y. Oren, et al., CF4 plasma-modified superhydrophobic PVDF membranes for direct contact membrane distillation,J. Memb.Sci.456(2014)155–161,http://dx.doi.org/10.1016/j.memsci.2014.01.013.

[115] Z.Ding,R.Ma,A.G.Fane,Anewmodelformasstransferindirectcontactmembrane distillation, Desalination 151 (2003) 217–227, http://dx.doi.org/10.1016/ S0011-9164(02)01014-7.

[116] C.-L.Lai,R.-M.Liou,S.-H.Chen,G.-W.Huang,K.-R.Lee,Preparationandcharacterization of plasma-modified PTFE membrane and its application in direct contact membranedistillation,Desalination267(2011)184–192,http://dx.doi.org/10.1016/j.desal.2010.09.024.

[117] D.Singh,K.K.Sirkar,Hightemperaturedirectcontactmembranedistillationbased desalinationusingPTFEhollowfibers,Chem.Eng.Sci.116(2014)824–833,http:// dx.doi.org/10.1016/j.ces.2014.05.042.

[118] J.Zhang,N.Dow,M.Duke,E.Ostarcevic,J.-D.Li,S.Gray,Identificationofmaterial andphysicalfeaturesofmembranedistillationmembranesforhighperformance desalination,J.Memb.Sci.349(2010)295–303,http://dx.doi.org/10.1016/j.memsci.2009.11.056.

[119] S.Roy,M.Bhadra,S.Mitra,Enhanceddesalinationviafunctionalizedcarbonnanotubeimmobilizedmembraneindirectcontactmembranedistillation,Sep.Purif. Technol.136(2014)58–65,http://dx.doi.org/10.1016/j.seppur.2014.08.009.

[120] L.F.Dumée,K.Sears,J.Schütz,N.Finn,C.Huynh,S.Hawkins, etal.,Characterization andevaluationofcarbonnanotubeBucky-papermembranesfordirectcontact membranedistillation,J.Memb.Sci.351(2010)36–43,http://dx.doi.org/10.1016/j.memsci.2010.01.025.

[121] L.Dumée,V.Germain,K.Sears,J.Schütz,N.Finn,M.Duke,etal.,Enhanceddurabilityandhydrophobicityofcarbonnanotubebuckypapermembranesinmembrane distillation,J.Memb.Sci.376(2011)241–246,http://dx.doi.org/10.1016/j.memsci.2011.04.024.

[122] M.Tian,Y.Yin,C.Yang,B.Zhao,J.Song,J.Liu,etal.,CF4plasmamodifiedhighly interconnective porous polysulfone membranes for direct contact membrane distillation(DCMD),Desalination369(2015)105–114,http://dx.doi.org/10.1016/j.desal.2015.05.002.

[123] Y.Peng,Y.Dong,H.Fan,P.Chen,Z.Li,Q.Jiang,Preparationof polysulfonemem- branesviavapor-inducedphaseseparationandsimulationofdirect-contactmembranedistillationbymeasuringhydrophobiclayerthickness,Desalination316 (2013)53–66,http://dx.doi.org/10.1016/j.desal.2013.01.021.

[124] M.Essalhi,M.Khayet,Surfacesegregationoffluorinatedmodifyingmacromolecule forhydrophobic/hydrophilicmembranepreparationandapplicationinairgapand directcontactmembranedistillation,J.Memb.Sci.417-418(2012)163–173, http://dx.doi.org/10.1016/j.memsci.2012.06.028.

[125] L.García-Fernández,M.C.García-Payo,M.Khayet,Effectsofmixedsolventsonthe structuralmorphologyandmembranedistillationperformance ofPVDF-HFPhollowfibermembranes,J.Memb.Sci.468(2014)324–338,http://dx.doi.org/10.1016/j.memsci.2014.06.014.

[126] S.Meng,Y.Ye,J.Mansouri,V.Chen,Crystallizationbehavior ofsaltsduringmembranedistillationwithhydrophobicandsuperhydrophobiccapillarymembranes,J. Memb.Sci.473(2015)165–176,http://dx.doi.org/10.1016/j.memsci.2014.09.024.

[127] S.R.Krajewski,W.Kujawski,M.Bukowska,C.Picard,A.Larbot,Applicationof fluoroalkylsilanes(FAS)graftedceramicmembranesinmembranedistillationpro- cess of NaCl solutions, J. Memb. Sci. 281 (2006) 253–259,http://dx.doi.org/10.1016/j.memsci.2006.03.039.

[128] Z.D. Hendren, J. Brant, M.R. Wiesner, Surface modification of nanostructured ceramicmembranesfordirectcontactmembranedistillation,J.Memb.Sci.331 (2009)1–10,http://dx.doi.org/10.1016/j.memsci.2008.11.038.

[129] L.D.Tijing,Y.C.Woo,W.G.Shim,T.He,J.S.Choi,S.H.Kim,et al., Superhydrophobic nanofibermembranecontainingcarbonnanotubesforhigh-performancedirect

[130] contact membrane distillation, J. Memb. Sci. 502 (2016) 158–170, http://dx.doi.org/10.1016/j.memsci.2015.12.014.

[131] A.Larbot,L.Gazagnes,S.Krajewski,M.Bukowska,W.Kujawski,Waterdesalination usingceramicmembranedistillation,Desalination168(2004) 367–372,http://dx.doi.org/10.1016/j.desal.2004.07.021.

[132] S.Cerneaux,I.Struzy??ska,W.M.Kujawski,M.Persin,A.Larbot,Comparisonofvar- ious membrane distillation methods for desalination using hydrophobic ceramic membranes,J.Memb.Sci.337(2009)55–60,http://dx.doi.org/10.1016/j.memsci.2009.03.025.

[133] X.Wei,B.Zhao,X.-M.Li,Z.Wang,B.-Q.He,T.He,etal.,CF4plasmasurfacemodificationofasymmetrichydrophilicpolyethersulfonemembranesfordirectcontact membranedistillation,J.Memb.Sci.407-408(2012)164–175,http://dx.doi.org/10.1016/j.memsci.2012.03.031.

[134] Rastegarpanah, H.R. Mortaheb, Surface treatment of polyethersulfone membranesforapplyingindesalinationbydirectcontactmembrane distillation,Desa- lination377(2016)99–107,http://dx.doi.org/10.1016/j.desal.2015.09.008.

[135] N.Hamzah,C.P.Leo,Foulingpreventioninthemembranedistillationofphenolic-richsolutionusingsuperhydrophobicPVDFmembraneincorporatedwithTiO2 nanoparticles,Sep.Purif.Technol.167(2016)79–87,http://dx.doi.org/10.1016/j. seppur.2016.05.005.

[136] K.He,H.J.Hwang,M.W.Woo,I.S.Moon,Productionofdrinkingwaterfromsaline waterbydirectcontactmembranedistillation(DCMD),J.Ind.Eng.Chem.17 (2011)41–48,http://dx.doi.org/10.1016/j.jiec.2010.10.007.

[137] X.Li,C.Wang,Y.Yang,X.Wang,M.Zhu,B.S.Hsiao,Dual-biomimetic superhydrophobicelectrospunpolystyrenenanofibrousmembranesformembranedistillation,ACSAppl.Mater.Interfaces6(2014)2423–2430,http://dx.doi.org/10.1021/am4048128.

[138] Y. Kong, X. Lin, Y. Wu, J. Chen, J. Xu, Plasma polymerization of octafluorocyclobutane and hydrophobic microporous composite membranes for membranedistillation,J.Appl.Polym.Sci.46(1992)191–199,http://dx.doi.org/10.1002/app.1992.070460201.

[139] Q.-M. Nguyen, S. Lee, Fouling analysis and control in a DCMD process for SWRO brine, Desalination 367 (2015) 21–27, http://dx.doi.org/10.1016/j.desal.2015.03. 039.

[140] J.Ge,Y.Peng,Z.Li,P.Chen,S.Wang,MembranefoulingandwettinginaDCMD process for RO brine concentration, Desalination 344 (2014) 97–107,http://dx. doi.org/10.1016/j.desal.2014.03.017.

[141] G.Naidu,S.Jeong,S.-J.Kim,I.S.Kim,S.Vigneswaran,Organicfoulingbehaviorin directcontactmembranedistillation,Desalination347(2014)230–239,http:// dx.doi.org/10.1016/j.desal.2014.05.045.

[142] G.Naidu,S.Jeong,S.Vigneswaran,Influenceoffeed/permeate velocityonscaling developmentinadirectcontactmembranedistillation,Sep.Purif.Technol.125(2014)291–300,http://dx.doi.org/10.1016/j.seppur.2014.01.049.

[143] L.D.Nghiem,T.Cath,Ascalingmitigationapproachduringdirectcontact membranedistillation,Sep.Purif.Technol.80(2011)315–322,http://dx.doi.org/10.1016/j.seppur.2011.05.013.

[144] G.Chen,X.Yang,Y.Lu,R.Wang,A.G.Fane,Heattransferintensificationandscaling mitigationinbubbling-enhancedmembranedistillationforbrineconcentration,J. Memb.Sci.470(2014)60–69,http://dx.doi.org/10.1016/j.memsci.2014.07.017.

[145] Z.Ding,L.Liu,Z.Liu,R.Ma,FoulingresistanceinconcentratingTCMextractbydirectcontactmembranedistillation,J.Memb.Sci.362(2010)317–325,http://dx.doi.org/10.1016/j.memsci.2010.06.040.

[146] M.Gryta,Foulingindirectcontactmembranedistillationprocess,J.Memb.Sci.325(2008)383–394,http://dx.doi.org/10.1016/j.memsci.2008.08.001.

[147] M.M.A.Shirazi,A.Kargari,M.Tabatabaei,EvaluationofcommercialPTFEmembranesindesalinationbydirectcontactmembranedistillation, Chem.Eng.Process.ProcessIntensif.76(2014)16–25,http://dx.doi.org/10.1016/j.cep.2013.11.010.

[148] A.Bahmanyar,M.Asghari,N.Khoobi,Numericalsimulationandtheoreticalstudy onsimultaneouslyeffectsofoperatingparametersindirectcontactmembranedistillation,Chem.Eng.Process.ProcessIntensif.61(2012)42–50,http://dx.doi.org/10.1016/j.cep.2012.06.012.

[149] G.Zuo,R.Wang,R.Field,A.G.Fane,Energyefficiencyevaluationandeconomic

analysesofdirectcontactmembranedistillationsystemusingAspenPlus,Desali-nation283(2011)237–244,http://dx.doi.org/10.1016/j.desal.2011.04.048.

[150] M.Su,M.M.Teoh,K.Y.Wang,J.Su,T.-S.Chung,Effectofinner-layerthermalconductivityonfluxenhancementofdual-layerhollowfibermembranesindirect contactmembranedistillation,J.Memb.Sci.364(2010)278–289,http://dx.doi.org/10.1016/j.memsci.2010.08.028.

[151] C.-L.Liu,Y.-F.Chen,W.-J.Sheu,C.-C.Wang,Effectofflowdeflectoronthefluxim-provement in direct contact membrane distillation, Desalination 253 (2010)16–21,http://dx.doi.org/10.1016/j.desal.2009.11.042.

[152] C.-D.Ho,C.-H.Huang,F.-C.Tsai,W.-T.Chen,Performanceimprovementondis- tillate flux of countercurrent-flow direct contact membrane distillation sys-tems,Desalination338(2014)26–32,http://dx.doi.org/10.1016/j.desal.2014.01.023.

[153] C.-D.Ho,H.Chang,C.-L.Chang,C.-H.Huang,Theoreticalandexperimentalstudies offluxenhancementwithroughenedsurfaceindirectcontactmembranedistilla-tiondesalination,J.Memb.Sci.433(2013)160–166,http://dx.doi.org/10.1016/j.memsci.2012.12.044.

[154] H. Hayer, O. Bakhtiari, T. Mohammadi, Simulation of momentum, heat and mass transferindirectcontactmembranedistillation:acomputationalfluiddynamics approach, J. Ind. Eng. Chem. 21 (2015) 1379–1382, http://dx.doi.org/10.1016/j. jiec.2014.06.009.

[155] G.Rao,S.R.Hiibel,A.Achilli,A.E.Childress,Factorscontributingtofluximprove- ment in vacuum-enhanced direct contact membrane distillation, Desalination 367(2015)197–205,http://dx.doi.org/10.1016/j.desal.2015.04.002.

[156] F.Suárez,S.W.Tyler,A.E.Childress,Atheoreticalstudyofadirectcontactmem- branedistillationsystemcoupledtoasalt-gradientsolarpondforterminallakes reclamation,WaterRes.44(2010)4601–4615,http://dx.doi.org/10.1016/j.watres.2010.05.050.

[157] R.B.Saffarini,E.K.Summers,H.A.Arafat,J.H.LienhardV,Economicevaluationof stand-alone solar powered membrane distillation systems, Desalination 299 (2012)55–62,http://dx.doi.org/10.1016/j.desal.2012.05.017.

[158] A.M.Karam,T.M.Laleg-Kirati,ElectricalThermalNetworksforDirectContact Membrane Distillation Modeling, 2014 IEEE Conf. Control Appl, IEEE 2014, pp.1563–1569,http://dx.doi.org/10.1109/CCA.2014.6981547.

[159] V.A.Bui,L.T.T.Vu,M.H.Nguyen,Simulationandoptimisationofdirectcontact membranedistillationforenergy efficiency,Desalination259(2010)29–37, http://dx.doi.org/10.1016/j.desal.2010.04.041.

[160] S.Lin,N.Y.Yip,M.Elimelech,Directcontactmembranedistillationwithheatrecov-ery:thermodynamicinsightsfrommodulescalemodeling,J.Memb.Sci.453 (2014)498–515,http://dx.doi.org/10.1016/j.memsci.2013.11.016.

[161] G.Guan,X.Yang,R.Wang,A.G.Fane,Evaluationofheatutilizationinmembrane distillationdesalinationsystemintegratedwithheatrecovery, Desalination366 (2015)80–93,http://dx.doi.org/10.1016/j.desal.2015.01.013.

[162] A.Saleh,J.A.Qudeiri,M.A.Al-Nimr,Performanceinvestigationofasaltgradient solarpondcoupledwithdesalinationfacilityneartheDeadSea, Energy36 (2011)922–931,http://dx.doi.org/10.1016/j.energy.2010.12.018.

[163] N.Palanisami,K.He,I.S.Moon,Utilizationofsolarenergyfordirectcontactmem-branedistillationprocess:anexperimentalstudyfordesalinationofrealseawater, KoreanJ.Chem.Eng.31(2014)155–161,http://dx.doi.org/10.1007/s11814-013-0250-1.

[164] W.G.Shim,K.He,S.Gray,I.S.Moon,Solarenergyassisteddirectcontactmembrane distillation(DCMD)processforseawaterdesalination,Sep.Purif.Technol.143 (2015)94–104,http://dx.doi.org/10.1016/j.seppur.2015.01.028.

[165] S.T.Bouguecha,S.E.Aly,M.H.Al-Beirutty,M.M.Hamdi,A.Boubakri,Solardriven DCMD:performanceevaluationandthermalenergyefficiency,Chem.Eng.Res. Des.100(2015)331–340,http://dx.doi.org/10.1016/j.cherd.2015.05.044.

[166] T.-C.Chen,C.-D.Ho,Immediateassistedsolardirectcontactmembranedistillation insalinewaterdesalination,J.Memb.Sci.358(2010)122–130,http://dx.doi.org/10.1016/j.memsci.2010.04.037.

[167] S.R.Selvi,R.Baskaran,Solarphotovoltaic-poweredmembranedistillationassustainablecleanenergytechnologyindesalination,Curr.Sci.109(2015)1247–1254.

[168] J.Koschikowski,M.Wieghaus,M.Rommel,Solarthermal-drivendesalination plantsbasedonmembranedistillation,Desalination156(2003) 295–304,http:// dx.doi.org/10.1016/S0011-9164(03)00360-6.

[169] H.E.S. Fath, S.M. Elsherbiny, A.A. Hassan, M. Rommel, M. Wieghaus, J. Koschikowski,etal.,PVandthermallydrivensmall-scale,stand-alonesolardesa-linationsystemswithverylowmaintenanceneeds,Desalination225(2008) 58–69,http://dx.doi.org/10.1016/j.desal.2006.11.029.

[170] J.Walton,H.Lu,C.Turner,S.Solis,H.Hein,SolarandWasteHeatDesalinationby Membrane Distillation, Denver, CO, USA,2004.

[171] J.BlancoGálvez,L.García-Rodríguez,I.Martín-Mateos,Seawaterdesalination by an innovative solar-powered membrane distillation system: the MEDESOL project, Desalination 246 (2009) 567–576, http://dx.doi.org/10.1016/j.desal.2008.12.005.

[172] Aquastill,Portfolio,http://aquastill.nl/portfolio2016accessedJanuary1,2016.

[173] M.T.Chan,A.G.Fane,J.T.Matheickal,R.Sheikholeslami,Membranedistillation crystallizationofconcentratedsalts-fluxandcrystalformation,J.Memb.Sci. 257(2005)144–155,http://dx.doi.org/10.1016/j.memsci.2004.09.051.

[174] X.Ji,E.Curcio,S.AlObaidani,G.DiProfio,E.Fontananova,E.Drioli,Membrane distillation-crystallizationofseawaterreverseosmosisbrines,Sep.Purif.Technol. 71(2010)76–82,http://dx.doi.org/10.1016/j.seppur.2009.11.004.

[175] F. Edwie, T.S. Chung, Development of simultaneous membrane distillation-crystallization(SMDC)technologyfortreatmentofsaturatedbrine,Chem.Eng. Sci.98(2013)160–172,http://dx.doi.org/10.1016/j.ces.2013.05.008.

[176] J.I.M.M.Khayet,M.P.Godino,Possibilityofnucleardesalinationthroughvarious membranedistillationconfigurations:acomparativestudy,Int.J.Nucl.Desalin.1 (2003)30–46,http://dx.doi.org/10.1504/IJND.2003.003441.

[177] A.E.Jansen,J.W.Assink,J.H.Hanemaaijer,J.VanMedevoort, MembraneDistillation ProducingHighQualityWaterfromSalineStreamsbyDeployingWasteHeat, 2007.

[178] J.Bundschuh,N.Ghaffour,H.Mahmoudi,M.Goosen,S.Mushtaq,J.Hoinkis,Low-CostLow-EnthalpyGeothermalHeatforFreshwaterProduction:InnovativeAppli-cationsUsingThermalDesalinationProcesses,Vol.43,2015196–206.

[179] A.ElAmali,S.Bouguecha,M.Maalej,Experimentalstudyofairgapanddirectcon-tactmembranedistillationconfigurations:applicationtogeothermalandseawater desalination, Desalination 168 (2004) 357, http://dx.doi.org/10.1016/j.desal.2004.07.020.

[180] A.Giwa,H.Fath,S.W.Hasan,Humidification–dehumidificationdesalinationpro-cessdrivenbyphotovoltaicthermalenergyrecovery(PV-

HDH)forsmall-scale sustainablewaterandpowerproduction,Desalination377(2016)163–171, http://dx.doi.org/10.1016/j.desal.2015.09.018.

[181] A.Giwa,N.Akther,A.AlHousani,S.Haris,S.W.Hasan,Recent advancesinhumid- ification dehumidification (HDH) desalination processes: improved designs and productivity, Renew. Sust. Energ. Rev. 57 (2016) 929–944,http://dx.doi.org/10.1016/j.rser.2015.12.108.

[182] P.Wang,T.Chung,Aconceptualdemonstrationoffreezedesalination–membrane distillation (FD–MD) hybrid desalination process utilizing liquefied natural gas (LNG)coldenergy,WaterRes.46(2012)4037–4052,http://dx.doi.org/10.1016/j.watres.2012.04.042.

[183] S.Mozia,A.W.Morawski,Theperformanceofahybridphotocatalysis–MDsystem forthetreatmentoftapwatercontaminatedwithibuprofen,Catal.Today193 (2012)213–220,http://dx.doi.org/10.1016/j.cattod.2012.03.016.

[184] M.Gryta,PurificationofoilywastewaterbyhybridUF/MD,WaterRes.35(2001) 3665–3669,http://dx.doi.org/10.1016/S0043-354(01)00083-5.

[185] K.Y.Wang,M.M.Teoh,A.Nugroho,T.Chung,Integratedforwardosmosis– membranedistillation(FO–MD)hybridsystemfortheconcentrationofprotein solutions,Chem.Eng.Sci.66(2011)2421–2430,http://dx.doi.org/10.1016/j.ces.2011.03.001.

★★★

STUDIES ON STRUCTURAL BEHAVIOUR OF REINFORCED CONCRETED FIBRE STUDIES

E SUJITH PRASAD

Asst Prof, Department of Mechanical Engineering NMIET BBSR

Abstract - With the headway of innovation and expanded field of utilizations of cement and mortars, the strength usefulness, sturdiness and different characters of the normal solid need adjustments to make it more appropriate for a by circumstances. Added to this is the need to battle the expanding cost and shortage of concrete. Under these conditions the utilization of admixtures is discovered to be a significant elective arrangement.

Toward this path, an endeavor has been made in the current examination to assess the usefulness, compressive strength, split elasticity and flexure strength on expansion of wood squander debris (0 – 30%) alongside pleated steel filaments (0-1%) in cement. Wood debris is an admixture: a pozzolana. Wood debris is created as a result of ignition in wood-terminated force plants, paper factories, and other wood consuming enterprises. In spite of the fact that a great deal of examination is centered in the most recent decade around utilization of different admixtures in delivering concrete, next to no data is accessible on wood squander debris added creased steel fiber strengthened cement. Standard 3D shapes of 150 X 150 X 150 mm have been projected and tried for getting 28 days compressive strength. Standard chambers of 150mm distance across and 300 mm tallness were projected and tried for Split rigidity. Standard Beams of 500mmx100mmx100mm were projected and tried for Flexural strength. M30 concrete has been utilized as reference blend. Results were dissected and ideal rates of Wood Waste Ash and Crimped Steel Fibers are discovered to be 20% and 0.75% separately. Nitty gritty portrayal about the outcomes was given assistance of charts, and future extension was examined.

Keywords - Steel Filaments, Admixture, Compressive Strength, Flexural Strength, Split Rigidity.

I. INTRODUCTION

The current boom in the construction industry has caused an exponential increase in the demand of cement, which is the primary constituent in the production of concrete. The production of cement needs a massive amount of raw material and energy, and at the same time releases carbon dioxide into the atmosphere. Researchers have shown that for every 600 kg of cement, approximately 400 kg of CO2 is released into the atmosphere. The increasing demand of cement leads to higher rate of environmental degradation and more exploitation of natural resources for raw material. Concrete is the world's most consumed man-made material. Also to produce 1 ton of Portland cement, 1.5 tons of raw materials are needed. These materials include good quality limestone and clay. Therefore, to manufacture 1.5 billion tons of cement annually, at least 2.3 billion tons of raw materials are needed. Over 5-million BTU of energy is needed to produce one tone of cement.

Regular concrete is the lay term describing concrete that is produced by following the mixing instructions that are commonly published on packets of cement, typically using sand or other common material as the aggregate, and often mixed in improvised containers. This concrete can be produced to yield a varying strength from about 10 MPa (1450 psi) to about 40 MPa (5800 psi), depending on the purpose, ranging from blinding to structural concrete respectively. Many types of pre-mixed concrete are available which include powdered cement mixed with aggregate, needing only water.

II. NEED FOR PRESENT INVESTIGATION

Though a lot of research is focused in the last decade on use of various admixtures in producing concrete, very little information is available on wood waste ash fiber reinforced concrete. As already mentioned, Wood ash is an admixture: a pozzolana as it is generated as a by-product of combustion in wood-fired power plants, paper mills, and other wood burning factories. Thus this new admixture has lot of potential for use in concrete. Hence, there is need to study the strength and workability characteristics of wood waste added concrete. Mixing of crimped steel fibres increases the various structural properties which improve its strength and durability. So far there is no work documented on the combined effect of addition of wood waste ash and crimped steel fibreson the strength and other characteristics. Hence it is necessary to study the effect of addition of wood waste ash and crimped steel fibreson the strength and other characteristics.

In this project work an attempt is made to study the properties of concrete like workability as well as compressive strength, split tensile strength, flexural strength of concrete with addition of wood waste ash and crimped steel fibres in varyingquantities.

III. MATERIALS USED

Experiments were conducted on concrete prepared by partial replacement of cement by wood waste ash of particle size 75µm at varying percentages and the mix design was prepared.

In all mixes the same type of aggregate i.e. crushed granite aggregate; river sand and the same proportion of fine aggregate to total aggregate are used. For each mix, 6 cubes of size 150 x 150 x 150 mm and 6 cylinders of 150 mm diameter & 300 mm height and 6 flexural beams of size 500 x100x100mm were cast and tested. The test programmed consisted of conducting Compressive tests on Cubes, Split Tensile tests on Cylinders and Flexural strength on beams.

CEMENT: Cement is a well-known building material and has occupied an indispensable place in construction works. Different varieties of cements are available in the market and each type is used under certain conditions due to its special properties. The cement commonly used is Portland cement, and the fine and coarse aggregates used are those that are usually obtainable, from nearby sand, gravel or rock deposits. In order to obtain a strong, durable and economical concrete mix, it is necessary to understand the characteristics and behavior of the ingredients. 53 grade OPC is used in this work

AGGREGATES: Aggregates are generally cheaper than cement and impart greater volume stability and durability to concrete. The aggregate is used primarily for the purpose of providing bulk to the concrete. To increase the density of the resulting mix, the aggregate is frequently used in two or more sizes. The aggregates provide about 75% of the body of the concrete and hence its influence is extremely important.

WATER: Generally, cement requires about 3/10 of its weight of water for hydration. Hence the minimum water-cement ratio required is 0.35. But the concrete containing water in this proportion will be very harsh and difficult to place. Additional water is required to lubricate the mix, which makes the concrete workable. This additional water must be kept to the minimum, since too much water reduces the strength of concrete. The water-cement ratio is influenced by the grade of concrete, nature and type of aggregates, the workability and durability. If too much water is added to concrete, the excess water along with cement comes to the surface by capillary action and this cement-water mixture forms a scum or thin layer of chalky material known as laitance this laitance prevents bond formation between the successive layers of concrete and forms a plane of weakness. The excess water may also leak through the joints of the formwork and make the concrete honeycombed. As a rule, the smaller the percentage of water, the stronger is the concrete subject to the condition that the required workability is allowedfor.

WOOD WASTE ASH: Wood Waste Ash (WWA) is the residue generated due to combustion of wood and wood products (chips, saw dust, bark, etc.). It is the inorganic and organic residue remaining after the combustion of wood or unbleached wood fiber. The physical and chemical properties of wood ash vary significantly depending on many factors. The physical and chemical of wood ash, which determining its beneficial uses, are dependent upon the species of the wood ash the combustion methods that include combustion temperature, efficiency of the boiler, and supplementary fuels used.

Typically, wood ash contains carbon in the range of 5-30% (Campbell, 1990). The major elements of wood ash include calcium (7-30%), potassium (3-4%), magnesium (1-2%), manganese (0.3-1.3%), phosphorus (0.3-1.4%) and sodium, (0.2-0.5%). Density of wood ash decreases with increasing carbon content. The chemical and physical properties depend upon the type of wood, combustion temperature, etc.

Typically wood burnt for fuel at pulp and paper mills and wood products industries may consist of saw dust, wood chips, bark and saw mill scraps, hard chips rejected from pulping, excess screenings such as sheaves and primary residuals without mixed secondary residuals.

STEEL FIBRES: Fibre reinforced concrete (FRC) may be defined as a composite materials made with Portland cement, aggregate, and incorporating discrete discontinuous fibres. We know that plain, unreinforced concrete is a brittle material, with a low tensile strength and a low strain capacity. The role of randomly distributes discontinuous fibres is to bridge across the cracks that develop provides some post-cracking “ductility”. If the fibres are sufficiently strong, sufficiently bonded to material, and permit the FRC to carry significant stresses over a relatively large strain capacity in the post- cracking stage. The real contribution of the fibres is to increase the toughness of the concrete, under any type of loading.

Although every type of fibre has been tried out in cement and concrete, not all of them can be effectively and economically used. Each type of fibre has its characteristic properties and limitations. Some of the fibres that could be used are steel fibres, polypropylene, nylons, asbestos, coir, glass and carbon. Fibre is a small piece of reinforcing material possessing certain characteristic properties. They can be circular or flat. The fibre is often described by a convenient parameter called “aspect ratio”. The aspect ratio of the fibre is the ratio of its length to its diameter.

Typical aspect ratio ranges from 30 to 150. Steel fibre is one of the most commonly used fibres. Generally, round fibresare used. The diameter may vary from 0.25 to 0.75 mm. The steel fibre is likely to get rusted and lose some of its strengths. But investigations have shown that the rusting of the fibres takes place only at the surface. Use of steel fibre makes significant improvements in flexural, impact and fatigue strength of concrete; it has been extensively used in various types of structures, particularly for overlays of roads, airfield pavements and bridge decks. Thin shells and plates have also been constructed using steelfibres.

IV. METHODOLOGY

To evaluate the strength characteristics in terms of compressive, split tensile and flexural strengths, a total of 16 mixes were tried with different percentages of wood waste ash (0,10,20 & 30%) and different percentages of crimped steel fibers (0,0.5,0.75 & 1%). In all mixes the same type of aggregate i.e. crushed granite aggregate; river sand and the same proportion of fine aggregate to total aggregate are used. The relative proportions ofcement, coarse aggregate, sand and water are obtained by IS - Code method. M30 is considered as the reference mix.(Appendix-I)

The strength parameters are studied for the following combinations:

With percentage of Wood Ash – 0, 10, 20 & 30%.
With percentage of Crimped Steel Fiber – 0, 0.5, 0.75 & 1%.

For each mix, 6 cubes of size 150 x 150 x 150 mm and 6 cylinders of 150 mm diameter & 300 mm height and 6 beams of size 500 x 100 x 100 mm were cast and tested. For all test specimens, moulds were kept on table vibrator and the concrete was poured into the moulds in three layers by tamping with a tamping rod and the vibration was effected by table vibrator after filling up moulds. The moulds were removed after twenty four hours and the specimens were kept immersed in clean water tank. After curing the specimens in water for a period of 7 days, 28 days the specimens were taken out and allowed for drying under shade before testing. The test programmed consisted of conducting Compressive tests on Cubes, Split Tensile tests on Cylinders and Flexural strength on beams at 28days.

V. RESULTS AND DISSUSSION COMPRESSIVE STRENGTH

Fibres do little to enhance the static compressive strength of concrete, with increases in strength ranging from essentially nil to perhaps 25%. Even in concrete members that contain conventional reinforcement in addition to the steel fibres, the fibres have little effect on compressive strength. However, the fibres do substantially increase the post-cracking ductility, or energy absorption of the material. The test results obtained from the compression of cubes under the compression test machine are given in the Table below. The variations of 28 days cube compressive strength of WWA- CSF mixes are presented in Figures below. From Figure it can be observed that the 28 days compressive strength increases with the increase in the percentage of wood waste ash up to 20% additionlevel.

Table 1: 28 days Compressive Strength values in N/mm^2

S.No	% of CSF	Compressive Strength (MPa)			
		0% WWA	10% WWA	20% WWA	30% WWA
1	0.00% CSF	38.9	41.1	42.9	33.0
2	0.50% CSF	40.1	43.8	45.6	33.9
3	0.75% CSF	42.9	45.3	48.0	36.7
4	1.00% CSF	41.6	44.8	46.9	35.3

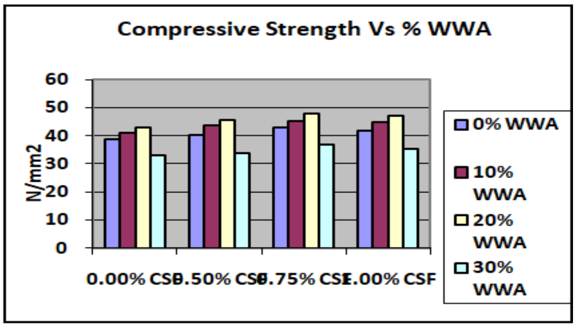

Figure 1 : 28 Days Compressive Strength Vs % of Wood Waste Ash

SPLIT TENSILE STRENGTH

Fibres aligned in the direction of the tensile stress may bring about very large increases in direct tensile strength, as high as 133% for 5% of smooth, straight steel fibres. In the present work crimped steel fibre were used and split tensile strength was tested with varying quantities of WWA and CSF.

Table 2: 28 days Split Tensile Strength values in N/mm^2

S.No	% of CSF	Split Tensile Strength (MPa)			
		0% WWA	10% WWA	20% WWA	30% WWA
1	0.00% CSF	4.26	4.67	4.76	3.65
2	0.50% CSF	5.45	5.61	5.91	4.43
3	0.75% CSF	5.57	5.90	6.33	4.65
4	1.00% CSF	5.32	5.72	6.10	4.45

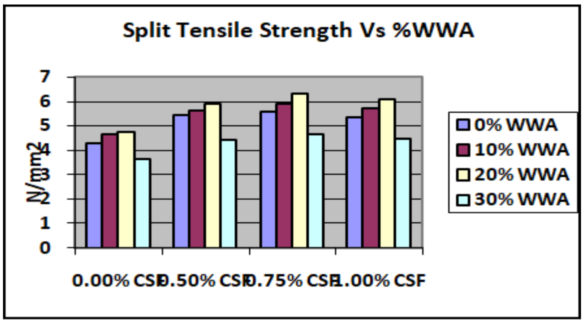

Figure 2: 28 Days Split Tensile Strength Vs % of Wood Waste Ash

FLEXURAL STRENGTH

Steel fibres are generally found to have aggregate much greater effect on the flexural strength of SFRC than on either the compressive or tensile strength, with increases of more than 100% having been reported. The increases in flexural strength are particularly sensitive, not only to the fibre volume, but also to the aspect ratio of the fibres, with higher aspect ratio leading to larger strength increases.

Table 3: 28 days Flexural Strength values in N/mm^2

S.No	% of CSF	Flexural Strength (Mpa)			
		0% WWA	10% WWA	20% WWA	30% WWA
1	0.00% CSF	5.25	5.56	5.62	4.33
2	0.50% CSF	6.23	6.56	6.81	5.21
3	0.75% CSF	6.67	6.89	7.33	5.72
4	1.00% CSF	6.52	6.67	7.21	5.51

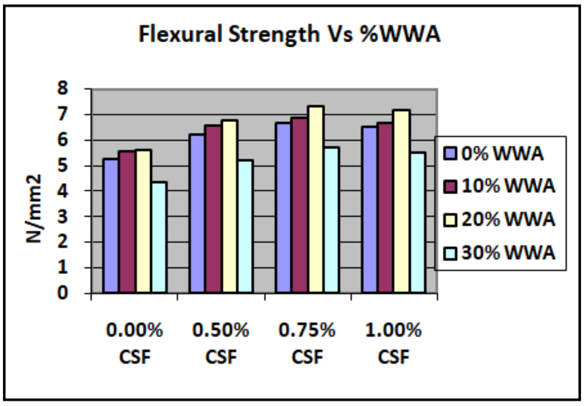

Figure 3: 28 Days Flexural Strength Vs % of Wood Waste Ash

VI. CONCLUSIONS

The following conclusions may be drawn from the experimental study on the characteristics of concrete with addition of wood waste ash (WWA) and crimped steel fibres(CSF). WWA is added at 0%, 10%, 20% and 30%, where as CSF is added at 0%, 0.5%, 0.75% and 1.0%.The workability of concrete with varying quantities of WWA and CSF are measured from compaction factor test. It was clearly understood from the test results that, as the percentage of wood waste ash and crimped steel fibre increases in the mix compaction factor decreases, and hence the workability decreases. This is due to the absorption of water from the mix by the WWA and subsequent loss of moisture from the mix, along with the obstruction and frictional resistance caused by the CSF in the concrete mixture. Hence it can be concluded that with the increase in the WWA and CSF content, workability decreases.The compressive strength of concrete cubes made with varying percentages of WWA and CSF were estimated using compression test machine after 28 days curing. From the test results it was found that compressive strength started increasing with addition of WWA and CSF; however this increase was found to be ceased after 20% increase of WWA and 0.75% increase of CSF.The increase in compressive strength due to addition of WWA is because of contribution of silica present in WWA to the CSH gel formation. The reduction of compressive strength with increase in percentage of WWA beyond 20% can be interpreted as the loss of water due to absorption by WWA and corresponding loss in degree of workability and hence compactability. The increase in compressive strength due to addition of CSF is because of contribution of fibres in bond and arresting the micro-crack development. The reduction of compressive strength with increase in percentage of CSF beyond 0.75 % is due to severe loss of degree of workability and there by poor compactability. It is also very clear that excess fibres will reduce the bond and integrity of the concrete mass. The flexural strength of the standard size beams tested under flexure after 28 days curing. The test results show that flexural strength of concrete got increased with increase in percentage of WWA and CSF. But the increase in flexural strength did not continued with increase in WWA and CSF content. Optimum percentages of WWA and CSF are 20% and0.75% respectively. Finally it was concluded that addition of WWA and CSF will reduce the workability. But the combined effect of both WWA and CSF will increase the compressive strength, split tensile strength and flexural strength. The optimum percentages of WWA and CSF are 20% and 0.75%respectively.

REFERENCES

[1] Alton G. Campbell (1990), “Recycling and Disposing of Wood Ash”, Tappi Journal, Pp.141- 146.
[2] Etiegni L, Campbell AG (1991), “Physical and Chemical Characteristics of Wood Ash”, Bio- resource Technology, Elsevier Science Publishers Ltd., Vol.37, No.2,Pp.173–178.
[3] S.Ezeldin and S.R.Lowe (1991), “Mechanical Properties of Steel Fibre Reinforced Rapid-set Materials”, ACI Materials Journals, Jul-Aug, Vol.88, No.4,Pp.384-389.
[4] Mukherji SK, Dan T K, Machhoya BB (1995), “Characterization and Utilization of Wood Ash in the Ceramic Industry”, International Ceramic Review, Vol.44, No.1,Pp.31-33.
[5] Naik TR (1999), “Tests of Wood Ash as a Potential Source for Construction Materials”, UWM Centre for By-Products Utilization, Report No.CBU-1999- 09, Pp.61.
[6] Naik TR, Kraus RN (2000), “Use of Wood Ash for Structural Concrete and Flowable”, Solid Waste Management and Research Program, CLSM, Report No. CBU-2000-31,Pp.121.
[7] Colin D. Johnston (2001), “Fiber Reinforced Cements and Concretes” Advances in Concrete Technology, Gordon and Breach Science publishes, Vol.3,Pp.105-108.
[8] Naaman, A.E., Sujivorakul (2001), “Pull-out Mechanisms of Twisted Steel Fibres Embedded in Concrete”, Proceedings of International Conference o Applications of Shotcrete,Pp.197-203.

[9] Nguyen Van Chanch (2002), “Steel Fibre Reinforced Concrete”,Pp108-116.

[10] TarunR.Naik (2002), “Greener Concrete Using Recycled Materials”, Concrete International, July, Pp.45-49.

[11] Naike, T R Kraus, R N (2003), “A New Source of Pozzolanic Material”, American Concrete Institute, ISSN: 0162-4075, OCLC: 4163061, Vol.25, No.12, Pp.55-62.

[12] TarunR. N., Rudolph N. K., and Rafat S.(2003), “Use of Wood Ash in Cement-based Materials”, A CBU Report, CBU-2003-19(REP-513).

★★★

MECHANICAL RESPONSES OF GFRP COMPOSITES WITH POXY-VINYLESTER INTERPENETRATING POLYMER NETWORK

[1]JAIN TONY B, [2]ALIVA MOHANTY, [3]GOUTAM MISHRA

[1]Department of Mechanical Engineering, NMIET, Bhubaneswar, 751019
[2]Department of Mechanical Engineering, REC Bhubaneswar
[3]Department of Mechanical Engineering, CEC Bhubaneswar
E-mail: [1]krusna.singh@nmiet.ac.in

Abstract -
Present investigation deals with development of glass fiber reinforced polymer (GFRP) composite with a matrix composed of a polymer blend of epoxy and vinyl ester. The evolved Interpenetrating polymer network (IPN) formedduetoblendingofthepolymersresultedinimprovedtensile,flexuralandinterlaminarshearproperties of the hybrid composite than that of both glass fiber/epoxy (GE) and glass fiber/vinyl ester (GVE)composites. Resinburn-offtestrevealedthattheglassfibervolumefractiontobealmostidenticalinallthreecomposite laminates,whichwas~45%. The role of curing temperatures (140,170,200and230◦C) on thecurekinetics of the composites wasexamined based ontheflexuralpropertiesofthecomposites,whichisalsosupportedwiththe dynamic mechanical thermal analysis (DMTA) results. The glass fiber reinforced epoxy-vinyl ester inter- penetrating polymer network (GEVIPN) composite led to 21.83%, 22.54% and 13.43% improvement in inter- laminarshearstrength(ILSS),tensileandflexuralstrengthrespectively, overGEcompositeatoptimalpostcure temperature.Further,chemicalrestructuringof GEVIPN composite was analysed by Fouriertransforminfrared spectroscopy (FTIR). From scanning electron microscopy (SEM), it was comprehended that strong interfacial bonding between the matrix and fiber made GEVIPN composite exhibit better mechanical properties.

Keywords - Mechanical Testing, Thermomechanical Testing, Fourier Transform, Infrared Spectroscopy Analysis, Interpenetrating Polymer Network (IPN), Fractography

I. INTRODUCTION

In the present generation, thermoset composites reinforced with fiberarerecognizedasoneofthemostimportantmaterials. Thereliable mechanical performance exhibited by Fiber-Reinforced Polymer(FRP) composites has gained huge acceptance because of its inherent proper- ties like high resistance to corrosion, high strength and modulus-to- weight ratio and improved fatigue resistance. These properties of FRP compositesaresuperiorbecausethesepropertiesrelyoninterfacial bondingandcrosslinksbetweenthematrixandthefiber[1–6].Buton the other hand, the thermoset FRP composites have lower toughness compared to that of ductile metals and alloys. The pertinent solution is tomodifythematrixsince,inFRPcomposites,toughnessisusually regulated by matrix [7–10]. Thermoset matrices like epoxy, vinylester, and polyester are commonly used as polymer matrices [11]. Among these,epoxyresinhasbeencommercializedasastructural adhesiveand as a polymer matrix for FRP composites. But the major concern onthe use of epoxy resin lies in the strength, which depends on the level of crosslinks influenced by the cure kinetics [12–16]. However, once the epoxy is cured with the hardener, the matrix exhibits brittle behavior [17], thus the resulting composite will be of lower toughness [18]. It has already been reported that in order to drive out the problemof lowertoughness, epoxyisusuallyblended witheitheranelastomeror with thermosetor withthermoplasticpolymer[19–21]. Typically,the epoxy resin modified by introducing various tougheners results in the loss of strength, stiffness and thermal properties [22–24]. Therefore thermoset-thermoset blends have emerged as better technique sinceit possesses higher strength and thermal stability [25,26]. The mixture of epoxy-vinyl ester results in the formation of Interpenetrating polymer networks (IPNs) consisting of two or more polymers wherein the network formed is held by permanent entanglements [25,27].
Karger-Kocsis et al. [26] have reported the toughening mechanism ontheformationof IPN resulting fromepoxy-vinylestermixtureandthe typeofepoxyaffectingthetoughnessoftheepoxy-vinylestersystem.

Their group found that cycloaliphatic or aliphatic epoxy yielded very hightoughnesswhen theepoxywascuredby thesamediamine. Jiaetal.[14] reported that the epoxy and vinyl ester polymer blend was pro- cessed by mixing of both polymers and respective hardeners simulta- neously using stirring process, and the resulting polymer blend enhanced the thermal stability, mechanical and damping ability prop- erties.M´esza´rosetal.[7] reportedthatbyusing thesimultaneously blended epoxy-vinyl ester polymer as matrix in carbon fiber reinforced composite, increment of 10% and 7% in flexural and impact strength, respectively, could be obtained compared to that when epoxy was used as matrix. Hence, it can be believed that reinforcing the glass fiber into the IPN-structured thermoset matrix would yield a composite of improved properties, especially mechanical properties compared tothat ofglassfiberreinforcedepoxy(GE)andglassfiberreinforcedvinylester (GVE)composites.Hereaftertheglassfiberreinforcedepoxy-vinylester interpenetrating polymer network will be abbreviated asGEVIPN.

On the other hand, the matrix being viscoelastic in nature, there is significant change in the properties with the change in temperature. Specifically, for IPN-structured thermoset matrix, the mechanical and thermomechanical properties are greatly affected by the curing process [28]. The curing process involves two steps i.e., gelation and vitrifica- tion [29]. During gelation, the liquid resin gets converted to gel once hardener is added and subsequently, if the curing temperature reaches the glass transition temperature (Tg), the polymer may then vitrify [25, 30]. K. Dean et al. [27] have reported that matrix made up of epoxy-vinyl ester system underwent premature vitrification because of the slower curing of the epoxy component during the low temperature isothermal curing. Their group also recognized that by post-curing the IPN system at elevated temperature, near full cure could be attained. Hence optimization of curing temperature for GEVIPN composite is required so that it yields a perfect crosslinked epoxy-vinyl ester IPN-structured matrix leading to enhanced mechanical properties. K. Deanetal.[27]alsoanticipatedthatbymixingtheepoxyresinandvinyl ester, both containing the bisphenol-A diglycidyl structure would enhance the miscibility in the IPN formed. In this research study, a matrixofepoxy-vinylesterIPN(EVIPN)systemwaspreparedbyusing bisphenol-Adiglycidylstructuredepoxyandvinylesterresinintheratio of 1:1. Then, the respective hardener and catalyst i.e., triethylenetetr- amine and peroxide were added to prepare a homogenous mixture. The present study deals with the effect of EVIPN matrix system on the me- chanical and thermomechanical response of the GFRP composite. Additionally, there is a dearth of open reports on the cure kinetics of GEVIPN composite. Therefore, the main aim of this work is to investigatetheeffectofcuretemperatureonflexuralbehaviourofGE,GVEand GEVIPNcomposites.Thecurekineticsstudyisalsodoneforobtainingthe optimalcuretemperatureofallexperimentedcomposites. Further,to identifythemechanicallybestperformingGFRPcompositematerial amongallexperimentedcomposites,comparativeanalysisofshortbeam shear (S.B.S), tensile and flexural tests were conducted at resulting optimal cured temperature. The chemical restructuring and post failure analysisofallexperimented composites wereconductedusing FTIR and SEM, respectively.

II. EXPERIMENTAL DETAILS

2.1. Materials

One of the resins used for mixing was bisphenol-A diglycidyl ether grade of epoxy polymer, for which the curing agent was triethylene- tetramine (TETA), available as Lapox L-12 and K-6 as trade names, respectively,suppliedbyAtulIndustriesLtd.,India.Anotherresinused was vinyl ester polymer (bisphenol-A diglycidyl based) and catalyst (free radical) was methyl ethyl ketone peroxide (MEKP), which were suppliedbyPliogripResins&ChemicalsPvt.Ltd,India.E-glassfiber(3K plainweave;15μmfilamentdiameter;arealdensity360gsm),purchased from Owens Corning, India, was used as reinforcement. Table1 represents theessential properties of the reinforcement and matrices.

Property	Material		
	E —Glassfiber	Epoxyresin	Vinyl ester resin
Tensilestrength(MPa)	3200	50–60	63–74
Tensilemodulus(GPa)	72.30	4.10	3.50
Strain atfailure(%)	4.60	1.50–3.00	4.00–5.00
Density(g/cm^3)	2.54	1.16	1.12

Table 1
Essential properties of the reinforcement and matrices.

2.2. Fabrication of compositelaminates

Threedifferenttypesofcomposites,i.e.,GE,GVEandGEVIPNwere fabricatedbythehandlay-upmethod.Alltheselaminatesconsistedof6 pliesofglassfibermatfortheflexural,tensile,DMTAandresinburnoff testwhereas,12pliesofglassfibermatfortheS.B.Stest.Inthecaseof epoxy matrix preparation, 10 wt % of curing agent TETA was mixedin theepoxypolymer,whileinthecaseofvinylestermatrixpreparation, 1.5 wt % of free radical MEKP was mixed in the polymer as per the in- structions provided by their respective manufacturers. Fig. 1represents the schematic of the fabrication of GEVIPN composite. The prepared laminates were then hot pressed for 20 min at 80 ◦C temperature with 10kg/cm2pressure[31–33].Thehotpresscompressionprocessprovides uniform thickness with a certain degree of cure temperature and appliedpressure,whichisessentialforfurtherhandlingofthecomposite laminates[34].

Epoxy and Vinyl ester polymers act as primary constituents in forming IPNs. The curing reactions of thermoset resin components do not interfere with one other, and that their relative amount is well balanced, close to the weight ratio of 1:1 for IPN formation with ther- moset resins, and this thermoset IPN system resulted in enhanced properties [26]. The other investigators also studied the cure, rheolog- ical and microstructural behaviour of epoxy/vinyl ester at 1:1 ratio-based thermosets of IPN network structure. Furthermore, they have suggested that the VE (vinyl ester)/EP(epoxy) systems at 1:1 ratio exhibited a clear IPN structure, which became more miscible with increasing curing temperature [25,27,35,36]. By consideration of re- ported advantages and reliable properties from literature, the same 1:1 wt ratio of epoxy and vinyl ester composition was used for the prepa- ration of the IPN matrix system. The preparation of IPN-structured thermoset matrix was done using the following steps:

In a flask, the weight ratio of epoxy resin and vinyl ester resin is maintained as 1:1 ratio.

ToprepareEVIPNmatrix,theepoxyresinispouredintoaflask.Then vinyl ester resin is also poured into the same flask. Then thecatalyst MEKPisaddedfirst,andhardenerTETAisalsothenpouredintothe flask.

By using stirrer, the suspension is mixed thoroughly until a homo- geneous mixture is obtained, which took approximately 5 min.

2.3. Post-curing

Before post-curing the samples, the diamond wheel cutter was employed to prepare the samples according to the ASTM standards for flexural (ASTM D7264), tensile (ASTM D3039), Dynamic mechanical thermal analysis (DMTA) (ASTM D7028), Short beam shear (S.B.S) (ASTMD2344)andResinburnoff(ASTMD3171)testsfromthefabri- catedlaminates followedbyfine polishingusingseriesofemerypapers. For post-curing purpose, all these composite samples were kept ina hot air oven. It is well recognized that the post-curing process is carriedout to increase the crosslinking density which results in improved mechanicalandthermomechanicalproperties.Therearetwo maincuring

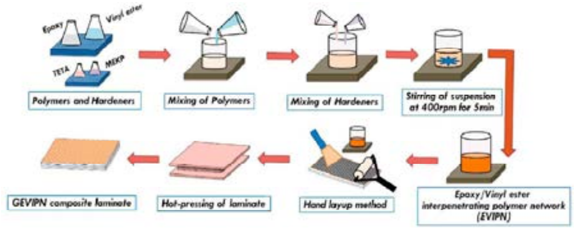

Fig. 1. Schematic of fabrication of GEVIPN composite.

parameters that shall determine the optimal post-curing process. One is the temperature and the other is the time. In this study, curing time was kept constant as 6 h and the post-curing temperature was varied. The reasonforkeepingthecuringtimeconstantfor6hisexplicitlyexplained by kumar et al. [29]. Their group varied both temperature and time,and reported that, at 140 ◦C temperature, there was no furtherimprovement inILSSofGEcompositeafter6hofcuring.Kumaretal.[29]groupalso reported that lower post cure temperature yielded lower ILSS of GE composite due to the unavailability of sufficient thermal energyto further enhance the fiber/matrix interface's wettability at before 140◦C postcuringtemperature,whichinturnresultedinalowerILSSvalueat 110 ◦C. Avadesh et al. [37] have investigated the effect of curekinetics onglassfiber/vinylestercomposite.TheyhavereportedthattheGVE composite exhibited better mechanical and thermal responses at 140◦C cure temperature with 6 h time duration than other cure temperaturesof 80◦Cand110◦C.Also,theystatedthatforobtainingoptimalglass transition (Tg) value, high cure temperature is the most favourable due to enhanced cross-linking among polymer chains. Dean et al. [38] reportedthattheslowercurebehaviouroftheDGEBAcomponentlowers theextentofcureoftheepoxysystemintheIPN.Moreover, post-curing at elevated temperature is favourable for attaining near full cure of the IPN system. Katherine et al. [25] suggested for a full/complete cure of IPNs is not available until the cure temperature is above the glass transition (Tg) of both epoxy and vinyl ester components. Aruniit etal.

[39] have reported that the low-temperature post cured composites exhibited relatively low performance than high-temperature post cured composites. Furtos et al. [40] group also suggested that the cure tem- perature significantly influences the mechanical and thermal properties of the GFRP composites. In order to ensure completereaction and obtaining the composite's optimal mechanical properties, it is required to post cure the composite at a higher temperature. Therefore, the optimization study was conducted by keeping the curing time constant andthepost-curingtemperaturesexperimentedwere140◦C,170◦C, 200 ◦C and 230 ◦C. After the completion of post-curing, the samples wereleftintheovenuntiltheroomtemperatureisreachedinorderto prevent the composite samples from thermal shock effects.

2.4. Materialcharacterization

2.4.1. Mechanical and thermomechanical characterization

Flexural testing was done to observe the influence of cure temperatureontheflexuralbehaviourofGE,GVEandGEVIPNcompositesasper ASTMD7264standardusinga3-pointbendingfixtureofInstron5967. Fortheflexuraltest,thetestspecimens'dimensionswere maintainedas 40 mm length 12.7 mm width 2 mm thick. The supported span-to-thicknessratioof16:1waskeptforallcompositeflexuralspecimens,and thespanlengthwassetat32mm.Theflexuraltestwascarriedoutatan ambient environment and at 1 mm/min cross head velocity. As per the

ASTMD7028,theviscoelasticpropertiesoftheGEVIPN compositepost- curedatdifferent temperatureswere evaluated using DMTA.Forthis analysis, therangeoftemperature chosenwasfrom40◦Cto200◦C and was performed at 5 ◦C/min heating rate. The frequency wasmaintained at1Hz.ThetensiletestofGE, GVEandGEVIPNcompositeswasconductedinuniversaltestingmachine(Instron5967)withtensilefixtureat 1 mm/min cross head velocity and at ambient environment. ILSS of GFRPcompositeswere evaluated fromS.B.Stestsusingthesamemachine asperASTMD2344.FortheS.B.Stest,thetestspecimens' dimensions were maintained as 32 mm length 8 mm width 4 mm thick. The supportedspan-to-thicknessratioof6:1waskeptforallcompositeS.B.S specimens,andthespanlengthwassetat24mm.Furthermore,theS.B.S test was carried out at an ambient environment and at 1 mm/min cross head velocity. According to their respective ASTM standards,five specimenswerechosenfromeachexperimentedcompositegroupofthe tests, as mentioned above [41–43]. Fourier transform infrared (FTIR) study helps in understanding the molecular components and chemical structure of materials by the infrared absorption bands. Using Fourier-transform infrared spectros- copy (Infra-red range: 350 to 7800 cm—1 Shimadzu IR P-21)chemical restructuring and material compounds of the GEVIPN composite was studied. The post failure analyses of fractured samples were conducted usingFieldEmissionScanningElectronMicroscope(FESEM),(FEINova nano SEM 450). Before performing the test, platinum coating wasdone on the fracture surface of the specimens using a sputter coater. This platinum coating makes the surface of tested samples conductive to prevent the static electric charge accumulation and is also done for better resolution of fractographs. The Resin burnoff test was performed toevaluatethevolumefractionoftheglassfiber(vf),matrix system(vm), and voids (vv) in all experimented GE, GVE and GEVIPNcomposites.

Fivetestsampleswerepreparedfromeachgroupoflaminateswith25x 25 mm2 and kept in cleaned ceramic crucibles. Later these ceramic crucibles were placed in a muffle furnace at 55015 ◦C for 6 h [44,45].

Furthermore, the calculated volume fraction of constituents and the presence of void content in all experimented composites are mentioned in Table 2. The volume fraction of glass fiber was obtained almost the same in all three experimented composites. Moreover, a slightdecrease invoidvolumefractioncanbeseeninGEVIPNcomposite materialthan other homopolymer based composite material. This lower voidcontent resultsfromtheexistenceofenhancedwettabilitybetweenfiberandthe hybrid IPN matrix system, which is essential for improving composite material's overallperformance.

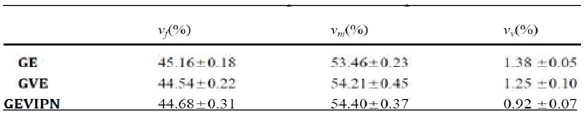

	v_f(%)	v_m(%)	v_v(%)
GE	45.16±0.18	53.46±0.23	1.38 ±0.05
GVE	44.54±0.22	54.21±0.45	1.25 ±0.10
GEVIPN	44.68±0.31	54.40±0.37	0.92 ±0.07

Table 2

Volumefractionofconstituentsintheexperimentedcomposites.

III. RESULTS AND DISCUSSION

3.1. Simultaneous IPN formation

Fig. 2shows the possible reaction between bisphenol-A diglycidyl structured epoxy and vinyl ester, which intimately take part in forming the networks and the crosslinks resulting into IPNs. To result into simultaneousIPNs,thecrosslinkersandthemonomersare presentatthe start ofpolymerisation. The vinyl ester resin is obtained by reacting the bisphenol-A diglycidyl ether grade of epoxy polymer with methacrylic acid. The reactive diluent used in such systems is styrene monomer of 30–50% byweight. Inthecaseofvinylester,crosslinkingcantakeplaceonlyatthechain ends because the reactive sites are positioned only at the ends of the molecularchain,whilestyrenehasonlyone.Therefore,styreneprovides only the linear chain extension, whereas crosslinking capacity and branch points are provided by the vinyl ester monomer[46,47].

Individually, the free radical copolymerization reaction is followed by vinyl ester curing, initiated by MEKP initiator [46], while a poly-additionmechanismisfollowedbyepoxycrosslinking,in whichTETAis used as the hardener. Because of these independent reactions, there is a possibility of development of simultaneous IPN structure [48]. However,somesidereactionsmaytakeplacebutKarger-Kocsisetal.[26]have reported that their effects are mostlynegligible. The reaction may take place in such a way that the secondary –OH groups present in vinyl ester may react with oxirane group of epoxy resin, resulting into chemical links between epoxy and vinyl ester [26]. ThisfactwillfurtherbesupportedwithFTIRanalysis.Furthermore,the combined effect of thermoset epoxy and vinyl ester hybrid resin is allowed to get strongly bonded to the glass fiber. Additionally, once proper wettability is achieved, there are chances of the thermoset based hybrid matrix interacting since the reinforcement material, i.e., glass fiber used is of a thin layer. This interaction results in the formation of IPN,theevidenceofwhichisexplainedinsubsequentsection3.8(FTIR analysis).So,theobtainedIPNwillfurtherassistindevelopingnetworks andcross-links,whichwillallowthemaximumstresstransferwithin the constituent materials of the GEVIPN composite, which is evident from section 3.7 (fractography analysis). This efficient stress transfer maybe ascribed to the resistance to crack generation and delay the crack propagation, resulting in the improved mechanical performance of GEVIPN compositematerial.

3.1.1. Impact of post cure temperature on flexuralbehaviour of GE

Fig. 3(a) represents the flexural stress-strain plot of GE composite post-cured at different temperatures. Increasing the post curing temperature from 140 ◦C to 170 ◦C does not seem to have anyappreciable impact on the flexural strength of GE composite. This can be attributed to the lower availability of thermal energy for it to exhibit better crosslinking.Butafterpost-curingtemperaturetheGEcompositeat 200 ◦C, there was significant improvement in the flexural strengthover 140◦C(Fig.3(b)).Thiscanbeduetotheenhancedwettabilitybetween fiberandmatrixattainedatthatpost-curingtemperatureresultinginto better interfacialbonding. Additionally, this can also be supported by the fact that at that high temperature there was sufficient amount of thermal energy for the crosslinking to take place between fiber and matrix. The GEcomposite was further subjected to high temperature post-curing, i.e., 230 ◦C,but theimprovementwhichcouldbeobtainedwasonly1.23% over200◦C. Ifthetestsampleswerepostcuredbeyond230◦C,itishighlyexpected thattherateofincrementwillbemuchlessduetoits slowcurerate behaviour [38,49]. At higher post cure temperature, the polymeric compositematerialhasledtohighercrosslinkingdensity. Nevertheless, such high crosslinking density is also not adequate since it results in brittle failure, and this results in the lower strain at the peak, which is evidentfromFig.3(d)[23,50].Straintofailureisoneofthe crucial characteristicsofthematerial. Ifitisdroppedthen thatmightbea threat to the material. Therefore 200 ◦C post-curing temperature can be considered as the optimum post-curing temperature for GE composite. The flexural modulus followed the same trend as that of flexural strength, buttherewasnosignificant variation (within~1GPaasshown in Fig.3(c)).

3.1.2. Impact of post cure temperature on flexuralbehaviour of GVE

The GVE composite was also post-cured at same temperatures in order to obtain the optimal post-curing temperature as can be seen in (Fig.4).Thetrendobtainedafterconductingtheflexuraltestofdifferent post-curedsamplesofGVEcompositewasalmostthesameasobtained in the GE composite case. This may be attributed by the fact that the mechanical response of composite material depends on various factors such as chemical bonding, wetting, adsorption, and exchange reaction bonding [33]. P Siva et al. [51] and Ganesh et al. [52] groups also reportedthattheflexuralandILSSresponsesofglassfiberreinforcedvinyl ester composite was significantly influenced by vinyl ester resin structure, chemical composition, reinforcement type and styrene content. Moreover, similar types of results were also reported by Murthy et al. [53].Theyfoundthatthereisnomuchdifferenceinflexural strengthof GE(glass/epoxy)andGVE(glass/vinylester)composites,whereasCVE (carbon/vinyl ester) based composite exhibited relatively higher strength than CE (carbon/epoxy) composite at ambienttemperature condition.Exceptatpost-curingtemperatureof230◦C,wheretheGVE composite exhibited drastic drop in the flexural strength of 329.38 1.87 MPa over 351.232.52 MPa at post-curing temperature of 200 ◦C. This can be explained due to the higher curing rate of GVE composite over GE composite [54]. Because of the high curing rate of GVE composite which happens at higher post-curing temperature, it attains highercrosslinkingdensitywithextremebrittleness[28]. Thisisevident from Fig. 4(c) and (d), where in it exhibits high flexural modulus and low strain to failure at post-curing temperature of 230 ◦C.

3.1.3. Impact of post cure temperature on flexural behavior of GEVIPN

Fig. 5(a) represents the flexural stress-strain plot of GEVIPN composite post-cured at different temperatures. The fact that crosslinking reactionrequiressufficienttemperaturecanbeobservedfromtheplotof flexuralstrengthversuspost-curetemperature(Fig.5(b))whereinthe 200 ◦C post-cured GEVIPN composite shows highest flexuralstrength compared to other post-curing temperatures. K. Dean et al. [27] have reported that to attain near full cure of epoxy-vinyl ester IPN system, hightemperaturepost-curingistobecarriedout.Additionally,toobtain such a remarkable effect on the flexural performance, chemical reactivationisrequiredwhichcanbeobtainedbyheatingthecomposite aboveglasstransitiontemperature(Tg)[30].Inthisregard,200◦C post-curing temperature acts as optimal temperature since higher chemical conversions are attained at that temperature within the epoxy-vinyl ester IPN-structured thermoset. As the post-curingtemperatureisincreasedfurtherto230◦C,theremightbechancesthatthe GEVIPNcompositemaypossesshighercrosslinkdensity.Butthebitter side of such higher crosslink density leads to lower flexural strength (Fig.5(b)).Thisaspectofcrosslinkingdensitywillbeexplainedmorein DMTA analysis, and it will be revealed that high temperature curing would lead to higher crosslinks.

Variation in the flexural modulus is insignificant and the trend followed by it is the same as that of flexural strength (Fig. 5(c)). For the synthesis of IPNs, the kinetics of the crosslinking is important due to its slow curing behaviour [38,55]. Higher synthesis is achieved at higher temperature which may result in the formation of higher entanglements, which in turn acts as the potential energy absorber [7]. These entanglements restrict the crack propagation and hence can be attributed for the higher failure strain of the 200◦C post-cured GEV IPN composite

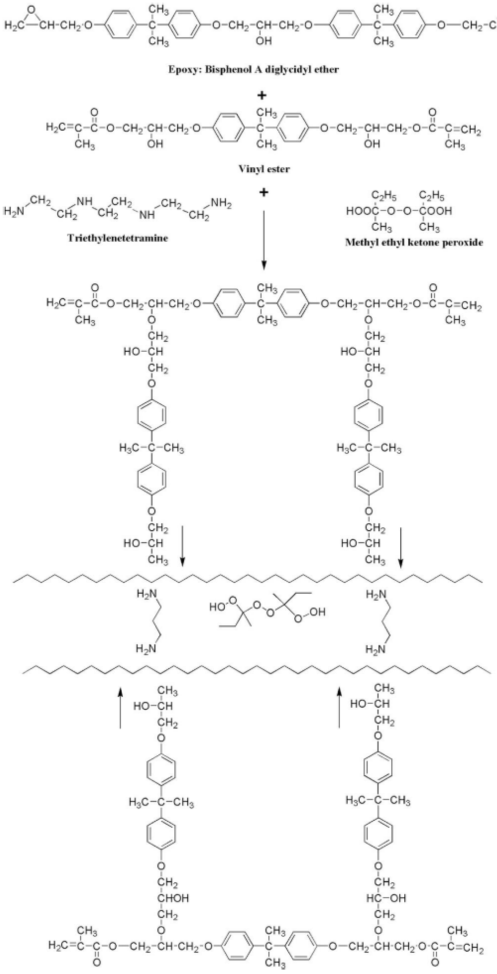

Fig. 2. Plausible chemical reaction which yields IPN structure.

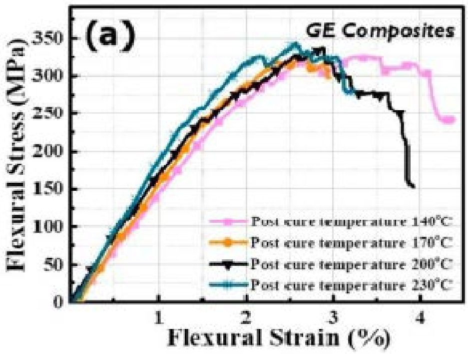

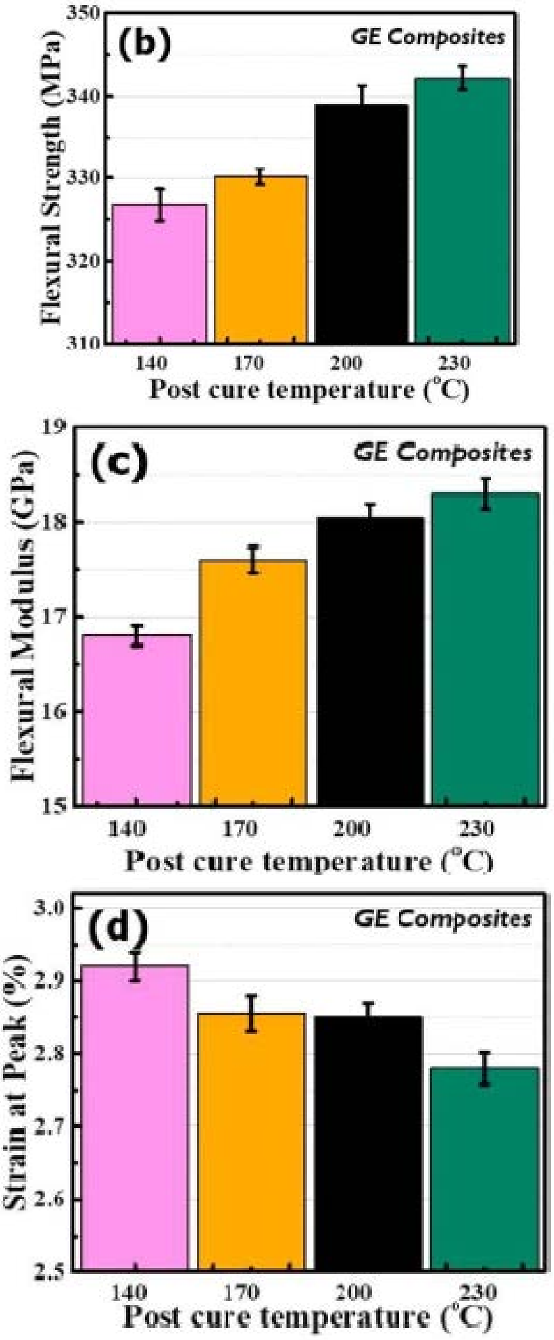

Fig.3.Flexural properties of GE composite at various post-curing temperatures (a)stress-strain curves (b)flexural strength (c)flexural modulus (d)strain at peak.

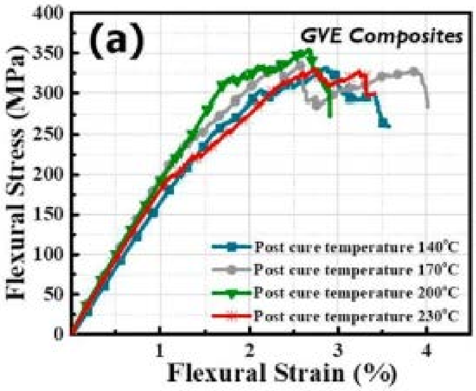

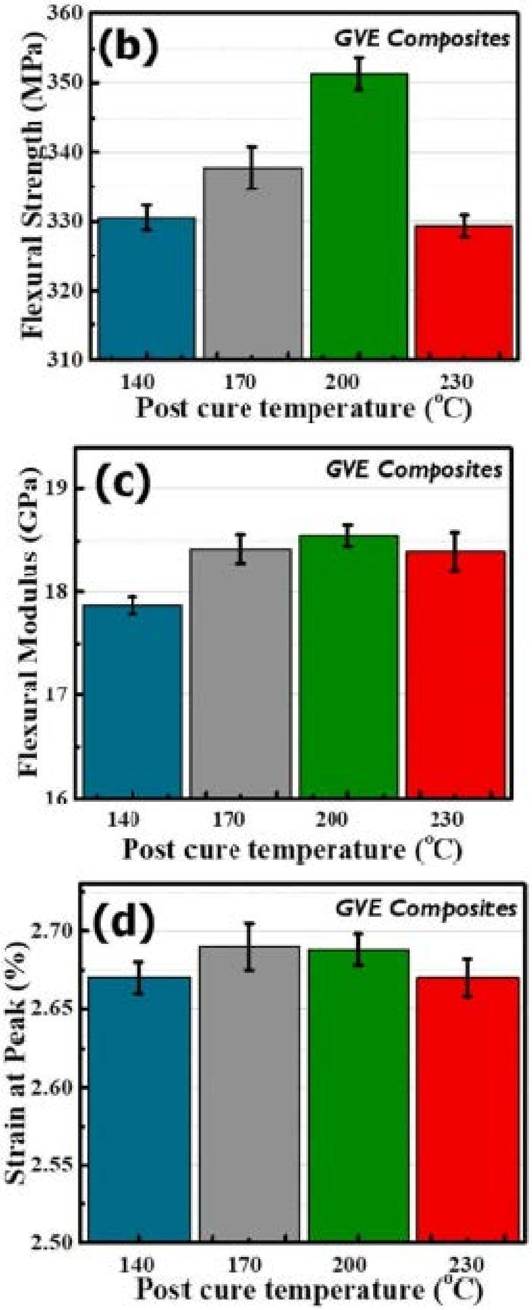

Fig.4.FlexuralpropertiesofGVEcompositeatvariouspost-curingtemperatures(a)stress-straincurves (b)flexuralstrength (c)flexuralmodulus (d)strainatpeak.

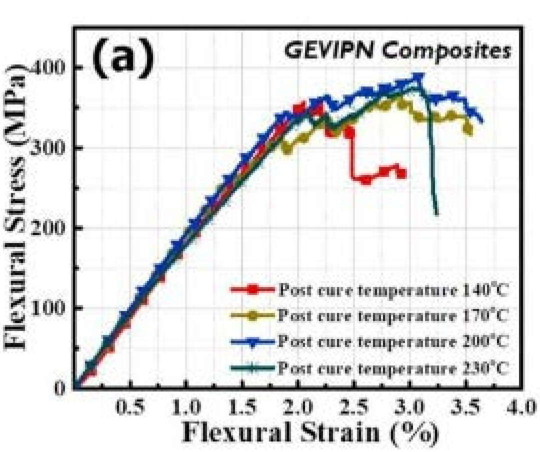

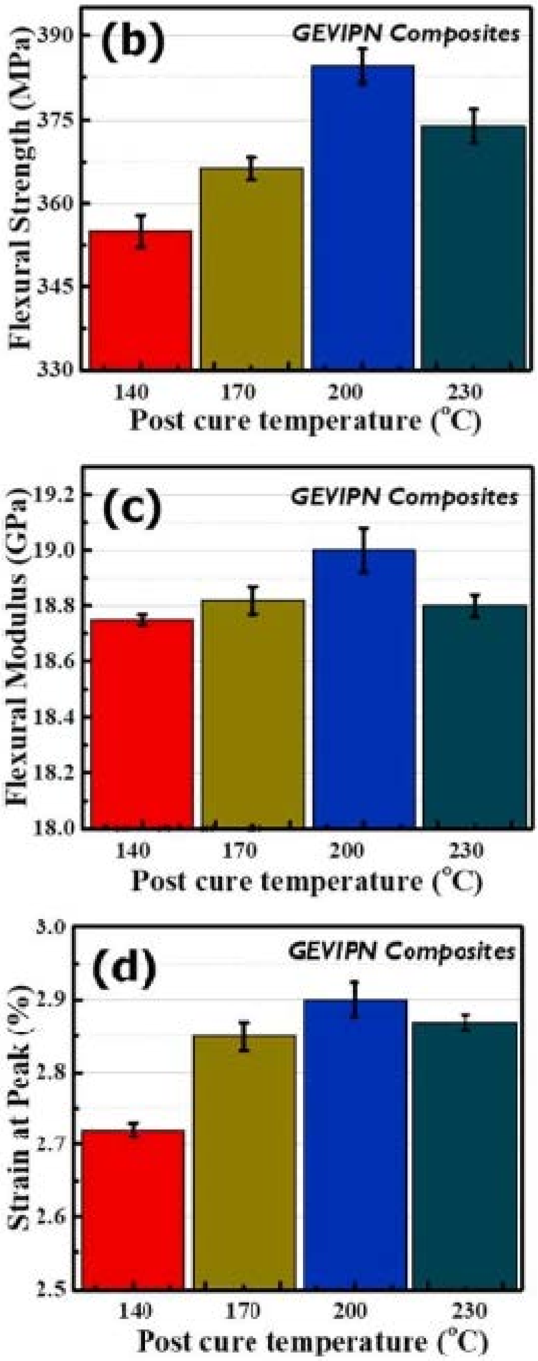

Fig. 5. Flexural properties of GEVIPN composite at various post-curing temperatures (a) stress-strain curves (b) flexural strength (c) flexural modulus (d) strain at peak.

(Fig. 5(d)). Therefore, it can be deduced that for all the composite sys- tems, 200 ◦C post-curing temperature acts as the optimal post-curing temperatureforthemtoexhibithigherflexuralstrength,whichisrepresented in Fig. 6. It also depicts that, the epoxy-based GE composite showedslightimprovementevenatahighercuretemperatureof230◦C due to its slow cure rate behaviour [38,49]. Moreover, the obtainedrate of increment is around 1.23%, which is very negligible. Whereas,vinyl ester based GVE composite exhibited poor performance at 230 ◦C cure temperatureover200◦Ccuretemperatureduetoitshighcurerate. Because of this difference in the cure rate behaviour of respective polymeric materials, the flexural strength trend of GE and GVE composites at post-curing temperature 230 ◦C is different from each other.” Moreover, at any of the post-curing temperatures, the GEVIPN compositealwaysexhibitedhighestflexuralstrengthover GE,andGVE composites.section3.6explainsmoreabouttheflexuralperformanceof fabricated composites and its comparativeanalysis.

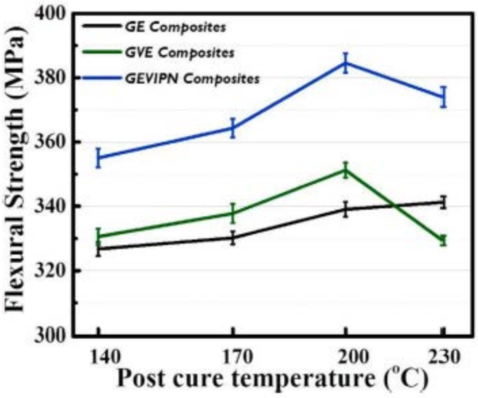

Fig. 6. Variation in flexural strength with post-curing temperature for GE, GVE and GEVIPN composites.

3.2. Dynamic mechanical thermal analysis(DMTA)

Viscoelastic properties of GEVIPN composite over the temperature rangefrom40◦Cto200◦C have been reportedinFig.7. DMTAisa perfect method to examine the viscoelastic behaviour of composite materials[56].InDMTA,theviscoelasticpropertiessuch asdamping factortanδ,storagemodulus(E′)andlossmodulus(E″)are obtainedby applying a dynamic stimulus to the composite material, and the corre- sponding dynamic displacement is recorded over the range of temperature. The plot of storage modulus (Fig. 7(a)) reveals that, all GEVIPN composite post-cured at different temperatures experience a transition from glassy state to rubbery state. But before the start of the transition, the trend shown by the storage modulus response remains identical as that of flexural modulus response which acts as reliable verification undoubtedly. The Tg is taken as that temperature when there is a maximum change in the storage modulus [57]. As the post-curing temperature is increased to higher temperatures in order to attain near full cure of epoxy-vinyl ester system, the Tg also increases (Fig. 7(d)) and accordingly explains that at higher temperatures higher cross- linking density is attained[28].

Fig.7(b)explainsthelossmodulus,anditrevealstheviscousnature of the polymeric composite. Usually, it is the matrix that dissipates maximum heat to the surrounding when the load is applied to the composite. But when the fiber is reinforced in the composite, then ma- trix present around it gets adsorbed on the fiber surface. This adsorbed matrix will not be available for heat dissipation since, after applying load,thedeformationofthis adsorbedmatrixis lesscomparedtothe

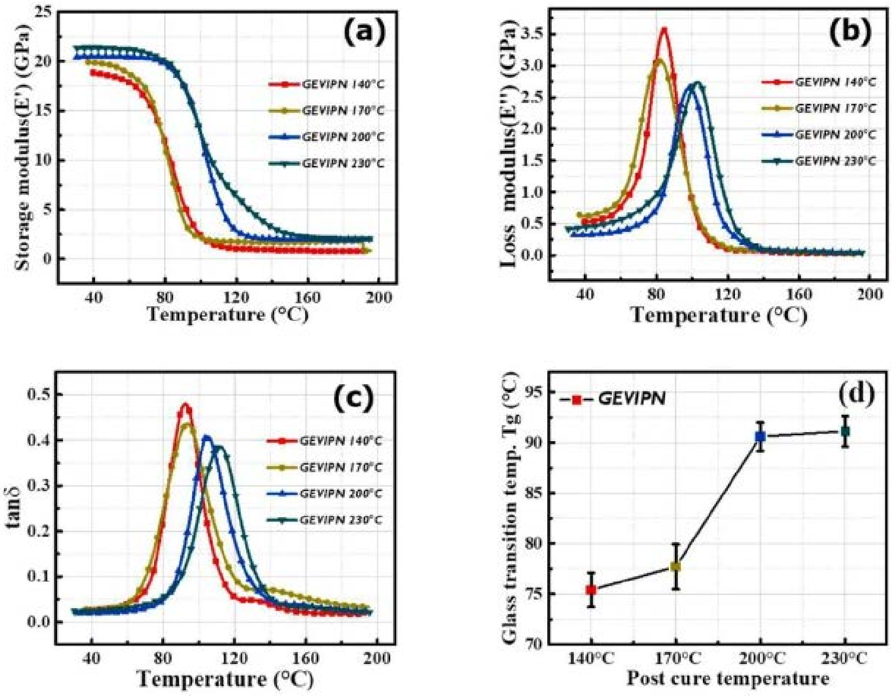

Fig. 7. DMTA results of GEVIPN composites post-cured at different temperatures.

bulk matrix [57]. So, if the curing temperature is higher, then more matrixgetsadheredto thefibersurface, whichisthereas on behindfor the200◦Cpost-curedGEVIPN compositetoexhibit lowerpeakheightof lossmodulus.Duetopost-curingat200◦C, onecannoticethatthereis a shift in Tg (Fig. 7(c)) toward higher temperatures, which indicates the formation of new crosslinks [26]. Additionally, the lower tanδ peak heightof200◦Cpost-curedGEVIPNrevealsgoodadhesionbetween matrix and fiber at the interface.

3.3. Short beam shear (S.B.S)testing

Thehistogram(Fig.8)depictsthattheuseofepoxy-vinylesterIPNas a matrix in glass fiber reinforced composite enhanced the ILSS of GEVIPNcompositecomparedtotheuseofhomopolymer asamatrixin glass fiber reinforced composite. The order of increment in the ILSSis GE, GVE and GEVIPN, respectively. The GEVIPN composite could exhibit a considerable improvement of 21.83% (37.83 0.33 MPa) of ILSS over (31.05 0.27 MPa) GE composite (Fig. 8(b)). It can be deduced that the matrix has a primary role on ILSS of the composite material [54]. Indeed, it is recognized that interlaminar shear failure between fiber and matrix is one of the critical failure modes [54]. Therefore, at the time of loading, generation of large interfacial shear stress between matrix and fiber results in the debonding between fiber and matrix [58]. On the basis of this theory, GE and GVE composites exhibited lower ILSS value owing to the lower generation ofinterfacial shear stress compared to that of GEVIPNcomposite.

For GEVIPN composite to exhibit such remarkable increment was due to the strong interfacial bond existing between the IPN matrix and fiber. Also, the ionic sites of silicon and oxygen atoms present on the surface of glass fiber in the form of silane sizing, impart strong polar active sites resulting into the strong glass fiber and IPN matrix inter- molecular adhesion [59].

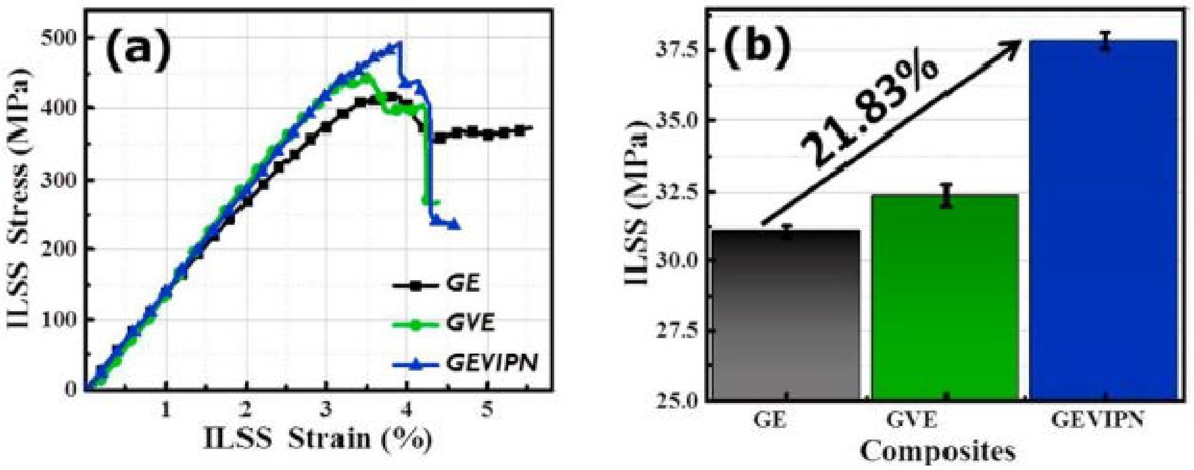

Fig. 8. S.B.S of various GFRP composites (a) stress-strain curve (b) ILSS.

Apart from the strong adhesion, the improved interlocking resulting from the synergism of the mutually entangled networks could also be one of the reasons for such increment [60,61]. The improvedinterfacial interactionresultingfromthepresenceoflowviscousIPN couldwetthe surfaceofglassfiberefficiently, whichcanbelaterconfirmedfrom SEM micrographs. Therefore, for the structures under bending loads where ILSS is considered as important design criteria [54], selection ofmatrix becomes very crucial and to which GEVIPN can act as a potential candidate.

3.4. Tensiletesting

Depicts the tensile response of the experimented GFRP composites. The tensile stress-strain plot is represented in Fig. 9(a) and the tensile strengthandmodulusarededucedfromthisplotandareshowninFig.9(b) and (c), respectively. The tensile test indicated that GEVIPN com- posite exhibited better tensile strength over GE and GVE composites. The increment in the tensile strength of GEVIPN composite was about 22.54% (423.20 3.0 MPa) over GE composite (345.34 1.90 MPa). This performance can be attributed to the formation of entanglements within epoxy-vinyl ester IPN which absorb sufficient energy before transferring it to the fiber during the tensile loading. Additionally, low viscosity of this hybrid resin would impart excellent wet-out on the fibrous surface leading to a better adhesion between fiber and matrix [62]. Although, tensile strength is mostly decided by the nature and volumepercentageofthefiberinthecomposite,buthowwellthematrix present around the fiber is adhered to it also plays a crucial role in the ultimate fiber pull out strength. Therefore, relatively low fiber/matrix adhesion was the reason for GE and GVE composites to exhibit lower tensile strength compared to GEVIPNcomposite.

On the other hand, 11.15% improvement in the tensile modulus (Fig. 9(c)) of GEVIPN composite can also be seen over GE composite.

This improvement can be due to the higher number of crosslinks be- tween the fiber and matrix and same can be the reason for the slight increment in the toughness (Fig. 9(a)) [63]. Additionally, tensile modulus of any composite depends on the modulus of matrix and modulusoffiberwhereinmodulusismaterial’sinherentproperty.Here, althoughthefiberusedwassameforallthe GFRPcompositesbutthe matrix used was different in the GFRP composites. Therefore, the potentialimprovementinthetoughnesscanalsobeduetothelowmodulus of the epoxy where in the crack may continue to grow in the epoxy networkleadingtobifurcationatthevinylesternetworkresultingintoa longer crack path [64]. Fig. 9(d) indicates that there is no significant change in the tensile strain to failure among the experimented GFRP composites.Although,slightimprovementincaseofGEVIPNcomposite can be due to the hindrance provided by the mutual entanglements of the network on the propagation of crack or due to the blunting of the crack as it propagates from vinyl ester network to low modulus epoxy domain[64].

3.5. Flexural testing

OneofthemechanicalperformanceofGEVIPNcompositeisevalu- ated by comparing the flexural properties of the fabricated composites and the details of which are illustrated in Fig. 10. It can be noticed that the effect of blending the polymers has a direct influence on the stress- straincurve(Fig.10(a)).Afterperformingthe3-pointbendtest,GEVIPN compositeyieldedthehighestflexuralstrengthcompared toGEandGVE composites (Fig. 10(b)). The increment in the flexural strength of GEVIPN composite was about 13.43% (384.58 2.20 MPa) over GE composite (339.02 2.30 MPa). The reason behind the GEVIPN com- posite exhibiting such high flexural strength solely depends on the formationofIPNssincetheentanglementsformedabsorbsufficientenergy before the breakage [7]. Additionally, it may even be becausethe crosslinksformedbetweentheepoxy-vinylestermatrixsystemandfiber allowsbetterstresstransferfromthematrixtothefiber.Similaristhe

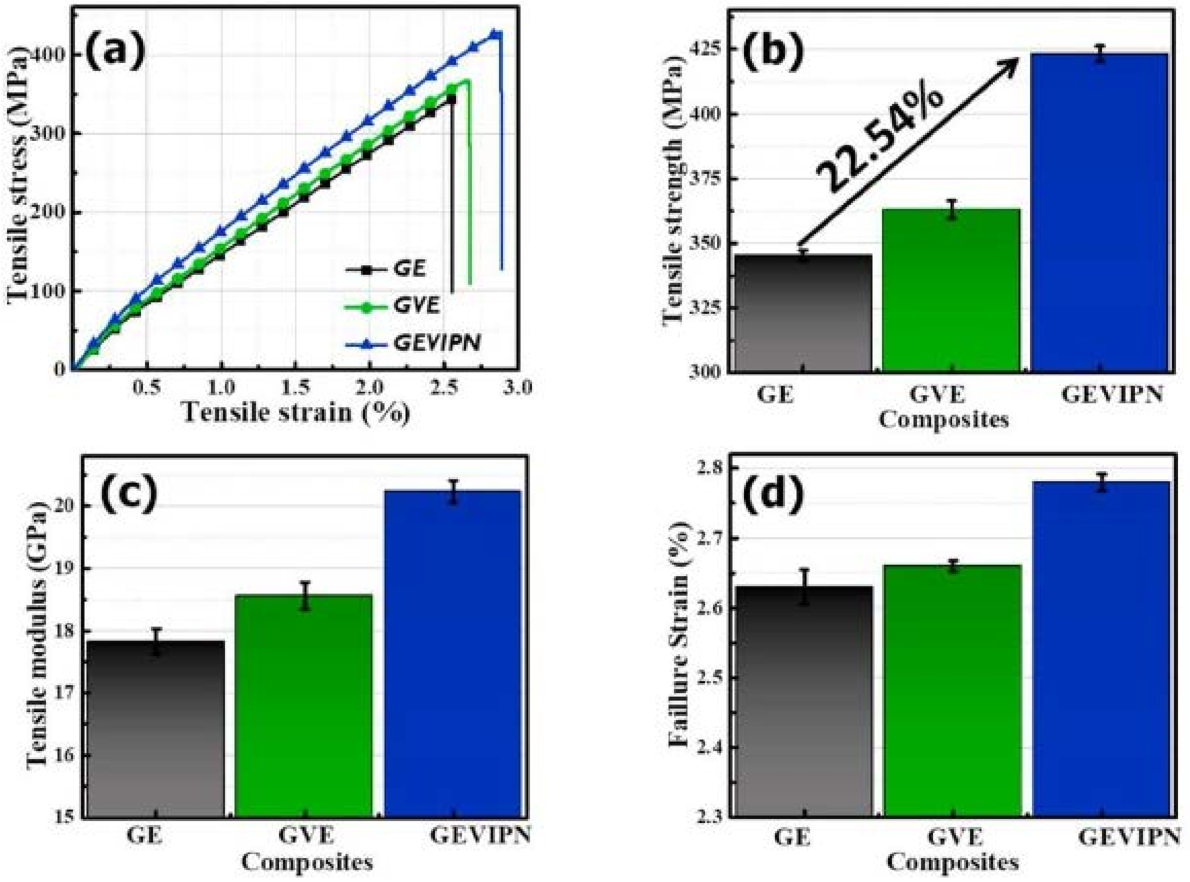

Fig. 9. Tensile properties of various GFRP composites (a) stress-strain curve (b) tensile strength (c) tensile modulus (d) failure strain.

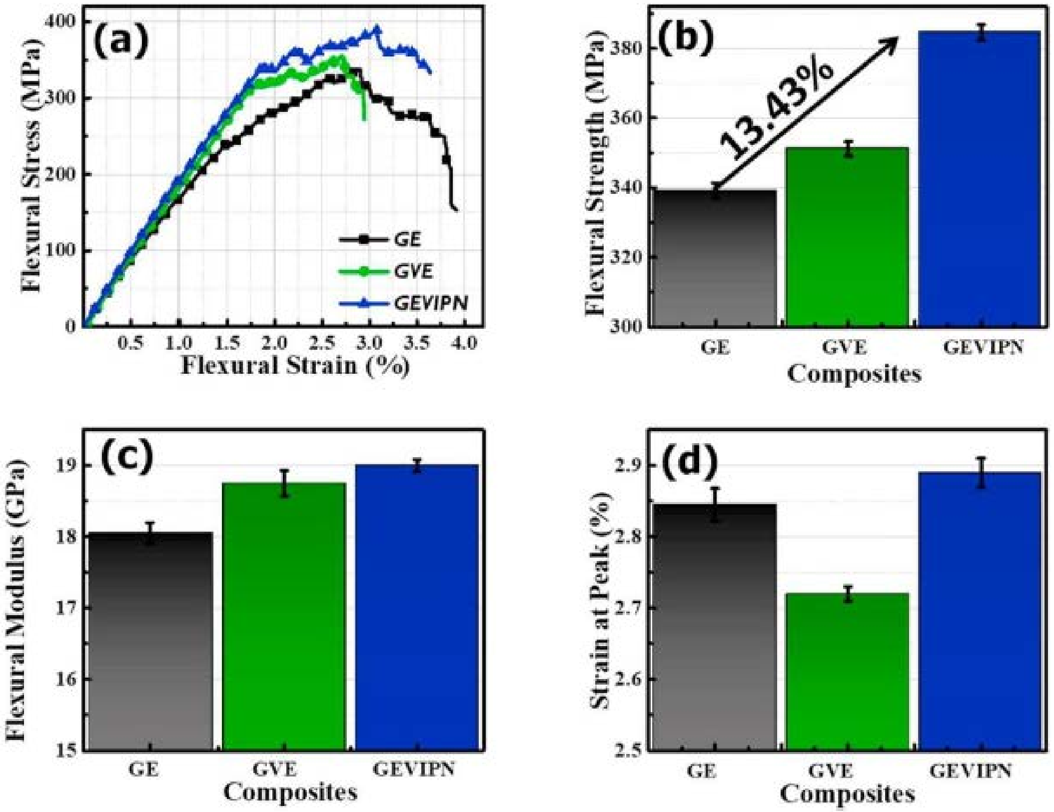

Fig. 10. Flexural properties of various GFRP composites (a) stress-strain curve (b) flexural strength (c) flexural modulus (d) strain at peak.

case in flexural modulus too (Fig. 10(c)) [28]. In case of strain at peak, the GVE composite exhibits lower strain to failure than the GE composite. However, compared to GVE composite, GEVIPN composite exhibited relatively higher value. Therefore, this suggests that vinylester network may fail prior to epoxy network failure. Hence as the system is deformed, the remaining epoxy network may lead to crack bridging and result in to additional energy absorption.

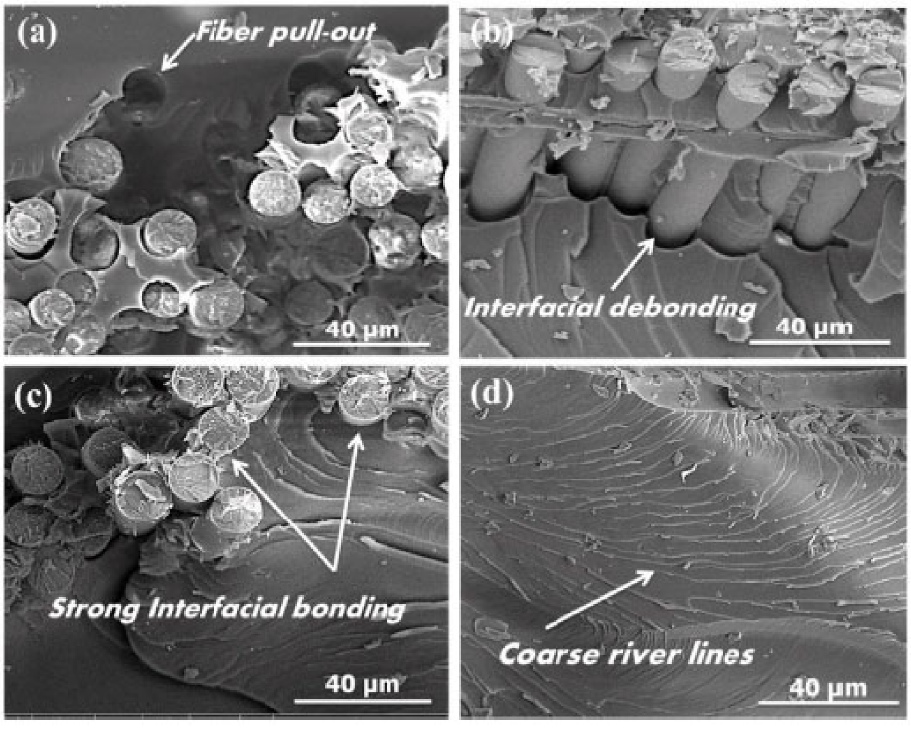

Fig. 11. Fractography images of Flexural tested samples of (a) GE (b) GVE (c) and (d) GEVIPN composites.

3.6. Fractography

The failure morphology of the flexural tested GFRP composites was studied by observing the fracture surface under SEM (Fig. 11). SEM micrograph clearly depicts that the failure of GE composite wasmainly duetofiberpull-out(Fig.11(a))becauseoftheweakinterfacialbonding between the matrix and fiber. Whereas, although GVE composite exhibitedbetterflexuralstrengththantheGEcompositebutasthe loading increased, GVE composite also experienced failure becauseof the interfacial debonding between the fiber and matrix (Fig. 11(b)).

Thesebothsuggestthatinorderforcompositetoexhibithigherflexural strength, strong interfacial bonding should exist between the matrix and fiber.Thiscanexistifthepolymerwetsthefibers'surfaceuniformlyand completely[65].Byblendingthepolymers,onecanseeinFig.11(c)that strong interfacial bonding existed between the fiber and matrix, which revealsthatblendexhibitedhigherwettabilitycomparedtotheindividual polymer. Also, in Fig. 11(d), coarse river lines indicate that the blend matrix underwent large deformation before failure revealing higher stress transfer from matrix to the fiber.

3.7. Fourier transform infrared spectroscopy(FTIR)

The presence of any organic compounds in a polymer can be easily detected from FTIR analysis. The FTIR spectra of GE, GVE and GEVIPN composites is shown in Fig. 12. In this study, the range analysed was mid-IR spectra. Table 3 shows various stretchings associated with the FTIR spectra of GE, GVE and GEVIPN composites.

The peaks at~2871 cm^{-1} and~2968 cm^{-1} of GE, the peaksat~2890cm^{-1} and~3000 cm^{-1} of GVE and the peaks at~ 2871 cm^{-1} and 2968 cm—1ofGEVIPNarethealiphaticC–Hstretching[66]. The presence of thepeakat~1725cm^{-1} confirmed theexistenceofC–Ostretchingofthe carbonyl group in GEVIPN composite. However, in the spectra of GEVIPN composite, the formation of the IPN-structured thermoset ma- trix is confirmed by witnessing the decrease in the peak intensity at 1508 cm—1,~ 1608 cm—1 and~ 3040 cm—1 [27]. Additionally, it is alsoconfirmed with the vanishing of the peak at~910 cm—1 of the C–Ostretching of the oxirane group of epoxy [19]. It may also be noticed that peak~3638 cm—1 resembling the –OH stretching of GVE composite, doesn't appear in GEVIPN FTIR spectra. Therefore, disappearance of the peaks at~910 cm—1 and~ 3638 cm—1 in GEVIPN FTIR spectra,explains that the –OH group of vinyl ester takes part in the reaction with oxirane group of epoxy to form simultaneous IPN structure.

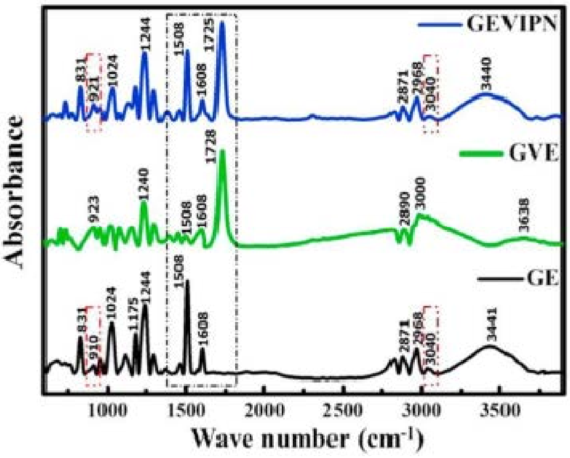

Fig. 12. FTIR spectra of various GFRP composites in the mid IR range.

Composite	Wavenumber (cm^{-1})	AssociatedStretching	References
GE	831	C–O–C stretching of the Oxirane group	[30]
	910	C–OstretchingoftheOxiranegroup	
	1024	Ether'sC–O–Cstretching	[66]
	1175	C–O stretching ofasymmetrical aliphaticgroup	
	1244	C–O stretching of asymmetrical aromaticgroup	
	1508	Aromatic ring's C–Cstretching vibration	[30]
	1608	's C–C stretching Aromatic ring vibration	
	3040	C–H stretching of the methylene group of the Oxirane group	
	3441	O–Hstretching	
GVE	923	Mono-substitutedC‾C stretching	[67]
	1240	C–Ostretching	
	1508	Aromatic ring's C–Cstretching vibration	[30]
	1608	Aromaticring'sC–Cstretching vibration	
	1728	C=O stretching vibration ofthe Carbonyl group	[67]
	3638	O–H stretching	
GEVIPN	831	Oxirane group'sC–O–Cstretching	[30]
	921	Mono-substitutedC–Cstretching	[67]
	1024	Ether'sC–O–Cstretching	[66]
	1175	C–O stretching of asymmetrical aliphaticgroup	
	1244	C–O stretching of asymmetrical aromaticgroup	
	1508	Aromatic ring's C–Cstretching vibration	[30]
	1608	's C–C stretching Aromatic ring vibration	
	1725	C=O stretching vibration ofthe Carbonylgroup	[67]
	3040	C–H stretching of the methylene group of the Oxirane group	[30]
	3440	O-Hstretching	

Table 3
Respective absorption wave numbers of GE, GVE and GEVIPN in the mid IR.

IV. CONCLUSIONS

The present investigation reports on how the formation of IPN in- fluences the overall performance of the GFRP composite. In this study, epoxy has been mixed simultaneously with vinyl ester, both having bisphenol-A diglycidyl structure, which resulted into the formation of IPN-structured thermoset matrix.

1. The experimental results suggested

thatEVIPNmatrixsystemismost suitable matrix for GFRP composite material, and this IPN matrix significantly enhanced overall performance of conventional GFRP composites by strong interpenetrated crosslinking network and possible potential IPN toughening mechanisms (crack bifurcation, crack bridging, network interactions, crack tip blunting), which was developedbyindependentpolymericreactionsandcuremechanism. Moreover,duetothereliableperformance,thisEVIPNmatrixsystem is appropriate and suggestable for other synthetic and natural fiber- basedcomposites.

2. Thecurekineticstudyon GE,GVEandGEVIPN compositeshasbeen done in order to know the optimal cure temperature. This cure ki- netic study is essential for obtaining optimal performance of experimented composites and acts as a base for furtherdevelopment in composite material. Among various post-curing temperatures, 200 ◦C post-curing temperature resulted into optimal flexural per- formance for all experimented composite materials.

3. Additionally, cure kinetic of GEVIPN composite was supported by DMTA analysis. It suggested that storage modulus trend beforethe onset of glass transition temperature was in sync with flexural modulus trend. It also favoured the results that at higher tempera- tures higher crosslinking density is attained.

4. TheformationofIPNwithinGEVIPNcompositemade it exhibitthe highestILSS,tensileandflexuralstrength, comparedtoGEandGVE composites at optimally cured temperature. A figures of 21.83%, 22.54% and 13.43% improvement in ILSS, tensile and flexural strength was recorded by GEVIPN composite over GE composite. Moreover, better reliability has been gained on GEVIPN composite over the homopolymer based composites due to strong interfacial bonding betweenconstituents.

5. The IPN matrix in the GEVIPN composite leads to effective stress transfer between constituents and enhances mechanical perfor- mance. Moreover, this thermoset IPN approach can yield the best solutionfordesignengineers,wherethehigh-performancestructural material with cost-saving is of primaryconsideration.

6. SEM results showed that strong interfacial bonding existedbetween the matrix and fiber for GEVIPN composite, since by blending the epoxy and vinyl ester polymers, proper wettability existed between the matrix andfiber.

7. FTIR spectra confirmed the existence of the reaction between–OH Groupofvinylester and oxiranegroupof epoxytoform simultaneous IPN structure. Italsoconfirmedthattherewasno910cm—1peakinGEVIPN spectra which resembled the C–O stretching of oxirane group ofepoxy.

CREDIT AUTHORSHIP CONTRIBUTION STATEMENT

B.N.V.S. Ganesh Gupta K: Conceptualization, Data curation, Investigation, Validation, Writing - original draft, Writing - review & editing.MritunjayMaharudrayyaHiremath:Datacuration,Valida-tion.BankimChandraRay:Supervision,Resources,Projectadminis-tration,Fundingacquisition.RajeshKumarPrusty:Conceptualization, Supervision, Resources, Project administration, Funding acquisition, Writing - review &editing.

DECLARATION OF COMPETING INTEREST

The authors declare that they have no known competing financial interests or personal relationships that could have appeared toinfluence the work reported in thispaper.

REFERENCES

[1] S.Yashiro,D.Nakashima,Y.Oya,T.Okabe,R.Matsuzaki,Particlesimulationofdual-scale flow in resin transfer molding for process analysis, Compos. Part A Appl. Sci. Manuf. 121 (2017) 283–288, https://doi.org/10.1016/j.compositesa.2019.03.038.

[2] G.Ryzin´ska,M.David,G.Prusty,J.Tarasiuk,S.Wron´ski,Effectoffibre architecture on the specific energy absorption in carbon epoxy composite tubes under progressive crushing, Compos. Struct. 227 (2017) 111292, https://doi.org/ 10.1016/j.compstruct.2019.111292.

[3] M.Sayer,N.B.Bektas¸,O.Sayman,M.Topçu,Anexperimentalinvestigationonthe impactbehaviourofglass/epoxyandhybridcompositeplates,Adv.Compos.Lett.18 (2009) 113–122, https://doi.org/10.1177/096369350901800401.

[4] B.N.V.S.GaneshGuptaK,A.Yadav,M.M.Hiremath,R.K.Prusty,B.C.Ray, Enhancementofmechanicalpropertiesofglassfiberreinforcedvinylestercomposites by embedding multi-walled carbon nanotubes through solution processing technique, Mater. Today Proc (2020) 1–6, https://doi.org/10.1016/j.matpr.2020.01.391.

[5] M.Sayer,N.B.Bektas¸,O.Sayman,Anexperimentalinvestigationontheimpact behavior of hybrid composite plates, Compos. Struct. 92 (2010) 1256–1262,https://doi.org/10.1016/j.compstruct.2009.10.036.

[6] S.Yashiro,Applicationofparticlesimulationmethodstocompositematerials:a review, Adv. Compos. Mater. 26 (2017) 1–22, https://doi.org/10.1080/ 09243046.2016.1222508.

[7] L.M´esz´aros,T.Turcs´an,Developmentandmechanicalpropertiesofcarbonfibre reinforcedep/vehybridcompositesystems,Period,Polytech.Mech.Eng.58 (2014) 127–133,https://doi.org/10.3311/PPme.7237.

[8] A.Tiwari,J.Wiener,F.Arbeiter,G.Pinter,O.Kolednik,Applicationofthematerial inhomogeneity effect for the improvement of fracture toughness of a brittle polymer, Eng. Fract. Mech. 224 (2020) 106776, https://doi.org/10.1016/j. engfracmech.2019.106776.

[9] B.N.V.S.GaneshGuptaK,M.M.Hiremath,R.K.Prusty,B.C.Ray,

Developmentof advanced fiber-reinforced polymer composites by polymerhybridization

[10] technique:emphasisoncurekinetics,mechanical,andthermomechanical performance, J. Appl. Polym. Sci. (2020) 1–11, https://doi.org/10.1002/app.49318.

[11] Yoshimura, T. Nakao, S. Yashiro, N. Takeda, Improvement on out-of-plane impactresistanceofCFRPlaminatesduetothrough-the-thicknessstitching,

[12] Compos. Part A Appl. Sci. Manuf. 39 (2008) 1370–1379, https://doi.org/10.1016/j.compositesa.2008.04.019.

[13] A.L.NazarethDaSilva,S.C.S.Teixeira,A.C.C.Widal,F.M.B.Coutinho,Mechanicalpropertiesofpolymercompositesbasedoncommercialepoxyvinylesterresinand glassfiber,Polym.Test.20(2001)895–899,https://doi.org/10.1016/S0142-9418(01)00018-6.

[14] M.M.Raj,L.M.Raj,P.N.Dave,Glassfiberreinforcedcomposites ofphenolic-urea- epoxy resin blends, J. Saudi Chem. Soc. 16 (2012) 241–246, https://doi.org/ 10.1016/j.jscs.2011.01.007.

[15] S.Ghorui,N.R.Bandyopadhyay,D.Ray,S.Sengupta,T.Kar,Useofmaleatedcastoroil as biomodifier in unsaturated polyester resin/fly ash composites, Ind. Crop. Prod. 34 (2011) 893–899, https://doi.org/10.1016/j.indcrop.2011.02.007.

[16] S. Stelzer, S. Ucsnik, G. Pinter, Composites : Part A Strength and damagetoleranceof composite – composite joints with steel and titanium through the thickness reinforcements, Compos. Part A. 88 (2016) 39–47, https://doi.org/10.1016/j.compositesa.2016.05.020.

[17] P.Jojibabu,Y.X.Zhang,A.N.Rider,J.Wang,B.GangadharaPrusty,Synergetic effects of carbon nanotubes and triblock copolymer on the lap shear strengthof epoxy adhesive joints, Compos. B Eng. 178 (2017) 107457, https://doi.org/ 10.1016/j.compositesb.2019.107457

[18] P.Jojibabu,Y.X.Zhang,B.G.Prusty,Areviewofresearchadvancesinepoxy-based nanocompositesasadhesivematerials,Int.J.AdhesionAdhes.96(2020),https:// doi.org/10.1016/j.ijadhadh.2019.102454.

[19] M.P.Raymond,V.T.Bui,Epoxy/castoroilgraftinterpenetratingpolymernetworks, J. Appl. Polym. Sci. 70 (1998) 1649–1659.

[20] D.J. Hourston, J.M. Lane, H.X. Zhang, Toughening of epoxy resins with thermoplastics: 3. An investigation into the effects of composition on thepropertiesof epoxy resin blends, Polym. Int. 42 (1997) 349–355, https://doi.org/10.1002/ (sici)1097-0126.

[21] J.Jia,Z.Huang,Y.Qin,Dynamicandmechanicalpropertiesofvinylester/epoxy interpenetrating polymer networks, High Perform. Polym. 25 (2013) 652–657,https://doi.org/10.1177/0954008313477878.

[22] H. Ke, L. Zhao, X. Zhang, Y. Qiao, G. Wang, X. Wang, Performance of high- temperature thermosetting polyimide composites modified with thermoplastic polyimide, Polym. Test. 90 (2020) 106746, https://doi.org/10.1016/j. polymertesting.2020.106746.

[23] A.L.N. Da Silva, F.M.B. Coutinho, Some properties of polymer blends based on EPDM/PP,Polym.Test.15(1996)45–52,https://doi.org/10.1016/0142-9418(95) 00012-7.

[24] R.A.Pearson,A.F.Yee,Tougheningmechanismsinelastomer-modifiedepoxies- Part3theeffectofcross-linkdensity,J.Mater.Sci.24(1989)2571–2580,https:// doi.org/10.1007/BF01174528.

[25] N.R. Paluvai, S. Mohanty, S.K. Nayak, Effect of nanoclay on the mechanical, thermal,andwaterabsorption propertiesofanUP-toughenedepoxynetwork,J. Adhes. 92 (2016) 840–861, https://doi.org/10.1080/00218464.2015.1047828.

[26] D.M.Laura,H.Keskkula,J.W.Barlow,D.R.Paul,Effectofglassfibersurfacechemistryonthemechanicalpropertiesofglassfiberreinforced,rubber-toughened nylon 6, Polymer 43 (2002) 4673–4687,https://doi.org/10.1016/S0032-3861(02)00302-6.

[27] K. Dean, W.D. Cook, L. Rey, J. Galy, H. Sautereau, Near-infrared and rheological investigations of epoxy-vinyl ester interpenetrating polymer networks, Macromolecules 34 (2001) 6623–6630,https://doi.org/10.1021/ma010438z.

[28] J.Karger-Kocsis,O.Gryshchuk,N.Jost,Toughnessresponseofvinylester/epoxy- based thermosets of interpenetrating network structure as a function of theepoxy resinformulation:effectsofthecyclohexylenelinkage,J.Appl.Polym.Sci.88 (2003) 2124–2131, https://doi.org/10.1002/app.11946.

[29] K.Dean,W.D.Cook,P.Burchill,M.Zipper,CuringbehaviourofIPNsformedfrom model VERs and epoxy systems: Part II. Imidazole-cured epoxy, Polymer 42(2001) 3589–3601, https://doi.org/10.1016/S0032-3861(00)00745-X.

[30] Y.Liu,Q.Wu,C.Wang,D.Zhou,R.Liang,Y.Kang,Curingbehaviors’characterization of strong and weak crosslinking systems by thermal and dynamic mechanical methods, Polym. Test. 70 (2018) 1–7, https://doi.org/10.1016/j.polymertesting.2018.06.022.

[31] D.S.Kumar,M.J.Shukla,K.K.Mahato,D.K.Rathore,R.K.Prusty,B.C.Ray,Effect of post-curing on thermal and mechanical behavior of GFRP composites, IOP Conf. Ser. Mater. Sci. Eng. 75 (2015), https://doi.org/10.1088/1757-899X/75/1/012012.

[32] M.G.Gonz´alez,J.C.Cabanelas,J.Baselga,ApplicationsofFTIRonepoxyresins-identification, monitoring the curing process, phase separation and water uptake, Infrared Spectrosc. - Mater. Sci. Eng. Technol. 2 (2012),https://doi.org/10.5772/36323.

[33] B.N.V.S.GaneshGuptaK,A.Yadav,M.M.Hiremath,R.K.Prusty,B.C.Ray, Enhancementofmechanicalpropertiesofglassfiberreinforcedvinylestercomposites by embedding multi-walled carbon nanotubes through solution processing technique, Mater. Today Proc. 27 (2020) 1–6, https://doi.org/10.1016/j.matpr.2020.01.391.

[34] R.K.Prusty,S.K.Ghosh,D.K.Rathore,B.C.Ray,Reinforcementeffectofgraphene oxideinglassfibre/epoxycompositesatin-situelevatedtemperatureenvironments: an emphasis on graphene oxide content, Compos. Part A Appl. Sci.Manuf. 95 (2017) 40–53,https://doi.org/10.1016/j.compositesa.2017.01.001.

[35] M.M.Hiremath,B.N.V.S.GaneshGuptaK,B.Sen,R.K.Prusty,B.C.Ray,Effectof in-situtemperaturevariationonmechanicalresponseofglass/vinylestercomposites, Mater. Today Proc. (2020) 1–5, https://doi.org/10.1016/j.matpr.2020.01.595.

[36] D.K. Rathore, R.K. Prusty, S.C. Mohanty, B.P. Singh, B.C. Ray, In-situelevatedtemperature flexural and creep response of inter-ply glass/carbon hybrid FRP composites, Mech. Mater. 105 (2017) 99–111, https://doi.org/10.1016/j.mechmat.2016.11.013.

[37] J. Karger-Kocsis, O. Gryshchuk, S. Schmitt, Vinylester/epoxy-based thermosets of interpenetrating network structure: an atomic force microscopic study,J. Mater.Sci. 38 (2003) 413–420, https://doi.org/10.1023/A:1021855228253.

[38] J.S.Szabo´,J.Karger-Kocsis,O.Gryshchuk,T.Czig´any,Effectoffibresurface treatment on the mechanical response of ceramic fibre mat-reinforced interpenetratingvinylester/epoxyresins,Compos.Sci.Technol.64(2004)1717–1723, https://doi.org/10.1016/j.compscitech.2004.01.006.

[39] A.Yadav,B.N.V.S.GaneshGuptaK,A.O.Fulmali,R.K.Prusty,B.C.Ray,Effectof cure kinetics and nanomaterials on glass fiber/vinyl ester composites: an assessment on mechanical, thermal and fracture morphology, Mater. Today Proc. (2020),https://doi.org/10.1016/j.matpr.2020.02.683.

[40] K. Dean, W.D. Cook, M.D. Zipper, P. Burchill, Curing behaviour of IPNsformedfrom model VERs and epoxy systems I amine cured epoxy, Polymer 42 (2001) 1345–1359, https://doi.org/10.1016/S0032-3861(00)00486-9.

[41] A.Aruniit,J.Kers,A.Krumme,T.Poltim¨ae,K.Tall,Preliminarystudyoftheinfluence of post curing parameters to the particle reinforced composite’s mechanicalandphysicalproperties,Medziagotyra18(2012)256–261,https://doi.org/10.5755/j01.ms.18.3.2435.

[42] G. Furtos, L. Silaghi-Dumitrescu, M.Moldovan, B. Baldea, R. Trusca,

[43] C.Prejmerean,Influenceoffiller/reinforcingagentandpost-curingontheflexural propertiesofwovenandunidirectionalglassfiber-reinforcedcomposites,J.Mater.

[44] Sci. 47 (2012) 3305–3314, https://doi.org/10.1007/s10853-011-6169-1.

[45] ASTM D7264/D7264M-07, Standard test method for flexural properties of polymermatrix composite materials, Annu. Book ASTM Stand. (2007) 1–11, https://doi.org/10.1520/D7264_D7264M-15, i.

[46] ASTMD2344,StandardTestMethodforShort-BeamStrengthofPolymerMatrix Composite Materials and Their Laminates, Annu. B. ASTM Stand. (n.d.) 1–8.https://doi.org/10.1520/D2344_D2344M-16.

[47] ASTM D3039, Standard test method for tensile properties of polymer matrix composite materials, Annu. B. ASTM Stand. (n.d.) 1–13. https://doi.org/10.1 520/D3039_D3039M-17.

[48] ASTM D3171, Standard test methods for constituent content of composite materials,ASTMB.Stand.(n.d.)1–10.https://doi.org/10.1520/D3171.

[49] B.N.V.S.GaneshGuptaK,A.Yadav,M.M.Hiremath,R.K.Prusty ,B.C.Ray, Enhancement of mechanical properties of glass fiber reinforced vinyl ester compositesbyembeddingmulti-walledcarbonnanotubesthroughsolutionprocessing technique, Mater. Today Proc. 27 (2020) 1045–1050, https://doi.org/10.1016/j.matpr.2020.01.391.

[50] R.P. Brill, G.R. Palmese, An investigation of vinyl-ester-styrene bulk copolymerizationcurekineticsusingFouriertransforminfraredspectroscopy,J. Appl. Polym. Sci. 76 (2000) 1572–1582, https://doi.org/10.1002/(SICI)1097-4628(20000606)76:10<1572::AID-APP12>3.0.CO;2-C.

[51] L.Rosu,C.N.Cascaval,D.Rosu,EffectofUVradiationonsomepolymericnetworksbased on vinyl ester resin and modified lignin, Polym. Test. 28 (2009) 296–300, https://doi.org/10.1016/j.polymertesting.2009.01.004.

[52] B.M. Sundaram, R.B. Mendez, M.L. Auad, H.V. Tippur, Quasi-static anddynamicmechanical behavior of transparent graft-interpenetrating polymer networks (graft-IPNs), Polym. Test. 70 (2018) 348–362, https://doi.org/10.1016/j.polymertesting.2018.06.032.

[53] R.A. Pethrick, Composite to Metal Bonding in Aerospace and Other Applications, Woodhead Publishing Limited, 2012, https://doi.org/10.1533/9780857098993. frontmatter.

[54] K.P.Unnikrishnan,E.T.Thachil,Tougheningofepoxyresins,Des .MonomersPolym. 9 (2006) 129–152, https://doi.org/10.1163/156855506776382664.

[55] P.Siva,I.K.Varma,D.M.Patel,T.J.M.Sinha,Effectofstructureon propertiesofvinylesterresins,Bull.Mater.Sci.17(1994)1095–1101,https://doi.org/10.1007/BF02757587.

[56] B.N.V.S.GaneshGuptaK,M.M.Hiremath,R.K.Prusty,B.C.Ray, Developmentof advanced fiber-reinforced polymer composites by polymer hybridization technique:emphasisoncurekinetics,mechanical,andthermomechanicalperformance, J. Appl. Polym. Sci. 137 (2020) 1–11, https://doi.org/10.1002/app.49318.

[57] H.N.NarasimhaMurthy,M.Sreejith,M.Krishna,S.C.Sharma,T. S.Sheshadri,Seawater durability of epoxy/vinyl ester reinforced with glass/carbon composites, J. Reinforc. Plast. Compos. 29 (2010) 1491–1499, https://doi.org/10.1177/0731684409335451.

[58] P.K.Mallick,Fibre-reinforcedCompositesMaterials, ManufacturingandDesign, 1989,https://doi.org/10.1016/0010-4361(89)90651-4.

[59] A.Anˇzlovar,I.Anˇzur,T.Malavaˇsiˇc,Kineticsofformationofpolyurethane/polymethylmethacrylate grafted semi-interpenetrating polymer networks based on the functional prepolymers, Polym. Bull. 39 (1997) 339–346, https://doi.org/10.1007/s002890050157.

[60] K. Jayanarayanan, N. Rasana, R.K. Mishra, Dynamic Mechanical Thermal Analysis of Polymer Nanocomposites, Elsevier Inc., 2017, https://doi.org/10.1016/B978-0- 323-46139-9.00006-2.

[61] M. Akay, Aspects of dynamic mechanical analysis in polymeric composites, Compos. Sci. Technol. 47 (1993) 419–423, https://doi.org/10.1016/0266-3538 (93)90010-E.

[62] M.J. Shukla, D.S. Kumar, D.K. Rathore, R.K. Prusty, B.C. Ray, An assessment of flexural performance of liquid nitrogen conditioned glass/epoxy composites with multiwalled carbon nanotube, J. Compos. Mater. 50 (2016) 3077–3088,https://doi.org/10.1177/0021998315615648.

[63] G.Suresh,L.S.Jayakumari,Evaluatingthemechanicalproperties ofE-Glassfiber/ carbon fiber reinforced interpenetrating polymer networks, Polimeros 25(2015) 49–57, https://doi.org/10.1590/0104-1428.1650.

[64] C.L. Qin, W.M. Cai, J. Cai, D.Y. Tang, J.S. Zhang, M. Qin, Damping propertiesand morphology of polyurethane/vinyl ester resin interpenetrating polymer network, Mater. Chem. Phys. 85 (2004) 402–409, https://doi.org/10.1016/j.matchemphys.2004.01.019.

[65] C.N. Cascaval, D. Rosu, L. Rosu, C. Ciobanu, Thermal degradation of semi- interpenetrating polymer networks based on polyurethane and epoxy maleateof

[66] bisphenol A, Polym. Test. 22 (2003) 45–49, https://doi.org/10.1016/S0142-9418 (02)00047-8.

[67] J. Karger-Kocsis, Simultaneous interpenetrating network structuredvinylester/epoxyhybridsandtheiruseincomposites.Micro-NanostructuredMultiph.Polym. BlendSyst.PhaseMorphol.Interfaces,CRCPress,2005,pp.273–294,https://doi.org/10.1201/9781420026542.ch8.

[68] S.A. Bird, D. Clary, K.C. Jajam, H.V. Tippur, M.L. Auad, Synthesis and characterization of high performance, transparent interpenetratingpolymer networkswithpolyurethaneandpoly(methylmethacrylate),Polym.Eng.Sci.53 (2013) 716–723,https://doi.org/10.1002/pen.23305.

[69] G.R. Weber, Interpenetrating polymer network adhesives, Univ. Washingt.42 (2012) 1–204, https://doi.org/10.1017/CBO9781107415324.004.

[70] R.H. Patel, P.H. Kachhia, S.N. Patel, S.T. Rathod, J.K. Valand, Studies on fabrication of glass fiber reinforced composites using polymer blends, AIP Conf. Proc. 1953 (2018),https://doi.org/10.1063/1.5032874.

[71] P. Maity, S.V. Kasisomayajula, V. Parameswaran, S. Basu, N. Gupta, Improvement in surface degradation properties of polymer composites due topre-processed

[72] nanometric alumina fillers, IEEE Trans. Dielectr. Electr. Insul. 15 (2008) 63–72,https://doi.org/10.1109/T-DEI.2008.4446737.

[73] G.H.Hamcdani,M.Ebrahimi,S.R.Ghaffarian,Synthesisandkineticsstudyofvinyl esterresininthepresenceoftriethylamine,Iran,Polym.J.(English Ed.15(2006) 871–878.

★★★

INVESTIGATION OF CALCIUM UPON ALUMINIUM MOLTEN METAL DENSITY

[1]KASINATH DASMOHAPATRA, [2]ANIL PANDA, [3]ABINASH PANDA

[1]Department of Mechanical Engineering, NMIET, Bhubaneswar, 751019
[2]Department of Mechanical Engineering, CEC, Bhubaneswar
[3]Department of Mechanical Engineering, REC, Bhubaneswar
E-mail: [1]bs.patro@nmiet.ac.in

Abstract - Aluminium molten metal used widely for making aluminium product. This study discusses an investigation into the metal composition effect upon the metal density. But other factor also involved inside it. In this experiment we changed metal composition and other factor remains constant than we find out the effect of composition element upon density.

Keywords- - Brass, Manganese, Silicon, Magnesium, Zinc, Chromium, Nickel

I. INTRODUCTION

Rotary degassing of liquid aluminium alloys is a widely used commercial process to control levels of hydrogen, alkali metals and inclusions in the melt prior to casting. A comprehensive theoretical understanding of the kinetics of aluminium degassing has been established in the past twenty years. Whilst there have been some published experimental tests of degassing theory in molten aluminium, in many cases key pieces of information are not reported or determined, such that a critical assessment of the underlying theory is compromised. Similarly, practical implementation of such understanding in usable shop-floor process models has met with difficulties owing to lack of knowledge concerning some key parameters. These include the stirring intensity dissipated in the melt, and its relationship to the average gas bubble size, and the mass transfer coefficient at the free surface of the melt. A selection of different degassing rotors have been characterised in a comprehensive experimental program. The study resulted in Internet based simulation software for the degassing processes in foundries; the elements of this simulation are presented. Density is the mass of an object per unit of volume. In other words metals with the same mass will occupy less or more space depending on their density. A metal with a high density will occupy a smaller space than a metal with a low density. A metal with a low density will occupy a larger space than a metal with a higher density. Density- Mass divided by volume. M=D/V Aluminum (also known as aluminium) is the most abundant metal element in the earth's crust. And it's a good thing , too, because we use a lot of it. About 41 million tons are smelted each year and employed in a wide arrange of applications. From auto bodies to beer cans, and from electrical cables to aircraft skins, aluminum is a very big part of our everyday lives.

Properties:

- Atomic Symbol:Al
- Atomic Number:13
- Element Category: Post-transitionmetal
- Density: 2.70g/cm3
- Melting Point: 1220.58 °F (660.32°C)
- Boiling Point: 4566 °F (2519°C)
- Moh's Hardness:2.75

Characteristics:
Aluminum is a lightweight, highly conductive, reflective and non-toxic metal that can be easily machined. The metal's durability and numerous advantageous properties make it an ideal material for many industrial applications.A major breakthrough in aluminum production came in 1886 when Charles Martin Hall discovered that aluminum could be produced using electrolytic reduction.Until that time, aluminum had been rarer and more expensive than gold. However, within two years of Hall's discovery, aluminum companies were being established in Europe and America.During the 20th century, aluminum demand grew substantially, particularly in the transportation and packaging industries.Although production techniques have not changed substantially, they have become notably more efficient. Over the past 100 years, the amount of energy consumed to produce one unit of aluminum has decreased 70%.

II. PROPOSED EXPERIMENTAL SETUP

Melt Treatment or liquid prior to pouring in to die plays an important role towards the quality of the casting in term of microstructure, strength, mach inability, freedom from porosity, etc. the melt treatment comprises of

1. Slag/ dross coagulation and their removal using cover fluxes /drossingfluxes.
2. Degassing using tablets or nitrogengas
3. Determination of hydrogencontent.
4. Grainrefining
5. Modification

2.1 EQUIPMENTSUSED

2.1.1 MTS (DEGASSINGMACHINE).

The main used of degassing m/c is to remove hydrogen content from melt. In this machine flow rate, degassing time, rotor r.p.m set early and these are changeable also. In this machine a rotor lance is also used in which inert gas coming from cylinder and its goes inside the melt.

2.1.2 N2 OR ARGONGAS

These two types of gas basically used in degassing process because of low cost and good output. In this process basically inert gas is used. The pressure range is 2-3 bar used according to other factor.

2.1.3 LADLE

Ladle is a vessel contains molten metal inside it. Its capacity 450-500 kg. The molten metal tapping inside the ladle for degassing purpose and then pouring inside the die.

2.1.4 DENSITY INDEX TESTER:- Two sample made one in air and another in vacuum . Air sample solid in air and vacuum sample 80 Mbar pressure and 4 minute time for solid. Density index tester measure gas content in the sample. Computer also connected with this density index tester for keeping record.

2.1.5 SPECTROMETER

The spectro meter is used for the composition checking of the metal. The spectro meter analysis the element percentage of the given sample. The spectrometer required room temp. 22- 28 degree. The metal sample granding first and then checking the composition.

2.1.6 MOLTEN METALCOMPOSITION

Composition of aluminium molten metal

ELEMENT	%
ALUMINIUM	89.5
SILICON	6.44
Fe	.55
Cu	2.52
Mn	.147
Mg	.468
Cr	.012
Ni	.0095
Zn	.268
Ti	.019
Ca	.450
Sr	.010

TOOL FOR METAL CLENAING AND SAMPLE MAKING.

1. Skimmer- it's used for metal cleaning and dross removing from metal.
2. Spoon with long handle it's used for sample taking from ladle.
3. Die is used for making sample for checking metal composition.
4. Grinding machine is also used for sample grinding for metal composition checked.

Element concentration: The element concentration is shown by the following data table in which different % of different components are shown.

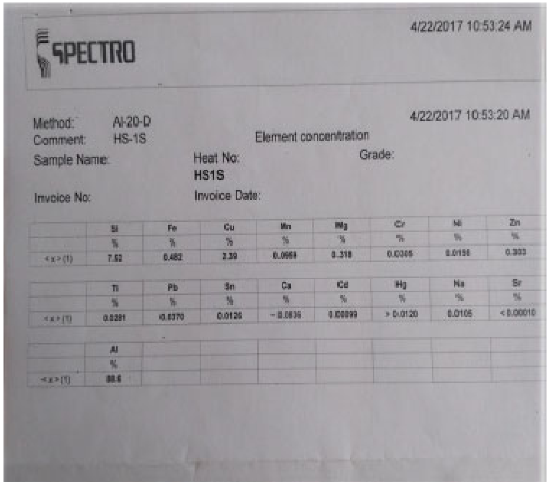

4/22/2017 10:53:24 AM

Method: Al-20-D
Comment: HS-1S
Sample Name:
Heat No: HS1S
Invoice No:
Invoice Date:

4/22/2017 10:53:20 AM

Element concentration

Grade:

	Si	Fe	Cu	Mn	Mg	Cr	Ni	Zn
	%	%	%	%	%	%	%	%
<x> (1)	7.52	0.482	2.39	0.0969	0.318	0.0305	0.0156	0.303

	Ti	Pb	Sn	Ca	Cd	Hg	Na	Sr
	%	%	%	%	%	%	%	%
<x> (1)	0.0281	<0.0370	0.0126	~0.0836	0.00899	> 0.0120	0.0105	< 0.00010

	Al
	%
<x> (1)	88.6

Fig.: element concentration

Additions Calculation:- (Req. Element % - actual element %) x total metal weight/100 . It is the formula used for the correction in metal composition.

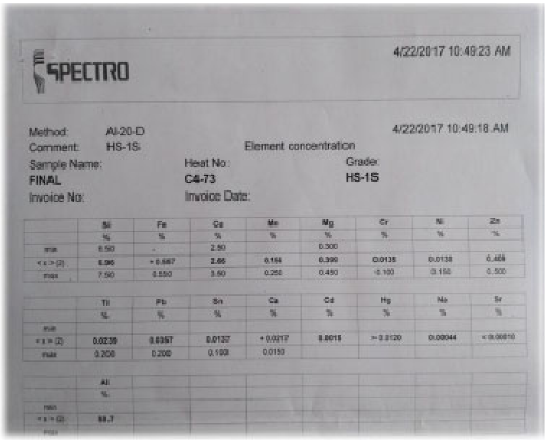

4/22/2017 10:49:23 AM

Method: Al-20-D
Comment: HS-1S
Sample Name: FINAL
Heat No: C4-73
Grade: HS-1S
Invoice No:
Invoice Date:

4/22/2017 10:49:18 AM

Element concentration

Fig.: element concentration with min. and max. value

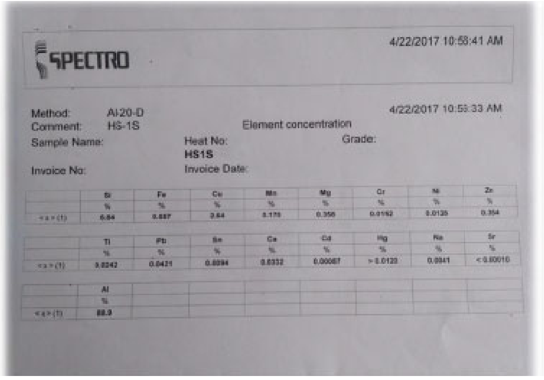

4/22/2017 10:58:41 AM

Method: Al-20-D
Comment: HS-1S
Sample Name:
Heat No: HS1S
Invoice No:
Invoice Date:

4/22/2017 10:53:33 AM

Element concentration

Grade:

Fig.: element concentration addition calculation

Sr.no.	Calcium %	Density index
1	0.0836	3~6
2	0.0606	2~5
3	0.0332	1~3
4	0.0217	1~2.5
5	0.0100	0~2.0
6	0.0040	0~1.5

Table: calcium %and density index come.

III. PROJECT RESULTS ANDDISCUSSIONS

After establishing the value of calcium with density index we can plot a graphical representation as following:

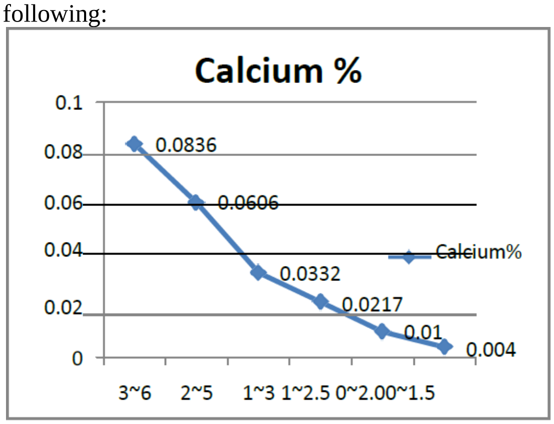

Fig: Density index & calcium %

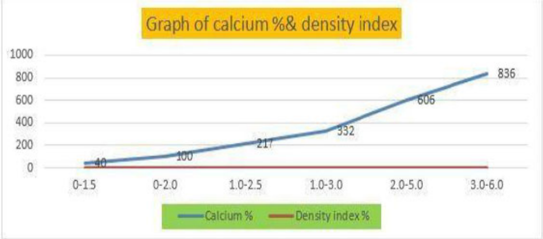

Fig: Graph of calcium % &density index up warding

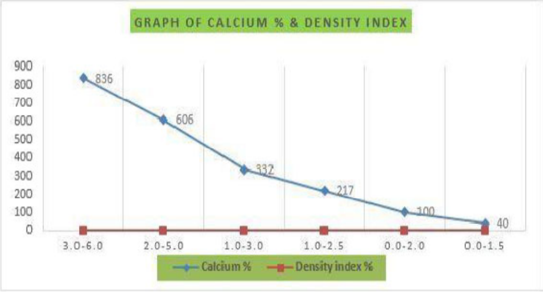

Fig: Graph of calcium % &density index down warding

IV. CONCLUSIONS

Based on the results obtained in this study, the following can be conclude;

1. When density index is less than 1% porosity defect eliminated completely
2. Calcium also found in the silicon with different -different range.
3. The aluminium molten metal composition in which calcium less than 100 % surface appearancegood.
4. Higher calcium % near 700 not good for densityindex.
5. Tensile strength increase when density index less than1%.
6. Influence of different alloy compositions on degassing efficiency.

Thus, it can be safely concluded that the output quality characteristic is greatly improved by the used of less than 100 % calcium in aluminium moltenmetal.
The project work is successfully completed.
It is clear from this study by every element in the aluminium molten metal composition having its impact upon the mechanical properties. From this study scope for future work in many field like

1. Automobile parts like cylinder head and other automobile parts.
2. In Aerospace manufacturing.
3. Construction (windows, doors, siding, building wire, sheathing, roofing,etc.).[
4. Transportation (automobiles, aircraft, trucks, railway, cars, marine vessels, bicycles, spacecraft, etc.) as sheet, tube, and castings.
5. Packaging (foil, frame ofetc.).

REFERENCES

[1] AluminiumAlloyCastings; JG Kaufman and EL Rooy(2005)
[2] The effects of Hydrogen in Aluminium and its Alloys; DEJ Talbot, Maney(2004)
[3] The treatment of Liquid Aluminium SiliconAlloys;
[4] JE Gruzleski and BM Closset, AFS
[5] Melting technology for aluminium gravity die casting
[6] Treatment ofaluminiummelt ;R.VApshankar
[7] Metallurgy of cast aluminium alloys ;Sharad Prakash
[8] L.F. Mondolfo, Aluminium alloy: Structure and properties, Butterworth and Co ltd, London, (1976) 253.
[9] X.Yang, J.D. Hunt and D.V. Edmonds, Aluminium, 69(2)(1993)158.
[10] B.Zluticanin, S.Duric, B.Jordovic andB.Radonjic,
[11] ―Characterization of Microstructure and properties of Al-CuMg alloy‖, Journal of mining and etallurgy,
[12] Vol39, 2003, 509526
[13] A.Garg and J.M. Howe, ―Grain boundary precipitation Al-CuMg-Ag alloy‖ Journal of actametarilia, Vol 40, 1992,2451-2462.
[14] F. Bron, J. Besson, A. Pineau, ― Ductile Rupture in thin sheets of two grades of 2024 aluminiumalloy‖,
[15] Journal of material science &EnggA,2004,356-364
[16] Yang C.Y., Lee S.L., Lee G.K., Lin J.G., Effect of Sr and Sb modifiers on the sliding behaviour of A357 alloy under varying pressure andspeed conditions, Wear, 2006, 261, p. 1348-1358.
[17] Harun M., TalibI.A., DaudA.R., Effect of element additions on wear property of Eutectic aluminium Silicon alloys, Wear, 1996, 194,p.54-59.
[18] DwivediD.K., Wear behaviour of cast hypereutectic aluminium silicon alloys, Mater Des., 2006, 27(7), p. 610-616.
[19] Davis F.A., Eyre T.S., The effect of silicon content and morphology on the wear of Aluminium-silicon alloys under dry and lubricated sliding conditions, Tribology International, 1994, 27(1), p.171-181.

★★★

FIBROBLAST/OSTEOBLAST CO-CULTURE DERIVED BIOACTIVE ECM WITH UNIQUE MATRISOME PROFILE FACILITATES BONE REGENERATION

[1]MOHAMMAD ISRAR, [2]KISHAN DASH, [3]BISWAJIT MOHAPATRA

[1]Department of Mechanical Engineering, NMIET, Bhubaneswar, 751019
[2]Department of Mechanical Engineering, REC Bhubaneswar
[3]Department of Mechanical Engineering, CEC Bhubaneswar
E-mail: [1]pradyut.swain@nmiet.ac.in

Abstract -
Extracellular matrix (ECM) with mimetic tissue niches was attractive to facilitate tissue regeneration in situ via recruitment of endogenous cells and stimulation of self-healing process. However, how to engineer the com- plicate tissue specific ECM with unique matrisome in vitro was a challenge of ECM-based biomaterials in tissue engineering and regenerative medicine. Here, we introduced coculture system to engineer bone mimetic ECM niche guided by cell-cell communication. In the cocultures, fibroblasts promoted osteogenic differentiation of osteoblasts via extracellular vesicles. The generated ECM (MN-ECM) displayed a unique appearance of mor- phology and biological components. The advantages of MN-ECM were demonstrated with promotion of multiple cellular behaviors (proliferation, adhesion and osteogenic mineralization) in vitro and bone regeneration in vivo. Moreover, proteomic analysis was used to clarify the molecular mechanism of MN-ECM, which revealed a specific matrisome signature. The present study provides a novel strategy to generate ECM with tissue mimetic niches via cell-cell communication in a coculture system, which forwards the development of tissue-bioactive ECM engineering along with deepening the understanding of ECM niches regulated by cells for bone tissue engineering.

Keywords - Cell Coculture, Bioactive ECM Matrisome, Bone mimetic microenvironment, Bone regeneration

I. INTRODUCTION

Tissue lost caused by disease, trauma or congenital abnormalities is often beyond self-healing and required transplantation to replace missing form and function [1,2]. Though auto-transplantation is con- sideredasthe“goldstandard”,thehighriskofdonorsitemorbidityand limited source of donor tissues still restricted its application in clinic [3]. To address this issue, tissue engineering was developed to recreate functional biological replacement tissues and organs for theirdamaged counterparts via constructions of biomaterials and signaling cues [4,5]. Among these, the tissue microenvironment has emerged as a key de- terminant of cell behavior and function for the development of func- tional and biomimetic materials [6]. The engineered constructs should provide physical support and biological signals, as well as mobilized endogenous cells for tissue repair [1,2]. Based on these, naturally de- rived materials with appropriate microenvironment are attractive due totheirbiophysicalandbiochemicalcues,andtheirpotentialin
modulation of cell-cell and cell-extracellular matrix (ECM) interactions [4,7–10].These biomaterials providing physiological fashion have been drawn attention as a new generation of biomaterial and biomaterial modification for tissue engineering to induce the formation of func- tional tissue by harnessing endogenous regenerative capacity in situ [3,11].

ECM, secreted by multiple cells in tissues or organs, is a naturally fibrous network of proteins, glycosaminoglycans and proteoglycans precisely arranged in a tissue-specific 3D architecture and provides specialized local microenvironments [12]. Increasing evidences de- monstrated advantages of ECM in tissue engineering and regenerative medicine [3,12,13]. Intrinsic biochemical and mechanical cues in ECM regulated cell phenotype and function in development, in homeostasis and in response to injury [12,14]. Communications between en- dogenous cells and matrix directed the process of tissue regeneration [15–17]. However, the challenge of ECM-based biomaterials is what kind of ECM is the most suitable for specific tissue regeneration and how to obtain the ECM preserving the tissue specific biochemical composition and ultra-structure to promote the formation offunctional tissues for clinical application. Many efforts have been made,including ECM fabrication from different kinds of cell culture, or from whole tissues and organs [18]. Compared with tissue-derived ECM, cell-cul- ture-derived ECM shows faster, easier, cheaper production and more controllable pattern [19]. Less vigorous decellularization also made muchmorepreservationofECMcomposition/structureincell-culture- derivedECM.

Though ECM from various cells (such as human dermal fibroblasts, pre-osteoblasts and BMSCs) have been applied to coat biomaterials for tissue engineering [12,14], the physiological niche in vivo should be a complex system which is comprised of complex ECM affected by cell- cell signaling networks, and further guides multi cellular tissue self-organization and regeneration [20,21]. ECM from single type of cells is hard to mimic tissue microenvironment without cell-cell signaling interactions. While it's common to understand that cellular neighbor- hoods during cell interactions influence cell behavior and have im- portance to stem cell biology and regeneration [21–24], the influence of cell-cell communication on ECM organization and the role of the gen- erated ECM on tissue regeneration was rarely investigated. Coculture system provides a possible way to investigate cell communication in direct or indirect manners [25–27].

Bone remodeling is a highly coordinated process involving com- munication between multiple cell types present in the bone tissue, in- cluding osteoblasts, osteoclasts, fibroblasts, endothelial cells and im- mune cells [28]. Amongst them osteoblasts forming a continuous membrane surrounding bone secrete bone organic matrix and control the matrix environment for mineralization [29]. Osteoblasts at the apical membrane continuously communicate with outsides, including multiple cell communication and signaling transportation, which fi- nally influence bone remodeling and bone regeneration in vivo. One of these influences should be fibroblasts, which are abundant around os- teoblasts in bone tissue and mass accumulated at the beginning ofbone regeneration. Moreover, ECM secreted by fibroblasts has also been demonstrated to promote tissue regeneration, including muscle, nerve, artery and bone tissue [3,30]. However, the communication between osteoblasts and fibroblasts and ECM secreted by them were rarely re- ported.

Here, we cocultured osteoblasts and fibroblasts at different ratios directly to generate complicated ECM to mimic bone local micro- environment. Arrangement and cell-cell communication between two celltypesweremonitoredduringcoculturing.Structureandmatrisome composition of the complicated bone mimetic ECM (BM-ECM) were characterized comprehensively. The effect of BM-ECM on cell pro- liferation, cell adhesion and osteogenic differentiation were in- vestigated respectively. Moreover, SIS scaffolds coated with BM-ECM wereimplantedintomousecalvarialdefectstoassesstheabilityofBM- ECM for bone regeneration invivo.

II. MATERIALS AND METHODS

2.1. Cell culture ANDGENERATION of DECELLULARIZEDECM

MC3T3-E1 cells were cultured in αMEM mediumsupplemented with10%fetalbovineserumandpenicillin(100U/ml)-streptomycin (0.1mg/ml).NIH/3T3cellswereculturedinDMEMmediumsupple- mented with 10% bovine calf serum, 0.1 mM NEAA (non essential amino acid) and penicillin (100U/ml)-streptomycin (0.1 mg/ml).To obtain the coculture of MC3T3-E1 and NIH/3T3 cells (MC/NIH co- cultures),thesetwokindsofcellsweretypsinizedintosinglecellsand mixed together in coculture medium (MC3T3-E1medium:NIH/3T3 medium=1:1,v/v)atthedensityof1.6×105cells/mlwithdifferent ratios of cell number (MC3T3-E1:NIH/3T3 = 9:1, 7:3, 5:5, 3:7,1:9).

The mixed cells were seeded and cultured in tissue culture plates for10 days.Freshmediumwaschangedeveryotherday DecellularizedECMfromMC3T3-E1,MC/NIHcoculturesandNIH/ 3T3 cells was prepared following the decellularization process as re- ported previously [19]. Briefly, Cells were treated with pre-heated triton X-100 at 37 °C for 5 min, and washed with PBS for 3 times. After that, cells were frozen at −80 °C for 40 min and thawed in pre-heated PBS at 37 °C for 40 min, following with PBS washing for 3 times. The freeze/thaw (−80 °C/37 °C) cycles was repeated twice again. All samples were treated with DNase (50 U/ml)/RNase (50 μg/ml) for 2hat37°C,andsubsequentlywashedwithPBSfor3times.

2.2. GeneexpressionASSAY(mRNAANDprotein)

Total mRNA isolation and real-time qPCR performance were oper- atedaspreviouslyreported[31].Briefly,cellswererinsed withPBSand lysed in RNA-Solv Reagent (R6830-02, Omega, Guangzhou, China) according to the manufacturer's instruction. The concentration and purity of mRNA were assessed by UV absorbance at 230 nm, 260 nm and 280 nm using a microplate spectrophotometer. The first-strand cDNAwassynthesizedusingtheTransScriptOne-StepgDNARemoval and cDNA Synthesis SuperMix kit (TransGen Biotech Co. Ltd, Beijing, China).TherelativegeneexpressiononmRNAlevelwasassessedby real-time qPCR with SYBR reagent from TransGen Biotech Co. Ltd and calculated by comparative Ct method (2-(ΔΔC(t))). Actin was introduced as an internal control.

Alkaline phosphatase (ALP) staining was used to assay the activity level of ALP protein in cells as described previously [31]. Immuno- fluorescence staining (IF) was used to visualize protein distribution pattern and protein expression level. Primary antibodies for COL1A1 (ab21286, Abcam, Shanghai, China) and Ocn (ab93876, Abcam) were used. F-actin for cell adhesion assay was stained by phalloidin (Beijing Solarbio Science & Technology Co., Ltd, China) following the manu- facturer's instruction. Working solution of phalloidin was 150 nM. SecondaryantibodiesconjugatedwithAlexaFluor®555 orAlexaFluor® 488 (CST, Shanghai, China) were applied. DAPI was used to show nu- clei,andantifadesolutionwasusedforsamplestocking.

2.3. Fluorescence protein LABELINGAND cell-cell

COMMUNICATIONASSAY

Toidentifytheintercellularcommunicationbetweenfibroblastsand osteoblasts, green fluorescence protein (GFP) and red fluorescence protein (RFP) were used to label cells. MC3T3-E1 and NIH/3T3 cells were cultured on a 24-well plate at the density of 3 × 104 cells/well.

Onnextday,300µLfreshmediumwereaddedintoeachwell, following with1µLauxiliarytransfectionreagentand10µLlentiviruscontaining GFP or RFP expression sequence (ViGene Biosciences, Shangdong, China). Three days later, the labeling cells were passaged and selected bypuromycin(MC3T3-E1,8µg/ml;NIH/3T3,2µg/ml)for7days.GFP- MC3T3-E1 and RFP-NIH/3T3 were imaged under fluorescence micro- scope.

To investigate intercellular communication in MC/NIH cocultures, flow cytometry and transwell-cell culture were introduced. For flow cytometry, GFP-MC3T3-E1 and RFP-NIH/3T3 were cocultured at the ratio of 9:1 (MC:NIH, cell number). The cells in four groups (GFP- MC3T3-E1, RFP-NIH/3T3 and labeled MC/NIH cocultures on day 1or day10)wereseededinto6-wellplate.Thecelldensitywas 1.6 × 105 cells/ml and 2 ml cell suspension solution was added into each well. The cells were typsinized into single cells after culturing and run in a flow cytometer (CytoFLEX, BECKMAN COULTER, CA, USA). The results were analyzed with Flowjo software. For transwell-cell culture, GFP-MC3T3-E1 cells were cultured on the wells in a 24-well plate, while RFP-NIH/3T3 cells were cultured in transwells. Reversely, RFP-NIH/3T3 cells on a 24-well plate and GFP-MC3T3-E1 cells in transwells were performed. The cells on plates were imaged under fluorescence microscope on desired time.

2.4. Morphology of ECMASSAY

Scanning electron microscope (SEM) and atomic force microscope (AFM) were used to observe the surface of ECM. Samples were fixedin 4% paraformaldehyde PBS for 30 min at room temperature, following with PBS washing. After that, the samples were dehydrated in 50%, 70%, 90%, 95% and 100% ethanol for 15 min each, and dried in a frozen vacuum. For SEM scanning, the samples were sputter-coated with platinum and examined under an SEM (SU-70, Hitachi, Japan). AFM (Oxford Instruments, Cypher S) was utilized to determine the height of ECMsurface.

2.5. QUANTIFICATION of ECM proteins ANDGLYCOSAMINOGLYCANS(GAG)

ThetotalECMproteins,collagenproteinsandGAGwerequantified respectively. The ECM from decellularized cells was mechanically de- tached from tissue culture plates, and UA buffer (8 M urea, 150 mM Tris-HCl, pH8.0) was added to lyse the ECM pallet under agitation at 37 °C for 2 h. After cooling, the lysate was sonicated (80W, 10 s on/15 s off, 10 cycles), and then boiled for 15 min. After centrifuged at 14,000 g for 40 min, the supernatant were transferred to a new tube and quan- tified with BCA Protein Assay Kit(Bio-Rad, USA).

CollagenousproteinswerestainedandquantifiedbySiriusRed/Fast Green collagen staining kit (Chondrex, Inc.) as previously [19]. ECM in a 24-well plate was fixed in Kahle fixative (26.7% ethanol/3.7% for- maldehyde/2% glacial acetic acid in distilled water) for 10 min at RT, stained with dye solution for 30 min at RT, and eluted with dye ex- traction buffer in the kit. OD540 and OD605 was measured and used to calculate the amount of collagenproteins.

For GAG content quantification, cells were cultured on a 24-well plate and decellularized. GENMED GAG quantification kit via DMMB (GENMEDscientificsInc.,Wilmington,DE)wasusedto determineGAG content in ECM according to the manufacturer's instructions. Standard GAG samples in the kit were assayed in the meantime to prepare a standardcurve.

2.6. PREPARATION of ECM/SISSCAffolds

Small intestinal submucossa (SIS), a natural collagenous ECM, was usedasanidealbiomaterialwithmultiplemodificationsforbonetissue engineering in our previous papers [32–36]. In the present study, wealso introduced SIS scaffold as a basic biomaterial to investigate the effects of coculture-ECM on bone regeneration in vivo. First, SIS scaf- folds were cut into round constructs measuring 4 mm in diameter by biopsy punches. Lyophilized SIS scaffolds (Cook Biotech, Inc., Weat Lafayette, IN) were rehydrated in complete culture medium for at least 24 h before cell culture. MC3T3-E1, MC/NIH and NIH/3T3 cells were seeded on SIS scaffolds in 96-well plates at 5 × 104 cells/well and culturedfor10days.M-ECM/SIS,MN-ECM/SISandN-ECM/SISscaf- folds were obtained after decellularization and stored at −80°C.

2.7. Mouse CALVARIAL defect model

Healthy adult male C57 mice (8 week) were purchased from SFP Biotechnology Co., Ltd. (Beijing, China). The mice were randomly di- vided into three groups (n = 5). The animals were anesthetized by an intraperitoneal injection of sodium pentobarbital (1%, 50 mg/kg) on a super clean bench. Critical-sized (4 mm) defects were created on the skull, following with implantation of different scaffolds. The mice were sacrificed at 3 and 6 weeks. After that, the skulls were collected sur- gically and fixed in formaldehyde (4%) overnight. Soft X-ray photo- graphs were taken for radiological analysis under IVIS® Lumina XRMS Series III.

2.8. ETHICALSTATEMENT

All experimental procedures involving animals in this study were conductedincompliancewiththeChineselegislationregardingtheuse and care of laboratory animals and were approved by the Animal Care and Use Committee of NingboUniversity.

2.9. SAMPLEHARVESTINGANDHISTOLOGICALSTAINING

The samples were rinsed with PBS and decalcified in 10% (w/v) sodium citrate/22.5% (v/v) formic acid (Morse's solution) for 2 days, neutralized with 5% sodium sulfate for 6 h, and washed with water for 6 h. The samples were then dehydrated, embedded in paraffin, and sectioned(5μm). Hematoxylinandeosin(H&E) stainingwasperformed under standard procedures. Masson's trichrome staining (MTS) was performed according to the manufacturer's instructions of staining kit (Solarbio).

2.10. TANDEMMASSTAG (TMT) technology for QUANTITATIVE proteomic ANALYSIS

TMTlabeledtechnologycouldprovideabetterunderstandingofthe relative expression levels of proteins and proportion of different componentsindifferentgroupsasawhole.ECMfromMC3T3-E1,MC/NIH coculturesandNIH/3T3werecarefullyscrappedfrom6cmplates, and lysed in UA buffer as described in the method of total ECM proteins quantification. The dissolved ECM solution was filtered with 0.22 μm filters and stored at −80 °C. The proteins were separated on a SDS- PAGE gel and visualized by coomassie blue staining. After that, the proteins were undergoing enzymolysis process following filter-aided sample preparation (FASP digestion) [37]. Peptide mixture of each sample (100 μg) was labeled using TMT reagent according to the manufacturer's instructions (Thermo Fisher Scientific). Pierce high pH reversed-phasefractionationkit(Thermo)wasusedtofractionateTMT- labeled digest samples into 10 fractions by an increasing acetonitrile step-gradient elution. Each fraction was injected for nano LC-MS/MS analysis on a Q Exactive mass spectrometer (Thermo) which was cou- pled to Easy nLC (Thermo) for 90 min. MS/MS spectra were in- vestigated with MASCOT engine (Matrix Science, London, UK) em- bedded into Proteome Discoverer 1.4. For GO mapping and functional annotation, the protein sequences of differentially expressed proteins were retrieved from UniProtKB database and locally explored against SwissProt database (mouse). Normalization (−1, 1) of the studied protein relative expression data was used to performing hierarchical clusteringanalysis.ShortTime-seriesExpressionMiner(STEM)analysis was used to investigate the expression tendency of ECM proteins in differentgroups.

2.11. STATISTICALANALYSIS

All quantitative data were expressed as the means ± standard deviation. Statistical analyses were performed using SPSS® software (Chicago, IL). Statistical significance was determined using a one-way analysisofvariance(ANOVA)followedbyaposthoctest(Bonferroni). Apvaluelessthan0.05wasconsideredstatisticallysignificant.

III. RESULTS

3.1. Coculture of OSTEOBLASTSwithfiBROBLASTSENHANCEDosteogenic diffERENTIATION

Osteoblasts and fibroblasts were cocultured directly on tissue cul- ture plates as illustrated in Fig. 1a. Morphology and osteogenic differ- entiation assay were valued at different time points. Special spatial arrangement in the cocultures was observed on day 2, which was not observed on the first day after cell seeding (Fig. 1b). Fibroblasts were

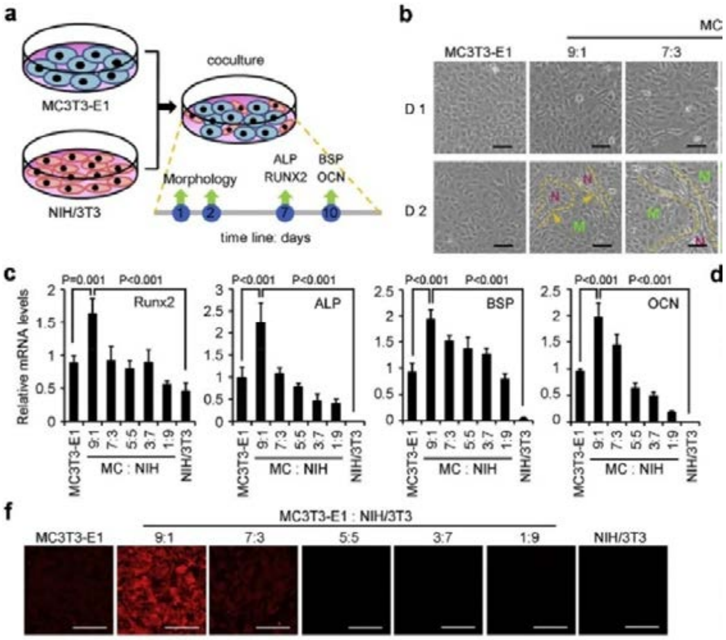

Fig.1.Cocultureofosteoblastsandfibroblastspromotedosteogenicdifferentiation.(a)SchematicdiagramofMC/NIHcocultures.MC3T3-E1(osteoblasts)andNIH/ 3T3 (fibroblasts) were cocultured and characterized as time lime shown. (b) Morphology of coculture cells at different ratios was imaged

by a phase contrast microscopeonday1and2.Green“M”indicatedMC3T3-E1cells;Red“N”indicatedNIH/3T3cells;yellowdottedlineindicatedtheedgebetweenMC3T3-E1and NIH/3T3cells.(c)Real-timeqPCRanalysisofosteogenicassociatedgenes(RUNX2,ALP,BSPandOCN)atdifferenttimepointsasindicatedin(a).MC:MC3T3-E1; NIH:NIH/3T3.ProteinlevelsofALP(blue)andOCN(red)wasanalyzedbyALPstaining(d)andIFstaining(f)respectively.TheactivityofALPindifferentgroupsin 24-well plates was quantified by ImageJ software (e). Images and data are representative of n = 3 individual experiments, and bar heights and error bars were represented as means ± SD. Scale bars: 100 μm(b&e).

presented as vimineous and tended to grow around osteoblast popula- tion. Osteoblasts were separated into smaller population along with higher ratio of fibroblasts. Moreover, osteogenic differentiation was also promoted by coculture, especially at the ratio of 9:1 (MC3T3- E1:NIH/3T3, MC/NIH). The expression of RUNX2 and osteogenic markers(ALP,BSPandOCN)wasthehighestintheMC/NIH(9:1)cells at mRNA levels (Fig. 1c–f). ALP staining was used to analyze the ac- tivity of ALP in different groups (Fig. 1d), and quantification of the staining showed the highest activity of ALP in MC/NIH (9:1) cells (Fig.1e).Consistently,theproteinlevelofOCNwashigherinMC/NIH (9:1) cells than other groups (Fig. 1f). Therefore, our later investigation wasmainlyfocusedonthecocultureofMC3T3-E1andNIH/3T3cellsat the ratio of 9:1 (MC:NIH), the abbreviation of which was MC/NIH co-cultures. However, mineralization was not obvious in all kinds of cell cultures yet (Fig. S1).

3.2. EXTRACELLULARvesiclesMEDIATEcell-cellCOMMUNICATIONfromfiBROBLASTS to OSTEOBLASTS incocultures

Cell-cell communication is essential for cell arrangement and cel- lular activities, and contributes specific ECM formation. To further investigate the intercellular communication in MC/NIH cocultures, os- teoblasts and fibroblasts were labeled with green fluorescence protein (GFP) and red fluorescence protein (RFP) respectively, following with coculture of labeled cells (Fig. 2a). As shown in Fig. 2b, little fibroblasts were found on the first day, while more fibroblasts were observed and arranged around osteoblast population on day 2 in cocultures, consistent with bright field images (Fig. 1b). Fibroblasts grew much faster than osteoblasts in cocultures with the special arrangement pattern until overgrowth on osteoblasts, and orange cells with both FPs (GFP andRFP)wereobservedonday10.However,theappearanceoforange cells may be caused by overlapped cells. To avoid the inaccuracy and makesuretheFPsexpressionprecisely,thecoculturedcellsonday10 were separated into single cells and double positive cells (GFP/RFP) were still visible (Fig. 2c). Moreover, flow cytometric analysis revealed that almost all fibroblasts retained their original red label, while more than half osteoblasts were shifted to become double positive (Fig. 2d&e). The results indicated osteoblasts absorbed RFPs from fibroblasts, which was further determined by transwell assay in Fig. 2f&g. Extracellular vesicles (EVs) with RFPs were secreted by fibroblasts, pene- trated through transwell membrane and observed around osteoblasts underlayer (Fig. 2f). Conversely, no EVs with GFPs were observed around fibroblasts underlayer (Fig. 2g). Moreover, double positive cells were observed in GFP-MC3T3-E1 cells underlayer (Fig. S2a), but still not observed in RFP-NIH/3T3 cells underlayer on day 26 (Fig. S2b). Thus, short distance in direct cocultures enhanced cell-cell commu- nication efficiency, compared with long distance in indirect cocultures (transwell coculture).

3.3. PREPARATIONAND CHARACTERIZATION ofMN-ECM

The specific cell arrangement, cell-cell communication and en- hancement of osteogenic differentiation in MC/NIH cocultures ne- cessarily affected ECM secretion and organization, which might be better to mimic microenvironment in vivo than ECM from single cell type.Todemonstratethehypothesis,ECMfromcocultureсellsorsingle cell type was obtained via decellularization after 10 days as illustrated by Fig. 3a. During decellularization, N-ECM showed low binding affi- nity to tissue culture plates and was easier to be washed away than other two kinds of ECMs. After that, the composition and structure of MN-ECMwerecharacterized(Fig.3b–g).ThemorphologyofMN-ECM was obviously different from M-ECM and N-ECM when scanned by bright field, SEM and AFM (Fig. 3b). Bright field showed most dense structureofMN-ECMbutmostloosestructureofN-ECM,whichreflects the difference of refraction index in ECMs. Under the SEM and AFM scanning,M-ECMwasdensewithroughsurface,whileN-ECMwasflat

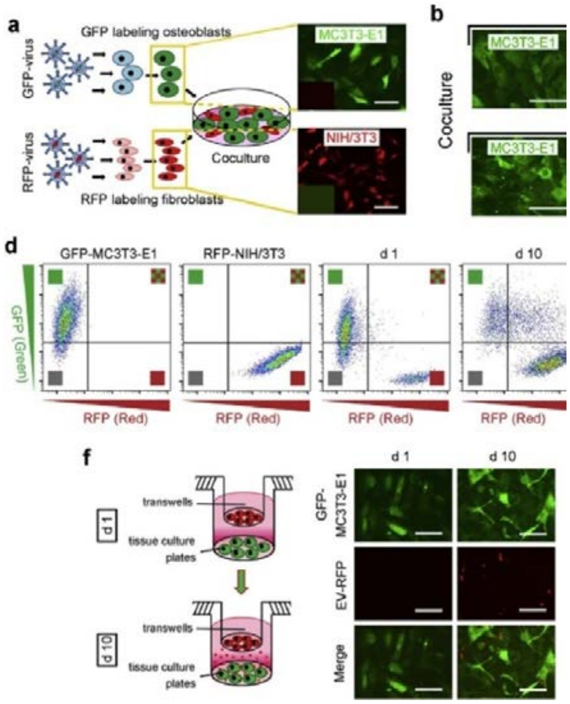

Fig. 2. Extracellular vesicles mediated cell-cell communication from NIH/3T3 to MC3T3-E1. (a) Fluorescence protein labeling of cells via virus transfection. MC3T3- E1 was labeled with GFP, and NIH/3T3 was labeled with RFP. (b) IF images of labeled coculture cells (MC/NIH) under a fluorescence microscope. Green cells were MC3T3-E1 (MC), and red cells were NIH/3T3 (NIH). (c) MC/NIH cocultures were tripsinized into single cells, and were imaged under a fluorescence microscope. Yellow arrows indicated double positive cells. (d–e) Flow cytometry analysis of GFP-MC3T3-E1, RFP-NIH/3T3 and GFP-MC/RFP-NIH cocultures on day 1 and 10. GFP-MC3T3-E1 cells in cocultures on day 10 were smeared, and shifted into double positive area (d), the number of which was ~20% (e). (f–g) GFP-MC3T3-E1 and RFP-NIH/3T3 were cocultured indirectly via transwell system: RFP-NIH/3T3 cells cultured in transwells and GFP-MC3T3-E1 cells cultured on tissue culture plates (f); or GFP-MC3T3-E1 cells cultured in transwells and RFP-NIH/3T3 cells cultured on tissue culture plates (g). Cells on tissue culture plates were imaged. Images and data arerepresentativeof n=3individualexperiments,andbarheightsanderrorbarsrepresentmeans±SD.Scalebars:100μm.

withlittleholes. MN-ECMcombinedandreorganizedthesetwokindsof ECMs.Consistently,thedistributionof COL1A1fibersinMN-ECMalso combineddenseappearanceinM-ECMandlooseappearanceinN-ECM withacertainorganization(Fig.3c).OCN,animportantECMproteinin bone tissue, was not expressed in N-ECM, and the distribution was distinct between M-ECM and MN-ECM. We further quantified total protein content (Fig. 3d) and GAG content (Fig. 3e) in three kinds of ECM. MN-ECM showed the highest level among them. Moreover, the distribution of whole collagen proteins were differed from each other (Fig. 3f) and the collagen content was quantified accordingly (Fig. 3g). The collagens were schistose in M-ECM, while they were loose in N-ECM. In MN-ECM, the collagens were presented as net shape with the highest content. The specific morphology and structure of MN-ECM might be caused by the alteration of cellular activities, which were affectedbycell-cellcommunicationinthecocultures.

3.4. Cell BEHAVIORS REGULATED by MN-ECM in vitro

To investigate the guiding effect of coculture ECM on cells in comparisontothatofECMfromsinglecelltype,BMSCsandosteoblasts were seeded on M-ECM, MN-ECM and N-ECM respectively and cell behaviors including cell proliferation, cell adhesion and osteogenic differentiation were assessed (Fig. 4a). At first, we assessed the effect of coculture ECM at different ratios (MC:NIH) on cell proliferation (Fig. 4b–c, Fig. S3). Consistent with cell behaviors in coculture system (Fig. 1a), MN-ECM at the ratio of 9:1 showed the best promotion on BMSCs proliferation on day 3 and 5 (Fig. 4b), and on osteoblasts proliferation on day 4 and 7 (Fig. 4c), compared with other ratios and single cell type secreted ECM. Proliferation rate was highest on MN-ECMat9:1inbothBMSCsandosteoblastsatearlyandmiddlestage, but was similar in all groups at a low level at late stage in osteoblasts (Fig. S3a&b). No significant difference was observed in fibroblasts cultured on different ECMs (Fig. S3c). Thus, we also mainly focused on guiding effects of cell behavior on MN-ECM at 9:1 ratio later.

Cell adhesion was assessed by F-actin staining at different time points (1 h, 4 h and 24 h) (Fig. 4d–i). Cells on MN-ECM exhibited specific appearance, which was different from that on other two kinds of ECMs. For BMSCs, much more pseudopodia were apparent in the cellsonMN-ECMthanthoseonM-ECMandN-ECMat4h(Fig.4d).By 24 h, the cells on MN-ECM were vimineous, while the cells on M-ECM andN-ECMwerespreading(Fig.4d).Consistently,perimeterof cellson MN-ECM was much longer than that on M-ECM or N-ECM (Fig. 4f), though no significant difference of area was observed between three groups(Fig.4e).SimilartoBMSCs,osteoblastsonMN-ECMalsoshowed a unique appearance which was vimineous at 24 h (Fig. 4g). The differencewasthatpseudopodiawereapparentinosteoblasts onMN-ECM asearlyas1h,whichwasmorethanthatonN-ECMandnotapparentin the cells on M-ECM. Moreover, statistical analysis showed higher area of osteoblasts on MN-ECM at 1 h, and lower area by 4 h and 24 h, compared with M-ECM group (Fig. 4h), while perimeter of cells was longest in MN-ECM group (Fig.4i).

Mineralization is important for osteogenic differentiation in vitro andboneregenerationinvivo.AlizarinredSstainingwasusedtoassess themineralizationinBMSCsandosteoblastsculturedondifferentECMs (Fig. 4j-m). MN-ECM significantly enhanced the mineralization of BMSCsat2and4weeks(Fig.4j&k).Forosteoblasts,calciumdeposition was also the highest in the cells on MN-ECM at 4 weeks, but the mi- neralization ability of osteoblasts was lower than that of BMSCs (Fig. 4l &m).

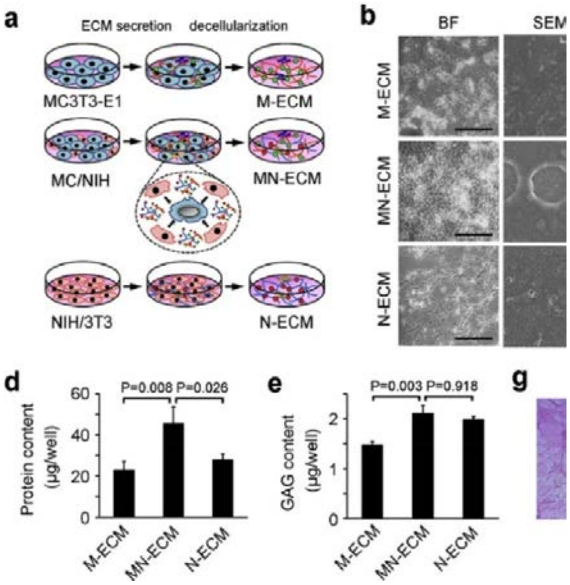

Fig. 3. Generation and characterization of ECM from secreted single cell type or cocultured cells. (a) Schematic diagram of cell-secreted ECM generation. Single cell type (MC3T3-E1 or NIH/3T3) or MC/NIH cocultures were cultured on tissue plates for 10 days to generate ECM. Complicated ECM was secreted by MC/NIH cocultures because of cell-cell communication. Decellularization was introduced to remove cells and ECM was left. (b) ECM morphology was characterized by phase contrastmicroscope(brightfield,BF),scanningelectronmicroscope(SEM)andatomicforcemicroscope(AFM).Scalebars:50μm(BF); 2μm(SEMandAFM). (c)IFstainingofCOL1A1andOCN.Scalebars:20μm. BothdenseandloosecollagenfiberswereobservedinMN-ECMandseparatedbywhitedottedline.(d–f)Total proteincontent (d)andGAGcontent (e) inECMson24-wellplateswereassessed. (f–g)Collagenfiberswerestainedasred(f).CollagencontentinECMson24-well plates was quantified according to the instructions of Sirius Red/Fast Green collagen staining kit. Scale bars: 40 μm. Images and data are representative of n = 3 individual experiments, and bar heights and error bars representmeans ± SD.

3.5. Bone REGENERATION promoted by ECM modified SCAffoldsinvivo

SISscaffoldswereornamentedwithM-ECM,MN-ECMandN-ECMin situ, and the complex constructs were implanted in a mouse calvarial defectmodel(Fig.5a).X-rayanalysisshowedsignificantcalcifyingnew bone formation in the middle of the defects with MN-ECM scaffolds implantation (Fig. 5b). Statistical analysis revealed MN-ECM was the most beneficial for calvarial bone regeneration in comparison to the ECMs secreted by single cell type (M-ECM and N-ECM) (Fig. 5c). His- tological evaluation with H&E (Fig. 5d) and Masson trichromestaining (MTS) (Fig. 5e) further demonstrated the promotion of MN-ECM in bone repair. The newly formed bone with typical structure as sparse osteocytes embedded in lacunas with osteoblasts lining the outer edge of the bone tissue was observed in all three ECM scaffolds at 6 weeks (Fig. 5d). However, marrow cavities or blood vessels were only pre- sented in the defects with MN-ECM scaffolds (Fig. 5d). Bone formation ratio was also higher after implantation of MN-ECM scaffolds, com- paredwithimplantationofM-ECMorN-ECMscaffolds(Fig.5f).Newly formed collagenous fibers in MN-ECM scaffolds were much more than thatinM-ECMandN-ECMscaffoldsat3weeks(Fig.5e&g).By6weeks, newlyformedcollagenousfiberswereobservedinallkindsofECMs(M- ECM, MN-ECM and N-ECM) (Fig. 5e). Consistent with H&E staining, marrowcavitiesorbloodvesselswereapparentinthedefectswithMN- ECM scaffolds (Fig. 5e). The results indicated MN-ECM provided the most suitable microenvironment to mimic bone tissue niche for bone regeneration invivo.

3.6. ECM secreted by MC/NIH cocultures DISPLAYEDA specific MATRISOME SIGNATURE

To investigate the molecular mechanism of the generated complex ECM in coculture system (MN-ECM), the protein composition inECMs was comprehensively characterized by proteomic analysis (Fig. 6). Quantitative proteomic approaches by labeling TMT was performed to evaluate the relative abundance of ECM proteins among three kinds of ECMs. Total 178 ECM proteins were identified, of which 80 proteins were core matrisome proteins and 98 proteins were matrisome-asso- ciated proteins (Fig. 6a). Though the number of core matrisome pro- teinswaslessthan50%,theproteinabundance(PSMs)oftheseproteins was more than 80%. In addition to the core matrisome proteins, the ECMs served as a reservoir for regulators, secreted factors and other ECM-affiliated proteins were less abundant but with more kinds of proteins. Statistical analysis showed 124 proteins were assessed with significant difference among three kinds of ECMs (M-ECM, MN-ECM and N-ECM) (Fig.6b).

The expression of ECM proteins was presented in the format of a heat map (Fig. 6c), and short time-series expression miner (STEM) was introduced to analyze the results (Fig. 6d). In the present study, the ECM proteins were separated into four clusters according to their ex- pressiontendency.Sixty-twoproteinswereexpressedhighestinM-ECM with major core matrisome proteins (cluster 1), while only 19 proteins were expressed highest in N-ECM with major matrisome-associated proteins (cluster 4).

Interestingly, 28 proteins were assessed as highest expression (cluster 2) and 12 proteins were assessed as lowest expres- sion (cluster 3) in MN-ECM. The STEM in each sub-category of ECM proteins was also presented and each ECM protein was listed (Figs. S4–S9). The ratio of proteins in cluster 2 was higher in collagens, proteoglycans, regulators, affiliated proteins and secreted factors than the ratio of that in total proteins, only except glycoproteins (Fig. S10). To further define the specific protein composition in MN-ECM, thefold change of ECM proteins in cluster 2 and cluster 3 was listed from high to low in Fig. 6e&f respectively. The top 17 ECM proteins expressed highest in MN-ECM were mainly matrisome-associated proteins, besides3corematrisomeproteins(VTN,DCNandCOL24A1).Theresults indicated core matrisome proteins mainly depended on cell type, and the expression of these proteins tended to be stable relatively without great changes. The function of MN-ECM might be mainly regulated by matrisome-associatedproteins.

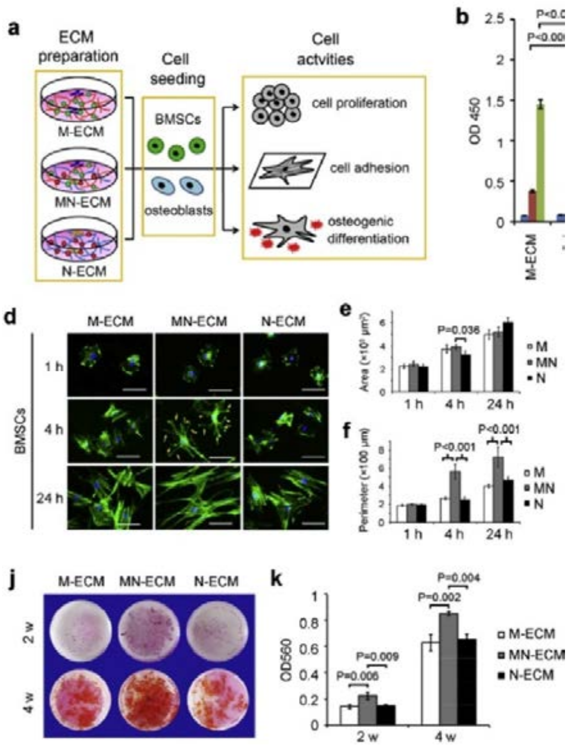

Fig. 4. Bone mimetic ECM engineered by cocultured cells facilitated cell proliferation, adhesion and osteogenic differentiation. (a) Schematic diagram of cellular guiding effects of ECM on cell proliferation, adhesion and osteogenic differentiation. M-ECM, MN-ECM and N-ECM were prepared, following with seeding of BMSCs and osteoblasts to assess the effects. (b–c) MN-ECM promoted cell proliferation of BMSCs (b) and MC3T3-E1 (c), especially at the ratio of 9:1 (MC:NIH) (n = 6). (d–i) Cell spreading morphology of BMSCs (d–f) and MC3T3-E1 (g–i) on MN-ECM (9:1) was unique. F-actin of BMSCs (d) and MC3T3-E1 (g) was stained by FITC-phalloidin. Representative images were shown. Scale bars represented 50 μm. Cell area (e&h) and cell perimeter (f&i) were calculated based on images by ImageJ software. Twenty cells (n = 20) were measured for each individual samples and four individual experiments (n = 4) were performed for each group. (j–m) MN-ECM (9:1) promoted osteogenic mineralization of BMSCs (j&k) (n = 3) and MC3T3-E1 (l&m) (n = 4). BMSCs were cultured in osteogenic induction medium (100 nM dexamethazone, 50 μg/ml ascorbic acid and 10 mM β-glycerophosphate). Mineralization was stained by Alizarin red S and captured by a camera (j&l). The stained dyewasextractedwithcetylpyridiniumchlorideandmeasuredat560nm(k&m).

GOanalysisofproteinsincluster2and3suggestedMN-ECMmight contribute to multiple biological process of cells (including biological adhesion, cell proliferation, cell differentiation, cell migration, angio- genesis and immune system) (Fig. 6g, Table S1&S2) and molecular functions (including protein binding, iron binding and ECM binding) (Fig. 6h, Table S3&S4). Moreover, 15 ECM proteins in cluster 2 and 3 were specifically associated with calcium iron binding among iron binding, which might contribute to osteogenic mineralization (Table S3 &S4).

IV. DISCUSSION

Accumulated researches introduced ECM-like scaffolds with tissue mimetic niches for tissue regeneration via recruitment of endogenous cells [2,38]. Compared with artificial ECM with single or a few com- positions, natural ECM secreted by cells harbored a complex network including collagen fibers, glycoproteins, cytokines and proteoglycans under ordered arrangement, and contributed the process. Here, we coculturedfibroblastsandosteoblaststogenerateacomplexECMunder guidance of unique cell arrangement and cell-cell communication (Figs. 1–4), which effectively regulated proliferation, attachment and osteogenicdifferentiationofBMSCsandosteoblastsinvitro (Fig.5),and enhanced bone regeneration in vivo (Fig. 6). The complex ECM gener- ated in a coculture system represents several unique advantages: (1) betterguidanceofmultiplecellarrangementthansinglecellculture; (2) tissue mimetic niche organized by multiple cells under cell-cell communication; (3) easy operability and controllability with low immunogenicity after implantation in vivo; (4) extensive application with different cell composition depended on tissue properties and (5) surface modification on multiple biomaterials as “off-shelf” implants after decellularization.

Tissues are composed of ECM with mechanical and physiological support, and multiple cells with accurate organization. The arrange- ment of different cells is essential for tissue ECM generation with un- ique microenvironment. In the present study, fibroblasts and osteo- blasts were cocultured together and unique cell arrangement was formed along with alteration of cellular activities (Fig. 1). In the co-culture system, fibroblasts grew fast around osteoblasts and osteogenic maturation of osteoblasts was stimulated by surrounding fibroblasts due to the specific cell order and cell-cell communication. Previously, a gold standard coculture model was tranwell culture. The model was beneficial to investigate paracrine pathways between different cells,but blockedcellinteractionandcellarrangementwhichlimitedapplication in tissue regeneration. Later studies ever did efforts to arrange different cells together in a specific order artificially. For example, HUVEC and MSCs were mixed into fibrin bioinks and printed HUVEC fibers and MSCs fibers alternately in a round shape [26]. Here, we found fibro- blasts and osteoblasts could form circle-surrounding construct sponta- neously via their own activities which should be closer to clarify cell- cell communication naturally. Accordingly, recent studies introduced coculture of multiple cells direct together to mimic tissues in vivo [27,39,40]. Myoblasts were cocultured with hMSCs to induce trans- differentiation under electric field stimulation [27]. Coculture of glioblastomacellsandendothelialcellsmimickedtumornichetoincrease glioblastoma cell proliferation and to decrease endothelial cell expres- sion of cell adhesion proteins [39].

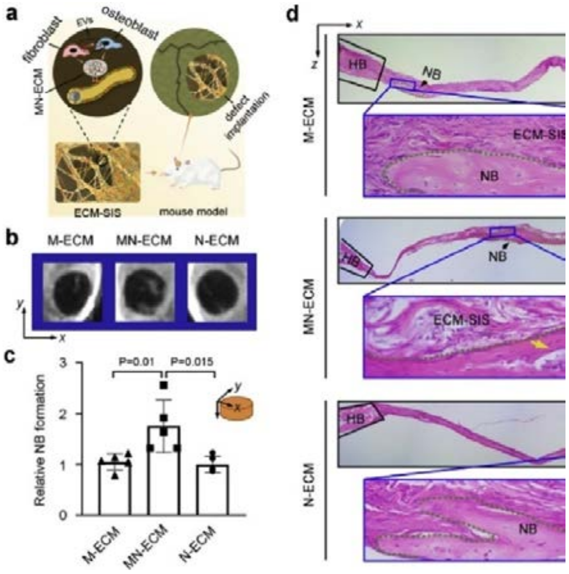

Fig. 5. Bone mimetic ECM engineered by cocultured cells enhanced bone regeneration in vivo. (a) Schematic diagram of ECM ornamented SIS scaffolds implanted into mouse cavarial defects (Φ = 4 mm). The tissues with defects were collected after 3 or 6 weeks. (b–c) X-ray images of defects implanted with ECM-SIS scaffolds (M-ECM, MN-ECM and N-ECM) (n = 5) at 6 weeks (b). The relative new bone formation was calculated by normalization to new bone formation area in the defects with M-ECM scaffolds at 6 weeks, which was measured by ImageJ software (n = 5) (c). (d) H&E staining of the cross-sections to show the histological morphology of the regenerated defects at 6 weeks. Green dotted region represented newly formed bone (NB) (black arrow). The blue boxes were magnified to present the details of NB. HB: host bone; yellow arrow: marrow cavity. (e) MTS staining of the cross-sections of the regenerated defects at 3 and 6 weeks. Newly formed collagens were visualized as blue and newly formed mature bones were visualized as red. (f) Bone formation ratio was measured by ImageJ software based on H&E staining of cross-sectionsofthedefectsat6weeks.Sectionswithnewlyformedbonewere measuredforeachmouseand5micewereanalyzedforeachgroup. (g)Collagenareawith blue color and the whole scaffold area were measured by ImageJ staining, and the ratio was calculated. Five random fields were measured for each mouse and 5 mice were analyzed for each group. Scale bars represented 50 μm.

The advantage of coculture in vitro is convenient to regulate the cell ratio to achieve the best effects. In this study, we designed multiple ratios of osteoblasts and fibroblasts, and 9:1 (MC:MIH) of the seeding ratio was demonstrated to be the best with the highest expression of osteogenic differentiation markers. The advantage of coculture in vitro is convenient to regulate the cell ratio to achieve the best effects. In this study, we designed multiple ratios of osteoblasts and fibroblasts, and 9:1(MC:MIH)oftheseedingratiowasdemonstratedtobethebestwith the highest expression of osteogenic differentiation markers. Inthe cocultures, osteoblasts and fibroblasts were undergoing different cell fates. Osteoblasts were mainly undergoing osteogenic differentiation, along with up-regulation of differentiation markers and alteration ofcell morphology (Figs. 1 and 2b). However, proliferation of osteoblasts was inhibited at the meantime. Then, fibroblasts in the cocultures were mainly undergoing cell proliferation (Fig. 2). The cellular activities of osteoblasts and fibroblasts during the coculturing led to the ratio al- teration as the higher ratio of fibroblats and lower ratio of osteoblasts on day 10 (Fig. 2d&e). Even though, the seeding ratio of 9:1 (M:N) was demonstrated with the highest activities of osteogenic differentiation (Fig. 1) and the derived ECM was considered as the best for cell pro- liferation (Fig. 5b&c).There are two possibilities: (1) A small amount of fibroblasts at the beginning is important to trigger the activities of os- teoblasts. Then, the proliferation of fibroblasts and cell-cell communications further promotes the events. (2) Osteoblasts secrete the major functional ECM proteins for bone regeneration. Higher amount of fi- broblasts diluted the roles of osteoblasts. Proper ratios of osteoblasts and fibroblasts are essential for the functionsof the cocultures.

IntheMC/NIHcoculturesystem,it'sinterestingtofindthat thecell- cell communication was not bi-directional, but mainly unidirectional from fibroblasts to osteoblasts via EVs (Fig. 2). Double staining cells mainly shifted from GFP-osteoblasts after absorbing RFP secretedby fibroblasts. Transwell coculture demonstrated EVs as messengers from fibroblasts to osteoblasts. However, the communication was much slower than coculture together (Fig. S2), which indicated other inter- actions occurred between the two cell types. It's common that cell-cell communication is the key for higher-order biological functions inmulticellular tissues [41,42]. Coculture system provides the opportu- nity to study the mechanisms of cell-cell communication and multicellular behaviors. In coculture system, cell fate in recipient cells was directed by the cell-cell communication to support a differentiated function, including paracrine, exosomes or EVs, and direct cell-cell interactions via transmembrane proteins [41]. Consistent with our study, juvenilechondrocytes(CHs)incoculturewithadultmesenchymalstem cells (MSCs) improved chondrogenesis of MSCs via EVs from CHs to MSCs and promoted cartilage engineering[25].

Our previous studies focused on the effects of single cell type behavior on ECM secretion and ECM-ornemented biomaterials for bone regeneration [34–36]. Compared with ECM from single cell type, ECM from multiple cells presented multiple advantages due to multiple cell organization and cell-cell communication mentioned above. Cumulative evidences have demonstrated the interactions between two cell typesimprovedECMremodeling[25,43].ECMprovidingcomplexlocal heterogeneous microenvironments modulated cellular activities via cell-matrix interactions [44,45]. The composition and structure of ECM dependedoncelltype,localenvironment,availabilityofsubstratesand shear forces [46,47]. Spatial, chemical and mechanical cues in ECM influencedcell-ECMinteractionsviaactivationofintracellularsignaling cascades and further affected cellular behaviors [48]. Consistently, our presentstudydemonstratedtheECMgeneratedbyMC/NIHcocultures possessed unique structure and molecular composition (Figs. 3 and 4) and was beneficial for cell proliferation, adhesion and osteogenic differentiation (Fig. 5), and further promoted bone regeneration in vivo (Fig.6).

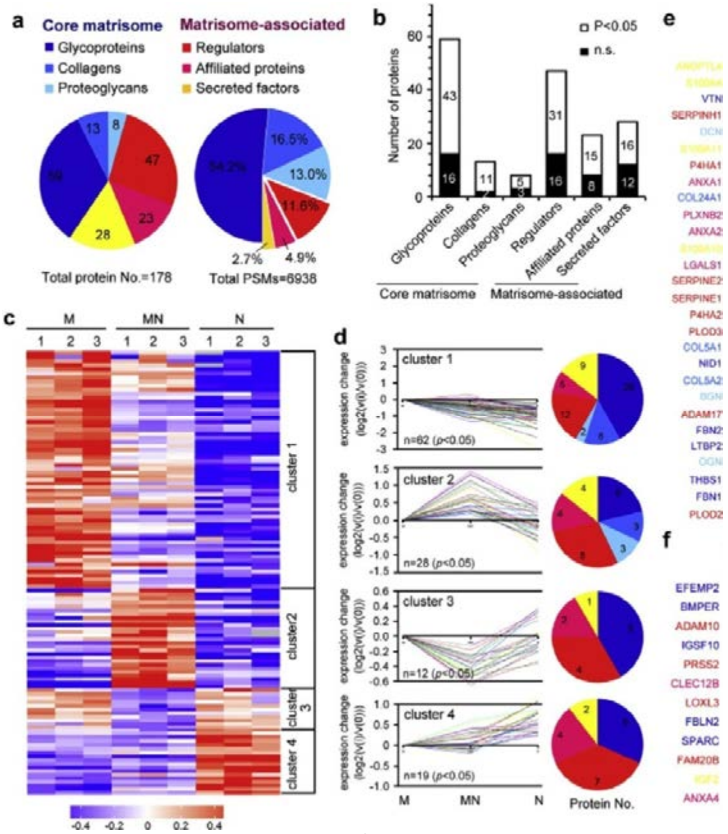

Fig. 6. Quantitative proteomic analysis of ECMs secreted by cocultured cells (MN-ECM) revealed a unique matrisome signature. (a) Matrisome signature of cell secreted ECM as presented by pie chart. Distribution of ECM proteins was calculated by protein numbers (left) and protein abundance (PSMs, right) of each matrisome protein sub-category, respectively. (b) Distribution of protein numbers with or without statistical significance among three kinds of ECM. (c) Heatmap of quantitative proteomics using TMT labeling. The fold-change in protein detection levels normalized to the mean of M-ECM in log2 scale was shown. (d) Short-time series expression miner (STEM) of ECM proteins with statistical significance. According to the expression tendency, ECM proteins were divided into four clusters. Distribution of protein numbers was presented for each cluster. (e–f) ECM proteins in cluster 2 (e) and cluster 3 (f) were listed from highest changes to lowest changes. The color of proteins was consistent with the sub-category in pie chart. (g–h) GO analysis of ECM proteins in cluster 2 and cluster 3, including biological process (g) and molecular function (h). Red color represents the ECM proteins expressed highest in MN-ECM in cluster 2 and blue color represents the proteins expressedlowestinMN-ECMincluster3.Triplicateindependentexperimentswereperformedforeachgroup.

Though ECM has been realized as a functional biomaterial with various biochemical components to recapitulate complicated microenvironments and broadly applied for tissue regeneration [49,50], the furtherquestionwaswhytheyworkedinspecificity.Many effortshave been made to rationalize the specific functionalities of ECM biomaterials, including proteomic analysis [51–53]. Proteomic analysisprovided a powerful way to understand ECM matrisome comprehensively, including the compositions and potential biological functions

[54,55]. Proteomic composition of stem cell-derived ECM has been character- ized, including ECM from bone-marrow-derived MSC [54], adipose- derived MSC [54] and osteoblast-differentiated MSCs [56]. However, proteomic composition of ECM from fibroblasts or osteoblasts, especiallycoculturedcells,wasrarelyreported.Here,wefigur edoutunique ECM matrisome from MC/NIH cocultures and single cell type (fibroblastsorosteoblasts)respectivelyviaproteomicanalysis. It'sinteresting that the levels of ECM proteins in MN-ECM were not only between M- ECMandN-ECM,butwithgreatchange.InMN-ECM,28proteinswere expressed highest and 12 proteins were expressed lowest. The results might be caused by the activity alteration of osteoblasts, which was guided by fibroblast in the cocultures (Fig. 2). The most abundance of ECM proteins in N-ECM were matrisome-associated proteins. Con- sistently, fibroblasts greatly increased matrisome-associated protein secretionofosteoblastsinthecocultures(Fig.6e),includingANGPTL4, S100A4, SERPINH1, S100A11 and so on (from high to low).These geneswerereportedtoplayessentialrolesinbiologicalprocessand might contribute to the function of MN-ECM. For example, ANGPTL4 was a key factor in the modulation of angiogenesis and in bone re- generation [57]. The expression of ANGPTL4 was increased in miner- alizing periodontal cells on day 14 of culture and was induced by hy- poxia in periodontal fibroblasts [58]. SERPINH1 encodes the collagen chaperone HSP47 that binds to the type I precollagen trimers and regulated the folding and stabilization of triple helical domain. SER- PINH1 mutations have been associated with osteogenesis imperfect [59]. Thus, the results also provided orientations to investigate ECM matrisome in depth in future.

V. CONCLUSIONS

In conclusion, the present study developed a novel strategy to generate tissue mimetic ECM with excellent bioactivities for bone re- generation. In the coculture system, existence of fibroblasts promoted osteoblasts undergoing osteogenic maturation. The cell communication betweendifferentcelltypesguided thetissuemimeticECMengineering with specific morphology and molecular components. The generated ECMfromcoculturecells provided uniquebiophysical andbiochemical cues for cell-matrix interactions and regulated cell behaviors. Furthermore, the complicated ECM ornamented scaffolds withsuitable microenvironment promoted collagen regeneration and new bone for- mation, which might be caused by the recruitment of endogenouscells and stimulation of self-healing process. The “off-shelf” products with higher bioactivities in ECM from multiple cell types than that from single cell type should be a bright choice for biomaterial decoration for tissue engineering and regenerative medicine.

FUNDING

This work was supported by the National Natural Science Foundation of China (Grant No. 31300800 and 81702625), the Zhejiang Province Welfare Technology Application Research Project (Grant No. 2017C33135), the Natural Science Foundation of Ningbo (Grant No. 2018A610202 and 2019A610309) and the K.C. Wong Magna Fund in NingboUniversity.

CREDIT AUTHORSHIP CONTRIBUTION STATEMENT

Mei Li: Formal analysis, Data curation, Writing - original draft. Anqi Zhang: Investigation. Jiajing Li: Investigation. Jing Zhou: Formal analysis. Yanan Zheng: Formal analysis. Chi Zhang: Formal analysis. Dongdong Xia: Formal analysis. Haijiao Mao: Formal ana- lysis. Jiyuan Zhao: Formal analysis, Data curation, Writing - original draft.

DECLARATION OF COMPETING INTEREST

The authors declara that they have no known competing financial interests or personal relationships that could have appaered influence the work reported in the papaer.

APPENDIX A: SUPPLEMENTARY DATA

Supplementary data to this article can be found online at https://doi.org/10.1016/j.bioactmat.2020.06.017.

REFERENCES

[1] K. Sadtler, A. Singh, M.T. Wolf, X.K. Wang, D.M. Pardoll, J.H. Elisseeff, Design, clinical translation and immunological response of biomaterials in regenerative medicine, Nat. Rev. Mater. 1 (7) (2016) 1–17, https://doi.org/10.1038/natrevmats.2016.40.

[2] H.M.Xia,X.Li,W.W.Gao,X.Fu,R.H.Fang,L.F.Zhang,K.Zhang,Tissuerepairand regeneration with endogenous stem cells, Nat. Rev. Mater. 3 (7) (2018) 174–193,https://doi.org/10.1038/s41578-018-0027-6.

[3] M.Zhu,W.Li,X.Dong,X.Yuan,A.C.Midgley,H.Chang,Y.Wang,H.Wang,

[4] K. Wang, P.X. Ma, H. Wang, D. Kong, In vivo engineered extracellular matrix scaffoldswithinstructivenichesfororientedtissueregeneration,Nat.Commun.10(1) (2017) 4620,https://doi.org/10.1038/s41467-019-12545-3.

[5] L. Moroni, J.A. Burdick, C. Highley, S.J. Lee, Y. Morimoto, S. Takeuchi, J.J. Yoo, Biofabricationstrategiesfor3Dinvitromodelsandregenerativemedicine(vol3,pg 21, 2018), Nat. Rev. Mater. 3 (5) (2018) 21–37, https://doi.org/10.1038/s41578- 018-0020-01.

[6] A.E. Stanton, X. Tong, F. Yang, Extracellular matrix type modulates mechanotransductionofstemcells,ActaBiomater.96(2017)310–320,https://doi.org/10. 1016/j.actbio.2019.06.048.

[7] G.Y. Huang, F. Li, X. Zhao, Y.F. Ma, Y.H. Li, M. Lin, G.R. Jin, T.J.Lu, G.M. Genin,

[8] F. Xu, Functional and biomimetic materials for engineering of the three-dimen- sional cell microenvironment, Chem. Rev. 117 (20) (2017) 12764–12850, https:// doi.org/10.1021/acs.chemrev.7b00094.

[9] Z.K. Cui, S. Kim, J.J. Baljon, B.M. Wu, T. Aghaloo, M. Lee, Microporous metha- crylatedglycolchitosan-montmorillonitenanocompositehydrogelforbonetissue engineering, Nat. Commun. 10 (1) (2017) 3523, https://doi.org/10.1038/s41467- 019-11511-3.

[10] A.M. Rosales, K.S. Anseth, The design of reversible hydrogels to capture extra-cellularmatrixdynamics,Nat.Rev.Mater.1(2)(2016)15012,https://doi.org/10. 1038/natrevmats.2015.12ARTN15012.

[11] M.R.Lutolf,F.E.Weber,H.G.Schmoekel,J.C.Schense,T.Kohler , R.Muller,

[12] J.A. Hubbell, Repair of bone defects using synthetic mimetics of collagenous ex- tracellular matrices, Nat. Biotechnol. 21 (5) (2003) 513–518, https://doi.org/10. 1038/nbt818.

[13] L.T.A. Hong, Y.M. Kim, H.H. Park, D.H. Hwang, Y. Cui, E.M. Lee, S. Yahn, J.K.Lee,

[14] S.C.Song,B.G.Kim,Aninjectablehydrogelenhancestissuerepairafterspinalcord injury by promoting extracellular matrix remodeling, Nat. Commun. 8 (2017),https://doi.org/10.1038/ s41467-017-00583-8ARTN533.

[15] E.S.Place,N.D.Evans,M.M.Stevens,Complexityinbiomaterials fortissue engineering, Nat. Mater. 8 (6) (2009) 457–470, https://doi.org/10.1038/Nmat2441.

[16] G.S.Hussey,J.L.Dziki,S.F.Badylak,Extracellularmatrix-basedmaterialsforre- generative medicine, Nat. Rev. Mater. 3 (7) (2018) 159–173, https://doi.org/10. 1038/ s41578-018-0023-x.

[17] G.G.Giobbe,C.Crowley,C.Luni,S.Campinoti,M.Khedr,K.Kretzschmar,M.M.De Santis,E.Zambaiti,F.Michielin,L.Meran,Q.Hu,G.vanSon,L.Ur bani,

[18] Manfredi, M. Giomo, S. Eaton, D. Cacchiarelli, V.S.W. Li, H. Clevers, P. Bonfanti,

[19] N. Elvassore, P. De Coppi, Extracellular matrix hydrogel derived from decellularized tissues enables endodermal organoid culture, Nat. Commun. 10 (1) (2017) 5658–5671, https://doi.org/10.1038/s41467-019-13605-4.

[20] Q.Xing,Z.C.Qian,W.K.Jia,A.Ghosh,M.Tahtinen,F.Zhao,Naturalextracellular matrix for cellular and tissue biomanufacturing, ACS Biomater. Sci. Eng. 3 (8) (2017) 1462–1476,https://doi.org/10.1021/acsbiomaterials.6b00235.

[21] J.Madhusoodanan,Matrixmimicsshapecellstudies,Nature566(7745)(2017) 563–565,https://doi.org/10.1038/ d41586-019-00681-1.

[22] U.H.Langen,M.E.Pitulescu,J.M.Kim,R.Enriquez-Gasca,K.K.Sivaraj,

[23] A.P. Kusumbe, A. Singh, J. Di Russo, M.G. Bixel, B. Zhou, L. Sorokin,

[24] J.M. Vaquerizas, R.H. Adams, Cell-matrix signals specify bone endothelial cells during developmental osteogenesis, Nat. Cell Biol. 19 (3) (2017) 189–201, https:// doi.org/10.1038/ncb3476.

[25] C.J. Li, G.H. Zhen, Y. Chai, L. Xie, J.L. Crane, E. Farber, C.R. Farber,X.H. Luo,

[26] P.S. Gao, X. Cao, M. Wan, RhoA determines lineage fate of mesenchymal stem cells by modulating CTGF-VEGF complex in extracellular matrix, Nat. Commun. 7 (2016) 11455, https://doi.org/10.1038/ncomms11455 ARTN 11455.

[27] M.C. Prewitz, S.F. Philipp, V.B. Malte, F. Jens, S.E. Aline, N. Christian, M.Katrin,

[28] Konstantinos, W. Claudia, H. Bernard, Tightly anchored tissue-mimetic matrices as instructive stem cell microenvironments, Nat. Methods 10 (8) (2013) 788–794,https://doi.org/10.1038/nmeth.2523.

[29] M. Li, T. Zhang, J. Jiang, Y. Mao, A. Zhang, J. Zhao, ECM coating modification generatedbyoptimizeddecellularizationprocessimprovesfunctionalbehaviorof BMSCs, Materials science & engineering, Mater. Biol. Appl. 105(2017) 110039, ,https://doi.org/10.1016/j.msec.2019.110039.

[30] S. Toda, L.R. Blauch, S.K.Y. Tang, L. Morsut, W.A. Lim, Programming self-orga-nizingmulticellularstructureswithsyntheticcell-cellsignaling,Science361(6398)(2018) 156–162,https://doi.org/10.1126/science.aat0271.

[31] L.A. Johnston, Competitive interactions between cells: death, growth, and geo- graphy, Science 324 (5935) (2009) 1679–1682, https://doi.org/10.1126/science. 1163862.

[32] J.H.Lee,D.H.Bhang,A.Beede,T.L.Huang,B.R.Stripp,K.D.Bloch,A.J.Wagers,

[33] Y.H.Tseng,S.Ryeom,C.F.Kim,Lungstemcelldifferentiationin micedirectedby endothelialcellsviaaBMP4-NFATc1-thrombospondin-1Axis,Cell156(3)(2014) 440–455,https://doi.org/10.1016/j.cell.2013.12.039.

[34] J.A.Zepp,W.J.Zacharias,D.B.Frank,C.A.Cavanaugh,S.Zhou, M.P.Morley,

[35] E.E. Morrisey, Distinct mesenchymal lineages and niches promote epithelial self- renewal and myofibrogenesis in the lung, Cell 170 (6) (2017) 1134–1148, https://doi.org/10.1016/ j.cell.2017.07.034.

[36] X. Zhang, C.A. Simmons, J. Paul Santerre, Paracrine signalling from monocytes enables desirable extracellular matrix accumulation and temporally appropriate phenotypeofvascularsmoothmusclecell-likecellsderivedfromadiposestromal cells, Acta Biomater. 103 (2020) 129–141, https://doi.org/10.1016/j.actbio.2017. 12.006.

[37] M.Kim,D.R.Steinberg,J.A.Burdick,R.L.Mauck,Extracellularvesiclesmediate improved functional outcomes in engineered cartilage produced from MSC/chon- drocyte cocultures, Proc. Natl. Acad. Sci. U. S. A. 116 (5) (2017) 1569–1578,https://doi.org/10.1073/pnas.1815447116.

[38] C.Piard,A.Jeyaram,Y.Liu,J.Caccamese,S.M.Jay,Y.Chen,J.Fisher,3Dprinted HUVECs/MSCs cocultures impact cellular interactions and angiogenesisdepending on cell-cell distance, Biomaterials 222 (2017) 119423, , https://doi.org/10.1016/j. biomaterials.2019.119423.

[39] S. Naskar, V. Kumaran, Y.S. Markandeya, B. Mehta, B. Basu, Neurogenesis-on-Chip: electricfieldmodulatedtransdifferentiationofhumanmesenchymalstemcelland mousemuscleprecursorcellcoculture,Biomaterials226(2020)1 19522,,https:// doi.org/10.1016/j.biomaterials.2019.119522.

[40] Y.V.Shih,S.Varghese,Tissueengineeredbonemimeticstostudy bonedisordersex vivo: role of bioinspired materials, Biomaterials 198 (2017) 107–121, https://doi. org/10.1016/j.biomaterials.2018.06.005.

[41] H.C.Blair,Q.C.Larrouture,Y.Li,H.Lin,D.Beer-Stoltz,L.Liu,R.S.Tuan,

[42] L.J. Robinson, P.H. Schlesinger, D.J. Nelson, Osteoblast differentiation and bone matrix formation in vivo and in vitro, Tissue Eng. B Rev. 23 (3) (2017) 268–280,https:// doi.org/10.1089/ten.TEB.2016.0454.

[43] I.G.Kim,M.P.Hwang,P.Du,J.Ko,C.W.Ha,S.H.Do,K.Park,Bioactivecell-derived matricescombinedwithpolymermeshscaffoldforosteogenesisandbonehealing, Biomaterials 50 (2015) 75–86, https:// doi.org/10.1016/j.biomaterials.2015.01. 054.

[44] M.Li,C.Zhang,X.Li,Z.Lv,Y.Chen,J.Zhao,Isoquercitrinpromotestheosteogenic differentiationofosteoblastsandBMSCsviatheRUNX2orBMPpathway,Connect. Tissue Res. (2018) 1–11,https:// doi.org/10.1080/03008207.2018.1483358.

[45] M.Li,C.Zhang,M.Cheng,Q.Gu,J.Zhao,Smallintestinalsubmucosa:apotential osteoconductiveandosteoinductivebiomaterialforbonetissueengineering,Mater. Sci. Eng. Mater. Biol. Appl. 75 (2017) 149–156, https://doi.org/10.1016/j.msec. 2017.02.042.

[46] M.Li,Q.Gu,M.Chen,C.Zhang,S.Chen,J.Zhao,Controlleddeliveryoficariinon smallintestinesubmucosaforbonetissueengineering,Mater.Sci.Eng.Mater.Biol. Appl. 71 (2017) 260–267,https://doi.org/10.1016/j.msec.2016.10.016.

[47] C.Zhang,M.Li,J.Zhu,F.Luo,J.Zhao,Enhancedbonerepairinducedbyhuman adipose-derived stem cells on osteogenic ECM ornamented small intestinal sub- mucosa, Regen. Med. 12 (5) (2017) 541–552, https://doi.org/10.2217/rme-2017-

[48] 0024.

[49] M. Li, C. Zhang, Y. Mao, Y. Zhong, J. Zhao, A cell-engineered small intestinal submucosa-basedbonemimeticconstructforboneregeneration,TissueEng.24 (13-14) (2018) 1099–1111,https://doi.org/10.1089/ten.TEA.2017.0407.

[50] M. Li, C. Zhang, Y. Zhong, J. Zhao, A novel approach to utilize icariin as icariin-derivedECMonsmallintestinalsubmucosascaffoldforbonerepair,Ann.Biomed. Eng. 45 (11) (2017) 2673–2682,https://doi.org/10.1007/s10439-017-1900-y.

[51] J.R. Wisniewski, A. Zougman, N. Nagaraj, M. Mann, Universal sample preparation method for proteome analysis, Nat. Methods 6 (5) (2009) 359–362, https://doi.org/ 10.1038/nmeth.1322.

[52] F.D. Miller, D.R. Kaplan, Mobilizing endogenous stem cells for repair and re- generation: are we there yet? Cell. Strm. Cell. 10 (6) (2012) 650–652, https://doi.org/10.1016/j.stem.2012.05.004.

[53] C.Wang,J.Li,S.Sinha,A.Peterson,G.A.Grant,F.Yang,Mimickingbraintumor- vasculature microanatomical architecture via co-culture of brain tumor and en- dothelialcellsin3Dhydrogels,Biomaterials202(2017)35–44,https://doi.org/10. 1016/j.biomaterials.2019.02.024.

[54] T.H.Qazi,D.J.Mooney,G.N.Duda,S.Geissler,Biomaterialsthat promotecell-cell interactions enhance the paracrine function of MSCs, Biomaterials 140 (2017) 103–114,https://doi.org/10.1016/j.biomaterials.2017.06.019.

[55] S.Toda,N.W.Frankel,W.A.Lim,Engineeringcell-cellcommunicationnetworks: programming multicellular behaviors, Curr. Opin. Chem. Biol. 52 (2017) 31–38,https://doi.org/10.1016/j.cbpa.2019.04.020.

[56] L. Sapir, S. Tzlil, Talking over the extracellular matrix: how do cells communicate mechanically? Semin. Cell Dev. Biol. 71 (2017) 99–105, https://doi.org/10.1016/j. semcdb.2017.06.010.

[57] C.D.Cook,A.S.Hill,M.Guo,L.Stockdale,J.P.Papps,K.B.Isaacson,

[58] D.A. Lauffenburger, L.G. Griffith, Local remodeling of synthetic extracellular matrix microenvironmentsbyco-culturedendometrialepithelialandstromalcellsenables long-term dynamic physiological function, Integr. Biol. Quantitat. Biosci. Nano. Macro 9 (4) (2017) 271–289,https:// doi.org/10.1039/c6ib00245e.

[59] M.Uroz,S.Wistorf,X.Serra-Picamal,V.Conte,M.Sales-Pardo,P.Roca-Cusachs, R. Guimera, X. Trepat, Regulation of cell cycle progression by cell-cell and cell- matrix forces, Nat. Cell Biol. 20 (6) (2018) 646–654, https://doi.org/10.1038/ s41556-018-0107-2.

[60] H.Koo,K.M.Yamada,Dynamiccell-matrixinteractionsmodulatemicrobialbiofilm and tissue 3D microenvironments, Curr. Opin. Cell Biol. 42 (2016) 102–112,https://doi.org/10.1016/j.ceb.2016.05.005.

[61] E.E. Mann, D.J. Wozniak, Pseudomonas biofilm matrix composition and niche biology, FEMS Microbiol. Rev. 36 (4) (2012) 893–916, https://doi.org/10.1111/j. 1574-6976.2011.00322.x.

[62] H.C.Flemming,J.Wingender,Thebiofilmmatrix,Nat.Rev.Microbiol.8(9)(2010) 623–633,https://doi.org/10.1038/nrmicro2415.

[63] I.L.S. Chua, H.W. Kim, J.H. Lee, Signaling of extracellular matrices for tissue re-generationandtherapeutics,TissueEng.Regen.Med.13(1) (2016)1–12,https:// doi.org/10.1007/s13770-016-9075-0.

[64] W. Han, N.K. Singh, J.J. Kim, H. Kim, B.S. Kim, J.Y. Park, J. Jang, D.W. Cho, Directeddifferentialbehaviorsofmultipotentadultstemcellsfrom decellularized tissue/organ extracellular matrix bioinks, Biomaterials 224 (2017) 119496, ,https://doi.org/10.1016/ j.biomaterials.2019.119496UNSP119 496.

[65] F. Pati, J. Jang, D.H. Ha, S. Won Kim, J.W. Rhie, J.H. Shim, D.H. Kim, D.W. Cho, Printing three-dimensional tissue analogues with decellularized extracellular matrixbioink, Nat. Commun. 5 (2014) 3935,https://doi.org/10.1038/ncomms4935.

[66] J.M. Aamodt, D.W. Grainger, Extracellular matrix-based biomaterial scaffolds and the host response, Biomaterials 86 (2016) 68–82, https://doi.org/10.1016/j. biomaterials.2016.02.003.

[67] R.Raghunathan,M.K.Sethi,J.A.Klein,J.Zaia,Proteomics,glycomics,andglyco- proteomics of matrisome molecules, Mol. Cell. Proteomics 18 (11) (2017) 2138–2148,https://doi.org/10.1074/mcp.R119.001543.

[68] H. Bi, K. Ye, S. Jin, Proteomic analysis of decellularized pancreatic matrix identifies collagen V as a critical regulator for islet organogenesis from human pluripotent stem cells, Biomaterials 233 (2020) 119673, , https://doi.org/10.1016/j. biomaterials.2019.119673.

[69] H.Ragelle,A.Naba,B.L.Larson,F.Zhou,M.Prijic,C.A.Whittaker,A.DelRosario,

[70] R. Langer, R.O. Hynes, D.G. Anderson, Comprehensive proteomic characterization of stem cell-derived extracellular matrices, Biomaterials 128 (2017) 147–159,https://doi.org/10.1016/j.biomaterials.2017.03.008.

[71] Q.Y. Li, B.E. Uygun, S. Geerts, S. Ozer, M. Scalf, S.E. Gilpin, H.C. Ott, M.L.Yarmush,

[72] L.M. Smith, N.V. Welham, B.L. Frey, Proteomic analysis of naturally-sourced bio- logical scaffolds, Biomaterials 75 (2016) 37–46, https://doi.org/10.1016/j. biomaterials.2015.10.011.

[73] M.Baroncelli,B.C.vanderEerden,Y.Y.Kan,R.D.Alves,J.A.Demmers,J.vande Peppel,J.P.vanLeeuwen,Comparativeproteomicprofilingofhu manosteoblast-derivedextracellularmatricesidentifiesproteinsinvolvedinmesenchymalstromal cell osteogenic differentiation and mineralization, J. Cell. Physiol. 233 (1) (2018) 387–395,https://doi.org/10.1002/jcp.25898.

[74] P. Zhu, Y.Y. Goh, H.F. Chin, S. Kersten, N.S. Tan, Angiopoietin-like 4: a decade of research, Biosci. Rep. 32 (3) (2012) 211–219, https://doi.org/10.1042/ BSR20110102.

[75] K.Janjic,A.Schellner,A.Engenhart,K.Kernstock,B.Schadl,A. Moritz,H.Agis, Angiopoietin-like4productionupontreatmentwithhypoxiaandL-mimosinein periodontal fibroblasts, J. Periodontal. Res. 54 (5) (2017) 489–498, https://doi. org/10.1111/jre.12649.

[76] U.Schwarze,T.Cundy,Y.J.Liu,P.L.Hofman,P.H.Byers,Compoundheterozygosity for a frameshift mutation and an upstream deletion that reduces expression of SERPINH1insiblingswithamoderateformofosteogenesisimperfecta,Am.J.Med. Genet.179(8)(2017)1466–1475,https://doi.org/10.1002/ajmg.a.61170.

★★★

ANALYSIS AND EXPERIMENTAL INVESTIGATION OF STAINLESS STEEL COMPOSITE BY METAL INJECTION MOULDING

[1]NITISH KUMAR , [2]BIBHH UTI BHUBASANA SABAT, [3]MANAS RANJAN DASH

[1]Department of Mechanical Engineering, NMIET, Bhubaneswar, 751019
[2]Department of Mechanical Engineering, CEC Bhubaneswar
[3]Department of Mechanical engineering, REC Bhubaneswar
E-mail: [1]anway.maiti@nmiet.ac.in

Abstract -
Metal injection moulding (MIM) is large scale manufacturing method, for creation of complex shapes and miniature parts by a combination of plastic injection moulding with the flexibility in sintering of metal particulates. In current investigation binder comprised of paraffin wax, polyethylene glycol, stearic acid and low-density polyethylene are developed for moulding of composite powders of SS316L+WC-CrC-Ni, and sintered at 1200°C under hydrogen purged atmosphere. Composites are characterised with respect to rheological, thermal properties and microstructure by scanning electron microscopy, microhardness and density. Properties of sintering temperature and heating rate on the above properties have been evaluated to obtain a defect- free composite.

Keywords - Metal Injection Moulding (MIM); Microstructure; SS316L+WC-CrC-Ni .

I. INTRODUCTION

In present trend, the manufacturing process is developed for a large amount of small and complex parts with increased production rate to full fill demands of various products for modern day to day life. The manufacturing methods and processing of metal components have general limitations of traditional process for fabrication of metal components and it encouraging for finding alternative process. Hence alternative method for producing near net shape metal component is Metal injection moulding (MIM). The MIM is a mishmash of powder metallurgy and plastic infusion shaping procedure. MIM can produce low-cost products at large number, close tolerance and shape complexity, good mechanical properties, compare to other technologies since it eliminates secondary operations and also material damages while in case intricate geometries for numerous applications in today's industry[1].

Nomenclature

MIM	Metal Injection moulding
MMC	Metal matrix composite
LDPE	Low-Density Polyethylene
PEG-600	Polyethylene Glycol600

Metal injection moulding (MIM) is a near-net shaping method that is predominantly beneficial for the users where intricate shape with high density and precision and accuracy in dimensions are mandatory [2].

In MIM process, binder acts as a brief vehicle for evenly pack the metal powder into the mould cavity at desired profile and then holding the particle till sintering process begins. The selection of binder great influence on mixing rheology, agglomeration, particle packing, moulding, debinding and dimensional correctness. The selected binder should be little viscosity at the initial moulding stage and sudden viscosity change through cooling. The binder essential free from toxic and it should be environmental friendly [3].

The technique involves in MIM is shown in Figure1. initially mixing of the fine metal powder with binders, the mixture is crushed to a suitable size(feedstock), for the injection moulding process by applying pressure and heat to feedstock from the pre-defined shape of core cavity in the mouldtool(green part). The green part undergoes debinding process where the binder is partially detached in solvent debinding and a reminder of the binder is removed in the thermal debindingprocess(brown part). Later debinding process the brown part exposed to sintering process which densifies the part to achieve good mechanical properties.

In current work, the metal matrix composite (MMC) contain SS316L and WC-CrC-Ni powders. SS316L compromises good corrosion resistance and mechanical properties. WC-CrC-Ni exhibits better hardness and wears resistance. By using the experimental trials for SS316L and WC-CrC-Ni powders, a set of suitable mixing technique, moulding parameters and debinding cycles were designed for minimum defects of MMC parts. Microhardness and density were evaluated with respect to sinteringfactors.

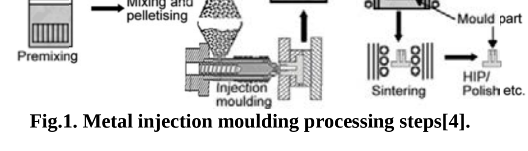

Fig.1. Metal injection moulding processing steps[4].

II. EXPERIMENTAL PROCEDURES

Stainless steel 316L and WC-CrC-Ni powders were utilized as a part of the present review with normal molecule estimate 2.6 and 38 µm, respectively. The composition of the metal powder was SS316L+WC-CrC-Ni.These powders (55 vol.%) and binders (45 vol.%) were warmed at 110°C and then mixed in a Sigma Z-blade mixer at 135°C for 3 h. Successively, the temperature was decreased and the mixture was removed and sliced to small granular size around 3-4 mm.The granular were prepared for injection moulding. The composition of binder was 52wt.% paraffin wax, 10wt.% PEG-600, 3wt.% stearic acid, and 35wt.% LDPE.Themoulding temperature and pressure were 170°C and 120 Mpa at the nozzle, respectively. The green parts were debound at 48° C for 5 h in hexane and then sintered at 1200 °C for 300 min. using a vacuum sintering furnace to achieve samples with higher density. Table1 represents the chemical composition of the metal powder. An etching reagent containing 1gm. picric acid, 5mlHCL and 100ml ethanol were used to etch the samples for microstructure examination. Vickers microhardness (H_V) was measured using a microhardness tester (Make:Omni Tech, Model:MVH- S Auto) with a load of 9.81 N. Total 10 indentation were performed at 0.4mm intervals and the average value was reported for eachsample.

	Ni	Cr	Mo	C	Fe	W
SS316L	10-14 %	16-18 %	2.0-3.0 %	2.0-3.0 %	Remainder	
WC-CrC-Ni	7.15%	19%	-	6.8%	-	Remainder

Table 1. The chemical composition of SS316L Powder, WC–CrC–Ni powder.

2.1 Analysis of Powder shape and particle size

The particle size of Metal powder and its distribution pattern have been investigated using a particle size analyser at 36°C and the dispersion medium used is ethylene glycol 49%. Figure 2. shows mixer of SS316L and WC-CrC-Ni , has been analysed through SEM. (Supplier -6380LA, JEOL).The Distribution of particle size given in Table2.

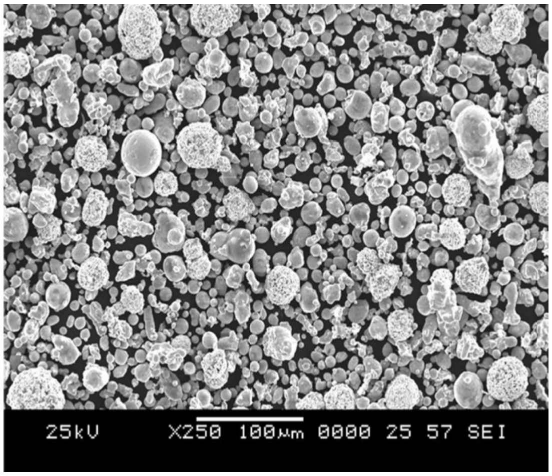

Fig.2. SEM micrograph of SS316L(70%)+WC-CrC-Ni(30%) powder Table 2 Distribution of particle size in (µm)

	Property Distribution Particle size (µm)			
Metal powder	D10(µm)	D50(µm)	D90(µm)	D97(µm)
SS316L	0.45	1.08	3.35	5.85
WC-CrC-Ni	0.42	1.07	17.68	31.56

Table 2: Distribution of Particle size in (µm)

2.2 Preparation of Feedstock and MIMspecimen

Feedstock has been framed with 56 vol.% SS316L (70%)+WC-CrC-Ni(30%), powder (manufactured by Innomet Pvt. Ltd, Hyderabad) and 44vol.% binder. The binder comprises of Paraffin Wax (PW) (Supplier: LOBACHEMIE Pvt. Ltd, Mumbai), Polyethylene Glycol 600(PEG-600) (Supplier:LOBACHEMIE Pvt. Ltd, Mumbai),Stearic Acid (SA) (Supplier: LOBACHEMIE Pvt. Ltd, Mumbai) and Low Density Polyethylene (LDPE) (manufactured by Indian Petrochemical Corporation Ltd, Gujrat). In the Table 3 Composition of the binder and in Table 4 Feedstock Composition is given for the SS316L (70%)+WC-CrC-Ni(30%). Figure 3. Shows the binders for the preparation of feedstock. Feedstock has been prepared in each batch as per composition designed with a sigma blade mixer at 135°C for 90 minutes at 35 rpm. Once mixing done thoroughly, the viscous feedstock is allowed to cool at a lower temperature. It gets to be distinctly strong at room temperature. In advance stage pelletized to supply feedstock to the injection mouldingmachine

Thermal properties of feedstock was evaluated by using Differential scanning calorimeter (DSC) (HICHAN- 2510) the temperature between 40° C to 170° C warming rate of 10° C/min, then allowed to cool from 170° C to 40° C at 10° C/min cooling rate in helium gas atmosphere.

Sl. No.	Elements	Wt. %
1	PW	52.0
2	PEG 600	10.0
3	LDPE	35.0
4	SA	3.0

Table 3 Binders composition

Sl. No.	Name of the elements	Wt. percentage
1	SS316L +WC-CrC-Ni	81
2	PW	9.8
3	PEG 600	1.9
4	LDPE	6.65
5	SA	0.57

Table 4 Feedstock Composition for the SS316L +WC-CrC-Ni

Fig.3 Binders for preparation of feedstock

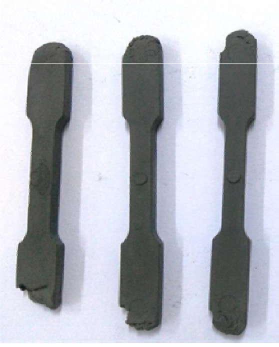

Fig.4 Defected tensile specimens at initial parameters.

The injection moulding was carried out in a permanent mould by 150-tonne injection mouldingmachine.To measure the injection pressure, a pressure sensor with a range 0 -100 bar has been put in the hydraulic line which pushes the injection screw inside the barrel. A standard 40 mm diameter screw and barrel assembly has been used for injection moulding. Multiple injection speed steps are adapted for injecting the feedstock into the mould. In the first set, injection speed is set 5% of the maximum injection speed (138 cc/s) for 7.5 % of the total injection time (4s) and injection speed 15% of the maximum injection speed (138 cc/s) for rest of the injection time at injection temperature of feedstock 120° C ,145° C and 160°C. Figure 4. Shows the tensile specimens for the first set of trial parameters. After several trials, the parameters selected for defect free tensile specimens are injection speed 41.4 cc/s , injection time 3.7s and feedstock velocity 5.85m/s at injection machine barrel temperature 160,165 170°C.

Debinding process was done in steps. In the main stage dissolvable debinding was executed by submersing the moulded specimen in n-hexane (C_6H_{14}) bath and heating the bath below the melting temperature of PW, where most of the PEG-600, PW and SA are removed by dissolving in n- hexane. In the second stage, warm debonding has been completed to evaluate all of the PEG-600, PW, SA and LDPE from the moulded sample. Solvent binding has been accomplished in a drying oven at different temperatures and time durations. After solvent debinding, the specimens are taken out of n-hexane and dried for 60 min, at 48 °C in a drying oven (DASS and Co- Howrah). Then thermal debinding was performed in a tube type furnace at different holding times and temperatures in a Hydrogen atmosphere with a warming rate of 1°C/min.

Sintering of the debound tensile specimens was kept in a tube type furnace in a hydrogen atmosphere. The specimens are heated at a temperature 1200°C warming rate of 1-5°C/min. and kept at that temp. for 30 minutes and then cooled to 200°C at a cooling rate of 5°C/min and then chilled down to room temperature through furnace cooling.

III. RESULTS ANDDISCUSSION

3.1 DSC Studies of feedstock and binder

The feedstock and binder thermal property provide the basic guidelines for handling subsequent steps in MIM. The DSC delivers the thermal properties binder and feedstock. Figure 5 shows DSC curves of MIM feedstock and two endothermic pinnacle were detected at 65.2°C and 96.9°C during warming cycle owing to tender of major binder elements. The main pinnacle at 65.2°C resembles the tender of SA, PW and PEG-600. The second pinnacle at96.9°C resembles the melting of LDPE. The DSC aftereffect of feedstock demonstrates that infusion temperature of the MIM feedstock should be above 96.9°C also, the temperature should be beneath 65.2°C for better injection moulding. For controlling mould temperature cooling channel were provided in the mould tool with inlet and outlet for cooling media circulation. In the study, the injection was performed above 96.9°C i.e. at 160°C and 170°C where binder in the feedstock meltscompletely.

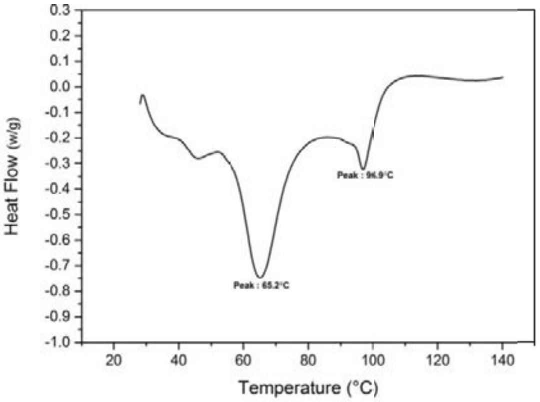

Fig.5 DSC curves of MIM feedstock

3.2 Feedstock density Measurement

Density measures how securely matter is packed together. One of the most common uses of density is how the material interacts with other materials when mixed together such as feedstock. The density of feedstock and binder measured at room temperature by Archimedes Principle. Density results are presented in table 5 and table 6 respectively. The density was measured by submerging in acetone and water respectively.

SL.No	Weight in air (g)	Weight in water (g)	Differenceinweight.(g)	Density (g/cc)	Average density(g/cc)
1.	3.768	0.613	3.155	0.943	0.916
2.	5.451	0.68	4.771	0.902	
3.	12.78	1.603	11.177	0.903	

Table 5. Binder density measurement

SL.No	Weight in air (g)	Weight in water (g)	Differenceinweight.(g)	Density (g/cc)	Average density(g/cc)
1.	16.519	13.266	3.253	5.08	5.093
2.	13.304	10.7	2.604	5.11	
3.	15.417	12.391	3.026	5.09	

Table 6. feedstock density measurement

3.3 Viscosity of MIM feedstock

A rotational rheometer. Rheological characteristic was developed at different temperatures in the range 160−170°C in 2 °C steps. For conducting experiments in rotational rheometer using parallel geometry some of the factors must be considered very close gaps must maintain in middle of the parallel plates to avoid intimal secondary flows, the capability to increase and decrease the shear rate quickly to reduce viscous heating. [5]. In the filling of the mould dies the feedstock rheological properties are vital types which impact the steady flow and even filling of the mould. The rheological property of feedstock evaluation is founded on the viscosity, shear sensitivity and temperature sensitivity Figure 6. shows the pseudoplastic behaviour of feedstock at an injection temperature of 160, 165 and 170 °C. Normally, the viscosity was decreasing when shear rate was increased. This is due to the fine powder contains reduced interstitial spaces than the coarse powder, thus it increases it's inter-particle friction. Besides that, the fine powder has greater particle surface contact area between powder particles[6]. A quick viscosity change could bring about under anxiety centres in formed parts, creating in splitting and twisting[7].

3.4 Debinding and sintering of MIMspecimens

In the current investigation binder is consist of PEG-600, PW, SA and LDPE. The binders are removed in steps because of selected multi-component binder system. It is important to have one of the binder segments no less than 30 per or more [8,9] to be detached first in the debinding to escape insulated sample of pores. The shaped green samples are characterised in two phases dissolvable depending followed by warm debinding. Since PEG- 600, PW and SA collectively constitute more than 30 percent and resolvable in n-hexane (C_6H_{14}) solvent, PEG 600, PW and SA have been expelled from the smaller by submerging the sample in n-hexane at various temperatures individually. Figure 7 shows that as the time and temperature increases, the rate of PEG 600, SA and PW removal increases. Similar results are reported in the literature [10].Because of opened up diffusivity and dissolvability at a higher temperature, more PEG 600, SA and PW condense in n-hexane and turn out from the specimen consequently setting off extra weight reduction. Essentially, as time builds, additional time is accessible to break down the binders.

Cracks are formed in solvent debinding above 52°C in the sample may be due to thermal expansion and reduction and same is observed in the experiment. The swelling of sample occurred due to insoluble backbone binder stay in n-hexane causes expansion in a long time [11,12]. At the point when compacts are taken out at a higher temperature amid solvent debinding results in solvent drain out and evaporate. This leads to the sudden temperature drop and expansion and rapid contraction encourages inside worries in the specimen and causes splitting as shown in Figure 8. It is likewise observed that dissolvable debinding above 60° C, sample sagging happens may be owing to unstiffening of binder component PEG 600, SA and PW. Since split and dense sagging arise beyond 50° C and few splits also arise in few samples which are solvent debound at 50° C, deformity free dissolvable debinding smaller temperature has been chosen at 48° C where no split (crack) or twisting has been seen in any samples.

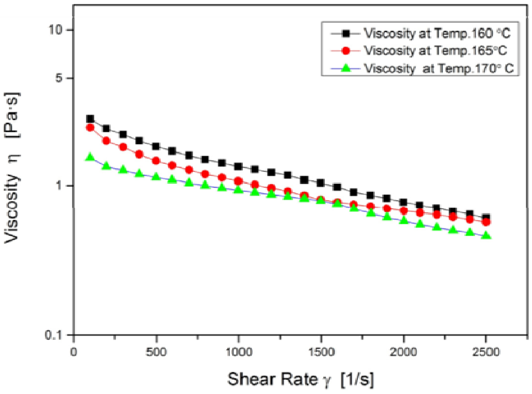

Fig.6 The relation between the viscosity of SS316L+WC-CrC-Ni feedstock and shear rate.

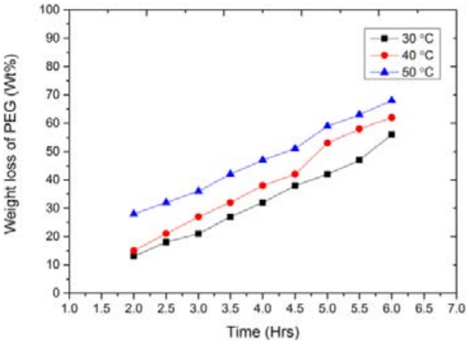

Fig. 7 Impact of debinding temperature on the weight reduction of MIM sample immersed in n-hexane for various times.

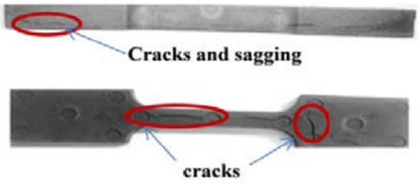

Fig. 8 shows the cracks and sagging on compact after debinding.

To create interconnected pores for backbone binder (LDPE) solvent debinding was performed, from interconnected pores the backbone binder evaporation takes place during thermal debinding and also its necessary to create interconnected pores at least 30 % at solvent debinding [13] and it is good to have more pores created during solvent debinding for stress-free subtraction of backbone binder in thermal debinding. In the meantime era of extra pores means expulsion of more PEG 600, SA and PW. Since at 48° C, around 60 % of PEG-600, PW and SA have been expelled and no issue in warm debinding of the samples is gone over, dissolvable debinding has been done up to 5 hours. Figure 9 and Figure 10 demonstrate the micrograph of infusion green sample before debinding and after dissolvable debinding at 48° C for 5 hours respectively. Figure 9 demonstrates that binder encompasses the powder particles. Because of the expulsion of the vast majority of the significant constituent of the binder, PEG 600, PW and SA, in dissolvable debinding, powder particles are not completely encompassed by binder found in Figure 10.

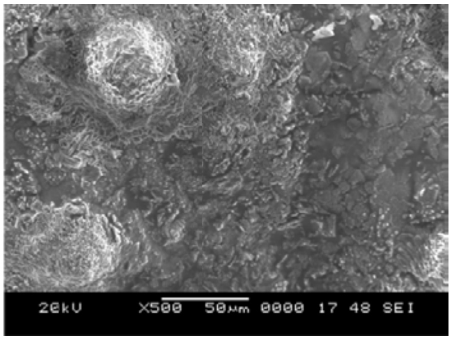

Fig.9. Micrograph of MIM green samplebeforedebinding.

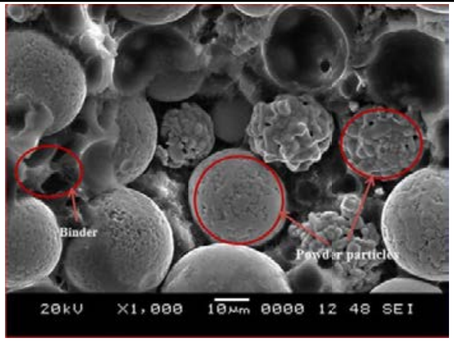

Fig.10. Micrograph of MIM sample after solventdebinding

The solvent debound sample has been thermally debound at various temperature and dwell time. In the thermal debounding the major backbone binder LDPE and the rest of the PEG-600, SA and PW which stay after after solvent debinding. are completely removed through previously created interconnected pores in solvent debinding. Normally, debinding time relies on upon the thickness of the green specimen and it is relative to the square of the green example thickness [14]. At temperature 500°C no binder is left following 5 hours of holding time. In this phase, the minimal is sensitive to deal with till sintered. Therefore, the samples those are sintered are all solvent debound at 48° C for 5 hrs in n-hexane followed by thermally debound at 500° C for 5 hours under hydrogen atmosphere. Figure 11. shows SEM Micrograph of a sample after thermaldebinding.

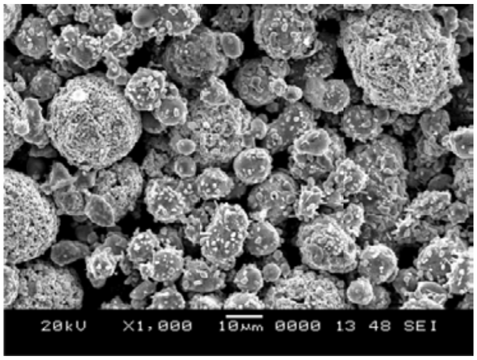

Fig. 11. Shows SEM Micrograph of a sample after thermal debinding. a) SS316L+WC-CrC-Ni

In the present investigation, thermal debound tensile compacts have been sintered. It is seen that as the temperature increases, density increases but beyond the formation of the liquid phase, compact shape starts distorting [15].Therefore, with a view to achieving maximum density and mechanical properties, sintering has been carried out at 1200 ° C and a pure hydrogen atmosphere has been used to avoid oxidation.In sintering cycle, the heating rate is varied from 1 to 5°C/min and also soaking time is allowed to remove remaining binders in the compactandtostabilisethefurnacetemperature.Initially, 2°C/minconstantheatingratemaintained upto1000°C followed by 80 min,80 min and 30 min soaking time at 250 °C, 400°C and 1000°C respectively. In the next stage 1°C/min heating rate is minted for densification of tensile specimen till 1200 °C, and also 5°C/min cooling cycle was adopted for 200 ° C than furnace cooling. The important of cooling cycle is for avoiding distortion in tensile specimen due to a sudden drop in thetemperature.

The tensile specimens of solvent decided compact and sintered at 1200° C has been shown in Figure 12, and the micrograph of the sintered tensile specimen shows Figure 13,it is observed that SS316L+WC-CrC-Ni tensile specimen micrograph showing fishbone structure that powder particles are bound together and it is also observed that isolated pores are separated from the grain boundary.

Fig. 12.Tensile specimen sintered at 1200 °C

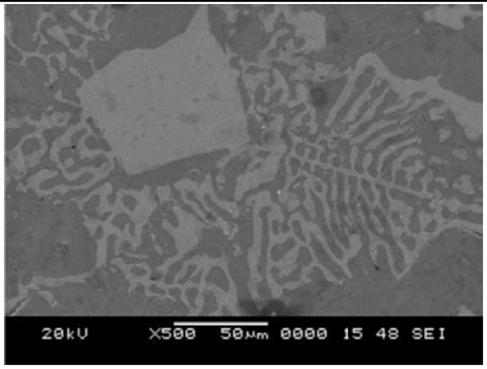

Fig. 13 Micrograph of the sintered tensile specimen a) SS316L+WC-CrC-Ni

A Clear sign of the occurrence of liquid phase during sintering cycle appears in the samples, heated up to 1200 °C viewing herringbone morphologies. The average values of Microhardness and density of sintered specimens have been given in table 7.

Material	Density (g/cc)	Microhardness (Hv)
SS316L+WC-CrC-Ni	7.76	459

Table:7 Mechanical properties of tensile specimen

Material	Length (Shrinkage %)	Width (Shrinkage %)	Thickness (Shrinkage %)
SS316L+WC-CrC-Ni	13.65to14.28	15.37to16.76	14.68 to 15.89

Table 8 Linear shrinkage

As the specimens are sintered, density increases by the elimination of pores and substantial shrinkage occur in the specimens[16]. Shrinkage upon sintering of the specimens has been measured in length wise, width wise and thickness wise that is, in X, Y and Z direction. Shrinkage varies given in table 8. Ideally, shrinkage should be equal in all directions in MIM, in this case, overall shrinkage varies.This variation of shrinkage may be attributed to the segregation of powder and binder phase in the specimen in the injection stage. Shrinkage variation is more in widthwise direction compared to the length and thickness-wise direction, more segregation of powder and binder phase widthwise direction. The bigger the powders are the greater the green density and lower the linear shrinkage [17]

IV. CONCLUSION

- Developed binders PW, LDPE and PEG-600 are successfully employed for defect free metal injection moulding component to selectedpowders.
- Injection parameters are optimised by several trails. Injection speed 41.4cc/s, injection time3.7s and feedstock velocity 5.85m/s at injection temperatures 160, 165,170° C.
- The binder is evacuated in two phases solvent depending took after by thermal debinding. In solvent debinding, as the temperature of the solvent expands the rate of PEG 600, PW and SA expulsion increments yet it is found that 48°C is ideal temperature.
- The rheological outcomes revealed that the feedstock of 56 vol.% powder loading exhibited pseudo-plastic behaviour i.e. as the shear strain rate increases viscosity decreases. SS316L+WC-CrC-Ni exhibits a viscosity within limits.
- Mechanical properties of sintered tensile specimens achieved the best density and microhardnessof
- SS316L+WC-CrC-Ni shows 7.76 g/cc and microhardness 457 Hv.

REFERENCES

[1] R. Jisa, S. Laumann, U. Cihak-Bayr, C. Tomastik, R. Eberle, M. Keppeler, U. Hofmann & F. Franek, Tribology - Materials, Surfaces &Interfaces,8.1(2014),p.27-34.

[2] J. M. Torralba, Int. J. Microstructure and Materials Properties,8(2013), p.87–96.

[3] Z. Y. Liu, N. H. Loh, S. B. Tor, K. A. Khor, Y. Murakoshi, and R. Maeda, Materials Letters, 48(2001), p. 31–38. [4] A. T. Sidambe, Materials 7(2014), p.8168–8188,

[4] L. Shu-quan, T. Yan, Z. Yong, and Z. Jie, J. Cent. South Univ. Technol,1(2007), p.378–381.

[5] R. M. German, ScriptaMaterialia,58(2008),p.295–298.

[6] N. H. M. Nor, N. Muhamad, M. H. Ismail, K. R. Jamaludin, S. Ahmad, and M. H. I. Ibrahim, International Journal of Mechanical and Materials Engineering,4 (2009), p.70-75.

[7] S. V Atre, R. M. German, and J. P. De Souza, Materials Science and Engineering,356(2003),p.337-344

[8] H. Abolhasani and N. Muhamad, J. Mater. Process. Tech., 210(2010), p.961–968.

[9] W. W. Yang, K. Y. Yang, M. C. Wang, and M. H. Hon, Ceram. Int.,29(2003),p.745–756.

[10] J. Hwang, S. Choi, S. Hong, and N. Kim, Journal of Mechanical Science and Technology, 27(2013), p.1815–1824.

[11] H. Guoxin, Z. Lixiang, F. Yunliang, and L. Yanhong, journal of materials processingtechnology,206(2008),p.395–399.

[12] M. German, Metal powder report,56(2001),p.18–22.

[13] J. Banhart, Progress inMaterialsScience,46(2001),p.559–632 .

[14] L.I.U.Xiang-quan,L.I.Yi-min,Y.U.E.Jian-ling,andL.U.O.Feng-hua,Trans.NonferrousMet.Soc.China,18(2007),p.278-284.

[15] K. R. Jamaludin, N. Muhamad, M. Nizam, A. Rahman, S. Y. M. Amin, M. Halim, I. Ibrahim, N. Hafiez, and M. Nor,Moulding Parameter, Proceedings of the World Congress onEngineering,1(2009),p.1–5.

[16] V. P. Onbattuvelli, R. K. Enneti, S. J. Park, and S. V. Atre, Int. J. Refract. Met. Hard Mater,36(2013),p.183–190.

★★★

FABRICATION OF NANOSTRUCTURED $Fe_{50}Ni_{25}Al_{25}$ POWDERS PREPARED BY MECHANICAL ALLOYING

[1]PRADYUT KUMAR SWAIN, [2]RATIKANTA SAHOO, [3]NALINIKANTA SWAIN

[1]Department of Mechanical Engineering, NMIET, Bhubaneswar, 751019
[2]Department of Mechanical Engineering, REC Bhubaneswar
[3]Department of Mechanical Engineering CEC Bhubaneswar
E-mail: [1]bharat.chede@nmiet.ac.in

Abstract - Nanostructured powders of Fe50Ni25Al25 were prepared by mechanical alloying in argon atmosphere from elemental Fe, Ni and Al powders. The obtained powders were characterized by, X-ray diffraction, Transmission Electron Microscopy and 57Fe Mossbauer Spectroscopy. A detailed analysis of the diffraction patterns reveals a fast decrease of the crystalline size in the first hour of milling, after we obtained a stationary state. The final lattice parameter of this structure is close to 0.2895 nm. For the first milling time, Mossbauer spectra are composed of magnetic contribution characteristic of alpha iron and paramagnetic contribution attributed to Fe-Al (rich in Al). The formation of disordered solid solution Fe50Ni25Al25 is complete after 48 hours of milling.

I. INTRODUCTION

Mechanical alloying MA is a process used to produce alloys at room temperature having a fine microstructure; furthermore, it can be applied to alloy incompatible materials. Also, MA is a promising route to synthesize nanocrystalline alloys, amorphous alloys, structural intermetallics, and ceramic materials [1-5], in other words, materials with unusual structural properties [6]. Several physical properties of materials are strongly affected by the grain size. For instance, in metallic systems the yield stress increases with decreasing grain size over a considerable range as described by the Hall–Petch equation [7]. An analogous effect is the strengthening of a ferromagnetic material, with decreasing grain size in the micrometer to the tens of manometer range. When the dimensions of the grains become comparable with the characteristic length of the physical phenomenon involved, conventional scaling laws often break down and may even reverse [8]. These results strongly suggest that both functional and mechanical properties can be adapted by controlling the grain size of the material. The intermetallic show a clearly better behavior in the high temperature range especially regarding their creep-resistance and strength connected with low density compared to conventional materials. The large number of technological fields where Fe-Ni-Al interrnetallic compounds, have found useful applications makes these systems particularly attractive from an experimental point of view. In the previous papers, phase formation and nanometer order grained microstructures and their formation process were reported for the Fe-Ni-Al alloys by Mechanical alloying. It was found that the process of gradual refinement into nanometer order of crystal size and the formation of homogeneous solid solution take place concurrently. Another aspect of the present work is the opportunity to study the availability of homogeneous synthesis by mechanical alloying, starting from multi-elemental initialcomponents.

Only, very few papers have been found to be concerned with mechanical alloying of more than two elementary initial components.

II. EXPERIMENTALPROCEDURE

In order to prepare the alloys required for these studies, a mixture of appropriate amounts of Fe (99.9%, powder, grain size <60 μm), Ni (99.9%, grain size <100 μm) and Al (99, 97 grain size <100 μm) powder, were ball milled in a vial with balls. Both the vials (45 ml in volume) and the balls (12 mm in diameter) were made stainless steel. The powders were sealed in the vials under a pure argon atmosphere. Mechanical alloying was performed with a planetary ball mill type Fritsch-Pulverisette 7 with powders to ball weight ratio R= 1/35 and a rotating speed of about 1000 rpm. The total milling time was either 48h, interrupted for either 15 min every 30mn, respectively, in order to minimise excessive temperature rise and to limit the adherence of the powders to the vial walls. The investigation methods were X-ray diffraction patterns (XRD) and Mössbauer Spectrometry. Structural characterization was done by means of X-ray diffraction (XRD) using Cu-Kα (λ =0.154056nm) radiation at room temperature in the 2θ range from 25° to 130°. We also used the MAUD procedure [9] for microstructural XRD analysis, based on RietVeld [10] method combined with Fourier analysis, which is well adapted for broadened diffraction peaks. This version permits a more detailed analysis of the material thus since it can take in account the anisotropy of shape of diffraction domains coherent and of micro-deformations [11] as well as possible effects of texture [12]. The RietVeld's method was successfully applied for determination of the quantitative phase abundances of the mixture powders [1]. There is a simple relationship between the individual scale factor determined, considering all refined structural parameters of individual phases of a multiphase sample, and the phase concentration in the mixture. The weight fraction for each phase was obtained from the refinement relation as adopted by earlier [13]. The structure refinement along with size-strain broadening analysis was carried out simultaneously by adopting the Maud procedure [9] as mentioned previously, The Maud procedure can take in account the anisotropy of shape of diffraction domains coherent and of micro-deformations by fitting the reflections of these phases with POPA anisotropic model [11]. For the powders milled more or equal than 4 hours, the crystallite size and microstain values of disordered phase -Fe (Ni, Al) are fitted with POPA anisotropic model [11]. Mossbauer spectroscopy, which probes the local atomic structure of the alloys, has proven to be useful in studies of mechanical alloying [14-17]. ^{57}Fe Mossbauer spectra were recorded at room temperature in transmission geometry with a constant acceleration apparatus. The spectra were analysed by means of the MOSFIT program developed by F. Varret et al [18], which extracts an hyperfine mean field distribution, P (H), from an experimental spectrum. The isomer shift (IS) at the ^{57}Fe nuclei is given relative to α-Fe at roomtemperature.

III. RESULTS ANDDISCUSSIONS

3. 1. X-rays analysis

X-ray diffraction spectra for the $Fe_{50}Ni_{25}Al_{25}$ powders are shown in Fig.1. Only narrow range of diffraction angles is presented (35-115°), but it contains the all lines of all components. The diffraction patterns indicate that the unmilled powders contains only the element Fe, Ni and Al. Analysis of X-rays patterns with MAUD program reveal that the concentrations of the elements Fe, Ni, and Al are close to the initial proportions i.e. 50%Fe, 25%Ni and 25%Al. For short milling time (30mn) (Fig.1), only relatively sharp diffraction peaks of elemental powders are observed on the XRD patterns and it's observed a fast decrease of the intensity of the (111) diffraction peak of -Al. For a powders mixture milled for 1h and 2h the X-rays diffraction patterns are fitted by using 3 components, because it takes into account the two various distributions of the Fe(Ni, Al) crystallites sizes and those is due to the fact that the lines diffraction peaks are asymmetrical and justify our choice clearly whatever the crystallite shapes, on the another hand, all the possibilities were explored to improve the fitting of mixture powders milled for 1h and 2h with two components but without success (fig.2). The broadening of the Bragg peaks with milling time (fig.3) indicates a progressive decrease in crystallite size and accumulation of microstrains induced by repeated fracturing and cold welding of the powder particles. After 1h of milling, crystal peaks of -Al seem to disappear and the peaks of -Fe become lower and broader, and the powders are mainly in the FCC form (-Ni (Fe, Al)) rich onNi, there is only 22% of Fe in the BCC form (- Fe(Ni, Al)) rich on Fe.

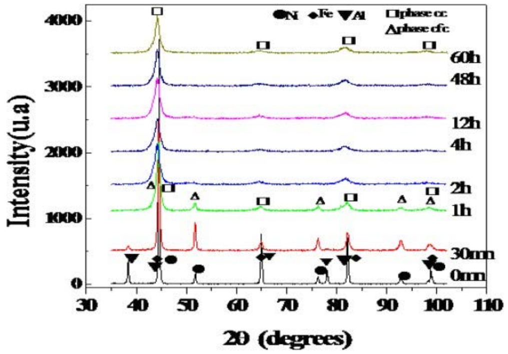

Figure 1: X-rays diffraction patterns of mechanically alloyed $Fe_{50}Ni_{25}Al_{25}$ powders milled at various times.

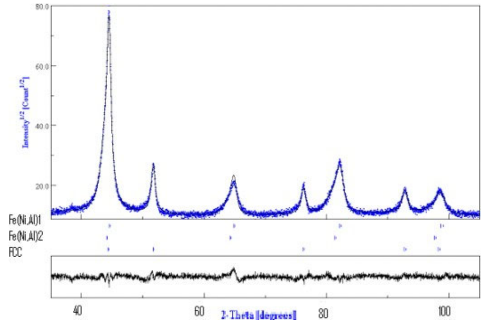

Fig.2: XRD patterns of mechanically alloyed $Fe_{50}Ni_{25}Al_{25}$ powdersmilledfor1hwith3components. Experimental(dots) and calculated (fullline).

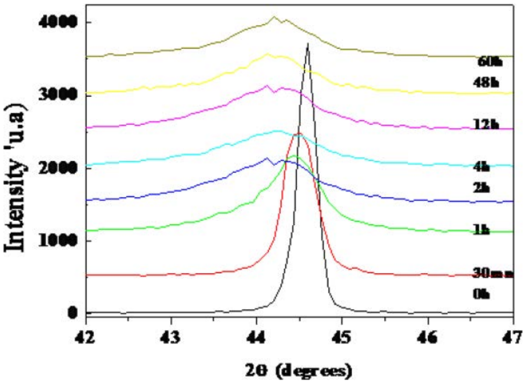

Fig.3: Evolution of the pick situated to the surrounding 45° as function of the milling time showing the broadening and the displacement toward the left of the peak.

The best fitting is obtained with 3 components: 1 FCC and 2 BCC with different crystallite sizes and microstrains. This means that some Fe atoms, which have the smaller atomic radius than Ni are diffused in Ni matrix, with Al atoms witch have better affinity with Fe atoms than Ni. Neither superstructure reflections nor peaks corresponding to DO3 structure or B2 ordered structure have observed in these mechanically alloyed $Fe_{50}Ni_{25}Al_{25}$ powders. We noted that the crystallite size is in nanometric range after only one hour of milling, and is about 10 nm for 48 hours of milling. The progress of alloying is illustrated in Fig.4, which shows the change of BCC and FCC lattice parameters for α-Fe(Ni, Al) and γ-Ni(Fe, Al). The γ-Fe(Ni, Al) lattice parameter increases strongly at the first hours of milling and approach a saturation value with longer processing, but the α-Fe(Ni, Al) lattice parameter increases until one hour of milling after its decreases and reached a quasi-stationary state . It is necessary to note that the percentage of γ-Fe(Ni,Al) phase decreases in a continuous way. This indicates that alloying takes place mainly within the first 4 hours, reaching a steady state after12heures.

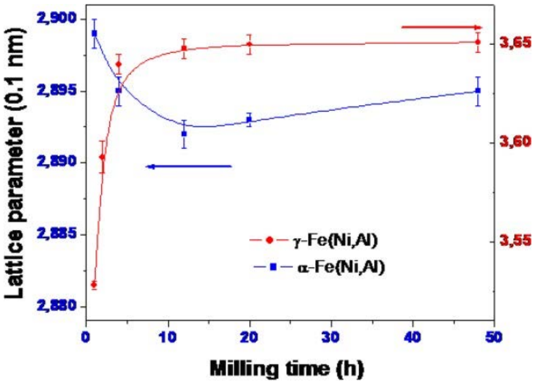

Fig.4: Lattice parameters of α-Fe(Ni,Al) and γ-Fe(Ni,Al) as function of milling time.

3.2 MET analysis

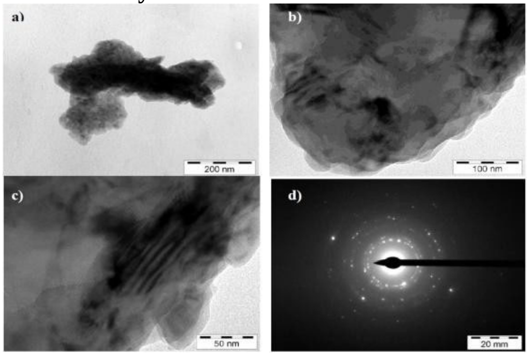

Fig.5: Bright field transmission electron micrographs (TEM) at different magnifications and of the $Fe_{50}Ni_{25}Al_{25}$ powder milled for 12hours and (d) selected area diffraction rings of the region in (c).

Direct observation of the individual grains within the deformed powder particles by TEM indicates that the crystallites sizes are in the manometer range. TEM bright-field micrographs of a particle of a $Fe_{50}Ni_{25}Al_{25}$powder milled for 12 h at different magnification are shown in Fig. 5. The presence of nanocrystallites in this particle is best evidenced considering that the selected area diffraction (SAD) pattern Fig.6 d shows a ring-like pattern due the distinct orientations of the crystallites. The corresponding SAD pattern shows whose radii agree with the bcc Fe structure and fcc Ni structure. Such as view of the diffraction pattern can brought about coexistence of amorphous and nanocrystalline phases, the latter of which is α-Fe and γ-Ni. Chemical compositions of the obtained milled products were analyzed using energy dispersive X-ray spectroscopy (EDS) methods, equipped in TEM. The EDS analysis have shown inhomogeneous Ni and Al distribution in the Fe particles formed (see Figure 6) indicating that the homogenous alloy is not closed.

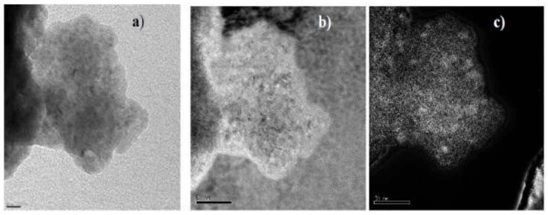

Fig.6: Bright field transmission electron micrographs (TEM) (a), map of Ni (b), and Al (c) of the $Fe_{50}Ni_{25}Al_{25}$ powder milled for 12 hours

3.3 Mossbauer analysis

Magnetic structure can be determined by Mossbauer spectroscopy that allowed obtaining information about local interactions between iron nuclei and their nearest-neighbourhood, observing the process of alloy formation and change of its magnetic properties at every stage of the milling. The Mossbauer spectra for $Fe_{50}Ni_{25}Al_{25}$ alloy prepared by high-energy ball milling process are shown in Fig.7.a for various milling times. Three mains components can be seen on these spectra. The observed Mossbauer spectrum is composed on two sextuplets and one doublet. At short milling times, the first sextuplet is characteristic of pure iron or iron slightly substituted, and it's predominant. The second sextuplet characterized by a hyperfine field lower than 330 kG and a broad line-width which increases with the milling time. This component is come significant gradually with increasing milling time. At the same time, the intensity of the first sextuplet decreases gradually. The doublet which characterizes the Fe largely substituted by Al, its intensity goes through a maximum at 1h. However, it is necessary to note that the doublet is unimportant at 4h of milling; it is no longer observed in powders ground for 12h and more. The variation of the average hyperfine field < H > according to the milling time is shown on Fig.7.c. That can be divided into three stages: a fast reduction at the beginning of milling indicating that the combination with aluminium is very important and a light increase indicating that the Ni atoms gradually integrate the first coordinate sphere of the Fe atoms, certainly in the BCC structure and finally quasi-stationary state. The process of MA, in binary alloys is generally made up of two stages which occur simultaneously: refinement of the grains and formation of the multi-layer structures (stage 1)and then finally formation of alloy (stage 2) as reported by several authors[19-21].

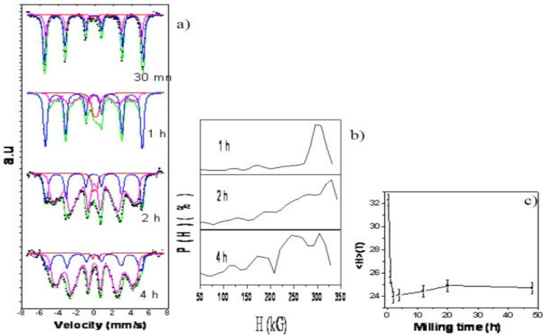

Fig.7: ^{57}Fe room temperature Mossbauer spectra (a) , some associated HFD (b) and average hyperfine field (c) ofpowders mixture FeNiAl as millingtime.

IV. CONCLUSION

The TEM and the electron diffraction results confirm the nanocrystallites nature of the as –prepared sample in accordance with both broads XRD peaks and hyperfine field distributions. On the basis of the X-rays analysis, transmission electron microscopy and Mossbauer Spectroscopy, the process of nanocrystallization appears to be composed by 3 stages: progressive refinement of elements Fe, Ni and Al grains within the sandwich type microstructure (stage 1), formation of the binary FeAl, FeNi and NiAl presumably at the interfaces between Fe, Al, Ni. (stage 2) followed by the formation of the ternary FeNiAl (stage 3).The X-rays and Mössbauer spectroscopy results showed that three stages take place almost simultaneously. The X-rays diffraction analysis indicates there is a rapid nanocrystallization of Al; the formation of ternary alloy occurs in a progressive way and Mössbauer spectrometry shows that the formation of FeAl tens to start after short milling times.

REFERENCE

[1] Djekoun, B.Bouzabata, A. Otmani, J.M.Grénèche, Catalysis Today, 89 (2004)319A.
[2] Y.Zou, K.Kiyoshi,S. Saji, Mat. Research Bulletin 37 (2002) 1307-1313.
[3] Albiter, E. Bedolla, R. Perez, Mat. Sci.Eng. A328 (2002) 80-86.
[4] X. J. Gu, F.Ye, F. Zhou, K. Lu , Mat. Sci. Eng. A278 (2000) 61-65.
[5] E. Jartych, J.K. Zurawicz, D. Oleszak, M. Pekala, J.Magn. Magn. Mater. 208 (2000)221.
[6] J.S. Benjamin, Mater. Sci. Forum 88–90 19921.
[7] F.J. Humphreys, P.B. Prangnell, R. Priester, Current Opinion in Sol. Stat. Mat. Sci. 5 (2001)15.
[8] E. Arzt, Acta Mater. 46 (1998)5611.
[9] L. Lutterotti, S. Matthies, H.R. Wenk, Proceding of the Twelfth Intenational Conference on Textures of Materials (ICOTOM-12), Vol.1 (1999)1599.
[10] H.M. Rietveld, J. Appl. Crystallogr., 2 (1996)65. [11] N.C. Popa, J.Apll.Cryst., 31 (1998)176.
[11] H. R. Wenk, S. Matthies, L. Lutterotti, Mater. Sci.Forum, 157-162 (1994)473-480.
[12] R.A. Young, D.B. Wiles, J. Appl. Cryst., 15 (1982)430..
[13] F.Z. Bentayeb, S.Alleg, B.Bouzabata, J.M. Grenèche, J.Magn. Magn. Mater., 288 (2005)282.
[14] N.Bensabaa, S. Alleg, J.M. Grenèche, J. Alloys and Compounds, 393 (2005)194.
[15] H. Moumeni, S. Alleg, F.Z. Bentayeb, J.M. Grenèche, J. Alloys and Compounds, 386 (2005)12..
[16] G. Le Caër, P. Delcroix, T.D. Shen, B. Malaman, Phys. Rev. B 54 (18) (1996)12775..
[17] F.Varet, J.Teillet, MOSFIT program, unpublished,(1976).
[18] K. Wolski, G. Le Caër, P. Delcroix, R. Fillit, F. Thévenot, J. Le Cose, Mat. Sci. Eng., A207 (1996)97.
[19] Otmani, B. Bouzabata, A. Djekoun, S.Alleg, Ann. Chim.Sci. Mat. 22 (1997)201.
[20] C.Lemoine, A. Fnidiki, D. Lemarchand, J. Teillet, J. Phys : Condens. Matter, 11 (1999)8341.

★★★

MULTI AXIS INDUCTIVE DISPLACEMENT SENSOR

[1]PRAJNA KAR, [2]SWASTI NAYAK, [3]ASHIS TRIPATHY

[1]Department of Mechanical Engineering, NMIET, Bhubaneswar, 751019
[2]Department of Mechanical Engineering, CEC Bhubaneswar
[3]Department of Mechanical Engineering, REC Bhubaneswar
E-mail: [1]mohammad.israr@nmiet.ac.in

Abstract - This paper presents a novel multi axis inductive displacement sensor design and analysis. The proposed sensor capable to measure the displacement and also tilt angle of the objects without contact. First, an analytical model is developed to express the measurement principle. Then 3D finite element analysis (FEA) is performed to verify analytical model by using Ansys Maxwell software. In the analysis, 0-5 mm linear movement and 0-3° tilt angle are considered. Finally, an experimental setup is built and performance tests are performed.

Keywords - Inductive Sensor, Displacement Measurement, Tilt Angle

I. INTRODUCTION

With developing technology, the need for accurate position and/or displacement measurement in the micrometer level has increased significantly. In the industry, different type of applications about position and displacement sensing can be found. For many of these, sensors based on mechanical contact are sufficient to position measurement. But, some of these applications are require non-contact measurement. Inductive displacement sensors are widely used for contactless measurement [1-3].

In the literature, many kinds of measurement applications were investigated using inductive and eddy current sensors for displacement and proximity sensing [3-10]. These studies mostly focused on thermal stabilities and electronical interfaces of the sensor to improve measurement quality of the sensors [4-7]. Moreover, most of the studies are dealt with single axis position measurement [4-6]. Although some studies have done about angular measurement and two axis tilt measurement by using multi coil printed circuit board technology and combining flux gate sensor principle with magnets [8-10], there is no study about multi axis tilt angle measurement by using inductive displacement measurementprinciple.

In this paper, a novel multi axis inductive displacement sensor which has one excitation coil and two sensing coils, will be presented. Firstly, sensor structure is introduced and analytical solution based on Lenz Law is carried out. Then the sensoris analyzed to verify the analytical results by using 3D finite elements method. Finally, a sensor is built and tests are carried out to verify the theoretical results.

II. ELECTROMAGNETIC ANALYSIS

A. System Description and Model Development

A novel structure has one excitation coil in the middle of the square base and two sensing coils at the corners as shown in Fig. 1. This structure allows us to sense tilt on the target metal by evaluating the voltage cause voltage induction on sensing coil. Induced voltage is amplified and then filtered to get linear analog output.

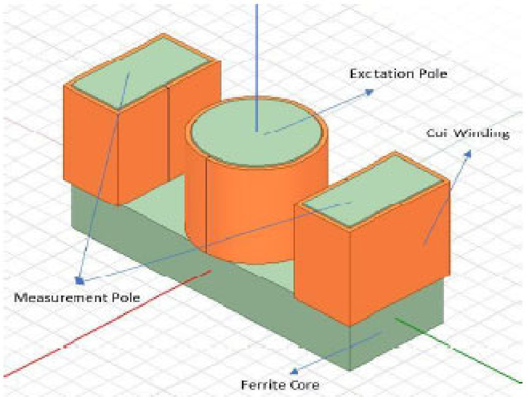

Fig 1: CAD model of the proposed sensor.

Any change in the magnetic environment of a coil of wire will cause a voltage (emf) to be "induced" in the coil. No matter how the change is produced, the voltage will be generated. The change could be produced by changing the magnetic field strength, moving a magnet or metal toward or away from the coil, moving the coil into or out of the magnetic field, rotating the coil relative to the magnet, etc. says Faraday's law and presents this phenomenon as follows;

$$e = \frac{d\lambda}{dt} \qquad (1)$$

where, λ is the flux linkage and defined as follows;

$$\lambda = N\phi \qquad (2)$$

where, $\phi$is magnetic flux and expressed as follows by assuming the magnetic resistance and the hysteresis of the sensor core, eddy currents, flux leakage and fringing effects areneglected;

The sensor gets excited by an excitation circuit which creates sine waves.

$$\phi = \frac{Ni}{R_{gap}} \qquad (3)$$

where, i is the excitation current and *Rgap*is the reluctance of airgap between sensor head and target can be calculated as follows;

$$R_{gap} = \frac{x}{\mu S} = \frac{1}{P_{gap}} \qquad (4)$$

where, x is length of the airgap, $\mu$is the permeability and S is the pole cross section area. Permeance can be defined as inverse of reluctance. Permeance values change by linear displacement and tilt angle of target represented as *z, α, β*. These permeances can be calculated by solving double-integrals as follows;

$$P_{gap1} = \iint_{a-b}^{b+a} \frac{\mu}{z - \tan\beta + x\tan\alpha} .dx.dy$$

$$P_{gap2} = \iint_{a-b}^{b+a} \frac{\mu}{z - \tan\beta + x\tan\alpha} .dx.dy \qquad (5)$$

In this study, magnetic circuit principle is used in order to derive induced voltages.
Magnetic circuit equivalent of the system can be seen from the Fig. 2.

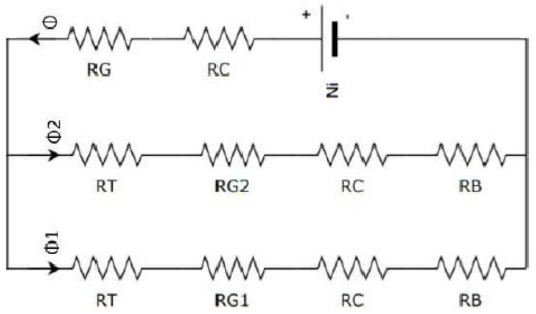

Fig 2: Equivalent Circuit

R_C, $R_B$and $R_T$are coil reluctance, core reluctance and target reluctance respectively. And reluctance of a material can be calculated asfollows;

$$R = \frac{l}{\mu_0 \mu_r A} \qquad (6)$$

where l is material length, μ_0 is air relative permeability, $\mu_r$is materila relative permeability and A is the material cross sectional area.

Analtical results are found by solving this equivalent circuit. And results are presented in section.

B. Finite Elements Analysis

Finite element analyses are performed using Ansys Maxwell Software. Linear displacement and tilt angle effects are examined. The model is designed on Ansys Maxwell. A ferrite core used as sensor base and coils are designed as solid copper whichhas 4mm thickness. To prevent the skin effect, steeltarget thickness has chosen as 5 mm in the analysis.

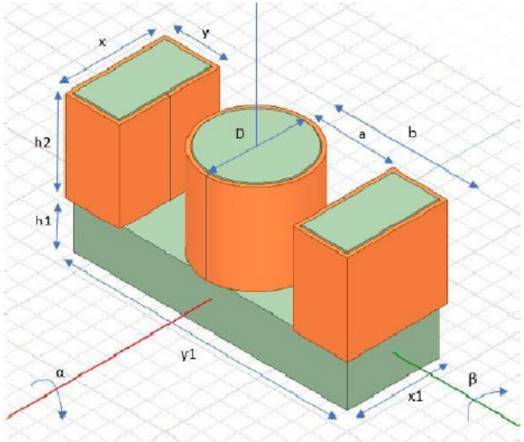

Fig 3: Symbolic representation of dimensions

After completing the design, mesh operations are performed separately on core, coil and target. And mesh parameters are listed on the following table. Mesh distribution on the sensor and the target is shown in theFig.4

Name	*Number of Additional Elements*
Body	1000
Coil	2000
Target	2000

TABLE I. MESH PAREMETERS

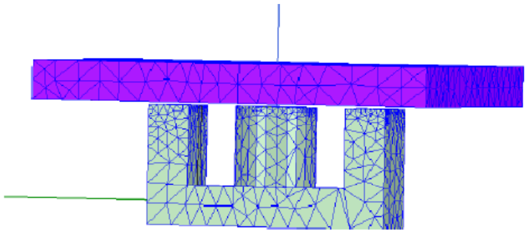

Fig 4: Mesh Distribution

After completing mesh operations and setting solving parameters, the analysis has been run.

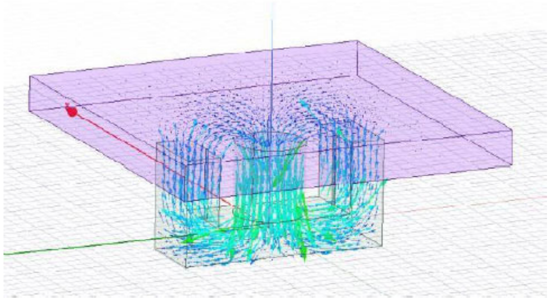

Fig 5: Magnetic Flux Distribution

When the excitation coil is excited magnetic flux is created and starts to flow form excitation coil through target, sensing coils and the sensor core respectively. Magnetic flux density is maximum on the excitation coil as expected and lowers down while going through target and sensor core. Finally, it increases when completing to circuitry as seen in the Fig.5.

III. EXPERIMENTAL SETUP

In this section experimental setup is presented. At first a sensor is built which has similar structure used in the analysis. The sensor structure built in for experimental tests has an excitation coil in the middle and two sensing coils around it. The sensor is built form a ferrite core and 0.4mm copperwire.

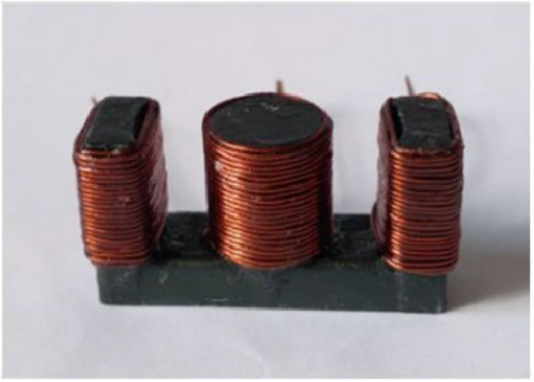

Fig 6: The Sensor Built for Experimental Tests

Dimensions of the excitation coil is Ø10x10mm, dimensions sensing coils are 5x10x10mm. Total length of the sensor is 30mm and all coils have 44 turns.

By using this sensor structure experimental tests are performed. A gauge tester which has 0.1mm thickness is used to measure the displacement.

A function generator is used as an excitation source and an oscilloscope is used to measure the voltage changes on sensing coils.

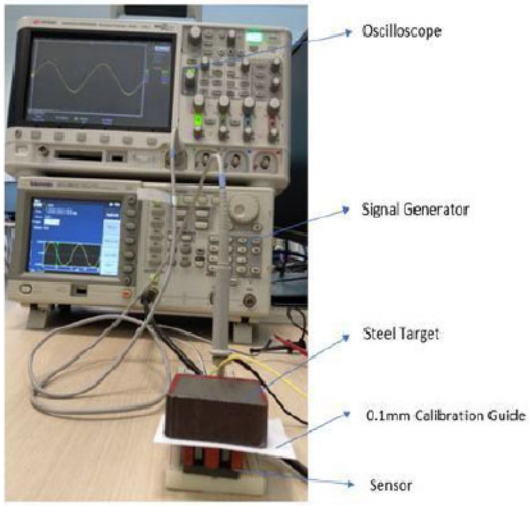

Fig 7: Experimental Setup

IV. RESULTS ANDDISCUSSION

In this section a detailed results of analytical model results, FEA results and test results are presented. Results achieved from these methods are compared and discussed.

FEA analysis and analytical model are performed for the parameters listed in the following Table 2 and Table 3.

Parameter	*Magnitude*	*Unit*
l_c	0.010	m
l_b	0.010	m
l_t	0.010	m
μ_0	4xπx10-7	-
μ_{rc}	2200	-
μ_{rb}	2200	-
μ_{rt}	100	-
A_c	50x10-6	m2
A_b	150x10-6	m2
A_t	150x10-6	m2
A_{ex}	78x10-6	m2

TABLE II. SENSORPARAMETERS

Parameter	*Magnitude*	*Unit*
x	10	mm
y	5	mm
D	10	mm
a	10	mm
b	15	mm
h1	5	mm
h2	10	mm
x1	10	mm
x2	30	mm

TABLEIII.SENSORDIMENSIONS

Parameter	*Magnitude*	*Unit*
i (excitation current)	10	mA
f (excitation frequency)	1	1kHz
N (number of turns)	44	-
z (linear displacement)	0.2-5	mm
α (tilt angle thorough x axis)	0-3	◦
β (tilt angle thorough y axis)	0	◦

TABLE IV. ANALYSIS PARAMETERS

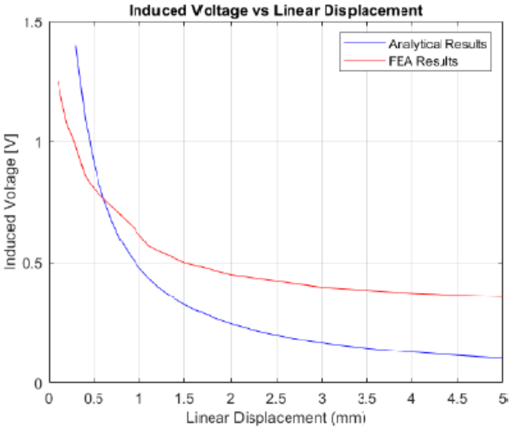

Fig 8: Comparison of FEA and Analytical Results – Induced Voltage vs Linear Displacement

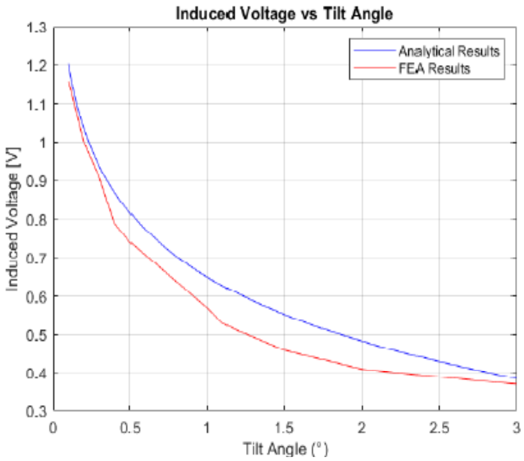

Fig 9: Comparison of FEA and Analytical Results – Induced Voltage vs Tilt Angle

Fig. 8. and Fig. 9. show comparison of the results between analytical and FEA results. It can be seen that there is difference between analytical and FEA results. In analytical results the mechanical instabilities, eddy current losses and other losses to environment doesn't considered and that caused that difference between these results which is expected.

Since two sensing coils are identical, the induced voltage on four sensing coils are also identical. But the induced voltage is nonlinear because of the Faraday's Law.

Fig. 9. shows the change the induced voltage on the sensing coils against tilt on target It also shows a nonlinear change on coils as expected. It is also expected that the excitation voltages on both coils should be decreasing because when one side of the target getting away from the sensing coil other side is also getting away as seen Fig.9. However, while the target gets far away from the one of the sensing coils (l), the displacement change on other target becomes really smaller (k). Because of the sensor resolution this change can not be observed; and the voltage change on that coil keeps constant.

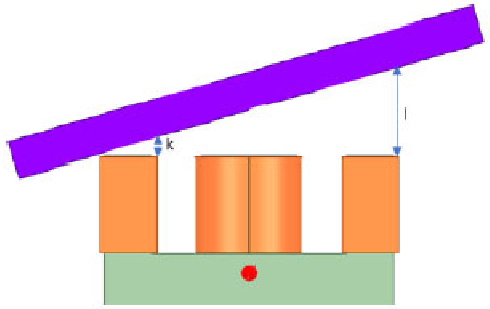

Fig 10: Tilt change of target -Exxagerated illustration

Fig. 11. shows the induced voltage on sensig coils against linear displacement. And it shows similar nonlinear characteristics as FEA and analytical results as expected.

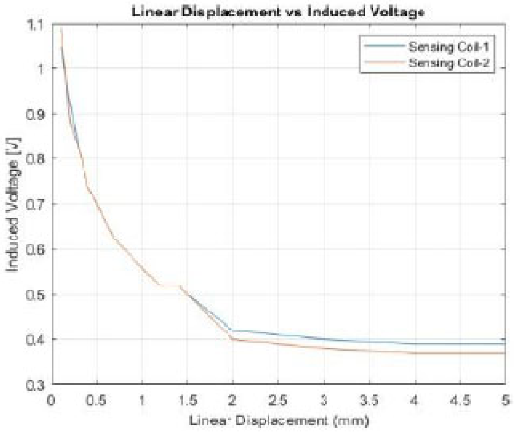

Fig11:TestResults–InducedVoltagevsLinearDisplacement

It can be seen from the Fig. 11. that builted sensor can be linearized between from 0-1.2mm. AndFig. 12.shows that voltage change against tilt on sensingcoils are almost linear up to 3°. Fig. 12. shows theinduced voltage on sensig coils against tilt anglechange on each coil separately. While performing tiltangle measurement, one side of the target kept fix asseen in Fig. 10. and voltage change on senging coilswere measured. So while the voltage on one of thesensing coil is decreasing other didn't change

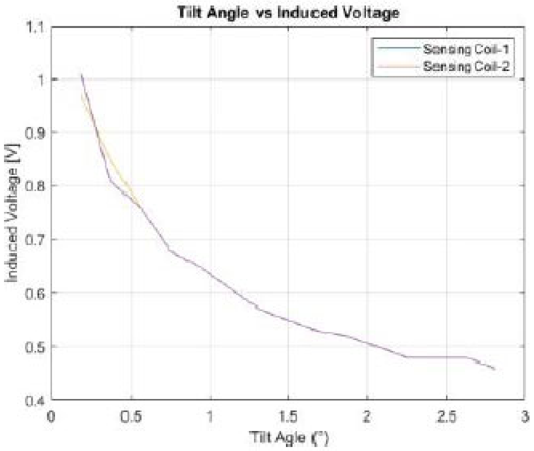

Fig 12: Test Results – Induced Voltage vs Tilt Angle

V. CONCLUSION

This paper presents a novel multi axis inductive displacement sensor analysis. The sensor is analyzed by analytically and FEA. Preliminary results show that the voltage output can be linearized for 0-1.5 mm displacement and for 0° to 3° tilt angle. Experimental results show thattheproposedstructureisachivable.

REFERENCE

[1] B. George, Tan. Z and S. Nihtianov. "Advances in capacitive, eddy current and magnetic displacement sensors and corresponding interfaces." IEEE Trans. Ind. Electron 64 2017, pp.9595-9607.

[2] S.Tumanski,—Inductioncoilsensors—Areview‖ Measurement

Science & Technology – vol. 18, no. 3,2007.

[3] M.R.NabaviandS.Nihtianov,―DesignStrategiesforEddy-Current Displacement Sensor Systems: Review and Recommendations‖, IEEE Sensors Journal, vol. 12, no. 12, 2012, pp.3346-3355.

[4] S. C. Chen, D. K. Le and V. S. Nguyen. "Inductive displacement sensors with a notch filter for anactive magnetic bearing system." Sensors 14.7 2014, pp. 12640-12657.

[5] SFericeanandRDroxler―Newnoncontactinginductive analog proximity and inductive linear displacement sensors for industrial automation‖, IEEE Sensors Jou., vol. 7, no. 11, 2007, pp.1538-1545.

[6] K Wang, L Zhang, Y Le, S Zheng, B Han and J.Yiang, ―Optimizeddifferentialself-inductancedisplacementsensor for magnetic bearings: Design analysis and experiment‖, IEEE Sensors Jou.., vol. 17, no. 14, 2017, pp.4378-4387.

[7] M.R.NabaviandS.Nihtianov,―Eddy-CurrentSensor Interface for Advanced Industrial Applications‖, Industrial Electronics, IEEE Transactions, vol. 58, no.9, 2011, pp 4414- 4423.

[8] R.Olaru,andD.Dragoi,―Inductivetiltsensorwithmagnets and magnetic fluid‖, Sensors and Actuators A: Physical, vol. 120,2005.

[9] L. Rovati and S. Cattini, ‖Contactless Two-Axis Inclination Measurement System Using Planar Flux-Gate Sensor‖, IEEE Trans. Instrumentation and Measure, vol. 59, no. 5, 2010, pp. 1284-1293.

[10] Z. Zhang, F.L. Ni, Y. Dong, J. Minghe, H. Liu,‖A novel absolute angular position sensor based on electromagnetism‖, Sensors and Actuators A: Physical, vol. 194, 2013, pp. 196 - 203.

★★★

INVESTIGATION OF LOAD-HAUL-DUMPER (LHD) MACHINE PERFORMANCE CHARACTERISTICS USING FEED-FORWARD-BACK-PROPAGATION ANN MODEL

[1]PRAKASH KATDARE, [2]SIDHARTH PRADHAN, [3]DEBASHIS MOHAPATRA

[1]Department of Mechanical Engineering, NMIET, Bhubaneswar, 751019
[3]Department of Mechanical Engineering, CEC Bhubaneswar
[3]Department of Engineering, REC Bhubaneswar
E-mail: [1]ahmad.omar@nmiet.ac.in

Abstract - Faced with intense global competition and to enhance the expected targets of production and productivity, every industry is constantly looking to maintain the equipment in an efficient and effective manner. Hence, it is more essential to predict the performance of the equipment. By keeping this in view, the present research work deals with an artificial neural network (ANN) modeling of the underground mining equipment such as load haul dumper (LHD) to predict the percentage of reliability, availability and preventive maintenance time schedules. The input data for network training was collected from the field visit. The prediction model was developed based on feed-forward-back-propagation Levenberg-Marquardt training algorithm. The performance of the equipment was validated by comparing computed data sets with predicted data. The predicted outcomes demonstrate that the ANN model provided good agreement with the computed data with highaccuracy.

Keywords - LHD, ANN, Performance, Reliability, Availability and Preventive Maintenance.

I. INTRODUCTION

In the present competitive business environment, all the industries have made the survival fight extremely tough due to serious competition among them. The increase in productivity aims at efficient and effective utilization of resources. As the production time has cost implications, many of the producers are motivated towards an additional reduction of time loss of production. [1]. In the meantime, as consumers are more worry about the safety and reliability of the systems the workers also desire a safe and sound work atmosphere [2]. In the time past, testing and investigation used to be strategies to measure reliability, this is no longer obtainable. The emphasis is on predicting the components that lead to breakdown and make sure that such factors are kept from occurring frequently using a robust design [3]. This can be accomplished by estimating the overall system performance of the equipment [4]. The investigation of execution attributes of any equipment in the industry plays a vital job in ensuring the smooth running of the production procedure since it ensures production continuity as well as product quality[5].

The performance analysis of Load-Haul-Dump (LHD) machines using analytic and statistic approaches will be taking more time to solve a complex problem as compared with software basis approach. Nowadays, soft computing techniques catch the attention of researchers for resolving a variety of non-linear problematical issues. Ingeneral, for such analysis, most of the conventional approaches cannot be resolved without the utilization of equations of fundaments, traditional correlations, or developing distinctive intends from investigational records through trial and error [6]. To maintain a strategic distance from these issues, the artificial neural network (ANN) technique has been executed in different sorts of confounding issues which are not comprehended by regular strategy and in different fields. This method processes information with not so much time but rather more precisely anticipated [7]. ANN has the capability to model both the linear and non-linear frameworks without the need to make suspicions as are understood in most customary measurable methodologies [8]. Hence, this tool has been becoming increasingly popular in various Engineeringfields.

II. CASE STUDY

The field investigation was carried out in one of the underground metal mines of the southern part of India. known as M/s The Hutti Gold Mines Company Limited and located in Raichur, Karnataka state, India. Drilling and blasting operations used to extract the ore, and for ore handling and transportation, LHDs are utilized as the major workhorse. LHDs are used to scoop the extracted ore, with a bucket, load it into the bucket, and dump it in the bottom of the mine to undergo a primary crushing operation before being hoisted to the surface out of the mine. Currently, the mine is operating with 7 numbers of LHDs with a capacity of each is about 3 Cu.M made by M/sEmico Elicon and Sandvick. A typical LHD machineatthe operating environment is shown in Fig1.

Fig 1. A typical LHD machine at the operating environment

III. DATA COLLECTION AND CLASSIFICATION

Before performing the analysis of a complex repairable system, it has to be categorized into a number of sub-assemblies in order to classify the breakdown modes. In the this investigation, each LHD was treated as an independent system and are named as LHD1, LHD2, LHD3, LHD4, LHD5, LHD6, and LHD7, and each LHD-system has been classified into eight numbers of sub-systems such as Sub-System of Engine (SSE), Sub-System of Braking (SSBr), Sub-System of Tyre (SSTy), Sub-System of Hydraulics (SSH), Sub-System of Electrical (SSEl), Sub-system of Transmission (SSTr) and Sub-System of Mechanical (SSM). Three major steps are known as the collection of required data, classification after collection and manipulation if necessary needs to be considered before performing the analysis. The collected data of Time Between Failures (TBF), Time To Repair (TTR) and Failure Frequency (FF) for each sub-system of the LHDs are given in TableI.

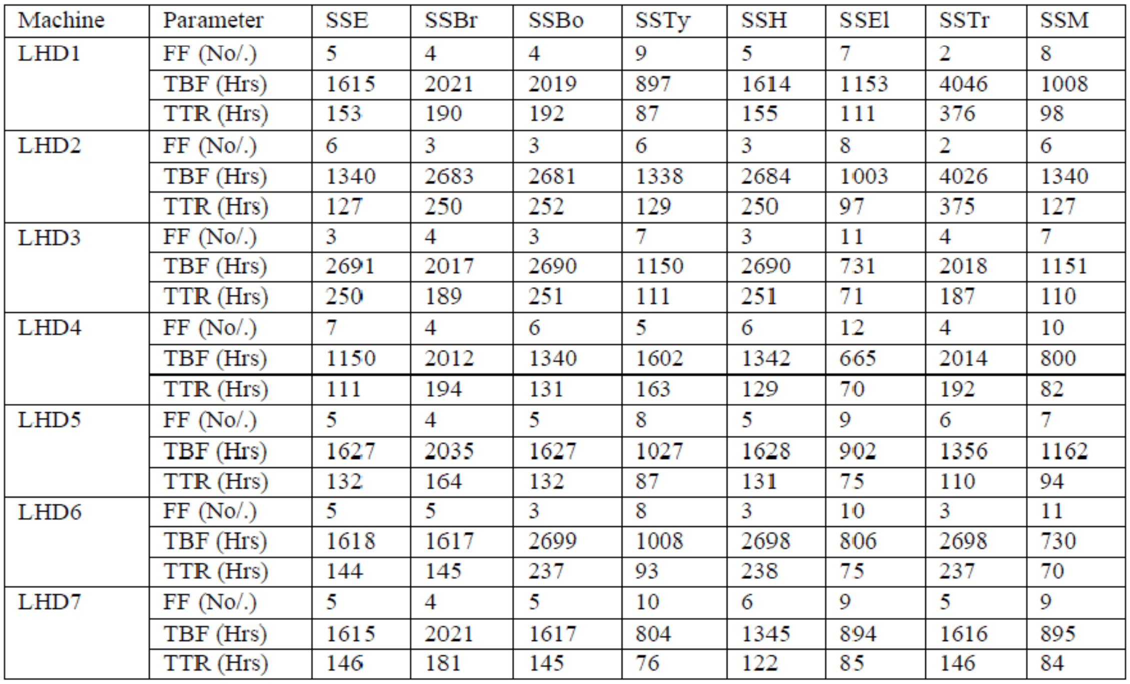

Machine	Parameter	SSE	SSBr	SSBo	SSTy	SSH	SSEl	SSTr	SSM
LHD1	FF (No/.)	5	4	4	9	5	7	2	8
	TBF (Hrs)	1615	2021	2019	897	1614	1153	4046	1008
	TTR (Hrs)	153	190	192	87	155	111	376	98
LHD2	FF (No/.)	6	3	3	6	3	8	2	6
	TBF (Hrs)	1340	2683	2681	1338	2684	1003	4026	1340
	TTR (Hrs)	127	250	252	129	250	97	375	127
LHD3	FF (No/.)	3	4	3	7	3	11	4	7
	TBF (Hrs)	2691	2017	2690	1150	2690	731	2018	1151
	TTR (Hrs)	250	189	251	111	251	71	187	110
LHD4	FF (No/.)	7	4	6	5	6	12	4	10
	TBF (Hrs)	1150	2012	1340	1602	1342	665	2014	800
	TTR (Hrs)	111	194	131	163	129	70	192	82
LHD5	FF (No/.)	5	4	5	8	5	9	6	7
	TBF (Hrs)	1627	2035	1627	1027	1628	902	1356	1162
	TTR (Hrs)	132	164	132	87	131	75	110	94
LHD6	FF (No/.)	5	5	3	8	3	10	3	11
	TBF (Hrs)	1618	1617	2699	1008	2698	806	2698	730
	TTR (Hrs)	144	145	237	93	238	75	237	70
LHD7	FF (No/.)	5	4	5	10	6	9	5	9
	TBF (Hrs)	1615	2021	1617	804	1345	894	1616	895
	TTR (Hrs)	146	181	145	76	122	85	146	84

Table I. Failure and repair data of LHDs from field investigation

IV. COMPUTING AND PREDICTION OF PERFORMANCECHARACTERISTICS

A. Kolmogorov-Smirnov (K-S)Test

The next step in this study is to analyze the goodness-of-fit (best-fit) approximation for TBF datasets. The best fit analysis was accomplished by utilizing the Kolmogorov-Smirnov (K-S) approach. The principle behind this is to see, how far the selected distribution is from the actual dataset, or in other words how well the selected distribution signifies the observed distribution. Four statistical probability distribution functions (Exponential, Weibull 1-Parameter, Weibull 2-Parameter, and Weibull 3-Parameter functions) were examined for the best-fit approximation.

The parameters for the appropriations were evaluated utilizing the Maximum Likelihood Estimate (MLE) strategy. These two tests were conducted by utilizing 'Isograph Reliability Workbench 13.0' software. The goodness of fit (best fit) approximations of the K-S test in accordance with TBF data and estimated factors of MLE are given in TableII.

Machine	K-S Statistics Dmax				ML Estimates of the Best Fit Parameters (η=Scale/life, β=Shape, γ=Location			Best Fit Model
	Exponential	Weibull 1P	Weibull 2P	Weibull 3P	ɳ	Β	γ	
LHD1	0.0610	0.0525	0.0468	0.0549	170.3	1	0	Weibull 2P
LHD2	0.1051	0.0640	0.0525	0.0864	200.9	1	0	Weibull 2P
LHD3	0.0799	0.0799	0.0799	0.0786	252.1	2.926	-45.44	Weibull 3P
LHD4	0.1901	0.17	0.0454	0.0467	151.2	2.874	0	Weibull 2P
LHD5	0.2236	0.2015	0.0634	0.0611	67.94	1.816	57	Weibull 3P
LHD6	0.1527	0.1361	0.0791	0.0745	124.8	1.201	47.11	Weibull 3P
LHD7	0.2075	0.1866	0.0789	0.0873	138.4	3.188	0	Weibull 2P

Table II. Kolmogorov-Smirnov (K-S) Test Results of LHDs

B. Estimation ofAvailability

Availability is one of the important measures in performance analysis. It can be measured by downtime losses, which includes any events that stop planned production for an appreciable length of time known as “breakdown time” and “idle time” such as machine failures, spare part shortages, and change over time.

$$\text{Availability}=\frac{\text{MTBF}}{\text{MTBF}+\text{MTTR}} \qquad (1)$$

Change over time may not be possible to eliminate but in most cases, it can be reduced. The remaining available time is called operating or working time [9]. On the basis of collected data, these were computed (Table III) as from (1) [10]. Due to maintenance and operational issues, the percentage of availability was reduced and observed as 70.00%(approximately).

Sl. No	Machine	MTBF(Hrs)	MTTR (Hrs)	Availability (%)
1	LHD1	326.6	30.95	71.34
2	LHD2	462.0	43.43	71.40
3	LHD3	360.4	33.80	71.42
4	LHD4	202.3	19.85	71.06
5	LIID5	231.9	18.87	72.47
6	LHD6	289.0	25.81	71.80
7	LHD7	203.9	18.58	71.64

Table III. Computed Results of Availability

C. Estimation of Reliability

Dependability is characterized as the likelihood of a machine or its parts can play out its pondered activity over a period of time in recognized conditions [11].

These were determined in Accordance with the best-fit approximation for particular an MTBF value.

From the computed results (Table IV) it was noticed that the highest reliability was observed as 78.28% (LHD3) and least level as 60.14% (LHD2) compared with others. Frequently occurring failures with fewer TBFs are the reasons for the drastic reduction of reliability percentage.

Sl. No	Machine	MTBF (Hrs)	η	β	γ	Reliability (%)
1	LHD1	326.6	170.3	1	0	64.78
2	LHD2	462.0	200.9	1	0	60.14
3	LHD3	360.4	252.1	2.926	-45.44	78.28
4	LHD4	202.3	151.2	2.874	0	58.18
5	LHD5	231.9	67.94	1.816	57	69.98
6	LHD6	289.0	124.8	1.201	47.11	65.44
7	LHD7	203.9	138.4	3.188	0	64.00

Table IV. Computed Results of Reliability

D. Estimation of Preventive Maintenance (PM) Schedules

Preventive maintenance can be characterized as the activities performed in an endeavor to hold the components in an indicated condition by giving an efficient assessment, identification furthermore avoidance from claiming early failure [12]. Forecasting of PM intervals is essential in order to improve the reliability. These were computed with respect to the expected reliability (Table V). From the results, it was understood that if the requirement of reliability as 90% for LHD1, then PM should be performed for every 18 hours. Similarly for LHD2 to LHD7 are 21, 71, 69, 77, 66 and 68 hours respectively.

Sl. No	Machine	Reliability (%)	η	β	γ	PM (Hrs)
1	LHD1	90.00	170.3	1	0	18
2	LHD2	90.00	200.9	1	0	21
3	LHD3	90.00	252.1	2.926	-45.44	71
4	LHD4	90.00	151.2	2.874	0	69
5	LHD5	90.00	67.94	1.816	57	77
6	LHD6	90.00	124.8	1.201	47.11	66
7	LHD7	90.00	138.4	3.188	0	68

Table V. Computed Results of PM Time Intervals

E. Neural Network Modelling

Artificial intelligence (AI) tools find vast applications in different forms for the mining industry. Especially, knowledge and expert-based systems are the most popular AI tools, that have a number of computer-based applications in day to day mining operations [13]. Nowadays, these techniques are utilized for the selection of machinery, optimization of operating procedures, decision making in a critical problem, etc. These AI frameworks together with a regularly expanding number of complex reason constructed PC programming bundles have made an entirely good condition for the presentation of one more dominant AI techniques, the Artificial Neural Network(ANN).

ANN is one of the simulation tools in MATLAB, intended to work with qualified functions as that of the working of brains in human beings [13]. The modeling and, the preparation of the system model was done utilizing the Neural Network Toolbox of MATLAB programming. The ANN displaying contains two stages: the primary stage is to prepare the system model, while the second stage is to approve the system model with new information which was not utilized for preparing. TheANN technique contains three numbers of layers: such as information layer for input, shrouded layer for mixing and yield layer for output. An example of a feed-forward ANN system is given in Fig 2 and demonstrated that each result of entering components (ai) and weights (wij) are feed to adding intersections and is added with bias (bj) of neurons.

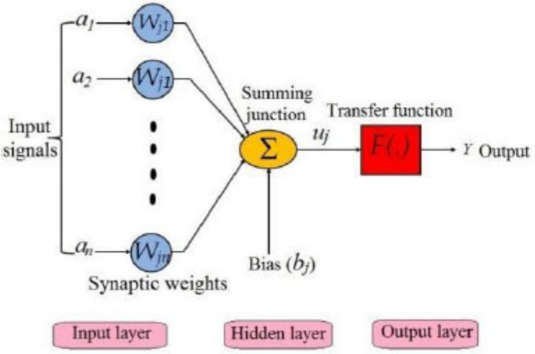

Fig 2. The basic structure of the ANN model (Source: [10])

ANN can also be defined as a complex information processing system, which is organized from interconnected segmental handling components, called neurons. These neurons discoverthe information data from different sources and perform commonly a non-linear operation on the outcome and after that give last outcomes as yield. A MATLAB based simulation tool can be utilized to estimate the responses from the modeled and trained input data. Infeed forward back propagation ANN model each component input data along with weights are fed to summing junction and summed with neurons of bias until it reaches to the threshold value given to (2) as follows [12]-[13]:

$$X = (^{n}{}_{i=1} Wij\ ai) + bj \qquad (2)$$

Where,
The total number input data are denoted as n, Wij be the interconnecting weights of input data (ai) and the bias for the neurons was denoted as bj. The value of X then passes through transfer function (F) of the model, referred to as in (3).

$$FX = ui = (^{n}{}_{i=1} Wij\ ai) + bj \qquad (3)$$

TANSIG and LOGSIG functions are the commonly used transfer functions for hidden layers. When the output response lies in between 0 to 1 SIGMOD non-linear activation function (4) has been used.

$$FX = \frac{1}{1+e^{-x}} \qquad (4)$$

The TANSIG transfer function has been utilized when there is an existence of any negative values in output response and is referred to as in(5):

$$FX = \frac{1-e^{-2x}}{1+e^{2x}} \qquad (5)$$

The representation of the performance index for various training algorithms was made based on the mean square error (MSE) and is represented as in (6):

$$MSE = \frac{1}{n} {}^{n}_{i=1} (Xai - Xbi)^{2} \qquad (6)$$

In this research work, availability, reliability and PM parameters of 10 numbers of LHDs were predicted from ANN tool (Fig 3 to 5). In order to assess the availability of the system, two numbers of parameters such as MTBF and MTTR were given as input. Whereas in the case of prediction of reliability, four numbers of parameters like MTBF, scale parameter (η), shape parameter (β) and location parameter (γ) were given as input. Similarly, for prediction of PM, percentage of reliability (R), scale parameter (η), shape parameter (β) and location parameter (γ) were given as input.

Hence these three predicted values from the output layer of MATLAB based ANN model were recorded for the discussion.

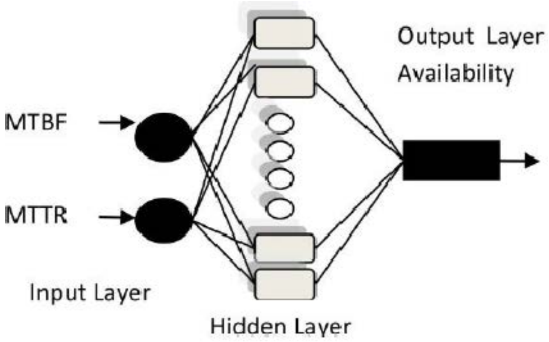

Fig 3. ANN model for availability

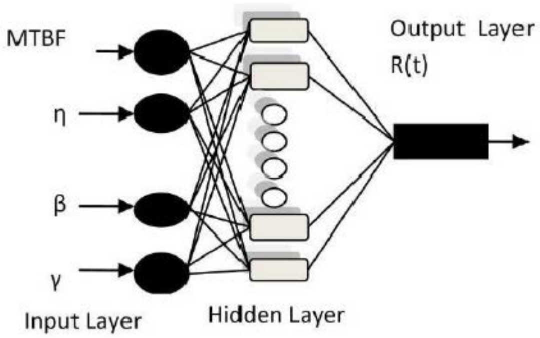

Fig 4. ANN model for reliability

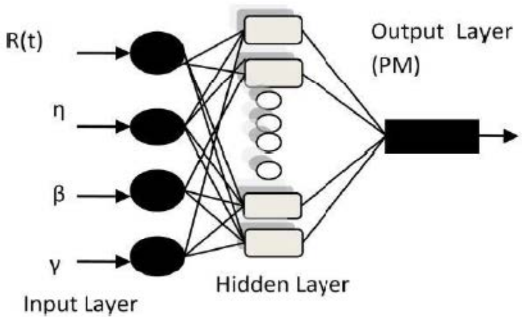

Fig 5. ANN model for PM

F. Development of ANN Simulation Model for Reliability

ANN model of reliability was developed by the utilization of MTBF and MTTR metrics. The learning function called as TRAINLM has been utilized for training procedure. Once the selection of training function was completed, the learning function known as Gradient Descent with momentum weight and bias learning function (LEARNGDM) has also been selected in this process. For hidden layer TANSIG transfer function and for output function linear function (PURELIN) was chosen. The model was tested by selecting the number of neurons as from 4 to 12 and trained up to 1000 iterations for obtaining the best optimum results. The selection of optimum value R2 was done based on the Root Mean Square Error (RMSE) (Eq.7) value. The developed network model for reliability is shown in Fig 6. From the results (Table VI) it was noticed that R2 (0.992) (Fig 7) was optimum at 0.1655 (RMSE) for LM-10.

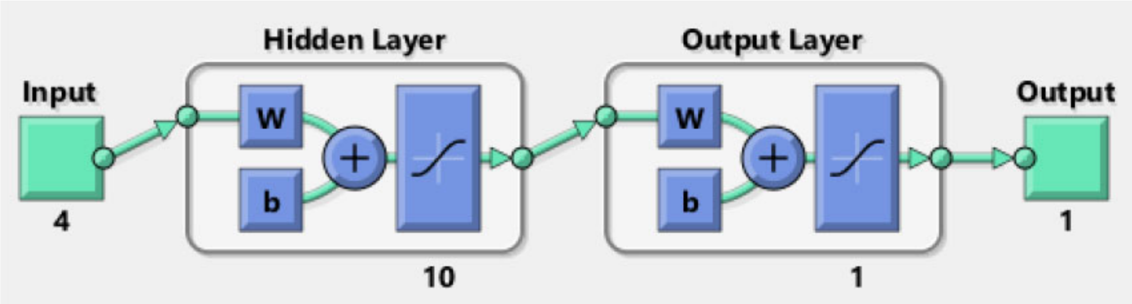

Fig 6. Developed an Optimum Network Model for Reliability

Sl.No	Number of Neurons	R^2	RMSE
1	4	0.9849	0.2267
2	5	0.8219	0.3780
3	6	0.8116	0.8957
4	7	0.8796	0.5242
5	8	0.5441	0.6833
6	9	0.9329	0.3094
7	10	0.9927	0.1655
8	11	0.7690	0.5462
9	12	0.8997	0.8876

Table VI. Trainined results of the reliability of various neurons

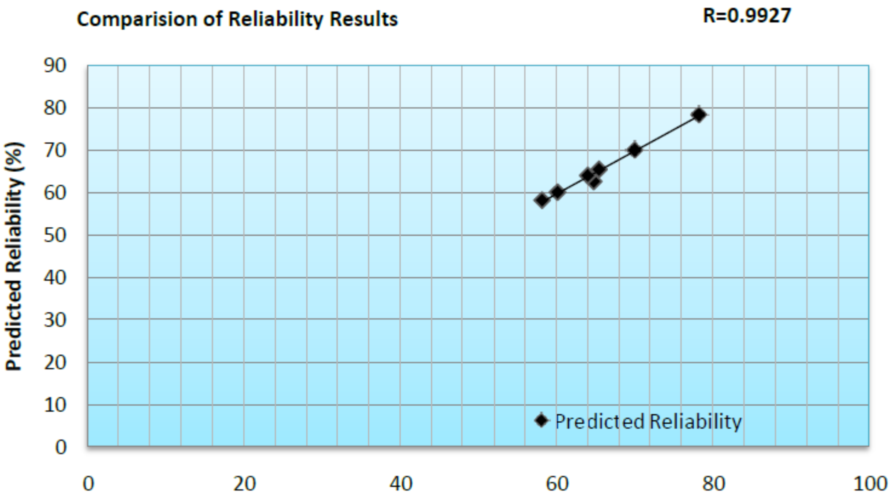

Fig 7. Regression plot of LM-10

G. Development of ANN Simulation Model for Availability

ANN model of availability was developed by the utilization of MTBF and MTTR metrics. The utilized functions for learning, training, testing, transfer, and output in this model are the same as that of the developed reliability model. The developed availability model was tested by selecting the neuron number from 2 to 9 and trained up to 1000 iterations to obtain the best optimum results. The selection of optimum R2 value was done based on the Root Mean Square Error (RMSE) value. The developed network model for reliability is shown in Fig 8. From the obtained results it was noticed that R2 (0.9988) (Fig 9) was optimum at 0.0226 (RMSE) for LM-3. The predicted values related to the optimum R2 are then recorded (Table VII) for the further validation process.

$$RMSE = \sqrt{\sum_{i-1}^{n} \frac{(y - y')^2}{n}} \qquad (7)$$

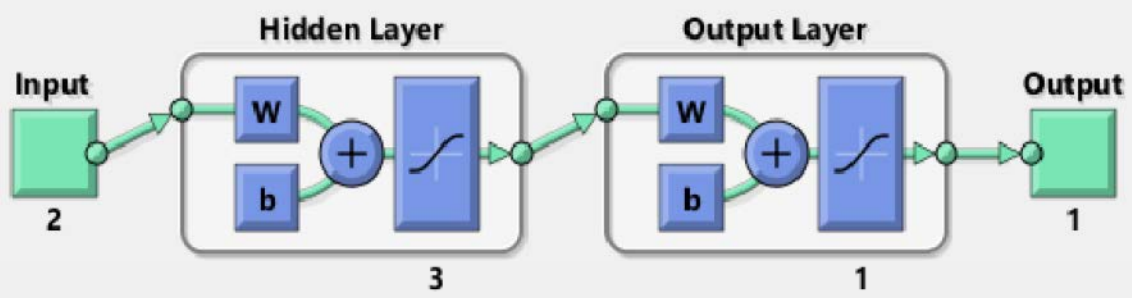

Fig 8. Developed an Optimum Network Model for Availability

Sl.No	Number of Neurons	R^2	RMSE
1	2	0.9139	0.3779
2	3	0.9988	0.0226
3	4	0.9642	0.1972
4	5	0.8436	0.5868
5	6	0.9980	0.0287
6	7	0.9039	0.3561
7	8	0.8914	0.3896
8	9	0.9183	0.3761

Table VII: Trained results of the availability of various neurons

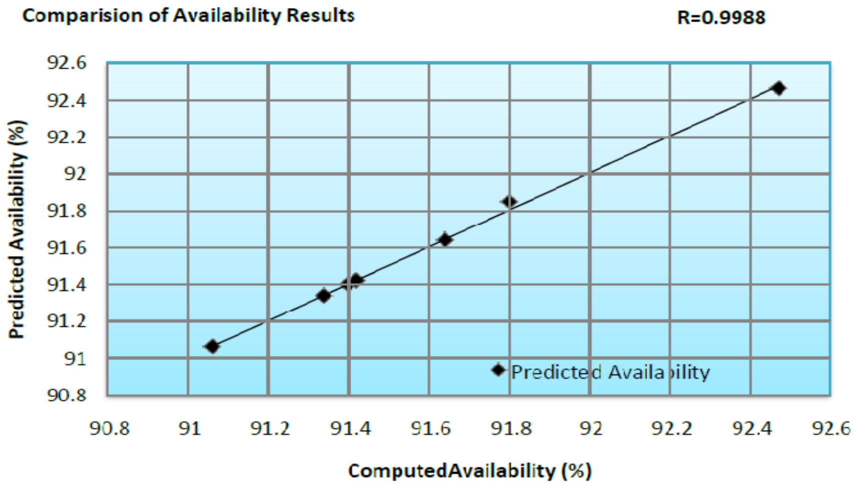

Fig 9. Regression plot of LM-3

H. Development of ANN Simulation Model for Preventive Maintenance(PM)

ANN model of PM was developed by the utilization of MTBF and MTTR metrics. The utilized functions for learning, training, testing, transfer, and output in this model are the same as that of developed reliability and availability model. The developed PM model was tested by selecting the number of neurons as from 4 to 11 and trained up to 1000iterations for obtaining the best optimum results. The selection of optimum R2 value was done based on the Root Mean Square Error (RMSE) value. The developed network model for reliability is shown in Fig 10. From the obtained results it was noticed that R2 (0.9993) (Fig 11) was optimum at 0.1311 (RMSE) for LM-9. The predicted values related to optimum R2 are then recorded (Table VIII) for the further validation process.

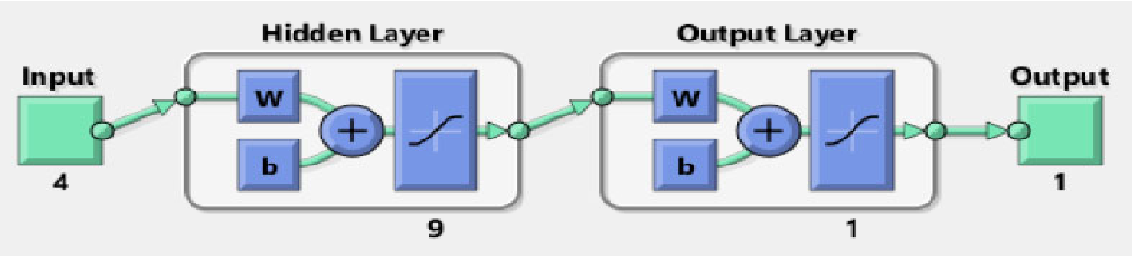

Fig 10. Developed an Optimum Network Model for PM

Sl.No	Number of Neurons	R^2	RMSE
1	4	0.9467	0.3216
2	5	0.9508	0.3401
3	6	0.8168	0.9966
4	7	0.9961	0.2507
5	8	0.9856	0.2090
6	9	0.9993	0.1311
7	10	0.8406	0.9877
8	11	0.9695	0.3211

Table VIII. Trained results of the PM for various neurons

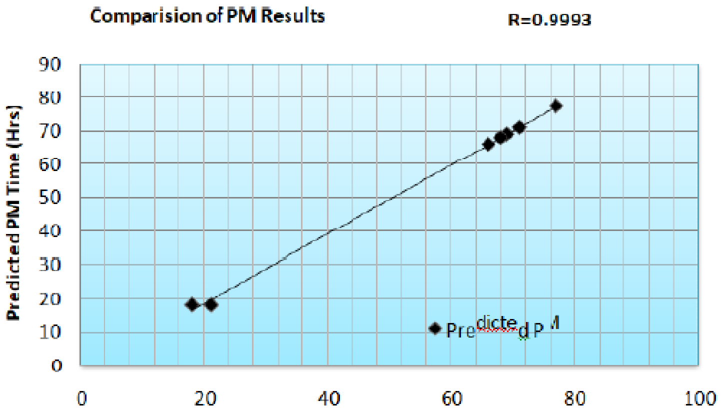

Fig 8. Regression Plot of LM-8

I. Validation of Computed Results with Predicted Results

After successful completion of development and simulation of performance characteristics (reliability, availability, and PM), the validation of computed results was made on the basis of MATLAB based ANN predicted values (Table IX). From the comparison, it was noticed that the computed and predicted values of performance characteristics were in satisfactory with the highest R2 value.

Sl. No	Machine	Computed values from Isograph Reliability Workbench 13.0			Predicted Values from MATLAB based ANN		
		Availability (%)	Reliability (%)	PM (Hrs)	Availability (%)	Reliability (%)	PM (Hrs)
1	LHD1	71.34	64.78	18	71.34	62.59	18.11
2	LHD2	71.40	60.14	21	71.40	60.04	18.05
3	LHD3	71.42	78.28	71	71.42	78.28	71
4	LHD4	71.06	58.18	69	71.06	58.18	69
5	LHD5	72.47	69.98	77	72.46	69.98	77
6	LHD6	71.80	65.44	66	71.85	65.44	66
7	LHD7	71.64	64.00	68	71.64	64.00	68

Table IX. Validation of Computed Results with ANN Predicted Results

IV. CONCLUSIONS

Enhancement of continuous operation of equipment can be achieved by the plan and organization suitable managerial practices. The following conclusions were made based on the analysis:

i. Availability is one of the Key Performance Indicators (KPI) of the machine. LHD5 (72.47%) has the highest availability percentage as compared with other systems. Unavailability and unproductive utilization lead to reduces production rates. This will be improved by strict adherence of PM schedules, effective management of equipment and crew, skilled operating team and effective and efficient management of machinery. This can be possible to increase at 25-30% by shiftoverlapping.

ii. Reliability estimation plays a vital role in performance evaluation. the highest reliability has observed as 78.28% (LHD3) and least level as 60.04% (LHD2). Frequently occurring failures with fewer TBFs are the reasons for the drastic reduction of reliability. Hence, it is recommended that poor efficiency equipment should be maintained at an adequate level by designing the optimal maintenance practices.

iii. Reliability-based PM time intervals were estimated to forecast the early failure of the system. If the reliability requirement is 90% for LH21, then PM should be performed for every 18 hours. Timely conduct of PM enables to achieve the projectedlife.

iv. For ANN reliability model R2 (0.9927) was optimum at 0.8655 (RMSE) for LM-10. For ANN availability model R2 (0.9988) was optimum at 0.0226 (RMSE) for LM-3. Similarly for ANN PM model R2 (0.999) was optimum at 0.1311 (RMSE) for LM-15. The predicted performance characteristics (availability, reliability, and PM) with the highest R2 value gives satisfactory results compared with computed results. It was concluded that ANN is an appropriate technique for the developed network models.

REFERENCE

[1] Paprocka, I. The model of maintenance planning and production scheduling for maximizing robustness. Int. J. Prod. Res. 2018,1–22.

[2] Zambon, I.; Andrea, P.; Matyjas-łysakowska, P.; Luca, S.; Danilo, M.; Andrea, C. Applied Research for a Safer Future: Exploring Recent Job Accidents in Agriculture, Italy (2012–2017). Processes 2018, 6,1–13.

[3] Vishnu, C.R.; Ravikumar, V. Reliability Based Maintenance Strategy Selection in Process Plants: A Case Study. Procedia Technol. 2016, 25,1080–1087.

[4] Swanson, L. An empirical study of the relationship between production technology and maintenance management. Int. J. Prod. Econ. 1997, 53,191–207.

[5] Adoghe, A.U.; Awosope, C.O.A.; Daramola, S.A. Critical Review of Reliability Centred Maintenance (RCM) for Asset Management in Electric Power Distribution System. Int. J. Eng. Technol. 2012, 2,1020–1026.

[6] Harish K. Ghritlahre, “Development of Feed-Forward Back-Propagation Neural Model to Predict the Energy and Exergy Analysis of Solar Air Heater”, Trends in Renewable Energy, 2018, Vol.4, No.2, 213-235. doi:10.17737/tre.2018.4.2.0078.

[7] Harish Kumar N. S., R. P. Choudhary, Ch. S. N. Murthy, “Reliability-based preventive maintainability analysis of the shovel-dumper system in a surface coal mine using ANN and isograph reliability workbench”, Journal of Mathematical Modelling of Engineering Problems, Vol.5, No.4, December 2018, PP.373-378.

[8] Shakhar S. and Haung Y., “Discovering spatial collocation patterns a summary of rules, Proc. of 7thInt. Symp. On Spatial and Temporal Database, L.A., CA, USA, PP:236-256; Jul.2001.

[9] Jordaan.J.T, “Bord-and-pillar mining in inclined ore bodies", The Journal of the South African Institute of Mining and Metallurgy, MARCH 2003, pp:101-110.

[10] Harish Kumar NS, Choudhary RP, Murthy ChSN. (2018). Failure rate and reliability of the Komatsu hydraulic excavator in a surface limestone mine. AIP Conference Proceedings 1-9.https://doi.org/10.1063/1.5029583

[11] Balaraju J, Govinda Raj M, Ch.S.N.Murthy, “Reliability analysis and failure rate evaluation of load haul dump machines using Weibull distribution analysis” Journal of Mathematical Modeling of Engineering Problems, Vol. 5, No.2, June 2018,pp.116-122.

[12] K. Kapageridis., (2002), “Artificial Neural Network Technology in Mining and Environmental Applications”, Mine Planning and EquipmentSelection.

[13] Ghritlahre HK, Prasad RK. (2017). Prediction of thermal performance of unidirectional flow porous bed solar air heater with optimal training function using Artificial Neural Network. Energy Procedia 109:369-376.https://doi.org/10.1016/j.egypro.2017.03.033.

★★★

AUTOMATIC SENSORY MONITORING SYSTEM FOR CONTINUOUS MONITORING OF MATERIAL AND STRUCTURE STATE

[1]PRAKHAR KHARWAR, [2]SATYA BEHERA, [3]DEBANANDA BEHERA

[1]Department of Mechanical Engineering, NMIET, Bhubaneswar, 751019
[2]Department of Mechanical Engineering, REC Bhubaneswar
[3]Department of Engineering, CEC, Bhubaneswar
E-mail: [1]kasinath.dasmohapatra@nmiet.ac.in

Abstract - The goals of this article it to solve problems of automated monitoring systems for industrial constructions. Within this article several NDT systems are analysed, that have the potential to be used for automated monitoring system, covered their main pros and cons. Based on the latest research the most cost effective solutions are covered.

Keywords - Non-Destructive Testing, Integrated Monitoring, Piezoelectric Sensor, Impedance.

I. INTRODUCTION

Any person on this planet comes into contact with various elements of infrastructure. We spend hours in tall building buildings made of concrete, we cross bridges made of concrete and steel. We use electricity received through high voltage power lines that stretch through countries. The electricity is generated with enormous turbines and nuclear power plants, thermoelectric power-plants even let us get warmth for our dwellings. Water and natural gas reaches us through complex net of pipelines. All units of this infrastructure, as well as any of the many more other buildings, every Thing that is Made will eventually brake, bend, skew or crash- will come to a faulty state.

To avoid this, this entire infrastructure has to be maintained; their state- monitored. We have to know, if the houses we live in, the bridges we cross are safe- If our lives are safe.

Monitoring of constructions is made "all the time", that is to say-any interval it is deemed necessary; from the point of view of statistics- when the variable "chance it all would crash" meets variable "this much money can be spent on inspection". So- some faults still occur. Manufacturing plants stop, trains derail, bridges collapse. To make such occurrences less often, automated monitoring systems should be introduced. Systems, that would really be able to monitor all the time- constantly and without any intervals; that would let us know when the first sign problem occurs instead of the best that can be done with manual maintenance at intervals- to find when actual problems have already showed up or even clustered together, forming a biggerproblem.

Inventing and introducing such systems always come with certain limitations. Firstly-he system should be safe, secondly- the monitoring system should cost considerably less than the object it will be monitoring.

This article will check on some methods that can be used to monitor the state of constructions and the base elements of these systems and their sensory elements.

II. SHORT REVIEW OF NON-DESTRUCTIVE TESTING (NDT)

2.1 Radiography

Use irradiation with radioactivity to make detailed scans of structure of the monitored construction. The method provides results with high precision and level of detail, making it highly reliable to determine the safety of the construction. Unfortunately the devices for irradiation and radioactive isotopes are expensive, bulky and there are various very strict limitations to use of such devices and elements. And a very large downside- radiation quickly reaches harmful state to living organisms, thus drastically limiting the use if this method to monitor the state of constructions. The method can be used for periodic monitoring of separate elements of the construction and in best case- inside specialized laboratory- much like x-ray is used inmedicine.

2.2 Eddy-currenttesting

A rather perspective method, the phenomenon it is based on was discovered back in 1824–1850 and still can be used to this day. As sensory elements are used Hall sensors and SQUID sensors (Superconducting Quantum Interference Device) that have up to a thousand times higher resolution. The principle does have its limitations- it can be only used on electro-conductive materials and it has strict limitations on depths of the measurements. The most limiting factor of this method is the limited area where each measurement can be made at a time. As a result- the surface would need to be "scanned" by making subsequent measurements one such small area after another small area till all the construction is combed.

2.3 Magnetic AdaptiveTesting

An interesting method based on magnetic induction. The principle used is very similar to how an isolating electric transformer functions Fig.1. The primary coil gives energy impulse and on the secondary coil it is received and measured on its clamps. In case of "Ideal transformer" the energy on primary and secondary coils would be identical. In an actual transformer there are losses of energy as well as impulse wave-form deformations. This is cause by active and reactive resistance of wires, losses caused by energy transmission from one form to another and crossing several surfaces of various electric and magnetic conductivity; hysteresis of the transformer core will cause both energy loss and wave-form deformations. The largest measureable difference to parameters would be caused by the changes in the state of transformer core- layering of the core material, change of its shape, integration of a layer of air that was not there originally (broken core) or mechanical stress applied to the core will affect the system strongly enough to have these changes noticeable when monitoring the Current and Voltage of the system. The method becomes less precise the larger the area that is monitored, it creates electromagnetic emission that can interfere with other devices while working and lastly- it would work only on ferromagnetic materials and can only be used where the existence of constant magnetism and thus, the fact any ferromagnetic dust would stick to the magnetised parts, would not be aproblem.

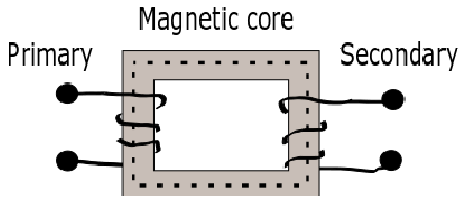

Fig.1. The magnetic induction method.

The method can be used for continuous monitoring of magnetically closed constructions. The method can monitor the construction constantly and with high safety, the system also has high longlivety as measurement impulse generation and reception is done with simple coils. However, to use this method, the construction need to be made to be used in tandem with this method, as adjusting an already installed construction to house this monitoring system can only be done by swapping the existing construction elements with ones that have this system elementsinstalled.

2.4 Electromechanical impedance (EMI) Technique

Emi- One of the relatively new NDT methods, known as the electromechanical impedance (EMI) Technique. The method consists of making measurements of the monitored elements within a set frequency range. When plotted as functions of frequency, these measurements constitute a unique signature of the structure. If there is a change in the monitored element, the signature of the structurealso changes. The method can rival Radiography with its precision; however, it is not widely used due to various factors. To use this method, extensive knowledge of the material and its behaviour in various natural circumstances is needed as well as equally extensive knowledge about the probable faults of said element. The parameters of the construction and its elements can change because of humidity and even ambient sound, not just faults, like, for example, micro-fractures. The devices used are complex and expensive, but, as this method is slowly getting more exposure, also more and more technical solutions become available on market with more attractive prices. Also more empiric results become available as more scientific research is done using said solutions. The results range from data for searching for faults in concrete to determining state of vegetables.

III. INTEGRATED NDTSOLUTIONS

Most commonly used EMI system is based onimpedance converter Fig.2 as AD5933 1 MSPS, 12-Bit converter and its evaluation hardware EVAL-AD5933EBZ. Pros to this system is comparatively low price, industrial temperature range of -40°C to +125°C; 2.7 V to 5.5 V power supply operation and serial I2C interface, thus allowing the elements not only be linked to a computer system, but also microcontroller systems, thus making the whole system and its costs more flexible.

As an alternative ADuCM350 can be used. It has 16-Bit Precision ADC; Low Power Meter On A Chip with Cortex-M3 and Connectivity. Impedances can be measured from 80 Hz to ~75, that is lower than AD5933 100 kHz, but it has a better 16-bit precision analogue-to-digital converter (ADC). The integrated Chip has factory pre-set for work with several problems. Can be programmed, has several channels with video/audio support for use of a Display. The communication range is very wide. Has 2.5V-3.6V active measurement range that has high compatibility with Li-ion accumulators. As a result this unit can be considered as a goodalternative.

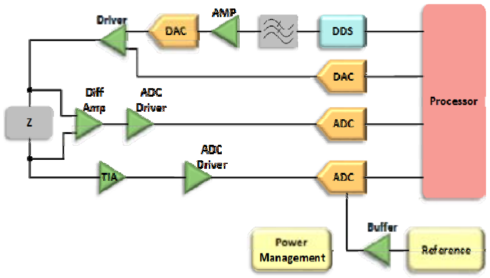

Fig.2. Impedance Converter.

Such microchips are mostly intended for medical, network uses so they are not ideal for use in construction monitoring. But, if the automated monitoring systems based on this method will become more common, more specialized systems will also become available.

During a research (Venu Gopal MadhavAnnamdas, 2010) a testing of concrete constructions was commenced using Embedded PZT Sensor, the research confirmed that 100 kHz frequency was optimal for the tests on the concrete and maximal measurement range was 200mm.

IV. CONCLUSION

By gathering information on various NDT methods, analysing their cons and pros; conclusion can be made, that Automated construction monitoring system with low costs and high safety is plausible, but their current limitations would make their use riddled with problems; most noticeable problem at the moment is lack of pre-set solutions based on empiric results from tests of actual constructions and materials. Results and, as a proxy, price, of any method used will highly depend on how well-placed sensory elements and modules would be and how effective would they work together. A similarity of the sensor placement can be drawn with demolition of constructions using explosives- well placed charges on well prepared for this task construction would drastically decrease material expenditure when compared to brute-forcing the process or guess-work of where to place charges. And we need it tolast.

REFERENCE

[1] Giurgiutiu, V., [Structural Health Monitoring with Piezoelectric Wafer Active Sensors], Elsevier Academic Press, Amsterdam & Boston, 760(2008).

[2] Yan, W., Chen, W. Q., Cai, J. B. and Lim, C. W., “Quantitative structural damage detection using high-frequency piezoelectric signatures via the reverberation matrix method,” Int. J. Num. Meth. Eng., 71(5), 505–528 (2007).

[3] Annamdas, V. G. M. and Soh, Ch. K., “Application of Electromechanical Impedance Technique for Engineering Structures: Review and Future Issues,” J. Intell. Mat. Syst. and Struct., 21, 41-59(2010).

[4] Pavelko, V. New Applications of a Model of Electromechanical Impedance for SHM. No: Health Monitoring of Structural and Biological Systems 2014, ASV, San Diego, 9.-13. marts, 2014. Bellingham: SPIE, 2014, 90640Y-1.-90640Y-15.lpp. ISBN978-0-8194-9990-5. Pieejams: doi:10.1117/12.2044260

[5] Pavelko, V. Application of the Fatigue Crack Opening/Closing Effect for SHM Using Electromechanical Impedance Technology. Applied Mechanics and Materials, 2015, Vol.811, pp.228-235. ISSN 1660-9336. e-ISSN 1662-7482.Available from: doi:10.4028/ www.scientific.net/AMM.811.228

[6] Pavelko, V. Application of the Fatigue Crack Opening/ Closing Effect for Aircraft SHM. In: 7th International Symposium on NDT in Aerospace: Proceedings, Germany, Bremen, 16-18 November, 2015. Bremen: 2016,pp.1-8. ISSN 1435-493

[7] Attila Sipeky, AmáliaIványi“Stress effects on magnetic properties under different shape of excitation”, ISEF 2005 - XII International Symposium on Electromagnetic Fields in Mechatronics,ElectricalandElectronicEngineeringBaiona, Spain, December 15-17, 2005

[8] Abdulwadood Al-Ali, Ahmed Elwakil, Abdelaziz Ahmad and Brent Maundy; "Design of a Portable Low-Cost Impedance Analyzer", Proceedings of the 10th International Joint Conference on Biomedical Engineering Systems and Technologies (BIOSTEC 2017), pages 104-109,2017

[9] Mohammed Omar, “Nondestructive Testing Methods and NewApplications”,JanezaTrdine9,51000Rijeka,Croatia, February, 2012

[10] Venu Gopal MadhavAnnamdas ,Yaowen Yang, Chee KiongSoh, “Impedance based Concrete Monitoring using Embedded PZT Sensors” , International journal of civil and structural engineering, Volume 1, No 3,2010

★★★

DESIGNING OPTIMAL VELOCITY FOR A STEPPED SOLAR STILL TO MAXIMIZE THE PRODUCTIVITY

[1]PRATEEK DAS, [2]RATNAMANJARI DAS, [3]MANASAN RANJAN PAL

[1]Department of Mechanical Engineering, NMIET, Bhubaneswar, 751019
[2]Department of Mechanical Engineering, REC Bhubaneswar
[3]Department of Mechanical engineering, CEC Bhubaneswar
E-mail: [1]smrutirekha.sen@nmiet.ac.in

Abstract- The Levenberg-Marquardt Method (LMM) is utilized to determine the optimum design variables for a stepped solar still with a glass cover water film cooling device to maximize the productivity of the distillate. The design algorithm is based on the minimization of the functional of the problem and estimation of the optimal design variables of glass cover water film cooling devices.

The accuracy of the present numerical solution for distillate is first verified by comparing the values with those provided by El-Samadony and Kabeel. Next, four different designs are considered in the present work, and the resultant daily amount of distillate for each stepped solar still with glass cover water film cooling device are examined. The results indicate that utilizing the optimal design variables for glass cover water film cooling devices can indeed increase the productivity of distillate, and the percentages of increase are calculated as 1.81%, 4.85%, 4.27%, 3.88%, and 2.93% for cases A, B, C, D, and E, respectively.

Keywords - Optimum Design, Stepped Solar Still, Maximize the Productivity

---

I. INTRODUCTION

Of the many types of solar stills, stepped solar stills were found to have better effectiveness than the conventional solar stills (El-Zahaby et al., 2010). Omara et al. (2013) experimentally found that the distillate production of the stepped solar still was higher by approximately 57% than that for conventional solar still. Abu-Hijlew and Mousa (1997) studied numerically that using glass cover water film cooling can improve the efficiency of a conventional solar still by approximately 20%. Additionally, Abu-Hijleh (1996) found numerically that poor combinations of design variables for a glass cover water film cooling device can reduce the still efficiency significantly.

Recently, El-Samadony and Kabeel (2014) considered theoretically the performance of a single basin stepped solar still with glass cover water film cooling. To obtain the best combinations of film cooling design variables, i.e., film cooling thickness, water film cooling volumetric flow rate and glass cover length, an optimization algorithm is utilized to yield the optimum design variables and thus the maximum distillate productivity.

The objective of this study is to re-examine the work of El-Samadony and Kabeel (2014) using the Levenberg-Marquardt method (LMM) (Marquardt, 1963) and seek a better combination of film cooling design variables. LMM was utilized as an efficient optimization algorithm because it has been proven to be a powerful tool for design problems in engineering applications. For example, Huang et al. (2015) applied LMM and a general purpose commercial code, CFD-ACE+ (CFD-ACE+ user's manual, 2005), in an optimal design problem to determine the optimum perforation diameters for a pin fin array. Huang and Wang (2017) used LMM in a design problem to design the optimal fin shape of LED lighting heat sinks. Therefore, the LMM is considered as the optimization algorithm in this work.

II. METHODOLOGY

2.1 The direct problem

A schematic diagram of a stepped type solar still with glass cover water film cooling device is shown in Figure 1. This module will be considered to illustrate the methodology for designing of optimum design variables for a glass cover water film cooling device to maximize the productivity of the stepped solar still by using the LMM [6] and CFD-ACE+.

The energy balance for the stepped-type solar still can be applied to four regions: (1) basin plate, (2) saline water, (3) glass cover and (4) film cooling regions. The basin plate temperature T_b, saline water temperature T_w, glass cover temperature T_g and water film temperature T_f can be evaluated accordingly.

The solar still is assumed to be in a steady-state condition, and the film cooling and glass cover are both assumed thin; as a result, no incident radiation will be absorbed by both of them, and evaporation from the film cooling is negligible.

The mathematical formulation of the steady-state energy balance equations for four regions can be obtained in El-Samadony and Kabeel (2014); therefore, they are not presented in this discussion paper.

The relevant parameters regarding the dimensions, material properties and ambient conditions are also identical to those utilized by El-Samadony and Kabeel (2014) and will be provided in Section 6 for calculation purpose.

The rate of mass evaporation m_{re} can be obtained as follows:

$$m_{re}=\frac{Q_e}{h_{fg}} \qquad (1)$$

and the daily amount of distillate of the solar still is obtainable using the following equation:

$$M_{re}=m_{re}t_{total} \qquad (2)$$

here, t_{total} represents the total operation time for each day. In the present study, the total operational time is from 09:00 to 18:00, i.e., nine hours per day.

The solutions of the coupled ordinary differential equations in four regions, i.e., the direct problem, can be solved using the Runge–Kutta method. The direct problem considered here is concerned with the determination of the temperatures for basin plate, saline water, glass cover and water film as well as the daily distillate productivity of the stepped solar still when the relevant parameters of computations are all given and known.

2.2 The design problem

Let the design variables, film cooling thickness x_f, water film cooling volumetric flow rate Vol_f and glass cover length L, be represented by **B**, i.e., $\mathbf{B}=B_i=\{B_1,B_2,B_3\}=\{x_f,Vol_f,L\}$. Thepurpose of the present discussion paper is to determine the optimum design variables for a glass cover water film cooling stepped solar still to achieve maximum productivity. Let the desired daily productivity of the solar still be denoted by δ; the glass cover water film cooling design problem can be given as follows: utilize the abovementioned desired productivity δ of the solar still and obtain the optimum design variables B_i for the glass cover water film cooling device for maximum productivity.

The objective function of this study to be minimized to yield the optimal variables B_i is

$$J[\theta_m(B_i)]=[M_{re}(B_i)-\delta]^2=U^TU \qquad (3)$$

here, M_{re} represents the estimated or computed productivity of the stepped solar still and can be obtained from the solution of the direct problem.

2.3 The Levenberg-Marquardt Method (LMM) for minimization

Equation (3) is minimized with respect to the design variables B_i to yield

$$\frac{\partial J[\theta_m(\mathbf{B})]}{\partial B_i}=2\left[\frac{\partial M_{re}(B_i)}{\partial B_i}\right][M_{re}-\delta]=0\text{; i=1 to 3} \qquad (4)$$

A Taylor series is utilized to linearize Equation (4) by expanding $M_{re}(B_i)$ and retaining the first order terms. Next, a damping parameter μ^n is added to the resultant equation to increase the rate of convergence. As a result, the Levenberg-Marquardt method can be obtained as follows:

$$(\mathbf{F}+\mu^n\mathbf{Z})\Delta\mathbf{B}=\mathbf{E} \qquad (5)$$

$$\mathbf{F}=\mathbf{\Psi}^T\mathbf{\Psi} \qquad (6)$$

$$\mathbf{E}=\mathbf{\Psi}^T\mathbf{U} \qquad (7)$$

$$\Delta\mathbf{B}=\mathbf{B}^{n+1}-\mathbf{B}^n \qquad (8)$$

Here, the superscripts T and n indicate the transpose matrix and iteration index, respectively, and **Z** is the identity matrix. **Ψ**denotes the Jacobian matrix and is defined as follows:

$$\mathbf{\Psi}=\frac{\partial M_{re}(\mathbf{B})}{\partial B_i} \qquad (9)$$

The Jacobian matrix **Ψ**can be obtained by perturbing the unknown design variables B_i, one at a time, and calculating the resultant change in productivity of the solar still from the solution of the direct problem.

Equation (8) is now rewritten in a form suitable for iteration:

$$\mathbf{B}^{n+1}=\mathbf{B}^n-(\mathbf{\Psi}^T\mathbf{\Psi}+\mu^n\mathbf{Z})^{-1}\mathbf{\Psi}^T\mathbf{U} \qquad (10)$$

To achieve rapid convergence, the steepest-descent method is applied first, i.e., $\mu^n\to\infty$. Finally, the Gauss-Newton method is used, i.e., $\mu^n=0$, to obtain the optimum productivity.

2.4 Iterative process

The iterative process of this work to determine the optimum productivity of the stepped solar still with the Levenberg-Marquardt method can be described as follows:

Step 1. Choose the optimum design variables for x_f, Vol_f and L given by El-Samadony and Kabeel (2014) as the initial guesses to start the design process.

Step 2. Solve the direct problem to obtain the estimated or computed productivity of the solar still.

Step 3. Compute the Jacobian matrix according to Equation (9).

Step 4. The design variables $\mathbf{B}^{n+1}$ are updated based on Equation (10), and then the new geometry of glass cover water film cooling device for the stepped solar still can beconstructed.

Step 5. Check the stopping criterion ν; if it is not satisfied, then go to Step 2 and iterate again.

III. RESULTS

The accuracy of the numerical solutions for the productivity of the stepped solar still plays an important role in this optimum design problem. For this reason, it is necessary to show that the accuracy of the computed productivity obtained in the present work is adequate by comparing it with the productivity provided by El-Samadony and Kabeel (2014).

The physical and operating parameters used in this study are identical to those used in El-Samadony and Kabeel (2014). The distribution function of the solar radiation with time was not given in (2014); it can be obtained directly from the Hong Kong Weather Website which is utilized in this study. The daily productivities given in Table 2 of El-Samadony and Kabeel (2014) are re-calculated in this work; the computed results are summarized in Table 1.

Table 1 reveals that the maximum error among five daily productivities is less than 2.22% because the function of solar radiation with time used in this study is not exactly identical to that utilized in Samadony and Kabeel (2014); however, the trends of the computed productivities are similar.

The objective of this work is to examine whether the use of the LMM can further improve the daily amounts of distillate of the stepped solar still. To illustrate the validity of the LMM in estimating the optimal design variables of the stepped solar still with glass cover water film cooling device by minimizing the objective functional, the numerical experiments used for determining the optimal design variables are presented below. The constraints for three design variables are as follows (Samadony and Kabeel, 2014):

$$2.5\times10^{-4}\ \mathrm{m} \le x_f \le 5.5\times10^{-4}\ \mathrm{m}\ ;$$

$$4\times10^{-5}\ \mathrm{m}^3/\mathrm{s} \le Vol_f \le 8.5\times10^{-5}\ \mathrm{m}^3/\mathrm{s}\ ;$$

$$2.0\mathrm{m} \le L \le 2.8\mathrm{m}$$

The stopping criterion is chosen as $= 10^{-3}$ and a 10% increase in the daily productivity of distillate of the stepped solar still from five initial design conditions, i.e., cases A to E, is required in the five design cases considered here. It is impossible to obtain the optimum design to yield the desired daily productivity δ; however, the optimal still variables with the best daily productivity can be obtained.

Table 2 presents the optimum design variables of the stepped solar still for cases A to E. The results show that film cooling thickness x_f will approach its lower limit whereas the water film cooling volumetric flow rate Vol_f and glass cover length L will both approach their upper limits for optimal still daily productivity. This result occurs because, as the film cooling thickness becomes thinner and film cooling volumetric flow rate becomes larger, more solar energy can penetrate to the saline water. When the glass cover length increases, the surface area for solar energy transfer increases; as a result, more solar energy can reach the saline water, thereby increasing the productivity of the stepped solar still.

The resultant daily productivities using the present optimal design variables and the design variables of Samadony and Kabeel (2014) for cases A to E are also given in Table 2. The optimal still daily productivity for cases A to E with different temperature difference, t_a-t_{f1}, are all the same. This implies that the variationoftemperaturedifference(t_a-t_{f1})considered in this work can hardly affect the productivity, whereas the design variables can indeed affect the productivity.

IV. CONCLUSION

The daily distillate productivity obtained in the present work is clearly better than that using the design variables of Samadony and Kabeel (2014). Based on the above results, it can be concluded that the present design algorithm can indeed increase the daily productivity of the distillate and the percentages of increasing distillate for cases A, B, C, D, and E are 1.81%, 4.85%, 4.27%, 3.88%, and 2.93%,respectively.

REFERENCE

[1] Abu-Hijleh Bassam AK., 1996. Enhanced solar still performance using water film cooling of the glass cover. Desalination 107,235–44.

[2] Abu-Hijlew Bassam AK, Mousa Hasan A., 1997. Water film cooling over the glass cover of a solar still including evaporation effects. Energy 22(1),43–48.

[3] CFD-ACE+ user's manual, 2005. ESI-CFDInc.

[4] El-Samadony YAF, Kabeel AE., 2014. Theoretical estimation of the optimum glass cover water film cooling parameters combinations of a stepped solar still. Energy 68, 744-750.

[5] El-Zahaby AM, Kabeel AE, Bakry AI, El-agouz SA, Hawam OM., 2010. Augmentation of solar still performance using flash evaporation. Desalination 257,58–65.

[6] Hong Kong Weather Watch Website (http://www.hkww.org/weather/index_

[7] main.html) 2018, Solar information for majorcities.

[8] Huang CH, Liu YC, Ay H., 2015. The design of optimum perforation diameters for pin fin array for heat transfer enhancement. International Journal of Heat and Mass Trans- fer 84,752–765.

[9] Huang CH, Wang GJ., 2017. A design problem to estimate the optimal fin shape of LED lighting heat sinks. International Journal of Heat and Mass Transfer 109,1205–1217.

[10] Marquardt DM., 1963. An algorithm for least-squares estimation of nonlinear parameters. J. Soc. Indust. Appl. Math. 11,431–41.

[11] Omara ZM, Kabeel AE, Younes MM., 2013. Enhancing the stepped solar still performance using internal reflectors. Desalination 314,67–72.

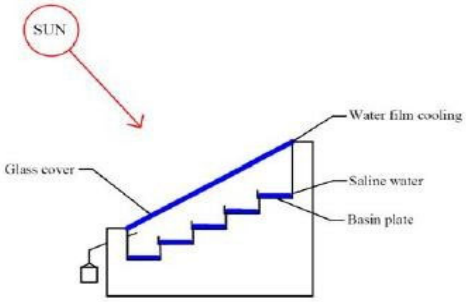

Figure 1. Schematic of the experimental setup

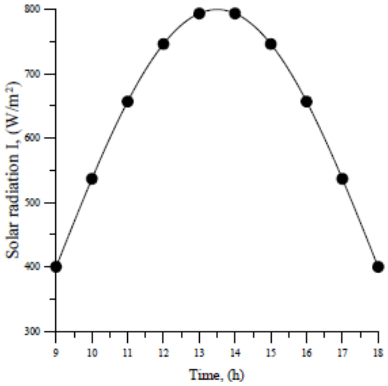

Figure 2. Solar radiation with time

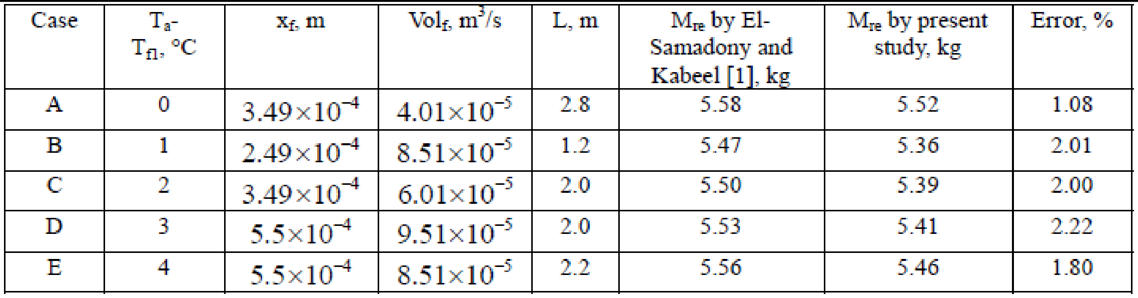

Case	T_a-T_{f1}, °C	x_f, m	Vol_f, m^3/s	L, m	M_{re} by El-Samadony and Kabeel [1], kg	M_{re} by present study, kg	Error, %
A	0	3.49×10^{-4}	4.01×10^{-5}	2.8	5.58	5.52	1.08
B	1	2.49×10^{-4}	8.51×10^{-5}	1.2	5.47	5.36	2.01
C	2	3.49×10^{-4}	6.01×10^{-5}	2.0	5.50	5.39	2.00
D	3	5.5×10^{-4}	9.51×10^{-5}	2.0	5.53	5.41	2.22
E	4	5.5×10^{-4}	8.51×10^{-5}	2.2	5.56	5.46	1.80

Table 1. Comparison of the daily productivities between El-Samadony and Kabeel [1] and the present study using the design variables of Reference [1]

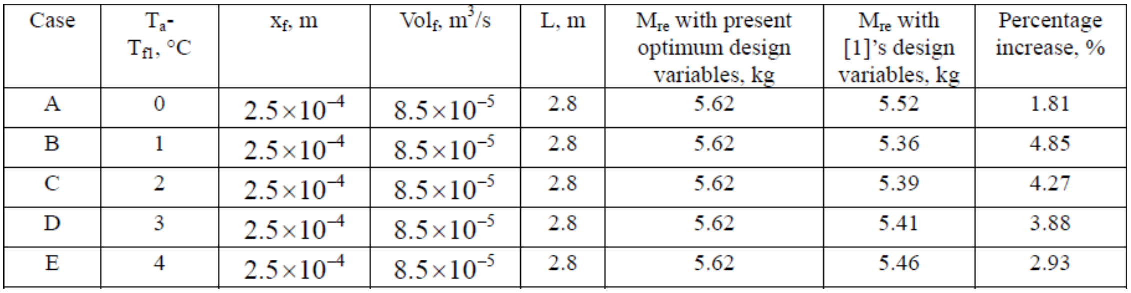

Case	T_a-T_{f1}, °C	x_f, m	Vol_f, m^3/s	L, m	M_{re} with present optimum design variables, kg	M_{re} with [1]'s design variables, kg	Percentage increase, %
A	0	2.5×10^{-4}	8.5×10^{-5}	2.8	5.62	5.52	1.81
B	1	2.5×10^{-4}	8.5×10^{-5}	2.8	5.62	5.36	4.85
C	2	2.5×10^{-4}	8.5×10^{-5}	2.8	5.62	5.39	4.27
D	3	2.5×10^{-4}	8.5×10^{-5}	2.8	5.62	5.41	3.88
E	4	2.5×10^{-4}	8.5×10^{-5}	2.8	5.62	5.46	2.93

Table 2. Comparison of the daily productivities between El-Samadony and Kabeel's [1] design variables and the present optimum design variables

★★★

ANALYSIS OF QUASICRYSTAL IN TI – BASED TI-ZR-NI-MG COMPOUND MATERIALS

[1]PUNITA KUMARI, [2]ITISHREE SWAIN, [3]ABINASH SAHOO

[1]Department of Mechanical Engineering, NMIET, Bhubaneswar, 751019
[2]Department of Mechanical Engineering, REC Bhubaneswar
[3]Department of Mechanical Engineering, CEC Bhubaneswar
E-mail: [1]s.arunachalam@nmiet.ac.in

Abstract - Various methods for hydrogen storage have been proposed by many researchers. Magnesium (Mg) was known as one of the most famous hydrogen reservoir materials due to its low cost and good stability when reacting with hydrogen. However, the energy and temperature used for hydrogen adsorption of Mg was quite high. In order to improve these disadvantages, alloying method was used by adding Mg into Ti-based quasicrystal (Ti-Zr-Ni) . The Ti-based quasicrystal was a high capability material for hydrogen absorption due to a large number of interstices in the icosahedral quasicrystal (i-phase).This study was to investigate the icosahedral quasicrystaland crystal phase of mixed materials between Ti-based quasicrystals(Ti-Zr-Ni)andMagnesium(Mg).Mechanicalalloyingprocesswasconductedundertwoconditionsincluding;
(i) rotation speed of 600 rpm with 20 hours milling time and (ii) rotation speed of 630 rpm with 30 hours milling time. The nominal composition was Ti45-xZr38Ni17Mgx (x = 2, 4).The results from XRD analysis indicated that i-phases and crystal phase were appeared for both conditions that the proposed materials could be used as a hydrogen storagematerial.

Keywords - Quasicrystal, Mechanical Alloying, Hydrogen Storage Material, Magnesium.

I. INTRODUCTION

The quasicrystalis a new type of translational long-range order; however, it is a non-crystallographic which shows rotational symmetry patterns. For tetrahedral interstitial sites of quasicrystals contain more than normal crystals due to the structure of quasicrystals has Bergman two-shell atomic cluster. Takasaki et al. [1, 2]indicatedthatBergman two-shell of quasicrystalscontain 20 tetrahedral interstitials within its inner shell and 120 between its inner and outer shells. A large number of interstices were also found in the icosahedral quasicrystal (i-phase)and these interstices may provide appropriate sites for hydrogen storage. This result was consistent with the result reported by Tomoki et al.[3], whichicosahedral quasicrystal was appropriate properties for hydrogen storage.

Quasicrystal was discovered by Shechtman et al.[1, 4, 5]. Ithas been found in an aluminum alloy and laterhave been found to be thermodynamicallystable in many alloys[4].One of the famous compound was a Ti-based quasicrystal (Ti-Zr-Ni. Ti-based quasicrystalwas the second largest group of the stable quasicrystals,which wasthe thermodynamic stability,strong chemical affinity with hydrogen and low cost. Especially, $Ti_{45}Zr_{38}Ni_{17}$shows a very high hydrogen storage capacity (H/M)of1.5[6,7].

There were two phases of Ti-based quasicrystal; (i) icosahedral quasicrystal and (ii) crystal phase (Ti_2Ni). Icosahedral quasicrystal contained large number of tetrahedral interstices which couldadsorbmore hydrogen than normal crystals. For crystal phase (Ti_2Ni),it contained a large number of interstitial sites for hydrogen storage[8]. However, crystal phase (Ti_2Ni) was sensitive to react with oxygen, thus controlling the oxygen in the process became critical parameter[1].

Magnesium (Mg) was known as one of the most famoushydrogen reservoir materials, in the form of MgH_2, due to its low cost and good stabilitywhen reacting with hydrogen. The structure of magnesium hydride (MgH_2) hadhigh thermodynamic stability ability to storage hydrogen of7.6 wt. %[9, 10].However,the energy and temperature for hydrogen adsorption were very high.In 2017,Wang et al.[9]has reportedthat there were manymethods for improving magnesium hydride including(i)alloying (ii) nano scaling (iii) nano confinement (iv) adding catalysts and (v) mixing with other metal hydrides. When Magnesiumwas added into Ti-based quasicrystal, Mg_2Ni crystal phase could be found to appearafter annealing process[11, 12].Thecrystallized phase (Mg_2Ni)was one of the most important hydrogen storagematerials. The advantage of$Mg_2Ni$was high hydrogen capacity up to 3.6 wt. % [12]. It was also reported thatabsorbing hydrogen of Mg_2Nihas relatively highkinetic compare to other form of Mg crystals. However,Mg_2Nicannot absorb hydrogen under normal conditions.The usual hydrogenation condition of $Mg_2Ni$was between 250 and 350°C.

This research was aimed to studythe appearing of quasicrystal in Ti-based Ti-Zr-Ni-Mg compound materials mixing by mechanical alloying method. The benefit of this research was to achievepotential of Ti-Zr-Ni-Mg compound materials as ahydrogen storage material.

II. MATERIALS ANDMETHODS

Commercially pure Ti (99.9%), Zr (99.9%), Ni (99.9%) and Mg (99.9%) elemental powders were used as starting materials. The nominal composition of compound was $Ti_{45-x}Zr_{38}Ni_{17}Mg_x$ (x = 2, 4). A weight of powder totally 10.34 g was weighted, mixed and poured into a stainless steel vial which contained five stainless steel balls. Weight of ball to powder ratio was 8:1. All the operations was performed under argon atmosphere. Allsamples were mechanically alloyed using planetary ball mill machine. The parameters for MA were given in Table 1. The structures of$Ti_{45-x}Zr_{38}Ni_{17}Mg_x$ (x = 2, 4)were analyzed by using X-ray diffraction (XRD).Takasaki et al. [13] reported that the i-phase cannot be obtained directly by MA. However, the amorphous phase wastransformed into i-phase andTi_2Ni crystal phaseafterannealingprocess.

The powders after MA were analyzedby using Differential Scanning Calorimetry measurements (DSC)under argon atmosphere.3 milligrams of the powder was usedfor DSC analysis. Heating rate of 5^oC/min was carried out in this study[14].The temperature for annealing process can be observed from the peak of DSC result.For annealing process, powder sample was annealed under vacuum condition for 2hours.

Quasicrystals (i-phase), crystal phase (Ti_2Ni) and (Mg_2Ni) of $Ti_{45-x}Zr_{38}Ni_{17}Mg_x$(x = 2, 4) after annealing process were analyzed by using X-ray diffraction (XRD).

Compositions	Parameters	
	Speed (rpm)	Milling time(hour)
$Ti_{43}Zr_{38}Ni_{17}Mg_2$	600	20
	630	30
$Ti_{41}Zr_{38}Ni_{17}Mg_4$	600	20
	630	30

Table1: Materials Composition and Parameters

III. RESULTS AND DISCUSSION

Figure 1 shows XRD patterns after MA of$Ti_{45-x}Zr_{38}Ni_{17}Mg_x$; (x = 2, 4) powders.The results indicatedthatno peak was observed in all compositions and conditions, the $Ti_{45-x}Zr_{38}Ni_{17}Mg_x$ samples wereamorphous after mechanical alloying process.The results fromDifferential ScanningCalorimetrymeasurements (DSC) analysiswere shown inFig. 2. The temperature for annealing process can be obtainedfrom the onset temperature of the peak of DSC results.Table 2summarizedtheobserved temperature at each condition for annealing process. It was obvious that the annealing temperature of sample with composition $Ti_{43}Zr_{38}Ni_{17}Mg_2$was lower than that of$Ti_{41}Zr_{38}Ni_{17}Mg_4$composition.

Figure 3 showed the XRD patterns of$Ti_{45-x}Zr_{38}Ni_{17}Mg_x$ after annealing process. It was found that quasicrystal was observed inall compositions and conditions inboth theicosahedral (i-phase) and crystal phases. For crystal phases, two types of crystal phases were appeared includingTi_2Ni and the Mg_2Ni.

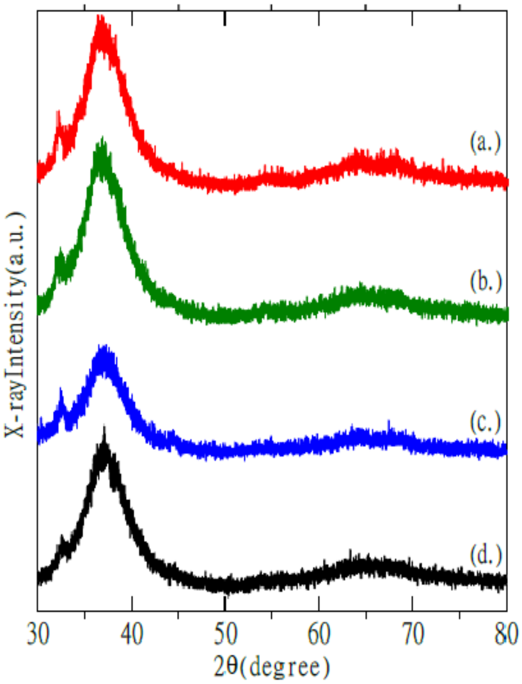

Fig.1 XRD patterns for $Ti_{45-x}Zr_{38}Ni_{17}Mg_x$; (x = 2, 4) powders after mechanical alloying process
(a.)$Ti_{43}Zr_{38}Ni_{17}Mg_2$ 600 rpm 20hr.,
(b.) $Ti_{43}Zr_{38}Ni_{17}Mg_2$ 630 rpm 30hr.,
(c.) $Ti_{41}Zr_{38}Ni_{17}Mg_4$ 600 rpm 20hr.,
(d.) $Ti_{41}Zr_{38}Ni_{17}Mg_4$ 630 rpm 30 hr.

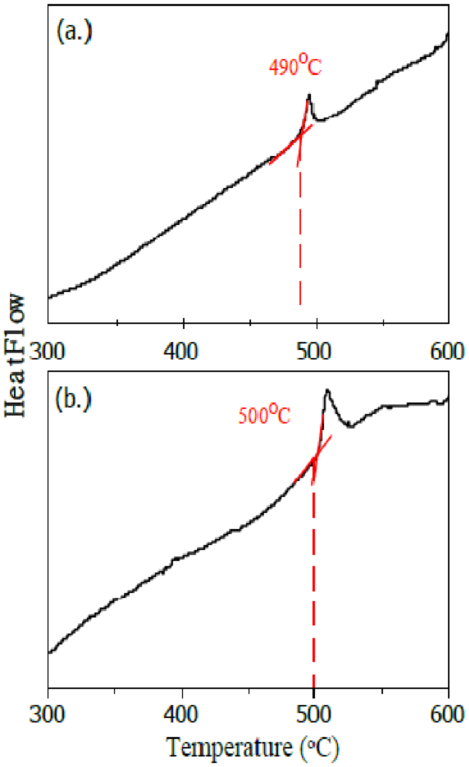

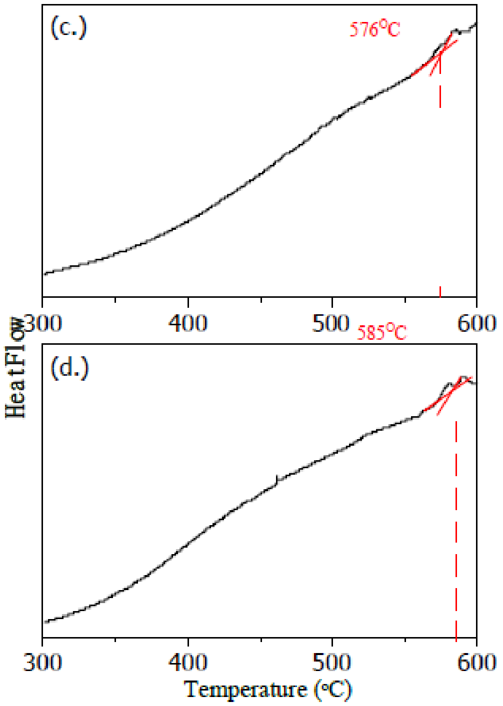

Fig.2 Differential scanning calorimetry for $Ti_{45-x}Zr_{38}Ni_{17}Mg_x$; ($x= 2, 4$) powders after mechanical alloying
(a.) $Ti_{43}Zr_{38}Ni_{17}Mg_2$ at 600 rpm 20 h,
(b.) $Ti_{43}Zr_{38}Ni_{17}Mg_2$ at 630 rpm 30 h,
(c.) $Ti_{41}Zr_{38}Ni_{17}Mg_4$ at 600 rpm 20 h,
(d.) $Ti_{41}Zr_{38}Ni_{17}Mg_4$ at 630 rpm 30 h.

Compositions	Parameter		Annealing Temperature (°C)
	Speed (rpm)	Milling time (h)	
$Ti_{43}Zr_{38}Ni_{17}Mg_2$	600	20	550
	630	30	500
$Ti_{41}Zr_{38}Ni_{17}Mg_4$	600	20	576
	630	30	585

Table2: The annealing temperature obtained from DSC analysis

It was also observed from the XRD patterns that the i-phase in $Ti_{45-x}Zr_{38}Ni_{17}Mg_x$:($x = 2, 4$) compoundcould be observed in all compositions and conditions, 35-40 degree. However, the peaks at about 65 degree and 76-78 degree were revealed that rotation speed of 600 rpm with20 hours milling time wasyielded higheri-phase thanusing rotation speed of 630 rpm with 30 hours milling time.

On the other hands, crystal phase(Ti_2Ni and the Mg_2Ni) were observed for all compositions and conditions. Therefore, on the view of i-phase amount, $Ti_{43}Zr_{38}Ni_{17}Mg_2$ compound with 600 rpm with 20 hours milling time results slightly higher amount than $Ti_{41}Zr_{38}Ni_{17}Mg_4$ compound. Thus, based on results of this study, it could be concluded that $Ti_{43}Zr_{38}Ni_{17}Mg_2$ compound with 600 rpm with 20 hours milling time showed potential as hydrogen storagematerials.

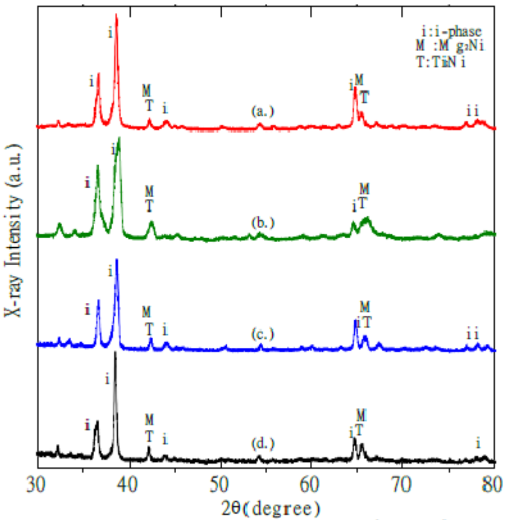

Fig.3XRD patterns for $Ti_{45-x}Zr_{38}Ni_{17}Mg_x$; ($x = 2, 4$) powders after annealing
(a.) $Ti_{43}Zr_{38}Ni_{17}Mg_2$ at 600 rpm 20 h 550°C,
(b.) $Ti_{43}Zr_{38}Ni_{17}Mg_2$ at 630 rpm 30 h 500°C,
(c.) $Ti_{41}Zr_{38}Ni_{17}Mg_4$ at 600 rpm 20 h 576°C,
(d.) $Ti_{41}Zr_{38}Ni_{17}Mg_4$ at 630 rpm 30 h 585°C.

IV. CONCLUSIONS

This research was undertaken to investigate the icosahedral quasicrystal (i-phase)and crystal phase of mixed materials between Ti-based quasicrystals (Ti-Zr-Ni) and Magnesium (Mg) by using mechanical alloyingprocess.

This process was conducted under two conditions including; (i)rotation speed of 600 rpm with 20 hours milling time and (ii) rotation speed of 630 rpm with 30 hours milling time.The followingconclusion can be drawn from thisstudy:

1. Theannealing temperature of $Ti_{43}Zr_{38}Ni_{17}Mg_2$compound was lower than that of $Ti_{41}Zr_{38}Ni_{17}Mg_4$compound.
2. The $Ti_{45-x}Zr_{38}Ni_{17}Mg_x$ compound was transformed from amorphous to icosahedral and crystal phase after annealingprocess.
3. The $Ti_{43}Zr_{38}Ni_{17}Mg_2$ compound with 600rpm with 20 hours milling time had potential as hydrogen storage materials.
4. In further study, hydrogenation process should be investigated for determination of hydrogen adsorption of the Ti-Zr-Ni-Mg compound.

REFERENCES

[1] Takasaki, A., and Kelton, K.: 'Hydrogen storage in Ti-based quasicrystal powders produced by mechanical alloying', International Journal of Hydrogen Energy, 2006, 31, (2), pp. 183-190

[2] Morozov, A.Y., Isaev, É.I., and Vekilov, Y.K.: 'Charge state anddiffusionofhydrogenintheTiZrNiicosahedralalloy',

[3] Physics of the Solid State, 2006, 48, (9), pp. 1625-1628

[4] Tominaga, T., Takasaki, A., Shibato, T., and Świerczek, K.: 'HREM observation and high-pressure composition isotherm measurement of Ti 45 Zr 38 Ni 17 quasicrystal powders

synthesized by mechanical alloying', Journal of Alloys and Compounds, 2015, 645, pp.S292-S294

[5] Samavat, F., Tavakoli, M.H., Habibi, S., Jaleh, B., and Ahmad, P.T.: 'Quasicrystals', Open Journal of Physical Chemistry, 2012, 02, (01), pp.7-14

[6] Shechtman, D., Blech, I., Gratias, D., and Cahn, J.W.: 'Metallic Phase with Long-Range Orientational Order and No Translational Symmetry', Physical Review Letters, 1984, 53, (20), pp.1951-1953

[7] Patrick, D.K., Takasaki, A., and Klimkowicz, A.: 'High discharge capacities of Ti-based quasicrystal electrodes synthesized by mechanical alloying', MRS Advances, 2018, 3, (38), pp.2271-2279

[8] Takasaki, A., Huett, V.T., and Kelton, K.F.: 'Hydrogenation of Ti–Zr–Ni quasicrystals synthesized bymechanical alloying', Journal of Non-Crystalline Solids, 2004, 334-335, pp. 457-460

[9] Zhao, X., Ma, L., Yao, Y., Ding, Y., and Shen, X.: 'Ti2Ni alloy: a potential candidate for hydrogen storage in nickel/metal hydride secondary batteries', Energy & Environmental Science, 2010, 3,(9)

[10] Wang, Y., and Wang, Y.: 'Recent advances in additive-enhanced magnesium hydride for hydrogen storage', Progress in Natural Science: Materials International, 2017, 27, (1), pp. 41-49

[11] Jain, I.P., Lal, C., and Jain, A.: 'Hydrogen storage in Mg: A most promising material', International Journal of Hydrogen Energy, 2010, 35, (10), pp.5133-5144

[12] REILLY, J.J., and WISWALL, R.H.: 'The Reaction of Hydrogen with Alloys of Magnesium and Nickel and the Formation of Mg2NiH4',1968

[13] Zaluski, L., Zaluska, A., and Strom-Olsen, J.O.: 'Hydrogen absorption in nanocrystalline Mg2Ni formed by mechanical alloying',1995

[14] Takasaki, A., Huett, V.T., and Kelton, K.F.: 'Hydrogen Pressure-Composition Isotherms for Ti45Zr38Ni17 Amorphous and Quasicrystal Powders Produced by Mechanical Alloying',2002

[15] Żywczak, A., Rusinek, D., Czub, J., Sikora, M., Stępień, J., Gondek, Ł., Gajewska, M., Takasaki, A., and Hoser, A.: 'Icosahedral hydrides of the Ti 45 Zr 38 Ni 17−x Co x nano-powders', Journal of Alloys and Compounds, 2016, 656, pp. 702-706

★★★

ANALYSIS OF ARTIFICIAL AGING ON MECHANICAL PROPERTIES OF ROLLING AND SEMI-SOLID CASTING ALUMINIUM ALLOY 2024

[1]RABI SANKAR PANDA, [2]PRIYABRATA JENA, [3]RANJAN KISHORE MALLICK

[1]Department of Mechanical Engineering, NMIET, Bhubaneswar, 751019
[3]Department of Mechanical engineering CEC BHUBANESWAR
[3]Department of Mechanical Engineering REC Bhubaneswar
E-mail: [1]tanusree.bera@nmiet.ac.in

Abstract - This work was aimed at investigate the mechanical properties of rolled and semi-solid casted aluminium alloy 2024, T6 heat treatment as follows : solution treated at 505 ºC for 4 h followed by quenching in water at room temperature and then artificially aged at 190 ºC for 12 h,15 h and 18 h, was carried out Rockwell hardness scale B (HRB) and tensile tests were investigated for mechanical properties. Optical Microscope was used to illustrate the microstructure. It was found that maximum hardness was observed at 15 hours aging time for both Al2024.Maximum strength of rolled Al2024 was found to higher than that of semi-solid casted Al2024. It might due to influence of cold work of the rolledAl2024.

Keywords - Aluminum alloy 2024, Aging, Precipitation, Mechanical property

I. INTRODUCTION

The use of aluminium alloys in industry are widely and replacing steel usage in aerospace and aviation industries owning to their light weight, excellent thermal stability, and good corrosion resistance and high strength/ density ratioetc. [1-2]

The strength of the Al alloys were usually come out with heat treatment processes.In heat treatment process, the second phase was precipitated within matrix phase. The values of hardness and strength increase as a result of a new precipitate due to period of time and heat from supersaturated solid solution.[2,3] Alloy 2024 is an aluminium alloy which containing copper, magnesium, manganese some minor alloying elements.

It's used in engineering applications widely such as aeroplane constructions, orthopaedic soles, rivet and pulling wheels.[2,4] The strength of alloys arises mainly from the nanoscaled precipitates as a results of natural or artificial aging. After solution treating, quenching and aging S phase (Al_2CuMg) was identified as the equilibrium phase of the aluminium alloy 2024. The several stages were typically given as the following sequence [5-7]:

SSS → G.P. zone → S''→ S'→S

The investigation of serveral aging times and temperature on mechanical properties of Aluminium alloy 2024 has been reported by Y.C. Lin et al [8]. However, studies of aging influence on semi-solid casted Aluminium Alloy is very rave. Therefore, the present study, influence of T6 heat treatment was investigated on rolled and semi-solid casted Al2024.

II. MATERIAL ANDMETHODS

2.1. Materials

Rolled 2024 Aluminium Alloy with a dimension of In the present study, the raw material with a dimension of 370 mm x 370 mm x 12 mm semi-solidcasted aluminium alloy with a dimension of 100 mm x 100 mm x 20 mm were used in this study.The composition of the rolled plate and semi- solid casted 2024 aluminium alloy was provided in Table 1. andTable 2.

Element	Cu	Mg	Mn	Si	Fe	Zn	Al
Content	4.56	1.57	0.65	0.50	0.50	0.04	Bal.

Table 1 :Chemical composition of Rolled 2024 aluminium alloy (wt%)

Element	Cu	Mg	Mn	Si	Fe	Zn	Al
Content	5.09	1.67	0.63	0.40	0.33	0.04	Bal.

Table 2 : Chemical composition of 2024 Semi-solid casted aluminium alloy (wt%)

2.2 Samples preparation

Artificial aging (T6) of the alloy was performed using an electric muffle furnace. The aging specimens were cut with a dimension of 10 mm x 20 mm x 12 mm by Horizontal Band Saw machine. Tensile test specimenswerecutbywire electrode into shape according to the ASTM E8 specification. The specimens were solution treated at 505 ºC for 4 hrs, and quenched in water at room temperature. Thereafter artificially aged at 190 ºC for 12, 15 and 18 hrs and quenched in water at room temperature was carriedout.

2.3 Characterization of materials

The sample for optical microscopic examination were prepared using conventional metallographic techniques and alumina powder. The aged specimens were evaluated in hardness, Rockwell Scale B, and tensile strength.

III. RESULTS AND DISCUSSION

Fig.1 showed microstructure of as receives (a) rolled Aluminium2024and (b)semi-solid casted aluminium 2024priorto process of heat treatment. It was obvious that microstructure was different. Fig.1a. Showed the columnar grains of rolled Aluminium while Fig.1b illustrated the globular structure of semi-solid casted Al2024.However, both structures were consisted of primary phase α-Al and eutectic mixture of Al and Cu surrounding around grain boundaries.

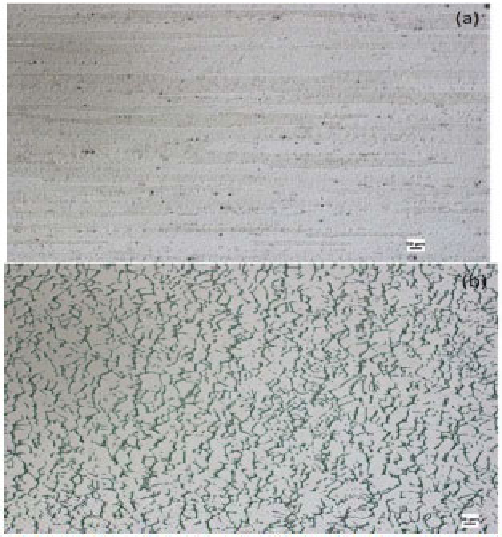

Fig.1.As receivesmicrostructure of (a)rolled Aluminium alloy 2024 and(b) semi-solid castedaluminium alloy 2024

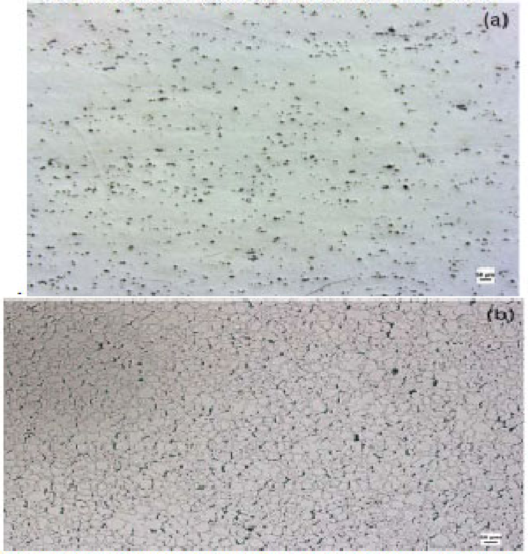

Fig.2. Microstructure of samples after solution treated (a) rolledAluminium Alloy 2024 and (b) semi-solid castedaluminium alloy 2024

Fig.2Show themicrostructure of samples after solution treated at 505 ºC for 4 hrs. Both microstructureswere consisted of α-Al and secondary phase (Al2Cu) in which secondary phase (Al2Cu)locatedalong the grain boundary becomes discontinuous and round in shape. It was considered that secondary phase (Al2Cu) was dissolved intothe α-Almatrix**.** After quenching the soluted atoms in the matrixwere in the supersaturated condition and tend to precipitate out duringfurther aging stage.It can be observed from Fig.3that specimen's hardness was increased as aging time increase due to increasing of precipitate phase. The hardness was found to reach the highest around 15 hours aging time with 81 HRB for rolled Aluminium2024.

Aging time (hrs)	Rockwell Hardness (HRB)	
	Rolled plate	Semi-solid cased
As received	76	36
12	76	72
15	81	80
18	69	73

Table 1 : Rockwell hardness (HRB) of rolled plated and semi-solid casted aluminium alloy 2024

Table 1 shows the Rockwell hardness scale B (HRB) of rolled and semi-solid casted aluminium alloy 2024 that was solution treated at 505 ºC for 4 hoursan followed by quenching in water temperature and aging at 190 ºC for 12, 15 and 18 hours. The hardness of rolled Al2024, as solution treated samples, was quite higher that of semi-solid cased Al2024. It should be due to cold work effect on the rolled Al2024. The hardness was becomed maximum at 15 hours aging time for both of Al2024 with closed value of maximum hardness. Then, when time aging further increaseto18 h,the hardness was revealed to over aging caused by coarsening of precipitate.

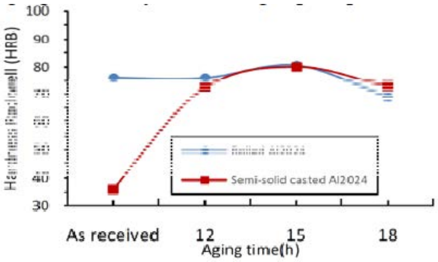

Fig.3.Effects of aging time on the Rockwell hardness (HRB) of rolledand semi-solid casted aluminium alloy 2024

The initial increase in hardness wasexplained by the diffusion from secondary phase (Al2Cu) particles. At the beginning of aging treatment the soluted atoms diffuse and locally cluster to form the GP-zone throughout in the matrix.The GP-zone yielded mechanical property improvement due to the higher stress required to force dislocation through the coherent zone.With increase aging time the GP-zone was transformed and the intermediate s′ precipitates might be formed. Along the aging time, the intermediate precipitate phases were growed and transformed, finally, to s phase incoherent.As the s phase growingnumber of dislocation was decreased and resulting to drop of hardness.[9]

Heat treatment	σ_{max}(Mpa)	EL(%)	HRB
As received Rolled of Al2024	470	18	75
SST at 505 ºC / 4h and 190 ºC / 15 h	483	15	81
As Casted of Semi-solid Al2024	230	33	37
SST at 505 ºC / 4h and 190 ºC / 15 h	395	11	80

Table 2 : Ultimate strength (σ), Elongation (EL) and Rockwell Hardness (HRB) of rolled and semi-solid casted aluminium alloy 2024

Fig.4 to Fig.5 showed the microstructure of samples aging for rolled and semi-solid cased aluminium alloy 2024, respectively. It was revealed that microstructure of solution treated specimens, Fig.4 (a) and Fig.4 (a) indicated the small eutectic phase along the grain boundary. The eutectic phase was considered to dissolve into α-Al during solution treatment. The phase transformation to form secondary phase (Al2Cu) during aging stage yield fine and disperse of secondary phase (Al2Cu) (Fig.4(b)(c) and Fig.5(b)(c)) until reaching the maximum at 15 hour aging time. Then, it was found that coarsening of secondary phase (Al2Cu) was illustrated in Fig.4(d) and Fig.5(d)and lead todroping of mechanical properties.Table 2 showed results of tensile testson as received samples and maximum cases. It was shown that the strength and hardness of semi-solid casted Al2024 were improved by huge effect compare to the rolledAl2024.

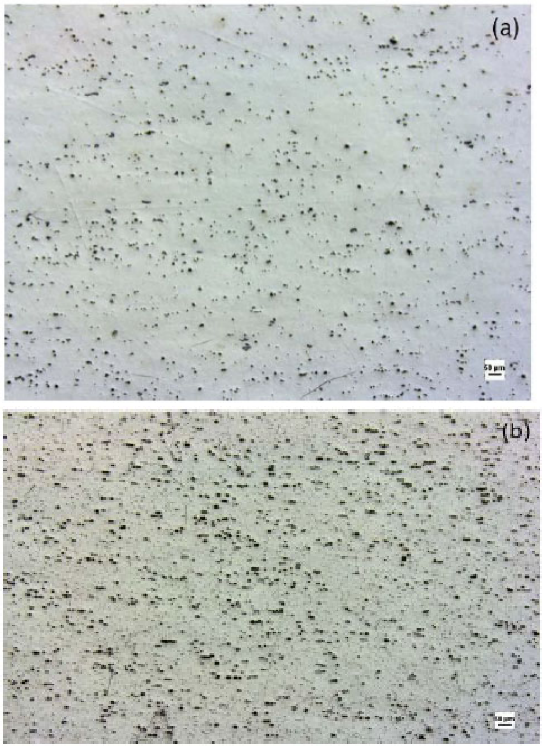

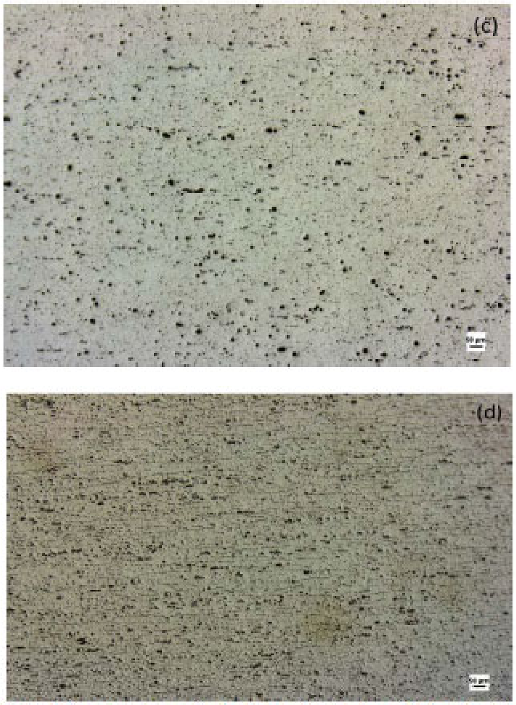

Fig.4. Microstructure of rolled aluminium alloy 2024 at the (a) Solution treated 505 °c/4h and different aging time at 190°c (b) 12 h, (c) 15 h and (d) 18 h (5X)

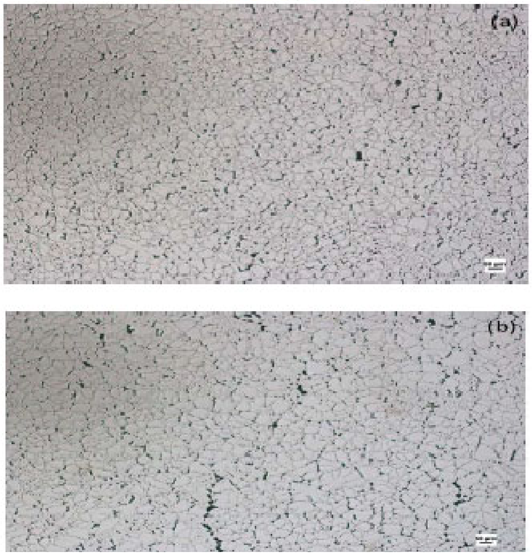

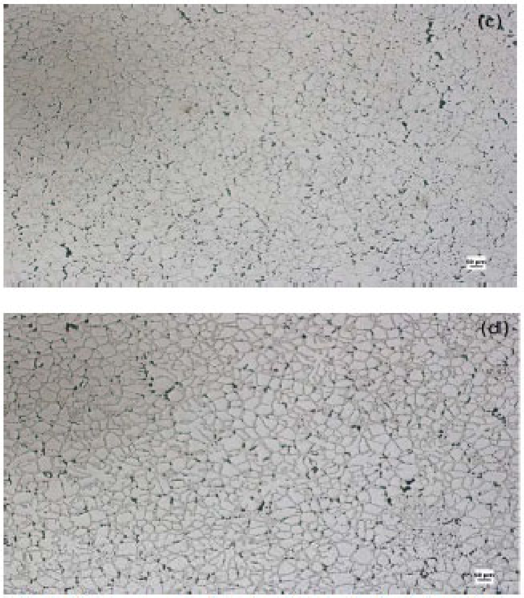

Fig.5. Microstructure of semi-solid casted aluminium alloy 2024 at the (a) Solution treated 505 °c/4h and different aging time at 190 °c (b) 12 h, (c) 15 h and (d) 18 h (5X)

It may due to influence of cold work on rolled Al2024 that resulted in quite high strength and hardness for as received rolled Al2024. Ductility of specimen was found to drop in proportion of increasing of strength. Consequently, rolled Al2024 exhibited remarkable higher strength than semi-solid casedAl2024.

IV. CONCLUSIONS

Rolled and semi-solid cased Al2024 were T6 treated, the following conclusions could be drawn from the tested results:

1. Strength and hardness of rolled and semi-solid casted Al2024 were increased as longer aging time and reached the maximum at 15 hours aging time
2. Rolled Al2024 exhibited higher strength than semi- solid casted Al2024 at 15 hours aging time. It could be considered as the influence of cold rolling processes.

REFERENCES

[1] D. A.P. Reis et al., "Effect of Artificial Aging on the Mechanical Properties of an Aerospace Aluminum Alloy 2024", Defect and Diffusion Forum, Vols. 326-328, pp. 193-198,2012

[2] Kaçar, Hülya, Enver Atik, and Cevdet Meriç. "The effect of precipitation-hardening conditions on wear behaviours at 2024 aluminium wrought alloy." Journal of Materials Processing Technology 142, no. 3 (2003):762-766.

[3] Scheuring, Jason N., and A. F. Grandt. "An Evaluation of Aging Aircraft Material Properties." ASME-PUBLICATIONS-AD 47 (1995):99-110.

[4] Tyouke, B., M. Larouech, Y. Tamraoui, and E. Saad. "microstructure and mechanical peoperties of Al-Cd binary alunminium alloy." Journal of Science and Arts 17, no. 1 (2017):131.

[5] Li, Hai, Wei Xu, Zhixiu Wang, Bijun Fang, Renguo Song, and Ziqiao Zheng. "Effects of re-ageing treatment on microstructure and tensile properties of solution treated and cold-rolled Al–Cu–Mg alloys." Materials Science and Engineering: A 650 (2016):254-263.

[6] Sun, Daren, Xi-chen Sun, Derek O. Northwood, and Jerry H. Sokolowski. "Thermoelectric power characterization of a 2024 aluminum alloy during solution treatment and aging." Materials characterization 36, no. 2 (1996):83-92.

[7] Alexopoulos, Nikolaos D., Zaneta Velonaki, Constantinos I. Stergiou, and Stavros K. Kourkoulis. "Effect of ageing on precipitation kinetics, tensile and work hardening behavior of Al-Cu-Mg (2024) alloy." Materials Science and Engineering: A700 (2017):457-467.

[8] Lin, Y. C., Yu-Chi Xia, Yu-Qiang Jiang, Hua-Min Zhou, and Lei-Ting Li. "Precipitation hardening of 2024-T3 aluminum alloy during creep aging." Materials Science and Engineering: A 565 (2013):420-429

[9] Song, Y. F., X. F. Ding, L. R. Xiao, X. J. Zhao, Z. Y. Cai, L. Guo, Y. W. Li, and Z. Z. Zheng. "Effects of two-stage aging on the dimensional stability of Al-Cu-Mg alloy." Journal of Alloys and Compounds 701 (2017):508-514.

★★★

DEVELOPMENT OF HEAT EXCHANGERS IN HIGH-TEMPERATURE USING ADVANCED MANUFACTURING TECHNOLOGIES

[1]RAGHU. T. S, [2]SAMARENDRA KUMARNAYAK, [3]CHANDAN KUMAR PRADHAN

[1]Department of Mechanical Engineering, NMIET, Bhubaneswar, 751019
[2]Department of Mechanical Engineering, REC Bhubaneswar
[3]Department of Mechanical Engineering, CEC Bhubaneswar
E-mail: [1]punita.kumari@nmiet.ac.in

Abstract - Experimental program Development of high-temperature heat exchangers using advanced manufacturing technologies, mechanical design and materials was focused on the prototype production of the heat exchangers by means of conventional and progressive manufacturing methods. Developments in the additive manufacturing (AM) processes and the introductionofnewand/or modifiedalloysgaveengineers libertynotonlyinthedesign. Metallographiccharacteristicsofthe nickel-based alloys were the main objectives of the research. The results will contribute to the design and construction of the plate heatexchanger.

Keywords - Heat Exchangers, Superalloys, Additive Manufacturing.

I. INTRODUCTION

The main objectives of the projectDevelopment of high-temperature heat exchangers using advanced manufacturing technologies, mechanical design and materials is to design new types of the high-temperature gas/gas heat exchanger for applicationsinindustrialandenergysectors,aswellas for the new generation of nuclear reactors. The materials,whichareappliedinthesesectors,areeither stainless steels or nickelsuperalloys.

Nickel-based alloys have become standard for high-temperatureapplications. These alloys generally offer high corrosion and wear resistance when exposed to high temperatures. Conventional production of these alloys is well established;however boom in the field of additive manufacturing has opened a new way of the manufacturing procedure. The investigated components were processed from Incoloy alloy 800 HT (1.4959) and Inconel 718, materials ideal for high-temperature applications such as gas turbine parts, instrumentation parts, power and process industry parts up to 700 - 800 °C[1] - [3].

Materials produced by AM exhibit specificities comparedtocommonlyproducedcomponents.Froma material perspective, AM products show a strong dependence on the process parameters.The entire process chain of the additive manufacturing, which will be in near future similarly important to conventional methods, also highly influences the microstructure of the component. AM products are composed of tiny weld beads so-called “melt pools”, generated by the laser. A certain pattern of texture can be expected due to the fast and directional solidification. The resultant heat transfer and fluid flow affect the size and shape of the meltpools, the cooling rate, and the transformation reactions in the melt pool and heat-affected zone[4] - [7]. Metallographic characteristics were performed by means of optical and scanning electron microscopy enhanced by electron backscattering diffraction analysis, a unique tool for assessing the material texture. After the literature search on the materials used nowadays for high-temperature heat exchangers, austenitic steels andnickelalloyswereproposedforthisresearch.This contribution will deal with the analysis of nickel alloys.

II. EXPERIMENT DESCRIPTION

The experiment consisted of two main parts. In the first part, microstructural characteristics of the conventionally produced nickel-iron-chromium alloy Incoloy 800 HT (1.4959), was tested and analysed in as - received and aged conditions at 650 and 850 °C with 150 hours holding time. As not every material was found to be suitable for additive manufacturing, further tests were performed withthe material Inconel 718. Direct Metal Laser Sintering (AM) methodwas involved in the second part of the experiment.The additively manufactured Inconel 718 was stress-relieved at 980 °C for 1 hour and air cooled.

The chemicalcomposition of the alloys was measured by optical emission spectrometer BRUKER Q4 TASMAN. The results are given in **Legend**: LM (Light microscopy). Hardness HV 10 was measured according to ISO 6507 – 1on Struers Durascan 50 (SeeTable II).

Legend: LM (Light microscopy)

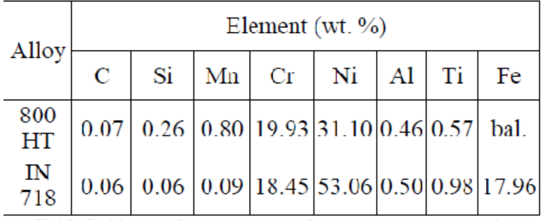

Alloy	Element (wt. %)							
	C	Si	Mn	Cr	Ni	Al	Ti	Fe
800 HT	0.07	0.26	0.80	19.93	31.10	0.46	0.57	bal.
IN 718	0.06	0.06	0.09	18.45	53.06	0.50	0.98	17.96

Table I. Chemical composition of experimental materials

A. Microstructural analysis

The analysed samples were subjected to standard metallographic preparation – i.e. grinding and subsequent polishing. The microstructure of thesample was revealed by etching in the V2A reagent and documented using a Carl Zeiss-Observer.Z1m optical microscope. The microstructure was also analysed by SEM analysis performed on the Jeol JSM 6380 scanning electron microscope. The local chemical composition was measured using the INCAx-sight EDX analyser.

The homogeneous microstructure of Incoloy 800 HT consists of an austenitic matrix with carbide precipitates in grains and at the borders of austenitic grains (Fig. 1). With increasing temperature and ageing, carbides precipitated inside the grain. Grain coarsening trend with increasing time and the ageing temperaturewasnotobservedinthisalloy(Fig.2,Fig. 3). Specimens were subjected to EDX analysis for identification of intermetallic particles and secondary phases.EDXanalysisofIncoloyrevealedthepresence ofcomplexcarbidescomposedofCr,NbandTiwithin the grains and chromium carbides (likely Cr23C6) on thegrainboundaries(Fig.4).Additivelymanufactured Inconel 718’smicrostructureconsisted of an austenitic matrix with small, uniformly dispersed γ’ and γ’’ precipitates, δ phase plates and discontinuous M23C6 grain boundary carbides (see Fig. 5 and Fig.6).

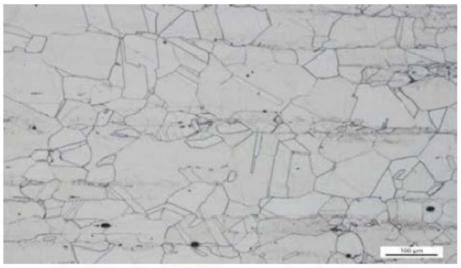

Fig. 1 Incoloy 800 HT _as_recieved state. LM

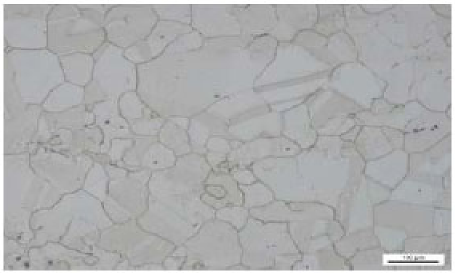

Fig. 2 Incoloy 800 HT 650°C - 150 h.LM

Fig. 3Incoloy 800 HT_850°C - 150 h.LM

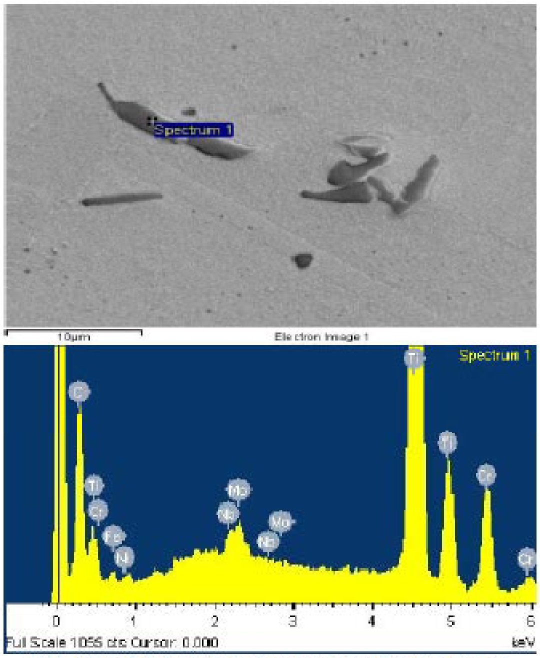

Fig. 4Results of EDX measurements on Incoloy 800HT specimen on particles within the grains

Fig. 5 IN 718_LM

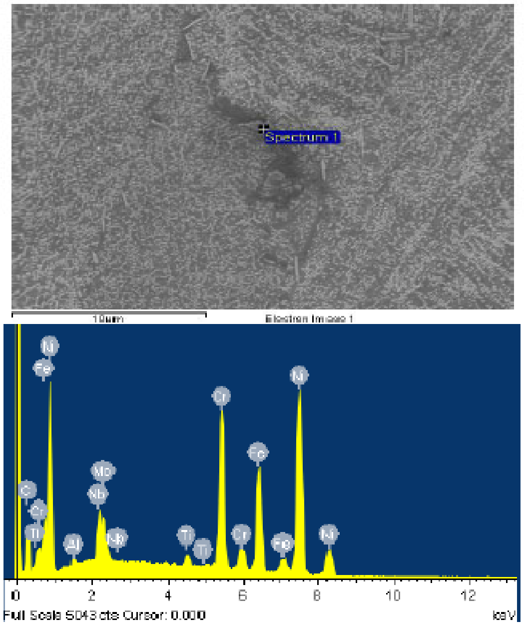

Fig. 6 Results of EDX measurements on Inconel 718

Specimen		HV10
Incoloy 800 HT	As received	120
	650°C - 150 h	183
	850°C – 150 h	142
Inconel 718	As received	387

Table II. Results of hardness testing

B. Electron Backscatter Diffraction Analysis (EBSD)

The microstructure of Inconel 718 consists of an austenitic matrix with thepresence of columnar grains intheZ-buildingdirection.Fig.7showsbandcontrast - image quality. This indicates the "sharpness" of the Kikuchi lines for each index point. The lighter the point in the image (in the grayscale), the diffraction pattern of the Kikuchi line is sharper at that point. By default, the smallest sharpness (and hence the darker points in the picture) is achieved by indexing at grain boundaries, phase intervals, pores, inclusions,etc.

Fig. 8 shows the orientation of the individual grains of phases using the Inverse Pole Figure (an inverted pole pattern). In the Inverse Pole Figure are projected spheres aligned with the directions of the crystals. Sketched directions are a stereographic design of the directions of the crystals parallel to the normal direction(ND), the parallel direction (RD) or the transverse direction (TD) in the sample. An inverse pole pattern can help to visualize certain types of textures. Thus we can determine that, for example,the grain has the same orientation of the crystal lattice as several grains coloured with an identical colour.Fast and directional coolingduring the AM processingresulted in a certain degree of texture, which is obvious from Fig.9.

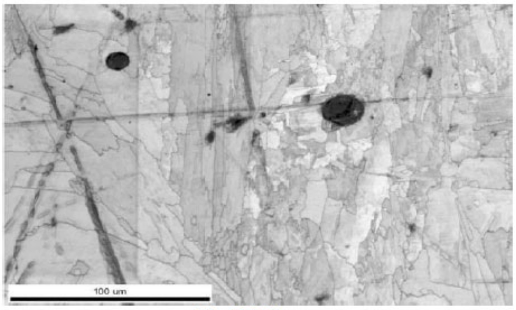

Fig. 7 IQImage

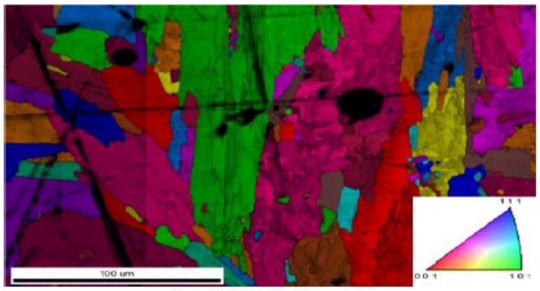

Fig. 8 IPF - IQ Image

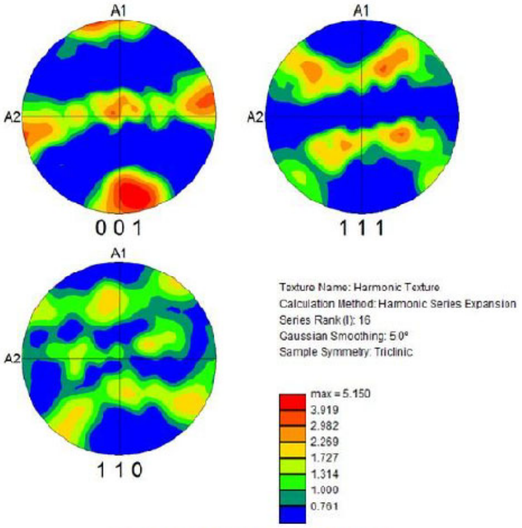

Fig. 9EBSD analysis pole figures

III. CONCLUSION

Two nickel alloys were selected for experiment dealing with microstructural properties of conventionally and additively manufactured superalloys.The grain size of conventionally manufactured Incoloy 800HT was not affected after ageingat two temperatures 650 and 850°C.Nevertheless, the precipitation of carbides within the grains and on the boundaries was observed in this material. The microstructure of additively manufactured materialconsiderably differed from that of conventionally produced alloy, as fast and directional coolingtook place during the processing. Presence of precipitatesin the nickel-chromium alloy Inconel 718 microstructure, contributed to the strengthening of the matrix, which was reflected in the increase in hardness values.The DMLS processed heat exchangerwill be tested in the experimental helium loop. The test results will serve mainly for the design and construction of a short-time service helium-helium heatexchanger.

REFERENCES

[1] J. R. Davis, “Nickel, cobalt and their alloys”,2000.

[2] Material data sheet. EOS NickelAlloy IN718. TMS, WEIL / 05.2014, EOS GmbH.,2014

[3] ASMHandbook, Volume 9, Metallography and Microstructure,2004.

[4] D.I.Wimpenny;P.M.Pandey,andL.J.Kumar,“Advancesin 3D Printing & Additive Manufacturing Technologies,” ISBN 978-981-10-0812-2, pp. 40 - 53,2017.

[5] T.S. Srivatsan, T.S. Sudarshan, “Additive Manufacturing: Innovations, Advances, and Applications,” ISBN 978-1-4987-1478-5, pp. 70 - 76,2016.

[6] M.Brandt,“LaserAdditiveManufacturing:Materials,Design, Technologies, and Applications,” pp. 55 - 70, ISBN 978-0-08-100434-0,2017.

[7] D.Gu, “Laser Additive Manufacturing of High – Performance Materials,” ISBN 978-3-662-46089-4, pp. 223 - 271,2015.

★★★

INVESTIGATION OF FUSED DEPOSITION TECHNOLOGY FOR THE PRODUCTION COMPONENTS OF THE SUPER-EFFICIENT SHELL ECO-MARATHON CAR

[1]RAMYARANJAN LENKA, [2]AMAR SETHY, [3]NILAKANTHA MOHAPATRA

[1]Department of Mechanical Engineering, NMIET, Bhubaneswar, 751019
[2]Department of Mechanical Engineering CEC Bhubaneswar
[3]Department of Mechanical Engineering REC BHUBANESWAR
E-mail: [1]prajna.kar@nmiet.ac.in

Abstract - Fused Deposition Modeling rapid prototyping technology consists in applying a melt of thermoplastic material with the print head layer by layer until the complete physical object is created. With the decrease of the 3D printers' price, FDM was also used in the production of final products or spare parts. Thanks to the low price of 3D printers and print materials for this technology, it is currently the most widespread 3D printing technology in the world. This paper presents the application of FDM technology for part production of the super-efficient car Eco Arrow 3.0 which took part in the Shell Eco Marathon competition in the prototype class. The use of 3D printing technology to produce many elements of the car designed especially for its construction allowed to significantly reduce the cost and time of their implementation at the stage of prototypes and finalmodels.

Keywords - 3D Printing, 3D Printing Costs, Fused Deposition Modeling, Additive Manufacturing, Shell Eco Marathon

I. INTRODUCTION

Fused Deposition Modeling (FDM) is one of the oldest 3D printing technologies, it was invented in 1988 by Scott Cramp who founded one of the most known companies in the 3D printing industry – Stratasys [1]. This rapid prototyping technology consists in applying a melt of thermoplastic material with the print head layer by layer until the complete physical object is created. Originally, due to the high prices of 3D printers, it was mainly used to manufacture prototypes in large industrial companies. At the beginning of the 21st century, with the expiration of key patents protection, much cheaper FDM printers began to appear on the market. With the decrease of the 3D printers' price, FDM was also used in the production of final products or spare parts. Thanks to the low price of 3D printers and print materials for this technology, it is currently the most widespread 3D printing technology in theworld.

This paper presents the application of FDM technology for part production of the super-efficient car Eco Arrow 3.0 which took part in the Shell EcoMarathon competition in the prototype class. This car was built by Iron Warriors – a team of students from the Technical University of Lodz. A characteristic feature of this type of projects is necessity to fabricate single copies of many different parts. It often happens that after testing it is essential to introduce some modifications in the component and remake it. The time needed to complete the production of parts is also important. Printing real models yourself, self-owned 3D printer is much faster than ordering the parts at an external company. It can takeseveralweekstosendthedocumentationofthe designed part to receive the finished product. This is much too long, especially for prototypes that may need iterative improvements. Service at external companies also generates high costs. Self-made parts on 3D printer are much cheaper solution. Using your own printer in the case of FDM technology, the only cost is electricity and print material as thermoplastic-material wire wound on a roll [1, 2].

II. PRINTED MODELS

Designing models for fabricating on a 3D printer gives a lot of freedom in their shape. The 3D printer makes it also possible to cheaply produce parts that cannot be produced using traditional methods or very expensive in single copies. An additional advantage of FDM technology is the ability to choose the internal structure of the model. In cases where high mechanical strength is required, a high filling density can be used, and when it is not necessary, can be low and a much lighter element is obtained, what further reduces the cost and time of its production. The use of low density of the model fill gives the greatest savings in the case of large volume components. For very slim models, the weight reduction when printing the hollow part will be small, due to the fact that in such a model, the surface to volume ratio is large, and the external parts of the model are printed with full filling to a depth of 1-2 mm. The space in which the low-density fill is applied will besmall.

Below we present examples of model parts with different characteristics and desirable properties that have been printed from one of the most popular materials used in FDM technology – ABS (Acrylonitrile butadiene styrene)[3]with the 3D Ultimaker 2 Extended 3D printer. They were used during the construction of a car competing in Shell EcoMarathon race. The winning aim is to achieve the least fuel consumption by a constructed vehicle.

2.1 Drive beltguard

The model shown in the Picture 1 is a part of the transmission system in the car. Six pairs of such elements connected with bolts protect against falling of the toothed drive belt from the receiving gearwheel. The modular design of the gearwheel with the use of printed parts enables cutting out a central part of the 40 cm in diameter sprocket with a flat sheet metal in 2D, which significantly reduces the cost of manufacturing such a large gearwheel. This model is characterized by very low thickness, so reducing the density of the filling does not significantly reduce the weight of the finished part. Due to the appearance of a large flat surface, this model has a large contact surface with the printer's work platform. The amount of necessary supports during printing was verysmall.

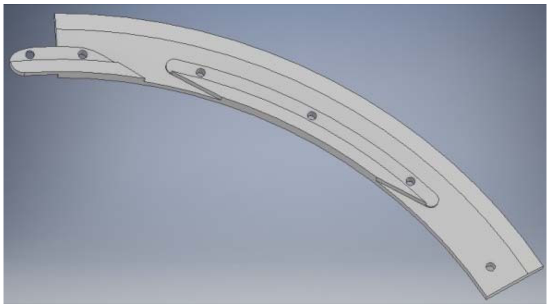

Picture 1. Drive belt guard design drawing.

2.2 Safety switchholder

In each car that competes in the Shell EcoMarathon competition, a safety switch must be placed to enable cut off power from the outside. Picture 2. present such a safety switch holder. This element has to have high mechanical strength due to its additional function: the top of the car’s body is partly based on it. Therefore, it has thick walls and struts, as well as it has been printed with a very high fillingdensity.

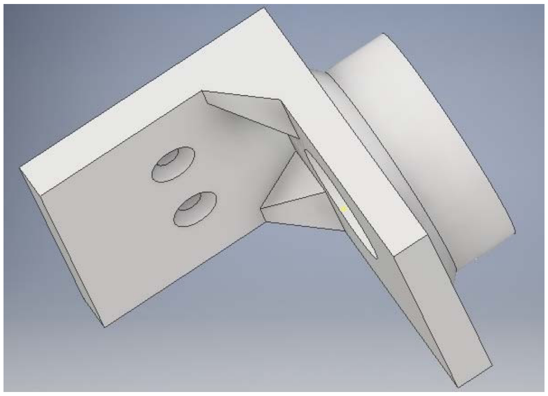

Picture 2. Safety switch holder design drawing.

2.3 Speed sensorholder

Model presented in the Picture 3 does not have to have high mechanical strength, but it has to maintain high rigidity, so that the sensor placed in it does not get vibrations which could disrupt its operation. It has been designed with relatively thick walls. However, it can be printed with a fairly low filling density that reduces its mass while not significantly reducing the rigidity of the part. This model has a simple geometry so it could be easily made using traditional methods, however, the use of 3D printing thanks to the low density of the model fill ensures lower mass of the finished part. The car has two such components with rotational speed sensors installed there to control the clutch that disconnects the rear wheel of the car when the engine in the vehicle is turned off and the car is rolling due toinertia.

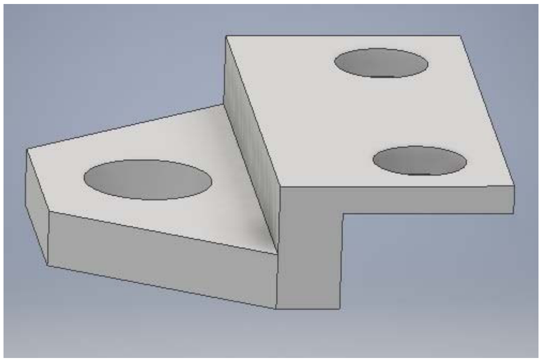

Picture 3. Speed sensor holder design drawing.

2.4 Magnet holder for speedsensor

The model shown in the Figure 4, similarly to the speed sensor holder, doesn’t have to have high mechanical strength, so it was printed with low filling density. Magnetic fields of the magnets mounted in it are received by the sensor placed in the speed sensor holder.

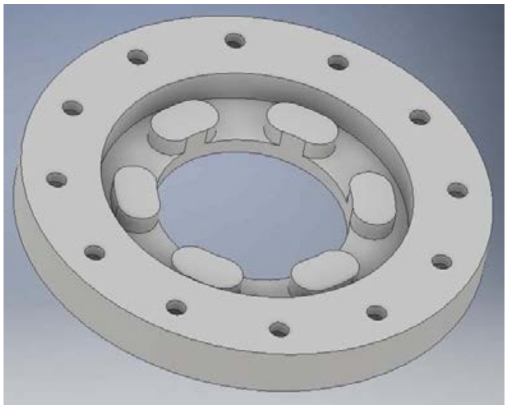

Picture 4. Magnet holder for speed sensor design drawing.

2.5 Servomotor holder

Servomotor holder presented in the picture 5 as the name suggests is used to mount servo in it, which is responsible for automatically disconnecting the drive while the vehicle's engine is not turned on. This aims to reduce the rolling resistance of the car. This part must have high mechanical strength, so they have been printed with a high filling density.

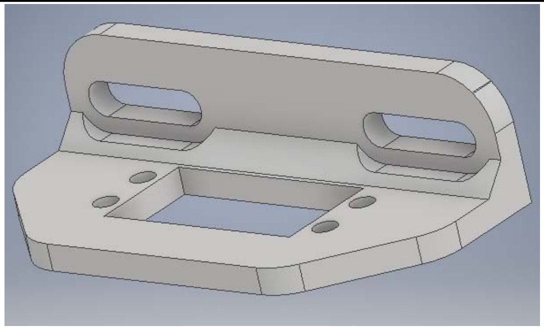

Picture 5. Servomotor holder design drawing.

2.6 Part of engine air intake system

Model presented in the Picture 6 is a part of engine air intake system. An air filter is mounted in this part to protect the engine from dirt. A characteristic feature of this element are thin walls, similarly to the drive belt guard reducing the density of the model filling, does not achieve a significant mass reduction. Another important feature of this part is a complicated geometry. For this model to be printed correctly it is necessary to use a large amount of supports. It is important to keep the flow resistance in this part as small as possible. To achieve that it is necessary to use low layer height, which gives a better surface quality, but unfortunately significantly extends the printing time. Due to the complicated shape of the model, manufacturing it with traditional methods is much more expensive than using additive technology.

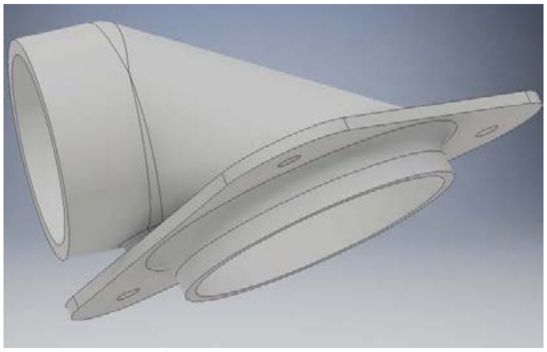

Picture 6. Part of engine air intake system design drawing.

2.7. Phone holder

The phone holder presented in the Picture 7 make possible to install the phone on the steering wheel as a speedometer and a counter helping the driverto control the travel time using a special mobile application. The grip with the phone is mounted on the steering wheel using magnets placed in the bottompartofthegrip. Itallowseasilyremoveit from the car if necessary. This model was printed with a low filling density which allowed to significantly reduce mass of thispart.

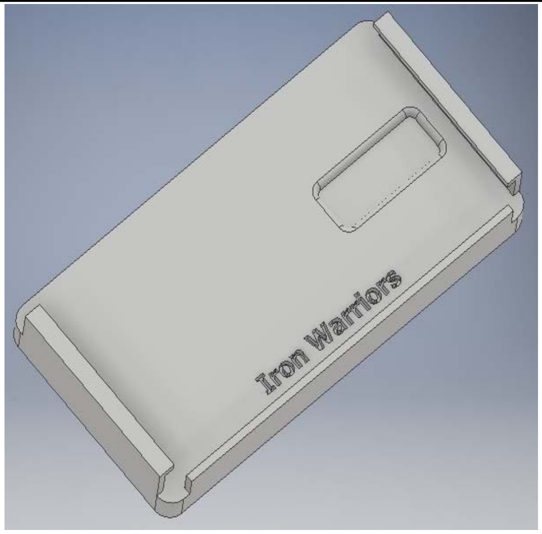

Picture 7. Phone holder design drawing.

III. COSTS, PRINTING TIME AND WEIGHT OF THEMODELS

Table 1 presents basic printing parameters for individual models. These values were selected to achieve optimal results depending on the desired characteristics of the part. The density value of the filling was set from 20% for mechanically unloaded parts up to 90% for parts that need to be durable. In case of printed parts with a low filling density, it was possible to achieve even more than 50% reduction in the weight of the printed part. Total weight reduction for all printed parts reached over 20% in comparison to parts made of solid ABS, and70% compared to parts made of aluminum. The height of the printed layer for the model with the desired surface quality was set at 0.1 mm, in the other models a 0.3 mm layer was used to achieve greater mechanical strength[4]. The use of a lower layer height of applied material results in a practically linear increase in printing time relative to the weight of the material used to print the model. The total printing time of all parts used for building a car sums up to almost 44 hours. The printing time of a single part depends on its size and set parameters. The shortest printing time of single part was about an hour, the maximum printing time was 12 hours. This is a time short enough that in the case of damage to any of the printed elements, the spare part is ready even on the same day. Using traditional methods this is in most cases impossible. Apart from the purchase price of a 3D printer and assuming self-service of the printer the total cost consists of the price of the material and electricity. The total cost of producing all of the presented parts was less than 15 USD. This price is many times lower than using traditional methods.

	Drive belt guard x12	Air intake part	Safety switch grip	Speed sensor holder x2	Magnet holder for speed sensor x2	Servomotor holder	Phone holder	Sum
Volume of the model [cm^3]	211	50	35	52	60	22	104	534
Infill density [%]	90	60	90	40	30	90	20	-
Layer height [mm]	0,2	0,1	0,3	0,3	0,3	0,3	0,3	-
Print time [min]	1212	716	134	139	160	77	185	2623
Model mass [g]	228	44	37	34	39	24	49	455
Used material [g]	230	76	42	43	40	25	50	506
Material cost [USD]	5,98	1,98	1,09	1,12	1,04	0,65	1,30	13,16
Electricity cost [USD]	0,61	0,36	0,07	0,07	0,08	0,04	0,09	1,31
Total cost [USD]	6,59	2,33	1,16	1,19	1,12	0,69	1,39	14,47

Table 1. Print parameters, parts features and costs

IV. CONCLUSIONS

All printed parts were mounted in the vehicle and successfully fulfilled their tasks while participating in the Shell EcoMarathon competition. ABS is a sufficiently durable material for many parts mounted in the Shell EcoMarathon vehicle. The use of 3D printing technology to produce many elements of the car designed especially for its construction allowed to significantly reduce the cost and time of their implementation at the stage of prototypes and final models. An additional advantage of using printed in 3D parts is their lower mass than parts made using traditional methods, thanks to which it was possible to reduce the weight of the car. An additional aspect that supports the use of additive technologies is the small amount of generated waste, which is beneficial for the natural environment.

REFERENCES

[1] Chee Kai Chua, Kah Fai Leong, Chu Sing Lim, Rapid Prototyping: Principles and Applications, ISBN: 978-981-277-897-0

[2] Ben Redwood, Filemon Schöffer, Brian Garret, The 3D Printing Handbook: Technologies, design andapplications,

[3] ISBN:978-908-274-850-5

[4] www.sculpteo.com/en/glossary/abs-definition

[5] www.my3dmatter.com/influence-infill-layer-height-pattern/#more-95

* * *

INVESTIGATIONS OF OVERBURDEN MECHANICAL PROPERTIES ON SUBSIDENCE CHARACTERISTICS

[1]S. ARUNACHALAM, [2]KRUSHNA MOHAN MOHAPATRA, [3]SOURAV PRAKSH PRADHAN

[1]Department of Mechanical Engineering, NMIET, Bhubaneswar, 751019
[2]Department of Mechanical Engineering REC Bhubaneswar
[3]Department of Mechanical Engineering CEC Bhubaneswar
E-mail: ranjan.kumar@nmiet.ac.in

Abstract - Numerical analyses is using Phase 2.8 program performed study the effects of overburden properties and opening depth on the subsidence configurations under sub-critical condition. The computer simulation results indicate that the maximum subsidence decrease with increasing roof thickness. The maximum subsidence is constant if the roof thickness-to-opening width ratio are more than 0.4. The trough width decreases with increasing elastic moduli of overburden and decreasing opening depths.

Keywords - Surface Subsidence, Trough, Finite Element, Overburden Stratum

I. INTRODUCTION

Surface subsidence due to underground mining can impact the environment and surface structures within the mine area [2]. In practice, the mining processesdo not allow collapse of the underground opening, the overburden however may deform and move due to mine extraction. In this case, the surface subsidence deformationdoesnotexceedthecriticalpoint,referred as sub-criticalcondition.

To minimize the adverse impacts of subsidence a reliable prediction is essential. Several parameters affect the magnitude and extent of subsidence that occur due to underground mining [3]-[7]. The observed data and theoretical research demonstrated that the subsidence of underground mining is related with the following factors: mining depth, mining thickness, degree of extraction, methods of working, near-surface geology, physical and mechanical properties of overburden strata and ore seam [8-10].

Overburden strata and ore seam properties is one of the important factors that can affect the surface subsidence characteristics [8]. Most researchers tried to correlate the subsidence characteristic (maximum subsidence and angle of draw) with overburden strata andoreseampropertiesforundergroundminingunder sub-critical, critical, and super-critical conditions using physical and numerical methods[11]-[13].

Thesearerresearchconsideredtheoverburdenstratato behomogenousandonlyonetypeofoverburdenrock. Multi-layers of overburden rock strata and the difference in their mechanical properties are not emphasizing as the key parameter for the study. Even though numerous studies have been carried out to analyze and simulate the surface subsidence as affected by configurations of underground opening, rare attempt has been made to assess the effects of overburden properties, in particular, modulus of deformation (for sub-critical condition).Theobjective of this study is to determine the relationships between the deformation modulus (E) of the overburden with the subsidence components (angle of draw (γ) and subsidence magnitude (S_{max})).

The tasks involve performing numerical simulations andtodeterminetherelationshipsabove.Theeffectof overburden inter-layer is alsostudied.

II. NUMERICALSIMULATION

The finite difference method program – Phase 2.8 [1] is used to simulate the surface subsidence profiles correlated with the overburden properties and underground opening configurations because of simplify of geometry creation.

The results are represented in term of the maximum subsidence (S_{max}), angle of draw (γ) and limit trough width (B). The limit trough width can be readily derived using a predefined subsidence limit with 1% of the maximumsubsidence.

III. MESHMODELS

To cover the entire range of the opening dimensions, over8,000mesheswithuniformmeshandthreenoded triangles element types have been constructed to obtain accurate simulation results. The analyses are performed in plane strain condition. The distance between the left and right boundaries edges from the center is 1010m.

The left and right boundaries are fixed in the x-axis, and the bottom boundary is fixed in the x, y – axis. The upper boundary can move freely in both directions,whereDisthedepthofopening,S_{max}isthe maximum subsidence, B is the limit trough wide, γ is the angle of draw, W is the width of opening and H is theheightofopening,tisthethicknessroofofopening

(Fig.1).

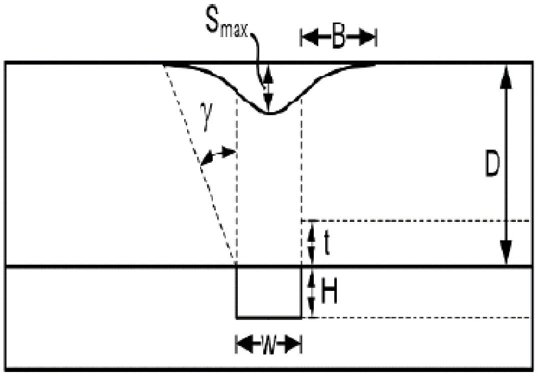

Fig. 1 Variables used in numerical model simulation

IV. MATERIAL PROPERTIES

Theinfluenceofthevariantoverburdenstrataandroof thickness (t_i) on surface subsidence is studied here. The elastic modulus and density (Table I) of the overburden selected in this study represent four different rock sequences in the northeast of Thailand where most salt mines have been developed. The model simulation as shown in Fig.2. The average modulus (E_{avg}) and density ($\square_{avg}$) are calculated as follow:

$$E_{ave} = \sum_{i=1}^{n} E_i\, t_i \,/ \sum_{i=1}^{n} t_i \qquad (1)$$

$$\rho_{ave} = \sum_{i=1}^{n} \rho_i\, t_i \,/ \sum_{i=1}^{n} t_i \qquad (2)$$

when t_i is thickness of rock unit from above calculation, the average elastic modulus is 7 GPa and the average rock density is 2,360 kg/m^3. The measurement results are presented in terms of the maximum subsidence (S_{max}) and trough width (B). Figure 3 compares the results obtained from the modelling of variant E of overburden strata (E_{each}) with those of the modelling of average E of overburden (E_{avg}). Two models show virtually identical relation (trends) between subsidence components and the opening configurations, especially when the t/w ratios are beyond 0.4. The maximum subsidence decreases with increasing roof thickness. The maximum subsidence are constant, when the roof thickness-to-opening width ratios are more than 0.4.

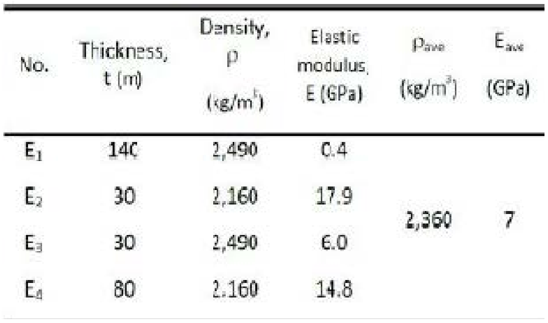

No.	Thickness, t (m)	Density, ρ (kg/m^3)	Elastic modulus, E (GPa)	ρ_{ave} (kg/m^3)	E_{ave} (GPa)
E_1	140	2,490	0.4	2,360	7
E_2	30	2,160	17.9		
E_3	30	2,490	6.0		
E_4	80	2,160	14.8		

Table I Estimation of average density (ρ_{ave}) and average elasticity (E_{ave}) for the study (Fig.3).

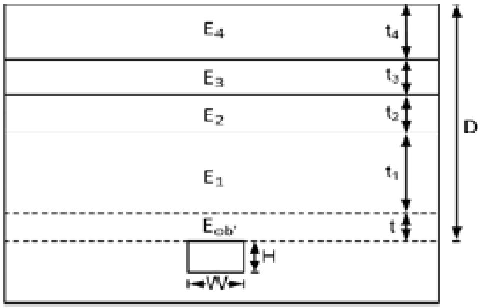

Fig. 2. Variables used in numerical model simulation

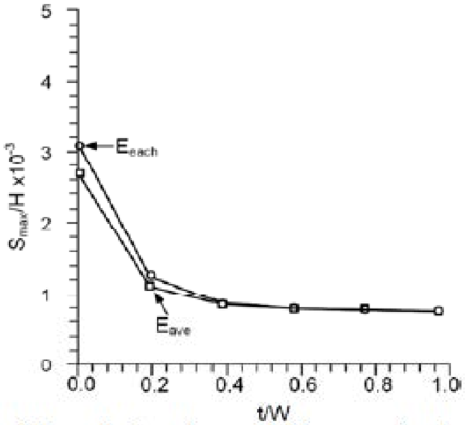

Fig. 3 Normalized maximum subsidence as a function of normalize roof thickness

V. EFFECT OF ELASTICMODULUS

Studying the effect of elastic modulus of overburden on subsidence limit characteristics has been carried out using a finite difference method program. The elastic modulus of overburden (roof of opening ($E_{ob'}$)) are 0.1, 0.5, 1, 5, and 10 GPa and the elastic modulus of ore is constant as 1 GPa. Figure 4 shows boundary condition for this study. The simulations are performed in plane strain condition. Figure 5 shows normalized maximum subsidence (S_{max}/H) as a function of normalized roof thickness (t/w) under various elastic modulus of ore ratios ($E_{ob}/E_{ob'}$) from 0.1 to 10 GPa. The results indicate that increasing of elasticmodulusoftheoverburdenreducethevaluesof maximum subsidence (figure5 and 6). The observation also agrees reasonably well with those obtained by Yao et al. [8] and Sartkaew et al.[12]

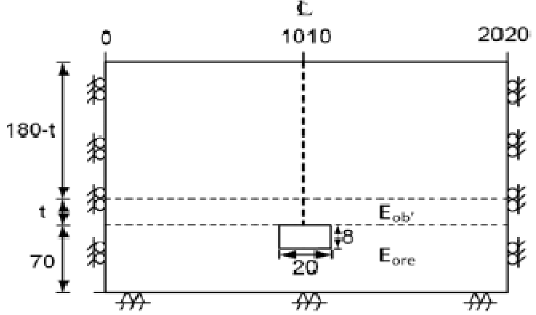

Fig. 4 boundary condition for simulation

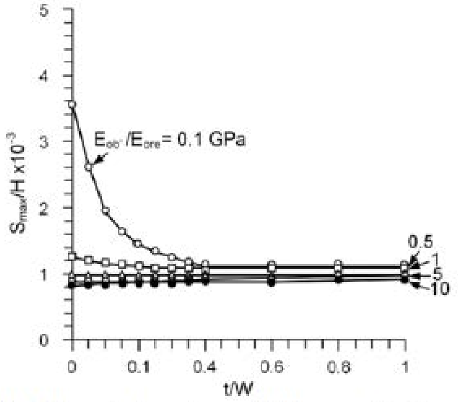

Fig. 5 Normalized maximum subsidence as a function of normalize roof thickness

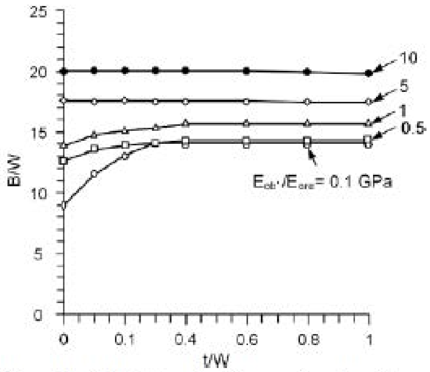

Fig. 6 Normalized limit trough wide as a function of normalize roof thickness

VI. EFFECT OF OPENING DEPTH

The computer simulation is performed to investigate the effects of opening depth. All cases are simulated under constant opening height at 8 m and opening width at 20 m. The depths of opening (D) are 80, 180, 280, 380, and 480 m (Fig.7). The results show that increasing of the opening depth would reduce the values of maximum subsidence (Fig.8 and 9). This agrees with the postulation given by Singh [14] which suggests that under sub-critical subsidence condition the angles of draw tends to be constant and the maximum subsidence sensitive to opening height, depth.

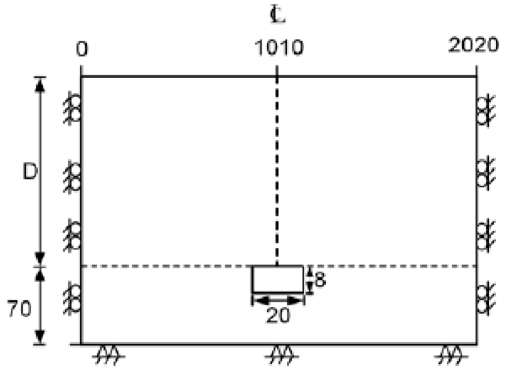

Fig. 7 boundary condition for simulation

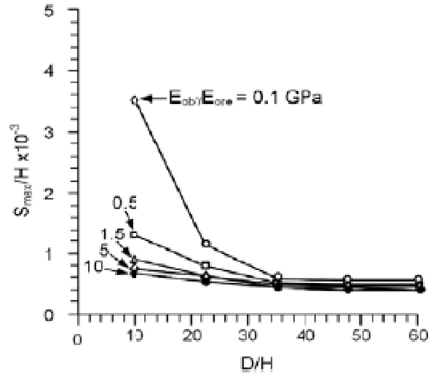

Fig. 8 Normalized maximum subsidence as a function of normalize opening depth

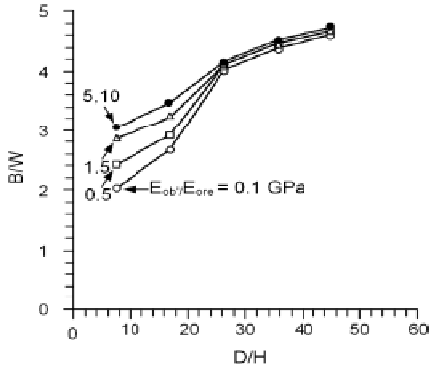

Fig. 9 Normalized limit trough wide as a function of normalize opening depth

VII. CONCLUSION

From the above analysis the following conclusions can be draw:

1. The maximum subsidence decreases with increasing roof thickness. When the roof thickness of opening-to-width of opening (t/W) are more than 0.4 times, the opening width and maximum subsidence will beconstant.
2. The main factor controlling the maximum subsidence are overburden properties and the opening depth, the function of elastic modulus of overburden to elastic modulus of ore ratio (Eob’/Eore).
3. The maximum subsidence decreases with increasing opening depths. Conversely, decreasing of opening depth tend to increase the extent of surface subsidence.
4. A function of elastic modulus of overburden to elastic modulus of ore ratio ($E_{ob'}/E_{ore}$) increase in the overburden tends to decrease the extent of subsidence at the surface.

ACKNOWLEDGMENT

This study is funded by NMIET and by the and National Research University of Thailand. Permission to publish this paper is gratefully acknowledged.

REFERENCES

[1] Rocscience Inc., Phase2 User’s Guide, Itasca Consulting Group Inc., Toronto, Canada,2001.

[2] sadi, A., Shahriar, K., Goshtasbi, K. and Najm, K., Development of new mathematical modepl for prediction of surface subsidence due to inclined coal-seam mining, J. of SouthernAfricanInstituteofMiningandMetallurgy,vol.105, no. 11, pp. 15-20,2005.

[3] Henry, L., Anciennes familles genevoises, étude démographique, XVIe-XXe siècle, Presses universitaires de France, vol. 26,1956.

[4] King, H. J., & Whetton, J. T., Mechanics of mine subsidence. In Proceedings European congress on ground movement, University of Leeds, Leeds, UK pp. 27-38, April1957.

[5] Oscar,E.M.,&Harry,S.L.,U.S.Patent,Washington,DC, U.S. Patent and Trademark Office, no. 3, 1963.

[6] Kermabon, A., & Cortis, U., A new Sphincter corer with a recoilless piston, Marine Geology, vol. 7, pp. 147-159,1969.

[7] Brooks, G. A., Brauner, K. E., & Cassens, R. G, Glycogen synthesis and metabolism of lactic acid after exercise. American Journal of Physiology-Legacy Content, vol. 224, no. 5, pp. 1162-1166,1973.

[8] Yao, X.L., Reddish, D.J. and Whittaker, B.N., Influence of overburdenmassbehaviouralpropertiesonsubsidencelimit characteristics. Mining Science and Technology. 13: 167-173, 1991.

[9] G.Ren,D.J.Reddish,andB.N.Whittaker.,Miningsubsidence and displacement prediction for incline seam, Mining Science and Technology, vol. 8, pp. 235-252,1989.

[10] Ghabraie, B., Ren, G., Smith, J., and Holden, L., Application of 3D laser scanner, optical transducers and digital image processingtechniquesinphysicalmodellingofmining-related strata movement, Int. J. of Rock Mechanics and Mining Sciences, vol. 80, pp. 219-230,2015b.

[11] Thongprapha, T., Fuenkajorn, K., and Daemen, J. J. K., Study of surface subsidence above an underground opening using a trap door apparatus, Tunnelling and Underground Space Technology, vol. 46, pp. 94-103,2015.

[12] Sartkaew, S., and Fuenkajorn, K., Verifications of empirical method and numerical simulation using physical model for subsidencepredictionofMahaSarakhamformation,Eng.J.of Research and Development, vol. 27, no. 3, pp. 17-27,2016.

[13] Saoanunt, N. and Fuenkajorn, K., Physical model simulations of super-critical subsidence as affected by mining sequence and excavation rate. In 9th SEATUC Symposium, Suranaree University of Technology, pp. 22-25,2015.

[14] Singh, M.M. (1992). Mine subsidence. In H.L. Hartman (ed). SME Mining Engineering Handbook. society for mining metallurgy and exploration. littleton, colorado. pp.938-971.

[15] Thongprapha, T., Fuenkajorn, K., and Daemen, J.J.K. (2015). Study of surface subsidence above an underground opening using a trap door apparatus. Tunnelling and Underground Space Technology. 46:94-103.

* * *

EFFECT OFMECHANICAL PROPERTIES OF EPOXY BASED KENAF/BANANA/GLASS FIBER HYBRID NANO COMPOSITES

[1]SANTOSH KUMAR SAHU, [2]KABI SAHOO, [3]RAMESH CHOUDHRY

[1]Department of Mechanical Engineering, NMIET, Bhubaneswar, 751019
[2]Department of Mechanical Engineering CEC Bhubaneswar
[3]Department of Mechanical Engineering REC Bhubaneswar
E-mail: [1]shashi.mohan@nmiet.ac.in

Abstract - Development of the polymer hybrid composite as a sustainable alternative materials for some engineering applications, particularly in aerospace application and automobile applications are being investigated. The role of natural fibers reinforced hybrid composite are growing in a field of engineering and technology due to favorable properties. In the present unsustainable environmental condition natural fibers are serving better materials in terms of biodegradability, low cost, high strength and corrosion resistance when compared to conventional materials. The main objective is to prepare the Kenaf/Glass fiber hybrid composite filled with graphene as nano filler and to investigate the mechanical properties of hybrid composites. The different types of hybrid composites laminates are fabricated without filler, 0.5, 1 & 1.5Wt % of graphene by using kenaf and glass fiber as reinforcing material with epoxy resin. The specimen were prepared as per the ASTM standards and results shows that the mixing of graphene in epoxy resin improves the mechanical properties of hybrid composites and also the performance of kenaf/glass fiber composites is more than banana/glass fibercomposites.

Keywords - Kenaf Fiber, Banana Fiber, Nano Filler, Hybrid Composite Material

I. INTRODUCTION

Since from past two decades, there is tremendous growth in development of FRP composites with high strength to weight ratios, as it has acquired the various fields of application, ranging from shipbuilding, aerospace, automotive, to recreation equipment, furniture, office products, biomedical devices and implants, construction and building industry etc. With the increase in requirements, there is a demand to develop the stronger and cost effective composites. The fiber/matrix interface plays a vital role in determining the mechanical properties of glass fiber composites[1]. When the addition of filler materials to Epoxy/Glass fiber composites is increased then the thermal expansion coefficient of the corresponding composite getsreduced[2].

The tensile strength and the tensile modulus of Glass fiber/Epoxy composite increases in fiber loading and the addition of Nano filler particles to the Glass fiber/ Epoxy composite increases the tensile strength and the tensile modulus of the composite. Also, the addition of Nano filler particles to the Glass fiber/Epoxy composites increase the flexural properties of the Glass fiber composite[3] It has been reported that the addition of Nanoclay to Glass fiber/Epoxy composites increases the interfacial shear strength tremendously[4].The fiber/matrix interface plays a vital role in determining the mechanical properties of glass fiber composites[5]. When the content of Nanoclay is increased beyond an optimal level then the mechanical properties of the resultant composites decreases[6]. The percentage of Nanoclay to be used should be restricted to 5 wt% in order to get good mechanical properties of thecomposites[7].

II. DETAILSEXPERIMENTAL

2.1. Materials used

Kenaf, banana and glass fiber with (0˚/ 90˚orientation) is used as reinforcing material, Epoxy resin (LY 556) and hardener (HY 951) is used as the matrix material and nano filler (Graphene) used as a filler material with different weight percentage to increase mechanicalproperties.

2.2 Preparation ofResin

A measured amount of epoxy is taken for different volume fraction of fiber and mixed with the hardener in the ratio of 100:10 and Graphene filler is added into that mixer with weight percentage of (without filler, 0.5, 1, 1.5wt.%)

2.3 Preparation of the reinforcingmaterial

The kenaf, banana and glass fabric is spread on the flat surface and required dimension of 300 mm x 300 mm is marked using the marker pen on the fabric spread and cut using a scissor manually. Required such layers of fabric were cut to get the required thickness oflaminate.

Fig.1. Kenaffibermat

Fig.2. Glass fiberMat

Sl.No	Material	Density (g/cm^3)	UTM (Mpa)	Modulus (Gpa)
1	Kenaf fiber	1.45	930	53
2	Glass fiber	1.9	2500	70
3	Graphene	0.2	130	1000
4	Epoxy	1.18	85	4.4

Table 1: Material properties

2.4. Hand layup technique

The composite laminates are fabricated by hand layup technique. Kenaf and glass fibers mat were cut into the dimensions of length and breadth is of 300×300mm and 4mm thick was used to prepare the laminate. The composite laminate consists of total 6 layers of glass fiber and 5 layers of kenaf fibers for the fabrication of different samples. The layers of fibers were fabricated by adding the required quantity of epoxy resin. The glass fiber is mounted on the table and then epoxy resin is applied on it. Before the resin gets dried, the second layer of kenaf fiber is mounted over the glass fiber. The process is repeated till six layers of glass fiber and five layers of kenaf fiber got over. The epoxy resin is applied to the entire surfacebymeansofaroller. Theairgapsformed during the processing between the layers were removed out. Finally these laminates are kept in press for over 24 hours to get the required shape and thickness. Two types of composite laminates were prepared with addition of graphene filler (0, 0.5, 1, 1.5, wt. %)

- Kenaf/Glass/Graphenecomposites
- Banana/Glass/Graphenecomposites

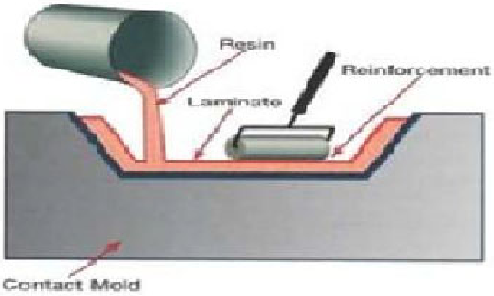

Fig.3. Hand layup technique

2.5 Preparation of test specimens

The test specimens are prepared as per ASTM standards from the composite laminates using water jet machine as shown in fig. 1, 2 &3.

Fig.4. Water Jetcutting

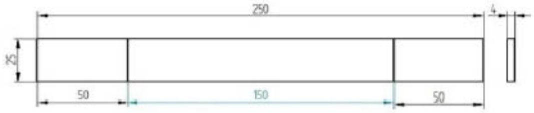

Figure 5(a)

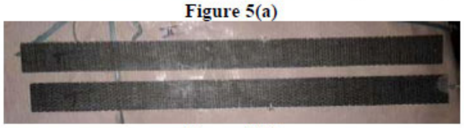

Figure 5(b)

Fig.5(a,b): Tensile test Dimensions & specimen - ASTM D3039

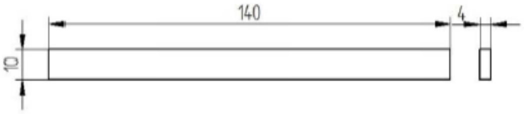

Figure6(a)

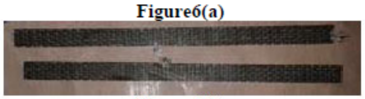

Figure6(b)

Fig.6(a,b): Compression test dimensions & specimen - ASTM D3410

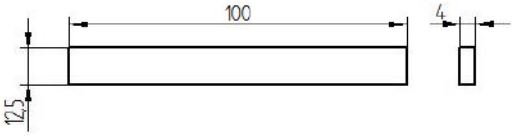

Figure 7(a)

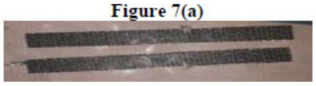

Figure 7(b)

Fig.7(a,b): Flexural test dimensions & specimen - ASTM D790-2

III. RESULTS AND DISCUSSION

All tests were carried out on tensometer as per the ASTM standards

3.1. Comparison of UTS for Kenaf/Glass and Banana/Glass fiber composites

Sl.No.	Graphene %	UTS(N/mm^2) for Kenaf hybrid Composites	UTS(N/mm^2) for Banana hybrid Composites
1	0	132.45	117.08
2	0.5	120.15	112.26
3	1	128.69	102.34
4	1.5	113.06	111.38

Table 2: Tensile test results

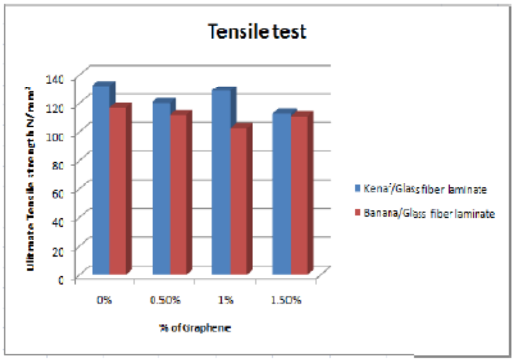

3.2. Comparison of compressive strength for Kenaf/Glass and Banana/Glass fibercomposites

Sl.No.	Graphene %	Compressive strength (N/mm^2)for Kenafhybrid Composites	Compressive strength (N/mm^2)for Banana hybrid Composites
1	0	22.76	13.82
2	0.5	12.36	16.6
3	1	28.95	21.84
4	1.5	15.54	23.94

Table 3: Compression test results

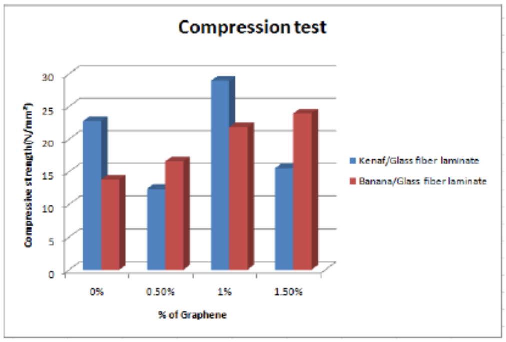

3.3. Comparison of flexural strength for Kenaf/Glass and Banana/Glass fibercomposites

Sl.No.	Graphene %	Flexural strength (N/mm^2) for Kenaf hybrid Composites	Flexural strength (N/mm^2) for Banana hybrid Composites
1	0	11.02	11.05
2	0.5	12	12.26
3	1	14.04	13.77
4	1.5	12.36	10.87

Table 4: Flexural test results

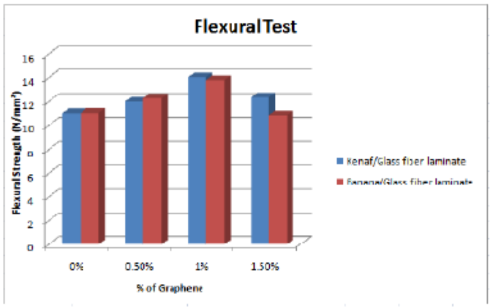

IV. CONCLUSIONS

- Fabrication of Kenaf/glass and Banana/glass fiber hybrid polymer composites withdifferent
- Better Compressive properties are obtained with kenaf/glass fiber composites than banana/glass fibercomposites.
- Kenaf/glass fiber reinforced with 1% graphene possesses good flexural strength of 14Mpa when compared to banana/glass fiber composites of13Mpa.

REFERENCES

[1] Mo-lin Chan, Kin-tak Lau, Tsun-tat Wong, Mei-po Ho, David Hui, "Mechanism of reinforcement in a nanoclay/polymer composite" Composites: Part B 42 (2011) PP1708–1712.

[2] Andrea Dorigato, Stefano Morandi and Alessandro Pegoretti, "Effect of nanoclay addition on the fiber/matrix adhesion in epoxy/glass composites" Journal of Composite Materials 46(12)PP1439–1451.

[3] Normasmira A. Rahman, Aziz Hassan, R. Yahya& R.A. Lafia-Araga, "Glass Fiber and Nanoclay Reinforced Polypropylene Composites: Morphological, Thermal and Mechanical Properties" SainsMalaysiana 42(4)(2013): PP537–546.

[4] K.Devendra, T. Rangaswamy, "Evaluation of thermal properties of E-Glass/ Epoxy Composites filled by different filler materials" International Journal Of Computational Engineering Research Vol. 2,Issue.5

[5] RafaelCeleghiniSantiago,RicardoLessaAzevedo,Antonio

[6] F. Avila, MarcilioAlves, "Mechanical characterization of Glass/Epoxy composite material with Nanoclays" 19th International Congress of Mechanical Engineering.

[7] Mo-lin Chan, Kin-tak Lau, Tsun-tat Wong, Mei-po Ho, David Hui, "Mechanism of reinforcement in a nanoclay/polymer composite, Composites": Part B 42 (2011) PP1708–1712.

[8] Amir HoomanHemmasi, Ismail Ghasemi, BehzadBazyar and Ahmad Samariha, "Influence of Nanoclay on the physical properties of recycled High-Density Polyethylene/Bagasse Nano Composite", Middle-East Journal of Scientific Research 8 (3): PP648-651,2011.

★★★

THE INFLUENCE OF AMOUNT OF LAYER ON THE BENDING STRENGTH BY LONGITUDINAL FINGER-JOINTING WOOD ELEMENTS

[1]SHASHI RANJAN MOHAN, [2]DAMBARUDHAR DAS, [3]SANJIB KUMAR DASH

[1]Department of Mechanical Engineering, NMIET, Bhubaneswar, 751019
[2]Department of Mechanical Engineering REC Bhubaneswar
[3]Department of Mechanical Engineering CEC Bhubanswar
E-mail: [1]deepikarani.swain@nmiet.ac.in

Abstract - Testofbendingstrengthsectionobtainedthroughlongitudinalconnectingwoodenelementswascarriedoutbyan experimental method. The test samples were formed of fir/spruce and using polyurethane adhesive PURBOND HB S609, a total of 243 samples has been formed. Testing the effects of the amount of adhesive on the bending strength of linear coupled sections was carriedoutonthreelevels(180,200, 220)g/m^2.Thispaperattemptstoproveassumptionthatexcessiveincreaseinthequantity of adhesive in theadhesive film comesto impairmentgluedjointstrength.

Keywords - Amount Of Adhesive Layer; Bending Strenght; Finger Joint; Glued Laminated Beams

---

I. INTRODUCTION

Length connecting of wood elements, among others, is performed in the production of laminated beams in the segment forming sections required length of the beams from shorter elements. Elements that enter into the process of forming sections should be formed without significant errors anatomical structure of wood and mistakes from previous processing. As part of production the laminated beams, especially when forming sections bonded through finger-jointing, an important parameter from the regime of bonding represents the amount of adhesive. This parameter directly reflects the strength of the bondedjoint.

The amount of adhesive that is applied to the surface of the wood should be sufficient to provide: the amount that penetrates into the wood, the amount that fills a variety of unevenness caused by surface processing and the amount which is necessary to achieve the joints thin, continuous and unbroken film of dried glue. The necessary amount of glue to be applied dependson:

- adhesive properties (dry substances content, viscosity and adhesiveproperties),
- properties of wood that is glued (structural unevenness, fines - surface roughness caused by processing, craters on the surface,etc.).

In addition, the strength of glued joint depends on the cohesion of the adhesive and its adhesion to wood, as well as the internal stresses in the bonded joint. Increasing the thickness of the adhesive layer reduces the cohesion and strength of the bondedjoint.

Considering the prominence of different sizes, craters, holes, etc. around the glued joints, glue shrinkage in percentage is similarly but also because of different thickness and volume of the glue in some places in absolute terms is very different. This means that the internal stress in the joints, because of shrinkage of the adhesive, is different. Bearing in mind the fact that the shrinkage is done across the width, length and thickness of the joint and the thickness in some places is very different, it is clear that the internal stress due to the shrinkage of the adhesive is complex and diverse. Therefore, maximum attention should be paid to the preparation of surfaces for bonding wood and ensure that the areas with the lowest possible roughness and unevenness. You also need to give maximum attention to the choice of adhesive should have adequate flexibility when cured, it can be successful without the destructionthataccompanies theirshrinkageanddeformationsduetoswellingorshrinkageofwood[1].

The quantity of deposited adhesive and the deformation of wood under the influence of external pressure significantly affects the temperature at which bonding is performed, which is directly or indirectly reflected in the necessary amount of glue and internal stress in the joints.

In the case of glued laminated beams for building construction should be applied (170 ÷ 220) g/m^2 glue. This amount is dependent on the type of used adhesive used, the content of dry substances and viscosity. Dry substances must be provided to create a continuous uninterrupted film of dried glue with sufficient penetration of the adhesive into thewood.

In previous research related to the amount of adhesive or adhesive film thickness was determined that an excessive amount of adhesive adversely affects the strength of the bonded joint. Interpreting the complementary effect, the amount of adhesive, it can be quite complex. [2] Below are presented some facts related to the impact of the amount of adhesive on the strength of adhesivejoint.

The nature and dimensions of the destruction caused by the low strength of the bonded joint can be different depending on the thickness of the adhesive film. Visual and microscopic evaluation of destruction can be significant for the assessment of this phenomenon. The structure of the adhesive film can vary depending on the amount of adhesive and bonding requirements. Heterogeneous temperature changes, such as different temperature distributions, are influenced by the distance from the thermally conductive substrate. Analyses of the heat balance and measuring the thermal properties of surfaces that come in contact with the glue joints can help solve the problem structure changes of adhesivefilm.

The interface between the substrate and the adhesive properties can be changed if it increases the thickness of the adhesive film. This may be caused by the internal stresses that develop in the joint with migration of oxide from surfaces for bonding or stoichiometric changes within the adhesive and substrate [3]. The results of this experiment confirmed that the technological process of gluing affects on the physical and mechanical properties of gluing elements [4]. The migration of oxide from surfaces for bonding or stoichiometric changes within the adhesive and substrate. Roche and associates are thoroughly investigated this phenomenon [5]. Many techniques are used to detect properties of interfaces, based on changes in the chemical state (infra-red spectroscopy or micro-thermal analysis) and mechanical testing (extraction, nano-indentation and laser-acoustic method). For bonded timber elements such as glued laminated timber beams, it is assumed that the adhesive in use does not significantly influence the resistance of structural timber beams.[6]

Energy of dissipation can be changed by changing the distance between the substrates. Careful mechanical testing can be used to introduce this phenomenon. By changing the geometry of the sample with increasing thickness of t adhesive layer can cause a change in the state of stress within the joint, so that the tests on samples of different sizes do not provide the same features bondedjoint.

II. MATERIALS AND EXPERIMENT

The paper examines through an experimental method the effect of the amount on adhesive strength of the adhesive finger joint in length connecting the wooden elements in sections for the production of glued laminated beams. Testing was carried out according to standard EN 408: Timber structures - Structural timber and glued laminated timber - Determination of some physical and mechanicalproperties.

During the experiment has been used glue PURBOND HB S609. PURBOND HB S609 is fluent, one-component, polyurethane adhesive based on isocyanatic prepolymers, without additives of solvent and admixture of formaldehyde. Bonding is done under the influence of humidity and moisture in the wood creating a strong adhesive joint that is not brittle. Under the influence of chemical reactions that occur in the process of bonding becomes a slightfoaming.

In the experiment has been used a fir/spruce timber. Relative humidity of the wood is reached (11 ± 2)%. Adjacent elements had no difference in moisture content greater than 3%. Bonding elements in sections is carried out at a temperature (20 ± 2) ° C and relative humidity (60 ± 5) %. Visual assessment of the class the sections was C24 (80%) and C30(20%).

Testing of bending strength as a function of the quantity of adhesive is done by forming 243 samples size (115x35x700) mm for the next levels of amount of adhesive:

- 180 g/m^2 : 81sample,
- 200 g/m^2: 81sample,
- 220 g/m^2: 81sample.

In addition to these sample groups, formed an additional group of 10 samples of solid wood size (115x35x700) mm in order to compare the results obtained by testing bending strength of finger joint. Dimensions of the finger (Figure 1) formed by used device are: length of finger: l = 10 mm, step of finger: p = 4 mm, thewidthofthegap :b_t=1mm,thelengthofthegap: l_t=1mm. Centrelineoffingerismarkedwith*1)*.

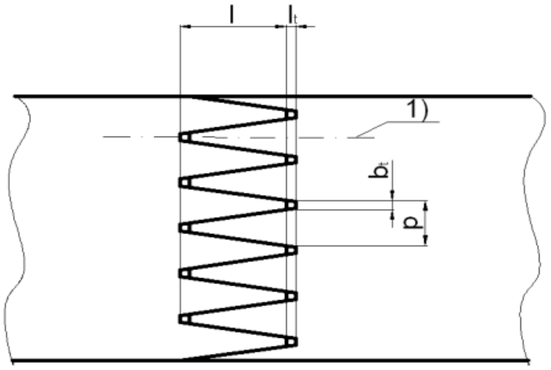

Fig. 1. Dimensions of the finger.

Testing of samples was performed in the climatic conditions in accordance with EN 408, temperature (20 ± 2) ° C and relative humidity (60 ± 5) %. Humidity test of samples (Figure 2.) amounted to (11 ± 2) %. During the testing process of bending strength were recorded visual assessment of destruction of samples.

Values obtained for bending strength was performed and statistical analysis of data using the student's t-test by testingtheequalityofmeans twobasicasetofasdoublesideddistribution (t-TweostS: aTmpleAssumingEqual Variances).

Fig. 2. The form of sections for samples and final appearance of samples.

Testing was carried out on the device Spanevello Tester KN 50. According to the standard EN 408, testing was done by properly positioning the samples on measuring device (Figure 3.). Samples dimensions and position of power in the process of testing the samples is a function of its thickness[7].

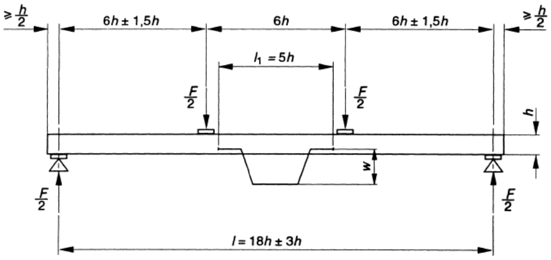

Fig. 3. Scheme of the test of samples for bending strength [7].

III. RESULTS AND DISCUSSION

In the process of testing the bending strenght of finger joint samples experiences some deformation and destruction. Destruction occurred in the followingforms:

- destruction ofwood,
- destruction of root thefinger,
- destruction of bonded jointor
- combination of prevous forms ofdestruction.

Table 1. presents the number and percentage of destructed samples from these forms of destruction.

Form of joint destruction	Wood	Root of finger	Joint	Combination r.o.f./j.	Combination r.o.f./w.	Σ
Number of samples	134	65	16	14	14	243
Percentage of samples [%]	55.14	26.75	6.58	5.76	5.76	100

Table 1. Number and percentage values of destruction during the testing of bending strength.

The amount of adhesive in the production practice is the most important parameter from regime of bonding to optimize the consumption of adhesive without adversely affects the final value of the strength of the bonded joint. Influence of the amount of adhesive on the strength of adhesive bonded joint in length connecting elements white finger joint connection is represented in the Figure4.

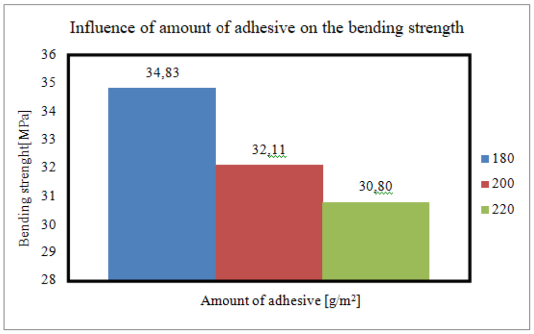

Fig. 4. Influence of amount of adhesive on the bending strength.

Based on the Fig. 4 it can be concluded that there are significant differences between the level of the amount of adhesive, and that the maximum value of bending strength reached a group of samples that are glued whit amount of adhesive in the value of 180 g/m^2. Results of *t*-test are presented in the following table 2.

	Level of significance	e α = 0,05	
Comparison of mean values	(180/200) g/m^2	(180/220) g/m^2	(200/220) g/m^2
t Stat	2.665115	3.343888	1.239583
t Critical two-tail	2.006647	2.006647	2.006647
Accepted hypothesis	H1 (5%)	H1 (5%)	H0

Table 2. *t*-Test: Two-Sample Assuming Equal Variances 95 % (for the levels of amount of adhesive).

Between different levels of quantity of adhesive there is a significant difference that is manifested on the final value of bending strength test of tested samples. In the present case, denies the null and alternative hypothesis is adopted. In order to determine the level of significance was carried out and the *t*-test for the level of confidence of 99%, in table3.

		Level of significance α = 0,01	
Comparison of mean values	(180/200) g/m^2	(180/220) g/m^2	(200/220) g/m^2
t Stat	2.665115	3.343888	1.239583
t Critical two-tail	2.673734	2.673734	2.673734
Accepted hypothesis	H1(5%)	H1 (1%)	H0

Table 3. *t*-Test: Two-Sample Assuming Equal Variances 99 % (for the levels of amount of adhesive).

Based on tables 2. and 3. for the tested samples can be concluded that between first and second level of amount of adhesive there is a significant difference, while the first and third level of amount of adhesive there is obtained a high significant difference. On the other hand, we can see that between the second and third level there was no significant difference (null hypothesis). Comparison of values of bending strength of finger joint with the values of bending strength of solid fir/spruce was performed in order to obtain the information that glued finger joints increases or decreases the value of strength of sections. For comparision has been taken 3 mean values of bending strenghtfromeverylevel amountofadhesive, sowehad9meanvalues. Thesevaluesarepresentedinfigure5.and 6. Based on the figure 5. and 6. it can be concluded that the strength of the finger joint conected sections becomes more uniformly and a few percent higher value of bending strenght than the value of the bending strength of solid wood.

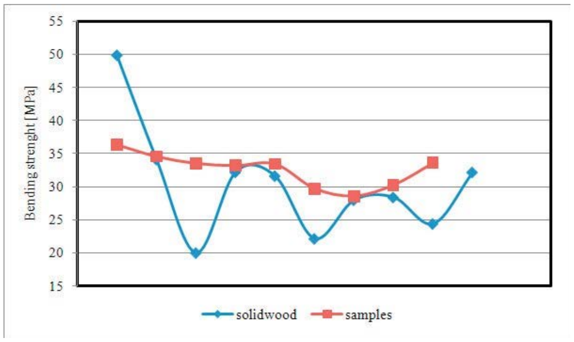

Fig. 5. Scattering of bending strength values of solid wood and finger joint samples.

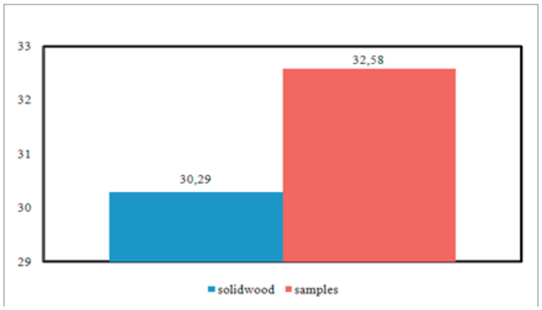

Fig. 6. Comparing the values of bending strength of solidwood and finger joint samples.

IV. CONCLUSION

On the basis of this study it can be concluded that the proven assumption that an excessive increase in the quantity of adhesive in the adhesive film is coming to a reduction in the value of the glued joint strength. The optimum value of the quantity of adhesive for a given test is 180 g/m^2. Increasing this value leads to a significant reduction in bending strength of adhesive joint. Compared to solid wood, length merging or forming finger glued joint is an increase in the value of bending strength with uniformlyvalues.

For a given sample, in future research should be oversized the finger joint and examine the lower levels of the amount of adhesive to establish the minimum allowable value of the quantity of adhesive to achieve maximum strength of the bonded joint in longitudinal connectingelements.

REFERENCES

[1] Backović,M.„Lijepljenjeutehnologijamapreradedrveta“(„Bondinginwoodprocessingtechnologies“),BosnaPublic,Sarajevo,1996.
[2] P.Davieset.al.„Influenceofadhesivebondlinethicknessonjointstrength“,InternationalJournalofAdhesionandAdhesives, Volume29, Issue 7,(2009), pp.724-736, ElsevierLtd.
[3] Nairn JA, “Energy release rate analysis for adhesive and laminate double cantilever beam specimens emphasizing the effect of residual stresses”, Int. J Adhesion & Adhesives, Volume 20, (2000), pp.59-70.
[4] Obucina, M.; Turk, G.; Dzaferović, E.; Resnik, J. “Influence of gluing technology on physical and mechanical properties of LVL” Journal Drvna industrija (Wood industry),Volume 64 number 1, (2013), pp.33-38.
[5] RocheAA, BouchetJ,BentadjineS,“Formationofepoxy-diamineinterphases,IntJAdhesionandAdhesives”,Volume22,(2002),pp.431- 441.
[6] KlippelM.;Frangi,A.;HugiE.,“ExperimentalAnalysisoftheFireBehaviorifFinger-JointedTimberMembers”,J.Struct.Eng.,
[7] 10.1061/(ASCE)ST.1943-541X.0000851, 04013063, Technical Papers (2013).
[8] EN408:Timberstructures–Structuraltimberandgluedlaminatedtimber–Determinationofsomephysicalandmechanicalproperties.

★ ★ ★

AN ENGINEERING MODEL FOR DYNAMIC WIND POWER PLANT FLOW

[1]SINGULURI SRINIVASAN, [2]ASITA RATH, [3]SATYAKAM ACHARYA

[1]Department of Mechanical Engineering, NMIET, Bhubaneswar, 751019
[2]Departyment of Mechanical Engineering REC Bhubaneswar
[3]Department of Mechanical Engineering CEC Bhubaneswar
E-mail: [1]asit.parida@nmiet.ac.in

Abstract -
An engineering method is developed for the prediction of dynamic flow through a wind power plant, in the presence of turbine control actions. The model is composed of a simplified steady-state boundary layer model of velocity deficits and turbulence, a dynamic wake model relating the rotor induction to an effective "dynamic" value of thrust, and a flow convection model which is simply a time delay function. A partial validation is conducted, using wake measurements at the Nørrekær Enge wind farm. The model is implemented in the STAS WPP program for wind power plant analysis.

Keywords - Wind Farm; Wind Power Plant; Control; Wakes

I. INTRODUCTION

To study the control of a wind power plant requires a model for the atmospheric flow, which is coupled with the operation of the wind turbines. There are two rather distinct flow regimes [1]. On the upwind side of the turbine array, a concentrated wake forms behind individual wind turbines, and this may impinge, or not, on the turbines immediately downwind. These local wakes are often modelled by a Gaussian-shaped velocity deficit [2], which decays as higher-velocity air is entrained by turbulent mixing. Deep in a large wind power plant, there are still local wakes, but the presence of the wind turbines is also felt throughout the atmospheric boundary layer, to an elevation much higher than the tops of the rotors. Energy recovery occurs "top-down" as higher-velocity air in the upper portion of the boundary layer is mixed into the lower levels.

Interestingly, methods based on boundary-layer analysis provide good predictions of the average velocity deficits, even near the upwind side of a wind power plant [1,3]. That is, the local wakes may meander back and forth, with the second row of turbines seeing a velocity deficit which fluctuates abruptly [4]; yet in the mean, the boundary layer experiences the turbines as, effectively, an increased surface roughness, like a forest canopy [5]. The influence of the local wake on stochastic loads may be approximated by an increased turbulence intensity[6].

The goal is to assemble, from existing parts, a simple engineering method for predicting the influence of turbine control actions on the flow through a wind power plant. The method must be compatible with a state-space model of the turbines, electrical grid, and controls comprising the wind power plant. CFD analyses of the complete flow domain are ruled out, for the time being. This leaves an approach based on one or both of the above perspectives: superposition of local wakes, or a simplified boundary-layer analysis.

Here it is proposed to use a method based partly on a two-dimensional boundary-layer analysis, specifically the Viper software [3]. The boundary-layer approach has the advantages of being scalable from small turbine arrays to large wind power plants, or even plant clusters; and of not attempting to explicitly resolve the local wake, where the result becomes sensitive to small changes in the wind direction. In other words, the control algorithms so developed will be applicable in bulk, rather than for specific wind directions.

II. STATE-SPACE REPRESENTATION OF FLOW

A state-space model of the flow is built up from the following elements:

a. The dynamic induced velocity, which is obtained from Øye's second-order filter model [7], built into the STAS Turbine module [8]. The second-order filter, like the real wake dynamics, has the feature that rapid control inputs have little influence on the wake flow: the amplitude decays with frequency in a realistic manner.[†]
b. A steady-state boundary layer analysis [3] relating the induction at an upwind location to the velocity deficit at a downwindlocation.
c. A convection model for signals (velocity deficits) in the flow. Convection is modelled as a state-space approximation of a time delay, based on the hub-height windspeed. As simple as the time-delay assumption is, it has been validated by wind tunnel experiments[10].
d. A model for the effective turbulence intensity including wake effects, based on Frandsen[6].

2.1 Transient induction and the boundarylayer

Let us begin the story with the induced velocity, and its connection to the flow, in the context of boundary layer analysis. Momentum balance applied to a control volume of air flowing through the rotor gives the well-known relationship

The theoretical relation (1) must be augmented with an empirical trend for values of a above about 0.4. Burton et al. [11] propose a linear trend, Alternative formulas for (3) are also available. Regardless, the main point here is that for steady flow there is a 1:1 correspondence between the rotor-average induced velocity and the thrust.

The relationships (1) through (3) between induced velocity and thrust do not hold under transient conditions. The induced velocity lags changes in the rotor loading, with an amplitude that decreases at high frequencies. Physically, this is due to the time it takes to convect the wake vorticity – which is responsible for the induced velocity – downstream away from the rotor. A slow fluctuation in the rotor load gives the wake time to develop, and the induced velocity follows the steady-state trend. A fast fluctuation in the rotor load produces a pattern of vorticity in the wake whose net effect tends to cancel out, except near the tips of the blades. A method attributed to S. Øye, described by Snel & Schepers [7], captures these trends by a second-order filter,

Here V_i satisfies (2) instantaneously, whereas the filtered V_i is taken as the true value at the rotorplane.

The time constants in (4) are a function of the radius, but the equations may be integrated, or an effective value at r R 0.7 taken, in order to represent the rotor average.

This same line of thought can be extended to boundary-layer analysis. Namely, that a slow fluctuation in the rotor load will produce a well-developed wake which, upon subsequent breakup and diffusion of the momentum deficit, will influence the atmospheric boundary layer; whereas a fast fluctuation in the rotor load will lead to local features in the flow which will tend to cancel out, from the broader perspective of the boundary layer. To put it another way, we connect the development of the boundary layer with the wake, represented by the induction,and not the instantaneous loading on the rotor. We suggest the use of (4) to obtain Vi , and then (2) to obtain a "wake- equivalent" value of rotor thrust, which is experienced by the boundary layer.

2.2 Steady-state perturbations in the boundarylayer

Totheextentthattheboundarylayerisinfluencedbytherotorthrust ,orequivalently ,thisdecayswiththe distance downstream. In other words, if one should begin with a boundary layer in a steady-state condition, make a constantperturbationtotherotorthrust = atsomelocation,andallowtheflowtoreachanewsteadystate, then the velocity profile of the perturbed flow will asymptotically approach the original, far downstream. The decay is due to the fact that, given a uniform rotor thrust loading, the boundary layer tends to reach an equilibrium over long distances. At equilibrium, the turbulent diffusion of momentum from the high-velocity air at altitude balances the momentum removed by the rotor thrust and surface friction. The higher the loading on the air at low altitudes, the greater the shear in velocity with height, and the greater the mixing in of momentum from above.

As an illustration, consider a wind power plant consisting of a uniform grid of DTU 10 MW wind turbines [12], with spacing $s_x = s_z = 8D$. (The X direction is along-wind, the Z direction is cross-wind, and the Y direction is straight up.) The remote incoming windspeed is 10 m/s. Figure 1 shows the hub-height velocity profile from the first through the 21st row of turbines. The velocity profile as a function of height, just upstream of Turbine Row 6, is also shown. The effect of shutting down Turbine Row 5 is illustrated by the dashed curves. Immediately downstream there is recovery of windspeed, which diminishes far downstream as the boundary layer approaches equilibrium.

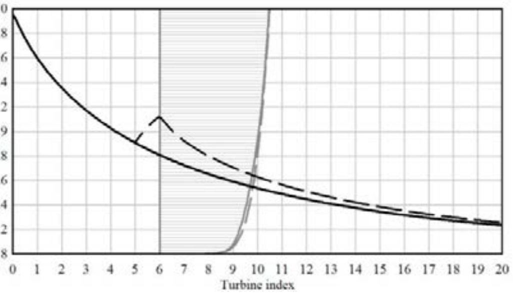

Figure 1: The hub-height velocity, and the velocity profile with altitude at Turbine Row 6, for two scenarios: one in which all the turbines are operating normally, and another (dashed lines) in which Turbine Row 5 is shut down. The velocity profile with altitude (shaded gray) does not correspond to the units on the axes. For an idea of scale, the uppermost elevation shown is 500 m, and the windspeed at 500 m is about 10.9 m/s.

The profiles in Fig. 1 are generated by solving nonlinear differential equations for a turbulent boundary layer. In order to make a useful low-order state-space model of the boundary-layer flow, we must identify simple linear models that capture the effect of perturbations about a given operating condition. Intuitively, and consistent with elementary boundary-layer theory, we can say that the perturbation in hub-height windspeed seen by the k^{th} turbine is some function of the loading, or induction, of the upstream turbines. Assuming that this relationship is linear for small enoughperturbations,

Equation (6) is global, in the sense that in order to solve for δV_k we would need to know all the influence coefficients $\partial V_k/\partial V_{i,j}$ and induced velocities $\delta V_{i,j}$ for the upstream turbines. In the steady-state case, this is a computation involving a lower-triangular matrix, which is no problem. However, it becomes a problem in the dynamic case, because there is a unique time delay between each upstream-downstream pair of turbines; and, as will be seen in Section 2.3, an accurate representation of a long time delay requires a lot ofstates.

It is much more convenient if we can write

$$\delta V_k$$

That is, if we associate with each wind turbine an incoming windspeed V_k and a (downstream-side) induced velocity $V_{i,k}$, and say that the windspeed at the next turbine downstream is a function of these. Indeed, (6) is recovered from (7), provided that and $\delta V_1 = 0$. In other words, (8) holds true if the decay in a perturbation is multiplicative as one proceeds from station to stationdownstream.

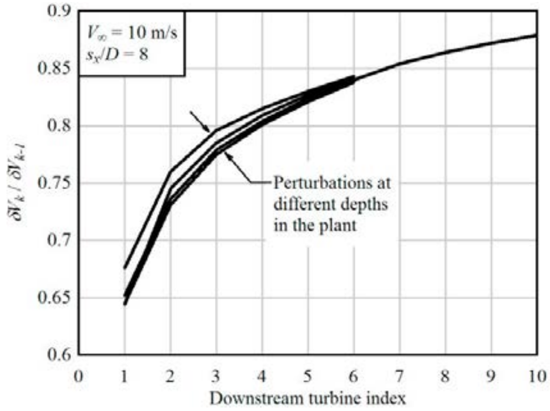

Figure 2: The station-to-station decay of a perturbation to the boundary layer. Multiple analyses were run, each time perturbing the operation of a different wind turbine. The downstream turbine index indicates the location relative to the turbine whose operation was perturbed. The trend is relatively independent of the depth in the wind power plant.

As it turns out, this is not strictly true; but it is close enough to be a useful assumption. Furthermore, the influence of a perturbation in turbine operating state $\delta V_{i,k}$ appears to be nearly independent of the downstream location. To illustrate this, consider again the example of a 10 m/s remote windspeed and a uniform 8*D* spacing. Figure 2 shows the results of introducing a perturbation in the operation of a wind turbine – specifically, decreasing the thrust by 10%. Referring to the indices of Fig. 2, the operation of Turbine -1 is perturbed, such that Turbine 0 experiences a change in the incomingwindspeed

The curve shows subsequent values of $\partial V_k/\partial V_{k-1}$ for $k = 1,2,\ldots$ The trend is nearly independent of the location in the plant at which the perturbation is introduced. The trend is also independent of the amplitude: Fig. 3 shows reductions in thrust from 10% to 100% (shut downturbine).

The value of $\partial V_k/\partial V_{i,k-1}$ is also remarkably consistent, and is equal to about 0.08 in the case of a 10 m/s remote windspeed and a uniform 8*D* spacing.

Still, Fig. 2 and Fig. 3 are not enough. If $\partial V_k/\partial V_{k-1}$ is a function of the downstream turbine index – relative to where the perturbation was introduced – then one still must formulate individual values for each upstream- downstream combination of turbines. We really need $\partial V_k/\partial V_{k-1}$ to be constant, such that we can say how the perturbation to the windspeed δV_{k-1} will evolve downstream into δV_k, independent of how δV_{k-1} was created. If we take the approximation $\partial V_k/\partial V_{k-1} \approx 0.75$, then this provides a good estimate of the flow over a distance of several turbines downstream of the perturbation. In addition, superposition applies. Figure 4 shows an example where the thrust of turbines 2, 5, and 10 has been reduced. The perturbation in hub-height windspeed is well-predicted by (7), with a constant $\partial V_k/\partial V_{k-1}$; except that the perturbation decays too fast far downstream.

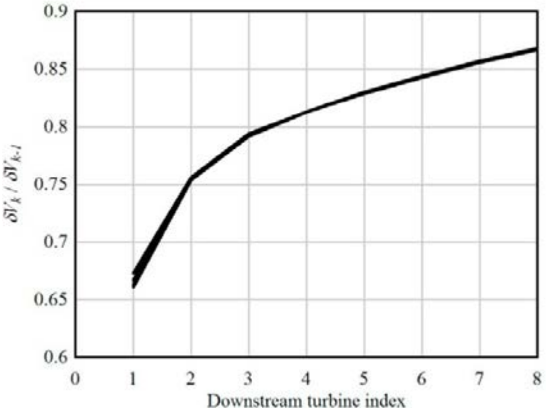

Figure 3: The influence, or lack thereof, of the perturbation amplitude on the trend in the station-to-station decay of the perturbed velocity.

The values of $\partial V_k/\partial V_{k-1}$ and $\partial V_k/\partial V_{i,k-1}$ may depend on the size of the wind turbine, the remote windspeed, and the spacing between turbines, and should be generated, or obtained from a database, for each load case being analyzed.

2.3 Convection of flowperturbations

The transmission of a signal – that is, a perturbation in the flow – from an upwind to a downwind turbine can be modelled as convection at the hub-height windspeed [10]. The frequency dependence is handled by the dynamic wake method of Section 2.1, while the diffusion part is handled by the boundary-layer calculations – or the simplified approximation – of Section 2.2. The convection model is therefore a pure time delay.

A time delay of τ is simple to model as a transfer

$$\frac{dy}{dx} = \exp(-s\tau)$$

function,

simple to model in (discrete) time domain simulations, although $x(T)$ must be stored for $t - \tau \leq T \leq t$; and difficult to model in state space. The storage requirement for (11) hints at the problem. How many values are required to store a segment of a continuous function? An infinite number; that is, an infinite number of states is required in order to represent (10) or (11) exactly. With a finite number of states, a time delay may be approximated by a rational transferfunction,

$$\frac{dy}{dx} \approx \frac{P_m(s\tau)}{Q_n(s\tau)}$$

$$P_m(x)=\sum_{k=0}^{m}\frac{(m+n-k)!m!}{(m+n)!(m-k)!k!}(-x)^k,\quad Q_n(x)=\sum_{k=0}^{n}\frac{(m+n-k)!n!}{(m+n)!(n-k)!k!}x^k$$

It is common to use $m = n$, as this gives a transfer function with a uniform unit amplitude. The alternative, $m < n$, results in a low-pass behavior.

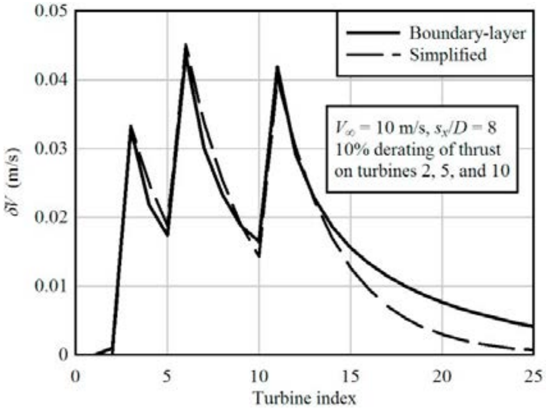

Figure 4: The approximation to the perturbed velocity that is obtained from (7), compared with the full boundary-layer analysis, for a case with multiple perturbations.

The higher the frequency of the signal to be transmitted, in relation to the delay time, the more states are required. The use of too few states, for a given frequency and time delay, will either transmit the signal with insufficient lag ($m = n$), or transmit nothing ($m < n$). Our situation is unfortunately one in which the time delay is long in comparison with the timescale of the signal. The latter is the timescale of the dynamic wake, which can be obtained from (4). (Higher frequencies are negligible due to the low-pass behavior.) In the present example of a 10 MW wind turbine, $\tau 1 \approx 16$ s. If the spacing between turbines is 8D, or 1426 m, and the windspeed is 10 m/s, then the time delay is 143 s, an order-of-magnitude greater. We now see why it is so important to use (7), instead of (6), even at the expense of some accuracy: we do not want to track a velocity perturbation over a distance farther than the separation betweenturbines.

A state-space form of (12), for $m = n$, is At high orders n – say, 10 or higher – (13) exhibits poor numerical conditioning. This effectively limits the bandwidth. Continuing with the example of a 10 m/s windspeed and 8D spacing, Fig. 5 compares the phase angle obtained using different orders of (13) against the exact value $\theta = -\omega s_X/V_\infty$. The maximum condition number C of the matrix $i\omega\mathbf{I} - \mathbf{A}$, representing a frequency-domain solution of the state equations, is also listed. This condition number is that obtained after employing a balancing operation, intended to improve the numericalconditioning.

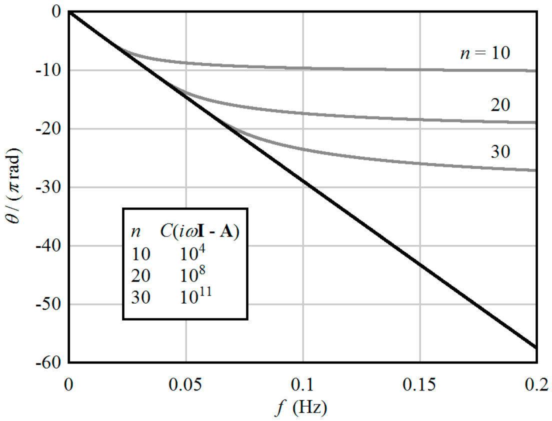

Figure 5: The phase angle, in multiples of π, of the time delay $\exp(-i\omega s_X/V_\infty)$, compared against different orders of the approximation (13)

The numerical conditioning can be greatly improved by breaking the spacing s_X between wind turbines into sub- intervals, and employing a low-order form of (13) over each sub-interval. The downside is an increase in the number of states required for a given accuracy ofapproximation.

The time delay must be accurately represented over the bandwidth of the wake dynamics. Figure 6 plots the magnitudeofthetransferfunction [illegible] from(4).Areasonablecriterionforaccuracyis,say,thatthe phaseof the time delay is within 1% of the exact value at a frequency of 0.1 Hz. Phase errors at a higher frequency than this will have a limited influence on the dynamic response of the wind turbines, since the relative magnitude of the velocity perturbations is small.

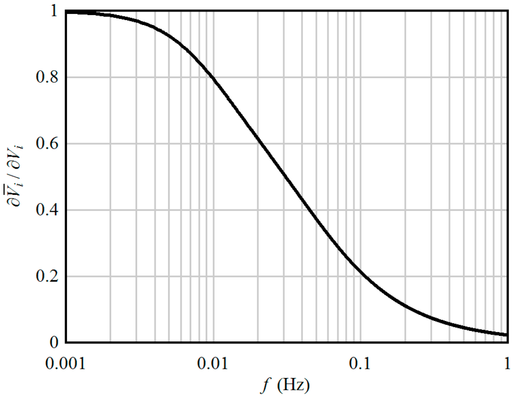

Figure 6: The magnitude of the transfer function between steady-state and transient induced velocity, according to (4), for a windspeed of 10 m/s.

Table I shows combinations of the number of sub-intervals N_S and the order of approximation n from (13) that satisfy the stated criterion for accuracy. The condition number is also shown. Increasing the number of sub-intervals improves the numerical conditioning. An increased number of states is required; but this has the additional benefit, seen in Fig. 7, that the accuracy is improved at higher frequencies.

N_s	n	N_x	$C(i\omega\mathbf{I}-\mathbf{A})$
2	27	54	10^7
3	19	57	10^6
4	15	60	10^5
5	13	65	10^4
6	11	66	10^4
7	10	70	10^4
8	9	72	10^4
10	8	80	10^4
12	7	84	10^4
15	6	90	10^3
19	5	95	10^3
28	4	112	10^3
49	3	147	10^3

Table I: Combinations of the number of sub-intervals N_S and order of approximation n that satisfy the criterion for accuracy.

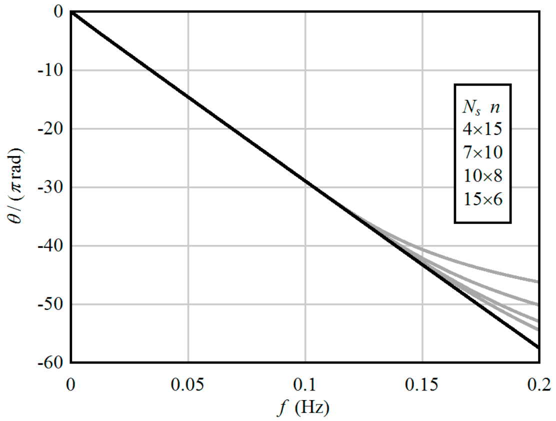

Figure 7: The approximate and true phase of a time delay, with various numbers of sub-intervals and orders of approximation, satisfying the criterion that the error in phase is less than 1% at a frequency of 0.1 Hz.

2.4 Turbulence

The level of turbulence within a wind power plant is a function of the terrain, atmospheric conditions, and turbine operation. Terrain effects are specific to each location; here we assume that the terrain is flat enough that its influence can be represented by an empirical surface roughness length y_0. Then, under conditions of neutral stability (no thermal convection or stabilization), the standard deviation of turbulent velocity fluctuations can be estimated as [6]

where h is the elevation above the ocean or land surface. In other words, if we know the wind shear $\partial V/\partial h$, then we may directly estimate the level of turbulence. The velocity profile with height, and hence the wind shear, is computed as part of the steady-state boundary-layer analyses of Section2.2.

Figure 8 shows an example of the levels of turbulence so obtained. The ambient value of the turbulence intensity is about 8%. Deep inside the wind power plant, it is around 13% to 14%, depending on how the effective value is computed from the profile. These values of turbulence intensity are based on the local mean hub-height windspeed, which is lower than the ambient value upwind of the turbine array. Relative to the ambient hub-height windspeed, the turbulence intensity is about 12%, which is in agreement with the value given by Frandsen [6] for an infinitely large turbinearray.

If the level of turbulence follows from the velocity profile, and the profile is convected dynamically at the mean hub-height windspeed, then it can be assumed that under dynamic conditions, the level of turbulence evolves according to the time delay functions of Section 2.3.

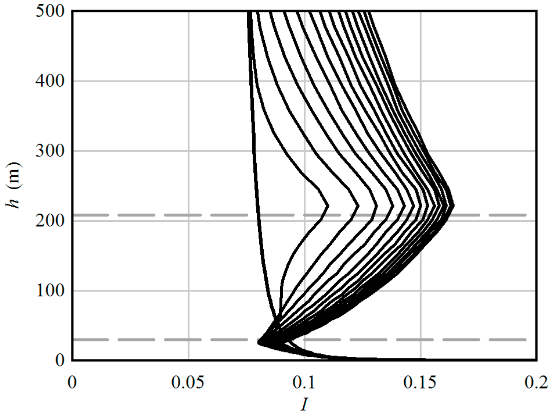

Figure 8: The turbulence intensity as a function of height, for turbines progressively deeper inside a large wind power plant. Here V_∞ = 10 m/s, s_X/D = 8, and y_0 = 0.001 m. The dashed gray lines indicate the bottom and top elevations of the rotor.

2.5 Preliminary comparison with data

The Nørrekær Enge wind power plant, described by Hansen [13], offers a partial field validation of the simple turbulence model (14). Frandsen [6] provides some normalized windspeed and turbulence measurements, as a function of elevation, for wind directions within ±15° of southwest. The plant layout is sketched in Fig. 9, with the axes in units of meters from the met mast at which data was collected. Two-dimensional boundary-layer analysis was performed along three lines: one oriented to the southwest, and one each at ±15°. Profiles of windspeed and turbulence intensity were obtained as averages from these three lines, weighting the middle linetwice.

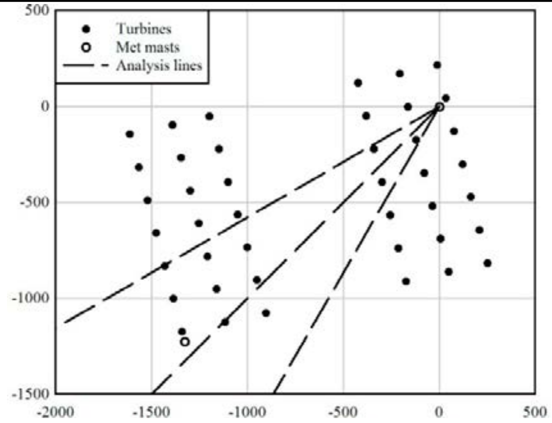

Figure 9: The layout of the Nørrekær Enge wind power plant, showing the met masts and lines along which boundary-layer analyses were conducted.

The measured and computed profiles are plotted in Fig. 10. There is some uncertainty in both the data and the analysis. In the case of the data, Frandsen gives profiles with height for ambient windspeed ranges of 8-9 m/s (plot at left) and 12-14 m/s (plot at right), and subsequently the same values at a single elevation of 58 m, for integer windspeeds between cut-in and cut-out. The values do not exactly agree, and no explanation is offered; presumably, they were based on different sets of measurements. Uncertainty in the analysis is related to the effective surface roughness length. The wind farm was located in grassy terrain. Some kilometers upstream the terrain was hilly, and closer upstream there were obstacles such as farm buildings. For comparison, the analysis was run with roughness values of 0.03 m, representative of flat grassy terrain, and 0.2 m, representative ofhedges.

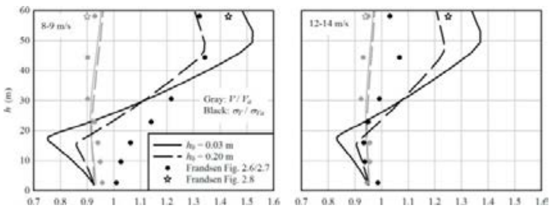

Figure 10: Windspeed and turbulence profiles as a function of elevation, presented as a ratio of the value measured within the wind turbine array to that measured immediately upstream of the array.

Overall, the comparisons in Fig. 10 indicate that the simplified boundary-layer analysis predicts reasonable trends in the development of wake velocity deficits and turbulence in a wind power plant. At the same time, there are clearly factors which influence the atmospheric flow, which are not taken into account.

Wind tunnel tests [14] also exhibit the pattern of turbulence predicted in Fig. 10. A full validation exercise is left to future work.

III. STEADY-STATE POWER SET-POINTS

Consider the problem of optimizing the pitch – or equivalently, the axial induction – of an array of wind turbines, in order to maximize the total production. Simplified methods based on local wake analysis, such as Jensen [15] and its derivatives, predict that the maximum power is obtained when the production of the upstream turbines is curtailed [16]. On the other hand, recent analyses using large eddy simulation [17] fail to reproduce this result: the maximum power of a two-turbine pair is obtained when both turbines are set to their respective maximum aerodynamic efficiencies. It is of interest to see how boundary-layer methodsfare.

According to the methods of Section 2, each turbine is represented as a distributed thrust over an equivalent volume of air. Lateral mixing of the wake is assumed to be negligible in comparison with vertical mixing, giving a two-dimensional boundary-layer flow. In the case considered, the layout consists of DTU 10 MW wind turbines arranged with a uniform 8*D* spacing, and the ambient windspeed is 10 m/s.

Figure 11 shows the results for a single upwind/downwind turbine pair. In this case, curtailing the operation of the upwind turbine is always detrimental to the totalproduction.

On the other hand, for a large wind power plant consisting of many rows of turbines, curtailing the operation of the upwind turbines may provide a slight benefit. Table II compares the baseline and optimal blade pitch set-points, to the nearest 0.2°, for a wind power plant with 11 turbine rows. The total power output is increased 0.5% by derating the upwind turbines. The turbulence intensity is also decreased by a couple percent. This hints that there may be something to be gained from the strategy; though the margin of uncertainty in the analysis is larger than the potential effect.

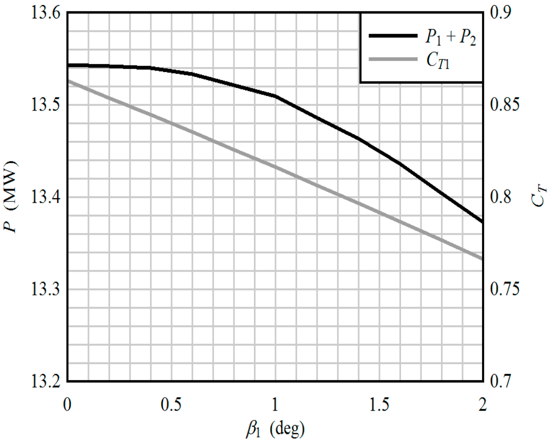

Figure 11: Axial induction control of a single upwind/downwind pair of turbine rows, according to the distributed-thrust boundary layer model of flow through a wind power plant.

IV. CONCLUSIONS

An engineering method has been developed for predicting the influence of control actions on the flow through a wind power plant. The physics are simplified, not by superposing axisymmetric wakes as in Jensen-type methods [15], but by representing the turbines as a distributed drag on the atmospheric boundary layer. This perspective – this way of representing the physics – gives windspeed and turbulence profiles which capture some of the important trends seen in experiments and high-fidelity CFD analyses. The resolution of the simplified boundary-layermethod is coarse, not accounting for the precise placement of turbines relative to the wind; rather, it gives results which are valid for winds averaged over a sector of some degrees. This is not as severe assumption as it may seem, since the wind direction in a large wind power plant is, in reality, not a perfectly consistent and definable quantity.

Turbine	β	V_h	I	P	β	V_h	I	P
1	0.0	10.00	0.086	7.106	1.0	10.00	0.086	7.033
2	0.0	9.60	0.101	6.371	1.0	9.62	0.101	6.344
3	0.0	9.36	0.113	5.902	1.0	9.39	0.111	5.900
4	0.0	9.17	0.121	5.563	1.0	9.21	0.119	5.576
5	0.0	9.03	0.127	5.301	1.0	9.07	0.125	5.326
6	0.0	8.91	0.131	5.094	1.0	8.96	0.129	5.126
7	0.0	8.81	0.134	4.926	0.6	8.86	0.132	4.992
8	0.0	8.72	0.137	4.787	0.6	8.77	0.134	4.845
9	0.0	8.65	0.138	4.670	0.4	8.70	0.136	4.734
10	0.0	8.59	0.140	4.571	0.0	8.63	0.138	4.639
11	0.0	8.54	0.141	4.485	0.0	8.57	0.140	4.538
Total				58.775				59.052

Table II: A comparison of default (at left) and optimal (at right, to the nearest 0.2 deg) pitch settings in a large turbine array, with the objective of maximizing production. The array is 11 turbines deep, and infinitely wide. The terrain is flat, the ambient hub-height windspeed is 10 m/s, and turbine spacing is a uniform 8*D*. Pitch angles are given in degrees, hub-height windspeed in m/s, and power in MW per column of turbines.

Approximating the influence from one turbine to the next by constant coefficients, whose values are a function of the particular turbine operation, spacing, and mean flow conditions, a linear approximation to the boundary-layer analysis is obtained. Dynamic flow is added to the linear steady-state analysis by, first, using an effective value of thrust, based on dynamic induced velocity in the rotor wake; and second, considering the convection delay from one turbine to the next.

The present engineering method is intended for preliminary design and tuning of wind power plant controllers, as well as for generating hypotheses which may be tested by experiments and more refined analyses.

REFERENCES

[1] Frandsen ST, *et al*. (2009). The making of a second-generation wind farm efficiency model complex. Wind Energy12:445-458.

[2] Ainslie JF (1988). Calculating the flowfield in the wake of turbines. Journal of Wind Engineering and Industrial Aerodynamics 27:213- 224.

[3] Merz KO (2014). VIPER: A tool for computing energy production from large offshore wind farms. Report TR A7382, SINTEF Energy Research, Norway.

[4] Larsen GC, *et al*. (2007). Dynamic wake meandering modeling. Report Risø-R-1607(EN), Risø National Laboratory,Denmark.

[5] Belcher SE, *et al*. (2003). Adjustment of turbulent boundary layer to a canopy of roughness elements. Journal of Fluid Mechanics 488:369-398.

[6] Frandsen ST (2007). Turbulence and turbulence-generated structural loading in wind turbine clusters. Report Risø-R-1188(EN), Risø National Laboratory,Denmark.

[7] Merz KO (2015). A linear state-space model of an offshore wind turbine, implemented in the STAS wind power plant analysis program. Report TR A7474, SINTEF Energy Research,Norway.

[8] Pedersen M (2016). Steady and transient inflow dynamics with actuator disk vortex theory. Manuscript submitted to WindEnergy.

[9] Annoni J, *et al*. (2016b). An experimental investigation on the effect of individual turbine control on wind farm dynamics. Wind Energy 19:1453-1467.

[10] Burton T, *et al*. (2001). *Wind Energy Handbook*. Chichester:Wiley.

[11] Snel H, Schepers JG (1995). Joint investigation of dynamic inflow effects and implementation of an engineering method. ReportECN-C--94-107, Energy Research Centre of the Netherlands.

[12] Bak C, *et al*. (2013). Description of the DTU 10 MW Reference Wind Turbine. DTU Wind Energy Report-I-0092, Technical University ofDenmark.

[13] Hansen KS (2013). Presentation of Nørrekær Enge wind farm and Nordtank 300kW wind turbine. Report by the Technical University of Denmark for IEA Wind Task 31:Wakebench.

[14] Chamorro LP, Porté-Agel F (2009). A wind-tunnel investigation of wind-turbine wakes: boundary-layer turbulence effects. Boundary- Layer Meteorology132:129-149.

[15] Jensen NO (1983). A Note on Wind Generator Interaction. Report Risø-M-2411, Risø National Laboratory,Denmark.

[16] Machielse LAH, *et al*. (2007). Evaluation of "Heat and Flux" Farm Control – Final Report. Report ECN-E--07-105, Energy Research Centre of theNetherlands.

[17] Annoni J, *et al*. (2016a). Analysis of axial-induction-based wind plant control using an engineering and a high-order wind plant model. Wind Energy19:1135-1150.

★★★

QUANTITATIVE RISK ANALYSIS APPLIED TO REFRIGERATION'S INDUSTRY USING COMPUTATIONAL MODELING

[1]SIVAKUMAR SUNDARAM, [2]SARADENDU BHUJABALA, [3] JYOTIKESH BARIK

[1]Department of Mechanical Engineering, NMIET, Bhubaneswar, 751019
[2]Department of Mechanical Engineering CEC Bhubaneswar
[3]Department of Mechanical Engineering REC Bhubaneswar
E-mail: [1]nitish.kumar@nmiet.ac.in

Abstract -
Ammoniahasbeenusedinrefrigerationinstallationsforyears.Itisanaturalrefrigerantandisreplacingother syntheticfluidsasithaszeroozonedepletionpotentialandnoglobalwarmingpotential;however,anammonia leakinarefrigerationplantcancausedamagetotheenvironmentandhumanhealthaswell.Hereweevaluatethe quantitative risk analysis of using ammonia in real industrial refrigeration in Rio de Janeiro. This work's methodologyusedPHASTtoachievetheassessmentmodelofsevenscenariosofammonialeakage,whichallowed theunderstandingofquantitativeriskforammonialeakage.Foreachscenario,threeammoniaconcentrations weresimulated,andthegasdispersiondistancesandtheirzoneofinfluencewereanalyzed.Resultsindicatedthe worstscenarioreached2677mand665mandallaccidentscenariosshowedthatindividualandsocietalriskwere abovethelimitallowedbytheRiodeJaneiroenvironmentalagency.Toreachthelimitstolerablebytheagency, twomitigationmeasureswereproposed,guaranteeingareductioninammoniadispersionbetween41and48% and 100% for each measure. Although the use of environmentally friendly refrigeration fluid is desired, the assessmentneedstoconsiderindividualandsocietalriskstoensurethatitwillnotaffectthefacility.

Keywords - Quantitative risk analysis Environmental risk Individual risk Societal risk FN Curves PHAST Industrial refrigeration

I. INTRODUCTION

Ammoniaisachemicalsubstanceusedinseveralchemical industry segments,suchasthefertilizer,pharmaceutical,textile,andindustrial refrigerationindustries.Ontheonehand,asarefrigerant,it hasseveral characteristics that make it extremely attractive. For example, it has betterheattransferproperties,thevolumetricrefrigeratingeffectis higherthanotherfluidswithsimilarvaporpressure,andhasnoozone depletionpotential(ODP)andextremelylowerGW.Ontheotherhand,it istoxicandcombustible[1].Besides,becauseitisanatural andenvironmentallyfriendlyrefrigerant,ammoniahasbeenusedtosubstitute halogenatedhydrocarbonsrefrigerantssuchasCFC,HCFC,andHFC.The firstonehadbeenbannedunderMontrealprotocol(1987), andtheother twohavebeenphasedoutasstipulatedbytheKyotoProtocol(1997).For thosereasons,researchershavebeenstudyingalternativerefrigerants[2] andammoniahaswidespreaduseasarefrigerantfluidinmediumand largefood,beverage,andpreservationindustry[3].Duetoitssmall molecularstructureandmolecularstrengthbetweenmolecules,itcan easilyspreadwhenreleasedintotheenvironment[4].Theleakageand dispersionofammoniacancausethesurroundingpopulation'spoisoning and result in severe environmental pollution [5]. Despite being an environmentallyfriendlyrefrigerant,itcancausemassive damageto the environmentandhumanhealthifanaccidentalreleaseoccurs.Thus,itis essentialtodevelopaquantitativeriskassessment(QRA) oftheriskof ammonia leakage in refrigerationinstallations.

Thereleaseanddispersionofammoniahavebeenstudiedfrequently. Itmainlyfocusesonthetoxicgasleakageanddispersionmodel,especiallysinceitisoneofthereplacementrefrigerantsforthecurrent halogenated hydrocarbons fluids used, HCFC and HFC [6,7]. According toPandyaetal.[7],thedispersionmodelscanbeclassifiedintothreemaincategories,rangingfromlesstomorecomplex:Gaussianmodels, integral-type models, and 3D or computational fluid dynamics(CFD) models.Thefirstoneisbasedonthediffusionequationand observations inexperimentalstudies.Thesecondoneisasimplification ofthecon- servation equations for mass, momentum and energy. ALOHA(Areal Locations of Hazardous Atmosphere), DEGADIS (DEnse GAs DISpersion), HEGADAS,andPHAST(ProcessHazardAnalysisSoftwareTool)arethe mostpopulardispersionintegral-typemodelsandwidelyusedinsafety engineering applications, which provide relatively easy and fast dispersionestimations.Thelastonehasbeendevelopedforyears andallows the users to have a three-dimension analysis. Some standard CFD codes are CFX, FLACS, FDS, and FLUENT[7].

Amongallthemodelspresented,ALOHA,PHASTandCFDcodesare themostcommonlyusedtostudythegasdispersion.Orozcoetal.[8] usedALOHAtoquantifytheeffectsofammoniareleaseandtheresults showedtheworstscenariowasthetoxicvaporcloud.Forinstance,Zhang etal.[9]combinescenariosetandcomputationalfluiddynamics(CFD) toevaluatingtheindividualriskduetotheammoniarelease.Rajeevetal. [10] evaluated and mapped the population vulnerability using the ALOHA software package and geographical information system (GIS).

PHASTisasoftwarethatgathersasetofcomprehensivemodelsand allowsthestudyofanaccidentsequence.Itanalyzesfromthereleaseof chemical material to the explosion and/or the toxic dispersion.Although itdoesnotrequirelargeamountsofinputdataandcalculationtimeisnot time-consuming,itstillgeneratestherequireddataandinformationfor evaluatingtheriskandsafety[11].PHASTsoftwareisamongthemost popularandwidelyusedinsafetyengineeringapplications.Besides,itis one of the most comprehensive computer programs for modeling acci- dental releases, used by companies and the competent authorities [7]. Many researchers have been using it to predict the gas dispersion of hazardousmaterial.Forinstance,Zhangetal.[12]usedPHASTtostudy thedispersionandtoxiceffectofliquefiedammoniainthecaseofan instantaneousrelease.Quetal.[13]alsoadoptedPHASTtoanalyzethe liquefied ammonia leakage accidents quantitatively. However, in both works,itwasevaluatedonlyonescenarioofleakageinatankfilledwith ammonia. Inordertoachieveaquantitativeriskanalysis,manyresearchersand engineershavebeenadoptingtheQRAmethod.Itisacommontoolused forplanningandapprovalofhigh-riskprocessfacilitiesglobally.The QRAresultsareanalyzedusingindividualriskcontoursandsocietalrisk contourorF–Ncurve[14].AvasthyandSiddiqui[15]estimatedtherisk offatalityduetoanoperationalammonialoadingfacilitysurroundedby aresidentialpopulation.Althoughthisstudyconsiderstheriskcontours, itonlyconsidersthreescenarioswithoneammoniaconcentrationfor eachone.Zolt´anetal.[16]discussedthepotentialthreatsposedby ammoniaincoldstoragefacilitiesanddescribedanexampleofapo- tential event involving ammonia dispersion and depicts it on a map togetherwiththesolution.Nevertheless,thisworkdidnotevaluatethe risk contourseffectively.

Thisarticleaimstofeatureaquantitativeriskanalysis(QRA)method in industrial facilities with toxic gas release hazards that combine the scenarios and PHAST software. Based on the subject matter experts (SME's)opinions,sevenpotentialequipmentfailures,andtoxicgas releasescenariosareconstructed.Theindividualandsocietalriskofeach releasescenarioareestimated.Furthermore,threeammoniaconcentrationlevelsaresimulated,andthedispersionfeaturesandimpacteddistanceofammoniaarepredicted.Theseoutcomesarecomparedwiththe tolerablelimitsfromtheregulatoragency–environmentstateinstitute (INEA)–inRiodeJaneiro.Besides,weproposemitigationmeasuresto reduce the distance of ammonia dispersion and reduce individual and societalrisk.Inthisstudy,arealcaseofacoldstorageunitcontaining ammoniaasrefrigerantfluidisprovidedtoillustratethismethod.Afood factoryindustrylocatedinanindustrialareaatCampos,RiodeJaneiro, Brazil,isselectedasanempiricalfieldofapplication.

Thisarticleaimstofillthegapsfoundinotherarticlesandprovide a completeanalysisofarealindustrialfacility,whichusesammoniaasa refrigerant.Thisarticle'snoveltyisthequantitativeanalysisofammonia throughout the refrigeration process, which takes into account different incidentsscenariosandthreelevelsofammoniaconcentration.

II. THEORETICAL FOUNDATION

Ammoniaisachemicalmaterialcomposedofonenitrogenatomand threehydrogenatoms,representedbythechemicalformulaNH3.AccordingtoReyes[17],ammoniahaschemicaladvantagesforitsusein refrigerationinstallationsduetoitslightmolecularweight (17.03g),low boilingpoint(28○F),andhighlatentheatofvaporization(1371.2J). Anotheradvantageisthatmanyresearchershavestudiedammoniasince the19thcentury,whichprovidesavastdomainoveritspropertiesand managementexperiences.

According to the document provided by the INEA [18],ammonia qualifiesinalmostallconceptsofagoodrefrigerantgasdespiteits toxicity.Themainconceptsthatmakeagasagoodrefrigerantareshown in Table1. Tofacilitatethetransportandstorageofammonia,itispressurizedto achievethestateofliquefiedammonia.Whenaleakageoccurs,theliquefiedammoniaisquicklyvaporized.Ammoniainitsgaseousstateisnot flammable,butifitisinlargequantitiesandthepresenceofanintense energysource,itcanbeignitedandcauseanexplosion.However,therisk offlammabilityofammoniamanifestsitselfonlyinextremefireconditionsandinconfinedplaces.Additionally,ifincontactwithwater,an exothermicreactionisproduced,producingheatthat,incontactwith othergases,cancausefireorexplosion.Ithastoxiccharacteristicsconcerninghumanhealthifinhaled,causingburnsandsevereinjuriestothe skin and eyes. Therefore, an ammonia leakage can have serious consequencesdependingontheconcentrationreleasedandtheextentofthe vaporcloud.

Althoughammoniaisnotconsideredaflammablesubstance,concentrationsinavolumeofaround15%and28%canformaflammable mixturecapableofignitingorexploding[7].Ammoniavaporisdifficult tobeignitedintheairatmospherebecauseofitshighMinimumIgnition Energy (MIE 680 mJ) [4]. However, the presence of oils or other combustible materials increases the risk of fires and explosions. Furthermore,ammoniaistoxic,combustible,possessesapungentodor andaggressivenesstocopperalloy[1].However,comparedtoother refrigerants, ammonia presents no damage to the ozone layer anddoes not intensify the greenhouseeffect.

Regardingthetoxicity,theregulatoryagencyarguesthatammoniaisabasewithmanyaffinitiesforwater,whichcancauseirritatingeffectsonthe eyes, skin, respiratory tract, and mucousmembranes of thenasalpassagesandlungs.Nevertheless,ammoniahasapowerfulcharacteristicodor, making it easy to recognize when breathed byhumans.Smallconcentrationsstartingat10ppm,ammoniaisalreadynoticeable.Intherangesbetween150and400ppm,italreadycausesirritationanddiscomfortinthenasalmucousmembranes,anditisverytoxicinconcentrationsabove1500ppmandcandestroytissuesofthenasalcavities.

Thebiggestconcernofcompaniesthatuseammoniaasarefrigerantshouldberelatedtoleaksthattriggertheformation oftoxicclouds,andthatcancauseexplosions.AccordingtoINEA,themostcommoncausesofaccidentsarefailuresinthedesignofthecoolingsystemanddamagetotheequipmentcausedbyheat,corrosion,andvibration,aswellasdueto impropermaintenanceorlackofmaintenanceofitscomponents,suchas relief valve pressure, compressors, condensers, pressure vessels, purging equipment, evaporators, pipes, pumps and instruments in general. INEA listssomeofthecausesthatusuallygenerateammonialeaks,asshownin Table2. AmmoniahasanODPandGWPcorrespondingtozero,whichmeans nodamagetotheozonelayerorcontributiontoglobalwarming. Therefore,ammoniaisanidealgastobeusedinrefrigerationsystems consideringonlytheenvironmentalriskrequirements.

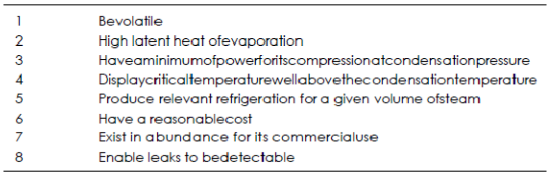

1	Bevolatile
2	High latent heat ofevaporation
3	Haveaminimumofpowerforitscompressionatcondensationpressure
4	Displaycriticaltemperaturewellabovethecondensationtemperature
5	Produce relevant refrigeration for a given volume ofsteam
6	Have a reasonablecost
7	Exist in abundance for its commercialuse
8	Enable leaks to bedetectable

Table 1
Maincharacteristicstobearefrigerant.

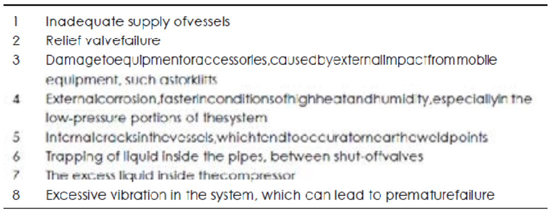

1	Inadequate supply ofvessels
2	Relief valvefailure
3	Damagetoequipmentoraccessories,causedbyexternalimpactfrommobile equipment, such asforklifts
4	Externalcorrosion,fasterinconditionsofhighheatandhumidity,especiallyin the low-pressure portions of thesystem
5	Internalcracksinthevessels,whichtendtooccuratornearttheweldpoints
6	Trapping of liquid inside the pipes, between shut-offvalves
7	The excess liquid inside thecompressor
8	Excessive vibration in the system, which can lead to prematurefailure

Table 2 Main causes of ammonia leakage

III. METHODOLOGY

The work methodology adopted in this study is composed of four phases,asindicatedinFig.1.Asaninitialstep,therefrigerationplant’s installationandprocessneedtobespecifiedbyanalyzingitsconstructive and operational aspects. Besides, the vicinity description is also essential toidentifyanyaspectthatmayinterfereinanyaccidentalscenario.

The second step herein is the identification and description ofthe accidentalscenariosofammonialeakage.Aftercompletingthehazards identificationstep,inthethirdstep,acriterionmustbeestablishedfor selectingaccidentalhypothesesthatwillbestudiedindetailinthenext stepsoftheAQR.Thecriterionmustbeestablished,consideringthe severityofthedamageresultingfromtheidentifiedfailure.Theselected accidentalhypotheseswillbestudiedintermsoftheirconsequences,that is,theirimpactsanddamagescausedduetoapossiblematerializationof theaccidentalscenarios.ThispartisperformedbyusingProbitfunction thatitdefinestheammoniaconcentrationthatwillreachtheprobabilitiesof1%and50%ofdeaths.Then,duetothecomplexityof thecal- culations involved, PHAST's computational models are run in order toestimatetheconsequencesofaccidentalscenarios.Inthispart,itispossibletoobservetheeffectsandthevulnerabilityoftheregionwhenit isexposedtoatoxiccloud.Theestimationofthefrequenciesofthe accidental scenarios requires the use of frequency calculation methods and models. This study is based on the use of the event tree and componentfailureratesinaccidentalscenarios.

Thelaststepconsistsofcalculatingandcomparingtheriskwiththe previously established criterion. The risk assessment results are expressedintermsofindividualrisk(IR)andsocietalrisk(SR),whichare comparedwiththelimitrequiredbytheRiodeJaneiroenvironmental agency,INEA.Itsguidanceforriskanalysis[19]establishesamethodto developariskanalysisstudy.Thedevelopmentofaquantitativerisk assessmentintermsofIRandSRisbasedontherelationbetweenthe inventoryoftoxicmaterialandthedistancetoaresidential area.The final project must exhibit lower IR and SR; if either fails, mitigation measures must be proposed[14].

Inthiswork,weanalyzedsevenpossiblescenariosofammonia leakageinarefrigerationinstallationinRiodeJaneiroandevaluatedthe extent of dispersion of the generated ammonia plume, the societal and individualrisk.WeusedPHASTRisksoftware(version7.01)toassess thesescenarios'effectsandevaluatetheregion'svulnerabilityaround the refrigerationinstallation.

3.1. Estimation of consequences

Estimationofconsequencesconsiderstheimpactanalysis,whichis appliedtoestimatethepotentialfordamageorinjuryfromspecificaccidents.Itallowscalculatinghumanexposuretoacloudoftoxicgas. Then,outcomescanbecomparedwithguidelinesorstandardstoestimatetheprobabilityofharmtoanexposedindividualorpopulation.The probabilityoffatalityiscalculatedusingtheappropriateprobitfunction toestimatetheprobabilityofdamageforeachexposuretype.Probit functions (Equation (1)) exist for almost any hazardous chemical but are typically available for thermal radiation, toxic gas release,andblastoverpressureeffects.Itestimatesthepercentageof injured persons living in the impacted areas [8]. In this study, the probability of fatality is calculated using the appropriate Probit function,described as[20]: (1)

WhereYisthevaluecorrespondingtotheprobabilityofdeath;Cisthe concentrationofthetoxicmaterial(ppm);tisthetimeofexposure (minutes);andn,K1,K2areconstants,whichareexclusive anddepend onthetypeofchemicalsubstanceevaluated. Inthisstudy,theequationfindstheconcentrationofammoniathat willreachthepointswithaprobabilityof1%and50%ofdeathsaround the refrigerationplant.

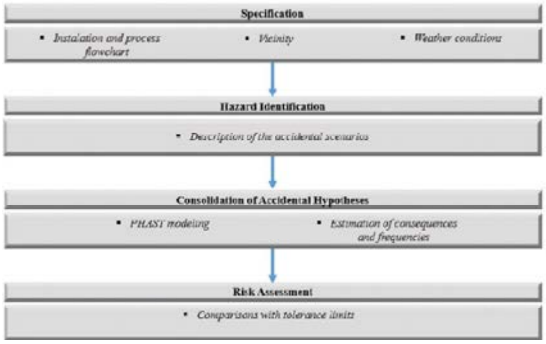

Fig. 1. Work methodology.

3.2. Estimation of frequencies

Frequencyestimationofaccidentalscenarioscanbeobtainedeither fromhistoricalrecordsmadeavailablebySME'sorfromanalyzesof previousaccidents.Thisdirecttechniqueprovidestheincidentfrequencyforthemaineventwithouttheneedfordetailedfrequencymodeling. However,mostaccidentsanalyzedinanAQRaresorarethatitis necessarytousefrequencycalculationmethodsandmodels. Eventtreesaretypicallyusedinriskassessmentstudiestoquantify thefrequencyofdifferentpossiblescenarios.Itconsistsofatechniqueto analyzetheconsequencesofanunwantedeventbydescribingthetem- poral sequence of the facts. To determine the frequency estimation ofa finalevent'soccurrence,itisnecessarytoperformtheproductofallthe probabilities of the branches previously covered. Therefore, a simple event tree of the refrigeration plant was developed to calculate the frequencyofaccidentalscenariosrelatedtotheammoniarelease.Thiswork usedtheequipmentfailureratestocalculatethefrequency ofinitiating events, as shown in Table3.

3.3. Estimation of individual and societalrisk

Individualrisk(IR)isdefinedastheprobabilityofdeathper yearifanindividualisexposedtoahazardinthevicinityofa ninstallation[10,22].IRisausefulcriteriontounderstanda ndmanagetheriskforaspecificperson or group of people according to the geographic locationofthesourceofthetoxicsubstancereleasedandth epeoplearoundthefacility.Thetotalindividualriskatage ographiclocationclosetoanindustrialplantwithcoordina tesx,yassumesthatisequaltothesumoftheindividualrisksatthatpoint.Then,thisinformationisusedtoge nerateindividualriskcontours.AccordingtoCCPS[23],thetotalin dividual risk can be calculated by Equation (2) and Equation (3):

$$IR_{x,y}¼\sum_{i¼1} IR_{x,y,i} \qquad (2)$$

Where,fiisthefrequencyofeachincidentandpf;iisthepro babilityofthe incident that will result infatality. Societalriskconsiderstheindividualrisktoestimatethepo pulation densityaroundthesourceofthereleasedhazardousmateri al.Itssignif- icance is in describing the severity of the accident, showing therelationshipbetweentheaccumulatedprobabilityandtheexp ectednumber ofdeaths,thenumberofpeopleaffectedforeachoftheriska reas.The societalriskisusuallyrepresentedbyF–Ncurves,whichisatypeofrisk indicatorthatplotsthevariablesF(annualfrequencyofacc idents involvingnandmorefatalities)andN(thenumberoffatalit ies)inatwo-

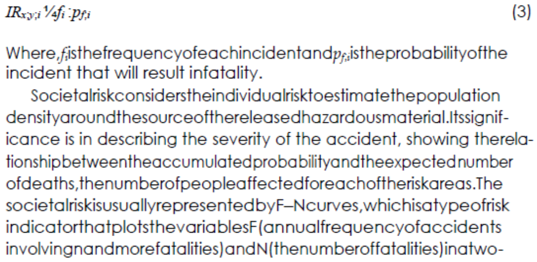

$$IR_{x,y,i}¼f_i\cdot p_{f,i} \qquad (3)$$

Where,$f_i$isthefrequencyofeachincidentand$p_{f,i}$istheprobabilityofthe incident that will result infatality.

Societalriskconsiderstheindividualrisktoestimatethepopulation densityaroundthesourceofthereleasedhazardousmaterial.Itssignificance is in describing the severity of the accident, showing therelationshipbetweentheaccumulatedprobabilityandtheexpectednumber ofdeaths,thenumberofpeopleaffectedforeachoftheriskareas.The societalriskisusuallyrepresentedbyF–Ncurves,whichisatypeofrisk indicatorthatplotsthevariablesF(annualfrequencyofaccidents involvingnandmorefatalities)andN(thenumberoffatalities)inatwo-

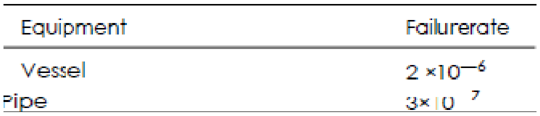

Equipment	Failurerate
Vessel	2×10^{-6}
ipe	3×10^{7}

Table 3
Equipment failure rate [21].

dimensionalcoordinatesystemtoexpresstherelationship betweenthem. Usually,riskcurvesareshowninalog-logplotwiththeannualfrequency ontheordinateaxisandthenumberoffatalitiesontheabsci ssaaxis[24, 25].Toassesstheseverityoffatalaccidentsinammonialea kage,the mostcommonlyusedmethodistoplottheF–Ncurve,showingthe relationbetweentheaccumulatedprobabilityandthenum berofdeaths, which can be provided as follows[26]:

Where,fNðxÞistheprobabilitydensityfunctionoftheann ualfatalities; FN x represents the cumulative probability distribution function ofthe annualfatalities,representingtheprobabilityoflessorequ altoxfatal- itiesperyear.Inreal-worldpractice,theprobabilityofaccidentsisusuallyreplacedbythefrequency,andtheaccidentsaregroup edaccording to the number ofdeaths.

IV. CASE STUDY

Thiswork’scasestudyisarefrigerationinstallationlocate dinRiode Janeiro,whoserefrigerantusedisammonia.Theinstallati onislocated 500mwestofapopulatedareawithapopulationuniformly distributed over 452 occupations, including residential occupations and small com- mercial establishments. Therefore, this work aims to assess individual andsocietalrisksgivensevenscenariosofliquefiedammo nialeakage.To estimatethenumberofpeoplepresentinthevicinityofthef acility,this workconsideredthepresenceof3.24inhabitantsperresid enceinthe studied region.

4.1. System description

Fig.2showstheprocessdiagramoftherefrigerationinstall ation usingammoniaastherefrigerantfluid.Themainreservoir (V-01)hasa storagecapacityof7700LofNH3.TheflowofNH3intheli quidphase leavesthemainreservoirandthenfeedstheseparatorvesse latatem- peratureof—10○C(V-02) andtheintermediatecooler,whichwillsupply theseparatorvesselatatemperatureof—35○C(V-03).Fromthesepa- rator vessels, the liquefied ammonia is pumped into the rooms of refrigeratedproductsat—10○Candfrozenproductsat—35○C.Afterthe heatexchangebetweentheammoniaandtherooms,NH3r eturnstothe separatorvessels.Fromtheseparatorvessels,NH3isaspir atedintothe compressorsystem,consistingoftwocompressorsforthe systemwitha temperatureof—10○Candtwoforthesystemwithatemperatureof—35 ○ C.Then,NH3leavesthecompressorsandissenttothecond ensation system composed of one condenser. Finally, NH3 leaves the condenser, goestothecoolingtower,andthenreturnstothemainreser voir.

4.1.1. Accidental scenarios and weatherconditions

Asstatedpreviously,sevenaccidentalscenariosweredefi nedbased ontheopinionsofSME’s.SME’sismadeupofrefrigeratio nplantworkers withexperienceintherefrigerationsystem.Table4shows theaccidental scenariostakingintoaccountthedifferentfailuremodesin thecooling system.Intypicalcases,accidentalreleaseofammoniaisusuallydueto releasesinvessels,suchascontinuousleakageorcatastrophicruptures [22,27]orduetobrokenpipeorequipment,andsoon[28].Itisassumed thatammoniaescapesintotheatmosphereindifferentsituationsinall scenarios,i.e.,ammonialeaksduetoruptureofthevesselor hole-s/ruptureinthepipeorequipment.Furthermore,whenanaccidentoc-curs,itisassumedthat100%oftheamountofammoniainthepipesor vessels is released into theatmosphere.

TorunthePHASTsoftware,eachleakscenariocanbedefinedbythe amountofhazardoussubstance,storagepressure,holediameter,the heightoftheleak,andweatherconditions.Therefore,alargenumberof releasescenarioscanbegeneratedbyvaryingtheseparameters[29].

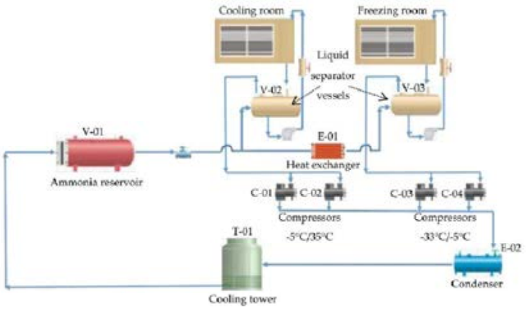

Fig. 2. Process flow diagram of the installation.

1	NH_3leakageinthepathbetweenthecondenserandthemainreservoir
2	NH_3 leakage in the main reservoir(V-01)
3	NH_3leakageintheseparatorvessel(V-02)
4	NH_3leakageintheseparatorvessel(V-03)
5	NH_3leakageinthepathbetweenthemainreservoirandtheseparatorvessels(V- 02 andV-03)
6	NH_3leakageinthepathbetweentheseparatorvessel(V-02)andtheroomof refrigeratedproducts
7	NH_3leakageinthepathbetweentheseparatorvessel(V-03)andtheroomof frozenproducts

Table 4 Accidental scenarios considering different modes of failure in the refrigeration plant.

Table5presentsthesevenpotentialaccidentscenarioswithammonia leakage. In each scenario, the conditions are specified, which was later insertedintoPHASTtoperformthemodeling.Thecalculationofthe massofammoniareleasedtookintoaccountsomefactors, suchasthe volumewithintheline(scenario1),thetotalvolumeofthe mainreser-voirV-01(scenario2–5)orthevolumeoftheseparatorvesselV-02and V-03 (scenario6–7).

Then,aspreviouslyindicatedintheflowchart(Fig.2),theindividual risk(IR)aroundtheinstallationneedstobeestimatedafterselectingthescenarios. PHAST software was used to calculate the population’s vulnerability levels if one of the seven release scenarios occurred.

Themeteorologicalinputforthemodelingwasmadeusing theaverage of climatological data gathered from Campos meteorologicalstationandisdepictedinTable6.DispersioncalculationsareexecutedassumingastabilityclassD.ThestabilityclassesarebasedonPasquill’s sixstabilityclasses,classesAtoF,todepictdifferentatmosphericturbulencelevels[30].Inthisstudy,classDcharacterizesaconditionof neutralstability,whichmeansthatthewindturbulencemaycause dispersionoftoxicgasoveragreaterdistancefromthereleasesource.

Parameter	Accidental scenarios						
	1	2	3	4	5	6	7
Physical state	Saturated liquid	Saturated liquid	Subcooled liquid	Subcooled liquid	Saturated liquid	Subcooled liquid	Subcooledliquid
Pressure (kgf/cm²)	18	18	15.69	15.69	18	18	18
Temperature (°C)	–	–	−10	−35	–	−10	−35
Leak height (m)	3	1	1	1	3	3	3
Pipeline diameter (in)	5"	–	–	–	1 ½"	2½"	2"
Volume (m³)	0.38	3.86	3.86	3.86	3.86	1.4	1.4
Released ammonia (kg)	215	2185	2185	2.185	2185	2185	2185

Table 5
Parameters to define the mass of ammonia released from each accident scenario

AirTemperature	23.7°C
AtmosphericPressure	1atm
Humidity	79.1%
Windspeed	2.0m/s

Table 6 Weather conditions.

4.1.2. Ammoniaconcentrations

Thisworktakesintoaccountthreeammoniaconcentrationlevels. The first level corresponds to the concentration Immediately Dangerous toLifeorHealth(IDLH)that,accordingtotheNationalInstitutefor Occupational SafetyandHealth (NIOSH),is300ppm.Theothertwo levelsconsidertheprobabilitiesofdeathof1%and50%ofthepopula-tionaroundtheinstallationfor30minofexposure.Table7showsthe ammoniaconcentrationlevelsforIDLHandthedeathprobabilitiesof1% and50%.Weevaluatedascenarioofatoxiccloudformationafterthe

CODE	Type	Conc. (mg/m³)	Conc. (ppm)	Scenario	Effect
A	IDLH	–	300	Toxic cloud formation	Toxic concentration
B	Death Probability 1%	1.693	2.435		
C	Death Probability 50%	5.428	7.807		

Table 7 Ammonia concentration levels.

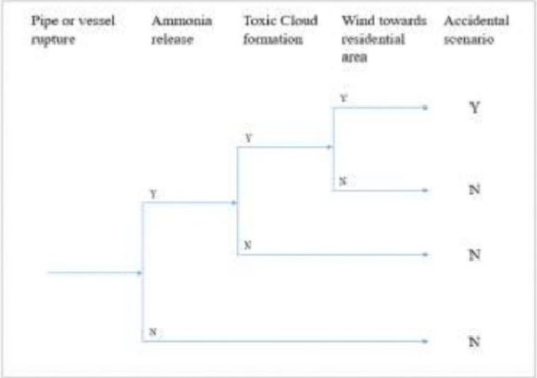

Fig. 3. Ammonia leakage event tree.

Accidentalscenarios	Frequency
1	3.38E—06
2	7.50E—07
3	7.50E—07
4	7.50E—07
5	1.13E—05
6	5.63E—05
7	5.63E—05

Table 8 Ammonia release frequency estimation.

ammonia leakage inside the plant for each level. The physicaleffect developedisthetoxicconcentrationofthiscloudthatcanleadtodeathif the population is exposed for a longtime.

4.1.3. Ammonia dispersionfrequencies

Thefrequencyofoccurrenceofaccidentalscenarioswasestimatedby applyingtheeventtreetechnique(Fig.3).Theestimationismadefrom thecompositionofthefrequencyofoccurrenceoftheinitiatingevents andthedifferentpossibilitiesfortheevolutionofaccidents.Thefrequencyestimationtakesintoaccounttheequipmentfailurerateandthe winddirectiontowardstheresidentialarea.Table8showsthefrequency estimation of accidentalscenarios.

V. RESULTS AND DISCUSSION

5.1. The distance achieved of the ammoniacloud

Basedonthedatapresentedabove,accidentalscenarioswerecharacterizedbymodelingandcalculatingthescopeoftheharmfulphysical effectsofatoxicammoniacloud.Table9showsthedistancesreachedby the ammonia concentrations specified for the accidental scenarios postulated.

Fromtheanalysisoftheresults,itcanbeseenthatthegreaterrangeoflethalconcentrationsisrelatedtotheoccurrence ofammoniareleaseinthe section between the separator vessel containing liquidammoniaat10○Candthecoldroomsduetoaholeoralinebreak,scenario6.Inthiscase, the level of ammonia concentration corresponding tothe1%probabilityoffatalityoftheexposedpopulationreaches665m,and50% of fatality reaches a distance of 428 m. Itappearsthattherearesensitiveoccupationswithintheraysofthe cloudforthedifferentlevelsofammoniaconcentration.

5.2. Individual and societalrisk

N°	Accidentalevents	Distances(m)		
		A	B	C
1	NH_3leakageinthepathbetweenthecondenserand the mainreservoir	440	292	241
2	NH_3 leakage in the main reservoir(V-01)	643	299	174
3	NH_3 leakage in the separator vessel(V-02)	674	321	219
4	NH_3 leakage in the separator vessel with(V-03)	772	195	137
5	NH_3leakageinthepathbetweenthemainreservoir and the separator vessels (V-02 and V-03)	845	534	400
6	NH_3leakageinthepathbetweentheseparatorvessel (V-02) and the chamber of refrigerated products	2677	665	428
7	NH_3leakageinthepathbetweentheseparatorvessel (V-03) and the chamber of frozenproducts	2034	518	302

Table 9
Distances reached by three ammonia concentrations

Individualrisk(/year)	Distance(m)
1.00E—05	479
1.00E—06	644
1.00E—07	667

Table 10
Distances corresponding to the individual risk

As previously stated, the individual risk (IR) reflects the annual

probabilityofanindividualdeathlocatedintheinfluenceareaofthe accidental scenarios’ effects postulated. The calculation of each accidentalscenario’scontributiontothetotalindividualriskrelatedtothe release of ammonia was made based on the results obtainedpreviously foritsfrequencyofoccurrenceandthereachofthelevelsof physical effects corresponding to the different probabilities of people death exposed.

Table 10 presents the calculated distances that correspond to the individualrisklevelswithoneorderofmagnitudevariation. Theindividual riskprofileachievedisshowninFig.4.Therefrigerationinstallation’s respectiveiso-riskcontoursareillustrated,wheretheprojectionofthe iso-riskcontourswaselaboratedfromthemachineroomsincethisareais associatedwiththemostcriticalaccidentalscenarios. Theobservationoftheiso-riskcontoursindicatesthattheindividual risklevelof1.00E06/year,consideredbyINEAasthetolerablelimit fornewinstallations,reachessensitiveresidentialoccupationsaround theinstallation.

Aspreviouslyindicated,thecalculationofsocietalriskis madefrom thefrequencyofeachaccidentalscenarioandtheestimateofthenumber ofdeathsamongtheexposedpopulation.Theresultsarepr esentedinan F–Ncurve,whichprovidesthecumulativefrequencyofaccidentswithN ormorefatalities.Theestimateofthenumberofdeathsamongthe populationexposedtothesescenarios’effectswasbasedontheestimateofthenumberofpeoplepresentintheinstallationsurroundings.

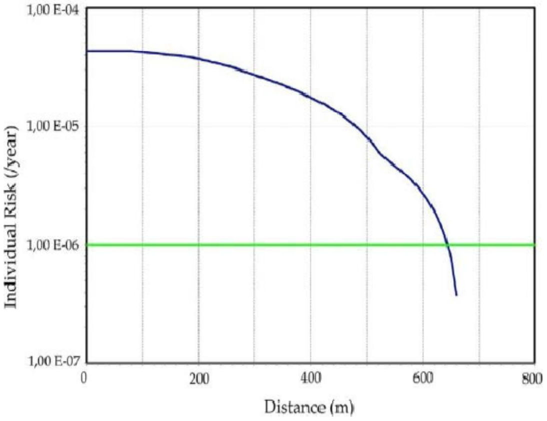

Fig. 4. Individual risk profile achieved.

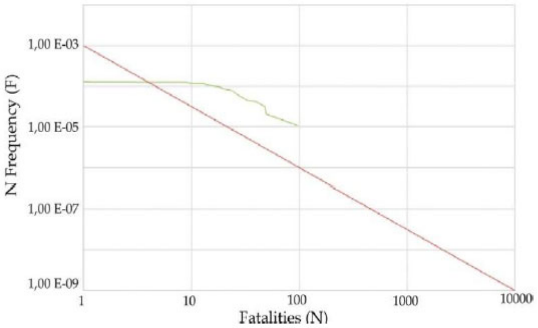

Fig. 5. F–N curve plotted for the model selected.

Theestimatednumberofdeathswasobtainedbyconsideringthe following probabilities: 75%probabilityofdeathforpeoplelocatedintheareacorresponding totheperimeterofthecircle,foreachdirectionconsidered, delimited bythescopeoftheconcentrationregardingtheprobability ofdeathof 50% of the exposed population; 25%probabilityofdeathforpeoplelocatedintheareacorresponding to the circle perimeter, relative to each direction considered, delimitedbytherangeofconcentrationsreferringtotheprobabilities ofdeathof50%and1%oftheexposedpopulation.

Fig.5showstherespectiveF–Ncurve.Thehorizontalaxisshowsthe numberofdeathsandtheverticalaxisshowstheprobabilityperyearfor anaccidentduetotheammoniareleasethatwouldcausemorethanthe numberofvictims.Thegraph’sobservationshowsthatthe curverepresentingthesocietalriskislocatedabovetheacceptabilitylimitfornew installations,accordingtothecriterionadoptedbyINEA.

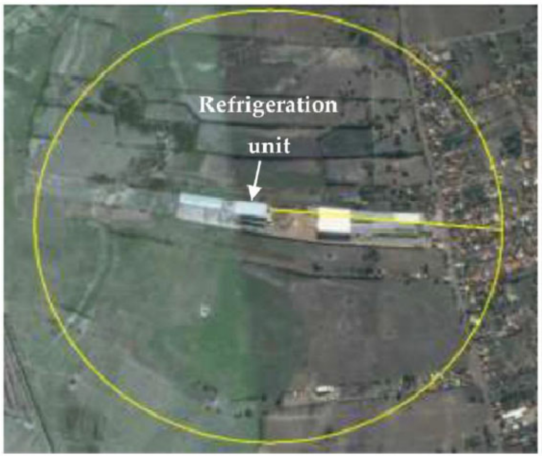

Fig. 6. Iso-risk curve concerning to distance of 644 m

5.3. Risk tolerability

Thecalculationoftheindividualriskindicatedthatthelevelof1.00 E06/year,consideredbyINEAasthelimitofacceptability fornew installations, reaches areas with the presence of sensitive residential occupations. The calculation of societal risk indicated that the acceptabilitylimitconsideredbyINEAfornewinstallationsisexceeded.Fig.6illustrates the 1.00 E 06/year radius plotted in Google Earth for the refrigerationplant.Therefore,duetoindividualandsocietalrisks,itwill be necessary to reassess the risks after the implementation of preventive and mitigatingmeasures.

5.4. Mitigating measures

Afterinvestigatingthedistancesreachedbythetoxicammoniacloud, two mitigating measures were proposed to reduce the extent of the cloud’sradiusofinfluenceoverthehabitablepartneartheinstallation boundary.Thefirstmitigationmeasure(MM1)representstheimplementationofleakcontainmentvalves.Table11showstheseven possible scenarios of ammonia release accidents with the implementation of the MM1measure.Fortheelaborationofthesescenarios,somefactorswere considered,suchasthereleasepressure,theamountoftotal ammonia and ammoniareleased. Thepressureofreleaseofthetoxicammoniacloudtookintoaccount theshutdownofpumpsandcompressors,reachingavalue of1kgf/cm2.

Thetotalammoniaamountwasconsideredthetotalmassofammoniain therefrigerationsystem,whichcorrespondsto3700kg.To calculatethe ammoniareleasedineachscenario,thevolumequantitywascalculated accordingtothespecificationsofthepipelineandthevessels’size. Afterdescribingthenewscenarioswiththeimplementationof MM1, thenewtoxicammoniacloudsweremodeled,andthedistancereached byeachofthescenarioswasobtained,ascanbeseeninTable12.From theanalysisoftheresults,itcanbeseenthatthegreaterrangeoflethal concentrationsafterMM1isrelatedtotheoccurrenceofNH3(l)release inthesectionbetweentheseparatorvesselat10○Candthecoldrooms duetoaholeorlinebreak.Inthiscase,theammoniaconcentrationlevel correspondingtothe1%probabilityoffatalityoftheexposedpopulation reachesadistanceof395m,andthe50%fatalityreachesadistanceof 255 m. The presence of sensitive occupations is verified withinthe ammoniaconcentrationlevels’reachaftertheimplantationofMM1.

The second mitigation measure 2 (MM2) consists of enclosing the installationusingagasabatementsystem.Aftertheimplementationof MM2,theaccidentalscenarioswereremodeled.Somepremiseswere consideredfortheapplicationofMM2,suchasshedimensionsof9000 m3,exhaustrateof3000m3/h,exhaustfandiameterof1200,exhaustion oftheabsorptiontowerfortheabatementsystem,andthereleaseofthe ammoniawillonlyoccuriftheabatementsystemfails.Asinapplyingthe firstmitigatingmeasure,Table13presentsthepropertiesconsideredfor

Parameter	Accidentscenarios						
	1	2	3	4	5	6	7
Physicalstate	Saturatedliquid	Saturatedliquid	Subcooledliquid	Subcooledliquid	Saturatedliquid	Subcooledliquid	Subcooledliquid
InitialPressure(kgf/cm^2)	18	18	15.69	15.69	18	18	18
ReleasePressure(kgf/cm^2)	1	1	1	1	1	1	1
Temperature(°C)	–	–	—10	—35	–	—10	35
PipelineDiameter(in)	5"	–	–	–	1½"	2½"	2"
Ammoniaavailableforrelease(kg)	3700	3700	3700	3700	3700	3700	3700
Volume(m^3)	0.38	3.86	1.4	1.4	0.114	1.57	1.00
ReleasedAmmonia(kg)	215	2185	910	954	64.5	1023	684

Table 11
Parameters to define the mass of ammonia released from each accident scenario applying MM1

N°	Accidental eventswithMM1	Distances(m)		
		A	B	C
1	NH_3leakageinthepathbetweenthecondenserand the mainreservoir	440	292	241
2	NH_3 leakage in the main reservoir(V-01)	545	229	136
3	NH_3 leakage in separator vessel(V-02)	407	188	130
4	NH_3 leakage in separator vessel with(V-03)	34	20	16
5	NH_3leakageinthepathbetweenthemainreservoir and the separator vessels (V-02 and V-03)	290	193	154
6	NH_3leakageinthepathbetweentheseparatorvessel (V-02) and the chamber of refrigerated products	1474	395	255
7	NH_3leakageinthepathbetweentheseparatorvessel (V-03) and the room of frozenproducts	237	77	35

Table 12
Distances reached by three ammonia concentrations applying MM1.

Parameter	Accidentscenarios						
	1	2	3	4	5	6	7
Physicalstate	Saturatedliquid	Saturatedliquid	Subcooledliquid	Subcooledliquid	Saturatedliquid	Subcooledliquid	Subcooledliquid
InitialPressure(kg/cm^2)	18	18	15.69	15.69	18	18	18
Temperature(°C)	–	–	—10	—35	–	—10	35
PipelineDiameter	5"	–	–	–	1½"	2½"	2"
Ammoniaavailableforrelease(kg)	3700	3700	3700	3700	3700	3700	3700
ReleasedAmmonia(kg)	3700	3700	3700	3700	3700	3700	3700

Table 13
Parameters to define the mass of ammonia released from each accident scenario applying MM2.

modeling in PHAST using MM2. Table14showsthedistancesreachedbythetoxicammoniacloudfor theaccidentalscenariospostulatedconsideringtheabatementsystem’s failure.Fromtheanalysisoftheresultsofthedistancesreachedwiththe implementationofMM2,itwasfoundthatthegreatestreachofthelevel ofammoniaconcentrationcorrespondingtothe1%probabilityoffatality oftheexposedpopulation(B)reachesthedistanceof48mand50% fatality(C)reachesadistanceof28m.Withthis,itappearsthatthereis nopresenceofsensitiveoccupationswithintheraysofreachofthelevels of ammoniaconcentration.

5.5. Reassessment of individual and societal risk with MM1 and MM2 measures

AfterimplementingthemitigatingmeasuresMM1andMM2,thein- dividual and societal risks were reassessed considering the imple- mentation of these measures in the refrigeration system. Table 15presentsthedistancescorrespondingtotheindividualrisklevelswithan orderofmagnitudevariationandtheirpercentagesrelatedtotheamount ofriskmitigatedbyMM1.Itcanbeseenthattheindividualriskprofile showninFig.7isinacertainpartabovethelevelofttoleranceadoptedby theenvironmentalagencyinRiodeJaneiro.Theobservationoftheiso-riskcontoursindicatesthattheindividualrisklevelof1.00

E06/year, consideredbyINEAasalimitofacceptabilityfornewinstallations, reachessensitiveoccupationsaroundtheinstallation.

A new model for societal risk was made according to theaccidental scenarios’frequenciesimplementingtheMM1measure. Thenumberof deathsestimationwasmadefromthenumberofpeoplepresentinthe rangeofaccidentalscenarios,consideringtheprobabilitiesof25%and 75%.Fig.8showstherespectiveF–Ngraphswiththeimplementationof MM1. The graph’s observation shows that the curve representing the societalriskislocatedbelowtheacceptabilitylimitfornew installations, accordingtothecriterionadoptedbyINEA.ThecalculationofsocietalriskafterMM1indicatedthattheacceptabilitylimitconsideredbyINEA for new installations is notexceeded.

AftertheimplementationofMM2,theindividualriskswereassessedandareshowninTable16,whichpresentsthedistancescorresponding to the individual risk levels with an order of magnitude variation.Fig.9presentstheindividualriskprofilewithMM2andthe tolerancecriterionadoptedbyINEA.Comparingtheindividualrisk profile,itisobservedthatitiswellbelowtheadoptedcriterionof1.00 E06;thelimitofacceptabilityfornewinstallationswasnot reached.

Therefore,thepercentageofmitigationforthevaluesfoundintheindividualrisk’sinitialprofilewas100%.ThesocietalriskafterMM2was notcalculatedduetotheabsenceofsensitiveoccupations withinreachof toxic ammoniaclouds.

ThisworkcarriedoutanammonialeakQRAbasedonthree different concentrationsofitandtookintoaccounttheindividualandsocietalrisk asindicatorsofthelevelofriskthatthepopulationneartheareaofthe facility was exposed to. First, seven possible ammonia leak scenarios were evaluated, which indicated the possibility of exposing the populationtoatoxicammoniacloudifoneoftheaccidentsoccurred.Although ammoniaisanaturalrefrigerant,exposureofpeopletoammoniaclouds in certain concentrations can have serious health consequences. Some

N°	Accidental eventswithMM2	Distance(m)		
		A	B	C
1	NH_3leakageinthepathbetweenthecondenserandthe mainreservoir	17	–	–
2	NH_3 leakage in the main reservoir(V-01)	155	48	27
3	NH_3 leakage in separator vessel(V-02)	149	46	28
4	NH_3 leakage in separator vessel with(V-03)	147	45	28
5	NH_3leakageinthepathbetweenthemainreservoirand the separator vessels (V-02 and V-03)	139	41	26
6	NH_3leakageinthepathbetweentheseparatorvessel(V-02) and the chamber of refrigerated products	137	40	26
7	NH_3leakageinthepathbetweentheseparatorvessel(V-03) and the room of frozen products	136	40	26

Table 14 Distances reached by three ammonia concentrations applying MM2

Individualrisk(/year)	Distance(m)	Mitigated risk (%)
1.00E—05	251	48
1.00E—06	382	41
1.00E—07	396	41
1.00E—08	479	100

Table 15 DistancescorrespondingtoindividualrisklevelsapplyingMM1andmitigation percentage.

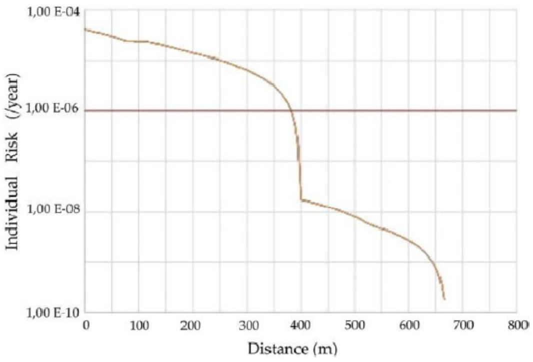

Fig. 7. Individual risk profile applying MM 1.

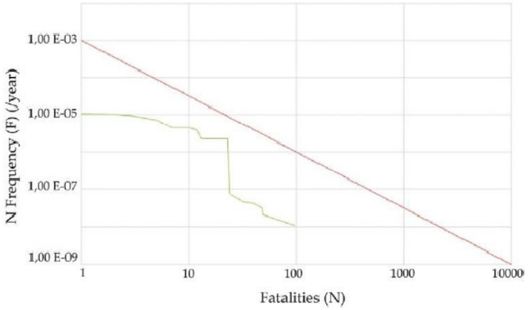

Fig.8.F–NcurvegraphapplyingMM1.

Individualrisk(/year)	Distance(m)	Mitigated risk (%)
1.00E—09	32	100
1.00E—10	39	100
1.00E—11	44	100
1.00E—12	47	100

Table 16 DistancescorrespondingtoindividualrisklevelsapplyingMM2andmitigation percentage.

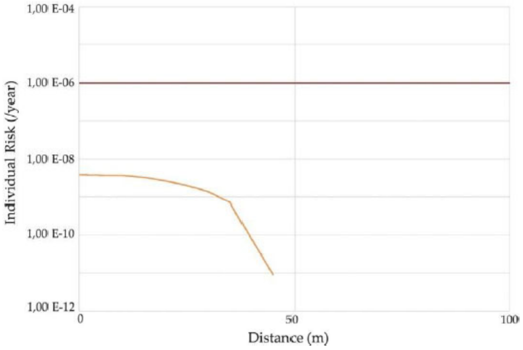

Fig. 9. Individual risk profile applying MM 2.

studiesusingQRAtoassesstheriskofaccidentsinvolving ammoniacan be found in the literature. For instance, Avasthy and Siddiqui [15] applied QRA to identify the accident scenarios of an ammonia loading facilitysurroundedbyaresidentialpopulation,andtheconsequencesof the predictions were compared with accepted internationalcriteria. OtherworkalsoappliedQRAtoevaluatethedispersionandtheeffectsof liquefiedammoniatankinthecaseofaninstantaneousrelease[12].Both worksdemonstratethatthisrefrigerationplantstudyisinlinewiththe procedurescarriedoutinotherworkswithtoxicmaterials, suchas ammonia. The former showed the maximum IR to which the general publicisexposedwasestimatedas4.03E-06/year,andSRfellmostly above and near the intolerable region. This study indicated that the maximumIRtowhichtheresidentialareaisexposedwasestimatedas 1.00E-05/year,andSRfellmostlyabovetheintolerableboundary.The latteronlytookintoaccountthetoxiceffectdistancesofthreeconcentrationsofammonia.AlthoughZolt´anetal.[16]describedanexampleof apotentialaccidentinvolvingammoniainacold-storagefacility,their workdidnotperformacompletequantitativeriskanalysis. Thisstudy presentedtheadvantageofanalyzingagreaternumberofaccidentscenariosandthreeammoniaconcentrationstoassesstheeffectsoftoxic cloud dispersion, which demonstrated that the toxic ammoniacloud reachedtheresidentialareawithoutmitigatingmeasures. Inthisstudy,itwasproposedtwomitigatingmeasures,whichare basedonapreliminaryriskanalysiscarriedoutbySME'sinrefrigeration plants.BotharecommonmeasuresandeasilyachievablebyBrazilian companies that use some type of gas in their process. The proposed mitigatingmeasuresaimedtoreducetheIRandSR.IftheSRisabovethe intolerableboundary,itisnecessarytoadoptmeasurestoreducetherisk. Theresponsibleenvironmentalagency-INEAdefinesthelimitsofboth IRandSR.Observationoftheiso-riskcontoursindicatesthattheindividualrisklevelof1.00E-06/year,consideredbyINEAasthelimitof acceptabilityfornewinstallations,reachestheresidential area.Ifthereis anysensitiveoccupationwithinthe1.00E-06/yeariso-riskboundary,the riskisconsideredunacceptablebyINEA,andmeasurestoreducetheriskaremandatory. Comparingthethreegraphsreferringtoindividualrisk,we verified thatonlythesimulationusingMM2presentsvaluesbelow theintolerable boundarystipulatedbyINEA.Theothertwosimulations withoutany measurementandusingMM1presentedacceptablevaluesonlywith distances greater than 644m and 382m, respectively. Therefore, the only acceptable condition is the case using MM2, as it presents all values belowthetolerancelimit.Regardingthesocietalriskindicatedbythe F–Ncurve,itisobservedthatonlythefirstsimulationindicatedvalues abovethelimitstipulatedbyINEA.TheuseofMM1andMM2reduced the extent of the risk, ensuring the absence of sensitive occupations withintheradiusofdistancereachedbythetoxicammonia cloud.

VI. CONCLUSIONS

Thisworkaimedtoevaluatetheriskofammonialeakage,usedasa refrigerantinanindustrialfacilitylocatedinRiodeJaneiro.Theanalysis usedPHASTcomputationalmodeling,wheresevenammonialeakscenarioswiththreedifferentconcentrationsweredescribedforthesimulation.Aftercalculatingtheriskanalysis,itwasfoundthattheriskof leakageandformationoftoxicammoniacloudamongthesevenscenariosisabovethetolerancelimitforindividualriskandsocietalrisk stipulated by INEA. The most critical scenario, indicating sensitiveoccupationswithintheradiusofthetoxiccloud,wastheaccidentalscenario with leakage between the separator vessel V-02 and the refrigeratedproductsroom.Thisscenarioreachedadistanceof2677m (IDLH), 665 m (1% probability death), and 428 m (50% probability death). The individual risk tolerance limit stipulated by the INEAof 1.00E-06/yearachievedadistanceof644m,indicatingthatitreached occupationsclosetotheinstallation.Besides,thesocietalriskgraphalso showedthattheF–Ncurvewasabovetheacceptablelimit. Thus,twomitigatingmeasureswereproposed(MM1and MM2)to reducetheriskuptothespecifiedtolerabilitylimitandweresimulated againinPHAST.MM1alsoreachedtheresidentialareaclosetothe installation,whichachievedthedistancesof1474m(IDLH),395m(1% probabilitydeath),and255m(50%probabilitydeath).TheIRlimitfor thiscasereachedadistanceof382m,anditalsoreachedtheresidential area.Nevertheless,theSRindicatedthattheF–

Ncurvewasbelowthe requiredlimit.Ontheotherhand,MM2showedamoresignificantrisk reduction and did not reach the residential area around the installation; themostcriticalscenariowasthescenariowiththeleakage inthemain reservoirandindicatedthedistancesof155m(IDLH),48 m(1%probabilitydeath)and27m(50%probabilitydeath).Besides,IRandSR indicatedvalueswaybelowthetolerancelimits.Therefore,MM2metthe limitsofINEAandensuredthateveninpossibleammonialeakagescenarios,toxicammoniacloudsdidnotreachtheresidentialareacloseto thefactory,whichindicatedgreatersafetyfortheuseofthis refrigerant in theinstallation. Thispaperdoesnotpresentananalysisofuncertaintyinthe analysis ofQRA,thereforeitpresentslimitationsrelatedtoasensitivityanalysis, which can generate great uncertainty. For future work, the authors suggestapplyingasensitivityanalysisorconsideringtheuseofother tools fortheanalysisoftoxicclouddispersion,suchasCFD.

FUNDING

Theauthorswanttoacknowledgethefinancialsupportfrom CNPq (Brazilian National Council for Scientific and Technological Development)andCNEFAPERJ(Fundaç~aodeAmparo`aPesquisadoEstadodoRio de Janeiro) 2017-E—26/202.568/2017(245,653). Credit author statement AnaRosa:Formalanalysis,Investigation,Validation,Datacuration, Writing–originaldraft.IvenioTeixeira:Formalanalysis,Investigation, Validation,Datacuration,Writing–originaldraft.AlexandreTerra: Formal analysis, Investigation, Validation, Data curation. Ahmed WA Hammad:Supervision,Validation,Writing–review&editing.Leandro TorresDiGrego´rio:Supervision,Writing–review&editing,Projectadministration. Elaine Vazquez: Supervision, Project administration, Funding acquisition. Assed Haddad: Conceptualization, Methodology, Project administration, Fundingacquisition. Declaration of competing interest Theauthorsdeclarenoconflictofinterest.Thefundershad norolein thestudy’sdesign;inthecollection,analyses,orinterpretationofdata;in thewritingofthemanuscript,orinthedecisiontopublishtheresults.

REFERENCES

[1] Z. Yang, X. Wu, Retrofits and options for the alternatives to HCFC-22, Energy 59(2013) 1–21,https://doi.org/10.1016/j.energy.2013.05.065.

[2] D.Calleja-Anta,L.Nebot-Andr´es,J.Catal´an-Gil,D.S´anchez,R.Cabello,R.Llopis,

[3] Thermodynamic screening of alternative refrigerants for R290 and R600a, Results Eng 5 (2020), https://doi.org/10.1016/j.rineng.2019.100081.

[4] N. Abas, A.R. Kalair, N. Khan, A. Haider, Z. Saleem, M.S. Saleem, Natural and synthetic refrigerants, global warming: a review, Renew. Sustain. Energy Rev. 90(2018) 557–569,https://doi.org/10.1016/j.rser.2018.03.099.

[5] W.Tan,H.Du,L.Liu,T.Su,X.Liu,Experimentalandnumericalstudyofammonia leakage and dispersion in a food factory, J. Loss Prev. Process. Ind. 47 (2017) 129–139,https:// doi.org/10.1016/j.jlp.2017.03.005.

[6] R.K.Gangopadhyay,S.K.Das,Ammonialeakagefromrefrigerationplantandthe management practice, Process Saf. Prog. 27 (2007) 15–20, https://doi.org/ 10.1002/prs.

[7] R.Bouet,S.Duplantier,O.Salvi,Ammonialargescaleatmosphericdispersion experiments in industrial configurations, J. Loss Prev. Process. Ind. 18 (2005) 512–519,https://doi.org/10.1016/ j.jlp.2005.07.016.

[8] N. Pandya, N. Gabas, E. Marsden, Sensitivity analysis of Phast’s atmospheric dispersionmodelforthreetoxicmaterials(nitricoxide,ammonia,chlorine),J.Loss Prev. Process. Ind. 25 (2012) 20–32,https://doi.org/10.1016/j.jlp.2011.06.015.

[9] J.L.Orozco,J.VanCaneghem,L.Hens,L.Gonz´alez,R.Lugo,S.Díaz,I.Pedroso,

[10] AssessmentofanammoniaincidentintheindustrialareaofMatanzas,J.Clean. Prod. 222 (2017) 934–941,https://doi.org/10.1016/j.jclepro.2019.03.024.

[11] B. Zhang, Y. Liu, S. Qiao, A quantitative individual risk assessment method in processfacilitieswithtoxicgasreleasehazards:acombinedscenariosetandCFD approach, Process Saf. Prog. 38 (2017) 52–60,https://doi.org/10.1002/prs.11979.

[12] K.Rajeev,S.Soman,V.R.Renjith,P.George,Humanvulnerabilitymappingof chemicalaccidentsinmajorindustrialunitsinKerala,Indiaforbetterdisaster mitigation, Int. J. Disaster Risk Reduct. 39 (2017) 101247, https://doi.org/ 10.1016/j.ijdrr.2019.101247.

[13] T.Ruiz-S´anchez,P.F.Nelson,J.L.François,M.J.Cruz-Go´mez,A.Mendoza, Applicationoftheaccidentconsequenceanalysisintheemergencysystemdesignof an SI cycle hydrogen production plant, Int. J. Hydrogen Energy 37 (2012) 6965–6975,https://doi.org/10.1016/j.ijhydene.2012.01.116.

[14] Z.-C. Zhang, H. Liu, S.-M. Sun, Analysis on dispersion and toxic effect of liquefied ammonia tank release based on PHAST, in: Energy Dev. Environ. Prot., 2016,https://doi.org/10.12783/dteees/edep2016/5872.

[15] F. Qu, K. Hao, H. Niu, Application of phast in the quantitative evaluation for the liquefiedammonialeakageaccidents,Adv.Mater.Res.706–708(2013)579–582.https://dx.doi.org/10.4028/www.scientific.net/AMR.706-708.579.

[16] R.Pitblado,M.Bardy,P.Nalpanis,P.Crossthwaite,K.Molazemi, M.Bekaert,

[17] V. Raghunathan, International comparison on the application of societal risk criteria,ProcessSaf.Prog.31(2012)363–368,https://doi.org/10.1002/prs.11525.

[18] Avasthy, N.A. Siddiqui, Quantitative estimation of risk to community near an ammonia rail wagon loading facility, in: Springer Trans. Civ. Environ. Eng., Springer, Singapore, 2018, pp. 115–122, https://doi.org/10.1007/978-981-10-7281-9_9.

[19] K.Zolt´an,D.Jo´zsef,K.Gyula,K.Eniko},Industrialsafetyanalysisofaccidentsinvolvingammonia,withspecialregardtocold-storagefacilities,AARMS14(2015) 273–284.

[20] G.Z.Reyes,LayerofProtectionAnalysisAppliedtoAmmoniaRefrigeration Systems, Universidad Nacional de Colombia,2008.

[21] INEA,Identificaç~aoegerenciamentodeatividadesderiscomenor,RiodeJaneiro, 2014.

[22] FEEMA, Technical Instruction for Environmental Impact

Study and Environmental Impact Report, Rio de Janeiro,2007.

[23] F.Lees,LossPreventionintheProcessIndustries:HazardIdentification,Assessment and Control, fourth ed., Butterworth-Heinemann, 2012 https://doi.org/10.1016/ C2009-0-24104-3.

[24] S. Mannan, Lees' Loss Prevention in the Process Industries, third ed., Elsevier, Oxford, UK,2005.

[25] N.S.Anjana,A.Amarnath,M.V.HarindranathanNair,Toxichazardsofammonia releaseandpopulationvulnerabilityassessmentusinggeographicalinformation system, J. Environ. Manag. 210 (2018) 201–209, https://doi.org/10.1016/ j.jenvman.2018.01.021.

[26] CCPS,GuidelinesforChemicalProcessQuantitativeRiskAnalysis,seconded.,AmericanInstituteofChemicalEngineers(AIChE), NewYork,2000.

[27] I.Benekos,D.Diamantidis,Onriskassessmentandriskacceptanceofdangerous goods transportation through road tunnels in Greece, Saf. Sci. 91 (2017) 1–10,https://doi.org/10.1016/J.SSCI.2016.07.013.

[28] J.Pei,G.Wang,S.Luo,Y.Luo,Societalriskacceptancecriteriafor pressure pipelines in China, Saf. Sci. 109 (2018) 20–26, https://doi.org/10.1016/ j.ssci.2018.05.006.

[29] S.N. Jonkman, P.H.A.J.M. Van Gelder, J.K. Vrijling, An overview of quantitative risk measures for loss of life and economic damage, J. Hazard Mater. 99 (2003) 1–30,https://doi.org/10.1016/S0304-3894(02)00283-2.

[30] H.W.M. Witlox, M. Fernandez, M. Harper, A. Oke, J. Stene, Y. Xu, Verification and validation of Phast consequence models for accidental releases of toxic or flammable chemicals to the atmosphere, J. Loss Prev. Process. Ind. 55 (2018) 457–470,https://doi.org/10.1016/j.jlp.2018.07.014.

[31] N.V.Namboothiri,A.R.Soman,Consequenceassessmentofanhydrousammonia release using CFD-probit analysis, Process Saf. Prog. 37 (2018) 525–534, https:// doi.org/10.1002/prs.11970.

[32] B.Wang,B.Chen,J.Zhao,Thereal-timeestimationofhazardousgasdispersionby the integration of gas detectors, neural network and gas dispersionmodels,

[33] J. Hazard Mater. 300 (2015) 433–442, https://doi.org/10.1016/j.jhazmat.2015.07.028.

[34] F.Pasquill,Theestimationofthedispersionofwindbornematerial, Meteorol.Mag. 90 (1961)33–49.

★★★

SUPERSONIC REFRIGERATION PERFORMANCES OF NOZZLES AND PHASE TRANSITION CHARACTERISTICS OF WET NATURAL GAS CONSIDERING SHOCK Wave Effects

[1]SMRUTIREKHA SEN, [2]SARAT KUMAR MISHRA, [3]SANTOSH KUMARA PATRA

[1]Department of Mechanical Engineering, NMIET, Bhubaneswar, 751019
[2]Department of Mechanical Engineering AIET Bhubaneswar
[3]Department of Mechanical Engineering REC Bhubaneswar
E-mail: [1]bhagwat.dhekwar@nmiet.ac.in

Abstract -
Lavalnozzleisthecriticalpartofsupersonicseparatortoproviderefrigerationenvironment.Due tothebackpressureattheoutletofsupersonicseparatorindehydrationprocess,thecondensation characteristicsofwatervaporandtherefrigerationperformancesofthenozzlesareaffectedby theshockwave.Herein,mathematicalmodelsforthesupersoniccondensationandflowofthe methane-watertwo-phaseflowmodelwereestablished,whichwereverifiedbytheexperimental data.Theeffectsofdifferentdivergentanglesontherefrigerationandcondensationbehaviorin theLavalnozzlewerestudiedconsideringshockwave.Theresultsshowthattherefrigeration performanceofthenozzlewillbeworsenunderthepresenceofshockwaves.Withthedivergent angleofthenozzleincreasedfrom2◦to8◦,thelowesttemperaturewasdecreasedfrom304.4Kto 291.8K,theliquidmassfractionatthenozzleoutletwasdecreasedfrom0.84%to0.133%,the maximumdropletradiusthatcanbeobtainedwasreducedfrom2.54×10—7mto1.69×10—7m duetotheforwardmovementsoftheshockwaves.Thedivergentangleofthenozzleisrecom-mendedtobedesignedto4◦–6◦inconsiderationoftherefrigerationperformance.

Keywords - Lavalnozzle Supersonic condensation Refrigeration Divergent angles Shock wave

---

I. INTRODUCTION

Innaturalgasextraction,alargeamountofsaturatedwater vaporisoftenaccompaniedwithnaturalgasflowingoutofthewell-head.Whenthetemperatureofnaturalgasislowerthanthe dewpointtemperature,thesaturatedwaterinthenaturalgasisseparated andthepipelineiscorrodedwiththeacidicgas.Thesupersonicseparatorisanemergingtechnologyinthefieldofnaturalgasprocessing[1,2],whichcanbeappliedfornaturalgasdehydration[3].Thewholeprocesshastheadvantagesofairtight,highefficiency, environmentalprotection,noadditionalchemicalagents, noexternalpower,etc.Thescholarshaveperformedextensiveresearchand furtherexpandedtheapplicationsofsupersonicseparatorinnaturalgasliquefaction[4,5],acidgasremoval[6,7],and heavyhy- drocarbons extraction[8,9].

Lavalnozzleandswirlingdevice[10]arecriticalpartsofthesupersonicseparator[11,12].ThedesignofLavalnozzle affectsthe gasexpansionandrefrigerationofthenozzle[13].Therefore,multipleexperimentalstudieshavebeenperformedonthesupersonic flowandcondensationofgasinthenozzle.Yellott[14]determinedthelocationofWilsonpointbystudyingtheflowofsupersaturated steamintheLavalnozzle.Prandtl[15]capturedthe“X-shock”shockwavephenomenonintheexperimentsviaflowvisualization methodandobservedtheflowfielddisturbanceduetocondensationinthenozzle.Wegener[16]andWyslouziletal.[17]usedLaval nozzlewithrectangularcross-sectiontoconductexperimentsandmeasurethecondensationandflowparametersinLavalnozzle.

Matsuoetal.[18]observedthecondensationshockwavethroughopticalexperimentsandclarifiedtheformationmechanismof condensationshockwave.Setoguchietal.[19]conductedanexperimentalstudyontheimpactofcondensationonshockwavesand boundarylayerinthesupersonicflowfieldandfoundthatcondensationhasasignificantinfluenceonthepositionofshockwaves.

MajidiandFarhadi[20]studiedtheeffectsofdifferentparametersontheshockwavepositionthroughexperimentsandnumerical simulationsandconcludedthatthecondensationefficiencyintheseparatorcanbeenhancedbyincreasingtheinletpressureand reducing the inlettemperature.

Intermsoftheoreticalresearchandnumericalcalculations[21,22],Ryzhov[23]studiedshockwavesintheLavalnozzleandanalyzedthecausesofshockwaves.Learetal.[24]simulatedthetwo-phaseflowintheLavalnozzleconsideringtheheattransfer betweenthephasesandthedissipationeffectsofsliding,andanalyzedthethermalanddynamiccharacteristicsofthetwo-phaseflowinthenozzle.Dykasetal.[25]consideredtheimpactoftheshockwaveintheLavalnozzleandexploredtheimpactofshockwavesontheevaporationofliquidphaseundersupersonicflow.Chengetal.[26,27]studiedtheaerod ynamiceffectsofcondensationandanalyzedtheinfluenceofcondensationflowfieldparameters.Wenetal.[28,29]establishedawetsteamcondensationmodeltostudytheinfluenceofshockwavesandcondensationphenomenaontheejectionefficiencyandentropylossesinthesteamejector,theestablishedmodelcouldaccuratelypredictthelowesttemperatureintheejector[30].Yangetal.[31,32]developedawatervaporcondensationmodeltostudythespontaneouscondensationphenomenoninsupersonicflows,atthesametime,thetwo-phaseflowcharacteristicsofwetsteaminthesteamejectorwerestudied.Yangetal.[33,34]performedsimulationsonthethermodynamic processesofspontaneouscondensation,dropletgrowth,andcondensationshockinLavalundernon-equilibriumconditions.Bianetal. [35–37]improvedthestructureoftheseparatortolowertheimpactoftheshockwaveontheflowfield.Also,fugacitywasintroducedtocalculatethechemicalpotentialdifferenceandtheinfluenceofactualgasoncondensationwasconsidered.ShooshtariandShahsavand[38]designedthenozzlestructurewithdifferentdivergentanglesandperformednumericalsimulationtoelucidatetherelationshipbetweentheoutletandinletpressureratioandshockwaveposition.Jassimetal.[39,40]studiedthenaturalgasflowcharacteristicsinLavalnozzleonthebasisofrealgaseffectandanalyzedtheimpactofnozzlestructureontheshockwaveposition.Intheactualproduction,tomaintainthepipelineconveyingpressuredownstreamofthesupersoniccyclone,acertainbackpressureisgenerallysetattheoutletofthesupersoniccyclone.ThebackpressuremaycauseshockwavesintheLavalnozzle[41],whichhasagreatimpactontheflowandcondensationcharacteristicsofwetnaturalgasinthenozzle.Whenthenozzlestructurechanges,thepositionoftheshockwaveswillmove,affectingthecondensationgrowthofdroplets.However,therearelimitedstudiesontheimpactofshockwavesonthesupersonicflowandcondensationcharacteristicsofwetnaturalgas.Herein,methaneandwaternon-equilibrium phase change numerical models were established considering the impact of the shock wave.Thesupersoniccondensationflowcharacteristicsofwetnaturalgasunderdifferentdivergentangleswereobtained.Also,thelocationofshockwaveinLavalnozzlewaselucidatedandtheeffectsofshockwaveongasnon-equilibriumcondensationflowparametersinthenozzlewerestudied.ThisworkcanprovidetheoreticalbasisfordesigningtheLavalnozzlelineandguidanceonthelocationoftheseparationdevice,thereby,reducingtheimpactofshockwavesondropletcondensationanddropletseparation,andimprovingtheseparation efficiency of the entire supersonic separator.

II. SIMULATION METHODOLOGIES

2.1. Detailed dimension and design for Laval nozzle

Lavalnozzlestructureprimarilyincludesfourparts,namelystraightsection,convergentsection,throat,anddivergentsection.The naturalgasflowisinahighdegreeofturbulenceinthepipeline,whichisnotconduciveforgascontractionintheconvergentsection.

Therefore,astraightsectionissetbeforethenozzleconvergentsectiontoensuretheuniformdistributionofinletvelocity.

TheWitozinskycurve,Bicubicparametriccurve,andQuinticcurvewereoftenadoptedinthedesignofconvergentsection[42].

TheWitozinskycurveshrinksfasteratthenozzleinletsection,andthecurveisgentlerwhenapproachingtheconvergentsection outlet.Thisisbeneficialforrectificationbeforethenozzlethroatandensuresuniformgasflowdistributionatthenozzlethroat.

Therefore,theWitozinskycurvewasemployedforthedesignoftheconvergentsection.Liuetal.[43]providedadetailedderivation forthethroatradiusoftheLavalnozzle.Herein,BWRSequationwasusedtocalculatethenozzlethroatbyconsideringtherealgas effectandthethroatradiuswasrt8.5mm.Theinletradiuswasdesignedtobe8timesthatoftheradiusofthenozzlethroat.The divergentsectionisoftendesignedwithcircularandstraightline,Foelsch[44]analyticalmethodandstraightline,andtaperedtube structure.ThetaperedtubestructuredesignedbyBianetal.[13]effectivelyenhancestheseparationperformanceofthesupersonic separatorbysmallerthedivergentangleoftheLavalnozzleandextendingthelengthofthedivergentsection.Therefore,thetapered tubestructurewasadoptedinthiswork.TheparametersofthenozzlearelistedinTable1,andthestructureispresentedinFig.1.

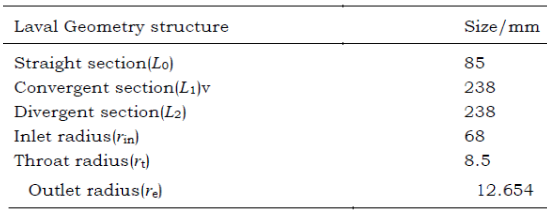

Laval Geometry structure	Size/mm
Straight section(L_0)	85
Convergent section(L_1)v	238
Divergent section(L_2)	238
Inlet radius(r_{in})	68
Throat radius(r_t)	8.5
Outlet radius(r_e)	12.654

Table 1 Detailed dimension for the Laval nozzle.

(1)ThegasreachesacriticalflowstatewhenflowsthroughtheLavalnozzlethroat,andtheMachnumberis1,andtheequationis expressed as follow[45]:

$$Ma = \frac{c_f}{c}$$

(2) Theconvergentsectionequation

$$r = \frac{r_t}{\sqrt{1 - \left[1 - \left(\frac{r_t}{r_{\text{in}}}\right)^2\right] \frac{\left(1 - \frac{x^2}{L_1^2}\right)^2}{\left(1 + \frac{x^2}{3L_1^2}\right)^3}}}$$

(3) Thedivergentsectionequation

$$L_2=\frac{r_e-r_t}{\tan\frac{\varphi}{2}}$$

2.2. Governingequationsofmathematicalmodel

Whensimulatinggascondensation,asourcetermwasneededinFluenttocalculatetheliquidflowofthecondensationdroplet. Therefore,User-DefinedScalar(UDS)wasrequiredtodefinethecondensationdroplet,andtheentirecondensationprocesswassimulatedbyaddingtheUser-DefinedFunction(UDF)[46].Asthewatervaporinthenaturalgascondensesintoliquiddrops,thegas andliquidflowcontrolequations[47,48]wereestablished separately.

(1)Thegasphasecontrolequationsareexpressedasfollows:

Continuity equation:

$$\frac{\partial \rho_g}{\partial t}+\frac{\partial}{\partial x_j}\left(\rho u_j\right)_g=S_m$$

Momentum equation:

$$\frac{\partial}{\partial t}\left(\rho u_i\right)_g+\frac{\partial}{\partial x_j}\left(\rho u_i u_j\right)_g+\frac{\partial p_g}{\partial x_i}-\frac{\partial}{\partial x_j}\left[\mu\left(\frac{\partial u_i}{\partial x_j}+\frac{\partial u_j}{\partial x_i}-\frac{2}{3}\delta\frac{\partial u_l}{\partial x_l}\right)\right]+\frac{\partial}{\partial x_j}\left(\rho\overline{u_i' u_j'}\right)_g=S_v$$

Energy Equation:

$$\frac{\partial}{\partial t}(\rho E)_v+\frac{\partial}{\partial x_j}\left(\rho u_j E+u_j p\right)_v=\frac{\partial}{\partial x_j}\left(k_{\mathrm{eff}}\frac{\partial T}{\partial x_j}+u_i\tau_{\mathrm{eff}}\right)+S_h$$

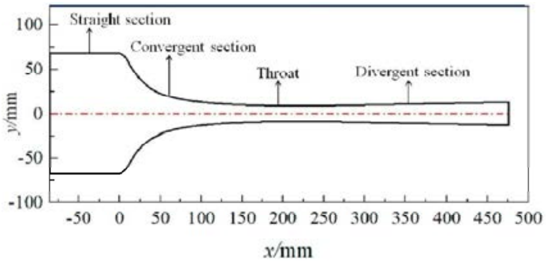

Fig. 1. Laval nozzle structure diagram.

(2)Theliquidphasecontrolequationsareexpressedasfollows:

$$\frac{\partial}{\partial t}(\rho_v Y)+\frac{\partial}{\partial x_j}\left(\rho_v u_j Y\right)=S_Y$$

$$\frac{\partial}{\partial t}(\rho_v N)+\frac{\partial}{\partial x_j}\left(\rho_v u_j N\right)=J$$

$$r_d=\sqrt[3]{\frac{3Y}{4\pi\rho_l N}}$$

(3)Thesourcetermintheequationsareexpressedasfollows:

$$S_m=-m_v$$

$$S_u=-m_v u$$

$$S_h=-m_v\left(h-h_{lv}\right)$$

(4)Inthisprogram,theUDSparametersusedinthecondensationmodelaremainlyInternallyConsistentClassicNucleationTheory model(ICCT)[49,50]anddropletgrowthrate,whichwereprogrammedintheUDFfunctiontoobtainotherparameters:

The ICCT model is expressed as follows:

$$J_{\mathrm{ICCT}}=\frac{1}{S}\frac{\rho_V^2}{\rho_L}\sqrt{\frac{2\sigma}{\pi m_0^3}}\exp\left(-\frac{16\pi}{3}\frac{\sigma^3}{k_B\rho_L^2 R_M^2 T^3(\ln S)^2}\right)\exp(\Theta)$$

The droplet growth rate is expressed as follows:

$$\frac{dr}{dt}=\frac{\lambda_V}{\rho_L h_{LV}}\frac{\left(T_s-T\right)\left(1-\frac{r_c}{r}\right)}{r\left(1+2\frac{\sqrt{8\pi}}{1.5\mathrm{Pr}_V}\frac{\gamma}{1+\gamma}\mathrm{Kn}\right)}$$

2.3. Turbulencemodel

SeveraltypesofturbulencemodelsareavailableinFluentsoftware,includingSpalart-Allmarasmodel,k-εmodel, andk-ωmodel

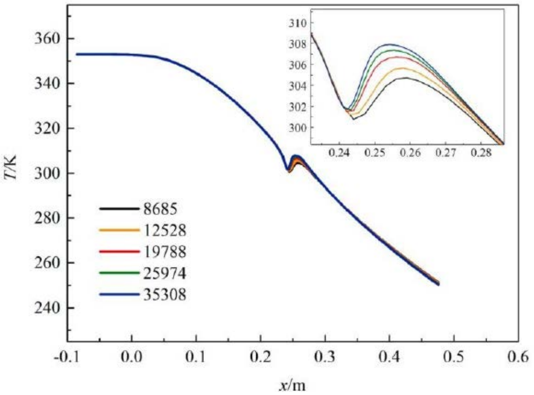

Fig. 2. Grid independence verification results.

[46].Themostwidelyusedturbulencemodelsmainlyincludestandardk-εmodel,realizablek-εmodel,standardk-ωmodel,Shear StressTransportmodel(SST)k-ω,ReynoldsStressmodel(RSM)etc.ThelowReynoldsnumberflowistakenintoaccountinthe standardk-ωmodel,andthecompressibilityandshearflowofthefluidwascorrected.Thestandardk-ωmodel[51]forcompressible gasflowinthenozzlehadhigheraccuracythanothermodels.Therefore,thestandardk-ωmodelwasadoptedinthispapertosimulate

thecondensationofwatervaporincompressiblenaturalgas.

2.4. Meshing and independenceverification

Thestructuredgridwasusedtomeshthetwo-dimensionalLavalnozzle.Asthenumberofgridsmayaffectthefinalcalculation,the 8,685,12,528,19,788,25,974,and35,308numberofgrids wererespectivelyusedtoverifythegridindependence.Thetemperature distributionatthenozzleaxisisshowninFig.2.Thetemperaturemeasurementerroronaxisatx0.256mforthegridnumber8685 and35,308was1.041%,whilethatthegridnumber19,788 and35,308wasonly0.368%.Theoveralldeviationwassmalland relativelyaccuratecalculationresultswereobtained.Consideringthecalculationefficiencyinactualoperation,thestructuredgrid withacellnumberof19,788wasusedinsimulations.

2.5. Experimentalvalidation

Themathematicalmodelandcalculationmethodwereemployedinthecalculations.ThenozzlestructureemployedbyMosesand Stein[52]wasusedinthespontaneouscondensationexperimentofwatervaporintheLavalnozzlefornumericalcalculations.Inthe experiment,anozzlewasusedbyMoses,whichthroatwas 0.010.01m(x0.0822m),asmoothtransitionofacirculararcwitha radiusof0.053mwasadoptedinthesubsonicsectionandthesupersonicsectionwascomposedofanarcwitharadiusof 0.686m.In thecase410,theinletwatervaporpressurewas70,727Pa,theinlettemperaturewas377K,andtheoutletbackpressurewas0Pa.The comparisonbetweenthecalculationresultsandexperimentaldataofMosesaredisplayedinFig.3andTable2.Atx0.103m,the phenomenonofsuddenincreaseinaxialpressurecausedbythewatervaporcondensationwaswell-capturedwiththenumerical simulationresults,whichisbasicallyconsistentwiththeexperimentalresults,indicatingthereliabilityofthesimulationresults.

III. RESULTS AND DISCUSSION

3.1. PerformanceanalysisoftheLavalnozzleunder backpressure

Whenthemixedgasnozzlereachedsupersonicspeedinthedivergentsection,theheatexchangebetweenthefluidinthenozzle andoutsidewasignoredatthistime,anditwasconsideredasanisentropicadiabaticflow.Thecalculationswereperformedbasedon thenumericalmodeldescribedinSection2,nozzleinletpressureas800,000Pa,inlettemperatureas353.15K,outlet pressureas 550,000Pa,methanemolefractionas95%,andwatervapormolefractionas5%.Theflowfielddistributionandcondensation parameterdistributioninthenozzleareshowninFig.4. ThedistributionsoftheflowparametersareshowninFig.4(a)–(d).Intheconvergentsectionofthenozzle,asthecross-sectional areaofthenozzlecontinuedtoshrink,theMachnumberincreased,andthepressureandtemperaturecontinuedtodecrease.The internalenergyandpressurepotentialenergygraduallytransformedintokineticenergyandtheMachnumberatthethroatreached1. Atthistime,thedegreeofsupercoolingofthenozzleincreasedcontinuously.Inthedivergentsectionofthenozzle,thegascontinuouslyexpandedandthedegreeofsupercoolingcontinuedtoincrease,atx=0.228m,thedegreeofsupercoolingreachedthe

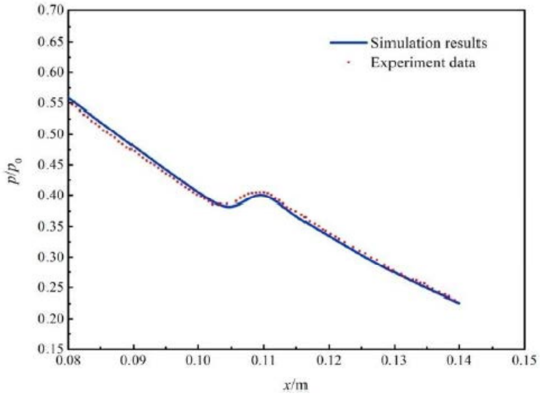

Fig. 3. Comparison of simulation and experimental results.

Distance from throat/m	p/p_0		Relative error
	Simulation	Experiment	
x_1= 0.084	0.528	0.518	0.019
x_2=0.103	0.385	0.387	0.005
x_3=0.122	0.319	0.325	0.018

Table 2
Relative error of p/p0 under different location between simulation and experimental data

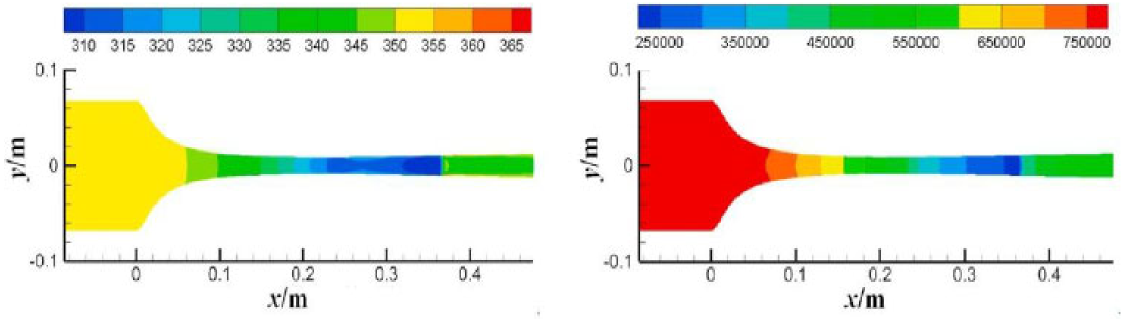

(a) Temperature/K **(b)** Pressure/Pa

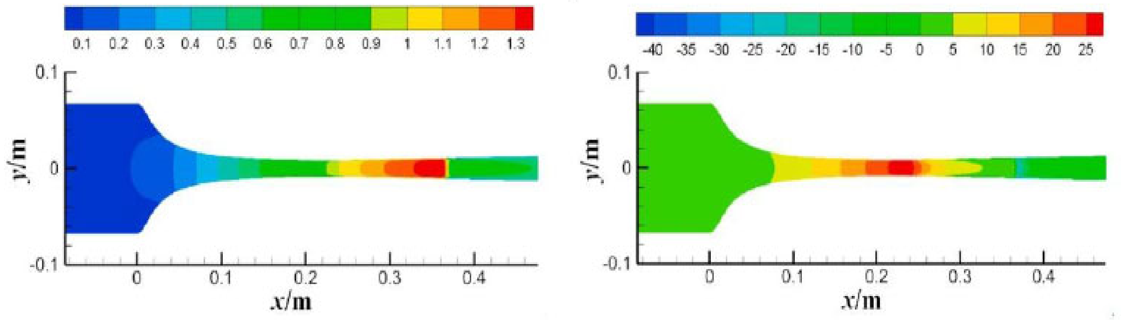

(c) Mach number/Dimensionless **(d)** Degree of supercooling/K

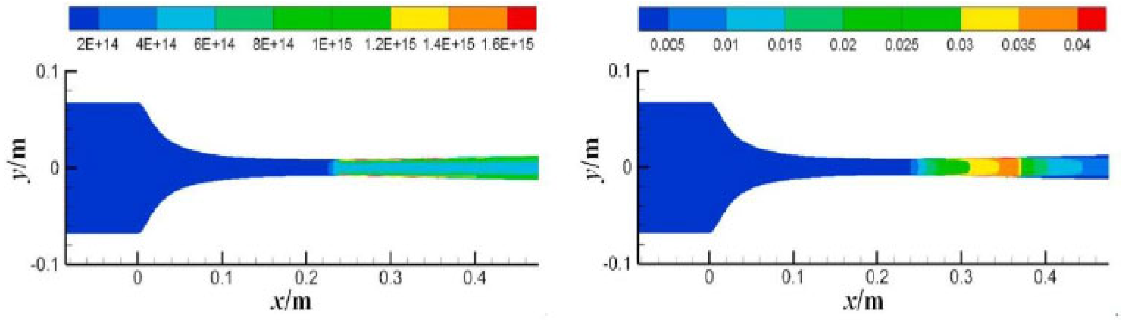

(e) Droplet number/kg^{-1} **(f)** Liquid mass fraction/Dimensionless

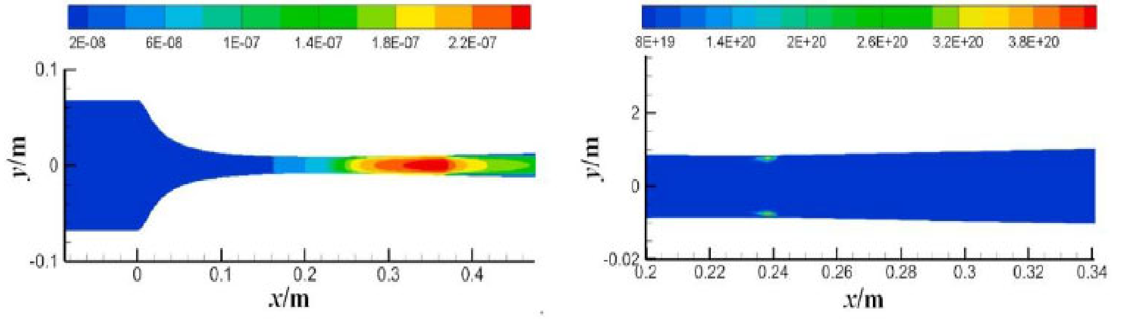

(g) Droplet radius/m **(h)** Nucleation rate/m$^{-3}\cdot$s^{-1}

Fig. 4. Distribution of flow and condensation parameters in Laval nozzle with 2◦ divergent angle.

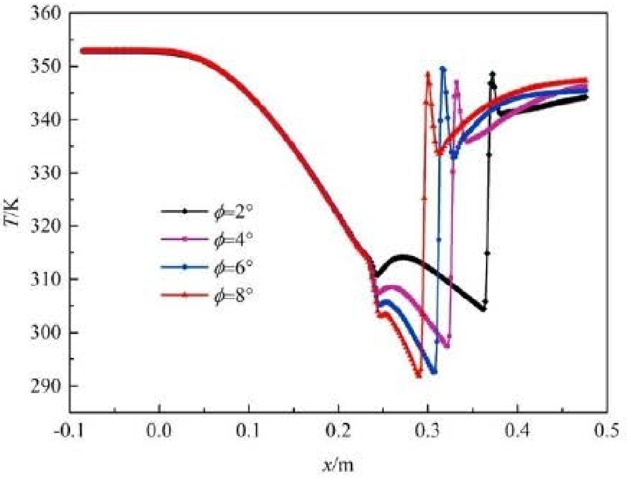

(a) Temperature/K

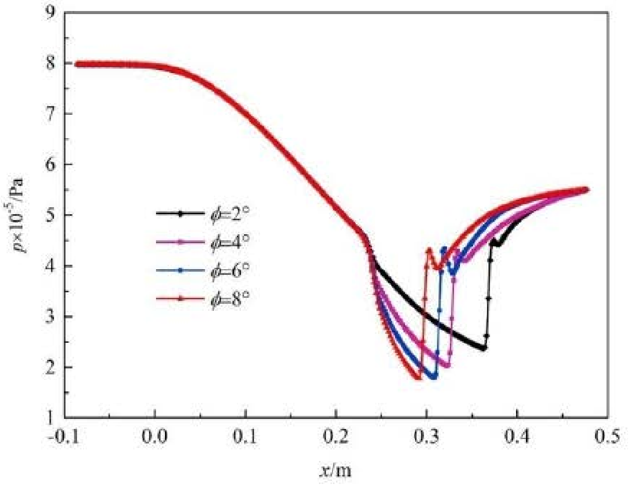

(b) Pressure/Pa

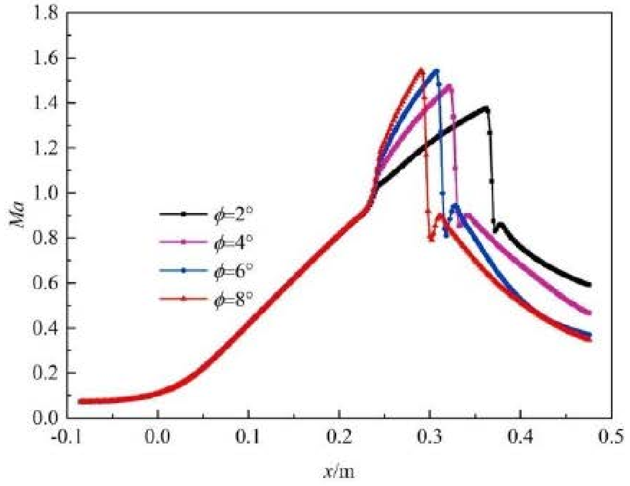

(c) Mach number/Dimensionless

Fig. 5. Axial flow parameters distribution diagram with different divergent angles.

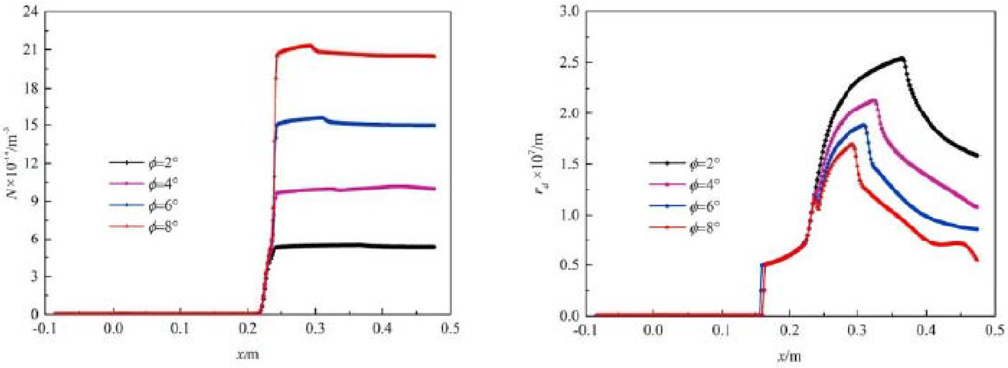

(a) Droplet number/kg^{-1}

(c) Droplet radius/m

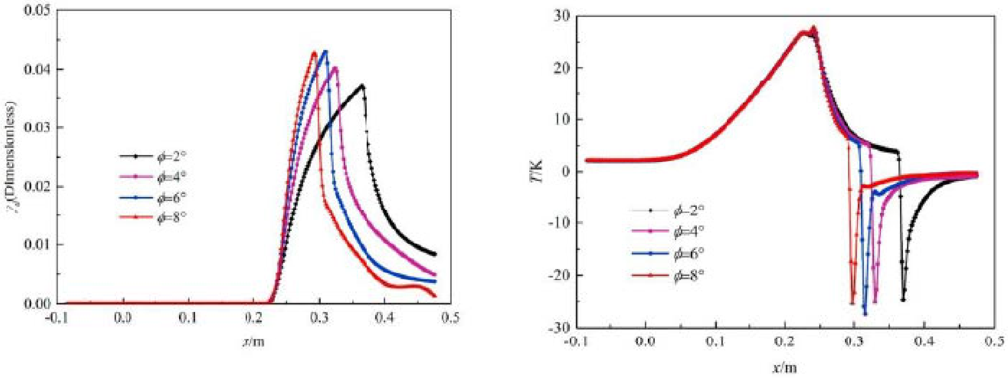

(b) Liquid mass fraction/Dimensionless

(d) Degree of supercooling/K

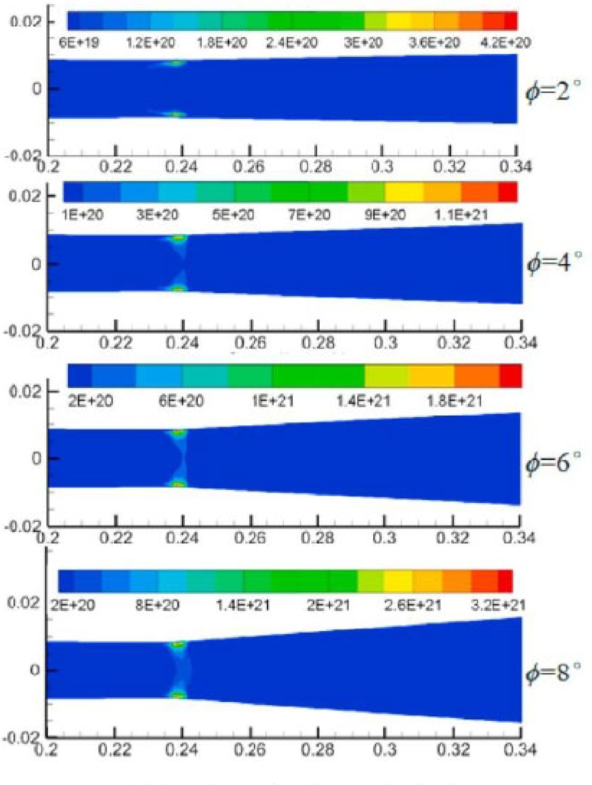

(e) Droplet nucleation rate/m$^{-3}\cdot$s^{-1}

Fig. 6. Distribution of condensation parameters at different divergent angles.

maximum26.8K.Thewatervaporinthemethane-watertwo-componentbecamesaturatedorevensupersaturatedfromtheunsaturatedstate,andthepressureandtemperaturecontinuedtodroptotheWilsonpoint.Therefore,thesteamreachedthenucleation condition.Asthegasexpandsnearthewallmorerapidlyandviolentlythanatthecentralaxis,thedegreeofsupercoolingatthewall washigherthanthatatthecentralaxis.Thewatervapornearthewallfirstreachedthenucleationconditions,condensedand nucleated(asshowninFig.4(h),themaximumnucleationratewas4.381020m—3s—1).Therewasareleaseofthelatentheatof condensation,whichdestroyedthenucleationconditions,andthenthenucleationratedroppedto0.Then,thegascontinuedto expandandthetemperaturedecreased,watervaporcontinuedtoaccumulateandgrowonthesurfaceofthecondensationnodules, andthedropletradiuscontinuedtoincreaseto2.5410—7m.Duetothenozzleoutletbackpressure,theshockwaveappearedatx 0.362mbehindthethroat,whichdestroyedtherefrigerationconditionsinthenozzle,leadingtotemperaturerise,pressurerise,Mach numberdrop,degreeofsupercoolingdrop,dropletevaporation,dropletradiusdecrease,andcontinuousloweringofliquidmass fraction.Tillthenozzleoutlet,theradiusofthedropletatthenozzleaxiswasreducedto1.58×10—7m.

3.2. Effectofdifferentdivergentanglesonflowparameter

Theboundaryconditionsofthenozzlearepresentedinsection3.1.Thepressure,temperature,Machnumber,andshockwave positionsintheLavalnozzleatdifferentdivergentangles wereanalyzed,andtheresultsaredisplayedinFig.5.

Thenozzlepressure,temperature,andMachnumberdistributionofdifferentdivergentangleswerebasicallythesameinthe convergentsection,buttherewerehugedifferencesinthedivergentsection.

AsshowninFig.5(a),whenthedivergentangleswere2◦,4◦,6◦,and8◦,thecorrespondingminimumtemperaturesatthenozzle axiswere304.4K,297.4K,292.6K,and291.8K,respectively.Withthelargerdivergentangle,thetemperaturedropinthenozzle continuedtoincreaseandthelowesttemperatureposition continuedtomovetowardsthenozzlethroat,whichcanprovidealow temperatureenvironmentfordropletnucleationandgrowthearlier.Undertheconditionofthenozzleoutletbackpressureof550,000 Pa,theshockwaveswereclearlygeneratedinthenozzle.Whenthedivergentangleswere2◦,4◦,6◦,and8◦,theshockwavelocations obtainedbynumericalsimulationswerex0.362m,0.322 m,0.306m,and0.290m.Theshockwavelocationsconstantlymoved towards the nozzlethroat.

AnalyzingthepressuredistributionatthenozzleaxisinFig.5(b),whenthedivergentangleincreasedfrom2◦to8◦,thecorrespondingminimumpressuredecreasedfrom237,080Pato177,816Pa.Asthedivergentangleincreased,therewasgreaterpressure dropinthenozzle.Howeverwhenthedivergentangleswere6◦and8◦,themaximumpressuredropdifferencewasonly1573Pa.

Fig.5(c)showsthedistributionofMachnumberatthenozzleaxis.Asthedivergentangleincreasedfrom2◦to8◦,themaximum Machnumberincreasedfrom1.38to1.54.Whenthedivergentanglesofthenozzlewere6◦and8◦,thehighestMachnumberinthe nozzlewasbasicallythesame.Inthelatterhalfofthedivergentsectionofthenozzle,theMachnumbercurvesofthetwonozzles almostcoincided.Increasingthedivergentanglecanleadtogreaterpressuredrop,thelowertemperature,andgreater Machnumber, whiletheMachnumberandtemperatureatthenozzleoutletgraduallyapproachedthesamevalue.

3.3. Effectofdifferentdivergentanglesoncondensationparameter

Thecondensationparametersandshockwavepositionsin Lavalnozzleswithdifferentdivergentangleswereanalyzed,andthe results are shown in Fig.6.

Fig.6(a)–(d)showthedistributionsofcondensationparametersfordifferentdivergentangles.Withthelargerdivergentangle,the numberofdropletsatthenozzleaxiskeptincreasing,themaximumliquidmassfractioncontinuedtorise,themaximumdropletradius thatcanbeobtainedcontinuedtodecrease,andthemaximumdegreeofsupercoolingwasalmostthesame.

Whenthedivergentanglesofthedivergentsectionwere2◦,4◦,6◦,and8◦,themaximumliquidmassfractionsthatcouldbe obtainedwere3.7%,4.02%,4.3%,and4.28%,respectively.Whenthedivergentanglewas8◦,themaximumliquidmassfractionwas slightlydecreasedrelativetothedivergentangleof6◦.Howeverwiththeincreaseinnozzledivergentanglefrom2◦to8◦,theliquid massfractionatthenozzleoutletwasdecreasedfrom0.84%to0.133%,andthemaximumdropletradiusthatcanbeobtainedwas reducedfrom2.5410—7mto1.6910—7m.Thisisbecausetheincreaseindivergentangleandtheforwardmovementoftheshock wavedestroyedthelowtemperatureenvironmentinthenozzleandreducedthedegreeofsupercooling.Whenthedivergentanglewas

2◦,thedegreeofsupercoolingwasfirstreducedtobelow0 Kat0.366m,andwhenthedivergentanglewas8◦,thedegreeof supercoolingwasfirstreducedtobelow0Katx0.294m,whichshortenedthedropletgrowthspaceandthemaximumdropletradius thatcouldbeobtainedwascontinuouslyreduced.Especially,aftershockwave,thedegreeofsupercoolingdroppedsharply,destroying therefrigerationenvironmentofdropletgrowth.Thedropletunderwentsecondaryevaporationandtheliquidmassfractionofthe outlet liquid phase was greatlyreduced.

Fig.6(e)showsthenucleationratedistribution.Withtheinletpressureandcontentofcondensablecomponentsremainingunchanged,thenucleationratepositionwasbasicallythesame.Thisisbecauseasthewatervaporcontentwasconstant,thewatervapor partialpressuredidnotchangeandthelocationinthenozzlereachedthesupersaturationdegreeofcondensation,hence,thelocation ofnucleationwasalmostunchanged.However,thelargerthedivergentangle,thehigherwasthedegreeofgasexpansioninthe divergentsection.Theminimumtemperaturethatcouldbeobtainedincreased,andthenucleationrateincreased.Whenthedivergent anglewas2◦,themaximumnucleationratewas4.38 1020m—3/s,whilewhenthedivergentanglewas8◦,themaximumnucleation rate was 3.31 1021 m—3/s, an increase in the nucleation rate by an order of magnitude.

Thelargerthedivergentangle,themoreintensethegasexpansion,whichcanprovidealowtemperatureenvironmentfordroplet nucleationandgrowthearlier,butitwillalsocausetheshockwavelocationsconstantlymovedtowardsthenozzlethroat,shortenthe lengthoftherefrigeratedsectioninthenozzle,andcausethecondenseddropletradiustodecreasesgradually,whichisnotconducive tosubsequentdropletseparation.Whenthedivergentangleis6◦and8◦,thehighestdegreeofsupercoolingis27.4Kand27.6K, respectively,themaximumMachnumberandminimumtemperatureatthenozzlegraduallyapproachedthesamevalue.Therefore, whenthereisbackpressureatthenozzleoutlet,thedivergentangleisrecommendedtobedesignedto4◦–6◦inconsiderationofthe subsequent swirling separation ofdroplets.

IV. CONCLUSION

Herein,numericalsimulationsofthenon-equilibriumphasetransitionofmethane-watertwo-componentwereperformed.By changingtheangleofthedivergentsection,therefrigerationperformancesofthenozzleandcondensationparametersofwatervapor werestudied.Also,theimpactoftheflowfieldandshockwavepositioninthenozzleunderdifferentdivergentangles wereanalyzed. The results showthat: Therefrigerationconditionsinthenozzlewouldbedestroyedbyshockwaves,leadingtotheriseoftemperatureandpressure,the dropofMachnumberanddegreeofsupercooling,andthedecreaseofdropletradiusandliquidmassfraction.

Withtheincreaseinnozzledivergentanglefrom2◦to8◦,theshockwavelocationsconstantlymovedfromx0.362mtox 0.290m,thelowesttemperaturewasdecreasedfrom304.4Kto291.8K,themaximumdropletradiusthatcanbeobtainedwas reducedfrom2.5410—7mto1.6910—7m.Aftershockwaves,thedegreeofsupercoolingdroppedsharply,destroyingthe refrigerationenvironmentofdropletgrowth.Thedropletunderwentsecondaryevaporationandtheliquidmassfractionatthenozzle outletwasgreatlyreducedfrom0.84%to0.133%.Therefore,whenthereisbackpressureatthenozzleoutlet,thedivergentangleof thedivergentsectioncanbedesignedto4◦–6◦inconsiderationofthesubsequentswirlingseparationofdroplets.

Intheactualproduction,thebackpressureofnozzleoutletwillcauseshockwavesintheLavalnozzle.Theshockwavescausethe watervaporpressureandtemperatureofwatervaportorisesharplyinashortduration,causingthecondenseddropletstore-evaporate.Bysimulatingtheperformanceofthenozzleunderdifferentdivergentangles,theimpactofshockwavesonthenozzle flowparameterswasanalyzed.Byreasonablycontrolling thedegreeofthedivergentangle,theshockwavepositioncanbemoved backwardtoensurethegrowthspaceofthedroplets,thereby,ensuringthedehydrationefficiencyoftheLavalnozzle. Therefore,some measuresmustbeadoptedtoeliminatetheinfluenceofenvironmentshockwave.Theeffectsofshockwavesshouldbeconsideredin the nozzledesign.

AUTHOR STATEMENT

Xuewen Cao: Conceptualization, Methodology, Investigation, Writing-Original draft preparation and Revising Yang Liu: Formal analysis and Reviewing XueruiZang:FormalanalysisandReviewing DanGuo:Numericalsimulation Jiang Bian: Conceptualization, Investigation, Revising and Editing

DECLARATION OF COMPETING INTEREST

Theauthorsdeclarethattheyhavenoknowncompetingfinancialinterestsorpersonalrelationshipsthatcouldhaveappearedto influence the work reported in thispaper.

ACKNOWLEDGEMENTS

ThisworkwassupportedbytheNationalNaturalScienceFoundationofChina(GrantNo.52074341)andNationalKeyR&D Program of China (Grants No.2016YFC0802302).

NOMENCLATURE

A	Laval nozzle section area(m^2)
c	local speed of sound(m/s)
c_f	gas flow rate(m/s)
dr_d/dt	droplet growth rate (ms^{-1})
E	total energy (Jkg^{-1})
h_{lv}	latent heat of condensation (Jkg^{-1})
J	nucleation rate ($m^{-3}s^{-1}$)
Kn	Kundsen number(—)
k_B	Boltzmann constant–()
k_{eff}	effective thermal conductivity ($W\ m^{-1}K^{-1}$)
L_0	straight section(mm)
L_1	convergent section(mm)
L_2	divergent section(mm)
m_o	mass of single molecule(g)
m_v	liquidmassperunitvolumeofcondensationinunittime($kgm^{-3}s^{-1}$)
Ma	Math number–()
N	droplet number per mass of gas(kg^{-1})
n	droplet number–()
p	pressure(Pa)
Pr_v	Prandtl number(—)
R_M	gas constant–()
r	Laval nozzle radius(m)
r_c	criticalradius(m)
r_d	droplet radius(m)
r_e	Laval nozzle outlet radius(m)
r_{in}	Laval nozzle inlet radius(m)
r_t	Laval nozzle throat radius(m)
S	degree of supersaturation ()
S_h	source term in energy equation ($Jm^{-3}\ s^{-1}$)
S_m	source term in continuity equation ($kgm^{-3}\ s^{-1}$)
S_u	source term in momentum equation ($kgm^{-2}\ s^{-2}$)
t	time(s)
T	temperature(K)
T_s	saturation temperature of vapor(K)
u	velocity(ms^{-1})
u'	velocityfluctuation(ms^{-1})
V	volume(m^3)
x	arbitrarylengthalongtheaxisofnozzle(m)
Y	liquid fraction(—)

Greek symbols

γ	specific heat ratio(—)
δ_{ij}	Kronecker delta–()
θ	dimensionless surface tension ()
μ	chemical potential ($Jmol^{-1}$)
ρ	density (kgm^{-3})
σ	droplet surface tension (Nm^{-1})
τ_{eff}	effective stress tensor–()
λ_v	gas thermal conductivity ($Wm^{-1}K^{-1}$)

Subscripts

t	Laval nozzlethroat
in	Laval nozzleinlet
e	Laval nozzleoutlet
i,j	x, $y$axis
l	liquidphase
v	vaporphase

REFERENCES

[1] Alfyorov,L.Bagirov,L.Dmitriev,V.Feygin,S.Imayev,Supersonicnozzleefficientlyseparatesnaturalgascomponents,OilGasJ.103(2005)53–58.

[2] F. Okimoto, J.M. Brouwer, Supersonic gas conditioning, World Oil 223 (2002)89–91.

[3] X.W.Cao,J.Bian,Supersonic separationtechnologyfornaturalgasprocessing:areview,Chem.Eng.Process136(2017)138–151.

[4] J.Bian,X.W.Cao,W.Yang,S.Gao,C.C.Xiang,Anewliquefactionmethodfornaturalgasbyutilizingcoldenergyandseparatingpowerofswirlnozzle,AIChEJ. 66 (2020)16811.

[5] J.Bian,X.W.Cao,L.Teng,Y.Sun,S.Gao,Effectsofinletparametersonthesupersoniccondensationandswirlingcharacteristicsofbinarynaturalgasmixture, Energy 188 (2017)116082.

[6] L.DeO.Arinelli,T.A.F.Trotta,A.M.Teixeira,J.L.DeMedeiros,F.A.O.DeQueiroz,OffshoreprocessingofCO_2richnaturalgaswith supersonicseparatorversus conventional routes, J. Nat. Gas Sci. Eng. 46 (2017)199–221.

[7] C.Wen,N.Karvounis,J.H.Walther,Y.Yan,Y.Feng,Y.Yang,AnefficientapproachtoseparateCO₂usingsupersonicflowsforcarboncaptureandstorage,Appl. Energy 238 (2017)311–319.

[8] D.Ghosh,D.Bergmann,R.Schwering,J.Wölk,R.Strey,S.Tanimura,B.E.Wyslouzil,Homogeneousnucleationofahomologousseriesof *n*-alkanes(C_iH_{2i2},

[9] *i* 7-10) in a supersonic nozzle, J. Chem. Phys. 132 (2010), 024307.

[10] R.Secchi,G.Innocenti,D.Fiaschi,Supersonicswirlingseparatorfornaturalgasheavyfractionsextraction:1DmodelwithrealgasEOSforpreliminarydesign, J. Nat. Gas Sci. Eng. 34 (2016)197–215.

[11] Y.Amini,M.Mokhtari,M.Haghshenasfard,M.B.Gerdroodbary,HeattransferofswirlingimpingingjetsejectedfromNozzleswithtwistedtapesutilizingCFD technique, Case Stud. Therm. Eng. 6 (2015)104–115.

[12] C.Wen,H.B.Ding,Y.Yang,Optimisationstudyofasupersonicseparatorconsideringnonequilibriumcondensationbehaviour,EnergyConvers.Manag.222 (2020)113210.

[13] K.A.Pathan,P.S.Dabeer,S.A.Khan,OptimizationofarearatioandthrustinsuddenlyexpandedflowatsupersonicMachnumbers,CaseStud.Therm.Eng.12 (2018)696–700.

[14] J.Bian,W.M.Jiang,L.Teng,Y.Liu,S.W.Wang,Z.F.Deng,Structureimprovementsandnumericalsimulationofsupersonicseparators,Chem.Eng.Process110 (2016)214–219.

[15] J.I. Yellott, Supersaturated steam, Trans. Am. Soc. Mech. Eng. 56 (1934)411–430.

[16] L. Prandtl, General considerations on the flow of compressible fluids, Volta Congress, December 30 - October 6, 1935. RomeItaly.

[17] P.P. Wegener, Nonequilibrium flow with condensation, Acta Mech. 21 (1975)65–91.

[18] B.E.Wyslouzil,J.L.Cheung,G.Wilemski,R.Strey,Smallangleneutronscatteringfromnanodropletaerosols,Phys.Rev.Lett.79(1997)431.

[19] K.Matsuo,S.Kawagoe,K.Sonoda,K.Sakao,Studiesofcondensationshockwaves:part1,mechanismsoftheirformation,Bull.JSME28(1985)1416–1422.

[20] T.Setoguchi,S.Matsuo,S.Yu,H.Hirahara,Effectofnonequilibriumhomogenouscondensationonflowfieldsinasupersonicnozzle, J.Therm.Sci.6(1997) 90–96.

[21] D.Majidi,F.Farhadi,Supersonicseparator'sdehumidificationperformancewithspecificstructure:experimentalandnumericalinvestigation,Appl.Therm. Eng. 179 (2020)115551.

[22] B.Elhub,S.Mat,K.Sopian,A.M.Elbreki,M.H.Ruslan,A.A.Ammar,PerformanceevaluationandparametricstudiesonvariablenozzleejectorusingR134A, Case Stud. Therm. Eng. 12 (2018)258–270.

[23] Y.Huang,P.Y.Wang,Y.Dou,F.Xing,Chemicalnon-equilibriumflowanalysisofH_2fueledscramjetnozzle,CaseStud.Therm.Eng.5(2015)89–97.

[24] O.S. Ryzhov, Shockwave formation in Laval nozzles, J. Appl. Math. Mech. 27 (1963)453–494.

[25] W.E.Lear,S.A.Sherif,J.R.Langford,Efficiencyandgasdynamicanalysisoftwo-phasemixturesinsupersonicnozzleswithinter-

phaseheattransferandslip, Acta Astronaut. 40 (1997)701–706.

[26] S.Dykas,A.Szymański,M.Majkut,Liquidphaseevaporationonthenormalshockwaveinmoistairtransonicflowsinnozzles,J.Therm.Sci. 26(2017)214–222.

[27] W. Cheng, X.S. Luo, M.E.H. Van Dongen, On condensation-induced waves, J. Fluid Mech. 651 (2010)145.

[28] Y.Cao,W.Cheng,X.Luo,J.Yang,NumericalinvestigationofhomogeneouscondensationinPrandtl–Meyerexpansionflows,ShockWaves27(2017)271–279.

[29] C.Wen,N.Karvounis,J.H.Walther,H.B.Ding,Y.Yang,Non-equilibriumcondensationofwatervapourinsupersonicflowswithshockwaves,Int.J.HeatMass Tran. 149 (2020)119109.

[30] C.Wen,L.Gong,H.BDing,Y.Yang,Steamejectorperformanceconsideringphasetransitionformulti-effectdistillationwiththermalvapourcompression (MED-TVC) desalination system, Appl. Energy 279 (2020)115831.

[31] C.Wen,H.B.Ding,Y.Yang,Performanceofsteamejectorwithnonequilibriumcondensationformulti-effectdistillationwiththermalvapourcompression (MED-TVC) seawater desalination system, Desalination 489 (2020)114531.

[32] Y.Yang,J.H.Walther,Y.Y.Yan,C.Wen,CFDmodelingofcondensationprocessofwatervaporinsupersonicflows,Appl.Therm.Eng.115(2017)1357–1362.

[33] Y.Yang,X.W.Zhu,Y.Y.Yan,H.B.Ding,C.Wen,Performanceofsupersonicsteamejectorsconsideringthenonequilibriumcondensationphenomenonfor efficient energy utilisation, Appl. Energy 242 (2017)157–167.

[34] Y.Yang,S.Q.Shen,X.S.Mu,R.Liu,S.H.Zhou,Investigationofthepressurecharacteristicsofasupersonicsteamflowwithnonequilibriumphasechange,Heat Tran. Res. 43 (2012)633–650.

[35] Y.Yang,S.Q.Shen,Numericalsimulationonnon-equilibriumspontaneouscondensationinsupersonicsteamflow,Int.Commun.HeatMass36(2009)902–907.

[36] J.Bian,X.W.Cao,W.Yang,X.D.Song,C.C.Xiang,S.Gao,Condensationcharacteristicsofnaturalgasinthesupersonicliquefactionprocess,Energy168(2017) 99–110.

[37] J.Bian,X.W.Cao,W.Yang,M.A.Edem,P.B.Yin,W.M.Jiang,SupersonicliquefactionpropertiesofnaturalgasintheLavalnozzle,Energy159(2018)706–715.

[38] J.Bian,X.W.Cao,W.Yang,D.Guo,C.C.Xiang,Predictionofsupersoniccondensationprocessofmethanegasconsideringrealgaseffects,Appl.Therm.Eng. 164 (2020)114508.

[39] S.H.R.Shooshtari,A.Shahsavand,Maximizationofenergyrecoveryinsidesupersonicseparatorinthepresenceofcondensationandnormalshockwave,Energy 120 (2017)153–163.

[40] E.Jassim,M.A.Abdi,Y.Muzychka,Computationalfluiddynamicsstudyforflowofnaturalgasthroughhigh-pressuresupersonicnozzles:part1.realgaseffects and shockwave, Petrol. Sci. Technol. 26 (2008)1757–1772.

[41] E.Jassim,M.A.Abdi,Y.Muzychka,Computationalfluiddynamicsstudyforflowofnaturalgasthroughhigh-pressuresupersonicnozzles:part2.nozzle geometry and vorticity, Petrol. Sci. Technol. 26 (2008)1773–1785.

[42] J.S. Pan, P. Peng, Fundamentals of Gasdynamics, National Defense Industy Press, 2011, pp.180–183.

[43] E.Witoszynski,ÜberStrahlerweiterungundStrahlablenkung,VorträgeausdemGebietederHydro-undAerodynamik(Innsbruck1922),Springer,1924,pp.248–251.

[44] H.W.Liu,Z.L.Liu,J.Zhang,Y.X.Feng,T.M.Yan,Nozzlethroatdesignunderrealgascondition,J.Eng.Thermophys.27(2006)862–864.

[45] K.Foelsch,TheanalyticaldesignofanaxiallysymmetricLavalnozzleforaparallelanduniformjet,J.Aeronaut.Sci.16(1949)161–166.

[46] J.X.Wang,Y.Z.Li,J.X.Li,C.Li,Y.Zhang,X.W.Ning,Agas-atomizedspraycoolingsystemintegratedwithanejectorloop:ejectormodelingandthermal performance analysis, Energy Convers. Manag. 180 (2017)106–118.

[47] Fluent Ansys, Fluent User's Manual, vol. 13, Software release,2006.

[48] G.J.Zhang,X.Z.Zhang,F.F.Wang,D.B.Wang,Z.L.Jin,Therelationshipbetweenthenucleationprocessandboundaryconditionson non-equilibrium condensing flow based on the modified model, Int. J. Multiphas. Flow 114 (2017)180–191.

[49] G.J.Zhang,F.F.Wang,D.B.Wang,T.Q.Wu,X.Qin,Z.L.Jin,Numericalstudyofthedehumidificationstructureoptimizationbasedonthemodifiedmodel, Energy Convers. Manag. 181 (2017)159–177.

[50] X.Han,W.Zeng,Z.Han,Investigationofthecomprehensiveperformanceofturbinestatorcascadeswithheatingendwallfences,Energy174(2017) 1188–1199.

[51] X.Han,W.Zeng,Z.Han,P.Li,J.Qian,Effectofthenonaxisymmetricendwallonwetsteamcondensationflowinastatorcascade,EnergySci.Eng.7(2017) 557–572.

[52] F.R. Menter, Two-equation eddy-viscosity turbulence models for engineering applications, AIAA J. 32 (1994)1598–1605.

[53] C.A.Moses,G.D.Stein,OnthegrowthofsteamdropletsformedinaLavalnozzleusingbothstaticpressureandlightscatteringmeasurements,J.Flu idEng.100 (1978)311–322.

★★★

COACTION OF THERMAL CONDUCTIVITY ENHANCEMENT IN BINARY POLYMER MATRIX BINARY NANO PARTICLE REINFORCED COMPOSITE

[1]SUJEET YADAV, [2]PRADYUT KUMAR SWAIN, [3]MANASI LENKA

[1]Department of Mechanical Engineering, NMIET, Bhubaneswar, 751019
[2]Department of Mechanical Engineering AIET BHUBANESWAR
[3]Department of Mechanical Engineering REC BHUBANESWAR
E-mail: [1]suryakant.parida@nmiet.ac.in

Abstract - In recent years, high strength and low cost conductive polymer composites have attracted a considerable attention of worldwide researchers due to their wide range of applications. Usually, they are being made by adding high volume fraction of conductive reinforcing fine particles in polymers, which is expensive and also causes some problems as it reduces the moldability and draw ability of the composites. Binary polymer matrix with binary conductive particle reinforced composite could be a solution to overcome the challenges. This study is designed to develop a conductive binary matrix polymer composites composed of polymers of high strength (polypropylene, PP) and soft but conductivity friendly (ethylene-co-vinyl acetate, EVA) with relatively lower amount of conductive binary nano filler materials (carbon black and alumina powder). For doing this, samples were prepared by mixing all ingredients (PP 60wt%, EVA 40wt%) and their thermal conductivity values were measured. After detailed experimental study, it has been revealed that the thermal conductivity of the developed binary nano particle reinforced composite is nearly 12 times higher than that of the pure PP and 10 times higher that of pure EVA, whereas the conductivity is significantly lower if the reinforcing particles (carbon and alumina) are usedseparately.

Keywords - Polypropylene, Ethylene-Co-Vinyl Acetate, Binary Matrix, Binary Filler, Thermal Conductivity

I. INTRODUCTION

Among different types of polymers used, polypropylene is light, low cost, easy of processing and excellent chemical stability with high mechanical strength [1,2]. This polymer is not only used in plastic industries, but it is also used in bulk volume as fibres in textile industries. On the other hand, polymers like polyanylene, polyvinyl alcohol, polyethylene-co-vinyl acetate, etc have moderate to high thermal conductivity. Conducting polymeric materials also have a wide range of uses for making antistatic coatings, electromagnetic shielding materials, biomaterials, semiconductors and batteries [3,4,7,8]. As we know, PP has good mechanical properties, however, its conductivity is relatively poor. On the other hand, compared to PP, EVA has better thermal and electrical conductivities, but it is relatively soft. In this situation, binary matrix (PP and EVA) polymer could be a good choice for a more balanced mechanical and thermal property combination [9-11]. EVA added PP binary polymer has also drawn considerable attention to be used in smart fabric, which can give comfortness as well as high durability because of its relatively high strength [3-7]. Different particles are increasingly being used as additives in polymers to simultaneously enhance a variety of properties without sacrificing other useful qualities of the base polymers. Carbon black,activated carbon and alumina, for example, have very high thermal and electrical conductivities. As a consequence,thesefillerscanbeusedto convertthermally and electrically insulating polymers into conductive materials [12-14].

II. MATERIALS AND EXPERIMENTAL PROCEDURE

For making binary polymer matrix PP and EVA along with two different fillers as carbon black and alumina powders were collected from the local market.

In development of the composite, at first, the ingredients of the binary polymer matrix (PP 60wt% and EVA 40wt%) along with 6wt% (compared to the total weight of PP and EVA) the nano filler particles (carbon black and alumina of particle size less than 100nm, Fig.1) singly or in combination (as binary filler material) were melted and blended in a simple polymer melting and blending unit having rotational speed range from 0 to 60 rpm and temperature range up to 450°C. To begin, all compounds ingredients were mixed at 190°C in the blending unit using a 30 rpm speed for 10min.

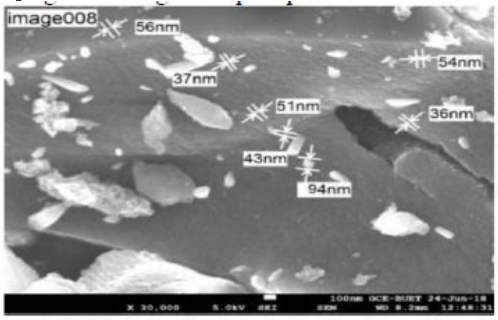

Figure 1: SEM photomicrograph showing the particle size of filler material.

The molten polymer from the blending machine was then transferred to an aluminum mold and the mold was then placed under a hot press. Thereafter, the samples were molded to plate shape by hydraulic compression press at a pressure of approximately 30kN for 5min at 190°C. After cooling, the cast sample was taken out from the mould (the overall operation in hot press is shown in Fig.2). The prepared samples were characterized by FTIR analysis, FEGSEM and thermal conductivitytests.

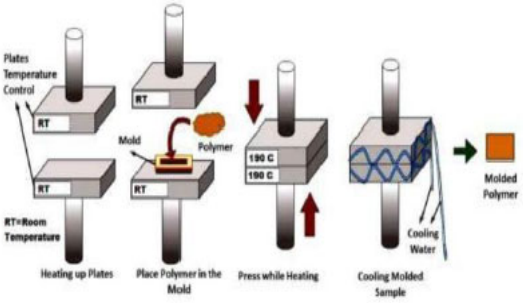

Figure 2: Schematic of sample preparation of compression molding in hot press.

III. RESULTS ANDDISCUSSION

3.1. FTIR Spectroscopy

Figure 3 represents the FTIR spectra for the blended PP/EVA and filler materials, where all characteristics peaks have been found. The peaks found like 2914cm-1, 2847cm-1, 1730cm-1, 1464cm-1, 1375cm-1, 1300cm-1 and 720cm-1, respectively, represent methylene asymmetric C–H stretching, methylene symmetric C–H stretching, aliphatic C=O ester group of EVA, methylene scissoring, methyl symmetrical C–H bending, methylene wagging and methylene rocking respectively. From the spectra resented in Fig.3 no new peak other that the characteristic peaks related to EVA and PP has been observed. This finding is a proof that after melting and blending of the binary polymer matrix of PP and EVA did not form any new type of polymer, rather than they just remain as co-continuous phases. Similar observation has also been mentioned by some other investigators [10,15].

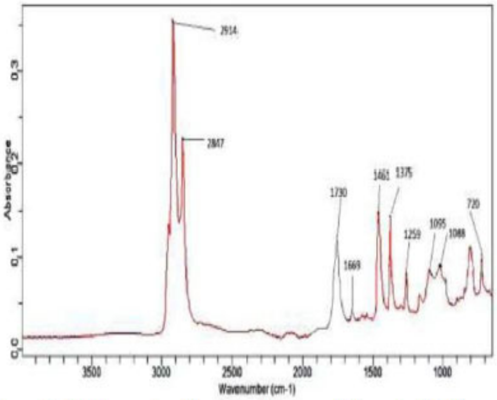

Figure 3: FTIR spectra binary polymer reinforced with binary particle.

Microstructural Observation in FEGSEM

The FEGSEM observation is presented in Fig.4. From this photomicrograph taken on tensile fracture surfaces, it is very clear that the two phases of PP and EVA are not in mixed condition, they just overlapped with each other creating a mating interface. PP is relatively brittle, which has been identified by its nature of brittle type of fracture, whereas EVA phase has been identified from its ductile nature of fracture mode. This observation figures out that these two polymers remain immiscible in the case of their binarymatrix.

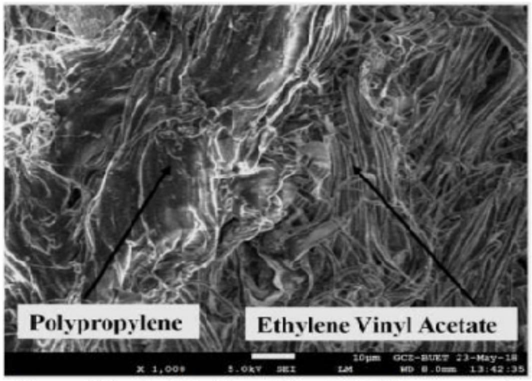

Figure 4: Immiscible phases PP and EVA binary matrix polymer.

Thermal Conductivity

Throughout the study binary matrix system of polypropylene (PP, 60 wt%) and ethylene vinyl acetate (EVA, 40 wt%) were used. The samples were designed in such way that single to binary particle effects on thermal conductibility of the developed composites could be possible to observe. Figure 5 indicates that the thermal conductivity of the binary polymer composites increase with the increase in the activated carbon filler content and that after adding about 8% of carbon particles the thermal conductivity increase from the value of base binary polymer matrix 0.16 to 0.9w/m.k. This increase might have been attributed due to continuous thermal pathways created in thecomposites.

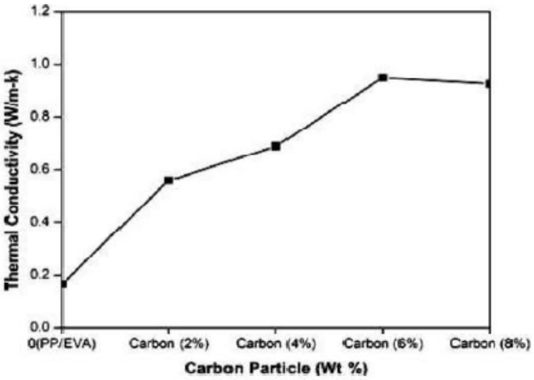

Figure 5: Variation of thermal conductivity with carbon particle content in PP and EVA binary matrix.

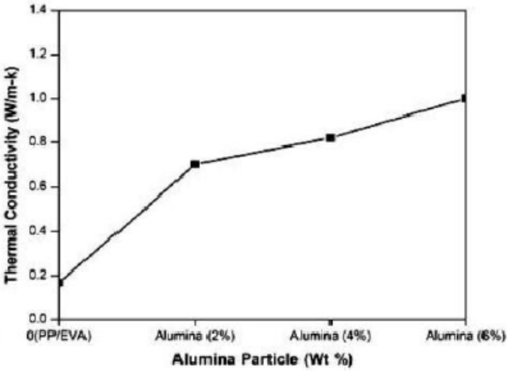

Figure 6: Variation of thermal conductivity with alumina particle content in PP and EVA binary matrix

Similar to activated carbon, alumina particle individually also has low effect on thermal conductivity of the composite (Fig.6), where the thermal conductivity increased from 0.16 to 1.0w/m.k after addition of 6% of filler particle. Slightly better conductivity increase has been possibly due to its higher thermal conductivity compared to that of the activated carbon particle. From Figs.5 and 6, it is clear that the effect of 6% alumina particle is very close to that of 8% carbonparticle.

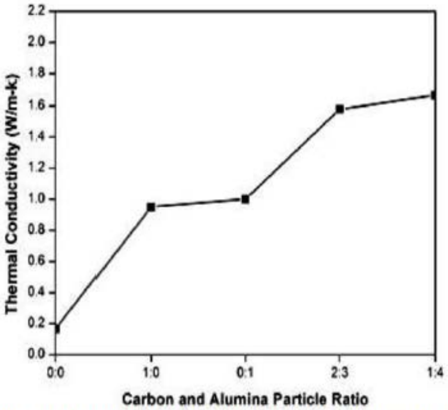

Figure 6: Variation of thermal conductivity of alumina and carbon binary particle content in PP and EVA binary matrix.

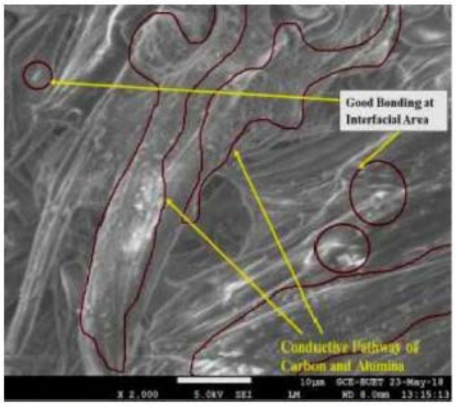

Figure 7: Easy conductive pathways in EVA phase in the binary PP and EVA polymer matrix

For binary polymer matrix with binary particle reinforcement composite system the seneriois somewhat different, Fig.7. In the latter case, initially the thermal conductivity increases slightly similar to the single particle reinforced composite due to isolated alumina particle segregation in activated carbon particle. However, the trend has been changed when the alumina content is gradually increased as higher alumina created more continuous networks in immiscible interfacial zone of EVA. This is because EVA is polar materials, whereas PP is non-polar, where alumina particles tend to remain preferentially distributed in EVA phase, Fig.7. Consequently, more and favourable easy thermal pathways have been created in the composite. The carbon particles also create more contact between the alumina networks, which also accelerated the thermal conductivity of the composite. In this case the thermal conductivity has been increased to 1.7w/m.k from the base value of 0.16w/m.k, which is about 12 time higher than that of pure PP and 10 higher than that of pure EVA. Some other researchers have also mentioned similar observation [15,16]. Here it is to be noted that the thermal conductivity of pure PP and EVA are, respectively, 0.14w/m.k and 0.16w/m.k[17].

IV. CONCLUSION

In the present research, binary matrix by single particle and binary matrix by binary particle composites were fabricated with hot press technique following pre melting and blending of fixed 6wt% of filler. After development of the composite; it was characterized by FTIR spectroscopy, FEGSEM and thermal conductivity tests. After the detail investigation the followings outcome can be concluded from thiswork:

a. The polymer composite containing single filler either organic particle (activated carbon) or inorganic particle (alumina) have lower effect on thermal conductivity of polymer composite than binaryparticle.

b. It is revealed from experimental result that in the binary matrix immiscible co-continuous phase of binary matrix of PP/EVA has been formed that helped to particle distribution in immiscible interfacial zones of the binary matrix. This creates thermal conductive pathways of filler that caused significant enhancement in the thermal conductivity. The ultimate thermal conductivity of this study is nearly twelve times of the pure PP and ten times of pure EVA having 6wt% of filler in the binary matrixsystem.

ACKNOWLEDGEMENT

The authors would like to express their gratitude to CASR of BUET to provide necessary fund and research facilities to conduct this research work. They also indebted to MME Departmant for ensuring the

use of all laboratory facilities.

REFERENCE

[1] Okada and A. Usuki, "Twenty years of polymer-clay nanocomposites,"Macromolecular Materials and Engineering, vol.291, no.12, pp.1449-1476,2006.

[2] Utracki, S. Maryam and E. Boccaleri, "Synthetic, Layered Nanoparticles for Polymeric Nanocomposites", Polymers for Advanced Technologies, vol.18, no.1, p.1-37,2007.

[3] Ramadan, R.A. Mohamed and K.H Mohamed ,"An Idea to Enhance the Thermal Performance of HDPE Pipes Used for Ground-source Applications", Thermal Engg., vol.109, pp.15-21,2016.

[4] Q. Li, J. Lu, X. Zeng, R. Sun, J. Wu, J.B. Xu, and C.P. Wong, "Enhanced Thermal Conductivity for Ag-deposited Alumina Sphere/Epoxy Resin Composites Through Manipulating Interfacial Thermal Resistance", Composites Part A: Applied Sci. and Manufacturing, vol.107, pp.561-569,2018.

[5] Agrawal and A. Satapathy, "Effects of Aluminium Nitride Inclusions on Thermal and Electrical Properties of Epoxy and Polypropylene: An Experimental Investigation", Composites Part A: Applied Sc. and Manufacturing, vol.63, pp.51-58, 2014.

[6] L. Liu, P. Li, L. Ding, W. Tong, F. Li and Y. Zhang, ”Utilization of Industrial Ultra-fine Carbon Ash as Filler of High-k Composites with High Density Polyethylene as Matrix”, Environmental Progress & Sustainable Energy, vol.36, no.6, pp.1719-1724,2017.

[7] Liming, “Intelligent Macromolecules for Smart Devices: from Materials Synthesis to Device Applications”, Springer Sci. & Business Media,2004.

[8] P. M. Ajayan and H. S. Nalwa, "Handbook of Nanostructured Materials and Nanotechnology", Academic Press, New York, 2000.

[9] Paul and C. Bucknall, "Introduction in Polymer Blends Formulation”, vol.1,2000.

[10] Laurent and L. Leibler, "A Model for Toughening of Semicrystalline Polymers", Macromolecules, vo.40, no.15, pp.5606-5611,2007.

[11] S. Surajit, “Model Aircraft”, Mega Hobby.com, 27 July 2013,www.megahobby.com/categories/model-aircraft.html.

[12] Orna and S. Uttandaraman, "Big Returns from Small Fibers: A Review of Polymer/Carbon Nanotube Composites, Polymer Composites, vo.25, no.6, pp.630-645,2004.

[13] N. James and P. Krzysztof, "Polymer Nanocomposites for Aerospace Applications", Advanced Engg. Materials, vol.5, no.11, pp.769-778,2003.

[14] R. S. Prasher, J.Y Chang, I. Sauciu, D. Chau, G. Chryslerand

[15] C. Hu, “Nano and Micro Technology-Based Next-Generation Package-Level Cooling Solutions”, J. Intel Tech., vo.9, no.4, pp.205-211, 2005.

[16] M. Sarikanat, K. Sever, Y. Seki, and I. Özdemir. "Preparation and Mechanical Properties of Graphite Filled HDPE Nanocomposites", Arch. Mater. Sci. Eng, vol.50, no.2, pp.120-124,2011.

[17] O. Abdollah and A.A. Rostami, "The Effects of Alumina Nanoparticle on the Properties of an Epoxy Resin System", Materials Chemistry and Physics, vo.114, no.1, pp.145-150, 2009.

[18] Properties of Polymers, Fourth Edition 2009, Elsevier Publisher.

★★★

MECHANICAL PROPERTIES, WEAR AND DETERIORATING PROPERTIES OF DUCTILE IRON CASTINGS

[1]SUNIL KUMAR YADAV, [2]BABITA MEHER, [3]RAKESH MOHANTY

[1]Department of Mechanical Engineering, NMIET, Bhubaneswar, 751019
[2]Department of Mechanical Engineering AIET Bhubaneswar
[3]Department of Mechanical Engineering REC Bhubaneswar
E-mail: [1]prakash.katdare@nmiet.ac.in

Abstract - Austempered Ductile Iron (ADI) has found vast applications in over the decades due to its high strength and hardness, coupled with essential ductility and toughness. Ductile iron replaced steel in most applications. The applications of ADI include the manufacture of crankshafts, engine mounts, camshafts, track guides for bulldozers, drive mechanism for carpet looms, camshafts, gears etc. Corrosion studies play an important role in the field of production industry. Various corrosion testing methods available are electrochemical test, salt spray test, total immersion tests etc. The selection of the corrosion testing method depends upon various factors such as condition of environment, condition of exposure, type of specimen etc. The wear test will be carried out on pin on disc type machine for different condition i.e. varying speeds at constant load and varying loads at constant speed. In the present research investigation, ductile iron castings conforming according to the ISO-standard No. 1083 (1976) there are four main grades of as-cast ductile iron denoted as 700/2 and 400/12 grade was examined in as cast and heat treated condition. The ductile iron castings were subjected to standard austempering heat treatment cycle to bring about the changes in the microstructure and hence the mechanical properties, wear and corrosion properties wereexamined.

Keywords - Austempered Ductile Iron (ADI), Ductile Iron (DI), Corrosion, Wear, Mechanical Properties.

I. INTRODUCTION

Ductile Iron consists of graphite in the form of nodules or spheroids in a matrix of either ferrite or pearlite. The properties of ductile iron combine the properties of cast iron and steel. Iron with varying microstructure can be obtained by varying the treatment conditions during melting, after treatment and also by heat-treating the castings. By altering any one of the parameters, a suitable iron as per requirements and application can be obtained. In order to improve the properties of ductile iron, the material can be treated with alloying elements or can be heat-treated to bring about change in the microstructure of the material. Commonly, austempering heat treatment is carried out on ductile iron; hence the name “Austempered Ductile Iron” or “ADI”. ADI has found its way in a wide range of components for many engineering sectors as in gears, crank shafts, transmissions, suspensions, earth-moving and construction equipment, railways etc[1].

Wear is an important property, which is evaluated in materials to find out its response to undergo loss of material. It is a progressive, unintentional loss of material when two surfaces come in contact under normal load and there is relative motion between the surfaces. Wet abrasive wear test is one method for evaluating the material behaviour to wet abrasive action [1]. Different corrosion testing methods are available viz. Electrochemical test, salt spray test, total immersion test etc. The choice of the corrosion testing methods as reported depends upon many factors such as nature of environment, nature of exposure, type of specimen etc. Salt Spray Fog test is one of the corrosion testing methods, whichinvolves the exposure of the specimens to fine spray as mist of a solution of sodium chloride at a specified temperature. The spray particles settle upon the test surface (which is preferably inclined) and constantly replenish and replace the film of solution on the surface. The extent and nature of the corrosion of the metal or coated surface after a specified period of exposure serve as a measure of quality/corrosion resistance. To accelerate corrosion the temperature of the media or the pH of the media or the concentration of the media can be varied [10].

Corrosion studies were carried out using standard salt spray fog type testing machine. Corrosion testing apparatus conforming to ASTM standard B117 specification was used. The corrosion rate of the specimen was calculated using the formula:

Corrosion Rate (mpy) = (534xW) / D A T Where
W = Weight loss inmg,
D = Density of the specimen in gm/cc, A = Area in squaremm,
T = Exposure time in hours mpy = mils per year

Weight loss method was employed to assess the corrosion of the specimen. At regular intervals, the specimen was taken out and the weight is determined for calculation of loss in weight or corrosion. The weight loss of specimen in as-cast condition is more than heat-treated condition for any given temperature. The weight loss in specimens subjected to corrosion at higher temperature is more. This may be attributed to higher reaction involved at higher temperature of the fog mixture. The corrosion rate for specimenin as-cast condition is more than heat-treated condition for any given temperature. The corrosion rate is more at higher temperatures of the fog mixture. This may be attributed to more resistance offered by the heat-treated specimens and higher reaction rate involved at higher temperature [10].

Much of the annual production of ductile iron is in the form of ductile iron pipe, used for water and sewer lines. Ductile iron is specifically useful in many automotive components. Other major industrial applications include off-highway diesel trucks, class 8 trucks, agricultural tractors, oil well pumps, fully machined piston for large marine diesel engine, bevel wheel, hydraulic clutch on diesel engine for heavy vehicle and Fittings overhead electric transmission lines[2]. If ductile iron is heated at 750^0C, then it is quenched (mineral oil or vegetable oil or water or any other quenching media), then its properties are vary depending upon the micro constituents present in particular metal. In general heat treatment processes involving heating, holding and continuous cooling, due to this graphite nodules are transformed into a ferrite matrix or upto 10% pearlite although it does not contain carbides[2].

	Tensile Strength (in N/mm^2)	Hardness (BHN)	Yield Stress (in N/mm^2)	%Elongation
Grade 600/3	610-650	200-265	525-555	3.1-3.9
Grade 500/7	507-565	165-225	455-465	7.2-17.8

Table 1 As cast ductile cast iron shows following values of the mechanical properties:

	Tensile Strength (in N/mm^2)	Hardness (BHN)	Yield Stress (in N/mm^2)	%Elongation
Grade 600/3	645-650	210-220	528-558	10.1-14.2
Grade 500/7	540-575	195-210	475-485	20-24.6

Table 2 Heat treated ductile cast iron shows following values of the mechanical properties:

Factor that affect heat treatment process:

- Austenising temperature andtime.
- Casting quality and size ofcastings.

II. HISTORY OF DUCTILE IRON

It was Chinese who first invented cast iron in the 5th century BC by archaeologists. To make ploughshare, pots and weapons they poured the cast iron into the mould which is the replica of the desired component.

Because production costs of pig iron are relatively low as compared with other alloys, and since no expensive refining process is necessary, cast iron is a cheap metallurgical material which is particularly useful where a casting requiring rigidity, resistance to wear or high compressive strength isnecessary.

Other useful properties of cast iron include:

1. Good machinability when a suitable composition is selected
2. High fluidity and the ability to make good castingimpressions
3. Fairly low melting range (1130-1250°C) as compared withsteel
4. The availability of high strengths when additional treatment is given to suitableirons,

e.g. spheroidal-graphite iron, compacted-graphite irons or pearlitic malleable irons.

The structure and physical properties of a cast iron depend upon both chemical composition and the rate at which it solidifies following casting [5].

III. PRODUCION OF DUCTILE IRON

Ductile iron is made by the treatment of molten iron with nodulizing (spheroidizing) material. During this treatment, graphite changes from flakes to nodules or spheres. The treatment process is a key operation in the production of ductile iron that ensures a predetermined microstructure, and mechanical and engineering properties of castings. Production of ductile iron is influenced by a large number ofmetallurgical, technological, heat transfer and designing parameters. The first step of the production of ductile iron castings is the careful selection of the charge materials. Manganese and chromium have the most influence on all mechanical properties [3]. For this reason, their concentration in metal is of particular importance. These elements arise in the charge from steel scrap, pig iron and foundry returns. It is a recommended practice to select steel scrap so that the average Cr content remains below 0.1%. Ideally, the same advice would be given for Mn but, unfortunately, all steel scraps contain Mn, the majority being at 0.5% level. The amount of steel scrap in the charge must be such that the castings produced are free of carbides as much as possible [3]. It is particularly important for the production offerritic ductile iron. Charge materials result in the average size of graphite spheroids. For instance, if the amount of steel scrap in the charge is higher than 50%, then an average spheroids diameter is 33 μm and if it is 30%, then the average diameter is 57 μm. The amount of steel scrap affects metallic matrix structure too. It increases the pearlite formation. The graphite structure is affected by the carbon content as well. If initial metal does not contain enough carbon then graphite particles will be of compact shape. The metallic matrix structure is affected not only by carbon equivalent but by C/Si ratio too. As this ratio increases in ductile iron, the proportion of ferrite decreases and the proportion of pearlite increase [3]. Ductile iron production accounts for about 42% of all iron castings and is still growing. While a number of elements, such as cerium, calcium and lithium are known to develop nodular graphite structures in cast iron, magnesium treatment is always used in practice. The base iron istypically:

%C	%Si	%Mn	%S	%P
3.7	2.5	0.3	0.01	0.01

Table 3: Determinants of base iron

Having high carbon equivalent value (CEV) and very low sulphur, sufficient magnesium is added to the liquid iron to give a residual magnesium content of about 0.04%, the iron is inoculated andcast.

IV. FAMILY OF DUCTILEIRON

With a high percentage of graphite nodules present in the structure, mechanical properties are determined by the Ductile Iron matrix. The importance of matrix in controlling mechanical properties is emphasized by the use of matrix names designate the following types of ductileiron.

Austenitic Ductile Iron: Alloyed to produce and austenitic matrix, this ductile iron offers good corrosion and oxidation resistance, good magnetic properties, and good strength and dimensional stability at elevated temperatures.

Ferritic Ductile Iron: Graphite spheroids in a matrix of ferrite provide and iron with good ductility and resistance and with a tensile and yield strength equivalent to a low carbon steel. Ferritic Ductile Iron can be produced “as-cast’ but may be given and annealing heat treatment to assure maximum ductility and low temperature toughness.

FerriticPearlitic Ductile Iron: These are the most common grade of Ductile Iron and are normally produced in the “as cast condition. The graphite spheroids are in a matrix containing both ferrite and pearlite. Properties are intermediate between ferritic and pearlitic grades, with good machinability and low production costs.

Pearlitic Ductile iron: Graphite spheroids in a matrixofpearlite result in an iron with high strength, good wear resistance, and moderate ductility and impact resistance. Machinability is also superior to steels of comparable physical properties. The preceding three types of ductile iron are the most common and are usually used in the as-cast condition, but Ductile iron can be also bealloyed and/or heat treated to provide the following grades for a wide variety of additionalapplications.

Martensitic Ductile iron: Using sufficient alloy additions to prevent pearlite formations, and a quench-and-temper heat treatment produces this type of ductile iron. The resultant tempered martensite matrix develops very high strength and war resistance but with lower levels of ductility and toughness.

Bainitic Ductile iron: This grade can be obtained through alloying and/or by heat treatment to produce a hard, wear resistantmaterial.

Austempered Ductile iron: ADI, the most recent addition to the Ductile Iron family, is a sub-group of ductile irons produced by giving conventional Ductile iron a special austempering heat treatment. Nearly twice as strong as pearlitic ductile Iron, ADI still retains high elongation and toughness. This combination provides a material with superior wear resistance and fatigue strength.

V. MICROSTUCTURE

Engineering applications of cast iron have been traditionally based upon gray (Flake graphite) irons providing a range of tensile strengths between about 150 N/mm^2 and 400 N/mm^{2}withrecommended design stresses in tensile applications of 0.25 × Tensile strength. Despite their limited strength gray irons provided very useful combinations of properties, which have ensured there wide continuing use. In fact gray irons still account for nearly 65 % of all iron castings produced. In contrast ductile irons have tensile strengths ranging from 350 to 1500N/mm^2 with good elongation and high toughness. They now account for about 30 % of iron casting production serving in safety critical applications where they have replaced steel casting, forging and fabrications with technical and cost advantage.[6] Ductile iron and gray iron differs in morphology of graphite present in the structure. Ductile iron has graphite in the form of spherical nodules which is achieved by suitable treatments on the melt. The major micro structural constituents of ductile iron are: the chemical and morphological forms taken by carbon, and the continuous metal matrix in which the carbon and/or carbides are dispersed[6].

The following important micro-structural components are found in ductile iron:

Graphite

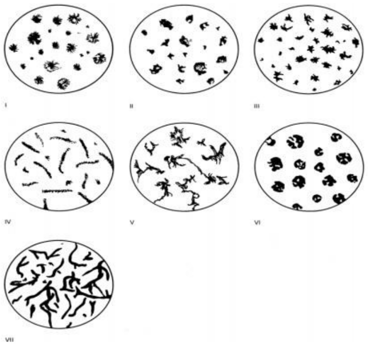

Fig.1 Typical shapes of graphite from ASTM A 247 standard. I) spheroidal graphite, II) imperfect spheroidal graphite,III) temper graphite, IV) compacted graphite, V) crabgraphite, VI) exploded graphite, VII) flake graphite

This is the stable form of pure carbon in cast iron. Its important physical properties are low density, low hardness and high thermal conductivity and lubricant property. Graphite shape, which can range from flake to spherical, plays a significant role in determining the mechanical properties of cast irons. Graphite flakes act like cracks in the iron matrix, while graphite spheroids act like “crack arresters”, giving the respective irons dramatically different mechanical properties [7].

Carbide:

Carbide, or cementite, is an extremely hard, brittle compound of carbon with either iron or strong carbide forming elements, such as Chromium, Vanadium or Molybdenum. Massive carbides increase the wear resistance of cast iron, but make it brittle and very difficult to machine. Dispersed carbides in either lamellar or spherical forms play in important role in providing strength and wear resistance in as-cast pearlitic and heat-treatedirons.

Ferrite

This is the purest in phase in a cast iron. In conventional Ductile iron ferrite produces lower strength and hardness, but high ductility and toughness. In Austempered Ductile Iron (ADI), extremely fine-grained acicular ferrite provides an exceptional combination of high strength with good ductility and toughness.

Bainite

When austenite is cooledto large super saturations below the nose of the pearlite transformation curve, a new eutectoid product called bainite is produced. Like pearlite, bainite is mixture of ferrite and carbide, but it is by microstructural behaviour quite distinct from pearlite and can be characterized by its own C curve on a TTT diagram. In plain carbon steels this curve overlaps with the pearlite curve so that at temperatures around 500°Cboth pearlite and bainiteformcompetitively.

In the case of pearlite the cementite and ferrite have no specific orientation relationship to the austenite grain in which they growing, whereas the cementite and ferrite in bainite do have an orientation relationship with the grain in which they are growing. Bainite is a mixture of ferrite and carbide, which is produced by alloying or heattreatment.

Pearlite

When austenite containing about 0.8% wtCarbon is cooled below the A1 temperature (710°C) it becomes simultaneously supersaturated with respect to ferrite andcementiteandaeutectoidtransformationresults, i.e. $\gamma \rightarrow \alpha + Fe_3C$.In the case of Fe-C alloys the resultant microstructure comprises lamellae, or sheets, of cementite embedded in ferrite. This is known as pearlite. Both cementite and ferrite form direly in contact with the austenite. Pearlite nodules nucleate on grain boundaries and grow with a roughly constant radial velocity into the surrounding austenite grains. At small undercooling below A1 the number of pearlite nodules that nucleate is relatively small, and the nodules can grow as hemispheres or spheres without interfering with each other. At larger undercooling the nucleation rate is much higher and site saturation occurs, that is all boundaries become quickly covered with nodules which grow together forming layers of pearlite outlining the prior austenite grain boundaries. A common constituents of cast irons, pearlite provides a combination of higher strength and with a corresponding reduction in ductility which meets the requirements of main engineeringapplications.

Martensite

Martensite is a supersaturated solid solution of carbon in iron produced by rapid cooling. In the untempered condition it is very hard and brittle. Martensite is normally “tempered”- heat treated to reduce its carbon by the precipitation of carbides-to provide a controlled combination of high strength and wear resistance.

Austenite

Normally, a high temperature phase consisting of carbon dissolved in iron, it can exist at room temperature in austenitic and austempered cast irons, in austenitic irons, and austenite is stabilized by nickel in the range 18-36%. In austmepred iron, austenite is produced by a combination of rapid cooling which suppresses the formation of pearlite and the super saturation of carbon during austempering, which depresses the start of the austenite-tomartensite transformation far below room temperature. In austenitic irons, the austenite matrix provides ductility and toughness at all temperatures, corrosion resistance and good high temperature properties, especially under thermal cycling conditions. In austempered Ductile Iron stabilized austenite, in volume fractions up to 38 % in lower strength grades, improves toughness and ductility and response to surface treatment such filletrolling.

VI. CONCLUSION

Ductile cast irons are materials having strength, impact toughness and ductility comparable to those of many grades of steel while exceeding by far those of standard gray irons. In addition, they have the same advantages of design flexibility and low cost casting procedures of cast irons. The combination of good mechanical properties and casting abilities of ductile cast iron makes it economical choice for many applications. This paper discusses about ductile iron and analysis of mechanical properties, wear and corrosion characteristics of different grades of ductile iron casting for its application in production industries. It also includes history of ductile iron, production of ductile iron and family of ductile iron and theirmicrostructures.

REFERENCE

[1] Prasanna, N. D., et al. "Mechanical Properties and Corrosion Characteristics of IS400/12 Grade Ductile Iron." Transactions of 57th International FoundrymenCongress.2009.

[2] Madtha, Lisa Shifani, and BR NarendhaBabu. "Experimental behavioural study of ductile cast iron microstructure and its mechanical properties." International Journal of Engineering Research and Applications 3.3 (2013):1470-1475.

[3] Olawale, J. O., S. A. Ibitoye, and K. M. Oluwasegun. "Processing Techniques and Productions of Ductile Iron: A Review." International Journal of Scientific & Engineering Research 7 (2016):397-423.

[4] US patent 2485760, Keith Millis, “Cast Ferrous Alloy”, issued1949-10-25

[5] Higgins.R.A., Engineering Metallurgy Applied Physical Metallurgy.London,EdwardArnold,Sixthedition1993.

[6] Karsay. S.I., Anderson.J.V., “Production ofS.G.Iron”,1996

[7] A guide to mechanical properties of ductile iron, Mid-Atlantic Castingservice.

[8] SiddarajuC, Dr. N. D. Prasanna and Dr. M. K. Muralidhara, June 2013. Abrasive wear studies on austempered ductile iron castins, International Journal of Emerging Technology and Advanced Engineering, Vol 03, Issue 06,124-130.

[9] Mohammad BabaZadesh, HaMiDPourAsiabiandHamed Pour asiabi, 2013. Wear characteristics of ADI; A comprehensive review on mechanisms and effective parameters,JournalofBasicandAppliedScientificResearch, Vol 03, Issue 02,646-656.

[10] C. Siddaraju, N. D. Prasanna, and M. K. Muralidhara, January 2013. Corrosion characteristics of ductile iron castings subjected to austempering heat treatment, Indian Foundary Congress, Vol 59, No 01,44-47.

★★★

DRAFT OF THE MEPS AND HEPS FOR INDUSTRIAL REFRIGERATION COMPRESSOR IN THAILAND

[1]TANUSREE BERA, [2]BHAGYASHREE PANDA, [3]SANJEET KUMAR

[1]Department of Mechanical Engineering, NMIET, Bhubaneswar, 751019
[2]Department of Mechanical Engineering AIET Bhubaneswar
[3]Department of mechanical engineering REC Bhubaneswar
E-mail: [1]prateek.das@nmiet.ac.in

Abstract -
This study aimed to find the high energy efficiency standard (HEPS) and minimum energy efficiency standard (MEPS) of industrial refrigeration compressors that suitable for Thailand. The energy efficiency data of each sample product was obtained from the specification providing by its manufacturer. The energy efficiency data of 1,006 products were found and used for study HEP and MEP values in this study. They were categorized into 2 groups consists of 344 products and 662 products for low and medium evaporating temperature groups, respectively. All of them were coefficient of performance (COP) measured according to the EN13771-1:2016 and describing the results in accordance with EN12900:2013. The results show that evaporating temperature has dominant effect on COP. It was found that the COPs of low and medium evaporating temperatures should not below 0.7911+0.7392 [Cooling capacity/(Cooling capacity × + 1.049)] and 1.3774 + 1×.2934 [Coolingcapacity/(Coolingcapacity+1.785)];respectively,forHEPsand0.4307+0.7392 × [Cooling capacity/(Cooling capacity+1.049×)]and0.8354+1.2934 [Cooling capacity/(Cooling capacity + 1.785)]; respectively, for MEPs. It is noted thatcoolingcapacity'sunitiskW.

Keywords - Refrigeration Compressor; High Efficiency Performance Standard; Minimum Efficiency Performance Standard

I. INTRODUCTION

The DEDE has a duty to promote and support the production, distribution and use of high-performancemachines, materials and equipment. Recently, the DEDE has studied more than 60 high-performance products for promoting the high efficiency products[1].

Industrial refrigeration compressor is an important component which consumes the largest portion of energy use in industrial refrigeration. It is commonly used in food and beverage industrial cluster in which the total energy saving potential is about 5370 ktoe/year or 62,453 GWh/year [2]. Therefore, the study to find the MEPS and HEPS ofrefrigerationcompressorisnecessaryforpromotingthe production,saleandusageofthehighefficiencyproducts. Hence,thecountryenergysavingpotentialcanbeachieve diftheHEPSandMEPShasbeenenforced.

II. METHODOLOGY

The technical and marketing information of the refrigeration compressors were surveyed. It was found that EN13771-1:2016[3]iswidelyusedby manymanufacturersfortestinganddescribingthecoefficientofperformance of their refrigeration compressors. The coefficient of performance (COP) Eq. (1) refers to a ratio of the amount of heatabsorbed(Q_L)fromtherefrigeratedspacetoaworkinput(W)andcanbeexpressas[4]

$$\mathrm{COP} = \frac{Q_L}{W}$$

The energy efficiency data of each sample product were obtained from the specification providing by its manufacturer. All of them were measured according to EN13771-1:2016 and describing the results in accordance with EN12900:2013 [5]. The results were lead to find the right MEPS and HEPS with the consent from the related. The methodology details are described as follow.

2.1 Datasurvey

There are 17 familiar brands of industrial refrigeration compressors in Thailand. In 2020, the data from the Custom Department reveal that the average cost and quantity for the past 5 years of imported industrial refrigeration compressors for selling in Thailand (HS-CODE 8414-3040 Refrigeration capacity exceeding 21.10 kW, or with a displacement per revolution of 220cc or more) were about 976,961,722 Baht per year and 36,107 unit per year, respectively [6]. However, it was insisted by related parties (e.g. dealers and importers) that only half of imported cost was industrial refrigeration compressors with cooling capacity exceeding 100 kW. Thus, the actual quantity of imported industrial refrigeration compressors would be 617 units per year as shown in Table 1.

Table 1. The quantity of imported industrial refrigeration compressor.

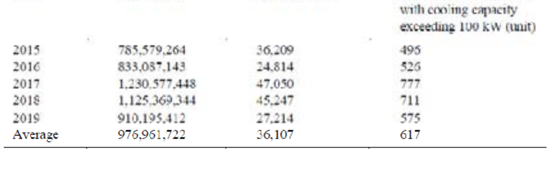

Year	Cost (Baht)	Quantity (unit)	Quantity of compressors with cooling capacity exceeding 100 kW (unit)
2015	785,579,264	36,209	495
2016	833,087,143	24,814	526
2017	1,230,577,448	47,050	777
2018	1,125,369,344	45,247	711
2019	910,195,412	27,214	575
Average	976,961,722	36,107	617

The energy efficiency data of 1006 products were found and used for study HEP and MEP values in this study. They were categorized into 2 groups consists of 344 products for low evaporating temperature group and 662 products for medium evaporating temperature group as shown in Table 2.

Table 2. The energy efficiency data samples.

Evaporating temperature	Cooling capacity (kW)	Number of models	% of total
Medium temperature	0.39–2676	662	65.8
Low temperature	0.72–6417	344	34.2
Total	0.39–6417	1006	100

2.2 Draft of MEPS andHEPS

To increase the energy efficiency of refrigeration compressors, the DEDE decided to support 30% of products that have the energy performance higher than HEPS and will be encouraged 5% of products that have the energy performancelowerthan MEPStoimprovetheproductefficiency.

III. RESULTS AND DISCUSSION

The total of 1006 energy efficiency data of refrigeration compressors categorized into low and medium evaporating temperature refrigeration compressor groups were analyzed. It was found that the average COPs were 1.37 W/with standard deviation of 0.2 and 2.39 with standard deviation of 0.32 for low and medium evaporating temperature groups, respectively. The distributions of energy efficiency data for each group are shown in Fig. 1.

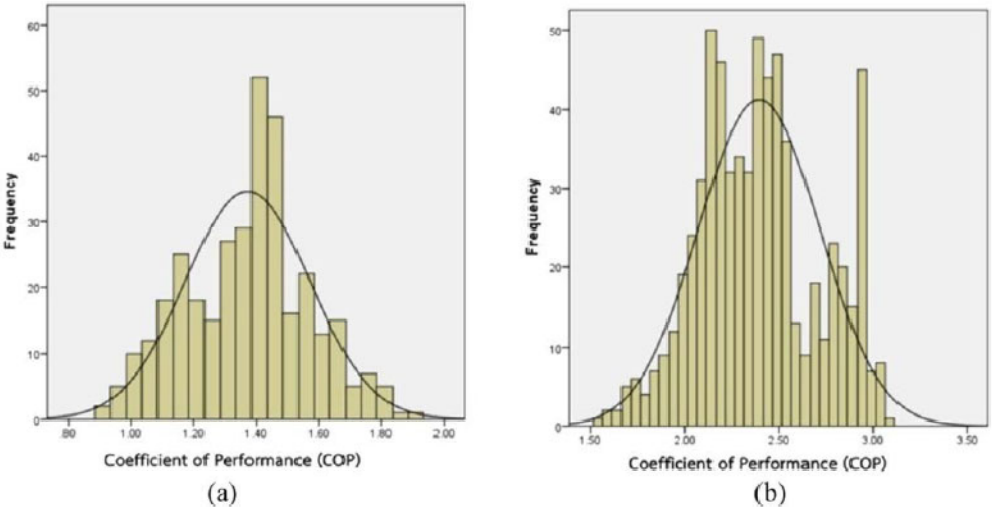

Fig. 1. Distributions of energy efficiency data for (a) low evaporating temperature and (b) medium evaporating temperature.

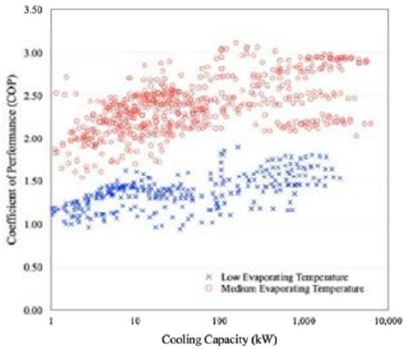

Fig. 2. The relationship between cooling capacity and COP of refrigeration compressor.

Fig. 2 show the relationship between cooling capacity and COP of refrigeration compressor for low and medium evaporating temperature groups.

It could be seen that COP increases when the cooling capacity increases. Thus, the average COPs should bebased on the refrigerating capacity of the compressor [7]. It is also clear that the evaporating temperature has dominant effect on COP so the average COPs were expressed in low and medium evaporating temperature according to EN13771-1:2016 by the equations shown inTable 3.

Table 3. The average coefficient of performance.

Group	Coefficient of performance(W/W)
Lowevaporatingtemperature	0.7259 + 0.7392 × [Cooling capacity/(Cooling capacity + 1.049)]
Mediumevaporatingtemperature	1.2386 + 1.2934 × [Cooling capacity/(Cooling capacity +1.785)]

Note: Cooling capacity's unit is kW.

To find the suitable HEPS and MEPS. The DEDE committee and related parties agree to define the HEPS by specifying HEP of refrigeration compressors as the COP values in which number of compressors lies in an area above HEP line is about 30% of total number of refrigeration compressors in the market. It was found that 103 models and 8 brands pass the HEP value for low evaporating temperature compressors. While there are 199 models and 7 brands pass the HEP value for medium evaporating temperature compressors.

Similarly, the committee and related parties decided to define the MEPS by specifying MEP of refrigeration compressors as the COP values in which number of compressors lies in an area below MEP line is about 5% of total number of refrigeration compressors in the market. It was found that 17 models and 4 brands do not meet the MEP value for low evaporating temperature compressors. While there are 33 models and 3 brands do not meet the MEP value for medium evaporating temperature compressors. The HEP and MEP lines of refrigeration compressors are shown in Fig.3.

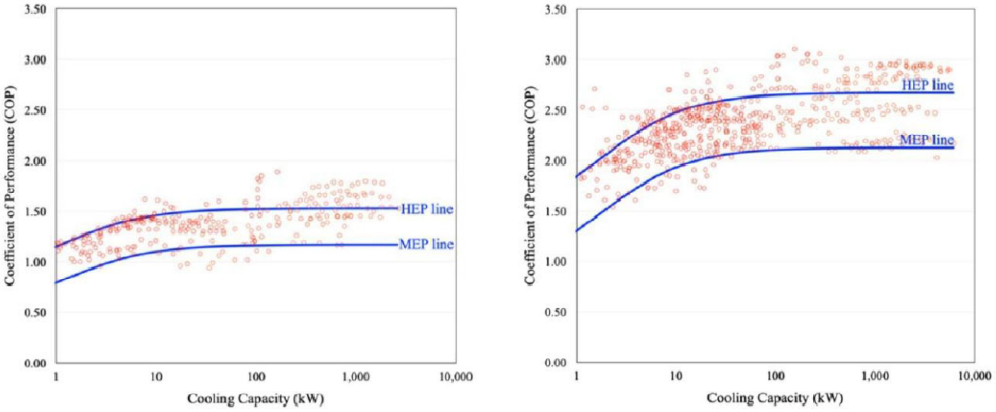

(a) (b)

Fig. 3. HEP and MEP lines for (a) low evaporating temperature and (b) medium evaporating temperature compressors.

The HEP and MEP values of refrigeration compressors are summarized in Table 4 and Table 5, respectively.

The difference between the minimum value of HEP and the average value of current COP was used to calculate the energy saving potential. It was estimated from the survey of 21 cold rooms that the average cooling capacity of refrigeration compressors for low and medium evaporating temperature were 331.18 kW and 558.31 kW; respectively, with the load factor of 1.00 and 0.46. If HEPS has been enforced, it is estimated that 6000 high energy efficiency compressors will be sold during the next 10 years and yearly electrical saving potential will be 606,177,751kWh/yearwhichequivalentto52.12kilotonsofoilequivalentperyearandequivalenttoCO$_2$reduction of 101,101 tons peryear.

IV. CONCLUSION

Fromthisstudy,theCOPsoflowandmediumevaporatingtemperaturesshouldnotbelow0.7911+0.7392[Coolingcapacity/(Coolingcapacity+1.049)]and1.3774+1.2934 [Cooling capacity/(Coolingcapacity+1.785)]; respectively, for HEPS and 0.4307 +0.7392[Coolingcapacity/(Coolingcapacity+1.049)]and0.8354 +1.2934[Coolingcapacity/(Coolingcapacity+1.785)];respectively,forMEPS.Itisnotedthatcooling capacity's unit iskW.

DECLARATION OF COMPETING INTEREST

The authors declare that they have no known competing financial interests or personal relationships that could have appeared to influence the work reported in this paper.

ACKNOWLEDGMENTS

This research was supported by Department of Alternative Energy Development and Efficiency (DEDE). We thank our colleagues from the Department of Mechanical Engineering, Chiang Mai

University who provided insight and expertise that greatly assisted the research.

REFERENCES

[1] Ministerialregulations.Thailand:Departmentofalternativeenergydevelopmentandefficiency,MinistryofEnergy.

[2] Thailand20-yearenergyefficiencydevelopmentplan(2011–2030).Thailand:MinistryofEnergy.

[3] European Standard (EN). EN13771-1:2016 Compressors and condensing units for refrigeration. Performance testing and test methods. Refrigerantcompressors.

[4] BorgnakkeClaus,SonntagRichardE.Fundamentalsofthermodynamics.JohnWiley&Sons;2012.

[5] European Standard (EN). EN12900:2013 Refrigerant compressors - Rating conditions, tolerances and presentation of manufacturer's performancedata.

[6] StatisticsReport.Thailand:ThaiCustomsDepartment,Ministryof Finance.

[7] Ellis Mark, et al. From the Cold, Strategies to increase the energy efficiency of non-domestic refrigeration in Australia and New Zealand, vol.2.Technicalreport,Australia:CouncilforEnergy;2009.

★★★

EXERGY PERFORMANCE AND OPTIMIZATION POTENTIAL OF REFRIGERATION PLANTS IN FREE COOLING OPERATION

[1]THANGARAJU S, [2]SATYAJEET MOHANTY, [3]GOPAL KRUSHNA SAHU

[1]Department of Mechanical Engineering, NMIET, Bhubaneswar, 751019
[2]Department of Mechanical Engineering AIET Bhubaneswar
[3]Department of Mechanical Engineering REC Bhubaneswar
E-mail: [1]raghu.s@nmiet.ac.in

Abstract -
Exergy analysis has been widely used to assess refrigeration systems by evaluating exergy losses or exergy efficiency. The latter is mostly used as an indicator to determine the system performance, whichrequires the comparison of the actual system with its idealized reversible version, but not the practical achievable efficiency. Therefore, a practice-oriented evaluation method for refrigeration plants in free cooling operation is proposed, based on exergy analysis and technical standards as baseline. By considering the exergy input of auxiliary devices, the overall design of hydraulic circuits can be assessed on subsystem level. The achievable optimization potential compared to the state of the art in technology and the performance is revealed with the introduced optimization potential index (OPI). The application is demonstrated on a case study, where the analysis reveals an adequate operation of the field plant in general.Mostcoolinglocationsshow potentialforimprovement,whichisindicatedbyanOPIsuperiorto zero. Moreover, the auxiliary electrical exergy input shows the same magnitude as the thermal exergy input, which emphasizes the importance of reducing the electrical energy usage of auxiliary devices in refrigeration plants to increase theperformance.

Keywords - Optimization potential assessment method Exergy analysis Refrigeration plants Free cooling Optimization potential index OPI

I. INTRODUCTION

In order to evaluate and reduce the energy consumption inbuildings, e.g. heating, ventilation and air-conditioning (HVAC)systems, different approaches were applied. One suitable method is the concept of exergy. In the last couple of years, several exergy-based investigations were carried out in the field of buildingtechnologies, namely heat pumps [1,2], HVAC [3,4], photovoltaics[5,6], building energy systems [7,8] and refrigeration systems [9,10].From a thermodynamic viewpoint, exergy can be seen as theunrestrictedly convertible portion of energy (maximum mechani-cal energy), which can be obtained from any form of energy byreversible interaction with the environment [11]. Exergy can also beidentified as the quality of energy or available energy. In compar-ison to energy, exergy is destroyed in real (irreversible) thermo-dynamic processes, such as heat transfer in a heat exchanger. Thisrepresents a loss in energy potential to produce work. Such lossesare the key for optimization, as their location and magnitude can be By comparing the measured (actual) cooling system power con- sumption to a simulated (reference) one, the key figure may be used to assess the cooling efficiency of the system or to realize a model-based fault detection, which reduces the risk of cooling device failure. Fan et al. evaluated the performance of an HVAC system in an airport terminal building and determined the influ- ence of different control strategies on the system performance [4]. By means of a simulation model of the building and HVAC system and exergy analysis, it was found that the air handling unit (AHU) has the highest optimization priority, followed by the chillers. In order to evaluate the system performance over a certain time period in the setting of different control strategies with respect to an ideal operating level, the control perfect index (CPI) was intro- duced. Three different control strategies were assessed, where the highest yearly CPI value of 0.82 was reached with the optimal load allocationstrategyincomparisonto 0.77withtheoriginalone.

II. NOMENCLATURE

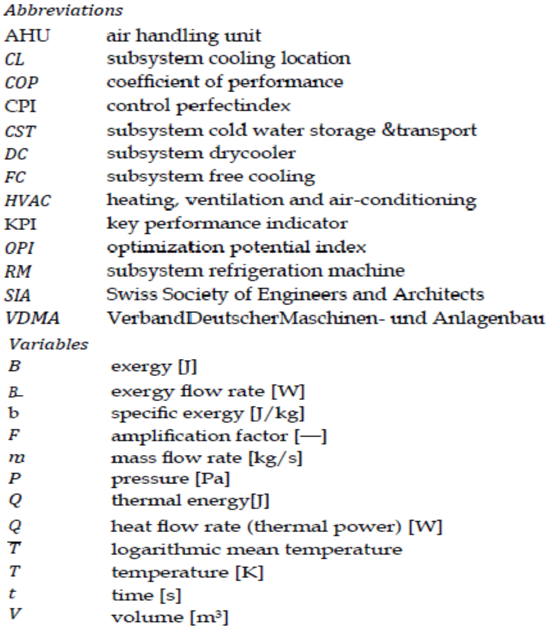

Abbreviations	
AHU	air handling unit
CL	subsystem cooling location
COP	coefficient of performance
CPI	control perfectindex
CST	subsystem cold water storage &transport
DC	subsystem drycooler
FC	subsystem free cooling
HVAC	heating, ventilation and air-conditioning
KPI	key performance indicator
OPI	optimization potential index
RM	subsystem refrigeration machine
SIA	Swiss Society of Engineers and Architects
VDMA	VerbandDeutscherMaschinen- und Anlagenbau
Variables	
B	exergy [J]
$\underline{B}$	exergy flow rate [W]
b	specific exergy [J/kg]
F	amplification factor [—]
m	mass flow rate [kg/s]
P	pressure [Pa]
Q	thermal energy[J]
Q	heat flow rate (thermal power) [W]
T	logarithmic mean temperature
T	temperature [K]
t	time [s]
V	volume [m^3]

W	electrical energy [J]
W	electrical power [W]

Subscripts

0	referencestateforexergyanalysis
amb	ambient
CL	coolinglocation
CP	circulatingpump
CPR	compressor
CST	cold water storage &transport
D	distribution
DC	drycooler
el	electrical
ex	exergetic
FC	freecooling
HE	heatexchanger
in	component/systeminput
kin	kinetic
L	loss/destroyed
m	mass
out	component/systemoutput
th	thermal
w	work

Superscripts

*	reference value according to technical standards

Greek letters

D*T*	temperature difference [K]
h	efficiency [—]

Regarding vapor compression refrigeration plants, the interest extents from the refrigeration machine itself to the neighboring system structures. In practice, a well-suited hydraulic integration of the chiller or free cooling module is crucial in order to achieve a highly performing plant. Furthermore, it can be beneficial to partition the refrigeration plant into different subsystems, where each of them can be assessed individually. The influence of auxil- iary devices on the exergy destruction was considered in a study of Kazanci et al., where different cooling systems were compared [15]. The authors showed that the electrical exergy input of auxiliary devices can be significant, which reveals the importance of reducing the latter to increase the system performance. Another studyinvestigatedtheenergysavingsifvariablefrequencydrives for cooling tower fans are implemented [16]. Results showed that with a variable frequency drive, the water consumption was shortened by 13% and for the same cooling load, the overall energy consumption of the refrigeration plant was reduced by 5.8%. The approach to partition the investigated system into subsystems was applied by Harrell et al. to assess the performance of a chilledwater system of a campus [9]. The authors found the highest system exergy efficiency of 13% at an evaporator cooling load of 70%. By dividing the refrigeration plant into four different subsystems, the most significant exergy losses of 42 and 31% were discovered in the stream turbine and refrigeration subsystem, respectively. A detailed exergy analysis of a ground-source heat pump was carried out by Menberg et al. [2]. The system was evaluated with 8 sub- systems in heating as well as 6 subsystems in cooling operation. The exergy flow path was examined from the input to the output, where the exergy consumption in cooling mode is mentioned to be approximately 2.71 kW compared to 7.62 kW in heating mode. The authors state the need of additional research regarding variable boundary and system conditions, the investigation of different reference environment definitions and dynamic exergy evaluation. Another study focused on measuring concepts in order to evaluate the efficiency of refrigeration plants with an exergy-based approach [17]. Typically, an exergy analysis requires an increased amount of measured quantities. Therefore, they suggest using adequate system boundaries for the calculation and to use thermodynamic relations to compute missing variables where possible. Further, they state the need of achievable reference values in order to allow an absolute comparison, as they can vary across different refrigerationplants.

Accordingtotheliteraturesearch,theinvestigatedrefrigeration systemsaremostlysplitintoreasonablesubsystemswithrespectto the available measurement data in order to allow a detailed assessment. The performance and optimization potential is then evaluatedintermsofkeyfigures.Typically,energyorexergyper-formanceindicatorsarereferredtoathermodynamicideal,which is not achievable in practice. However, it is relevant for plantop-eratorstoidentifytherealizableimprovementsandtohave refer- ence values for an absolute comparison. Optimization potentials shouldberevealed,asmeasureswhichimprovethesystem effec-tivenessmostlikelypreventfrequentshortcomingsduringrefrig-erationplantoperation.Itshouldnotrequirespecialistsinorderto determinewhetherthereisaneedtotakeactiononaninstallation. Therefore, a practice-oriented assessment method with technical standards as baseline is applied [18]. The objective of the present work is to introduce the method for refrigeration plants in free coolingoperation,which,tothebestofourknowledge,has never beenappliedbeforetosuchsystems.Toensureabroadapplicability in practice and to avoid high retrofitting costs by installing addi-tionalmeasurementequipment,thepresentedevaluation method aims to consider the most common measuring concepts of real refrigeration plants. First, the plant is divided into four different subsystems:drycooler,freecooling,coldwaterstorage&transport andcoolinglocation.Anexergyanalysisisthencarriedout andthe optimizationpotentialindex(OPI)isproposedforthefree cooling configuration.Thisallowsastraightforwarddeterminationofthe performanceandoptimizationpotentialofeachsubsystemin the refrigerationplant.WiththeOPI,acomparisonbetweendifferent refrigeration systems is possible and the reference can vary depending on the technological requirements, which is of great importance in practice. The assessment system is applied and its functionality demonstrated on a field plant as a casestudy.

II. REFRIGERATION PLANT

Fig. 1 shows schematically a typical refrigeration plant with coldwater distribution and free cooling. Usually, multiple refrigeration machines are set up in parallel (e.g. redundancy) and multiple cooling locations are present. The piping &instrumentation diagramisnotintendedtoshowtheidealconfiguration,buttoreveal theassignmentoftheauxiliarydevicestothedifferentsubsystems. The definition of the latter is based on investigations regarding existing systems but can be chosen differently according to the needed degree of detail. The present study focusses only on the refrigerationsystem,meaningotherbuildingcomponentssuchas ventilationsystemsorthebuildingenvelopearenotconsidered. In refrigeration machine operating mode, the cooling is realized by a refrigeration cycle (subsystem refrigeration machine RM), where the chilled water is distributed over a secondary hydraulic circuit (subsystem cold water storage &transport CST) to the cooling locations, e.g. air-handling units (subsystem cooling locationCL).Theheatfromthecycleprocessisdischargedoveranother secondary hydraulic circuit (subsystem dry cooler DC) with the aid of dry coolers. If the surrounding air temperature is substantially lower than the temperature in the refrigeration system, the use of free cooling is feasible. Typically, a free cooling module (subsystem freecoolingFC),inthesimplestformconsistingofaheatexchanger, is arranged in parallel to the chillers. In free cooling operation, the couplingofthesubsystemdrycooler(DC)andcoldwaterstorage&transport (CST) allows an indirect cooling of the cooling location (CL) without the use of the refrigeration machines (RM). Thus, the electrical energy of the compressors can be economized. This free cooling operating mode is mostly present in the colder monthsover theyearandissubjectofthepresentanalysis.

Moreover, the exergies of every subsystem in free cooling operationaswellasthemeasuredquantitiesforthecomputation are depicted in Fig. 1(for details see Tables 1 and 2). The arrows indicatetheexergyflowsandBLdescribestheexergylossinevery subsystem.Thecoolinglocationanddrycoolerthermalexergy,BCLand BDC, are not needed for the assessment but shown for completeness. Tambrepresents the ambient airtemperature.

For the present study, a field plant is examined, from which measurements were collected during the year 2018. The refrigerationplantislocatedinWinterthur,Switzerlandandincorporates

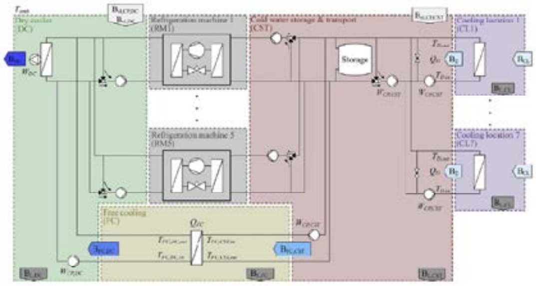

Fig. 1. Simplified piping &instrumentation diagram of a typical refrigeration plant with cold water distribution and free cooling divided into different subsystems. The exergy inputs and outputs in free cooling operation are depicted with arrows and measured variables shown in italic (for details see Tables 1 and 2).

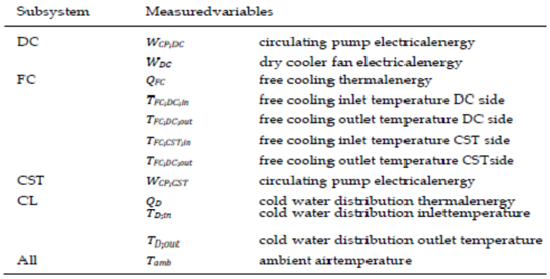

Subsystem	Measuredvariables	
DC	$W_{CP;DC}$	circulating pump electricalenergy
	W_{DC}	dry cooler fan electricalenergy
FC	Q_{FC}	free cooling thermalenergy
	$T_{FC;DC;in}$	free cooling inlet temperature DC side
	$T_{FC;DC;out}$	free cooling outlet temperature DC side
	$T_{FC;CST;in}$	free cooling inlet temperature CST side
	$T_{FC;DC;out}$	free cooling outlet temperature CSTside
CST	$W_{CP;CST}$	circulating pump electricalenergy
CL	Q_D	cold water distribution thermalenergy
	$T_{D;in}$	cold water distribution inlettemperature
	$T_{D;out}$	cold water distribution outlet temperature
All	T_{amb}	ambient airtemperature

Table 1
Measuredvariablesineachsubsystemfortheexergycalculation

five refrigeration machines with a total cooling power of approxi- mately 5 MW and ammonia (R717) as refrigerant. The plant sup- plies seven buildings with chilled water, where the cooling locations represent air-handling units of ventilation systems in the different buildings, three of which were integrated into the system inApril2018.Thetemperaturerequirementofallcoolinglocations isanaveragevalueofz13○Cbetweenthecoldwatersupply and return flow according to the design. Additionally, 12 circulating pumps are present, from which three are winter pumps for thefree cooling operation, in order to transport the cold water through the underground distribution network. One free cooling heat exchanger is integrated to the system, while three dry coolers discharge the heat to the environment. As a result, 10 different subsystems are defined to analyze the free cooling operation. No data was registered of the circulating pumps in free cooling oper- ation (winter pumps). As an approach, the electrical energy input is calculated under the assumption that they behave similarly as the circulating pumps in refrigeration machine operation.

III. ASSESSMENT APPROACH

3.1. Exergy balance and keyfigures

The rate of change of exergy dB/dt over a control volume, e.g. over a subsystem in the refrigeration plant, can be written as [19,20]:

$$\frac{dB}{dt} = \underbrace{\sum_i \left(1-\frac{T_0}{T_i}\right) Q_i}_{B_{th}} - \underbrace{\left(W - p_0 \frac{dV}{dt}\right)}_{B_w} + \underbrace{\sum_j m_{in,j} b_{in,j} - \sum_k m_{out,k} b_{out,k}}_{B_m} - B_L$$

The three underlined terms correspond to the exergy transfer by heat B_{th}, work B_w and massflow B_m, where

- Q_i representsaheatflowrateinoroutofthecontrolvolume,
- T_i is the temperature at which the heat transfer takesplace,
- T_0 corresponds to the referencetemperature,
- W representsmechanicalorelectricalpowerinoroutofthecontrolvolume,
- p_0 is the referencepressure,
- dV/dt corresponds to the rate of change of the controlvolume,
- $m_{in,j}$ and $m_{out,k}$ representthemassflowratesinandoutofthe controlvolume,
- $b_{in,j}$ and $b_{out,k}$ are the incoming and outgoing specific flow exergies, and,
- B_L correspondstotheexergyflowratelossesinthecontrol volume due to irreversibilities.

By definition, mechanical energy is pure exergy, as it can befully transformed into any other form of energy (e.g. heat). In contrast, thermal energy contains only a portion of exergy and cannot be fully transformed. By assuming steady-state, incompressible flow (liquid in the hydraulic circuits) and neglecting pressure lossesover thesystemboundaries, Eq.(1)canbe expressedasfollows[8,21]:

$$0 = \sum_i \left(1-\frac{T_0}{T_i}\right) Q_i - W + \sum_l \left(1-\frac{T_0}{\bar{T}_l}\right) Q_l - B_L \quad (2)$$

wheretheexergytransferbymassflowisnowexpressedbythenet heat Q_l transportedoverthesystemboundarywiththeincoming andoutgoingmassflowandthelogarithmicmeantemperature $\bar{T}_l$ definedas:

$$\bar{T}_l = \frac{T_{in,l} - T_{out,l}}{\ln \frac{T_{in,l}}{T_{out,l}}} \quad (3)$$

with $T_{in,l}$ the temperature of the incoming and $T_{out,l}$ the tempera- ture of the outgoing mass flow, respectively. With the intention of ensuring a broad applicability of the presented method, the simplifications mentioned above are considered tolerable. While the pressure losses are not explicitly treated for the exergy transfer between the subsystems, they are indirectly considered on subsystem level by assessing the exergy input of the circulatingpumps in the exergy analysis. A detailed hydraulic evaluation could be carried out in a further evaluation step, assuming that the required technical data is available. The exergy efficiency hex is mostly used to assess the exergy performance of thermodynamic systems. The key figure can be evaluated by balancing the total exergy output B_outtotheinputB_in[22]:

$$\eta_{ex} = \frac{B_{out}}{B_{in}} = 1 - \frac{B_L}{B_{in}} \quad (4)$$

which indicates how much exergy leaves the system compared to the input. The key figure reaches a value of 0 if the energy is completely degraded (only losses present) and 1 if a thermody- namic ideal process (no exergy losses) is considered. Since every real process is irreversible, exergy losses are to be expected and the need to know the best process possible is appearing. This indicator allows a relative comparison between different processes with re- gard to the thermodynamic ideal, but there are no reference values available stating which exergy efficiency should be achieved with a certain process. Thus, the quantification of the performance and possible optimization potentials according to the state of the art in technology is problematic, which is of great importance in practice. For this reason, the optimization potential index (OPI) is applied which has the following general form [18]:

$$OPI = 1 - \frac{\eta_{ex}}{\eta^*_{ex}} = 1 - \frac{\frac{B_{out}}{B_{in}}}{\frac{B_{out}}{B^*_{in}}} = 1 - \frac{B^*_{in}}{B_{in}} \quad (5)$$

The OPI balances the effective exergy efficiency hex according to measurement data with a reference efficiency h*. The key figure describes the behavior of the real system in comparison with a reference system under identical operation conditions while the sameexergyoutputB_outisachieved.Thus,theevaluationofasubsystemiscarriedoutwiththeassumptionthattheadjacent *subsystems perform identically. B_ andB_ describe the actual exergy input according to

Subsystem	Exergyinput		Exergyoutput	
DC	$B_{el,CP,DC}$	circulating pump exergy	B_{DC}	dry coolerexergy
	$B_{el,DC}$	dry cooler fanexergy		
	$B_{FC,DC}$	free cooling exergy DCside		
FC	$B_{FC,CST}$	free cooling exergyCSTside	$B_{FC,DC}$	free cooling exergy DC side
CST	$B_{el,CP,CST}$	circulating pump exergy	$B_{FC,CST}$	free cooling exergy CSTside
	B_D	cold water distributionexergy		
CL	B_{CL}	cooling locationexergy	B_D	cold water distributionexergy

Table 2
Exergy inputs and outputs of each subsystem

measurements and the reference exergy input, respectively. As a first approach, the reference values are defined according to technical standards (see subsection 3.3). This represents an achievable technological baseline, where the specified conditions can be fulfilled or exceeded if the refrigeration plant is properly engineered and maintained. Typically, such standards are specified in tenders or contracts and should be fulfilled at the stage of commissioning. Any other appropriate standards or limits (e.g. performance parameters) could find application, i.e. the baseline can depend on the technological requirements in different countries orregions.

With the OPI, the results are straightforward to interpret (see Fig. 2). No specialists are required to reveal eventual issues or improvement potentials, which is of great importance in practice.

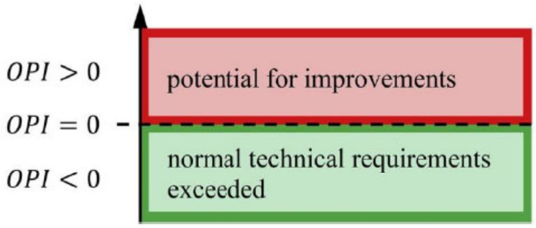

Fig. 2. OPI scale with the corresponding operating conditions.

For example, plant operators can easily evaluate the system operation by tracking the key figure over time. A colored indicator as depicted in Fig. 2 could be realized and implemented in monitoring systems, which helps also to raise awareness for an efficient refrigeration plant operation. If the actual exergy input of the subsystem is larger than the reference (meaning an increased input is required to achieve the same output), the OPI is larger than 0 and points out improvement potential. For example, assuming a fouled heat exchanger of the dry cooler. As a consequence, the cooler fans needtooperateatahigherfrequencytoensuretheneededheat transfer, while consuming an increased amount of electricalenergy.

The actual exergy input of the subsystem DC will be larger compared to the reference and the OPI reveals the issue with a value superior to 0. Conversely, if the dry cooler is correctlymaintained and operated, the actual exergy input is lower than the reference, where the OPI delivers a value inferior to 0. Thus, no optimization potential according to the state of the art in technologyispresent. AnOPIof0indicatesthatthetechnicalrequirements are met. Therefore, the OPI delivers a first localization of eventual issues and optimization potentials on subsystem level. In a second evaluation step, the malfunction can be further narrowed down with a more detailed analysis. Eventually, by including a cost analysis, it is revealed if adjustments to the system are worthwhile, not only from a technical but also an economical aspect. Plant operators can then initialize the appropriate corrective measures by specialists.

As for technical reasons, typically no physical data is available in real systems for the calculation of B (see Fig. 1) of the subsystem CL.Therefore,analternative approachisappliedforthelatterin freecoolingoperation.Namely,theexergyinputissettobe the sameintheactualandinthereference condition,whiletheexergy output varies according to the technical standards. The latter is plausiblefromathermodynamicviewpoint,asitisfavorablefor the subsystem, if more exergy is extracted compared to the reference operating condition. Thus, the interpretation of the OPI remains the same for the subsystemCL.

3.2. Reference environment

Exergy describes the energy potential with respect to an environmental reference. Therefore, exergy evaluations require a proper definition of the latter. Torío et al. investigated different reference states for the building environment, where they recommend using the surrounding ambient air as reference [23]. The variable outdoor temperature was applied in other studies [24,25]. However, other research stated to use a fixed and constant reference in order to carry out a consistent and reliable exergy analysis [26,27]. Therefore, as a first approach, a constant referencetemperatureT_0of5○C isusedinthepresentstudy,whichrepresents theaveragedoutdoortemperatureofthemonthsJanuaryto April andNovembertoDecember2018, accordingtomeasurementsfrom the investigated field plant. While the definition of the reference environment may influence the absolute values of the exergy,the effect on the OPI is assumed to be small, as the same reference temperature is used for the actual and reference exergy.

3.3. Subsystemevaluation

With the goal to achieve a daily assessment of refrigeration plants in free cooling operation, as the cooling load in air-conditioning applications typically exhibits a daily rhythm, a quasi-stationary approach is chosen. The exergy flow rates are determined and balanced over each subsystem. The needed quantities are calculated from measurement data, obtained with reference values from technical standards or determined with an

Subsystem	Optimization potentialindex	
DC	$OPI_{DC} = 1 - \frac{\sum_{t=0h}^{24h}\left[\dot{B}^{*}_{FC,DC} + \sum_i \dot{B}^{*}_{el,CP,DC,i} + \sum_j \dot{B}^{*}_{el,DC,j}\right]}{\sum_{t=0h}^{24h}\left[\dot{B}_{FC,DC} + \sum_i \dot{B}_{el,CP,DC,i} + \sum_j \dot{B}_{el,DC,j}\right]}$	(6)
FC	$OPI_{FC} = 1 - \frac{\sum_{t=0h}^{24h} \dot{B}^{*}_{FC,CST}}{\sum_{t=0h}^{24h} \dot{B}_{FC,CST}}$	(7)
CST	$OPI_{CST} = 1 - \frac{\sum_{t=0h}^{24h}\left[\sum_i \dot{B}^{*}_{D,i} + \sum_j \dot{B}^{*}_{el,CP,CST,j}\right]}{\sum_{t=0h}^{24h}\left[\sum_i \dot{B}_{D,i} + \sum_j \dot{B}_{el,CP,CST,j}\right]}$	(8)
CL	$OPI_{CL} = 1 - \frac{\sum_{t=0h}^{24h} \dot{B}_{D}}{\sum_{t=0h}^{24h} \dot{B}^{*}_{D}}$	(9)

Table 3 Proposed OPI definitions of every subsystem in free cooling operation of the refrigeration plant.

exergy balance (see Eq. (2)). Subsequently, the exergy flow rates are numerically integrated with the trapezoidal rule over the present measurement interval of 5 min. The corresponding exergies of each interval are then summed up over 24 h and the optimization potential index is evaluated on a daily basis. Each subsystem of the field plant in free cooling operation is assessed separately with the described procedure. Table 3 lists the proposed definitions of the optimization potential index of each subsystem under consideration, with the exergies according to Table 2. The exergies marked with an asterisk represent reference values computed with technical standards. The detailed approach is introduced below using the subsystem dry cooler (DC) as an example, whereby the OPI for the other subsystems is determined similarly using the corresponding measured variables from Table 1. The OPI DC is proposed according to Eq. (6) (see Table 3), where the electrical exergy input of each present circulating pump and dry cooler fan is summed up. The free cooling exergy on the DC side $B_{FC;DC}$ is defined as:

$$B_{FC;DC} = Q_{FC}\left(1 - \frac{T_0}{\overline{T}_{FC;DC}}\right) \tag{10}$$

where Q_{FC} represents the free cooling thermal energy, T_0 the reference temperature and $\overline{T}_{FC;DC}$ the logarithmic mean temperature of the secondary circuit of the heat exchanger according to:

$$\overline{T}_{FC;DC} = \frac{T_{FC;DC;in} - T_{FC;DC;out}}{\ln\left(\frac{T_{FC;DC;in}}{T_{FC;DC;out}}\right)} \tag{11}$$

with the inlet and outlet temperature $T_{FC;DC;in}$ and $T_{FC;DC;out}$ of the heat exchanger on the dry cooler side. By definition, electrical energy is pure exergy, and thus, the exergy of the dry cooler fans $B_{el;DC}$ is given by:

$$B_{el;DC} = W_{DC} \tag{12}$$

with the dry cooler fan electrical energy W_{DC}. Correspondingly, the exergy of circulating pumps $B_{el;CP;DC}$ is defined by:

$$B_{el;CP;DC} = W_{CP;DC} \tag{13}$$

with $W_{CP;DC}$, the respective electrical energy input of the circulating pumps. The reference exergy of the free cooling on the DC side $B^{*}_{FC;DC}$ is given by:

$$B^{*}_{FC;DC} = Q_{FC}\left(1 - \frac{T_0}{T^{*}_{FC;DC}}\right) \tag{14}$$

where $T^{*}_{FC;DC}$ represents the reference temperature of the free cooling module. As no reference temperatures for the inlet and outlet of the free cooling module according to technical standards are available, a definition similarly to Eq. (11) is not possible. Therefore, a calculation with the ambient air temperature as a basis and temperature differences according to technical standards as well as available measurements is proposed as a first approach:

$$T^{*}_{FC;DC} = T_{amb} + \Delta T_{HE} + \frac{T_{FC;DC;out} - T_{FC;DC;in}}{2} \tag{15}$$

where T_{amb} is the ambient air temperature and ΔT_{HE} the temperature difference between the secondary hydraulic circuit medium and the ambient air in the dry cooler heat exchanger. According to the technical standard VDMA 24247-8 [28], a desirable temperature difference ΔT_{HE} of 6 K is defined. The reference exergy of the dry cooler fans $B^{*}_{el;DC}$ is proposed as follows:

$$B^{*}_{el;DC} = \frac{1}{f_{el;th;DC}} Q_{FC} \tag{16}$$

with the electro-thermo amplification factor for dry cooler fans $f_{el;th;DC}$ (see Table 4). This factor determines the desirable amount of electrical energy consumed by auxiliary devices with respect to the transferred thermal energy. Similarly, the reference exergy of the circulating pumps $B^{*}_{el;CP;DC}$ is given by:

$$B^{*}_{el;CP;DC} = \frac{1}{f_{el;th;CP;DC}} Q_{FC} \tag{17}$$

where $f_{el;th;CP;DC}$ represents the electro-thermo amplification factor for circulating pumps (see Table 4). The amplification factors are defined in the technical standard SIA 382/1 [29] with respect to the thermal energy of the condenser and evaporator of the integrated refrigeration machine. As an approach, the thermal energy of the free cooling module is used for the computation of the reference exergies of the auxiliary devices, as the refrigeration machines are turned off in free cooling operation.

Concerning the other subsystems, the reference exergy of the circulating pumps $B^{*}_{el;CP;CST}$ in the subsystem CST is computed similarly to Eq. (17) with the electro-thermo amplification factor $f_{el;th;CP;CST}$ according to Table 4. The reference exergy of the free cooling module $B^{*}_{FC;CST}$ on the CST side is determined by an exergy balance of the reference exergies in the subsystem CST. The cold water distribution reference exergy B^{*}_{D} of the subsystem CL is calculated according to Eq. (14), but with the cold water distribution thermal energy Q_D. The cold water distribution reference temperature T^{*}_{D} is determined similarly to Eq. (11) with temperatures of the secondary side hydraulic circuit according to the technical standard SIA 382/1 [29]. A cold water distribution reference inlet temperature $T^{*}_{D;in}$ of 10 °C and a cold water distribution reference outlet temperature $T^{*}_{D;out}$ of 16 °C is specified, representing the temperature level for an air-conditioning application with partial dehumidification.

Subsystem	Electro-thermo amplification factor		Threshold value
DC	dry cooler fan	$f_{el;th;DC}$	≤28
	circulating pump	$f_{el;th;CP;DC}$	≤85
CST	circulating pump	$f_{el;th;CP;CST}$	≤65

Table 4
Amplification factors for auxiliary devices according to the technical standard SIA 382/1 [29].

IV. RESULTS AND DISCUSSION

The investigated field plant exhibits free cooling operation if the measured compressor electrical energy W_{CPR} is equal to and the free cooling thermal energy Q_{FC} larger than 0 J, respectively. This is the case from January to mid-March as well as from end of October to December 2018. Mixed operation of the refrigeration machines and the free cooling module, e.g. precooling overnight, is not considered in the present work. The daily OPI (y-axis) of every subsystem in the refrigeration plant in function of the date (x-axis) is depicted in Fig.3.

4.1. Subsystem FC

To begin with, the subsystem FC shows an average OPIFCof 0.30 and exhibits almost a steady-state behavior over the investigated time period (see Fig. 3a). The minimum of 0.45 is achieved on December 25th and the maximum of 0.21 on November 21st. The key figure is 100% of the time lower than 0 and thus, the technical requirements according to the applied technical standards are exceeded. This leads to the assumption that the implemented heat exchanger is well designed according to the specifications, which results in an adequate operation and performance.

4.2. SubsystemCST

The subsystem CST reveals a similar behavior, where the tech- nical requirements are fulfilled. The OPICSTis 100% of the investi- gated time period lower than 0 and shows an average value of 0.30 (see Fig. 3a). The hydraulic circuit is apparently well designed and the circulating pumps correctly operated, resulting in a low electrical power consumption and a low exergy input compared to the reference, respectively. Interestingly, the performance indicator reveals an increase of approximately 0.2 from mid- March to end of October. A possible reason are the three additional coolinglocationswhichwereintegratedattheendofApril, and thus, the actual exergy input of the subsystem is increased. Most likely, the circulating pumps exhibit an increased electrical energy usage,duetotheadditionalpipinginstalledinthehydrauliccircuit.

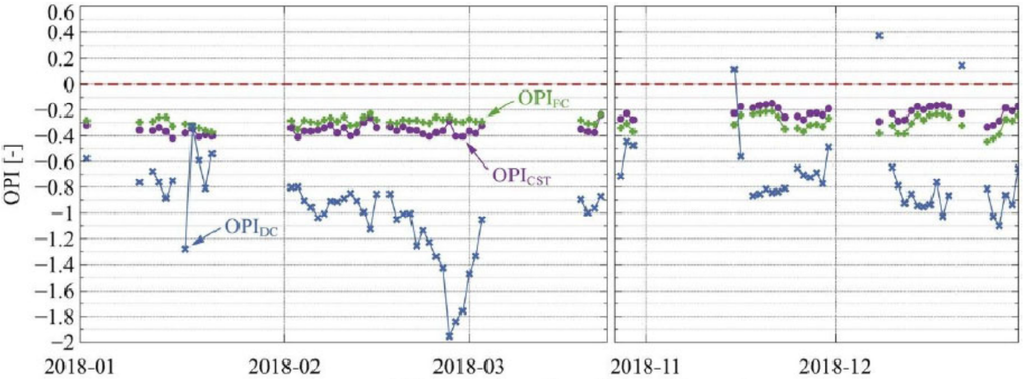

(a) Dry cooler, free cooling, cold storage & transport

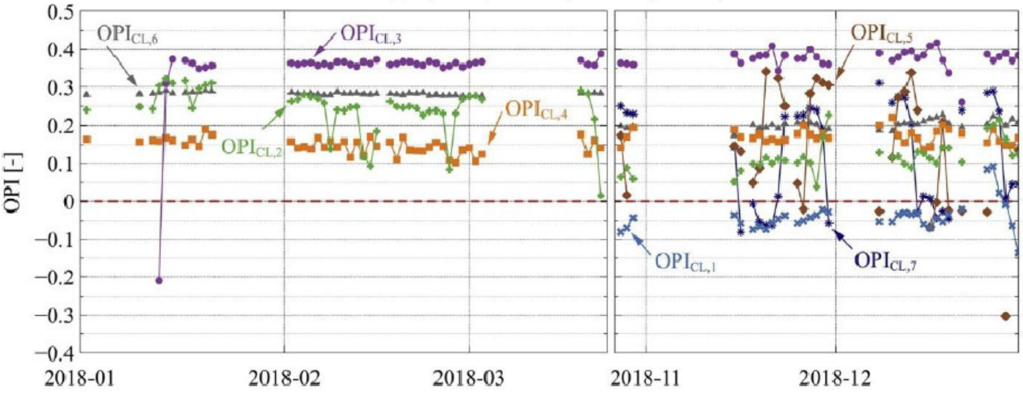

(b) Cooling location

Fig. 3. Optimization potential index (OPI) of the subsystem DC, FC and CST (a) as well as subsystems CL,1 to CL, 7 (b).

4.3. SubsystemCL

The cooling locations CL reveal a differentiated behavior (see Fig.3b).Coolinglocation1performsbest,hasanaveraged OPICL;1of approximately 0.04 and is 92% of the time lower than 0. Cooling locations 2, 4, 5 and 7 operate close to the technicalrequirements with an average OPI of 0.19, 0.16, 0.13 and 0.12, respectively. Accordingly, these cooling locations should be observed closely during further operation. An increase of the key figure would indicate a possible malfunction. In contrast, the cooling location 3 performs worst with an average OPICL;3 of 0.36 and cooling location 6 reveals an averaged OPICL;6 of 0.25. Therefore, both cooling loca- tions show an increased potential for improvement. A possible reason can be a fouled or suboptimal heat exchanger, which results in a decreased cold water distribution temperature to achieve the needed heat transfer, compared to the chosen reference (see subsection 3.3). Also, a different dimensioning might be present in the refrigeration plant compared to the initial design, meaning that the cooling locations supply an air-conditioning application with a different temperature level as assumed in the reference conditions (e.g. an air-conditioning application without dehumidification). Asa consequence, the mentioned cooling locations should be inspected to determine eventual issues and to initiate counter-measures in order to achieve an increased performance.

4.4. SubsystemDC

The subsystem DC operates according to the technical requirements,similarlytothesubsystemsFCandCST,andexhibitsan average OPIDCof 0.87 (see Fig. 3a). Three outliers with a value superior to 0 are present on November 15th as well as December 8th and 21st. However, such outliers should not be overly considered, as only a constantly high or rising key figure is a possible indication of a faulty operation. By investigating the daily exergy sums, the reason for the adequate performance of the subsystemDC is revealed (see Fig.4).

The exergy input of the circulating pumps (see Fig. 4b) is all the time lower than the reference. Also, the exergy input of the dry cooler fans (see Fig. 4c) is substantially, around factor 2, lower than the reference. This is favorable for the refrigeration plant operation. The actual dry cooler fan input is increased by approximately a factor of 6 the same days the OPI reveals a potential for improve- ment, and thus, the behavior of the dry cooler fans determines the outcome. The thermal exergy input of the free cooling module (see Fig. 4a) exhibits values according to the technical standards. It is revealed, that a decreased electrical exergy input is more favorable for the subsystem than an adequate temperature level. The refer- ence electrical exergy is roughly factor 2 higher than the reference thermal exergy and, interestingly, the actual electrical exergy in- puts of the auxiliary devices exhibit a similar magnitude as the actual thermal exergy input. In energetic considerations, their input would account only for roughly 4.7% of the thermal load according to technical standards. This outcome emphasizes to reduce the auxiliary electrical energy input where possible, e.g. with an adaptivespeedcontrolofthecirculatingpumpsanddrycoolerfans, inordertoachieveahighlyperformingrefrigerationplant.

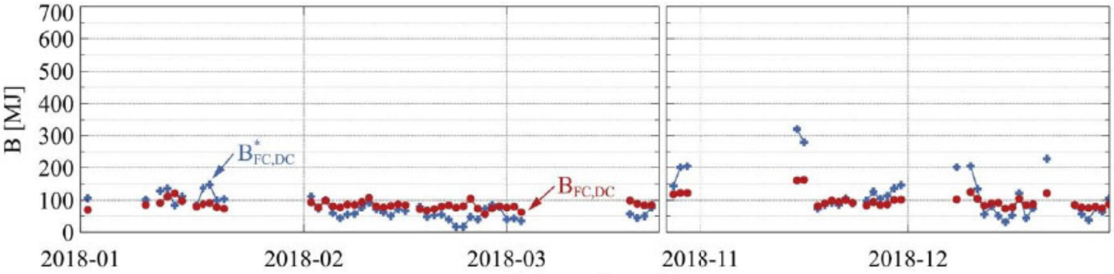

(a) Free cooling module

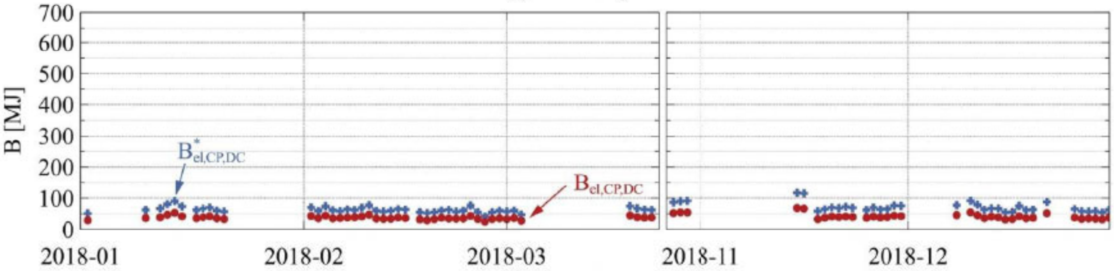

(b) Circulating pumps

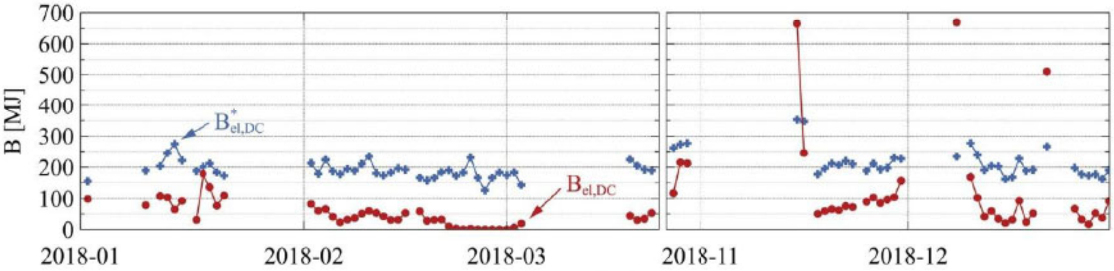

Fig. 4. Daily exergy sum of the subsystem DC input from the free cooling module (a), circulating pumps (b) and dry cooler fans (c).

5. Conclusions andoutlook

The introduced optimization potential indices for free cooling operation of refrigeration plants allows an assessment of the per- formance and the corresponding optimization potential in every subsystem at a glance. The identification of possible optimization potentials is relevant, as measures which improve the system effectiveness most likely prevent frequent shortcomings during refrigeration plant operation. The functionality of the methodology was shown by applying it with experimental data from an existing field plant as a case study. With defined reference values according to the state of the art in technology, an absolute comparison be- tween different refrigeration plants is feasible. The interpretation of the results is straightforward, which is of great importance in practice. Laypersons can easily determine the system operating state and initiate countermeasures by specialist if needed. A simple red/green indicator could be realized to facilitate the monitoring of the plant operation. Furthermore, the exergy-based assessment system helps to sensitize all involved actors, e.g. plant operators, regarding an efficient operation of refrigeration plants. The pre- sented method finds possibly also application in other building energy systems, such as heatpumps. The investigated field plant reveals a performance according to the technical requirements in general, whereby it can be concluded that the overall design of the hydraulic circuits is adequate and the auxiliary devices properly controlled. Two out of seven cooling locations show significant potential for improvement. The latter could be realized by e.g. ameliorating the heat transfer or including another hydraulic circuit for the cold water distribution on the desired temperature level according to the air-conditioning appli- cation. Moreover, the analysis shows the importance of reducing the energy usage of auxiliary devices to achieve an adequate per-formance of theplant. Further investigations are needed regarding the determination of the cooling location exergy. As no measurements were available for the present study, an alternative approach was used for the subsystem cooling location to determine the optimization potential index. To allow a consistent definition of the latter, the temperature and the corresponding air humidity of the cooling location circuit(e.g. ventilation system) needs to be measured in the future. This includes the determination of the exergy of humid air, which is typically present in air-conditioning applications or evaporative coolers, e.g. cooling towers. Likewise, if further technical informa- tion would be available, a hydraulic analysis could be integrated to the proposed method in order to evaluate the specific flow exergies and to consider occurring pressure losses in detail. While no cost analysis was considered in the present work, it could be carried out in a subsequent evaluation step in order to determine if the found optimization potential is also worthwhile from an economic point of view. Furthermore, the exergy-based assessment system should be applied to other field plants, preferably with a different cooling power and other subsystems such as heat utilization. This helps to identify interrelationships between various refrigeration systems and to use them for future evaluations. Further technical reference values should be determined, as it is currently not possible to es- timate which values of the optimization potential index close tothe limit of 0 still represent a permissible operation. Ideally, these limits are specified with statistically sound, representative mea- surements and with the help of experts. Not only technical and methodical but also strategic aspects have to be considered together with all actors in the industry. This involves long term investigations of different real systems. In addition, future in- vestigations should analyze the influence of the reference envi- ronment on the optimization potentialindex. CRediT authorship contribution statement Lorenz Brenner: Methodology, Formal analysis, Investigation, Writing - original draft, Visualization. Frank Tillenkamp: Conceptualization, Validation, Writing - review &editing, Super- vision, Funding acquisition. Christian Ghiaus: Validation, Writing - review &editing, Supervision. Declaration of competing interest The authors declare that they have no known competing financial interests or personal relationships that could have appeared to influence the work reported in this paper. Acknowledgements This study was partially funded by the Swiss Federal Office of Energy (SFOE). Appendix A. Supplementary data

Supplementary data to this article can be found online at https://doi.org/10.1016/j.energy.2020.118464.

REFERENCES

[1] Wu D, Hu B, Wang R. Performance simulation and exergy analysis of a hybrid source heat pump system with low GWP refrigerants. Renew Energy2018;116:775e85.https://doi.org/10.1016/J.RENENE. 2017.10.024.

[2] Menberg K, Heo Y, Choi W, Ooka R, Choudhary R, Shukuya M. Exergy analysis of a hybrid ground-source heat pump system. Appl Energy 2017;204:31e46.https://doi.org/10.1016/J.APENERGY.2017. 06.076.

[3] Razmara M, Maasoumy M, Shahbakhti M, Robinett R. Optimal exergy controlof building HVAC system. Appl Energy 2015;156:555e65. https://doi.org/ 10.1016/J.APENERGY.2015.07.051.

[4] Fan B, Jin X, Fang X, Du Z. The method of evaluating operation performance of HVAC system based on exergy analysis. Energy Build 2014;77:332e42.https://doi.org/10.1016/j.enbuild.2014.03.05 9.

[5] Fudholi A, Zohri M, Jin GL, Ibrahim A, Yen CH, Othman MY, Ruslan MH, Sopian K. Energy and exergy analyses of photovoltaic thermal collector with

[6] ∇-groove. Sol Energy 2018;159:742e50. https://doi.org/10.1016/J.SOLENER.2017.11.056.

[7] Agrawal S, Tiwari G. Energy and exergy analysis of hybrid micro-channel photovoltaic thermal module. Sol Energy 2011;85(2):356e70. https:// doi.org/10.1016/J.SOLENER.2010.11.013.

[8] Sangi R, Müller D. Exergy-based approaches for performance evaluation of building energy systems.

Sustainable Cities and Society 2016;25:25e32.https://doi.org/10.1016/J.SCS.2016.04.002.

[9] Saloux E, Teyssedou A, Sorin M. Development of an exergy-electrical analogy for visualizing and modeling building integrated energy systems. Energy Convers Manag 2015;89:907e18. https://doi.org/10.1016/J.ENCONMAN.2014.10.056.

[10] Harrell J, Mathias J. Improving efficiency in a campus chilled water system using exergy analysis. Build Eng2009;115(1):507e22.

[11] Yang M-H, Yeh R-H. Performance and exergy destruction analyses of optimal subcooling for vapor-compression refrigeration systems. Int J Heat Mass Tran2015;87:1e10.https://doi.org/10.1016/J.IJHEATMASSTRANSFER.2015.03.085.

[12] FratzscherW,BrodjanskijVM,MichalekK.Exergie-TheorieundAnwendung. Leipzig: DeutscherVerlagfürGrundstoffindustrie;1986.

[13] Shan K, Wang S, Gao DC, Xiao F. Development and validation of an effective and robust chiller sequence control strategy using data-driven models. AutomConStruct2016;65:78e85.https://doi.org/10.1016/j.autcon.2016.01.005.

[14] Dong K, Li P, Huang Z, Su L, Sun Q. Research on free cooling of data centers by using indirect cooling of open cooling tower. Procedia Engineering 2017;205: 2831e8.https://doi.org/10.1016/J.PROENG.2017.09.902.

[15] Sorrentino M, Rizzo G, Trifiro A, Bedogni F. A model-based key performance index for energy assessment and monitoring of telecommunication cooling systems. IEEE Transactions on Sustainable Energy 2014;5(4):1126e36.https://doi.org/10.1109/TSTE.2014.2334365.

[16] Kazanci OB, Shukuya M, Olesen BW. Theoretical analysis of the performanceof different cooling strategies with the concept of cool exergy. Build Environ2016;100:102e13.https://doi.org/10.1016/J.BUILDENV.2016.02.013.

[17] Al-Bassam E, Alasseri R. Measurable energy savings of installing variable frequency drives for cooling towers' fans, compared to dual speed motors. Energy Build 2013;67:261e6.https://doi.org/10.1016/j.enbuild.2013.07.081.

[18] Eisenhauer S, Hauck T, Arnemann M. SystematischeErstellung und Anwendung messtechnischerKonzeptezurenergetischenUntersuchungvon Ka€lteanlagen.Dresden:DKV-Tagung;2015.

[19] Brenner L, Tillenkamp F, Krütli M, Ghiaus C. Optimization potential index (OPI): an evaluation method for performance assessment and optimization potential of chillers in HVAC plants. Appl Energy 2020;259. https://doi.org/10.1016/j.apenergy.2019.114111.

[20] Moran MJ, Shapiro HN, Boettner DD, Bailey MB. Fundamentals of engineering thermodynamics:SIversion.NewYork:JohnWiley;2010.

[21] BejanA,TsatsaronisGG,MoranMJ.Thermaldesignandoptimization.Wiley; 1996.

[22] Ducoulombier M, Sorin M, Teyssedou A. Thermodynamic bounds for fooddeep chilling tray tunnel operation. Int J ThermSci 2007;46(2):172e9. https://doi.org/10.1016/J.IJTHERMALSCI.2006.05.001.

[23] Çengel YA, Boles MA. Thermodynamics: an engineering approach. Boston: McGraw-Hill;2005.

[24] Torío H, Schmidt D. Annex 49final report: energy Conservation in Buildings andCommunitySystems(ECBCS)-lowexergysystemsforhigh-performance buildingsandcommunities.Tech.rep.Stuttgart:FraunhoferIBP; 2011.

[25] MartinaitisV, BielskusJ, Januˇseviˇciusк,BareikaP.Exergyefficiencyofa ventilation heat recovery exchanger at a variable reference temperature.Mechanics 2017;23(1):70e7.https://doi.org/10.5755/j01.mech.23.1.1767.

[26] Zhou Y, Gong G. Exergy analysis of the building heating and cooling system from the power plant to the building envelop with hourly variable reference state. Energy Build 2013;56:94e9. https://doi.org/10.1016/J.ENBUILD.2012.09.041.

[27] Bonetti V. Dynamic exergy analysis for the built environment:fixed or vari- able reference?. Proceedings of the 9th exergy, energy and environment symposium.Split,Croatia:FESB,UniversityofSplit;2017.p.924e39.

[28] Pons M. On the reference state for exergy when ambient temperature fluc- tuates. Int J Therm 2009;12(3):113e21. https://doi.org/10.5541/ IJOT.1034000246.

[29] VereinDeutscherMaschinen-undAnlagenbau(VDMA).EnergieeffizienzvonKlimak€alteanlagen.Teil8:Komponenten-Wa€rmeübertrager(VDMA24247-8). Beuth;2011.

[30] Swiss Society of Engineers and Architects (SIA). Lüftungs- und Klimaanlagen -AllgemeineGrundlagen und Anforderungen (SIA 382/1). SIA;2014

★★★

DUAL ROLL CASTING OF HIGH Mg CONTAINED ALUMINUM ALLOY

[1]VELMURUGAN G, [2]SURYAKANTA DASH, [3]SRIKANT KUMAR SAHOO

[1]Department of Mechanical Engineering, NMIET, Bhubaneswar, 751019
[2]Department of Mechanical Engineering, REC Bhubaneswar
[3]Department of Mechanical Engineering, AIET Bhubaneswar
E-mail: [1]velmurugan.g@nmiet.ac.in

Abstract - Twin roll strip casting of aluminum alloy AC7B using commercial scale machine was operated. Twin roll casting process is able to produce a strip from molten metal directly. Thus this process has a possibility to reduce total cost of sheet making comparing to conventional rolling process. Strip casting process has some disadvantages. Casting speed depends on the material properties. It is difficult to determine the casting conditions. Theaimsofthisstudyistoinvestigatetheeffectoftheinitialrollgaponthestrip.Continuousstripcouldnotbeproducedatthe rollspeedof10m/min.Continuousstripwasproducedattherollspeedof20m/min.Thestripconsistedofanopaquepartand a metallic luster part. However, cracks were observed. Continuous strip was produced at a roll speed of 30 m/min. However, cracks were observedtoo.

Keywords - Twin Roll Casting Process, Aluminum Alloy AC7B, Castability, Surface Condition, Strip Thickness

I. INTRODUCTION

It is important that the improvement of fuel efficiency of transport machine such as automobile through the viewpoint of the global environment and the resource protection. The methods of improving fuel efficiency are the several ways such as improving of power drive system and reduction of running resistance and weight. Among them, weight saving of car weight is an effective method of improving fuel efficiency. Therefore, Aluminum for car structural material is attracted attention from the view point of the weight reduction. The Demand of aluminum is increasing for recent years in Japan. Especially the demand of aluminum for transport machine is increasing in last years. [1] Therefore, it is necessary to reduce the cost of manufacturing Aluminum strip.

This paper describes a vertical type twin roll strip casting process for producing aluminum alloy strip of AC7B. Aluminum strip[2] is generally produced by multi process such as DC casting, scalping,hot rolling of 200 mm ~ 600 mm thickness slab, repeated cold rolling and annealing. Form the above, the manufacturing cost of Aluminum strip become high because of the number ofprocesses.

Theverticaltwinrollstripcasterwasusedinthisstudy. It is possible to produce an Aluminum strip continuously from molten metal directly by twin roll strip casting. The molten metal was solidified on the roll surface and formed to strip. Strip thickness is about1~3mm.Stripcastingprocessisarapidcooling solidification process. So that the mechanical properties improve. The roll speed is generally high in twin roll casting such as 60 ~ 150 m/min. Thus, it is possible to reduce the strip manufacturing cost compared with the conventional rolling process because of the highly productivity. Strip casting process has some disadvantages. Casting speed depends on the material properties. It is difficultto determine the casting conditions.

Aluminum alloy AC7B is contained high Mg. A lot of studyoftwinrollcastingisreported[3]-[6]. Inthisstudy, continuous casting method of vertical twin roll strip of aluminum alloy AC7B using large equipment for practical use of strip casting was studied. In this study, the influence of the roll speed was investigated. The continuity, surface condition, sheet thickness, rolling load, internal structure of the strip wereevaluated.

II. EXPERIMENTAL DEVICE AND CONDITION

Fig. 1 (a), (b) and (c) show photographs of the experimentalapparatus.Fig.1(a)isafrontviewofthe device. Fig. 1 (b) is a top view. Fig. 1 (c) is an overall view. This device was manufactured by IHI Co., Ltd. and transferred to Gunma University Ota Campus. This device was manufactured for magnesium alloys. In this time, some modifications were made in conducting experiments on aluminum alloys. The roll material is SKD 61, the roll diameter is 1,000 mm,the roll width is 240 mm, it is a solid material. The maximum rolling load on the design is 75 tons, and it is possible to apply loads up to 312.5kgf / mm when converted per unit width. The roll gap is fixed type. The roll speed is variable using an inverter and can be variedfrom3m/minto100m/min.Thecapacityofthemotoris3phases400V,80kW,andtherollisrotated through the gear box and the universal joint. Fig. 2 showsaphotographoftheloadcell.Twoloadcellsare installed and it is possible to successively measure the rollingloadduringtwinrollcastingthatchangesevery minute. In this study, only the maximum load in the experimentisshown.Fig.3showsaphotographofthe side dam. The side dam is formed from a mild steel strip and five layers of heat resistant cloth. Heat resistant cloth was pasted to mild steel strip using spray glue

(3M, 88). Approximately 2 kg ofAC7B alloy was melted in a crucible furnace. Fig.4 shows a photograph of the pouring mechanism. We installed a wire in the crucible box and pour the molten metal by tilting the box by pulling the wire from the mezzanine level of the laboratory for safety. Fig. 5 shows a photograph of the nozzles. The nozzles are formed of aluminum sheet and heat resistant cloth. The nozzle was used to control the coagulation distance. No release agent to the roll was used. The experimental conditions are shown in Table 1. The initial roll gap was 2.0 mm. Roll gap was adjusted by tightening the nut. We checked it with thickness gauge. The pouring temperature was 611 ° C (5 ° C on the liquidus). The roll speed were 10 m/min, 20 m/min and 30 m/min.

(a) Front view (b) Top view

(c) Overall view

Fig. 1 Twin roll strip casting machine

Fig.2 Load cell

Fig. 3 Side dam plate

Fig. 4 Pouring device

Fig. 5 Nozzle

Material	AC7B
Pouring temperature [℃]	611
Initial roll gap [mm]	2.0
Solidification length [mm]	100
Roll speed [m/min]	10, 20, 30

Table 1 Experimental conditions

III. RESULTS ANDDISCUSSION

Fig. 6(a), (b), and (c) show photographs of the produced strips. Table 2 shows the measurement results of thickness, length and maximum load of the strips. The width of the strips are the same as the roll width. At the roll speed of 10 m/min, no cracks were observed and the surface condition of the strip is metallic luster.

At the roll speed of 20m/min, the surface condition of the strip is metallic luster part and white turbid part. Fig7and8showtheenlargedphotographsofthestripsurfaceat20m/min.Fig.7showstheedgeoftheplate, andhotcrackswereobservedatthemetalliclusterpart of the edge.That is because the amount of solidification near the edge increased. Therefore partial draft increased. Fig. 8 shows a white turbid part. Solidification cracks were observed in the white turbid part. In the turbid part, the contact between the rollandthemoltenmetalisinsufficient,sothecooling becomes insufficient.

It is considered that cracks occurred because the solidification was not completed and the rolling force oftherollwasreceived. Attherollspeedof30m/min, the strip was composed of the white turbid. This is because there was a difference between the roll speed and the speed of discharged strip.

Thereforethefillingofthemoltenmetalinthegapwas insufficient. Solidification cracks were observed too. The initial roll gaps were differfrom the strip thicknesses because of insufficient skill in the equipment. It is considered that this problem can be solved by setting the initial roll gap to the target strip thicknessinconsiderationoftheelasticdeformationofthe device.

Roll speed [m/min]	10	20	30
Strip length [mm]	185	1082	1027
Strip thickness [mm]	3.03	2.55	2.18
Rolling load [t]	80.21	41.69	10.40

Table 2 Strip thickness and rolling load

(a) 10 m/min

(b) 20 m/min

(c) 30 m/min

Fig. 6Produced strip

Fig.7 Hot rolled crack

Fig. 8 Solidification crack

ACKNOWLEDGMENT

This work was supported by the subsidy of the association for the advancement of Science & Technology, Gunma University. And this study was operated at Monodukuri Innovation Center, Gunma, Japan. And this study was supported by the Light Metal Educational Foundation, Inc..

REFERENCE

[1] Light Metal Society edition: Microstructure and properties of aluminum(1991)
[2] Engler,C.Schäfer,H.J.Brinkman,J.Brecht,P.BeiterandK. Nijhof, Journal of Materials Processing Technology, 229 (2016),139-148.
[3] T.Haga,H.Inui,H.WatariandS.Kumai,JournalofMaterials Processing Technology, 191, 1-3 (2007),238-241.
[4] T. Haga, M. Ikawa, H. Watari and S. Kumai, Journal of Materials Processing Technology, 172, 2 (2006),271-276.
[5] T.Haga,K.Takahashi,M.IkawaandandH.Watari,Journalof Materials Processing Technology, 153-154 (2004),42-47.
[6] T. Haga and S. Suzuki, Journal of Materials Processing Technology, 143-144 (2003),895-900.

★★★

RESEARCH ON MECHANICAL PROPERTIES OF EPOXY BASED KENAF/BANANA/GLASS FIBER HYBRID NANO COMPOSITES

[1]VENUGOPAL T, [2]ISWARANJAN BISWAL, [3]KRUSHNAPRIYA MOHAPATRA

[1]Department of Mechanical Engineering, NMIET, Bhubaneswar, 751019
[2]Department of Mechanical Engineering AIET Bhubaneswar
[3]Department of Mechanical Engineering REC Bhubaneswar
E-mail: [1]subhasis.sarkar@nmiet.ac.in

Abstract - Development of the polymer hybrid composite as a sustainable alternative materials for some engineering applications, particularly in aerospace application and automobile applications are being investigated. The role of natural fibers reinforced hybrid composite are growing in a field of engineering and technology due to favorable properties. In the present unsustainable environmental condition natural fibers are serving better materials in terms of biodegradability, low cost, high strength and corrosion resistance when compared to conventional materials. The main objective is to prepare the Kenaf/Glass fiber hybrid composite filled with graphene as nano filler and to investigate the mechanical properties of hybrid composites. The different types of hybrid composites laminates are fabricated without filler, 0.5, 1 &1.5Wt % of graphene by using kenaf and glass fiber as reinforcing material with epoxy resin. The specimen were prepared as per the ASTM standards and results shows that the mixing of graphene in epoxy resin improves the mechanical properties of hybrid composites and also the performance of kenaf/glass fiber composites is more than banana/glass fibercomposites.

Keywords - Kenaf Fiber, Banana Fiber, Nano Filler, Hybrid Composite Material

I. INTRODUCTION

Since from past two decades, there is tremendous growth in development of FRP composites with high strength to weight ratios, as it has acquired the various fields of application, ranging from shipbuilding, aerospace, automotive, to recreation equipment, furniture, office products, biomedical devices and implants, construction and building industry etc. With the increase in requirements, there is a demand to develop the stronger and cost effective composites. The fiber/matrix interface plays a vital role in determining the mechanical properties of glass fiber composites[1]. When the addition of filler materials to Epoxy/Glass fiber composites is increased then the thermal expansion coefficient of the corresponding composite getsreduced[2].

The tensile strength and the tensile modulus of Glass fiber/Epoxy composite increases in fiber loading and the addition of Nano filler particles to the Glass fiber/ Epoxy composite increases the tensile strength and the tensile modulus of the composite. Also, the addition of Nano filler particles to the Glass fiber/Epoxy composites increase the flexural properties of the Glass fiber composite[3] It has been reported that the addition of Nanoclay to Glass fiber/Epoxy composites increases the interfacial shear strength tremendously[4].The fiber/matrix interface plays a vital role in determining the mechanical properties of glass fiber composites[5]. When the content of Nanoclay is increased beyond an optimal level then the mechanical properties of the resultant composites decreases[6]. The percentage of Nanoclay to be used should be restricted to 5 wt% in order to get good mechanical properties of thecomposites[7].

II. DETAILS EXPERIMENTAL

2.1. Materials used

Kenaf, banana and glass fiber with (0˚/ 90˚orientation) is used as reinforcing material, Epoxy resin (LY 556) and hardener (HY 951) is used as the matrix material and nano filler (Graphene) used as a filler material with different weight percentage to increase mechanicalproperties.

Preparation of Resin

A measured amount of epoxy is taken for different volume fraction of fiber and mixed with the hardener in the ratio of 100:10 and Graphene filler is added into that mixer with weight percentage of (without filler, 0.5, 1, 1.5wt.%)

Preparation of the reinforcing material

The kenaf, banana and glass fabric is spread on the flat surface and required dimension of 300 mm x 300 mm is marked using the marker pen on the fabric spread and cut using a scissor manually. Required such layers of fabric were cut to get the required thickness oflaminate.

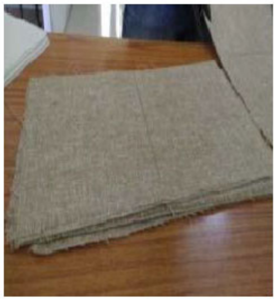

Fig.1. Kenaffibermat

Fig.2. Glass fiberMat

Sl.No	Material	Density (g/cm$^{3)}$	UTM (Mpa)	Modulus (Gpa)
1	Kenaf fiber	1.45	930	53
2	Glass fiber	1.9	2500	70
3	Graphene	0.2	130	1000
4	Epoxy	1.18	85	4.4

Table 1: Material properties

2.4. Hand layup technique

The composite laminates are fabricated by hand layup technique. Kenaf and glass fibers mat were cut into the dimensions of length and breadth is of 300×300mm and 4mm thick was used to prepare the laminate. The composite laminate consists of total 6 layers of glass fiber and 5 layers of kenaf fibers for the fabrication of different samples. The layers of fibers were fabricated by adding the required quantity of epoxy resin. The glass fiber is mounted on the table and then epoxy resin is applied on it. Before the resin gets dried, the second layer of kenaf fiber is mounted over the glass fiber. The process is repeated till six layers of glass fiber and five layers of kenaf fiber got over. The epoxy resin is applied to the entire surfacebymeansofaroller.Theairgapsformed during the processing between the layers were removed out. Finally these laminates are kept in press for over 24 hours to get the required shape and thickness. Two types of composite laminates were
prepared with addition of graphene filler (0, 0.5, 1, 1.5, wt. %)

- Kenaf/Glass/Graphenecomposites
- Banana/Glass/Graphenecomposites

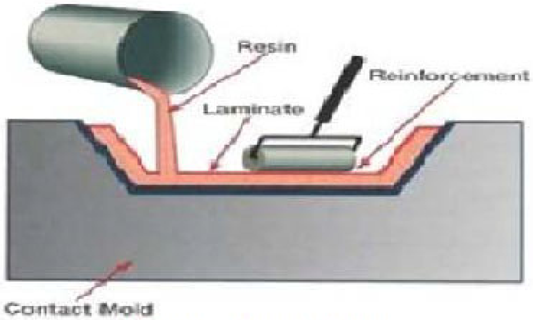

Fig.3. Hand layup technique

Fig.4. Water Jetcutting

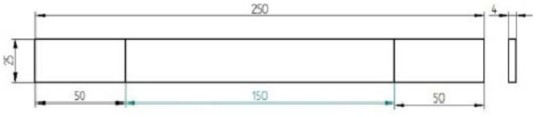

Figure 5(a)

Figure 5(b)

Fig.5(a,b): Tensile test Dimensions & specimen - ASTM D3039

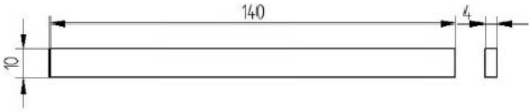

Figure6(a)

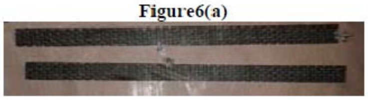

Figure6(b)

Fig.6(a,b): Compression test dimensions & specimen - ASTM D3410

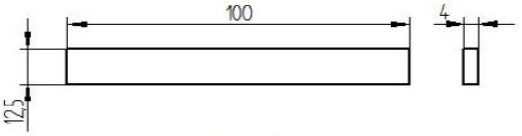

Figure 7(a)

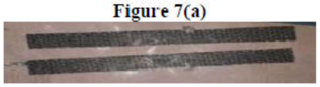

Figure 7(b)

Fig.7(a,b): Flexural test dimensions & specimen - ASTM D790-2

2.5 Preparation of test specimens

The test specimens are prepared as per ASTM standards from the composite laminates using water jet machine as shown in fig. 1, 2 &3.

III. RESULTS ANDDISCUSSION

All tests were carried out on tensometer as per the ASTM standards

3.1. Comparison of UTS for Kenaf/Glass and Banana/Glass fiber composites

Sl.No.	Graphene %	UTS(N/mm^2) for Kenaf hybrid Composites	UTS(N/mm^2) for Banana hybrid Composites
1	0	132.45	117.08
2	0.5	120.15	112.26
3	1	128.69	102.34
4	1.5	113.06	111.38

Table 2: Tensile test results

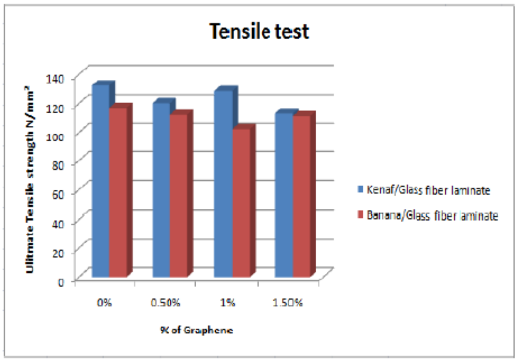

3.2 Comparison of compressive strength for Kenaf/Glass and Banana/Glass fibercomposites

Sl.No.	Graphene %	Compressive strength (N/mm^2)for Kenafhybrid Composites	Compressive strength (N/mm^2)for Banana hybrid Composites
1	0	22.76	13.82
2	0.5	12.36	16.6
3	1	28.95	21.84
4	1.5	15.54	23.94

Table 3: Compression test results

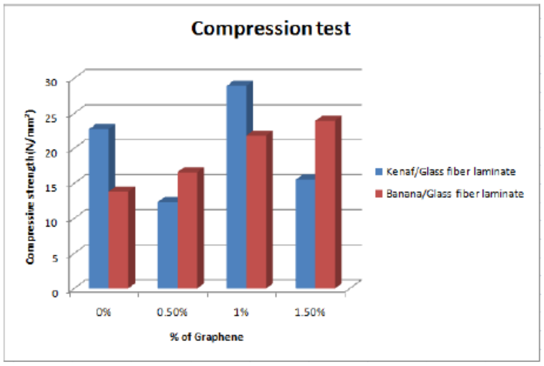

3.3 Comparison of flexural strength for Kenaf/Glass and Banana/Glass fibercomposites

Sl.No.	Graphene %	Flexural strength (N/mm^2) for Kenaf hybrid Composites	Flexural strength (N/mm^2) for Banana hybrid Composites
1	0	11.02	11.05
2	0.5	12	12.26
3	1	14.04	13.77
4	1.5	12.36	10.87

Table 4: Flexural test results

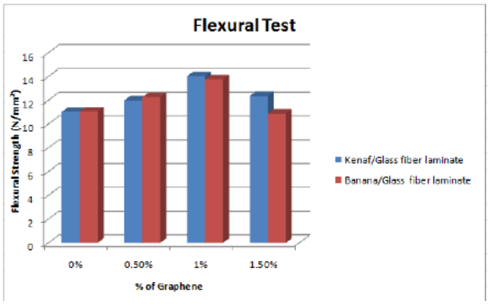

IV. CONCLUSIONS

- Fabrication of Kenaf/glass and Banana/glass fiber hybrid polymer composites withdifferent percentage of graphene were prepared successfully by hand lay-up process.
- Performance of kenaf/glass fiber composites is more than banana/glass fiber composites with graphene.
- Kenaf/glass fiber reinforced with 0% graphene possesses good ultimate tensile strength of 130Mpa when compared to banana/glass fiber composites of117Mpa.
- Better Compressive properties are obtained with kenaf/glass fiber composites than banana/glass fibercomposites.
- Kenaf/glass fiber reinforced with 1% graphene possesses good flexural strength of 14Mpa when compared to banana/glass fiber composites of13Mpa.

ACKNOWLEDGMENTS

I would like to express my sincere thanks to my Ph.D Guide Dr. H. K. Shivanand, Professor, Department of Mechanical Engineering, UVCE, Bengaluru for their encouragement and suggestions which helped me a lot in the completion of this research work and I am also extremely thankful to Dr.K.S.Narayanaswamy, Director, School of Mechanical Engineering, REVA University for his constant encouragement, directions and support throughout thecourse.

REFERENCES

[1] Mo-lin Chan, Kin-tak Lau, Tsun-tat Wong, Mei-poHo, David Hui, "Mechanism of reinforcement in a nanoclay/polymer composite" Composites: Part B 42 (2011) PP1708–1712.

[2] Andrea Dorigato, Stefano Morandi and Alessandro Pegoretti, "Effect of nanoclay addition on the fiber/matrix adhesion in epoxy/glass composites" Journal of Composite Materials 46(12)PP1439–1451.

[3] Normasmira A. Rahman, Aziz Hassan, R. Yahya& R.A. Lafia-Araga, "Glass Fiber and Nanoclay Reinforced Polypropylene Composites: Morphological, Thermal and Mechanical Properties" SainsMalaysiana 42(4)(2013): PP537–546.

[4] K.Devendra, T. Rangaswamy, "Evaluation of thermal properties of E-Glass/ Epoxy Composites filled by different filler materials" International Journal Of Computational Engineering Research Vol. 2,Issue.5

[5] RafaelCeleghiniSantiago,RicardoLessaAzevedo,Antonio

[6] F. Avila, MarcilioAlves, "Mechanical characterization of Glass/Epoxy composite material with Nanoclays" 19th International Congress of Mechanical Engineering.

[7] Mo-lin Chan, Kin-tak Lau, Tsun-tat Wong, Mei-poHo, David Hui, "Mechanism of reinforcement in a nanoclay/polymer composite, Composites": Part B 42 (2011) PP1708–1712.

[8] Amir HoomanHemmasi, Ismail Ghasemi, BehzadBazyar and Ahmad Samariha, "Influence of Nanoclay on the physical properties of recycled High-Density Polyethylene/Bagasse Nano Composite", Middle-East Journal of Scientific Research 8 (3): PP648-651,2011.

★★★

POROSITY REDUCTION AND DEVELOPMENT OF MECHANICAL PROPERTIES OF DIE-CAST BRASS PRODUCTS USING TAGUCHI METHOD

[1]JYOTI PRASAD PATRA, [2]DIBYA KISHORE PRUSTY, [3]TAPAN KUMR MOHANTY

[1]Department of Electrical Engineering, NMIET, Bhubaneswar, 751019
[2]Department of Mechanical Engineering REC Bhubaneswar
[3]Department of Mechanical Engineering AIET Bhubaneswar
E-mail: [1]shakyasingha.sahoo@nmiet.ac.in

Abstract - By increasing the growth of various industries such as automotive industries as well as the need to build more parts with improved properties and a decrease in production costs, the die-casting method is more concerned. The die-casting method is capable of producing complex parts, reducing machining time and high-speed production rate. The aim of this paper is producing brass parts by pressure casting method then improving its mechanical properties by reducing its porosity. For this purpose, the effective parameters such as alloying elements, molten temperature, and injection pressure were improved by utilizing Orthogonal Array L9 of the Taguchi method and using Minitab software. It was found that lower molten temperature (1000 ° C), moderate injection pressure (140-ton), and 60% Cu had the best fulfilling, and lower porosity.

Keywords - Die-Casting Process, Brass Alloy, Taguchi Method, Injection Pressure, Molten Temperature, Casting Defects

I. INTRODUCTION

Die casting is a popular casting process that is specified by forcing liquid metal under high pressure into the mold cavity. These castings are made from light alloys, especially magnesium, copper, aluminum, zinc, etc. by use of the hot or cold-chamber machine. Not only this process is suited for rapid production rates, but also it has some other benefits such as very good surface finish, excellent dimensional accuracy, and reduced final machining[1].

One of the prominent problems in the die casting process is porosity in final products so the main objectives of this study are decreasing porosity percentage and increasing mechanical properties of brass parts in this process by use of the Taguchi method. Firstly, it was attempted to understand the effects of process parameters on the die casting process. It was found that alloying elements, molten temperature, and injection pressure have the most influential effects on the process[2&3]. Hence to solve the problem of high porosity and low mechanical properties of brass parts, it was decided to optimize the parameters by using the Taguchi method. Then, by doing some experiments and analyzing casting samples, obtained results were verified.

II. EXPERIMENTAL DETAILS

This research is divided into three main sections including experiment design, conducting experiments and analyzing them.

Orthogonal array L9 of the Taguchi method was utilized with Minitab software as a statistical and process improvement tool to analyze data and approach the most effective parameters on output [4].Taguchi designs is based on signal-to-noise ratio Control factors are those design parameters that can be controlled but noise factors are uncontrollable factors that should be minimized. It means higher values of the signal-to-noise ratio (S/N) identify control factor settings that minimize the effects of the noise factors [5].These parameters arealloying elements (55%, 60%, 65% Cu), molten temperature (9000c, 10000c, 11000c), and injection pressure (120, 140, 160 ton). Based on these influential parameters and their interaction, practical experiments then microstructural and mechanical tests were conducted.All designed experiments according to the Taguchi method are given in table l. By using this method not only time and costs of experiments were saved but also more accurate results were obtained.

Sample number	Cu%	PT(^{0}c)	IP (ton)
1	55	900	120
2	55	1000	140
3	55	1100	160
4	60	900	140
5	60	1000	160
6	60	1100	120
7	65	900	160
8	65	1000	120
9	65	1000	140

Table1: Designed experiments according to Taguchi method
Cu%= Copper percentage (%), PT=pouring temperature (^{o}C), IP=injection pressure (ton)

A prepared copper-zinc alloy according to table 2 specification was melted in an induction furnace. The melt temperature was measured by the use of type K thermocouple inside the furnace and also before pouring it into the chamber. Then the liquid metal was poured into the chamber of the horizontal cold chamber machine with 200-ton capacity and the filling was adjusted by plunger speed. The mold was machined from hot work tool steel (H13) and the inner surface was coated by Nano-coating. After cooling, the casting was removed from themold.

Element	Cu	Zn	Sn	Fe	Ni	Al	Si
Composition (Wt %)	55	45	0.183	0.311	0.187	1.424	0.030
	60	40	0.195	0.356	0.189	1.410	0.060
	65	35	0.205	0.355	0.180	1.323	1.322

Table 2: Casting alloy elemental analysis

In the next step, cast samples were extensively analyzed for casting integrity, microstructure and hardness test [6]. For casting integrity, all castings were evaluated by the naked eye and also a digital camera to detect surface defects, incomplete filling, deficient edges and corners (Fig 1).

Fig 1: casting defects

Then, samples were prepared by cutting them in halves, grinding and polishing them, then porosities were detected and evaluated by equipped microscope with Image analyzer software.The microstructural analysis was focused on examining the main features such as internal shrinkage, area fraction and percentage of internal porosity (Fig 2). To find information about the mechanical behavior of the samples, a hardness test through cross-section of it was performed according to the Rockwell hardness test B scale.

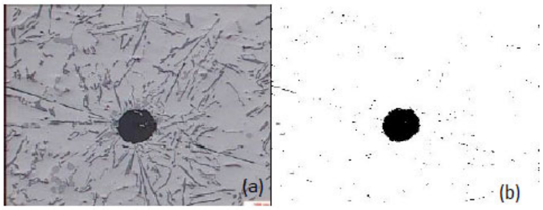

Fig 2: Determining method for porosity area fraction; a) captured image, b) detected porosity

III. RESULTS ANDDISCUSSION

In this section, the results of the Taguchi method in addition to experimental results will be introduced, analyzed and explained. For this purpose, influential parameters including casting defects, porosity percentage and hardness tests will be presented separately. Table 3 illustrates experiment results including porosity percentage and hardness.

Sample number	1	2	3	4	5	6	7	8	9
Porosity (%)	4.5	4	6.2	4.62	4.8	5.6	5.1	5	4.8
Hardness (HRB)	88.2	86.3	82.5	92.1	87.2	83.4	93.8	86.1	88

Table 3: Experiment results including porosity percentage and hardness

3.1. Effect of Copper percentage on casting defects, porosity and hardness

Percentage of Copper is one of the influential parameters to determine the characteristic of liquid metal and brass final products. It directly affects on pouring temperature, the fluidity of molten metal and mechanical properties. By increasing Cu percentage, the brass melting point is increased that causes increasing ofmelt fluidity and finally creates turbulence during injection into the mold.This phenomenon decreases the solidification rate and as results die casting defects will be increased. Fig 3 illustrates theS/N ratio of casting defects for different percentages of Cu.

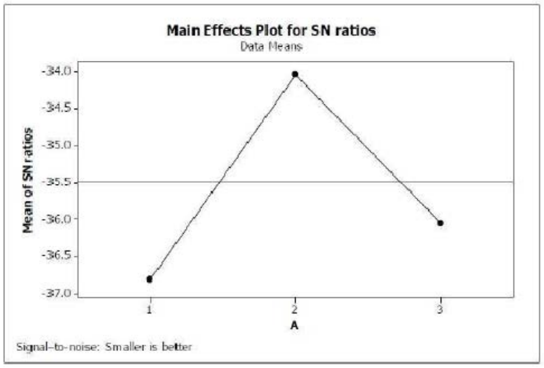

Fig 3: S/N ratio of casting defects for different percentage of Cu, 1:55%, 2:60%, 3:65% Cu

As can be seen, 60% Copper has the optimum value, it may be explained in this way that Brass is a mixture of Zn and Copper, so by decreasing Cu, the percentage of Zn will be increased. Furthermore, Zn has a lower melting point whichtempered mold evaporates parts of it that creates remained gases in the final product [7].

Moreover, by increasing Cu in the alloy, the porosity percentage in casting is increased. Even though increasing Cu results in decreasing other alloying elementsand less produced gas in the mold, but a higher amount of Cu in the liquid metal needs more temperature for adequate fluidity that by increasing more fluidity leads to a higher percentage of porosity in the final products [8].

Alloy hardness not only depends significantly on Cu percentage but also depends on other effective parameters such as grain size, microstructure, and porosity percentage. According to table 3, a lower percentage of Cu has the highest amount of hardness because of the existence of other alloys such as Zn, Al, Pb, etc. It also can be noticed that Cu has a highheat transfer coefficient that causes higher solidification rate and as a result finer grain size and better mechanical properties [3]. By putting all the results together, it can be concluded that 60% of Copper is the best percentage for this experiment.

3.2. Effect of Pouring temperature on casting defects, porosity and hardness

Brass casting is mainly a mixture of Cu and Zn so the pouring temperature should be selected based on a higher melting point (Cu) and due to the huge difference between the melting point of alloying elements, this parameter is an influential factor on producing casting defect. In one hand increasing pouring temperature, cause the Cu to be melted easily thatincreasesfluidity but on the other hand, other alloying elements with a lower melting point will be evaporated to gas and smog in the mold[7]. Fig 4 shows the S/N ratio of casting defects for different pouring temperatures.

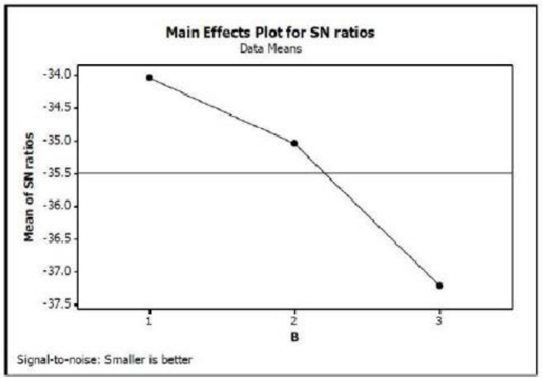

Fig 4: S/N ratio of casting defects for different pouring temperature, 1:9000c, 2:10000c, 3:11000c

From fig 4, it is obvious that by increasing temperature,casting defects have been increased which is due to increased evaporated elements in the alloy as well as higher turbulence in the liquid metal. Furthermore, lower temperature causesan inadequate mixture of alloy elements as well as a shortage of fluidity which all of these lead to more porosity.

According to obtained results, the pouring temperature of 10000c has the optimum amount of hardness. By increasing temperature, liquid turbulence, as well as solved gas in it, will be increased which leads to lower mechanical properties. Qualified property in 10000c temperature refers to the optimized fluidity of alloying elements in this temperature.

3.3. Effect of injection pressure on casting defects, porosity andhardness

Injection pressure is a required pressure for the die casting process and is an effective parameter in this process. This pressure causes the mold to be filled by molten metal. During injection pressure, liquid metal flows with turbulence which decreases the casting quality. By increasing this pressure, the force on liquid metal is increased significantly and this means higher turbulence during mold filling which leads to more entrapped gases. Fig 5 shows the S/N ratio of casting defects for different injection pressure.

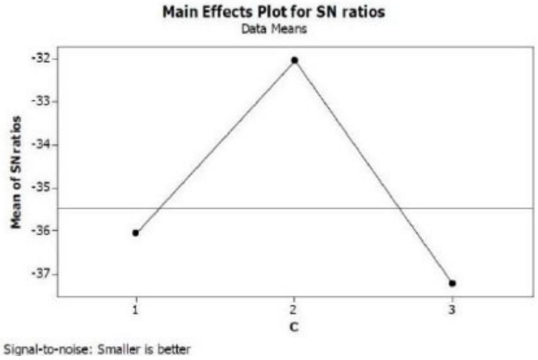

Fig 5: S/N ratio of casting defects for different injection pressure, 1: 120 ton, 2:140 ton, 3:160 ton

The dropin sample number 1 can be explained by the lack of pressure to force the liquid metal to flow into the mold which finally causes misrun and defects. According to table 3, in 120-ton injection pressure there will be a higher amount of porosity in final casting because there is not enough force for evacuating gas porosity from the liquid metal or pressing them [8]. On the other hand, in 160-ton pressure, due to increased turbulence in liquid metal and more entrapped gases, the porosity percentage will increase and hardness decrease.

It should be noticed that an increase in injection pressure should be applied based on the casting dimensions and alloying elements. By applying optimized pressure, most of the entrapped gases will be evacuated and some of them will be compressed during pressure process, therefore less porosity percentage in the final casting will remain [7]. Finally by comparing Taguchi design and experimental results, it can be said that the optimized injection pressure for this research is 140 tons.

IV. CONCLUSION

In this research, effective parameters of the die casting process including alloying elements, molten temperature, and injection pressure were improved by utilizing the Taguchi method. Then, by doing experiments and analyzing casting samples, obtained results were verified.

From the obtained results it can be concluded higher turbulence and evaporated gases may be created by a lower percentage of Cu, higher pouring temperature and high injection pressure. On the other hand, a lower amount of these parameters may lead to misrun and unfilled mold so both situations can cause more casting porosity and less mechanical properties. Finally, it was found that lower molten temperature (1000 ° C), moderate injection pressure (140-ton), and 60% Cu had the best fulfilling, and lower porosity.

ACKNOWLEDGMENTS

The authors would like to thank the Islamic Azad University of Khomini Shahr for providing experimental facilities and KarizZob Pars foundry for financial support.

REFERENCE

[1] Y.Qiang,B.Fanqiang,M.Fanzhi,Q.Xin,Z.Deping,Z.Tian,
[2] X. Liu, Meng, Jian, “The improved effects by the combinative addition of lanthanum and samarium on the microstructures and the tensile properties of high-pressure die-cast Mg–4Al-based alloy”, Materials Science & Engineering, A 628, pp.319-326,2015.
[3] M.Vogel, O.Kraft, G.Dehm and E. Arzt. “Quasi-crystalline grain-boundary phase in the magnesium die-cast alloy”ScriptaMaterialia, vol. 85, pp.517-524,2001
[4] S.Ji, W.Yang, F.Gao, D.Watson, Z.Fan, “Effect of iron on the microstructure and mechanical property of Al–Mg–Si–Mn and Al–Mg–Si diecast alloys” Materials Science & Engineering, A 564, pp.130–139,2013.
[5] ASM, “Casting Design Handbook” Ohio, American Society forMetals,1962
[6] G.Campatelli, A.Scippa, “Heuristic approach to meet geometric tolerance in High Pressure Die Casting” Simulation Modelling Practice and Theory, Vol22, pp. 109–122,2012
[7] ASM, “Metals Handbook”, 9th. ed., Vol.15, Ohio, American Society forMetals
[8] L.Wang, P.Turnley, G.Savage, “Gas content in high pressure die castings” Journal of Materials ProcessingTechnology, Vol211, pp. 1510-1515, 2011
[9] J.P.Weiler, J.T. Wood, R.J.Klassen, E. Maire, R.Berkmortel, G. Wang “Relationship between internal porosity and fracture strength of die-cast magnesium AM60B alloy” Materials Science and Engineering, A 395, pp. 315-322, 2005.

★★★

ALTERATION AND PERFORMANCE ENERGY ANALYSIS OF FOUR STROKE ENGINE TO SIX STROKE ENGINE

[1]ANJAN KUMAR SAHOO, [2]TAPAN KUMR MOHANTY, [3]MANOJ KUMAR PATTNAIK

[1]Department of Electrical and Electronics Engineering, NMIET, Bhubaneswar, 751019
[2]Department of Mechanical Engineering ZAIET Bhubaneswar
[3]Department of Mechanical Engineering REC Bhubaneswar
E-mail: [1]shakyasingha.sahoo@nmiet.ac.in

Abstract - Modern four stroke engines are used on large scale because the power to weight ratio and reliableness of four stroke engines are greater. The disadvantages of the four stroke engine are that there is excess amount of heat energy produced. This heat energy has been wasted through the walls of the container of the engine and ejected as the additional energy during the exhaust stroke of the cycle. To increase the efficiency of the 4 stroke engine there is need to develop a six stroke internal combustion engine which uses the heat energy for additional power stroke. So to raise the brake thermal efficiency of the engine, few of the fundamental changes have been performed in four stroke internal combustion engine. The changes are also made to reduce the pollution and for betterscavenging.

Keywords – Heat Energy, Scavenging, Brake Thermal Efficiency, Pollution

---

I. INTRODUCTION

With the passage of time, it is understood that the fossil oil and residual oil would not be sufficient and they would be expensive. Different experiments are performed for the betterment of fuel efficiency of engines. As the demand and availability of diesel and petrol is not balanced and there is a need to balance that is happened due to increase in number of vehicles. If the same scenario continues then petrol and diesel would be prove more expensive and restricted. Now a days much of the importance has been given to the secondary fuels with enhanced usage and the consumption of the remainingfuels.

In the cylinder of the piston the additional energy from the four stroke engine has been used as the second power ad exhaust stroke in the initial method. For the second power stroke, air can be used as the working fluid. Similarly the engine is cooled by second power stroke second power stroke cools the engine and removes the need for a cooling system and increase 40% brake thermal efficiency over the Otto or diesel cycle. For each insertion of the fuel the piston goes to the top and bottom six times in the six stroke engine. There are 2 power strokes in these six stroke engines: One by fuel that is first power stroke and second is by fuel that is the working fluid. In second method there is another conflicted piston that drives off at half the cylinder rate of the main piston that brings about six motions of piston per cycle. The second piston exchanges the valve mechanism of the schematic engine and the compression ratio is increased.

II. LITERATUREREVIEW

In the six stroke engines high octane fuels are preferred to increase the efficiencies of the engines. Due to high efficiency, less fuel is consumed and low atmospheric emissions are produced by the engines. In six stroke engines methanol is a preferred fuel because high engine efficiency is obtained by these fuels. In six stroke engine, the power to weight ratio and power to volume ratio is increased.[1]
The investigation and research for an engine having same or greater power and higher fuel efficiency has led to the concept of a six stroke engine. Almost all of the internal combustion engines have one feature in common, combustion occurs after compression, which is resulted in the expansion of gas that acts directly on the piston and is limited to 180 degrees of the crankshaft angle. On the worldwide sector, the automotive industry has adopted the discipline. There will be a great effect on the worldwide sector. This technology has been resulted in minimizing the fuel depletion up to 40% and the pollution is also reduced up to 60% to 90%. This pollution is dependent on the kind of fuel used.[2]

In the internal combustion engine, two totally diverse formulation has been briefly explained by the theory of six stroke engine that were formulated in 1990 so that the efficiency of the engine might become better and the radiations are also minimized. This engine results in the dramatic reduction of pollution as well as fuel consumption. In order to get the more work per cycle, the fuel efficiency of the engine can be raised and also the valve timing can be efficaciously ordered.[3] Four strokes engines have high power to weight ratio and are reliable. In four strokes engines excess amount of heat energy is released from the cylinder walls and this heat energy is eliminated as additional energy during the exhaust stroke of the cycle. In six stroke engine there is less fuel is consumed and less polluted.[4]

One of the major and necessary concerns in engines is to raise the brake thermal efficiency of an engine.
Four stroke diesel engines and those working on the

Otto cycle has very less brake thermal efficiency because large amount of energy gets missed in the exhaust stroke due to which engine is cooled. Better scavenging becomes possible due to the air intake occurring in the 5th stroke and exhaust stroke in the 6th stroke.[5]

Six stroke engines are developed because there is a need to raise the efficiency of the engine by reducing the fuel consumption and contamination of the engine without any influence on the performance of the engine. In six stroke engine, two additional strokes are fifth stroke also called water injection stroke and sixth stroke is called exhaust stroke. As power of sixth stroke engine is more than that of four strokes so it is more efficient and it reduces pollution. In six stroke engine, 60%-90% pollution and 40% fuel consumption of engine is reduced. In six stroke engine compression ratio is increased by valve mechanism.[6]

There must be two power strokes in the six stroke engine. The scope of development is huge in six stroke engine. Six stroke engines have huge influence on the economy of the world. According to the mechanical design of six stroke engine, combustion does not occur in the cylinder. The combination of two stroke and four stroke engine is named as six stroke engine. The six stroke engine helps in the betterment of the world economy and support the advancement of automobile industry. [7]

Six stroke engine produces more power and it has high efficiency than four stroke engines. Six stroke engines are used in heavy load carrying vehicles where focus is on load carrying capacity than fuel economy. The two additional strokes in these engines raised the work which has been removed per unit input of energy which causes an energy efficiency of up to 30% higher than that of four stroke engine.[8]

III. TYPES OF SIX STROKEENGINE

A. Single pistondesigns

In single piston designs, single piston per cylinder is used which is similar to two stroke or four stroke engine. A minor non-fulminating coolant is added in to the assembly and the heat which is remained from the combustion process causing the assembly to spread out for a second power stroke carried out by another exhaust stroke.

A.1 Griffin six-strokeengine

The important law of working of Griffin six stroke engine was heated exhaust-jacketed outward vaporizer. The fuel was dispersed in the heated exhaust-jacketed outward vaporizer. The temperature of the vaporizer was kept around 550 °F. This temperature is quite enough to evaporate the oil but at this temperature the oil was not split up chemically. The use of dense oil fuels is held by the fractional distillation. The useless tars and minerals throwing out in thevaporizer.

A.2 Bajulaz six-strokeengine

The design of Bajulaz six stroke engine is same as systematic combustion engine. There are, still, alternations to the cylinder head, with two secondary attached volume assemblies:

Above every container there is a combustion assembly and an air preheating assembly. The combustion assembly gets an assess of warm air by the container; the thermal efficiency is increased by the constant volume (isochoric) ignition of the fuel as compared to the ignition in thecontainer.

A.3 Velozeta six-strokeengine

Warm air is vaccinated into the container during the exhaust stroke in the Velozeta engine. This warm air spreads by the heat and due to this piston takes an extra stroke. The intersection of the valves havebeencut off and for better gas scavenging, two extra strokes are supplied by using thevaccination.

A.4 NIYKADO Six StrokeEngine

This engine is classified as a fully working model. In 2004, the first model was formulated. This model had used only two valves. In 2007, another model was formulated. This model had cleared the design by using four valves.

A.5 Crower six-strokeengine

Bruce Crower developed a six stroke engine in the United States. After the exhaust stroke, water is vaccinated into the container and the water is immediately converted in to vapors. The vapors disperse and due to this dispersion, an extra power stroke is taken by the piston. So, useless heat is seized which is needs an air or water cooling system to eject in most of the engines.

B. Opposed pistondesigns

The two pistons per container are used by this type of design which are working at different rates with explosion occurring between the pistons.

B.1 BeareHead

Malcolm Beare, the discoverer of the Beare Head coined the term six stroke engine. The profession unite a four stroke engine bottom part with a conflict piston in the container head working at fifty percent of the alternating rate at the lower position of the piston. Practically, the valve mechanism is substituted by the second piston of a schematicengine.

B.2 M4+2

The M4+2 engines are quite similar to the Beare Head engines, uniting two opposite pistons in the identical container. One piston works at fifty percent alternating rate of the other piston, so the important role of the other piston in a Beare Head engine is to substitute the valve mechanism of a schematic four stroke engine, the M4+2 assumes the law one more step.

B.3 Piston chargerengine

The Piston charger engine has the design which is similar to the Beare head, a "piston charger" alternates a valve design. The work of charging the important container is conducted by the piston charger and at the same time the internal and external opening is controlled by thepiston charger that results in no utilization of air and fuel in the exhaust stroke. The ignition process is held as in two stroke engine in the main container, and coating similar the four-stroke engine.

Fuel vaccination could be occur in the piston charger, in the fuel delivery passage or in the ignition assembly.

IV. WORKING OF SIX STROKE ENGINE

Different working strokes of a six stroke engine are:

1st stroke (suction stroke)

The air-fuel mixture or solution has been drawn from the carburetor in to the container by the inlet valve and motion of the piston is from top dead center position to the bottom dead center position during the first stroke.

2nd stroke (compression stroke)

During the second stroke both inlet and outlet valves are closed and piston moves from BDC to TDCduring which the mixture of air and fuel remains tight. The compression ratio remains same as in 4 strokeengine.

3rd stroke (1st power stroke)

In power stroke, because of the combustion of the tight air-fuel mixture power is obtained using a spark plug. Both valves remains closed as motion of the piston is from top dead center to the bottom dead center.

4th stroke (exhauststroke)

In this stroke exhaust valve remains open as burnt gases are eliminated through the container. In 4th stroke the motion of the piston is from bottom dead center to the top deadcenter.

5th stroke (2nd power stroke)

In that stroke exhaust valve remains closed while working fluid valve that is either steam or water is opened. So fresh working fluid from the inlet valve enters the cylinder through the secondary air simulation system. In the 5th stroke the motion of the piston is from top dead center to bottom dead center.

6th stroke (2nd exhaust stroke)

In that stroke air exhaust valve is opened so that air induced during the fifth stroke is expelled to the atmosphere through the exhaust valve. Piston moves from BDC to TDC and six stroke cycle is completed.

V. CONCEPT OF SIX STROKEENGINE

Six stroke internal combustion engine is advancement over four stroke internal combustion engine which works also on the same principle. In six stroke the heat exhausted in the exhaust stroke is used as the second power stroke input which moves the piston downward so by spinning the crankshaft for another half cycle. In 4th stroke engine the demand for a cooling system is excluded as the heat evolved in the 4th stroke engine is not lost.

In six stroke engine, the fuel injection or fuel vaccination occur only once in after 3 full cycles of the crank shaft and it is best at any rate as compared to four stroke engine where fuel injection or fuel vaccination occur in after 2 full cycles of the crankshaft. It should be known that six stroke engine has higher brake thermal efficiency as compared to the four stroke engine. Working fluid used in six stroke engine are either air orsteam.

VI. BASIC PARTSMODIFICATION

1. Crankshaft to camshaft ratio Modification:

In four stroke internal combustion engine crankshaft rotates 720 degree while the camshaft rotates 360 degree in six stroke engine to complete one cycle so crankshaft must rotate 1080 degree to rotate the camshaft 360 degree and complete cycle. Hence crankshaft to camshaft ratio is 3:1.

Figure 01 Crankshaft modification

2. CamshaftModification:

Since camshaft rotates 360 degree in six stroke engine so it can be divided as 60 degree. In six stroke engine exhaust cam has two lobes one to open the exhaust valve at 4th stroke (first exhaust stroke) and also at the six stroke to expel out the hotsteam.

Figure 02 Camshaft modification

3. Cam follower Modification:

In four stroke engine the regular follower has a flat pattern of bottom shape which is suitable. While in six stroke engine due to reducing the valve opening from 9000 to 6000 the shape of the follower must be changed from flat to roller or sphericalshape.

4. Modification in Inlet and Exhaust Manifold:

There is a pipe by which the needed amount of air is drawn from the region by the motion of the piston and mixed with the fuel for ignition in the four stroke engine.

Figure 03 Inlet and Outlet exhuast modification

The common internal piping of four stroke engine as shown in diagram the common inlet manifold of four-stroke engine parted by fastening a plate between the common internal piping.

There are two cylinders in six stroke engine. In the first cylinder, fuel is provided. The fuel is not provided in the second cylinder. The internal piping of the second cylinder is used to deliver the exhaust system of the first cylinder to the secondcylinder.

VII. RESULTS

The results of analysis are given below in graphs.

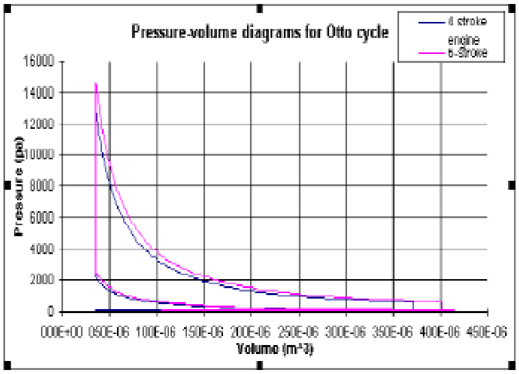

Figure 04. Comparison of PV diagram of 4- stroke and 6-stroke engine for Otto cycle.

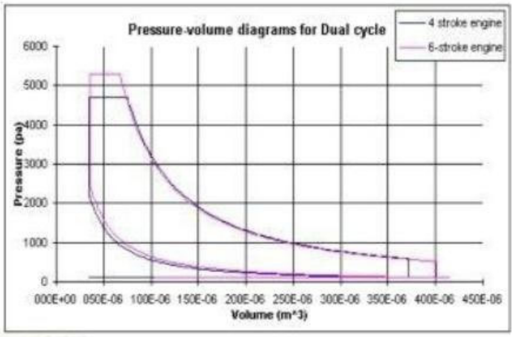

Figure 05. Comparison of PV diagram of 4- stroke and 6-stroke engine for Dual cycle.

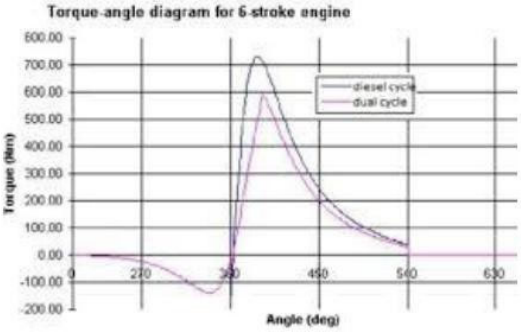

Figure 06. Torque angle diagram of 6-strokeengine.

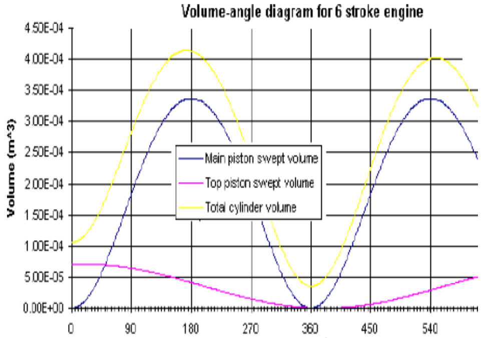

Figure 07. Volume angle diagram of 6-strokeengine.

VIII. CONCLUSION

There is no wonder solution for the replacement of the inner combustion engine. Solely enhancements of the present technology will facilitate it progress inside affordable time and money limits. The sixstroke engine fits absolutely into this read. Its adoption by the auto trade would have an amazing impact on the surroundings and world economy. The six stroke engine guarantees dramatic reduction of pollution and fuel consumption of an indoor combustion engine. Assuming up to 40% reduction in the fuel consumption and 60% to 90% in polluting emissions, depending on the type of fuel being used and the second piston replaces the valve mechanism of a conventional engine and also it increases the compression ratio. After modifications to four stroke engine the results differences are veryeffective i.e. thermal brake efficiency, torque transmitted, pollution effects, fuel consuming capability etc. results can also be verified with the help ofgraphs.

REFERENCES

[1] George Marchetti and Gilles Saint-Hilaire “A Six- Stroke, High- Efficiency Quasiturbine Concept Engine with Distinct, Thermally-Insulated Compression and Expansion Componets.”

[2] SHWETA KANDARI et.al, Six Stroke Engine, October 2013

[3] KAPIL N. KARIYA AND et.al, Velozeta Six Stroke Engine, May2014.

[4] TEJASKUMAR U. KOTHARI et.al, Design and Analysis of Six stroke Internal Combustion Engine,2014.

[5] VISHAL KUMAR TYAGI, Study and Analysis of Six Stroke Engine, May2015.

[6] VIRENDRA KUMAR PATEL, et.al, A study on basic theory of six stroke engine,2015.

[7] S.VGURAO, Six Stroke Engine,2016.

[8] MOHSIN RAZA, Study and analysis of six stroke internal combustion engine,2017.

★★★

ELECTRO CHEMICAL DISCHARGE MACHINING: PROCEEDING CAPABILITIES

IRANI MAJUMDAR, [2]GANESH PANDA, [3]SURAJ KUMAR PATEL

[1]Department of EEE Engineering, NMIET, Bhubaneswar, 751019
[2]Department of Mechanical Engineering REC Bhubaneswar
[3]Department of Mechanical Engineering AIET Bhubaneswar
E-mail: [1]hemant.nayak@nmiet.ac.in

Abstract - Electro Chemical Discharge Machining (ECDM) process has combined characteristic of ECM and EDM that enables to machine electrically conductive materials at a rate five to fifty times higher than ECM& EDM irrespective of the typical properties of newer materials such as chemical inertness and high strength high temperature resistance (HSHTR) by electro chemical dissolution (ECD) and by electric discharge erosion (EDE) simultaneously. The novelty of this process is that electrically non conductive HSHTR materials that are difficult to machine by conventional methods can also be machined by this process. Though this process itself imposes certain limitations such as low machining efficiency, heat affected zone, radial overcut etc. especially while machining some of the electrically non conductive materials but on the other hand this process has been successfully utilized with different conventional machining processes and named as hybrid machining. This paper explains the insight of the mechanism evolved while machining electrically conductive and non conductive materials and focused on the process capabilities of ECDM that has been explored by many researchers and proposed its usage in various forms.

Keywords - Electro-Chemical Discharge Machining (ECDM), High Strength High Temperature Resistant Materials (HSHTR), Electro Chemical Dissolution (ECD), Electric Discharge Erosion (EDE), Hybrid Machining Processes (HMP).

I. INTRODUCTION

ECM is considered as one of the most versatile method of producing stress free machining on various kinds of metal and alloys. ECM occurs at high current density (greater than 200 amps / cm^2) causing rapid dissolution of the anode, and characterized by high surface integrity, improved surface finish, high machining rate and the absence of tool (cathode) wear. But as compared with EDM, it has low accuracy of reproducing the shape of the tool electrode into the workpiece. On the other hand EDM can provide a high surface finish only with a low productivity and an increase in machining rate results in a significantly increased roughness and deeper damaged surface layer, while a reduction in surface roughness leads to increased tool wear. In order to make use of the mutually enhanced advantages of both the processes for gaining high machining rate and improved dimensional accuracy, a hybrid process is in use which is known as electrochemical arc machining (ECAM). This process involves electric discharge erosion (EDE) and electrochemical dissolution (ECD). In ECAM, electric discharge in electrolyte occurs due to electrical breakdown of the vapour-gas layer which causes large number of cratersonthe workpiece surface, simultaneously these surface irregularities (roughness caused by craters) are reduced by electrochemical dissolution. Hence high material removal rate compared to ECM / EDM and better quality of the surface finish is obtained. This process has potential to machine electrically conductive materials at a rate, five to fifty times higher than ECM& EDM [1] with better dimensional accuracy and good surface finish (provided that the parameters areproperly selected), and has been well accepted by the industries to machine HSHTR alloys. Due to high machining efficiency of this process, continual research is being carried out to incorporate better control of the system by adaptive fuzzy logic [2, 3], by intelligent gap width controller [4], by intelligent pulse classification system [5], by computer based real time process monitoring system [6, 7] etc. This process has been effectively used for hole drilling, die sinking and cutting heat resistance alloys, those having tensile strength more than 1500 N/mm^2 with machining capacity of the order $10^4 mm^3/min$, accuracy of 0.04-0.2 mm and surface roughness of $Ra = 1.25\text{-}2.5\ \mu m$. McGeough [8-12] et al. have contributed a lot to understand the mechanism of ECAM and ECDM.

Unlike ECAM, ECDM is used for machining electrically non conductiveHSHTR materials. The workpiece which is kept in the vicinity of electrical discharge that occurs at smaller size tool electrode i.e., cathode-electrolyte interface instantly generates a machined cavity over the workpiece surface depending upon the tool configuration and parametric values of an electrochemical cell, while counter electrode i.e. anode which is much larger in size compared to cathode acts as an auxiliary electrode and is just used to complete the electrical circuit as shown in figure1.

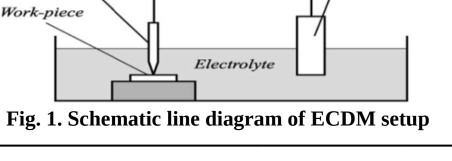

Fig. 1. Schematic line diagram of ECDM setup

Following are the reactions that take place at cathode and at anode in an electrochemical cell when appropriate potential is reached between the inter-electrode gap.

Reactions at the cathode (Tool) Plating of metal ions:
$M^+ + e^- \rightarrow M$, where M represents any anode material.
Evolution of hydrogen gas:
$2H^+ + 2e^- \rightarrow H_2 \uparrow$ (in acidic solution)
$2H_2O + 2e^- \rightarrow 2(OH)^- + H_2 \uparrow$ (in alkaline solution)
Reactions at anode (auxiliary electrode) Dissolution of metal ions:
$M \rightarrow M^+ + e^-$ (in acidic solution) Evolution of oxygen gas:
$2H_2O \rightarrow O_2\uparrow + 4H^+ + 4e^-$ (in acidic solution) $4(OH)^- \rightarrow 2H_2O + O_2 \uparrow + 4e^-$ (in alkaline solution)

II. MECHANISM OF DISCHARGE GENERATION

The phenomenon of discharge generation in an electrolytic system could be explained as, "in view of high supply voltage compared to ECM process, hydrogen bubble density increases substantially to constrict the current path at cathode (tool)-electrolyte interface. This constriction causes an increase in the resistance and ohmic heating of electrolyte solution in the local region and hence leads to blanketing of the tool by vapour generation and hydrogen gas bubbles. At a critical value of applied potential, this insulating bubble bridge blows off instantly due to intense heating. Consequently, the current suddenly drops to zero through the circuit and discharge takes place along the locations of the bubble bridge" and the process repeats. To have an overview of these three situations in an electrolytic medium, Ghosh A. [13] showed the range of current density Vs voltage used in ECM, ECAM&ECDM processes with their respective state of applied potential (Figure 2a&2b).

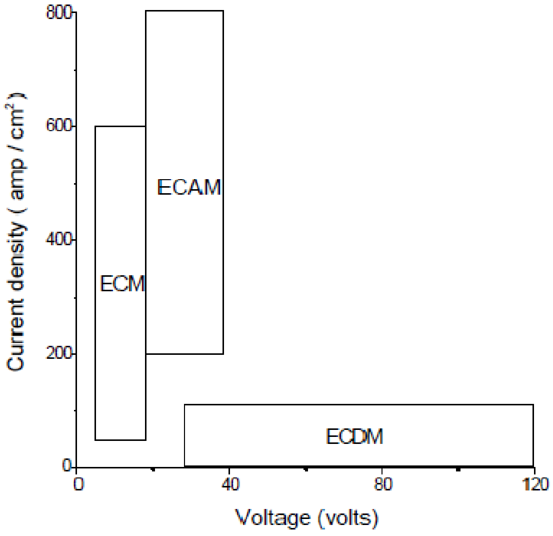

(a)

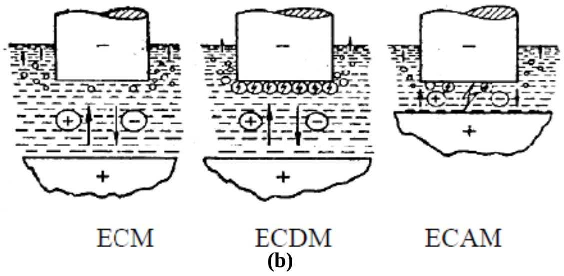

(b)

Fig. 2. (a) Voltage and current density ranges used in electrolytic process. (b) Different state of applied potential in an electrochemical cell [13].

Mechanism of discharge generation in an electrolyte is a complex phenomenon; confusion often arises over the difference between arc and discharge which influences surface integrity and dimensional accuracy of the machined surface to a great extent. The principle and application of ECDM process for machining electrically conductive materials was first reported by Rudroff [14]. ECD phenomenon was described as a sudden transient and noisy spark of approximately 1μs - 1ms duration, randomly positioned between the two electrodes, while an arc is a thermionic phenomenon of approximately 0.1s duration and occurs at fixed position between the two electrodes. McGeough [15], analyzed EDE process more precisely as electrochemical spark discharge (ECSD) & electrochemical arc discharge (ECAD). The frequency and distribution of discharge among spark and arc affects the material removal rate and the surface finish. High frequencies lead to a more condensed energy over a short period of time resulting in a small crater volume, i.e. a smooth surface and thin heat affected zone on the machined part.

Crichton and McGeough [16-17] explained that both spark and arc discharges were possible in the electrolyte across localized region of gas and / or electrolyte vapour. The type of discharge may have to be distinguished from the energy of the emitted radio frequencies or by the study of the light emitted. Crichton and McGough [17] performed streak photography to get insight into the various stages of discharge by applying the 85 V pulse for a duration of 200 μs. They concluded that the electrical discharge between cathode tool and electrolyte interface occurred due to: (i) generation of electrolytic gas at the surface of electrodes; (ii) the growth of layers of low ionic concentration near the electrodes and formation ofoxide films on the anode surface;and (iii) the local variations in the electrolyte flow pattern caused by flow stagnation and eddy. They also categorized the electrochemical action followed by discharge between the electrodes (i.e. ECAM) into four stages, i.e. (i) high frequency oscillations (160-170 KH_z), (ii) high rate ECM at 30 volts and 50 ampere, (iii) low rate ECM due to gas generation and (iv) electric discharge action,asshowninfigure3. Stage 1 represents un-productive period, which can beeliminated by circuit configuration. Stage 2 & 3 together represent an ECM phase. Stage 4 represents an EDM phase. The durations of these phases respectively increase and decrease with increasing the gap width and vary with electrolyte type, concentration and conductivity. Hence, these phases could be controlled to get the desired effect on the components machined by ECDM as shown in figure 3.

Basak [18] proposed that the electrical discharge in electrolyte occurred due to switching action and not due to dielectric break down of the medium. In view of high supply voltage compared to ECM, hydrogen gas bubbles density increases substantially to constrict the current path at tool-electrolyte interface. This constriction causes an increase in the resistance and ohmic heating of electrolyte solution in the local region and hence leads to blanketing of the tool by vapour generation and hydrogen bubbles. At a critical value of applied potential, this insulating bubble bridge blows off instantly due to intense heating. Consequently, the current suddenly drops to zero through the circuit and discharge takes place along the locations of the bubble bridge. This has been claimed as analogous to switching-off effect of an electrical circuit (Figure 4 (a) & (b)), based on Paschen's Curve from an electric contacttheory.

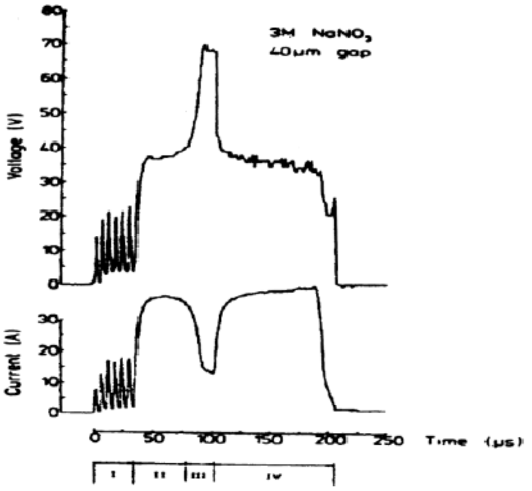

Fig. 3. Electrical phenomenon during ECAM with a square wave pulse [17].

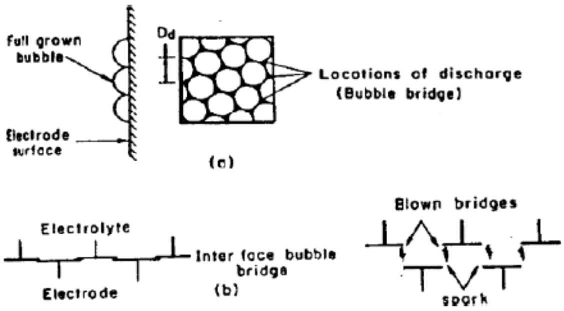

Fig.4. (a) Discharge locations with bubble distributionat critical condition. (b) Idealized switching-off situation[18].

Jain [19] claimed that the switching-off theory proposed by Basak [18] had certain inconsistencies and proposed "Valve Theory" with several assumptions regarding diameter of the bubble, electric field intensity, frequency of spark, etc. in conjugation with the finite element method to compute material removal rate. They considered each gas bubble as a valve, which after its breakdown due to high electric field produced discharge in the form of arc. The process was explained by constructing an equivalent circuit and it was concluded that the sparking during ECSM process was the result of arc discharge. Kulkarni [20], proposed that ECD was a discrete phenomenon. The breakdown is similar to the one that occurs in a gas due to a large electric field of the order of 10^7V/m which gets generated locally. By a time-varying current measurement method it has been observed that when an isolating film of hydrogen gas bubbles cover the cathode tip portion in the electrolyte, a large dynamic resistance is created and the current through the circuit becomes almost zero. A high electric field of the order of 10^7 V/m gets generated across the cathode tip and isolated electrolyte causing an arc discharge within the gas layers covering the tip. The electrons flow towards the workpiece kept near the cathode tip. This flow of electron is seen as a current spike of about 20 A or more for a short duration of few milliseconds. This bombardment of electrons raises the temperature of the workpiece momentarily and then the temperature decreases due to quenching.

It could be observed that due to complexity involved in this process, different theories have been used to explain the ECD phenomenon. Despite this, the mechanism of material removed in electrically conductive materials has been well explained in the literature by different machining methods (i.e., drilling & die sinking) [21-26] while for electrically non conductive materials, thermo-mechanical and chemical action have been considered by many researchers which depend very much on the property of the material being processed. The studies related to mechanism of material removal from electrically conductive and non-conductive materials have been discussed in this section to identify the influential parameters in ECDM while machining electrically non-conductive HSHTR engineering ceramics.

III. MECHANISM OF MATERIAL REMOVAL IN ELECTRICALLY CONDUCTIVE MATERIALS

The experimental investigation of ECAM for drilling hole on mild steel plate with high feed rate i.e. 15 mm/min to 25 mm/min (max. as high as 80 mm/min) was carried out by Kubota [21]. It was suggested that the bulk of metal removal is achieved by a sparking action in an electrolyte, whilst electrochemical action act as finishing operation which depends on the quality of electrolyte used. In a parametric study, Drake [65] reported that the ferocity of the sparks in ECAM could cause greater metallurgical damage to the workpiece than that normally associated with EDM. The dimensional accuracy achieved by ECAM was poor compared to EDM, the reason being, former process produced sparks / arc of greater intensity than those found usually in EDM to erode metal.

In an extensive study on drilling holes on different alloys (low carbon chrome steel, cobalt alloy, nickel alloy, low alloy steel), De Silva [23] reported similar findings i.e., material removal at the frontal gap was due to electric discharge erosion while at the side gap electro chemical dissolution of the material occurred. The metallurgically damaged layers, caused by the discharge erosion phase, were wholly or partially removed by the electrochemical dissolution phase. Therefore, a right balance of EDE &ECD controls the surface integrity (Figure 5) and produce smooth, damage free surface finish without sacrificing the metal removal rate.

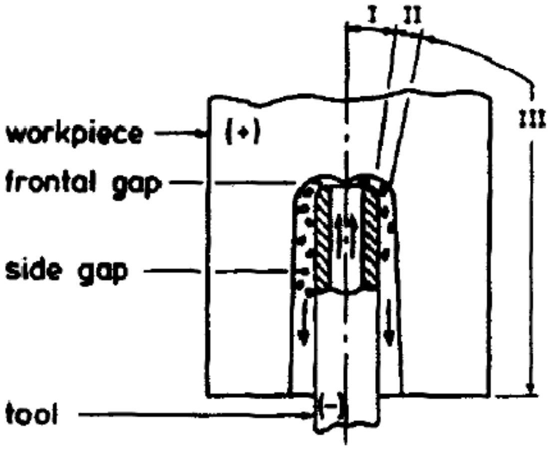

Fig. 5. Electrochemical arc drilling, (I) almost EDE, (II) combined ECD and EDE and (III) almost ECD [23].

The experimental verification of the above facts were further studied to have better control on the process by investigating the effect of different process parameters such as machining voltage, frequency and amplitude of tool oscillation, electrolyte type and concentration and the relationship between the tool oscillation and the voltage waveform on surfacefinish and surface integrity of moulds and dies [24- 26]. It was reported that machining at 12 -16 volts improved the flatness of the machined surfaces, while above 16 volts showed the evidence of tool wear & undercut on the machined surface, metal removal efficiency increased with increase in frequency oftooloscillation while it decreased with the increase in amplitude of tool oscillation. Under the effect of 20 wt% concentration of $NaNO_3$, single phase full-wave rectified unsmooth DC (0-60 V., 200 Amps.) showed high surface finish with low metal removal rate while low surface finish with high metal removal rate was observed with smooth DC (0-30 V., 200 Amps.). The phase relationship between the tool vibrationand machining voltage was shown to be an influential factor in ECAM. To enhance machining, ignition of the discharge was made to occur just before the voltage reached its maximum value on each cycle, this ensured stable machining in which discharges and high current density ECM occurred simultaneously.

IV. MECHANISM OF MATERIAL REMOVAL IN ELECTRICALLY NON CONDUCTIVE MATERIALS

Mechanism of material removal in electrically non conductive materials such as glass, quartz, composite, ceramics, etc., has been explained with the help of ECDM phenomenon. Similar to ECAM, mixed state of electric discharge (ED) and electro chemical (EC) machining which includes thermo-mechanical (vaporization, melting, erosion, cavitation, pitting, etc.) and chemical (chemical etching, dissolution) action depending upon the nature of material being processed has been proposed.

The phenomenon of electrical discharge in electrolyte was first utilized by Kurafugi and Suda [27] in 1968. Holes upto the depth of 0.31 mm was drilled on glass plate with cell voltage of 34 volts at 15wt% concentration of NaOH electrolyte. However, the mechanism of material removal was not identified but later it was proved as the most suitable process to machine non conductive materials. In an extensive study on machining of glass and other non conductive materials, Cook et al. [28] reported the process to be polarity dependent and electrolyte sensitive. It was observed that machining rate and depth of cut increased with the increase in supply voltage, electrolyte concentration and temperature, but for a given voltage the rate of machining was found to decrease with time (Fig. 6). The possible mechanism of material removal was explained as thermo mechanical, chemical, electric field and due to some other unknown effects. Experiments were conducted with DC pulsed power supply, where pulse in micro second range increased by a factor two and also produced better surface finish compared to smooth DC power supply.

Allesu [29], conducted an extensive experimental study on ECDM process while machining glass and categorized the mechanism of material removal process into three phases:

i) Electrochemical phase, where the current is carried by the electrolyte without any discharge (Figure 7(a)).

ii) Discharge phase, where the discharge occurs across the vapour / bubble, the surface activity operates because of the adsorbed electrolyte layer on the work surface. The current flows through the adsorbed layer and discharge takes place across the gas bubble (Figure 7(b)).

iii) Electrochemical phase occurs when the impressed voltage approaches zero (at the end of the pulse), the electrolyte is back into its original state. The hot surface of the glass undergoes quenching leading to thermal cracking or thermal spalling (Figure 7 (c)). This shows that mechanism depends very much on the workpiece material where thermal heating, cavitation and electro chemical action removes thematerial.

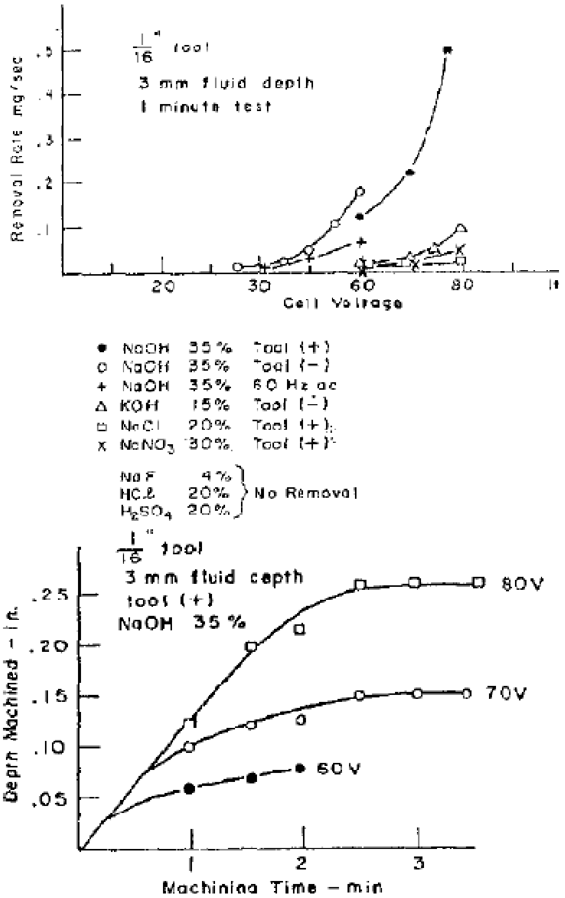

Fig. 6. Effect of parameters on material removal rate and machined depth while machining glass [28].

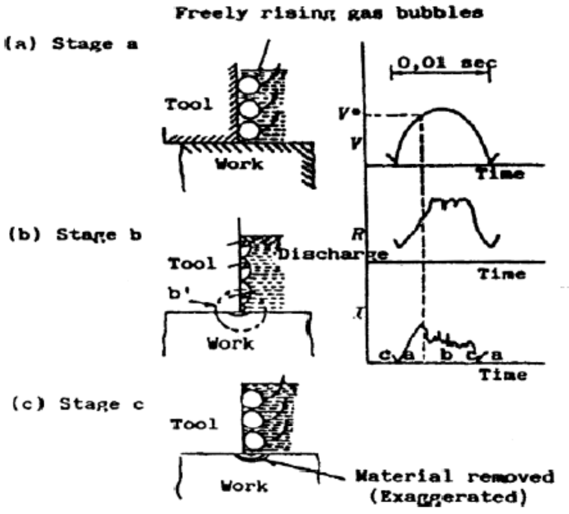

Fig. 7. Proposed mechanism of material removal in glass by ECDM process [29].

Apart from this, Allesu [30] discussed associated problems like "limiting depth characteristic" in ECDM. It was explained as a result of loss of potential between the tool electrode and bulk electrolyte with the tool penetration in the workpiecs, which was caused by the accumulation of gas bubbles, machined debris and electrolyte under confined conditions inside the hole. It was reported that discharge voltage increased with the increase in flow of electrolyte and upward shifting of discharge zone was observed when tool depth inside the electrolyte / workpiece increased. Basak [31], formulated a mathematical model to predict the material removal rate by varying input parameters and explained that, "machining occurs due to the transmission of a fraction of the spark energy to the workpiece, which raises the temperature of the spot quickly to a very high value and melts the work material spontaneously. A part of the molten portion of the workpiece is removed from the region due to the mechanical shock resulting from sudden phase change and the electrical shock due to the discharge. Figure 8 shows the mechanism of material removal in glass by ECDM process which is based on idealized model of discharge (switching-off situation [18]). In addition, the effect of inductance (in external circuit) on material removal rate was studied to improve the efficiency of the process[32].

Based on ECD phenomenon i.e. "evolution of heat due to sparking", Jain et al. [33] reported that the material removal process in glass-epoxy and Kevlar-epoxy composites involved evaporation, melting, mechanical erosion due to cavitation (rupture of gas bubble on the workpiece surface) and electrochemical reactions. It was reported that material removal rate, tool wear rate and overcut increased with increase in applied voltage and increase in specific conductivity of electrolyte. Specific conductance of NaOH increased upto 15wt% concentration, beyond that it decreased gradually. They reported the need of further investigation into the mechanism of this process. Material removal mechanism while machining ceramics is more difficult to explain, because they disintegrate instead of melting at high temperature.

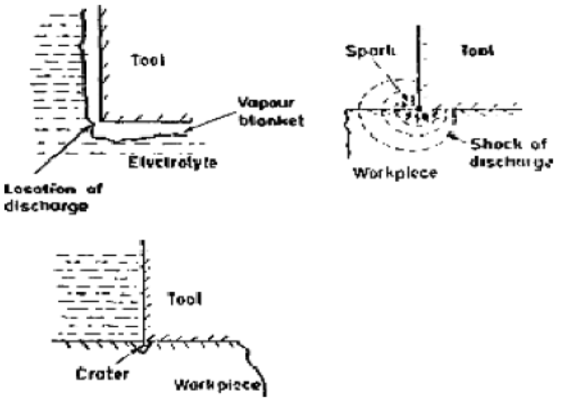

Fig. 8. Mechanism of material removal while machining glass by ECDM process [31].

Tokura et al. [34] reported that material removal in ceramics could be due to chemical etching and spalling (cavitation) effect. This is greatly influenced by the applied voltage, so it could not be increased beyond a certain value as ceramics show susceptibility towards crack due to thermal shocks at high voltage. With a stationary gravity fed Ni electrode of 0.5 mm diameter as cathode, a small pit formation was noticed under the influence of full wave rectified DC. Results obtained showed that the pit could be formed on ceramics (Al_2O_3&SiC) while its depth apparently varied with the ceramic material. It was observed that the volume of material removed, size and depth of the pit increased with increase in voltage and electrolyte concentration. 20wt% concentration of NaOH was found to result in maximum material removed. However, the rate of machining was found to be very low while machining ceramics and concluded that deep drilling of fine holes may not be feasible due to occurrence of abrupt spark which increased with the increase in tool depth inside theelectrolyte.

Bhattacharya et al. [35], reported that the machining in ceramics took place mainly due to spark discharge action across the gas bubble layers formed on the workpiece surface. Each electrical discharge causes a focussed stream of electrons to move with a very high velocity and acceleration from the cathode (or tool) towards the workpiece and ultimately creates compressive shock waves on the workpiece surfaces. The phenomenon is accomplished within a few microseconds and the temperature of the spot hit by electrons could rise to a very high value. As this temperature reach above the melting point of the workpiece material, it melts and finally evaporates the material. The high pressure of the compressive shock waves creates a blast, causing metallic vapours to form wear products in the shape of metallic globules, leaving craters in the workpiece surface. The material removal from the workpiece surface during electrical spark discharge is proportional to the pulse energy of the spark, which is released as heat during machining. Some researchers have pointed out that the heat generated by the electrical sparking rather than melting of the hard and brittle ceramics may cause the ceramic materials to spall. This phenomenon is known as thermal spalling, where the material removed is due to mechanical failure without melting. A complex temperature gradient is established due to the sudden temperature change in the machining area of the ceramic materials. It creates internal stresses that may be sufficient to overcome the bond strength of the ceramic grains, resulting in mechanical erosion. The proposed gas bubble formation and sparking phenomenon are exhibited in figure 9. They conducted an experimental study on Al_2O_3 to find the effect of applied voltage (70-90 V), electrolyte concentration (i.e., NaOH at 20wt%, 25wt%, 30wt% concentration) and tool tip shape(i.e.,flat front – straight side wall / taper side wall, curvature front – taper side wall shown in figure 10) on material removal rate and radial overcut under the effect of pulsed DC. It was observed that material removal rate & radial overcut increased with the increase in applied voltage & the increase in electrolyte concentration.

Machining at high voltage developed micro-crack while at higher concentration, overcut was increased. The effective range of parametric combination for moderately higher machining rate and dimensional accuracy was centered around 80 V applied voltage and 25wt% NaOH electrolyte solution. Similar results were obtained while machining ZrO_2 and Si_3N_4 with NaOH / KOH electrolytes [36-39]. It was observed that applied voltage had more significant effect on MRR, ROC and HAZthan other parameters [40]. Tool tip was also reported as a prominent factor for controlling spark generation in ECDM. Taper side wall-curvature front tool tip causes maximum amount of electrolyte availability in sparking zone which creates maximum number of sparks and thus increases MRRcompared to flat front - straight side wall tool tip / flat front – taper side wall tool tip where the availability of electrolyte in the gap between tool and job is very less as they are always in contact with each other due to the gravity feed force and thus causing occurrence of lower number of sparks.

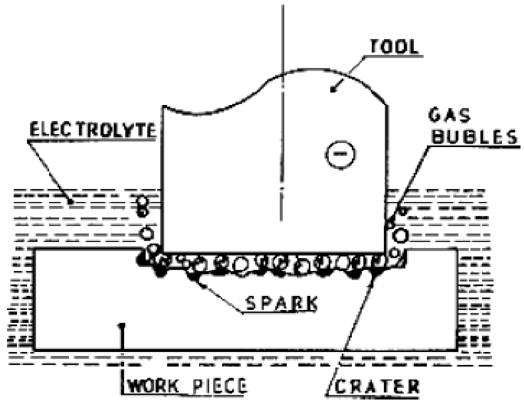

Fig. 9. Material removal mechanism of ECDM operation.

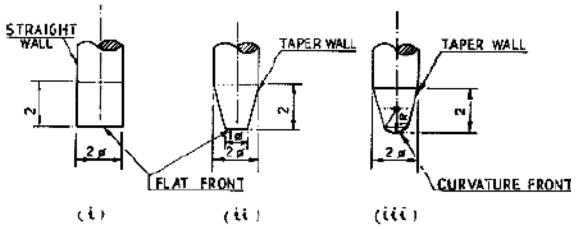

Fig. 10. Different geometrical shapes of the tool tip used [35].

Moreover, the mechanism of material removal in the ECDM process is very complex in nature and is governed by various process parameters that are still not very clear to researchers. In order to achieve effective and controlled machining, researchers have reported various predominant input parameters while machining low temperature materials such as glass, quartz, composites etc. using different machining techniques like drilling, grooving, cutting / slicing etc. On the other hand machining of ceramics is more difficult because they do not have melting characteristic and pose high hardness, high brittleness, chemical inertness at elevated temperature and also susceptible towards crack at highvoltage.

Wire electrochemical discharge machining of glass and ceramics was first reported by Tsuchiya [41]. Similar to the concept of wire EDM, wire ECDM was used to study the effect of polarity of electrodes, duty factor, supply voltage, electrolyte concentration and electrolyte flow rate on cutting rate and overcut was examined. It was observed that negative polarity of wire gave higher cutting rate than positive polarity. Cutting rate increased with the increase in voltage and electrolyte concentration. At high voltage & electrolyte concentration, MRRincreases but wire melts frequently at high voltage & low concentration and the micro cracks appeared over the machined surface. Cutting rate also increased with increase in duty factor and it became larger with low pulse rate. Glass (soda-lime, silica and borosilicate) and ceramic (Al_2O_3, Si_3N_4 and SiC) plates of 1.2 mm thickness were cut in the range of 2.5 mm / min to 4.0 mm / min and 0.12 mm / min to 0.14 mm / min respectively. Similar findings were reported by Jain et al. [42] while machining piezoelectric ceramic material (i.e. lead zirconatetitanate) of 2–3 mm thickness. MRRwas found maximum at 22.5wt% concentration of NaOH and average diametric overcut was reported as 0.67mmwith 0.5 mm diameter ofwire.

In order to increase the volume of material removed and machined depth in ceramics, researchers have tried different machining possibilities such as step drilling [43], vibrating tool [44], gas filled ECDM with side insulated tool [45], introducing external inductor into the circuit for constant supply of power input [46], SiC / graphite powder mixed electrolyte [47-48], rotary and trepanning action of copper electrode [49], etc. and were able to show some improvement. It was observed that rotary motion of electrode gave better results than stationary electrode. This electrode configuration was further modified to machine larger size holes on Al_2O_3& Quartz [50] by the orbital motion (trepanning) of the tool with comparatively smaller size electrode.

Jain et al. [51] used abrasive electrode with rotary motion under smooth DC voltage to drill holes on Al_2O_3. Results showed that the volume of material removed and depth of cut increased with the increase in supply voltage and electrolyte temperature. But the volume of material removed could not exceed 20 mg at 70 volts and the material showed tendency to cracking beyond these operating conditions. However, these limitations were partially relaxed by introducing pulsed DC power supply with an abrasive electrode that has reduced the tendency of crackingat high voltage and has reduced the taper on vertical surface while drilling deep holes in ceramics. Results obtained indicate that volume of material removed from the workpiece increases with increase in supply voltage, duty factor and electrolyte conductivity. The pulsating nature of current has reduced the could have helped in eroding the work material by intermittent focusing of thermal shocks while the use of an abrasive electrode simultaneously removed the recast layer at the local region and provides additional electrical discharge beneath the tool electrode which improves the machining conditions [52].

Apart from these findings, researcher also tried to develop mathematical models (based on different assumptions) to estimate the critical voltage & critical current using different electrolytes [53], temperature measurement at different radii of the workpiece [54] and electrolytic concentration & energy partition over material removal rate by finite element method [55]. It was observed that with the increase in electrolyte concentration from 10% to 30%, and with the increase in energy partition, material removal rate increased significantly especially in soda lime glass while machining Al_2O_3, similar trend had been observed with low variation in results due to its high hardness at elevatedtemperature.

On the other end, this process has also shown the different possibilities to machine electrically non-conductive HSHTR materials when the configuration of electrodes is modified. Though comparatively low machining efficiency was obtained, but researchers have made successful use of this process to machine such materials by different techniques like, 3D micro structuring of glass (Fig. 11) [56-60], slicing (cutting) of glass / quartz / glass &kevlarfibre epoxy composites (Fig. 12) [61-64], drilling of composites / glass / quartz (Fig. 13) [64-71], chemical engraving of glass (Fig. 14) [72-76] etc. Apart from machining / trueing & dressing of metal bonded diamond grinding tools by centerless grinding (Fig. 15) [77-79], micro welding (Fig. 16) [80] and ECD fused deposition for rapid prototyping (Fig. 17) [81, 82] are the variants of ECDM that is used for developing precision 3D micro structureslayerby layer similar to additive manufacturing, but they are less discussed in the literature.

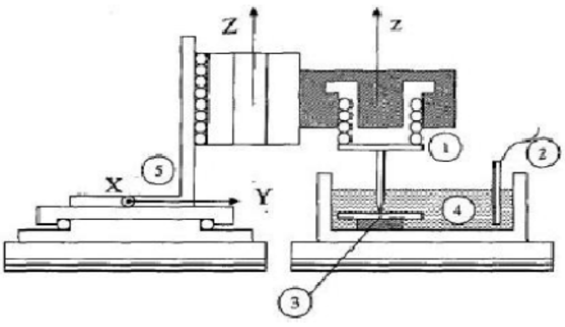

Fig. 11. 3D micro structuring of glass: (1) tool electrode with the holder mounted on a voice coil motor, (2) anode (3) glass sample.(4) electrolyte (5) XYZ stage [56].

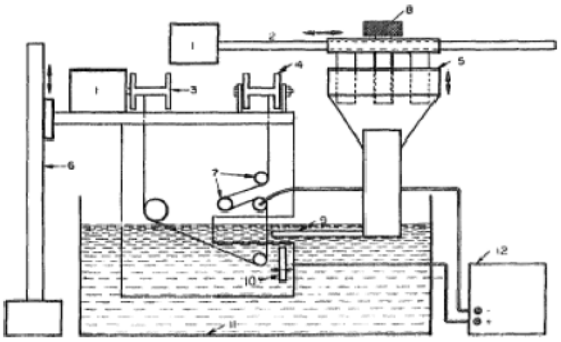

Fig. 12. Schematic line diagram of the ECDMwirecut experimental setup for slicing / cutting [63].

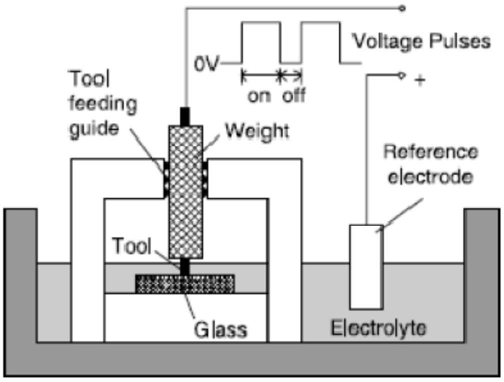

Fig. 13. Schematic diagram of the ECDM experimental apparatus for drilling [71].

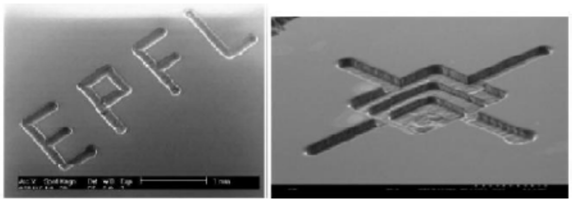

Fig. 14. Chemical engraving of glass by ECD phenomenon [74].

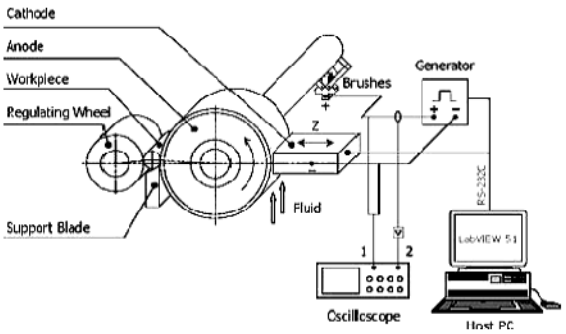

Fig.15. Schematic diagram of the ECDM Centerless Grinding[79].

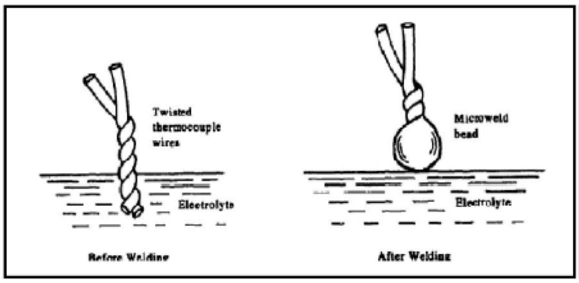

Fig.. 16. Micro welding by ECD phenomenon [80]

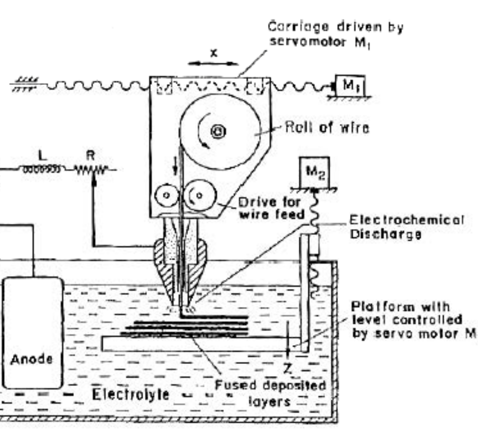

Fig.17. Scheme of electrochemical fused deposition for rapid prototyping[81].

V. HYBRID MACHINING PROCESSES

Compared to electrically conductive materials, machining of HSHTR engineering ceramics is more difficult because they pose high hardness and brittleness at high temperature. Despite their outstanding characteristics, applications of these ceramics is limited to only specialized fields due to inherent machining problems such as, low material removal rate, high tool wear rate, possible damage to the workpiece, high surface roughness and poor dimensional accuracy. Due to these reasons, efficient processes like electrochemical machining (ECM) and electric discharge machining (EDM) are not suitable to machine these ceramics, while other non-traditional / hybrid machining processes need thorough investigation on important aspects like surface integrity, dimensional accuracy, heat-affected zone, etc. of the machined surface.

The recent trend of combining different physiochemical action on the material being removed has shown improvement in machining. In particular a mechanical action, which is used in conventional material removal processes can be combined with respective interactions applied in unconventional manufacturing processes to make use of the combined or mutually enhanced advantages, and to reduce some adverse effects the constituent processes produce when they are individually applied. This trend of hybrid machining process (HMP) has now been extended to develop the processes like abrasive electric discharge grinding (AEDG), abrasive electro chemical grinding (AECG), abrasive electric discharge machining (AEDM) / powder mixed electric discharge machining (PMEDM), ultrasonic assisted electrical discharge machining (USEDM), ultrasonic assisted electro chemical machining (USECM), electro chemical discharge machining (ECDM), abrasive electro chemical discharge machining (AECDM), powder mixed electro chemical discharge machining (PMECDM), etc. for improved productivity / diversified applications, as shown in thefigure18.

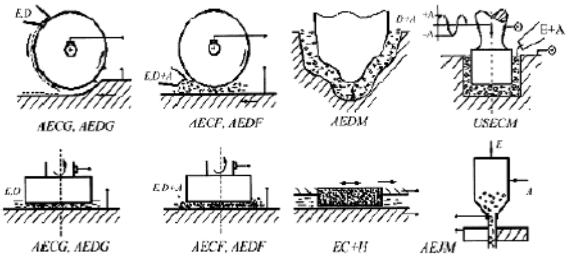

Fig.18. Schematic diagram of some methods of abrasive electrical machining.

Abrasive assisted electrical machining methods are becoming popular, as it facilitates additional cutting action, removal of recast layer / oxide film and improved surface finish during machining. This technique is now been effectively used by many researchers to machine electrically conductive &non conductiveHSHTR materials such as carbide / magnetic alloy / steel / titanium alloy / metal matrix composite / Al-SiC / cemented carbide by AEDG [83-85], sintered carbides / creep resisting alloys / titanium alloys / metallic matrix composites (e.g. PCD-Co, Al-SiC, Al-Al_2O_3) by AECG [86, 87], ferrous alloys by PMEDM [88, 89] and by AECF [90].

Among these methods, abrasives assisted ECDM process is gaining more popularity especially in micro machining of electrically non conductive materials, because it involve combined action of electrical discharge, chemical etching and abrasive cutting. Yang et al. [47] claims that loose abrasives particles disrupt the bubble accumulation to form an isolating layer around the tool electrode in ECDM. As a result, the measured critical voltage is higher in the electrolyte with abrasives than in the pure electrolyte. More energy is wasted in the bubble isolation layer and less energy is released during the removal of material by discharge heating, thus it reduces the overcut. It is observed that diametric overcut and surface roughness increased with increase in grit size. Material removal rate also increased with increase in abrasive concentration but saturates beyond 100gm/L. Smaller abrasive grit size improves the dimensional accuracy and surface finish of the product. Higher power frequency with smaller size abrasives also helps to refine / remove the micro-cracks and the melted zone formed by the discharge heat. The lapping force exerted by the relative motion between the abrasives and the workpiece promotes surface finish. Thus quality of slit produced on Pyrex glass by wire ECDM can be well controlled (KOH with 300g/L SiC, #200, 100Hz, Duty factor0.25).

Min et al. [48] claims that the use of fine abrasive graphite powder in ECDM helps to improve the surface integrity of the machined surface. By the use of 1.0 wt% graphite powder concentration in 30% NaOH, the number of microcracks was significantly reduced and the surface roughness was improved from 4.86 to 1.44 µm. Graphite powderpossesses good thermal and electrical conductivity therefore it intensifying the local electric field that reduces the spark initiation voltage [91]. The dielectric strength of hydrogen film depends on the condition of conductive particle such as number, size, chain shape of the particles [92]. When a particle is subjected to an electric force, it tends to detach itself from the electrode [93]. This charged particle attached to or moves between the electrodes, the potential between the electrodes decreases [94]. A micro discharge is caused if the detached particle approaches to the opposite electrode and likewise successive micro discharges in the hydrogen film results in the electrical breakdown [95] Figure19.

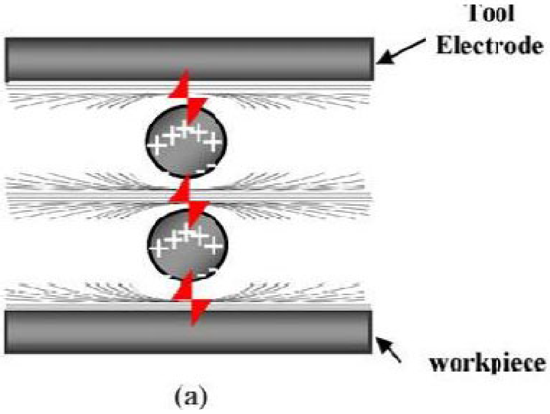

Fig. 19. Schematic diagram of series discharge in powder mixed electric discharge machining process (PMEDM) [95].

VI. CONCLUSION

This study reveals that much has been discussed about the electrochemical discharge phenomenon and its application while machining electrically conductive and electrically non conductivematerials. Since material removal in ECAM has been well explained, continuous improvement for its development is in progress and it is being effectively used to machine electrically conductive HSHTR materials with higher material removal rate and improved dimensional accuracy than ECM& EDM. This discharge phenomenon has also been used to machine electrically non conductive materials and the process was named as ECDM. It was observed that ECDM had low machining efficiency due to inherent machining problems, therefore materials like glass, quartz, composites etc. those having ability to melt(at discharge temperature) were machined by this process. Researchers have also reported that ECDM could be a viable solution for machining electrically non conductiveHSHTR ceramics, but realizing low efficiency of the process hybrid machining especially involving abrasives or electrically conductive powder mixed electro chemical discharge machining may further improve the machining performance. This process could be used for diversified applications such as 3D micro structuring, electro chemical discharge based fused deposition for rapid prototyping, slicing / grooving of glass / quartz/composites, trueing / dressing / centerless grinding of metal bonded diamond grinding tools, micro welding etc.

REFERENCES

[1] A.K. De Silva, “Process developments in electrochemical arc machining”, Ph.D. Thesis, University of Edinburgh, 1988.

[2] T.K.K.R. Mediliyegedara, A.K.M. De Silva, D.K. Harrison, J.A. McGeough, “An adaptive fuzzy inference system for the process control of electro chemical discharge machining (ECDM) process”, in: Proceedings of the fourth International Conference on Monitoring and Automatic Supervision in Manufacturing (AC’04), Zakopane, Poland, (2004)1-7.

[3] Skrabalak G., Skrabalak M. Z., Ruszaj A., “Building of rules base for fuzzy-logic control of the ECDM process”, Journal of Materials Processing Technology, Vol. 149 (2004)530–535.

[4] T.K.K.R. Mediliyegedara, A.K.M. De Silva, D.K. Harrison, J.A. McGeough, “An intelligent gap width controller for electro chemical discharge machining (ECDM) machine”, in: Proceedings of the Fourth CIRP Seminar on Intelligent Computation in Manufacturing Engineering (ICME 2004), Sorrento, Italy, (2004) 473– 478.

[5] T.K.K.R. Mediliyegedara, A.K.M. De Silva, D.K. Harrison, J.A. McGeough, An intelligent pulse classification system for electro chemical discharge machining (ECDM)—a preliminary study, Journal of Material Processing Technology, Vol. 149 (2004) 499– 503.

[6] A.K.M. De Silva, A.B. Khayry, J.A. McGeough, Process monitoring and control of electroerosion-dissolution machining. IMechE Conference Transactions, in: Proceedings of the 11th International Conference on Computer-Aided Production Engineering, (1995) 73–78.

[7] T.K.K.R. Mediliyegedara, A.K.M. De Silva, D.K. Harrison, J.A. McGeough, “New developments in the process control of the hybrid electro chemical discharge machining (ECDM) process”, Journal of Materials Processing Technology, Vol. 167 (2005)338–343.

[8] Crichton I. M., McGeough J. A., Munro W., White C., “Comparative studies of ECM, EDM and ECAM”, Journal of Precision Engg. Vol. 3 (3) (1981)155-160.

[9] Khayry A. B. M., McGeoughJ. A., “Modelling of Electrochemical Arc Machining by use of Dynamic Data Systems”, Proc. of the International Machine Tool Design and Research Conference, Birmingham, (1985)321-328.

[10] Khayry A. B. M., McGeoughJ. A., “Analysis of Electrochemical Arc Machining by Stochastic and Experimental methods”, Proc. Royal Society of London, A 412 (1987) 403 –429.

[11] Ni X., McGeough J. A., Greated C. A., “An analysis of Electrochemical Arc Machining”, Proc. Inst. of Mech. Engg., Part-B, Vol. 204 (1) (1990)23-28.

[12] McGeough J.A., Bhalla S., “Modelling and experiments on combined electrochemical and electro discharge machining of metals”, Proceeding of CAPE, (2001) 3-14, Wuhang, China.

[13] Ghosh Amitabha, “Electrochemical Discharge Machining. A New Process with Many Possibilities”, Journal of Inst. of Engrs. India, Vol. 70 (1) (1989)14-18.

[14] RudrofD.W., “Principles and applications of spark machining”, Proc. Inst. Mech. Engg., Vol. 17 (1957) 495-507.

[15] Mc Geough J.A., KhayryA.B.M., Munro. W., “Theoretical and experimental investigation of the relative effect of spark erosion and electrochemical dissolution in ECAM,” Annals of the CIRP, Vol. 32 (1) (1983)113-116.

[16] Crichton I.M., McGeough J.A., “Theoretical, Experimental and Computational aspects of the electrochemical arc machining process”, Annals of the CIRP, Vol. 33 (2) (1984) 429-432.

[17] Crichton I.M., Mc Geough J.A., “Studies of the discharge mechanism in electro-chemical are machining,” Journal of Applied Electrochemistry, Vol. 15 (1985)113-119.

[18] Basak I., Ghosh A., “Mechanism of Spark Generation during Electrochemical Discharge Machining: A Theoretical Model and Experimental Verification”, Journal of Materials Processing Technology, Vol. 62 (1) (1996)46-53.

[19] Jain V. K., Dixit P. M., Pandey P. M., “On the Analysis of the Electrochemical Spark Machining Process”, Int. Journal of Machine Tools and Manufacture, Vol. 39 (1) (1999)165-186.

[20] Kulkarni A., Sharan R., Lal G. K., “An Experimental Study of Discharge Mechanism in Electrochemical Discharge Machining”, Int. Journal of Machine Tools and Manufacture, Vol. 42 (10) (2002)1121-1127.

[21] Kubota M., Tamura Y., “ECDM drills a steel plate with high feed rate”, Bulletin, Japan society of precision engineering, Vol. 7 (4) (1973) 114 –117.

[22] Drake T. H., McGeough J. A., “Aspects of Drilling by Electrochemical Arc Machining”, Proceedings of the 22nd International Machine Tool Design and Research Conference, London, (1982)361-369.

[23] De Silva A., McGeough J. A., “Surface Effects on Alloys Drilled by Electrochemical Arc Machining”, Proc. Inst. Mech. Engg., Part-B, Vol. 200 (4) (1986)237-246.

[24] Levy N. M., McGeoughJ. A., Munro W., “Investigations of Surface Finishing of Dies and Moulds by Electrochemical Arc Machining”, Proc. of the 7th International Symposium, Birmingham, (1983)265-275.

[25] De Silva, A. K. and McGeough, J .A., “The Production of Full Die Shapes by Electrochemical Arc / Electrochemical Machining”, Proceedings of the ISEM, Vol. 9 (1989) 107-110.

[26] De Silva, A. and McGeough, J. A., “Hybrid Electrodischarge-Electrochemical Process for Roughing and Finishing Dies and Moulds”, Proceedings of the ISEM, Vol.12 (1998)397-406.

[27] Kurafugi H., Suda H., “Electrical discharge drilling of glass,” Annals of the CIRP, Vol. 16 (I) (1968)415-419.

[28] Cook N.H., Foot G.B., Jordan P., KalyaniB.N., “Experimental studies in electro-machining,” Trans. ASME, Journal of Engg. for Industries, Vol. 96 (1973) 945-950.

[29] Allesu K. Ghosh A., Muju M. K., “Preliminary qualitative approach of a proposed mechanism of material removal in electrical machining of glass”, European Journal of Mech. Engg., Vol. 36 (3) (1991)201-207.

[30] Allesu K., Ph.D. Dissertation, I. I. T. Kanpur, India,1988.

[31] BasakIndrajit, Ghosh Amitabha, “Mechanism of Material Removal in Electrochemical Discharge Machining: A Theoretical Model and Experimental Verification”, Journal of Materials Processing Technology, Vol. 71 (3) (1997)350-359.

[32] Basak I., Ph. D. Dissertation, I. I. T. Kanpur,India,1992.

[33] Jain V. K., Rao P. Sreenivasa, ChoudharyS.K., Rajurkar

[34] K. P., “Experimental Investigations into Traveling Wire Electrochemical Spark Machining (TW-ECSM) of composites”, Trans. ASME. Journal of Engg. for Industry, Vol. 113 (1) (1991) 75-84.

[35] Tokura H., Kondoh I., Yoshikaswa M., “Ceramic material processing by electrical discharge in electrolyte,” Journal of Material Science, Vol. 24 (1989)991-998.

[36] Doloi B., Bhattacharyya B., SorkhelS.K., “Experimental investigations into electrochemical discharge machining (ECDM) of non conductive ceramic materials”, J. of material processing technology, Vol. 95 (1999)145-154.

[37] Doloi B., Bhattacharyya B., Sorkhel S. K., “Experimental studies on electro chemical discharge machining (ECDM) characteristics for machining engineering ceramics”, 18thAIMTDR Conf. I.I.T. Kharagpur, (1998)322-327.

[38] Doloi B., Bhattacharyya B., Sorkhel S. K., “Electrochemical Discharge Machining of Non-Conducting Ceramics”, Defence Science Journal, Vol. 49 (4) (1999) 331-338.

[39] Doloi B., Bhattacharyya B., Sorkhel S. K., “Experimental Studies on Electrochemical Discharge Machining (ECDM) of

Silicon Nitride Ceramic Material", Proc. of 19thAIMTDR Conf., (2000)185-190.

[40] Doloi B., Bhattacharyya B., Sorkhel S. K., "Optimization of Electrochemical Discharge Machining Process for Machining Silicon Nitride Ceramics", Proc. of National Symposium on Manufacturing in twenty firstcentury, I.I.T. Kanpur, (2001) 117-120.

[41] Sarkar B. R., Doloi B., Bhattacharya B., "Parametric analysis on electrochemical discharge machining of silicon nitride ceramics", Int. Journal of Advance Manufacturing Technology, Vol. 28 (2007)873-881.

[42] Tsuchiya H., Inoue T, Miyazaki M., "Wire Electro- Chemical Discharge Machining of Glasses and Ceramics", Japan Soc. of Precision Engineering, Proc. of 5th ICPE, Tokyo, Japan, (1984)413-417.

[43] Singh Y. P., Jain V. K., Prashant K., Agrawal D. C., "Machining Piezoelectric (PZT) Ceramics using an Electrochemical Spark Machining (ECSM) process", Journal of Materials Processing Technology, Vol. (58) (1) (1996)24-31.

[44] Allesu K., Umesh K. N., Muju M. K., Ghosh A., "Some investigations into the spark machining of non-conducting materials", 12th AIMTDR Conf. I.I.T. Delhi, (1986) 521-524.

[45] Chikamori K., "Grooving on Silicon Nitride Ceramics with Arc Discharge in Electrolyte", Int. J. Japan Soc. of Precision Engineering, Vol. 25 (2) (1991)109-110.

[46] Yonghong L., Zhixin J., Jinchun L., "Study on hole machining of non-conducting ceramics by gas-filled electro-discharge and electro-chemical compound machining", J. of Material Processing Technology, Vol. 69 (1997)198-202.

[47] RaghuramV., Pramila T., SrinivasaY.G., Naryanaswamy K., "Effect of the circuit parameters in the electrolytes in the electrochemical discharge phenomenon," Journal of Materials Processing Technology, Vol. 52 (1995)289-300.

[48] Yang C. T., Song S. L., Yan B. H., Huang F. Y., "Improving machining performance of wire electrochemical discharge machining by adding SiC abrasive to electrolyte", Int. Journal of Machine Tools & Manufacture, Vol. 46 (15) (2006) 2044 - 2050.

[49] Min-Seop Han, Byung-Kwon Min, Sang Jo Lee, "Improvement of surface integrity of electro-chemical discharge machining process using powder-mixed electrolyte", Journal of Material Processing Technology, Vol. 191 (2007)224-227.

[50] Gautam-N., Jain V.K., "Experimental Investigations into ECSD process using various tool kinematics", Int. Journal of Machine Tools and Manufacture, Vol. 38 (1) (1998) 15- 27.

[51] Jain V.K., Chak-S.K., "Electrochemical Spark Trepanning of Alumina and Quartz", Int. Journal of Machining Science and Technology, Vol. 4 (2) (2000)277-290.

[52] Jain V.K., Choudhury S.K., Ramesh K.M., "On the machining of Alumina and Glass", Int. Journal of Machine Tools and Manufacture, Vol. 42 (2002)1269-1276.

[53] Chak, S.K., Rao, P.V. 'Drilling of Al2O3 using pulsed DC supply with rotary abrasive electrode by electro-chemical discharge (ECD) process', Int. Journal of Advanced Manufacturing Technology, Vol. 39, No. 7, 2008 pp.633–641.

[54] Dutta A., Basak I., "Electrochemical Discharge: A potential tool for machining electrically non conducting materials", Institution of Engg. Prod. Engg., Vol. 80 (1999) 38-41.

[55] Kulkarni A. V., Karnik M. G., "Experimental Measurements and Theoretical Ectimation of Temperature in ECDM Process", Proceedings of the International Conference on MEMS, NANO and Smart Systems (ICMENS'04),(2004).

[56] Fascio V., Wuthrich R., ViqueratD. Langen H., "3D microstructuring of glass using electrochemical discharge machining (ECDM)", Int. Symposium on Micromechatronics and Human Science (MHS'.99), (1999)179-183.

[57] H. Langen, V. Fascio, R. Wu¨thrich, D. Viquerat, "Three-dimensional structuring of pyrex glass devices—trajectory control", International Conference of the European Society for Precision Engineering and Nanotechnology (EUSPEN) 2 Eindhoven, (2002)435–438.

[58] R. Wuthrich, H. Bleuler, "Glass microstructuring with spark assisted chemical engraving", The Fourth Korea–Switzerland Joint Symposium, Les Diablerets, Switzerland, Feb. 1-3, 2004,51–54.

[59] L.A. Hof, A. Lal, K. Fujisaki, R. Wu¨thrich, H.H.Langen, H. Bleuler, "3D Micro structuring of glass with an AFM", The Fourth EUSPEN International Conference, Glasgow, UK, May 30th–3rd June 2004, 98–99.

[60] Zhi-Ping Zheng, Wei-Hsin Cheng, Fuang-Yuan Huang, Bilng-Hwa Yan, "3D microstructuring of Pyrex glass using the electrochemical discharge machining process", Journal of Micromechanics and Microengineering, Vol. 17 (2007)960-966.

[61] Peng W. Y., Liao Y. S., "Study of electrochemical discharge machining technology for slicing non- conductive brittle materials" J. of material processing technology, Vol. 149 (2004)363-369.

[62] Jain V. K., "ECSM-A New Way to Machine Polymer Composites", Proc. INCARF-93, (1993)359-368.

[63] Nesarikar V. V., Jain V. K., Choudhury S.K., "TW-ECSM of Thick Sheet of Kevlar-Epoxy Composites," Proc. of16thAIMTDR Conf., (1994)672-677.

[64] Tandon S., Jain V. K., Kumar P., Rajurkar K. P., "Investigations into Machining of Composites", Journal of Precision Engg., Vol. 12 (4) (1990)227-238.

[65] Zhi-Ping Zheng, Wei-Hsin Cheng, Fuang-Yuan Huang, Bilng-Hwa Yan, "The tool geometrical shape and pulse- off time of pulse voltage effects in a Pyrex glass electrochemical discharge microdrilling process", Journal of Micromechanics and Microengineering, Vol. 17 (2007) 265-272.

[66] H. Langen, I. Ceausoglu, M. van der Meer, E.Lehmann, H. Bleuler, Ph. Renaud, "Electrochemical micromachining of glass using Mico-EDMedMicrotools, Proceedings of Ultraprecision in Manufacturing Engineering, Braunsweig, May 26–30, 1997, 672-679.

[67] H. Langen, J.-M. Breguet, H. Bleuler, Ph. Renaud, T. Masuzawa, "Micro electrochemical discharge machining of glass", International Journal of Electrical Machining, Vol. 3, (1998)65–69.

[68] R. Wuthrich, V. Fascio, D. Viquerat, H. Langen, "In situ measurement and micro-machining of glass", International Symposium on Micromecatronics and Human Science (MHS'99), Nagoya, 1999,185–191.

[69] C.T. Yang, S.S. Ho, B.H. Yan, "Micro hole machining of borosilicate glass trough electrochemical discharge machining (ECDM)", Key Engineering Materials, Vol. 196 (2001)149–166.

[70] H.-J. Lim, Y.-M. Lim, S.H. Kim, Y.K. Kwak, "Self- aligned micro tool and electrochemical discharge machining (ECDM) for ceramic materials", Proceedings of SPIE 4416, (2001)348–353.

[71] Kim D. J., Ahn Y., Lee S. H., Kim Y. K., "Voltage pulse frequency and duty ratio effects in an electrochemical discharge micro drilling process of Pyrex glass", Int. Journal of Machine Tools & Manufacture, Vol. 45 (10) (2006) 1064 – 1067.

[72] R. Wuthrich, "Spark assisted chemical engraving—a stochastic modeling approach", Dissertation Thesis (2776), Swiss Federal Institute of Technology, EPF Lausanne, 2003.

[73] V. Fascio, R. Wuthrich, K. Fujisaki, D. Viquerat, H. Langen, H. Bleuler., "Spark assisted chemical engraving: a novel technology for glass microstructuring", Invited lecture in European Congress on Advanced Materials and Processes (EUROMAT), Lausanne,2003.

[74] Fascio V., Wuthrich R., Bleuler H., "Spark assisted chemical engraving in the light of electrochemistry", ElectrochimicaActa, Vol. 49 (2004)3997-4003.

[75] Wuthrich R., FascioV., "Machining of non-conducting materials using electrochemical discharge phenomenon – an overview", Int. Journal of Machine Tools & Manufacture, Vol. 45 (2005) 1095 –1108.

[76] Wuthrich R., Hof L. A., "The gas film in spark assisted chemical engraving (SACE) – A key element for micro-machining applications", Int. Journal of Machine Tools & Manufacture, Vol. 46 (2006)828-835.

[77] Kramer D., Rehsteiner F., Schumacher B., “ECD (Electrochemical In-Process Controlled Dressing), a New Method for Grinding of Modem High-Performance Cutting Materials to Highest Quality”, Annals of theCIRP. Vol. 48 (1) (1999)265-268.

[78] Nebashi N., Wakabayashi K., Yamada M., Masuzawa T., “In-Process Trueing/Dressing of Grinding Wheels by WEDG and ELID”, International Journal of Electrical Machining, No. 3 (1998)33-38.

[79] Schopf M., Beltrami I. Boccadoro M., Kramer D., “ECDM (Electro Chemical Discharge Machining), a New Method for Trueing and Dressing of Metal-Bonded Diamond Grinding Tools”, Annals of the CIRP Vol. 50 (1) (2001) 125-128.

[80] Ghosh A., MujuM.K., Pasrija S., Allesu K., “Micro- Welding using Electrochemical Discharge”, Int. Journal of Machine Tools and Manufacture, Vol. 37 (9) (1997)1303- 1312.

[81] Ghosh Amitabha, “Electrochemical Discharge Machining: Principle and Possibilities”, Sadhana Academy, Proceedings in Engineering Sciences, Vol. 22 (3) (1997) 435-447.

[82] Saraf A., Saha P., Mishra P. K., Ghosh A., “A feasibility study of using electrochemical deposition for rapid prototyping”, 18thAIMTDR Conference, I.I.T. Kharagpur, India, Dec. 1998,328-333.

[83] Jerzy Kozak and Kazimierz E. Oczo, “Selected problems of abrasive hybrid machining”, Journal of Materials Processing Technology, Vol. 109 (3) (2001)360-366.

[84] K.P. Rajurkar, B. Wei, J. Kozak, S.R. Nooka, Abrasive electro-discharge grinding of advanced materials, in: Proceedings of the International Symposium for Electro-Machining ISEM-11, Lousanne, (1995),863-870.

[85] Philip Koshy, V. K. Jain and G. K. Lal, “Grinding of cemented carbide with electrical spark assistance”, Journal of Materials Processing Technology, Vol. 72 (1) (1997) 61-68.

[86] J. Kozak, “Selected problems of hybrid electro-mechanical machining”, Arch. Mech. Technol. Automatization, Vol. 16 (1996) 59-65 (inPolish).

[87] J. Kozak, “The analysis of the interactions of mechanical abrasion and electrochemical dissolution processes in AECG”, in: Proceedings of the 19th Science Symposium on Abrasive Machining, (1996) 275-282 (inPolish).

[88] Y.S. Wong, L.C. Lim, I. Rahuman, W.M. Tee, “Near- mirror-finish phenomenon in EDM using powder-mixed dielectric, Inernational. Journal of Advance Manufacturing. Technology, Vol. 79 (1998)30–40.

[89] H. K. Kansal, Sehijpal Singh, P. Kumar, “Parametric optimization of powder mixed electrical discharge machining by response surface methodology”, Journal of Materials Processing Technology, Vol. 169 (2005) 427– 436.

[90] H. Kamada, K. Tamiya, “A study on electrolytic-abrasive mirror finishing”, Bulletin. Japan. Society of Precision Engineering, Vol. 16 (2) (1982)109-110.

[91] L. Dascalescu, R. Tobazeon, P. Atten, “Behaviour of conducting particles in corona-dominated electric fields”, J. Phys. D: Appl. Phys. Vol. 28 (1995)1611-1618.

[92] L. Dascalescu, A. Samuila, R. Tobazeon, : Size of solid contaminants and formation of particle chains: two factor affecting the dielectric strength of insulating gases”, J. Electrostatics Vol. 40-41 (1997)419-424.

[93] L. Dascalescu, A. Samuila, R. Tobazeon, “Dielectric behavior of particle-contaminated air-gaps in the presence of corona”, J. Electrostatics Vol. 36 (1996)235-275.

[94] P. Felsenthai, B. Vonnegut, “Enhanced charge transfer in dielectric fluids containing conducting particles, Br. J. Appl. Phys. Vol. 18 (1967) 1801-1806.

[95] W. S. Zhao, Q. G. Meng, Z. L. Wang, “ The application of research on powder mixed EDM in rough machining”, J. of Material Processing Technology, Vol. 129 (2002) 30- 33.

★★★

THE RESULT OF HEAT TREATMENT ON THE MECHANICAL BEHAVIOR OF FE-CR-AL BASED OPH ALLOY

[1]KHIROD KUMAR ROUT, [2]SASHIKANT KANTA ACHARYA, [3]SMRUTIREKHA GIRI

[1]Department of Electrical and Electronics Engineering, NMIET, Bhubaneswar, 751019
[2]Department of Mechanical Engineering REC Bhubaneswar
[3]Department of Mechanical Engineering AIET Bhubaneswar
E-mail: sujeet.yadav@nmiet.ac.in

Abstract - The Fe-Al Oxide Precipitation Hardened (OPH) alloy is new generation of Oxide Dispersion Strengthened (ODS) alloys which is famous group of material based on their high temperature properties. The general production process of OPH alloys consists of a mechanical alloying process to create a material with a ductile matrix and hard oxide dispersion. Two variants of Fe-Cr-Al based OPH alloys developed by the authors to investigate the thermomechanical properties under different conditions. The results show that the heat treatment has a significant role on the mechanical properties of OPH alloys as well as microstructure development. It can improve the ultimate tensile strength (UTS) up to 100% while improving the elongation to almost20%.

Keywords - OPH Alloys, Fe-Al, Heat Treatment, ODS Alloys

I. INTRODUCTION

Iron Aluminum based OPH alloys are so nowadays interested because of low-cost and improved mechanical properties. By additional Cr contents of around 15 wt.%, it could be one of the leading candidates for structural components of future power plants [1-3]. Several advantages are considered when employing ferretic Fe-Cr-Al alloys in high temperature applications. In addition of lower raw material and preparation costs and of course superior oxidation resistance, the alloys have a higher melting point, lower density and lower thermal expansion compare to the current nickel or cobalt base alloys [4, 5]. Besides the oxidation resistance of Fe-Cr-Al ODS alloys is attributed to the presence of the yttrium as a reactive element and in fact this element leads to the formation of an adherent and slow growing Al2O3 film exhibiting highly protective properties for the underlying material up to 1200^{o}C [6]. However, the mechanical strength of these alloys in the cast and wrought condition at elevated temperatures were too low to make them outstandingforsuch a purpose, that's why the dispersion strengthening with stable oxide particle used to improve their higher temperature strength without sacrificing the excellent surface stability of the matrix alloy [7, 8]. ODS steels usually have reasonable creep resistance rather than their non-reinforced counterparts, however it usually suffer from poor toughness[9-11]. Therefore it is very important to optimize the microstructure of ODS steels to achieve an improved thermomechanical behavior. The author's previous experience showed that the use of Y_2O_3 is effective to adjust the oxygen content in Fe-Cr-Al OPHAlloys[12, 13]. In addition, this could also enhance the impact properties of OPHferritic steels [14]. However, there exists little information about the annealing effect on the microstructure and tensile properties of these materials at elevated temperatures. Thustheauthors tried to manufacture two variants of Fe-Cr-Al OPH alloys differing in milling time to investigate the effect of annealing on the thermomechanical properties of this group ofalloys

II. EXPERIMENTALPROCEDURE

The OPH alloy was prepared based on Fe-Cr-Al matrix under a controlled mechanical alloying (MA) process. A particular advantage of the process is that the stored energy introduced to powders by high energy milling, can contribute to the production of a large elongated grain structure during subsequent high temperature heat treatments. However, special care should be considered for the milling time and rotation speed. The components consist of (wt.)%71Fe-15Cr-6Al-3Mo-1Ta-4Y_2O_3 in a form of atomized powder which then mixed with the specific amount of O2 in form of gas in a low energy ball mill. The mill which is developed by the authors is capable of evacuation and filling by oxygen in addition of adjusting rotation speed. The milling lasted for 150 h for first variant (V1) and 230 h for the second variant (V2), both at 70 rpm. Then the powder became a solid solution and transferred to the rolling container in a vacuum condition. At the same time, it has been evacuated by suction pump and then sealed by means of welding. The final semi products went through two step hot rolling at 900oC and the final thickness of 6 mm covered by 1 mm steel container was achieved. Based on the type of tests, the desired sample shape then cut by means of waterjet, parallel to the rollingdirection.

In order to investigate the effect of annealing on the thermomechanical properties of OPH alloys more in details, both variants were put under heat treatment described on table 1.Both variants then went through the tensile and hardness tests at room temperature (RT) to see how they were effected from the different heat treatment. A metallographic analysis was also made to go more in depth through the microstructure of these alloys

Variant	Temperature (°C)	Holding time (hours)
V1	1000	5, 10
	1100	5, 10
	1200	1, 5, 10
V2	1000	5, 10
	1100	5, 10
	1200	1, 5, 10

Table 1: Annealing plan

III. RESULTS ANDDISCUSSIONS

The mechanical properties after heat treatment of both materials were investigated by performing the tensile test using a thermomechanical simulator which could keep the constant desire strain rateof $0.003\ s^{-1}$during the whole test. Fig. 1 to Fig. 3 show the flow curves for both V1 and V2 under different annealing conditions which described in Table 1. It should be noted that all the tensile tests were done at RT. It can be seen that both UTS and elongation are significantly sensitive to heat treatment. In case of UTS, the best result achieved for V1 after 20 hours of annealing at 1000 °C while the best elongation achieved for the same variant at 1200 °C after same holding time.

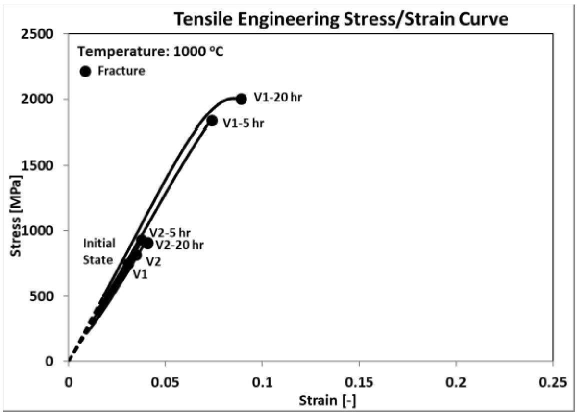

Figure 1: Flow curves after annealing at 1000 °C

On the other hand, annealing at higher temperature, increased the ductility of OPH alloy while at lower temperature, higher strength could achieved, regardless of milling time. Compare to initial state (IS), the improvement in UTS could be varied from 20% after annealing at 1200°C (Fig. 3) to more than 100% after annealing at 1000°C (Fig. 1). The most effective one for V1, happened at 1100 oCholding for 20 hours, which increase the UTSfor almost 50% while the elongation increased to10%.

Besides, the results confirmed that higher milling time, caused less improvement on the mechanical properties of OPH Alloy, even after annealing at elevated temperatures. The UTS improvement for V2 (higher milling time) after 20 hours annealing at 1000°C and 1100°C is almost 15% to 29%, respectively compare to initial state while no improvement in elongation was observed. It seems that the improvement for V2 started at 1100 °C after 20 hours of annealing (Fig. 2) which then increased by increasing the annealing temperature to 1200 °C (Fig. 3). UTS increased almost by 30% and 43% after 5 and 20 hours respectively, compare to initialstate.

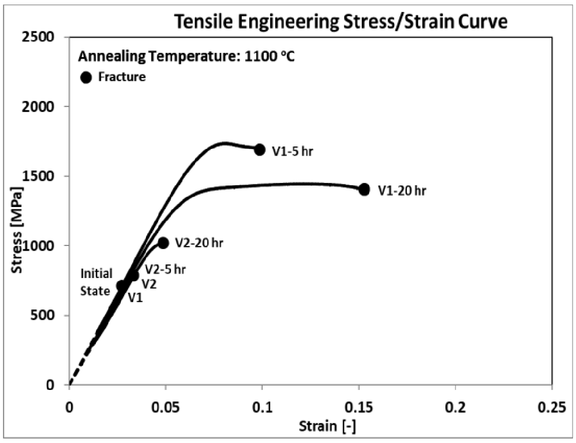

Figure 2: Flow curves after annealing at 1100°C

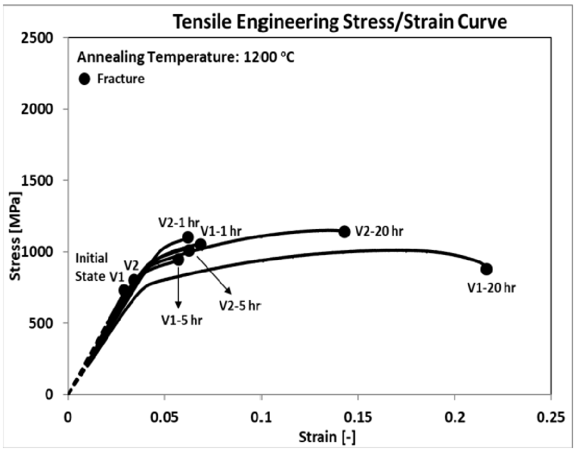

Figure 3: Flow curves after annealing at 1200°C

Figure 4 shows the hardness (HV10) results for both materials on the initial state and on the samples after annealing under heat treatment at 1000 C, 1100 C and 1200°C holding within the time described in table1. The hardness test according to Vickers was performed by using a ZWICK/ROELLZ2.5 hardness tester with a load of 10 kg and loading time 11 s on the surface fracture area ofpolished samples. The average value was calculated from three measurements. The hardness of samples demonstrates the ability of OPH alloys to resist plastic deformation at various elevated temperatures. As the ODS ferritic steels possess remarkable mechanical properties such as high tensile and creep strength, OPH steels surely possess extremely hard surface and strength. Thus, Vickers hardness test is the standard method to measure the hardness of this group of materials compared to other hardness measurement methods such as Rockwell andBrinell.

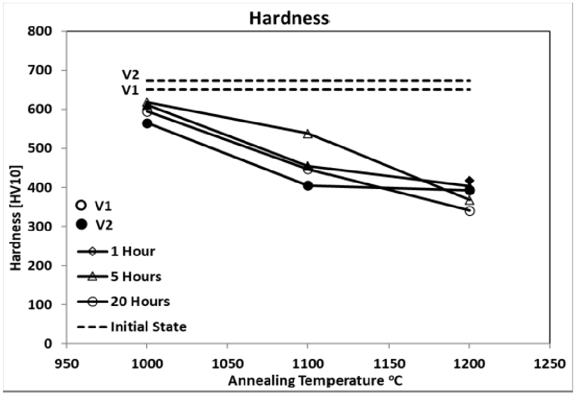

Figure 4: Hardness (HV10) at different conditions

The results show that the annealing also effected the hardness on both variants of OPH alloys. Compare to initial state, elevating temperature up to 1200°C decreases the hardness almost 30% while at 1000°C it decreases maximum 10%. Besides, V1 after 5 hours annealing at 1100°C shows less reduction in HV10compare to the V2 at the same condition. The reason could be attributed to the recrystallization process which may not started in this situation for V1 [15]. On the other hand, the decrease in HV10is more considerable at the first step of annealing from 1000°C to 1100°C, however on the second step from 1100°C to 1200°C, less reduction happened. On the other hand, longer holding time has more influence on the hardness value of OPH alloys. Holding for 20 hours up to 1100°C decreases the hardness 2 times more compare to similar condition with less holding time while at 1200°C, longer holding time has the same influence as lowertime.

In order to go more in depth, the microstructure of both OPH variants with different annealing conditions were investigated. Fig. 5 to 11 show the microstructure of all both V1 and V2 material using optical microscope. It could be seen that after the rolling (initial state), the microstructure of both materials consisted of solid solution with very fine oxides with different chemical composition. The microstructure was homogeneous without visible cracks after rolling. This microstructure keeps its formation with almost no changes in the main structure up to annealing at 1100 °Cfor5 hours, especially for V2 (Fig. 7b). However, recrystallization did not take place in the entire material volume. Very small grains were still visible in the microstructure.

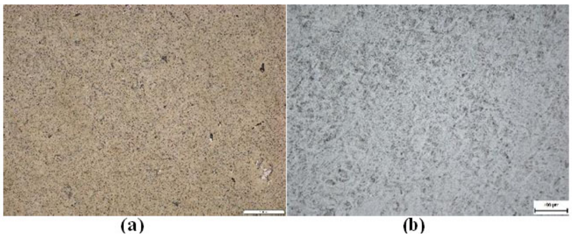
(a) (b)

Figure 5: OPH alloys microstructure (Initial State), (a) V1 and (b)V2

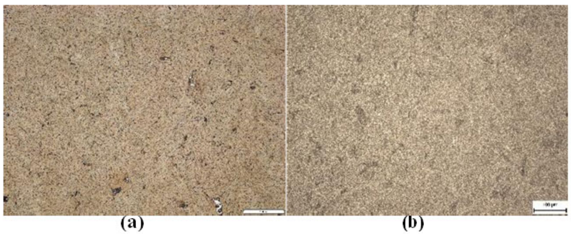
(a) (b)

Figure 6: OPH alloys microstructure (1000°C, 5 hours), (a) V1 and (b) V2

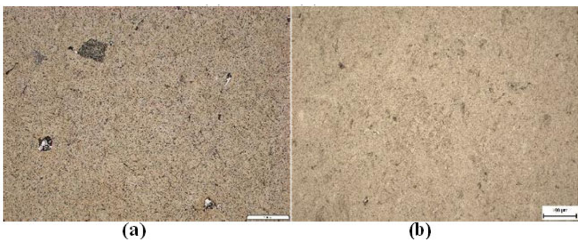
(a) (b)

Figure 6: OPH alloys microstructure (1000°C, 20 hours), (a) V1 and (b) V2

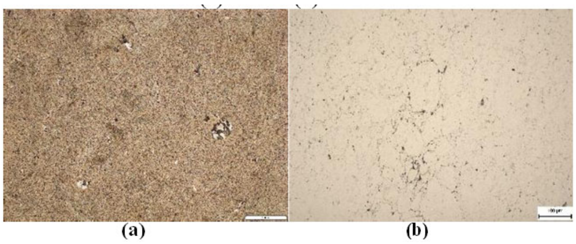
(a) (b)

Figure 7: OPH alloys microstructure (1100°C, 5 hours), (a) V1 and (b) V2

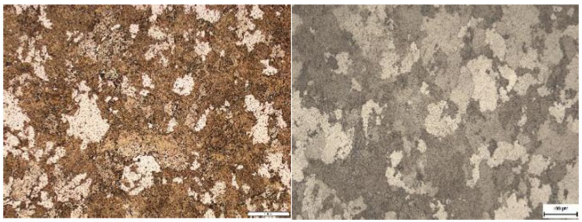
(a) (b)

Figure 8: OPH alloys microstructure (1100°C, 20 hours), (a) V1 and (b) V2

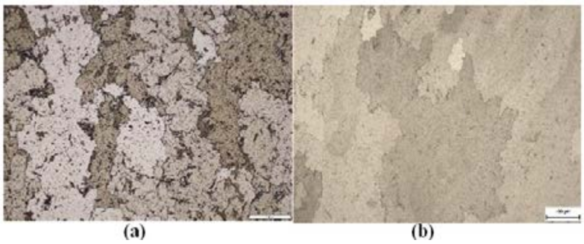
(a) (b)

Figure 9: OPH alloys microstructure (1200°C, 1 hour), (a) V1 and (b) V2

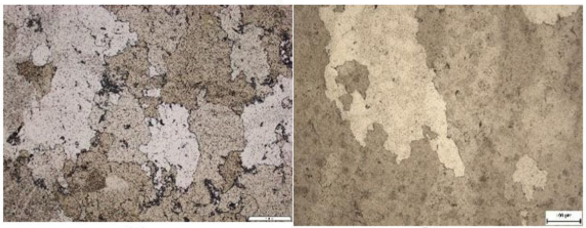
(a) (b)

Figure 10: OPH alloys microstructure (1200°C, 5 hours), (a) V1 and (b)V2

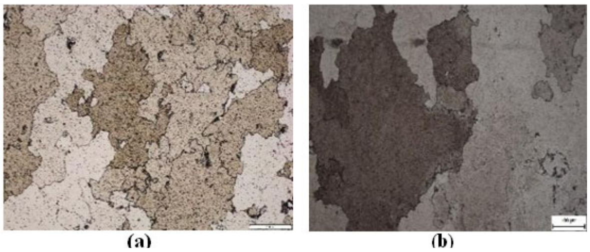

Figure 11: OPH alloys microstructure (1200^{o}C, 20 hours), (a) V1 and (b)V2

Following Fig. 8, the recrystallization also starts for V1 holding at 1100^{o}Cfor 20 hours (Fig. 8a) while it was started at the same temperature for 5 hours for V2 (Fig. 7b). The recrystallization progress almost completed for both variants after 1 hours at 1200oC (Fig. 9) and followed by Fig. 11 that shows the longest holding time of 20 hours at 1200°C, which the structure was completely recrystallized. The results also showed that the grain size is bigger for theV2 materials with longer millingtime.

To have a better understanding of chemical composition of the occurring particles in the microstructure of initial state, an EDS spectrum analysis were performed on both variants using scanning electron microscope (Zeiss Crossbeam 340-47-44) (Fig. 12, Fig. 13) In the material V1 two types of particles were found. The bigger particles were darker and the EDS analysis showed that they are molybdenum, chromium, aluminum rich (Fig. 12). The second type were smaller lighter particles, which also contained tantalum.

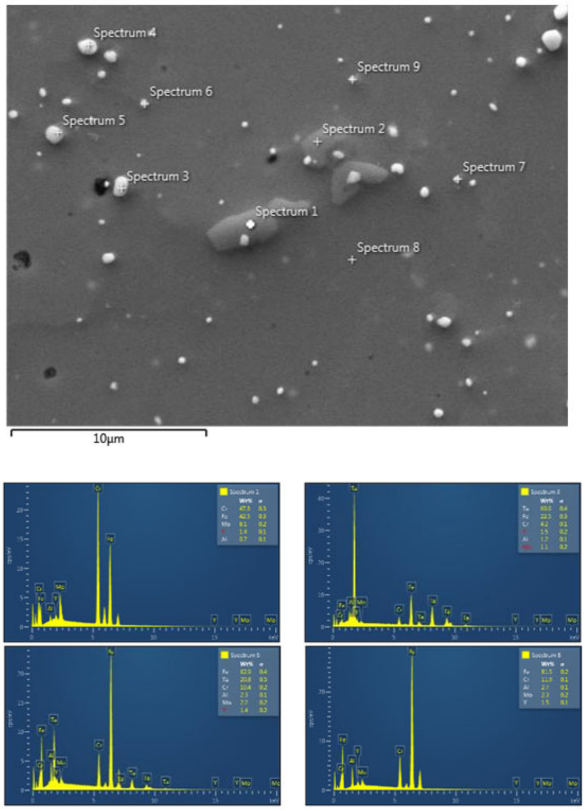

Figure 12: EDS spectrum analysis results for V1

On the other hand, the bigger particles in V2 (Fig. 13) were tantalum rich and the rest of the particles were are Fe-Cr-Al rich. Molybdenum and chromium as a refractory element increases significantly the cohesive strength of the grain boundaries, stabilize bcc-lattice and increase the oxidation resistance at high temperatures. However, both elements increase the stability of carbides precipitating at grain boundaries provoking intergranularfracture.

Figure 13: EDS spectrum analysis results for V2

IV. CONCLUSION

This paper described a preliminary investigation on the effect of annealing on the thermomechanical properties, hardness and microstructural of two variants of OPH alloys, differing in milling time, using a number ofdifferent tests. The results show that the heat treatment at elevated temperatures has a significant role on the mechanical properties as well as microstructure development of these alloys. The optimum annealing condition could be reported as 1100^{o}Cfor 20 hours which has the optimum effect on both UTS and elongation. Besides, it was found out that longer milling time (V2) has a negative influence on the mechanical properties which caused the late starting of recrystallization process. Base on that, the V2showed less sensitive to heat treatment even at higher temperature with longer holding time. On the other hand, the hardness value (HV10), shows a decrease to almost 50% of initial value while the heat treatment temperature increased from 1000^{o}C to 1200^{o}C. Also higher reduction was observed from the second step of temperature increasing (1100^{o}C to

1200°C) compare to the first step (1000°C to 1100°C). The microstructure observation showed that the recrystallization, which leads to grain growth, started after holding for 5 hours (V1) and 20 hours (V2) at 1100°C. Before this critical temperature, the structure was composed from very fine grains of about 100 nm. Over critical annealing temperature, a full recrystallized structure with coarse grains was obtained. Besides, the EDS analysis confirmed the presence of chromium and molybdenum in the biggest particles and tantalum was found in the smaller, which showed a positive behavior within the microstructures of OPHalloys.

ACKNOWLEDGMENT

This paper includes results created within the project 17-01641S Improvement of Properties and Complex Characterization of New Generation Fe-Al-O Based Oxide Precipitation Hardened Steels subsidized by the Czech Science Foundation from specific resources of the state budget of the Czech Republic for research anddevelopment.

REFERENCES

[1] O. Khalaj, H. Jirková, T. Janda, L. Kucerova, and J. Svoboda, "Improving the High Temperature Properties of a New Generation of Fe-Al-O Oxide Precipitation Hardened Steels," Materials and technology, vol. 53, no. 4, pp. 495-504,2019.

[2] R. L. J. J. o. N. M. Klueh, "Reduced-activation steels: Future development for improved creep strength," vol. 378, no. 2, pp. 159-166,2008.

[3] J. Svoboda et al., "Microstructure Evolution in ODS Alloys with a High-Volume Fraction of Nano Oxides," vol. 8, no. 12, p. 1079,2018.

[4] O. Khalaj, H. Jirková, B. Masek, P. Hassasroudsari, T. Studecky, and J. Svoboda, "Using thermomechanical treatments to improve the grain growth ofnew-generation ODS alloys," Materials and technology, vol. 52, no. 4, pp. 475-482, 2018.

[5] S. Ohtsuka, S. Ukai, M. Fujiwara, T. Kaito, T. J. J. o. p. Narita, and c. o. solids, "Nano-structure control in ODS martensitic steels by means of selecting titanium and oxygen contents," vol. 66, no. 2-4, pp. 571-575,2005.

[6] G. Merceron, R. Molins, and J. L. Strudel, "Oxidation behaviour and microstructural evolution of FeCrAl ODS alloys at high temperature," Materials at High Temperatures, vol. 17, no. 1, pp. 149-157, 2000/01/012000.

[7] B.Masek,O.Khalaj,H.Jirkova,J.Svoboda,andD.J.M.I.

[8] T. Bublikova, "Influence of thermomechanical treatment on the grain-growth behaviour of new Fe-Al based alloys with fine Al2O3 precipitates," vol. 51, no. 5, pp. 759-768, 2017.

[9] K. Murty and I. J. J. o. N. M. Charit, "Structural materials for Gen-IV nuclear reactors: Challenges and opportunities," vol. 383, no. 1-2, pp. 189-195,2008.

[10] O. Khalaj, B. Masek, H. Jirkova, A. Ronesova, and J. Svoboda, "Investigation on New Creep and Oxidation Resistant Materials," Materials and technology, vol. 49, no. 4, pp. 645–651,2015.

[11] G. Odette, M. Alinger, and B. J. A. R. M. R. Wirth, "Recent developments in irradiation-resistant steels," vol. 38, pp. 471-503,2008.

[12] J. Svoboda and P. J. A. M. Lukáš, "Creep deformation modelling of superalloy single crystals," vol. 48, no. 10, pp. 2519-2528,2000.

[13] O. Khalaj, H. Jirková, B. Mašek, and J. Svoboda, "Microstructure Evaluation of New ODS Alloys with Fe-Al Matrix and Al2O3 Particles," in Proceedings of the 2017 International Conference on Industrial Design Engineering, 2017, pp. 11-15:ACM.

[14] H. J. Xu, Z. Lu, D. M. Wang, Z. W. Zhang, Y. F. Han, andC.

[15] M. Liu, "Structure and composition of oxides in FeCrAl ODS alloy with Zr addition," (in English), Materials Science and Technology, vol. 33, no. 15, pp. 1790-1795, 2017.

[16] Z. Oksiuta, M. Lewandowska, P. Unifantowicz, N. Baluc,K.

[17] J. F. E. Kurzydlowski, and Design, "Influence of Y2O3 and Fe2Y additions on the formation of nano-scale oxide particles and the mechanical properties of an ODS RAF steel," vol. 86, no. 9-11, pp. 2417-2420, 2011.

[18] F.M.Shamsudin,S.Radiman,Y.Abdullah,andN.A.J.S.

[19] M. Hamid, "The effect of annealing to the hardness of high Y2O3-oxide dispersion strengthened (ODS) ferritic steels," vol. 47, no. 1, pp. 189-193, 2018.

★★★

CONFIGURATION OF THE TEG-THERMOSYPHON WITH SIMILAR HEATSINK AND STORAGE TANK LEVELS

[1]MD UMAR FARUK, [2]SMRUTIREKHA GIRI

[1]Department of Electrical and Electronics Engineering, NMIET, Bhubaneswar, 751019
[2]Department of Mechanical Engineering, AIET Bhubaneswar
E-mail: [1]Sunil.yadav@nmiet.ac.in

Abstract - One of the useful areas for power generation is employing thermoelectric generators that can convert the temperature difference to electrical energy. The efficiency of thermoelectric generators (TEGs) can be enhanced by providing the conditions for raising the temperature difference between the hot and cold poles. There are various ways to raise thisrequired temperature difference, among which the use of natural convection is of great importance due to its low initial costs. However, TEGs, which utilize natural convection, suffer from low efficiency. Furthermore, to the best of our knowledge, all thermosyphons have the disadvantage that the storage tank needsto be elevated slightly higher than the heat sink to increase the efficiency. In the present numerical study, the effect of using a thermal sink, made of a flat plate withcylindrical finson the thermal efficiency of the natural convection heat transfer is investigated and the optimum fin height is determined.

In addition, the effect of tank storage height on the heat transfer has been evaluated, and the optimum height is determined. A new design with a similar level of the storage tank and heat sink is introduced, which has a comparable efficiency with traditional designs.

Keywords - Thermoelectric Generator, Thermosyphon Storage Tank, Heatsink, Natural Convection, Cylindrical Fins

---

I. INTRODUCTION

The production of environmental pollutants caused by fossil fuel burning has promoted researchers to step up the energy efficiency of systems [1].Many researchers study ways to produce energy without using fossil fuels such as solar and photovoltaic cells, wind energy and thermoelectric generators (TEGs).Thermoelectric generators fall in a solid-state and semiconductor material category, which can convert temperature difference and thermal flux directly to electricity, known as the Seebeck effect method [2]. If a temperature difference is present atthe poles of a semiconductor, they will act like batteries, and if they are connected to a battery, there would be a temperature difference between them.The function of the TEG is similar to thermal engines, with the difference that their heat sink can be provided using the exhaust heat of cars or power plants or other wasted heats[3].

Compared to conventional heat engines, TEGs haveat least three advantages: i)they have no moving components and are completely silent, ii) their total thermal efficiency can be readily increased by increasing temperature difference iii) theyare small in size and are environmentally friendly components[4]. The main disadvantage of the TEGs is their low efficiency[5].Moreover,the storage tank needs to be placed higher than the heat sink, to provide the head needed for the circulation of the fluid. This is considered as a thermosyphon problem, which has remained unstudied [5, 6] andimposes a constrainton the component configuration of a TEG. This situation is similar to photovoltaic cells. Thebest and easiest way to improve the efficiency of TEGs is to provide a higher temperature difference between hot and cold poles. Moreover, if thermoelectric semiconductors are placed in such a way that they are electrically connected in series, but are thermally parallel, they provide a suitable voltage for amplifying the efficiency. The temperature difference between the poles and the height difference between the heat sink and storage tank are both drivers of water circulation in the system. As it will be shown later, the temperature difference could be sufficient for the circulation of the flow in the thermosyphon-heat sink, hence, the tank storage and heat sink can be placed at the samelevel.

The fluid in thermosyphon-heatsink structures can be circulated by active or passive means. The active method requires pumping power and is not a cost-effective way.In the passive method, fluid derives its momentum from the buoyancy and temperature difference. This methodis both reliable for fluid circulationand has almost no cost. Although the active method is not economical, it is still widely used in the TEGs. The active method is used for instance in solar cells[7]. Besides, the active method is also commonly utilized in other areas including cooling systems requiring forced convection for different purposes such as vehicles[8], marine [9], industrialand householdapplications.Achieving high efficiency for TEGs coupled with active forced air convection cooling systems requiresa high flow rate for the cooling fluid, which needs more energy [11].In some cases, thisenergy could bemore than the electricity produced by theTEG.

Use of natural water-flow convection method, as a coolant of a TEG, was first investigated by Champier et al. [10].An aluminum heat sink with fins, which well absorbs the heat generated by the hot air from the combustion of fossil fuels was used in their study. It is worth mentioning that the heat sink was located lower than the water storage tank. Ashwin et al. [11] investigated energy efficiency and performance of TEGs by air cooling through three different methods and compared the results. They found that the use of fins and bare plates through the heat pipes, allowed lower temperaturesto be reached at cold pole of the TEG. As reported by Elghool et al. [12], under identical conditions, the natural convection heat transfer coefficient of a liquid coolant is much higher than that of a gaseous fluid for cooling TEGs.Deasy et al. [5],both experimentally and numericallydesigned a passive pure water thermosyphon system for cooling TEGs.They observed that the passive method could provide appropriate and effective cooling. Ahmed et al. [13], experimentally investigated the performance of TEGs by three different passive cooling liquids. In their study, natural convection by air, water, and vapor were studied. They used rectangular fins that had been parallel with the coolant flow for better heat dissipation from the TEG. They found that vapor phase change aided by fins showed the best performance compared to othertechniques.

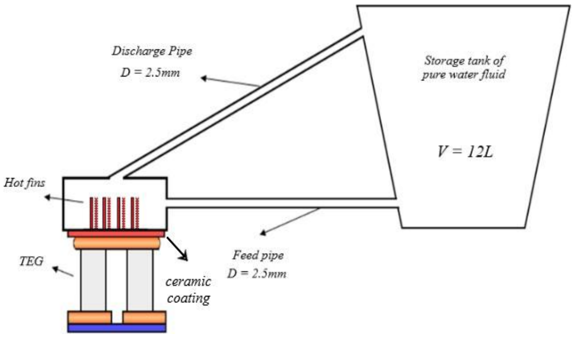

Fig. 1. Schematic of the TEG-thermosyphon geometry.

Purpose of this study

Anobjective in this study, is to find the optimum height of the storage tank relative to the lower surface of the heat sink and to address this height difference problem, which has not been examined for the TEGs before. Another aim, is to examine the impact of different fin heights, with the same circular cross-section, on the performance. In addition, an appropriate fin height for the presented configuration is determined.

The remaining of the paper is organized as follows. In section 2, problem definition is given. Numerical method is presented in section 3. Results are discussed in section 4, followed by the concluding remarks in section5.

II. PROBLEMDEFINITION

2.1. Schematic and boundary conditions

A schematic of thecurrent thermosyphon geometry is shown in Fig.1. This thermosyphon benefits from a passive cost-effective approach. In this approach, the fluid circulates between the thermosyphon and the heat sink using the buoyancy effect. The storage tank in the thermosyphon has a volume of 12 liters, filled with pure water.

The heatsink is shown in blueat the bottom leftin Fig.1. A constantheat flux is applied to the ceramic coated section in the hot part of the thermoelectric generator,seeFig.1. Hence, the heat flux is applied at the hot surface of the thermosyphon-TEG system,referred to as the heatsink. The heatsink has 32 pin fins mounted separately. The fins havea height of 9.625 mm and a hydraulic diameter of 1.25 mm.To investigate the influence of the fin height,valuesfrom 2.5 mm to 14.5 mm with 2.5 mm intervals are used.A schematic of the height changes is shown in Fig.2.

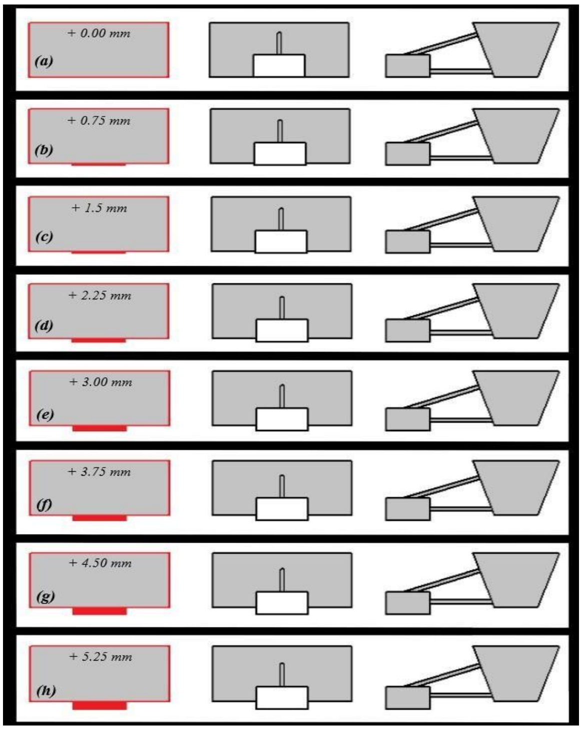

Fig.2. Schematic view of the extent of the storage tank elevation (a) 0.00 mm, (b) 0.75 mm, (c) 1.50 mm, (d) 2.25 mm, (e) 3.00 mm, (f) 3.75 mm, (g) 4.50 mm and (h) 5.25 mm.

The heat flux, generated by the fins, enters the fluid in the thermosyphon-heatsink system. A wall is considered above the surface of the storage tank. To consider the fluid evaporation at this surface, an approach similar to the oneused by Deasy et al. [5] is employed, wherea constant heat transfer coefficient, 80 W / m^2 K in this case, is assumed. On this basis, the evaporation heat at the surface of a given wall in contact with air, $Q_{evaporation}$ with no shear stressis assumed.The lateral walls of thestorage tank are isothermal with the ambient temperature. The feed and thermosyphon discharge pipes, as shown in Fig.1., have a diameter ofD=2.5 mm. The TEGis located at the bottom of the heat sink, whose pole is connected to the heat sink by a ceramic coated part.

The semiconductors presented in the TEGs of this research, are chosen as Bi_2Te_3. All components of the thermosyphon-heatsink are made of alumina. The selection of this alloy is due to the suitable heat transfer of aluminum within the operating temperature range.

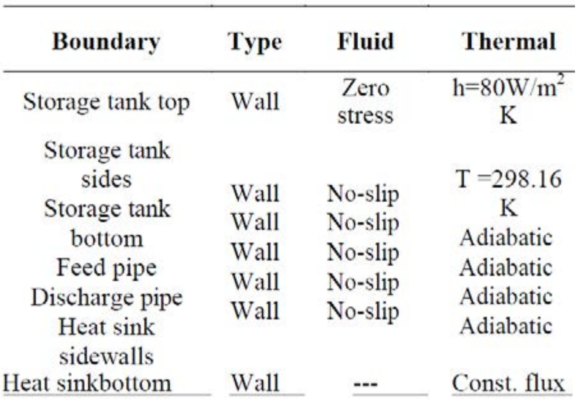

Boundary	Type	Fluid	Thermal
Storage tank top	Wall	Zero stress	h=80W/m^2 K
Storage tank sides	Wall	No-slip	T =298.16 K
Storage tank bottom	Wall	No-slip	Adiabatic
Feed pipe	Wall	No-slip	Adiabatic
Discharge pipe	Wall	No-slip	Adiabatic
Heat sink sidewalls	Wall	No-slip	Adiabatic
Heat sinkbottom	Wall	---	Const. flux

Table 1: Boundary condition description

The boundary conditions are given in Table 1. It is worth noting that adiabatic conditions are used for both heatsink sides as well as the feed and discharge pipes, which is identical to those found in prevalent thermosyphon-heatsink systems. The bottom area of the heatsink is 25mm×30mm.The lateral part of the hot pole of the TEG iskept at 70°C.It is worth noting that the Bi_2Te_3 alloy, used in the present TEG, can endure temperatures up to 300°C [5]. The cooling system efficiency, based on the heat transfer to the fluid by natural convection, of the TEG was evaluatedusing different fin heights, with a fixed finarrangement. Auniform flux with a temperature of 70 °C is applied to the lower part of the heat sink.

The expansion coefficient $\beta = 0.00044\ (1/K)$ is used for water in the simulations, which is based on the average ambient temperature (26 °C) and hot part of the heat sink temperature (70 °C) . Other water properties are considered to betemperature dependent.

III. NUMERICALMETHOD

Although the problem has a transient-state behavior, the results are similar to a steady simulation. This has also been verified previously [5]. Hence, simulations are carried out as steadystate.

3.1. Governing equations

The significant temperature differencesin the TEG,produces buoyancy forces that helps the fluid to circulatein the thermosyphon system.The fluid flow inside the thermosyphon is single-phase, laminar, incompressible and Newtonian.The density, thermal conductivity, viscosity and specific heat vary with temperature.

The continuity, momentum and energy equations using the Boussinesq approximation are as follows[14]:

$$\nabla.(\rho V) = 0 \quad (1)$$

$$\nabla.(\rho VV) = -\nabla P + \nabla.(\mu \nabla V) \quad (2)$$

$$\nabla.(\rho V C_p T) = -\nabla.PV + \nabla.\{k \nabla T\} \quad (3)$$

Where ρ is the fluid density,V is the velocity vector, $P$is the pressure, $\mu$is the dynamic viscosity, $C_p$is the specific heat at constant pressure, $K$is the thermal conductivity and $T$is the temperature.

3.2 Flow parameters

Due to the small Grashof number, the flow is laminar

$$Gr = \frac{g\beta\left(T_{ws} - T_{feed}\right)L^3}{\nu^2} \approx 1-3\times10^3 \quad (4)$$

Moreover, Newton’s cooling law is used to calculate the average heat transfer coefficient for the heat sink as

$$h_{ave} = \frac{\square Q}{A_{ws}\left(T_{ws} - T_{feed}\right)} \quad (5)$$

where, Q is the heat flux from the TEG, A_{ws} isthe wetted surface area of the heat sink, T_{feed} is the temperature of the water in the feed pipe and $T_{ws}$is the average temperature inthe wetted regionof the heatsink.

3.3 Numerical scheme

The finite volume method is used for the discretization of equations (1-3). The numerical code used in this study, has a second-order accuracy in time and space with the QUICK scheme used for the convective terms.

3.4 Validation of the numerical method and Grid independence examination

To assess the validity of the numerical method for the current problem, simulations are carried out for the geometryof the experiment carried out in [5].The experimental data is for constant heat fluxes of 60, 120, and 180 W, thermal convection heat transfer with h=80 W/m^2 K at top of the storage tank, and adiabatic conditions for other boundaries. Comparison of the results with the experimental data, given in Table 2, shows a reasonable agreement.

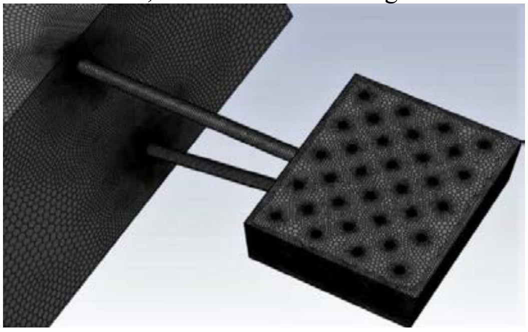

Fig.3. Bottom view of the selected fins polyhedral mesh with a polygonal mesh for the circular fin shape geometry.

Heat flux (W)	Experimental [5] R_{th}(W/K)	Numerical R_{th}(W/K)	Error (%)
60	0.099	0.092	7.0
120	0.080	0.074	7.5
180	0.073	0.069	5.5

Table 2: Comparison between experimental [5] and present numerical results for the thermal resistance of the heat sink

In this work, the effect of height difference between the heat sink and storage tank on the heat transfer performance is examined. Hence, in comparison with the experiment in [5], the heat sink is replaced with a new configuration. Furthermore, circular fins are used in a staggered configuration to increase the heat transfer and reduce the thermal resistance.A sample view of the mesh is given in Fig. 3, showing the polyhedral meshused.

Name	Elements	Mesh size (×10^{-6} mm)	Discharge Temperature (°C)	Error (%)
A	2314158	7.6	52.65	0.84
B	2858272	5.1	52.34	0.59
C	3402687	3.26	52.21	0.0

Table 3: Discharge temperature and error for different grids

To examine the mesh dependence of the simulation results, three different meshes are used, see Table 3.Simulations are carried out at the operating thermal heat fluxof 180 W. The differences in discharge temperature predictions for grids A, B and C are less than 1%.

IV. RESULTS ANDDISCUSSION

4.1 Velocity and temperature contours

Velocity contour plot for a lateral cross section is given in Fig.4. Figure shows a maximum velocity of 0.022m/s. Water flows from the storage tank to the heat sink.

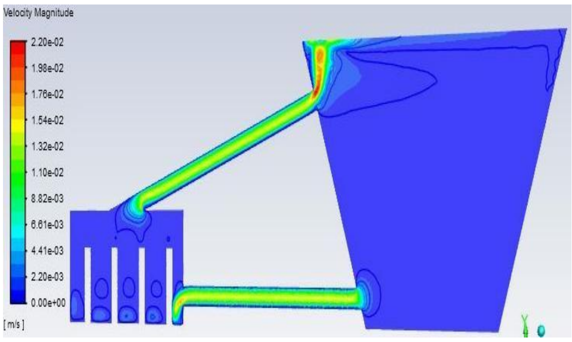

Fig.4. Velocity magnitude contours in a lateral cross section.

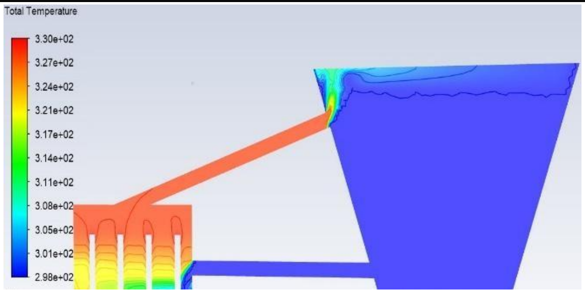

Fig.5. Temperature contours in a lateral cross section.

In Fig.5, a contour plot of the temperature is given. Figure shows that cold water enters the heat sink. After cooling the heat sink, water at a higher temperature enters the storage tank. This process is due to the buoyancy forces and natural convection mechanism. The hot water flowing out from the discharge pipe entersthestorage tank, where its temperature drops to almost the ambient condition. This process goes until a steady-state is reached.

4.2 Effect of the finheight

Effect of the fin height on the average convection heat transfer coefficient for the coolant is shown in Fig. 6. The efficiency increases monotonically with the fin height. An economically optimum fin height of 9.5 mm is indicated in thefigure.

4.3 Effect of the storage tankelevation

In Fig.7, variation of the average heat transfer coefficient with the storage tank elevation is given. Figure shows that the average heat transfer coefficient drops with increasing tank storage elevation. A minimum value occurs for an elevation of about 5.2 mm, which is the optimum value, where thermosyphon-heat sink system has its maximum efficiency.

Thermal resistance variation with respect to the storage tank elevation, see Fig.8, shows almost the same behavior as the average heat transfer coefficient in Fig.7.

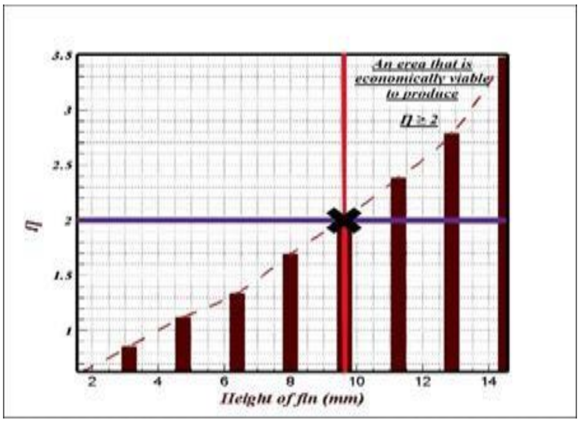

Fig.6. Effect of the fin height on the average heat transfer coefficient.

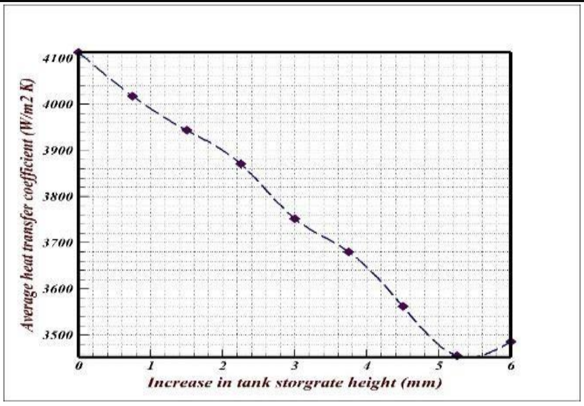

Fig.7. Effect of storage tank elevation on the on the average heat transfer coefficient.

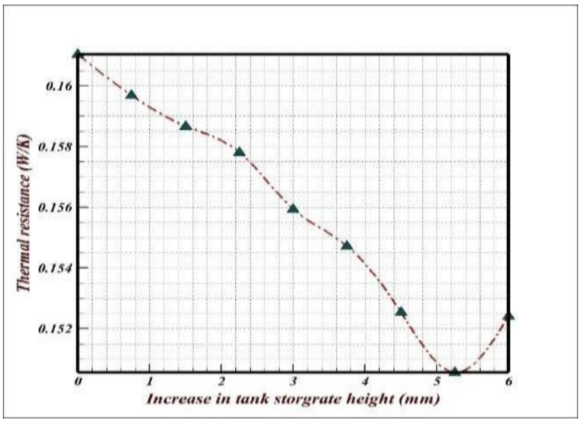

Fig.8. Effect of storage tank elevation on the thermal resistance.

Thermal resistance variation with respect to the storage tank elevation, see Fig.8, shows almost the same behavior as the average heat transfer coefficient in Fig.7. Similarly, a minimum value occurs at about 5.2 mm tank elevation.

In Fig.9. the efficiency is given with respect to the storage tank elevation. The efficiency increases and reaches a maximum at about 5.2 mm storage tank elevation. A further increase in elevation, decreases the efficiency.

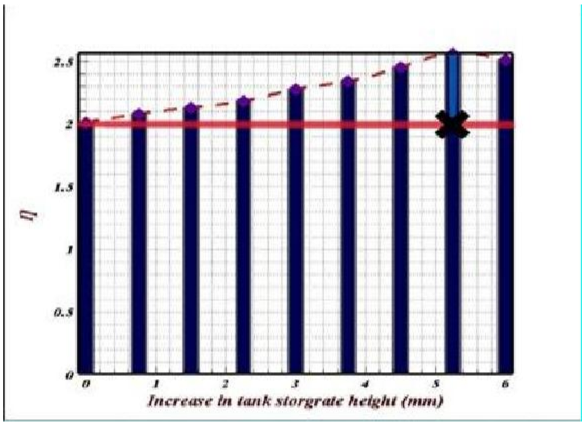

Fig.9. Effect of the storage tank elevation on the efficiency.

As can be observed, the increase inefficiency due to the change in the storage tank elevation, ismuch less than the efficiency changes due to the increase in the fin height in the thermosyphon-heat sink. This suggests that the change in elevation has a rather small influence on the entire system efficiency.Hence, the storage tank and heat sink can be place at almost the same level and maintain an optimum efficiency. This new configuration is more suitable, optimal, less bulky and more efficient, compared to other thermosyphon configuration[5,6].

V. CONCLUDING REMARKS

In this study, the effect of storage tank level on the heat transfer performance of thermosyphon-TEGheat sink was numerically investigated. It was found that the optimum efficiency for the thermosyphon-TEG heat sink, considered in this study, was reached for a storage tank elevation of 5.2 mm.A new design, where the storage tank and heat sink are placed at almost the same level was proposed and numerically tested. The new design would allow for a better configuration of the TEG components.

Furthermore, to increase the heat transfer efficiency of the passive cooling system, a staggered configuration of circular fins was employed in the cooling system and its efficiency was numerically tested.

REFERENCE

[1] N. Adroja-S. B. Mehta, and P. Shah, “Review of thermoelectricity to improve energy quality,” Int. J. Emerg. Technol. Innov. Res, vol. 2, pp. 847-850,2015.

[2] C. Goupil, Continuum theory and modeling of thermoelectric elements: John Wiley & Sons,2015.

[3] R. L. Cataldo, and G. L. Bennett, "US space radioisotope power systems and applications: past, present and future," Radioisotopes-Applications in Physical Sciences: IntechOpen,2011.

[4] M. Sajid-I. Hassan, and A. Rahman, “An overview of cooling of thermoelectric devices,” Renewable and Sustainable Energy Reviews, vol. 78, pp. 15-22,2017.

[5] M. Deasy-N. Baudin-S. O'Shaughnessy, and A. Robinson, “Simulation-driven design of a passive liquid coolingsystem for a thermoelectric generator,” Applied energy, vol. 205, pp. 499-510, 2017.

[6] M. Deasy-S. O'Shaughnessy-L. Archer, and A. Robinson, “Electricity generation from a biomass cookstove with MPPT power management and passive liquid cooling,” Energy for sustainable development, vol. 43, pp. 162-172,2018.

[7] R. Singh-S. Tundee, and A. Akbarzadeh, “Electric power generation from solar pond using combined thermosyphon and thermoelectric modules,” Solar Energy, vol. 85, no. 2, pp. 371-378,2011.

[8] S. Yu-Q. Du-H. Diao-G. Shu, and K. Jiao, “Start-up modes of thermoelectric generator based on vehicle exhaust waste heat recovery,” Applied energy, vol. 138, pp. 276-290,2015.

[9] N. Kristiansen-G. Snyder-H. Nielsen, and L. Rosendahl, “Waste heat recovery from a marine waste incinerator using a thermoelectric generator,” Journal of electronic materials, vol. 41, no. 6, pp. 1024-1029,2012.

[10] D. Champier-J.-P. Bédécarrats-T. Kousksou-M. Rivaletto-F. Strub, and P. Pignolet, “Study of a TE (thermoelectric) generator incorporated in a multifunction wood stove,” Energy, vol. 36, no. 3, pp. 1518-1526,2011.

[11] Date-A. Date-C. Dixon-R. Singh, and A. Akbarzadeh, “Theoretical and experimental estimation of limiting input

heat flux for thermoelectric power generators with passive cooling," Solar Energy, vol. 111, pp. 201-217,2015.

[12] Elghool-F. Basrawi-T. K. Ibrahim-K. Habib-H.Ibrahim, and D. M. N. D. Idris, "A review on heat sink for thermo-electric power generation: Classifications and parameters affecting performance," Energy conversion and management, vol. 134, pp. 260-277, 2017.

[13] S. Ahmed-M. Mousa, and A. Hegazi, "Performance analysis of a passively cooled thermoelectric generator," Energy conversion and management, vol. 173, pp. 399-411,2018.

[14] Kleinstreuer, Engineering fluid dynamics: an interdisciplinary systems approach: Cambridge University Press,1997.

★★★

SUSTAINABILITY AND INNOVATION DYNAMICS IN MANUFACTURING: A STRUCTURAL EQUATION MODELLING APPROACH

[1]MRUTYUNJAY SENAPATI, [2]BIMAL SARANGI, [3]CHANDRABHANU MALLA

[1]Department of Electrical and Electronics Engineering, NMIET, Bhubaneswar, 751019
[2]Department of Mechanical Engineering, REC Bhubaneswar
[3]Department of Mechanical Engineering, AIET Bhubaneswar
E-mail: prakhar.kharwar@nmiet.ac.in

Abstract - Much has been said in research literature about how innovation contributes to sustainability of business both in service and manufacturing contexts. Nevertheless, not many of those researches consider the influence of these two aspects on organizational performance. To address this gap, this research focusses on the role played by innovation in promoting organizational performance in manufacturing industries with sustainability as the mediating factor. The research is based on positivist paradigm and has adopted empirical approach for testing nine hypotheses using structural modelling technique using a sample size of 211 based on convenience sampling. The respondents for the questionnaire survey were managers from manufacturing industries. The hypothesis testing has indicated that while both product and process innovation contribute to social, economic and environmental sustainability, only economic sustainability contributes to the organizational performance. Based on the results, implication have been drawn to the managers of manufacturing industries to enhance their organizational performance.

Keywords - Manufacturing Performance, Product Innovation, Process Innovation, Social Sustainability, Economic Sustainability, Environmental Sustainability, Organizational Performance

I. INTRODUCTION

One of the prime areas of research in manufacturing management today is sustainability as manufacturing is associated with environmental, social, and economic aspects. While manufacturing is essential to the economic growth of any country, it is also necessary that the process does not affect the environment adversely, alter the valued social norms and disturb the wellbeing of the members of the society. In an attempt to meet these challenges, the manufacturing management philosophy has shifted focus from production management, to flexible manufacturing and now to lean, clean and green manufacturing (Herrmann et al., 2014). It also makes manufacturing multi-disciplinary subject as it demands creativity in thinking and imagination, understanding of scientific phenomena, knowledge of material science, abilities to create value through optimized processes and latest technologies, imagination about tangible and intangible products, and ideas about the possible services which can be associated with manufactured products (Abdullahi& Abdullah, 2015; Tonelli, Evans &Taticchi,2013).

The challenges to be faced by the manufacturing sector in the years to come are umpteen. To name a few, it is estimated that by the year 2050, manufacturing industries are expected to double their output using only half of current resources by generating only 20% of current Carbon Dioxide (Tonelli, Evans &Taticchi, 2013). The mandate of Kyoto Protocol is a legal commitment from the manufacturers to reduce greenhouse gases emission at least 5% each year (Wiktorsson, Bellgran, & Jackson, 2008). Looming labour shortage would be a challenge as Baby Boomer generation is now on the verge of retirement and they take their vast experience in manufacturing with them and it is estimated that by the year 2025 there would be a shortage of 3.5 million jobs in the field of manufacturing (Deloitte, 2017). So, filling the manufacturing skill gap would be a challenge. Meeting stiff timelines of product delivery would pose a challenge to sustainability of the manufacturing industry in the years to come (Xu, David & Kim, 2018). Replacing the traditional value proposition by sustainable value proposition would pose another challenge to manufacturing (Tonelli et al., 2013). In addition to all these challenges to be faced by the sustainable manufacturing: minimization of resource consumption in all stages of manufacturing; lesser material usage in production, package, distribution and recovery; extension of product life-cycle; improving the perceptions of the customers about the product on a continual basis; extension of modular designs; usage of highly standardized interfaces to facilitate assembly; increased use of smart-materials; and increased use of biodegradable materials would be the challenges to be faced by the sustainable manufacturing in the years to come.

The solution to all these aforementioned challenges would be to constantly innovate and find newer ways of doing things which would contribute to all the dimensions of sustainability. In the manufacturing scenario there are two distinct innovations, namely product innovation and process innovation both of which have been tried very widely. Innovation in general focuses on newer methods, practices, processes and technology in manufacturing. Product innovation specifically refers to the upgradation of manpower utilization, material saving, machine upgradation and utilization and method refinements to bring about newer products (Romero et al., 2017). Product innovation also deals with re-engineering and developing an organizational culture which is sensitive to the issues related to lean and green manufacturing (Jaw, Chen & Chen, 2012). On the other hand, process innovation deals with the development of newer technical principles and production modes so as to minimize energy consumption and manufacture goods and services in a sustainable manner (Wang et al., 2017).

II. LITERATURE REVIEW

Research in manufacturing innovation and sustainability have taken many different forms. The research focus in these researches have been mainly based on the context in which the research has been undertaken. While one group of researchers have focussed on manufacturing efficiency enhancement, in contrary to it another group has focussed on environmental protection. While one group of researchers have focussed on innovative ways of manufacturing, in contrary to it another group has focussed on sustainability of such newer ways of manufacturing. A brief review of literature in the context of research constructs of specific interest to this research has been given in the subsequent paragraphs.

Wang et al., (2017) have designed a hierarchy evaluation index system for process innovation using fuzzy linguistic computing in micro-turbine machining. The model helps in process innovation through the evaluation of the existing knowledge related to the problem solving in the manufacturing scenario with sustainability in focus. The computing tool has successfully identified the core value of knowledge in manufacturing innovations and successfully met the need of rapid evaluation and selection of relevant knowledge from high volume multiple knowledge available in innovation environments.

Jaw, Chen & Chen (2012) through their exploratory study provided a cultural dimension for product innovation in creative industries. The focus was on product innovation and found that it is not technological innovations alone which provide sustainability, but the three interrelated management practices: organizational development, customer interface and optional technology application have a role to play in promoting sustainability. The research has provided a comprehensive framework with a wider perspective on innovation leading to sustainability.

Protogerou, Kontolaimou & Caloghirou (2017) have undertaken a comparative study of production and process innovation in both creative and non-creative industries. The findings through the empirical investigation was that Creative industries outperform the Non-creative industries in product innovation; however, the latter shows better performance in process innovation. The key finding in this study is that human capital of founders have a major role to play in promoting innovation leading to the sustainability of business.

Padilha & Gomes (2016) focused on the cultural influence on both production and process innovation leading to sustainability of manufacturing. The empirical study was based on 287 respondents from textile industry chosen based on simple random sampling. Analysis was based on structural equation modelling and results indicated a positive correlation between culture and both production and process innovation. Further, innovation culture was found to have a greater influence on process innovation than on Product innovation. It was also revealed that both production and process innovation were independent of the size of the manufacturingorganization.

Soni, Lilien& Wilson (1993) were among the pioneers who adopted structural equation modelling to study the innovation dynamics. The approach was to study the influence of innovation on firm performance leading to sustainability. Sample was drawn from 40 chemical industries. The results indicated that on the overall basis innovation drives firms' performance; however, intermediate levels of market concentration promote performance. Smaller firms as well as less diversified firms indicated higher levels of innovation leading towardssustainability.

Tomoyose, Santos &Faria (2017) used the PINTEC 2014 innovation survey data to study the influence of open innovation on sales of the new products using SEM. As anticipated open innovation did have an influence on sales of the new products; however, there were mediating factors: product quality and expansion of new portfolios, involved in the enhancement of sales particularly in domestic environment. It was found that among 5,107 firms manufacturing clothing and accessories which had adopted open innovation about 78% of the firms had shown higher performance in sales of their products.

Çakir (2017) conducted a comparative study between the generation of new knowledge and industrial innovation activities on their relative impact on innovation outcomes in the chosen manufacturing industries in European Union. The results indicated that the Networked Readiness Indicator (NRI) which included several factors including – business and non-business sector expenditures, number of doctorates, government expenditure on education, number of scientific publication etc., was the major predictors of innovation outcome. Innovation activities in the manufacturing firms also has a direct influence on innovation outcomes and also larger impact on the innovation outcome than that of the generation of new knowledge factor.

Behnam &Cagliano (2017) conducted an extensive research using the data collected from 860 manufacturing plants in 22 countries using self-administered questionnaire. Their study revealed that innovation and sustainability were positively correlated. The study was based on the three dimensions of innovation and sustainability: priority, action programme and performance. The results indicated that innovation and sustainability were related significantly at all the three dimensional levels. Further, it was also observed that innovation action programmes and sustainability action programs, and also, innovation performance and sustainability performance relationships were bidirectional which means the higher the innovation action programmes the better would be sustainability action programs and the higher the innovation performance the better would be the sustainability performance.

Cherrafi et al., (2018) studied the moderating influence of process innovation between lean management and green practices on green supply chain performance using the SEM approach. The sample of 374 was collected from 11 manufacturing industries spread across 13 countries. The results indicated that process innovation had a statistically significant moderating influence on individual as well as collective basis between the two endogenous variables: lean management and green practices and the exogenous variable supply chain performance.

Hami, Muhamad &Ebrahim (2015) used the survey data collected from 150 Malaysian manufacturers to empirically investigate the relationships among sustainable manufacturing practice (internal and external), innovation performance (product, process, organizational and marketing), and economic sustainability using the SEM approach. Results indicated that external sustainable manufacturing practice and economic sustainability relationship was not significant on the overall basis; however, product and process innovations had significant influence on economic sustainability.

Research literature in the field of sustainability are diversified into various domains and there is evidence that innovation has been linked to sustainability in the context of manufacturing. It can be noted that both innovation and sustainability are multi-dimensional constructs. While there are several dimensions in use primarily in the context of manufacturing Product innovation and process innovation have emerged out to be the dimensions which have been researched into depth. Similarly, in case of sustainability it is economic sustainability, social sustainability and environmental sustainability which are widely being considered. In the aforementioned articles, while some have developed models to link innovation to sustainability (e.g., Wang et al., 2017). Another group of researchers has undertaken exploratory research on specific dimension of innovation such as Product innovation and linked it to sustainability (e.g., Jaw et al., 2012). There are also research studies which have compared the two dimension of innovation in the context of manufacturing (e.g., Protogerou et al., 2017). Researchers have also explored the antecedents of innovation and it has been identified that cultural aspects also have a role to play on the effectiveness of the dimensions of innovation (e.g., Padilha& Gomes, 2016). While both qualitative and quantitative approaches have been adopted in the research on sustainability, Structural Equation Modelling (SEM) is becoming popular and researchers have made attempts to test the relationships between the dimension of innovation and sustainability using this tool (e.g., Çakir, 2017; Soni et al., 1993; Tomoyose et al., 2017). However, there is a need to explore further on the organizational performance with innovation and sustainability as its determinants. This is because, while sustainability in terms of its three dimensions is necessary and research shows that dimensions of innovation have the ability to meet these sustainability requirements, it is the organizational performance which the manufacturing industries look forward to achieve. Unless the organizational performance is ensured, the former two would only be the statutory requirements to the manufacturing industries. Thus, in this research an attempt is made to fill this research gap by investigating the interrelationships between the dimensions of innovation, sustainability and organizational performance.

III. OBJECTIVES

The main objective of this research is to study if innovation can drive organizational performance under the mediating effect of social, economic and environmental sustainability. Specifically, following are the target objectives of this research:

- Explore the linkages between the dimensions of innovation, sustainability and organizational performance.
- Determine the significance of relationships between the above referreddimensions.
- Make suggestions to the managers of manufacturing industries to enhance organizational performance.

IV. RESEARCH METHODOLOGY

4.1 Conceptual Model and Hypotheses

The conceptual model of the research has been developed based on the research literature which included both qualitative and quantitative studies which have made attempts to link the various dimensions of the research constructs.

Following are some of the prominent studies which have related the dimensions of innovation and sustainability in both service and manufacturing industries.

Innovation and Social Sustainability

Buchegger & Ornetzeder (2000) on studying the 230 project initiatives in Ausria, Germany and Switzerland found that innovation can contribute to the social sustainability. Piccarozzi (2017) found that start-ups in Italy have contributed to social sustainability through Social Impact Assessment and the innovative measures to contribute towards sustainability. It was observed that among the 61 start-ups which were considered for the analysis 89% could contribute towards social sustainability through innovation. Several authors including Dawson & Daniel (2010) and Morais & Silvestre (2018) have associated innovation and social sustainability as innovation often considers the community goals as one of the objectives to be achieved through it. However, literature has no much of evidence on the empirical investigation of the impact of innovation on social sustainability at its dimensional level and the following hypotheses have been formulated.

H1: Product innovation has positive significant relationship with social sustainability in manufacturing industries.
H2: Process innovation has positive significant relationship with social sustainability in manufacturing industries.

Innovation and Economic Sustainability

Brettel & Cleven (2011) theorize that innovations come through external knowledge from all the stake holders of business and it has the potential to contribute to the economic sustainability of business. Chesbrough (2003) suggested that diverse range of collaboration partners in open innovation can contribute to the economic sustainability. Rauter et al., (2017) have proved that open innovation had a positive significant correlation with economic sustainability in manufacturing context. The manufacturing industries considered included the research automation, industrial electronics, construction, automobile, food, information technology, and timber. The recommendation of the research was that collaborating with customers, universities, and other stakeholders in innovation initiatives would enhance the economic sustainability to a considerable extent. Matthies et al., (2017) have established a strong positive linkage between innovation and economic sustainability in the context of both product and service organizations. Despite these studies there is no evidence on the investigation of the influence of innovation at its dimensional level on economic sustainability in manufacturing sector. Thus, following hypotheses have been formulated in the context of manufacturing companies.

H3: Product innovation has positive significant relationship with economic sustainability in manufacturingindustries.
H4: Process innovation has positive significant relationship with economic sustainability in manufacturingindustries.

Innovation and Environmental Sustainability

Joyce & Paquin (2016) have found that as innovation demands the bringing of the entire supply chain in manufacturing and by and large the society together towards a common goal it has the potential to contribute to environmental sustainability in business. Srivastava (2007) claims that innovations in manufacturing have green innovation as a component of their innovation process and thus it can contribute to environmental sustainability. Silvestre &Ţîrcă (2017) have proposed a detailed typology on how innovation can lead to environmental sustainability both in the service as well as manufacturing contexts. Kishawy, Hegab&Saad (2018) claim that all three types of innovation (product, process, and system) have the potential to contribute to the environmental sustainability because all the three have their bearing on one way or the other on environment and innovative efforts do consider the environmental impact during the design. Despite these studies there is little evidence on the study of the impact of innovation at the dimensional level on environmental sustainability and hence the following hypotheses have been formulated.
H5: Product innovation has positive significant relationship with environmental sustainability in manufacturing industries.
H6: Process innovation has positive significant relationship with environmental sustainability in manufacturing industries.

Sustainability and Organizational Performance

Akram et al., (2018) opine that knowledge and resource based views promote innovating abilities and sustainability of business which can provide a boost to the organizational performance. Maletič et al., (2014) have provided empirical evidence to the point that sustainability oriented innovative practices can lead to the organizational performance. Côté, Booth & Louis (2006) have found that process innovation can result in reduced consumption of energy and materials thus contributing to sustainability, which can lead to environmental sustainability. Rennings et al., (2006) have identified that Product innovation can enhance rework, recycle and remanufacturing thus contributing to sustainability which can lead to the environmental protection. There are many such studied which have established the path of linkage between innovation, sustainability and organizationalperformance; however, there is no empirical evidence for the relationships at the dimensional level and hence the following hypotheses have been formulated.
H7: Social sustainability has positive significant relationship with organizational performance in manufacturing industries.
H8: Economic sustainability has positive significant relationship with organizational performance in manufacturing industries.
H9: Environmental sustainability has positive

significant relationship with organizational performance in manufacturing industries.

Considering the earlier studies, it is evident that both product and process innovation have bearing on the three types of sustainability which in turn has the potential to drive organizational performance. Drawing from this the following hypothetical (Figure 1) model has been developed in this research.

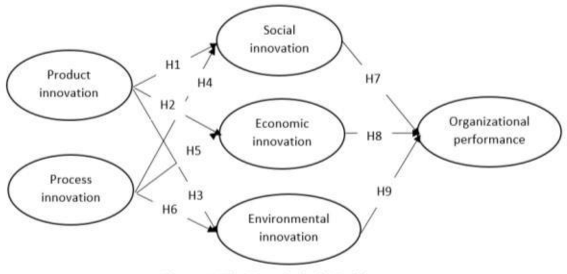

Figure 1: The Hypothetical Model

The Metric Development

4.2The Metric Development

As most of the dimensions used in this research are very well established dimensions with readily available scales of measurement the items have been chosen from those scales. But some of these scales were used in many different contexts other than manufacturing and in different geographic location and time. So, these scales have been subjected to confirmatory factor analysis to confirm their representativeness in the present context.

Dimension	Contributing Authors	Description
1. Product innovation	Arkolakis et al., (2018), Breznitz &Cowhey (2012), Löfgren, &Williams (2016), Lundvall (2002), Tohidi& Jabbari(2012), Wejnert(2002)	Re-engineering the entire system and organisational culture so as to bring out the new products/services which are sustainable.
2. Process innovation	Amit, Zott (2012); Andraszewicz et al., (2015); Belvedere et al.,(2013), Länsisalmi et al.,(2006), Snihur&Wiklund (2017)	It is the introduction of a new technology/method for manufacturing to gain competitive advantageand aim towards sustainability.
3. Social sustainability	Bacon at al., (2012); Colantonio & Dixon (2011); Dempsey at el., (2011); Dillard et al., (2011); Eizenberg &Jabareen (2017); Griessler & Littig (2015); Woodcraft (2015);	Is a state in which formal and informal processes, systems, policies, structures, and relationships are in alignment with the needs of current and future generations.
4. Economic sustainability	Armeanu et al., (2018); Bockermann et al., (2005); Hanushek &Woessmann (2008); Spangenberg (2008); Tomislav (2018).	It is the practices that provide long- term economic growth without adversely affecting social, environmental, and cultural aspects ofthe community.
5. Environmental sustainability	Abatenh et al., (2018); Abhilash et al., (2016); Arora et al., (2018); Di Vaio, &Varriale (2018); Giddings et at;, (2018); Puig et al., (2015)	It is the ability to meet the needs of the present without compromising the ability of future generations to meet their own needs without adversely affecting earth's ecosystem.
6. Organizational Performance	Kutucuoglu et al. (2001) and Wordsworth (2001), Jung &Hong (2008), (Salaheldin, 2009), Kumar, Garg and Garg 2009), Chiang Han, & Chuang (2012).	It is the indicators of performance of an organization can be broadly categorized in to Operational performance, Financial performance and Non- financial performance factors

The initial questionnaire had 30 items of measurement and a pilot study was undertaken using a sample size of 30 to test the questionnaire and make sure the items did not have jargons of management and was easy to understand in the context of manufacturing company. The data was subjected to confirmatory factor analysis to test the reliability and validity and was reduced to 18 simple questions which were easy to answer and a quick response can be ensured without losing its ability to measure what the metric was intended tomeasure.

4.3 Research design

This is basically an empirical study with quantitative approach based on convenience sampling. The research is cross-sectional type of design and the method of data collection is through self-administered questionnaire. This research design has been chosen specifically as this research aims to explore the interrelationships of the dimensions of innovation, sustainability and organizational performance. The exploration is facilitated through the testing of the hypotheses which have been developed based on the existing literature in the area of study. The analysis of the data is through SEM which essentially has: Measurement Model and Structural mode. While the former provides the reliability of the data and validates the metric the latter tests the hypotheses using the partial least square technique. SEM has been very successful in addressing the issue of multi-collinearity that exists between the variables of study and hence been used in thisresearch.

4.4 Sample Design

The data used in this research is from randomly chosen manufacturing companies which are medium scale industries located in Bangalore the capital of Karnataka State in India. There are 1618 registered medium scale industries with in Bangalore which include agro based, soda based, cotton textile, jute based, ready-made garments, wooden furniture, paper products, chemical products, rubber and plastic products, minerals, steel fabrication and electrical machineries. From these industries according to the standard sample size formula (Igwenagu, 2016), 169 industries were randomly chosen and the questionnaire were distributed through the HR Managers to the manufacturing managers. In the first round a total of 400 questionnaires were served and 124 filled questionnaires were received. But as SEM demands a minimum sample of 180 which is based on the principle of ten times the number of manifest variables in research (Kline, 2001). So in the second round again 200 questionnaires were served and after repeated visits to these industries a sample size of 227 could be achieved out of which 211 were selected and the rest were discarded as they were either incomplete orerroneous.

V. RESULTS AND ANALYSIS

5.1 Measurement Model

The Cronbach's alpha coefficient (Table 2) in this research varies from 0.7 to 0.8, and composite reliability estimate also ranges from 0.6 to 0.9, both indicating a moderate to high level of internal consistency (cut off value of 0.6 for both these measures) (Ahmad, Zulkurnain & Khairushalimi 2016). The convergent validity is assessed through factor loading and in the present research they are above 0.6 which indicate a strong effect of the factor on the variable of study (cut off 0.6 Ahmad et al., 2016) (Table 3, Figure 2). Table 4 shows acceptable discriminant validity as the square roots of average variance extracted of a dimension is greater than the correlation of the item with the remaining dimensions. Thus, the measurement model indicates that the data has the required reliability and the metric has the desirevalidity.

	Cronbach's Alpha	rho_A	Composite Reliability	Average Variance Extracted (AVE)
ECS	0.67	0.68	0.82	0.60
ENS	0.66	0.68	0.81	0.59
ORS	0.66	0.69	0.71	0.48
POI	0.71	0.67	0.66	0.42
PRN	0.67	0.79	0.77	0.54
SCS	0.78	0.69	0.74	0.48

Table 2: Reliability and Validity

	ECS	ENS	ORS	POI	PRN	SCS
ECS1	0.77					
ECS2	0.80					
ECS3	0.76					
ENS1		0.81				
ENS2		0.81				
ENS3		0.69				
ORS1			0.81			
ORS2			0.79			
ORS3			0.85			
POI1				0.91		
POI2				0.73		
POI3				0.70		
PRN1					0.61	
PRN2					0.79	
PRN3					0.79	
SCS1						0.76
SCS2						0.63
SCS3						0.70

Table 3: Factor Loading

	ECS	**ENS**	**ORS**	**POI**	**PRN**	**SCS**
ECS	**0.78**					
ENS	**0.56**	**0.77**				
ORS	**0.46**	**0.32**	**0.69**			
POI	**0.45**	**0.40**	**0.38**	**0.65**		

PRN	**0.31**	**0.28**	**0.30**	**0.25**	**0.73**	
SCS	**0.34**	**0.18**	**0.25**	**0.30**	**0.48**	**0.70**

Table 4: Discriminant validity Values in bold indicate the square root of AVE

5.2 Structural Model

The structural model in SEM facilitates the testing of the hypotheses (Table 5, Figure 3). The path coefficients between the latent variables is shown in Figure 2.

The following hypotheses are supported:

H1: Product innovation has positive significant relationship with social sustainability in manufacturingindustries.

H2a: Process innovation has positive significant relationship with social sustainability in manufacturingindustries.

H3: Product innovation has positive significant relationship with economic sustainability in manufacturingindustries.

H4: Process innovation has positive significant relationship with economic sustainability in manufacturingindustries.

H5: Product innovation has positive significant relationship with environmental sustainability in manufacturingindustries.

H6: Process innovation has positive significant relationship with environmental sustainability in manufacturingindustries.

H8: Economic sustainability has positive significant relationship with organizational performance in manufacturing industries.

Following hypotheses are not supported:

H7: Social sustainability has positive significant relationship with organizational performance in manufacturing industries.

H9: Environmental sustainability has positive significant relationship with organizational performance in manufacturing industries.

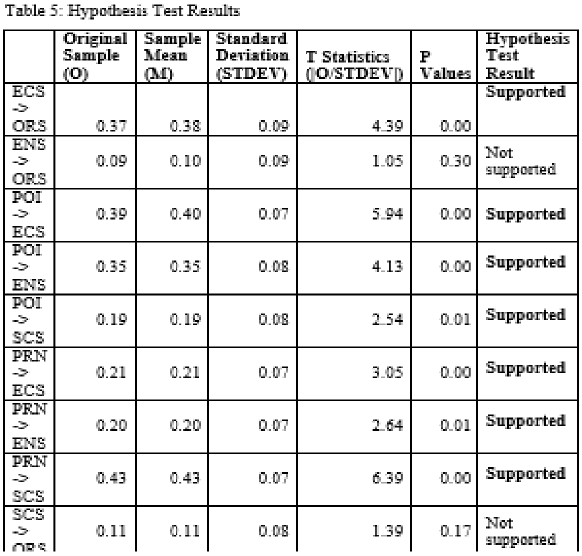

Table 5: Hypothesis Test Results

	Original Sample (O)	Sample Mean (M)	Standard Deviation (STDEV)	T Statistics (|O/STDEV|)	P Values	Hypothesis Test Result
ECS -> ORS	0.37	0.38	0.09	4.39	0.00	Supported
ENS -> ORS	0.09	0.10	0.09	1.05	0.30	Not supported
POI -> ECS	0.39	0.40	0.07	5.94	0.00	Supported
POI -> ENS	0.35	0.35	0.08	4.13	0.00	Supported
POI -> SCS	0.19	0.19	0.08	2.54	0.01	Supported
PRN -> ECS	0.21	0.21	0.07	3.05	0.00	Supported
PRN -> ENS	0.20	0.20	0.07	2.64	0.01	Supported
PRN -> SCS	0.43	0.43	0.07	6.39	0.00	Supported
SCS -> ORS	0.11	0.11	0.08	1.39	0.17	Not supported

Table 5: Hypothesis TestResults

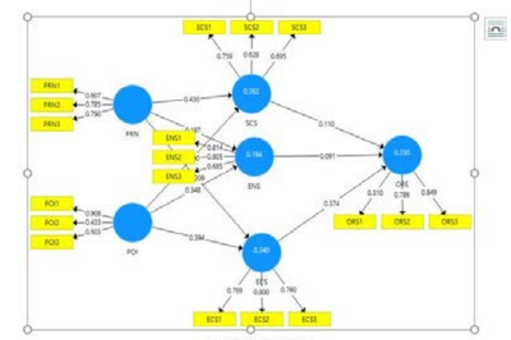

Figure 2: Path Model

Fig 2: Path Model

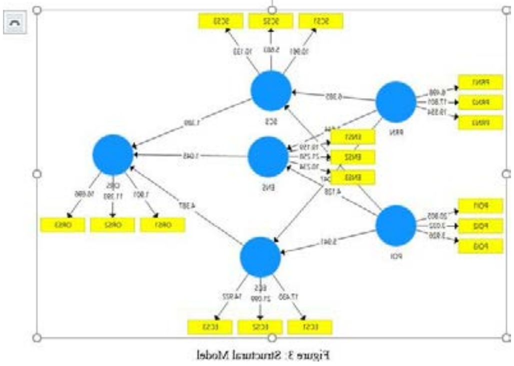

Fig 3:Structural Model

VI. IMPLICATIONS TO THE MANUFACTURING MANAGERS

Hypothesis testing has indicated that both product innovation and process innovation have positive significant relationship with social sustainability, economic sustainability and environmental sustainability in manufacturing industries. This finding is in agreement with some earlier studies in various other contexts (e.g., Brettel & Cleven, 2011; Buchegger & Ornetzeder, 2000; Morais & Silvestre, 2018; Rauter et al., 2017; Matthies et al., 2017). The implication of this study is that if the company has to achieve sustainability in their business they need to strengthen both product and process innovation. Speaking about product innovation, the managers in manufacturing industries need to bear in mind the concept of user-centric-innovation in both product and process innovation through a well-defined innovation strategy (Pisano, 2015). An effective strategy should start with specific objectives and the objectives need to incorporate all the three dimensions of sustainability in the formulation stage itself. It has been observed that while many manufacturing organizations have a very highly matured innovation strategy the missing factor is sustainability of aspects. This is one of the reason why many of the fortune 500 companies of the past have lost their market standing and have been forced to adopt exit strategy. The need of the hour is to have a paradigm shift from the over emphasis laid on technology to the social, economic and environmental aspects of manufacturing. The demands of the customers keep changing from time to time and as the products evolve the demands of the customers also keep changing and today's customers are more conscious about the environmental, social as well as cultural aspects associated with the product. So, the innovation strategy with objectives linked to sustainability issues could enable the manufacturing companies to ensure competitive advantage in the market.

Value creation to the customers during the product and process innovation could be another aspect which needs attention in the present manufacturing scenario. Value creation to the customers not only refers to the higher level of performance of the product, but ensure healthy environment with clean water, fresh air, healthy food and harmony in the society. These are the demands of present day customers as it has been realized that manufacturing industries have been responsible for the pollution of environment and WHO has declared some of the major destinations of the world to be not safe anymore for healthy living (WHO, 2017). Thus, the product innovation should necessarily consider making the product cheaper, durable, reliable, serviceable, and reusable but at the same time sensitive to the social, economic and environmental issues.

Finally, manufacturing industries need to focus more on disruptive innovation, which is not mere technological in nature, but more of business model re-engineering (Pisano, 2015). The product and process innovation should essentially disrupt the existing way of doing things the best example being Android as an operating system which is also free and inbuilt to the mobile. So, there is a need for the manufacturers to have a paradigm shift from radical innovation to disruptive innovation for the simple reason that sustainability is better addressed in the latter.

It was surprising to note through the results of the study that only the economic sustainability had a significant positive influence on organizational performance and both social and environmental sustainability had no significant influence on the organizational performance. The finding does not mean that only economic sustainability should be the target of the manufacturing managers to achieve higher level of organizational performance, but it is evident that it has a higher level of contribution. This result is in agreement with the findings of many researchers who have proved that economic sustainability has higher contribution to organizational performance because it is mainly technology driven. The higher the technology the better is the economic sustainability and higher the organizational performance (Maletic et al., 2015; Pisano, 2015; Wagner, 2010). The implication to the managers is that they may give higher focus on to the economic sustainability aspects of manufacturing without sacrificing the social andenvironmental aspects of manufacturing. Some researchers have also proved that economic sustainability and environmental sustainability are inversely proportional (Schaltegger, S., &Synnestvedt, 2002). Even though social and environmental sustainability does not contribute significantly to the organizational performance as indicated through this research they cannot be ignored completely as they are statutory requirements and also controlling the license to operate.

VII. CONCLUSION

This research is an attempt to provide a holistic model of innovation, sustainability and business performance. While the research literature is inundated with studies on individual aspects of these three research constructs not much has been done to study the interdependencies of these three constructs at their dimensional level. So, this research is a step forward in that direction.

Through this study it was found that innovation in the context of manufacturing was a multi-dimensional construct and the product and process innovation cannot be studied in isolation but they need to be holistically linked to the dimensions of sustainability. Thus, the conceptual model related the product and process innovations to the social, economic and environmental dimensions. It was found that in the context of manufacturing industries there were studies which have empirically tested the relationships between innovation and sustainability, but the linkage can be complete only when sustainability was linked to organizational performance. That provided completeness to the hypothetical model provided in thisresearch.

Through the quantitative analysis using questionnaire survey with a sample size of 211 spread over the medium scale manufacturing industries in Bangalore which is the capital of Karnataka State of India, it could be concluded through the hypothesis testing that while both product and process innovation contributed to social, economic and environmental sustainability, only economic sustainability contributed to the organizational performance. Accordingly, implications were drawn for the benefit of the managers of manufacturing industries so as to enhance their organizational performance. Two important aspects of innovation: innovation strategy and value creation have been briefed for the benefit of managers highlighting the need for a change in the existing radical innovation which is focussing mainly on technology ignoring other aspects for sustainability.

In today's customer driven market of manufacturing, it is important for the manufacturers to be mindful about the social, economic and environmental awareness of the customers and align their products as well as manufacturing processes to meet the customer demands. It can be concluded that while economic sustainability should be the main aim of the manufacturers to achieve organizational performance but the importance of social and economic sustainability should not be undermined as they are indirectly the ‘license to operate’. Well-planned corporate social responsibility demonstrated through clearly defined action plans and measures taken to demonstrate sensitiveness to environmental protection could surely pave the way tosucceed.

REFERENCE

[1] Abatenh, E., Gizaw, B., Tsegaye, Z., & Tefera, G. (2018). Microbial Function on Climate Change-A Review. Environ Pollut Climate Change, 2(147),10-4172.

[2] Abdullahi, T., & Abdullah, S. S. (2015). Sustainability Considerations in Manufacturing and Operation Management. International Journal of Scientific Engineering and Applied Science,1.

[3] Abhilash, P. C., Dubey, R. K., Tripathi, V., Gupta, V. K., & Singh, H. B. (2016). Plant growth-promoting microorganisms for environmental sustainability. Trends in biotechnology, 34(11),847-850.

[4] Ahmad, S., Zulkurnain, N. N. A., &Khairushalimi, F. I. (2016). Assessing the validity and reliability of a measurement model in Structural Equation Modeling (SEM). Journal of Advances in Mathematics and Computer Science, 1(1)1-8.

[5] Akram, M., Goraya, M., Malik, A., &Aljarallah, A. (2018). Organizational Performance and Sustainability: Exploring the Roles of IT Capabilities and Knowledge Management Capabilities. Sustainability, 10(10),3816.

[6] Amit, R., Zott, C., (2012). New business models—creating value through business model innovation. MIT Sloan Management Review, 53(3),41.

[7] Andraszewicz, S., Scheibehenne, B., Rieskamp, J., Grasman, R., Verhagen, J., &Wagenmakers, E. J. (2015). An introduction to Bayesian hypothesis testing for management research. Journal of Management, 41(2),521-543.

[8] Arkolakis, C., Ramondo, N., Rodríguez-Clare, A., &Yeaple,

[9] S. (2018). Innovation and production in the global economy. American Economic Review, 108(8), 2128-73.

[10] Armeanu, D., Vintilă, G., &Gherghina, Ş. (2018). Empirical study towards the drivers of sustainable economic growth in EU-28 countries. Sustainability, 10(1),4.

[11] Arora, N. K., Fatima, T., Mishra, I., Verma, M., Mishra, J., & Mishra, V. (2018). Environmental sustainability: challenges and viable solutions. Environmental Sustainability, 1(4), 309-340.

[12] Bacon, N., Cochrane, D., Woodcraft, S., & Brown, J. (2012). Creating strong communities: how to measure the social sustainability of new housing developments. The Berkeley Group: London,UK.

[13] Behnam, S., &Cagliano, R. (2017). Be sustainable to be innovative: An analysis of their mutual reinforcement. Sustainability, 9(1),17.

[14] Belvedere, V., Grando, A. & Ronen, B. (2013). Cognitive Biases, Heuristics, and Overdesign: An Investigation on the Unconscious Mistakes of Industrial Designers and on Their Effects on Product Offering. Behavioral Issues in Operations Management: New Trends in Design, Management, and Methodologies, pp.125-139.

[15] Bockermann, A., Meyer, B., Omann, I., &Spangenberg, J. H. (2005). Modelling sustainability: Comparing an econometric (PANTA RHEI) and a systems dynamics model (SuE). Journal of Policy Modeling, 27(2),189-210.

[16] Brettel, M., &Cleven, N. J. (2011). Innovation culture, collaboration with externalpartners and NPD performance. Creativity and Innovation Management,20(4),253–272.

[17] Breznitz, D., &Cowhey, P. (2012). America's two systems of innovation: innovation for production in fostering USgrowth. Innovations: Technology, Governance, Globalization, 7(3), 127-154.

[18] Buchegger, B., &Ornetzeder, M. (2000). Social innovations on the way to sustainable development. In ESEE Conference Proceeding, Vienna.

[19] Çakir, s. (2017). Modeling national innovation systems of EU countries using partial least squares structural equation modeling (PLS-SEM). HacettepeÜniversitesiİktisadiveİdariBilimlerFakültesiDergisi , 35(3), 19-41.

[20] Cherrafi, A., Garza-Reyes, J. A., Kumar, V., Mishra, N., Ghobadian, A., &Elfezazi, S. (2018). Lean, green practices and process innovation: A model for green supply chain performance. International Journal of Production Economics, 206,79-92.

[21] Chesbrough, H. (2003). Open innovation. The new imperative for creating and profiting from technology. Boston: Harvard Business SchoolPress.

[22] Chiang, H., Han, T., & Chuang, J. (2011). The relationship between high-commitment HRM and knowledge-sharing behavior and its mediators, International Journal of Manpower, 32(5/6), 604 –622.

[23] Colantonio, A., & Dixon, T. (2011). Urban regeneration and social sustainability: Best practice from European cities. John Wiley &Sons.

[24] Côté, R., Booth, A. & Louis, B. (2006). Eco-efficiency and SMEs in Nova Scotia, Canada. Journal of Cleaner Production, 14, 542-55,http://dx.doi.org/10.1016/j.jclepro.2005.07.004

[25] Dawson, P., Daniel, L., (2010) Understanding social innovation: a provisional framework. Int. J. Technol. Manag. 51 (1),9–21.

[26] Deloitte (2017). The Deloitte Global Millennial Survey 2017: Optimism, trust reach troubling low levels. Retrieved on 5/12/2017 from:

[27] https://www2.deloitte.com/global/en/pages/about-deloitte/articles/millennialsurvey.html.

[28] Dempsey, N., Bramley, G., Power, S., & Brown, C. (2011). The social dimension of sustainable development: Defining urban social sustainability. Sustainable development, 19(5), 289-300.

[29] Di Vaio, A., &Varriale, L. (2018). Management innovation for environmental sustainability in seaports: Managerial accounting instruments and training for competitive green ports beyond the regulations. Sustainability, 10(3),783.

[30] Dillard, J., Dujon, V., & King, M. C. (Eds.). (2008). Understanding the social dimension of sustainability. Routledge.

[31] Eizenberg, E., &Jabareen, Y. (2017). Social sustainability: A new conceptual framework. Sustainability, 9(1),68.

[32] Giddings, B., Hopwood, B., &O'brien, G. (2002). Environment, economy and society: fitting them together into sustainable development. Sustainable development, 10(4), 187-196.

[33] Griessler, E., &Littig, B. (2005). Social sustainability: a catchword between political pragmatism and social theory. International Journal for Sustainable Development, 8(1/2), 65-79.

[34] Hami, N., Muhamad, M. R., &Ebrahim, Z. (2015). The impact of sustainable manufacturing practices and innovation performance on economic sustainability. Procedia CIRP, 26, 190-195.

[35] Hanushek, E. A., &Woessmann, L. (2008). The role of cognitive skills in economic development. Journal of economic literature, 46(3),607-68.

[36] Herrmann, C., Schmidt, C., Kurle, D., Blume, S., &Thiede, S. (2014). Sustainability in manufacturing and factories of the future. International Journal of precision engineering and manufacturing-green technology, 1(4),283-292.

[37] Igwenagu, C. (2016). Fundamentals of research methodology and data collection,.LAP Lambert Academic Publishing (2016-04-19), ISBN:978-3-659-86884-9

[38] Jaw, Y. L., Chen, C. L., & Chen, S. (2012). Managing innovation in the creative industries–A cultural production innovation perspective. Innovation, 14(2),256-275.

[39] Jaw, Y. L., Chen, C. L., & Chen, S. (2012). Managing innovation in the creative industries–A cultural production innovation perspective. Innovation, 14(2),256-275.

[40] Joyce, A., Paquin, R.L., (2016). The triple layered business

model canvas: a tool to design more sustainable business models. J. Clean. Prod. 135 (1),1474–1486.

[41] Jung, J.Y. & Hong, S., (2008). Organizational citizenship behaviour (OCB), TQM and performance at the maquiladora, International Journal of Quality & Reliability Management, 25(8), 793 –808.

[42] Kishawy, H. A., Hegab, H., &Saad, E. (2018). Design for sustainable manufacturing: Approach, implementation, and assessment. Sustainability, 10(10),3604.

[43] Kline, R. B. (2001). Principles and practices of structural equation modelling, NY: GilfordPress.

[44] Kumar, R., Garg, D. and Garg, T.K. (2009). Total quality management in Indian industries: relevance, analysis and directions, The TQM Journal, 21(6),607-22.

[45] Kutucuoglu, K. Y., Hamali, J., Irani, Z., & Sharp, J. M. (2001). A framework for managing maintenance using performance measurement systems. International Journal of Operations & Production Management, 21(1/2),173-195.

[46] Länsisalmi, H., Kivimäki, M., Aalto, P., &Ruoranen, R. (2006). Innovation in healthcare: a systematic review of recent research. Nursing Science Quarterly, 19(1),66-72.

[47] Löfgren, H., & Williams, O. (Eds.). (2016). The new political economy of pharmaceuticals: production, innovation and TRIPS in the global south.Springer.

[48] Lundvall, B. Å., Johnson, B., Andersen, E. S., &Dalum, B. (2002). National systems of production, innovation and competence building. Research policy, 31(2),213-231.

[49] Maletič, M., Maletič, D., Dahlgaard, J. J., Dahlgaard-Park, S. M., &Gomišček, B. (2014). The relationship between sustainability–oriented innovation practices and organizational performance: empirical evidence from slovenian organizations. Organizacija, 47(1),3-13.

[50] Maletic, M., Maletic, D., Dahlgaard, J., Dahlgaard-Park, S. M., &Gomišcek, B. (2015). Do corporate sustainability practices enhance organizational economic performance?. International Journal of Quality and Service Sciences, 7(2/3), 184-200.

[51] Matthies, A. L., Stamm, I., Hirvilammi, T., &Närhi, K. (2017). Ecosocial Innovations and Their Capacity to Integrate Ecological, Economic and Social Sustainability Transition. Sustainability, 11(7),2107.

[52] Morais, D.O., Silvestre, B.S., (2018). Advancing social sustainability in supply chain management: lessons from multiple case studies in an emerging economy. J. Clean. Prod. 199,222–235.

[53] Padilha, C. K., & Gomes, G. (2016). Innovation culture and performance in innovation of products and processes: a study in companies of textile industry. RAI Revista de Administração e Inovação, 13(4),285-294.

[54] Piccarozzi, M. (2017). Does Social Innovation Contribute to Sustainability? The Case of Italian Innovative Start-Ups. Sustainability, 9(12),2376.

[55] Pisano, G. P. (2015). You need an innovation strategy. Harvard Business Review, 93(6),44-54.

[56] Protogerou, A., Kontolaimou, A., &Caloghirou, Y. (2017). Innovation in the European creative industries: a firm-level empirical approach. Industry and Innovation, 24(6),587-612.

[57] Puig, M., Wooldridge, C., Michail, A., &Darbra, R. M. (2015). Current status and trends of the environmental performance in European ports. Environmental Science & Policy, 48,57-66.

[58] Rauter, R., Globocnik, D., Perl-Vorbach, E., &Baumgartner, J. (2017). Open innovation and its effects on economic and sustainability innovation performance. Journal of Innovation & Knowledge, 4(4), 226-233.

[59] Rennings, K., Ziegler, A., Ankele, K., & Hoffmann, E. (2006). The influence of different characteristics of the EU environmental management and auditing scheme on technical environmental innovations and economic performance. Ecological Economics, 57(1),45-59.

[60] Romero, D., Larsson, L., Rönnbäck, A. Ö., &Stahre, J. (2017, December). Strategizing for Production Innovation. In IFIP International Conference on Advances in Production Management Systems (pp. 3-12). Springer,Cham.

[61] Salaheldin, S.I. (2009). Critical success factors for TQM implementation and their impact on performance of SMEs, International Journal of Productivity and Performance Management, 58(3), 215 –237.

[62] Schaltegger, S., &Synnestvedt, T. (2002). The link between 'green'and economic success: environmental management as the crucial trigger between environmental and economic performance. Journal of environmental management, 65(4), 339-346.

[63] Seliger, G. (Ed.). (2012). Sustainable Manufacturing: Shaping Global Value Creation. Springer Science & Business Media.

[64] Silvestre, B. S., &Ţîrcă, D. M. (2017). Innovations for sustainable development: Moving toward a sustainable future. Journal of Cleaner Production, 208,325-332.

[65] Snihur, Y., &Wiklund, J. (2017). Searching for innovation: Product, process, and business model innovations and search behavior in established firms. Long Range Planning, 52(3), 305-325.

[66] Soni, P. K., Lilien, G. L., & Wilson, D. T. (1993). Industrial innovation and firm performance: A re-conceptualization and exploratory structural equation analysis. International Journal of Research in Marketing, 10(4),365-380.

[67] Spangenberg, J. H. (2005). Economic sustainability of the economy: concepts and indicators. International journal of sustainable development, 8(1-2),47-64.

[68] Srivastava, S.K., (2007). Green supply-chain management: a state-of-the-art literature review. Int. J. Manag. Rev. 9 (1), 53–80.

[69] Tohidi, H., & Jabbari, M. M. (2012). Product innovation performance in organization. Procedia Technology, 1, 521-523.

[70] Tomislav, K. (2018). The Concept of Sustainable Development: From its Beginning to the Contemporary Issues. Zagreb International Review of Economics & Business, 21(1), 67-94.

[71] Tomoyose, F. H., Santos, I. C. D., &Faria, A. C. D. (2017). The influence of open innovation on domestic sales in Brazilian industry: an analysis of the Innovation Survey 2014 based on structural equation modeling. BBR. Brazilian Business Review, 16(3),222-238.

[72] Tonelli, F., Evans, S., &Taticchi, P. (2013). Industrial sustainability: challenges, perspectives, actions. International Journal of Business Innovation and Research, 7(2),143-163.

[73] Wagner, M. (2010). The role of corporate sustainability performance for economic performance: A firm level analysis of moderation effects. Ecological Economics, 69(7), 1553-1560.

[74] Wang, G., Tian, X., Hu, Y., Evans, R. D., Tian, M., &Wang, (2017). Manufacturing process innovation-oriented knowledge evaluation using MCDM and fuzzy linguistic computing in an open innovation environment. Sustainability, 9(9),1630.

[75] Wejnert, B. (2002). Integrating models of diffusion of innovations: A conceptual framework. Annual review of sociology, 28(1),297-326.

[76] WHO (2017). Air pollution, World Health Organization Report, Retrieved on 13/12/209 from: https://www.who.int/health-topics/air-pollution#tab=tab_1

[77] Wiktorsson, M., Bellgran, M., & Jackson, M. (2008). Sustainable manufacturing-challenges and possibilities for research and industry from a swedish perspective. In Manufacturing Systems and Technologies for the New Frontier (pp. 119-122). Springer,London.

[78] Woodcraft, S. (2015). Understanding and measuring social sustainability. Journal of Urban Regeneration & Renewal, 8(2),133-144.

[79] Wordsworth, P. (2001). Lee's Building Maintenance Management, 4th ed., Oxford:Blackwell.

[80] Xu, M., David, J. M., & Kim, S. H. (2018). The fourth industrial revolution: opportunities and challenges. International journal of financial research, 9(2),90-95.

★★★